UNIVERSITAT ROVIRA I VIRGILI

MECHANISTIC STUDIES OF WATER OXIDATION CATALYZED BY HOMOGENEOUS IRON AND RUTHENIUM COMPLEXES AND LIGHT-DRIVEN ORGANIC REDUCTIONS WITH A DUAL COBALT/COPPER CATALYTIC SYSTEM

Carla Casadevall Serrano

UNIVERSITAT ROVIRA i VIRGILI

Mechanistic Studies of Water Oxidation Catalyzed by Homogeneous Iron and Ruthenium Complexes and Light-driven Organic Reductions with a Dual Cobalt/Copper Catalytic System

CARLA CASADEVALL SERRANO

DOCTORAL THESIS
2019

MECHANISTIC STUDIES OF WATER OXIDATION CATALYZED BY HOMOGENEOUS IRON AND RUTHENIUM COMPLEXES AND LIGHT-DRIVEN ORGANIC REDUCTIONS WITH A DUAL COBALT/COPPER CATALYTIC SYSTEM

Carla Casadevall Serrano

UNIVERSITAT ROVIRA I VIRGILI

MECHANISTIC STUDIES OF WATER OXIDATION CATALYZED BY HOMOGENEOUS IRON AND RUTHENIUM
COMPLEXES AND LIGHT-DRIVEN ORGANIC REDUCTIONS WITH A DUAL COBALT/COPPER CATALYTIC SYSTEM
Carla Casadevall Serrano

Carla Casadevall Serrano

Mechanistic Studies of Water Oxidation Catalyzed by Homogeneous Iron and Ruthenium Complexes and Light-driven Organic Reductions with a Dual Cobalt/Copper Catalytic System

DOCTORAL THESIS

Supervised by Prof. Dr. Julio Lloret Fillol

Institute of Chemical Research of Catalonia

UNIVERSITAT
ROVIRA i VIRGILI

ICIQ
Institut
Català
d'Investigació
Química

Tarragona
2019

UNIVERSITAT ROVIRA I VIRGILI
MECHANISTIC STUDIES OF WATER OXIDATION CATALYZED BY HOMOGENEOUS IRON AND RUTHENIUM
COMPLEXES AND LIGHT-DRIVEN ORGANIC REDUCTIONS WITH A DUAL COBALT/COPPER CATALYTIC SYSTEM
Carla Casadevall Serrano

Prof. Dr. Julio Lloret Fillol, Research Professor of the Catalan Institution for Research and Advanced Studies (ICREA) and Group Leader at the Institute of Chemical Research of Catalonia (ICIQ)

I STATE that the present study, entitled "Mechanistic Studies of Water Oxidation Catalyzed by Homogeneous Iron and Ruthenium Complexes and Light-driven Organic Reductions with a Dual Cobalt/Copper Catalytic System", presented by Carla Casadevall Serrano for the award of the degree of Doctor, has been carried out under my supervision in my group at the Institute of Chemical Research of Catalonia (ICIQ) and fulfills all the requirements for the International Doctor Distinction.

Tarragona, May 8th, 2019

Doctoral Thesis Supervisor

Prof. Dr. Julio Lloret Fillol

UNIVERSITAT ROVIRA I VIRGILI
MECHANISTIC STUDIES OF WATER OXIDATION CATALYZED BY HOMOGENEOUS IRON AND RUTHENIUM
COMPLEXES AND LIGHT-DRIVEN ORGANIC REDUCTIONS WITH A DUAL COBALT/COPPER CATALYTIC SYSTEM
Carla Casadevall Serrano

Dedicated to my family and friends

"A la yaya"

"You never fail until you stop trying."

Albert Einstein

"The woman who follows the crowd will usually go no further than the crowd. The woman who walks alone is likely to find herself in places no one has ever been before."

Albert Einstein

"I was taught that the way of progress is neither swift nor easy."

Marie Curie

UNIVERSITAT ROVIRA I VIRGILI

MECHANISTIC STUDIES OF WATER OXIDATION CATALYZED BY HOMOGENEOUS IRON AND RUTHENIUM
COMPLEXES AND LIGHT-DRIVEN ORGANIC REDUCTIONS WITH A DUAL COBALT/COPPER CATALYTIC SYSTEM
Carla Casadevall Serrano

ACKNOWLEDGEMENTS

I would like to acknowledge all the people that have made this thesis possible.

Primer de tot vull donar les gràcies al meu director de tesi, el Prof. Julio Lloret. Julio, des de que vaig començar els meus "pinitos" en la investigació durant la carrera a Girona, sempre m'has motivat i empès a superar-me. La teva passió i curiositat per la ciència i per voler entendre sempre més els processos que estudiem es inexhaurible. Durant els més de 6 anys que he treballat al teu costat he tingut el privilegi de poder aprendre directament de tu i m'has transmet aquesta actitud i manera de treballar fent les coses bé i anant al detall; indagant en el perquè dels fenòmens i en no quedar-se content amb els primers resultats. M'has ensenyat a ser crítica, que potser és una de les coses que més t'ha costat i amb la que ambdós hem hagut de tenir més paciència. A més, mai deixarà de sorprendre'm la gran capacitat que tens per pensar noves idees i per fer raonaments complexos de manera ràpida. Com diria en Zoel, "los cracks son los cracks". També, l'experiència de començar un nou grup aquí a l'ICIQ justament en començar la tesi també ha estat molt enriquidora. No només per haver après a muntar de zero el laboratori els dos sols i per haver hagut d'organitzar tot de nou sinó per tot lo que implica. Veure l'evolució d'un grup de recerca com el nostre de zero fins ara ha sigut molt didàctic. De no tenir res, hem construït els nostres propis fotoreactors i hem iniciat moltes línies d'investigació al grup. Gràcies a això he tingut la oportunitat d'estar involucrada en molts projectes i aprendre moltes tècniques i competències que, d'altra banda no crec que hagués après. T'estic molt agraïda per haver confiat en mi per ser la teva primera estudiant de doctorat com a professor independent. Em sento molt orgullosa i agraïda d'haver fet el meu doctorat al teu grup i que m'hagis ensenyat tantes coses i m'hagis donat sempre tants bons consells.

També vull donar les gràcies especialment al Prof. Miquel Costas. Miquel, de fet vas ser tu que em vas introduir en el món de la recerca al teu grup del QBIS quan era estudiant de 3er de carrera. Gràcies a això vaig poder descobrir la meva passió: la investigació. A més sempre m'has donar molt bons consells i hem continuat col·laborant al llarg de la tesi, pel que he pogut també aprendre de tu. Sempre t'estaré molt agraïda Miquel.

També vull fer una especial menció a en Zoel Codolà ja que amb ell vaig començar al QBIS mentre ell era estudiant de doctorat i jo feia les pràctiques de la carrera. De tu he après molt i sempre has sigut un model a seguir durant la tesi. A

més recordo molts bons moments al lab durant la meva etapa de recerca al QBIS. Era un fart de riure juntament amb l'Olaf, en Sabi, l'Arnau, en Ferran, en Joan, la Irene, la Mercè, la Tere, la Mònica i la Carlota.

Vull agrair també als meus companys de l'ICIQ i que ara ja no estan al grup. Especialment a l'Arnau, que va ser la primera persona que va arribar mentre ja entrenava per parlar amb les provetes després d'estar 4 mesos sola. Arnau va ser un suport compartir els inicis amb tu. La química del cobalt la he après de tu, m'ha agradat molt anar a tope treballant al teu costat. Recordo alguna nit treballant els 3 fins les tantes i anat a sopar a les hamburgueses porqué "esto hay que tenerlo ya". Arnau ets únic i sempre em feies riure amb les teves històries. Per altra banda també vull agrair especialment a Vlad, thanks a lot buddy for all you incondicional suport and being always there. You have played a very important role in the whole thesis since we have worked a lo together. Plus you are my friend. I miss you a lot. Wanna do another 24 h EPR measurements? ☺ També vull agrair a en Fede que es un encant i apart de ser un gran científic del que he pogut aprendre moltíssim durant els 3 anys que hem compartit laboratori, és una gran persona. Et desitjo molta sort en la nova etapa. ☺ També als altres companys que ja hn marxat: Alicia, Kaia i Felix, molta sort en la els nous projectes que heu iniciat!

També penso en "mi ovejita". El nostre passat infantil veient "cine de barrio" i el nostre apreci a Carmen Sevilla va fer que rebategés a en Sergi amb aquest nom. Tot i que hem xocat alguna vegada al lab, t'aprecio moltíssim i et trobaré a faltar quan marxi. M'ha agradat molt treballar amb tu i anar a "beam trips" fins i tot quan ens barallàvem per posar les mostres. Sempre recordaré els nostres moments de locura quan em vas vneir a vuere a Suècia mentre feia l'estada. ☺ Geyla, mi cubanita favorita, que llegaste al lab y lo llenaste de positivismo. Gracias por tener siempre una frase buena, una buena cara, una sonrisa y ayudar. Eres un encanto y estoy muy contenta de haberte conocido y haber trabajado contigo estos años. Pucci (Alberto) gracias por ayudarme siempre y por estar ahí cuando lo he ncesitado y por hacernos reir con tus historietas. También quiero agradecer a David, mi padawan, por la paciencia que ha tenido en esta última etapa de mi tesis. Ahora ya puedes con todo. Mucha suerte en tu tesis! Noufal, we have been working for a long time together already, thanks for all the suport. Klaudia and Miguel thanks a lot for the time shared and, you are the next ones in finishing the thesis, good luck! ☺ Suvendu thanks for sharing your expertise and these years in the lab. Jordi "el ruiseñor del lab" moltes

gracies per aquesta etapa al lab i molta sort. Et portaré "Cacaolat" el dia de la defensa! Luis hemos coincidido poco pero te deseo mucha suerte! Bea, yo que ya lloraba el primer día solo de pensar que me iría en algun momento, muchas gracias por todo. Y fuera del grupo, también quiero agradecer a Cristina y Andrea del grupo de JR por trabajar juntos y por vivir tan divertidos momentos en ICIQ y fuera de él. Crsitina sin tin no hubiese sido lo mismo! Al grupo de Pau, que son los vecinos y quiereras que no, simpre nos hemos hecho más, Guilia, Luís, Guillem, Ricardo, Dragos, Lluís, Felipe, simpre compartiendo cosas del lab y ayudándonos en muchas ocasiones, muchas gracias! ☺ Y a tu Gemma, la súper coordinator del Pau i la meva companya d'oficina en aques últims mesos tants durs d'escriptura de tesis i de tancament de projectes, gràcies pel suport moral i els aclariments tècnics! Os echaré de menos a tod@s!

I also acknowledge Dr. Marten Alquist to give me the opportunity to do my first doctoral stay in the KTH in Stockholm to learn about EPR calculations. Also, Prof. Giovanna Ghirlanda, for giving me the opportunity to do my second doctoral stay in the Arizona State University, where I got insight on working with metalloproteins and protein film electrochemistry. I am very thankful for this experience. In this line, I want to thank Prof. Wesley R. Browne for the collaboration to perform the Raman studies on the Ru intermediates in WO. Wes thanks a lot for teaching me Raman and being so supportive and kind to me. Thanks as well for the advice. Finally, I want to thank Prof. Serena DeBeer and Dr. Olaf Rüdiger the opportunity to perform a short stay in the MPI-CEC for the characterization of a Ru intermediate. This was a wonderful experience and I learnt a lot. Thanks as well for letting me give a talk in the seminar program of the institute.

I also want to acknowledge the ICIQ Research Support Area, specially Jordi Benet and Noemí Cabello for the support given along some of the measurements. Xavi and Leon, because without them some of the experiments would not have been possible. Noemí, tantas cinéticas juntas te he cogido mucho cariño, ya lo sabes, te mandaré paquetitos de te desde Cambridge. ☺ Xavi y León ya sabéis que para mi sois uno de los grandes pilares del ICIQ. Gracias a vosotros, he podido trabajar con montajes únicos e incluso hemos desarrollado nuestros fotoreactores a medida. Muchas gracias, soys unos máquinas! ☺ Xavi sé que malgrat et portava tubs young per reparar dia si i dia també en el fons em tens molta estima. ☺

També vull donar gràcies als meus amics Anna, Montse, Guillem, Raquel, Valentina i Ester per entendre'm i dornar-me suport en tot moment. Sé que sobretot en els darrers anys de la tesi ens hem vist poc, gràcies per respectar-ho i entendre que ara necessitava dedicar cert temps a això i a la meva vida professional. I a les meves companyes de pis per compartir aquests gairebé 5 anys de vida a Tarragona! ☺

Finalment, vull agrair especialment a la meva família per donar-me suport durant aquests anys, especialment en aquesta última etapa, que ha estat la més dura. Als avis, pares, oncles, cosins i germans. Vull fer especial èmfasi al meu germà Sergi per animar-me i estar orgullós de mi. I del qual jo també estic orgullosa per haver-se tret el batxillerat! ☺ A l'àvia Fina i al meu avi Josep que està molt orgullós de mi perquè sempre diu que "la nena és llesta com l'avi"! I a la meva "yaya Rosario", que gràcies a ella i al meu avi que al cel sia sóc la persona en la que m'he convertit. Malgrat ara ja fa un temps que estàs perdent la memòria per culpa de l'Alzheimer, sé que estàs mot orgullosa de mi i que t'emociona veure que he complert un dels meus objectius. Sempre has cregut en mi i gracies al teu amor he pogut arribar on sóc ara, per això et dedico aquesta tesi. Te quiero mucho yaya!

LIST OF PUBLICATIONS

"A Unified Electro- and Photocatalytic CO_2 to CO Reduction Mechanism with Aminopyridine Cobalt Complexes. Identification of Key Intermediates to Overcome Bottlenecks";
S. Fernández, F. Franco, **C. Casadevall**, V. Martin-Diaconescu, J.M. Lluis, J. Lloret-Fillol; *submitted.*

"Improved Activity and Stability of an Electro- and Photocatalytic Water Reduction Cobalt Catalyst by Supramolecular Confinement in Streptavidin";
A. Call*, **C. Casadevall***, A. Romero-Rivera, D. J. Sommer, S. Osuna, G. Ghirlanda, and J. Lloret-Fillol; (* equal contribution), ACS catalysis, ASAP, doi.org/10.1021/acscatal.8b04981.

"Water Oxidation Catalysis with Well-defined Molecular Iron Complexes"
C. Casadevall, A. Bucci, M. Costas, J. Lloret-Fillol; Review, AINC, 74, chapter 5, 2019, doi.org/10.1016/bs.adioch.2019.03.004, *in press, corrected proof*, doi.org/10.1016/bs.adioch.2019.03.004.

"Design of Iron Coordination Complexes as Highly Active Homogenous Water Oxidation Catalysts by Deuteration of Oxidation Sensitive Sites.";
Z. Codolà, I. Gamba, F. Acuña-Parés, **C. Casadevall**, J. M. Lluis, M. Costas, J. Lloret-Fillol; *J. Am. Chem. Soc.,* 2019, 141 (1), 323.

"Dual cobalt-copper light-driven catalytic reduction of aldehydes and aromatic ketones in aqueous media";
A. Call*, **C. Casadevall***, F. Acuña-Parés, A. Casitas, J. Lloret-Fillol; Chem. Sci., 2017, 8 (7), 4739. (* stands for equal contribution). Front cover, Highlighted in Chemistry World and Chemistry Views and Among the most downloaded articles of 2017.

Patent 2: "Photoreactor",
J. Lloret-Fillol, **C. Casadevall**, J. L. León, A. Call, A. Casitas, J. J. Pla, J. P. Hernández, F. X. Caldentey; Fundació privada Institut Català d'ivestigació Química (ICIQ), reference: 17382313.9-1370; 2017.

Patent 1: "A photocatalytic reduction procedure and a catalytic composition for the procedure"

J. Lloret-Fillol, A. Call, **C. Casadevall**, A. Casitas; ICIQ, ref PCT/ES2017/070314, PCT international, 16/05/2017.

"Catalizadores para la conversión de la energía solar en enlaces químicos"

C. Casadevall, A. Call, Z. Codolà, F. Acuña-Parés, J. Lloret-Fillol; Anales de Química, 2016, 112 (3), 133.

"Spectroscopic, Electrochemical and Computational Characterization of Ru Species Involved in Catalytic Water Oxidation: Evidence for a $[Ru^V(O)(Py_2Metacn)]$ Intermediate"

C. Casadevall, Z. Codola, M. Costas, J. Lloret-Fillol: Chem. Eur. J.; 2016, 22 (29), 10111.

Articles in preparation

"Isolation of an $\eta2$-$[Ru^{IV}$-$OO]^{2+}$ intermediate after the rate determining step in the water oxidation reaction. A direct evidence of a O-O bond formation from a metal-oxo moiety";

C. Casadevall, V. Martin-Diaconescu, W. R. Browne, F. Franco, N. Cabello, J. Benet-Buchholz, B. Lasalle-Kaiser, J. Lloret-Fillol; *in preparation*.

"A cobalt-copper dual light-driven catalytic system for the reduction of aromatic olefins in aqueous media"; **C. Casadevall**, D. Pascual, A. Casitas, A. Call, J. Lloret-Fillol; *in preparation*.

"Characterization of Reduced $[Co^{II}(Py_2^{Ts}tacn)L]$ Intermediates. The Unexpected Non-innocent Character of the Pyridine in Water Reduction."

C. Casadevall, A. Call, F. Acuña-Parés, V. Martin-Diaconescu, F. Franco, C. Sáenz de Pipaón, J. R. Galán-Mascarós and J. Lloret-Fillol; *in preparation.*

"A new N-pentadentate iron (II) complex as an active homogeneous catalyst for water oxidation"

C. Casadevall, Z. Codolà, F. Acuña-Parés, V. Martin-Diaconescu, J. M. Lluis, M. Costas, J. Lloret-Fillol; *in preparation*.

"Photoelectrochemical Water Splitting with Cobalt Cytochrome c integrated-ATO Photoanode";

Z. Bahrami, **C. Casadevall**, H. Zhang, S. Chen, D. J. Sommer, G. F. Moore, D. Seo, G. Ghirlanda; *in preparation.*

GLOSARY OF ABBREVIATIONS

Å: Angstrom

AcOEt: Ethyl acetate

aq: Aqueous

AQ^{Me2}tacn: 2-(4,7-dimethyl-1,4,7-triaazacyclononan-1-yl)-*N*-(quinolin-8-yl)acetamide

bpy: 2,2'-bypyridine

cal: Calorie

CAN: cerium(IV) ammonium nitrate

cat: Catalyst

Co-cat: Cobalt catalyst

Cp: Cyclopentadienyl

Cp*: Pentamethylcyclopentadienyl

CV: Cyclic voltammetry

δ: Chemical shift

DFT: Density functional theory

DIPEA: *N,N*-diisopropylethylamine

DLS: Dynamic Light Scattering

DMF: Dimethyl formamide

Dpaq: 2-[bis(pyridine-2-ylmethyl)]amino-*N*-quinolin-8-yl-acetamido

E1/2: Thermodynamic potential

EPR: Electron paramagnetic resonance

ESI-MS: Electrospray Ionization Mass Spectroscopy

Et_2O: Diethyl ether

eV: Electronvolt

EXAFS: Extended X-Ray Adsorption Fine Structure

FT-IR: (Fourier Transform) Infrared spectroscopy

GC: Gas chromatography

K: Kelvin

Kcal: Kilocalorie

KIE: Kinetic isotope effect

HAT: Hydrogen atom transfer

J: Joule

Kg: Kilogram

KIE: Kinetic isotopic effect

KRA: Ketyl radical anion

KIE: Kinetic isotopic effect

L: Liter

LED: Light emitting diode

LLCT: Ligand-to-ligand charge transfer

L-XTA: Laser - X-ray Transient Absorption Spectroscopy

M: Molar

Mcp = *N,N'*-dimethyl-*N,N*'-bis-(pyridin-2-ylmethyl)cyclohexane-1,2-diamine

MeCN: Acetonitrile

MeOH: Methanol

MJ: Mega joules= 106 joules= 106 W/s

MLCT: Metal-to-ligand charge transfer

Mol: Mole

MS: Mass spectrometry

$NaIO_4$: Sodium periodate

NMR: Nuclear Magnetic Resonance

NP: Nanoparticles

N4Py: *N,N'*-bis(2-pyridylmethyl)-*N*-(bis-2-pyridylmethyl)amine

NTA: Nanoparticle Tracking Analysis

η: Overpotential

ORTEP: Oak Ridge Thermal Ellipsoid Plot Program

OTf: Trifluoromethansulfonate anion

P: Pressure

PCET: Proton-coupled electron transfer

PDP: N,N'-bis(2-pyridylmethyl)2,2'-bypyrrolidine

Ph: Phenyl group

PPh_3: Triphenyl phosphine

ppm: Part per million

PSI: Photosystem I

PSII: Photosystem II

PS_{Cu}: [Cu(Bathocuproine)(Xantphos)]PF_6
photosensitizer

PS_{Ir}: [Ir^{III}(ppy)$_2$(bpy)]PF_6 photosensitizer

PS_{Ru}: [Ru(bpy)a]$^{2+}$ photosensitizer

ppy: 2-phenylpyridine

PS: Photosensitizer

Py: Pyridine

rds: Rate-determining step

RNILs: Redox non-innocent ligands

RT: Room temperature, 298 K

SET: Single electron transfer

SCE: Saturated Calomel Electrode

tacn: 1,4,7-triazacycononane

Ts: Tosyl moiety

TCD: Thermal conductivity detector

TEA: Triethylamine

TEMPO: 2,2,6,6-tetramethyl-1-piperidinyloxy free radical

TEOA: Triethanolamine

TFA: Trifluoroacetic acid

THF: Tetrahydrofurane

TOF: Turnover frequency (TON · h-1)

TON: Turnover number, (number the molecules of product)/(number of molecules of catalyst used)

TPA: Tris(2-pyridylmethyl)amine

TS: Transition state

UV-Vis: Ultraviolet-visible spectroscopy

V: Volt

VT-^{1}H-NMR: ^{1}H-NMR at varied temperatures

WO: Water oxidation

WR: Water reduction

WS: Water splitting

XANES: X-ray absorption near edge structure

XAS: X-ray absorption spectroscopy

SCHEME OF CATALYSTS EMPLOYED IN THIS THESIS

Fe and Ru WOCs

α-[Fe(OTf)₂(mcp)]
1αFe

D₄−α-[Fe(OTf)₂(mcp)]
D₄-1αFe

β-[Fe(OTf)₂(mcp)]
1βFe

D₄−β-[Fe(OTf)₂(mcp)]
D₄-1βFe

D₆−β-[Fe(OTf)₂(mcp)]
D₆-1βFe

[Ru(OH₂)(Py₂Metacn)](PF₆)₂
1RuII-OH₂

[Ru(OH)(Py₂Metacn)](PF₆)₂
1RuIII-OH

[Ru(O)(Py₂Metacn)](PF₆)₂
1RuIV=O

[Ru(O)(Py₂Metacn)](PF₆)₃
1RuV=O

η2-[Ru(OO)(Py₂Metacn)](PF₆)₂
η2-1RuIV-OO

[Fe(OTf)(Py₂Metacn)]OTf
1FeII-OTf

[Fe(OH₂)(AQMetacn)]OTf
1Fe
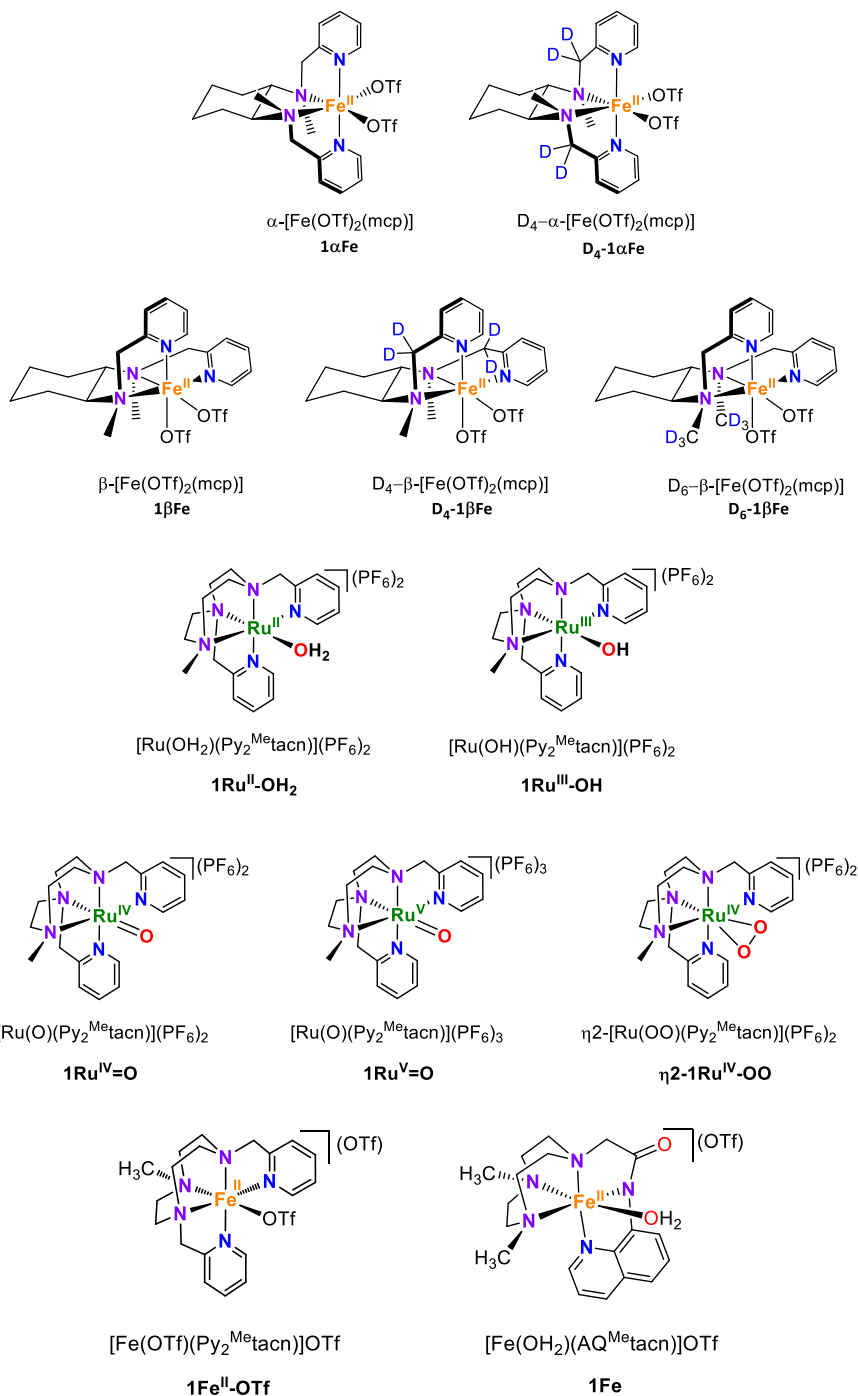
Co catalysts for light-driven organic reductions

$[Co^{II}(OTf)(Py_2^{Ts}tacn)](OTf)$

1$_{Co}$

$[Co^{II}(OTf)(^{Me,OMe}Py_2^{Ts}tacn)](OTf)$

1$^{DMM}_{Co}$

$[Co^{II}(OTf)(^{H,CO2Et}Py_2^{Ts}tacn)](OTf)$

1$_{Co}^{CO2Et}$

$[Co^{I}(Cl)(Py_2^{Ts}tacn)]$

1$_{Co}{}^{I}{}_{Cl}$

$[Co^{II}(Cl)(Py_2^{Ts}tacn)](Cl)$

1$_{Co}{}^{II}{}_{Cl}$

$[Co^{III}(Cl)(Py_2^{Ts}tacn)](Cl)(BF_4)$

1$_{Co}{}^{III}{}_{Cl}$

$[Co^{I}(Py_2^{Ts}tacn)(CH_3CN)](OTf)$

1$_{Co}{}^{I}{}_{CH3CN}$

$[Co^{II}(Py_2^{Ts}tacn)(CH_3CN)](OTf)$

1$_{Co}{}^{II}{}_{CH3CN}$

$[Co^{III}(Py_2^{Ts}tacn)(CH_3CN)](OTf)_2(BF_4)$

1$_{Co}{}^{III}{}_{CH3CN}$

$[Co^{II}(^{Me,OMe}Py_2^{Ts}tacn)(CH_3CN)](OTf)_2$

1$^{DMM}_{Co}{}^{II}{}_{CH3CN}$

$[Co^{II}(Cl)(^{Me,OMe}Py_2^{Ts}tacn)](Cl)$

1$^{DMM}_{Co}{}^{II}{}_{Cl}$

$[Co^{I}(Cl)(^{Me,OMe}Py_2^{Ts}tacn)]$

1$^{DMM}_{Co}{}^{I}{}_{Cl}$

$[Co^{II}(^{H,CO2Et}Py_2^{Ts}tacn)(CH_3CN)](OTf)_2$

1$^{CO2Et}_{Co}{}^{II}{}_{CH3CN}$

$[Co^{II}(Cl)(^{H,CO2Et}Py_2^{Ts}tacn)](Cl)$

1$^{CO2Et}_{Co}{}^{II}{}_{Cl}$

$[Co^{I}(Cl)(^{H,CO2Et}Py_2^{Ts}tacn)]$

1$^{CO2Et}_{Co}{}^{I}{}_{Cl}$

[Co^{II}(OTf)(DPA-Bpy)](OTf)
2

[Co^{II}(OTf)(H-CDPy$_3$)](OTf)
3
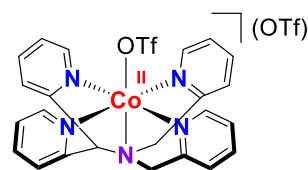
[Co^{II}(OTf)(N4Py)](OTf)
4
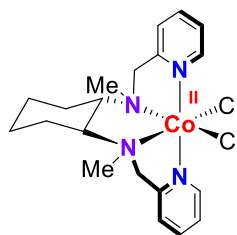
[Co^{II}(Cl)$_2$(BpcMe)]
5
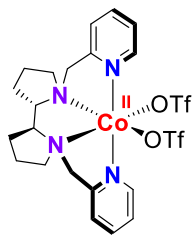
[Co^{II}(OTf)$_2$(PDP)]
6
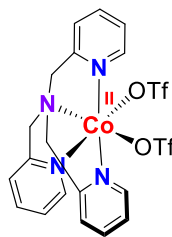
[Co^{II}(OTf)$_2$(TPH2A)]
7
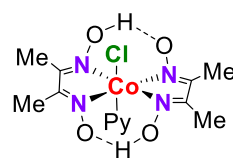
[Co^{III}(Cl)(Py)(Glyoxim)]
8
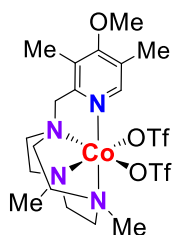
[Co(OTf)$_2$(^{Me,OMe}Py^{Me2}tacn)]
9
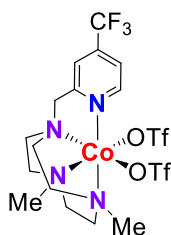
[Co(OTf)$_2$(^{H,CF3}Py^{Me2}tacn)]
10
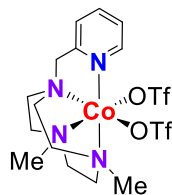
[Co(OTf)$_2$(^{H,H}Py^{Me2}tacn)]
11
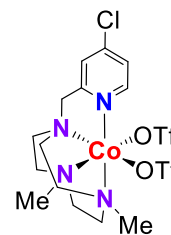
[Co(OTf)$_2$(^{H,Cl}Py^{Me2}tacn)]
12
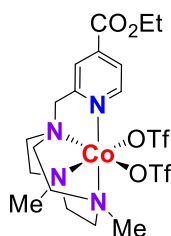
[Co(OTf)$_2$(^{H,CO2Et}Py^{Me2}tacn)]
13
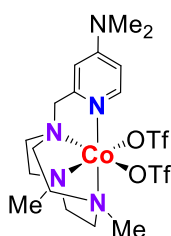
[Co(OTf)$_2$(^{Me,OMe}Py^{Me2}tacn)]
14
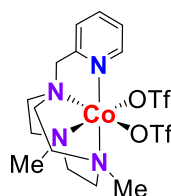
[Co(Py^{Me2}tacn)(CH$_3$CN)$_2$](OTf)$_2$
2$_{Co}^{II}_{CH3CN}$
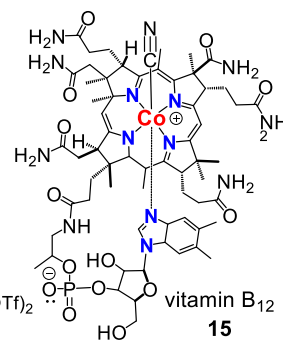
vitamin B$_{12}$
15

Photoredox catalysts for light-driven organic reductions
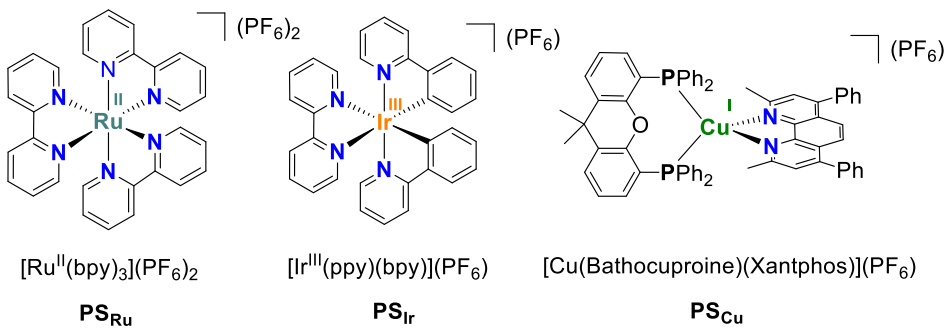
$[Ru^{II}(bpy)_3](PF_6)_2$

PS$_{Ru}$

$[Ir^{III}(ppy)(bpy)](PF_6)$

PS$_{Ir}$

$[Cu(Bathocuproine)(Xantphos)](PF_6)$

PS$_{Cu}$

GRAPHICAL ABSTRACT

CHAPTER III. Identification of the Molecular Nature of the Active Species in Water Oxidation with a Well-defined N-Tetracoordinate Fe Catalyst: the fate of the ligand (page 111)
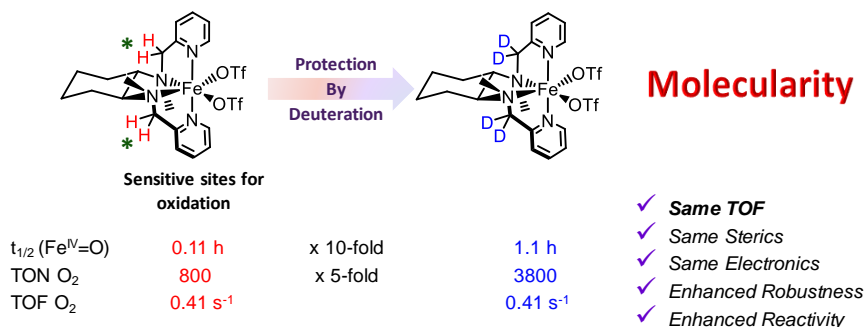
CHAPTER IV. Mechanistic Investigations of Water Oxidation Catalyzed by Ru Complexes Based on Aminopyridyl Ligands (page 137)
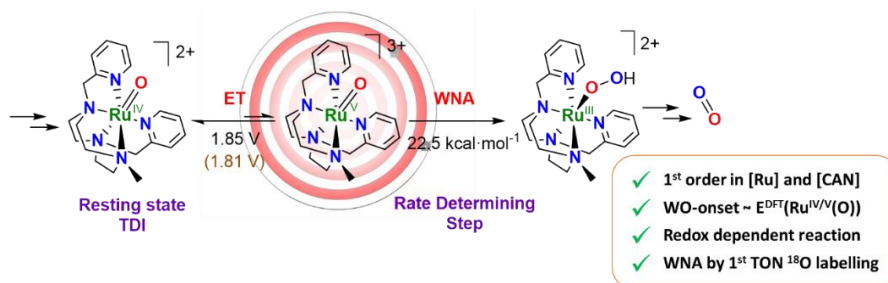
CHAPTER V. Computational Study of the Mechanisms Involved in Water Oxidation Catalyzed by Ru Complexes Based on Aminopyridyl Ligands: Understanding the Differences in Reactivity Between Analogous Ru and Fe Complexes (page 175)
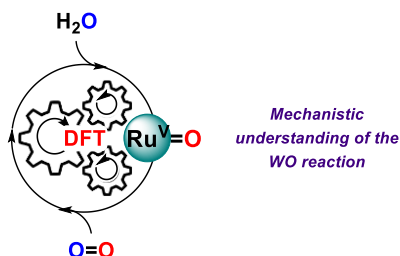
CHAPTER VI. After the O-O Bond Formation in Ruthenium Catalyzed Water Oxidation: a Missing Link (page 199)

CHAPTER VII. Development of a New N-Pentadentate anionic Fe Complex as an active catalyst for WO: the influence of the ligand scaffold and the accessibility of Fe^V species (page 249)

TABLE OF CONTENTS

CHAPTER II

CHAPTER VI

CHAPTER IX

UNIVERSITAT ROVIRA I VIRGILI

MECHANISTIC STUDIES OF WATER OXIDATION CATALYZED BY HOMOGENEOUS IRON AND RUTHENIUM
COMPLEXES AND LIGHT-DRIVEN ORGANIC REDUCTIONS WITH A DUAL COBALT/COPPER CATALYTIC SYSTEM

Carla Casadevall Serrano

SUMMARY

The transition to a green and sustainable energy-based scheme is one of the most important challenges that faces our society. Natural photosynthesis is the process by which sunlight energy is stored into chemical bonds to sustain life, producing only O_2 as a by-product. Therefore, an appealing approach is the application of artificial photosynthetic (AP) schemes to produce the so-called solar fuels and fine solar chemicals from CO_2 and water using sunlight as driving force. However, both CO_2 reduction and water oxidation (WO) are challenging processes and remain bottlenecks for the development of efficient AP. In addition, a viable artificial photosynthetic approach should also rely on inexpensive and long-lasting photocatalytic materials. In this regard, new sustainable, modular, robust and efficient catalytic platforms are needed. Moreover, it is important to notice that to design efficient and robust artificial photosynthetic systems, a fundamental understanding of the factors that control both the catalytic activity and selectivity is necessary.

Therefore, this thesis entails a fundamental understanding of the mechanisms involved in AP schemes and their application to produce fine chemicals. In this regard, we describe the synthesis and characterization of well-defined molecular iron and ruthenium WO catalysts, which, led to a better mechanistic understanding of how to access and stabilize the high oxidation states required at the metal center for O-O bond formation. Ultimately, this work resulted in the isolation and comprehensive characterization the key intermediates, as well as a thorough experimental and theoretical description of the catalytic cycle. Of particular note is the isolation and direct characterization of a high-valent Ru^{IV}-peroxo intermediate after the O-O bond formation in ruthenium catalyzed WO. Furthermore, the development of light-driven selective organic transformations based on a dual copper-cobalt photocatalytic system is also described. To remark is the unprecedented selectivity for the reduction of aromatic ketones in front of aliphatic aldehydes. Here, mechanistic studies point to a substrate-dependent mechanism for the reactivity of the postulated [Co-H] species, which is dependent on the reduction potential of the substrate. Detailed reactivity and mechanistic studies based on spectroscopic techniques (UV-vis, XAS, NMR, etc.) together with DFT calculations point to the formation of a Co^I intermediate, which followed by protonation forms the [Co-H] active species. These examples pave the way for novel sustainable light-driven reductive transformations using earth-abundant elements as catalysts.

RESUM

La transició cap a un model energètic sostenible i respectuós amb el medi ambient és un dels majors reptes socials actuals. La fotosíntesi natural és el procés pel qual les plantes emmagatzemen l'energia solar en forma d'enllaços químics per sustentar-se, produint tan sols O_2 com subproducte. Així doncs, una de les alternatives més atractives és l'aplicació d'esquemes fotosintètics artificials per a la producció de combustibles solars i productes solars d'alt valor afegit utilitzant CO_2 i aigua com a matèria prima i llum solar com a font d'energia. No obstant, tant la reducció de CO_2 com l'oxidació de l'aigua són processos limitants per l'eficient desenvolupament de la fotosíntesi artificial. A més, pel correcte desenvolupament de la fotosíntesi artificial calen materials fotocatalítics barats i d'alta durabilitat. En aquest sentit, s'han de desenvolupar nous catalitzadors que siguin sostenibles, modulars, robustos i eficients. Tanmateix, cal destacar que pel disseny de sistemes artificials eficients i robustos, és fonamental entendre els paràmetres que controlen l'activitat i l'estabilitat dels catalitzadors.

Per tant, aquesta tesi es basa en l'estudi fonamental dels mecanismes involucrats en la fotosíntesi artificial i la seva aplicació en la producció de compostos químics. Així, es descriu la síntesi i caracterització de complexos moleculars de ferro i ruteni per a la oxidació de l'aigua. El seu estudi mecanístic porta a entendre millor com accedir i estabilitzar alts estats d'oxidació al centre metàl·lic per a formar l'enllaç O-O. Finalment, aquest estudi ha resultat en l'aïllament i caracterització d'intermedis clau, així com en la detallada descripció experimental i teòrica del cicle catalític. Cal destacar la intercepció i caracterització d'un intermedi clau Ru^{IV}-peroxo després de la formació de l'enllaç O-O en la WO catalitzada per Ru. A més, també es descriu el desenvolupament de transformacions orgàniques selectives fotocatalitzades mitjançant un sistema catalític dual basat en cobalt i coure. Cal remarcar la selectivitat única en la reducció de cetones aromàtiques davant d'aldehids alifàtics. Estudis mecanístics apunten cap a un mecanisme dependent del substrat per a la reactivitat de l'espècie putativa de [Co-H], que depèn del potencial redox del substrat. Estudis de reactivitat i mecanístics basats en diferents tècniques espectroscòpiques (UV-vis, XAS, NMR, etc.) juntament amb càlculs DFT suggereixen la formació d'un intermedi de Co^I que es protona donant lloc a l'espècie activa [Co-H]. Aquests exemples inicien el camí pel desenvolupament de metodologies orgàniques sostenibles utilitzant catalitzadors basats en elements abundants.

RESUMEN

La transición hacia un modelo energético sostenible y respetuoso con el medio ambiente es uno de los mayores retos sociales actuales. Mediante la fotosíntesis natural las plantas almacenan energía solar en forma de enlaces químicos para sustentarse, produciendo O_2 como subproducto. Así, una de las alternativas más atractivas es la aplicación de esquemas fotosintéticos artificiales (FA) para la producción de combustibles solares y productos solares de alto valor añadido utilizando CO_2 y agua como materia prima y luz solar como fuente de energía. Sin embargo, tanto la reducción de CO_2 como la oxidación del agua son procesos limitantes para el desarrollo de la FA. Además, para el correcto desarrollo de la FA se necesitan materiales fotocatalíticos baratos y de alta durabilidad. En este sentido, se deben desarrollar nuevos catalizadores que sean sostenibles, modulares, robustos y eficientes. Sin embargo, cabe destacar que para el diseño de sistemas artificiales eficientes y robustos, es fundamental entender los parámetros que controlan la actividad y la estabilidad de los catalizadores.

Por lo tanto, esta tesis se basa en el estudio de los mecanismos involucrados en la FA y su aplicación en la producción de compuestos químicos. Así, se describe la síntesis y caracterización de complejos moleculares de hierro y rutenio para la oxidación del agua. Su estudio mecanístico permite entender mejor el acceso y estabilización de altos estados de oxidación en el centro metálico para formar el enlace O-O. Finalmente, se han aislado y caracterizado intermedios claves, y se ha propuesto una descripción detallada experimental y teórica del ciclo catalítico. Cabe destacar la intercepción y caracterización de un intermedio Ru^{IV}-peroxo después de la formación del enlace O-O en la WO catalizada por Ru. Además, también se describe el desarrollo de transformaciones orgánicas selectivas fotocatalizadas mediante un sistema catalítico dual basado en cobalto y cobre. Hay que remarcar la selectividad única en la reducción de cetonas aromáticas ante aldehídos alifáticos. Estudios apuntan hacia un mecanismo dependiente del sustrato para la reactividad de la especie putativa de [Co-H], dependiente del potencial redox del sustrato. Estudios de reactividad y mecanísticos basados en diferentes técnicas espectroscópicas (UV-vis, XAS, NMR, etc.) junto con cálculos DFT sugieren la formación de un intermedio de Co^I que se protona dando lugar a la especie activa [Co-H]. Estos ejemplos inician el camino para el desarrollo de metodologías orgánicas sostenibles utilizando catalizadores basados en elementos abundantes.

UNIVERSITAT ROVIRA I VIRGILI

MECHANISTIC STUDIES OF WATER OXIDATION CATALYZED BY HOMOGENEOUS IRON AND RUTHENIUM
COMPLEXES AND LIGHT-DRIVEN ORGANIC REDUCTIONS WITH A DUAL COBALT/COPPER CATALYTIC SYSTEM
Carla Casadevall Serrano

CHAPTER I.

GENERAL INTRODUCTION

UNIVERSITAT ROVIRA I VIRGILI
MECHANISTIC STUDIES OF WATER OXIDATION CATALYZED BY HOMOGENEOUS IRON AND RUTHENIUM
COMPLEXES AND LIGHT-DRIVEN ORGANIC REDUCTIONS WITH A DUAL COBALT/COPPER CATALYTIC SYSTEM
Carla Casadevall Serrano

UNIVERSITAT ROVIRA I VIRGILI
MECHANISTIC STUDIES OF WATER OXIDATION CATALYZED BY HOMOGENEOUS IRON AND RUTHENIUM
COMPLEXES AND LIGHT-DRIVEN ORGANIC REDUCTIONS WITH A DUAL COBALT/COPPER CATALYTIC SYSTEM
Carla Casadevall Serrano

CHAPTER I   GENERAL INTRODUCTION

I. GENERAL INTRODUCTION

I.1. World energy demand

One of the most challenging problems of our society is the fast rate of consumption of fossil fuels (Figure I.1.), which is not only leading to higher concentrations of greenhouse gases in the atmosphere and enhancing the global warming but also contributing to the depletion of unrenewable resources. At this stage, the reduction of CO_2 to biomass by photosynthesis cannot keep pace with production with the result that nature has lost control of the global carbon cycle. The increase of the CO_2 concentration in the atmosphere is behind the raise of global surface temperature during the last century, 0.74 ± 0.18 ºC, and is causing new extreme weather patterns, the rise of the sea level, expansion of deserts and retreat of the glaciers.[1,2] World energy demand projections show an increase in the energy consumption of about 48% from 2015 to 2040, where 80% is coming from fossil fuels. Consequently, the current energetic and environmental scenario forces to replace the carbon-based energy fuels for more sustainable ones.
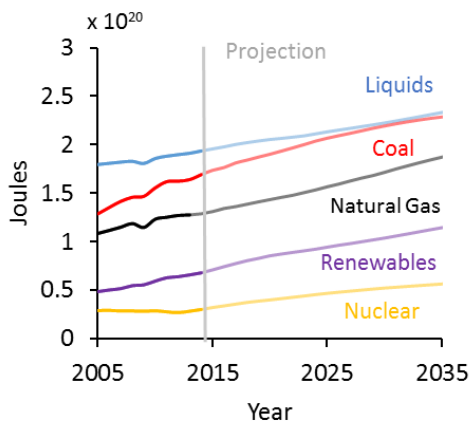
Figure I.1. Left) Projection of world energy use by fuel type, 2005-2030. Energy consumption (in Joules) comprises commercially traded fuels only. Excluded are fuels such as wood, peat and animal waste which are unreliably documented in terms for consumption statistics. Right) Projection of the worldwide energy consumption of OECD and non-OECD members. Adapted with permission from IEO2013.[3]

UNIVERSITAT ROVIRA I VIRGILI
MECHANISTIC STUDIES OF WATER OXIDATION CATALYZED BY HOMOGENEOUS IRON AND RUTHENIUM
COMPLEXES AND LIGHT-DRIVEN ORGANIC REDUCTIONS WITH A DUAL COBALT/COPPER CATALYTIC SYSTEM
Carla Casadevall Serrano

CHAPTER I   GENERAL INTRODUCTION

Therefore, non-polluting carbon-neutral and sustainable energy sources, economically comparable to the current ones, are required to substitute fossil fuels in large scale. In this line, solar energy is an optimum energy source to be used for multi-TON applications since it is readily available and abundant. Indeed, in one hour of irradiation it arrives all the energy consumed in one year. The Earth insolation resource base exceeds all other renewable energy sources combined and it is exploitable in mostly all planet regions. Nevertheless, the requirement of a permanent supply is a difficult task because of the day/night cycles of energy production. To overcome the out-of-phase sunlight energy consumption/production, a convenient energy storage system is required. In this line, the application of artificial photosynthetic schemes that allow storing sunlight energy into chemical bonds is highly desirable.

I.2. Solar energy to chemical energy conversion in Nature: Natural Photosynthesis

Evolution has come up with a very smart and complex system to harvest solar energy and to convert it into chemical energy, which is stored into carbohydrates (sugars) by the CO_2 fixation (Eq. I.1), using water as source of electrons and protons and solar energy as driving force, the Natural Photosynthesis. This complex natural machinery consists of two main processes the light reactions and the light-independent reactions and takes place in the thylakoid membrane of chloroplasts.

$$H_2O + CO_2 \xrightarrow{h\nu} [CH_2O] + O_2 \qquad \textbf{(Eq. I.1)}$$

$$2H_2O + 2NADP^+ + 3ADP + 3P_i \xrightarrow{h\nu} 2H^+ + O_2 + 2NADPH + 3ATP \qquad \textbf{(Eq. I.2)}$$

$$6CO_2 + 18ATP + 12NADPH + 12H_2O \rightarrow C_6H_{12}O_6 + 18ADP + 18P_i + 12NADP^+ + 6H^+ \qquad \textbf{(Eq. I.3)}$$

8

UNIVERSITAT ROVIRA I VIRGILI
MECHANISTIC STUDIES OF WATER OXIDATION CATALYZED BY HOMOGENEOUS IRON AND RUTHENIUM
COMPLEXES AND LIGHT-DRIVEN ORGANIC REDUCTIONS WITH A DUAL COBALT/COPPER CATALYTIC SYSTEM
Carla Casadevall Serrano

CHAPTER I   GENERAL INTRODUCTION

Figure I.2. General scheme of the principle components of natural photosynthesis, from *left* to *right*: photosystem II (PSII), plastoquinone (PQ), cytochrome b_{6f} (cyt b_{6f}), plastocyanin (PC), photosystem I (PSI), ferredoxin (Fd) and ferredoxin NADP$^+$ reductase.

In green plants, algae and cyanobacteria, light-dependent reactions of photosynthesis are performed by 3 enzymes embedded in the thylakoid membrane of the chloroplasts; Photosystem II (PSII), Cytochrome b_6f (Cyt b_6f) and Photosystem I (PSI) (Figure I.2-3).[4,5] PSII is the first enzyme involved in the light-dependent reactions, which start when a photon is captured by chlorophylls present in the light-harvesting complexes I and/or II (LHCI, LHCII) of PSII (Figure I.3). The energy of the photon is transferred to chlorophyll P680, which gets excited to form chlorophyll P680*, which is one of the strongest oxidants in biology. Excited chlorophyll P680* transfers one electron to the pheophytin (Ph, the primary acceptor), recovering chlorophyll P680 that at the same time oxidizes tyrosine Try 161 (Yz $\rightarrow$ Yz$^+$). Finally, Yz$^+$ triggers the oxidation of the Oxygen Evolving Complex (OEC). The OEC is metalloenzyme that can store up to four oxidizing equivalents, until reduced by the oxidation of a water molecule to dioxygen, releasing 4 electrons and 4 protons, which facilitate the proton gradient generation that triggers ATP synthesis.[6] Subsequently, electrons coming from water oxidation are transferred to different redox mediators (that get subsequently oxidized and reduced) from PSII to PSI through the so-called electron transport chain (Figure I.3). First, electrons from WO reduce plastoquinone (PQ) to plastoquinol (PQH$_2$). Then, cytochrome b_6f catalyzes the electron transfer from PQH$_2$ to plastocyanin (PC, a Cu-containing protein), linking the two light-dependent enzymes, PSII and PSI, whereby introducing protons into the

thylakoid space upon PQ recovery. Finally, PSI activation proceeds via a mechanism analogous to that of PSII: the energy of a photon excites chlorophyll P700 that at the same time generates a charge separation. The electron is then transported through ferredoxin (Fd, an iron-sulfur protein) to ferredoxin $NADP^+$ reductase (FNR), which reduces $NADP^+$ to NADPH (Figure I.3). In addition, the proton gradient created across the chloroplast membrane is used by ATP synthase for the concomitant synthesis of ATP (Eq. I.2). The energy stored into the chemical bonds of ATP and NADPH is used in the light-independent reactions to reduce CO_2 to hydrocarbons in the Calvin cycle and fuel the organisms' biologic activities (Figure I.3, Eq. I.3). This reserves energy into the primary energy-store, i.e. carbohydrates, which are consumed when recombined with O_2. The electronic recovery of the mechanism is achieved by oxidizing water, a process taking place in PSII (Figure I.2).
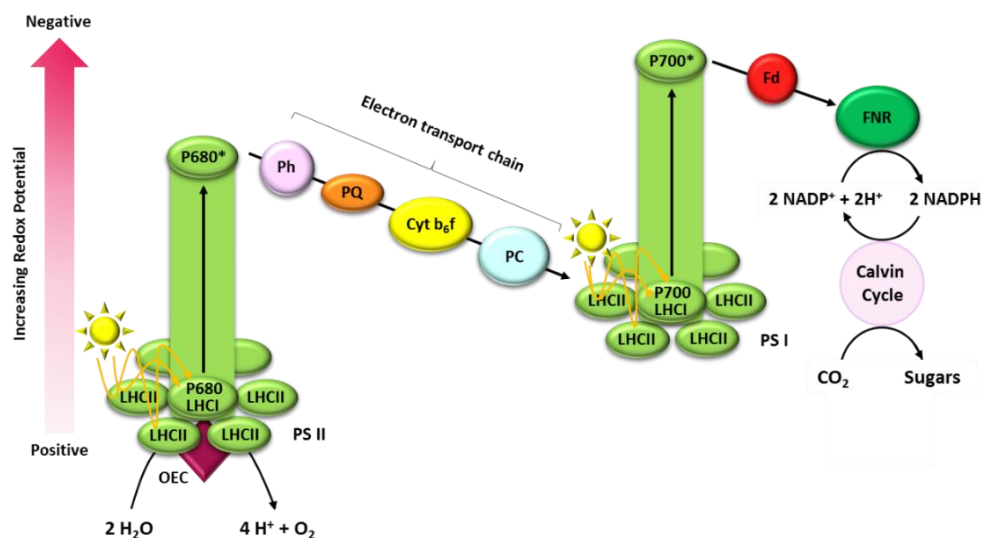
Figure I.3. Simplified scheme of the "Z-scheme" of the photosynthesis that describes the oxidation/reduction changes during the light-dependent reactions for the synthesis of NADPH. The vertical axis represents the reduction potential of a particular species. Ph = Pheophytin, PQ = Plastoquinone, PC = Plastocyanin, b_6f = Cytochrome b_6f, Fd = ferredoxin, FNR = Ferrodoxin-$NADP^+$ reductase, LHCII =light-harvesting complex II, LHCI-P680 and P700 = light-harvesting complexes containing reaction centres, located in PSII and PSI respectively.

UNIVERSITAT ROVIRA I VIRGILI
MECHANISTIC STUDIES OF WATER OXIDATION CATALYZED BY HOMOGENEOUS IRON AND RUTHENIUM
COMPLEXES AND LIGHT-DRIVEN ORGANIC REDUCTIONS WITH A DUAL COBALT/COPPER CATALYTIC SYSTEM
Carla Casadevall Serrano

CHAPTER I   GENERAL INTRODUCTION

I.3. Towards artificial photosynthesis

Natural photosynthesis elegantly transforms solar energy into chemical energy, obtaining the chemical products plants need to sustain their life. In this regard, one of the most important challenges is to mimic this process artificially to develop sustainable and greener synthetic organic methodologies to produce solar fuels and fine chemicals based on the application of artificial photosynthetic schemes.[2,7] However, both CO_2 reduction and water oxidation (WO) are challenging processes and still remain bottlenecks for the development of efficient artificial photosynthesis. A large number of accessible reaction pathways with similar thermodynamic reduction potential (Eq. I.6-8)[8,9] and the multi-proton-electron transformations involved in the CO_2 reduction difficult the selectivity.[10] On the other hand, WO (Eq. I.4) is a highly endergonic process that requires the access of very high oxidation states at the metal center, which often leads to oxidative damage side reactions. In addition, a viable artificial photosynthetic approach should also rely on inexpensive, non-toxic and robust photocatalytic materials.[11] In this regard, new sustainable, modular, robust and efficient catalytic platforms are needed. Moreover, it is also important to notice that to design efficient and robust artificial photosynthetic systems, a fundamental understanding of the factors that control both the catalytic activity and selectivity is necessary.[12]

WO half reaction: an energetic "uphill" reaction

$$2H_2O \xrightarrow{h\nu} O_2 + 4H^+ + 4e^-$$

$E^o = 1.23$ V
$\Delta G^o = 4.92$ eV
(113 Kcal·mol^{-1})

(**Eq. I.4**)
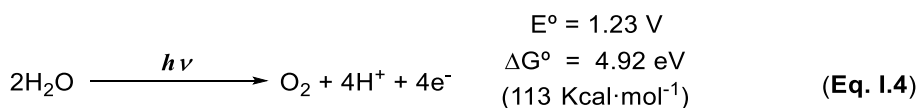
Proton and selected CO_2 reduction half reactions

$$4H^+ + 4e^- \longrightarrow 2H_2 \qquad E^o = 0.0 \text{ V} \qquad (\textbf{Eq. I.5})$$

$$CO_2 + 2H^+ + 2e^- \longrightarrow CO + H_2O \qquad E^o = -0.53 \text{ V} \qquad (\textbf{Eq. I.6})$$

$$CO_2 + 2H^+ + 2e^- \longrightarrow HCO_2H \qquad E^o = -0.61 \text{ V} \qquad (\textbf{Eq. I.7})$$

$$CO_2 + 6H^+ + 6e^- \longrightarrow CH_3OH + H_2O \qquad E^o = -0.38 \text{ V} \qquad (\textbf{Eq. I.8})$$

Despite all the studies related to understanding all the processes in natural photosynthesis in detail, still, there are some mechanisms that remain not fully understood, such as the O-O bond formation in water oxidation (WO) by the OEC. The study of photosynthesis despite being challenging due to the high amount of simultaneous multi-proton and electron transfer processes is needed to understand how this natural process works so that it can be mimicked and even improved. A better understanding of the essential components is still required to construct efficient artificial photosynthetic systems: i) light harvesting, ii) charge separation, iii) water oxidation (Eq. I.4), iv) proton and electron transport, v) proton reduction (Eq. I.5) and vi) CO_2 fixation (Eq. I.6-7). In this line, the study of the mechanisms involved in "natural" photosynthesis very much benefit from the development of (semi)synthetic models mimicking the natural machinery that allows for the investigation of the different processes involved in such complex transformation individually, such as light harvesting, charge transfer and separation, water oxidation and reductive transformations.

To be able to fully develop systems for artificial photosynthesis it is necessary to understand the mechanisms that govern WO and reduction chemistry separately to be able to finally combine both mechanisms so that water can be used as the ultimate source of electrons and solar energy as driving force. In the case of WO, we need to learn how to generate and stabilize high oxidation states at the metal centers needed to form the O-O bond formation and to understand how this process takes place so that we can develop robust and efficient systems. In the case of the reductive processes, the artificial photosynthetic scheme can be simplified to the water splitting scheme, in which water is oxidized to O_2 and then the electron and protons are recombined to produce H_2, which can be directly used as fuel. But it can also be generalized, and we can think about using the electron from WO to reduce other molecules such as CO_2 (as in photosynthesis) or organic molecules to produce added value chemicals. In this line, it is important to understand how we can generate the reductive equivalents using light as driving force (mimicking photosynthesis) and access low valent metal species and stabilize them to promote reductive transformations (scheme I.1).
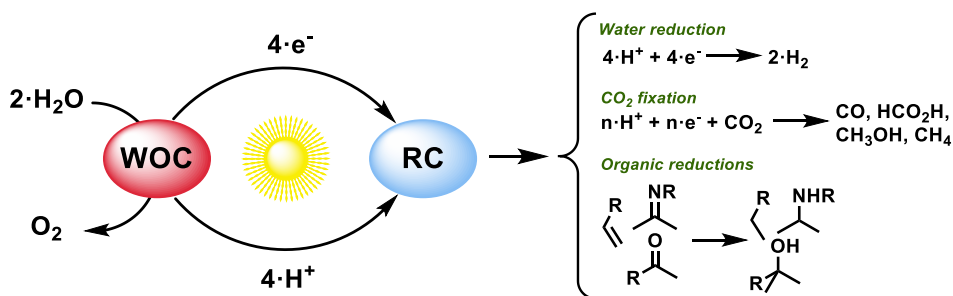
Scheme I.1. Simplified extended artificial photosynthetic scheme representing the use of electron from the oxidation of water to perform reductive transformations. WOC stands for Water Oxidation Catalysts and RC stands for Reduction Catalysts.

I.3.1. Catalysts and reactivity

Both the production of solar fuels and fine chemicals from the application of artificial photosynthetic schemes require the use of catalysts. Catalysts must be cheap, based on earth-abundant elements, robust and able to work efficiently for long periods of time. In the synthesis of solar fuels, efficiency, which is valued in the number of catalytic cycles per molecule of catalyst (TON, should be higher than 10^8) and time (TOF, should be higher than $10^3\,s^{-1}$, is very important to maximize the catalyst activity. In contrast, in the production of fine chemicals, the most important aspects are the yield and the selectivity of the transformation, since in these reaction products formed usually have a substantially higher added value.

I.3.2. Methods to evaluate and study the catalytic activity

The evaluation of the catalytic activity of catalysts requires the change in the oxidation state (oxidation/reduction) of the active centers. There are mainly 3 approaches to modify the oxidation state of the metal center and study with detail the reaction intermediates and their catalytic activity. First, we can use sacrificial agents (chemical oxidants or chemical reductants) with the desired chemical potential but with a slow reaction kinetics regarding the reaction to be catalyzed. This method enables for TON and TOF determination and for identification of reaction intermediates and mechanistic studies of the reactions. In the case of WO, the most widely used one electron sacrificial

oxidant is cerium(IV) ammonium nitrate (CAN, ~1.75 V *vs* SHE at pH 0.9, at about 50 mM concentration), which can be used to follow reaction kinetics by means of UV-Vis spectroscopy due to its strong absorption band at around 300 nm.[13] But the latter is renders acidic pH (pH < 1), limiting its use to acid-tolerant systems. Another oxidant that can be used is $[Ru(bpy)_3]^{3+}$ (~1.26 V *vs* SHE) from intermediate pHs (slightly acid to slightly basic). Alternatively, $NaIO_4$ (1.60 V vs SHE) and $KHSO_5$ (Oxone®, 1.82 V vs SHE) are used as 2 electron sacrificial oxidants.[14] Despite $NaIO_4$ is stable in aqueous solutions in wider pH range 2 – 7.5, it contains relatively labile oxygen atoms, enabling it to react as an Oxo-transfer sacrificial oxidant, which can have mechanistic implications. The use of chemical reductants has been less explored, due to their faster reaction kinetics and their instability. It is worth to note that sacrificial oxidants/reductants can act beyond simple electron acceptors/donors and get actively involved in the reactions.
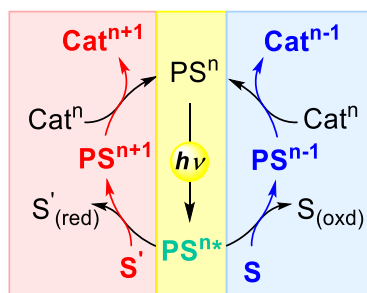
Figure I.4. General scheme of the possible photocatalytic cycles with a photoredox catalyst (PS), which allows the oxidation (red) or reduction (blue) of the metal complex that acts as the ultimate oxidation or reduction catalyst. S and S' are the sacrificial oxidants or reductants, respectively. Cat stands for the catalyst.

The other option, which is closer to the natural photosynthetic systems, consists on the combination of a photoredox catalyst (PS, chromophore, light absorption), electron donor (or acceptor) and a catalyst. Irradiation of PS generates the excited species PS*, that is a highly oxidizing (or reducing) species (Figure I.4). PS* transfers (or accepts) an electron to the sacrificial agent (S) generating the oxidized species PS^+ (or reduced). This charge separation resembles the charge separation that takes place in natural photosynthesis in PSII and PSI. The oxidized PS (or reduced) oxidizes (or reduces) the catalyst to promote the catalytic activity. In WO, the most commonly used PS/S

UNIVERSITAT ROVIRA I VIRGILI
MECHANISTIC STUDIES OF WATER OXIDATION CATALYZED BY HOMOGENEOUS IRON AND RUTHENIUM
COMPLEXES AND LIGHT-DRIVEN ORGANIC REDUCTIONS WITH A DUAL COBALT/COPPER CATALYTIC SYSTEM
Carla Casadevall Serrano

CHAPTER I   GENERAL INTRODUCTION

combination is $[Ru(bpy)_3]^{2+}$ and $Na_2S_2O_8$.[15,16] On the other hand, in the case of water reduction, the most commonly used PS/S couples are $[Ru(bpy)_3]^{2+}$ / ascorbic acid and $[Ir(ppy)_2(bpy)]^+$ / Et_3N.[17] This methodology enables the detailed study of the catalytic activity of molecular complexes under photocatalytic conditions. Nevertheless, the low efficiency for light absorption of those photoredox catalysts together with their stability in the reaction media and the difficult electron transfer between them in the solvent used for catalysis, limit the efficiency of the catalyst. The support of complexes onto solid photoelectrodes normally improves both parameters.[18]

Another method to change the oxidation state of the catalysts is by using (photo)electrochemical techniques.[19] This strategy allows for the mechanistic investigation of the speciation, the redox potential to access the active species in catalysis and evaluate the overpotential (the difference between the potential that must be applied in the electrochemical cell to promote catalysis and the thermodynamic potential) and the current intensity (related to the reaction kinetics). In this case, the most important advantage of those studies is that the reaction conditions are similar to the ones expected in the production of solar chemicals.

I.4. Dioxygen production in nature: the oxygen evolving complex

The photosynthetic protein complex PSII oxidizes water to molecular oxygen at an embedded inorganic cluster composed of four manganese ions and one calcium ion bridged by oxo or hydroxo ligands (Mn_4CaO_5), the OEC, which is placed in the light harvesting complex I (LHCI). The OEC oxidizes water generating molecular oxygen as a by-product at a rate above 300 O_2 molecules·s^{-1} (per unit of OEC).[20] This multi-metallic cluster can accumulate up to four oxidizing equivalents from tyrosine (Y_Z), generating enough driving force to oxidize water and recover the initial state. WO, then, occurs upon the subsequent oxidation of the Mn metal centers of the catalytic site, which is known as the Kok cycle and consists in 5 stages (S-states) to accumulate four oxidizing equivalents (from S_0 to S_4) and a light-independent O_2 release in the spontaneously decaying S_4 state ($S_4 \rightarrow S_0$), being S_1 (2 Mn^{III}, 2 Mn^{IV}), the dark-stable state (Scheme I.2). Despite all the

UNIVERSITAT ROVIRA I VIRGILI
MECHANISTIC STUDIES OF WATER OXIDATION CATALYZED BY HOMOGENEOUS IRON AND RUTHENIUM
COMPLEXES AND LIGHT-DRIVEN ORGANIC REDUCTIONS WITH A DUAL COBALT/COPPER CATALYTIC SYSTEM
Carla Casadevall Serrano

CHAPTER I   GENERAL INTRODUCTION

studies that have been performed to unravel the mechanism of WO in nature, the mechanism of the O-O bond formation is still far from being understood and the oxidation state of the Mn atoms at the S_4 state is not clear, being one of the missing pieces in the puzzle of biological WO. Even the dark-stable state S_1 is still incompletely understood because the available structural models do not fully explain the complexity revealed by spectroscopic investigations. Resolving the geometric and electronic structure of this cluster in its highest metastable catalytic state is a prerequisite for understanding the mechanism of O-O bond formation.[21-24] Two possible mechanistic scenarios have been proposed for the O-O bond formation: i) the nucleophilic attack of the water to a highly electrophilic $Mn^V=O$ species (or Mn^{IV}-oxyl radical), and ii) the biradical coupling between two highly electrophilic $Mn^V=O$ species (or Mn^{IV}-oxyl radical), which is one of the most accepted proposals.[24-27] The two mechanisms differ in the formation of the S_3-state. For the biradical coupling pathway, an additional water molecule must bind to the cluster, triggering an expansion of the structure. The additional water substrate forms the Mn^{IV}-oxyl radical in S_4 (Siegbahn model).[24] The evolution of the latter species until O_2 release is postulated to occur through the formation of a peroxide intermediate species, although the exact mechanism is not known. Despite the exact role of the calcium atom is not fully understood, its presence is fundamental for WO to take place.[28-30]
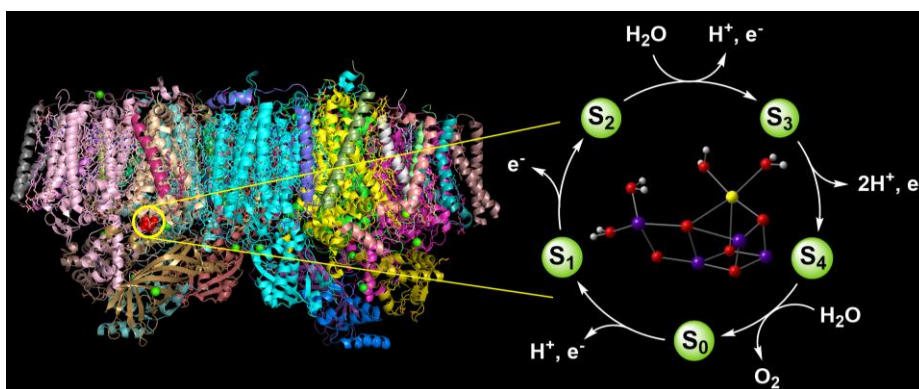
Scheme I.2. *Left*) Overall structure of PSII dimer from *T. vulcanus* at a resolution of 1.9Å extracted from the protein data bank base from ref 15; view from the direction perpendicular to the membrane normal. The protein subunits arecolored individually in both monomers. *Right*) the OEC cycle (Kok cycle) of five oxidation states Si (i = 0–4); inset, the structure of the Mn_4CaO_x cluster that has been built from crystallographic data reported on ref 15.

Nowadays, the catalytic structure of the OEC still remains elusive. The improved understanding of the structure of the OEC for the experimentally accessible catalytic states often creates a more complex picture of the system than previously imagined, while the various strands of evidence cannot always be unified into a coherent model.[22] In 2004, a cubane Mn_3O_4Ca cluster bridged by oxo atoms and connected with the fourth Mn via one of the μ-oxo groups was reported by Ferreira and coworkers.[31] Afterward, different positions of metal ions and ligands were determined with high precision energy density maps.[32] Following concerns that the OEC is being reduced during data collection, Extended X-ray Absorption Fine Structure (EXAFS) experiments with lower X-ray exposure were performed. Nevertheless the large amount of metal atoms in the OEC difficult data interpretation and three possible geometries were proposed by Yano *et al*.[33] Our present structural understanding of the OEC was decisively shaped by the 2011 most accurate crystal structure determination ever performed of PSII dimer from *T. vulcanus* by Umena *et al.*, with a resolution of 1.9Å. This disqualified a number of hypothesis and EXAFS interpretations and clarified assignments regarding the number and connectivity of oxygen bridges and the coordination and orientation of aminoacid side chains. In this structure, a distorted cubane-like Mn_3O_4Ca cluster remains as the most plausible conformation of the OEC core, which is bound to an additional manganese atom by and oxo bridge that fulfill the oxygen evolving center cluster (Mn_4CaO_5, Scheme I.2).[21] In the OEC surrounding, molecules of water were found coordinated to the metal centers and linking the Mn cluster to Yz and the last one to a nearby histidine (D1-His 190). D1-His190 seems to play a crucial role in the photosynthesis providing an exit pathway for protons and rendering the water oxidation process thermodynamically favorable (ΔG = -8.4kcalmol^{-1}).[34] Despite the high precision, authors admit that data is still insufficient in order to reveal the detailed structure of the water-splitting catalytic center. Indeed, distances obtained by X-ray crystallography and EXAFS are slightly different, suggesting that the cluster may also suffer from photoreduction by radiation and the data does not represent exclusively the structure of the S_1-state, but a superposition of reduced states.[24]

In order to understand the WO mechanism, investigations beyond the OEC multi-metallic core are currently on going, because the distinctive features of this natural catalysts also depend on its environment, the role of the protein matrix, the channels and secondary interactions, which altogether regulate mechanisms for coordinating the proton-coupled electron transfer processes (PCET) and binding, positioning, activation and O-O bond formation. The carboxylate groups from the aminoacid residues close to the metal cluster and the oxo bridging ligands are essential to stabilize the high oxidation state of the Mn centers of the Mn_4CaO_5 cluster. Understanding this latter event is very important for a technological point of view since it would provide a widespread criterion for the development of globally deployable biomimetic model systems for water splitting catalysis. Therefore, a lot of effort has been put in the development of synthetic models to study this complex machinery, although those artificial mimics still struggle to imitate the function and performance of the OCE.[22,35,36] PSII manages the whole catalytic reaction dealing with the inevitable side-reactions occurring when O_2 is accumulated. To prevent over-oxidation, Nature has developed a self-healing mechanism.[37,38] This feature represents a major issue for the development of synthetic and stable functional models.

I.5. State of the art of water oxidation catalysts

Water is the most desired electron donor to be used at multi-TON scale for the synthesis of solar fuels due to its abundance and availability. Moreover, its oxidation only produces O_2 as a by-product. However, WO is a highly endergonic process at room temperature and pressure and thus is considered as the bottleneck for the development and application of artificial photosynthetic schemes. The thermal decomposition of water occurs at temperatures higher than 2200 ºC. In addition electrolysis of water electrochemically suffers from very slow reaction kinetics and requires very high overpotentials.[39] The very high potential required for the ideally-uncatalyzed stepwise water oxidation makes the process energetically inefficient and economically unfeasible. Therefore, the use of a catalyst is absolutely required to

accomplish the reaction at lower overpotentials and high rates, and hopefully close to the thermodynamic energetic parameters of the 4-electron water oxidation to O_2 (1.23 V vs SHE). With this objective in hand, tremendous efforts have focused on the development and study of efficient water oxidation catalysts (WOCs) in the last decades.

Initial considerations must be taken into account for rational design of the optimum WOC: i) the multi-proton/electron nature of WO, ii) the synergy between metal centers, iii) the stabilization effect of the first coordination sphere and the ligand environment, iv) substrate-catalyst interaction and v) the thermodynamic stabilization of the protein environment in the O-O bond formation event. Water oxidation is a multi-step redox process and, thus, redox active compounds would be ideal platforms to assist this process by storing oxidizing equivalents and avoid the formation of highly reactive radical species. In this line, metal oxides and coordination complexes based on transition metals (TM) open a wide range of redox possibilities. In addition, the accumulation of oxidizing power by the TM catalyst can very much benefit from the stepwise proton-coupled electron-transfer (PCET) processes, which lower the thermodynamic energy by avoiding highly charged intermediates. In the case of TM coordination complexes, the ligand environment can play a very important role in stabilizing the different oxidation states at the metal centers. Indeed, basic ligands can stabilize high valent intermediates due to the significant electron density injection to the metal center. In the same group of stabilizing ligands, we can find anionic or redox non-innocent ligands. Anionic donor ligands constitute good scaffolds to achieve a great stabilization of the high oxidation states, but they tend to hydrolyze easily. Besides, redox non-innocent ligands have the advantage of facilitating the delocalization of the positive charge of a highly oxidized metal center, to enable the accumulation of oxidizing equivalents. Nevertheless, it is very important to find the right balance between stabilization and reactivity of the active species to prevent an overstabilization that hampers the O-O bond formation.

Catalysts based on biomimetic systems of the OEC, coordination complexes and organometallic complexes are the most suitable ones for the mechanistic study of water oxidation. Those systems have allowed to shed some light in the mechanisms for WO and develop efficient and fast catalysts with rates comparable or even higher to that of PSII.[40-42] One of the most challenging factors in the development and study of those systems is the identification of the exact nature of the catalytic activity. The strong oxidizing conditions required for the water oxidation can promote site oxidation reactions on the organic ligand scaffolds, leading to significant structural modifications and hinder further mechanistic investigations. Alternatively, the direct use of inorganic ligands, which are called polyoxometalates, has emerged as a competent possibility in the recent years.[43] Polyoxometalates are discrete metal-oxides of nanometric size at half way between molecular complexes and metal oxides. Nevertheless, they can also be hydrolyzed under catalytic conditions. Therefore, from a technological point of view, heterogeneous metal oxides have more potential as efficient and robust catalysts for industrial applications, since they are more stable under catalytic conditions. But it is important to note that regarding mechanistic understanding, molecular catalysts present lots of advantages such as high catalytic activities, the possibility of rational design and accessible mechanistic investigations.

As overall, the ideal catalyst should consist of a highly-oxidizing core, together with a robust and basic ligand that facilitates the O-O bond formation (structurally) and the concomitant O_2 release (electronically). To this end, the development of efficient and robust WOCs very much benefits from the detailed mechanistic study of WO.

I.5.1. Proposed mechanisms for the O-O bond formation

The study of molecular systems enables to shed some light in the catalytic cycle of water oxidation. Likewise, two key steps have been determined in the water oxidation reaction: a) the oxidation of the metal center, generating M=O or M-O˙ reactive species, and b) the O-O bond formation event, which is in most of the cases

UNIVERSITAT ROVIRA I VIRGILI
MECHANISTIC STUDIES OF WATER OXIDATION CATALYZED BY HOMOGENEOUS IRON AND RUTHENIUM
COMPLEXES AND LIGHT-DRIVEN ORGANIC REDUCTIONS WITH A DUAL COBALT/COPPER CATALYTIC SYSTEM
Carla Casadevall Serrano

CHAPTER I   GENERAL INTRODUCTION

the rate-determining step (RDS). Analogously to the OEC in PSII, two main mechanistic scenarios have been proposed for the O-O bond formation: i) a water nucleophilic attack over a highly electrophilic metal-oxo species (M=O), resulting in a 2e$^-$ reduction of the metal center (acid base mechanism, Scheme I.3, AB) and ii) the interaction of two metal-oxyl radical units (M-O$^\cdot$), resulting in a 1e$^-$ reduction per metal center (direct coupling, Scheme I.3, DC). The AB mechanism is favored with electron-withdrawing ligands, which make the metal-oxo more electrophilic and therefore more susceptible to suffer the nucleophilic attack of a water molecule. Moreover, the assistance of an internal (being part of the ligand scaffold) or external proton acceptor, binding the water molecule, can facilitate the proper orientation to the attack. On the other hand, the DC mechanism is favored by increasing the spin density on the oxygen atoms generating radical species and facilitating (electronic and sterically) the dimeric interaction.

Acid Base mechanism
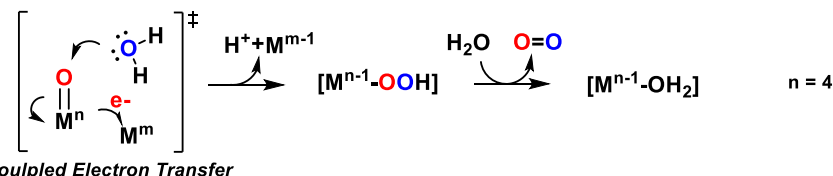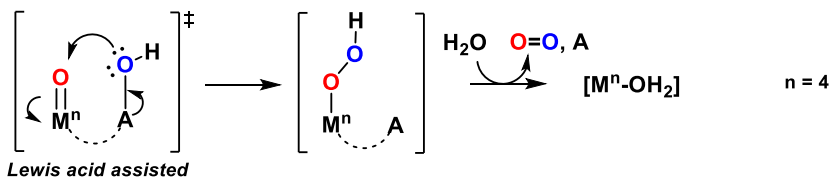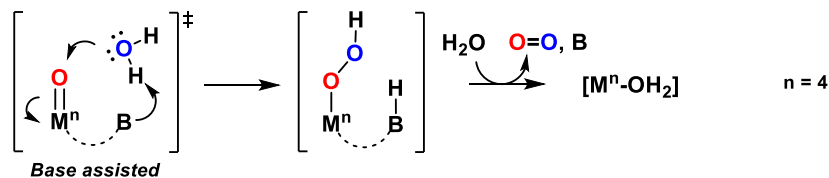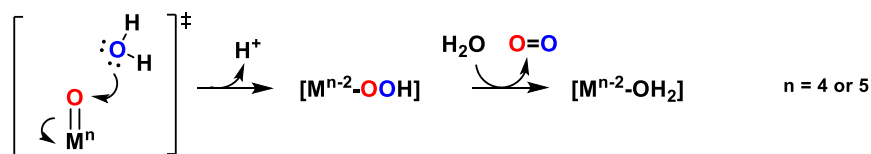
Direct Coupling mechanism
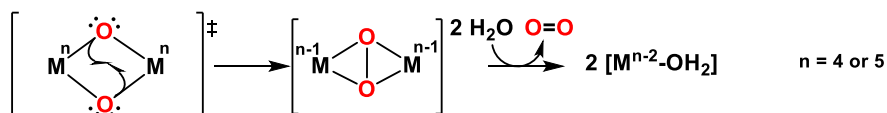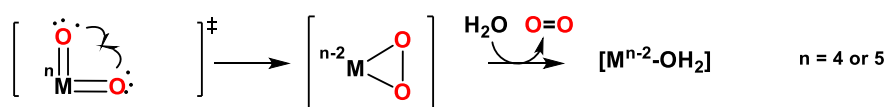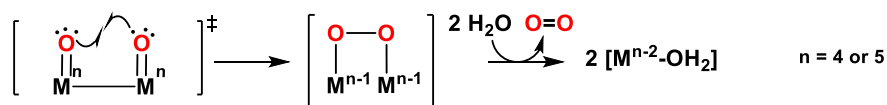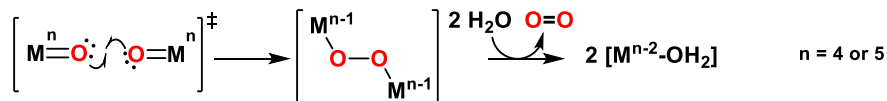
Scheme I.3. Mechanistic proposals for the O-O bond formation in the acid-base (AB) and direct coupling (DC) scenarios. Dashed lines indicate cooperation in both internal (being part of the ligand) or external scenarios.

After the O-O bond formation, reductive elimination of dioxygen is crucial to recover the catalyst, which can be also the RDS of the reaction. Electronics, the stability of the intermediate and subsequent oxidation potentials are the determining factors of the energy barrier for this step, although it is usually less energetically demanding.

I.5.2. Water oxidation catalysts based on noble metals

Understanding natural water oxidation is the most challenging aspect for the efficient and successful application of artificial photosynthesis. Moreover, the study of WO allows for the rational design of much more efficient and robust water oxidation catalysts (WOCs), which is the bottleneck for the development of efficient water splitting devices (WS). This very much benefits from the study of molecular complexes as mimic models of the natural machinery. In this line, many molecular and material WOCs, based on both noble metals, have been developed over the last decades. From the point of view of technological applications, heterogeneous materials are leading the field, albeit limited mechanistic understanding. Therefore, development and study of molecular homogeneous systems are essential to identify the intermediates involved in the WO catalytic cycle and understand the O-O bond formation event. Nevertheless, identification of the nature of the active species is not trivial and has been found particularly difficult and, sometimes, even misleading. Molecular systems are especially prone to undergo irreversible structural modifications under the strongly acidic catalytic conditions, leading to the transformation of the initially homogeneous complex into heterogeneous metal oxide species that are the actual active species. In this case, the initial metal complexes merely act as a precursor for the *in situ* formation of metal oxides that might be the true active catalytic species. In this regard, only a limited number of catalysts have been shown to proceed through well-defined molecular entities.

In the last 40 years, important discoveries have been achieved in the field of WO. Indeed, there has been a dramatic growth in activity. From the earliest "blue dimer" from Meyer and coworkers with a TOF of 0.004 s^{-1} to the mononuclear

23

UNIVERSITAT ROVIRA I VIRGILI
MECHANISTIC STUDIES OF WATER OXIDATION CATALYZED BY HOMOGENEOUS IRON AND RUTHENIUM
COMPLEXES AND LIGHT-DRIVEN ORGANIC REDUCTIONS WITH A DUAL COBALT/COPPER CATALYTIC SYSTEM
Carla Casadevall Serrano

CHAPTER I   GENERAL INTRODUCTION

ruthenium WOC from Sun and co-workers with a TOF of 380 s^{-1} in water oxidation, we are coming closer to the reaction rate of 100–400 s^{-1} 1 of the OEC of PSII (Figure I.5). Seminal studies on earth's scarce ruthenium[44,45] and more recently iridium[46-48] metals, both combined with the development of novel organic ligand frameworks, have led to the discovery of highly effective WOCs, with TON and TOF similar to the Natural OEC.[20,49]
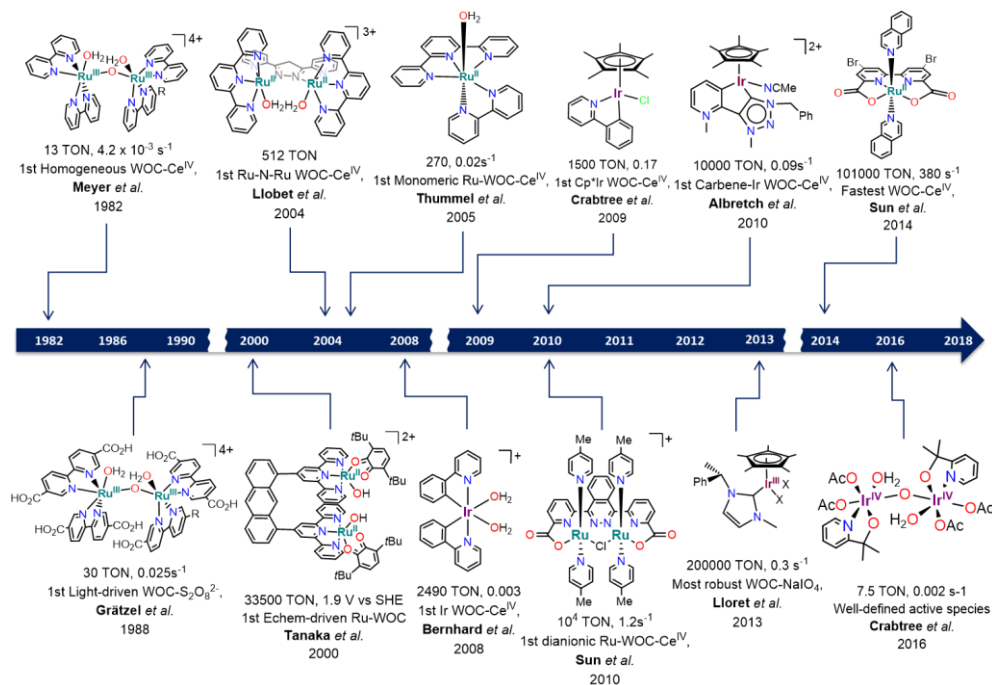
Figure I.5. Timeline with the most emblematic Ruthenium and Iridium WOCs. TON, TOF (s^{-1}), the relevance of the discovery, the corresponding author and the year or publication are included. Echem-driven stands for electrochemical driven water oxidation.

I.5.2.1. Ruthenium water oxidation catalysts

Considerable progress has been made in the development of water oxidation catalysts in the last decades. Many of these catalysts are based on ruthenium complexes based on polypyridyl ligands, and most of these complexes can be classified into dinuclear[50-55] or mononuclear[47,56-60] catalysts.

I.5.2.1.1. Dinuclear Ru WOCs

The oxidation of water by ruthenium complexes has been studied for over 30 years. The first example of a homogeneous ruthenium WOC was reported by the Meyer group in 1982 and it is known as the "blue dimer" (Figure I.6, 1a)[50,61] This dinuclear complex $[Ru_2(\mu-O)(bpy)_4(H_2O)_2](ClO_4)_4 \cdot 4H_2O$ (bpy = 2,2'-bipyridine) showed oxygen evolution using CAN as sacrificial oxidant in 0.1 M $HClO_4$ aqueous solution, with a TON O_2 of ca. 13. Under electrochemical conditions, 4.6 TON O_2 were obtained after 2 h of bulk electrolysis at 1.58 V vs SHE applied potential (pH 1, TfOH). The analogous phenanthroline dimer was also found active. The mechanism for chemically driven WO catalyzed by "the blue dimer" has been widely investigated and despite a large number of mechanistic studies performed with this system, there is still controversy. The most accepted mechanism is the nucleophilic attack of a water molecule on a highly electrophilic $Ru^{IV,V}$ or $Ru^{V,V}$ (acid base mechanism, Scheme I.4. WNA), which has been proposed on the bases of kinetic and ^{18}O isotopic labeling studies.[58,62] A significant increase in the catalytic activity was obtained by the inclusion of carboxylic groups in the 5',5' positions of the bipyridine, which lowered the WO-onset* to 1.3-1.4 V (Figure I.6, **1b**). For the thermal water oxidation, up to 75 TON were reported by using Co^{3+} ions as electron acceptor (H_2SO_4 1M). In this case, a mechanism involving the formation of a μ-peroxo complex $[Ru_2^{III}\text{-}O\text{-}O\text{-}Ru_2^{III}]$ from $[Ru^{IV}\text{-}OH]_2$ was also proposed (DC pathway). Taking advantage of the lower overpotential† of **1b**, light-driven oxygen evolution was achieved in aqueous buffered solution (pH 7) using $[Ru^{II}(^{COMe}bpy)_3]^{2+}$ (^{COMe}bpy = 4,4'-dicarboethoxy-2,2'-bipyridine) as photosensitizer and $Na_2S_2O_8$ as a sacrificial electron acceptor obtaining 30 TON O_2.[63]

---

* The onset potential is the potential at which the catalytic current starts.
† Overpotential (η) is referred to the difference between the potential experimentally observed for a catalytic event and the thermodynamically determined reduction potential for this process (in this case for the WO, which V_{thermo} = 1.23 - 0.059·pH).

UNIVERSITAT ROVIRA I VIRGILI
MECHANISTIC STUDIES OF WATER OXIDATION CATALYZED BY HOMOGENEOUS IRON AND RUTHENIUM
COMPLEXES AND LIGHT-DRIVEN ORGANIC REDUCTIONS WITH A DUAL COBALT/COPPER CATALYTIC SYSTEM
Carla Casadevall Serrano

CHAPTER I   GENERAL INTRODUCTION
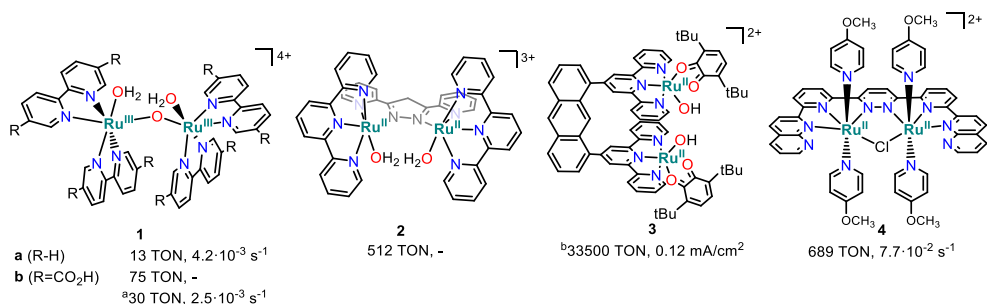
Figure I.6. Selected dimeric Ru complexes active in the water oxidation reaction. TON (moles of O_2 generated per moles of complex) and TOF (TON·s^{-1}) are indicated below the structures when available. TON and TOF values are based on Ce^{IV}-driven water oxidation unless stated. [a] Light-driven water oxidation conditions ([Ru(bpy)$_3$]$^{2+}$ as PS and Na$_2$S$_2$O$_8$ as SO). [b] Electrochemical-driven water oxidation, at 1.9 V vs SHE.

An approach to improve the efficiency of μ-oxo diruthenium complexes involved the use of dinucleating ligands to favor the O-O bond formation by means of spatial arrangement. Besides, the lack of oxo bridging motif prevents catalyst decomposition by reductive cleavage of the bridge or by the formation of the thermodynamically favored *trans*-dioxo structure. One of the first examples using this approach is the dinuclear ruthenium complex [Ru$_2$^{II}(μ-OAc)(bpp)(terpy)$_2$]$^{3+}$ (terpy = 2,2':6',2'' - terpyridine) reported by Llobet and co-workers, where the two metal atoms were connected by a Hbpp (2,2'-(pyrazole-3,5-diyl)dipyridine) ligand (Figure I.6, **2**). In this system, the two putative terminal oxo moieties [Ru^{IV}(O)] have the right orientation and are in the needed proximity to favor a direct coupling mechanism for the O-O bond formation.[53] Indeed, mechanistic studies by means of isotopic labeling proved that the O-O bond formation occurs intramolecularly[53] (Scheme I.4, **DC**) and the efficiency in water oxidation attained by this strategy slightly improved the pioneer Meyer's blue dimer. TON was substantially enhanced up to 250 when the catalyst was supported in Nafion[64] and up to 512 TON O_2 were obtained upon further optimization.[65]

UNIVERSITAT ROVIRA I VIRGILI
MECHANISTIC STUDIES OF WATER OXIDATION CATALYZED BY HOMOGENEOUS IRON AND RUTHENIUM
COMPLEXES AND LIGHT-DRIVEN ORGANIC REDUCTIONS WITH A DUAL COBALT/COPPER CATALYTIC SYSTEM
Carla Casadevall Serrano

CHAPTER I   GENERAL INTRODUCTION
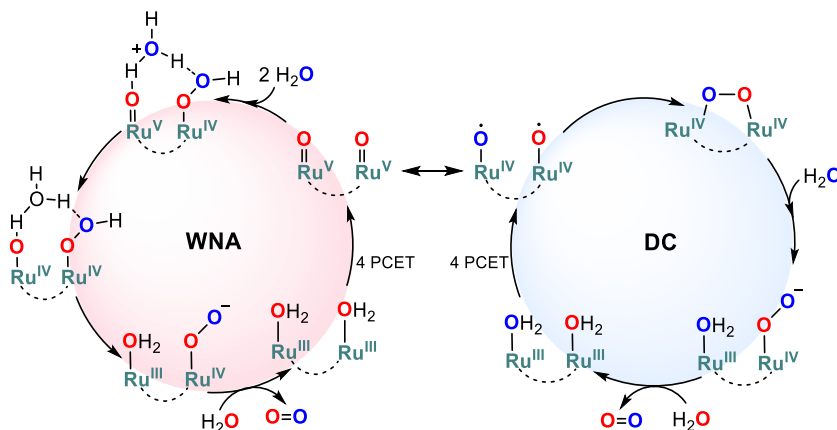
Scheme I.4. Scheme of the two general mechanistic proposals, including the acid base (left)[66,67] and the direct coupling (right, intra or intermolecular) pathways for the O-O bond formation.[68]

Inspired by complex $[Ru(OH_2)(quinone)(terpy)]^{2+}$ that releases protons from the aqua ligand in function of the pH without the formation of a μ-oxo dimer,[69] the same authors Tsuge and Tanaka developed a dinuclear complex $[Ru_2(OH)_2(Q)(btpyan)]^{2+}$ (btpyan = (1,8-bis(2,2':6',2''-terpyridyl)anthracene, Q = 3,6-di-*tert*-butyl-1,2-benzoquinone) by linking the terpy backbones to an anthracene moiety (Figure I.6, **3**) to favor the close proximity of two adjacent M=O moieties towards the O-O bond formation.[70,71] Due to solubility reasons, the complex was supported on an ITO (indium tin oxide) electrode to study its redox behavior in aqueous media. Up to 6730 TON O_2 were obtained after 40 h of electrolysis at 1.7 V vs SHE applied potential at pH4 (the pH was readjusted along with the electrolysis). Further optimization yielded 33500 TON O_2 at 1.9V vs SHE applied potential. An intramolecular DC mechanism was proposed since the redox non-innocent quinone ligand facilitates the Ru-OH oxidation to Ru=O by an intramolecular ET, inducing radical character in the oxo ligand, and facilitating the direct coupling to form Ru-O-O-Ru. Subsequent two single electron oxidations, a first one localized at the quinone and a second at the metal afford $[(Q)Ru^{III}-O-O-Ru^{III}(Q)]^{4+}$, from where O_2 dissociates with the concomitant binding of two H_2O molecules to the reduced Ru^{II} centers. Concordantly, DFT calculations in gas phase supported an O-O bond formation *via* a DC mechanism where the formal oxidation state of the Ru atoms remains

UNIVERSITAT ROVIRA I VIRGILI
MECHANISTIC STUDIES OF WATER OXIDATION CATALYZED BY HOMOGENEOUS IRON AND RUTHENIUM
COMPLEXES AND LIGHT-DRIVEN ORGANIC REDUCTIONS WITH A DUAL COBALT/COPPER CATALYTIC SYSTEM
Carla Casadevall Serrano

CHAPTER I   GENERAL INTRODUCTION

unchanged at II and the redox process are ligand-centered. After the removal of 4 protons and the 4 electron oxidation from the starting complex, $[(Ru^{II})_2(O_2^-)(Q)_2(btpyan^{.+})]^4$ is formed, from which O_2 release occurs recovering $[(Ru^{II})_2(Q)_2(btpyan)]^{4+}$ initial complex.[54]

R	TON O_2	TOF (s^{-1})
a OCH$_3$	689	$7.7 \cdot 10^{-2}$
b t-butyl	561	$4.9 \cdot 10^{-2}$
c C$_6$H$_5$	80	$1.5 \cdot 10^{-3}$
d CF$_3$	116	$5.2 \cdot 10^{-3}$
e NMe$_2$	112	$2.7 \cdot 10^{-2}$
f 3,5-Me$_2$	443	$4.8 \cdot 10^{-2}$
g CH$_3$	538	$4.6 \cdot 10^{-2}$

R	TON O_2	TOF (s^{-1})
a CH$_3$	459	$4.1 \cdot 10^{-2}$
b OCH$_3$	601	$7.0 \cdot 10^{-2}$

R	TON O_2	TOF (s^{-1})
a CH$_3$	512	$5.1 \cdot 10^{-2}$
b OCH$_3$	610	$7.2 \cdot 10^{-2}$

TON O_2	TOF (s^{-1})
597	$4.0 \cdot 10^{-2}$
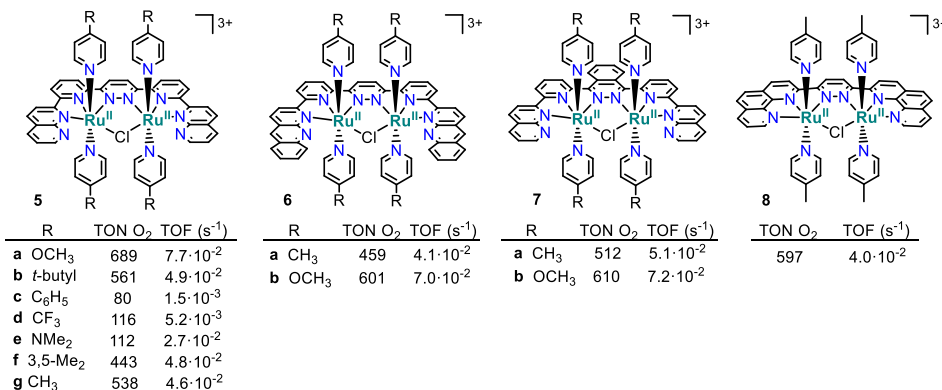
Figure I.7. Dimeric Ru^{2+} WOCs reported by Thummel and coworkers.[72]

In the same line, Thummel *et al.* reported a series of dimeric Ru^{II} WOCs with neutral bis-tridentate nitrogen-based ligands (Figure I.6, **6** and Figure I.7).[56,72] These ligand scaffolds favor the positioning of the two metal centers in the same plane of the backbone, which are linked by a chloride bridge that appears to be very stable. Up to 690 TON O_2 and $7.7 \cdot 10^{-2}$ s^{-1} (TOF) were reported when having methoxy groups in the para position of the monodentate axil pyridine ligand.

Later on, Sun *et al.* included a negatively charged biscarboxylato bridging ligand aiming to decrease the oxidation potential needed for WO. Complexes $[Ru^{II}_2(cppd)(pic)_6]^+$ and $[Ru^{II}_2(cpph)(pic)_4(\mu\text{-Cl})]^{2+}$ (H$_2$cppd = 1,4-bis(6'-carboxylate-pyrid-2'-yl)-pyridazine acid, pic = 4-picoline and H$_2$cpph = 1,4-bis(6'-carboxylate-pyrid-2'-yl)-phthalazine acid, Figure I.7, **9** and **10**).[73,74] Up to 10400 TON O_2 were obtained with complex **10** when using CAN as sacrificial oxidant at pH 1, whereas 4740 TON O_2 were achieved with complex **9**, even though they only differ in the *cis* and *trans* orientation of the two Ru centers. The difference in reactivity was ascribed to the different mechanism for the O-O bond formation: facilitated DC for **10** and AB or even an intermolecular DC was expected for **9**. The

catalysts were also tested under photochemical conditions using different types of $[Ru(bpy)_3]^{2+}$ as photoredox catalyst and $Na_2S_2O_8$ as a sacrificial electron acceptor, but the obtained TON O_2 was lower in all cases.[74,75] A similar DC mechanism was reported by Llobet and co-workers with complexes *trans*-$[[Ru^{II}(tpym)(H_2O)]_2(\mu$-bpp)]$(PF_6)_3$ (Figure I.8, **11**) and *cis*-$[[Ru^{II}(terpy)(H_2O)]_2(\mu$-bpp)]$(PF_6)_3$ (Figure I.6, **2**) (tpym = tris-(2-pyridyl)methane, bpp = 3,5-bis(2-pyridyl)pyrazolate).[76] Monitorization of the O_2 evolved during the first TON of the reaction between the Ru^{IV}=O dimer with excess of CAN in ^{18}O labelled water showed the formation of $^{16}O_2$ in about 100 %, confirming that the O-O bond formation takes place via a DC mechanism. This fitting was possible because the Ru=O exchange with water is below 10%. Modification of the pyrazolate bridge (μ-bpp, **2** to μ-Mebbp = 6,6''-(4-methyl-1H-pyrazole-3,5-diyl)di-2,2'-bipyridine Figure I.7, **12**) improved complex stability and robustness, despite no significative enhancement of the catalytic activity was observed (22.6 and 6.8·10^{-2} s^{-1} TON and TOF of **12** and 18.3 and 1.5·10^{-2} s^{-1} TON and TOF of **2**). However, ^{18}O labeling studies pointed to an AB mechanism for the O-O bond formation for complex **12**.[77,78]

	9	10	11	12
	4740 TON, 0.28 s^{-1}	10400 TON, 1.2 s^{-1}	9.6 TON, 3.1 x 10^{-2} s^{-1}	22.6 TON, 6.8 x 10^{-2} s^{-1}
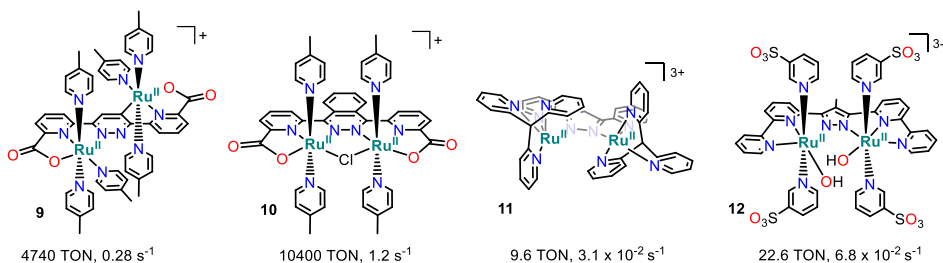
Figure I.8. The most actives dimeric Ru-WOCs, reported by Sun and coworkers (**9**, **10**) and complexes employed by Llobet and coworkers (**11**, **12**) for mechanistic studies.

As it can be seen, rational ligand design very much benefits from mechanistic studies of the intermediates formed before and after the O-O bond formation and the mechanism through which the latter step is achieved, and vice versa. This enables for the development of complexes topologically disposed to facilitate a DC between Ru=O, facilitating O_2 evolution. Moreover, the introduction of negative charges in the organic ligand reduces the redox potential needed to access the active species.

I.5.2.1.2. Mononuclear Ru WOCs

Initially, it was thought that more than one metal center was required to enable the critical O-O bond.[79] More recently, it has been discovered that dioxygen can be produced by the nucleophilic interaction of a water molecule with a single Ru=O, and this finding has generated some interesting mechanistic interpretations. The first example of monomeric ruthenium complex active in WO was reported in 2005 by Zong and Thummel.[56] The Ru complex (Figure I.9, **13**) was synthesized by using 2,2'-(4-(tert-butyl)pyridine-2,6-diyl)bis(1,8-naphthyridine) as the backbone ligand and 4-substituted pyridines occupying the axial positions.[56] A sterically hindered complex, containing 7'-^{t}Bu substituted 1,8-naphthyridine ligand afforded the same activity (Figure I.10, **28**), suggesting a mononuclear process. In light of this, and because no ligand exchange was detected after the catalysis (^{1}H-NMR, ESI-MS), a tentative mechanism was proposed involving a 7th coordinated Ru^{IV} species generated by the coordination of a water molecule to a highly electrophilic 16e$^-$ Ru^{IV} intermediate. The concomitant 18e$^-$ species was further oxidized to Ru^{VI}=O by the SO and the O-O bond formation took place at the following step.

260 TON, 1.4 x 10^{-2} s^{-1}
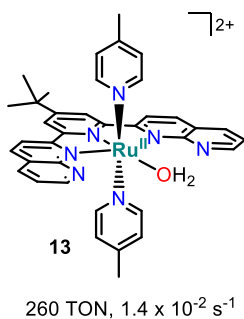
Figure I.9. The ruthenium monomer complex reported by Thummel and coworkers.

Then, Thummel's group followed up with a systematic study of the catalytic activity of several mononuclear Ru complexes based on aminopyridyl ligands. The first group was formed by complexes with the structure [Ru(tpy)(NN)Cl] (tpy = terpyridine, NN = bipyridine or other related diamine chelating ligands; Figure I.10. **14b**, **14h**, **15a-d**, **16b**, **19d**, **20e-f**, **21**), from which only complexes **14b, 14h, 15a-d**

UNIVERSITAT ROVIRA I VIRGILI
MECHANISTIC STUDIES OF WATER OXIDATION CATALYZED BY HOMOGENEOUS IRON AND RUTHENIUM
COMPLEXES AND LIGHT-DRIVEN ORGANIC REDUCTIONS WITH A DUAL COBALT/COPPER CATALYTIC SYSTEM
Carla Casadevall Serrano

CHAPTER I   GENERAL INTRODUCTION

and **19d** showed moderate activities. Parallel studies by Sakai and co-workers showed significant induction time prior to the onset of water oxidation in the presence of excess of CAN,[80] suggesting that the chloride complexes are not active in water oxidation, but rather they serve as precatalysts that undergo Cl$^-$/H$_2$O substitution, as seen by NMR,[81,82] to generate the catalytically active aquo complex. In this lines, Meyer and Sakai groups independently reported analogous mononuclear Ru-WOCs ([Ru(terpy)(NN)(OH$_2$)]$^{2+}$ (NN = bpy (Sakai) and NN = 2,2'-bipyrimidine (Meyer)) with aqua ligands, which did not show any induction time prior to O$_2$ evolution. They proposed a WNA mechanism for those complexes based on electrochemical data and UV-visible spectroscopy, suggesting the attack of the water molecule onto a transient [Ru^V=O]$^{3+}$ species followed by the formation of Ru^{III}-OOH, whose concomitant oxidation by CAN released dioxygen, closing the catalytic cycle (Scheme I.5).[81,83,84] In this line, parallel studies by Meyer and Berliguette groups separately reported O$_2$ evolution to be zeroth order with respect to [Ce^{IV}] when using 30-200 equivalents of CAN. But Masaoka and Sakai reported a first order regarding [Ce^{IV}] when using 10 equivalents. Therefore, it is still not conclusive if the rate determining step is the O-O bond formation or the O$_2$ release in excess of CAN. Indeed detection of an unexpected O$_2$ isotopic distribution in labelling experiments together with the detection of a possible Ru-O-Ce intermediate by ESI-MS which was fragmented into [Ru^{III}-OO]$^+$ by MS/MS experiments, the authors concluded that Ce^{IV} ion may play a role in weakening the N-O bond, allowing the O-O bond formation between the ruthenyl species and a nitrate anion.[85]
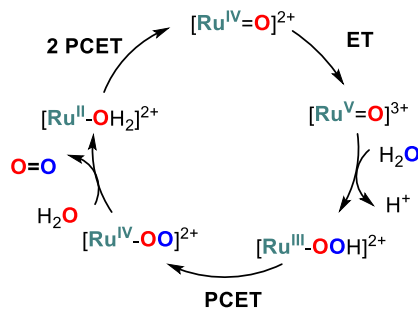
Scheme I.5. WNA mechanistic proposal by Meyer et al. for the [Ru(terpy)(NN)(OH$_2$)]$^{2+}$ type of complexes.[83]

The electronic effects on both the bipyridine and the terpyridine ligands were studied for [Ru(terpy)(bpy)(OH$_2$)]$^{2+}$ (**14**, **15**) and the catalytic activity was remarkably improved by including different groups (up to 701 TON O$_2$ when using ^{t}Bu at the in the terpy, **14f**).[86] There is a strong correlation between catalyst activity and stability depending on the position and identity of the substituent group on the ligands. Higher TON but lower TOF were achieved by electron withdrawing groups in the bpy, while electron donating groups accelerated the rate by decreasing the catalyst robustness.[82,85] However, the contrary effect was observed for the substituted terpy. This was rationalized by the π-back bonding to the most labile group, which was bpy. Thus, a fine balance between electron density at the metal and π-back bonding to the most labile ligand is key for a fast and robust complex. Further modifications on the tridentate (NNN) and bidentate (NN) ligand scaffolds of the original catalyst (**14a**) gave rise to several active mononuclear ruthenium catalysts for WO based on aminopyridyl ligands (Figure I.10).[81,84,87,88,89] In addition, the ligand *2,2´:6´,2´´:6´´,2´´´´*-quaterpyridine (qtpy) was used in order to minimize the *trans*-to-*cis* conversion of trans-[Ru(bpy)$_2$L$_2$]$^{2+}$ complexes,[90-94] although the rotation around the central C(sp^2)-C(sp^2) bond, which leads to the formation of dinuclear species, where each half of the ligand coordinates a single ruthenium atom. To overcome this problem, Thummel's group synthesized Ru complexes with the 2,9-di-(2´-pyridyl)-1,10-phenanthroline (dpp) ligand (catalyst **28,** Figure I.10), which prevents any rotation around the central C(sp^2)-C(sp^2) bond and enables tetradentate coordination to ruthenium.[95] This catalyst performed better than most of the other Ru complexes based on polypyridyl ligands with 416 TON O$_2$ using CAN as sacrificial oxidant. Despite this ligand has two pyridines in the axial positions, the mechanistic hypothesis is that a Ru^{IV} (16 e$^-$ complex) would be sufficiently electrophilic to accommodate a water molecule as a 7th coordination ligand to form a 18 e$^-$ pentagonal bipyramidal intermediate, which was further supported by DFT calculations.[87]

Analogously to the incorporation of anionic ligands into dinuclear systems of Thummel, Sun and co-workers applied the same strategy for complex [Ru^{II}(ONNO)(pic)$_2$] (ONNO = 2,2'bipyridine-6,6'-dicarboxylate, catalyst **29**, Figure

I.11), which lowered the redox potentials over a wide range of pH with the WO onset at ~ 1.05 V. This allowed for light-driven WO using tris-(2,2'-bipyridine)ruthenium^{2+} ($[Ru(bpy)_3]^{2+}$) as photoredox catalyst and sodium persulfate ($Na_2S_2O_8$) as electron acceptor,[96] although the activity was not as impressive as for the Ce^{IV}-driven catalysis. Moreover, a 7th coordinated Ru^{IV}-hydroxo intermediate μ-(HOHOH)-$[Ru^{IV}(ONNO)(pic)_2]^{3+}$ species was isolated and characterized with X-ray diffraction by Sun and coworkers after the addition of 2 equivalents of CAN to **29** (Figure I.11).[97] Due to the low oxidation potential required to achieve the Ru^{IV}=O species (0.57 V vs SHE), the Ru^{IV}=O intermediate was isolated from catalytic experiments (by precipitation with NH_4PF_6) with low amounts of sacrificial oxidant (60 eq). The wide O-Ru-O angle may encourage the coordination of a water molecule as a 7th ligand. Further modifications in the axial ligands of catalyst **29** yielded a new family of complexes with different catalytic activities (**30-36**, Figure I.11).[98,99] For example, the replacement of the axial 4-picoline ligands with isoquinoline ligands (catalysts **30**, Figure I.11) improved the catalytic activity by 4 fold.[20]

UNIVERSITAT ROVIRA I VIRGILI
MECHANISTIC STUDIES OF WATER OXIDATION CATALYZED BY HOMOGENEOUS IRON AND RUTHENIUM
COMPLEXES AND LIGHT-DRIVEN ORGANIC REDUCTIONS WITH A DUAL COBALT/COPPER CATALYTIC SYSTEM
Carla Casadevall Serrano

CHAPTER I   GENERAL INTRODUCTION
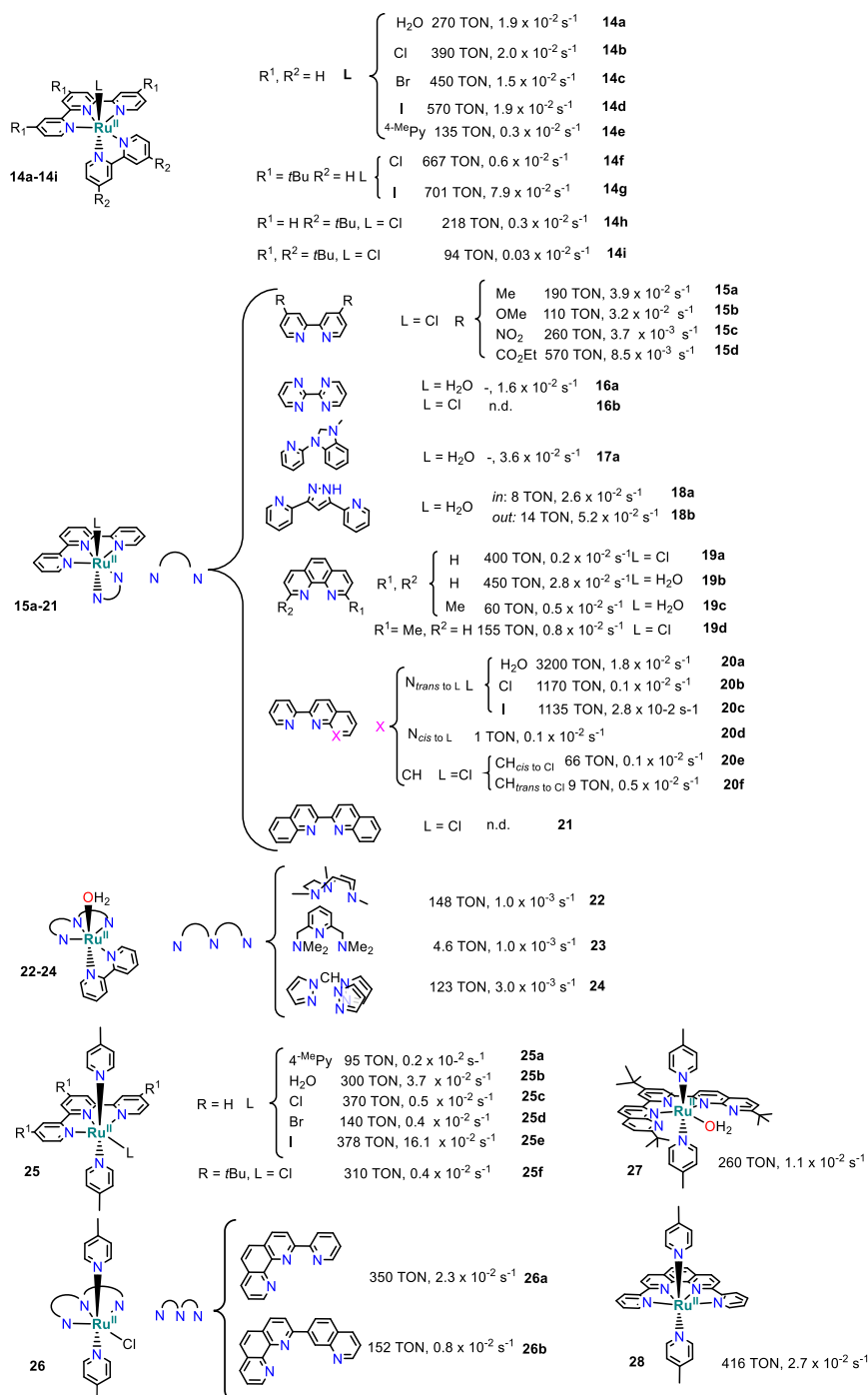
Figure I.10. Selected mononuclear ruthenium WOCs type [Ru(NNN)(NN)L], [Ru(NNN)(pic)$_2$] and [Ru(NNNN)(pic)$_2$] with different polypyridyl ligands. TON and TOF are obtained from different literature sources and they are not suitable for comparisons due to the different experimental conditions. CAN was used as SO.

UNIVERSITAT ROVIRA I VIRGILI
MECHANISTIC STUDIES OF WATER OXIDATION CATALYZED BY HOMOGENEOUS IRON AND RUTHENIUM
COMPLEXES AND LIGHT-DRIVEN ORGANIC REDUCTIONS WITH A DUAL COBALT/COPPER CATALYTIC SYSTEM
Carla Casadevall Serrano

CHAPTER I   GENERAL INTRODUCTION

29
2010 TON, 14.7 s^{-1}
[a] 100 TON, 6 x 10^{-2} s^{-1}

30
8360 TON, 120 s^{-1}
[b] 218 TON, 0.3 s^{-1}

31
[c] 4563 TON, 31s^{-1}

32
[c] 1702 TON, 70 s^{-1}

33
[c] 55400 TON, 286 s^{-1}
[b] 232 TON, 0.3 s^{-1}

34
[d] 336 TON, 9.2 x 10^{-2} s^{-1}

[e]35
a R^1,R^2 = H   2032 TON, 137 s^{-1}
b R^1= Me, R^2 = H   2365 TON, 146 s^{-1}
c R^1= H, R^2 = Me   550 TON, 150 s^{-1}
d R^1= Me, R^2 = Br 4050 TON, 176 s^{-1}

[e] 36
a R^1 = H, R^2 =NO$_2$ 1094 TON, 3.4 s^{-1}
b R^1= Me, R^2 = Br 150 TON, 4.5 s^{-1}

Figure I.11. Selected catalyst resulting from the modification of the axial ligand in complex [Ru^{II}(ONNO)(pic)$_2$] (ONNO = 2,2'bipyridine-6,6'-dicarboxylate, catalyst **29**. [a] Light-driven WO, using [Ru(bpy)$_3$]$^{2+}$ as PS and [Co(NH$_3$)$_5$Cl]Cl$_2$ as SO. [b] Light-driven WO, using [Ru(bpy)(4,4'-CO$_2$Et-bpy)$_2$]$^{2+}$ as PS and Na$_2$S$_2$O$_8$ as SO. [c] TON and TOF are not recorded under the same conditions, thus they are not comparable. [d] Under the same conditions, complex **30** performance was 1200 TON, 4.5 s^{-1} (TON, TOF). [e] Under the same conditions, complex **30** performance was 2000 TON with a TOF of 41.2 s^{-1}.

Investigation of complex **25a** ([Ru(terpy)(pic)$_3$]), showed that one picoline ligand was exchanged by H$_2$O to generate an octahedral intermediate.[100] Therefore, depending on the catalyst employed, the mechanistic proposals from Thummel and Meyer could be both feasible. In this line, the isolated 7th coordinated Ru^{IV}=O intermediate derived from complex **30** together with DFT calculations served to propose a mechanism for the O-O bond formation that pointed towards an intermolecular interaction between two monomeric units,[101] which was further supported by kinetics and DFT calculations.[20] In addition, electrochemical studies together with EPR and X-ray absorption spectroscopy have allowed getting a mechanistic insight of the intermediates formed with this type of catalysts.[102-104] Indeed, under acidic conditions, EPR spectra after electrolysis of the starting Ru(II) complex at 0.9 and 1.7 V revealed signals for Ru(III) and Ru(V), respectively. Further extended X-ray absorption fine structure (EXAFS) determined the formation of a 7th coordinate [Ru^V(O)(ONNO)(pic)$_2$] (Ru(V)=O) intermediate.[104]

Later on, it was envisioned that the direct coupling mechanism could be facilitated by the substitution of the axial picoline ligands by isoquinolines, taking advantage of the π-stacking interaction between the aromatic rings, lowering the barrier for the radical coupling of the Ru-O species (Scheme I.6). Indeed, complex **31** achieved a TOF of 300 s^{-1} under optimized conditions, which is within the order of the activity of PSII (100 – 400 s^{-1}).
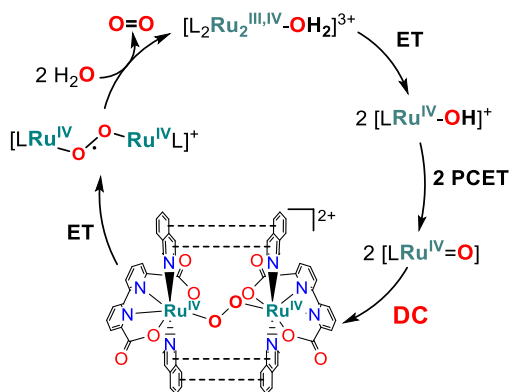
Scheme I.6. Proposed catalytic cycle for complex **31** and illustration of the π-stacking intermolecular interactions between isoquinoline moieties to favor the O-O bond formation by a DC mechanism.[20]

The introduction of substituents in the para position of the axial pyridine ligands (CO_2Et-, Br-, H-, MeO-, Me_2N- and $Ph(CH_2)_3$-) allowed for the study of electronic effects. It was observed that electron withdrawing groups enhance the WO activity while electron donating enhanced the longevity of the catalyst.[105] However, the observed non-covalent interaction[20] was definitively more effective than pure electronic effects.

Further modifications in the ligand backbone in the axial position using a spacer to favor the intermolecular interaction between monomeric unites resulted in a series of [Ru(ONNO)(N)$_2$] derivative complexes with high activities (1000-20000 TON O$_2$, Figure I.12). Indeed, the catalytic activities were in all cases one order of magnitude higher than its monomeric precursor. Mechanistic studies based on kinetics and electrodeposition experiments, point towards an intramolecular DC mechanism.[106]

UNIVERSITAT ROVIRA I VIRGILI
MECHANISTIC STUDIES OF WATER OXIDATION CATALYZED BY HOMOGENEOUS IRON AND RUTHENIUM
COMPLEXES AND LIGHT-DRIVEN ORGANIC REDUCTIONS WITH A DUAL COBALT/COPPER CATALYTIC SYSTEM
Carla Casadevall Serrano

CHAPTER I   GENERAL INTRODUCTION
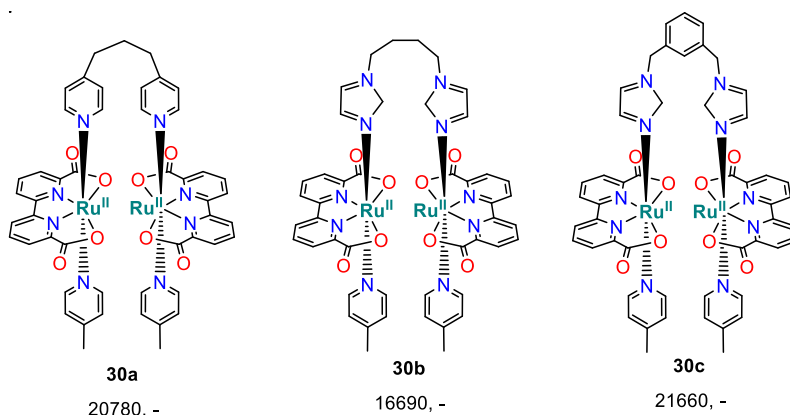
Figure I.12. Dimerized structures of the ruthenium WOC 30 by using different methylene spacers. TON values were obtained upon addition of the catalyst (0.05 μM) to an aqueous solution of HOTf (pH 1), containing CAN (5mM). TOF values were not available.

The field of WO has very much benefitted from the study of Ru-WOCs. Indeed, it has evolved significantly since the first report of "the blue dimer" in the early 80s. First, it was thought that two metal sites were needed to develop active systems. Later on, the findings encountered upon ligand design have brought new understanding into structure-activity relationships and their effect in the O-O bond formation mechanism. With the report of Thummel and Zong, it was proved that monomeric systems could be also active. And the first mechanistic investigation on a monomeric system reported by Meyer in 2008 provided a new vision in the field of WO. Even though there is not still a clear mechanistic trend for a given system because there many structural factors that play a role, all the lessons learned with those systems have allowed to extrapolate them to develop efficient WOCs based on other transition metals.

I.5.2.2. Iridium water oxidation catalysts

Despite the development of WOCs based on ruthenium has been really fruitful in the las decades,[40,57,107] the field has moved on also to develop WOCs based on iridium. Indeed, ruthenium and iridium oxides benefit from stability even at low pH values, therefore, they are currently found in commercial proton-exchange membrane (PEM) electrolyzers.[108] Moreover, iridium oxide materials have been proven to be among the

most active and stable for WO, showing both very high electrochemical and photochemical rates.[109-116] In this line, in 2008 Bernhard and coworkers reported the first molecular iridium complex active for water oxidation $[Ir^{III}(ppy)_2(OH_2)]^+$ (ppy = 2-phenylpyridine), which was at the same time the first organometallic active system.[46] Later on, Ir complexes with the general formula $[Cp^*IrL_n]$ (Cp* = 1,2,3,4,5-pentamethylcyclopentadienyl) have showed remarkable activity (TON > 10^4).[117,118] However, with this type of complexes the rationalization of kinetic data is not straightforward due to the oxidative transformation that the ligand undergoes, which exacerbates the identification of the real nature of the active species in WO.[119]

I.5.2.2.1. Ir WOCs without Cp* ligand

In the presence of CAN, a family of $[Ir^{III}(ppy)_2(OH_2)]^+$ derivatives (ppy=2-phenylpyridine) produced O_2 with a slow rate but for a long period of time (6 - 8 days). Indeed, through ligand modifications, the energy of the HOMO was found to be highly tunable and consequently, it was argued that the oxidation potentials could be easily controlled. The increase of $Ir^{III/IV}$ redox potential was associated with a decline of the electronic density at the metal center, which led to a slight increase of the catalytic activity, from 2200 TON up to 2760 TON and from $0.3 \cdot 10^{-2}$ to $0.4 \cdot 10^{-2}$ s^{-1} (TOF). DFT studies concluded that the ability to tune the electronics of both catalyst and photosensitizer may facilitate photo-driven half reactions or full water-splitting devices.[46]

37a	$R_1, R_2 = H$	2490, 10.8 s^{-1}
37b	$R_1 = Me, R_2 = H$	2270, 15.6 s^{-1}
37c	$R_1 = Me, R_2 = Ph$	-, 4.2 s^{-1}
37d	$R_1 = Me, R_2 = F$	2760, 15.6 s^{-1}
37e	$R_1 = Me, R_2 = Cl$	-, 4.2 s^{-1}
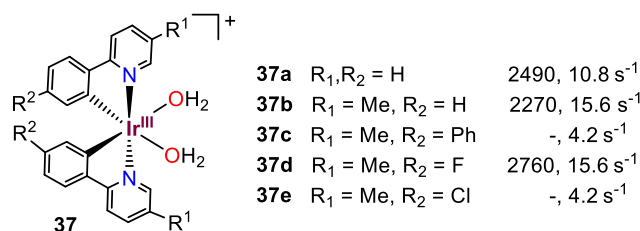
Figure I.13. Molecular structure of the cyclometalated Ir complexes reported by Bernhard and coworkers.[46] TON and TOF values are reported using CAN as sacrificial oxidant. TOF relative to the first 45 min of reaction.

Beller and coworkers reported 5 dimeric and a monomeric complexes (Figure I.14).[120] However, only the initial catalytic activity is attributed to the molecular species, which along reaction time form active nanoparticles, as confirmed by absorption spectroscopy, X-ray, XRD and STEM.

38 -, 0.27 s^{-1} **39** -, 0.10 s^{-1} **40** -, 0.09 s^{-1}

41 -, 0.13 s^{-1} **42** -, 0.14 s^{-1} **43** -, 0.17 s^{-1}
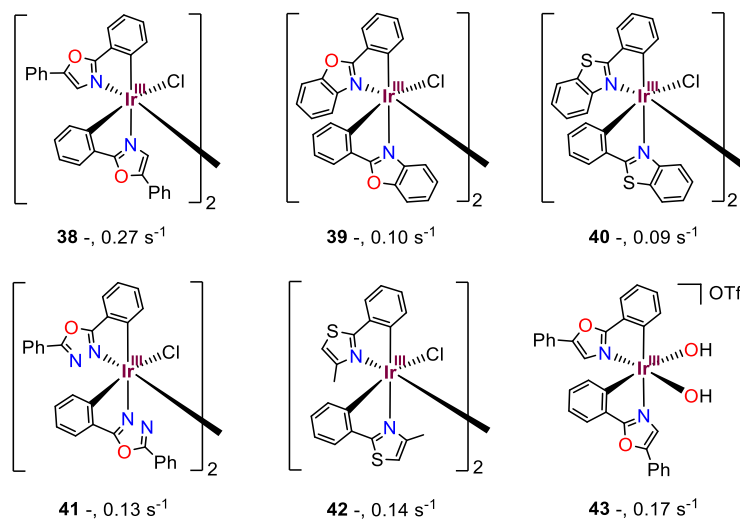
Figure I.14. Molecular structure of the cyclometalated Ir complexes reported by Beller and coworkers.[120] TON and TOF values are reported using CAN as sacrificial oxidant.

Other complexes based on aminopyridyl ligands were reported by Goldsmith, Bernhard and coworkers to be active in CAN driven WO (Figure I.15, **44**-**46**).[121] In this case, electrochemical quartz crystal microbalance (EQCM) and dynamic light scattering (DLS) studies excluded nanoparticle formation under catalytic conditions. Likewise, [(cod)ClIr(μ-bpi)Ir(cod)]PF$_6$ (bpi = (pyridine-2-ylmethyl) (pyridine-2-ylmethylene) and cod = 1,5-cyclooctadiene) complexes reported by de Bruin and coworkers (TON = 1000, and TOF = 0.94 s^{-1}) (Figure I.17, **47** and **48**), show a first order kinetics on both Ir and Ce^{IV}.[122] Macchioni *et al.* reported Ir complexes containing dicarboxylate ligands, analogous to the Ru ones (Figure I.17, **50** and **51**). Complex **51** was more robust, reaching up to 12000 TON O$_2$ with using CAN as SO.[78,123]

44 3540 TON, 27 s^{-1} **45** 2000 TON, 12.6 s^{-1} **46** 245 TON, 32.4 s^{-1}

47 1000 TON, 0.94 s^{-1} **48** 100 TON, 372 s^{-1} **50** 500 TON, 300 s^{-1} **51** 12000 TON, - s^{-1}
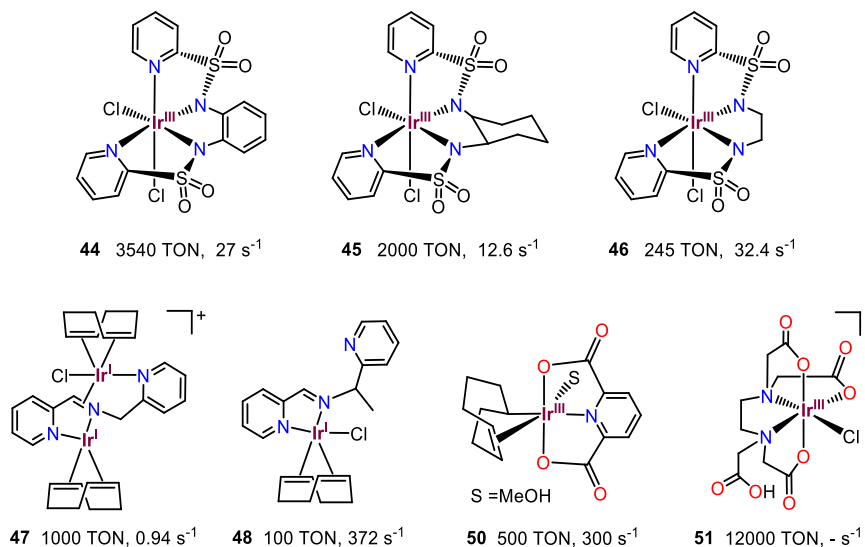
Figure I.15. Molecular structure of the Cp* free Ir complexes. TON and TOF values are reported using CAN as sacrificial oxidant. Initial TOF reported.

I.5.2.2.2. Ir WOCs based on Cp* ligands

Later on, Crabtree, Macchioni and coworkers and subsequently many other groups have explored the versatility of Cp*Ir complexes in WO (Cp* = 1,2,3,4,5-pentamethylcyclopentadiene). The "half-sandwich" iridium complexes showed an enhanced catalytic efficiency with regard to the previously described organometallic compounds (Figure I.16).[124-126]

40

UNIVERSITAT ROVIRA I VIRGILI
MECHANISTIC STUDIES OF WATER OXIDATION CATALYZED BY HOMOGENEOUS IRON AND RUTHENIUM
COMPLEXES AND LIGHT-DRIVEN ORGANIC REDUCTIONS WITH A DUAL COBALT/COPPER CATALYTIC SYSTEM
Carla Casadevall Serrano

CHAPTER I   GENERAL INTRODUCTION

52a Z = Cl, Y = ∅   349 TON, 0.17 s^{-1a}
52b Z = OTf, Y = ∅   -, 0.17 s^{-1a}
52c Z = NO$_3$, Y = ∅   500 TON, 0.23 s^{-1}

53 Z = Cl, Y = ∅   500 TON, 0.18 s^{-1a}

54 Z = CH$_3$CN, Y = OTf   1000 TON, 0.29 s^{-1a}

55 Z = Cl, Y = ∅   0.06TON, -,

56a Z = Cl, Y = Cl   320 TON, 0.24 s^{-1a}
56b Z = H$_2$O, Y = ∅   7200, 0.28 s^{-1}
56c Z = I, Y = NO$_3$ 738 TON, 0.15 s^{-1a}
56d Z = I, Y = PF$_6$ -, 0.13 s^{-1a}

57a R = OH, Z = H$_2$O, Y = ∅   500 TON, 0.75 s^{-1a}
57b R = OH, Z = Cl, Y = ∅   -, 0.37 s$^{-1b,d}$
57c R = OMe, Z = H$_2$O, Y = ∅   -, 0.27 s^{-1c}
57d R = OMe, Z = Cl, Y = ∅   -, 0.02 s$^{-1b,d}$
57e R = Me, Z = H$_2$O, Y = ∅   -, 0.16 s^{-1c}
57f R = COOH, Z = H$_2$O, Y = ∅   -, 0.05 s^{-1c}

58a R^1 = OH, R^2 = H, Z = H$_2$O, Y = ∅   6700 TON, 3.75 s^{-1b}
58b R^1 = OH, R^2 = H, Z = Cl, Y = ∅   -, 0.37 s$^{-1b,d}$

59a Z = Cl, Y = Cl   -, 0.06 s^{-1a}
59b Z = H$_2$O, Y = ∅   6700, 5.19 s^{-1b}

60 Z = Cl, Y = Cl   -, 0.14 s^{-1a}

61 Z = Cl, Y = Cl   -, 0.11 s^{-1a}

62a Z = Cl, Y = ∅   -, 0.21 s^{-1}
62b Z = NO$_3$, Y = ∅   168, 0.11 s^{-1b}

63a Y = SO$_4$ 281, 0.09 s^{-1a}
63b Y = (NO$_3$)$_2$ -, 0.63 s^{-1}

64 -, 0.2 s^{-1}

65 -, 0.17 s^{-1a}

66 -, 0.06 s^{-1a}

67 -, 0.05 s^{-1a}

68 6720, 3.5 s$^{-1a,b}$

69a X = Cl, Y = H, Z = H   1200, 2.1 s^{-1}
69b X = NO$_3$, Y = H, Z = H   2000, 1.85 s^{-1}
69c X = Cl, Y = H, Z = COOH   750, 0.38 s^{-1}
69d X = Cl, Y = COOH, Z = H   1300, 0.28 s^{-1}

Figure I.16. Molecular structure of the selected Cp* Ir complexes.[127] TON and TOF values are reported using CAN as sacrificial oxidant, unless otherwise noticed (b). TON and TOF values are highly sensitive, and very dependent on the concentration of both catalyst and oxidant. Values belonging to different sources are not directly comparable. Nevertheless, a qualitative comparison is informative. Initial TOF values are reported, unless otherwise indicated. [a] TOF relative to the first 30 s of the reaction. [c] TOF relative to the first 20 min of the reaction. [d] TOF relative to the first 240 s of the reaction.

UNIVERSITAT ROVIRA I VIRGILI
MECHANISTIC STUDIES OF WATER OXIDATION CATALYZED BY HOMOGENEOUS IRON AND RUTHENIUM
COMPLEXES AND LIGHT-DRIVEN ORGANIC REDUCTIONS WITH A DUAL COBALT/COPPER CATALYTIC SYSTEM
Carla Casadevall Serrano

CHAPTER I   GENERAL INTRODUCTION

I.5.2.2.3. Ir WOCs based on Cp* and Carbene-type ligands

The introduction of N-heterocyclic carbenes (NHCs) as ancillary ligands has been exploited by many groups.[119] Indeed, the use of bidentate carbene ligands has led to a raise of one order of magnitude in the TON of the Ir WOCs (Figure I.17, **73** - **79**). It was suggested that the high electronic flexibility (resonance) of the carbene-type ligand could stabilize both the low oxidation state species (carbene acts as a neutral ligand) and the oxidized species (zwitterionic form).[48] Another carbene-based complex reported by Bernhard, Albrecht and coworkers, compound **80**, has the highest TON achieved for any Ir WOC, using CAN as SO.[128] This complex was also found photo-electrochemically active. Using hematite as a photoanode, a pH-dependent light-induced current was observed at 1.23V.[128]

69a X = Cl, 2000 TON, 1.5 s^{-1}
69b X = OH, 2000 TON, 1.5 s^{-1}

70a n = 1, TON, s^{-1}
70b n = 2, TON, s^{-1}
70c n = 3, TON, s^{-1}
70d n = 4, TON, s^{-1}

71a X = I, TON, s^{-1}
71b X = Cl, TON, s^{-1}
71b X = OTf, TON, s^{-1}

72 TON, s^{-1}

73 -, 0.13 s^{-1}

74 -, 0.13 s^{-1}

^{a} **75** -, 0.13 s^{-1}

^{a} **76** -, 0.2 s^{-1}

77a n =1 ^{a} 1419 TON, 0.1 s^{-1}
77b n =2 ^{a} 2779 TON, 0.2 s^{-1}
         ^{b} 691 TON, 0.12 s^{-1}

78 8350 TON, 0.01 s^{-1}

79 10000 TON, 0.09 s^{-1}

80 22800, 0.03 s^{-1}
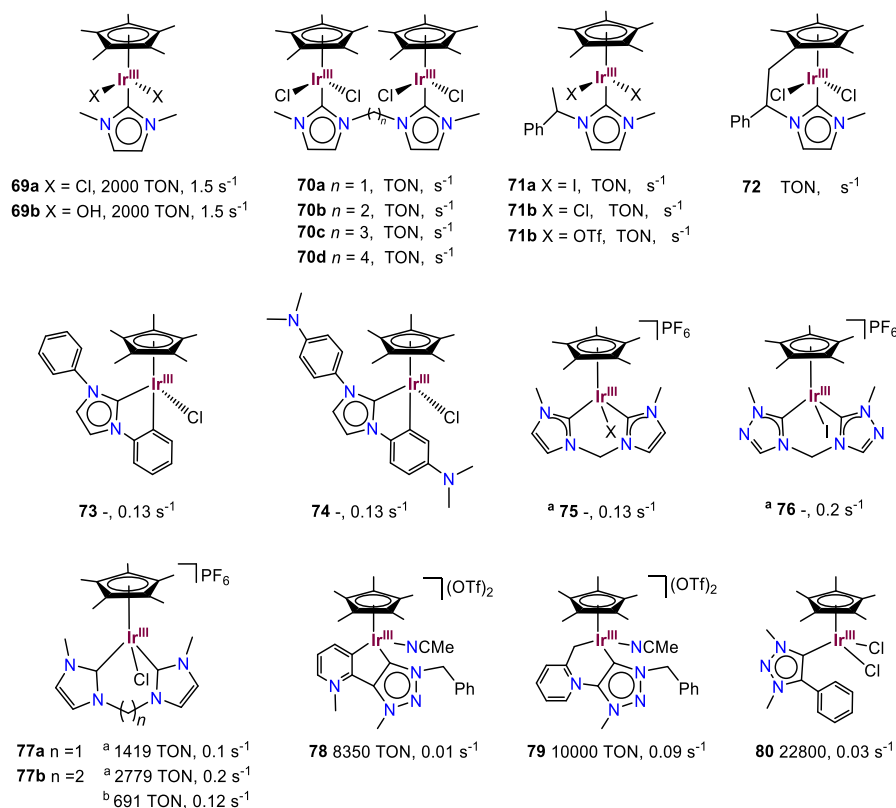
Figure I.17. Carbene based Ir complexes.

UNIVERSITAT ROVIRA I VIRGILI
MECHANISTIC STUDIES OF WATER OXIDATION CATALYZED BY HOMOGENEOUS IRON AND RUTHENIUM
COMPLEXES AND LIGHT-DRIVEN ORGANIC REDUCTIONS WITH A DUAL COBALT/COPPER CATALYTIC SYSTEM
Carla Casadevall Serrano

CHAPTER I   GENERAL INTRODUCTION

Crabtree, Brudvig and coworkers also reported an analogous example, $Cp*Ir(k^2,C^2,C^2-NHC)Cl$ ($k^2,C^2,C^2-NHC = k^2,C^2,C^2-1,3$-diphenylimidazol-2-ylidene) with a C-chelate carbene (Figure I.17, **73**). Kinetic studies showed almost 2nd order on Ir, and authors suggested that NHC may be lost under catalytic conditions forming compound **63**, which contributes to the catalysis when using CAN as SO. Therefore, WO activity was also tested using the milder SO $NaIO_4$, exhibiting a higher initial rate for O_2 evolution (~ 0.25 s^{-1}). To shed some light into these two different behaviors, insights on the WO intermediates were obtained by the CV of complex **73** in MeCN. A quasi-reversible wave was observed at 0.9 V, pointing towards a partially stable Ir^{IV} intermediate, which was chemically generated from Ir^{III} by the addition of $[Ru(bpy)_3]^{3+}$ and analyzed by EPR. A metastable low-spin d^5 Ir^{IV} with S = 1/2 was detected, which decomposed into EPR silent byproducts. In contrast, complex **63** did give any EPR signal, concluding that the NHC ligand provided greater stability to the high-valent $[Cp*Ir^{IV}(NHC)Cl]^+$ intermediate.[129]

Analogous to the successful introduction of anionic ligands (pyridine carboxylate) Ru WOCs, new complexes $[Cp*Ir(\kappa^2-N,O)X]$ (k^2-N,O = 2-pyridinecarboxylic acid, 2,4-pyridinecarboxylic acid or 2,6-pyridinecarboxylic acid, X = Cl$^-$ or NO_3^-) were also reported as active WOCs. While long-term activities were found similar to the previous examples, initial TOF were outstanding, being $[Cp*Ir(\kappa^2-N,O)Cl]$ the fastest Ir WOC reported so far using CAN as SO (TOF 4.8 s^{-1}, conditions: [Ir]= 0.5 μM, [Ce^{IV}] = 20 mM).[123]

I.5.2.2.4. The nature of the active species in Ir WOCs: Heterogeneous vs Homogeneous

Iridium oxides are well known water oxidation catalysts.[109-116] Despite iridium forms very stable organometallic and coordination complexes, the harsh catalytic conditions imposed by WO (especially when using CAN or/and acidic pH) can lead to oxidative transformations of the complexes or ligands.[130-133] This is the case of Cp*Ir compounds in which decomposition of the Cp* ligand takes place via initial oxidation of the C_q of the -C-CH$_3$ moiety of Cp*, followed by formation of -

CH_2OH.[132] In this line, oxidation of complex **62** upon subsequent addition of CAN was monitored by ESI-MS. The mass spectra showed oxidized species related to $[IrCp^* = O]^+$, $[IrCp^*(OH)_3]^+$, $[IrCp^* = O·2Na]^+$ and $[IrCp^*(O)_2·2Na]^+$.[134] Later on, Macchioni and coworkers, based on NMR and ESI-MS studies using CAN, $NaIO_4$ and H_2O_2 as SO, showed that these oxidations were not at the metal center, but on the Cp* moiety, which was oxygenated at different levels. They were able to intercept 3 intermediates during the oxidative transformation of the Cp* ligand (Scheme I.7).[135] Different oxidants (H_2O_2, CAN and $NaIO_4$) triggered the oxidation to an unconventional epoxide Ir^{III}-O-Cp* species, which after addition water evolves to double ketone-functionalized $Cp^*(O)_2$-Ir complex. Further unidentified oxidative transformations end up with the complete degradation of the Cp*. The isolated epoxide species, a mixture of intermediates, and the initial compound produced O_2 in a similar TOF (CAN as SO), suggesting a common single molecular species which provides most of the catalytic activity.[136,137]
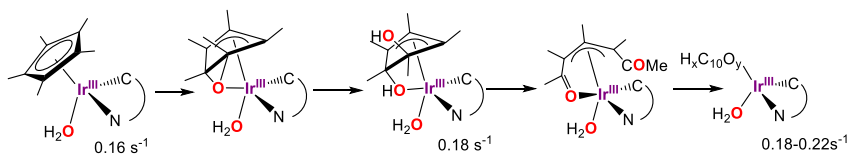
Scheme I.7. Initial complex and oxidized intermediates detected from the oxidative transformation of **62**. TOF of the starting compound (left), the isolated intermediate (center) and of mixtures resulting from the oxidative process with different eq. of CAN or H_2O_2 (right) detected.

Likewise, other interesting Ir complexes resulting from the oxidation of the Cp* ligand were reported by Batista and coworkers based on EXAFS and HEXS studies (Scheme I.8).[117]
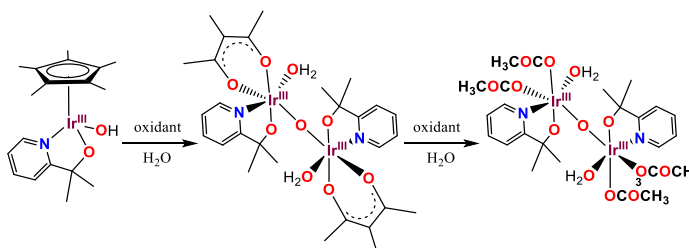
Scheme I.8. Starting precatalyst and oxidatively degraded C3- and C1- iridium complexes.

UNIVERSITAT ROVIRA I VIRGILI
MECHANISTIC STUDIES OF WATER OXIDATION CATALYZED BY HOMOGENEOUS IRON AND RUTHENIUM
COMPLEXES AND LIGHT-DRIVEN ORGANIC REDUCTIONS WITH A DUAL COBALT/COPPER CATALYTIC SYSTEM
Carla Casadevall Serrano

CHAPTER I   GENERAL INTRODUCTION

Despite Cp* was oxidatively damaged, ancillary ligands L_1L_2 accompanying Cp* in [Cp*IrL_1L_2X] complexes seemed to be more stable. Fukuzumi and coworkers reported complexes [Cp*Ir(4,4'-R$_2$-bpy)(H$_2$O)]$^{2+}$ (R = -OH, -OMe, -Me and -COOH) with potentially attackable ancillary ligands.[138] They found that [Cp*Ir(4,4'-OH-bpy)(H$_2$O)]$^{2+}$ was a highly active WOC with a TOF of 45 min^{-1}. However, further studies pointed out that the WO activity was due to the formation of iridium hydroxide nanoparticles. Likewise, Fujita and coworkers also reported nanoparticle formation from complex [Cp*Ir(6,6'-(OH)$_2$-bpy)(H$_2$O)]$^{2+}$ by DLS.[139-141]. And so did Crabtree et al. when using complex [Ir(CO)$_2$(pyalc)] as precatalyst with NaIO$_4$ as SO.[142] However, no NPs formation was detected by Crabtree and coworkers when using [Cp*$_2$Ir$_2$(µ-OH)$_3$]OH nor for catalysts bearing bpy, ppy or pyalc in addition to Cp* ligand in NaIO$_4$ driven WO.[143] Additionally, in some other studies with Ir WOCs NPs formation has also been excluded with successful efficiencies of the reported catalysts.[119,121,137,144,145]

I.5.3. Water oxidation catalysts based on first-row transition metals

In the current energetic scenario, the field has also evolved to the development of WOCs based on first-row transition metals (Mn, Fe, Co, Cu and Ni).[42,108]
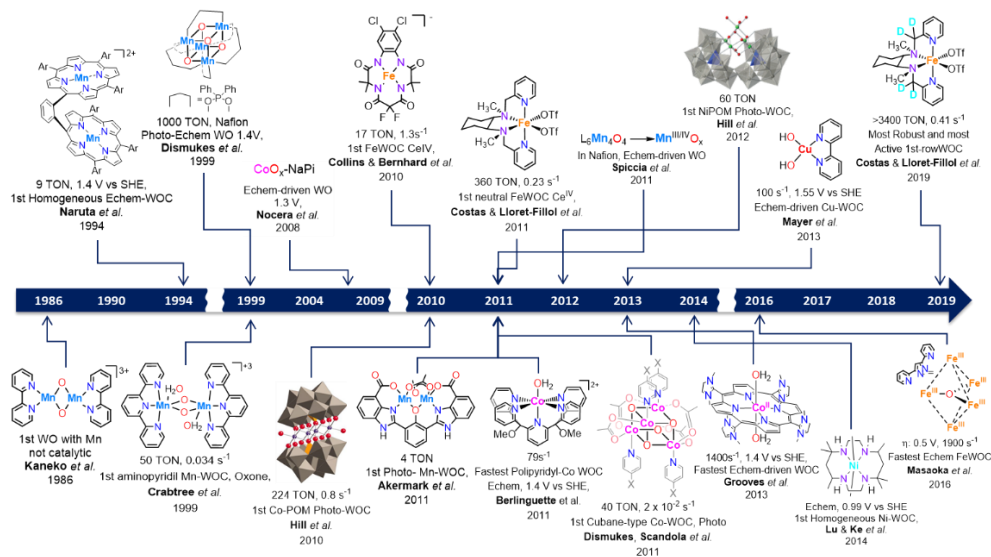
Figure I.18. Time line with the most emblematic Manganese, Iron, Cobalt. Copper and Nickel WOCs. TON, TOF (s^{-1}), relevance of the discovery, the corresponding author and the year or publication are included. Echem-driven stands for electrochemical driven water oxidation.

I.5.3.1. Water oxidation catalysts based on manganese

I.5.3.1.1. Bioinspired Mn_4O_4 models of the OEC

Due to the role of Mn in natural photosynthesis, the understanding of the mechanism of natural WO benefits from the study of biomimetic and bioinspired synthetic Mn coordination complexes as models. The first structural models of the OEC were robust tetranuclear manganese complexes with the general formula $L_6Mn_4O_4$ (L^- = diarylphosphinate ligand, $(p\text{-R-}C_6H_4)_2PO_2^-$ (R = H, alkyl, OMe)), that have the following reactivity (Scheme I.9): i) abstraction of four hydrogen atoms from amines or phenols, yielding two water molecules by triggering a notable structural change on the cubane, forming the so-called "pinned butterfly" $[L_6Mn_4O_2]$;[146,147] ii) O_2 photo-release with a concomitant loss of a bridging anion $(Ph_2PO_2^-)$, generating the "butterfly complex $[L_5Mn_4O_2]^+$.[148,149] Inspired by these reactivities, Dismukes and coworkers reported the support of the $L_6Mn_4O_4$ cluster on Nafion for the production of O_2 from water along the reverse mechanism i. This allowed the system to function in the presence of water. Photoelectrochemical driven water oxidation was observed at 1 - 1.4 V vs SHE. 1000 TON O_2 per cluster were obtained after 65h electrolysis.[150]
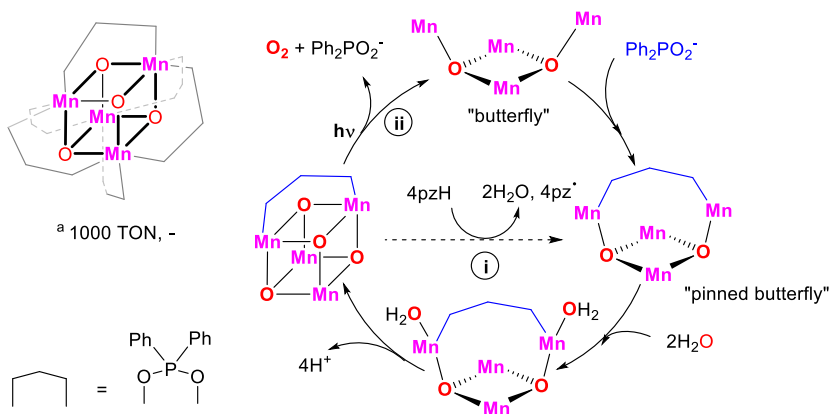
Scheme I.9. Proposed structural rearrangement of the manganese cluster during the water oxidation. Only one phosphinate ligand (in blue) was included in the catalytic cycle to emphatize the coordination/decoordination process. pzH is phenothiazine. [a] Photoelectrochemical TON obtained for the $L_6Mn_4O_4$ cluster supported on Nafion after 65h at 1.4V.

UNIVERSITAT ROVIRA I VIRGILI
MECHANISTIC STUDIES OF WATER OXIDATION CATALYZED BY HOMOGENEOUS IRON AND RUTHENIUM
COMPLEXES AND LIGHT-DRIVEN ORGANIC REDUCTIONS WITH A DUAL COBALT/COPPER CATALYTIC SYSTEM
Carla Casadevall Serrano

CHAPTER I   GENERAL INTRODUCTION

Later on, Spiccia and coworkers proved that $L_6Mn_4O_4$ clusters supported on Nafion are transformed into Mn^{2+} (birnessite), which is electro-oxidized into $Mn^{III/IV}$-O_x nanoparticles (NP), active species of WO by EXAFS studies.[151,152] Indeed, a number of molecular compounds initially considered to be homogeneous WOCs are not stable under the harsh oxidizing WO catalytic conditions, decomposing into heterogeneous materials that are the real active species.

A step further in mimicking PSII was the preparation of structural analogs of the OEC containing a calcium atom with the aim to clarify its role, which is challenging. The first example was reported in 2005 when Christou *et al.* with complex, $[Ca_2Mn_{13}O_{10}(OH)_2(OMe)_2(O_2CPh)_{18}(H_2O)_4]$; ($Mn^{IV}$, Mn^{III}_{10}, Mn^{II}_2) possessing two Mn_4O_4 cubes attached to a central, planar Mn_3O_4 unit, to which two Mn-Ca are attached above and below the plane.[153,154] Within this structure, a subunit possessing a distorted Mn_3CaO_4 cubane-like topology, analogous to the native OEC. The [Mn3CaNa] cluster was tested as WOC and it was found able to produce small amounts of dioxygen when oxone, NaOCl or tert-butyl hydrogen peroxide (*t*BuOOH) were used as sacrificial oxidants (< 4 TON, calculated from the reported plots obtained by the Clark electrode). But the closest rational synthetic approach to the real structure of the OEC, a $[Mn_3CaO_4]^{6+}$ model, was successfully described by Agapie and coworkers.[155] These authors included different Lewis acid ions in the cluster structure and evaluated their electrochemical properties. Reduction potentials were found dependent on the Lewis acidity of the redox-inactive metal incorporated, supporting the redox modulator role of Ca^{2+} in the OEC.[156-158] The lower the pK_a of the $M(aqua)^+$ ion (proportional to the Lewis acidity of the redox-inactive metal), the higher the redox potential of the Mn centers, due to the lower electron density on the metal.[157] However, a deviation from the trend (Sr^{2+} and Ca^{2+} exhibit the same redox) and the intriguing observation that only the replacement of Ca^{2+} for Sr^{2+} partially maintain the function of the enzyme,[159] remain puzzling observations awaiting an explanation. The incorporation of an external Mn atom to fully reproduce the OEC structure remains a challenge for synthetic inorganic chemists.

I.5.3.1.2. Manganese coordination complexes

Manganese coordination complexes for WO have been widely explored.[160] But in this chapter some representative examples will be described. In this line, Brudvig and coworkers reported that $[Mn_2^{III,IV}(\mu\text{-}O)_2(terpy)_2](NO_3)_3$ (terpy = 2,2´:6´,2´´-terpyridine, Scheme I.10) produced O_2 by using OCl^- or oxone as SOs (4 TON and > 50 TON O_2, respectively) but not when using CAN.[161,162] Mechanistic showed a complex scenario (Scheme I.10). Kinetic studies show a first-order dependence of reaction rates in the concentration of $[Mn_2^{III,IV}(\mu\text{-}O)_2(terpy)_2]^{3+}$ and zero order on oxone. The initial $[Mn_2^{III,IV}(\mu\text{-}O)_2(terpy)_2]^{3+}$ complex is the resting state, as determined by UV–Vis) and EPR spectroscopy. The thermodynamically favorable coordination of Oxone led to the formation of two possible isomers, produced by the two coordination vacancies available at the two metals cores (Mn^{III} or Mn^{IV}), initiating different reaction paths; despite preferring the interaction with the more electrophilic site (Mn^{IV}). However, the high energetic barrier for the O-O bond cleavage and the concomitant two-electron oxidation of Mn^{IV} to Mn^{VI} inhibits the reaction, accumulating an inactive Mn^{IV} species $[(terpy)Mn^{III}(\mu\text{-}O)_2Mn^{IV}\text{-}(HSO_5)(terpy)]^{3+}$. In equilibrium to this inactive species, the energetically less favored intermediate $[(terpy)\ (HSO_5)\text{-}Mn^{III}(\mu\text{-}O)_2Mn^{IV}(terpy)]^{3+}$, which is catalytically competent, was oxidized to $[(terpy)Mn^V(O)(\mu\text{-}O)_2Mn^{IV}(terpy)]^{3+}$ (best described as $Mn_2^{IV/IV}$-oxyl radical) and this further reacted with water evolving O_2. O-O bond cleavage to form a formal Mn^V intermediate is the rds under excess of oxone (Scheme I.10).[163,164] DFT calculations together with isotopic labeling studies showing the incorporation of ^{18}O from $H_2^{18}O$ into the evolved O_2, support this mechanistic picture.[163]
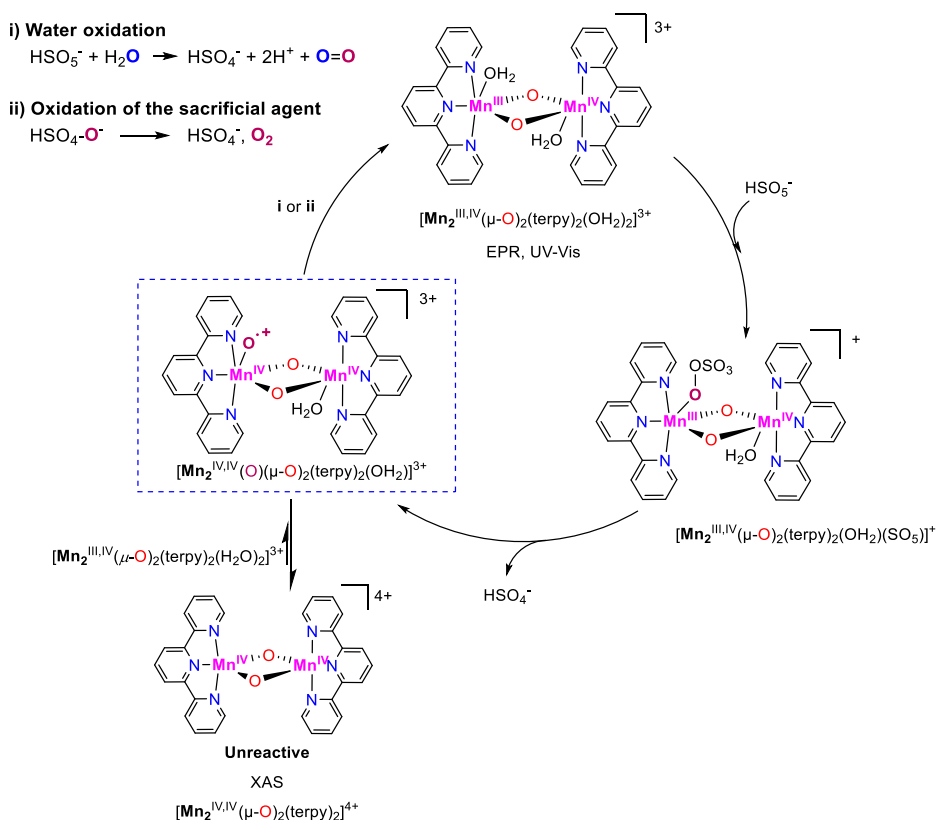
Scheme I.10. The mechanism proposed for the oxidation of water with $[Mn_2^{III,IV}(\mu\text{-}O)_2(terpy)_2(H_2O)_2]^{3+}$ (terpy = 2,2':6,2''-terpyridine) when using Oxone as oxidant. The proposed intermediate responsible for the oxygen release has been highlighted.

The use of CAN as an outer sphere single electron oxidant is preferred to avoid parallel sources of O_2 not arising from H_2O. However, the low pH of Ce^{IV} solutions is an important issue for the stability and few ligands can maintain its stability under these harsh conditions. Complex $[Mn_2^{III,IV}(\mu\text{-}O)_2(terpy)_2(H_2O)_2]$ is unstable under these conditions. To surpass this problem, Yagi and Narita adsorbed the Mn complex into different layered compounds (e.g. kaolin or mica). A maximum TON of 14 was observed and the stability of the entire $[Mn_2^{III,IV}(\mu\text{-}O)_2(terpy)_2]^{3+}$ / clay material after 30min of treatment with CAN was confirmed by EXAFS.[165,166] This was a remarkable result since it indicates a real catalytic water oxidation activity. Despite the nature of the active species was difficult to be identified.

Another type of Mn coordination complexes are those based on Porphyrin and corrole-type ligands, due to their capacity to stabilize high oxidation states.[167] The first report of their application in the water oxidation reaction was reported by Naruta and coworkers in 1994. The authors introduced a family of dimeric Mn-porphyrin complexes formed with two units of tetraarylporphyrins (aryl moieties = 4-tBuC$_6$H$_4$, 2,4,6-Me$_3$C$_6$H$_2$, and C$_6$F$_5$) linked by a 1,2-phenylene bridge and produced oxygen electrochemically when the potential was set up above 1.4 V vs SHE (Scheme I.11). The highest activity reported, 9.2 TON, was observed for the C$_6$F$_5$ aryl-substituted Mn-porphyrin at 2 V. The origin of the activity was related to the spatial disposition of the two Mn-porphyrin units, which facilitated a face to face intramolecular interaction between the two Mn=O units.[168] Detection and characterization of a Mn^V-porphyrin intermediate ([Mn^V=O TMPyP], TMPyP = tetra(N-methylpyridyl)porphyrinato) remained elusive until 1997,[169] when Mn$_2^V$=O(OH) was detected (by UV-Vis, resonance Raman (rR) and EPR spectroscopy) and characterized as the responsible species of the O-O bond formation.[170]

ᵃ 9 TON, 2.5 x 10⁻³
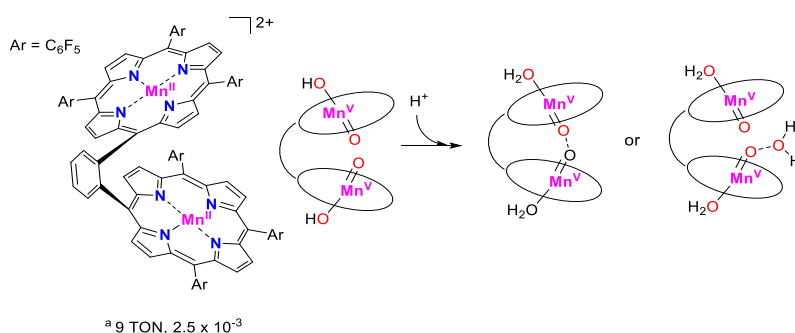
Scheme I.11. *Left*) First homogenous WOC based on first row transition metals. The active species for the water oxidation was suggested to be Mn^V. Ar = C$_6$F$_5$. *Right*) Proposed acid base mechanism for the water oxidation with Mn corrole-type complexes. ᵃ Electrochemical-driven water oxidation at 1.4V vs SHE. n.c. Not catalytic. Numbers reported in the figure stands for TON and TOF values.

The first pure homogeneous Mn WOC catalyst working in the presence of an outer sphere single electron transfer oxidant ([Ru(bpy)$_3$]$^{3+}$ (bpy = 2,2'-bipyridine)) was the dimeric [Mn$_2$(dCIP)(OMe)(CH$_3$CO$_2$)] (dCIP = 2-(3-(7-carboxy-1H-3λ^4-benzol[d]imidazol-2-yl)-2-hydroxyphenyl)-1H-benzo[d]imidazole-4-carboxylic

acid), with a TON of 25 and TOF of 0.027 s^{-1}.[171] Additionally, crystallization in hot methanol yielded a tetrameric structure of the compound, reminiscent of the OEC cluster (Figure I.19). Labeling studies with 5.8% ^{18}O-enriched water were in agreement with a WO process and the catalyst was found competent for the light-driven WO with a TON of 4 ($Na_2S_2O_8$ as SO and $[Ru(bpy)_3]^{2+}$ or $[Ru(bpy)_2(4,4'-CO_2Et-bpy)](PF_6)_2$ as photosensitizers).

25 TON, 2.7 x 10^{-2} s^{-1}

^{a} 4 TON, -
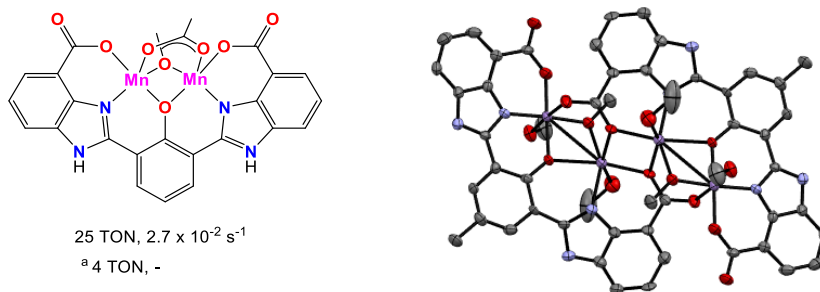
Figure I.19. Left) Line drawing of the first homogeneous Mn-WOC working with monoelectronic oxidants. Right) X-ray crystal structure at 50% probability level of the biomimetic complex formed upon refluxing in MeOH.[171] ^{a} Light-driven conditions ($[Ru(bpy)_2(4,4'-CO_2Et-bpy)](PF_6)_2$ as PS and $Na_2S_2O_8$ as SO, in NaPi buffer, pH 7.2)

I.5.3.2. Water oxidation with molecular iron catalysts

It is almost unnecessary to say that from sustainability and technologic point of view iron is the ideal metal – iron is the second most abundant metal in the earth crust (about 5 %, Figure I.20), it is cheap, and not only environmental benign but biocompatible. From a chemical point of view, the wide range of accessible oxidation states (-1 to +6) provides the potential for the development of a broad variety of chemical transformations, such as Lewis catalysis and catalytic reductions, being the most relevant is its oxidation chemistry. Certainly, FeNi mixed-metal oxides are excellent candidates for technological applications for WO.[172-175] Almost any oxidation reaction can be translated into iron catalysis, i.e. olefin epoxidation,[176] cis-dihydroxylation and C-C oxidative cleavage, C-H hydroxylation,[177-181] alcohol oxidation,[182-185] sulfide and sulfoxide oxidation,[186-189] and more recently WO.[190,191] Iron also has a privileged position at mediating oxidation processes at biological entities; just to name a few biological processes: biosynthesis of metabolites, O_2

UNIVERSITAT ROVIRA I VIRGILI
MECHANISTIC STUDIES OF WATER OXIDATION CATALYZED BY HOMOGENEOUS IRON AND RUTHENIUM
COMPLEXES AND LIGHT-DRIVEN ORGANIC REDUCTIONS WITH A DUAL COBALT/COPPER CATALYTIC SYSTEM
Carla Casadevall Serrano

CHAPTER I   GENERAL INTRODUCTION

transport and sensing, degradation of xenobiotics, DNA repair and antibiotic biosynthesis.[192-199] Interestingly, there is no reciprocity of water oxidation based on iron in biology, where Nature chose Mn for this function despite the parallel reactivity patterns in their oxidation chemistry.

Figure I.20. Relative abundance of the chemical elements in Earth's upper continental crust as a function of atomic number. Rare earth elements are labeled in blue ref (U.S. Geological Survey, 2005, USGS Fact Sheet 087-02. E. Generalic, https://www.periodni.com/rare_earth_elements.html)

The parallel reactivity between Mn and Fe is paramount in non-heme enzymes,[200,201] and in coordination complexes.[202,203] However, there are also inherent differences between their properties that have been discussed in terms of the preference of Nature for manganese to accomplish the water oxidation reaction in the biological Natural photosynthesis.[204] Under the same conditions, manganese-oxo species in oxidation states IV or V tend to be accessible at lower redox potentials and less reactive than the iron-oxo equivalent species. The different oxophilicity between them primes characteristic multinuclear O-bridged Mn(III) clusters, while in the case of iron the Fe^{III}-O-Fe^{III} species is very stable, which leads instead to the formation of lattices, when possible.[205] Clearly, it is of relevance to discover and design well-defined water oxidation catalysts (WOCs) based on Fe, to study how to control their reactivity by implementing strategies to facilitate both the formation of high

oxidation states and the O-O bond formation event, while mimicking parts of the natural photosynthesis machinery. Impressive progress on synthetic models, developed during the last decade, gave rise to the production of molecular catalysts with extraordinary TOFs, and heterogeneous materials with notable robustnesses.[160,206-209] However, none of them reproduces all the features of the OEC. On the other hand, the study of synthetic models has provided examples of operative water oxidation mechanisms and strategies that facilitate the process. The most extensive mechanisms involve the nucleophilic attack of water upon a metal oxo species in high oxidation state and then the coupling of metal oxo groups, with usually radical character. Effective strategies beyond the electronic tuning of the metal, such as charge delocalization within several metals, the water activation by an internal Lewis acid or a base and supramolecular interactions, have been found to facilitate the water oxidation reaction.

The first evidence that iron complexes catalyze the oxidation of water were reported by Elizarova and co-workers in the early 1980s,[190] and the subject was revisited by Kaneko and co-workers in 1998.[191] The subject experienced significant interest since the appearance of a report by Bernhard and Collins in 2010, describing a fast catalytic oxidation with a molecular iron catalyst.[210] Since then, different families of homogeneous water oxidation catalysts based on iron have been described (Figure 21). Although the field is still relatively new, these amenable systems of study already have revealed interesting intermediates within the water oxidation mechanism[211] and furthermore alternative chemical structures to consider.[212] In addition, their catalytic activities are among the most effective molecular water oxidation catalysts based on first-row transition metal complexes when using Ce^{IV} as a sacrificial oxidant, and the reactions are also faster under electro-catalytic conditions. In this review, we have classified the water oxidation catalysts in mononuclear, multinuclear, supported and heterogenized categories, with a focus on the water oxidation mechanism.
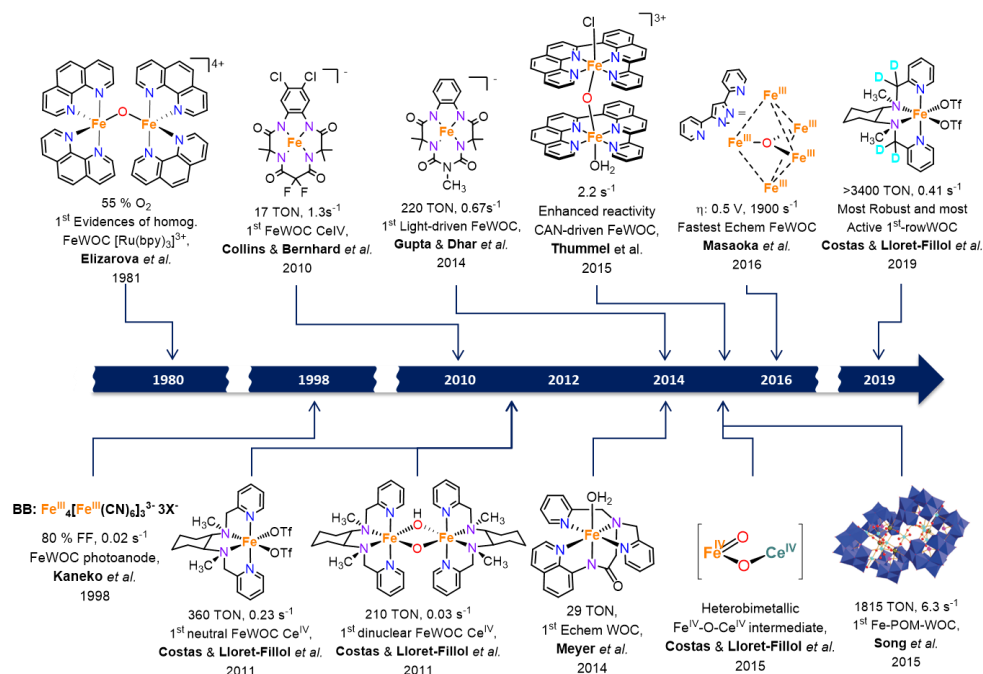
Figure 21. Timeline with selected Fe-WOCs. TON, TOF (s^{-1}), WO study and corresponding authors are included. Echem stands for electrochemical driven water oxidation.

15.3.2.1. Mononuclear Fe WOCs

Mononuclear complexes represent the majority of the reported active catalysts. Many of these Fe-WO complexes were previously studied with the aim to yield efficient and selective catalytic oxidation of organic substrates.[202,213,214] It is already well-known that they react with oxygen transfer oxidants such as peroxides or high valent iodide species, producing Iron-Oxo species in high valent state (IV or V) capable to yield selective oxidations, including the hydroxylation reaction of inert C-H bonds, the epoxidation and cis-diol formation from the oxidation of double bonds.[36]

Iron complexes described in this section are organized in terms of the basicity of the ligand: neutral, mono-anionic and polyanionic. As expected, the electron donor nature of the ligand dictates the metal stabilization in high oxidation states and therefore in oxidation catalysis, but also influences the hydrolysis particularly at low

UNIVERSITAT ROVIRA I VIRGILI
MECHANISTIC STUDIES OF WATER OXIDATION CATALYZED BY HOMOGENEOUS IRON AND RUTHENIUM
COMPLEXES AND LIGHT-DRIVEN ORGANIC REDUCTIONS WITH A DUAL COBALT/COPPER CATALYTIC SYSTEM
Carla Casadevall Serrano

CHAPTER I   GENERAL INTRODUCTION

pH values. In addition we have compared the relative catalytic activities between equivalent iron and ruthenium complexes.

15.3.2.1.1. Mononuclear Fe WOCs based on TAMLs type ligands

In 2010, Bernhard and Collins reported the first example of a well-defined homogeneous Fe-WOC, which were based on tetraamido macrocyclic ligands (Fe^{III}-TAMLs, see Figure I.22). Previously, tetraanionic tetraamido macrocyclic ligands (TAMLs) were already recognized as privileged ligand scaffolds to stabilize transition metals in high oxidation states, since they are quite robust against oxidation and showed efficient activation of O_2 to form Fe-oxo species.[215-218] In addition, their robust nature against oxidation translates into extraordinary stability, without compromising their oxidation reactivity, serving as very powerful peroxidase mimics for oxidative degradation of pollutants.[219]
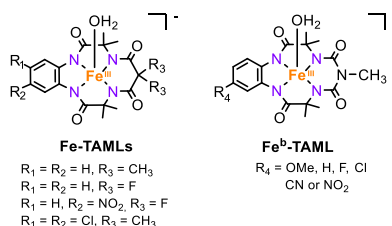
Figure I.22. Schematic representation of TAMLs Fe-WOCs.

In general, TAMLs complexes show an oxygen evolution activity with a fast turnover frequency (TOF) at low pH values. A peak of a TOF of 1.3 s^{-1} was found for the chloro-substituted TAML ligand when using cerium(IV) ammonium nitrate (CAN) as the oxidant, but only produced a total amount of 16 TONs.[210] This work provided evidence for the feasibility of Fe complexes to catalyze WO with a rapid rate. The fast deactivation observed was attributed to the acidity that CAN solution imposed (pH = 0.7). The pH-dependent WO catalytic tests with $NaIO_4$ showed a 2-fold increase in the reaction rates from pH 0.7 to 5.5. In a different study, the acid-induced ejection of iron(III) electron-rich TAML ligands has been shown.[220] With the intention of improving the performance a study of iron TAMLs complexes under electrocatalytic conditions for WO was carried out.[221] Fe-TAML complex

immobilized in Vulcan XC-72 carbon black / Nafion carbon-based electrodes (glassy carbon and carbon paper) registered a constant current of 5 mA with estimate TOF-O_2 of 0.081 s^{-1} at 50 min, with an empirical Faradaic efficiency of 45% (fluorescent oxygen sensor) at pH 1. CO_2 was also detected after electrolysis. Based on X-ray Photoelectron Spectroscopy (XPS) experiments, the observed CO_2 was attributed to the oxidation of the carbonaceous electrode, and it was proved that the catalyst was stable despite the oxidation of its supporting materials. Kinetic studies showed the first-order rate in O_2 evolution regarding catalyst concentration, which suggested a single site WO catalysis. Spectroscopic data pointed towards the formation of $Fe^V(O)$ species under catalytic conditions, although their kinetic competence was not clarified. For this system, the only mechanism information is based on DFT calculations. Independent studies by Cramer and co-workers, and Liao and co-workers suggested that the further oxidized $[TAML^{+\bullet}\text{-}Fe^V=O]$, where the ligand is oxidized by one electron, was responsible for the O–O bond formation *via* a water nucleophilic attack.[222,223] The refined total energy value obtained for the O-O bond formation barrier of 15.4 kcal·mol^{-1} is consistent with the experimental reaction rate constant of 1.3 s^{-1}, thus showing excellent agreement More details of the mechanism hypothesis are giving in figure I.23.
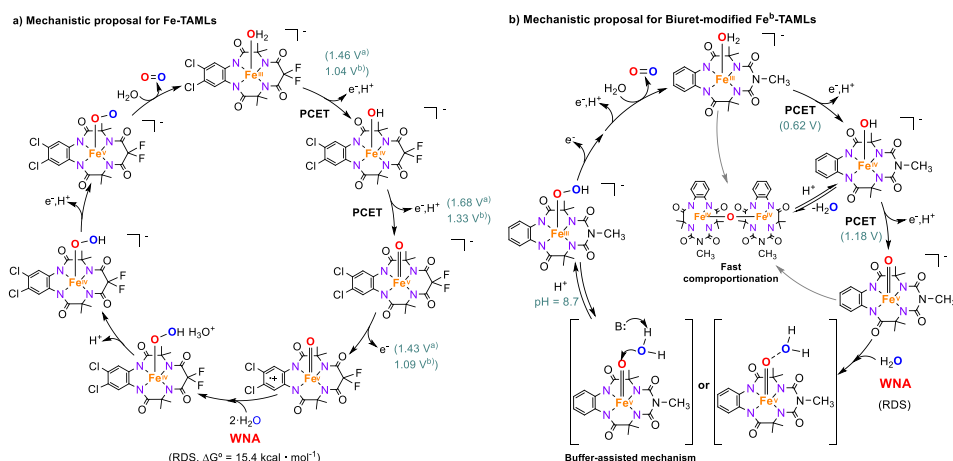
Figure I.23. Proposed mechanism for water oxidation with a) Fe-TAML complexes (computational) and b) Biuret-modified Fe-TAML complexes (experimental). Redox values are reported versus NHE. [a)] Redox calculated at B3LYP*-2D level of theory by Liao and co-workers.[222] [b)] Redox calculated at M06L level of theory by Cramer and co-workers.[223]

Biuret-modified **Fe-TAML** complexes (**Fe-^{b}TAML**, Figure I.22 and I.23) show higher operational stability, which leads to the identification and characterization of the first example of a light-driven WO with a well-defined iron complex. Dhar and co-workers reported a remarkable photocatalytic activity upon irradiation at 440 nm (TON = 220) when using $[Ru(bpy)_3]^{2+}$ as photosensitizer and $Na_2S_2O_8$ as sacrificial electron acceptor.[224-226] Of particular note, its high TOF value (0.76 s^{-1}), which is consistent with a highly reactive high valent iron intermediate. The improved stability under photocatalytic conditions facilitated the spectroscopic characterization of reaction intermediates during catalysis. The formation of a μ-oxo-Fe^{IV} dimer that evolves into a Fe^V(O) species was proposed based on EPR, UV-Vis and High-Resolution Mass Spectrometry (HRMS) studies. Neither the μ-oxo-Fe^{IV} dimer nor the resultant Fe^{IV}(O) monomer was kinetically competent to oxidize water and, thus, further oxidation of the latter appears necessary for generating the active species, in a scenario that resembles the one occurring for Fe-TAML complexes. Based on this mechanistic study the WO reaction is proposed as a single-site water nucleophilic attack on Fe^V(O) for the O-O bond formation followed by deprotonation to form the monomeric Fe^{III}-hydroperoxo species.[224,227] Additional mechanistic insights were provided by electrochemical studies.[226] Under electrochemical conditions (pH $\approx$ 7.2, 15 mM phosphate buffer, I = 0.1 M, NaNO$_3$) the O-O bond-formation event occurs by nucleophilic attack of H_2O on the Fe^V(O) species with a first-order relationship with water. Kinetic isotopic effects (3.2) and the critical role of the pKa of the buffer suggest an atom-proton transfer (APT) mechanism. The electronic effects on the ligand substituent modulate the kinetic rate constant and onset potential for the WO from 0.7 M^{-1} s^{-1} and 170 mV to 6.1 M^{-1} s^{-1} and 540 mV, resulting in values among the lowest overpotentials for complexes based on first-row transition metals.

15.3.2.1.2. Mononuclear Fe WOCs based on aminopyridine ligands

The larger family of well-defined iron-based water oxidation catalysts is based on aminopyridine ligands. Iron complexes bearing aminopyridine ligands were earlier designed to mimic the catalytic oxidation activity of the enzymes that have the

term, iron non-heme enzymes. In this context, the non-heme iron complexes have been proven to be highly resilient to oxidation conditions, to stabilize high oxidation states, such as Fe^{IV} and Fe^{V}, and to catalyze the challenging oxidation of inert C-H bonds.[214,228-234] This family of metal complexes is very versatile regarding the potentially accessible structures. There are literally hundreds of potential iron non-heme complexes, viable by possessing an appropriate combination of amines, pyridines and other nitrogen-based heteroaromatic moieties.[213,235,236] A natural extension of neutral aminopyridine ligands is the inclusion of negatively charged chelating groups, that can be developed in a straightforward manner and facilitate the access of high oxidation states.[237] Nevertheless, a judicious selection of the ligand configuration is essential to observe a significant WO catalytic activity. In this regard, the stability of the coordination complex under the water oxidation conditions is, as expected, decisive. Reaction conditions are highly oxidant and oxidative damage of the molecular catalysts is expected. In addition, when using CAN as a sacrificial oxidant, the highly acidic working pH values renders ligands prone to hydrolysis. An increase in the chelation capacity of the ligand can be determinant. In this respect, ligand architectures that reduce hydrolysis are desirable, especially in the case of N and O base anionic ligands. A more amenable alternative for the stability of the mononuclear iron WOCs based on aminopyridine ligands could be the use of $NaIO_4$ at higher pHs. However, this oxidant can engage in oxygen transfer processes masking the real water oxidation activity. Likewise, photoredox catalysts and sacrificial electron donors can also operate at higher pHs, preventing hydrolysis. Although photoredox catalysts can be a more amenable alternative, this is usually challenging since under typical photoredox catalytic conditions the driving force is lower than that obtained by chemical oxidants such as CAN. An additional drawback is also the potential generation of highly reactive radical species from the action of the photosensitizer that can seriously contribute to the oxidative damage of the ligand framework. Electrochemical conditions also open the possibility to undertake studies at higher pHs. In this case, factors such as the electron transfer kinetics catalyst-electrode may well play an important role and need to be considered.

UNIVERSITAT ROVIRA I VIRGILI
MECHANISTIC STUDIES OF WATER OXIDATION CATALYZED BY HOMOGENEOUS IRON AND RUTHENIUM
COMPLEXES AND LIGHT-DRIVEN ORGANIC REDUCTIONS WITH A DUAL COBALT/COPPER CATALYTIC SYSTEM
Carla Casadevall Serrano

CHAPTER I   GENERAL INTRODUCTION

From the results of the water oxidation studies under chemical conditions, when CAN is used as a chemical oxidant, we can sum up that the catalytic activity is highly dependent on the nature of the ligand scaffold. From all studies, a defined structure-activity pattern can be inferred in the case of neutral multidentate aminopyridyl ligands, and the best catalytic activity is obtained with iron complexes that contain tetradentate ligands with two *cis*-labile sites, while complexes with other neutral ligands such as those of bidentate, tridentate or pentadentate character are virtually inactive (Figure I.24). In addition, complexes that contain tetradentate ligands with *trans*-labile sites present, also yield poor activity, or are inactive, with the exception of iron complexes containing flat and rigid polypyridyl ligands, which nevertheless can be considered essentially a different family of iron coordination complexes.

The first examples of Fe complexes based on aminopyridyl ligands were reported in 2011, proving highly active for WO using chemical oxidants.[238-247] Among them, the complexes **[Fe(OTf)$_2$(^{Me2}Pytacn)]** (Figure I.24, **12**) and α-**[Fe(OTf)$_2$(mcp)]** (Figure I.24, **9**) are particularly interesting because they exhibit remarkable stability against hydrolytic and oxidative decomposition pathways under the chemically driven water oxidation reactions (at low pH). Under these conditions high valent reaction intermediates accumulate under catalytic conditions enabling mechanistic studies. In particular, **α-[Fe(OTf)$_2$(mcp)]** presents remarkable figures of merit, reaching TON values up to 360 (TOF$_{max}$ = 0.23 s^{-1}) and > 1000 (TOF$_{max}$ = 0.06 s^{-1}) when using CAN (pH 1) and NaIO$_4$ (pH 2) as chemical oxidants, respectively.[238] Unfortunately, these complexes are not competent in electrocatalytic or photochemically driven water oxidation processes. In the latter case, as Lau and co-workers first proposed, they undergo rapid decomposition forming iron-oxide nanoparticles that are then the active species.[243,248-250]

UNIVERSITAT ROVIRA I VIRGILI
MECHANISTIC STUDIES OF WATER OXIDATION CATALYZED BY HOMOGENEOUS IRON AND RUTHENIUM
COMPLEXES AND LIGHT-DRIVEN ORGANIC REDUCTIONS WITH A DUAL COBALT/COPPER CATALYTIC SYSTEM
Carla Casadevall Serrano

CHAPTER I   GENERAL INTRODUCTION
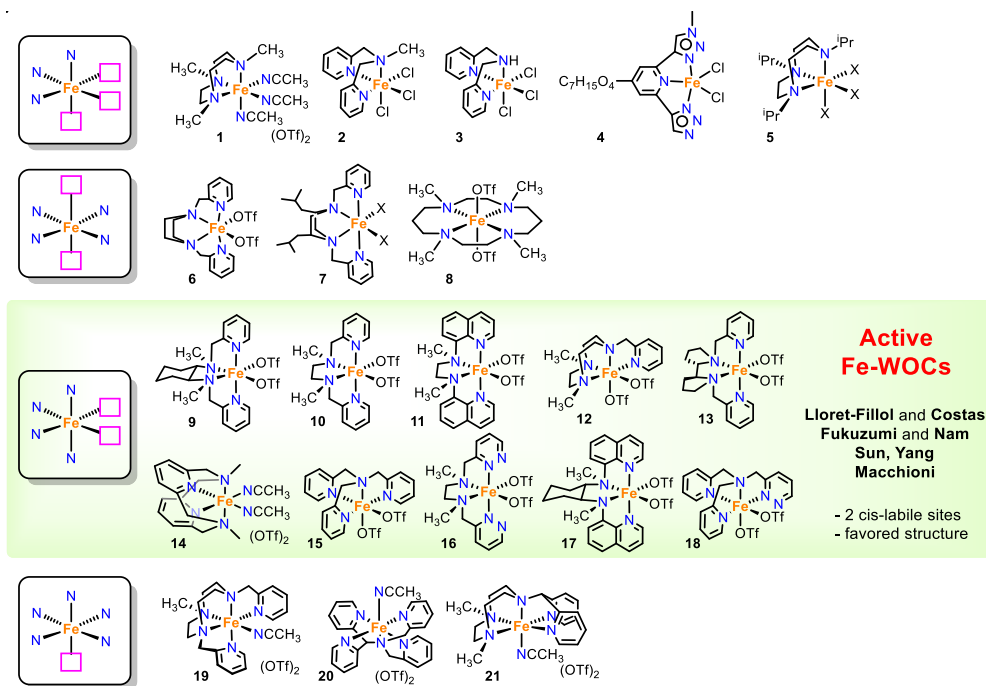
Figure I.24. Selected examples of well-defined iron water oxidation catalysts bearing neutral aminopyridyl ligands. Highlighted are the catalytically most active iron complexes for the water oxidation reaction.

A detailed mechanistic study allowed an understanding of the chemically-driven WO reactions. One insight; ^{18}O isotopic labeling studies with complexes [Fe(OTf)$_2$(L)] (L = ^{Me2}Pytacn and mcp) indicate that the evolved O_2 originates exclusively from water. Moreover, CO_2 was not produced as it was not detected in the gas formed during the WO reactions. In addition, Dynamic Light Scattering (DLS) and Nanoparticle-Tracking Analysis (NTA) experiments showed no evidence of nanoparticle formation. These results discard a complete ligand oxidative degradation with the production of iron oxides as active species, but instead, they are indicative of a homogeneous process. Most significantly, [Fe^{IV}(O)(H$_2$O)(L)]$^{2+}$ was identified as the resting state of the catalytic cycle, and O_2 evolution only occurs when this species is still present in solution. Interestingly, once this species is consumed, O_2 evolution ceases despite the presence of an excess of oxidant. Kinetic studies of WO mediated by CAN show that [Fe^{IV}(O)(H$_2$O)(L)]$^{2+}$ is kinetically incompetent to

activate the water molecule. Furthermore from kinetics studies both CAN consumption and $[Fe^{IV}(O)(H_2O)(L)]^{2+}$ showed first-order dependence. However, when using large amounts of oxidant (CAN > 20 eq) a saturation of the reaction rates was observed together with the formation of a new UV-Vis chromophore,[239] which was attributed to the reversible formation of $[Fe^{IV}\text{-}O\text{-}Ce^{IV}]$ intermediate before the rate-determining step. In this regard, Sakai, Masaoka *et al* .reported an alternative oxo-hydroxocerium (IV) radical coupling mechanism for the O-O bond formation for Ru complexes $[Ru(terpy)(bpy)(OH_2)]^{2+}$ and $[Ru(tpzm)\text{-}(R_2bpy)(OH_2)]^{2+}$ (R=H, Me, and OMe, R_2bpy=4,4′-disubstituted-2,2′-bipyridines) (where terpy = 2,2′:6′,2″-terpyridine, bpy=2,2′-bipyridine and tpzm=tris(1-pyrazolyl)methane).[251] Other indications that high valent M=O motifs could interact with Lewis acid are found in the literature. The interaction between Sc^{3+} and the oxoiron(IV) unit in $[Fe^{IV}(O)(tmc)]^{2+}$ (tmc = tetramethylcyclam) was documented by Fukuzumi, Nam and co-workers.[252,253] In addition, studies of Brudvig, Crabtree and co-workers also suggest $Mn\text{-}O\text{-}Ce^{IV}$ interactions to promote O_2 evolution, a mimic of the role of Ca^{2+} in PSII.[254] More recently, Que and co-workers identify the facile and reversible formation of $Fe^{III}\text{-}O\text{-}Ce^{IV}$ complexes in organic solvents.[255]

In order to obtain further insights into the high valent intermediate before the rate-determining step and O-O bond formation by iron complexes based on neutral tetracoordinate aminopyridyl ligands, Lloret-Fillol and Costas and co-workers studied the effect of the modification of electronic character around the metal center. The modularity of the TACN (1,4,7-triazacyclononane) derived ligands allows for systematic modification of electronic effects.[238,239,256] As a result, the catalytic activity for the iron complexes with the electron-withdrawing substituents at the *para*-position of the pyridine ring increases, with the **[Fe(OTf)$_2$(Me$_2$^{NO2,H}Pytacn)]** complex being the most active of the series (180 TON, Figure I.25). In contrast, substituents in the *ortho*-position of the pyridine showed a dramatic decrease in the catalytic activity independent of the electronic effect. Mechanistic and kinetic studies for these complexes pointed towards the formation of an $[Fe^{IV}\text{-}O\text{-}Ce^{IV}]$ intermediate, that upon inner-sphere oxidation by Ce^{IV} would yield the active species

$[Fe^V(O)(OH)(Me_2^{R1,R2}Pytacn)]$. Spectroscopic monitoring of the reactions with CAN yielded the formation of the characteristic UV-Vis band at a λ_{max} between 754 – 780 nm, symptomatic of the formation of $Fe^{IV}(O)$ S = 1 species. Additionally, CryoSpray-Injection High-Resolution Mass Spectrometry (CSI-HRMS) studies concur with the formation of these species. Interestingly, the addition of an excess of CAN (catalytic conditions, 5 to 75 equivalents) to previously generated $Fe^{IV}(O)$ species, promoted the shift of the characteristic UV-Vis band corresponding to the $Fe^{IV}(O)$ moiety to lower wavelengths ($-\Delta\lambda_{max}$ between 8–10 nm) and the increase of the corresponding ε_{max} from 10% to 25%. Several control experiments supported that the change in UV-Vis spectrum most likely indicates the formation of a novel species from the reaction between $[Fe^{IV}(O)(OH_2)(Me_2^{R1,R2}Pytacn)]^{2+}$ and Ce^{IV}. Kinetic studies of catalytic water oxidation reactions showed initial reaction rates with a first-order dependence on the concentration of $Fe^{IV}(O)$ species, for the iron complexes studied. However, the dependence on the concentration of CAN was more complex; first-order at CAN concentrations < 5 mM, and saturation of the rate at higher values. By considering prior equilibrium, the kinetic data were fitted[239] obtaining values for K_{eq} and k_2. Interestingly, the value of K_{eq} decreases with the increase of the electron-withdrawing character of the Py substituent while k_2 increases, verifying excellent agreement with the Hammett parameters. This finding was associated with the existence of a $Fe^{IV}=O$ / Ce^{IV} pre-equilibrium (K_{eq}) before the rate-determining step; k_2 associated with the nucleophilic attack of the water molecule. These results not only explain the higher WO activity upon increasing the electron-withdrawing character at the metal center and provide evidence of the molecularity of the active species but also clearly point to the formation of a relevant intermediate in the course of the reaction before the RDS.[239] DFT calculations suggested that the O-O bond formation is performed by an iron(V) intermediate $[Fe^V(O)(OH)(Me_2^{R1,R2}Pytacn)]^{2+}$ containing a *cis*-$Fe^V(O)(OH)$ unit. Under catalytic conditions (Ce^{IV}, pH 0.8) the high oxidation state Fe^V is only thermodynamically accessible through a Proton-Coupled Electron Transfer (PCET) process from the cis-$[Fe^{IV}(O)(OH_2)(Me_2^{R1,R2}Pytacn)]^{2+}$ resting state. Interestingly, the cis-OH ligand can act as an internal base, accepting a proton with concomitant

UNIVERSITAT ROVIRA I VIRGILI
MECHANISTIC STUDIES OF WATER OXIDATION CATALYZED BY HOMOGENEOUS IRON AND RUTHENIUM
COMPLEXES AND LIGHT-DRIVEN ORGANIC REDUCTIONS WITH A DUAL COBALT/COPPER CATALYTIC SYSTEM
Carla Casadevall Serrano

CHAPTER I   GENERAL INTRODUCTION

formation of the O-O bond. These results showed that the *cis*-labile coordinative sites in iron complexes have a beneficial key role in the O-O bond-formation process.[257]

Cat.		R_1	R_2	TON[a]	TOF[b]	K_{eq}[c]	k_2[c]
[Fe(OTf)$_2$(Me$_2$^{H,H}Pytacn)]	(**1**)	H	H	82	0.06	230 (20)	1.2 (0.1)
[Fe(OTf)$_2$(Me$_2$^{Cl,H}Pytacn)]	(**2**)	Cl	H	102	0.11	190 (20)	1.4 (0.1)
[Fe(OTf)$_2$(Me$_2$^{CO2Et,H}Pytacn)]	(**3**)	CO$_2$Et	H	143	0.16	130 (20)	1.8 (0.4)
[Fe(OTf)$_2$(Me$_2$^{NO2,H}Pytacn)]	(**4**)	NO$_2$	H	180	0.23	50 (10)	2.8 (0.4)
[Fe(OTf)$_2$(Me$_2$^{H,F}Pytacn)]	(**5**)	H	F	25	0.02	-	-
[Fe(OTf)$_2$(Me$_2$^{H,Me}Pytacn)]	(**6**)	H	Me	-	-	-	-

Proposed mechanism
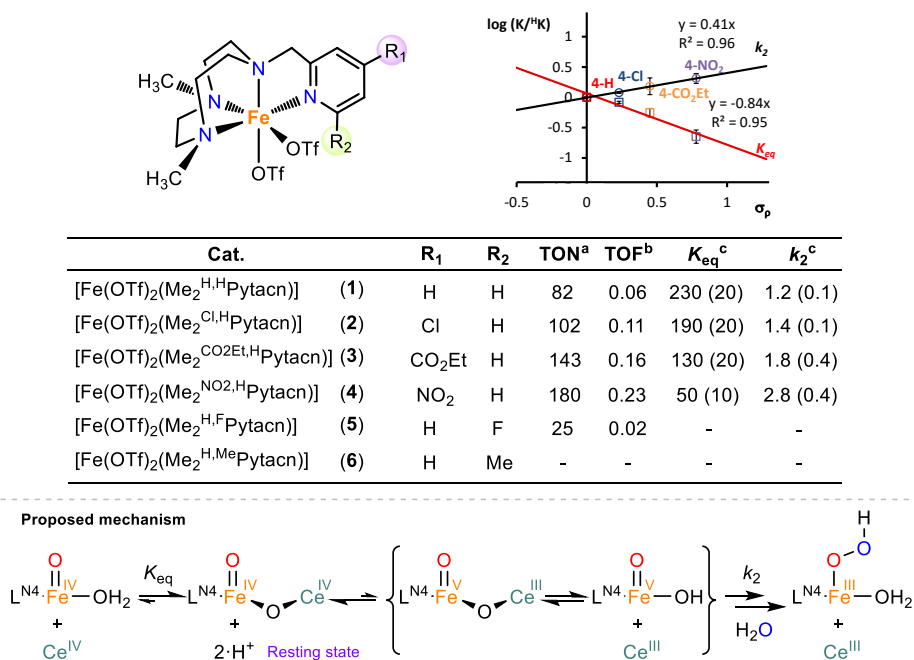
Figure I.25. Study of the electronic effects on the family of Fe-WOCs [Fe(OTf)$_2$(Me$_2$^{R1,R2}Pytacn)]. Top *left*) scheme of the series of Fe complexes; *right)* Hammett plot for the apparent association (K_{eq}, squares) and rate constants (k_2, circles) against the σ_p Hammett parameters for 1-4. Middle: table with the reactivity parameters TON and TOF and K_{eq} and k_2 values of 1-Fe^{IV}(O)-4-Fe^{IV}(O) complexes. a) TON = (n(O$_2$)/n(Cat.)). b) TOFs calculated at max. TON/t ratio in s^{-1}. c) Constants calculated by fitting k_{obs} values to saturation kinetics model (Michaelis-Menten fitting), $K_{eq} \approx 1/K_M$. Bottom: proposed mechanism for WO.

A few years later, a new study revealed the spectroscopic characterization of the **[(mcp)Fe^{IV}(O)-O-Ce^{IV}]** intermediate species under catalytic conditions in the WO reactions performed with the α**-[Fe(OTf)$_2$(mcp)]** complex. CSI-HRMS studies showed the formation of a heterobimetallic Fe^{IV}-Ce^{IV} intermediate with two exchangeable O atoms and no exchangeable protons. The CSI-HRMS in D$_2$O show the same peak pattern at the same m/z value, but in H$_2$^{18}O the peak was shifted by +4 units (see Figure I.26 a and c). In addition, solution resonance Raman (rR) studies in H$_2$O:MeCN (1:1) led to the formulation of the connectivity between the metal centers

and the O atoms. The rR spectrum (λ_{ex} 413.1 nm, 100 mW at -8 ºC) of $[Fe^{IV}(O)(H_2O)(L)]^{2+}$ generated after the addition of CAN (3 eq.) to α-$[Fe^{IV}(O)(H_2O)(mcp)]^{2+}$ showed a band at 822 cm^{-1} that downshifts to 782 cm^{-1} on replacing H_2O by $H_2^{18}O$ (Figure I.26 d, grey area), which is in agreement with the $\upsilon_{Fe=O}$ of α-$[Fe^{IV}(O)(H_2O)(mcp)]^{2+}$. Likewise, the rR spectrum (λ_{ex} 413.1 nm, 100 mW at -8 ºC) of the Fe^{IV}-Ce^{IV} intermediate generated after the addition of CAN (9 eq.) to α-$[Fe^{IV}(O)(H_2O)(mcp)]^{2+}$ showed two features. On the one hand, a band at 822 cm^{-1} that downshifts to 782 cm^{-1} on replacing H_2O by $H_2^{18}O$ was observed (Figure I.26 d, down). Comparison of the intensity of the nitrate feature at 762 cm^{-1} from CAN, together with the binding constant of Ce^{IV} to α-$[Fe^{IV}(O)(H_2O)(mcp)]^{2+}$ extracted from the kinetic studies, allowed for the association of this feature to the newly formed Fe^{IV}-Ce^{IV} intermediate, which must possess a Fe=O bond. On the other hand, the second feature of similar intensity was observed at 677 cm^{-1}, which was the only feature observed and enhanced when the intermediate was probed with 514.5 nm excitation (UV-Vis absorption of the Fe^{IV}-Ce^{IV} intermediate). This band was downshifted to 643 cm^{-1} in $H_2^{18}O$ (Figure 7 d, down). This feature is in agreement with the formation of a Fe-O bond. rR experiments in 1:1 H_2O:$H_2^{18}O$ showed the exclusive formation of bands at 677 and 643 cm^{-1}, discarding a possible $Fe^{IV}(\mu$-$O)_2Ce^{IV}$ core formation, and indicating the formation of a heterometallic $[Fe^{IV}(O)(\mu$-$O)Ce^{IV}]$ species (Figure 7 b). Indeed formation of similar intermediates was further proposed with other systems, which is the case for the $[Cp*Ir(dpa)Cl]Cl$ WOC (dpa = 2 2'-dipyridylamine), reported by Macchioni and co-workers.[258] This heterometallic species can be understood as an inner-sphere intermediate of the single-electron oxidation of $[Fe^{IV}(O)(H_2O)(L)]^{2+}$ species by Ce^{IV} to form a $Fe^V(O)(OH)$ species where the O-O bond is formed by undergoing a water nucleophilic attack (Figure I.27).

UNIVERSITAT ROVIRA I VIRGILI
MECHANISTIC STUDIES OF WATER OXIDATION CATALYZED BY HOMOGENEOUS IRON AND RUTHENIUM
COMPLEXES AND LIGHT-DRIVEN ORGANIC REDUCTIONS WITH A DUAL COBALT/COPPER CATALYTIC SYSTEM
Carla Casadevall Serrano

CHAPTER I   GENERAL INTRODUCTION
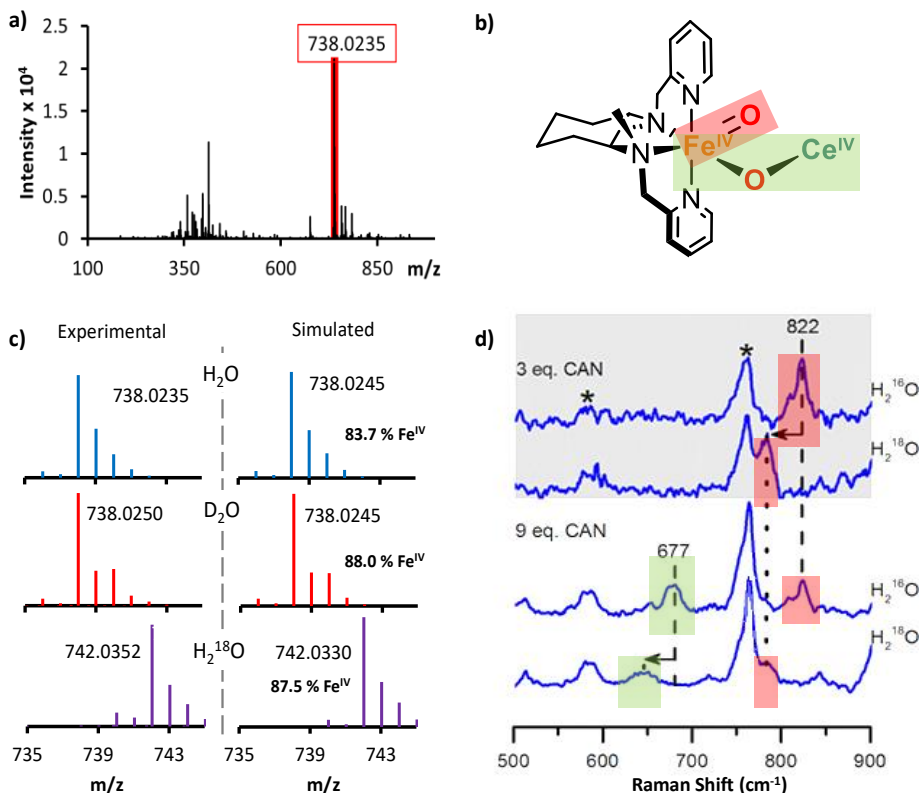
Figure I.26. Characterization of the $Fe^{IV}(\mu\text{-}O)Ce^{IV}$ intermediate by CSI-HRMS and resonance Raman spectroscopy. a) CSI-HRMS spectrum obtained after the addition of CAN (75 eq.) to α-$[Fe^{IV}(O)(H_2O)(mcp)]^{2+}$ species. b) Proposed structure of the $Fe^{IV}(\mu\text{-}O)Ce^{IV}$ intermediate. c) CSI-HRMS spectra of $Fe^{IV}(\mu\text{-}O)Ce^{IV}$ species generated in H_2O, D_2O and $H_2^{18}O$ at 25 °C. d) solution (in H_2O:MeCN, 1:1) rR spectra (λ_{ex} 413.1 nm, 100mW at -8 °C) of, from top to bottom, α- $[Fe^{IV}(O)(H_2O)(mcp)]^{2+}$ generated after the addition of CAN (3 eq.) to a solution of α-$[Fe(OTf)_2(mcp)]$ (5mM) (in grey); and of $Fe^{IV}(\mu\text{-}O)Ce^{IV}$ intermediate after the addition of CAN (9 eq.) to a solution of α-$[Fe(OTf)_2(mcp)]$ (5mM). Asterisks denote features arising from CAN.

UNIVERSITAT ROVIRA I VIRGILI
MECHANISTIC STUDIES OF WATER OXIDATION CATALYZED BY HOMOGENEOUS IRON AND RUTHENIUM
COMPLEXES AND LIGHT-DRIVEN ORGANIC REDUCTIONS WITH A DUAL COBALT/COPPER CATALYTIC SYSTEM
Carla Casadevall Serrano

CHAPTER I   GENERAL INTRODUCTION
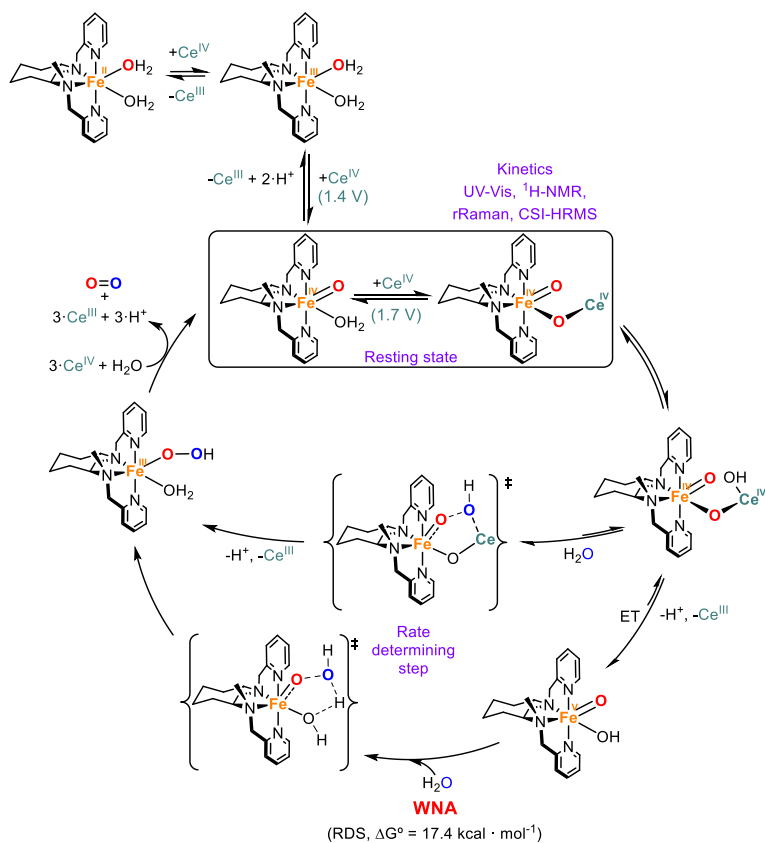
Figure I.27. The postulated mechanism for WO with complex α-[Fe(OTf)$_2$(mcp)] and analogous Fe complexes.

Interestingly, Che and co-workers proposed a different mechanism for the O–O bond formation for complex **[Fe(LN$_4$Py$_2$)Cl$_2$]$^+$** (LN$_4$Py$_2$ = *N,N′*-dimethyl-2,11-diaza[3,3](2,6)pyridinophane) (Figure I.24, **14**) when using Oxone, as well as CAN or NaIO$_4$ as sacrificial oxidants. Their mechanistic studies by means of high-resolution electrospray ionization mass spectrometry (ESI-MS), UV-Vis absorption spectroscopy, ^{18}O-labelling experiments, kinetic studies, cyclic voltammetry (CV), EPR analysis, and DFT pointed to the generation of a Fe^V=O intermediate as the active species. But in their case, no evidence of a Fe^{IV}(μ-O)Ce^{IV} intermediate was observed and it was proposed that [Fe^{IV}(O)(OH)(LN$_4$Py$_2$)]$^+$ is directly oxidized to [Fe^V(O)(O)(LN$_4$Py$_2$)]$^+$ (S = 3/2), which engages in the O-O bond formation through a WNA mechanism (figure I.28).[244]

66
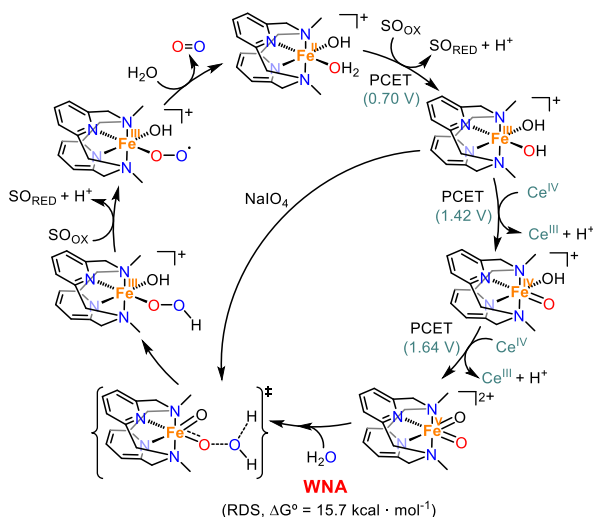
Figure I.28. Postulated mechanism for WO with complex **[Fe(LN₄Py₂)Cl₂]⁺** Fe complexes.

Another example that illustrates a key feature for active Fe complexes based on neutral amino ligands was reported by Hetterscheid and co-workers. The complex ***cis*-[Fe(cyclam)Cl₂]Cl** (figure 10) was shown to be an active electrocatalyst for WO in aqueous mixtures. Electrochemical studies on this system in aqueous mixtures showed a first reversible wave at 0.7 V vs NHE that was assigned to the $Fe^{II/III}$ redox couple and a catalytic peak starting at 1.7 V vs NHE.[259] Online electrochemical mass spectrometry (OLEMS) studies as a function of the applied potential showed the formation of O_2 starting at 1.7 V vs NHE. Moreover, immediate O_2 evolution was detected without induction time and no CO_2 formation before the onset of O_2 evolution. However, CO_2 evolution was observed at lower potentials than for WO, which is in agreement with ligand decomposition under the highly oxidative conditions. Likewise, when using a chemical oxidant, no significant turnover numbers of O_2 were observed, but strong catalyst deactivation occurred. In contrast, the complex ***trans*-[Fe(cyclam)Cl₂]** (figure 10) showed no significant WO activity neither with chemical oxidants nor under electrochemical conditions. Later on Ruffo, Macchioni and co-workers reported a series of differently substituted cross-bridged cyclam complexes **[Fe(CBC-R,R′)Cl₂]PF₆** (Figure I.29). The WO activity was found

to depend markedly on the steric hinderance of the ligand substituent. Up to 111 TON O_2 (TOF = 1.4 min^{-1}) were obtained using $NaIO_4$ as a sacrificial oxidant in water with **[Fe(CBC-Me,Et)Cl$_2$]PF$_6$**, whose steric substitution has the best compromise in terms of accessibility and protection of the metal center. Moreover, the lack of induction time before O_2 evolution suggests that the starting complex is the real molecular species.[247]
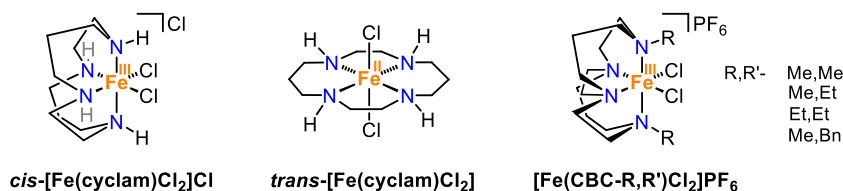
Figure I.29. Structure of iron complexes *cis*-**[Fe(cyclam)Cl$_2$]Cl**,*trans*-**[Fe(cyclam)Cl$_2$]** and cross-bridged cyclam complexes **[Fe(CBC-R,R′)Cl$_2$]PF$_6$**.

Among all the mechanistic studies performed on these systems, there are different proposed intermediates and reaction events in which there is an expectation of potential involvement of PCET processes. In this regard, Yang and co-workers studied the effect of introducing pendant bases at a coordinated pyridine or by introducing another coordinating heteroaromatic group. Tested catalysts such as **[Fe(OTf)$_2$(mep^b)]** and **[Fe(OTf)$_2$(tpa^b)]** (mep^b = *N,N′*-dimethyl-*N,N′*-bis(pyridazin-3-ylmethyl)ethane-1,2-diamine and tpa^b = 1-(pyridazin-3-yl)-*N,N′*-bis(pyridin-2-ylmethyl)methanamine, Figure I.24, **16** and **18**, respectively)[241] produced equivalent catalytic activity (67 and 20 TON O_2, respectively) to the parent complexes (72 and 14 TON O_2, respectively) under the same catalytic conditions. Although this strategy did not have a significant effect, as a basis of mechanistic studies, the presence of pendant bases in close proximity to the metal center could be beneficial.

A determination of the real nature of the catalyst is essential for the validation of the mechanistic studies. Especially for water oxidation studies where the severity of the reaction conditions can easily degrade the catalysts to give oxidized species that could act as well, as catalysts. In this regard, different studies have provided solid arguments toward establishing the molecularity of this family of water oxidation

UNIVERSITAT ROVIRA I VIRGILI
MECHANISTIC STUDIES OF WATER OXIDATION CATALYZED BY HOMOGENEOUS IRON AND RUTHENIUM
COMPLEXES AND LIGHT-DRIVEN ORGANIC REDUCTIONS WITH A DUAL COBALT/COPPER CATALYTIC SYSTEM
Carla Casadevall Serrano

CHAPTER I   GENERAL INTRODUCTION

catalysts. First, Lau and co-workers studied complex α-**[Fe(OTf)$_2$(mcp)]** at different pHs and they observed a duality in behavior.[248] At high pH and under photocatalytic conditions, using $[Ru(bpy)_3]^{2+}$ (bpy = 2,2′-bipyridine) as a photoredox catalyst, $Na_2S_2O_8$ as sacrificial electron acceptor and α-**[Fe(OTf)$_2$(mcp)]** as WOC, they found that the formation of metal oxide nanoparticles triggers the WO catalysis. Significantly enough, the exposure of those iron oxide nanoparticles under acidic conditions did not deliver any catalytic activity when using CAN as oxidant. The same type of experiments was reported by Sakai and co-workers, but using $NaIO_4$ as the sacrificial oxidant.[243] In contrast, to the previous reports, and additional reports it was found that under low pH values (0 - 4.5), forced by the sacrificial oxidants CAN and $NaIO_4$, water oxidation by iron complexes bearing multidentate *N*-donor ligands such, as the complex α-**[Fe(OTf)$_2$(mcp)]**, there was no evidence for the formation of iron oxide nanoparticles.[211,243,248] Actually this is expected based on thermodynamics; at low pH values $[Fe(OH_2)_6]^{3+}$ is the stable Fe^{III} species rather than Fe_2O_3. On the other hand, $[Fe(OH_2)_6]^{3+}$ cannot catalyze WO either by CAN or by $NaIO_4$. Despite that $[FeO_4]^{2-}$ is a well-known strong oxidant ($E°(Fe^{4+}/Fe^{3+})$ = 2.2 V) for WO, CAN and $NaIO_4$ are not capable of oxidizing Fe^{3+} to $[FeO_4]^{2-}$. This means that at low pH values, even if some ligand dissociation would occur, the resulting $[Fe(OH_2)_6]^{3+}$ ion would not be able to catalyze WO.

Fukuzumi, Nam, Llobet and co-workers reported the non-heme iron complexes **Fe(BQEN)(OTf)$_2$** and **Fe(BQCN)(OTf)$_2$** (BQEN = *N,N′*-dimethyl-*N,N′*-bis(8-quinolyl)-ethane-1,2-diamine and BQCN = *N,N′*-dimethyl-*N,N′*-bis(8-quinolyl)cyclohexanediamine, Figure I.24, **11** and **17**, respectively) for WO which produced 80 and 20 TON O_2, respectively using CAN as a sacrificial oxidant.[249] In addition, significant amounts of CO_2 were also detected during WO reactions under the acidic catalytic conditions derived from the use of CAN. This result suggests ligand dissociation[260] and oxidation under acidic conditions by CAN yielding CO_2, which compete with the O_2 evolution reaction. These results indicate that a wise selection of the ligand is the key to obtain robust WOC. Nevertheless, isotopic

labeling experiments also pointed towards the homogeneous nature of the active species. Conducting experiments under similar light-driven WO conditions, they observed the formation of iron hydroxide nanoparticles, derived from the decomposition of the Fe complexes, which were characterized as the active species.
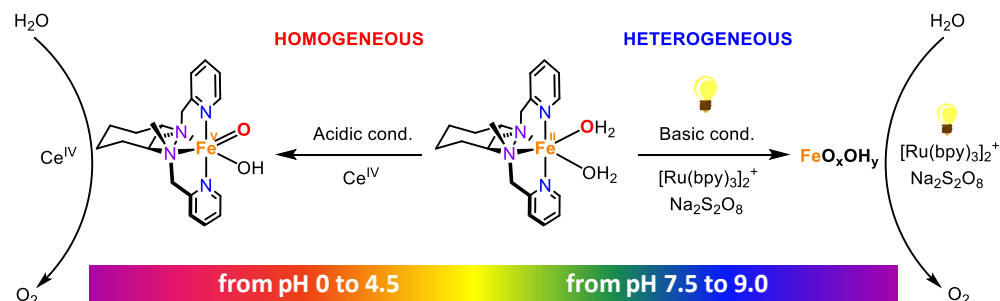
Figure I.30. Two different scenarios for water oxidation catalyzed by iron complexes bearing neutral tetradentate aminopyridyl ligands, such as **α-[Fe(OTf)₂(mcp)]**.

According to these studies, there are two regimes in WO reactions mediated by these systems: i) homogeneous WO by the molecular Fe complexes under acidic conditions (pH 0-4.5) when using CAN or NaIO$_4$ as sacrificial oxidants and ii) heterogeneous WO mediated by iron nanoparticles under the strongly basic (pH 7.5-9) photocatalytic conditions; it is worth noting that these nanoparticles are not active in CAN-driven WO (Figure I.30).[248,249]

Despite all the advances, there are still questions to be addressed regarding the real nature of the oxidizing species. The correlation between decomposition paths and O$_2$ evolution, or the direct evidence of O$_2$ evolution from a metal-oxo species, is a central problem that remains to be solved in many WO systems.

15.3.2.1.3. Iron complexes with anionic polypyridineamine ligands

A particularly interesting extension of the use of neutral tetradentate ligands is the introduction of an anionic coordinating moiety, which, by increasing the ligand basicity, would be expected to facilitate the formation of the high oxidation state Fe^V(O). In this vein, Meyer and co-workers reported that the **[Fe^{III}(dpaq)(H$_2$O)]$^{2+}$** (dpaq = 2-[bis(pyridine-2-ylmethyl)]amino-*N*-quinolin-8-yl-acetamido, Figure I.31)

UNIVERSITAT ROVIRA I VIRGILI
MECHANISTIC STUDIES OF WATER OXIDATION CATALYZED BY HOMOGENEOUS IRON AND RUTHENIUM
COMPLEXES AND LIGHT-DRIVEN ORGANIC REDUCTIONS WITH A DUAL COBALT/COPPER CATALYTIC SYSTEM
Carla Casadevall Serrano

CHAPTER I   GENERAL INTRODUCTION

complex, was the first electrocatalytic WOC. Sustained water oxidation catalysis in propylene carbonate–water mixtures yielded 29 TON-O_2 over a 15 h controlled potential electrolysis (CPE) with a 45% Faradaic yield. Kinetic analysis of the electrocatalytic process suggests the formation of a $Fe^V(O)$ species at 1.52 V vs NHE that then undergoes bimolecular water oxidation (Figure I.32) since the peak current displays a first-order dependence on the catalyst concentration.[256] However, no electrochemical WO activity was observed in aqueous solution nor when using CAN as a sacrificial oxidant as reported by Sun and co.[245]

[Fe(dpaq)(H₂O)]²⁺   **[Fe(BPG)Cl₂]**   **[Fe(BPH)Cl₂]**   **[Fe(cyclamacetate)Cl]**
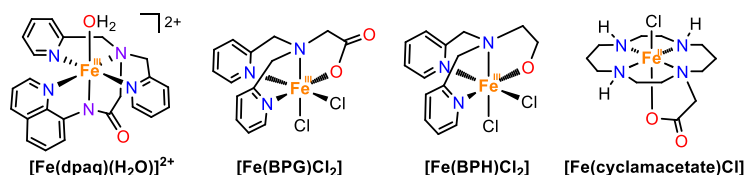
Figure I.31. Inactive WOC with monoanionic ligands when using CAN as sacrificial oxidation.
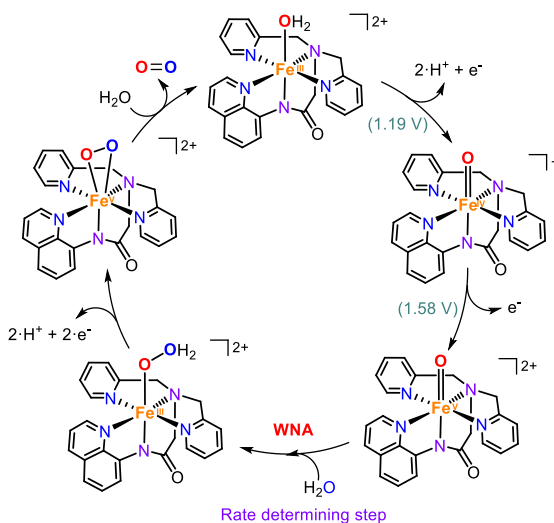
Figure I.32. The postulated mechanism for water oxidation with complex [Fe^{III}(dpaq)(H_2O)]²⁺. Redox values are reported versus NHE.

Another electrocatalyst for WO with a complex containing a monoanionic ligand was reported by Hetterscheid and co-workers, **[Fe(cyclamacetate)Cl]** (Figure I.31). Electrochemical studies on this system in aqueous mixtures showed a first

reversible wave at 0.7 V vs NHE that was assigned to the $Fe^{II/III}$ redox couple and catalytic peak starting at 1.8 V vs NHE. [259] To obtain more information about the WO onset potential, OLEMS studies as a function of the applied potential showed the formation of O_2 starting at 1.8 V vs NHE. Moreover, immediate O_2 evolution was detected without induction time and no CO_2 formation. CO_2 evolution was observed from 1.3 to 1.8 V vs NHE after the onset for WO, suggesting ligand decomposition under electrocatalytic conditions. Likewise, when using a chemical oxidant, no significant turnover numbers of O_2 were observed but strong catalyst deactivation. Likewise, monoanionic complexes **[Fe(BPG)Cl₂]** and **[Fe(BPH)Cl₂]** (BPG = (bis(2-pyridylmethyl)amino)acetate), and BPH = *N,N*-bis(pyrid-2-ylmethyl)-*N*-(2-hydroxyethyl)amine)) have been found to be inactive for WO employing CAN as a sacrificial oxidant (Figure I.31).[245] Presumably, the inactivity of this family of complexes under acid conditions may suggest a ligand labilisation *via* protonation of the anionic fragment.

15.3.2.2. Dinuclear and polynuclear Fe WOCs

15.3.2.2.1. Dimeric Fe WOCs based on polyaminopyridyl ligands

Another level of complexity has been introduced in the attempt to make more viable the O-O bond formation step, and this involves the use of molecular architectures with higher nuclearity. For iron complexes, straightforward access to binuclear complexes is *via* the formation of oxo-bridges between ferric centers. However, oxo-bridged diferric complexes are labile and may form monoferric species under the low pH conditions related to the water oxidation with chemical oxidants, complicating the study.

$[(tpa)(OH_2)Fe(\mu\text{-}O)Fe(OH_2)(tpa)]^{4+}$ $[(tpa)Fe(\mu\text{-}O)(\mu\text{-}SO_4)Fe(tpa)]^{2+}$ $[(tpa)(Cl)Fe(\mu\text{-}O)Fe(Cl)(tpa)]^{2+}$
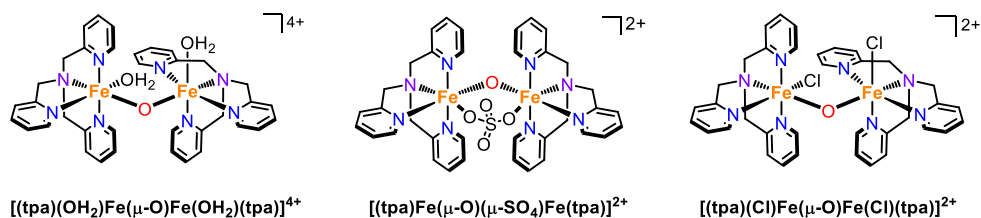
Figure I.33. Structures of the dinuclear Fe complexes based on the tpa ligand.

Fe dimers based on the TPA (TPA = tris(2-pyridylmethyl)amine) ligand are the most often investigated. Studies by Najafpour,[256] Sakai[243] and Ma[261] showed that a wide range of chemistry can be produced just by tuning the Fe-oxo core (Figure I.33). Indeed, the complex $[(tpa)(OH_2)Fe(\mu-O)Fe(OH_2)(tpa)]^{4+}$ reported by Najafpour et al.,[262] surpasses the performance of the monomer analog[238,263] tested in the presence of the same oxidant (Ce^{4+}). DLS studies exclude the formation of iron NPs. In-depth kinetic investigations indicated that O–O bond formation occurs within the dinuclear framework since the reaction rate was found to be first-order in both Ce(IV) and catalyst. Sakai *et al.*[243] reported an analogous dimer to $[(tpa)(OH_2)Fe(\mu-O)Fe(OH_2)(tpa)]^{4+}$ in which, in parallel with the μ-oxo bridge, a sulfate anion replaced the water molecule. Interestingly, the reaction rate was found to increase when lowering the pH in the range 3-7 suggesting that the reduced anation that occurs under acidic conditions affects the position of a monomer-dimer equilibrium before the rate determining step. The authors used this explanation to justify such an uncommon occurrence since a low pH should disfavor the rate-limiting water nucleophilic attack. Ma *et al.*[261] studied the activity of $[(tpa)(Cl)Fe(\mu-O)Fe(Cl)(tpa)]^{2+}$ (Figure 16) in acetate buffer in the presence of Oxone as a sacrificial oxidant; in this case the reaction occurs under less acidic conditions (pH 4.5). Under this condition, the performance is remarkable (TON = 2380 and TOF = 2.2 s^{-1}) and HRMS studies allowed to identify $[(tpa)Fe(\mu-O)(\mu-OAc)Fe(tpa)]^{3+}$ as a crucial species for such activity. They suggested that acetate coordinates and bridges two Fe moieties, highlighting that the two free coordination sites are constrained in a *cis* fashion. More mechanistic studies are needed to identify promising dinuclear reaction pathways.

A particular interesting example is the one reported by Thummel[262] and co-workers The $Fe_2^{III/III}$ $[(ppq)(OH_2)Fe(\mu-O)Fe(Cl)(ppq)]^{3+}$ (ppq = 2-(pyrid-2′-yl)-8-(1″,10″-phenanthrolin-2″-yl)-quinoline)) complex (Figure I.34) yielded an extraordinary catalytic activity (TON of 1000 and a TOF of 2.2 s^{-1}). The interplay between the two metal centers was evidenced by electrochemistry means. Two redox features appeared in the CV, one wave at ca. +0.21 V *vs* NHE associated with the

reversible $Fe_2^{III/III}(OH_2)$ → $Fe_2^{IV/IV}(OH_2)$ two-electron oxidation. The second was a *quasi*-reversible wave at ca. +0.69 V *vs* NHE, ascribed to a successive electron and proton transfers resulting in the following disproportionation: $Fe_2^{IV/IV}(OH_2)$ → $Fe^{III}Fe^V=O + 2\ H^+$.
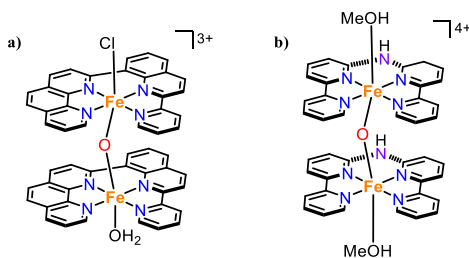
Figure I.34. a) Structure of the dinuclear $[(ppq)(OH_2)Fe(\mu\text{-}O)Fe(Cl)(ppq)]^{3+}$ complex reported by Thummel *et al*. b) $[(MeOH)Fe(Hbbpya)\text{-}\mu\text{-}O\text{-}(Hbbpya)Fe(MeOH)](OTf)_4$ complex reported by Hetterscheid *et al*.

Que and co-workers described a (μ-oxo)diiron(IV) complex supported by a pentadentate ligand, namely $[Fe(\mu\text{-}O)L_2]^{2+}$ (with L = *N,N*-bis-(3′,5′-dimethyl-4′-methoxypyridyl-2′-methyl)-N′-acetyl-1,2-diaminoethane) (Figure I.35).[246] The electrochemical activity of this Fe_2(IV) dimer is exceptional, since in pure CH_3CN, the $E_{1/2}$ of the $Fe^{IV/IV}/Fe^{III/IV}$ couple, is the highest measured for a diiron complex (2.14 V vs NHE), making it the very first example of a (μ-oxo)diiron(IV) oxidant capable of cleaving the O–H bond (2.13 V vs NHE). The authors proposed that water gets oxidized to the hydroxyl radical *via* a rate-limiting PCET that involves, according to the kinetic law, two water molecules (second-order with respect to H_2O and first-order with respect to the diiron dimer). The resulting third-order reaction rate constant was interpreted as a mechanism involving direct attack of the catalyst to the first water molecule, resulting in the OH cleavage, whereas the second one acts as an internal base that accepts the proton. The marked KIE of 2.3 unambiguously identified this PCET as the rate- determining step. Subsequently, the hydroxyl radical remains trapped by the solvent, rather than forming the O–O bond, consistent with the detection of acetamide in a 60% yield.
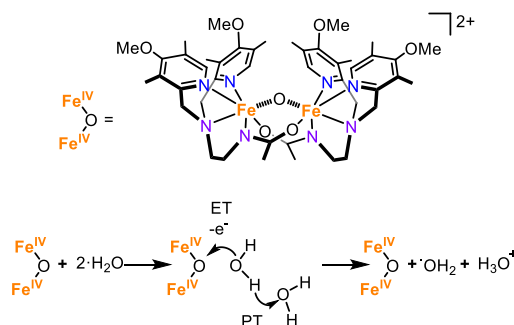
Figure I.35. The upper panel reports the structure of the Fe^{IV}_2 complex by Que *et al.* The lower panel is the proposed mechanism of –OH oxidative cleavage.

More recently, Hettersheid and co-workers, synthesized an analogous complex in which iron binds the Hbbpya (Hbbpya = N,N-bis(2,2′-bipyrid-6-yl)amine) ligand. The resulting [(MeOH)Fe(Hbbpya)-μ-O-(Hbbpya)Fe(MeOH)](OTf)$_4$ is structurally similar to the Thummel catalysts.[264] Interestingly, the performance is markedly dependent on the nature of the working electrode used, in particular, the onset potential is remarkably lower when a glassy carbon electrode is used instead of a Au one, thus indicating that the mechanism should not involve surface oxides. Conversely, the authors proposed π-π stacking interactions between the aromatic ligand and the sp^2 C surface of the electrode as the key for the increased activity. Detailed electrochemical quartz crystal microbalance (EQCM) experiments excluded the possible formation of a solid deposit on the electrode surface, demonstrating the molecular nature of the real active species.

The results reported here highlight how increasing the nuclearity of the catalytic systems may result in the enhancement of the performance with respect to simpler monomer counterparts, since the synergy between more metal centers acts directly in the rate-limiting O-O bond formation step.[251,265,266]

15.3.2.2.2. Polynuclear Fe WOCs

The use of polynuclear iron complexes initiates the possibility of engaging in multinuclear water oxidation pathways. Such complexes have been proposed to be

beneficial in reducing the energy barrier of the O-O bond formation in the case of Ru complexes, via a direct coupling mechanism between two M-Oxo (or M-Oxyl) moieties. The accumulation of the four oxidative equivalents required for the water oxidation reaction to yield O_2 can be facilitated in multinuclear complexes. In this regard, Åkermark *et al*. described two molecular complexes, a dimeric (Fe(III,III)) and a nonanuclear cluster, using the bio-inspired dinucleating ligand 2,2′-(2-hydroxy-5-methyl-1,3-phenylene)bis(1H-benzo[d]imidazole-4-carboxylic acid).[267] Both catalysts were found to be active toward photo-catalytic water oxidation assisted by $[Ru(bpy)_3]^{3+}$ in phosphate buffer. DFT calculations ruled out that the methoxide and acetate ligands of the dimeric precursors are only placeholders and they are replaced in the active species by a hydroxide bridge and a phosphate anion. Nevertheless, due to the neutral pH and the poor stability of the photosensitizer, the dimer is able to run only 4 TONs, with a first-order rate constant relating to catalyst concentration. The authors highlighted that the O-O bond is formed by the intramolecular coupling of two high-valent Fe units. During attempts to crystallize the dimer in warm DMSO, the authors crystallized the more aggregated species, constituted by nine iron atoms and six ligands cluster. These new catalysts exhibit even higher performance than the previous example, increasing by almost seven times the number of cycles performed (TON = 27), suggesting how the increment of the nuclearity in a highly-ordered ligand framework can represent a valid strategy for further developments.

The continuing endeavors aimed at achieving higher complexity led Masaoka *et al*. to develop a very elegant pentanuclear iron complex with outstanding performance.[268] The structure of this catalyst consists of five iron ions $[Fe^{II}_4Fe^{III}(\mu_3\text{-}O)(\mu\text{-}L)_6]^{3+}$ (LH = 3,5-bis(2-pyridyl)pyrazole). The overall complex has quasi-D_3 symmetry and consists of a triangular $[Fe_3(\mu_3\text{-}O)]$ core wrapped by two $[Fe(\mu\text{-}L)_3]$ units in the apical position. The two Fe at the apical positions are hexa-coordinated by three L^- with distorted octahedral geometries, whereas the three iron ions in the triangular core are pentacoordinated by two L^- and an O^{2-} anion with distorted trigonal bipyramidal geometries, resulting in unsaturated coordination of the core.

UNIVERSITAT ROVIRA I VIRGILI
MECHANISTIC STUDIES OF WATER OXIDATION CATALYZED BY HOMOGENEOUS IRON AND RUTHENIUM
COMPLEXES AND LIGHT-DRIVEN ORGANIC REDUCTIONS WITH A DUAL COBALT/COPPER CATALYTIC SYSTEM
Carla Casadevall Serrano

CHAPTER I   GENERAL INTRODUCTION

The cyclic voltammetry in acetonitrile reveals five reversible redox waves related to as many single electron transfers occurring on each iron ion of the cluster, thus describing six different redox states. In the presence of water, a large anodic current appears due to O_2 evolution and the relative metrics are outstanding (TON $\approx$ $10^6 - 10^7$ for 120 min and TOF = 140 – 1400 s^{-1}). The authors proposed a mechanism analogous to the one occurring in PSII, which foresees the accumulation of positive charge at the cluster until O_2 is generated by the formation of two terminal iron-oxo units (Figure I.36). Indeed, passing from the S0 state ($Fe^{III}Fe^{II}_4$) to S4 (Fe^{III}_4) no water molecule attack occurs, since no obvious changes in the redox waves can be observed. In the original paper, the proposed mechanism foresaw two water molecules attacking as many iron ions from the Fe-oxo core, followed by the O-O bond formation from a state $Fe^{II}_2Fe^{III}Fe^{IV}_2$. In a very recent paper,[269] a novel mechanism was proposed on the basis of DFT calculations. According to these, the first H_2O coordinates one Fe of the core from the state Fe^{III}_5 with a barrier of 18.8 kcal·mol^{-1}. The resulting species is sufficiently acidic to release an H^+, giving a hydroxo species in which O bridges two adjacent Fe of the core, while at 1.6 V, a PCET leads to the formation of the first oxo unit. Subsequently, a second water molecule insertion with a calculated barrier of 13.2 kcal·mol^{-1} precedes the one electron and two protons oxidation that gives the second Fe=O unit at a potential of 1.66 V. The coupling of two terminal oxo groups with a barrier of only 8.8 kcal·mol^{-1} produces the superoxide from which O_2 is released. The overall O-O bond formation requires 17.3 kcal·mol^{-1} of activation, which is slighter smaller than the first H_2O insertion, but the authors suggested that the water attack barrier could be an overestimate since an experimentally determined one would be 13 kcal·mol^{-1} using classical TS theory.
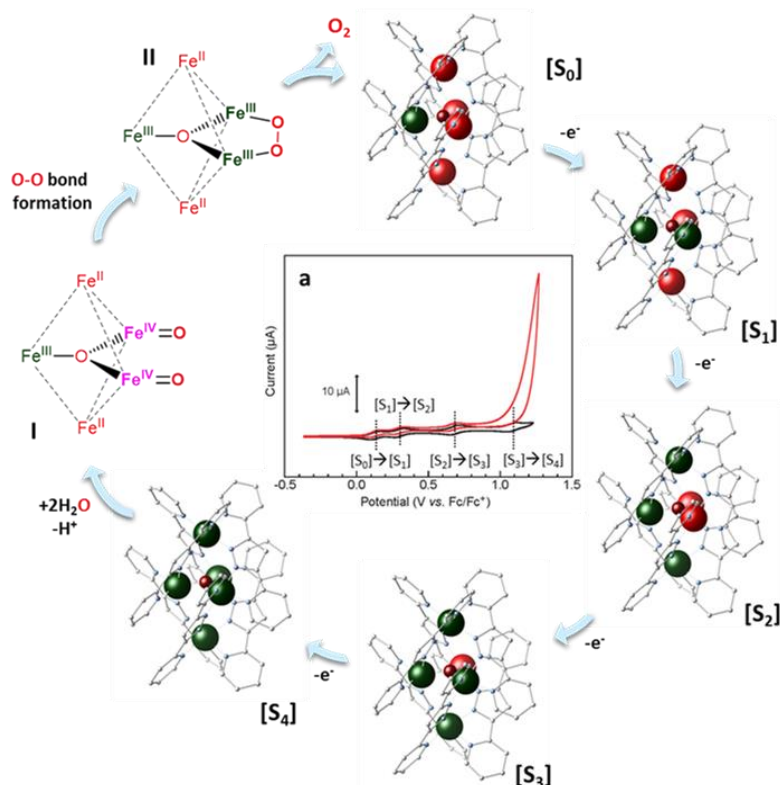
Figure I.36. Structure of the penta-iron complex catalyst and mechanism proposed for water oxidation. Inset a: CVs of 1 (0.2 mM) in acetonitrile solutions with Et_4NClO_4 (0.1 M) at a scan rate of 10 mV s−1 with 5 M of H_2O (red line) and without water (black line).

Recently, Ray *et al*. presented an advance in the field of multinuclear iron complexes, by reporting the one-pot synthesis of $[Fe_8(\mu_4\text{-}O)_4(\mu\text{-}4\text{-}R\text{-}pz)_{12}X_4]$ clusters (with R = CH_3, H, and Cl; X = Cl, Br; pz = pyrazolate).[270] The complex molecular structure is constituted by four outer $Fe(\mu\text{-}4\text{-}tBu\text{-}pz)_3$ moieties that tetrahedrally surround the inner Fe_4O_4 inner cubane core. The electrochemical properties of this cluster are unique, since the CV shows two *quasi*-reversible one electron reduction waves at $E_{1/2}$ = -0.28 V and -0.56 V, and one two-electron reduction at -0.99 V (*vs* Fc/Fc+), and generally octanuclear complexes show four one electron waves shifted of 100-300 mV to a more negative potential.[271] However, the performance of this catalyst when some water is added to it in dry acetone is not exceptional and the authors find that the cluster is only able to perform the two-electron oxidation of

water to H_2O_2 with 30% yield irrespective of initial catalyst concentration, invoking the hydroxyl radical as the principal active species involved in the O-O bond formation.

I.5.3.3. Cobalt water oxidation catalysts

Until 2008, water oxidation research was mainly focused on ruthenium and manganese. While those systems remained in solution during electrocatalysis, allowing their mechanistic study, cobalt salts precipitated after few catalytic cycles, complicating its mechanistic study. But in 2008 cobalt reemerged, held on by Nocera's group, showing that those precipitates arising from cobalt complexes or cobalt phosphate salts ("CoPi") are active WOCs in water.[272] Interestingly, modified electrodes obtained by electrodeposition of these precipitates exhibited a highly improved long-term water oxidation activity. In light of this, Co-complexes was relaunched and several research groups have developed homogeneous Co. Nevertheless, like Ir WOCs, simple Co(II) ions and cobalt-oxides are an active catalyst for WO and, thus, a great effort is usually needed to distinguish between homogeneous and heterogeneous systems. Currently, several Co complexes based on polyoxometalates, porphyrin, phthalocyanine, corrole, TAML, polypyridine, polyamine, polypyridinamine and salen ligands have been reported as active WOCs.[160,167] However, in this section we only show representative examples of the field.

In an early work, Elizarova *et al.* found that cobalt phthalocyanines or porphyrins catalyzed the oxidation of water by $[Ru(bpy)_3]^{3+}$.[273] A bilayer of an n-type semiconductor (PTCBI = 3, 4, 9, 10-perylenetetracarboxylic acid bisbenzimidazole) and the cobalt phthalocyanine (Co-Pc) supported on ITO showed a high photoanodic current at 0.2 V under the presence of TEA. This current was not observed in the dark or using an ITO/Co-Pc electrode. Further investigations indicate that the light was exclusively absorbed by the PTCBI, acting as the photosensitizer. At pH 11 (NaOH), the water-splitting took place very efficiently at an applied bias potential of 0.5 V *vs* SHE (η = -0.08 V, 2000 TON in 1 hour).[274]

Later on, a "xanthene-hangman" corrole, $[Co^{III}(bpfxc)]$ (Figure I.37, bpfxc = 5, 15-bis-(pentafluorophenyl)-10-(2,7-di-tert-butyl-5-carboxy-9,9-dimethyl-9H-xanthene-4-yl)corrole) was also found electrochemically active when immobilized in Nafion films, with a TOF close to 0.8 s^{-1} when the potential was setup to 1.6 V vs SHE (pH =7).[275] The authors argued that the hanging moiety assists in the intramolecular proton transfers by preorganizing the water molecule within the system, having a decisive role for water oxidation. The homogeneity of the system was reinforced because the onset was above the expected for CoO_x NPs. The porphyrin complex, $[Co^{II}(TDMImp)(OH_2)]$ ([Co-5,10,15,30-tetrakis-(1,3-dimethylimidazolium-2-yl)porphyrin]) was also found active in electrochemical WO at an onset potential of 1.4 V (vs SHE) in neutral water (0.2M NaPi buffer, pH 7), showing up to of 1400 s^{-1}(Figure I.37).[266] EDTA or ion exchange resins did not affect the catalytic activity, indicating that cobalt oxides are not formed during the reaction. This was supported by dispersive X-ray spectroscopic analysis of the electrode surface. Polipyridylamino Cobalt Complexes

Pyridyl-amino ligands have been widely used as ideal platforms for the oxidation chemistry due to their strong chelation, robustness and high electron-donation. Initially, Berlinguette and coworkers reported complex $[Co^{II}(PY5)(OH_2)](ClO_4)_2$ (Figure I.37), which showed irreversible oxidation at ~1.4 V (at pH 9.2) in aqueous media assigned to the formation of a $[Co^{IV}OH]^{3+}$ species. The complex was stable over the 7.6-10.3 pH range, without leading to film deposition under electrochemical conditions. The reaction rate coefficient (k_{cat}) was found 79s^{-1}, but the contribution of nanoparticles was not completely ruled out.[276] The stability of the complex, the i$_{cat}$-pH-independent behavior and the observation that repeated scans do not lead into electrodeposition seemed in agreement with homogeneous catalysis.[276] pH-dependent studies showed small different trends for the complex and Co^{2+}(aq) ions, suggesting that probably part of the current may arise from a molecular compound. However, diluted Co^{2+} (aq) ions showed similar behavior. Towards a better understanding, kinetics showed first order on cobalt and on [OH$^-$], suggesting that the RDS is the electrophilic attack of a high valent [Co^{IV}-

UNIVERSITAT ROVIRA I VIRGILI
MECHANISTIC STUDIES OF WATER OXIDATION CATALYZED BY HOMOGENEOUS IRON AND RUTHENIUM
COMPLEXES AND LIGHT-DRIVEN ORGANIC REDUCTIONS WITH A DUAL COBALT/COPPER CATALYTIC SYSTEM
Carla Casadevall Serrano

CHAPTER I   GENERAL INTRODUCTION

OH]$^{3+}$ to [OH$^-$], with an observed KIE of 4.7.[277] Likewise, the Ott and Thapper groups have explored the electro- and photocatalytic activity of the related [Co^{II}(PY5OH)(Cl)](BF$_4$) complex, showing a similar WO overpotential with 51 TON in the photocatalytic WO ([Ru(bpy)$_3$]$^{2+}$/Na$_2$S$_2$O$_8$ at pH 8, borate buffer).NPs formation in the pH 7.5-10 range was discarded based on DLS experiments, but not at pH > 10.[278]

Later on, Nam, Fukuzumi, and coworkers reported a clear example were the heterogeneous material was the real catalyst.[279] Under photocatalytic conditions at pH 7-10, complexes [Co^{II}(Me$_6$tren)(OH$_2$)]$^{2+}$, [Co^{III}(Cp*)(bpy)(OH$_2$)]$^{2+}$, [Co^{II}(12-TMC)]$^{2+}$, and [Co^{II}(13-TMC)] $^{2+}$ (Me$_6$tren = tris(N,N'-dimethylaminoethyl)amine, Cp* = η^5-pentamethylcyclopentadientyl, 12-TMC = 1,4,7,10-tetramethyl-1,4,7,10-tetraazacyclododecane, 13-TMC = 1,4,7,10-tetramethyl-1,4,7,10-tetraazacyclotriecane) were found active WOCs. However, after 3 min of irradiation, DLS and TEM showed the formation of different sized NPs (20-200 nm, depending on the precatalyst), the surface of each was mainly composed of cobalt hydroxide (XPS). Cobalt hydroxides could be converted to active species containing high-valent cobalt ions during the photocatalytic water oxidation. Therefore CoO$_x$ species was the true catalyst. The different activity observed among the catalysts was explained by TG/DTA (thermogravimetric/differential thermal analysis) measurements, revealing that the presence of different amounts of carbon on the NP surfaces modifies the O$_2$ production.
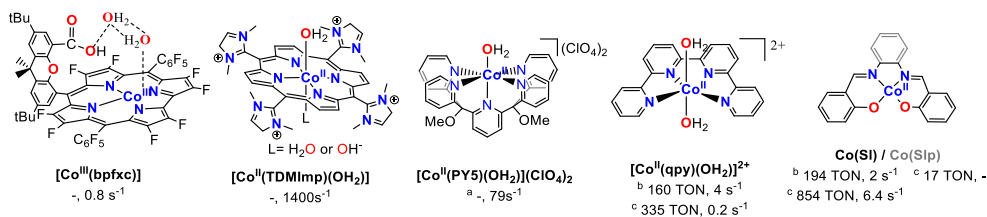
Figure I.37. Summary of corrole, porphyrin, polypyridylamino and polyamine cobalt complexes for WO. TOF reported here were all under electrochemical conditions.

This was not the case for [Co^{II}(qpy)(OH$_2$)$^{2+}$] (Figure I.37), qpy = 2,2':6',2'':6'',2'''-quaterpyridine) which homogeneously catalyzed the light-driven

UNIVERSITAT ROVIRA I VIRGILI
MECHANISTIC STUDIES OF WATER OXIDATION CATALYZED BY HOMOGENEOUS IRON AND RUTHENIUM
COMPLEXES AND LIGHT-DRIVEN ORGANIC REDUCTIONS WITH A DUAL COBALT/COPPER CATALYTIC SYSTEM
Carla Casadevall Serrano

CHAPTER I   GENERAL INTRODUCTION

$[Ru(bpy)_3]^{2+}$ water oxidation (335 TON after 1.5h irradiation at 457nm, pH 8).[280] The entire complex was detected by ESI-MS, and DLS discarded the presence of NPs. The O_2 yield for the thermal WO was 67%, with an initial TOF of $4s^{-1}$.

Salophen-based cobalt complexes (CoSlp, Slp = N,N'-bis(salicylaldehyde)-1,2-phenylenediamine, Figure I.37) were reported as active catalysts for photochemical WO (onset 1.1 V vs SHE, at pH 7.1 NaPi buffer).[281] The low overpotential observed ($\eta_{90b} = 0.3$ V, $\eta_{Co2+} = 0.5\text{-}0.6$ V) strongly supports the homogeneous catalysis. 17 TON and ~10-15% quantum yield were reported, and catalyst stability was confirmed by UV-Vis, DLS, and EPR. Laser flash photolysis studies showed a double ET *per* Co center, pointing towards $Co^{IV}=O$ as the active species. Analogously, the Co(Sl) complex (Figure I.37, Sl = N,N'-Bis(salicylidene)ethylenediaminecobalt (II)) was also found an effective light-driven WOC, yielding 854 TON and TOF of 6.4 s^{-1}, with a quantum yield of 38.6 % (borate buffer, pH 9).[282]

I.5.3.4. Copper water oxidation catalysts

30 years after the earlier work of Elizarova and coworkers about the first evidence for the water oxidation meditated by copper ($CuCl_2$, $Cu(bpy)_2Cl_2$ and $Cu(bpy)_3Cl_2$) in presence of $[Ru(bpy)_3]^{3+}$,[113,273] the first detailed report of WO catalyzed by Cu was described by Mayer and coworkers. Simple $[(bpy)Cu(\mu\text{-}OH)]_2^{2+}$ salts exhibited a large irreversible current at 750mV overpotential at high pHs (pH > 12). The monomeric $[(bpy)Cu(OH)_2]^{2+}$ (Figure I.38) was the dominant species in solution (EPR, CV) and a TOF_{max} of $100s^{-1}$ was observed. Catalyst electrodeposition and NP formation were discarded in favor of a homogeneous process.[283] Furthermore, kinetics showed a first order on copper (see the mechanistic proposal by T.J. Meyer *et al*. in Figure I.38). The 6,6'-OH substituted bipyridyl ligand was later designed to facilitate PCET during catalysis and also to facilitate oxidation of the copper center by electron donation.[284] Effectively, the overpotential was reduced by 200 mV when compared to the unsubstituted system. Catalyst stability was supported by UV-Vis

UNIVERSITAT ROVIRA I VIRGILI
MECHANISTIC STUDIES OF WATER OXIDATION CATALYZED BY HOMOGENEOUS IRON AND RUTHENIUM
COMPLEXES AND LIGHT-DRIVEN ORGANIC REDUCTIONS WITH A DUAL COBALT/COPPER CATALYTIC SYSTEM
Carla Casadevall Serrano

CHAPTER I   GENERAL INTRODUCTION

and NMR (>90% of the ligand was recovered after acidification) and a TON of 400 was reported during a bulk electrolysis at 1.1 V vs SHE (pH 12.4, 0.1M NaOAc/NaOH) in a fritted cell (the counter electrode was separated with a membrane to avoid the reduction of the catalyst), with a TOF of $0.4s^{-1}$.
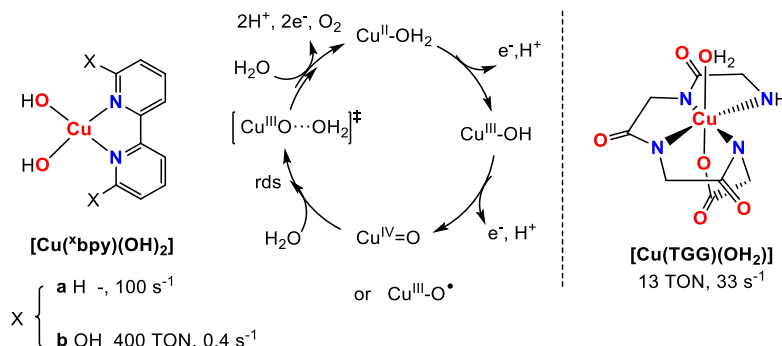
Figure I.38. Schematic representation of the Cu-WOCs, $[(bpy)Cu(\mu\text{-}OH)]_2^{2+}$ (left) and $[(TGG)Cu^{II}\text{-}OH_2]^{2-}$ (right) and the mechanistic proposal for the electrochemical acid-base water oxidation.[285]

An electrocatalytic oxidation wave with an onset at 1.1 V (vs SHE in NaPi electrolyte, pH 11) was also observed for a triglycylglycine Cu^{II} complex $[Cu(TGG)OH_2]^{2-}$ (Figure I.38).[285] The current was almost stable for long-time-electrolysis and no changes were observed due to electrodeposition, or catalyst decomposition, favoring a robust homogeneous system. Kinetics agree with a single site process, being a formal $Cu^{IV}=O$ the active species where the rate-determining O-O bond formation step takes place with a $k_{O\text{-}O}$ of $33s^{-1}$, which corresponds to the TOF of the catalytic reaction.

I.5.3.5. Nickel water oxidation catalysts

Nickel-based complexes have been studied to a very little extend in WO, although the situation is changing since recent discoveries of Ni-based materials as efficient WOCs.[167]

Strong evidence in favor of a single site nickel-based water oxidation catalyst operating in homogeneous phase was first provided for macrocyclic complex **[Ni(meso-L)]$^{2+}$** (Figure I.39).[286] The complex is isolated and crystallographically characterized as a four-coordinate nickel complex with the macrocyclic ligand enforcing a square planar coordination geometry. In water solution, the complex is in equilibrium with the octahedrally coordinated **[Ni(meso-L)(H$_2$O)$_2$)]$^{2+}$,** where the two water molecules occupy the axial positions. In phosphate buffer (but also operates in carbonate and acetate buffers) at neutral pH, **[Ni(meso-L)(H$_2$O)$_2$)](ClO$_4$)$_2$** electrocatalysis the oxidation of water at a relatively low overpotential (Epa = 1.41 V vs NHE) using a GC or an ITO electrode. The cyclic voltammetry of the complex exhibits two oxidation waves; the first one corresponds to oxidation from **[Ni^{II}(meso-L)(H$_2$O)$_2$)]$^{2+}$** to **[Ni^{III}(meso-L)(OH)(H$_2$O))]$^{2+}$** and the second one, that corresponds to the electrocatalytic wave was assigned to oxidation from **[Ni^{III}(meso-L)(OH)(H$_2$O))]$^{2+}$** to **[Ni^{IV}(meso-L)(O)(H$_2$O))]$^{2+}$** or **[Ni^{III}(meso-L)(O·)(H$_2$O))]$^{2+}$,** which is then responsible for the water oxidation reaction, presumably via a Ni(IV)-Ni(II) cycle. Insights into the reaction mechanism were elucidated by DFT methods. Two main points deserve a special consideration; a) Isomerization from a *trans*-(H$_2$O)Ni(O) to a *cis*-Ni(OH)$_2$ is facile (they differ in < 2 Kcal/mol), and b) O-O bond formation occurs via a HO-OH coupling, resulting in a **[Ni^{II}(meso-L)(H$_2$O$_2$)]$^{2+}$** intermediate that is further oxidized to produce O$_2$.
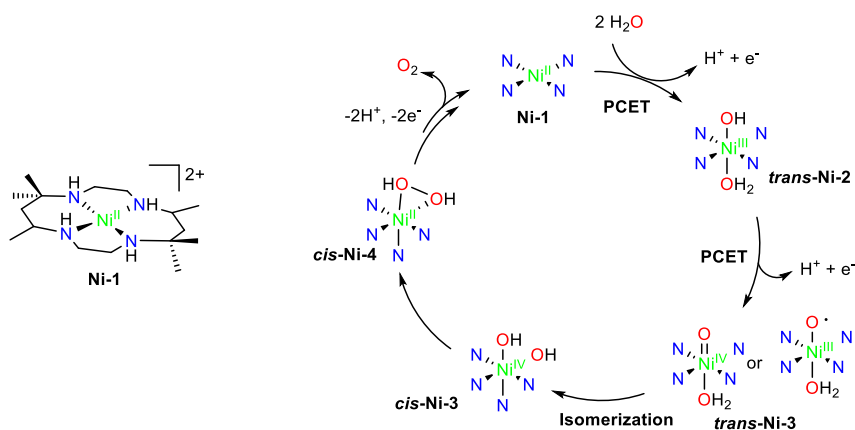
Figure I.39. Mechanism of electrocatalytic water oxidation proposed for **[Ni(meso-L)(H$_2$O)$_2$)](ClO$_4$)$_2$.**

Since the presence of two *cis*-labile sites appears to be a crucial element in the O-O bond formation step, the same authors have studied electrocatalytic water oxidation with nickel complexes **[Ni(mep)(H₂O)₂]²⁺** and **[Ni(mcp)(H₂O)₂]²⁺** (Figure I.40) based in tetradentate aminopyridine ligands.[287,288] Both complexes exhibit electrocatalytic behavior at low overpotential, very much resembling **[Ni(meso-L)(H₂O)₂)](ClO₄)₂**, although they proved somewhat less active.
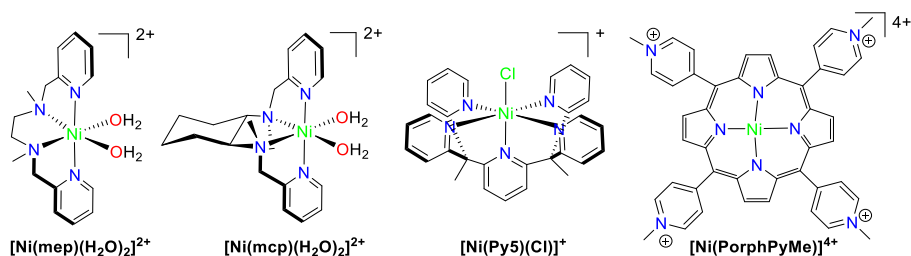
Figure I.40. Ni complexes employed as water oxidation catalysts.

A nickel complex with a pentapyridine ligand **([Ni(Py5)(Cl)]⁺)** has been also described by Sun and co-workers.[289] This compound also acts as an electrocatalyst in phosphate buffer, and in this case, water oxidation is presumed to take place *via* a nucleophilic attack of the water molecule over a high valent Ni^V-oxo species, being the O-O formation assisted by proton transfer to HPO_4^{2-}. Of interest, the reaction rate of this complex is highly enhanced by the proton acceptor base HPO_4^{2-}, reaching remarkably high rates (1820 s⁻¹). Structurally distinct is the Ni-porphyrin complex **[Ni(PorphPyMe)]⁴⁺**,[290] which also acts as WO electrocatalysts, operating in a range of pHs from 2.0 to 8.0, and at low overpotentials (onset at 1.0 V at neural pH). Inspection of the electrode, scanning electron microscope and energy dispersive X-ray spectroscopy (EDX) demonstrate that NiOx is not deposited over the electrode, and suggest a molecular nature of the catalyst. The mechanism of O-O bond formation was investigated by DFT methods, CV and by determining KIE's. The crucial O-O bond formation is proposed to occur via reaction of a Ni(III)-O·species that reacts with a water molecule via an oxygen atom transfer, coupled with a

UNIVERSITAT ROVIRA I VIRGILI
MECHANISTIC STUDIES OF WATER OXIDATION CATALYZED BY HOMOGENEOUS IRON AND RUTHENIUM
COMPLEXES AND LIGHT-DRIVEN ORGANIC REDUCTIONS WITH A DUAL COBALT/COPPER CATALYTIC SYSTEM
Carla Casadevall Serrano

CHAPTER I   GENERAL INTRODUCTION

hydrogen atom transfer from the water molecule to a second water molecule or a base (acetate of phosphate).[290]

I.6. State of the art of catalytic systems for light-driven organic reductions

The production of fine chemicals has less scaling and economic restrictions than the synthesis of energy carriers. The last goal is to apply artificial photosynthesis (AP) for the production of solar fine chemicals, by using water and CO_2 as primary feedstock and sunlight as driving force. In this line, in the last years, the field of photoredox catalysis has emerged as a powerful tool to develop synthetic methodologies to activate and transform organic molecules.[291] In a general view, this approach relies on the ability of metal complexes, semiconductors or organic dyes to engage single-electron transfer processes with organic substrates or to a second catalyst upon excitation by visible-light. Additionally, the capacity of some substrates to generate radicals allows the extension of the photochemical reactivity beyond the substrate reduction, such as dehalogenation,[292,293] olefin isomerization,[294] cross-coupling,[295] radical cyclizations,[296] C-H functionalization,[297] arylations, hydroaminations,[298] amine functionalization,[299] etc…. In addition, photoredox catalysts or semiconductor materials have also been employed to reduce organic substrates by SET. However, the latter is limited to the redox potential of the chromophore. Actually, the use of high-energy light (UV) is often needed, normally decreasing the selectivity of the reactions.[300]

To overcome these drawbacks, the combination of photoredox catalysts with well-defined molecular complexes or biocatalytic systems is a powerful approach towards light-driven reduction of organic molecules.[291,301] These catalytic systems can act as co-catalysts, activated by the reduced excited state of the photosensitizer *via* photoinduced electron transfer processes (PET) and then trigger catalytic reactions with the substrates (Scheme I.12). This strategy presents the following advantages: i) it facilitates the charge separation process in space; ii) reduces the energy barrier of reactants by multistep electron/proton-transfer processes (PCET processes in solution); iii) allows for better control of the selectivity through the

UNIVERSITAT ROVIRA I VIRGILI
MECHANISTIC STUDIES OF WATER OXIDATION CATALYZED BY HOMOGENEOUS IRON AND RUTHENIUM
COMPLEXES AND LIGHT-DRIVEN ORGANIC REDUCTIONS WITH A DUAL COBALT/COPPER CATALYTIC SYSTEM
Carla Casadevall Serrano

CHAPTER I   GENERAL INTRODUCTION

modification of the photosensitizer (lifetime and redox potential) and the active sites of the (bio)catalysts by rational ligand design, and iv) lets to rationally design the reactions according to the activity of the catalyst. Thus, cooperative photoredox catalysis merges the best of both a light-dependent cycle and a light-independent cycle in order to achieve a synergic photochemical system for the organic substrate transformation. Moreover, sustainable methodologies can be envisioned if earth abundant elements are employed for the development of catalytic systems.[291,302] Therefore, using catalytic systems derived from AP to perform selective organic transformations is highly appealing.[303-314]
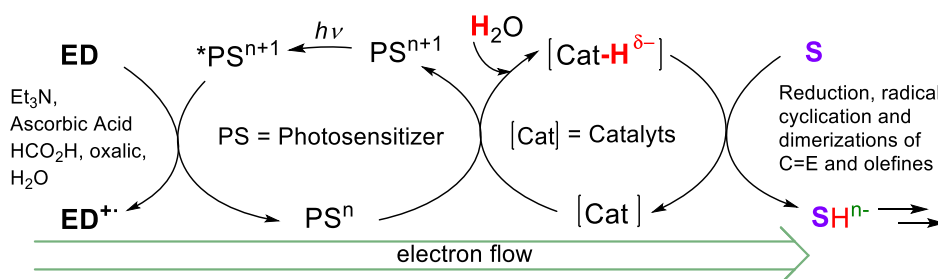
Scheme I.12. General scheme for the light-driven organic reductions via merging photoredox catalysis with TM-catalysis or biocatalysis, represented by [Cat] in the scheme above.

I.6.1. Photocatalytic reduction of ketones and aldehydes

Semiconductor materials, such as TiO_2 or CdS, provide very lower redox potentials promoting direct reduction reactions *via* one or two photoinduced electron transfer processes, but at expense of using UV light, novel metals or/and obtaining low to moderate selectivity.[315-321] The asymmetric reduction of acetophenones and α-ketoglutarate has been achieved coupling i) a sacrificial electron donor, ii) a photosensitizer, iii) a noble-metal-based catalyst, iv) an electron carrier and v) an enzyme that carries out the enantioselective transformation.[303-305,313,322] Results of the latter case show that selective light-driven reduction of organic substrates using water, as a formal dihydrogen source, is a feasible transformation, albeit limited to a

UNIVERSITAT ROVIRA I VIRGILI
MECHANISTIC STUDIES OF WATER OXIDATION CATALYZED BY HOMOGENEOUS IRON AND RUTHENIUM
COMPLEXES AND LIGHT-DRIVEN ORGANIC REDUCTIONS WITH A DUAL COBALT/COPPER CATALYTIC SYSTEM
Carla Casadevall Serrano

CHAPTER I   GENERAL INTRODUCTION

specific substrate.[303-308,313] On the other hand, due to the complexity of these catalytic systems, optimization and mechanistic studies are difficult. For instance, the coupling photoredox catalysis with biocatalysis, Baeg, and co-workers combined the photocatalytic activity of a graphene-porphyrin-based photocatalyst (converted graphene coupled with the organic dye multianthraquinone-substituted porphyrin CCGCMAQSP) with the reductive activity of an alcohol dehydrogenase enzyme (alcohol dehydrogenase from Lactobacillus kefir, LKADH) (Scheme I.13). Upon visible light irradiation ($\lambda = 420$ nm) the dual system was able to reduce acetophenone in 99 % ee.[303] The reaction started with the reductive quenching of visible-light-excited CCGCMAQSP (PS) by TEOA, resulting in the oxidation of TEOA to TEOA$^{.+}$ and the transfer of electrons to the Rh complex *via* SET, which regenerates the NADPH cofactor. Then, the enzyme LKADH consumes the reduced NADPH to perform the chiral reduction of aromatic ketones. Both enzymatic and photoredox catalysis occurs at the buffered aqueous phase, while the chiral alcohol products are formed in the organic one. Although this is a very complicated scheme as is limited to few substrates, it is one of the best schemes to demonstrate the concept of biocatalytic reactions for challenging synthesis fine chemicals.
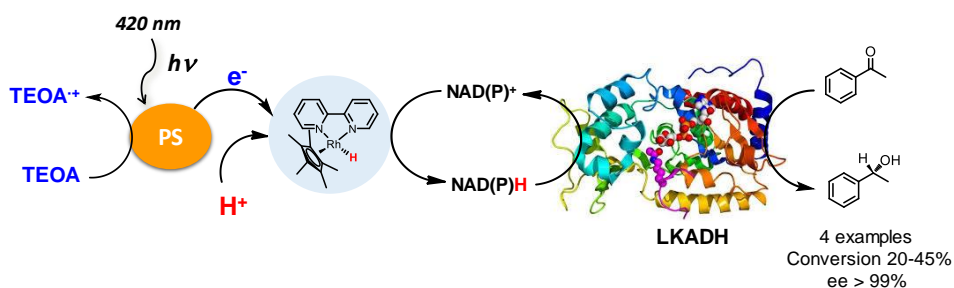
Scheme I.13. Scheme for the light-driven organic reductions via merging photoredox catalysis with TM-catalysis or biocatalysis, represented by [Cat] in the scheme above.

In another example a semiconductor ($W_2Fe_4Ta_2O_{17}$) combined with $[Rh(bpy)(Cp^*)H_2O]^{2+}$ as a hydrogenation catalyst, selectively regenerates the NADH cofactor. Then, NADH is used by the L-glutamate dehydrogenase enzyme for the

conversion of α-ketoglutarate to L-glutamate in the biocatalytic cycle (Scheme I.14).[323] Therefore, as in the previous example, the catalytic cycles couples integrally the work of an inorganic system with an enzyme yielding ultimately the aminoacid. In this case, the electrons are providedd by EDTA which acts as a sacrificial electron donor.
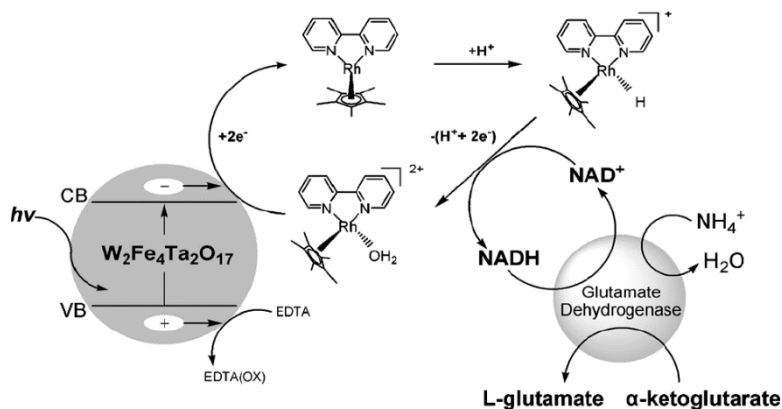
Scheme I.14. Schematic diagram of photochemical cofactor regeneration using an inorganic photosensitizer and their connection with L-glutamate dehydrogenase for the synthesis of L-glutamate from α-ketoglutarate. Reprinted with permission from ref 325. Copyright 2012 John Wiley and Sons.

The introduction of a photoredox catalytic cycle potentially enables the use of water and an electron donor as reductive equivalents, while organometallic or coordination complexes can serve as selective hydrogenation catalysts with a broad scope. In this regard, coordination complexes based on Rh,[314] Ru,[324] and Ir[325] have been explored. A remarkable example is the one reported by König and co-workers for the selective visible light photoreduction ($\lambda = 455$ nm) of aldehydes to alcohols in the presence of ketones. This catalytic system consists of proflavine (PF) as photocatalyst and [Cp*Rh^{III}(bpy)Cl]Cl as a well-known hydrogenation catalyst in the presence of triethanolamine (TEOA) as a sacrificial electron donor.[314] Nevertheless, while aldehydes can be easily reduced using this system, ketones are not suitable substrates (Scheme I.15). Mechanistic studies revealed that the photoreduced PF reacted with the rhodium catalyst leading to the formation of a Rh^{III}-H species, which is the active intermediate for substrate reduction (Scheme I. 10, Top). Moreover, the

UNIVERSITAT ROVIRA I VIRGILI
MECHANISTIC STUDIES OF WATER OXIDATION CATALYZED BY HOMOGENEOUS IRON AND RUTHENIUM
COMPLEXES AND LIGHT-DRIVEN ORGANIC REDUCTIONS WITH A DUAL COBALT/COPPER CATALYTIC SYSTEM
Carla Casadevall Serrano

CHAPTER I   GENERAL INTRODUCTION

photoredox catalytic production of Rh^{III}-H is very slow, which could kinetically distinguish between aldehydes and ketones. However, in the absence of the aldehyde compound, the catalytic system was not able to reduce ketones efficiently neither (acetophenone was reduced only in 7 % yield after 15 hours of irradiation). The authors attributed the latter to the low reactivity of the Rh^{III}-H towards the substrate reduction.
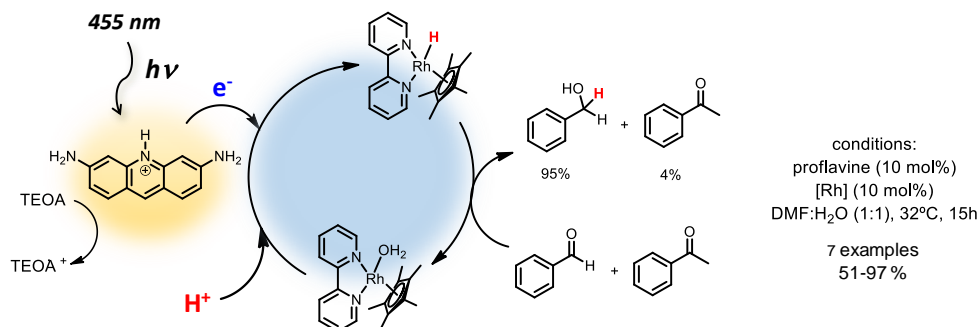
Scheme I.15. Schematic representation of the catalytic system of König and coworkers.

I.6.2. Photocatalytic reduction of alkenes

Semiconductor materials such as TiO_2 and CdS have been used for the light-driven hydrogenation of electron deficient olefins, despite using UV light ($\lambda = 365$ nm), noble metals and obtaining low/moderate selectivity[325-327]

Other examples use Co-B_{12} complex (cyanoaquacobyrinic acid) embedded on the surface of TiO_2 (B_{12}-TiO_2 hybrid) heterogeneous catalyst for the UV light-driven reduction of alkenes to alkanes.[328,329] However, such highly energetic conditions led to the important formation of dimeric products, which harm the selectivity.[330] An example of that is the photocatalytic reduction of olefins reported by Shimakoshi and Hisaeda.[331] They embedded the vitamin B_{12} on the surface of TiO_2 for the construction of a B_{12}-TiO_2 hybrid heterogeneous catalyst (Scheme I.16). During the UV irradiation ($\lambda = 365$ nm), and in the presence of EDTA as electron donor, the

semiconductor material absorbed light facilitating the reduction of the cobalt system to Co^I intermediate. The authors proposed that the latter gets protonated to form Co^{III}-H as the active species. The likely radical character of Co^{III}-H lets to a hydrogen radical attack at the β-position of the alkene, in order to minimize the steric effects imposed by the α-position substituents. However, an important generation of dimeric products derived from the radical coupling between olefins was also observed. For instance, styrene was reduced to ethylbenzene in 10 % yield with 82 % yield of 2,3-diphenylbutane as a dimeric byproduct. The authors also noted that during the irradiation time H_2 was evolved from the solution at 1 $TON \cdot h^{-1}$, and the amount of H_2 was more significant in the absence of olefin, suggesting competing paths between water and olefin reduction promoted by UV light.
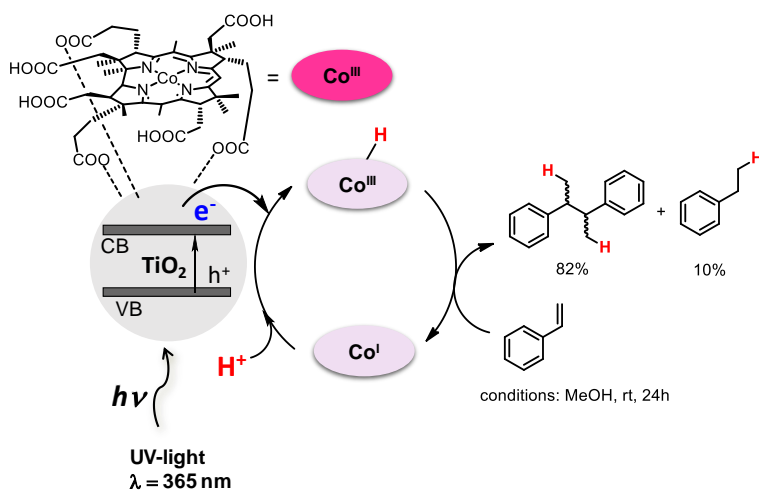
Scheme I.16. Schematic representation of the catalytic system of Hisaeda and coworkers.

A step forward was reported by Holland, Corma and co-workers, who achieved the stereoselective hydrogenation of the conjugated C=C bond of ketoisophorone combining the photocatalytic activity of Au nanoparticles supported on TiO_2 with the enzymatic activity of oxidoreductases by means of FAD^+ as mediator and cofactor (Scheme I.17).[305] Likewise, Hartwig, Zhao and coworkers reported a cooperative chemoenzymatic reaction that combines the isomerization activity of C=C of an

iridium photoredox catalyst with the hydrogenation activity of ene-reductases to selectively reduce electron deficient aromatic olefins to their corresponding alkanes in high enantiomeric excess (88-99 % ee).[331] These results show that selective light-driven reduction of organic substrates using water as hydrogen source is a feasible transformation, albeit very limited in substrate scope.[303-308,313,331]
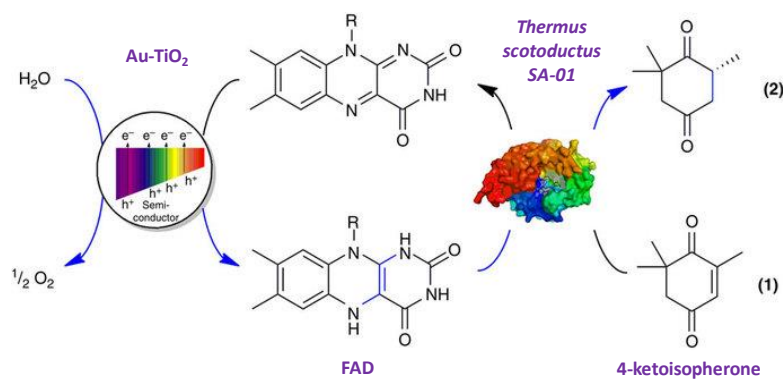
Scheme I.17. Schematic representation of the catalytic system of Corma and coworkers.

I.7. Computational studies of the mechanism involved in WO and light-driven reduction of organic substrates.

Due to the inherent complexity of the metal catalyzed water oxidation and light-driven reduction of organic substrates transformations and the limited information provided by spectroscopic techniques in paramagnetic species characterization, either when high-valent and low-valent metal species are formed, computational modeling of the possible intermediates that are generated under catalytic conditions can provide useful insights into the fundamentals of the mechanism of the transformations. On the other hand, Density Functional Theory (DFT) makes a good balance between the accuracy of the results obtained and the low computational cost makes it very attractive and because of that, it has become the most widely used methodology in computational studies of chemical reactivity.

The approach that DFT gives for solving the Schrödinger equation is based on the Honhenberg and Kohn (HK) theorems, which were formulated in 1964. The first

HK theorem states that the electronic density can fully determine the energy of a non-degenerated electronic ground state.[332] In fact, there exists a one-to-one relationship between the electronic density and the Hamiltonian, therefore not only the energy but also other observable properties of the system can be determined. The second Hohenberg and Kohn (HK) theorem provides the variational principle for the energy and establishes that the energy of the system $E[\rho]$ is a minimum (E_0) when the exact electronic density of the system ρ is considered.

$$E_0 = E_v[\rho] \leq E_v[\rho'] \tag{7}$$

The proof of the second theorem of Hohenberg-Kohn is based on the fact that, as it is proved by the first theorem of Hohenberg-Kohn, ρ' determines $v'(r)$, $\hat{H}'$ and ψ'. ρ' is the approximate one electron density of the chemical system. Therefore, ψ' is an approximate wavefunction of the molecule described by the Hamiltonian $\hat{H}$. And thus, the energy functional applied to any one electron density different from the exact one electron density functional leads to an energy value higher than the exact one.

This theorem (equation 7) is only satisfied if $\rho(r) \geq 0$, and its integral extended to the whole space is equal to the number of electrons of the system. Thus, the total energy of the ground state is a density functional that can be split into the kinetic energy functional $T[\rho]$, the electron-nucleus attraction potential energy functional $V_{Ne}[\rho]$ and the electron-electron interaction potential energy functional $V_{ee}[\rho]$:

$$E_0 = E_v[\rho] = T[\rho] + V_{Ne}[\rho] + V_{ee}[\rho] = F_{HK}[\rho] + V_{Ne}[\rho] \tag{8}$$

Hohenberg and Kohn pooled the functionals that do not depend on the external potential $v(r)$ into the one called Hohenberg-Kohn functional($F_{HK}[\rho]$), which is defined as the sum of the kinetic energy functional and the electron-electron interaction potential energy functional. Therefore, the energy functional of the system can be easily obtained as follows:

$$E[\rho] = F_{HK}[\rho] + V_{Ne} = F_{HK}[\rho] + \int \rho(r)\, v(r)\, dr \tag{9}$$

However, one of the problems of DFT is that the expression of the Hohenberg-Kohn functional $(F_{HK}[\rho])$ is not known, so (equation 9) does not allow us to calculate the energy E from the density ρ. Nevertheless, as $F_{HK}[\rho]$ does not depend on $v(r)$, it has the same form for any chemical system. Then, if the expression for this functional could be found, it would be able to be applied to any chemical system. Hence, one of the most active research lines in the field of the computational chemistry is finding more accurate expressions for $F_{HK}[\rho]$.

Kohn and Sham devised a practical method to calculate ρ and $E[\rho]$[333]. They considered a fictitious reference system of n non-interacting particles moving in a local effective external potential, $v_{eff}(r)$ or $v_s(r)$, called *Kohn-Sham* potential. Then, then exact ground state electronic energy E of a system of n interacting electrons can be written as:

$$E[\rho] = -\frac{\hbar^2}{2m_e}\sum_{i=1}^{n}\int \psi_i^*(r_1)\nabla_1^2\psi_i(r_1)dr_1 - \sum_{I=1}^{N}\int \frac{Z_I e^2}{4\pi\varepsilon_0 r_{I1}}\rho(r_1)dr_1 +$$

$$\frac{1}{2}\int \frac{\rho(r_1)\rho(r_2)e^2}{4\pi\varepsilon_0 r_{12}}dr_1 dr_2 + E_{XC}[\rho] \qquad (10)$$

Where the first term in (equation 10) represents the kinetic electronic energy of the reference system of the non-interacting electrons $(T_s[\rho])$; the second is the electron-nucleus attraction with the sum over all N nuclei with index I and atomic number Z_I the third term is the Coulomb repulsion between the total charge distribution at r_1 and r_2 and the last term is the exchange-correlation energy that takes into account all non-classical interactions between the electrons. E_{XC} can be expressed as:

$$E_{XC}[\rho] = (T[\rho] - T_s[\rho]) + (V_{ee}[\rho] - J[\rho]) \qquad (11)$$

Where $T[\rho]$ is the exact kinetic energy interaction and $J[\rho]$ is the exact electron-electron interaction energy. E_{XC} is the unique term that we cannot calculate exactly, so we have to use approximate forms. The nature of this approximation is the origin of the different DFT functionals. Kohn and Sham developed a very simple method to calculate $T[\rho]$ that leads to quite accurate values for the electronic kinetic

UNIVERSITAT ROVIRA I VIRGILI
MECHANISTIC STUDIES OF WATER OXIDATION CATALYZED BY HOMOGENEOUS IRON AND RUTHENIUM
COMPLEXES AND LIGHT-DRIVEN ORGANIC REDUCTIONS WITH A DUAL COBALT/COPPER CATALYTIC SYSTEM
Carla Casadevall Serrano

CHAPTER I   GENERAL INTRODUCTION

energy. Furthermore, as the reference system is formed by electrons that do not interact with each other, the Hamiltonian of the reference system does not contain an electron-electron potential interaction term. Then, the exact wavefunction can be expressed as the product of the one electron wavefunctions, such as orbitals. In addition, as the electrons are fermions, the exact wavefunction must be antisymmetric. Thus, the Slater determinant is the exact wavefunction of the reference system, and the one-electron spatial orbitals from which the Slater determinant is made of are the *Kohn-Sham* (*KS*) *orbitals* $\chi_i(x_i)$.

$$\psi_s(x_1, x_2, \ldots, x_n) = \frac{1}{\sqrt{n!}} |\chi_1(x_1)\chi_2(x_2)\ldots\chi_n(x_n)| \tag{12}$$

The density $\rho(r)$ of the reference system at given point is given by the sum over all the occupied KS orbitals and it is known once these orbitals have been computed:

$$\rho(r) = \sum_{i=1}^{n} |\psi_i(r)|^2 \tag{13}$$

The KS equations can be derived by applying the variational principle to the electronic energy $E[\rho]$ with the density given by (equation 13) and they have the form:

$$\hat{H}\psi_i(r_1) = \varepsilon_i\psi_i(r_1) \tag{14}$$

$$\left\{-\frac{\hbar^2}{2m_e}\nabla_1^2 + v_{eff}(r_1)\right\}\psi_i(r1) = \varepsilon_i\psi_i(r_1) \tag{15}$$

Where: $$v_{eff}(r1) = \sum_{I=1}^{N}\frac{Z_Ie^2}{4\pi\varepsilon_0 r_{I_1}} + \int\frac{\rho(r_2)e^2}{4\pi\varepsilon_0 r_{12}}dr_2 + V_{XC}(r_1) \tag{16}$$

And ε_i are the KS orbital energies and V_{XC} the exchange-correlation potential, which is a functional derivative of the exchange-correlation energy:

$$V_{XC}[\rho] = \frac{\delta E_{XC}[\rho]}{\delta\rho} \tag{17}$$

If $E_{XC}[\rho]$ is known, then $V_{XC}[\rho]$ can be obtained. Thus, the KS equations are solved in a self-consistent fashion as in the HF method. However, as for the HF

95

spinorbitals energies, the sum of the KS spinorbital energies does not lead to the total electronic energy of the real system.

I.7.1. Advantages of DFT methods

DFT has many advantages over the other computational methods that make it a very useful tool to study the mechanisms involved in several catalytic transformations. The main advantage of DFT is that one has to work with the three-dimensional electron density $\rho(r)$ as the basic variable, instead of the more complicated wavefunction Ψ. Moreover, since the 90s the approximations used in theory were greatly refined to better model the exchange and correlation interactions. The computational cost of DFT is relatively low compared to traditional methods such as HF and post-HF methods. Additionally, DFT determines the geometries, frequencies, activation barriers and dipole moments much more accurately than HF. Moreover, unrestricted DFT spin contamination (mixing of different electronic spin-states) is often lower than in unrestricted HF.

As a general overview, there is a strong agreement between the distances and angles calculated with DFT and experimental methods. In the case of transition metal atoms coordinated to ligands, in the best cases, that is when using hybrid functionals and saturated closed shell complexes, the deviations lie around $\pm\,0.05$ Å for bond distances. With Hartree Fock methods (HF) the deviation increases to $\pm\,0.1$ Å, while the Møller-Plesset perturbation theory 2 (MP2) gives values comparable to those obtained with the best DFT functionals, although it depends on the situation of the electronic system. Therefore, it is not surprising that DFT calculations are used by default in the prediction of molecular structures. Currently, DFT calculations are sufficiently accurate and speedy for applications in the study of reaction mechanisms.[334,335]

I.8. References

(1) Eisenberg, R.; Nocera, D. G. *Inorg. Chem.* **2005**, *44*, 6799.
(2) Lewis, N. S.; Nocera, D. G. *Proc. Natl. Acad. Sci. U. S. A.* **2006**, *103*, 15729.

(3) Conti, J.; Holtberg, P.

(4) Barber, J. *International Journal of Photoenergy* **2004**, *6*, 43.

(5) Ferreira, K. N.; Iverson, T. M.; Maghlaoui, K.; Barber, J.; Iwata, S. *Science* **2004**, *303*, 1831.

(6) Biesiadka, J.; Loll, B.; Kern, J.; Irrgang, K.-D.; Zouni, A. *Phys. Chem. Chem. Phys.* **2004**, *6*, 4733.

(7) Lewis, N. S. *Science* **2016**, *351*, 353.

(8) Liu, Q.; Wu, L.; Jackstell, R.; Beller, M. *Nat. Commun.* **2015**, *6*, 5933.

(9) Centi, G.; Perathoner, S. *Catalysis Today* **2009**, *148*, 191.

(10) Qiao, J.; Liu, Y.; Hong, F.; Zhang, J. *Chem. Soc. Rev.* **2014**, *43*, 631.

(11) Jessop, P. G.; Ikariya, T.; Noyori, R. *Chem. Rev.* **1995**, *95*, 259.

(12) Lee, K. J.; Elgrishi, N.; Kandemir, B.; Dempsey, J. L. *Nature Reviews Chemistry* **2017**, *1*, 0039.

(13) Wasylenko, D. J.; Ganesamoorthy, C.; Henderson, M. A.; Berlinguette, C. P. *Inorg. Chem.* **2011**, *50*, 3662.

(14) Parent, A. R.; Crabtree, R. H.; Brudvig, G. W. *Chem. Soc. Rev.* **2012**, *42*, 2247.

(15) Kärkäs, M. D.; Verho, O.; Johnston, E. V.; Åkermark, B. *Chem. Rev.* **2014**, *114*, 11863.

(16) Duan, L.; Xu, Y.; Zhang, P.; Wang, M.; Sun, L. *Inorg. Chem.* **2010**, *49*, 209.

(17) Singh, W. M.; Baine, T.; Kudo, S.; Tian, S.; Ma, X. A. N.; Zhou, H.; DeYonker, N. J.; Pham, T. C.; Bollinger, J. C.; Baker, D. L.; Yan, B.; Webster, C. E.; Zhao, X. *Angew. Chem. Int. Ed.* **2012**, *51*, 5941.

(18) Gao, Y.; Ding, X.; Liu, J.; Wang, L.; Lu, Z.; Li, L.; Sun, L. *J. Am. Chem. Soc.* **2013**, *135*, 4219.

(19) Andreiadis, E. S.; Chavarot-Kerlidou, M.; Fontecave, M.; Artero, V. *Photochem. Photobiol.* **2011**, *87*, 946.

(20) Duan, L.; Bozoglian, F.; Mandal, S.; Stewart, B.; Privalov, T.; Llobet, A.; Sun, L. *Nat Chem* **2012**, *4*, 418.

(21) Umena, Y.; Kawakami, K.; Shen, J.-R.; Kamiya, N. *Nature* **2011**, *473*, 55.

(22) Pantazis, D. A. *ACS Catal.* **2018**, *8*, 9477.

(23) Cox, N.; Retegan, M.; Neese, F.; Pantazis, D. A.; Boussac, A.; Lubitz, W. *Science* **2014**, *345*, 804.

(24) Cox, N.; Pantazis, D. A.; Neese, F.; Lubitz, W. *Acc. Chem. Res.* **2013**, *46*, 1588.

(25) Betley, T. A.; Surendranath, Y.; Childress, M. V.; Alliger, G. E.; Fu, R.; Cummins, C. C.; Nocera, D. G. *Philosophical Transactions of the Royal Society B: Biological Sciences* **2008**, *363*, 1293.

(26) Nilsson, H.; Rappaport, F.; Boussac, A.; Messinger, J. *Nat Commun* **2014**, *5*, 1.

(27) Gao, Y.; Akermark, T.; Liu, J.; Sun, L.; Akermark, B. *J. Am. Chem. Soc.* **2009**, *131*, 8726.

(28) Hillier, W.; Wydrzynski, T. *Coord. Chem. Rev.* **2008**, *252*, 306.

(29) Hendry, G.; Wydrzynski, T. *Biochemistry* **2003**, *42*, 6209.

(30) Kanady, J. S.; Tsui, E. Y.; Day, M. W.; Agapie, T. *Science* **2011**, *333*, 733.

(31) Ferreira, K. N.; Iverson, T. M.; Maghlaoui, K.; Barber, J.; Iwata, S. *Science* **2004**, *303*, 1831.

(32) Kamiya, N.; Shen, J.-R. *Proc. Natl. Acad. Sci.* **2003**, *100*, 98.

(33) J. Yano; J. Kern; K. Sauer; M. J. Latimer; Y. Pushkar; J. Biesiadka; B. Loll; W. Saenger; J. Messinger; A. Zouni; Yachandra, V. K. *Science* **2006**, *314*, 821.

(34) Sartorel, A.; Bonchio, M.; Campagna, S.; Scandola, F. *Chem. Soc. Rev.* **2013**.

(35) Xiaobo Chen; Shaohua Shen; Liejin Guo; Mao, S. S. *Chem. Rev.* **2010**, *110*, 6503.

(36) Ann Magnuson; Magnus Anderlund; Olof Johansson; Peter Lindblad; Reiner Lomoth; Tomas Polivka; Sascha Ott; Karin Stensjö; Stenbjörn Styring; Villy Sundström; Hammarström, L. *Acc. Chem. Res.* **2009**, *42*, 1899.

(37) Rutherford, A. W.; Osyczka, A.; Rappaport, F. *FEBS Letters* **2012**, *586*, 603.

(38) Aro, E.-M.; Suorsa, M.; Rokka, A.; Allahverdiyeva, Y.; Paakkarinen, V.; Saleem, A.; Battchikova, N.; Rintamäki, E. *J. Exp. Bot.* **2005**, *56*, 347.

(39) Neagu, C.; Jansen, H.; Gardeniers, H.; Elwenspoek, M. *Mechatronics* **2000**, *10*, 571.

(40) Duan, L.; Wang, L.; Li, F.; Li, F.; Sun, L. *Acc. Chem. Res.* **2015**, *48*, 2084.

(41) Wang, L.; Duan, L.; Ambre, R. B.; Daniel, Q.; Chen, H.; Sun, J.; Das, B.; Thapper, A.; Uhlig, J.; Dinér, P.; Sun, L. *J. Catal.* **2016**, *335*, 72.

(42) Kärkäs, M. D.; Åkermark, B. *Dalton Trans.* **2016**, *DOI:10.1039/c6dt00809g*.

(43) Geletii, Y. V.; Botar, B.; Kögerler, P.; Hillesheim, D. A.; Musaev, D. G.; Hill, C. L. *Angew. Chem. Int. Ed.* **2008**, *47*, 3896.

(44) Tong, L.; Duan, L.; Xu, Y.; Privalov, T.; Sun , L. *Angew. Chem. Int. Ed.* **2011**, *50*, 445.

(45) Yagi, M.; Tokita, S.; Nagoshi, K.; Ogino, I.; Kaneko, M. *Faraday Transactions* **1996**, *92*, 2457.

(46) McDaniel, N. D.; Coughlin, F. J.; Tinker, L. L.; Bernhard, S. *J. Am. Chem. Soc.* **2008**, *130*, 210.

(47) Hull, J. F.; Balcells, D.; Blakemore, J. D.; Incarvito, C. D.; Eisenstein, O.; Brudvig, G. W.; Crabtree, R. H. *J. Am. Chem. Soc.* **2009**, *131*, 8730.

UNIVERSITAT ROVIRA I VIRGILI
MECHANISTIC STUDIES OF WATER OXIDATION CATALYZED BY HOMOGENEOUS IRON AND RUTHENIUM
COMPLEXES AND LIGHT-DRIVEN ORGANIC REDUCTIONS WITH A DUAL COBALT/COPPER CATALYTIC SYSTEM
Carla Casadevall Serrano

CHAPTER I   GENERAL INTRODUCTION

(48) Lalrempuia, R.; McDaniel, N. D.; Müller-Bunz, H.; Bernhard, S.; Albrecht, M. *Angew. Chem. Int. Ed.* **2010**, *49*, 9765.

(49) Codolà, Z.; M. S. Cardoso, J.; Royo, B.; Costas, M.; Lloret-Fillol, J. *Chem. Eur. J.* **2013**, *19*, 7203.

(50) Gersten, S. W.; Samuels, G. J.; Meyer, T. J. *J. Am. Chem. Soc.* **1982**, *104*, 4029.

(51) Ishida, H.; Tanaka, K.; Tanaka, T. *Organometallics* **1987**, *6*, 181.

(52) Wada, T.; Tsuge, K.; Tanaka, K. *Inorg. Chem.* **2001**, *40*, 329.

(53) Sens, C.; Romero, I.; Rodríguez, M.; Llobet, A.; Parella, T.; Benet-Buchholz, J. *J. Am. Chem. Soc.* **2004**, *126*, 7798.

(54) Muckerman, J. T.; Polyansky, D. E.; Wada, T.; Tanaka, K.; Fujita, E. *Inorg. Chem.* **2008**, *47*, 1787.

(55) Hurst, J. K. *Coord. Chem. Rev.* **2005**, *249*, 313.

(56) Zong, R.; Thummel, R. P. *J. Am. Chem. Soc.* **2005**, *127*, 12802.

(57) Tseng, H.-W.; Zong, R.; Muckerman, J. T.; Thummel, R. *Inorg. Chem.* **2008**, *47*, 11763.

(58) Concepcion, J. J.; Jurss, J. W.; Templeton, J. L.; Meyer, T. J. *Proc. Natl. Acad. Sci.* **2008**, *105*, 17632.

(59) Concepcion, J. J.; Tsai, M.-K.; Muckerman, J. T.; Meyer, T. J. *J. Am. Chem. Soc.* **2010**, *132*, 1545.

(60) Shigeyuki, M.; Ken, S. *Chemistry Letters* **2009**, *38*, 182.

(61) Gilbert, J. A.; Eggleston, D. S.; Murphy, W. R.; Geselowitz, D. A.; Gersten, S. W.; Hodgson, D. J.; Meyer, T. J. *J. Am. Chem. Soc.* **1985**, *107*, 3855.

(62) Moonshiram, D.; Alperovich, I.; Concepcion, J. J.; Meyer, T. J.; Pushkar, Y. *Proc. Natl. Acad. Sci.* **2013**, *110*, 3765.

(63) Rotzinger, F. P.; Munavalli, S.; Comte, P.; Hurst, J. K.; Gratzel, M.; Pern, F. J.; Frank, A. J. *J. Am. Chem. Soc.* **1987**, *109*, 6619.

(64) Mola, J.; Mas-Marza, E.; Sala, X.; Romero, I.; Rodríguez, M.; Viñas, C.; Parella, T.; Llobet, A. *Angew. Chem.* **2008**, *120*, 5914.

(65) Bozoglian, F.; Romain, S.; Ertem, M. Z.; Todorova, T. K.; Sens, C.; Mola, J.; Rodríguez, M.; Romero, I.; Benet-Buchholz, J.; Fontrodona, X.; Cramer, C. J.; Gagliardi, L.; Llobet, A. *J. Am. Chem. Soc.* **2009**, *131*, 15176.

(66) Bianco, R.; Hay, P. J.; Hynes, J. T. *J Phys Chem A* **2011**, *115*, 8003.

(67) Bianco, R.; Hay, P. J.; Hynes, J. T. *J Phys Chem B* **2013**, *117*, 15761.

(68) Li, X.; Chen, G.; Schinzel, S.; Siegbahn, P. E. M. *Dalton. Trans.* **2011**, *40*, 11296.

(69) Tsuge, K.; Tanaka, K. *Chemistry Letters* **1998**, *27*, 1069.

(70) Wada, T.; Tsuge, K.; Tanaka, K. *Inorg. Chem.* **2000**, *40*, 329.

(71) Wada, T.; Tsuge, K.; Tanaka, K. *Angew. Chem. Int. Ed.* **2000**, *39*, 1479.

(72) Deng, Z.; Tseng, H.-W.; Zong, R.; Wang, D.; Thummel, R. *Inorg. Chem.* **2008**, *47*, 1835.

(73) Xu, Y.; Åkermark, T. r.; Gyollai, V.; Zou, D.; Eriksson, L.; Duan, L.; Zhang, R.; Åkermark, B. r.; Sun, L. *Inorg. Chem.* **2009**, *48*, 2717.

(74) Xu, Y.; Fischer, A.; Duan, L.; Tong, L.; Gabrielsson, E.; Åkermark, B.; Sun, L. *Angew. Chem. Int. Ed.* **2010**, *49*, 8934.

(75) Xu, Y.; Duan, L.; Tong, L.; Akermark, B.; Sun, L. *Chem. Commun.* **2010**, *46*, 6506.

(76) Maji, S.; Vigara, L.; Cottone, F.; Bozoglian, F.; Benet-Buchholz, J.; Llobet, A. *Angew. Chem. Int. Ed.* **2012**, *51*, 5967.

(77) Neudeck, S.; Maji, S.; López, I.; Meyer, S.; Meyer, F.; Llobet, A. *J. Am. Chem. Soc.* **2013**, *136*, 24.

(78) Savini, A.; Bellachioma, G.; Bolano, S.; Rocchigiani, L.; Zuccaccia, C.; Zuccaccia, D.; Macchioni, A. *ChemSusChem* **2012**, *5*, 1415.

(79) Collin, J. P.; Sauvage, J. P. *Inorg. Chem.* **1986**, *25*, 135.

(80) Kamdar, J. M.; Grotjahn, D. B. *Molecules* **2019**, *24*, 494.

(81) Masaoka, S.; Sakai, K. *Chemistry Letters* **2009**, *38*, 182.

(82) Wasylenko, D. J.; Ganesamoorthy, C.; Koivisto, B. D.; Henderson, M. A.; Berlinguette, C. P. *Inorg. Chem.* **2010**, *49*, 2202.

(83) Concepcion, J. J.; Jurss, J. W.; Templeton, J. L.; Meyer, T. J. *J. Am. Chem. Soc.* **2008**, *130*, 16462.

(84) Concepcion, J. J.; Jurss, J. W.; Norris, M. R.; Chen, Z.; Templeton, J. L.; Meyer, T. J. *Inorg. Chem.* **2010**, *49*, 1277.

(85) Wasylenko, D. J.; Ganesamoorthy, C.; Henderson, M. A.; Koivisto, B. D.; Osthoff, H. D.; Berlinguette, C. P. *J. Am. Chem. Soc.* **2010**, *132*, 16094.

(86) Yagi, M.; Tajima, S.; Komi, M.; Yamazaki, H. *Dalton. Trans.* **2011**, *40*, 3802.

(87) Tseng, H.-W.; Zong, R.; Muckerman, J. T.; Thummel, R. *Inorg. Chem.* **2008**, *47*, 11763.

(88) Yoshida, M.; Masaoka, S.; Sakai, K. *Chemistry Letters* **2009**, *38*, 702.

(89) Kaveevivitchai, N.; Zong, R.; Tseng, H.-W.; Chitta, R.; Thummel, R. P. *Inorg. Chem.* **2012**, *51*, 2930.

(90) Concepción, J.; Loeb, B.; Simón-Manso, Y.; Zuloaga*, F. *Polyhedron* **2000**, *19*, 2297.

(91) Coe, B. J.; Meyer, T. J.; White, P. S. *Inorg. Chem.* **1993**, *32*, 4012.

(92) Walsh, J. L.; Durham, B. *Inorg. Chem.* **1982**, *21*, 329.

(93) Durham, B.; Wilson, S. R.; Hodgson, D. J.; Meyer, T. J. *J. Am. Chem. Soc.* **1980**, *102*, 600.

(94) Chan, C.-W.; Lai, T.-F.; Che, C.-M. *Journal of the Chemical Society, Dalton Transactions* **1994**, 895.

(95) Zong, R.; Thummel, R. P. *J. Am. Chem. Soc.* **2004**, *126*, 10800.

(96) Duan, L.; Xu, Y.; Zhang, P.; Wang, M.; Sun, L. *Inorg. Chem.* **2009**, *49*, 209.

(97) Duan, L.; Fischer, A.; Xu, Y.; Sun, L. *J. Am. Chem. Soc.* **2009**, *131*, 10397.

(98) Duan, L.; Araujo, C. M.; Ahlquist, M. S. G.; Sun, L. *Proc. Natl. Acad. Sci.* **2012**, *109*, 15584.

(99) Wang, L.; Duan, L.; Stewart, B.; Pu, M.; Liu, J.; Privalov, T.; Sun, L. *J. Am. Chem. Soc.* **2012**, *134*, 18868.

(100) Duan, L.; Xu, Y.; Tong, L.; Sun, L. *ChemSusChem* **2011**, *4*, 238.

(101) Nyhlén, J.; Duan, L.; Åkermark, B.; Sun, L.; Privalov, T. *Angew. Chem.* **2010**, *122*, 1817.

(102) Planas, N.; Vigara, L.; Cady, C.; Miró, P.; Huang, P.; Hammarström, L.; Styring, S.; Leidel, N.; Dau, H.; Haumann, M.; Gagliardi, L.; Cramer, C. J.; Llobet, A. *Inorg. Chem.* **2011**, *50*, 11134.

(103) Pineda-Galvan, Y.; Ravari, A. K.; Shmakov, S.; Lifshits, L.; Kaveevivitchai, N.; Thummel, R.; Pushkar, Y. *J. Catal.* **2019**, *375*, 1.

(104) Lebedev, D.; Pineda-Galvan, Y.; Tokimaru, Y.; Fedorov, A.; Kaeffer, N.; Copéret, C.; Pushkar, Y. *J. Am. Chem. Soc.* **2018**, *140*, 451.

(105) Duan, L.; Wang, L.; Inge, A. K.; Fischer, A.; Zou, X.; Sun, L. *Inorg. Chem.* **2013**, *52*, 7844.

(106) Jiang, Y.; Li, F.; Zhang, B.; Li, X.; Wang, X.; Huang, F.; Sun, L. *Angew. Chem. Int. Ed.* **2013**, *52*, 3398.

(107) Concepcion, J. J.; Jurss, J. W.; Norris, M. R.; Chen, Z.; Templeton, J. L.; Meyer, T. J. *Inorg. Chem.* **2009**, *49*, 1277.

(108) Blakemore, J. D.; Crabtree, R. H.; Brudvig, G. W. *Chem. Rev.* **2015**, *115*, 12974.

(109) Kiwi, J.; Grätzel, M. *Angew. Chem. Int. Ed.* **1978**, *17*, 860.

(110) Kiwi, J.; Grätzel, M. *Angew. Chem. Int. Ed.* **1979**, *18*, 624.

(111) Mills, A. *Journal of the Chemical Society, Dalton Transactions* **1982**, 1213.

(112) Kiwi, J.; Gratzel, M.; Blondeel, G. *Journal of the Chemical Society, Dalton Transactions* **1983**, 2215.

(113) Elizarova, G. L.; Matvienko, L. G.; Lozhkina, N. V.; Parmon, V. N.; Zamaraev, K. I. *React Kinet Catal Lett* **1981**, *16*, 191.

(114) Kiwi, J.; Grätzel, M. *Angew. Chem.* **1979**, *91*, 659.

(115) Lehn, J. M.; Sauvage, J. P.; Ziessel, R. *Nouv. J. Chim.* **1979**, *3*, 423.

(116) Youngblood, W. J.; Lee, S.-H. A.; Maeda, K.; Mallouk, T. E. *Acc. Chem. Res.* **2009**, *42*, 1966.

(117) Yang, K. R.; Matula, A. J.; Kwon, G.; Hong, J.; Sheehan, S. W.; Thomsen, J. M.; Brudvig, G. W.; Crabtree, R. H.; Tiede, D. M.; Chen, L. X.; Batista, V. S. *J. Am. Chem. Soc.* **2016**, *138*, 5511.

(118) Thomsen, J. M.; Huang, D. L.; Crabtree, R. H.; Brudvig, G. W. *Dalton. Trans.* **2015**, *44*, 12452.

(119) Macchioni, A. *Eur. J. Inorg. Chem.* **2019**, *2019*, 7.

(120) Junge, H.; Marquet, N.; Kammer, A.; Denurra, S.; Bauer, M.; Wohlrab, S.; Gärtner, F.; Pohl, M. M.; Spannenberg, A.; Gladiali, S.; Beller, M. *Chem.—Eur. J.* **2012**, *18*, 12749.

(121) Li, M.; Takada, K.; Goldsmith, J. I.; Bernhard, S. *Inorg. Chem.* **2016**, *55*, 518.

(122) Dzik, W. I.; Calvo, S. E.; Reek, J. N. H.; Lutz, M.; Ciriano, M. A.; Tejel, C.; Hetterscheid, D. G. H.; de Bruin, B. *Organometallics* **2011**, *30*, 372.

(123) Bucci, A.; Savini, A.; Rocchigiani, L.; Zuccaccia, C.; Rizzato, S.; Albinati, A.; Llobet, A.; Macchioni, A. *Organometallics* **2012**, *31*, 8071.

(124) Hull, J. F.; Balcells, D.; Blakemore, J. D.; Incarvito, C. D.; Eisenstein, O.; Brudvig, G. W.; Crabtree, R. H. *J. Am. Chem. Soc.* **2009**, *131*, 8730.

(125) Blakemore, J. D.; Schley, N. D.; Balcells, D.; Hull, J. F.; Olack, G. W.; Incarvito, C. D.; Eisenstein, O.; Brudvig, G. W.; Crabtree, R. H. *J. Am. Chem. Soc.* **2010**, *132*, 16017.

(126) Savini, A.; Bellachioma, G.; Ciancaleoni, G.; Zuccaccia, C.; Zuccaccia, D.; Macchioni, A. *Chem. Commun.* **2010**, *46*, 9218.

(127) Corbucci, I.; Macchioni, A.; Albrecht, M.

(128) Petronilho, A.; Rahman, M.; Woods, J. A.; Al-Sayyed, H.; Müller-Bunz, H.; MacElroy, J. M. D.; Bernhard, S.; Albrecht, M. *Dalton Trans.* **2012**, *41*, 13074.

(129) Brewster, T. P.; Blakemore, J. D.; Schley, N. D.; Incarvito, C. D.; Hazari, N.; Brudvig, G. W.; Crabtree, R. H. *Organometallics* **2011**, *30*, 965.

(130) Savini, A.; Belanzoni, P.; Bellachioma, G.; Zuccaccia, C.; Zuccaccia, D.; Macchioni, A. *Green Chem.* **2011**, *13*, 3360.

(131) Grotjahn, D. B.; Brown, D. B.; Martin, J. K.; Marelius, D. C.; Abadjian, M. C.; Tran, H. N.; Kalyuzhny, G.; Vecchio, K. S.; Specht, Z. G.; Cortes-Llamas, S. A.; Miranda-Soto, V.; van Niekerk, C.; Moore, C. E.; Rheingold, A. L. *J. Am. Chem. Soc.* **2011**, *133*, 19024.

(132) Zuccaccia, C.; Bellachioma, G.; Bortolini, O.; Bucci, A.; Savini, A.; Macchioni, A. *Chem. Eur. J.* **2014**, *20*, 3446.

(133) Zuccaccia, C.; Bellachioma, G.; Bolaño, S.; Rocchigiani, L.; Savini, A.; Macchioni, A. *Eur. J. Inorg. Chem.* **2012**, 1462.

(134) Hetterscheid, D. G. H.; Reek, J. N. H. *Chem. Commun.* **2011**, *47*, 2712.

(135) Savini, A.; Belanzoni, P.; Bellachioma, G.; Zuccaccia, C.; Zuccaccia, D.; Macchioni, A. *Green Chemistry* **2011**, *13*, 3360.

(136) Zuccaccia, C.; Bellachioma, G.; Bortolini, O.; Bucci, A.; Savini, A.; Macchioni, A. *Chem. Eur. J.* **2014**, n/a.

(137) Wang, C.; Wang, J. L.; Lin, W. *J. Am. Chem. Soc.* **2012**, *134*, 19895.

(138) Hong, D.; Murakami, M.; Yamada, Y.; Fukuzumi, S. *Energy Environ. Sci.* **2012**, *5*, 5708.

(139) Lewandowska-Andralojc, A.; Polyansky, D. E.; Wang, C. H.; Wang, W. H.; Himeda, Y.; Fujita, E. *Phys. Chem. Chem. Phys.* **2014**, *16*, 11976.

(140) DePasquale, J.; Nieto, I.; Reuther, L. E.; Herbst-Gervasoni, C. J.; Paul, J. J.; Mochalin, V.; Zeller, M.; Thomas, C. M.; Addison, A. W.; Papish, E. T. *Inorg. Chem.* **2013**, *52*, 9175.

(141) Nahor, C. S.; Hapiot, P.; Neta, P.; Harriman, A. *J. Phys. Chem.* **1991**, *95*, 616.

(142) Huang, D. L.; Beltrán-Suito, R.; Thomsen, J. M.; Hashmi, S. M.; Materna, K. L.; Sheehan, S. W.; Mercado, B. Q.; Brudvig, G. W.; Crabtree, R. H. *Inorg. Chem.* **2016**, *55*, 2427.

(143) Hintermair, U.; Hashmi, S. A.; Elimelech, M.; Crabtree, R. H. *J. Am. Chem. Soc.* **2012**, *134*, 9785.

(144) Zhang, T.; deKrafft, K. E.; Wang, J. L.; Wang, C.; Lin, W. B. *Eur. J. Inorg. Chem.* **2014**, 698.

(145) Zoel Codolà, J. M. C., Beatriz Royo, Miquel Costas, Julio Lloret-Fillol *Chem. Eur. J.* **2013**, *19*, 7203.

(146) Ruettinger, W.; Yagi, M.; Wolf, K.; Bernasek, S.; Dismukes, G. C. *J. Am. Chem. Soc.* **2000**, *122*, 10353.

(147) Carrell, T. G.; Bourles, E.; Lin, M.; Dismukes, G. C. *Inorg. Chem.* **2003**, *42*, 2849.

(148) Ruettinger, W.; Dismukes, G. C. *Inorg. Chem.* **2000**, *39*, 1021.

(149) Yagi, M.; Wolf, K. V.; Baesjou, P. J.; Bernasek, S. L.; Dismukes, G. C. *Angew. Chem. Int. Ed.* **2001**, *40*, 2925.

(150) Brimblecombe, R.; Swiegers, G. F.; Dismukes, G. C.; Spiccia, L. *Angew. Chem. Int. Ed.* **2008**, *47*, 7335.

(151) Hocking, R. K.; Brimblecombe, R.; Chang, L.-Y.; Singh, A.; Cheah, M. H.; Glover, C.; Casey, W. H.; Spiccia, L. *Nat Chem* **2011**, *3*, 461.

(152) Takashima, T.; Hashimoto, K.; Nakamura, R. *J. Am. Chem. Soc.* **2011**, *134*, 1519.

(153) Mishra, A.; Wernsdorfer, W.; Abboud, K. A.; Christou, G. *Chem. Commun.* **2005**, *0*, 54.

(154) Mishra, A.; Yano, J.; Pushkar, Y.; Yachandra, V. K.; Abboud, K. A.; Christou, G. *Chem. Commun.* **2007**, *0*, 1538.

(155) Kanady, J. S.; Tsui, E. Y.; Day, M. W.; Agapie, T. *Science* **2011**, *333*, 733.

(156) Kanady, J. S.; Mendoza-Cortes, J. L.; Tsui, E. Y.; Nielsen, R. J.; Goddard, W. A.; Agapie, T. *J. Am. Chem. Soc.* **2012**, *135*, 1073.

(157) Tsui, E. Y.; Tran, R.; Yano, J.; Agapie, T. *Nat Chem* **2013**, *5*, 293.

(158) Siegbahn, P. E. M. *Phys. Chem. Chem. Phys.* **2014**.

(159) Brudvig, G. W. *Philosophical Transactions of the Royal Society B: Biological Sciences* **2008**, *363*, 1211.

(160) Karkas, M. D.; Akermark, B. *Dalton. Trans.* **2016**, *45*, 14421.

(161) Limburg, J.; Brudvig, G. W.; Crabtree, R. H. *J. Am. Chem. Soc.* **1997**, *119*, 2761.

(162) Limburg, J.; Vrettos, J. S.; Liable-Sands, L. M.; Rheingold, A. L.; Crabtree, R. H.; Brudvig, G. W. *Science* **1999**, *283*, 1524.

(163) Limburg, J.; Vrettos, J. S.; Chen, H.; de Paula, J. C.; Crabtree, R. H.; Brudvig, G. W. *J. Am. Chem. Soc.* **2000**, *123*, 423.

(164) Tagore, R.; Crabtree, R. H.; Brudvig, G. W. *Inorg. Chem.* **2008**, *47*, 1815.

(165) Yagi, M.; Narita, K. *J. Am. Chem. Soc.* **2004**, *126*, 8084.

(166) Narita, K.; Kuwabara, T.; Sone, K.; Shimizu, K.-i.; Yagi, M. *J Phys Chem B* **2006**, *110*, 23107.

(167) Lloret-Fillol, J.; Costas, M. In *Adv. Organomet. Chem.*; Academic Press: 2019.

(168) Naruta, Y.; Sasayama, M.; Sasaki, T. *Angew. Chem. Int. Ed.* **1994**, *33*, 1839.

(169) Groves, J. T.; Lee, J.; Marla, S. S. *J. Am. Chem. Soc.* **1997**, *119*, 6269.

(170) Shimazaki, Y.; Nagano, T.; Takesue, H.; Ye, B.-H.; Tani, F.; Naruta, Y. *Angew. Chem. Int. Ed.* **2004**, *43*, 98.

(171) Karlsson, E. A.; Lee, B.-L.; Åkermark, T.; Johnston, E. V.; Kärkäs, M. D.; Sun, J.; Hansson, Ö.; Bäckvall, J.-E.; Åkermark, B. *Angew. Chem.* **2011**, *123*, 11919.

(172) Fabbri, E.; Schmidt, T. J. *ACS Catal.* **2018**, *8*, 9765.

(173) Rana, M.; Mondal, S.; Sahoo, L.; Chatterjee, K.; Karthik, P. E.; Gautam, U. K. *ACS Appl. Mater. Interfaces* **2018**, *10*, 33737.

(174) Song, F.; Bai, L.; Moysiadou, A.; Lee, S.; Hu, C.; Liardet, L.; Hu, X. *J. Am. Chem. Soc.* **2018**, *140*, 7748.

(175) Suen, N.-T.; Hung, S.-F.; Quan, Q.; Zhang, N.; Xu, Y.-J.; Chen, H. M. *Chem. Soc. Rev.* **2017**, *46*, 337.

(176) Company, A.; Feng, Y.; Güell, M.; Ribas, X.; Luis, J. M.; Que Jr, L.; Costas, M. *Chem. Eur. J.* **2009**, *15*, 3359.

(177) Company, A.; Gómez, L.; Güell, M.; Ribas, X.; Luis, J. M.; Que, L.; Costas, M. *J. Am. Chem. Soc.* **2007**, *129*, 15766.

(178) Garcia-Bosch, I.; Codolà, Z.; Prat, I.; Ribas, X.; Lloret-Fillol, J.; Costas, M. *Chem. Eur. J.* **2012**, *18*, 13269.

(179) Serrano-Plana, J.; Acuña-Parés, F.; Dantignana, V.; Oloo, W. N.; Castillo, E.; Draksharapu, A.; Whiteoak, C. J.; Martin-Diaconescu, V.; Basallote, M. G.; Luis, J. M.; Que Jr, L.; Costas, M.; Company, A. *Chem. Eur. J.* **2018**, *24*, 5331.

(180) Milan, M.; Salamone, M.; Costas, M.; Bietti, M. *Acc. Chem. Res.* **2018**, *51*, 1984.

(181) Dantignana, V.; Milan, M.; Cussó, O.; Company, A.; Bietti, M.; Costas, M. *ACS Central Science* **2017**, *3*, 1350.

(182) Sinha, S.; Das, S.; Sikari, R.; Parua, S.; Brandaõ, P.; Demeshko, S.; Meyer, F.; Paul, N. D. *Inorg. Chem.* **2017**, *56*, 14084.

(183) Olivo, G.; Giosia, S.; Barbieri, A.; Lanzalunga, O.; Di Stefano, S. *Organic & Biomolecular Chemistry* **2016**, *14*, 10630.

(184) Bae, J. M.; Lee, M. M.; Lee, S. A.; Lee, S. Y.; Bok, K. H.; Kim, J.; Kim, C. *Inorg. Chim. Acta* **2016**, *451*, 8.

(185) Chàvez, J. E.; Crotti, C.; Zangrando, E.; Farnetti, E. *Journal of Molecular Catalysis A: Chemical* **2016**, *421*, 189.

(186) Strieker, M.; Nolan, E. M.; Walsh, C. T.; Marahiel, M. A. *J. Am. Chem. Soc.* **2009**, *131*, 13523.

(187) Hudlicky, T.; Reed, J. W. *Synlett* **2009**, 685.

(188) Boyd, D. R.; Sharma, N. D.; Allen, C. C. R. *Current Opinion in Biotechnology* **2001**, *12*, 564.

(189) Gibson, D. T.; Parales, R. E. *Current Opinion in Biotechnology* **2000**, *11*, 236.

(190) Elizarova, G. L.; Matvienko, L. G.; Lozhkina, N. V.; Maizlish, V. E.; Parmon, V. N. *React. Kinet. Catal. Lett.* **1981**, *16*, 285.

(191) Abe, T.; Shiroishi, H.; Kinoshita, K.; Kaneko, M. *Macromolecular Symposium* **1998**.

(192) Chowdhury, R.; Hardy, A.; Schofield, C. J. *Chem. Soc. Rev.* **2008**, *37*, 1308.

(193) Bruijnincx, P. C. A.; Koten, G. v.; Gebbink, R. J. M. K. *Chem. Soc. Rev.* **2008**, *12*, 2716.

(194) Bugg, T. D. H.; Ramaswamy, S. *Curr. Op. Chem. Biol.* **2008**, *12*, 134.

(195) Kovaleva, E. G.; Lipscomb, J. D. *Nature Chemical Biology* **2008**, *4*, 186.

(196) Krebs, C.; Galonić Fujimori, D.; Walsh, C. T.; Bollinger, J. M. *Acc. Chem. Res.* **2007**, *40*, 484.

(197) Vaillancourt, F. H.; Yeh, E.; Vosburg, D. A.; Garneau-Tsodikova, S.; Walsh, C. T. *Chem. Rev.* **2006**, *106*, 3364.

(198) Kryatov, S. V.; Rybak-Akimova, E. V.; Schindler, S. *Chem. Rev.* **2005**, *105*, 2175.

(199) Costas, M.; Mehn, M. P.; Jensen, M. P.; Que, L., Jr. *Chem. Rev.* **2004**, *104*, 939.

(200) Oliw, E. H.; Jerneren, F.; Hoffmann, I.; Sahlin, M.; Garscha, U. *Biochimica Et Biophysica Acta-Molecular and Cell Biology of Lipids* **2011**, *1811*, 138.

(201) Oliw, E. H.; Cristea, M.; Hamberg, M. *Lipids* **2004**, *39*, 319.

(202) Company, A.; Lloret, J.; Gómez, L.; Costas, M. In *Alkane C-H Activation by Single-Site Metal Catalysis*; Pérez, P. J., Ed.; Springer Netherlands: Dordrecht, 2012, p 143.

(203) Codola, Z.; Lloret-Fillol, J.; Costas, M. In *In Progress in Inorganic Chemistry* 2014; Vol. 59.

(204) Armstrong, F. A. *PHILOSOPHICAL TRANSACTIONS OF THE ROYAL SOCIETY B: BIOLOGICAL SCIENCES* **2008**, *363*, 7.

(205) Kepp, K. P. *Inorg. Chem.* **2016**, *55*, 9461.

(206) Han, L.; Dong, S.; Wang, E. *Adv. Mater.* **2016**, *28*, 9266.

(207) Liu, T.; Zhang, B.; Sun, L. *Chem.—Asian J.* **2019**, *14*, 31.

(208) Fukuzumi, S.; Jung, J.; Yamada, Y.; Kojima, T.; Nam, W. *Chem.—Asian J.* **2016**, *11*, 1138.

(209) Blakemore, J. D.; Crabtree, R. H.; Brudvig, G. W. *Chem. Rev.* **2015**, *115*, 12974.

(210) Ellis, W. C.; McDaniel, N. D.; Bernhard, S.; Collins, T. J. *J. Am. Chem. Soc.* **2010**, *132*, 10990.

(211) Fillol, J. L.; Codola, Z.; Garcia-Bosch, I.; Gomez, L.; Pla, J. J.; Costas, M. *Nat. Chem.* **2011**, *3*, 807.

(212) Okamura, M.; Kondo, M.; Kuga, R.; Kurashige, Y.; Yanai, T.; Hayami, S.; Praneeth, V. K.; Yoshida, M.; Yoneda, K.; Kawata, S.; Masaoka, S. *Nature* **2016**, *530*, 465.

(213) Company, A.; Lloret-Fillol, J.; Costas, M. In *Comprehensive Inorganic Chemistry II (Second Edition)*; Reedijk, J., Poeppelmeier, K., Eds.; Elsevier: Amsterdam, 2013, p 487.

(214) Que Jr, L.; Tolman, W. B. *Nature* **2008**, *455*, 333.

(215) Collins, T. J. *Acc. Chem. Res.* **2002**, *35*, 782.

(216) Ghosh, A.; de Oliveira, F. T.; Yano, T.; Nishioka, T.; Beach, E. S.; Kinoshita, I.; Münck, E.; Ryabov, A. D.; Horwitz, C. P.; Collins, T. J. *J. Am. Chem. Soc.* **2005**, *127*, 2505.

(217) Oliveira, F. T. d.; Chanda, A.; Banerjee, D.; Shan, X.; Mondal, S.; Lawrence Que, J.; Bominaar, E. L.; Münck, E.; Collins, T. J. *Science* **2007**, *315*, 835.

(218) Chanda, A.; Shan, X.; Chakrabarti, M.; Ellis, W. C.; Popescu, D. L.; de Oliveira, F. T.; Wang, D.; Que, L.; Collins, T. J.; Münck, E.; Bominaar, E. L. *Inorg. Chem.* **2008**, *47*, 3669.

(219) Collins, T. J.; Ryabov, A. D. *Chem. Rev.* **2017**, *117*, 9140.

(220) Mills, M. R.; Shen, L. Q.; Zhang, D. Z.; Ryabov, A. D.; Collins, T. J. *Inorg. Chem.* **2017**, *56*, 10226.

(221) Demeter, E. L.; Hilburg, S. L.; Washburn, N. R.; Collins, T. J.; Kitchin, J. R. *J. Am. Chem. Soc.* **2014**, *136*, 5603.

(222) Liao, R.-Z.; Li, X.-C.; Siegbahn, P. E. M. *Eur. J. Inorg. Chem.* **2014**, *2014*, 728.

(223) Ertem, M. Z.; Gagliardi, L.; Cramer, C. J. *Chemical Science* **2012**, *3*, 1293.

(224) Panda, C.; Debgupta, J.; Díaz Díaz, D.; Singh, K. K.; Sen Gupta, S.; Dhar, B. B. *J. Am. Chem. Soc.* **2014**, *136*, 12273.

(225) Das, D.; Pattanayak, S.; Singh, K. K.; Garai, B.; Sen Gupta, S. *Chem Commun (Camb)* **2016**, *52*, 11787.

(226) Pattanayak, S.; Chowdhury, D. R.; Garai, B.; Singh, K. K.; Paul, A.; Dhar, B. B.; Gupta, S. S. *Chem. Eur. J.* **2017**, *23*, 3414.

(227) Singh, K. K.; Tiwari, M. K.; Dhar, B. B.; Vanka, K.; Sen Gupta, S. *Inorg. Chem.* **2015**, *54*, 6112.

(228) Comba, P. In *Molecular Catalysts* 2014.

(229) Costas, M.; Mehn, M. P.; Jensen, M. P.; Que, L. *Chem. Rev.* **2004**, *104*, 939.

(230) Lyakin, O. Y.; Bryliakov, K. P.; Talsi, E. P. *Coord. Chem. Rev.* **2019**, *384*, 126.

(231) Olivo, G.; Lanzalunga, O.; Di Stefano, S. *Adv. Synth. Catal.* **2016**, *358*, 843.

(232) Que, L., Jr. *Bulletin of Japan Society of Coordination Chemistry* **2013**, *62*, 30.

(233) Solomon, E. I.; Brunold, T. C.; Davis, M. I.; Kemsley, J. N.; Lee, S.-K.; Lehnert, N.; Neese, F.; Skulan, A. J.; Yang, Y.-S.; Zhou, J. *Chem. Rev.* **2000**, *100*, 235.

(234) Sono, M.; Roach, M. P.; Coulter, E. D.; Dawson, J. H. *Chem. Rev.* **1996**, *96*, 2841.

(235) Oloo, W. N.; Que, L. *Acc. Chem. Res.* **2015**, *48*, 2612.

(236) Vicens, L.; Costas, M. *Dalton. Trans.* **2018**, *47*, 1755.

(237) McDonald, A. R.; Que, L. *Coord. Chem. Rev.* **2013**, *257*, 414.

(238) Lloret-Fillol, J.; Codolà, Z.; Garcia-Bosch, I.; Gómez, L.; Pla, J. J.; Costas, M. *Nat. Chem,* **2011**, *3*, 807.

(239) Codolà, Z.; Garcia-Bosch, I.; Acuña-Parés, F.; Prat, I.; Luis, J. M.; Costas, M.; Lloret-Fillol, J. *Chem. Eur. J.* **2013**, *19*, 8042.

(240) Codolà, Z.; Gómez, L.; Kleespies, S. T.; Que Jr, L.; Costas, M.; Lloret-Fillol, J. *Nat. Commun.* **2015**, *6*, 5865.

(241) Hoffert, W. A.; Mock, M. T.; Appel, A. M.; Yang, J. Y. *Eur. J. Inorg. Chem.* **2013**, *2013*, 3846.

(242) Detz, R. J.; Abiri, Z.; Kluwer, A. M.; Reek, J. N. H. *ChemSusChem* **2015**, *8*, 3057.

(243) Parent, A. R.; Nakazono, T.; Lin, S.; Utsunomiya, S.; Sakai, K. *Dalton. Trans.* **2014**, *43*, 12501.

(244) To, W.-P.; Wai-Shan Chow, T.; Tse, C.-W.; Guan, X.; Huang, J.-S.; Che, C.-M. *Chemical Science* **2015**, *6*, 5891.

(245) Zhang, B.; Li, F.; Yu, F.; Cui, H.; Zhou, X.; Li, H.; Wang, Y.; Sun, L. *Chem.—Asian J.* **2014**, *9*, 1515.

(246) Wang, D.; Que, L. *Chem. Commun.* **2013**, *49*, 10682.

(247) *Eur. J. Inorg. Chem.* **2018**, *2018*, 3283.

(248) Chen, G.; Chen, L.; Ng, S.-M.; Man, W.-L.; Lau, T.-C. *Angew. Chem. Int. Ed.* **2013**, *52*, 1789.

(249) Hong, D.; Mandal, S.; Yamada, Y.; Lee, Y. M.; Nam, W.; Llobet, A.; Fukuzumi, S. *Inorg. Chem.* **2013**, *52*, 9522.

(250) Horiuchi, Y.; Toyao, T.; Miyahara, K.; Zakary, L.; Van, D. D.; Kamata, Y.; Kim, T.-H.; Lee, S. W.; Matsuoka, M. *Chem. Commun.* **2016**, *52*, 5190.

(251) Yoshida, M.; Masaoka, S.; Abe, J.; Sakai, K. *Chem.—Asian J.* **2010**, *5*, 2369.

(252) Morimoto, Y.; Kotani, H.; Park, J.; Lee, Y.-M.; Nam, W.; Fukuzumi, S. *J. Am. Chem. Soc.* **2011**, *133*, 403.

(253) Fukuzumi, S.; Morimoto, Y.; Kotani, H.; Naumov, P.; Lee, Y.-M.; Nam, W. *Nat. Chem.* **2010**, *2*, 756.

(254) Gao, Y.; Crabtree, R. H.; Brudvig, G. W. *Inorg. Chem.* **2012**, *51*, 4043.

(255) Draksharapu, A.; Rasheed, W.; Klein, J. E. M. N.; Que Jr, L. *Angew. Chem. Int. Ed.* **2017**, *56*, 9091.

(256) Coggins, M. K.; Zhang, M.-T.; Vannucci, A. K.; Dares, C. J.; Meyer, T. J. *J. Am. Chem. Soc.* **2014**, *136*, 5531.

(257) Acuña-Parés, F.; Codolà, Z.; Costas, M.; Luis, J. M.; Lloret-Fillol, J. *Chem. Eur. J.* **2014**, *20*, 5696.

(258) Bucci, A.; Menendez Rodriguez, G.; Bellachioma, G.; Zuccaccia, C.; Poater, A.; Cavallo, L.; Macchioni, A. *ACS Catal.* **2016**, *6*, 4559.

(259) Kottrup, K. G.; Hetterscheid, D. G. H. *Chem. Commun.* **2016**, *52*, 2643.

(260) Klepser, B. M.; Bartlett, B. M. *J. Am. Chem. Soc.* **2014**, *136*, 1694.

(261) Liu, Y.; Xiang, R.; Du, X.; Ding, Y.; Ma, B. *Chem. Commun.* **2014**, *50*, 12779.

(262) Wickramasinghe, L. D.; Zhou, R.; Zong, R.; Vo, P.; Gagnon, K. J.; Thummel, R. P. *J. Am. Chem. Soc.* **2015**, *137*, 13260.

(263) Makhlynets, O. V.; Oloo, W. N.; Moroz, Y. S.; Belaya, I. G.; Palluccio, T. D.; Filatov, A. S.; Müller, P.; Cranswick, M. A.; Que, L.; Rybak-Akimova, E. V. *Chem. Commun.* **2014**, *50*, 645.

(264) Kottrup, K. G.; D'Agostini, S.; van Langevelde, P. H.; Siegler, M. A.; Hetterscheid, D. G. H. *ACS Catal.* **2018**, *8*, 1052.

(265) Barnett, S. M.; Goldberg, K. I.; Mayer, J. M. *Nat. Chem,* **2012**, *4*, 498.

(266) Wang, D.; Groves, J. T. *Proc. Natl. Acad. Sci.* **2013**, *110*, 15579.

(267) Das, B.; Lee, B.-L.; Karlsson, E. A.; Akermark, T.; Shatskiy, A.; Demeshko, S.; Liao, R.-Z.; Laine, T. M.; Haukka, M.; Zeglio, E.; Abdel-Magied, A. F.; Siegbahn, P. E. M.; Meyer, F.; Karkas, M. D.; Johnston, E. V.; Nordlander, E.; Akermark, B. *Dalton. Trans.* **2016**, *45*, 13289.

(268) Okamura, M.; Kondo, M.; Kuga, R.; Kurashige, Y.; Yanai, T.; Hayami, S.; Praneeth, V. K. K.; Yoshida, M.; Yoneda, K.; Kawata, S.; Masaoka, S. *Nature* **2016**, *530*, 465.

(269) Liao, R.-Z.; Masaoka, S.; Siegbahn, P. E. M. *ACS Catal.* **2018**, 11671.

(270) Deutscher, J.; Corona, T.; Warm, K.; Engelmann, X.; Sobottka, S.; Braun-Cula, B.; Sarkar, B.; Ray, K. *Eur. J. Inorg. Chem.* **2018**, *2018*, 4925.

(271) Chakraborty, I.; Baran, P.; Sanakis, Y.; Simopoulos, A.; Fachini, E.; Raptis, R. G. *Inorg. Chem.* **2008**, *47*, 11734.

(272) Kanan, M. W.; Nocera, D. G. *Science* **2008**, *321*, 1072.

(273) Elizarova, G. L.; Matvienko, L. G.; Lozhkina, N. V.; Maizlish, V. E.; Parmon, V. N. *React Kinet Catal Lett* **1981**, *16*, 285.

(274) Abe, T.; Nagai, K.; Kabutomori, S.; Kaneko, M.; Tajiri, A.; Norimatsu, T. *Angew. Chem. Int. Ed.* **2006**, *45*, 2778.

(275) Dogutan, D. K.; McGuire, R.; Nocera, D. G. *J. Am. Chem. Soc.* **2011**, *133*, 9178.

(276) Wasylenko, D. J.; Ganesamoorthy, C.; Borau-Garcia, J.; Berlinguette, C. P. *Chem. Commun.* **2011**, *47*, 4249.

(277) Wasylenko, D. J.; Palmer, R. D.; Schott, E.; Berlinguette, C. P. *Chem. Commun.* **2012**, *48*, 2107.

(278) Das, B.; Orthaber, A.; Ott, S.; Thapper, A. *Chem. Commun.* **2015**, *51*, 13074.

(279) Hong, D.; Jung, J.; Park, J.; Yamada, Y.; Suenobu, T.; Lee, Y.-M.; Nam, W.; Fukuzumi, S. *Energy & Environmental Science* **2012**, *5*, 7606.

(280) Leung, C.-F.; Ng, S.-M.; Ko, C.-C.; Man, W.-L.; Wu, J.; Chen, L.; Lau, T.-C. *Energy & Environmental Science* **2012**, *5*, 7903.

(281) Pizzolato, E.; Natali, M.; Posocco, B.; Montellano Lopez, A.; Bazzan, I.; Di Valentin, M.; Galloni, P.; Conte, V.; Bonchio, M.; Scandola, F.; Sartorel, A. *Chem. Commun.* **2013**, *49*, 9941.

(282) Fu, S.; Liu, Y.; Ding, Y.; Du, X.; Song, F.; Xiang, R.; Ma, B. *Chem. Commun.* **2013**, 2167.

(283) Barnett, S. M.; Goldberg, K. I.; Mayer, J. M. *Nat Chem* **2012**, *4*, 498.

(284) Zhang, T.; Wang, C.; Liu, S.; Wang, J.-L.; Lin, W. *J. Am. Chem. Soc.* **2013**.

(285) Zhang, M.-T.; Chen, Z.; Kang, P.; Meyer, T. J. *J. Am. Chem. Soc.* **2013**, *135*, 2048.

(286) Zhang, M.; Zhang, M. T.; Hou, C.; Ke, Z. F.; Lu, T. B. *Angew. Chem. Int. Ed.* **2014**, *53*, 13042.

(287) Wang, J. W.; Zhang, X. Q.; Huang, H. H.; Lu, T. B. *ChemCatChem* **2016**, *8*, 3287.

(288) Luo, G. Y.; Huang, H. H.; Wang, J. W.; Lu, T. B. *Chemsuschem* **2016**, *9*, 485.

(289) Wang, L.; Duan, L. L.; Ambre, R. B.; Daniel, Q.; Chen, H.; Sun, J. L.; Das, B.; Thapper, A.; Uhlig, J.; Diner, P.; Sun, L. C. *Journal of Catalysis* **2016**, *335*, 72.

(290) Han, Y. Z.; Wu, Y. Z.; Lai, W. Z.; Cao, R. *Inorg. Chem.* **2015**, *54*, 5604.

(291) Larsen, C. B.; Wenger, O. S. *Chem. Eur. J.* **2018**, *24*, 2039.

(292) Narayanam, J. M. R.; Tucker, J. W.; Stephenson, C. R. J. *J. Am. Chem. Soc.* **2009**, *131*, 8756.

(293) Maji, T.; Karmakar, A.; Reiser, O. *J Phys Chem* **2011**, *76*, 736.

(294) Meng, Q.-Y.; Schirmer, T. E.; Katou, K.; König, B. *Angew. Chem. Int. Ed.* **2019**, *58*, 5723.

(295) Ryu, D.; Primer, D. N.; Tellis, J. C.; Molander, G. A. *Chem. Eur. J.* **2016**, *22*, 120.

(296) Claros, M.; Ungeheuer, F.; Franco, F.; Martin-Diaconescu, V.; Casitas, A.; Lloret-Fillol, J. *Angew. Chem. Int. Ed.* **2019**, *58*, 4869.

(297) Jin, J.; MacMillan, D. W. C. *Nature* **2015**, *525*, 87.

(298) Nguyen, T. M.; Nicewicz, D. A. *J. Am. Chem. Soc.* **2013**, *135*, 9588.

(299) Beatty, J. W.; Stephenson, C. R. J. *Acc. Chem. Res.* **2015**, *48*, 1474.

(300) Shiragami, T.; Pac, C.; Yanagida, S. *J Phys Chem* **1990**, *94*, 504.

(301) Lang, X.; Zhao, J.; Chen, X. *Chem. Soc. Rev.* **2016**, *45*, 3026.

(302) Wenger, O. S. *J. Am. Chem. Soc.* **2018**, *140*, 13522.

(303) Choudhury, S.; Baeg, J. O.; Park, N. J.; Yadav, R. K. *Angew. Chem. Int. Ed.* **2012**, *51*, 11624.

(304) Lee, S. H.; Kim, J. H.; Park, C. B. *Chem. Eur. J.* **2013**, *19*, 4392

(305) Mifsud, M.; Gargiulo, S.; Iborra, S.; Arends, I. W.; Hollmann, F.; Corma, A. *Nat. Commun.* **2014**, *5*, 3145.

(306) Kim, J. H.; Nam, D. H.; Park, C. B. *Current Opinion in Biotechnology* **2014**, *28*, 1.

(307) Liu, J.; Huang, J.; Zhou, H.; Antonietti, M. *ACS Appl. Mater. Interf.* **2014**, *6*, 8434.

(308) Bachmeier, A.; Murphy, B. J.; Armstrong, F. A. *J. Am. Chem. Soc.* **2014**, *136*, 12876.

(309) Palmisano, G.; Augugliaro, V.; Pagliaro, M.; Palmisano, L. *Chem. Commun.* **2007**, 3425.

(310) Galian, R. E.; Pérez-Prieto, J. *Energy & Environmental Science* **2010**, *3*, 1488.

(311) Barber, J.; Tran, P. D. *J. R. Soc. Interface* **2013**, *10*, 20120984.

(312) Andreiadis, E. S.; Chavarot-Kerlidou, M.; Fontecave, M.; Artero, V. *Photochem. Photobiol.* **2011**, *87*, 946.

(313) Macia-Agullo, J. A.; Corma, A.; Garcia, H. *Chem. Eur. J.* **2015**, *21*, 10940.

(314) Ghosh, T.; Slanina, T.; König, B. *Chem. Sci.* **2015**, *6*, 2027.

(315) Joyce-Pruden, C.; Pross, J. K.; Li, Y. *J. Org. Chem.* **1992**, *57*, 5087.

(316) Yanagida, S.; Yoshiya, M.; Shiragami, T.; Pac, C.; Mori, H.; Fujita, H. *J. Phys. Chem.* **1990**, *94*, 3104.

(317) *Photocatalytic Hydrogenation on Semiconductor Particles*; Kohtani, S.; Yoshioka, E.; Miyabe, H., Eds.; InTech, Chapters published 2012.

(318) Füldner, S.; Mild, R.; Siegmund, H. I.; Schroeder, J. A.; Gruber, M.; König, B. *Green Chemistry* **2010**, *12*, 400.

(319) Ke, X.; Sarina, S.; Zhao, J.; Zhang, X.; Chang, J.; Zhu, H. *Chem. Commun.* **2012**, *48*, 3509.

(320) Yanagida, S.; Ishimaru, Y.; Miyake, Y.; Shiragami, T.; Pac, C.; Hashimoto, K.; Sakata, T. *J. Phys. Chem.* **1989**, *93*, 2576.

(321) Kohtani, S.; Kurokawa, T.; Yoshioka, E.; Miyabe, H. *Applied Catalysis A: General* **2016**, *521*, 68.

(322) Choudhury, S.; Baeg, J.-O.; Park, N.-J.; Yadav, R. K. *Green Chemistry* **2014**, *16*, 4389.

(323) Park, C. B.; Lee, S. H.; Subramanian, E.; Kale, B. B.; Lee, S. M.; Baeg, J.-O. *Chem. Commun.* **2008**, 5423.

(324) Liu, X.; Sun, D.; Yuan, R.; Fu, X.; Li, Z. *J. Catal.* **2013**, *304*, 1.

(325) Li, F.; Zhang, B.; Li, X.; Jiang, Y.; Chen, L.; Li, Y.; Sun, L. *Angew. Chem., Int. Ed.* **2011**, *50*, 12276.

(326) Imamura, K.; Okubo, Y.; Ito, T.; Tanaka, A.; Hashimoto, K.; Kominami, H. *RSC Advances* **2014**, *4*, 19883.

(327) Yamataka, H.; Seto, N.; Ichihara, J.; Hanafusa, T.; Teratani, S. *J. Chem. Soc., Chem. Commun.* **1985**, 788.

(328) Shimakoshi, H.; Hisaeda, Y. *ChemPlusChem* **2014**, *79*, 1250.

(329) Tian, H.; Shimakoshi, H.; Imamura, K.; Shiota, Y.; Yoshizawa, K.; Hisaeda, Y. *Chem. Commun.* **2017**, *53*, 9478.

(330) Shiragami, T.; Pac, C.; Yanagida, S. *J. Phys. Chem.* **1990**, *94*, 504.

(331) Litman, Z. C.; Wang, Y.; Zhao, H.; Hartwig, J. F. *Nature* **2018**, *560*, 355.

(332) Hohenberg, P. K., W. 1964; Vol. 136.

(333) kohn, W. S., Lu Jeu *Phys. Rev.* **1965**, *140*, A1133.

(334) Siegbahn, P. E. *Wiley, Chichester* **1996**.

(335) Ziegler, T. *Springborg, M (ed.), Wiley, Chichester.* **1997**.

CHAPTER II.

MAIN OBJECTIVES

MECHANISTIC STUDIES OF WATER OXIDATION CATALYZED BY HOMOGENEOUS IRON AND RUTHENIUM
COMPLEXES AND LIGHT-DRIVEN ORGANIC REDUCTIONS WITH A DUAL COBALT/COPPER CATALYTIC SYSTEM

Carla Casadevall Serrano

II.   MAIN OBJECTIVES

The transition to a green and sustainable energy-based scheme is one of the most important challenges that faces our society. In Nature, photosynthesis is the process by which sunlight energy is stored into chemical bonds to sustain life, producing only O_2 as a by-product. Therefore, an appealing approach is the application of artificial photosynthetic schemes to produce solar fuels and fine chemicals from CO_2 and water using sunlight as the driving force (Scheme 1). However, both CO_2 reduction and water oxidation (WO) are challenging processes and remain bottlenecks for the development of efficient artificial photosynthesis. WO is a highly endergonic process that requires the access of very high oxidation states at the metal center, which often leads to oxidative damage side reactions. In addition, a viable artificial photosynthetic approach should also rely on inexpensive, robust sustainable, modular and efficient materials. To this end, fundamental understanding of the parameters that control both the catalytic activity and selectivity is necessary.
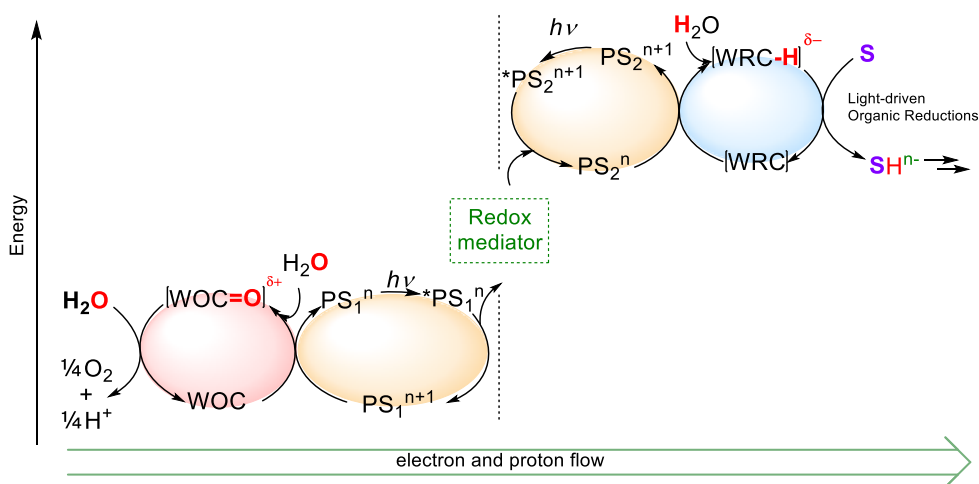
Scheme II.1. Simplified extended artificial photosynthetic scheme representing the use of electrons from the WO to perform reductive transformations. WOC stands for Water Oxidation Catalysts and WRC stands for Water Reduction Catalysts that can be used for organic reductions.

The study of the mechanisms involved in natural photosynthesis very much benefits from the development of synthetic models mimicking the natural machinery. Important processes to be understood are light harvesting, charge transfer and separation, water oxidation catalysis, as well as, how to couple it to reductive transformations in an efficient manner. In this line, the general objectives of the present Ph.D. Thesis are: i) on the one hand, the development of coordination complexes for water oxidation with well-defined iron and ruthenium complexes and the thorough analysis of the reaction mechanisms; and ii) on the other side, the development and mechanistic study of a dual cobalt-copper catalytic system coupling transition metal catalysis with photoredox catalysis for the light-driven reduction of organic substrates. This would allow us to advance in the identification of the factors that determine the activity and stability under catalytic conditions, as well as to elucidate the intermediates involved in both transformations. Altogether, we envision that mechanistic proposals for the water oxidation reactions with the Fe and Ru complexes of study, as well as for the dual Co/Cu catalytic system in the light-driven reductions will allow for the understanding and development of catalytic platforms for the production of fine chemicals by artificial photosynthesis.

Accordingly to the general objectives above mentioned, the first part of the thesis (chapters III – VII) is focused on the development of aminopyridine Fe and Ru complexes for WO and their mechanistic study. And the second part of the thesis (chapters VIII – X) is focused on the reactivity, selectivity and mechanistic studies of a dual Co/Cu catalytic system based on a cobalt aminopyridine complex and a copper photoredox catalyst for the light-driven reduction of aromatic ketones, aromatic and aliphatic aldehydes and aromatic olefins.

The thesis opens (chapter III) with the study of the decomposition paths in Fe WOCs based on the mcp ligand (Figure II.1) with the aim of not only to understand key aspects of the catalytic activity but to improve the catalytic activity by rational ligand design.
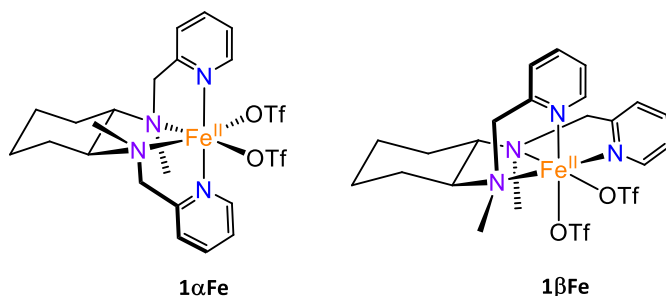
Figure II.1. **α**-[Fe(OTf)$_2$(mcp)] (mcp = *N*,*N*′-dimethyl-*N*,*N*′-bis(pyridin-2-ylmethyl)cyclohexane-1,2-diamine, OTf = trifluoromethanesulfonate anion), (**1α**) and **β**-[Fe(OTf)$_2$(mcp)], (**1β**) complexes studies in chapter III.

Then, in chapters IV and V, the study is focused in the understanding of the differences in the WO catalytic activity of analogous [Fe^{II}(OTf)(Py$_2^{Me}$tacn)](OTf) and [Ru^{II}(OH$_2$)(Py$_2^{Me}$tacn)](PF$_6$)$_2$ complexes. A detailed mechanistic study based on experimental *in situ* (chapter IV) and computational (chapter V) characterization of the intermediates involved in the WO reaction is performed (Figure II.2). We envision that this study can be important in the future to translate the ruthenium WO activity to homologous iron systems.
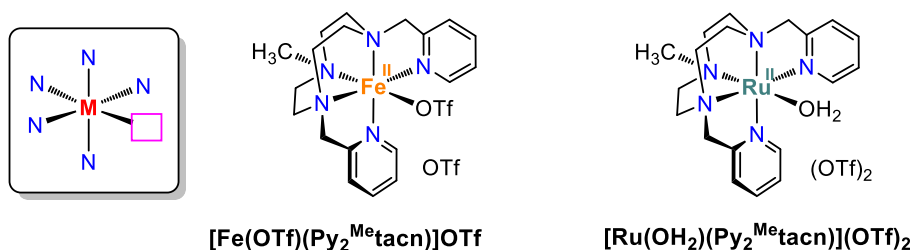
Figure II.2. [Fe^{II}(OTf)(Py$_2^{Me}$tacn)](OTf) and [Ru^{II}(OH$_2$)(Py$_2^{Me}$tacn)](PF$_6$)$_2$ complexes studied in chapters IV and V.

An important objective in the WO reaction is to further understand the O-O bond formation event beyond the state of the art. Therefore, in chapter VI a detailed mechanistic study of the O-O bond formation event in WO catalyzed by complex [Ru^{II}(OH$_2$)(Py$_2^{Me}$tacn)](PF$_6$)$_2$ is carried out.

UNIVERSITAT ROVIRA I VIRGILI
MECHANISTIC STUDIES OF WATER OXIDATION CATALYZED BY HOMOGENEOUS IRON AND RUTHENIUM
COMPLEXES AND LIGHT-DRIVEN ORGANIC REDUCTIONS WITH A DUAL COBALT/COPPER CATALYTIC SYSTEM
Carla Casadevall Serrano

CHAPTER II   MAIN OBJECTIVES

Finally, in chapter VII, due to the inactivity of *N*-pentadentate Fe complexes based on neutral aminopyridine ligands for WO, we seek to modify the first coordination sphere by the introduction of an anionic moiety in the tacn ligand (Figure II.3). We envision that this strategy would lower the redox potential to access the postulated active species Fe^V.
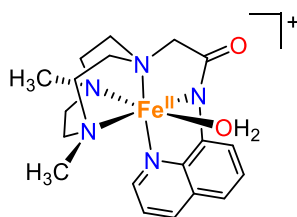
Figure II.3. [$Fe^{II}(OTf)(AQ_2{}^{Me2}tacn)$]$^+$ complex developed in chapter VII.

Regarding the reductive part, in chapters VIII and IX, we will explore the light-driven reduction of aromatic ketones, aromatic and aliphatic aldehydes (chapter VIII) and aromatic olefins (chapter IX) by a dual catalytic system based on an aminopyridine Co catalyst (Figure II.4). We hypothesized that the same Co catalysts used for H_2 production (shared low valent Co intermediates) can be used to trigger organic reductions, developing new organic methodologies. Moreover, mechanistic studies will be performed to shed light in the mechanisms of action in both chapters. Additionally, in chapter X, an important effort will be performed to study the key intermediates involved in the catalytic cycle of light-driven organic reductions. We aim to synthesize and characterize the putative low valent Co(I) species generated from complex **1** and study its reactivity and the electronic effects in its stabilization.

Figure II.4. [$Fe^{II}(OTf)(Py_2{}^{Me}tacn)$](OTf) and [$Ru^{II}(OH_2)(Py_2{}^{Me}tacn)$]($PF_6$)$_2$ complexes studied in chapters IV and V.

CHAPTER III

Identification of the Molecular Nature of the Active Species in Water Oxidation with a Well-defined *N*-Tetracoordinate Fe Catalyst: the Fate of the Ligand

Part of this chapter corresponds to the following publication:

MECHANISTIC STUDIES OF WATER OXIDATION CATALYZED BY HOMOGENEOUS IRON AND RUTHENIUM
COMPLEXES AND LIGHT-DRIVEN ORGANIC REDUCTIONS WITH A DUAL COBALT/COPPER CATALYTIC SYSTEM

Carla Casadevall Serrano

III. Identification of the Molecular Nature of the Active Species in Water Oxidation with a Well-defined *N*-Tetracoordinate Fe Catalyst: the Fate of the Ligand

III.1. General insight

Water oxidation (WO) is one of the most important reactions of natural photosynthesis and it is regarded as one of the bottlenecks to be mastered towards the development of artificial photosynthesis for solar fuel production. At the same time, WO has interest *per se* because of its multi-electron and proton nature. Mechanistic understanding of WO reactions very much benefit from the study of molecular catalysts that operate under homogeneous conditions.[1-3] However, proving the nature of the catalytic species is not straightforward due to the harsh oxidizing species, which compromise the stability of molecular catalysts *via* oxidative damage.[4-87,9-12] Oxidation of precatalysts can lead to novel discrete complexes that can be also active catalysts under homogeneous conditions. On the contrary, in several cases, initial oxidation of the molecular precatalysts can result in the formation of metal-oxide or hydroxide nanoparticles, which may be also active WO catalysts. In some cases, WO may occur via parallel paths originating from molecular catalysts operating in a homogeneous regime, and metal-oxide nanoparticles that act as heterogeneous catalysts. In these cases, elucidation of the active species becomes very complicated.

Special effort has been put in the development of water oxidation catalysts (WOCs) based on 1st row transition metals (TM), due to their readily available nature and abundancy.[13-17] However, WOCs based on 1st row TM are generally believed to be particularly sensitive to the oxidative and usually acidic catalytic conditions of water oxidation reactions. Moreover, the usually labile nature of metal-ligand bonds for this class of compounds is believed to critically undermine their ability to act as long-lasting WO catalysts, and there is a rich and lively debate on the exact nature of the species responsible for the catalytic activity. Iron complexes based on

aminopyridyl ligands have been explored as WO catalysts employing chemical, electrochemical and photochemical conditions.[18-37] Studies described so far have shown that the nature of the active species appears to be dependent on the nature of the catalysts, the oxidant and also the reaction conditions. Among all the studies performed, an interesting observation is that iron complexes based on neutral aminopyridyl ligands must have two *cis*-free coordination sites to be active.[20,38,39] Lloret, Costas and coworkers reported the catalysts **α**-[Fe(OTf)$_2$(mcp)] (mcp = *N,N′*-dimethyl-*N,N′*-bis(pyridin-2-ylmethyl)cyclohexane-1,2-diamine,   OTf   = trifluoromethanesulfonate anion), (**1α**) and **β-**[Fe(OTf)$_2$(mcp)]**, (1β)**, which despite of because being topological isomers, they exhibit important differences in their catalytic activity.[18,20] **1α** is a particularly efficient WO catalyst when employing chemical oxidants such as cerium ammonium nitrate (CAN) and NaIO$_4$ under acidic conditions, but it rapidly degrades under photochemical and or basic conditions.[18,22] On the other hand, **1β** is poorly active with chemical oxidants and it is very rapidly degraded under acidic conditions.

   The reaction mechanism proposed for these catalysts operating in acidic media using CAN as sacrificial oxidant entails the oxidation of Fe^{II}-OH$_2$ to Fe^{IV}(O) species. the latter is the resting state of the catalytic cycle (Figure III.1).[19,38] Further reaction with Ce^{IV} generates a Fe^{IV}-O-Ce^{IV} complex, which has been spectroscopically characterized by a combination of UV-Vis, resonance Raman and high resolution mass-spectrometry (HRMS).[18] Similar M-O-Ce adducts (M = Ru and Ir) have been also proposed.[40-43] Then, it evolves into the formation of Ce^{III} and the highly electrophilic Fe^{V}(O)(OH), which is the active species. Computational studies showed that the WNA is assisted by an initial coordination of the reactive water molecule to the *cis*- hydroxide ligand.[38,44]

UNIVERSITAT ROVIRA I VIRGILI
MECHANISTIC STUDIES OF WATER OXIDATION CATALYZED BY HOMOGENEOUS IRON AND RUTHENIUM
COMPLEXES AND LIGHT-DRIVEN ORGANIC REDUCTIONS WITH A DUAL COBALT/COPPER CATALYTIC SYSTEM
Carla Casadevall Serrano

CHAPTER III   Mechanistic study of Fe WOCs: molecularity of the active species
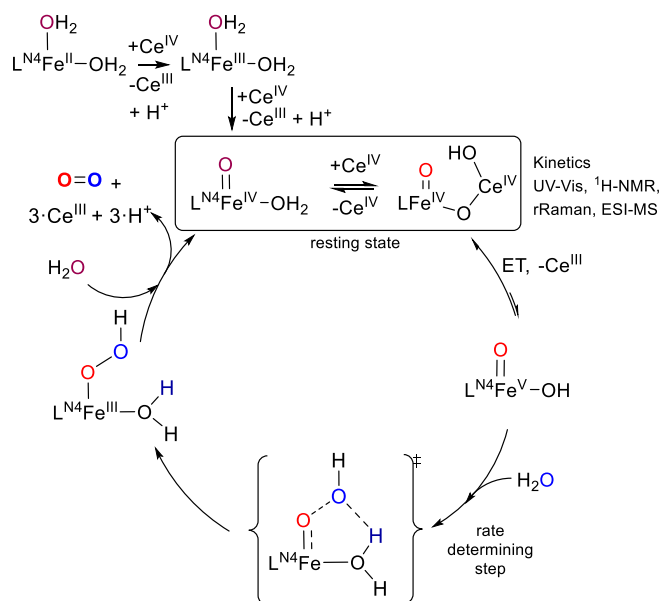
Figure III.1. Reaction mechanism proposed for iron aminopyridyl complexes operating in acidic media with CAN as sacrificial oxidant.[18] The charges of the different species have been omitted for clarity.

Despite there is a body of experimental evidence that supports this mechanistic proposal,[18] the molecular nature of the catalysts has been questioned on the basis of the observation that structurally related iron complexes undergo rapid decomposition,[45] and the lack of evidence of the formation of high valent iron-oxo species in a molecular Fe-WOC, so far. Therefore, the target of the group was to characterize the resting state of the catalysts **1α** and **1β** in water oxidation reactions with chemical oxidants and study their decay paths under catalytic conditions by a combination of experimental and computational methods. Previous studies in the group have let to the identification of the ligand oxidation sensitive sites for those complexes. And further catalytic and mechanistic studies that will be explained in this chapter have confirmed the two different oxidative mechanisms according to the topology of the catalyst. This knowledge has served to design extraordinarily robust catalysts by deuteration of these sites, overall providing compelling evidence that WO under these conditions takes place *via* molecular, high valent oxo-iron species.[46]

III.2. Precedents in the group

Previous studies in the group proposed high valent oxo-iron species α-$[Fe^{IV}(O)(H_2O)(mcp)]^{2+}$ (2α) and β-$[Fe^{IV}(O)(H_2O)(mcp)]^{2+}$ (2β) to be the resting state in WO on the basis of their distinctive UV-Vis spectra (λ_{max} = 769 nm, ε = 270 M^{-1} cm^{-1} for 2α; λ_{max} = 778 nm, ε = 280 $M^{-1}cm^{-1}$ for 2β), ESI-MS spectra (m/z = 413.162 ± 0.003 assigned to $[Fe^{IV}(O)(OH)(mcp)]^+$, in $H_2^{18}O$ and D_2O a + 4 and a + 1 shifts observed, respectively) and by resonance Raman for 2α (λ_{exc} = 413.1 nm, 822 cm^{-1}, downshifted by 40 cm^{-1} with the use of $H_2^{18}O$).[18] Later on, Mössbauer analysis performed after freeze quenched 2α and 2β samples suggest the presence of a mixture of Fe^{IV} and Fe^{III} species, what was confirmed by experiments conducted at 4.5 K under weak (0.06 T) and strong (7 T) magnetic fields applied parallel to the γ-rays (Figure A.I. 4). Particularly, the Fe^{IV} components characterize 2α and 2β as *bona fide* S=1 $Fe^{IV}=O$ species (Table A.I.1). These complexes are not stable and decay rapidly to Fe^{III} species (Figures A.I.3 and A.I.4). Thus, decomposition of $Fe^{IV}(O)L^{N4}$ is linked with the depletion of the catalytic activity, as previously observed by Lloret, Costas and coworkers.[18-20] Therefore, identification of the decay paths of 2α and 2β would be useful in designing more robust catalysts.

Towards this end, they studied the decay of 2α and 2β under aqueous acidic conditions analogous to WO by UV-Vis (1 mM, pH = 1, 25 ºC).[46] Analysis of the reaction head space after the decay of the iron-oxo(IV) species showed no traces of O_2, or CO_2 (in the gas phase, measured by GC-TCD and manometry) or H_2O_2 (in solution, measured by titration with the peroxotitanyl method)[47] were detected; suggesting that the degraded species is not catalytically active. Analysis and identification and quantification of the ligand fragments in solution after the decay was performed by Cryospray High Resolution Mass Spectrometry (CSI-HRMS) together with HPLC-MS (Figures III.2 and III.3). This analysis correlates the water oxidation activity of 1α and 1β with stability against oxidative damage of the ligand *via* aliphatic C-H oxidation (Figure III.2, b and c). The site of degradation and the

relative stability against oxidative degradation is shown to be dependent on the topology of the catalyst. [46] In the case of **2α**, ligand fragments arise from the oxidation of the benzylic positions (339.21 ([$C_{20}H_{26}N_4O$]+H^+) and 234.19 m/z ([$C_{14}H_{23}N_3$]+H^+) assigned to [**mcp(+O-2H)**]+H^+ and [**mcp-CH$_2$Py+H**]+H^+, respectively, depicted in Figure III.3a and III.3c). Instead, the main peak observed after decay of **2β** (Figure III.3b and III.3d) results from the loss of a methyl group, presumably through oxidation of the N-methyl position (311.22 m/z ([$C_{19}H_{26}N_4$]+H^+) assigned to [**mcp(-Me+H)**]+H^+). Oxygenation of a methylene from the benzylic position (m/z = 339.21) is also observed as a minor path.
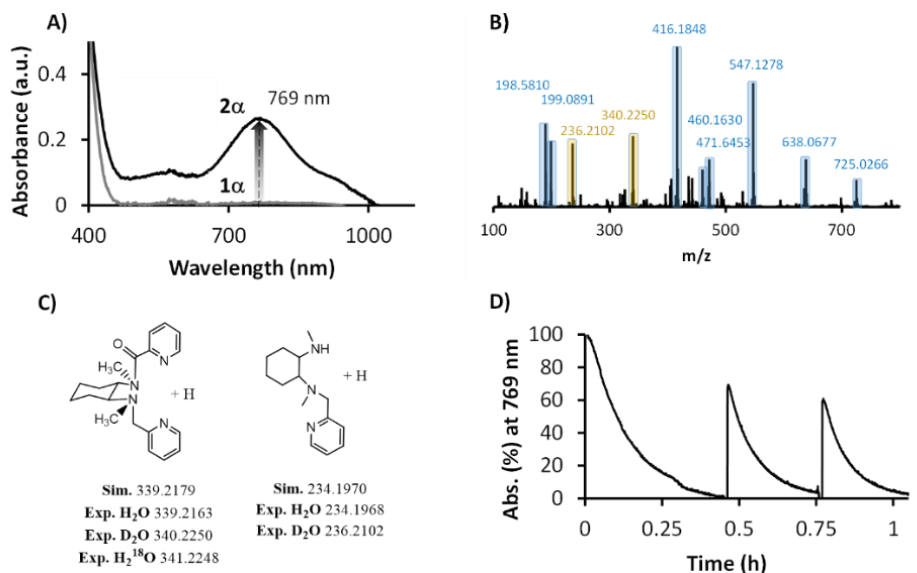
Figure III.2. A) UV-Vis spectrum of **2α** (black) in water formed by reaction of **1α** (gray) (1 mM) with 3 eq. of CAN in HOTf (final pH = 1, 25 ºC) and B) CSI-HRMS recorded 1.5 hour after of the addition of CAN (3 eq., 50 µL) to **1α** (4.5 mM, 0.5 mL) in D$_2$O. Blue peaks correspond to iron species while brown peaks correspond to ligand fragments. C) Ligand fragmentation observed by CSI-HRMS in reactions performed in H$_2$O, D$_2$O and H$_2$^{18}O. D) Evolution of the **2α** chromophore monitored at 769 nm after the addition of 1 eq. of CAN (x 3 times).[46]

Likewise, analysis of the decay of **1α** and **1β** with 75 mM of Ce^{IV}, conditions that are catalytically relevant for WO[20] showed more ligand oxidative degradation (Figure III.3). Even so, 60% of the **mcp** ligand was still recovered at the end of the decay of **2α** by HPLC-MS. However, the decay of **1β** leads to the almost complete

decomposition of the **mcp** ligand, and identifiable fragments account only for roughly 30-35% of the original amount of ligand. In addition, multiple minor products formed by multiple oxidative degradations, are observed (Figure III.3).[46]
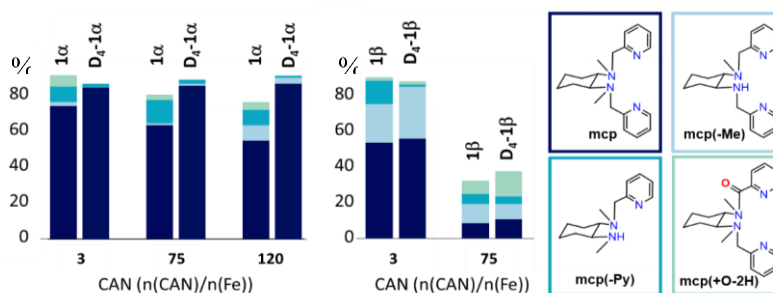
Figure III.3. Quantification of the ligand degradation products (in % respect to the theoretical amount) after reaction of **1β, D₄-1β** (1 mM) in water with CAN (3, 75 or 100 mM), demetalation and ligand extraction. Ligand fragments were identified by HPLC-MS and by comparison with independently prepared products. See experimental for details.

According to the explained above, the methylene benzylic sites are the sensitive sites for oxidative degradation for **1α**. Therefore, provided the molecular nature of the catalyst, and due to the sensitiveness of the WO reaction to the ligand scaffold,[20] deuteration of these sites will provide stronger C–H bonds, while retaining the electronic and structural properties of the catalyst. Following on this reasoning, tetradeutero **D₄-mcp** ligand was prepared by reacting **mcp** with NaH in CD₃CN, and the corresponding complexes α-D₄-[Fe^{II}(CF₃SO₃)₂(mcp)], **D₄-1α**, and β-D₄-[Fe^{II}(CF₃SO₃)₂(mcp)], **D₄-1β**, were prepared and kindly provided by Dr. Zoel Codolà and Dr. Ilaria Gamba (Figure III.4). Characterization of **D₄-1α** and **D₄-1β**, and in particular deuteration of the benzylic sites was confirmed by ¹H-NMR spectroscopy (see Figure A.I.1 and A.I.2) and MS analysis (See S.I. Section 3).[46] Interestingly, deuteration of the benzylic methylene sites in **1α** has a very important impact in the inertia of **D₄-2α.**
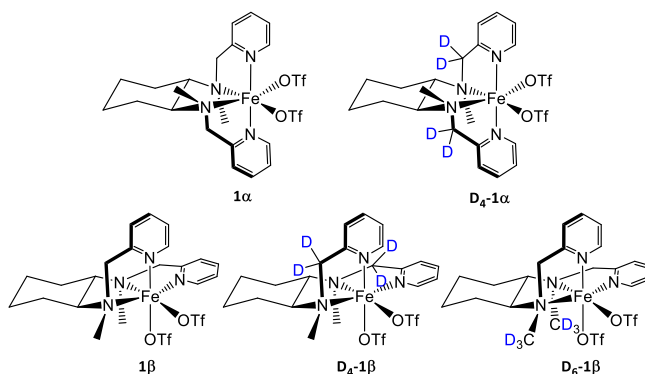
Figure III.4. Iron complexes evaluated in this study.

First of all, the half-life time of **D₄-2α** was enhanced by 10-fold (Figure SI.14-15)[46], from 0.11 h to 1.1 h with regard to **2α**. However, for **D₄-2β**, the same half-life of **2β** was observed (Figure SI.16-17).[46] In all cases, **D₄-1α** leads to almost quantitative recovery of the intact ligand (~ 85%), demonstrating that ligand degradation is basically ligated to oxidation of this site, and most remarkably, the process is hampered by deuteration. Moreover, in the case of **D₄-2α**, the recovery of the intact ligand increases from 69% (**2α**) to 79% (D₄-**2α**) (Figure III.3).[46] In contrast, the percentage of intact ligand recovered after the decay of **D₄-2β** does not change upon deuteration, but the relative amounts of products resulting from either the loss of a methylpyridine arm (**mcp(-Py)**) or a methyl group (**mcp(-Me)**) change, with the later increasing at the expenses of the former upon deuteration, suggesting competing paths leading to the two products (Figure III.3, Table S.I.7).[46]

As a summary, Mössbauer spectroscopy provides definitive evidence that **1α** and **1β** generate oxoiron(IV) species **2α** and **2β** respectively, as the resting state at low concentration of Ce[IV], as early proposed on the basis of UV-Vis, resonance Raman and mass-spectrometry. Decomposition paths of the catalysts under WO catalytic conditions have been investigated by identifying and quantifying ligand fragments that form upon catalyst degradation. The site of degradation and the relative stability against oxidative degradation is shown to be dependent on the topology of the catalyst, being oxidation of the benzylic positions and *N*-methyl

groups for **1α** and **1β**, respectively. This information has served as the basis for creating a novel family of catalysts where sensitive C-H bonds have been replaced by C-D bonds. Consequently, deuterated analogs, **D₄-1α**, **D₄-1β** and **D₆-1β** (where *N*-Me groups are deuterated), were prepared. Resulting in an increase of the robustness of the complexes; concretely, a 10-fold enhancement of the lifetime of **D₄-2α** with respect of **2α** and a 6-fold enhancement of the lifetime of **D₆-2β** with respect of **2β** were obtained.

As showed in the results described above, the substitution of C-H bonds by C-D bonds in the sensitive sites for oxidation has led to more robust complexes. Remarkably, this has improved the stability of the complexes without modifying the steric nor the electronic effects. In this regard, it would be very interesting to provide evidence on the effect of stability into the WO catalytic activity. In this line, we hypothesize that if the active species is molecular and is connected to the oxoiron(IV) resting state, the increase in its half lifetime, should be translated into an increase in the lifetime of the WO catalysis with regard to the previously reported protio analogs.[20] Moreover, the initial rate for O_2 evolution for complexes **1α** and **D₄-1α** should be the same, since both systems are equal regarding their steric and electronic nature. Therefore, all complexes have been evaluated under WO catalytic conditions, and the gas evolved along the reaction time has been monitored by manometry and analyzed and quantified by gas chromatography. In addition, online GC-MS studies have been performed to identify and analyze the initial rate of the gaseous products evolved from the reaction, discarding a possible connection between the decomposition paths and the WO catalytic activity. Moreover, the fact that the topology of the complex determines the degradation path has interest *per se*. We envision that the topology-dependence decomposition mechanism for **1α** and **1β** could be related to the accessibility of the C-H bonds by the Fe=O moiety. Thus, we expect that valuable mechanistic information can be obtained *via* computational modeling of the decay paths. These new studies are presented in this chapter and altogether have enabled to pinpoint the nature of the active species.

III.3. Results and discussion

III.3.1. Manometry and GC-MS on-line studies of the gases evolved in the chemically driven WO

The catalytic activity of the series of complexes, including protio and deuterio for the α and β isomer analogs was studied in parallel in order to ensure proper comparison among them. O_2 produced in the reactions was monitored by manometry (pressure sensors transducer, see the experimental section for further details) and also by gas chromatography, by subjecting an aliquot of the reaction head space to chromatographic analysis in a TCD-GC (thermal conductivity detector-gas chromatograph). Values determined by the two methods are in good agreement (see Table 1). For example, under catalytic conditions, manometric measurements indicate that **1α** and **D₄-1α** yield 379 ± 3 and 1730 ± 90 TON O_2, respectively (Table 1, entries 1 and 2), which are in good agreement with the values determined by GC (400 ± 10 and 1900 ± 110).[18,20] Indeed, GC-TCD analyses of the gas at the headspace of the reactions confirmed that the gas formed is essentially O_2 (Table 1).

Most remarkably, these values indicate that deuteration creates a much more active catalyst, yielding approximately a 5 - fold increase in TONs for **D₄-1α** (from 379 to 1730 TON O_2 upon deuteration). The O_2 produced for **D₆-β-Fe(OTf)₂(mcp)** (**D₆-1β**) (161 ± 2 TON O_2) is also roughly 4 - fold increased with respect to **D₄-β-Fe(OTf)₂(mcp)** (**D₄-1β**) and **β-Fe(OTf)₂(mcp)** (**1β**) (39 and 30 TON O_2, respectively), although this is still modest when compared to **1α** and **D₄-1α.** In the case of the beta isomer, the analysis of the decomposition paths after the decay of **2β**, pointed towards the oxidation of the *N*-methyl groups as responsible of the degradation of the catalyst. This is in reasonable agreement with the improved catalytic activity of **D₆-1β**, in which deuteration of the N-methyl groups prevents their degradation, in front of **1β** and **D₄-1β**, which, concordantly, did not have any effect in the catalytic outcome. None of the complexes showed induction time in the O_2 evolution catalytic traces (see Figure III.6). It is particularly interesting that **D₄-1α**

121

and **1α** have the same initial rate for oxygen evolution (See Table 1, entries 1 and 2 and Figure III.6 a, b). This has important mechanistic implications since the metal center in both **D$_4$-1α** and **1α** complexes have the same electronic and steric properties. Equivalent initial O_2 evolution rates strongly evidence catalytic species only differing on the isotopic nature of the pseudobenzylic positions.

Table 1. Water oxidation catalytic activities for the studied iron complexes.[a]

Entry	Complex	[CAN] (mM)	[Cat] (μm)	TOF (h^{-1})[b]	TON O$_2$[b]	TON O$_2$[c]	Yield O$_2$ (%)	TON CO$_2$[c]
1	**1α**[d]	125	12.5	850	379 ± 3	400 ± 10	16	<1
2	**D$_4$-1α**[d]	125	12.5	820	1730 ± 90	1900 ± 110	76	<1
3	**1β**[d]	125	12.5	33	30 ± 1	46 ± 1	2	<1
4	**D$_4$-1β**[d]	125	12.5	37	39 ± 2	52 ± 3	2	<1
5	**D$_6$-1β**[d]	125	12.5	214	161 ± 2	151 ± 2	6	<1
6	**[Fe(OTf)$_2$(mcp-Me)]**[d,h]	125	12.5	-	0	<1	-	<1
7	**[Fe(OTf)$_2$(mcp-Py)]**[d,h]	125	12.5	-	0	<1	-	<1
8	**1α**[e]	75	1000	150	12	-	64	-
9	**D$_4$-1α**[e]	75	1000	200	17	-	91	-
10	**1β**[e]	75	1000	74	9	-	48	-
11	**1α**[f]	125	1	1470[f]	670 ± 10	800 ± 90	3	-
12	**D$_4$-1α**[f]	125	1	1480[f]	3330 ± 150	3800 ± 100	12	-

[a]Reactions performed in MilliQ water at 25 ºC under vigorously stirring. [b]Results obtained by manometry studies after 20 h of reaction. TOF is calculated after 5 min of the addition of the catalyst. [c]Results from the analysis of an aliquot of the head-space by GC-TCD after 20 h of reaction. [d]Reaction conditions A: The catalyst (0.5 ml, final concentration 12.5 μM) was injected through a septum into the reaction vial containing CAN aqueous solution (9.5 ml, 131 mM, final concentration 125 mM). Initial pH is 0.8. [e]Reaction conditions B: CAN (0.8 ml of stock solution in HOTf:H$_2$O 3:10 solution, final concentration 75 mM) was injected through a septum into the reaction vial containing the catalyst aqueous solution (3.2 ml, final concentration 1 mM) pH is 1. [f]Reaction conditions C: The catalyst (0.5 ml, final concentration 1 - 3 μM) was injected through a septum into the reaction vial containing CAN aqueous solution (14.5 ml, 129.3 mM, final concentration 125 mM). TOF was calculated after 1 min of the addition of the catalyst. [g]TOF was calculated after 200 sec. of the addition of the catalyst.

Moreover, iron complexes prepared with the ligands that come from the different degradation fragments of the mcp ligand (See Figure III.5) do not show appreciable water oxidation catalytic activity (Table 1, entries 6 and 7 and Figure A.I.5). In addition, iron complexes where the methyl groups of the mcp ligand are

replaced by protons or with the two pyridyl positions oxidized are also catalytically incompetent.[48] These results strongly support that the initial O_2 evolution should come from the intact molecular species before degradation. Altogether strongly indicates the molecularity of the catalytic system and that the original molecular complex is the active species. The same trend was observed for the pair **1β** and **D$_4$-1β** but they are somewhat different for **D$_6$-1β.** Presumably, initial rates measured for **1β** and **D$_4$-1β** are already contaminated by rapid catalyst degradation (Table 1 entries 8-10 and Figure III.6 and III.7).

[Fe(OTf)$_2$(mcp-Me)]   **[Fe(OTf)$_2$(mcp-Py)]**   **[Fe(Cl)$_2$(mcp+O-2H)]**
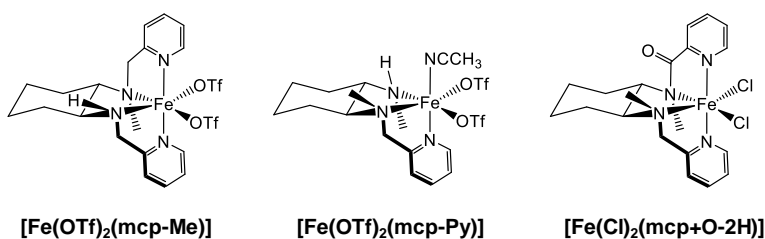
Figure III.5. Iron complexes of the fragmented ligands, tested under standard water oxidation catalysis conditions.

Important information regarding the gases formed in the reaction headspace at initial reaction times can be extracted from direct GC-MS online-analysis. This technique also allows for identification of the relative rates for O_2 and CO_2 evolution from the very beginning of the reaction to hundreds of seconds. In all cases the rates for O_2 evolution are much higher than the rates measured for CO_2 production, being the latter only produced in trace levels (Figure III.7). Thus, the measured reaction rates by manometry experiments are ascribed only to O_2 evolution. Likewise, catalyst decomposition is not connected with O_2 evolution. The sum of these results indicates that the higher activity of **D$_4$-1α** results from a more robust character. In combination with the HPLC analysis of the degradation paths, we can conclude that deuteration of the pseudobenzylic positions blocks the most important deactivation path, conferring stability to the catalyst.
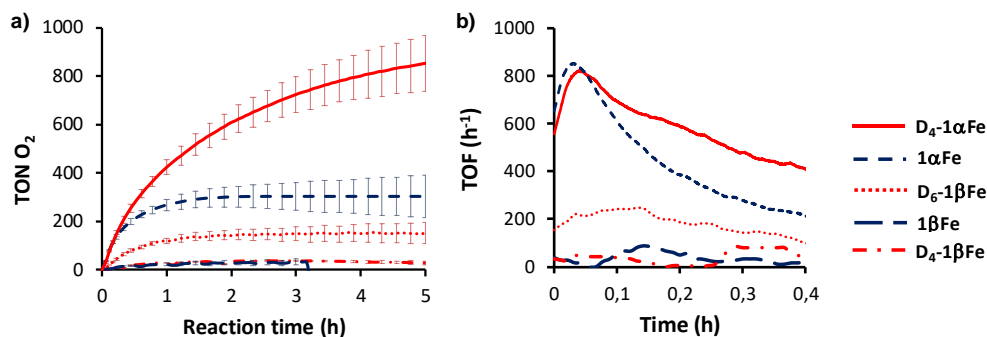
Figure III.6. a) Gas traces and b) initial TOF (h^{-1}) of the manometry monitorization when the iron catalyst (α-**Fe(OTf)₂(mcp)** (short-dashed line), **D₄-α-Fe(OTf)₂(mcp)** (straight line), **β-Fe(OTf)₂(mcp)** (long-dashed line), **D₄-β-Fe(OTf)₂(mcp)** (dotted-short-dashed line) and **D₆-β-Fe(OTf)₂(mcp)** (dotted line)) (0.5 ml of a stock solution, final concentration 12.5 μM) is added to a stirred solution of CAN (9.5 ml, final concentration 1000 equiv., 125 mM) in Milli-Q water at 25ºC and initial pH 0.8. Vertical lines represent the error bars from standard deviation between replicates.
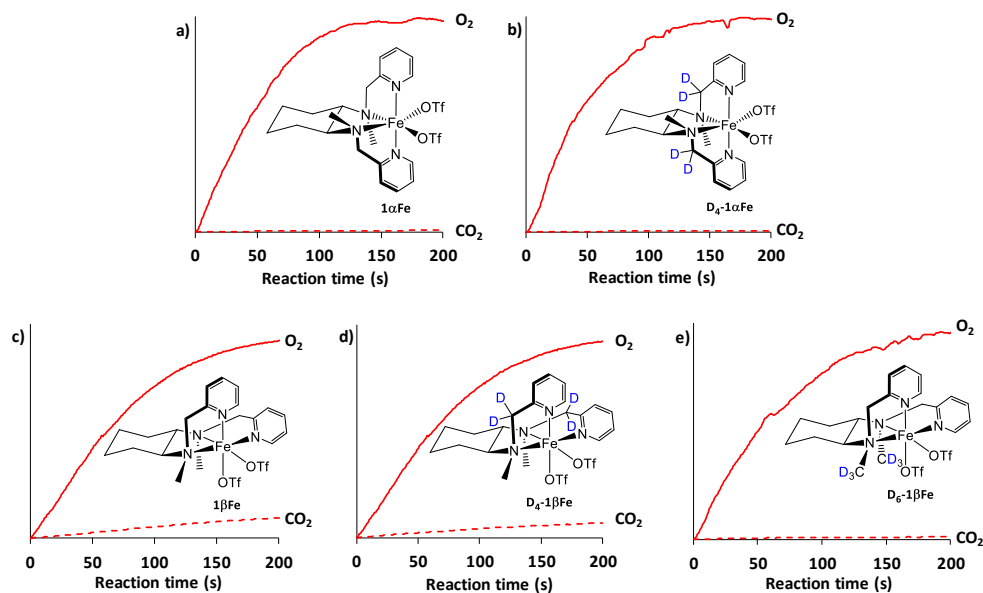
Figure III.7. Qualitative MS-online analysis (ion counting normalized for clarity) of the O_2 (straight line) and CO_2 (dashed line) evolved when CAN (75 equiv., 75 mM) is added to a strongly stirred solution of: a) **1αFe**, b) **D₄-1αFe**, c) **1βFe**, d) **D₄-1βFe** and e) **D₆-1βFe**, (final concentration 1 mM) in degassed Milli-Q water at 25ºC and pH 1. Results are the average of at least two duplicates.

III.3.2. Multiple oxidant addition experiments

The increase in TON (about 5-fold) obtained with **D₄-1α** with respect to **1α** nicely translates into substantially better yields of O₂ produced (76% *vs* 16%). However, this 5-fold increase appears modest when comparing the 10-fold improvement in the half-life time of **D₄-2α** in comparison with **2α.** Furthermore, while significant catalyst degradation is observed for **1α**, ligand recovery experiments showed minimum degradation of **D₄-1α.** This data let us consider that the end of catalytic activity observed in **D₄-1α** does not respond to a catalyst degradation process. Further optimization by lowering the catalyst concentration to 1 μM yields more than 3400 TON O₂ (see table 1, entry 12), which is about one order of magnitude higher than previously reported values with **1α** (table 1, entry 1). These observations indicate that the catalytic activity, at 12.5 μM, with the most robust catalyst of the series (**D₄-1α**) stops not as a result of catalyst degradation, but instead because of Nernstian effects in the Ce^{III}/Ce^{IV} ratio, which is related to the redox potential in solution (equation 1). Considering the ratio of $[Ce^{III}/Ce^{IV}]$ at which O₂ evolution stops after the first addition of CAN, we can determine a potential threshold of 1.62 V *vs* NHE for catalytic activity. The same value was consistently obtained when reactions were initiated with different amounts of CAN. Noticeable, this value is in reasonable agreement with the DFT computed value (1.73 V *vs* NHE) for the PCET from $[Fe^{IV}(O)(OH_2)(mep)]^{2+}$ to $[Fe^{V}(O)(OH)(mep)]^{2+}$ (mep = *N,N'*-bis(2-pyridylmethyl)-*N,N''*-dimethyl-1,2-diaminoethane),[38] suggesting that access to the active $Fe^{V}(O)(OH)$ oxidant becomes unfavorable at this $[Ce^{IV}]/[Ce^{III}]$ ratio.
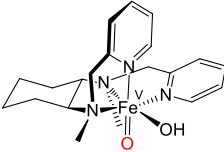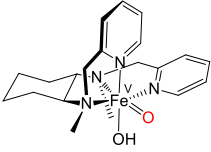
$$E = E^0 - \frac{R \cdot T}{n \cdot F} \cdot log\left(\frac{Ce^{III}}{Ce^{IV}}\right) \qquad (1)$$

III.3.3. DFT modeling of the decomposition pathways

DFT calculations have been conducted to evaluate the feasibility of the methylene/methyl oxidation mechanism by **1α** and **1β** topological isomers. The

geometry of the early proposed $Fe^V(O)(OH)$ WO active species, **3** was first optimized

for the two topological isomers (See *A.I.4. DFT modeling of the degradation paths*

and the catalytic cycle). In the case of **3β** complex, two *cis*-tautomers may exist in

which the $Fe^V=O$ moiety is parallel (**3β-a**) or perpendicular (**3β-b**) to the methyl

groups of the mcp ligand (Table 2). According to the free energy differences between

the β isomers, the intermediate **3β-a** in the S = 3/2 ground spin state is the most stable

form. Thus, **3β-a** was chosen to carry out the mechanistic study.

Table 2. Spin states relative free energies (kcal·mol^{-1}) of the $Fe^V(O)(OH)$ intermediates for complex **1β** in the two *cis*-tautomers **3β-a** and **3β-b.**

	3β-a	**3β-b**
S = 1/2	13.0	15.6
S = 3/2	0.0[a]	2.7

[a] Free energies respect to the most stable structure.

Both possible decomposition mechanisms were calculated for the α and β

isomers, that is: i) the oxidative degradation via methylene oxidation of the benzylic

positions; and ii) the oxidative degradation via *N*-methyl groups oxidation. The

methyl groups in **3β-a** are close to the oxo moiety (Figure III.8A). The latter together

with the experimental observations suggest that the decomposition of the mcp ligand

may start with the oxidation of a CH_3 group. Indeed, the $Fe^V=O$ in the quartet spin

state surface directly hydroxylates the CH_3 with a free energy barrier of 18.7

kcal·mol^{-1} with respect to β-[$Fe^V(O)(OH)(mcp)$]$^{2+}$ (**3β-a**) species, which can be

reached under catalytic conditions (See Figure III.8 and *A.I.4. DFT modelling of the*

degradation paths and the catalytic cycle for further details). This result is in good

agreement with the experimentally observed methyl decomposition product after the

decayed reaction mixture. Finally, the free energy profile for the O-O bond formation

was also calculated to determine if the decomposition reaction pathway prevails in solution (Figure III.10A). In this case, the water nucleophilic attack on the Fe^V=O moiety follows a stepwise mechanism, as has been described previously,[5] and the O-O bond formation event presents the highest in energy transition state ($\Delta G^{\ddagger} = 18.9$ kcal·mol^{-1}; Figure III.8A). The methyl oxidation barrier is only 1.2 kcal·mol^{-1} lower than the O-O bond formation one. These results suggest that the oxidation of the ligand may compete with the O-O bond formation event, providing a rational explanation for the origin of the reduced WO activity of **3β-a**.

For comparative reasons, the same calculations were performed also for **3α** (Figure III.8B). In this case, the methylene position is easier to oxidize ($\Delta G^{\ddagger} = 20.5$ kcal·mol^{-1}) than the methyl group ($\Delta G^{\ddagger} = 25.6$ kcal·mol^{-1}, see Figure A.I.9). This result is consistent with the methylene oxidation product detected by analysis of the decayed reaction mixture from **2α**. Most remarkably, in contrast with **3βa**, the transition state for the degradation path *via* oxidation of the methylene benzylic position is 3.1 kcal·mol^{-1} higher than the barrier for the O-O bond formation event (Figure III.8B). Therefore, computational studies indicate that nucleophilic attack of the water molecule over the electrophilic $Fe^V(O)$ species leading to the O-O bond formation is favored over ligand degradation via hydrogen atom transfer (HAT) from the benzylic C-H bond in **3α**. Instead, HAT from the *N*-Me group effectively competes with O-O bond formation in **3β-a.** This analysis has obvious consequences that are directly related with the experimental observations; i) **1α** is a more robust WOC than **1β**; ii) deuteration of the benzylic positions in **1α** protects its more sensitive site for ligand oxidation due to the stronger nature (ligand degradation becomes energetically more demanding) of the C-D over the C-H bond; iii) the most favorable site for ligand degradation in **1β** is the *N*-Me groups, and consistently, their deuteration limits the oxidative degradation and enhances its catalytic activity. Deuteration of the pseudobenzylic methylenes, in this case, does not have a positive effect because these positions are not the most favorable oxidizable sites.
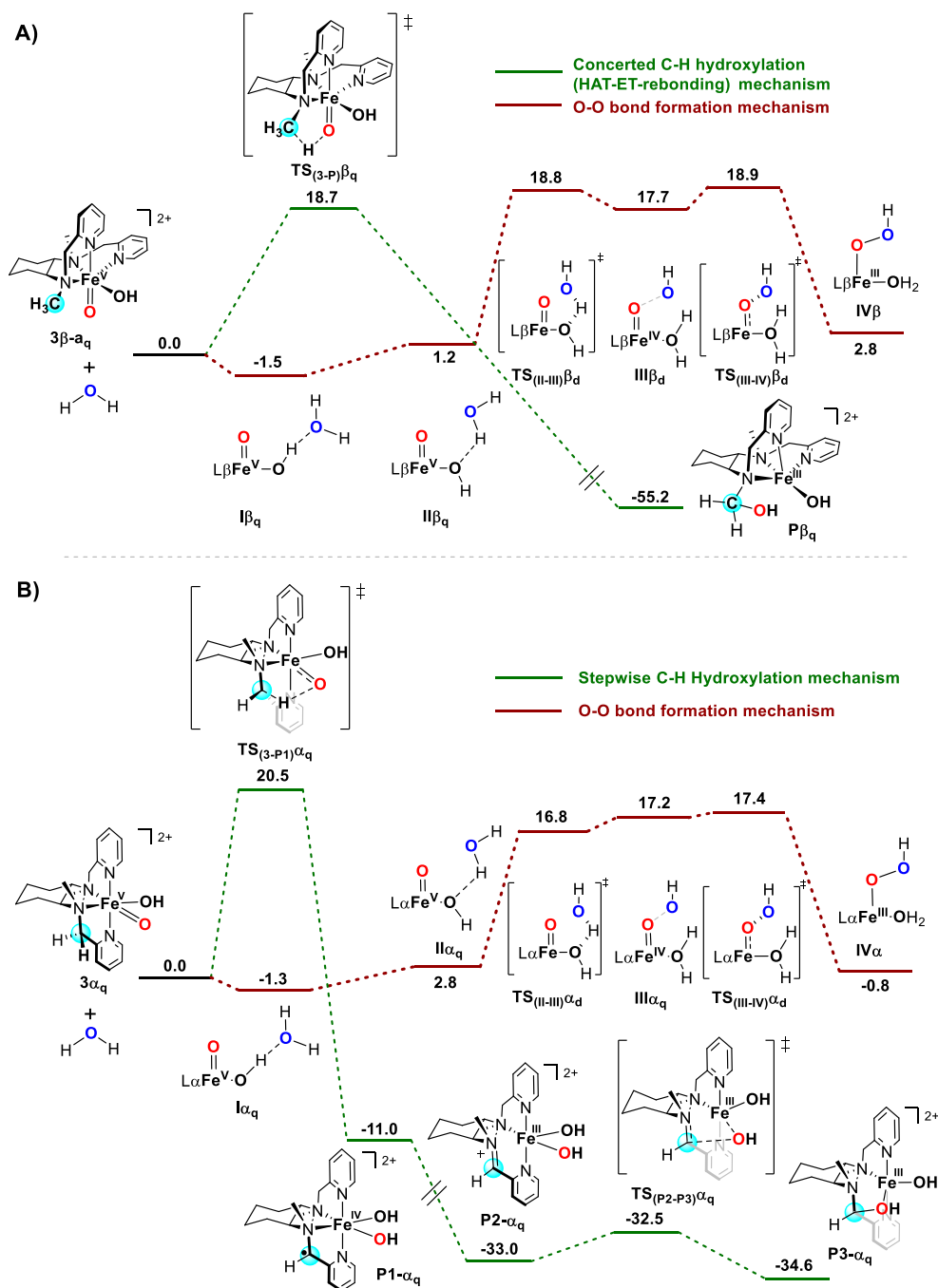
Figure III.8. A) Comparison between the O-O bond formation and methyl oxidation mechanisms for 3**β**a. B) Comparison between the O-O bond formation and methylene oxidation mechanisms for 3**α**. Gibbs energies are in kcal·mol^{-1}. L stands for the mcp ligand.

III.4. Conclusions

In this work, the deactivation paths for iron water oxidation catalysts **1α** and **1β** have been studied. High valent $Fe^{IV}(O)$ complexes **2α** and **2β** have been spectroscopically characterized, providing for the first time Mössbauer evidence for the implication of a high valent iron species in water oxidation reactions with homogeneous catalysts. **2α** and **2β** have been shown to degrade via processes that entail C-H oxidation of specific positions of the ligand. Interestingly, the locus of C-H oxidation is dependent on the nature of the catalyst, strongly suggesting that this is an intramolecular process, governed by the particular structure of the catalyst. Identification of the deactivation sites has been employed in the rational design of more robust catalysts by means of the deuteration of the ligand-sensitive sites.

In this regard, deuteration of the benzylic positions at **1α** leads to **D₄-1α**, which is an extraordinarily robust and active catalyst. Deuteration does not affect the water oxidation reaction rate nor the electronic nature of the catalyst, but the deuterated complex is more robust towards oxidation, maintaining the catalytic activity longer, and translating into larger TON > 3400 TON O_2, which represents the largest numbers for a 1st row TM. In addition, the lack of induction time in the O_2 evolution studies, and the much higher rate for O_2 evolution than for CO_2 production at initial reaction times strongly suggest that the catalytically active species is molecular. Under specific conditions, using the most robust **D₄-1α** complex, catalytic activity stops not because of catalyst degradation, but instead because of Nernst effects in the red-ox potential of the Ce^{III}/Ce^{IV} couple, setting a minimum redox potential in solution of 1.62 V for the generation of the water oxidation species with this catalyst.

III.5. Experimental section

III.5.1. Materials and reagents

Reagents and solvents used were commercially available and purchased from Panreac, Scharlau and Aldrich. Preparation and handling of air-sensitive materials

were carried out in a N_2 drybox (MBraun ULK 1000) with O_2 and H_2O concentrations < 1 ppm. Cerium(IV) ammonium nitrate (CAN) ≥99.99% trace metals basis and triflic acid were purchased from Sigma-Aldrich®. Solvents were purchased from SDS and Scharlab, purified and dried by passing through an activated alumina purification system (MBraun SPS-800). Water (18.2 MΩ·cm) was purified with a Milli-Q Millipore Gradient AIS system.

III.5.2. Physical methods and experimental procedures

UV-VIS-NIR spectra were recorded on an Agilent 8453 diode array spectrophotometer (190-1100 nm range) in 1 cm quartz cells. A cryostat from Unisoku Scientific Instruments was used for the temperature control.

High-Resolution Mass Spectra (HRMS) were recorded on a Bruker MicroTOF-Q IITM instrument with ESI or Coldspray ionization sources at Serveis Tècnics of the University of Girona. Samples were introduced into the mass spectrometer ion source by direct infusion using a syringe pump and were externally calibrated using sodium formate. The instrument was operated in the positive ion mode.

High-pressure liquid chromatography identification and quantification of ligand oxidation fragments. HPLC-MS analyses were performed with an Agilent Technologies 1200 HPLC system equipped with a G1315D DAD VL detector and coupled to a 6120 series-quadrupole analyzer. The instrument was operated in the positive ESI(+) ion mode. The HPLC conditions used were: Solvent A was 0.1% aqueous HCOOH and solvent B was 0.1% HCOOH in CH_3CN; 5-50% B linear gradient over 35 min at a flow rate of 1.0 mL/min. The analysis was carried out with a Kromasil 100 C18 (4.6 mm × 40 mm, 3.5 μm) column and the detection was performed at 247 nm (pyridine chromophore).

GC identification and quantification of dioxygen. An aliquot of gas captured from the headspace (100 μL) was analyzed with an Agilent 7820A GC

System equipped with columns Washed Molecular Sieve 5A, 2m x 1/8" OD, Mesh 60/80 SS and Porapak Q, 4m x 1/8" OD, SS. Mesh: 80/100 SS and a Thermal Conductivity Detector. The O_2 amount obtained was calculated by the difference between air-O_2 and reaction measured, considering N_2 as constant. O_2/N_2 calibration was performed using previously prepared different O_2/N_2 mixtures.

On-line MS monitoring experiments. The head space of the vial containing the reaction was monitored with an atmospheric pressure quadrupole mass spectrometer apparatus (Omnistar GSD 320 C Pfeiffer, m/z 28, 29, 30, 31, 32, 34, 36, 40, 44, 45, 46, 47, 48 and 49 were monitored).

General procedure employed in the chemically-driven WO reactions monitored by manometry (catalytic conditions, 1000 eq CAN). In a crimped 20 ml vial CAN (685.29 mg, 1000 eq, final concentration = 125 mM), was dissolved in Milli-Q water (9.5 mL) at room temperature leading to an orange solution. The head space of the vial containing the resulting solution was monitored with an atmospheric pressure sensor transducer. After equilibration of the pressure signal, complex **1αFe** (0.5 ml of a stock solution of 2 mg in 11.79 ml Milli-Q water, final concentration = 12.5 μM, the same concentration was used for all the studied complexes and the complexes derived from the ligand fragments, unless otherwise noticed) was added and the evolved gas was monitored along the reaction time. Then, an aliquot of the head space (150 μl) was analyzed in the GC-TCD to confirm the presence of O_2 and/or CO_2 in the head space. $V_{total}(H_2O) = 10$ mL.

General procedure employed in the chemically-driven WO reactions monitored by manometry (lower concentration of catalyst). In a crimped 20 ml vial CAN (1.03 g, 1000 eq, final concentration = 125 mM), was dissolved in Milli-Q water (14.5 mL) at room temperature leading to an orange solution. The head space of the vial containing the resulting solution was monitored with an atmospheric pressure sensor transducer. After equilibration of the pressure signal, complex **1αFe** (0.5 ml of a stock solution of 0.2 mg in 9.8 ml Milli-Q water, final concentration = 1

µM, unless otherwise noticed) was added and the evolved gas was monitored along the reaction time. Then, an aliquot of the head space (150 µl) was analyzed in the GC-TCD to confirm the presence of O_2 and/or CO_2 in the head space. $V_{total}(H_2O) =$ 15 mL.

General procedure employed in the chemically-driven WO reactions in the conditions used for the decay UV-vis studies monitored by manometry (75 eq. CAN). In a crimped 10 ml vial complex **1αFe** (2.71 mg, $4 \cdot 10^{-3}$ mmol, final concentration = 1 µM) was dissolved in degassed Milli-Q water (3.2 mL) at room temperature leading to a pale greenish solution. The head space of the vial containing the resulting solution was monitored with an atmospheric pressure sensor transducer. After equilibration of the pressure signal, CAN (75 eq, 0.8 ml of a solution of CAN (205.58 mg, 0.3 mmol, final concentration = 75 mM), in HOTf:Milli-Q (3:10) (1 mL, degassed)) was added and the evolved gas was monitored for 300 s (5 minutes) after which time an aliquot of the head space (150 µl) was analyzed in the GC-TCD confirming the presence of O_2. $V_{total}(H_2O) = 3.2$ mL, $V_{total}(HOTf:Milli-Q (3:10)) =$ 0.8 mL. $V_{final} = 4.0$ mL.

General procedure employed in the chemically-driven WO reactions monitored by online GC-MS (75 eq. CAN). In a crimped 10 ml vial complex **1αFe** (2.71 mg, $4 \cdot 10-3$ mmol, final concentration = 1 mM, the same concentration was used for all the studied complexes unless otherwise indicated) was dissolved in degassed Milli-Q water (3.2 mL) at room temperature leading to a pale greenish solution. The reaction vial was connected to an atmospheric pressure quadrupole mass spectrometer apparatus (Omnistar GSD 320 C Pfeiffer). After equilibration of the MS signal, CAN (75 equiv., 0.8 ml of a solution of CAN (205.58 mg, 0.3 mmol, final concentration = 75 mM), in HOTf:Milli-Q (3:10) (1 mL, degassed)) was added and the reaction was monitored (m/z 28, 29, 30, 31, 32, 34, 36, 40, 44, 45, 46, 47, 48 and 49 were monitored) for 300 s (5 minutes). $V_{total}(H_2O) = 3.2$ mL, $V_{total}(HOTf:Milli-Q (3:10)) = 0.8$ mL. $V_{final} = 4.0$ mL.

III.5.3. Computational details

Density functional theory (DFT) calculations were performed with the Gaussian09 software package.[48] All geometries were optimized with the hybrid B3LYP exchange-correlation functional,[49-51] using the 6-31G* 6d basis set for all atoms. The solvent effect of water was included in the geometry optimizations using the polarizable continuum IEFPCM-SMD model of Truhlar and coworkers.[52] The nature of the stationary points was confirmed by a vibrational analysis, where minima have no imaginary frequencies and transition states have only one. Intrinsic reaction coordinate (IRC) calculations were performed with Gaussian at B3LYP/6-31G* 6d basis set for all atoms level of theory.

The potential energies were further refined by single point calculations on B3LYP geometries with the dunning cc-pVTZ 6d basis set, including solvent effects ($E_{cc\text{-}pVTZ}$). Dispersion effects were also introduced through the Grimme-D_2 correction ($E_{disp.}$).[53] This combination of different levels of theory for geometry optimizations and free energies evaluation has been previously used to explore the water oxidation reaction mechanism by a group of non-heme iron complexes, reproducing the observed reactivity trends.[38]

The final free energies (G) were computed as:

$$G = E_{cc\text{-}pVTZ} + G_{corr} + E_{disp.} \quad (1)$$

where the G_{corr} term includes the thermal corrections obtained from the thermostatistical analysis in the solvent phase. The free energy change associated with moving from a standard-state gas phase pressure of 1 atm to a standard state gas phase concentration of 1 M for solutes was also included in the final free energy differences.[54] For the explicit solvent water molecules, a 55.6 M standard state was employed. The free energy associated with the phase change is 1.9 kcal·mol⁻¹ for 1 M standard state solutes and 4.3 kcal·mol⁻¹ for 55.6 M standard state explicit water molecules.

III.6. References

(1)   Blakemore, J. D.; Crabtree, R. H.; Brudvig, G. W. *Chem. Rev.* **2015**, *115*, 12974.
(2)   Karkas, M. D.; Verho, O.; Johnston, E. V.; Akermark, B. *Chem. Rev.* **2014**, *114*, 11863.
(3)   Meyer, T. J.; Sheridan, M. V.; Sherman, B. D. *Chem. Soc. Rev.* **2017**, *46*, 6148.
(4)   Blakemore, J. D.; Crabtree, R. H.; Brudvig, G. W. *Chem. Rev.* **2015**, *115*, 12974.
(5)   Stracke, J. J.; Finke, R. G. *ACS Catal.* **2014**, *4*, 909.
(6)   Fukuzumi, S.; Jung, J.; Yamada, Y.; Kojima, T.; Nam, W. *Chem.—Asian J.* **2016**, *11*, 1138.
(7)   Crabtree, R. H. *Chem. Rev.* **2015**, *115*, 127.
(8)   Zuccaccia, C.; Bellachioma, G.; Bortolini, O.; Bucci, A.; Savini, A.; Macchioni, A. *Chem. Eur. J.* **2014**, *20*, 3446.
(9)   Fukuzumi, S.; Hong, D. C. *Eur. J. Inorg. Chem.* **2014**, 645.
(10)   Li, J.; Güttinger, R.; Moré, R.; Song, F.; Wan, W.; Patzke, G. R. *Chem. Soc. Rev.* **2017**, *46*, 6124.
(11)   Wu, X.; Li, F.; Zhang, B.; Sun, L. *J. Photochem. Photobiol., C* **2015**, *25*, 71.
(12)   Macchioni, A. *Eur. J. Inorg. Chem.* **2018**.
(13)   Parent, A. R.; Sakai, K. *ChemSusChem* **2014**, *7*, 2070.
(14)   Hunter, B. M.; Gray, H. B.; Muller, A. M. *Chem. Rev.* **2016**, *116*, 14120.
(15)   Singh, A.; Spiccia, L. *Coordination Chemistry Reviews* **2013**, *257*, 2607.
(16)   Najafpour, M. M.; Renger, G.; Holynska, M.; Moghaddam, A. N.; Aro, E. M.; Carpentier, R.; Nishihara, H.; Eaton-Rye, J. J.; Shen, J. R.; Allakhverdiev, S. I. *Chem. Rev.* **2016**, *116*, 2886.
(17)   Karkas, M. D.; Akermark, B. *Dalton. Trans.* **2016**, *45*, 14421.
(18)   Codola, Z.; Gomez, L.; Kleespies, S. T.; Que, L., Jr.; Costas, M.; Lloret-Fillol, J. *Nat. Commun.* **2015**, *6*.
(19)   Codolà, Z.; Garcia-Bosch, I.; Acuña-Parés, F.; Prat, I.; Luis, J. M.; Costas, M.; Lloret-Fillol, J. *Chem. Eur. J.* **2013**, *19*, 8042.
(20)   Fillol, J. L.; Codolà, Z.; Garcia-Bosch, I.; Gómez, L.; Pla, J. J.; Costas, M. *Nature Chemistry* **2011**, *3*, 807.
(21)   Tan Peng, K. H.-K. L. T.-C. *ChemComm* **2014**, *50*, 12779.
(22)   Chen, G.; Chen, L.; Ng, S. M.; Man, W. L.; Lau, T. C. *Angew. Chem. Int. Ed.* **2013**, *52*, 1789.
(23)   To, W.-P.; Wai-Shan Chow, T.; Tse, C.-W.; Guan, X.; Huang, J.-S.; Che, C.-M. *Chemical Science* **2015**, *6*, 5891.
(24)   Hong, D.; Mandal, S.; Yamada, Y.; Lee, Y. M.; Nam, W.; Llobet, A.; Fukuzumi, S. *Inorganic Chemistry* **2013**, *52*, 9522.
(25)   Das, B.; Lee, B.-L.; Karlsson, E. A.; Akermark, T.; Shatskiy, A.; Demeshko, S.; Liao, R.-Z.; Laine, T. M.; Haukka, M.; Zeglio, E.; Abdel-Magied, A. F.; Siegbahn, P. E. M.; Meyer, F.; Karkas, M. D.; Johnston, E. V.; Nordlander, E.; Akermark, B. *Dalton. Trans.* **2016**, *45*, 13289.
(26)   Wickramasinghe, L. D.; Zhou, R.; Zong, R.; Vo, P.; Gagnon, K. J.; Thummel, R. P. *J. Am. Chem. Soc.* **2015**, *137*, 13260.
(27)   Coggins, M. K.; Zhang, M.-T.; Vannucci, A. K.; Dares, C. J.; Meyer, J. *J. Am Chem. Soc.* **2014**, *136*, 5531−5534.
(28)   Marelius, D. C.; Bhagan, S.; Charboneau, D. J.; Schroeder, K. M.; Kamdar, J. M.; McGettigan, A. R.; Freeman, B. J.; Moore, C. E.; Rheingold, A. L.; Cooksy, A. L.; Smith, D. K.; Paul, J. J.; Papish, E. T.; Grotjahn, D. B. *Eur. J. Inorg. Chem.* **2014**, 676.
(29)   Klepser, B. M.; Bartlett, B. M. *J. Am. Chem. Soc.* **2014**, *136*, 1694.
(30)   Panchbhai, G.; Singh, W. M.; Das, B.; Jane, R. T.; Thapper, A. *Eur. J. Inorg. Chem.* **2016**, *2016*, 3262.
(31)   Najafpour, M. M.; Safdari, R.; Ebrahimi, F.; Rafighi, P.; Bagheri, R. *Dalton. Trans.* **2016**, *45*, 2618.
(32)   Annunziata, A.; Esposito, R.; Gatto, G.; Cucciolito, M. E.; Tuzi, A.; Macchioni, A.; Ruffo, F. *Eur. J. Inorg. Chem.* **2018**, *2018*, 3304.
(33)   Das, B.; Orthaber, A.; Ott, S.; Thapper, A. *ChemSusChem* **2016**, *9*, 1178.
(34)   Coggins, M. K.; Zhang, M.-T.; Vannucci, A. K.; Dares, C. J.; Meyer, T. J. *J. Am. Chem. Soc.* **2014**, *136*, 5531.
(35)   Kottrup, K. G.; Hetterscheid, D. G. H. *Chem. Commun.* **2016**, *52*, 2643.
(36)   Wang, Z.-Q.; Wang, Z.-C.; Zhan, S.; Ye, J.-S. *Applied Catalysis A: General* **2015**, *490*, 128.

(37) Kottrup, K. G.; D'Agostini, S.; van Langevelde, P. H.; Siegler, M. A.; Hetterscheid, D. G. H. *ACS Catal.* **2018**, *8*, 1052.

(38) Acuna-Pares, F.; Codola, Z.; Costas, M.; Luis, J. M.; Lloret-Fillol, J. *Chem. Eur. J.* **2014**, *20*, 5696.

(39) Casadevall, C.; Bucci, A.; Costas, M.; Lloret-Fillol, J. In *Adv. Inorg. Chem.*; Academic Press: 2019.

(40) Yoshida, M.; Masaoka, S.; Abe, J.; Sakai, K. *Chem.—Asian J.* **2010**, *5*, 2369.

(41) Kimoto, A.; Yamauchi, K.; Yoshida, M.; Masaoka, S.; Sakai, K. *Chem. Commun.* **2012**, *48*, 239.

(42) Stull, J. A.; Britt, R. D.; McHale, J. L.; Knorr, F. J.; Lymar, S. V.; Hurst, J. K. *J. Am. Chem. Soc.* **2012**, *134*, 19973.

(43) Bucci, A.; Menendez Rodriguez, G.; Bellachioma, G.; Zuccaccia, C.; Poater, A.; Cavallo, L.; Macchioni, A. *ACS Catal.* **2016**, *6*, 4559.

(44) Acuña-Parés, F.; Costas, M.; Luis, J. M.; Lloret-Fillol, J. *Inorganic Chemistry* **2014**, *53*, 5474.

(45) Sala, X.; Maji, S.; Bofill, R.; García-Antón, J.; Escriche, L.; Llobet, A. *Acc. Chem. Res.* **2014**, *47*.

(46) Codolà, Z.; Gamba, I.; Acuña-Parés, F.; Casadevall, C.; Clémancey, M.; Latour, J.-M.; Luis, J. M.; Lloret-Fillol, J.; Costas, M. *J. Am. Chem. Soc.* **2019**, *141*, 323.

(47) Garcia-Bosch, I.; Company, A.; Frisch, J. R.; Torrent-Sucarrat, M.; Cardellach, M.; Gamba, I.; Guell, M.; Casella, L.; Que, L.; Ribas, X.; Luis, J. M.; Costas, M. *Angew Chem. Int. Ed.* **2010**, *49*, 2406.

(48) Gaussian 09, R. A., M. J. Frisch, G. W. Trucks, H. B. Schlegel, G. E. Scuseria, M. A. Robb, J. R. Cheeseman, G. Scalmani, V. Barone, B. Mennucci, G. A. Petersson, H. Nakatsuji, M. Caricato, X. Li, H. P. Hratchian, A. F. Izmaylov, J. Bloino, G. Zheng, J. L. Sonnenberg, M. Hada, M. Ehara, K. Toyota, R. Fukuda, J. Hasegawa, M. Ishida, T. Nakajima, Y. Honda, O. Kitao, H. Nakai, T. Vreven, J. A. Montgomery, Jr., J. E. Peralta, F. Ogliaro, M. Bearpark, J. J. Heyd, E. Brothers, K. N. Kudin, V. N. Staroverov, R. Kobayashi, J. Normand, K. Raghavachari, A. Rendell, J. C. Burant, S. S. Iyengar, J. Tomasi, M. Cossi, N. Rega, J. M. Millam, M. Klene, J. E. Knox, J. B. Cross, V. Bakken, C. Adamo, J. Jaramillo, R. Gomperts, R. E. Stratmann, O. Yazyev, A. J. Austin, R. Cammi, C. Pomelli, J. W. Ochterski, R. L. Martin, K. Morokuma, V. G. Zakrzewski, G. A. Voth, P. Salvador, J. J. Dannenberg, S. Dapprich, A. D. Daniels, Ö. Farkas, J. B. Foresman, J. V. Ortiz, J. Cioslowski, and D. J. Fox, Gaussian, Inc., Wallingford CT. **2009**.

(49) Becke, A. D. *J Chem Phys* **1993**, *98*, 5648.

(50) Becke, A. D. *J Chem Phys* **1993**, *98*, 1372.

(51) Lee, C.; Yang, W.; Parr, R. G. *Physical Review B* **1988**, *37*, 785.

(52) C. J. Cramer, A. V. M., D. G. Truhlar *J. Phys. Chem. B* **2009**, *113*, 6378.

(53) Grimme, S. *J. Comput. Chem.* **2006**, *27*, 1787.

(54) C. P. Kelly, C. J. C., D. G. Truhlar, *J. Phys. Chem. A* **2006**, *110*, 2493

UNIVERSITAT ROVIRA I VIRGILI
MECHANISTIC STUDIES OF WATER OXIDATION CATALYZED BY HOMOGENEOUS IRON AND RUTHENIUM
COMPLEXES AND LIGHT-DRIVEN ORGANIC REDUCTIONS WITH A DUAL COBALT/COPPER CATALYTIC SYSTEM
Carla Casadevall Serrano

CHAPTER IV

Mechanistic Investigations of Water Oxidation Catalyzed by Ru Complexes Based on Aminopyridyl Ligands
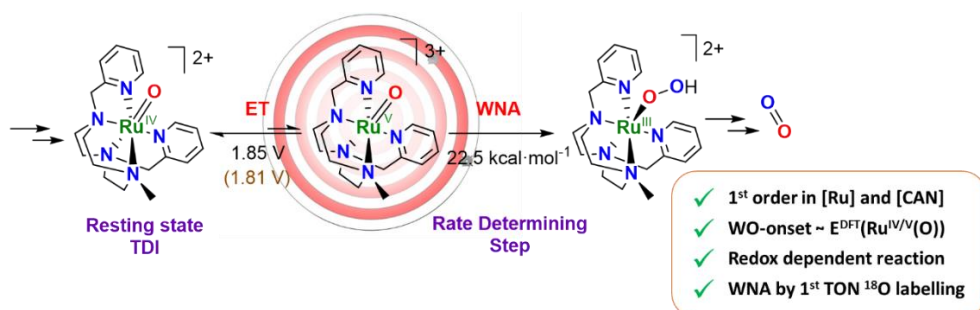
Part of this chapter corresponds to the following publication:

"Spectroscopic, Electrochemical and Computational Characterization of Ru Species Involved in Catalytic Water Oxidation: Evidence for a [Ru^V(O)(Py$_2$Metacn)] Intermediate"

C. Casadevall, Z. Codola, M. Costas, J. Lloret-Fillol: Chem. Eur. J.; 2016, 22 (29), 10111.

MECHANISTIC STUDIES OF WATER OXIDATION CATALYZED BY HOMOGENEOUS IRON AND RUTHENIUM
COMPLEXES AND LIGHT-DRIVEN ORGANIC REDUCTIONS WITH A DUAL COBALT/COPPER CATALYTIC SYSTEM

Carla Casadevall Serrano

IV. Mechanistic Investigations of Water Oxidation Catalyzed by Ru Complexes Based on Aminopyridyl Ligands

IV.1. General insight

Fundamental understanding of metal-catalysed water-oxidation (WO) mechanisms on a molecular scale is essential for its development and catalyst design.[1-9] In this line, mechanistic understanding of WO reactions very much benefit from the study of molecular catalysts that operate under homogeneous conditions. Several metal complexes of Ru,[10-13] Ir,[14-18] Mn,[19,20] Fe,[21-32] Co[33-38] and Cu[39-41] have been developed and studied to this end.[2]

In the family of monometallic ruthenium complexes with neutral ligands, after building up the right oxidation state at the metal centre two main O-O bond formation mechanisms have been elucidated: i) a water nucleophilic attack to a M(O) group forming a metal hydroperoxo species; and ii) a direct coupling of two M(O) groups forming a metal peroxo species (Scheme IV.1).[1,42] The O-O bond formation usually is identified as the rate-determining step, which is also responsible for the viability of the entire process. Although there is a collective agreement that for ruthenium complexes based on neutral nitrogen ligands the active species that leads to the O-O formation is the high oxidation state $Ru^V(O)$,[4] the evidence is not fully conclusive. Recently, an alternative scenario has been proposed, which is the formation of an O-O through a WNA (Water Nucleophilic Attack) coupled with an electron transfer, being the active species $Ru^{IV}(O)$.[43] This alternative mechanism under debate has the benefit to *bias* the need for reaching the high oxidation state of Ru^V. This viable alternative is in line with the mounting evidence of the existence of Ru-Ce[44-47] and Fe-Ce[22-24] complexes when Ce^{IV} is used as sacrificial oxidant, and therefore deserves some attention. The need for additional insights on the oxidation state responsible for the O-O bond formation in ruthenium complexes encourages us to explore strongly

chelating and basic neutral ligands previously successfully employed to study iron high oxidation states.[44,48-53]

Direct Coupling mechanism (DC)
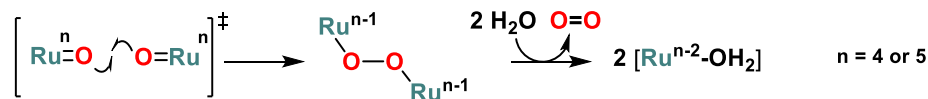
Acid Base mechanism (WNA)
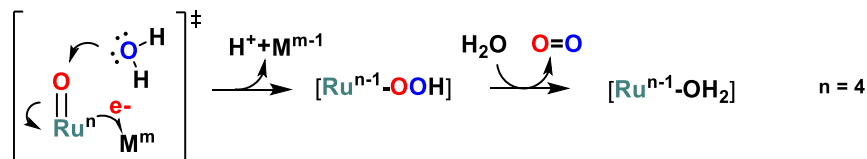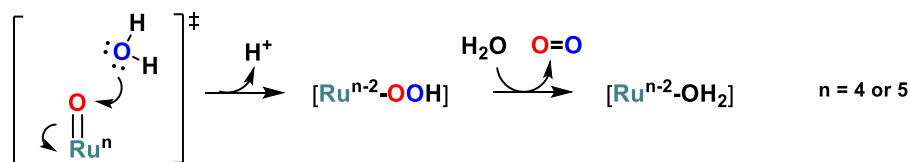
Coulpled Electron Transfer

Scheme IV.1. Main discussed mechanisms for the O-O bond formation.

Iron complexes have been also shown to be an excellent alternative as molecular WO catalysts to study the operating mechanism.[21-27,49,54,55] In particular, iron complexes based on the 1,4,7-tryazacyclononane (tacn) moiety have been proved to be very robust and stable towards ligand oxidation.[55-58] Furthermore, tacn based ligands are highly modular and can stabilise high oxidation states. Proof of that is the development of excellent catalysts for selective oxidation catalysis with either first or second row transition metals.[22,23,56,58-61] Some examples of ruthenium complexes based on the tacn fragment have been confirmed as active catalysts in olefin epoxidation,[62] dihydroxylation to *cis*-diols[63-66] and C-H oxidation when using Cerium(IV) ammonium nitrate (CAN) as oxidant.[67]

UNIVERSITAT ROVIRA I VIRGILI
MECHANISTIC STUDIES OF WATER OXIDATION CATALYZED BY HOMOGENEOUS IRON AND RUTHENIUM
COMPLEXES AND LIGHT-DRIVEN ORGANIC REDUCTIONS WITH A DUAL COBALT/COPPER CATALYTIC SYSTEM
Carla Casadevall Serrano

CHAPTER IV   Mechanistic Investigations of WO Catalyzed by Ru Complexes
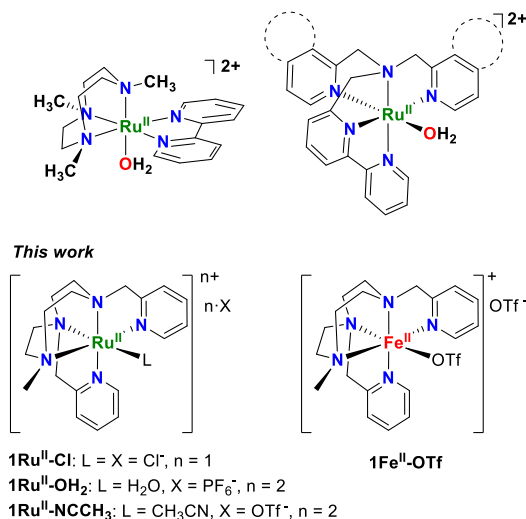
Figure IV.1. Top: selected aminopyridine ruthenium complexes previously studied for chemical mediated water oxidation. Bottom: ruthenium and iron complexes studied in this work.

Sakai *et al.* studied the catalytic water oxidation activity of the *N*-pentacoordinated $[Ru(Me_3\text{-}tacn)(bpy)(H_2O)]^{2+}$ complex ($Py_2^{Me}tacn$ = *N*-methyl-*N,N*-bis(2-picolyl)-1,4,7-triazacyclononane) (bpy = bipyridine), affording up to 148 TON after 40 h (with 3.6 h^{-1} TOF) when using CAN as sacrificial oxidant.[47] On the other hand, X. Zhao and C. E. Webster *et al*[68] reported a remarkable difference in activity between *N*-pentacoordinated $[Ru(DPA\text{-}Bpy)(H_2O)]^{2+}$ (DPA-Bpy = N,N-bis(2-pyridinylmethyl)-2,2'-bipyridine-6-methanamine) (c.a. 20 TON) and *N*-tetracoordinated complexes $[Ru(Me_3TPA)(H_2O)_2]^{2+}$ (TPA = tris(2-pyridylmethyl)amine) (< 1 TON) and $[Ru(TPA)(H_2O)_2]^{2+}$ (c.a. 2 TON) virtually inactive in WO. On the contrary, we have observed that *cis*-labile iron complexes with *N*-tetradentate ligands are highly active for water oxidation while *N*-pentacoordinated complexes, such as $[Fe^{II}(OTf)(Py_2^{Me}CH\text{-}tacn)](OTf)$, are not active when using CAN nor NaIO$_4$ as chemical oxidants. Nevertheless, under catalytic conditions the $[Fe^{IV}(O)(Py_2^{Me}CH\text{-}tacn)]^{+2}$ species is formed in high yield with a half-life time higher than 2 days at room temperature without evidence of O$_2$ evolution.[22,23,49]

Motivated by the differences between iron and ruthenium water oxidation catalysis we have studied new pentadentate ruthenium complexes based on our previous reports on pentadentate iron complexes. Herein we report the new $[Ru^{II}Cl(Py_2^{Me}tacn)]Cl$ (**1Ru^{II}-Cl**), $[Ru^{II}(OH_2)(Py_2^{Me}tacn)](PF_6)_2$ (**1Ru^{II}-OH$_2$**), and $[Ru^{II}(NCCH_3)(Py_2^{Me}tacn)](OTf)_2$ (**1Ru^{II}-NCCH$_3$**) ($Py_2^{Me}tacn = $ *N*-methyl-*N,N*-bis(2-picolyl)-1,4,7-triazacyclononane) pentadentate complexes (Figure IV.1). We have studied the WO activity and the mechanism of these new homogeneous ruthenium water oxidation catalysts. We also provide insights for the sharp differences in reactivity between the *N*-pentacoordinated iron and ruthenium complexes, as well as new kinetic and thermodynamic evidence for the need of Ru^V species in the O-O bond formation.

IV.2. Results and discussion

IV.2.1. Synthesis and characterization of a new family of ruthenium complexes with tacn-based derivative ligands

The pentadentate nitrogen donating ligand $Py_2^{Me}tacn$ was synthesised following the described procedure, by functionalization of the basic 1,4,7-triazacyclononane (tacn) structure as it is shown in Figure IV.2.[69] Complex $[Ru^{II}Cl(Py_2^{Me}tacn)]Cl$ (**1Ru^{II}-Cl**) was obtained by equimolar reaction of $Py_2^{Me}tacn$ with $RuCl_2(dmso)_4$ in refluxing ethanol during 24 h under N_2 atmosphere. The ^{1}H nuclear magnetic resonance spectrum (^{1}H-NMR) of **1Ru^{II}-Cl** in CDCl$_3$ presented new signals that expand from 0 to 14 ppm, which is indicative of a diamagnetic low-spin d^6 Ru^{II} centre. Based on the 8 new ^{1}H-NMR signals, with the same relative intensities, found in the aromatic region (6.9-9.4 ppm) we determined that upon coordination to the ruthenium centre the ligand is desymmetrized leading to two inequivalent pyridines. In addition, the characteristic high downfield peak at 9.23 ppm is an indication of an ortho-pyridine proton influenced by a coordinated ruthenium center (see Figure A.I.1). Bidimensional NMR (2D-NMR correlation spectra (See Figure A.I.2-5) are also in agreement with the formation of **1Ru^{II}-Cl**

complex. Finally, a cryospray high resolution mass spectrometric (CSI-HRMS) analysis of the bulk solid dissolved in water showed a molecular peak at m/z 462.1014 with the same m/z and pattern as the simulated for $[Ru^{II}Cl(Py_2^{Me}tacn)]^+$ (Figures A.I.6-7).

In addition, orange crystals suitable for single crystal X-ray diffraction were obtained by slow diffusion of Et$_2$O into a CH$_2$Cl$_2$ solution of the complex at room temperature (Figure IV.3). The X-ray diffraction data was refined as a racemic twin in the space group P2$_1$. The X-ray structure confirms the spectroscopic assignment in solution. The complex contains a Ru^{II} metal center coordinated to a Py$_2^{Me}$tacn pentadentate ligand, and a chloride anion in an octahedral environment. Distances between the ruthenium atom and the coordination environment are in the expected range for a polypyridine amine ruthenium(II) complex with a S = 0 spin state (d(Ru-Cl) = 2.454 (2) Å and d(Ru-N) = 2.056 (6) – 2.124 (5) (Å).
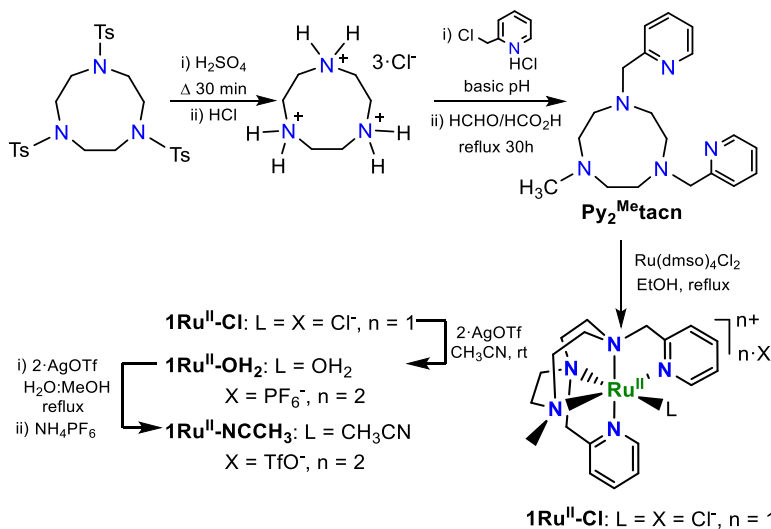
Figure IV.2. Synthetic pathway for the preparation of the Py$_2^{Me}$tacn ligand and the derivative ruthenium complexes.[68,70]
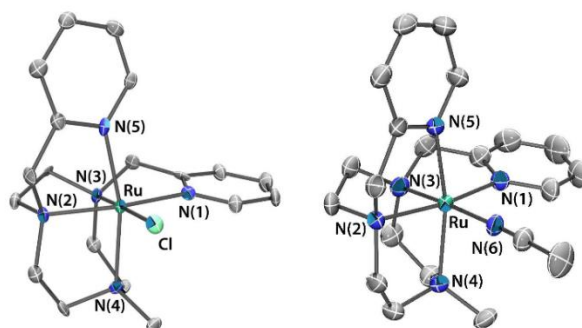
Figure   IV.3.   Thermal   ellipsoid   plot   of   **1Ru^{II}-Cl**   (50%   probability,
([RuCl(Py$_2^{Me}$tacn)]Cl)$_2$(H$_2$O)$_2$(CH$_2$Cl$_2$)$_3$)   and   **1Ru^{II}-NCCH$_3$**   (30%   probability,
[Ru(NCCH$_3$)(Py$_2^{Me}$tacn)](OTf)$_2$). Hydrogen atoms, solvent molecules and counterions have been
omitted for clarity. Selected bond lengths [Å] and angles [º] for **1Ru^{II}-Cl**: Ru-Cl 2.454(2), Ru-N(1)
2.056(6), Ru-N(2) 2.078(7), Ru-N(3) 2.072(7), Ru-N(4) 2.124(6), Ru-N(5) 2.082(7), N(1)-Ru-N(2)
167.7(3), N(3)-Ru-Cl 178.1(2), N(4)-Ru-N(5) 164.2(3). Selected bond lengths [Å] and angles [º] for
1Ru^{II}-NCCH$_3$: Ru-N(1) 2.072(4), Ru-N(2) 2.072(4), Ru-N(3) 2.065(5), Ru-N(4) 2.116(4), Ru-N(5)
2.070(4), Ru-N(6) 2.027(4), N(1)-Ru-N(2) 166.6(2), N(3)-Ru-N(6) 177.0(2), N(4)-Ru-N(5) 165.9(2).

Complex [Ru^{II}(OH$_2$)(Py$_2^{Me}$tacn)](PF$_6$)$_2$ (**1Ru^{II}-OH$_2$**) was prepared by reaction
of **1Ru^{II}-Cl** with AgOTf in refluxing MeOH:H$_2$O followed by precipitation with
NH$_4$PF$_6$ in water. In addition, the replacement of the chloride anion by acetonitrile
yielded complex [Ru^{II}(CH$_3$CN)(Py$_2^{Me}$tacn)](OTf)$_2$ (**1Ru^{II}-NCCH$_3$**), which was also
studied to compare the effect of the auxiliary ligand (Cl$^-$, H$_2$O and CH$_3$CN) in
catalysis. NMR studies of the new obtained complexes are in agreement with the
formation of the expected products (See Figures A.I.8-11 and 13-17). CSI-HRMS
analysis of **1Ru^{II}-OH$_2$** shows a base peak at m/z 227.5681 corresponding to
[Ru^{II}(Py$_2^{Me}$tacn)N$_2$]$^{+2}$. The formation of the N$_2$ adduct in the ionization environment
of the spectrometer (T = 25 ºC) suggests that the water molecule attached to the metal
centre is quite labile under the ionization conditions. In the case of **1Ru^{II}-NCCH$_3$**,
CSI-HRMS analysis shows a molecular peak at m/z 234.0794 corresponding to
[Ru^{II}(CH$_3$CN)(Py$_2^{Me}$tacn)]$^{2+}$, corroborating the formation of a dicationic complex.
Besides, a prominent peak at m/z 227.5689 is also observed for **1Ru^{II}-NCCH$_3$** (See
Figures S.I.12 and 19). The bulk solid composition is also in agreement with the
characterization as judged by the elemental analysis of both complexes. Finally,
yellow crystals of **1Ru^{II}-NCCH$_3$** suitable for X-ray diffraction studies were grown

UNIVERSITAT ROVIRA I VIRGILI
MECHANISTIC STUDIES OF WATER OXIDATION CATALYZED BY HOMOGENEOUS IRON AND RUTHENIUM
COMPLEXES AND LIGHT-DRIVEN ORGANIC REDUCTIONS WITH A DUAL COBALT/COPPER CATALYTIC SYSTEM
Carla Casadevall Serrano

CHAPTER IV   Mechanistic Investigations of WO Catalyzed by Ru Complexes

from slow diffusion of Et_2O in CH_3CN at room temperature (See Figure IV.3). The X-ray structure shows an octahedral Ru^{II} metal center coordinated to a $Py_2^{Me}tacn$ pentadentate ligand and an acetonitrile molecule (d(Ru-N) = 2.027(4) – 2.116(4) Å) as was also established by the spectroscopic assignment in solution.

IV.2.2. Water oxidation catalytic trials

The oxygen evolution catalytic activity of **$1Ru^{II}$-Cl**, **$1Ru^{II}$-OH_2** and **$1Ru^{II}$-$NCCH_3$** was tested using CAN and $NaIO_4$ as sacrificial oxidants in pure Milli-Q water (Table IV.1, Tables A.I.1-2).[22,23] Although the three ruthenium complexes only differ in the monocoordinated ligand, this has a pronounced effect in the catalytic outcome. The chloride **$1Ru^{II}$-Cl** complex (35 μM) yielded 19 ± 2 TON of O_2 when using CAN (125 mM). Analysis of the gas at the reaction headspace by gas chromatography (GC) showed that the main product was O_2, while CO_2 formation was negligible. The replacement of the chloride anion by an aquo ligand (**$1Ru^{II}$-OH_2**) leads to almost three- and a four-fold increase in the total amount of O_2 generated (51 ± 2 TON) and reaction rate ($4 \cdot 10^{-3}$ TOF), respectively. Similar results were obtained for **$1Ru^{II}$-Cl** in the presence of AgOTf, suggesting that the chloride anion is scavenged and exchanged by water. Indeed, when heating the stock solution of the catalyst (3 h at 60 ºC) prior starting the reaction, a significant increase in the TON was obtained (43 ± 4, see Table A.I.3). However, the chloride-water exchange is relatively slow as judged by NMR (See Figure IV.s 4 and A.I.20). After two hours in D_2O there is still around 27% of **$1Ru^{II}$-Cl** and exchange does not proceed further. This is in agreement with the observed differences in reactivity.[71] On the other hand, insignificant amounts of O_2 (1 ± 1 TON) were detected when **$1Ru^{II}$-$NCCH_3$** was tested under standard catalytic conditions. This suggests that even a small quantity of a co-solvent such as acetonitrile can extinguish the catalytic activity, and caution should be taken with similar ruthenium complexes. Indeed, the preparation of a stock solution of **$1Ru^{II}$-OH_2** in CH_3CN or the addition of 200 eq of CH_3CN drops to zero

its catalytic activity. Even the addition of only one equivalent of CH_3CN reduces the catalytic activity to half (Table A.I.3).

Table IV.1. Selected WO catalytic tests for complexes $[Ru^{II}Cl(Py_2^{Me}tacn)]Cl$ (**1Ru^{II}-Cl**), $[Ru^{II}(H_2O)(Py_2^{Me}tacn)](PF_6)_2$ (**1Ru^{II}-OH$_2$**) and $[Ru^{II}(CH_3CN)(Py_2^{Me}tacn)](OTf)_2$ (**1Ru^{II}-NCCH$_3$**). [a]

Catalyst	TON – O$_2$[b]	TON - CO$_2$[c]	TOF (s^{-1})[d]
1Ru^{II}-Cl	19±2	n.d.	$1 \cdot 10^{-3}$
1Ru^{II}-Cl[e]	36±1	0.2±0.1	$2 \cdot 10^{-3}$
1Ru^{II}-NCCH$_3$	1±1	n.d.	-
1Ru^{II}-OH$_2$	51±2	0.1±0.1	$4 \cdot 10^{-3}$
1Ru^{II}-OH$_2$[f]	38±3	n.d.	$7 \cdot 10^{-3}$
1Fe^{II}-OTf	<5	n.d.	-

[a] The reactions were carried out by addition of CAN (125 mM, pH = 1.1, final concentration) to a solution with the corresponding catalysts (35 μ^iM) in Milli-Q water (10 mL, 18.2 MΩ·cm). [b] TON-O$_2$ (n(O$_2$) / n(Cat)). [c] TON-CO$_2$ (n(CO$_2$) / n(Cat)) were measured by calibrated GC-TCD. [d] TOF (turnover frequency) = [n(O$_2$) / n(Cat)·t] for the initial rate regime. [e] Ag(OTf) (70 μM, 2 eq.). [f] [HOTf] = 1 M, pH = 0.

Informative is the fact that all attempts to use NaIO$_4$ (125 mM) as oxidant with **1Ru^{II}-Cl**, **1Ru^{II}-OH$_2$** and **1Ru^{II}-NCCH$_3$** lead to the generation of very low levels of O$_2$ (c.a. 1 TON), even at low pH values (from 0 to 9). In fact, this inactivity can be rationalized based on the low redox potential that NaIO$_4$ can provide (c.a. 1.6 V *vs* SHE at pH 1) in comparison with Ce^{IV} (~1.75 V vs SHE at pH 0.9, at about 50 mM concentration).[69] In support to this hypothesis, we found that at pH = 0 the **1Ru^{II}-OH$_2$** WO activity when using Ce^{IV} (E(Ce$^{IV/III}$) > 1.75 V *vs* SHE at pH 0) is faster than at pH 1.1 (see Table IV.1). Under these highly acidic conditions (pH = 0) it is known that the redox potential of Ce^{IV} is higher,[72] also pointing towards a possible electron transfer prior the O-O bond formation. For comparative purposes we have also studied the homologous $[Fe^{II}(OTf)(Py_2^{Me}tacn)](OTf)$ (**Fe^{II}-OTf**) complex, resulting inactive in WOC.
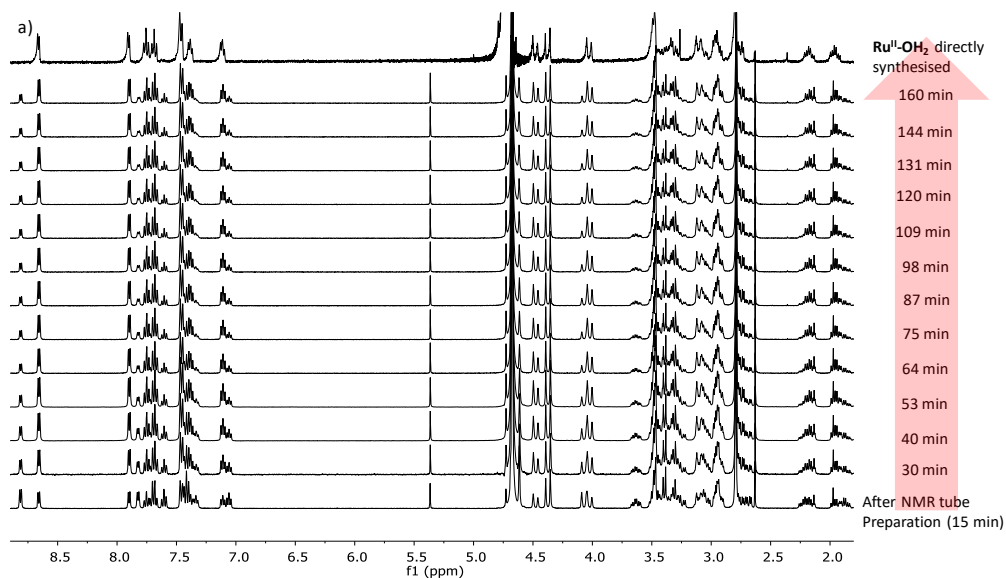
Figure IV.4. ^{1}H-NMR monitoring of the Cl/H$_2$O exchange in complex [Ru^{II}Cl(Py$_2$^{Me}tacn)]Cl (**1Ru^{II}-Cl**) after dissolution in D$_2$O *vs* time. On the top of the stacked spectra is the ^{1}H-NMR spectrum of pure [Ru^{II}(OH$_2$)(MePy$_2$tacn)](PF$_6$)$_2$ (**1Ru^{II}-OH$_2$**) complex dissolved in D$_2$O.

IV.2.3. Water Oxidation mechanistic studies of ruthenium complexes

We became interested in gaining a deeper understanding of the differences in the WO activity between the Py$_2$^{Me}tacn iron and ruthenium complexes. In particular, we were interested in the reason for the water oxidation capacity of **1Ru^{II}-OH$_2$** compared with the inactivity of **1Fe^{II}-OTf**.

As introduced above, several scenarios can be initially envisioned for the O-O bond formation by **1Ru^{II}-OH$_2$** after the generation of a Ru^{IV}(O): i) the O-O bond is formed through a direct coupling mechanism (DC) between two M^{IV}-oxo groups; ii) Ru^{IV}(O) suffers a water nucleophilic attack (WNA) forming a Ru^{II}-OOH species; and iii) a channel involving a WNA to a Ru^{IV}(O) coupled with an electron transfer giving Ru^{III}-OOH. However, there might be also the need to reach a higher oxidation state (Ru^V(O)) before the O-O bond formation takes place. In this regard, the possible mechanisms are: iv) *via* a direct coupling (DC) or v) WNA leading to Ru^{III}-OOH species. Recently Y. Pushkar *et al.* proposed the mechanistic scenario iii) as an

alternative to the highly reactive putative $Ru^V(O)$ species.[43-47] In addition, Sakai *et al.,* based on kinetic studies*,* proposed Ru-Ce intermediates as responsible for the O-O bond formation.[47]

To discard some of the possibilities and to provide evidence in favor of the molecular nature of the metal species responsible for the O-O bond formation event, we have first analyzed the reaction order by studying the initial rates of the O_2 evolution. The range of concentrations explored for $\mathbf{1Ru^{II}\text{-}OH_2}$ was 25 – 1000 µM and for CAN 25 – 150 mM (Figure IV.5). The double ln-plot shows first order O_2 evolution in both $\mathbf{1Ru^{II}\text{-}OH_2}$ and CAN at pH 0.7 (adjusted with perchloric acid) and 25 ºC. It is important to remark that under the same reaction conditions, for non-heme tetradentate iron complexes $[Fe^{II}(OTf)(^XPy^{Me2}tacn)]^{2+}$ (X = -NO_2, -CO_2Et, -H, -Cl) and $[Fe^{II}(OTf)(mcp)]^{2+}$ a saturation of the rate was found upon increasing the oxidant concentration. This behavior was attributed to the formation of a $Fe^{IV}(O)\text{-}Ce^{IV}$ intermediate[73-76] recently spectroscopically characterized.[75,76] The absence of saturation of the Ce^{IV} consumption rates in the studied range of [CAN] suggests that an analogous $Ru^{IV}(O)\text{-}Ce^{IV}$ intermediate, if formed, does not accumulate in solution.
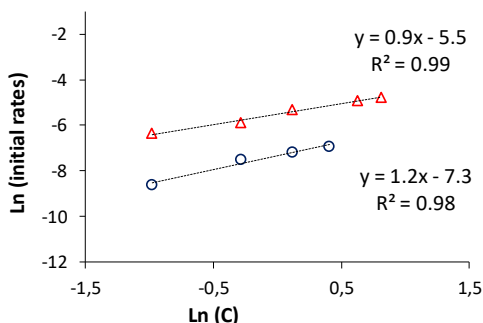
Figure IV.5. Double Ln-plot of initial rates (µmol $O_2 \cdot s^{-1}$) *vs* CAN (µmol, red triangles) and [$\mathbf{1Ru^{II}\text{-}OH_2}$] (µmol, dark blue circles) in water (25 ºC, pH 0.7, adjusted by HClO_4). Dotted lines represent the least square root data fittings. C stands for CAN or $\mathbf{1Ru^{II}\text{-}OH_2}$ in µmol as indicated.

In addition, valuable information can be obtained from a different analysis of the *on-line monitorization traces of the O_2 evolution.* O_2-traces show that both TON and TOF increase with the CAN concentration as expected (Figure IV.5.a). However,

a deep analysis of the Ce^{III}/Ce^{IV} ratio *versus* time (Figure IV.6 and A.I.22), is much more interesting. Actually, the Ce^{III}/Ce^{IV} ratio is related to the redox potential of the solution by the Nernst equation. Independently on the initial [CAN] the O_2 evolution basically stops at about the same redox potential (1.64 V, which corresponds to a Ce^{III}/Ce^{IV} ratio of c.a. 0.3, see Figure A.I.21.b). We could rationalize that the total amount of O_2 produced is mainly governed by the oxidation power of the solution, rather than by the exhaustion of the catalyst. In other words, Ce^{IV} is not fully consumed and there is still a large quantity of active catalyst in solution (though at some extend degradation is always occurring). Indeed, equivalent TON and TOF were obtained after the addition of the same initial amount of Ce^{IV} in a second run, confirming our hypothesis (Figure IV.6.c).

With this data in hand, we cannot truly identify this redox event nor the species responsible for the O-O bond formation. However, we can argue that the WO is redox-controlled, and define ~1.64 V as the minimum redox potential for the generation of a significant amount of the active species. In fact, it is in agreement with the value 1.81 V ($E^{V/IV}$ vs. SHE, Figures IV.7 and IV.12 and AI.28 c) and 29) found by electrochemical studies. The data thus strongly suggests that a $[Ru^V(O)(MePy_2tacn)](PF_6)_3$ (**$1Ru^V=O$**) needs to be formed in order to accomplish the O-O bond formation and that its formation affects the rate of the water oxidation raction. In concordance, when increasing the catalyst concentration, at a fixed CAN concentration (75 mM), the Ce^{III}/Ce^{IV} ratio increases (Figure IV.6.d-e and S.I.21.e), since the redox equilibrium is modified due to the higher concentration of catalytically active species.
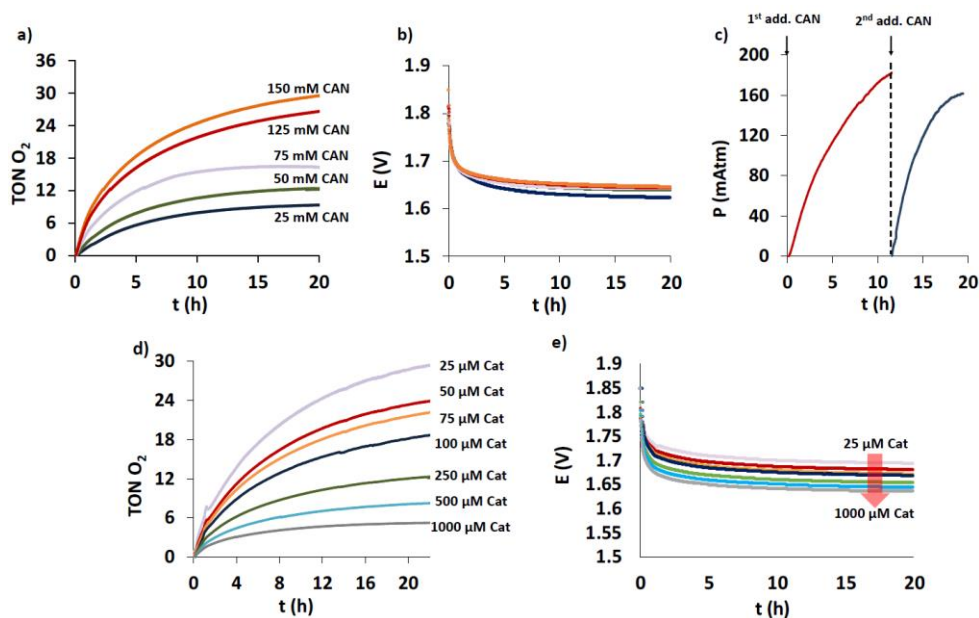
Figure IV.6. O*n-line monitorization of the O₂ evolution* either varying the [CAN] while keeping fixed the [catalyst] (250 µM) and varying the [catalyst] while keeping fixed the [CAN] (75 mM).a) Plot of TON O₂ *vs.* time at different [CAN] (250 µM **1Ru^{II}-OH₂**, pH 0.7, 25 ºC). b) Plot of the potential of the reaction (E (V)) vs. time at different [CAN] (250 µM **1Ru^{II}-OH₂**, pH 0.7, 25 ºC). c) Plot of the on-line pressure trace monitoring of the O₂ evolution vs. time after two subsequent additions of the same amount of CAN (75 mM CAN, 250 µM **1Ru^{II}-OH₂**, pH 0.7, 25 ºC). d) Plot of TON O₂ vs. time at different [**1Ru^{II}-OH₂**] (75 mM CAN, pH 0.7, 25 ºC). e) Plot of the redox potential of the reaction (E (V)) vs. time at different [**1Ru^{II}-OH₂**] (75 mM, pH 0.7, 25 ºC.
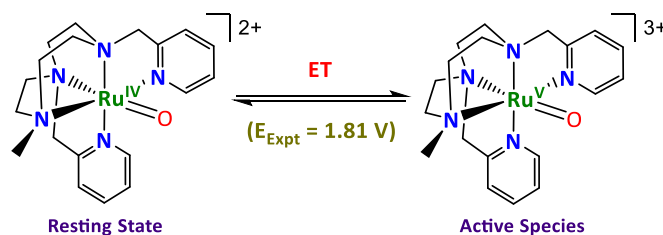
Figure IV.7. Proposed redox equilibrium between [Ru^{IV}(O)(MePy₂tacn)](PF₆)₂ (**1Ru^{IV}=O**) and [Ru^{V}(O)(MePy₂tacn)](PF₆)₃ (**1Ru^{V}=O**) prior to the WNA. The experimental redox potential value was estimated based on electrochemical studies with **1Ru^{II}-OH₂** in water (pH 0.7). The theoretical value was obtained by DFT modeling.

With the aim to clarify and get further insights into the mechanism of the WO reaction, we decided to investigate in detail all detectable intermediates and model the catalytic cycle by DFT (see chapter IV for further details).

IV.2.4. Characterization of water oxidation intermediates

First, we monitored the oxidation of **1Ru^{II}-OH$_2$** under catalytic conditions by means of UV-Vis, ^{1}H-NMR spectroscopy and CSI-HRMS spectrometry.

Oxidation of 1Ru^{II}-OH$_2$ to 1Ru^{III}-OH/1Ru^{III}-OH$_2$. A titration of complex **1Ru^{II}-OH$_2$** (0.28 mM, in Milli-Q water at 25 ºC) with CAN under non-buffered solution (pH = 2.9) (Figure IV.7.a) reveals the formation of new species. The initial two bands at a λ_{max} 249 nm (ε = 6419 M^{-1}cm^{-1}) and 397 nm (ε = 5345 M^{-1}cm^{-1}) with a shoulder at 369 nm (ε = 5107 M^{-1}cm^{-1}) decrease in intensity upon titration with CAN (up to 2 eq.), leading to new bands at 249 nm (ε = 5970 M^{-1}cm^{-1}), 266 nm (ε = 4107 M^{-1}cm^{-1}) and 297 nm (ε = 3506 M^{-1}cm^{-1}). However, the new bands are not well-defined due to the intense UV absorption of CAN in the 200 - 350 nm range (Figures IV.8.a,b, IV.9.a and A.I.22-23.a,b). CSI-HRMS of the resulting solution showed a prominent peak at m/z 222.0675 in milli-Q water with the pattern of **1Ru^{III}-OH** species. Deuterium oxide and ^{18}O labeling studies confirmed the presence of a labile OH group (See ^{18}O Labeling studies and Figure A.I.24.a-c) by CSI-HRMS.

At pH 0.7 the behavior is different. Titration of **1Ru^{II}-OH$_2$** with CAN leads to the formation of a new band at λ_{max} of 260 nm (ε = 7000 M^{-1}cm^{-1}). Such differences are indicative of a **1Ru^{III}-OH$_2$** - **1Ru^{III}-OH** acid-base equilibrium, with a pKa around 2 (according to NMR and UV-vis titration studies, Figure A.I.23.a). Titration of complex **1Ru^{II}-OH$_2$** (0.25 mM, in Milli-Q water at 25 ºC) with NaIO$_4$ (additions of 0.1 eq. up to 0.6 eq., Figure IV.7.b), proceeds with three different isosbestic points suggesting a clean transformation from complex **1Ru^{II}-OH$_2$** to a new species with λ_{max} at 233 nm (ε = 4362 M^{-1}cm^{-1}), 249 nm (ε = 4220 M^{-1}cm^{-1}), 266 nm (ε = 4242 M^{-1}cm^{-1}) and 297 nm (ε = 3166 M^{-1}cm^{-1}). CSI-HRMS studies with and without deuterium oxide and ^{18}O labeled water corroborate the observation of **1Ru^{III}-**

OH species (Figure IV.9.a-c). At pH 1.4 the band formed at λ_{max} of 260 nm (ε = 5810 $M^{-1}cm^{-1}$) confirmed the presence of **1Ru^{III}-OH$_2$** species (Figure A.I.23.b), as observed with CAN. In addition, analogous ^{1}H-NMR titrations corroborate the formation of different intermediates (Figure IV.11.a). Titration of **1Ru^{II}-OH$_2$** (2 mM, in degassed D$_2$O at 25 ºC, under Ar) with NaIO$_4$ (additions of 0.2 eq. dissolved in degassed D$_2$O) in an NMR tube showed the complete evolution of the initial diamagnetic Ru^{II} species to the well-defined paramagnetic **1Ru^{III}-OH** species after the addition of 0.6 eq. of NaIO$_4$.
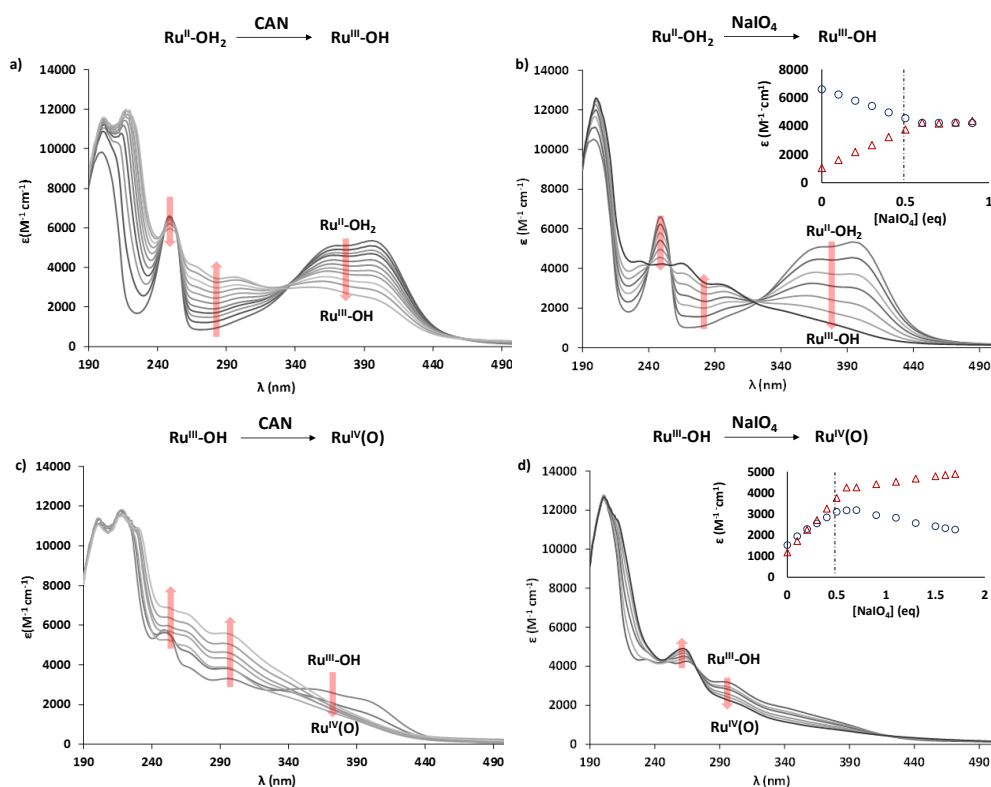
Figure IV.8. UV-Vis titration of **1Ru^{II}-OH$_2$** (3 ml of 0.28 mM (left) and 0.25 mM (right) under N$_2$ atm.) at 298 K with **a)** CAN (additions of 10 µl, 0.2 eq. each) and **b)** NaIO$_4$ (additions of 5 µl, 0.1 eq. each) to generate the **1Ru^{III}-OH** species. Inset: ε *versus* NaIO$_4$ equivalents at 249 nm (blue circles) and 266 nm (red triangles). The continued titration from **a)** and **b)** is shown in figures **c)** and **d)**, respectively. **c)** CAN (additions of 20 µl, 0.4 eq. each) and **d)** NaIO$_4$ (additions of 5 µl, 0.1 eq. each) to generate the **1Ru^{IV}=O** species. Inset: ε *versus* NaIO$_4$ eq. at 263 nm (red triangles) and 297 nm (blue circles). The baseline was corrected to 0 by abs. average of the 700 - 1100 nm range. The abs values were corrected taking into account the total volume after each aliquot addition.
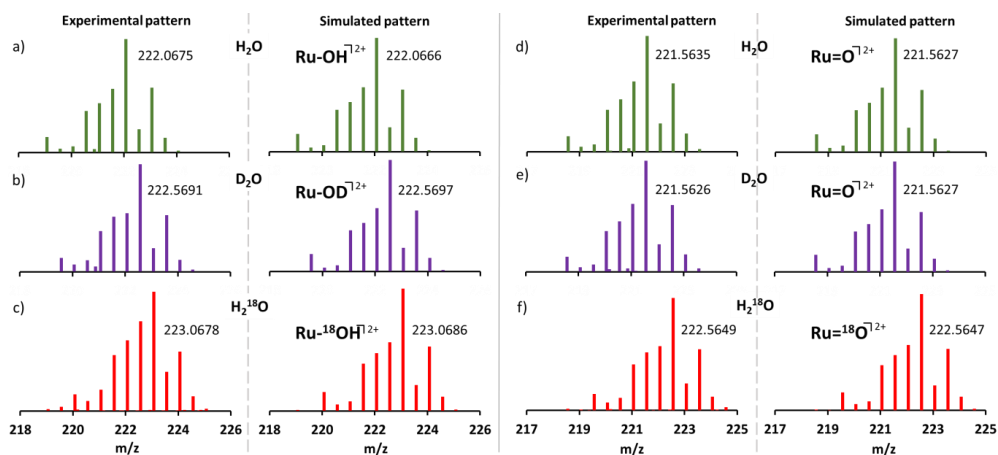
Figure IV.9. CSI-HRMS (298 K) of [Ru^{II}Cl(Py$_2^{Me}$tacn)]Cl with left) 0.5 eq of NaIO$_4$ in a), Milli-Q water, b) D$_2$O and c) H$_2^{18}$O (97% ^{18}O) and right) 1.5 eq. of NaIO$_4$ in d), Milli-Q water, e) D$_2$O and f) H$_2^{18}$O (97% ^{18}O). (For further experimental details see the experimental section).
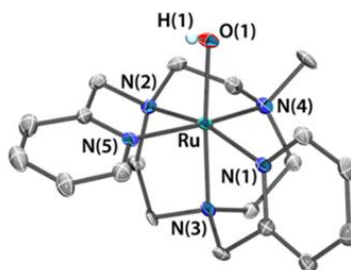
Figure IV.10. Thermal ellipsoid plot of [Ru^{III}(OH)(Py$_2^{Me}$tacn)](PF$_6$)$_2$ (**1Ru^{III}-OH**) (30% probability). Hydrogen atoms, solvent molecules and counterions have been omitted for clarity. Selected bond lengths [Å] and angles [°]: Ru−O 1.943(7), Ru−N(1) 2.063(7), Ru−N(2) 2.044(7), Ru−N(3) 2.098(8), Ru−N(4) 2.107(7), Ru−N(5) 2.074(7), N(1)-Ru-N(2) 165.1(3), N(3)-Ru-O 175.1 (3), N(4)-Ru-N(5) 166.5 (3).

Finally, single crystals suitable for X-ray diffraction of complex [Ru^{III}(OH)(Py$_2^{Me}$tacn)](PF$_6$)$_2$ were obtained by recrystallization (CH$_3$CN:Et$_2$O at -20 ºC). The Ru-O bond distance is 1.943(7) Å and it is within the range expected for a **1Ru^{III}-OH** unit (Figure IV.10). Likewise, the material obtained from the oxidation of **1Ru^{II}-Cl** with 0.5 eq of NaIO$_4$ yields suitable crystals for X-ray diffraction of [Ru^{III}(Cl)(Py$_2^{Me}$tacn)](PF$_6$)$_2$ complex (Figure A.I.31).

Oxidation of 1Ru^{III}-OH to 1Ru^{IV}=O. The subsequent addition of more equivalents of NaIO$_4$ makes the bands associated with **1Ru^{III}-OH** species

slowly disappear. In contrast, a new band at λ_{max} 263 nm ($\varepsilon = 4893$ $M^{-1}cm^{-1}$) arises, which may be associated with the formation of a **1Ru^{IV}=O** species. Indeed, further reaction with ascorbic acid regenerates the spectroscopic features of **1Ru^{III}-OH** and **1Ru^{II}-OH$_2$**, subsequently. Altogether, reactivity, UV-Vis, CSI-HRMS and NMR studies point to the formation of **1Ru^{IV}=O** species (See ^{18}O Labeling studies and Figure IV.8.b, IV.9.d-f and IV.11). Titration of **1Ru^{III}-OH** with Ce^{IV}, is partially masked by the Ce^{IV} absorbance (see CAN blank experiments, Figure A.I.22). Nevertheless, the formation of the same CSI-HRMS and NMR signatures (Figure A.I.25 and 27, respectively) assigned to **1Ru^{IV}=O** were observed. No indication of Ru^{IV}(O)-Ce^{IV} adducts were obtained by CSI-HRMS studies.

Treatment of 1Ru^{IV}=O with an excess of oxidant. No further oxidized ruthenium species were observed with an excess of CAN or NaIO$_4$. Remarkably, **1Ru^{IV}=O** is the predominant species detected by CSI-HRMS and NMR under catalytic conditions suggesting that under this conditions **1Ru^{IV}=O** is the resting state of the water oxidation catalytic cycle (Figure A.I. 27).

Labeling studies of in-situ generated 1Ru^{III}-OH and 1Ru^{IV}=O species by CSI-HRMS. To further confirm the formation of both **1Ru^{III}-OH** and **1Ru^{IV}=O** species CSI-HRMS studies in presence of D$_2$O and H$_2$^{18}O were performed. Addition of 0.5 eq of NaIO$_4$ or 1 eq of CAN to a **1Ru^{II}-OH$_2$** solution in Milli-Q H$_2$O leads to a prominent peak at m/z 222.0675 associated to [(Py$_2$^{Me}tacn)Ru^{III}-OH]$^{2+}$. This peak suffers an m/z 0.5 and 1 upshift in D$_2$O and H$_2$^{18}O, respectively. Further addition of 1 eq of NaIO$_4$ or 3 eq of CAN in Milli-Q H$_2$O leads to a new prominent peak at m/z 221.5635 corresponding to [(Py$_2$^{Me}tacn)Ru^{IV}(O)]$^{2+}$, which suffers a m/z 1 upshift in H$_2$^{18}O, but remains unchanged in D$_2$O (Figure IV.9.b-e and A.I.24-25)). These experiments point out the presence of one exchangeable proton and oxygen atom for **1Ru^{III}-OH** and one oxygen atom for **1Ru^{IV}=O**.
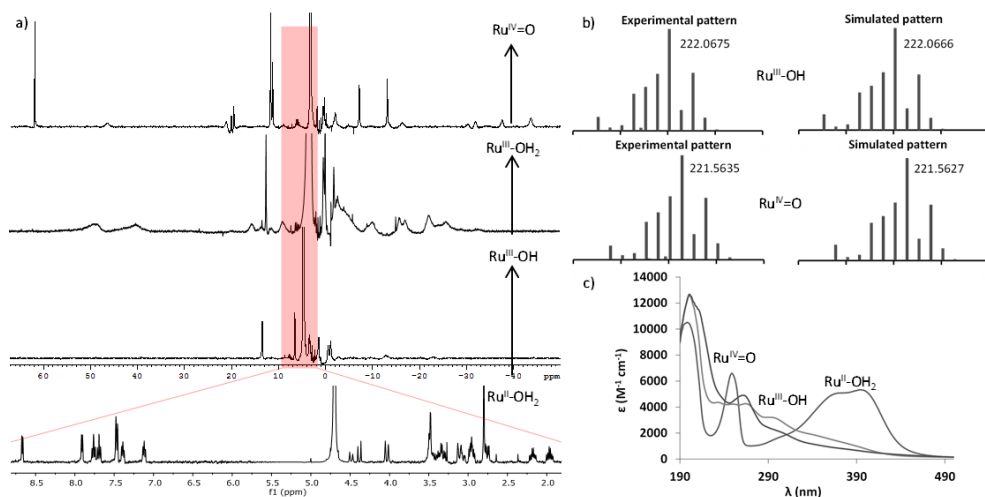
Figure IV.11. Summary of the spectroscopic and spectrometric features for $1Ru^{III}$-OH and $1Ru^{IV}$=O species. a) ^{1}H-NMR (400 MHz, D_2O, 298 K) of the solution of $1Ru^{II}$-OH_2 (2 mM in D_2O) in an NMR tube (bottom) 0.5 eq of $NaIO_4$ leads to the formation of paramagnetic $1Ru^{III}$-OH species. Subsequent addition of HOTf (final concentration 0.07 M, pH ~ 1.1) forms $1Ru^{III}$-OH_2 and further addition of 1 eq of $NaIO_4$ leads to the $1Ru^{IV}$=O species (top). b) CSI-HRMS studies of a $1Ru^{II}$-OH_2 solution (298 K, 0.25 mM, Milli-Q H_2O) after the addition of 0.5 eq (top) and 1.5 eq (bottom) of $NaIO_4$. c) UV-Vis of $1Ru^{II}$-OH_2, $1Ru^{III}$-OH, and $1Ru^{IV}$=O species (0.25 mM at 298 K in Milli-Q H_2O).

CSI-HRMS $H_2^{18}O$ labeling experiments are very informative about the course of the oxidation reaction with $NaIO_4$. When starting from $1Ru^{II}$-Cl dissolved in $H_2^{18}O$, the addition of 0.5 eq. of $NaI^{16}O_4$, initially forms a 2:1 mixture of $1Ru^{III}$-^{16}OH, $1Ru^{III}$-^{18}OH species and $1Ru^{III}$-Cl, which rapidly evolves (in 2 or 3 minutes) to give rise to $1Ru^{III}$-^{18}OH (peak at m/z 223.0678), as judged by the simulated pattern (see Figure A.I.26 for further details).
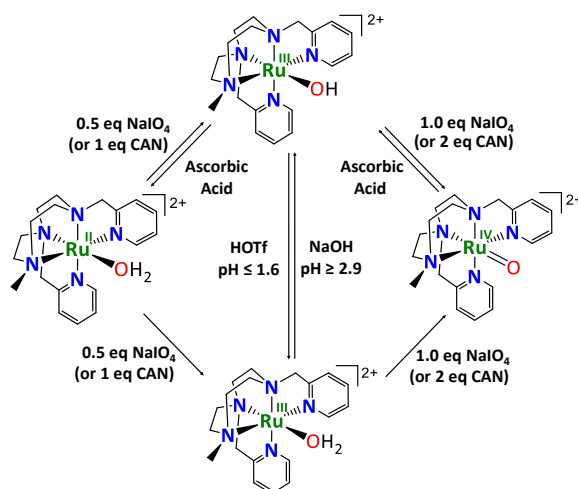
Figure IV.12. Summary of the reactivity that connects the **1Ru^{II}-OH$_2$**, **1Ru^{III}-OH$_2$**, **1Ru^{III}-OH** and **1Ru^{IV}=O** species.

This fact suggests that sodium periodate acts mainly as an oxygen transfer oxidant (going through the formation of **1Ru^{IV}=O** species, which rapidly comproportionates with the Ru^{II} species) rather than a 1e$^-$ oxidant. In addition, we were able to observe a rapid OH$^-$ exchange with the solvent. Interestingly, with both oxidants, it could be seen that once the **1Ru^{IV}=^{18}O** species had been generated, its ^{18}O could not be exchanged by ^{16}O on a WO reaction time scale with H$_2$^{16}O. After 24 hours of reaction, the exchange was << 1 %. This result opens the door to study the mechanism of the reaction by labeling experiments.

IV.2.5. Electrochemical and spectroelectrochemical studies

To get further insights into the nature of the oxidizing species in catalysis we have studied the pH-redox-potential-dependence of the **1Ru^{II}-OH$_2$** complex by CV (cycle voltammetry), DPV (differential pulse voltammetry) and SWV (square wave voltammetry) in the pH 1-12 range (Figure IV.13 and A.I.29-30). The redox-pH plot (Pourbaix diagram) shows the following redox processes **1Ru^{II}-OH$_2$** → **1Ru^{III}-OH** → **1Ru^{IV}=O**. Both redox processes,

UNIVERSITAT ROVIRA I VIRGILI
MECHANISTIC STUDIES OF WATER OXIDATION CATALYZED BY HOMOGENEOUS IRON AND RUTHENIUM
COMPLEXES AND LIGHT-DRIVEN ORGANIC REDUCTIONS WITH A DUAL COBALT/COPPER CATALYTIC SYSTEM
Carla Casadevall Serrano

CHAPTER IV   Mechanistic Investigations of WO Catalyzed by Ru Complexes

Ru^{III}/Ru^{II} ($E^{III/II}_{1/2}$ = 0.47 V at pH 7) and Ru^{IV}/Ru^{III} ($E^{IV/III}_{1/2}$ = 1.08 V at pH 7), are pH dependent (-62 mV/pH, -52 mV/pH, respectively) in the pH range from 2-12. This behavior is consistent with a proton-coupled electron transfer process (PCET) which enables the formation of a high-valent **$1Ru^{IV}=O$** species. Similar patterns have been reported for related pentadentate complexes such as [Ru(DPA-Bpy)] (DPA-Bpy = *N,N*-bis(2-pyridinylmethyl)-2,20-bipyridine-6-methanamine)[72] and [Ru(tacn)(bpy)](ClO_4)$_2$ (bpy = 2,2'-bipyridine).[62] In addition, it can be seen that at pH < 2 there is a pH-independent process attributed to the **$1Ru^{III}-OH_2/1Ru^{II}-OH_2$** redox couple ($E^{III/II}_{1/2}$ = 0.75 V). This is consistent with the **$1Ru^{III}-OH_2$ - $1Ru^{III}-OH$** (pK$_a$ ~ 2) acid-base equilibrium observed in the UV-Vis and NMR spectroscopy titration studies (Figure A.I.23). Moreover, from **$1Ru^{III}-OH_2$** to **$1Ru^{IV}(O)$** there is the transference of two protons and one electron as judged by the slope of -103 mV/pH. In contrast, $E^{(V/IV)}$ = 1.81 V for the **$1Ru^{IV}=O/1Ru^{V}=O$** redox pair is not pH dependent (~ 0 mV/pH) (Figure A.I.28 c)). Those results are in good concordance with our DFT-calculated Pourbaix diagram for the presented processes (see Computational studies in chapter IV).
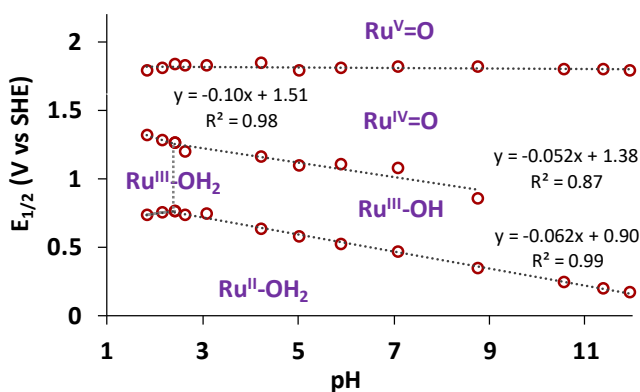
Figure IV.13. Pourbaix diagram for complex **$1Ru^{II}-OH_2$** (0.5 mM, 298 K) in aqueous Britton-Robinson buffer (0.1 M) and KNO_3 as electrolyte (0.1 M) from pH 1-12 ($E_{1/2}$ *vs* SHE). Points indicate the pH values in which the electrochemistry study has been done; dotted lines are the trend lines for each redox process.

To give confidence to the assignment of the electrochemical processes observed and match them with the characterized intermediates involved in the WO catalytic cycle by means of different spectroscopic and spectrometric techniques we have performed spectroelectrochemical studies. These were performed at pH 7 (in a 0.1 M solution of Britton-Robbinson buffer).

At a potential of 0 V the UV-Vis spectrum matches that of the **1Ru^{II}-OH$_2$** species with bands at 249 and 397 nm and a shoulder at 369 nm (see Figures IV.8 and IV.14). Then, upon increasing the voltage we can see the decrease of those initial bands and the appearance of new bands characteristic of **1Ru^{III}-OH** species (233, 249, 267 and 297 nm). The transformation is completed at a redox potential about 0.5 V (Figures IV.8 and A.I.30). Indeed, this potential matches with that of the **1Ru^{III}-OH$_2$** obtained in the electrochemical studies at the same pH (0.47 V, see Figure IV.13). The increase of the voltage from 0.5 to 1.2 V promotes the formation of a species with a new band at around 263 nm, which is consistent with that obtained for **1Ru^{IV}=O** species in the UV-Vis titration studies (Figures IV.8 and A.I.30). Likewise, this value of potential is also in agreement with the one obtained in the electrochemical studies (1.08 V, Figures IV.13 and IV.14). Attempts to explore voltages above 1.8 V produced large quantities of bubbles (O$_2$ originating from electrocatalytic water oxidation) precluding a useful reading of the UV-Vis spectra.
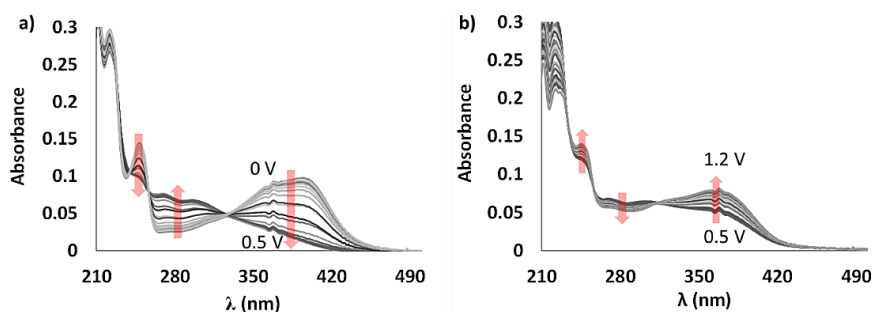
Figure IV.14. Characterization of intermediates by spectroelectrochemistry in 0,1 M of Britton-Robbinson buffer at pH 7 and 0,1 M of KNO$_3$ as electrolyte at 298 K, all the intermediates observed in the UV-Vis spectrum are those corresponding to the oxidized species by the application of a determined potential: a) **1Ru^{II}-OH$_2$** (2 mM) after the subsequent increase of the applied potential from 0 to 0.5 V (Ag/AgCl) and so that, forming **1Ru^{III}-OH$_2$** species. b) **1Ru^{II}-OH$_2$** (2 mM) after the subsequent increase of the applied potential from 0.5 to 1.2 V (Ag/AgCl) and thus, forming the **1Ru^{IV}=O** species.

IV.2.6. ^{18}O labeling water oxidation experiments

First, we analyzed the activity of $1Ru^{II}$-OH_2 as water oxidation catalyst under suitable conditions to perform ^{18}O labeling experiments. The addition of c.a. 100 eq of CAN (at pH 1.0) to a concentrated solution of $1Ru^{II}$-OH_2 (2.5 mM) produces about 1 TON of O_2 after 400 s, which was monitored by on-line MS and manometry, as shown in Figures IV.15 and A.I.30 negligible amount of CO_2 was recorded by on-line MS.

These experiments, together with an oxo-water slow exchange observed for $1Ru^{IV}$=O (studied by CIS-HRMS) unambiguously demonstrates that the mechanism of water oxidation can be reliably interrogated by ^{18}O labeling experiments.[73] To get robust evidence of the mechanism two different labeling experiments were carried out. In both cases, we monitored the dioxygen molecule isotopomers $^{32}O_2$, $^{34}O_2$ and $^{36}O_2$ evolved from the reaction. First, we carried out the addition of 100 eq of CAN dissolved in $H_2^{18}O$ to a 2.5 mM of $1Ru^{IV}$=^{16}O in $H_2^{16}O$ (previously generated) giving a final 16.7 % $H_2^{18}O$ content in 0.1 M triflic acid solution. In a second experiment, we added 100 eq of CAN dissolved in $H_2^{16}O$ to a 2.1 mM of $1Ru^{IV}$=^{18}O in $H_2^{18}O$ (previously generated) giving a final 26.4 % $H_2^{18}O$ content in 0.1 M triflic acid solution. Both experiments are summarized in Figures IV.15 and A.I.30. Three possible scenarios could be considered: a) a faster exchange of the oxo group, b) a water nucleophilic attack (WNA) mechanism and c) a direct bimolecular coupling of two Ru=O units (DC). In order to better analyze the outcome from the experiments, we have transformed the ratios between O_2 isotopes into the percentage of the three different possible mechanisms. Indeed, as a practical approach, we considered that the observed isotopic distribution is a linear combination of the three possible scenarios. This produces a three equations three variable system which can be easily solved using matrices and the Cramer's rule (see experimental section *IV.4.7. ^{18}O labeling Studies* for details). This method allows to study the dominant mechanism *versus* time and leads to

UNIVERSITAT ROVIRA I VIRGILI
MECHANISTIC STUDIES OF WATER OXIDATION CATALYZED BY HOMOGENEOUS IRON AND RUTHENIUM
COMPLEXES AND LIGHT-DRIVEN ORGANIC REDUCTIONS WITH A DUAL COBALT/COPPER CATALYTIC SYSTEM
Carla Casadevall Serrano

CHAPTER IV   Mechanistic Investigations of WO Catalyzed by Ru Complexes

some important advantages: i) broad applicability of the labeling experiments since there is no need to analyze stoichiometric experimentsd, ii) it improves significantly the sensibility and iii) the study can be done under catalytic conditions.

In Figure IV.15 it is shown the on-line values and the obtained mechanism percentages after the analysis of the ion counting. Regardless of the starting point, $\mathbf{1Ru^{IV}{=}^{16}O}$ or $\mathbf{1Ru^{IV}{=}^{18}O}$, after the addition of an excess of Ce^{IV} (c.a. 100 eq) the water nucleophilic attack mechanism contribution is significantly higher than exchange or DC contributions to the final O_2 isotopic distribution. A small contribution of the latter mechanism can be attributed to atmospheric O_2 contamination, especially at the beginning of the O_2 evolution. Indeed, this is clearly illustrated at negative times and at the very beginning of the reaction. Initial traces of $^{32}O_2$ and $^{36}O_2$ observed before the addition of the excess of CAN are reflected in the mechanism and they are rapidly overpassed by the O_2 produced. As the reaction advances the exchange mechanism gains importance due to the consumption of the initial $\mathbf{1Ru^{IV}{=}O}$ to give O_2. The new formed $\mathbf{1Ru^{IV}{=}O}$ has the isotopic distribution derived from the reaction media, which will give rise to more O_2. Therefore, we can safely conclude that the main reaction mechanism operation of $\mathbf{1Ru^{II}\text{-}OH_2}$ is the water nucleophilic attack.

UNIVERSITAT ROVIRA I VIRGILI
MECHANISTIC STUDIES OF WATER OXIDATION CATALYZED BY HOMOGENEOUS IRON AND RUTHENIUM
COMPLEXES AND LIGHT-DRIVEN ORGANIC REDUCTIONS WITH A DUAL COBALT/COPPER CATALYTIC SYSTEM
Carla Casadevall Serrano

CHAPTER IV   Mechanistic Investigations of WO Catalyzed by Ru Complexes
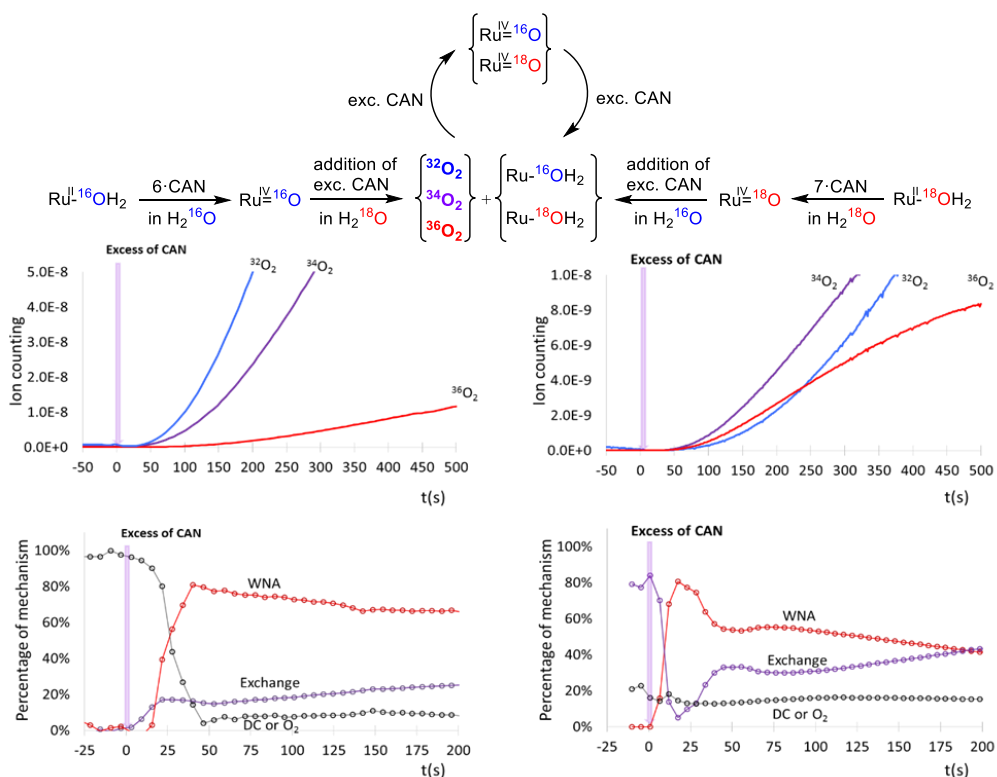
Figure IV.15. top) on-line values and bottom) mechanism percentage obtained after analysis of the m/z 32 (blue), 34 (purple) and 36 (red) ion counting monitored from the vial head space after the addition of c.a. 100 eq of CAN dissolved in left) $H_2^{18}O$ to a solution of **1Ru^{IV}=^{16}O** in $H_2^{16}O$ right) $H_2^{16}O$ to a solution of **1Ru^{IV}=^{18}O** in $H_2^{18}O$.

IV.3. Conclusions

The new synthesized *N*-pentadentate ruthenium complex **1Ru^{II}-OH$_2$** exhibits a significant WO activity (up to 51 ± 2 TON) while **1Fe^{II}-OTf** is inactive. Studies by means of catalytic, kinetics, spectroscopic, spectrometric, electrochemical and spectroelectrochemical techniques, pointed out that the water oxidation reaction follows a water nucleophilic attack mechanism. Our data suggest that the O-O bond formation affects the rate of the reaction and it occurs at the Ru^{V}(O) intermediate that can only be reached when the redox potential in solution is high enough under catalytic conditions ([Ce^{IV}/Ce^{III}] $\approx$ E(Ru$^{IV/V}$)). This Ru^{V}(O) intermediate is accessible under catalytic conditions

UNIVERSITAT ROVIRA I VIRGILI
MECHANISTIC STUDIES OF WATER OXIDATION CATALYZED BY HOMOGENEOUS IRON AND RUTHENIUM
COMPLEXES AND LIGHT-DRIVEN ORGANIC REDUCTIONS WITH A DUAL COBALT/COPPER CATALYTIC SYSTEM
Carla Casadevall Serrano

CHAPTER IV   Mechanistic Investigations of WO Catalyzed by Ru Complexes

through an ET process from $Ru^{IV}(O)$ ($E_{1/2} \sim 1.81$ V *vs* SHE) by the driving force provided by CAN ($E(Ce^{IV/III}) > 1.75$ V *vs* SHE at pH 0). Moreover our kinetic studies also suggest that the formation of the putative $Ru^V(O)$ as the also modifies the reaction rate. Additionally, the kinetic experiments indicate that the formation of a $[(Py_2^{Me}tacn)Ru^{IV}\text{-}O\text{-}Ce^{IV}]$ adduct is unlikely. These results shed some light in the mechanism involved in the molecular Ru-catalysed WO.

On the other hand, altogether suggests that the inactivity of the homologous iron complex could be linked to the inaccessibility of $Fe^V(O)$ under reaction conditions rather than other scenarios. Nevertheless, we performed DFT calculations to better understand the differences in reactivity. This detailed study is reported in the next chapter (chapter V).

IV.4. Experimental Section

IV.4.1. General Procedures

Materials. Reagents were purchased from commercial sources and used as received, without any further purification. Ceric ammonium nitrate (CAN) (≥99.99%) and trifluoromethanesulfonic acid (ReagentPlus grade ≥99%) were purchased from Sigma-Aldrich®. Solvents were purchased from SDS and Scharlab, purified and dried by passing through an activated alumina purification system (MBraun SPS-800) and stored in an anaerobic glovebox under N_2. Water (18.2 MΩ·cm) was purified with a Milli-Q Millipore Gradient AIS system.

Physical Methods. Nuclear magnetic resonance (NMR) spectra were recorded on BrukerDPX300 and DPX400 spectrometers using standard conditions (298 K). All ^1H chemical shifts are reported in ppm and have been internally calibrated to the residual protons of the deuterated solvent. The ^{13}C

UNIVERSITAT ROVIRA I VIRGILI
MECHANISTIC STUDIES OF WATER OXIDATION CATALYZED BY HOMOGENEOUS IRON AND RUTHENIUM
COMPLEXES AND LIGHT-DRIVEN ORGANIC REDUCTIONS WITH A DUAL COBALT/COPPER CATALYTIC SYSTEM
Carla Casadevall Serrano

CHAPTER IV   Mechanistic Investigations of WO Catalyzed by Ru Complexes

chemical shifts have been internally calibrated to the carbon atoms of the deuterated solvent. The coupling constants were measured in Hz. UV-VIS-NIR spectra were recorded on an Agilent 8453 diode array spectrophotometer (190-1100 nm range) in 1 cm quartz cells. A cryostat from Unisoku Scientific Instruments was used for temperature control. Elemental analyses were performed using a CHNS-O EA-1108 elemental analyzer from Fisons. UV-Vis spectra were recorded on an Agilent 8453 diode array spectrophotometer (190-1100 nm range) in 1 cm quartz cells. A cryostat from Unisoku Scientific Instruments was used for the temperature control. The pH of the solutions was determined by a pHmeter (XS Instruments) calibrated before measurements through standard solutions at pH= 4.01, 7.00 and 10.00.

The amount of gas generated was measured with a differential pressure transducer sensor (Honeywell-ASCX15DN, ±15 psi, see Annex II Figure A.II.33). Each reaction had its own reference reaction, which was connected to the other port of the sensor. Further details of the equipment are available elsewhere.[5b,28] Gases at the headspace were analyzed with an Agilent 7820A GC System equipped with columns Washed Molecular Sieve 5A, 2m x 1/8'' OD, Mesh 60/80 SS and Porapak Q, 4m x 1/8'' OD, SS. Mesh: 80/100 SS and a Thermal Conductivity Detector. The quantification of the O_2 obtained was measured through the interpolation of a previous calibration using known O_2/N_2 mixtures.

IV.4.2. Synthesis of complexes and characterization

Synthesis of [Ru^{II}Cl(Py$_2^{Me}$tacn)]Cl (1Ru^{II}-Cl). Ru^{II}Cl$_2$(dmso)$_4$ (90 mg, 0.2 mmol) was solved in absolute ethanol (30 ml) in a 50 ml flask. Then, 1-methyl-4,7-bis(pyridyl-2-methyl)-1,4,7-triazacyclononane, Py$_2^{Me}$tacn (0.20 g, 0.2 mmol) was solved in absolute ethanol (5 ml) in a vial and, under nitrogen, it was injected to the ruthenium precursor. The mixture was refluxed at 85ºC for 24h. After cooling to room temperature, the solvent was removed under

reduced pressure and the obtained residue was solved in the minimum amount of CH_2Cl_2 and precipitated with diethyl ether affording an orange solid. Suitable crystals for X-ray diffraction were obtained by slow diffusion of Et_2O in CH_2Cl_2 yielding 80 mg (0.2 mmol, 85%) of $[Ru(Cl)(Py_2^{Me}tacn)]_2(Cl)_2(CH_2Cl_2)_3(OH_2)_2$. Finally, the sample was ground and kept under vacuum overnight. ^{1}H-NMR ($CDCl_3$, 400MHz, 300 K) δ, ppm: 9.23 (d, $J = 5.2$ Hz, 1H, PyH_α), 7.81 (d, $J = 5.6$ Hz, 1H, PyH_α'), 7.65 (t, $J = 7.6$ Hz, 1H, PyH_β), 7.56 (t, $J = 8$ Hz, 1H, PyH_β'), 7.45 (d, $J = 7.6$ Hz, 1H, PyH_δ), 7.33 (d, $J = 7.6$ Hz, 1H, PyH_δ'), 7.29 (t, 1H, $J = 6.4$ Hz, PyH_γ), 7.04 (t, 1H, $J = 6.8$ Hz PyH_γ'), 5.00 (d, $J = 14.8$ Hz, 1H, Py-CH_2), 4.68 (d, $J = 14.8$ Hz, 1H, Py-CH_2), 4.44 (d, $J = 15.2$ Hz, 1H, Py-CH_2), 4.43-4.32 (m, 1H, N-CH_2-CH_2), 4.16-4.04 (m, 1H, N-CH_2-CH_2), 3.96 (d, $J = 15.2$ Hz, 1H, Py-CH_2), 4.01-3.87 (m, 2H, N-CH_2-CH_2), 3.65 (dd, $J = 12$ Hz, $J = 4.8$ Hz 1H, N-CH_2-CH_2), 3.51-3.49 (m, 1H, N-CH_2-CH_2), 3.23 (dd, $J = 15.4$ Hz, $J = 6$Hz, 1H, N-CH_2-CH_2), 3.12 (dd, $J = 15.4$ Hz, $J = 6$ Hz, 1H, N-CH_2-CH_2), 3.02-3.01 (m, 1H, N-CH_2-CH_2), 2.97 (s, 3H, N-CH_3), 2.91 (dd, $J = 12.8$ Hz, $J = 5.2$ Hz, 1H, N-CH_2-CH_2), 2.18 (td, $J = 16$ Hz, $J = 8$ Hz, 1H, N-CH_2-CH_2), 1.83 (td, $J = 16$ Hz, $J = 8$ Hz, 1H, N-CH_2-CH_2). Samples for combustion analysis were prepared by grinding the crystals and keep then under vacuum ($> 10^{-2}$ matm) for 12 h. Analysis calculation for $C_{19}H_{27}Cl_2N_5Ru\cdot 3H_2O$ (MW = 551.47 g/mol): N, 14.07; C, 45.87; H, 5.47 %. Found: N, 12.70; C, 41.38; H, 6.03 %. We noticed that complex **Ru^{II}-Cl** was highly hygroscopic, which accounts for the elemental analysis deviation. CSI-HRMS: m/z calcd for $[Ru^{II}Cl(Py_2^{Me}tacn)]^+$ is 462.0998; found 462.1014.

Synthesis of $[Ru^{II}(CH_3CN)(Py_2^{Me}tacn)](OTf)_2$ (1Ru^{II}-NCCH$_3$). Inside the glovebox $[Ru^{II}Cl(Py_2^{Me}tacn)]Cl$ (20 mg, 0.04 mmol) were stirred in a vial with 2 equivalents of silver trifluoromethanesulfonate, AgOTf, (21 mg, 0.08 mmol) in 1 ml of anhydrous acetonitrile. Then the mixture vial was covered with silver paper and left stirring overnight. Then the mixture was filtered

UNIVERSITAT ROVIRA I VIRGILI
MECHANISTIC STUDIES OF WATER OXIDATION CATALYZED BY HOMOGENEOUS IRON AND RUTHENIUM
COMPLEXES AND LIGHT-DRIVEN ORGANIC REDUCTIONS WITH A DUAL COBALT/COPPER CATALYTIC SYSTEM
Carla Casadevall Serrano

CHAPTER IV   Mechanistic Investigations of WO Catalyzed by Ru Complexes

through a celite plug with acetonitrile and the slow diffusion of diethyl ether over the resultant orange solution afforded, in few days, 22 mg of a pale yellow solid (0.03 mmol, 76 %). ^{1}H-NMR (CD$_3$CN, 400MHz, 300 K) δ, ppm: 8.75 (d, J = 8 Hz, 1H, Py**H$_\alpha$**), 7.87 (td, J = 8 Hz, J = 1.6 Hz, 1H, Py**H$_\gamma$**), 7.82 (td, J = 7.6 Hz, 1H, Py**H$_\gamma$**$'$), 7.70 (d, J = 5.6 Hz, 1H, Py**H$_\alpha$**$'$), 7.55 (t, J = 7.6 Hz, 2H, Py**H$_\delta$** and Py**H$_\delta$**$'$), 7.46 (t, J = 6.8 Hz, 1H, Py**H$_\beta$**), 7.22 (t, 1H, J = 6.4 Hz, Py**H$_\beta$**$'$), 4.70 (d, J = 15.6 Hz, 1H, Py-CH$_2$), 4.57 (d, J = 7.6 Hz, 1H, Py-CH$_2$), 4.53 (d, J = 8.4 Hz, 1H, Py-CH$_2$), 4.16 (d, J = 15.6 Hz, 1H, Py-CH$_2$), 3.60-3.30 (m, 8H, N-CH$_2$-CH$_2$), 3.20-3.05 (m, 4H, N-CH$_2$-CH$_2$), 2.83 (s, 3H, N-CH$_3$). Analysis calculation for C$_{23}$H$_{30}$F$_6$N$_6$O$_6$RuS$_2$ (MW = 765.71 g/mol): N, 10.98; C, 36.08; H, 3.95 %. Found: N, 10.86; C, 35.84; H, 3.93 %. CSI-HRMS: m/z calcd for [Ru^{II}(CH$_3$CN)(Py$_2^{Me}$tacn)]$^{2+}$ is 234.0788; found 234.0794.

Synthesis of [Ru^{II}(H$_2$O)(Py$_2^{Me}$tacn)](PF$_6$)^2 (1Ru^{II}-OH$_2$). [Ru^{II}Cl(Py$_2^{Me}$tacn)]Cl (100 mg, 0.2 mmol) and AgOTf (170 mg, 1.0 mmol) were heated at reflux in 8 ml of degassed MilliQ H$_2$O:MeOH (1:1) for 2 hours under inert atmosphere. The reaction mixture turned green and after 2 hours it was filtered hot through a bed of celite under an inert atmosphere. MeOH was removed in the vacuum line. Then, the green aqua complex was precipitated by addition of a saturated solution of ammonium hexafluorophosphate. ^{1}H-NMR (CD$_3$OD, 400 MHz, 300 K) δ, ppm: 8.80 (d, J = 8 Hz, 1H, Py**H$_\alpha$**), 8.12 (d, J = 5.6 Hz, 1H, Py**H$_\alpha$**$'$), 7.96-7.85 (m, 2H, Py**H$_\delta$** and Py**H$_\delta$**$'$), 7.63 (t, J = 8 Hz, 2H, Py**H$_\gamma$** and Py**H$_\gamma$**$'$), 7.56 (t, J = 5.6 Hz, 1H, Py**H$_\beta$**), 7.33 (t, 1H, J = 5.6 Hz, Py**H$_\beta$**$'$), 4.63 (d, J = 15.6 Hz, 1H, Py-CH$_2$), 4.53 (d, J = 15.6 Hz, 1H, Py-CH$_2$), 4.14 (d, J = 15.6 Hz, 1H, Py-CH$_2$), 3.80-3.40 (m, 6H, N-CH$_2$-CH$_2$), 3.25-3.15 (m, 2H, N-CH$_2$-CH$_2$), 3.15-3.00 (m, 2H, N-CH$_2$-CH$_2$), 2.20-2.10 (m, 2H, N-CH$_2$-CH$_2$), 2.86 (s, 3H, N-CH$_3$). ^{1}H-NMR (D$_2$O, 500 MHz, 298 K) δ, ppm: 8.64 (d, J = 5.5 Hz, 1H, Py**H$_\alpha$**), 7.88 (d, J = 5.5 Hz, 1H, Py**H$_\alpha$**$'$), 7.73 (td, J = 1.5 and 7.8 Hz, 1H, Py**H$_\delta$**), 7.66 (td, J = 1.5 and 7.8 Hz, 1H, Py**H$_\delta$**$'$), 7.44 (d, J = 7.9 Hz, 2H, Py**H$_\gamma$** and Py**H$_\gamma$**$'$), 7.37-7.33 (m, 1H, Py**H$_\beta$**), 7.11-7.06 (m, 1H,

UNIVERSITAT ROVIRA I VIRGILI
MECHANISTIC STUDIES OF WATER OXIDATION CATALYZED BY HOMOGENEOUS IRON AND RUTHENIUM
COMPLEXES AND LIGHT-DRIVEN ORGANIC REDUCTIONS WITH A DUAL COBALT/COPPER CATALYTIC SYSTEM
Carla Casadevall Serrano

CHAPTER IV   Mechanistic Investigations of WO Catalyzed by Ru Complexes

PyH_β'), 4.45 (d, J = 15.6 Hz, 1H, Py-CH$_2$), 4.35 (d, J = 15.6 Hz, 1H, Py-CH$_2$), 4.00 (d, J = 15.6 Hz, 1H, Py-CH$_2$), 3.48-3.27 (m, 5H, N-CH$_2$-CH$_2$), 3.10-2.99 (m, 2H, N-CH$_2$-CH$_2$), 2.96-2.87 (m, 2H, N-CH$_2$-CH$_2$), 2.77 (s, 3H, N-CH$_3$), 2.74-2.68 (m, 1H, N-CH$_2$-CH$_2$), 2.20-2.09 (m, 1H, N-CH$_2$-CH$_2$), 1.98-1.87 (m, 1H, N-CH$_2$-CH$_2$). Analysis calculation for C$_{19}$H$_{29}$F$_{12}$N$_5$OP$_2$Ru· NH$_4$PF$_6$ (MW = 897.47 g/mol): N, 9.36; C, 25.43; H, 3.71 %. Found: N, 8.55; C, 25.26; H, 3.70 %. CSI-HRMS: m/z calcd for [Ru^{II}(F)(Py$_2$Metacn)]$^+$ is 446.1294; found 446.1306.

IV.4.3. Water oxidation reactions

Water-oxidation reactions (8/run) were performed in a 15 ml vial capped with septa and equipped with stir bars. Each of the volume-calibrated vials that contained the oxidant–Milli-Q water solution (125 mM of NaIO$_4$ or 125 mM of CAN in 9.5 ml otherwise mentioned) were connected to one port of a differential pressure transducer sensor. Each reaction had its reference reaction, which was connected to the other port of the differential pressure transducer sensors. Both vials were kept under the same experimental conditions. Stock solutions were prepared by weighting the ruthenium catalysts inside of the glovebox to prevent them from hydration due to their high hygroscopicity. Once all the sensors were connected, 0.5 ml (otherwise mentioned) of the stock solution of the WO catalyst were added to the Milli-Q water-oxidant solution to start the on-line monitoring of the O$_2$ evolution. The oxygen evolution of the reactions was monitored by recording the headspace pressure increase (one second intervals). The oxygen contained in each of the reaction vials was measured by analysing an aliquot of the gas captured at the headspace (0.1 ml) by GC-TCD.

IV.4.4. Electrochemical Studies

All electrochemical experiments were performed with a Biologic VSP potentiostat, using a three-electrode cell configuration. Glassy carbon disk (ϕ = 3 mm, S = 0.07 cm^2) was used as working electrode, Pt wire as counter electrode and Hg/Hg$_2$SO$_4$ (K$_2$SO$_4$ saturated) as reference electrode (potentials were converted to NHE by adding 0.65 V). CVs and DPVs were iR compensated by the potentiostat in all the measurements. Glassy carbon electrodes were polished with 0.05 micron alumina (Al$_2$O$_3$) and washed water before every measurement.

IV.4.5. UV-Vis titration studies

The characterization of the WO intermediates by UV-Vis spectroscopy was done at 25 ºC and under N$_2$ using either NaIO$_4$ and CAN as sacrificial oxidants. To a 3 ml solution of **1Ru^{II}-OH$_2$** (0.25 mM) in MilliQ-water under N$_2$ atmosphere in a quartz UV-vis cell, subsequent additions of either NaIO$_4$ and CAN in aliquots of 5 μl (15 mM, 0.1 eq. respect to the ruthenium complex) led the formation of **1Ru^{III}-OH** and further titration **1Ru^{IV}=O** species. After each addition of oxidant, the UV-Vis spectrum was let to stabilize before further titration. When studying the **1Ru^{III}-OH$_2$** speciation the pH was fixed at 0.7 by using HOTf (1.1 M final concentration).

IV.4.6. High resolution mass spectrometry (HRMS)

All HRMS were recorded on a Bruker MicrOTOF-Q IITM instrument with ESI or Coldspray ionization sources at Serveis Tècnics of the University of Girona. Samples were introduced into the mass spectrometer ion source by direct infusion using a syringe pump and were externally calibrated using sodium formate. The instrument was operated in the positive ion mode. The characterization of the WO intermediates by HRMS was done at 25 ºC. From a solution of [Ru^{II}(H$_2$O)(Py$_2^{Me}$tacn)](PF$_6$)$_2$ (**1Ru^{II}-OH$_2$**) (8 mM) in water (250

µl of MilliQ, D_2O or $H_2^{18}O$, depending on the experiment) under N_2 an aliquot was firstly analyzed. Then the sample was titrated with an oxidant (0.5 eq. of $NaIO_4$ and 1 eq. of CAN) to form the **$1Ru^{III}$-OH** species. Further titration with oxidant (up to 1.5 eq. of $NaIO_4$ and 4 eq. of CAN) led to the formation of the **$1Ru^{IV}=O$** species.

IV.4.7. ^{18}O labeling Studies

a) O_2 MS-monitoring of the in situ formation of the $1Ru^{IV}=^{16}O$ and subsequent reaction with an excess of CAN in $H_2^{18}O$. In a crimped vial the **$1Ru^{II}$-$^{16}OH_2$** (6.7 mg, $9.2 \cdot 10^{-3}$ mmol, final concentration = 2.5 mM) complex was suspended in $H_2^{16}O$ (0.6 mL, degassed Milli-Q water). The mixture was heated for 5 h to 70 ºC leading a green-yellow solution. The head space of the vial containing the resulting solution was monitored with an atmospheric pressure quadrupole mass spectrometer apparatus (Omnistar GSD 301 C Pfeiffer, m/z 28, 32, 34, 36, 40, 44, 46, 48 were monitored). After equilibration of the MS signal, three subsequent additions of CAN (2 eq, 0.8 mL of a solution of CAN (11 mg, 0.02 mmol), CF_3SO_3H (270 µL) in $H_2^{16}O$ (0.89 mL, degassed Milli-Q water)) in intervals of 30 min to quantitative form of $Ru^{IV}(^{16}O)$ complex *in situ*. Then, CAN (c.a. 100 eq., 0.65 mL of a [CAN] solution in degassed water 97% isotopically labelled) was added. $V_{total}(H_2^{18}O) = 0.65$ mL, $V_{total}(H_2^{16}O) = 3.04$ mL. $V_{(final)} = 3.69$ mL. This produces a final concentration of catalyst of 2.5 mM and a final $H_2^{18}O$ content of 16.7%.

b) O_2 MS-monitoring of the In situ formation of the $1Ru^{IV}=^{18}O$ and subsequent reaction with an excess of CAN in $H_2^{16}O$. In a crimped vial the **$1Ru^{II}$-$^{16}OH_2$** (3.5 mg, $4.8 \cdot 10^{-3}$ mmol, final concentration = 2.1 mM) complex was suspended in $H_2^{18}O$ (0.5 mL, 97% isotopically labelled). The mixture was heated for 5 h to 70 ºC to *in situ* generate **$1Ru^{II}$-$^{18}OH_2$** (97% labelled) leading to a green-yellow solution. The head space of the vial containing the resulting solution was monitored with an atmospheric pressure quadrupole mass

spectrometer apparatus (Omnistar GSD 301 C Pfeiffer, m/z 28, 32, 34, 36, 40, 44, 46, 48 were monitored). After equilibration of the MS signal, three subsequent additions of CAN (2 eq, 50 µL of a solution of CAN (21 mg, 0.038 mmol), CF_3SO_3H (16 µL) in $H_2^{18}O$ (200 µL at 97%)) in intervals of 30 min and a final additional CAN (1 eq) were added to quantitative form of $\mathbf{1Ru^{IV}{=}^{18}O}$ complex *in situ*. Then, CAN (c.a. 103 eq., 1.75 mL of a [CAN] solution in degassed Milli-Q water) was added. $V_{total}(H_2^{18}O) = 0.675$ mL, $V_{total}(H_2^{16}O) = 1.75$ mL. This produces a final concentration of catalyst of 2.1 mM and a final $H_2^{18}O$ content of 26.4 %.

c) Mathematical treatment. For a final concentration of $H_2^{18}O$, taking into account the three possible mechanistic scenarios for the O-O bond formation and their contribution to the final O_2 isotopic distribution evolved from the reaction, we can construct a system of three equations and three variables. The latter is the result of considering the observed O_2 isotopic distribution as a linear combination of the three possible scenarios (Figure IV.16 and Scheme IV.2). Solving the system of equations by applying the Cramer's rule, allows finding the contribution of each mechanism along the reaction time.

169
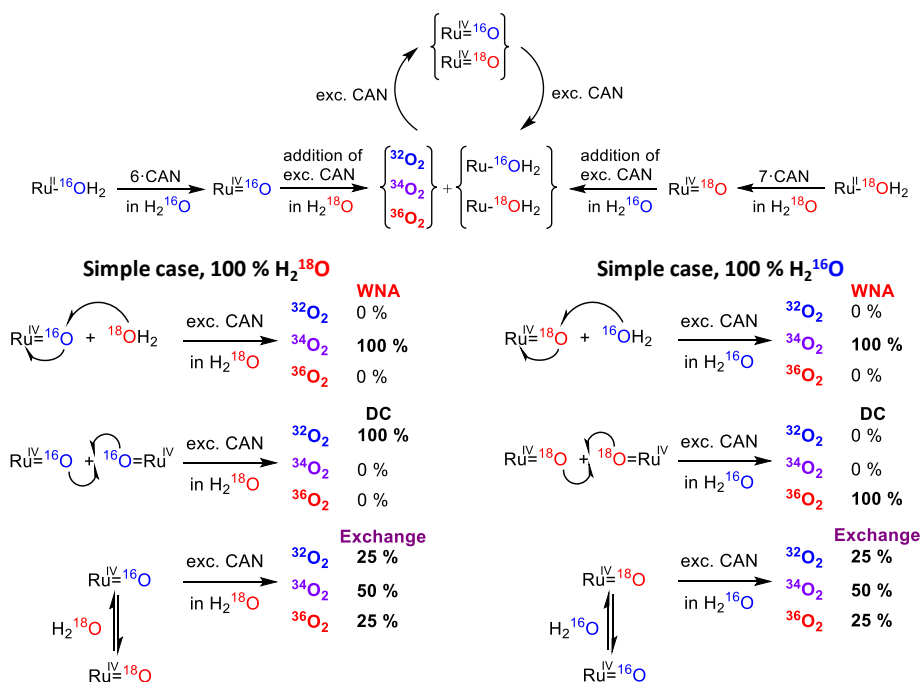
Figure IV.16. Possible isotopic O_2 distribution and percentage of the contribution of each mechanism in the simple case when having 100 % of ^{16}O or ^{18}O.

$$^{32}O_{2(WNA)} \cdot \textbf{WNA} + {}^{32}O_{2(DC)} \cdot \textbf{DC} + {}^{32}O_{2(EXC)} \cdot \textbf{EXC} = {}^{32}\textbf{O}_2$$

$$^{34}O_{2(WNA)} \cdot \textbf{WNA} + {}^{34}O_{2(DC)} \cdot \textbf{DC} + {}^{34}O_{2(EXC)} \cdot \textbf{EXC} = {}^{34}\textbf{O}_2$$

$$^{36}O_{2(WNA)} \cdot \textbf{WNA} + {}^{36}O_{2(DC)} \cdot \textbf{DC} + {}^{36}O_{2(EXC)} \cdot \textbf{EXC} = {}^{36}\textbf{O}_2$$

Scheme IV.2. Three equations with three variables system generated by taking into account the three possible mechanisms for the O-O bond formation event and their contributions to each of the three possible dioxygen isotopomers evolved from the reaction.

I.5. References

(1) Sala, X.; Maji, S.; Bofill, R.; García-Antón, J.; Escriche, L.; Llobet, A. *Acc. Chem. Res.* **2014**, *47*.

(2) Blakemore, J. D.; Crabtree, R. H.; Brudvig, G. W. *Chem. Rev.* **2015**, *115*, 12974.

(3) Ashford, D. L.; Gish, M. K.; Vannucci, A. K.; Brennaman, M. K.; Templeton, J. L.; Papanikolas, J. M.; Meyer, T. J. *Chem. Rev.* **2015**.

(4) Karkas, M. D.; Verho, O.; Johnston, E. V.; Akermark, B. *Chem. Rev.* **2014**, *114*, 11863.

(5) Chu, S.; Majumdar, A. *Nature* **2012**, *488*, 294.

(6) Lewis, N. S.; Nocera, D. G. *Proc. Natl. Acad. Sci. U.S.A.* **2006**, *103*, 15729.

(7) Blankenship, R. E.; Tiede, D. M.; Barber, J.; Brudvig, G. W.; Fleming, G.; Ghirardi, M.; Gunner, M. R.; Junge, W.; Kramer, D. M.; Melis, A. *Science* **2011**, *332*, 805.

(8) Dismukes, G. C.; Brimblecombe, R.; Felton, G. A. N.; Pryadun, R. S.; Sheats, J. E.; Spiccia, L.; Swiegers, G. F. *Acc. Chem. Res.* **2009**, *42*, 1935.

UNIVERSITAT ROVIRA I VIRGILI
MECHANISTIC STUDIES OF WATER OXIDATION CATALYZED BY HOMOGENEOUS IRON AND RUTHENIUM
COMPLEXES AND LIGHT-DRIVEN ORGANIC REDUCTIONS WITH A DUAL COBALT/COPPER CATALYTIC SYSTEM
Carla Casadevall Serrano

CHAPTER IV   Mechanistic Investigations of WO Catalyzed by Ru Complexes

(9) Wasylenko, D. J.; Palmer, R. D.; Berlinguette, C. P. *Chem. Commun.* **2013**, *49*, 218.

(10) Romain, S.; Vigara, L.; Llobet, A. *Acc. Chem. Res.* **2009**, *42*, 1944.

(11) Sala, X.; Romero, I.; Rodríguez, M.; Escriche, L.; Llobet, A. *Angew. Chem., Int. Ed.* **2009**, *48*, 2842.

(12) Gersten, S. W.; Samuels, G. J.; Meyer, T. J. *J. Am. Chem. Soc.* **1982**, *104*, 4029.

(13) Mola, J.; Mas-Marza, E.; Sala, X.; Romero, I.; Rodríguez, M.; Viñas, C.; Parella, T.; Llobet, A. *Angew. Chem., Int. Ed.* **2008**, *47*, 5830.

(14) Zoel Codolà, J. M. C., Beatriz Royo, Miquel Costas, Julio Lloret-Fillol *Chem. Eur. J.* **2013**, *19*, 7203.

(15) Thomsen, J. M.; Huang, D. L.; Crabtree, R. H.; Brudvig, G. W. *Dalton. Trans.* **2015**, *44*, 12452.

(16) Hull, J. F.; Balcells, D.; Blakemore, J. D.; Incarvito, C. D.; Eisenstein, O.; Brudvig, G. W.; Crabtree, R. H. *J. Am. Chem. Soc.* **2009**, *131*, 8730.

(17) McDaniel, N. D.; Coughlin, F. J.; Tinker, L. L.; Bernhard, S. *J. Am. Chem. Soc.* **2008**, *130*, 210.

(18) Savini, A.; Bellachioma, G.; Ciancaleoni, G.; Zuccaccia, C.; Zuccaccia, D.; Macchioni, A. *Chem. Commun.* **2010**, *46*, 9218.

(19) Limburg, J.; Brudvig, G. W.; Crabtree, R. H. *J. Am. Chem. Soc.* **1997**, *119*, 2761.

(20) Limburg, J.; Vrettos, J. S.; Liable-Sands, L. M.; Rheingold, A. L.; Crabtree, R. H.; Brudvig, G. W. *Science* **1999**, *283*, 1524.

(21) Ellis, W. C.; McDaniel, N. D.; Bernhard, S.; Collins, T. J. *J. Am. Chem. Soc.* **2010**, *132*, 10990.

(22) Fillol, J. L.; Codolà, Z.; Garcia-Bosch, I.; Gómez, L.; Pla, J. J.; Costas, M. *Nat. Chem.* **2011**, *3*, 807.

(23) Codolà, Z.; Garcia-Bosch, I.; Acuña-Parés, F.; Prat, I.; Luis, J. M.; Costas, M.; Lloret-Fillol, J. *Chem. Eur. J.* **2013**, *19*, 8042.

(24) Zoel Codolà, L. G., Scott T. Kleespies, Lawrence Que Jr, Miquel Costas & Julio Lloret-Fillol *Nat. Commun.* **2015**, *6*.

(25) Acuna-Pares, F.; Codola, Z.; Costas, M.; Luis, J. M.; Lloret-Fillol, J. *Chem. Eur. J.* **2014**, *20*, 5696.

(26) Kundu, S.; Annavajhala, M.; Kurnikov, I. V.; Ryabov, A. D.; Collins, T. J. *Chem.—Eur. J.* **2012**, *18*, 10244.

(27) Demeter, E. L.; Hilburg, S. L.; Washburn, N. R.; Collins, T. J.; Kitchin, J. R. *J. Am. Chem. Soc.* **2014**, *136*, 5603.

(28) Zhang, B.; Li, F.; Yu, F.; Cui, H.; Zhou, X.; Li, H.; Wang, Y.; Sun, L. *Chem.—Asian J.* **2014**, *9*, 1515.

(29) Coggins, M. K.; Zhang, M.-T.; Vannucci, A. K.; Dares, C. J.; Meyer, T. J. *J. Am. Chem. Soc.* **2014**, *136*, 5531.

(30) To, W.-P.; Wai-Shan Chow, T.; Tse, C.-W.; Guan, X.; Huang, J.-S.; Che, C.-M. *Chemical Science* **2015**, *6*, 5891.

(31) Wickramasinghe, L. D.; Zhou, R.; Zong, R.; Vo, P.; Gagnon, K. J.; Thummel, R. P. *J. Am. Chem. Soc.* **2015**, *137*, 13260.

(32) Okamura, M.; Kondo, M.; Kuga, R.; Kurashige, Y.; Yanai, T.; Hayami, S.; Praneeth, V. K. K.; Yoshida, M.; Yoneda, K.; Kawata, S.; Masaoka, S. *Nature* **2016**, *530*, 465.

(33) Nakazono, T.; Parent, A. R.; Sakai, K. *Chem. Commun.* **2013**, *49*, 6325.

(34) Wang, D.; Groves, J. T. *Proc. Natl. Acad. Sci. U.S.A.* **2013**, *110*, 15579.

(35) Yin, Q.; Tan, J. M.; Besson, C.; Geletii, Y. V.; Musaev, D. G.; Kuznetsov, A. E.; Luo, Z.; Hardcastle, K. I.; Hill, C. L. *Science* **2010**, *328*, 342.

(36) Goberna-Ferrón, S.; Vigara, L.; Soriano-López, J.; Galán-Mascarós, J. R. *Inorg. Chem.* **2012**, *51*, 11707.

(37) Wasylenko, D. J.; Ganesamoorthy, C.; Borau-Garcia, J.; Berlinguette, C. P. *Chem. Commun.* **2011**, *47*, 4249.

(38) Berardi, S.; La Ganga, G.; Natali, M.; Bazzan, I.; Puntoriero, F.; Sartorel, A.; Scandola, F.; Campagna, S.; Bonchio, M. *J. Am. Chem. Soc.* **2012**, *134*, 11104.

(39) Barnett, S. M.; Goldberg, K. I.; Mayer, J. M. *Nat. Chem.* **2012**, *4*, 498.

(40) Zhang, T.; Wang, C.; Liu, S.; Wang, J. L.; Lin, W. *J. Am. Chem. Soc.* **2013**, *136*, 273.

(41) Zhang, M. T.; Chen, Z. F.; Kang, P.; Meyer, T. J. *J. Am. Chem. Soc.* **2013**, *135*, 2048.

(42) Shaffer, D. W.; Xie, Y.; Concepcion, J. J. *Chem. Soc. Rev.* **2017**, *46*, 6170.

(43) Pushkar, Y.; Moonshiram, D.; Purohit, V.; Yan, L.; Alperovich, I. *J. Am. Chem. Soc.* **2014**, *136*, 11938.

(44) Kimoto, A.; Yamauchi, K.; Yoshida, M.; Masaoka, S.; Sakai, K. *Chem. Commun.* **2012**, *48*, 239.

(45) Masaoka, S.; Sakai, K. *Chem. Lett.* **2009**, *38*, 182.

(46) Yoshida, M.; Kondo, M.; Torii, S.; Sakai, K.; Masaoka, S. *Angew. Chem.* **2015**, *54*, 7981.

(47) Yoshida, M.; Masaoka, S.; Abe, J.; Sakai, K. *Chem.—Asian J.* **2010**, *5*, 2369.

(48) Que, L.; Tolman, W. B. *Nature* **2008**, *455*, 333.

(49) Anna Company, G. S., María González-Béjar, Laura Gómez, Martin Clémancey, Geneviève Blondin, Andrew J. Jasniewski, Mayank Puri, Wesley R. Browne, Jean-Marc Latour, Lawrence Que , Jr., Miquel Costas, Julia Pérez-Prieto, and Julio Lloret-Fillol *J. Am. Chem. Soc.* **2014**, *136*.

(50) Ray, K.; Heims, F.; Schwalbe, M.; Nam, W. *Curr Opin Chem Biol* **2015**, *25*, 159.

(51) Puri, M.; Que, L. *Acc. Chem. Res.* **2015**, *48*, 2443.

(52) Company, A.; Lloret-Fillol, J.; Costas, M. In *Comprehensive Inorganic Chemistry II*; Poeppelmeier, J. R. a. K., Ed.; Elsevier: Oxford, 2013; Vol. 3.

(53) Casadevall, C.; Bucci, A.; Costas, M.; Lloret-Fillol, J. In *Adv. Inorg. Chem.*; Academic Press: 2019.

(54) Acuña-Parés, F.; Costas, M.; Luis, J. M.; Lloret-Fillol, J. *Inorg. Chem.* **2014**, *53*, 5474.

(55) Garcia-Bosch, I.; Codolà, Z.; Prat, I.; Ribas, X.; Lloret-Fillol, J.; Costas, M. *Chem. Eur. J.* **2012**, *18*, 13269.

(56) Prat, I.; Mathieson, J. S.; Güell, M.; Ribas, X.; Luis, J. M.; Cronin, L.; Costas, M. *Nat. Chem.* **2011**, *3*, 788.

(57) Irene Prat, A. C., Teresa Corona, Teodor Parella, Xavi Ribas, and Miquel Costas *Inorg. Chem.* **2013**, *52*, 9229.

(58) Anna Company; Irene Prat; Jonathan R. Frisch; Ruben Mas-Ballest; Mireia Güell; Gergely Juhász; Xavi Ribas; Eckard Münck; Josep M. Luis; Lawrence Que, J.; Costas, M. *Chem. Eur. J.* **2011**, *17*, 1622.

(59) A. L. Gott, P. C. M., T.J. Podesta, C.W. Tate *Inorg. Chim. Acta* **2004**, *357*, 689.

(60) W.P. Yip, C. M. H., N.Zhu, T.C. Lau, C.M. Che *Chem. Asian J.* **2008**, *3*, 70.

(61) C.M. Che, W. P. Y., W.Y. Yu *Chem. Asian J* **2006**, *1*, 453.

(62) Cheng, W. C.; Yu, W. Y.; Cheung, K. K.; Che, C. M. *J. Chem. Soc., Dalton Trans.* **1994**, *1*, 57.

(63) Yip, W.-P.; Yu, W.-Y.; Zhu, N.; Che, C.-M. *J. Am. Chem. Soc.* **2005**, *127*, 14239.

(64) Wai-Hung Cheung, W.-Y. Y., Wing-Ping Yip, Nian-Yong Zhu, Chi-Ming Che *J. Org. Chem.* **2002**, *67*, 7716.

(65) Koichiro Jitsukawa, Y. O., Syuhei Yamaguchi and Hideki Masuda *Inorg. Chem.* **2004**, *43*, 8119.

(66) M. Yamaguchi, H. K., S. Izawa, Y. Ichii, T. Kumano, D. Masui, and T. Yamagishi *Inorg. Chem.* **2006**, *45*, 8342.

(67) E. McNeill, J. D. B. *Chem. Sci.* **2012**, *3*, 1810.

(68) B. Radaram, J. A. I., W. M. Singh, R. M. Grudzien, J. H. Reibenspies, C. E. Webster and X. Zhao *Inorg. Chem.* **2011**, *50*, 10564.

(69) Parent, A. R.; Crabtree, R. H.; Brudvig, G. W. *Chem. Soc. Rev.* **2013**, *42*, 2247.

(70) Anna Company; Yan Feng; Mireia Güell; Xavi Ribas; Josep M. Luis; Lawrence Que, J.; Costas, M. *Chem. Eur. J.* **2009**, *15*, 3359.

(71) Gilbert, J. A.; Eggleston, D. S.; Murphy, W. R.; Geselowitz, D. A.; Gersten, S. W.; Hodgson, D. J.; Meyer, T. J. *J. Am. Chem. Soc.* **1985**, *107*, 3855.

(72) *Ber. Bunsen-Ges. Phys. Chem* **1977**, *81*, 245.

(73) Sala, X.; Ertem, M. Z.; Vigara, L.; Todorova, T. K.; Chen, W.; Rocha, R. C.; Aquilante, F.; Cramer, C. J.; Gagliardi, L.; Llobet, A. *Angew. Chem., Int. Ed.* **2010**, *49*, 7745.

(74) Marenich, A. V.; Cramer, C. J.; Truhlar, D. G. *J Phys Chem B* **2009**, *113*, 6378.

(75) A. K. Vardhaman, C. V. S., D. Kumar, S. P. de Visser, *Chem. Commun.* **2011**, *47*, 11044.

(76) S. P. de Visser, M. G. Q., B, Martín, P. Comba, U. Ryde, *Chem. Commun.* **2014**, *50*, 262.

UNIVERSITAT ROVIRA I VIRGILI
MECHANISTIC STUDIES OF WATER OXIDATION CATALYZED BY HOMOGENEOUS IRON AND RUTHENIUM
COMPLEXES AND LIGHT-DRIVEN ORGANIC REDUCTIONS WITH A DUAL COBALT/COPPER CATALYTIC SYSTEM
Carla Casadevall Serrano

MECHANISTIC STUDIES OF WATER OXIDATION CATALYZED BY HOMOGENEOUS IRON AND RUTHENIUM
COMPLEXES AND LIGHT-DRIVEN ORGANIC REDUCTIONS WITH A DUAL COBALT/COPPER CATALYTIC SYSTEM

Carla Casadevall Serrano

CHAPTER V

Computational Study of the Mechanisms Involved in Water Oxidation Catalyzed by Ru Complexes Based on Aminopyridyl Ligands: Understanding the Differences in Reactivity Between Analogous Ru and Fe Complexes

Part of this chapter corresponds to the following publication:

UNIVERSITAT ROVIRA I VIRGILI

MECHANISTIC STUDIES OF WATER OXIDATION CATALYZED BY HOMOGENEOUS IRON AND RUTHENIUM
COMPLEXES AND LIGHT-DRIVEN ORGANIC REDUCTIONS WITH A DUAL COBALT/COPPER CATALYTIC SYSTEM

Carla Casadevall Serrano

V. Computational Study of the Mechanisms Involved in Water Oxidation Catalyzed by Ru Complexes Based on Aminopyridyl Ligands: Understanding the Differences in Reactivity Between Analogous Ru and Fe Complexes

V.1. General insight

This chapter is the follow up of chapter IV and has been separated to better illustrate and describe the computational study of these systems. In this chapter, with the aim to clarify and get further insights into the mechanism of the WO reaction catalyzed by $[Ru^{II}(OH_2)(Py_2^{Me}tacn)]^{2+}$ and the differences in reactivity between Ru and Fe complexes, we decided to investigate in detail all detectable intermediates and model the catalytic cycle by DFT.

Due to the inherent complexity of the metal catalysed water oxidation transformation and the limited information provided by spectroscopic techniques in paramagnetic species characterization, computational modelling provides useful insights into the fundamentals of the transformation. Recently, theoretical studies using Density Functional Theory (DFT)[1-10] have shed light in the WO mechanisms by providing highly detailed structural and energetic data of the key intermediates involved in the catalytic cycle.[11]

As mentioned in chapter IV, several scenarios can be envisioned for the O-O bond formation by **1Ru^{II}-OH$_2$** complexes after the generation of **1Ru^{IV}=O** or **1Ru^{V}=O** active species, which are mainly summarized as a direct coupling (DC) or water nucleophilic attach mechanism (WNA). In the DC scenario, O-O bonding occurs between two Ru^{IV}-oxyl groups. Therefore, the O-O bonding orbital arises from the combination of two Ru-O orbitals with $\pi*$ character. Extensive DFT studies have been reported by Muckerman and co-workers for two-site ruthenium catalysts that have shed light in the proposed intermediates.[1] On the other hand, in the WNA mechanistic proposal, a nucleophilic oxygen from a water molecule or a hydroxide

UNIVERSITAT ROVIRA I VIRGILI
MECHANISTIC STUDIES OF WATER OXIDATION CATALYZED BY HOMOGENEOUS IRON AND RUTHENIUM
COMPLEXES AND LIGHT-DRIVEN ORGANIC REDUCTIONS WITH A DUAL COBALT/COPPER CATALYTIC SYSTEM
Carla Casadevall Serrano

CHAPTER IV   Computational Study of WO mechanisms: Ru *vs* Fe

moiety attacks an electrophilic Ru^V-oxo group. That is, a σ orbital (HOMO) from a water molecule (or hydroxide moiety) attacks the π∗ Ru-O orbital (LUMO), leading to the formation of a σ O-O bond while breaking one of the π Ru-O bonds.

V.2. Results and discussion

V.2.1. Interrogating the active species and O-O bond formation event

We became interested in gaining a deeper mechanistic understanding of both: i) the intermediates involved in the catalytic cycle of WO catalysed by complex $[Ru^{II}(OH_2)(Py_2^{Me}tacn)]^{2+}$, and ii) the differences in the WO activity between the $Py_2^{Me}tacn$ iron and ruthenium complexes. To this end, we have performed a computational study of the full catalytic cycle. We have optimized the Cartesian geometries at a DFT uM11/6-31G(d) (SDD basis set for Ru) level including the solvent effect of water with the polarizable continuum model PCM-SMD.[12] In this work, we have used the new functional M11 to compute the catalytic cycle of the WO reaction. The use of this functional is justified on the basis of several published results of Thrular[13,14] and Cramer.[15] Truhlar and co-workers optimized M11 parameters against a broad database of energetic chemical properties and compared its performance to that of well-known functionals, including previous Minnesota functionals.[13] M11 introduces a Hartree-Fock exchange of 100 % at large interelectronic distance and an optimum percentage of 42.8 at short range. The comparison was done between M11 functional with common GGA and meta-GGA approximations by mean unsigned errors (MUEs) for the BC332 database and its subdatabases. The considered functionals were PBE[16] and SOGGA11[17] (GGA functionals), B3LYP[18-21] and B97-3[22] (hybrid GGAs), ωB97X[23] and ωB97X-D[24] (RSH-GGAs), and all eight previous Minnesota functionals, M05,[25] M05-2X,[26] M06-L,[27] M06,[28] M06-2X,[28] M06-HF,[29] M08-SO,[30] and M08-HX.[30] In terms of overall performance, M11 is the best functional of all those considered. From the results reported in the study,[13] it is clear that GGA functionals cannot

provide consistently good results for all components of such a broad database. M11 has especially good performance for main-group atomization energies, proton affinities, electron affinities and for ionization potentials.

As a result, we have found a good agreement between the experimental X-ray (from chapter IV) and the theoretical bond distances (see tables V.1, V2 and A.II.1). Energies have been further refined by single point calculations with the cc-pVTZ dunning basis set for all atoms (see *V.4.1. Theoretical Methods* section for details). We have examined the relative energies of all the possible spin multiplicities for all ruthenium species in all the target oxidation states to identify the ground spin state in each case. The methodology used herein uM11/cc-pVTZ//uM11/6-31G(d), including solvent (SMD = water), spin contamination and Gibbs corrections has been previously benchmarked, and it has shown a notable agreement with experimental data.[31,32] Labels **I**, **II**, **III**, **IV**, **V**, **VI**, **VIII** and **TS** are used as short nomenclature of the successive intermediates and transition states involved in WO mechanism catalyzed by complex $[Ru^{II}(OH_2)(Py_2{}^{Me}tacn)]^{2+}$. Besides, subscripts **s**, **d**, **t**, **q**, **quint** and **sext** are used to specify the singlet, doublet, triplet, quadruplet, quintuplet and sextuplet spin state of the metal centre in the previous structures.

Table V.1. Comparison of bond distances between X-ray diffraction and DFT modelled coordinates for $[Ru^{II}Cl(Py_2{}^{Me}tacn)]Cl$ (left) and $[Ru^{III}Cl(Py_2{}^{Me}tacn)]Cl_2$ structures.
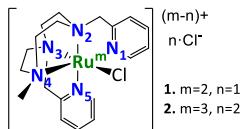
Bond distances	X-ray structures data		DFT data	
	$1Ru^{II}$-Cl	$1Ru^{III}$-Cl	$1Ru^{II}$-Cl	$1Ru^{III}$-Cl
d(Ru-Cl)	2.454(2)	2.327(3)	2.464	2.349
d(Ru-N$_1$)	2.056(6)	2.077(8)	2.065	2.101
d(Ru-N$_2$)	2.078(7)	2.074(8)	2.095	2.087
d(Ru-N$_3$)	2.072(7)	2.083(7)	2.097	2.117
d(Ru-N$_4$)	2.124(6)	2.122(9)	2.163	2.152
d(Ru-N$_5$)	2.082(7)	2.091(8)	2.059	2.100

Theoretically modelled distances of the most stable spin states. Bond distances are given in Å.

Table V.2. Comparison between selected bond distances for solid-state X-ray diffraction and the DFT modelled structures.

1: L = H$_2$O, X = PF$_6^-$, n = 2
2: L = H$_2$O, X = PF$_6^-$, n = 3
3: L = OH, X = PF$_6^-$, n = 2
4: L = O, X = PF$_6^-$, n = 2
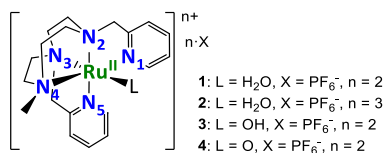
Bond distances	X-ray data	DFT data			
	1Ru^{III}-OH	1Ru^{II}-OH$_2$	1Ru^{III}-OH$_2$	1Ru^{III}-OH	1Ru^{IV}=O
d(Ru-O/N)	1.943(7)	2.234	2.194	1.931	1.762
d(Ru-N$_1$)	2.074(7)	2.097	2.126	2.100	2.095
d(Ru-N$_2$)	2.044(7)	2.096	2.101	2.089	2.085
d(Ru-N$_3$)	2.098(8)	2.065	2.071	2.143	2.234
d(Ru-N$_4$)	2.107(7)	2.156	2.142	2.146	2.159
d(Ru-N$_5$)	2.063(7)	2.100	2.091	2.098	2.091

Theoretically modelled distances of the most stable spin states. Bond distances are given in Å.

Mechanistic studies on the basis on kinetics, spectroscopic, ^{18}O labelling and electrochemical studies, have pointed towards a water nucleophilic attack over a metal-oxo species, most likely a **1Ru^V=O** ([Ru^V(O)(Py$_2^{Me}$tacn)]$^{2+}$) to form the O-O bond, which is the rate-determining step (RDS). In addition, titration studies monitored by NMR and UV-Vis spectroscopy confirmed that [Ru^{IV}(O)(Py$_2^{Me}$tacn)]$^{2+}$ is the resting state of the catalytic cycle. By monitoring the Ce^{IV} consumption, we have found that the O$_2$ evolution rate is redox-controlled and independent of the initial concentration of Ce^{IV}.

As a first step to unravel the WO mechanism catalysed by [Ru^{II}(OH$_2$)(Py$_2^{Me}$tacn)]$^{2+}$ complex, we investigated the potential speciation in the presence of Ce^{IV}. Therefore, we have evaluated the pKa, reduction potential and proton-coupled electron transfer (PCET) processes for the different aquo/hydroxo/oxo Ru$^{II/III}$, Ru$^{III/IV}$ and Ru$^{IV/V}$ redox couples, respective transformations. This analysis allowed us to establish by DFT the dominant species under catalytic conditions. It is worth to note that we have examined the relative energies of all possible spin multiplicities for the ruthenium species in oxidation states II, III, IV and V, to identify the ground spin state in each

case (see Table V.3). Moreover, we have directly compared the theoretical values of the possible redox processes in solution with the electrochemical experimental values in the pH rage of 2 to 12 by the construction of a Pourbaix diagram with the experimental and theoretical values (Figure V.1). The Pourbaix diagram gives information of the accessibility of determined species at a given redox potential and pH, which can be correlated with the catalytic conditions given by Ce^{IV}.

Table V.3. Relative energies for the possible spin states of the Ru complexes involved in the catalytic cycle of the water oxidation reaction. The same calculations have been done with the analogous $Fe^{IV}(O)$ and $Fe^{V}(O)$ intermediates.

Complex 1Ru^{II}-OH₂		[(Py₂^{Me}tacn)Ru^{III}-OO·]²⁺ (IV_s)	

Complex 1Ru^{II}-OH$_2$		**[(Py$_2^{Me}$tacn)Ru^{III}-OO·]$^{2+}$ (IV$_s$)**	
Spin state	ΔG (kcal·mol^{-1})[a]	$S = 0$	0.0
[(Py$_2^{Me}$tacn)Ru^{II}-OH$_2$]$^{2+}$ (VIII$_s$)		$S = 1$	8.1
$S = 0$	0.0	**[(Py$_2^{Me}$tacn)Ru^{IV}-OO]$^{2+}$ (IV'$_s$)**	
$S = 1$	35.7	$S = 0$	0.0
[(Py2Metacn)Ru^{III}-OH$_2$]$^{2+}$ (VI$_s$)		$S = 1$	37.0
$S = 1/2$	0.0	**[(Py$_2^{Me}$tacn)Ru^{III}-O$_2$]$^{2+}$ (V$_{quad}$)**	
$S = 3/2$	31.8	$S = 1/2$	25.3
[(Py$_2^{Me}$tacn)Ru^{III}-OH]$^{2+}$ (VII$_d$)		$S = 3/2$	0.0
$S = 1/2$	0.0	$S = 5/2$	18.2
$S = 3/2$	33.3		
[(Py$_2^{Me}$tacn)Ru^{IV}=O]$^{2+}$ (I$_t$)			
$S = 0$	16.2	**Complex 1Fe^{II}-OTf**	
$S = 1$	0.0	Spin state	ΔG (kcal·mol^{-1})[a]
$S = 2$	33.5	**[(Py$_2^{Me}$tacn)Fe^{IV}=O]$^{2+}$ (t)**	
[(Py$_2^{Me}$tacn)Ru^{V}=O]$^{3+}$ (II$_d$)		$S = 0$	29.5
$S = 1/2$	0.0	$S = 1$	0.0
$S = 3/2$	12.6	$S = 2$	6.6
[(Py$_2^{Me}$tacn)Ru^{III}-OOH]$^{2+}$ (III$_d$)		**[(Py$_2^{Me}$tacn)Fe^{V}=O]$^{3+}$ (quad)**	
$S = 1/2$	0.0	$S = 1/2$	6.9
$S = 3/2$	34.2	$S = 3/2$	0.0

[a]The free energy differences are computed using the methodology described in the "Computational details" section of the main text. For the **Ru^{IV}=O** and **Ru^{V}=O** the explicit water molecules have been taken into account in these calculations.

Starting from **1Ru^{II}-OH$_2$** the theoretical red-ox and proton-coupled electron transfer (PCET) processes have been studied to connect **1Ru^{II}-OH$_2$**, **1Ru^{III}-OH$_2$**, **1Ru^{III}-OH**, **1Ru^{IV}=O** and **1Ru^{V}=O**, previously found as intermediates in the catalytic cycle of the WO reaction (chapter IV).[33] Both redox processes, Ru^{III}/Ru^{II} and Ru^{IV}/Ru^{III}, are pH dependent (-62 mV/pH, -52 mV/pH, respectively) in the pH range from 2 - 12. This behaviour is consistent with a proton-coupled electron transfer process (PCET) which enables the formation of a high-valent **1Ru^{IV}=O** species. Similar patterns have been reported for related pentadentate complexes such as [Ru(DPA-Bpy)] (DPA-Bpy = *N,N*-bis(2-pyridinylmethyl)-2,20-bipyridine-6-methanamine)[34] and [Ru(tacn)(bpy)](ClO$_4$)$_2$ (bpy = 2,2'-bipyridine).[35] In addition, it can be seen that at pH < 2 there is a pH-independent process attributed to the **1Ru^{III}-OH$_2$/1Ru^{II}-OH$_2$** redox couple (E$^{III/II}_{1/2}$ = 0.75 V). This is consistent with the **1Ru^{III}-OH$_2$ - 1Ru^{III}-OH** (pKa$_{exp}$ ~ 2 and pKa$_{theor}$ ~ 4) acid-base equilibrium observed in the UV-Vis and NMR spectroscopy titration studies and the theoretical one. Moreover, from **1Ru^{III}-OH$_2$** to **1Ru^{IV}=O** there is the transference of two protons and one electron as judged by the slope of -103 mV/pH. In contrast, E$^{(V/IV)}_{expt}$ = 1.81 V and E$^{(V/IV)}_{theor}$ = 1.85 V for the **1Ru^{IV}=O/1Ru^{V}=O** redox pair is not pH dependent (~ 0 mV/pH) (Figure V.1).
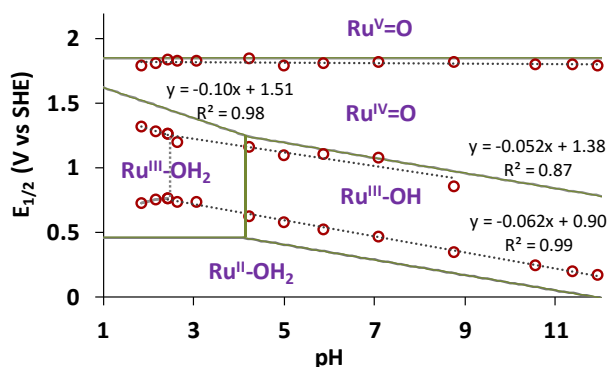
Figure V.1. Pourbaix diagram for complex **1Ru^{II}-OH$_2$** (0.5 mM, 298 K) in aqueous Britton-Robinson buffer (0.1 M) and KNO$_3$ as electrolyte (0.1 M) from pH 1-12 (E$_{1/2}$ *vs* SHE). Points indicate the pH values in which the electrochemistry study has been done; dotted lines are the trend lines for each redox process and the solid lines show the theoretical Pourbaix diagram obtained by DFT calculations.

Moreover, under catalytic conditions given by 125 mM Ce^{IV} the calculated one electron transfer (ET) process and the PCET are in reasonable agreement with the experimental values (Figures V.1 and V.2). **ET**: $E°(Ru^{II/III})_{exp}$ = 0.74 V, $E°(Ru^{II/III})_{theo}$ = 0.45 V; $E°(Ru^{IV/V})_{exp}$ = 1.81 V, $E°(Ru^{IV/V})_{theo}$ = 1.85 V and **PCET**: $E°(Ru^{II/III})_{exp}$ = 0.86 V, $E°(Ru^{II/III})_{theo}$ = 0.66 V; $E°(Ru^{III/IV})_{exp}$ = 1.34 V, $E°(Ru^{III/IV})_{theo}$ = 1.45 V at pH 0.7 and 25 ºC.

Therefore, the dominant species in solution before the O-O bond formation is **$1Ru^{IV}=O$**. The theoretical results are in agreement with the titration experiments with oxidants (CAN and $NaIO_4$) showing the **$1Ru^{II}-OH_2$** → **$1Ru^{III}-OH$** → **$1Ru^{IV}=O$** processes and suggesting that the latter is the resting state of the catalytic cycle. These species were spectroscopically characterised by means of UV-Vis and CSI-HRMS (chapter IV).
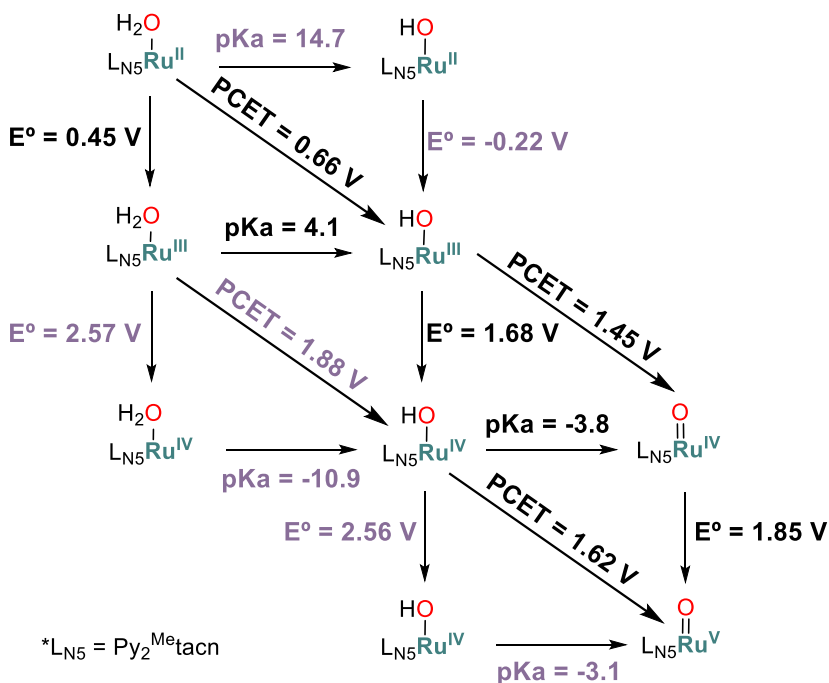
Figure 2. E^0, $E_{1/2(PCET)}$ and pK_a values of the thermodynamic cycle involving L_5Ru^n/L_5Ru^{n+1} transformations (pH 0.7 and 25 ºC). Redox values correspond to the standard redox potentials relative to the SHE. Values in purple represent not possible steps.

183

We theoretically evaluated the option of having **1Ru^{IV}=O** as a promoter for the O-O bond formation through a water nucleophilic attack. To simulate the O-O bond formation, a cluster of four water molecules was used since it previously gave excellent results for similar systems, together with the driving force of Ce^{IV} (CAN, ~1.75 V *vs* SHE)[36] at 298 K and pH 0.7.[11,37-40] The addition of three extra water molecules was needed to account for the hydrogen bonds, otherwise undescribed in the solvent model used (SMD), leading to unrealistic values for the O-O bond formation step. The strongly endergonic thermodynamics (ΔG = 44.4 kcal·mol^{-1}) and the high energy barrier ($\Delta G^{\ddagger}$ = 54.5 kcal·mol^{-1}) obtained for the O-O bond formation clearly discard **1Ru^{IV}=O** as the active species under catalytic conditions (Figure V.3).
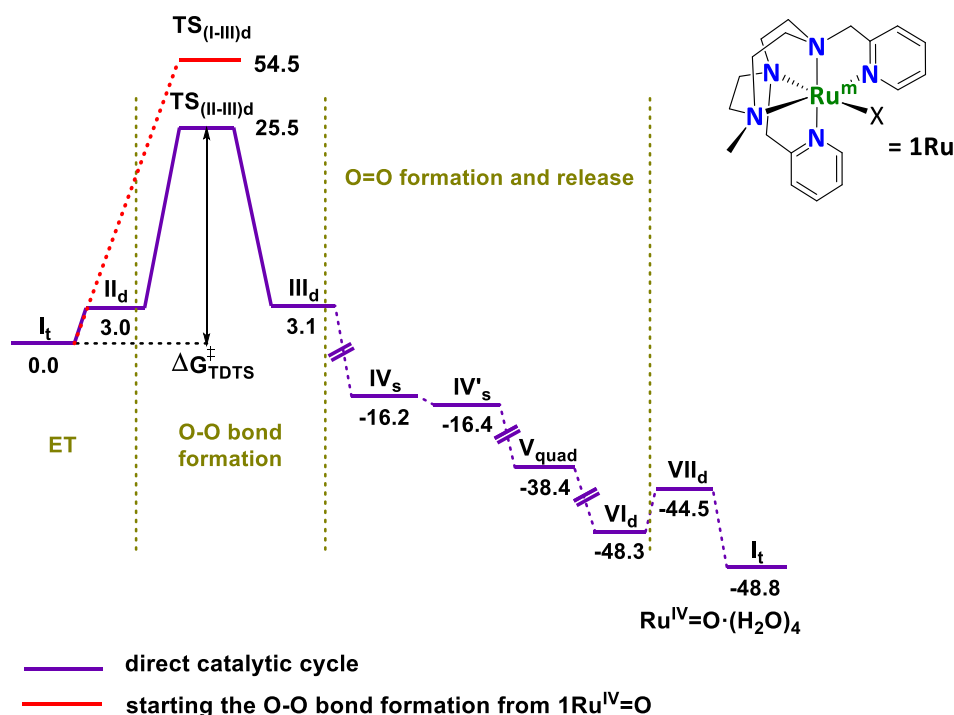
Figure V.3. Energy profile for the catalytic cycle starting from the **1Ru^{IV}=O** (**I$_t$**) species and comparing the free energy barrier for the O-O bond formation starting from **1Ru^{V}=O** (25.5 kcal·mol^{-1}) with that starting from **1Ru^{IV}=O** (54.5 kcal·mol^{-1}), which is over the kinetic limit indicating that this processes is not accessible within the catalytic conditions.

UNIVERSITAT ROVIRA I VIRGILI
MECHANISTIC STUDIES OF WATER OXIDATION CATALYZED BY HOMOGENEOUS IRON AND RUTHENIUM
COMPLEXES AND LIGHT-DRIVEN ORGANIC REDUCTIONS WITH A DUAL COBALT/COPPER CATALYTIC SYSTEM
Carla Casadevall Serrano

CHAPTER IV   Computational Study of WO mechanisms: Ru *vs* Fe

We found that the experimental and theoretical Ru$^{IV/V}$ redox values are well correlated (E$_{(WO\ onset)}$ =1.81 V at pH 0.7 and 298 K; E°(Ru$^{IV/V}$)$_{theo}$ = 1.85 V, Figure V.4). This redox potential is significantly higher than that provided by CAN (~ 1.75 V *vs* SHE, pH 0.7) and much higher than the one provided by NaIO$_4$ (~1.6 V *vs* SHE, at pH 0.7).[36] This is in agreement with our incapacity to experimentally quantitatively characterize the oxidation of [Ru^{IV}(O)(Py$_2^{Me}$tacn)]$^{2+}$ (**I$_t$**) to [Ru^{V}(O)(Py$_2^{Me}$tacn)]$^{3+}$ (**II$_d$**), the WO inactivity when using NaIO$_4$ and the redox dependence of the WO reaction catalysed by complex **1Ru^{II}-OH$_2$**. Therefore, WO presumably involves a highly electrophilic Ru^V oxo species. At this point, if we evaluate the electronic structure of **I$_t$** and **II$_d$**, we observe a significant spin density at the oxo group (ρ(O) ≈ 0.77 and 0.47, respectively) due to the location of unpaired electrons in the π* orbitals (Figure V.5). However, both are well-described as metal-oxo species, therefore it is expected a WNA mechanism *via* a Ru^V-oxo (Figure V.3).
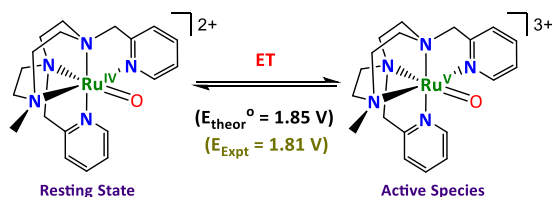
Figure V.4. Proposed redox equilibrium between **1Ru^{IV}=O** and **1Ru^V=O** prior to WNA. The experimental redox potential value was estimated based on electrochemical studies with Ru^{II}-OH$_2$ in water (pH 0.7). The theoretical value was obtained by DFT modelling.
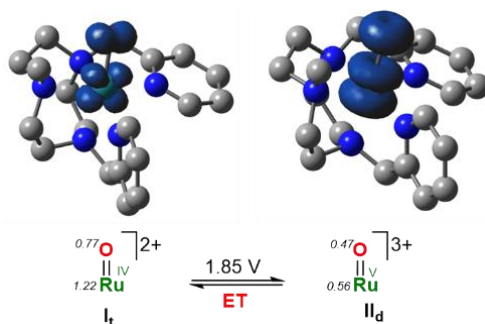
Figure V.5. Spin densities (isovalue = 0.005) calculated for **1Ru^{IV}=O** (**I$_t$**) and **1Ru^V=O** (**II$_d$**). Blue and green regions indicate α and β spin density, respectively.

The corresponding Gibbs free-energy profile showed in Figure V.3 has been constructed taking into consideration the experimental driving force introduced by Ce^{IV} (CAN, ~1.75 V *vs* SHE at pH 0.9, at about 50 mM concentration)[36] at 298 K and pH 0.7.[37,38] Analogously to the construction of the Gibbs free-energy profile having **$1Ru^{IV}=O$** as a promoter for the O-O bond formation, we have also introduced the extra cluster of three water molecules to account for the hydrogen bonding. Optimization of the $[Ru^V(O)(Py_2^{Me}tacn)]^{3+}$ species in the presence of a tetrahedral cluster of water molecules yields a distorted octahedral ruthenium complex $[Ru^V(O)(Py_2^{Me}tacn)]^{3+} \cdot (H_2O)_4$ (**II_d**), in which the oxo moiety of the complex is interacting with the cluster (see Figure V.6). The reaction is initiated by a water molecule reorientation. A water molecule H-bonded to the oxo ligand is disposed in such a way that the oxygen atoms of the oxo ligand and of the water molecule are located in an ideal spatial disposition to form the O-O bond, which happens during the transition state formation (**$TS_{(II-III)d}$**) from the reaction complex **II_d** (Figures V.3 and V.6). The Gibbs energy values for the O-O bond formation barrier are 22.5 kcal·mol^{-1} and 25.5 kcal·mol^{-1} starting from $[Ru^V(O)(Py_2^{Me}tacn)]^{3+} \cdot (H_2O)_4$ (**II_d**) and $[Ru^{IV}(O)(Py_2^{Me}tacn)]^{3+} \cdot (H_2O)_4$ (**I_t**), respectively (see Figure V.3). The later energy O-O formation barrier (**I_t**) was calculated considering the redox processes $Ce^{IV/III}$ (1.75 V) and $Ru^{V/IV}(O)$ (see Figure V.3). The value of 22.5 kcal·mol^{-1} corresponds to the TOF-determining transition state (TDTS), as judged by the full DFT calculated catalytic cycle (Figure V.6). This value is in the range of the kinetic limit but in concordance with the low initial TOF ($4.4 \cdot 10^{-3}$ s^{-1}) observed. Indeed, an energy barrier of about 21 kcal·mol^{-1} is expected for a TOF value of $4.4 \cdot 10^{-3}$ s^{-1}, calculated by the transition state theory (TST), which is within the error of DFT.
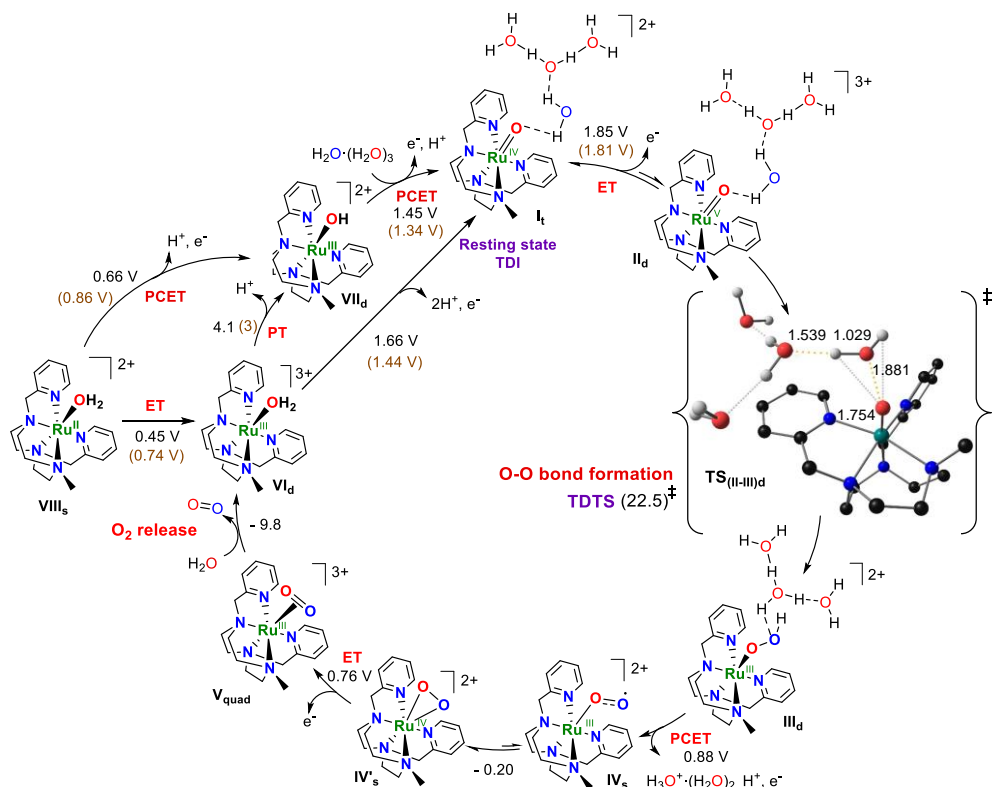
Figure V.6. Summary of the computed WO catalytic cycle for complex [$Ru^{II}(OH_2)(Py_2^{Me}tacn)$]($PF_6$)$_2$ (**1Ru^{II}-OH$_2$**). Values represent the redox potential for the ET, the PCET (at pH 0.7) or the pKa values for the PT [V] at 298 K. Subscripts indicate the spin multiplicity. Energies represent elementary steps and they are given in kcal·mol^{-1} (See Figure V.8 for the energy profile). TDTS = TOF-determining transition state. TDI = TOF-determining intermediate.

The O-O bond formation event leads to the Ru^{III} hydroperoxo [Ru^{III}(O-OH)(Py$_2^{Me}$tacn)]$^{2+}$·{(H$_2$O)$_2$(H$_3$O)$^+$} intermediate (**III$_d$**). Further oxidation coupled with a proton transfer leads first to an O-O end-on Ru^{III} superoxo species in a singlet state (**IV$_s$**, d(O-O) = 1.30 Å). A O-O closed-shell side-on ruthenium (**IV'$_s$**, S = 0) is located 0.2 kcal·mol^{-1} lower in energy with an O-O bond distance of 1.35 Å, characteristic of a peroxo species (see Figures V.7 and V.8).[41] Indeed, all attempts to obtain a S = 0 superoxo Ru^{III} lead to a closed shell electronic structure which formally better describes a Ru^{IV} peroxo structure (that will be further isolated and fully characterized in chapter V).

Additional one electron oxidation leads to a dioxygen Ru^{III} complex ($\textbf{V}_{\textbf{quad}}$) which exchanges the O_2 molecule by a H_2O molecule (-9.8 kcal·mol^{-1}) regenerating the initial state of the catalytic cycle (Figures V.6 and V.7). The O-O bond distance is shortening in the following sequence $[Ru^{III}(O-OH)(Py_2{}^{Me}tacn)]^{2+}$ → $Ru^{IV}(O-O)(Py_2{}^{Me}tacn)]^{2+}$ → $[Ru^{III}(O=O)(Py_2{}^{Me}tacn)]^{2+}$ (1.432, 1.299 and 1.198 Å, respectively), suggesting an increase in the O-O bond order upon oxidation, (Figure V.8). Indeed, after the O-O bond formation, all the intermediates are very low in energy (Figure V.3). Therefore we can only rely on DFT calculations to get mechanistic information oft he species that are being formed since experimental detection is very challenging.[1]
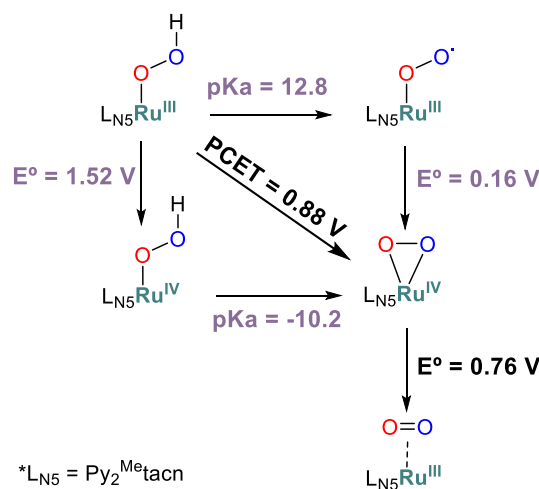
Figure V.7. E^0 , $E_{1/2(PCET)}$ and pK$_a$ values of the thermodynamic cycle involving $L_{N5}Ru^{III}/L_{N5}Ru^{IV}$ transformations (pH 0.7 and 25 ºC). Redox values correspond to the standard redox potentials relative to the SHE. Values in purple represent not possible steps.

As a summary, theoretical calculations and experimental studies (chapter IV) are consistent with two consecutive proton-coupled electron transfer (PCET) oxidations from $\textbf{1Ru}^{\textbf{II}}\textbf{-OH}_2$ to $\textbf{1Ru}^{\textbf{IV}}\textbf{=O}$ and a further oxidation to $\textbf{1Ru}^{\textbf{V}}\textbf{=O}$ under catalytic conditions, which is then attacked by a water molecule to form the O-O bond (WNA mechanism). Then, a ruthenium hydroperoxo intermediate ($\textbf{1Ru}^{\textbf{III}}\textbf{-O-OH}$) is formed, which can be further oxidised under the strong oxidising catalytic conditions to release dioxygen (Figure V.7).
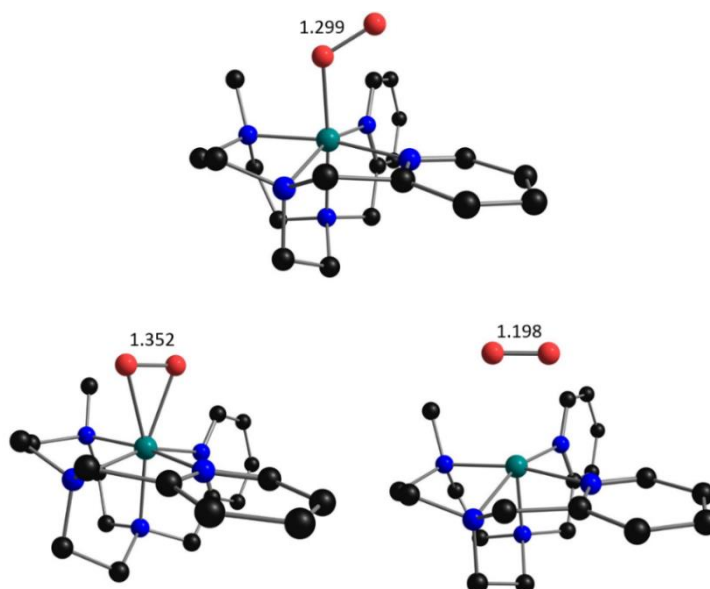
Figure V.8. Optimised geometries for [Ru^{III}(OO$^{\cdot}$)(Py$_2$^{Me}tacn)]$^{2+}$ (**IV$_s$**, singlet, broken symmetry), [Ru^{IV}(OO)(Py$_2$^{Me}tacn)]$^{2+}$ (**IV'$_s$**, singlet) and [Ru^{III}(O=O)(Py$_2$^{Me}tacn)]$^{3+}$ (**V$_{quad}$**, quadruplet). O-O bond distances are given in Å. Hydrogen atoms have been omitted for clarity.

V.2.2. Effect of the redox potential in the energy barrier for the O-O bond formation

In chapter IV, on the basis of kinetic studies changing the initial concentration of CAN while keeping fix the concentration of the ruthenium catalyst, we observed that the WO reaction is redox-controlled and defined ~1.64 V as the minimum redox potential for the generation of the active species (see section *III.2.3. Water Oxidation mechanistic studies of ruthenium complexes* and Figure V.6 from chapter IV). In order to shed some more light in this behaviour we studied how the redox potential in solution (related to the [Ce^{III}]/[Ce^{IV}] ratio in solution through the Nernst equation (1)) affects the energy barrier for the O-O bond formation (Figure V.9).

$$E = E^0 - \frac{R \cdot T}{n \cdot F} \cdot log\left(\frac{Ce^{III}}{Ce^{IV}}\right) \qquad (V.1)$$
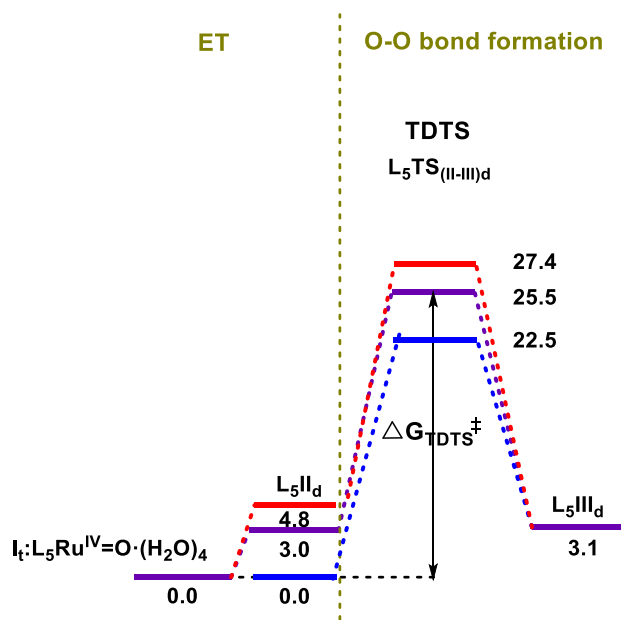
Figure V.9. Effect of the $[Ce^{III}]/[Ce^{IV}]$ ratios, (or redox potential), in the free energy barrier for the O-O bond formation when starting from **1Ru^{IV}=O**. Selected ratios: $[Ce^{III}]/[Ce^{IV}] = 0.3$ (1.64 V, red lines), $[Ce^{III}]/[Ce^{IV}] = 0.01$ (1.72 V, purple lines), $[Ce^{III}]/[Ce^{IV}] = 0.001$ (1.85 V vs SHE, blue lines).

We can envision 3 scenarios:

i) *Initial stage of the reaction:* at the very beginning, when all Ce^{IV} is intact, since the system is far from the equilibrium the redox potential proportionated by the CAN should be significantly greater than the $E_{1/2}$ of CAN (following the Nernst Equation a $[Ce^{III}]/[Ce^{IV}] = 0.001$ ratio should give ≈ 1.85 V *vs* SHE), enough to drive the formation of the WO active species, called as **1Ru^V=O** (**II$_d$**), this gives a DFT calculated energy barrier of $\Delta G^{\ddagger} = 22.5$ kcal·mol^{-1} for the O-O bond formation (Figure V.9, blue line).

ii) *Reaction at the kinetic limit*: in the middle of the course of the reaction as the catalytic reaction has advanced the $[Ce^{III}]/[Ce^{IV}]$ increases, decreasing the redox potential in solution. At a $[Ce^{III}]/[Ce^{IV}] = 0.01$ we have a redox potential in solution of about 1.75 V *vs* SHE, which gives a DFT calculated energy barrier of $\Delta G^{\ddagger} = 25.5$ kcal·mol^{-1} for the O-O bond formation (Figure V.9, blue line).

iii) _Reaction beyond the kinetic limit_: as the catalytic reaction advances the $[Ce^{IV}]$ drops increasing the $[Ce^{III}]/[Ce^{IV}]$ and thus decreasing the redox potential in solution. Since the redox potential of the $Ru^{IV/V}(O)$ redox couple (1.81 V *vs* SHE) is higher than the $Ce^{III/IV}$ (1.75 V *vs* SHE) the Ce^{IV} consumption produces an effective increase in the energy differences between the $Ru^{IV}(O)$ and $Ru^{V}(O)$. At high reaction times, when the reaction stops at about 20 h, we have an approximate $[Ce^{III}]/[Ce^{IV}] = 0.3$, which gives ≈ 1.64 V *vs* SHE, this gives a DFT calculated energy barrier of $\Delta G^{\ddagger} = 27.4$ kcal·mol^{-1} for the O-O bond formation (Figure V.9, red line).

V.2.3. Understanding of the inactivity of the $[Fe^{II}(OTf)(Py_2{}^{Me}tacn)](OTf)$ complex.

For comparative purposes, we have studied the homologous $[Fe^{II}(OTf)(Py_2{}^{Me}tacn)](OTf)$ (**1Fe^{II}-OTf**) complex under catalytic conditions where it was inactive. Analysis of the reaction media showed the near-IR band characteristic of **1Fe^{IV}=O** S = 1 complexes, at 715 nm ($\varepsilon = 240$ M^{-1}cm^{-1}). This feature was previously assigned to the formation of the $[Fe^{IV}(O)(Py_2{}^{Me}tacn)]$ (**1Fe^{IV}=O**) complex.[42] The half-life time of $[Fe^{IV}(O)(Py_2{}^{Me}tacn)]$ was estimated to be higher than 20 h under catalytic conditions.

In order to understand the sharp differences between *N*-pentadentate Fe and Ru complexes in water oxidation and taking into account that **1Fe^{IV}=O** was found to be stable and the main species present under catalytic conditions,[43,44] we have also studied the Fe$^{IV/V}$–oxo redox process for $[Fe^{II}(OTf)(Py_2{}^{Me}tacn)](OTf)$ (**1Fe^{II}-OTf**) by DFT calculations. A value of 2.15 V *vs* SHE was found using the same level of theory as for the analogous Ru system (Figure V.13). This value is in concordance with that obtained for the homologous $[Fe^{II}(OTf)(Py_2CH^{Me2}tacn)](OTf)$ complex (2.17 V *vs* SHE), also inactive in WO. At this point it is important to remark that previous DFT studies indicated that the free energy barrier for the O-O bond formation by a

water molecule attack to $[Fe^V(O)(Py_2CH^{Me2}tacn)]$ was less than 15 kcal·mol^{-1}, clearly feasible at room temperature.
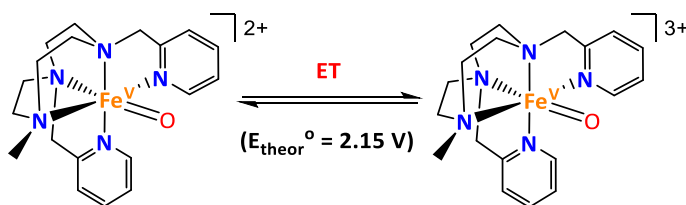
Figure V.10. Proposed redox equilibrium between **1Fe^{IV}=O** and **1Fe^V=O** prior to WNA. The theoretical value was obtained by DFT modelling

These facts, together with the high stability of the **Fe^{IV}(O)** suggest that the inactivity in water oxidation of $[Fe^{II}(OTf)(Py_2^{Me}tacn)](OTf)$ is mainly due to the insufficient redox potential that the sacrificial oxidant can proportionate (CAN 1.75 V *vs* SHE at pH 0.9) to achieve the intermediate responsible for the O-O bond formation. That is to say, $[Fe^V(O)(Py_2^{Me}tacn)]^{+3}$ cannot be reached with neither CAN nor NaIO$_4$. Therefore, it is reasonable to propose that the *N*-pentadentate neutral-redox-innocent ligands (such as Py$_2^{Me}$tacn and Py$_2$CH^{Me2}tacn) cannot stabilize enough the Fe^V -oxo to be accessed by CAN.

As a summary, the main reason for the difference in reactivity between **[M^{II}(OTf)(Py$_2^{Me}$tacn)]$^+$ (M = Fe** and **Ru)** complexes results from the distinct redox potential necessary to achieve the M^V(O) active species. In both cases, complexes **M^{IV}=O** species can be detected and characterized. However, the potential for the **M$^{IV/V}$(O)** redox couple in the Fe complex is 0.34 V (E$_{theo}$ 2.15 V *vs* SHE) higher than for the Ru (E$_{expt}$ = 1.81 V *vs* SHE).

V.3. Conclusions

In this chapter, mechanistic studies based on computational modelling using DFT have shed light in the catalytic cycle of the WO reaction catalysed by the new synthesized *N*-pentadentate ruthenium complex **1Ru^{II}-OH$_2$**. There is a good agreement between catalytic, kinetic, spectroscopic, spectrometric,

electrochemical and computational studies. Altogether points out that the water oxidation reaction follows a water nucleophilic attack mechanism. Our data suggest that the O-O bond formation is one of the rate determining steps ($\Delta G^{\ddagger}$ = 25.5 kcal·mol^{-1}) and it occurs at the Ru^{V}(O) intermediate, whose formation also limits the rate of the reaction. This Ru^{V}(O) intermediate is accessible under catalytic conditions through an ET process from Ru^{IV}(O) ($E_{1/2(exp)} \sim 1.81$ and $E_{1/2(theor)} \sim 1.85$ V *vs* SHE).

On the other hand, altogether indicates that the inactivity of the homologous iron complex **1Fe^{II}-OTf** is linked with the inaccessibility of Fe^{V}(O) ($E_{1/2(theor)} = 2.15$ V *vs* SHE) under reaction conditions rather than other scenarios.

The results from chapters III to V shed some light in the mechanisms involved in the molecular metal-catalyzed WO. Moreover, in chapters IV and V we make a link between iron and ruthenium WO mechanisms. We envision that these results will aid in the future development of new and more effective WO catalysts.

V.4. Experimental Section

V.4.1. Theoretical Methods

All the geometries were optimized using Density Functional Theory (DFT) at the uM11[45] level in conjunction with the SDD basis set for the Ru[15,46] and 6-31G(d) basis set[47] for the rest of the atoms, including the effect of water solvent with polarizable continuum model PCM-SMD[48-50] of Truhlar and co-workers as implemented in the Gaussian 09d01[12] software. Stationary points were verified by frequency analysis (see section S.I.7. Cartesian coordinates of the optimized structures).

In other previous studies[44] it was found that taking into account solvent effects in the optimization was essential to reproduce the experimental data.[43] The energies were further refined by single-point calculations with the cc-pVTZ dunning basis set for all atoms (E_{cc_pVTZ}). All calculations employed the spin-unrestricted formalism and spin-contaminated energies were systematically corrected by using the following equations (V.2) and (V.3):

$$E_{spin\ corr} = \frac{E_{cc-pVTZ} - a \cdot E_{cc-pVTZ/(S+1)}}{1-a} \tag{V.2}$$

$$a = \frac{\langle S^2 \rangle - S \cdot (S+1)}{\langle S^2_{(S+1)} \rangle - S \cdot (S+1)} \tag{V.3}$$

in which $E_{spin\ corr}$ is the spin corrected electronic energy, $E_{cc-pVTZ}$ and $\langle S^2 \rangle$ are the cc-pVTZ electronic energy and square total spin angular momentum, respectively, obtained from the structure optimized at the uM11/6-31G(d) level; and $E_{cc-pVTZ/(S+1)}$ and $\langle S^2_{(S+1)} \rangle$ are the energy and square total spin angular momentum of the afterward unpaired spin state (S+1), respectively, computed at the same level of theory and geometry.[51]

Gibbs energy corrections at 298.15 K were obtained from gas phase frequency calculations at uM11/6-31G(d) level (G_{corr}). The solvent effects were computed at the same level by performing gas phase and solvent phase calculations and taking the difference of the resulting energies (G_{solv}).[52] All calculated solvation free-energies use a standard state of an ideal gas at a gas-phase concentration of 1 mol·L^{-1} dissolving as an ideal dilute solution at a liquid-phase concentration of 1M, but for water itself a 55.6M standard state was employed. Thus, as it has been indicated by Cramer et al.,[11,39,40,53-55] we calculated the free-energy change associated with moving from a standard-state gas-phase pressure of 1 atm to a standard-state gas-phase concentration of 1M (55.6M for water), $\Delta G^{o/*}$. The value of $\Delta G^{o/*}$ at 298 K is 1.9 kcal·mol^{-}

[1] for 1M standard state solute and 4.3 kcal·mol^{-1} for 55.6M standard state water. The total Gibbs free energy (G) was obtained by adding the previous corrections to the spin-corrected electronic energy $E_{spin\ corr}$ (equation V.4):

$$G = E_{spin\ corr} + G_{corr} + G_{solv} + \Delta G^{o/*} \qquad (V.4)$$

All energies given in this work are referred to Gibbs energies G, unless otherwise noted. Since the lowest-energy spin state for transition-metal complexes is not obvious, all spin-states for each species were calculated and the respective geometries were optimized. The nature of the stationary points was established by frequency calculations in the solvent-phase, in which minima have no imaginary frequencies and transition states have one and only one. Finally, the connectivity of all transition states was confirmed by relaxing the transition state geometries towards both the reactants and the products through intrinsic reaction coordinate (IRC) calculations.

Standard reduction potentials, relative to the standard hydrogen electrode (SHE), were calculated by (equation V.5):

$$E^o = -\frac{\Delta G^o - \Delta G^o_{SHE}}{nF} \qquad (V.5)$$

where ΔG^o is the free energy change associated with reduction at standard conditions, n is the number of electrons involved in the redox reaction, F is the Faraday constant and ΔG^o_{NHE} is the free energy change associated with the reduction of a proton (-4.28 eV).[56] Some oxidation events are characterized by proton-coupled electron transfer (PCET), where electron transfer and proton transfer to the solvent occur simultaneously. Thus, we must include in ΔG^o the standard free energy of a proton in solution (equation V.6):

$$G^{H+}_{aq} = G^{H+}_{gas} + G^{H+}_{solv} \qquad (V.6)$$

where the free energy of solvation of a proton (G_{solv}^{H+}) was taken as -265.9 kcal·mol^{-1},[56] and the gas-phase Gibbs free energy of a proton (G_{gas}^{H+}) is -6.3 kcal·mol^{-1}. The aqueous pK_a associated to the general reaction: ($XH_{aq} \rightarrow X_{aq}^- + H_{aq}^+$) were computed according to (equation V.7):

$$pK_a = \frac{\Delta G^*}{RT \ln(10)} \tag{V.7}$$

where T is the temperature and R is the universal gas constant.[57] ΔG^* is expressed in terms of the standard free energies of the acid XH and its conjugate base X$^-$ (equation V.8):

$$\Delta G^* = G^o(X^-) + G_{aq}^{H+} - G^o(XH) + \Delta G_*^{\underline{o}} \tag{V.8}$$

V.5. References

(1) Muckerman, J. T.; Polyansky, D. E.; Wada, T.; Tanaka, K.; Fujita, E. *Inorg. Chem.* **2008**, *47*, 1787.

(2) Tseng, H. W.; Zong, R.; Muckerman, J. T.; Thummel, R. *Inorg. Chem.* **2008**, *47*, 11763.

(3) Liu, F.; Concepcion, J. J.; Jurss, J. W.; Cardolaccia, T.; Templeton, J. L.; Meyer, T. J. *Inorg. Chem.* **2008**, *47*, 1727.

(4) Bartolotti, L. J.; Pedersen, L. G.; Meyer, T. J. *Int. J. Quantum Chem* **2001**, *83*, 143.

(5) Yang, X.; Baik, M. H. *J. Am. Chem. Soc.* **2004**, *126*, 13222.

(6) Yang, X.; Baik, M. H. *J. Am. Chem. Soc.* **2006**, *128*, 7476.

(7) Batista, E. R.; Martin, R. L. *J. Am. Chem. Soc.* **2007**, *129*, 7224.

(8) Valdés, Á.; Kroes, G. J. *J Chem Phys* **2009**, *130*, 114701.

(9) Yang, X.; Baik, M. H. *J. Am. Chem. Soc.* **2008**, *130*, 16231.

(10) Bozoglian, F.; Romain, S.; Ertem, M. Z.; Todorova, T. K.; Sens, C.; Mola, J.; Rodríguez, M.; Romero, I.; Benet-Buchholz, J.; Fontrodona, X.; Cramer, C. J.; Gagliardi, L.; Llobet, A. *J. Am. Chem. Soc.* **2009**, *131*, 15176.

(11) L. Wang, Q. W., T. V. Voorhis *Inorg. Chem.* **2010**, *49*, 4543

(12) C. J. Cramer, A. V. M., D. G. Truhlar *J. Phys. Chem. B* **2009**, *113*, 6378.

(13) Truhlar, R. P. a. D. G. *J. Phys. Chem. Lett.* **2011**, *2*, 2810.

(14) Truhlar, R. P. a. D. G. *J. Phys. Chem. Lett.* **2012**, *3* 117−124.

(15) Aleksandr V. Marenich, A. M., Michelle Lenz, Christopher J. Cramer, and Donald G. Truhlar *Angew. Chem. Int. Ed.* **2012**, *51*, 12810

(16) Perdew, J. P. B., K.; Ernzerhof, *M.Phys. Rev. Lett.* **1995**, *77*, 3865.

(17) Peverati, R. Z., Y.; Truhlar *J. Phys. Chem. Lett.* **2011**, *2*, 1991.

(18) Becke, A. D. *Phys. ReV. A* **1988**, *38*.

(19) Becke, A. D. *J. Chem. Phys.* **1992**, *98*, 5648.

(20) Lee, C. Y., W.; Parr, R. G. *Phys. Rev. B* **1987**, *37*, 785.

(21) Stephens, P. D., F.; Chabalowski, C.; Frisch, M. J. *J. Phys. Chem. A* **1993**, *98*, 11623.

(22) Keal, T. T., D. *J. Chem. Phys.* **2005**, *123*, 121103.

(23) Chai, J.-D. H.-G., M. *J. Chem. Phys.* **2008**, *128*, 084106.

(24) Chai, J.-D. H.-G., M. *Phys. Chem. Chem. Phys.* **2007**, *10*, 6615.

(25) Zhao, Y. S., N. E.; Truhlar, D. G. *J. Chem. Phys.* **2005**, *123*, 161103.

(26) Zhao, Y. S., N. E.; Truhlar, D. G. *J. Chem. Theory Comput* **2005**, *2*, 364.

UNIVERSITAT ROVIRA I VIRGILI
MECHANISTIC STUDIES OF WATER OXIDATION CATALYZED BY HOMOGENEOUS IRON AND RUTHENIUM
COMPLEXES AND LIGHT-DRIVEN ORGANIC REDUCTIONS WITH A DUAL COBALT/COPPER CATALYTIC SYSTEM
Carla Casadevall Serrano

CHAPTER IV   Computational Study of WO mechanisms: Ru *vs* Fe

(27) Zhao, Y. T., D. G. *J. Chem. Phys.* **2005**, *125*, 194101.

(28) Zhao, Y. T., D. G. *Theor. Chem. Acc.* **2008**, *120*, 215.

(29) Zhao, Y. T., D. G. *J. Phys. Chem. A* **2005**, *110*, 13126.

(30) Zhao, Y. T., D. G. **2007**, *4*, 1849.

(31) A. K. Vardhaman, C. V. S., D. Kumar, S. P. de Visser, *Chem. Commun.* **2011**, *47*, 11044.

(32) S. P. de Visser, M. G. Q., B, Martín, P. Comba, U. Ryde, *Chem. Commun.* **2014**, *50*, 262.

(33) Casadevall, C.; Codolà, Z.; Costas, M.; Lloret-Fillol, J. *Chem. Eur. J.* **2016**, *22*, 10111.

(34) *Ber. Bunsen-Ges. Phys. Chem* **1977**, *81*, 245.

(35) Cheng, W. C.; Yu, W. Y.; Cheung, K. K.; Che, C. M. *J. Chem. Soc., Dalton Trans.* **1994**, *1*, 57.

(36) Parent, A. R.; Crabtree, R. H.; Brudvig, G. W. *Chem. Soc. Rev.* **2013**, *42*, 2247.

(37) Ferran Acuña-Pares, Z. C., Miquel Costas, Josep M. Luis, and Julio Lloret-Fillol *Chem. Eur. J.* **2014**, *20*, 1.

(38) Acuña-Parés, F.; Costas, M.; Luis, J. M.; Lloret-Fillol, J. *Inorg. Chem.* **2014**, *53*, 5474.

(39) R. Bianco, P. J. H., J. T. J. Hynes, *J. Phys. Chem. A* **2011**, *115*, 8003.

(40) M. Hirahara, M. Z. E., M. Komi, H. Yamasaki, C. J. Cramer, M. Yagi, *Inorg. Chem.* **2013**, *52*, 6354

(41) Holland, P. L. *Dalton. Trans.* **2010**, *39*, 5415.

(42) Anna Company, G. S., María González-Béjar, Laura Gómez, Martin Clémancey, Geneviève Blondin, Andrew J. Jasniewski, Mayank Puri, Wesley R. Browne, Jean-Marc Latour, Lawrence Que , Jr., Miquel Costas, Julia Pérez-Prieto, and Julio Lloret-Fillol *J. Am. Chem. Soc.* **2014**, *136*.

(43) Z.Codolà; I. Garcia-Bosch; F. Acuña; I. Prat; J. M. Luis; M. Costas; Lloret-Fillol, J. *Chem. Eur. J.* **2013**, *19*, 8042.

(44) Acuña-Parés, F.; Codola, Z.; Costas, M.; Luis, J. M.; Lloret-Fillol, J. *Chem.—Eur. J.* **2014**, *20*, 5696.

(45) Call, A.; Codola, Z.; Acuna-Pares, F.; Lloret-Fillol, J. *Chemistry* **2014**, *20*, 6171.

(46) Runhua Kang, J. Y., and Hui Chen *J. Chem. Theory Comput.* **2013**, *9*, 1872−1879.

(47) M. Dolg, U. W., H. Stoll, H. Preuss *J. Chem. Phys.* **1987**, *86*, 866

(48) W. J. Hehre, R. D., J. A. Pople *J. Chem. Phys.* **1972**, *56*, 2257.

(49) P. C. Hariharan , J. A. P. *Theoret. Chimica Acta* **1973**, *28*, 213.

(50) M. Suensson, S. H., R. D. J. Froese, T. Matsubara, S. Sieber, K. Morokuma *J. Phys. Chem.* **1996**, *100*, 19357.

(51) Gaussian 09, R. A., M. J. Frisch, G. W. Trucks, H. B. Schlegel, G. E. Scuseria, M. A. Robb, J. R. Cheeseman, G. Scalmani, V. Barone, B. Mennucci, G. A. Petersson, H. Nakatsuji, M. Caricato, X. Li, H. P. Hratchian, A. F. Izmaylov, J. Bloino, G. Zheng, J. L. Sonnenberg, M. Hada, M. Ehara, K. Toyota, R. Fukuda, J. Hasegawa, M. Ishida, T. Nakajima, Y. Honda, O. Kitao, H. Nakai, T. Vreven, J. A. Montgomery, Jr., J. E. Peralta, F. Ogliaro, M. Bearpark, J. J. Heyd, E. Brothers, K. N. Kudin, V. N. Staroverov, R. Kobayashi, J. Normand, K. Raghavachari, A. Rendell, J. C. Burant, S. S. Iyengar, J. Tomasi, M. Cossi, N. Rega, J. M. Millam, M. Klene, J. E. Knox, J. B. Cross, V. Bakken, C. Adamo, J. Jaramillo, R. Gomperts, R. E. Stratmann, O. Yazyev, A. J. Austin, R. Cammi, C. Pomelli, J. W. Ochterski, R. L. Martin, K. Morokuma, V. G. Zakrzewski, G. A. Voth, P. Salvador, J. J. Dannenberg, S. Dapprich, A. D. Daniels, Ö. Farkas, J. B. Foresman, J. V. Ortiz, J. Cioslowski, and D. J. Fox, Gaussian, Inc., Wallingford CT. **2009**.

(52) M. Swart, M. G., J. M. Luis, M. Solà *J. Phys. Chem. A* **2010**, *114*, 7191.

(53) M. Z. Ertem, L. G., C. J. Cramer *Chem. Sci.* **2012**, *3*, 1293

(54) L. Vigara, M. Z. E., N. Planas, F. Bozoglian, N. Leidel, H. Dau, M. Haumann, L. Gagliardi, C. J. Cramer, A. Llobet, *Chem. Sci.* **2012**, *3*, 2576

(55) Sameera, W. M. C.; McKenzie, C. J.; McGrady, J. E. *Dalton. Trans.* **2011**, *40*, 3859.

(56) C. P. Kelly, C. J. C., D. G. Truhlar, *J. Phys. Chem. A* **2006**, *110*, 2493

(57) Winget, P.; Cramer, C. J.; Truhlar, D. G. *Theor. Chem. Acc.* **2004**, *112*, 217.

UNIVERSITAT ROVIRA I VIRGILI
MECHANISTIC STUDIES OF WATER OXIDATION CATALYZED BY HOMOGENEOUS IRON AND RUTHENIUM
COMPLEXES AND LIGHT-DRIVEN ORGANIC REDUCTIONS WITH A DUAL COBALT/COPPER CATALYTIC SYSTEM
Carla Casadevall Serrano

CHAPTER VI

After the O-O Bond Formation in Ruthenium Catalyzed Water Oxidation: a Missing Link
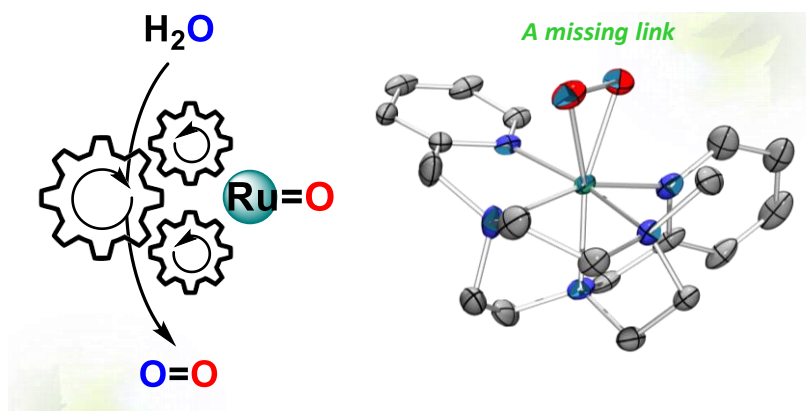
This chapter corresponds to the following publication:

"Isolation of a $[\eta^2\text{-Ru}^{IV}\text{-OO}]^{2+}$ intermediate after the rate determining step in the water oxidation reaction. Direct evidence of an O-O bond formation from a metal-oxo moiety";

C. Casadevall, V. Martin-Diaconescu, W. R. Browne, F. Franco, N. Cabello, J. Benet-Buchholz, B. Lasalle-Kaiser, J. Lloret-Fillol; *in preparation*.

UNIVERSITAT ROVIRA I VIRGILI
MECHANISTIC STUDIES OF WATER OXIDATION CATALYZED BY HOMOGENEOUS IRON AND RUTHENIUM
COMPLEXES AND LIGHT-DRIVEN ORGANIC REDUCTIONS WITH A DUAL COBALT/COPPER CATALYTIC SYSTEM
Carla Casadevall Serrano

VI. After the O-O Bond Formation in Ruthenium Catalyzed Water Oxidation: a Missing Link

VI.1. General insight

Water oxidation to dioxygen is pivotal in the natural photosynthesis, a process occurring in the oxygen evolving center (OEC) located in the photosystem II (PSII), that supports life on earth,[1-3] and inspires the development of global sustainable technologies for the synthesis of renewable fuels and chemicals.[4,5] Nevertheless, the natural mechanism is still not fully understood.[1] In this line, the study of homogeneous catalysts could greatly benefit to our understanding of WO. This view triggered the study of the fundamental understanding needed to design efficient water oxidation catalysts. Since the first report on the blue dimer a large effort has been placed in designing molecular catalysts, and in the characterization of the mechanisms and intermediates that govern the water oxidation reaction.[6-15] In this line, in the last decades, mononuclear ruthenium complexes based on amino- and polypyridyl ligands have grown rapidly in importance as water oxidation catalysts (WOCs).[16-21]
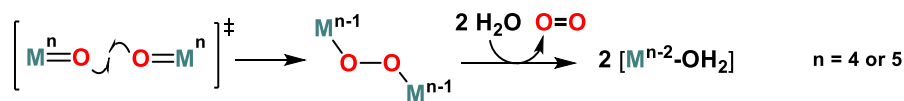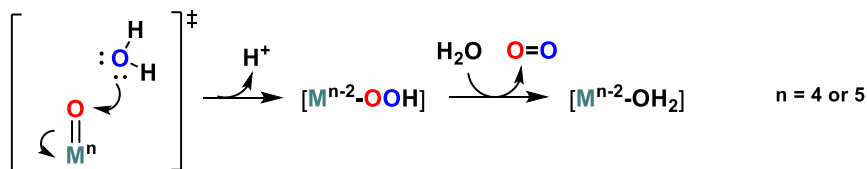
Figure VI.1. Main discussed mechanisms for the O-O bond formation.

201

Discovered mechanisms of water oxidation with molecular catalysts have influenced the interpretation of how the OEC can oxidize the water molecule.[1,3,8] Nevertheless, the debate about the operative mechanism in the OEC is still open. In general, the formal mechanisms considered are the coupling between two radical M=O (or M-oxyl) species and the acid base mechanism where a water molecule attacks an electrophilic metal oxo (Figure VI.1). In both cases, the formation of the O-O bond is usually the step that controls the rate of the reaction, and therefore facilitating the O-O bond formation translates in better efficiencies. However, despite the mounting evidence for both mechanisms, the pieces of evidence for the O-O bond formation step, the direct formation of the O-O bond from a M=O moiety are circumstantial.[22-25] In part, the challenge is to characterize the intermediates after the O-O bond formation step; paramount when this is the rate-determining step of a reaction, which is usually the case.
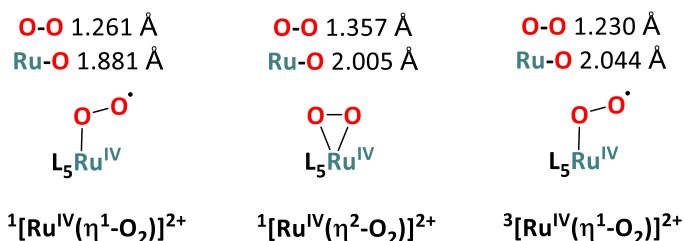
Figure VI.2. Possible coordination and reported averaged distances for Ru-peroxo/superoxo intermediates.

In this regard, several mechanistic studies point to the formation of [Ru-OO]$^{2+}$ species after the O-O bond formation step, followed by the release of molecular O_2 to restore the catalytic species.[22-24,26-28] Nevertheless, due to the intrinsic difficulty to elucidate the intermediates after the rate-determining step (O-O bond formation), [Ru-OO]$^{2+}$ has yet to be isolated and its electronic and geometric structures fully characterized. As such all the reported evidence of the existence of such species still do not clarify unequivocally its nature. Computational studies propose the formation of three close-in-energy structures: i) a singlet end-on η^1, ii) a singlet side-on η^2 or iii) a triplet end-on η^1 coordinated intermediate,[22,29-32] with the triplet η^1 structure

being the most stable in most of the cases (Figure VI.2).[22,27,33] In contrast, some evidence in solution and gas phase point to the formation of a singlet end-on η^1 peroxo species or even a Ru^{III}-superoxo species.[22,23] For example, Concepcion and coworkers reported a band at 1015 cm^{-1} in the resonance Raman spectrum of the oxidation of complex $[Ru(Mebimpy)(bpy)(H_2O)]^{2+}$ (Mebimpy = 2,6-bis(1-methylbenzimidazol-2yl)pyridine) with cerium ammonium nitrate (CAN).[23] In the same line, Polyansky et $al.$ showed a resonance Raman vibration of a solution of $[Ru(NPM)(pic)_2(O_2)]^{2+}$ (NPM = 4-tert-butyl-2,6-di(1',8'-naphthyrid-2'-yl)pyridine; pic = 4-picoline) corresponding to a Ru-O stretch.[33] On the basis of DFT calculations, in both cases, they associated the observed bands to the formation of a singlet η^2–OO intermediate, although the calculations pointed to a triplet η^1 structure as the lowest in energy.[23,33] More recently, Garand and coworkers reported the mass spectroscopic generation and cryogenic ion IR spectroscopy of the $[Ru(tpy)(bpy)(O_2)]^{2+}$ complex (tpy = terpyridine; bpy = bipyridine) in gas phase from the reaction of $[Ru(tpy)(bpy)]^{2+}$ with 1% O_2 in He in an 80 K ion trap.[22] They observed a weak band at 1150 cm^{-1} that shifted towards 1085 cm^{-1} in the presence of $^{18}O_2$, therefore they assigned those features to the ^{16}O-^{16}O and ^{18}O-^{18}O stretches, respectively. Despite DFT calculations at the B3LYP/def2-TZVP/ZORA pointed towards the triplet $^3[Ru(tpy)(bpy)(\eta^1$-$O_2)]^{2+}$ intermediate as the lowest in energy structure, the IR bands at 1150 cm^{-1} and 1085 cm^{-1} were closer to the ones calculated for the $^1[Ru(tpy)(bpy)(\eta^2$-$O_2)]^{2+}$ structure, suggesting that the latter is the experimentally detected species.[22] Therefore, putative peroxo species have been a topic of debate during last decades and their nature still remains unclear. Thus, the intrinsic difficulty to generate this intermediate under conditions relevant to water oxidation together with the lack of experimental evidence to characterize it, make this intermediate one of the missing links after the O-O bond formation in the mechanism of water oxidation.

In this regard, in this chapter we report, under catalytic water oxidation conditions, evidence for the direct formation of the O-O bond from a M=O (Ru=O),

and the isolation and full characterization of the elusive Ru(IV) side-on peroxo complex $[Ru^{IV}(OO)(Py_2^{Me}tacn)](PF_6)_2$ (η^2-**1Ru^{IV}-OO**) after the O-O bond formation. For comparative purposes, in this chapter we have also synthesized, isolated and fully characterized complex $[Ru^{II}(OH_2)(Py_2^{Me}tacn)](PF_6)_2$ (**1Ru$_{II}$-OH$_2$**), and intermediates $[Ru^{III}(OH)(Py_2^{Me}tacn)](PF_6)_2$ (**1Ru^{III}-OH**), $[Ru^{IV}(O)(Py_2^{Me}tacn)](PF_6)_2$ (**1Ru^{IV}=O**) and η^2-$[Ru^{IV}(OO)(Py_2^{Me}tacn)](PF_6)_2$ (η^2-**1Ru^{IV}-OO**). Moreover, electrochemical evidence of the formation of the $[Ru^V(O)(Py_2^{Me}tacn)](PF_6)_3$ (**1Ru^V=O**), which has been characterized as the active species, are also provided. A detailed mechanistic study for the formation of the η^2-**1Ru^{IV}-OO** from the resting state **1Ru^{IV}=O** using Raman spectroscopy together with coldspray high-resolution mass spectrometry (CSI-HRMS) isotopic labeling kinetic studies and experiments connecting η^2-**1Ru^{IV}-OO** with the proposed catalytic cycle are reported.

VI.2. Results and discussion

VI.2.1. Synthesis of complexes and characterization
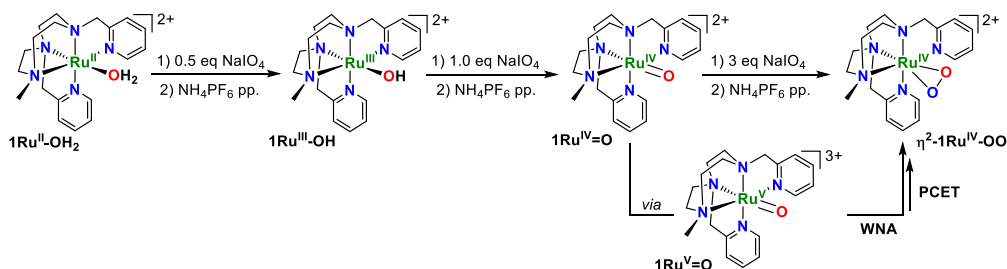
Scheme VI.1. Synthesis of the ruthenium intermediates **1Ru^{III}-OH**, **1Ru^{IV}=O** and η^2-**1Ru^{IV}-OO** involved in WO catalyzed by complex **1Ru^{II}-OH$_2$**.

The pentadentate nitrogen donating ligand Py$_2^{Me}$tacn and complex $[Ru^{II}(OH_2)(Py_2^{Me}tacn)](PF_6)_2$ (**1Ru^{II}-OH$_2$**) were synthesized as described previously in chapter IV.[21] Intermediates $[Ru^{III}(OH)(Py_2^{Me}tacn)](PF_6)_2$ (**1Ru^{III}-OH**) and $[Ru^{IV}(O)(Py_2^{Me}tacn)](PF_6)_2$ (**1Ru^{IV}=O**) were prepared by reacting $[Ru^{II}(OH_2)(Py_2^{Me}tacn)](PF_6)_2$ (**1Ru^{II}-OH$_2$**) with 0.5 and 1.5 equiv. NaIO$_4$ in H$_2$O at rt., respectively (Scheme VI.1). Then the desired products were collected through

precipitation with a saturated solution of ammonium hexafluorophosphate (NH_4PF_6) at 5 ºC for 15 minutes, filtered and dried under vacuum and analyzed by ^{1}H-NMR and CSI-HRMS (Figures VI.3 and VI.4, A.IV.20 and A.IV.21). The ^{1}H-NMR spectrum of **1Ru^{III}-OH** presents new signals with respect to that of the diamagnetic complex **1**[21] in the paramagnetic region expanding from 14 to -2 ppm, which is in agreement with the formation of a paramagnetic Ru(III)-hydroxo species (Figure VI.3). Moreover, a crystal structure of **1Ru^{III}-OH** was already reported in chapter IV, confirming its structure.[21] In, contrast, the ^{1}H-NMR spectrum of **1Ru^{IV}=O** shows signals expanding from 65 to -15 ppm, which is also in agreement with the formation of a paramagnetic Ru(IV)-oxo species (Figure VI.4). Likewise, crystals suitable for X-ray diffraction were obtained from **1Ru^{IV}=O** by slow evaporation of D_2O from an NMR tube. The asymmetric unit contains one molecule of the metal complex and two PF_6 anions. The X-ray structure clearly confirms the isolation of the **1Ru^{IV}=O** intermediate (Figure VI.5 and Annex A.IV section A.IV.2.1. X-ray characterization of Ru(IV) oxo species: **1Ru^{IV}=O** for details).
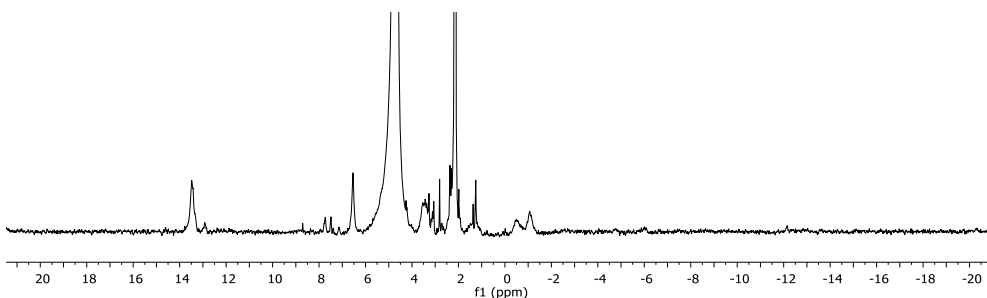
Figure VI.3. ^{1}H-NMR (400 MHz, 298 K, D_2O) spectrum of the isolated $[Ru^{III}(OH)(Py_2^{Me}tacn)](PF_6)_2$ (**1Ru^{III}-OH**) intermediate.
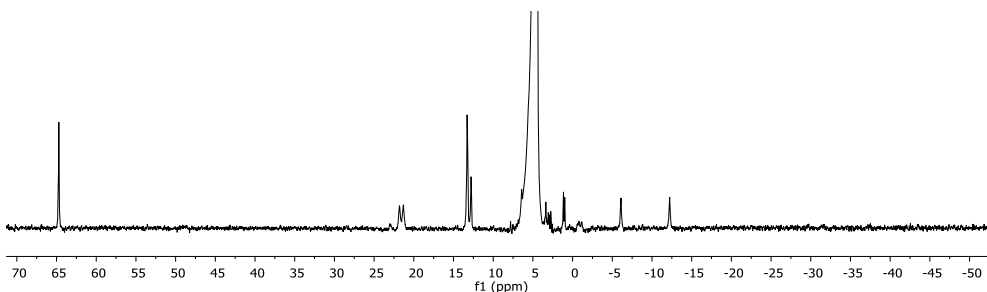
Figure VI.4. ^{1}H-NMR (400 MHz, 298 K, D_2O) spectrum of the isolated $[Ru^{IV}(O)(Py_2^{Me}tacn)](PF_6)_2$ (**1Ru^{IV}=O**) intermediate.
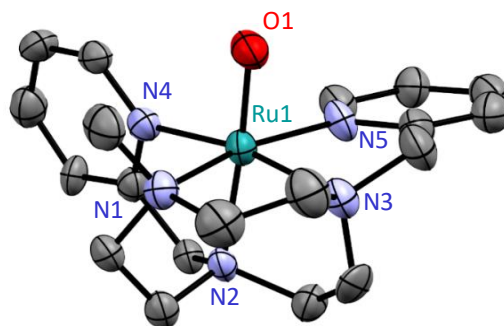
Figure VI.5. ORTEP drawing (thermal ellipsoids are drawn at a 50 % probability level) showing the structure of **1Ru^{IV}=O**. PF$_6$ anions and hydrogen atoms have been omitted in the sake of clarity. Selected bond lengths (Å): Ru-O1 1.807(8), Ru-N1 2.114(11), Ru-N3 2.062(12), Ru-N4 2.057(11), Ru-N2 2.135(10), Ru-N5 2.079(11). Selected angles (°): O1-Ru-N1 93.4(5), O1-Ru-N2 175.1(4), O1-Ru-N3 96.8(5), O1-Ru-N4 98.0(5), O1-Ru-N5 89.9(5).

Intermediate η^2-[Ru^{IV}(OO)(Py$_2^{Me}$tacn)](PF$_6$)$_2$ (**η^2-1Ru^{IV}-OO**) was prepared indistinctively from complexes **1Ru^{II}-OH$_2$**, **1Ru^{III}-OH** and **1Ru^{IV}=O** by changing the number of equivalents of sacrificial oxidant added (NaIO$_4$) to the starting complex (see VI.2. Experimental section, VI.4.2.3. Synthesis of η^2-[Ru^{IV}(OO)(Py$_2^{Me}$tacn)](PF$_6$)$_2$: **η^2-1Ru^{IV}-OO** for further details). **η^2-1Ru^{IV}-OO** was prepared by reacting [Ru^{II}(OH$_2$)(Py$_2^{Me}$tacn)](PF$_6$)$_2$ (**1Ru^{II}-OH$_2$**) with 4.5 equiv. NaIO$_4$ at rt for 2 h (Scheme VI.1). Then, a saturated solution of ammonium hexafluorophosphate (NH$_4$PF$_6$) in H$_2$O was added and the reaction mixture was left standing at 5 °C for 2 days. At that time, tinny needle-shaped crystals had appeared as a precipitate, which was filtered and collected for analyses. Additionally, if less than two equivalents of a saturated solution of NH$_4$PF$_6$ in H$_2$O were added, crystals with a different counterion were obtained (see below). The ^{1}H-NMR spectrum of **η^2-1Ru^{IV}-OO** presents new signals with respect to that of the diamagnetic complex **1Ru^{II}-OH$_2$**[21] but also in the diamagnetic region expanding from 9 to 1 ppm, which is in agreement with the formation of a closed shell diamagnetic Ru(IV)-peroxo species (Figure VI.6).
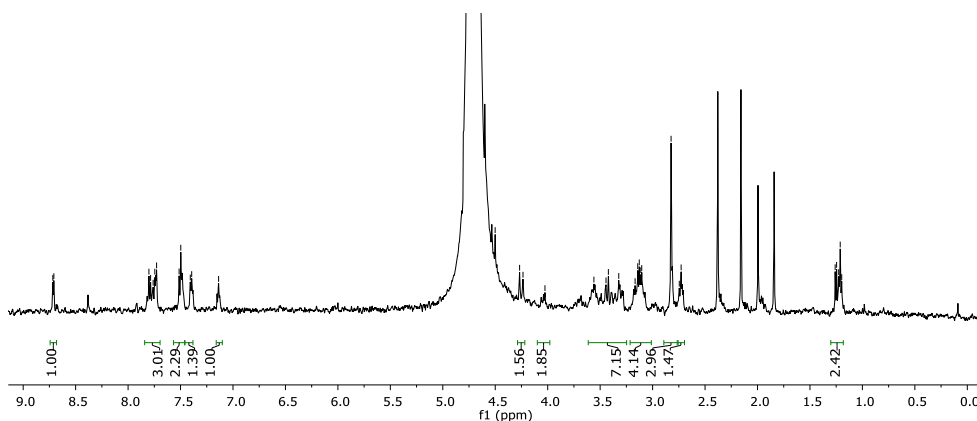
Figure VI.6. ^{1}H-NMR (400 MHz, 298 K, D$_2$O) spectrum of the isolated [Ru^{IV}(OO)(Py$_2^{Me}$tacn)](PF$_6$)$_2$ (**η^2-1Ru^{IV}-OO**) complex.

In addition, several crystal structures of different synthesis could be isolated and were suitable for X-ray diffraction analysis. However, among all, in this chapter, we report the CIF of two crystals of two different syntheses (Figure VI.7 and Figures A.IV.4 and A.IV.5 from Annex IV and section A.IV.2.1. X-ray characterization of Ru(IV) peroxo species: η^2-1^{IV}-OO for further details). Both crystals show an asymmetric unit that contains one molecule of the metal complex and two counterions. However, one of the crystals contains one and a half PF$_6$ and half IO$_3$ anion, and the other two PF$_6$ anions, both coming from the salts used during the synthesis of the intermediate (NaIO$_4$ and NH$_4$PF$_6$). The X-ray crystal structures of **η^2-1Ru^{IV}-OO** unequivocally revealed the mononuclear side-on heptacoordinate configuration of the Ru center. The complex displays a distorted squared-based bipyramid geometry, which arises from the coordination of the peroxo moiety. The density map clearly shows two oxygen atoms coordinated to the Ru center and the occupancy obtained for both atoms is exactly 1.0, which corresponds to two full oxygen atoms so that a single disordered oxygen atom can also be discarded. The O-O distance of the isolated crystals is 1.353(10) and 1.367(9) Å, respectively, which is in agreement with the reported distances of other organometallic Ru-O$_2$ complexes (1.36-1.41 Å)[29-32] and it is indicative of the peroxo character of the O-O coordinated moiety, as supported by Raman and XAS spectroscopy and DFT modeling (further discussed below). O-O is symmetrically bound to ruthenium with Ru-O distances

being $d_{(Ru-O1)} = 1.996(6)$ and $d_{(Ru-O2)} = 2.004(6)$ and $d_{(Ru-O1)} = 1.988(7)$ and $d_{(Ru-O2)} = 1.995(7)$, respectively. The O1-Ru-O2 angle is found to be 40.0º. These values are in excellent agreement with the averaged Ru-O distances (1.958-2.040 Å) and O-Ru-O angles (39.7º) reported for analogous organometallic complexes.[29-32]
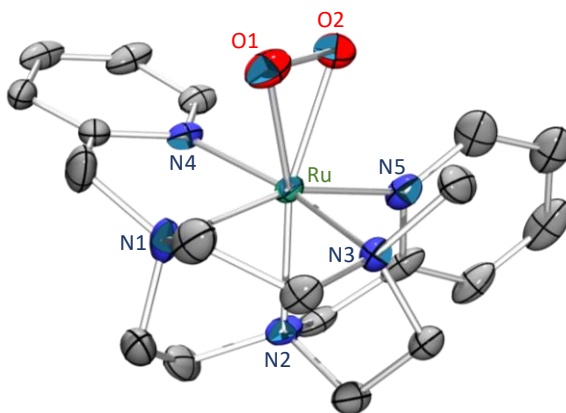
Figure VI.7. ORTEP drawing (thermal ellipsoids are drawn at a 50 % probability level) showing the structure of $[Ru^{IV}(OO)(Py_2^{Me}tacn)](PF_6)_{1.5}(IO_3)_{0.5}$ (**η^2-1Ru^{IV}-OO**). PF_6 anions and hydrogen atoms have been omitted in the sake of clarity. Selected bond lengths (Å): Ru-O2 1.996(6), Ru-O1 2.004(6), Ru-N4 2.075(7), Ru-N1 2.091(8), Ru-N3 2.093(7), Ru-N5 2.112(7), Ru-N2 2.118(7), O1-O2 1.367(9). Selected angles (º): O2-Ru-O1 40.0(3), O2-O1-Ru 69.7(4), O1-O2-Ru 70.3(4).

DFT calculations already performed in chapter V of this thesis pointed to the formation of a **η^2-1Ru^{IV}-OO** intermediate after the O-O formation step. Moreover, to get more insight in the electronic nature of the **η^2-1Ru^{IV}-OO** intermediate DFT calculations were carried out at a uM11/cc-pVTZ//uM11/6-31G(d) (SDD basis set for Ru) level including the solvent effect of water with the polarizable continuum model PCM-SMD in Gaussian.[34] In this line, we have calculated all the possible spin states and coordination modes for this intermediate by DFT (the η^1 and η^2 coordination for the singlet spin state and the η^1 coordination for the triplet spin state, see Annex IV, Figure A.IV.53). Altogether, the theoretical study pointed towards the singlet η^2 intermediate as the most stable among the calculated possibilities by 4.3 kcal·mol^{-1}. Indeed, if we overlap the X-ray structure of the isolated crystal of the **η^2-1Ru^{IV}-OO** intermediate with the optimized geometry by DFT for the η^2 coordination

for the singlet spin state and the η^1 coordination for the triplet spin state, respectively, we can see that there is a good agreement with the bond distances found for the isolated crystal and the lowest in energy found singlet η^2 closed shell DFT optimized structure: $d_{(O-O)theor} = 1.352$ Å for a singlet **η^2-1Ru^{IV}-OO** complex and $d_{(O-O)exp} = 1.353$ and 1.367 Å found for the two diffracted crystal structures form two different reactions (see Figure VI.8, A.IV.53 from the annex and Table VI.1). This suggests that the DFT level is good enough to describe the electronic nature of the metal center, which has also been a topic of debate.[22,23,28,33]
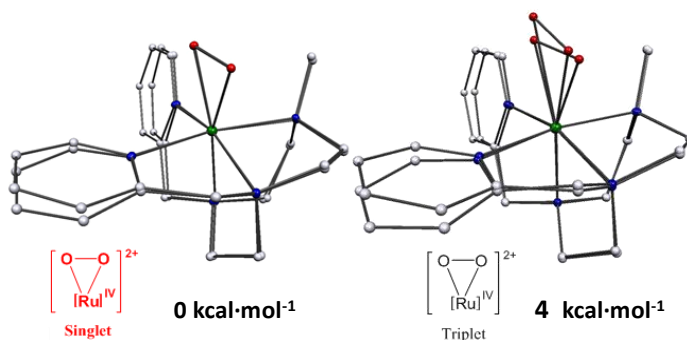
Figure VI.8. Overlap between the X-ray structure crystal structure of Figure VI.7 and the DFT optimized geometries for the **^{1}[η^2-1Ru^{IV}-OO]** and **^{3}[η^1-1Ru^{IV}-OO]** possible coordination modes and spin states.

Table VI.1. Comparison between selected bond distances for solid-state X-ray diffraction and the DFT modeled structures.

Bond dist.[a]	X-ray structures data η^2-1Ru^{IV}-OO	DFT data ^{1}[η^2-1Ru^{IV}-OO]	^{1}[η^1-1Ru^{IV}-OO]	^{3}[η^1-1Ru^{IV}-OO]
Ru-O$_1$	1.988(7)[b], 1.996(6)[c]	2.001	2.084	2.076
Ru-N$_1$	2.062(9)[b], 2.075(7)[c]	2.108	2.127	2.126
Ru-N$_2$	2.092(8)[b], 2.091(8)[c]	2.101	2.080	2.079
Ru-N$_3$	2.112(8)[b], 2.118(7)[c]	2.109	2.101	2.115
Ru-N$_4$	2.101(8)[b], 2.093(7)[c]	2.127	2.130	2.111
Ru-N$_5$	2.128(9)[b], 2.112(7)[c]	2.131	2.172	2.142
O$_1$–O$_2$	1.353(10)[b], 1.367(9)[c]	1.352	1.289	1.306
Ru-O$_2$	1.995(7)[b], 2.004(6)[c]	2.012	-	-

The theoretically modeled distances of the optimized geometries of all possible spin states. [a] bond distances are given in Å. [b] crystal with two PF$_6$ as counterions. [c] crystal with 1.5 PF$_6$ and 0.5 IO$_3$ as counterions.

VI.2.2. EPR characterization

In order to get further insights into the electronic nature of the isolated η^2-**1Ru^{IV}-OO** intermediate and collect more experimental evidence to further confirm the formation of a closed shell Ru(IV)-peroxo species, EPR spectra were measured for the isolated η^2-**1Ru^{IV}-OO** species together with the isolated intermediates **1Ru^{III}-OH** and **1Ru^{IV}=O** for comparative purposes. The EPR spectrum of a solid sample of **1Ru^{III}-OH** in perpendicular mode shows a rhombic signal ($g_z = 2.385$, $g_y = 2.17$ and $g_x = 1.885$) associated to a low spin (LS) Ru(III) $S = \frac{1}{2}$ species (Figure VI.9), which is in agreement with the formation of a LS d^5 Ru(III)-hydroxo species and with the lowest in energy intermediate $S = \frac{1}{2}$ found in our DFT calculations in chapter V.[21] In contrast, no signal was obtained for **1Ru^{IV}=O** in perpendicular mode, which is in agreement with the formation of a LS d^4 Ru(IV)-oxo species $S = 1$, which cannot be detected under this conditions. This is in agreement with the triplet structure as the lowest in energy intermediate also found in our DFT calculations in chapter V.[21] Likewise, η^2-**1Ru^{IV}-OO** was EPR silent, this is in agreement with the formation of a closed shell Ru(IV)-peroxo species with no unpaired electrons ($S = 0$), which is in good agreement with our DFT calculations supporting the **^{1}[η^2-1Ru^{IV}-OO]** as the lowest in energy intermediate.
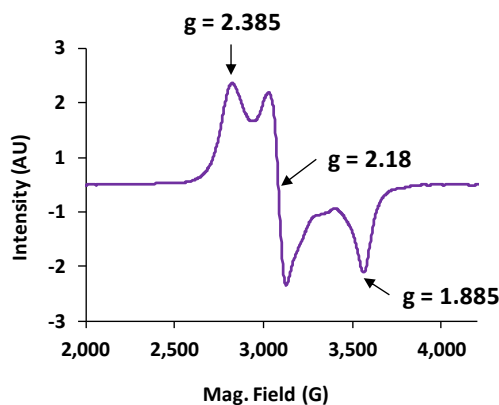
Figure VI.9. EPR spectrum of **1Ru^{III}-OH** ($g_z = 2.385$, $g_y = 2.17$ and $g_x = 1.885$) measured as solid at 77K; Mod. amp. 10 G; Mod. Freq. 100KHz, Resonance Freq. 9.404696 GHz and 33dB microwave power attenuation.

UNIVERSITAT ROVIRA I VIRGILI
MECHANISTIC STUDIES OF WATER OXIDATION CATALYZED BY HOMOGENEOUS IRON AND RUTHENIUM
COMPLEXES AND LIGHT-DRIVEN ORGANIC REDUCTIONS WITH A DUAL COBALT/COPPER CATALYTIC SYSTEM
Carla Casadevall Serrano

CHAPTER VI   After the O-O in Ru Catalyzed WO: a Missing Link

VI.2.3. Ru L₃-edge XAS characterization

X-ray absorption spectroscopy (XAS) is very informative regarding the determination of the local geometry and electronic structure of compounds. Therefore, to further explore their electronic structure η^2-**1Ru^{IV}-OO** and **1Ru^{IV}=O** were probed as solids with Ru L₃-edge spectroscopy which is a sensitive probe of the Ru d-manifold, and hence oxidation state and ligand field, as it results from dipole allowed p→d transitions (excitation of 2p electrons to d orbitals) (Figure VI.10). In addition, data were also collected on **1Ru^{II}-OH$_2$** and **1Ru^{III}-OH** isolated intermediates for comparative purposes (Figure VI.10). Moreover, the experimental data were fitted and correlated to theoretically calculated spectra due to the good correlation between theoretical transition energies and intensities and experimental ones (Annex IV Figures A.IV.6 – A.IV.8). In this line, experiment and theory are in agreement and as expected, within a molecular orbital picture for each compound, there is a direct correlation of the intensity of the transition with the percent d character of the acceptor orbitals in each case (Figure VI.10).[35]
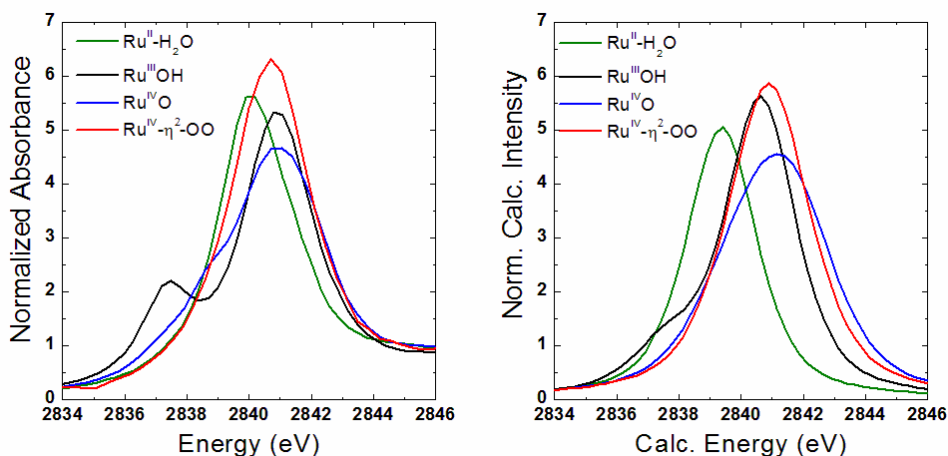
Figure VI.10. Comparison of experimental and calculated Ru L₃-edge spectra for complexes **1Ru^{II}-OH$_2$** (green line), **1Ru^{III}-OH** (black line), **1Ru^{IV}=O** (blue line) and η^2-**1Ru^{IV}-OO** (red line). The calculated spectra energies and intensities were correlated to experiment to facilitate comparison as described in Figure A.IV.7 (energy shift +16.6 eV; intensity scaled by a factor of 408). The calculated spectra intensities were broadened with experimentally determined FWHM and approximated as Gaussian-Lorentzian area sum peaks with 30% Gaussian character as shown in Figures VI.11 – VI.14.

The XAS spectrum of **1Ru^{II}-OH$_2$** shows a single intense feature at 2837.6 eV consistent with a low spin octahedral center where only the e$_g$ orbitals are accessible (Figure VI.11). The Ru L$_3$-edge spectrum of **1Ru^{III}-OH**, on the other hand, has an intense feature at 2838.3 eV due to p$_{3/2}$ → e$_g$ transitions with a well resolved, less intense feature at 2834.7 eV due to p$_{3/2}$ transitions to the singly occupied d$_{xy/yx}$ orbital of the t$_{2g}$ manifold (Figure VI.12).[36,37] In contrast, the p$_{3/2}$ to e(d$_{xz/yz}$) transitions in the spectrum of **1Ru^{IV}=O**, form a shoulder at 2836.0 eV and might be expected to increase in intensity due to the additional electron "hole" in the t$_{2g}$ manifold (Figure VI.13).[38] However the intensity of this transition is not significantly greater than in **1Ru^{III}-OH** and can be rationalized in terms of a highly covalent interaction with the oxo moiety resulting in significant p mixing into the valence orbitals and a lowering of d-character. This conclusion is supported both experimentally by a significant shift (~1.3 eV) to higher energy due to a more destabilized d$_{xz/yz}$ manifold as a result of the stronger Ru-O interaction, as well as by theoretical calculations which show relatively low d-character for this orbital set. It is important to note that this change in energy seems to be dominated by the Ru-oxo interaction, rather than oxidation state, as the main feature of **1Ru^{IV}=O**, which arises from transitions to the d$_x^2$-$_y^2$ and d$_z^2$ orbitals, experiences only a modest shift to a higher energy of ~0.1 eV relative to **1Ru^{III}-OH**. Lastly, the Ru L$_3$-edge spectrum of **η^2-1Ru^{IV}-OO** shows a single intense feature at 2838.0 eV, consistent with a closely spaced d-manifold as might be expected from a seven-coordinate metal center (Figure VI.14). The electronic structure derived is the S = 0 geometry, which is in agreement with the diamagnetic species observed by ^{1}H-NMR and the fact that it is EPR silent, together with our DFT calculations. Furthermore, the electronic structure of the **η^2-1Ru^{IV}-OO** bond alludes to a peroxo moiety where the O-O species interacts with the metal through an O$_{2\,\pi*}$ - Ru d$_{xy}$ interaction as previously reported for metal peroxo complexes.[39] The Ru(IV)-O$_2^{-2}$ character is further shown by the (O$_{2\,\pi*}$)^2(Ru d$_{xz/yz}$)^4(O$_{2\,\pi*}$)^2(Ru d$_{xy}$)^0(Ru d$_{x2-y2}$)^0(Ru d$_{z2}$)^0 electronic arrangement which effectively translates to a single bond character for the O-O bond. Altogether supports that the isolated intermediate is a well defined closed shell heptacoordinate Ru(IV)-peroxo species (**η^2-1Ru^{IV}-OO**).
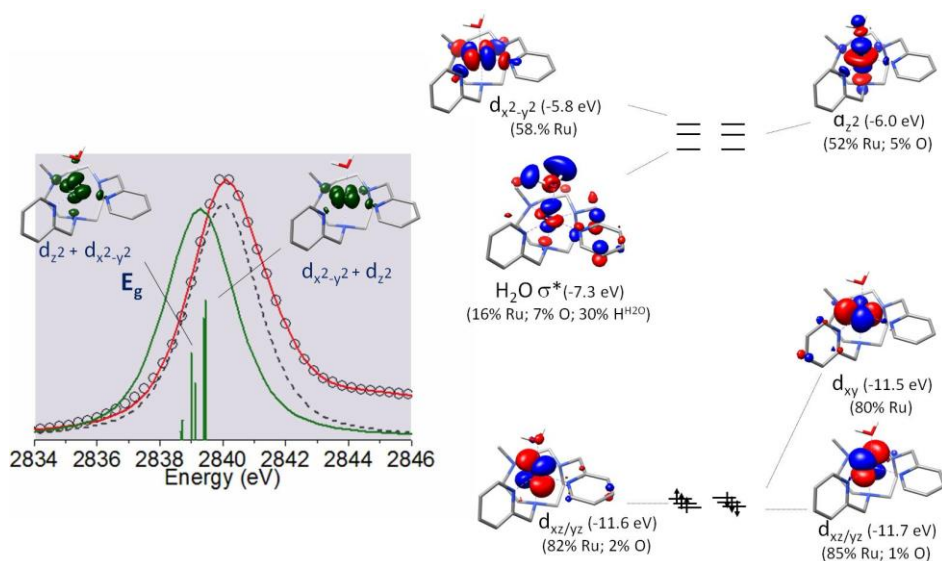
Figure VI.11. For **1Ru^{II}-OH$_2$**: (*left*) XANES region of Ru L$_3$-edge spectra showing edge and background subtracted experimental data (*circles*) overall fit (*red*) and fitted components (*dashed gray*) overlaid with scaled theoretical spectra having FWHM 2.6 eV and showing representative transition difference density maps (isovalue 0.01), with labels and symmetry for the orbitals involved. The geometry at the metal center is approximated as O$_h$ (*green*); *(right)* Schematic of the Ru 3d manifold showing metal and oxygen contributions (isovalue 0.05).
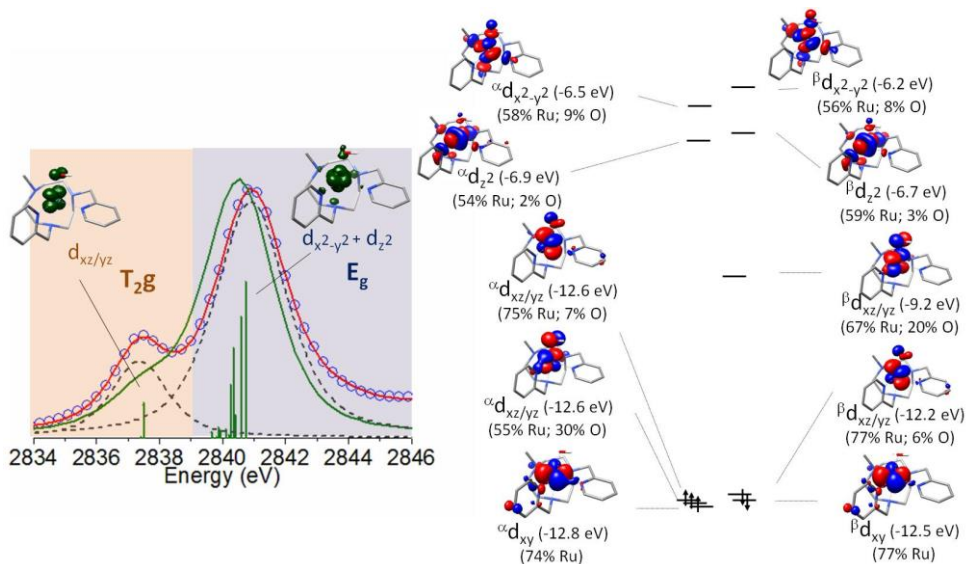
Figure VI.12. For **1Ru^{III}-OH**: (*left*) XANES region of Ru L$_3$-edge spectra showing edge and background subtracted experimental data (*circles*) overall fit (*red*) and fitted components (*dashed gray*) overlaid with scaled theoretical spectra having FWHM 2.6 eV and showing representative transition difference density maps (isovalue 0.01), with labels and symmetry for the orbitals involved. The geometry at the metal center is approximated as O$_h$ (*green*); *(right)* Schematic of the Ru 3d manifold showing metal and oxygen contributions (isovalue 0.05).
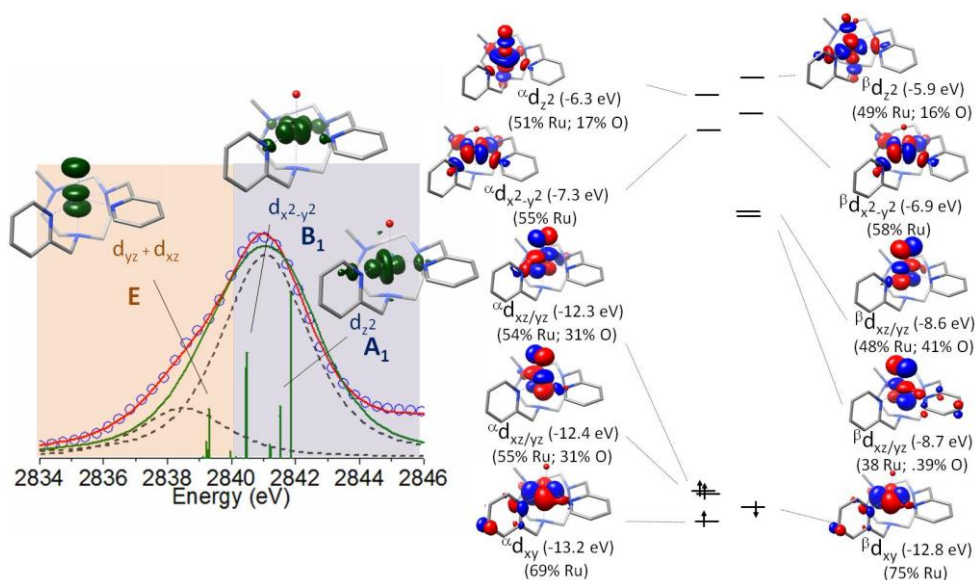
Figure VI.13. For **$1Ru^{IV}=O$**: (*left*) XANES region of Ru L_3-edge spectra showing edge and background subtracted experimental data (*circles*) overall fit (*red*) and fitted components (*dashed gray*) overlaid with scaled theoretical spectra having FWHM 3.2 eV and showing representative transition difference density maps (isovalue 0.01), with labels and symmetry for the orbitals involved. The geometry at the metal center is approximated as C_{4v} (*green*); *(right)* Schematic of the Ru 3d manifold showing metal and oxygen contributions (isovalue 0.05).
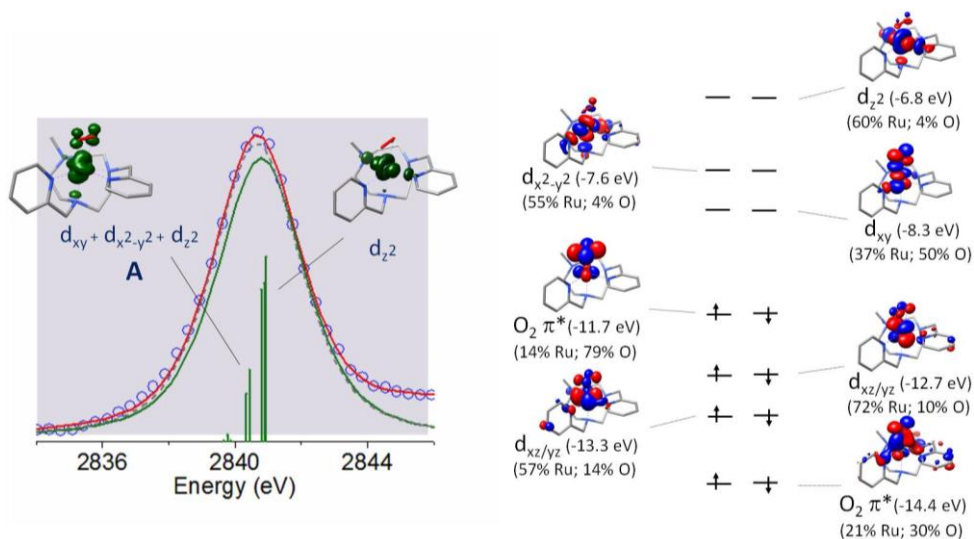
Figure VI.14. For **η^2-$1Ru^{IV}$-OO**: (*left*) XANES region of Ru L_3-edge spectra showing edge and background subtracted experimental data (*circles*) overall fit (*red*) and fitted components (*dashed gray*) overlaid with scaled theoretical spectra having FWHM 3.1 eV and showing representative transition difference density maps (isovalue 0.01), with labels and symmetry for the orbitals involved. The geometry at the metal center is approximated as distorted C_{2v}/D_{5h} (C_2)(*green*);[39] *(right)* Schematic of the Ru 3d manifold showing metal and oxygen contributions (isovalue 0.05).

214

Furthermore, the possibility of having triplet structures (S = 1) such as: i) $^3[\eta^1$-1Ru^{IV}-OO] and ii) $^3[\eta^2$-1Ru^{IV}-OO] species was considered. In the case of a $^3[\eta^2$-1Ru^{IV}-OO] (having the singlet geometry) the resulting calculated XAS spectra is a clear mismatch with the experimental data (Figure A.IV.10). For $^3[\eta^1$-1Ru^{IV}-OO], on the other hand, a much broader peak is expected to result from a $t_{2g} - e_g$ d-orbital manifold splitting with a shoulder at lower energy from the $p_{3/2}$ to e_g transitions. This again has a poorer correlation with experimental data both in terms of energy and overall intensity than the singlet description (Figure A.IV.11).

VI.2.4. Raman spectroscopic characterization

To shed more light on the coordination mode of the Ru(IV)-peroxo species, solid and solution Raman studies were performed for **η²-1Ru^{IV}-OO** together with all the isolated intermediates (**1Ru^{II}-OH₂, 1Ru^{III}-OH** and **1Ru^{IV}=O**) for comparative reasons. First, the UV-Vis spectra of the isolated complexes were measured as aqueous solutions (0.25 mM concentration in degassed MilliQ water) to know their absorption features so that we choose the most appropriate lasers for the Raman studies (Figure VI.15). The UV-Vis spectrum of **1** has been already described in chapter IV,[21] showing two bands at λ_{max} 249 nm (ε = 6419 M^{-1}·cm^{-1}) and 397 nm (ε = 5345 M^{-1}·cm^{-1}). The UV-Vis spectrum of **1Ru^{III}-OH** shows three bands at λ_{max} 233 nm (ε = 4360 M^{-1}·cm^{-1}), 249 nm (ε = 4220 M^{-1}·cm^{-1}), 266 nm (ε = 4240 M^{-1}·cm^{-1}) and 297 nm (ε = 3200 M^{-1}·cm^{-1}), which resembles the one of the *in situ* generated **1Ru^{III}-OH** upon oxidation of **1Ru^{II}-OH₂** with CAN or NaIO₄ reported in chapter IV.[21] Likewise, the spectrum of **1Ru^{IV}=O** shows a band at 263 nm (ε = 4800 M^{-1}·cm^{-1}), which is in agreement with the one of the *in situ* generated **1Ru^{IV}=O** from chapter IV.[21] In contrast, the spectrum of **η²-1Ru^{IV}-OO** shows two bands at 242 nm (ε = 9400 M^{-1}·cm^{-1}) and 360 nm (ε = 6500 M^{-1}·cm^{-1}). Therefore, all species have some absorbance in the region between 300 and 460 nm. Thus, solution Raman measurements were performed at λ_{exc} = 355 and 457 nm and solid measurements were performed at λ_{exc} = 632.8 nm, to get the best compromise between data quality and

avoiding rapid photodamage of the samples during the measurement time. All spectra were compared to the theoretical ones calculated by DFT at a uM11/6-31G(d) (SDD basis set for Ru) PCM-SMD (H_2O) level in Gaussian.[34]
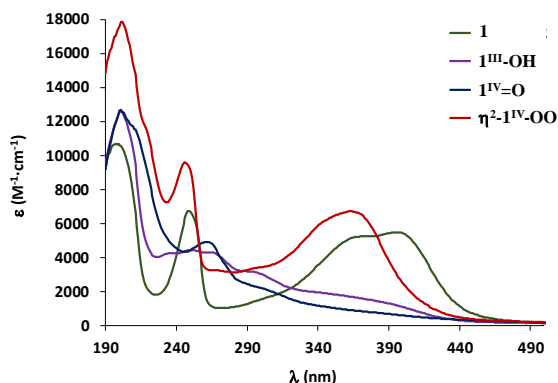
Figure VI.15. UV-Vis spectra of the isolated complexes **1Ru^{II}-OH$_2$** (green line) **1Ru^{III}-OH** (purple line) **1Ru^{IV}=O** (blue line) and **η^2-1Ru^{IV}-OO** (red line) at 0.25 mM concentration measured at 298 K in degassed MilliQ water.

The solution (dashed red line *top* spectrum), solid state (straight red line *middle* spectrum) and DFT calculated (dotted red line *bottom* spectrum) Raman spectra of complex **1Ru^{II}-OH$_2$** are shown in Figure VI.16. The solid-state Raman spectrum of **1Ru^{II}-OH$_2$**, shows the expected mode of the Ru-O stretch at 308 cm^{-1}, which is in agreement with the observed band at 329 cm^{-1} in the calculated spectrum. In addition, the stretch of the Py mode of the Py$_2^{Me}$tanc ligand can be seen at around 1020 cm^{-1} together with other vibrational modes of the Py$_2^{Me}$tanc ligand at upper and lower in energy shifts. In contrast, solution (red and green dashed line spectra *a* and *b*, generated upon the addition of CAN and NaIO$_4$ to **1Ru^{II}-OH$_2$**) and solid state Raman spectra of **1Ru^{III}-OH**, show the expected mode of the Ru-O stretch for a coordination of a hydroxy ligand at 576 cm^{-1}, which is in agreement with the observed band at 566 cm^{-1} in the DFT calculated spectrum (*d*) (Figure VI.17). In addition, the stretch of the Py mode from the Py$_2^{Me}$tanc ligand can be seen at around 1012 cm^{-1} together with other vibrational modes of the Py$_2^{Me}$tanc ligand at upper and lower in energy shifts. In general, there is a good correlation between the experimental and the DFT calculated Raman spectra (Figures VI.16 and VI.17).
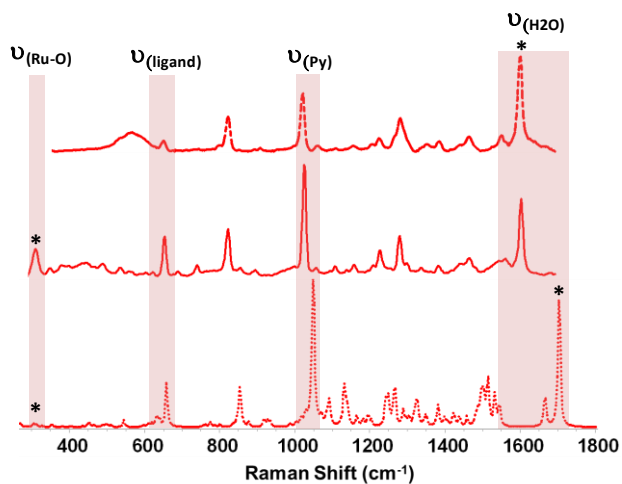
Figure VI.16. Raman spectra of $[Ru^{II}(OH_2)(Py_2{}^{Me}tacn)](PF_6)_2$ (**1Ru^{II}-OH$_2$**): *Top*) in H_2O (red dashed line) measured at λ_{exc} = 457 nm (50 mW power, rt); *Middle*) isolated solid (red straight line)measured at λ_{exc} = 632.8 nm (12 mW power, rt); and *Bottom*) DFT calculated Raman spectra of **1Ru^{II}-OH$_2$** (red dotted line). The most significant bands have been highlighted in red.
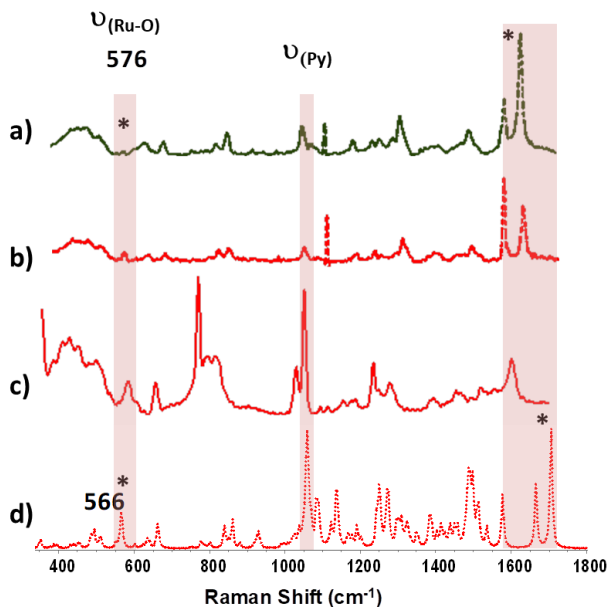
Figure VI.17. Raman spectra of $[Ru^{III}(OH)(Py_2{}^{Me}tacn)](PF_6)_2$ (**1Ru^{III}-OH**). Green dashed line spectrum *a* corresponds to the solution Raman spectra of **1Ru^{III}-OH** generated after the addition of CAN (1 eq) to **1** in H_2O (2 mM concentration) measured at λ_{exc} = 355 nm (10 mW power, rt). Red dashed line spectrum *b* corresponds to the solution Raman spectrum of **1Ru^{III}-OH** generated after the addition of NaIO$_4$ (0.5 eq) in H_2O (2 mM concentration) measured at λ_{exc} = 355 nm (10 mW power, rt). Spectrum *c* corresponds to the solid Raman spectra of **1Ru^{III}-OH** measured at λ_{exc} = 632.8 nm (12 mW power, rt). Spectrum *d* correspond to the DFT calculated Raman spectra of **1Ru^{III}-OH** with ^{16}O.
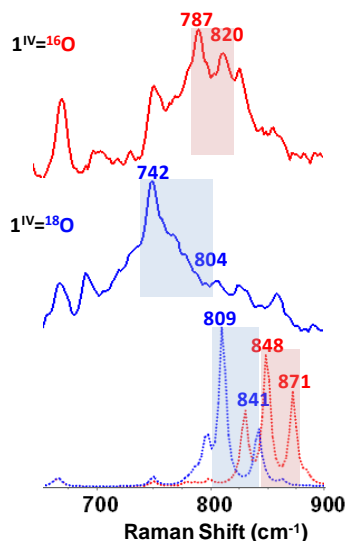
Figure VI.18. Solid Raman spectra of $[Ru^{IV}(O)(Py_2^{Me}tacn)](PF_6)_2$ (**$1Ru^{IV}=O$**) with ^{16}O (red) and ^{18}O (blue) isotopic substitution in the measured region (λ_{exc} = 632.8 nm, 12 mW power, rt), respectively.

On the other hand, the Raman spectrum of the isolated ^{16}O-labeled **$1Ru^{IV}=O$** intermediate (at λ_{exc} = 632.8 nm, 12 mW power, Figure VI.18, *top*) shows a Fermi doublet with two bands at 787 and 820 cm^{-1}, respectively, that exhibit an isotope shift of -45 and -16 cm^{-1}, respectively, upon ^{18}O-substitution (**$1Ru^{IV}=^{18}O$**) (from 787 to 742 cm^{-1}, $\Delta^{16,18}$(DFT-calcd) = 39 cm^{-1}, and from 820 to 804 cm^{-1}, $\Delta^{16,18}$(DFT-calcd) = 30 cm^{-1} Figure VI.18, *middle*) and is assigned to the Ru-O stretch, which is in agreement with the DFT calculated spectra (Figure VI.18, *bottom*, ^{16}O-red and ^{18}O-blue spectra, see also Annex A.IV Figure A.IV.12). It is worth to be noticed that there is an enhancement of the Ru-O stretch in the Raman collected of the in situ generated **$1Ru^{IV}=O$** and **$1Ru^{IV}=^{18}O$** intermediates upon the addition of NaIO$_4$ (1.5 eq.) to **$1Ru^{II}$-OH$_2$** and **$1Ru^{II}$-$^{18}OH_2$** in H$_2$O and H$_2^{18}$O, respectively (Figures A.IV.13 and A.IV.14, spectra *b* and *e*, respectively, λ_{exc} = 457 nm, 50 mW power, rt). In addition, the same bands are observed in the generation of **$1Ru^{IV}=O$** upon the addition of CAN (3 eq.) to **1** in H$_2$O (λ_{exc} = 355 nm, 10 mW power, rt, green dashed spectrum *c*, Figure A.IV.14). The features observed in the experimental spectra well correlate with the DFT calculated spectra for this intermediate (Figure A.IV.14, *f*).

218
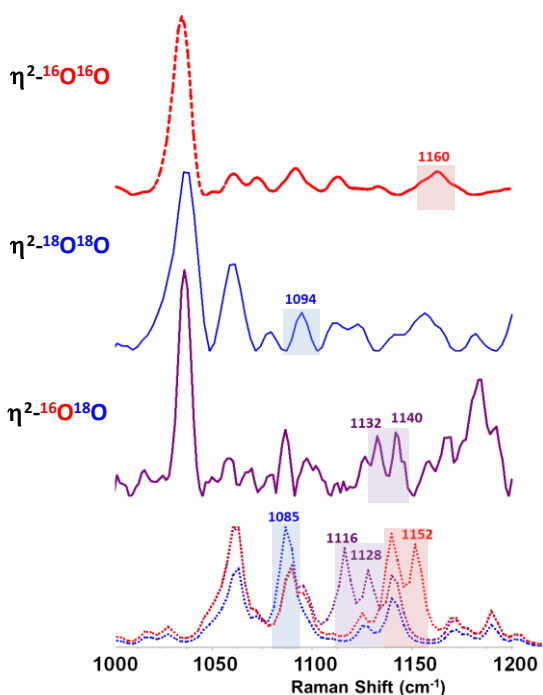
Figure VI.19. Comparison of the solution and DFT Raman spectra of η^2-**1Ru^{IV}-OO** in the Ru-O stretching region. Raman spectra of η^2-**1Ru^{IV}-OO** generated after the addition of NaIO$_4$ (6.5 eq) to **1Ru^{II}-OH$_2$** in Milli-Q H$_2$O (2 mM concentration) with ^{16}O (*top,* red) measured at λ_{exc} = 457 nm, (50 mW power, rt). Raman spectra of η^2-**1Ru^{IV}-^{18}O^{18}O** generated after the addition of NaI^{18}O$_4$ (6.5 eq, previously exchanged) to **1Ru^{II}-OH$_2$** in H$_2$^{18}O (2 mM concentration) (*middle*, blue) measured at λ_{exc} = 457 nm (50 mW power, rt). Raman spectra of η^2-**1Ru^{IV}-O^{18}O** generated after the addition of NaIO$_4$ (6.5 eq) to **1^{IV}=^{18}O** in D$_2$O (2 mM concentration) (purple) measured at λ_{exc} = 457 nm (50 mW power, rt). DFT calculated Raman spectra of η^2-**1Ru^{IV}-OO** (red dotted line), η^2-**1Ru^{IV}-^{18}OO** (purple dotted line) and η^2-**1Ru^{IV}-^{18}O^{18}O** (blue dotted line) in the regions of study (*bottom*).

The Raman spectrum of the ^{16}O η^2-**1Ru^{IV}-OO** in Milli-Q water (λ_{exc} = 457 nm, 50 mW power, rt) generated after the addition of 6.5 equivalents of NaIO$_4$ to **1** shows a band at 1160 cm^{-1} that exhibits an isotope shift of 66 cm^{-1} upon ^{18}O-substitution (1094 cm^{-1}, $\Delta^{16,18}_{(DFT\text{-}calcd)}$ = 66 cm^{-1}) and is assigned to the O-O stretch (Figure VI.19, *top* red and subsequent blue spectra and Figure A.IV.15). This frequency is within the range of the O-O stretch of many related M-O$_2$ complexes[22,23,40,41] and about 400 cm^{-1} lower than the 1580 cm^{-1} stretch of an isolated O$_2$ molecule and 90 cm^{-1} higher than the 1074 cm^{-1} stretch of a free superoxide radical anion (O$_2^-$). Moreover, the observed O-O st is in agreement with the formation of a closed shell heptacoordinated η^2-**1Ru^{IV}-OO** intermediate, as supported by the DFT calculated Raman spectra at the

uM11/cc-pVTZ//uM11/6-31G(d) (SDD basis set for Ru), PCM-SMD (H_2O) level of theory (Figure VI.19, *bottom*, red spectrum). The O-O st of the singlet η^2-**1Ru^{IV}-OO**, the lowest in energy intermediate, appears at 1152 cm^{-1}, whereas a O-O st at 1297 cm^{-1} is observed for the triplet η^1-**1Ru^{IV}-OO** structure (Figure VI.20, green *dotted* spectrum). This suggests that this level of theory well describes the spectroscopic features and electronic nature and structure of η^2-**1Ru^{IV}-OO**. The same O-O stretching was observed in the solid measurement (λ_{exc} = 632.8 nm, 12 mW power, rt, Figure A.IV.16, *c*) of η^2-**1Ru^{IV}-OO** and the in situ generated η^2-**1Ru^{IV}-OO** upon the addition of CAN to **1Ru^{II}-OH$_2$** (λ_{exc} = 355 nm, 10 mW power, rt, Figure A.IV.16, *a*). In addition, the Raman spectrum of the ^{18}O η^2-**1Ru^{IV}-^{18}O^{18}O** in $H_2{}^{18}$O generated after the addition of 6.5 equivalents of NaI^{18}O$_4$ to **1Ru^{II}-OH$_2$** shows a band at 1094 cm^{-1} that exhibits the expected isotopic shift ($\Delta^{16,18}{}_{(exp)}$ = 66 cm^{-1}, $\Delta^{16,18}{}_{(DFT-calcd)}$ = 67 cm^{-1}, Figure VI.19, blue spectra). Moreover, the Raman spectrum of the *in situ* generated ^{16}O-^{18}O-labeled η^2-**1Ru^{IV}-O^{18}O** in D_2O (after the addition of 5 eq NaIO$_4$ to **1Ru^{IV}=^{18}O** in D_2O) shows two bands at 1132 and 1140 cm^{-1} that are shifted in 28 and 20 cm^{-1} to lower energies from the non-labelled η^2-**1Ru^{IV}-OO** intermediate which are associated to the O-O stretching for the mix labelled η^2-**1Ru^{IV}-O^{18}O** intermediate (purple line spectrum in Figure VI.19), which is in concordance with the bands observed in the DFT calculated Raman spectrum for η^2-**1Ru^{IV}-O^{18}O** (1116 and 1128 cm^{-1}, $\Delta^{(16-16)-(16-18)}{}_{(DFT-calcd)}$ = 36 and 24 cm^{-1}, Figure VI.19, *bottom* purple dotted spectrum).

Additionally, in all spectra we can also see the pyridyl vibrational modes at around 1040 cm^{-1} that do not shift which also appear in the DFT calculated spectra at around 1060 cm^{-1} (Figure VI.19). In general, the shape and the features observed in the experimental spectra are well reproduced by the theoretical ones. The Ru-O stretching region is more complicated to analyze due to the several bands of similar intensities observed for each intermediate according to the possible labeling (see Annex IV Figures A.IV.16 – A.IV.19 for details). Altogether is in agreement with the peroxo coordination in a side-on manner, thus, having the singlet η^2-**1Ru^{IV}-OO**.
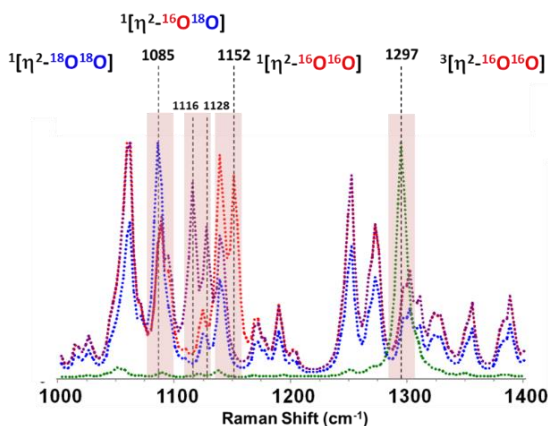
Figure VI.20. DFT calculated Raman spectra of η^2-**1Ru^{IV}-OO** (red dotted line), η^2-**1Ru^{IV}-^{18}OO** (purple dotted line), η^2-**1Ru^{IV}-^{18}O^{18}O** (blue dotted line) and the triplet structure of η^2-**1Ru^{IV}-OO** (η^1-**1Ru^{IV}-OO**) (green dotted line), in the O-O stretching region.

VI.2.5. CSI-HRMS labeling and kinetic studies

Raman studies show that the characterization of the solid crystalline η^2-**1Ru^{IV}-OO** matches the one from the generated η^2-**1Ru^{IV}-OO** under catalytic conditions after the addition of an excess of CAN or NaIO4 as sacrificial oxidants. Therefore, to further confirm the characterization in solution and the "*in situ*" formation of the η^2-**1Ru^{IV}-OO** intermediate after the WNA, CSI-HRMS labeling and kinetic studies in the presence of Milli-Q H$_2$O, D$_2$O and H$_2$^{18}O were performed. Those experiments are very informative regarding the course of the oxidation reaction of **1Ru^{IV}=O** with either NaIO$_4$ or Ce^{IV}. The reaction is slow, so an excess of oxidant is required to accelerate it, as in the Raman studies (see the experimental section for further details).

First, analysis of the isolated crystals of η^2-**1Ru^{IV}-OO** by CSI-HRMS was performed by dissolving the crystals in a D$_2$O:MeCN (1:10) solvent mixture. The mass spectrum shows a peak at *m/z* 604.0885 that is associated with the **[η^2-1Ru^{IV}-OO-(PF$_6$)]$^+$** complex (Figure VI.21). Other peaks corresponding to **1Ru^{IV}=O** and the coordination of MeCN most likely due to oxygen release during manipulation and analyses were also observed in the mass spectrum (see Annex IV figures A.IV.22 – A.IV.26 and Table A.IV.8 for details).

221
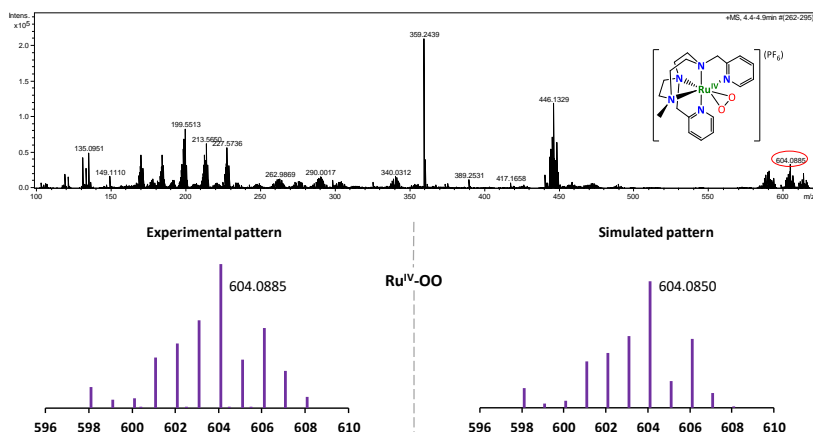
Figure VI.21. Characterization of the isolated crystal of complex $^2\eta$-$[Ru^{IV}(OO)(Py_2^{Me}tacn)](PF_6)_2$ (0.001 mM) by CSI-HRMS at 25ºC in D_2O:MeCN (1:10) solvent mixture.

In addition, the same peaks at *m/z* 604.0885 and 634.0086 associated to $[\eta^2\text{-}1Ru^{IV}\text{-}OO\text{-}(PF_6)]^+$ and $[\eta^2\text{-}1Ru^{IV}\text{-}OO\text{-}(IO_3)]^+$ where also observed after the addition of $NaIO_4$ (5 eq.) to $1Ru^{II}\text{-}OH_2$ (Figure A.IV. 27).
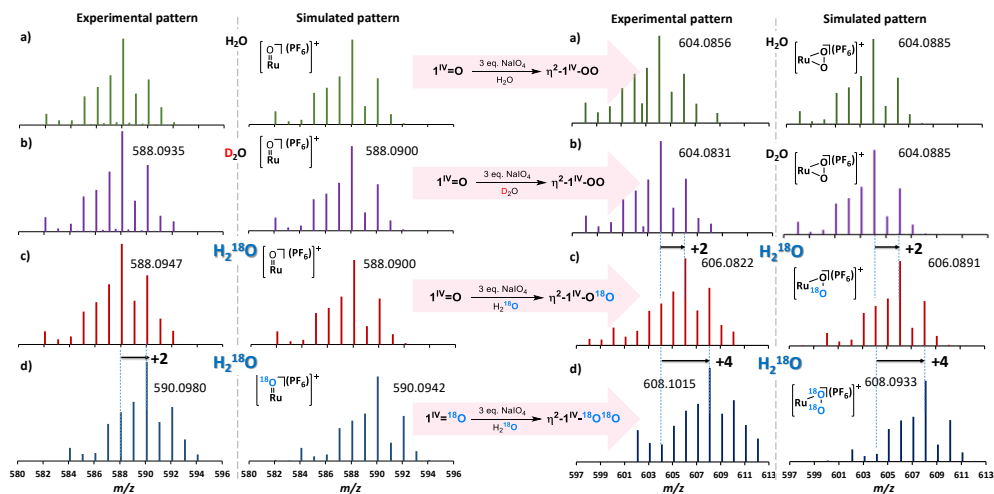
Figure VI.22. CSI-HRMS (293 K) of the monocharged $[Ru\text{-}OO\text{-}PF_6]^+$ species of a) η^2-$1Ru^{IV}$-OO generated in MilliQ H_2O after addition of $NaIO_4$ (5 eq.) to $1Ru^{IV}$=O (green), b) η^2-$1Ru^{IV}$-OO generated in D_2O after addition of $NaIO_4$ (5 eq.) to $1Ru^{IV}$=O (purple), c) η^2-$1Ru^{IV}$-^{18}OO generated in $H_2^{18}O$ after addition of $NaIO_4$ (5 eq.) to $1Ru^{IV}$=O (red) and d) η^2-$1Ru^{IV}$-$^{18}O^{18}O$ generated in $H_2^{18}O$ after addition of $NaIO_4$ (5 eq.) to $1Ru^{IV}$=^{18}O (blue) (see experimental section for further details).

Figure VI.23. CSI-HRMS (293 K) of the monocharged [Ru-OO-IO$_3$]$^+$ species of a) η^2-**1Ru^{IV}-OO** generated in MilliQ H$_2$O after addition of NaIO$_4$ (5 eq.) to **1Ru^{IV}=O** (green), b) η^2-**1Ru^{IV}-OO** generated in D$_2$O after addition of NaIO$_4$ (5 eq.) to **1Ru^{IV}=O** (purple), c) η^2-**1Ru^{IV}-^{18}OO** generated in H$_2$^{18}O after addition of NaIO$_4$ (5 eq.) to **1Ru^{IV}=O** (red) and d) η^2-**1Ru^{IV}-^{18}O^{18}O** generated in H$_2$^{18}O after addition of NaIO$_4$ (5 eq.) to **1Ru^{IV}=^{18}O** (blue) (see experimental section for further details).

Additionally, CSI-HRMS labeling studies of the generation of η^2-**1Ru^{IV}-OO** after the addition of NaIO$_4$ (5 eq.) to **1Ru^{IV}=O** in MilliQ H$_2$O, D$_2$O and H$_2$^{18}O together with the addition of NaIO$_4$ (5 eq.) to **1Ru^{IV}=^{18}O** in H$_2$^{18}O were performed. Addition of NaIO$_4$ (5 eq) to a solution of **1Ru^{IV}=O** (2 mM) in MilliQ H$_2$O leads to the formation of a prominent peak at *m/z* 634.0100 and a less intense peak at *m/z* 604.0885 that are associated to [η^2-**1Ru^{IV}-OO-(IO$_3$)**]$^+$ and [η^2-**1Ru^{IV}-OO-(PF$_6$)**]$^+$ complexes respectively (Figures VI.22 and VI.23), which is in agreement with the peaks observed during CSI-HRMS analysis of a water solution of η^2-**1Ru^{IV}-OO** crystals (Figure VI.21). In addition, a low intense peak at *m/z* 229.5601 that corresponds to the dicharged [η^2-**1Ru^{IV}-OO**]$^{2+}$ complex can be observed (A.IV.28). These peaks remain intact in D$_2$O but they are upshifted by *m/z* 8, 2 and 1 in H$_2$^{18}O (*m/z* 642.0313, 606.0822 and 230.5621) and by *m/z*, 10. 4 and 2 (*m/z* 644.0280, 608.1015 and 231.5686) when NaIO$_4$ (5 eq) is added to a solution of **1Ru^{IV}=^{18}O** (2 mM) in H$_2$^{18}O, respectively, which are associated to the formation of [η^2-**1Ru^{IV}-O^{18}O-(I^{18}O$_3$)**]$^+$, [η^2-**1Ru^{IV}-O^{18}O-(PF$_6$)**]$^+$ and [η^2-**1Ru^{IV}-O^{18}O**]$^{2+}$, and [η^2-**1Ru^{IV}-**

$^{18}O^{18}O$-($I^{18}O_3$)]$^+$, [η^2-1Ru^{IV}-$^{18}O^{18}O$-(PF$_6$)]$^+$ and [η^2-1Ru^{IV}-$^{18}O^{18}O$]$^{2+}$ respectively (Figures VI.22, VI.23 and A.IV.28). These experiments indicate the presence of one exchangeable oxygen atom for η^2-1Ru^{IV}-OO. Since the oxygen atom from the starting 1Ru^{IV}=O intermediate cannot be exchanged for an ^{18}O atom from H$_2$$^{18}O$ as we have seen in chapter IV,[21] the formation of ^{18}O-labelled complexes derived from η^2-1Ru^{IV}-OO suggests a nucleophilic attack of a ^{18}O atom to the rapidly formed 1Ru^V=O from 1Ru^{IV}=O (or 1Ru^V=^{18}O from 1Ru^{IV}=^{18}O) under an excess of oxidant.

Likewise, CSI-HRMS kinetic studies to monitor the "*in situ*" formation of the η^2-1Ru^{IV}-OO intermediate after the WNA in Milli-Q H$_2$O, D$_2$O and H$_2$^{18}O were performed (see Figure A.IV.29 and the experimental section for details). Initial monitoring of the addition of NaIO$_4$ (5 eq) to a solution of 1Ru^{IV}=O (2 mM) in MilliQ H$_2$O leads to the formation of a prominent peak at m/z 634.0100 and a less intense peak at m/z 604.0885 that are associated to [η^2-1Ru^{IV}-OO-(IO$_3$)]$^+$ and [η^2-1Ru^{IV}-OO-(PF$_6$)]$^+$ complexes, respectively (Figure VI.24 *left*). Interestingly, the trace of the peak associated to [η^2-1Ru^{IV}-OO-(PF$_6$)]$^+$ (m/z 604.0885) increases along the reaction time due to the slow accumulation of the intermediate until it reaches a plateau after approximately 2 hours of reaction due to crystal formation and precipitation of [η^2-1Ru^{IV}-OO-(PF$_6$)]$^+$ as observed in the microscope (Figure VI.25 and Figure A.IV.29). In addition, a new peak at m/z 229.5601 that corresponds to the dicharged [η^2-1Ru^{IV}-OO]$^{2+}$ complex appears at long reaction times. The same kinetic trend and peaks where observed in D$_2$O but they are upshifted by m/z 8, 2 and 1 in H$_2$^{18}O (m/z 642.0313, 606.0944 and 230.5649), respectively, which are associated to the formation of [η^2-1Ru^{IV}-O^{18}O-(I^{18}O$_3$)]$^+$, [η^2-1Ru^{IV}-O^{18}O-(PF$_6$)]$^+$ and [η^2-1Ru^{IV}-O^{18}O]$^{2+}$, respectively (Figures A.IV.30 – A-IV.32). These kinetic studies confirm the immediate formation of the Ru(IV)-peroxo species after the O-O bond formation.
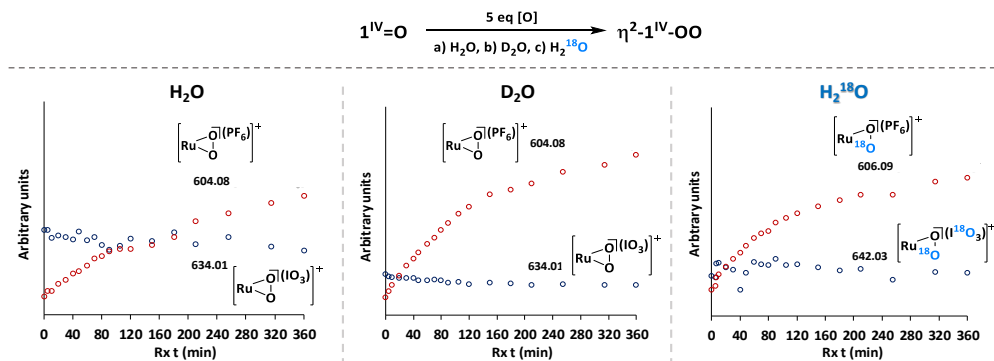
Figure VI.24. CSI-HRMS (293 K) monitoring of the reaction kinetics of **1Ru^{IV}=O** with NaIO$_4$ (5 eq) in *left*) MilliQ water, *middle*) D$_2$O and *right*) H$_2$^{18}O (97 % ^{18}O). For further details see Annex IV section A.IV.5.4. and experimental section.
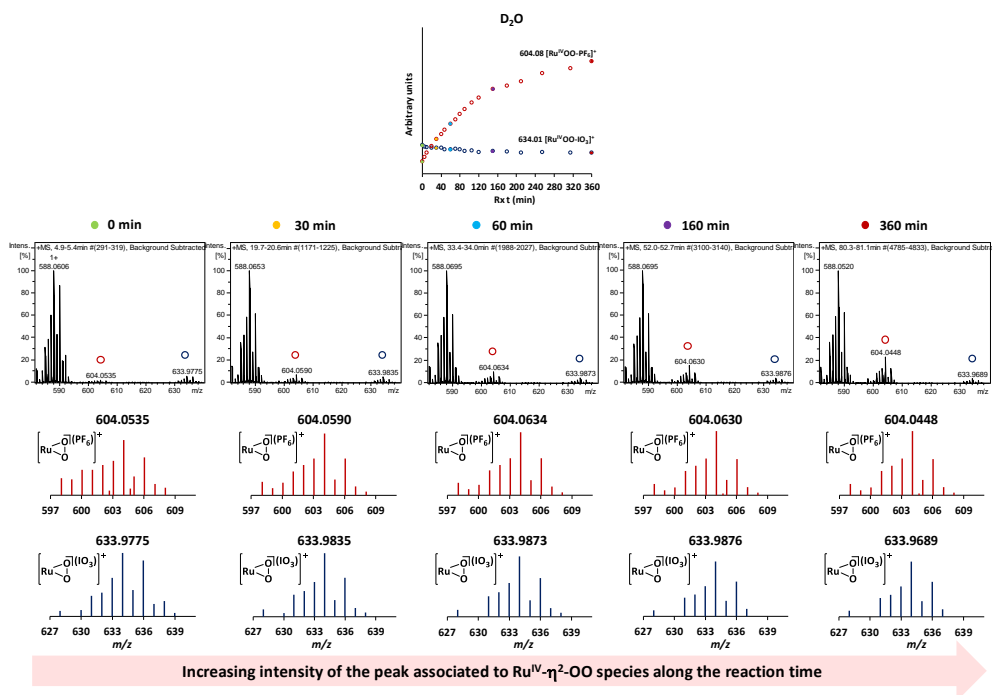
Figure VI.25. Snapshots of the CSI-HRMS (293 K) monitoring of the reaction kinetics of **1Ru^{IV}=O** with NaIO$_4$ (5 eq) in D$_2$O. For further details see Annex IV section A.IV.5.4. and the experimental section.

In order shed more light in the generation of the peroxo species form the Ru-oxo, we monitored its formation by using Ce^{IV} (analogous to the Raman studies and the SO mostly used in our catalytic studies in chapter IV) so that avoiding the use oxo-transfer reagents as $NaIO_4$. The use of CAN in mass spectrometry studies masks the region of study between m/z 500 and 700 to monitor the formation of **η^2-1Ru^{IV}-OO**. Therefore, $Ce(OTf)_4$ was used instead since the more labile triflate ligands give rise to cleaner mass spectra. Addition of $Ce(OTf)_4$ (5 eq) to a solution of **1Ru^{IV}=O** (2 mM) in D_2O shows the formation of a peak at m/z 608.0828 which is associated to the formation of **[η^2-1Ru^{IV}-OO-(PF$_6$)]$^+$** and **[η^2-1Ru^{IV}-OO-(OTf)]$^+$** in a 1:3 ratio (sum of two peaks at m/z 604.0878 and 608.0828). Those peaks are upshifted 2 units in $H_2^{18}O$ due to the formation of **[η^2-1Ru^{IV}-O^{18}O-(PF$_6$)]$^+$** and **[η^2-1Ru^{IV}-O^{18}O-(OTf)]$^+$** in a 1:1 ratio (sum of two peaks at m/z 606.0856 and 610.0734). This experiment, together with the experiments with $NaIO_4$, unequivocally proof that labeled and non-labeled **η^2-1Ru^{IV}-OO** intermediates are formed via a WNA of an H_2O molecule (D_2O or $H_2^{18}O$) to a most likely **1Ru^V=O** (electrochemically characterized in the section below), rapidly formed in solution under excess of oxidant. This is supported by the absence of any O-O exchange of the coordinated Ru(IV)-peroxo moiety upon the addition of $H_2^{18}O$ to a solution of **η^2-1Ru^{IV}-OO** in H_2O.
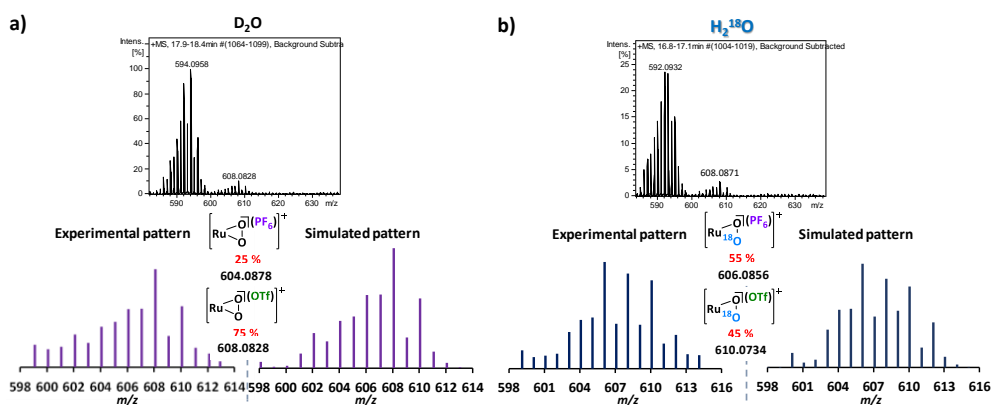
Figure VI.26. CSI-HRMS (293 K) of the reaction of **1Ru^{IV}=O** with $Ce(OTf)_4$ (5 eq) in a) D_2O, and b) $H_2^{18}O$ (97 % ^{18}O). For further details see Annex IV section A.IV.5.4. and the experimental section.

VI.2.6. Mechanistic studies with η^2-1Ru^{IV}-OO

Further mechanistic studies were performed in order to undoubtedly connect η^2-1Ru^{IV}-OO with the WO catalytic cycle. First, the decay of η^2-1Ru^{IV}-OO crystals in acetonitrile solution was observed ^{1}H-NMR, generating Ru(II) species. Indeed the ^{1}H-NMR of η^2-1Ru^{IV}-OO in MeCN-d$_3$ is comparable to that of 1Ru^{II}-MeCN from chapter IV (Figure VI.27 and Figure A.IV.1 and A.IV.2 and figure VI.28).
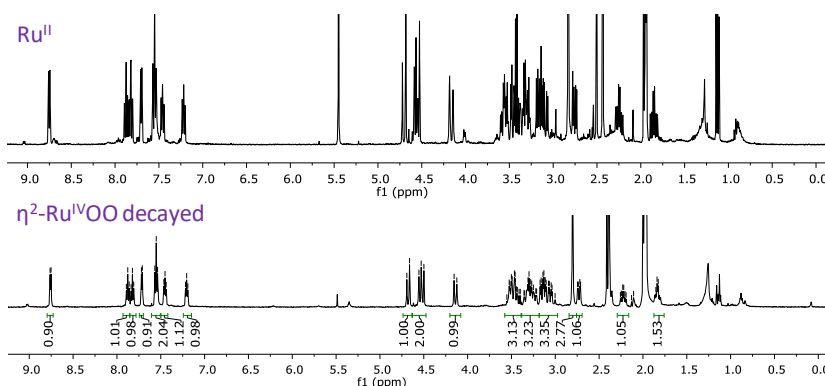
Figure VI.27. ^{1}H-NMR (500 MHz, 233 K, MeCN-d$_3$) spectrum of the isolated [Ru^{IV}(OO)(Py$_2^{Me}$tacn)](PF$_6$)$_2$ (η^2-1Ru^{IV}-OO) complex.
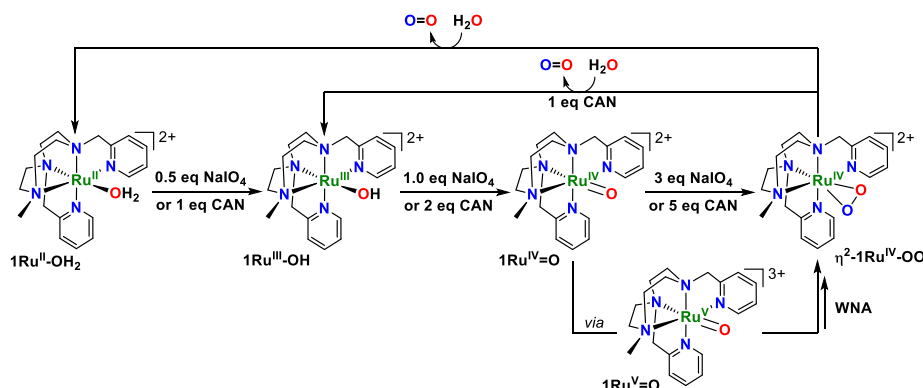
Figure VI.28. Interconnection and reactivity of ruthenium intermediates involved in WO.

In addition, the addition of CAN to η^2-1Ru^{IV}-OO in water (0.25 mM) monitored by UV-vis and pressure transducer sensors yield the formation of Ru(III) species with concomitant O$_2$ release (about 1 TON by pressure sensors and TCD-GC

227

analyses) (Figure A.IV.40). Although the formation of Ru(III) species was not clean since CAN has a strong absorbance in the $200 - 350$ nm region.[21] In addition, the oxygen evolution from the isolated η^2-**1Ru^{IV}-OO** was also further confirmed by GC-MS, showing the quantitative formation of $^{32}O_2$.

Moreover, WO catalytic tests from all the isolated intermediates **1Ru^{II}-OH$_2$**, **1Ru^{III}-OH**, **1Ru^{V}=O**, and η^2-**1Ru^{IV}-OO** show similar TON O_2 (around 50 TON O_2) and initial TOF (Table VI.2 and Figure VI.29), confirming the participation of them in the catalytic cycle.

Table VI.2. Water oxidation catalytic activities for the isolated ruthenium intermediates.

Entry	Complex	[CAN] (mM)	[Cat] (μM)	TOF (h^{-1})^a	TON O_2^{a}	TON O_2^{b}	TON CO_2^{b}
1	**1Ru^{II}-OH$_2$**^{c}	125	35	14	53 ± 7	53 ± 5	n.d.
2	**1Ru^{III}-OH**^{c}	125	35	13	45 ± 1	45 ± 3	n.d.
3	**1Ru^{IV}=O**^{c}	125	35	13	45 ± 5	47 ± 3	n.d.
4	η^2-**1Ru^{IV}-OO**^{c}	125	35	15	42 ± 2	42 ± 4	n.d.

Reactions performed in MilliQ water at 25 ºC under vigorous stirring. Reaction conditions: the catalyst (0.5 ml, final concentration 35 μM) was injected through a septum into the reaction vial containing CAN aqueous solution (9.5 ml, 131 mM, final concentration 125 mM. a) Results obtained by manometry studies after 20 h of reaction. TOF is calculated after 8 min of the addition of the catalyst. b) Results from the analysis of an aliquot of the head-space by GC-TCD after 20 h of reaction.
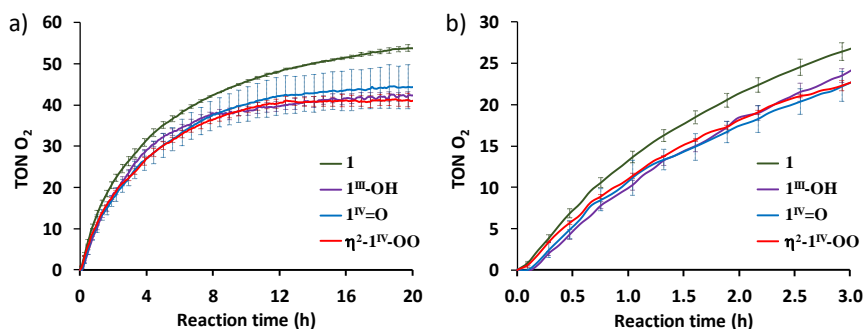
Figure VI.29. a) and b) Gas traces of the manometry monitorization when the ruthenium intermediate (**1Ru^{II}-OH$_2$** (green line), **1Ru^{III}-OH** (purple line), **1Ru^{IV}=O** (blue line) and η^2-**1Ru^{IV}-OO** (red line) (0.5 ml of a stock solution, final concentration 35 μM) is added to a stirred solution of CAN (9.5 ml, final concentration 125 mM) in Milli-Q water at 25ºC and initial pH 0.8. Vertical lines represent the error bars from the standard deviation between replicates.

Additionally, attempts to generate η^2-**1Ru^{IV}-OO** by the reaction of **1Ru^{II}-OH$_2$** with O_2 at 200 bar in either D_2O or acetone as solvents in a pressurized NMR tube,

did not yield η^2-**1Ru^{IV}-OO**. Neither did the reaction of hydrogen peroxide (H_2O_2) with **1**, discarding the formation of η^2-**1Ru^{IV}-OO** upon peroxide species formed during WO catalysis.

In order to get more insight of the formation of the η^2-**1Ru^{IV}-OO** intermediate DFT calculations were carried out at a uM11/cc-pVTZ//uM11/6-31G(d) (SDD basis set for Ru) level including the solvent effect of water or acetonitrile with the polarizable continuum model PCM-SMD in Gaussian.[34] We investigated the potential speciation in the presence of Ce^{IV}. Therefore, we have evaluated the pKa, reduction potential and proton-coupled electron transfer (PCET) processes for the different hydroperoxo/peroxo/superoxo Ru$^{III/IV}$ redox couples, respective transformations. It is worth to note that we have examined the relative energies of all possible spin multiplicities for the ruthenium species in oxidation states III and IV, to identify the ground spin state in each case. Starting from Ru(III)-hydroperoxo species (**1Ru^{III}-OOH**) the theoretical red-ox and proton-coupled electron transfer (PCET) processes have been studied to connect Ru(III)-hydroperoxo species (**1Ru^{III}-OOH**), Ru(III) end-on peroxo and superoxo species (η^1-**1Ru^{III}-OO** and η^1-**1Ru^{IV}-OO**) and Ru(IV) side-on peroxo species (η^2-**1Ru^{IV}-OO**), previously found as intermediates in the catalytic cycle of the WO reaction (chapter V).[21] Under catalytic conditions (pH 0.7, 25 ºC), **1Ru^{III}-OOH** can be oxidized to Ru(IV)-hydroperoxo species **1Ru^{IV}-OOH** ($E^{(III/IV)}_{theor}$ = 1.52 V vs SHE) via one electron transfer process (ET) or directly to Ru(III) end-on superoxo species (η^1-**1Ru^{IV}-OO**) via synchronous proton-coupled electron transfer process (PCET), which is more favorable ($PCET^{(III/IV)}_{theor}$ = 0.88 V vs SHE under catalytic conditions at pH 0.7 and 298 K). The latter intermediate is only 2.9 kcal·mol^{-1} higher in energy than the Ru(IV) side-on peroxo intermediate (η^2-**1Ru^{IV}-OO**) and rapidly rearranges to yield it. Alternatively, η^2-**1Ru^{IV}-OO** can be accessed by a PCET from **1Ru^{IV}-OOH** ($PCET^{(III/IV)}_{theor}$ = 0.15 V vs SHE under catalytic conditions at pH 0.7 and 298 K). Therefore, the formation of η^2-**1Ru^{IV}-OO** is accessible under catalytic conditions and thermodynamically feasible (Figure VI.30).
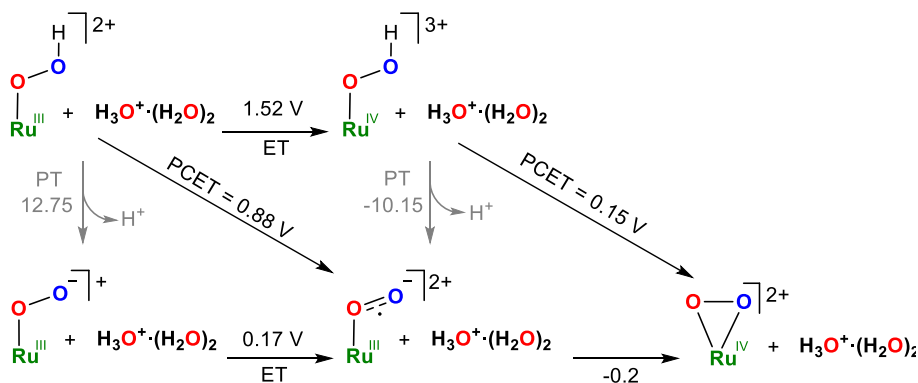
Figure VI.30. E^0, $E_{1/2(PCET)}$ and pK$_a$ values of the thermodynamic cycle involving L5Run/L5Run+1 transformations (pH 0.7 and 25 ºC) involved in the formation of the η^2-**1Ru^{IV}-OO** intermediate. Redox values correspond to the standard redox potentials relative to the SHE. Values in purple represent not possible steps.

In addition, the stability if the Ru(IV)-peroxo intermediate in either water or acetonitrile has been also studied at the same level of theory to try to rationalize the observed decay in solution with concomitant O_2 release. In this line, the high instability of η^2-**1Ru^{IV}-OO** in solution can be rationalized by the thermodynamically favorable reductive decoordination of the peroxo moiety from the metal center to yield $[Ru^{II}\text{-}OH_2]^{2+}$ or $[Ru^{II}\text{-}NCCH_3]^{2+}$ species, respectively, with concomitant O_2 release either in H_2O and MeCN (-0.44 and 22.9 Kcal·mol^{-1}, respectively, Figure A.IV.54).

VI.2.7. Full WO catalytic cycle

All the data support the formation of a closed shell η^2- $[Ru^{IV}(OO)(Py_2^{Me}tacn)](PF_6)_2$ complex under catalytic conditions after the WNA of a water molecule onto a Ru-oxo species, most likely the $[Ru^V(O)(Py_2^{Me}tacn)](PF_6)_3$, as evidenced by kinetic (chapter IV) and electrochemical studies. The labeling (CSI-HRMS) and spectroscopic studies (EPR, XAS, Raman) together with the observed reactivity of η^2-**1Ru^{IV}-OO** evidence its connection with the other previously *in situ* characterized and now isolated WO intermediates and with the catalytic cycle (Figure VI.31), as an intermediate formed after the rate-determining step in Ru catalyzed WO.
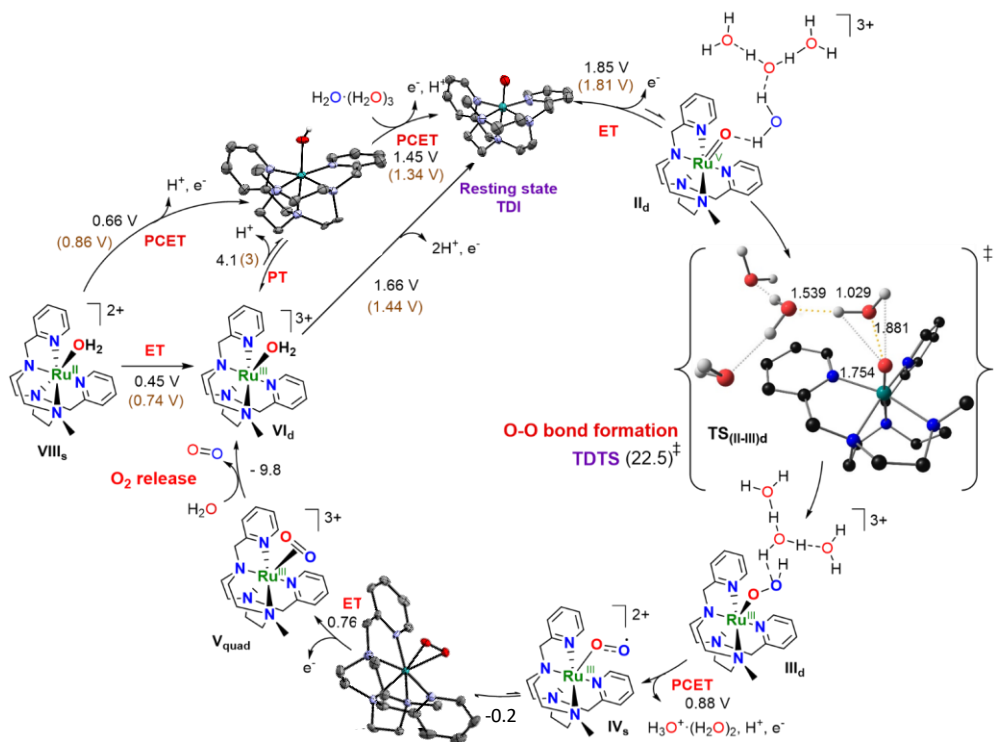
Figure VI.31. Summary of the computed WO catalytic cycle for complex **1Ru^{II}-OH$_2$** with experimental and theoretical redox values and X-ray structures when available. Values represent the redox potential for the ET, the PCET (at pH 0.7) or the pKa values for the PT [V] at 298 K. Subscripts indicate the spin multiplicity. Energies represent elementary steps and they are given in kcal·mol^{-1}. TDTS = TOF-determining transition state. TDI = TOF-determining intermediate.

VI.3. Conclusions

In this chapter, we have evidence of the O-O formation from a M=O species. We have crystallized and isolated a η^2-[Ru^{IV}(OO)(Py$_2^{Me}$tacn)](PF$_6$)$_2$ complex, one of the key intermediates generated after the rate-determining step in WO catalyzed by complex [Ru^{II}(OH$_2$)(Py$_2^{Me}$tacn)](PF$_6$)$_2$. All the solid-state and solution characterization techniques, as well as Raman and CSI-HRMS labeling experiments, point towards coordination of a peroxo moiety in a side-on manner forming an heptacoordinate Ru(IV)-peroxo complex (**η^2-1Ru^{IV}-OO**). In addition, we have provided here direct experimental evidence (NMR, EPR, X-ray and XANES) of the formation of a low-spin **η^2-1Ru^{IV}OO** intermediate, which is in good agreement with

the lowest in energy DFT optimized intermediate found after the O-O bond formation event. This highlights the fact that DFT calculations at the uM11/cc-pVTZ//uM11/6-31G(d) level of theory describe well the $Ru-O_2$ interaction. Overall, the isolation and characterization of such intermediate enable further understanding of the intermediates formed after the WNA in WO catalyzed by Ru and other metal complexes analogous to the previously reported $[Ru^{II}(OH_2)(Py_2Metacn)](PF_6)_2$ catalyst and sheds some light into the understanding of the O-O formation event.

VI.4. Experimental section

VI.4.1. General Procedures

Materials. Reagents were purchased from commercial sources and used as received without any further purification. Ceric ammonium nitrate (CAN; ≥99.99%) and trifluoromethanesulfonic acid (ReagentPlus grade ≥99%) were purchased from Sigma–Aldrich®. Solvents were purchased from SDS and Scharlab, purified and dried by passing through an activated alumina purification system (MBraun SPS-800) and stored in an anaerobic glovebox under N_2. Water (18.2 MWcm) was purified by using a Milli-Q Millipore Gradient AIS system.

Physical Methods. NMR spectra were recorded by using BrukerDPX300 and DPX400 spectrometers under standard conditions (298 K) unless otherwise indicated. All ^1H chemical shifts are reported in ppm and have been internally calibrated to the residual protons of the deuterated solvent. The ^{13}C chemical shifts have been internally calibrated to the carbon atoms of the deuterated solvent. The coupling constants were measured in Hz. ^1H-NMR experiments performed with the High-Pressure NMR tube under 200 bar of O_2 pressure were performed by purging and then charging the High-Pressure NMR tube in a high-pressure room with a O_2 pressurized system and then performing the NMR kinetic monitoring. For the Electron Paramagnetic Resonance (EPR) an EMX Micro X-band EPR spectrometer from Bruker was used to collect data on solid samples using a finger Dewar at 77 K. Data were acquired in perpendicular mode with a modulation frequency of 100 KHz,

modulation amplitude of 10 G, a Frequency of 9.404696 GHz and 33 dB microwave power attenuation. Spectra were simulated using the EasySpin software package.[43] UV/VIS/NIR spectra were recorded in 1 cm quartz cells by using an Agilent 8453 diode array spectrophotometer (λ =190–1100 nm range). A cryostat from Unisoku Scientific Instruments was used for temperature control. Elemental analyses were performed by using a CHNS-O EA-1108 elemental analyzer from Fisons. The pH of the solutions was determined by using a pHmeter (XS Instruments) that was calibrated by using standard solutions at pH 4.01, 7.00 and 10.00 before measurement. The amount of gas generated was measured by using a differential pressure transducer sensor (Honeywell-ASCX15DN, œ15 psi).[44] Each reaction had its own reference reaction, which was connected to the other port of the sensor. Further details of the equipment are available elsewhere.[44] Gases at the headspace were analyzed by using an Agilent 7820A GC System equipped with columns of washed molecular sieves (5A, 2m x 3mm OD, Mesh 60/80 SS) and Porapak Q (4 m x 3 mm OD, Mesh: 80/100 SS) and a thermal conductivity detector. The quantification of O_2 obtained was measured through the interpolation of a previous calibration by using known O_2/N_2 mixtures.

VI.4.2. Synthesis and characterization of the Ru intermediates

[Ru^{II}(OH$_2$)(Py$_2$^{Me}tacn)](PF$_6$)$_2$ was synthesized according to our previously published procedure.[21]

VI.4.2.1. Synthesis of [Ru^{III}(OH)(Py$_2$^{Me}tacn)](PF$_6$)$_2$ species: 1Ru^{III}-OH

[Ru^{II}(OH$_2$)(Py$_2$^{Me}tacn)](PF$_6$)$_2$[21] (25 mg, 0.03 mmol) were dissolved in 3.5 ml degassed MilliQ water (9.7 mM final concentration) under vigorously stirring until complete dissolution under argon atmosphere. Then, the addition of NaIO$_4$ (0.5 equiv., 25 μl of a solution of 145.23 mg in 1 ml degassed water) turned the initial green solution to pale green. Then, the compound was precipitated by the addition of 1.5 ml of an ammonium hexafluorophosphate saturated solution in degassed MilliQ water and cooling it down to 5 ºC. The compound was left stand for 15 min until

complete precipitation of a greenish solid (but the mother liquid was still having color). Then the solid was filtered cold through a cannula and washed with cold degassed MilliQ water and dried with diethyl ether. The solid was dried under vacuum for a couple of hours to achieve **1Ru^{III}-OH** as an intense green solid powder (15.7 mg, 63% yield). The solid was kept at -40 ºC in the freezer of the glovebox. ^{1}H-NMR (D$_2$O, 400 MHz, 300 K) δ: 13.49 (broad), 6.54 (broad), 3.44 – 3.11 (m), 2.88 - 2.81 (m), 2.37 (s), 1.57 (s), 1.20 (broad), -0.52 (broad), -1.06 (broad). CSI-HRMS: m/z calcd. for $[Ru^{III}(OH)(Py_2^{Me}tacn)](PF_6)^+$: 589.0979; found: 589.0951.

VI.4.2.2. Synthesis of $[Ru^{IV}(O)(Py_2^{Me}tacn)](PF_6)_2$ species: 1Ru^{IV}=O

$[Ru^{II}(H_2O)(Py_2^{Me}tacn)](PF_6)_2$[21] (25 mg, 0.03 mmol) was dissolved in 3.5 ml degassed MilliQ water (9.7 mM final concentration) under vigorously stirring until complete dissolution under argon atmosphere. Subsequent aliquots of NaIO$_4$ (0.2 equiv. each 10 μl addition of a solution of 145.23 mg in 1 ml degassed water) were added and the reaction was monitored by ^{1}H-NMR. A total of 1.5 equivalents of NaIO$_4$ were added to have the complete and clean formation of **1Ru^{IV}=O** after 20 minutes stirring at rt. Then, the compound was precipitated by the addition of 1.5 ml of an ammonium hexafluorophosphate saturated solution in degassed MilliQ water and cooling it down to 5 ºC. The compound was left standing for 15 min until complete precipitation of a yellow-greenish solid (but the mother liquid was still having color). Then the solid was filtered cold through a cannula and washed with cold degassed MilliQ water and dried with diethyl ether. The solid was dried under vacuum for a couple of hours to achieve **1Ru^{IV}=O** as a light greenish solid powder (18 mg, 72 % yield). The solid was kept at -40 ºC in the freezer of the glovebox. ^{1}H-NMR (D$_2$O, 400 MHz, 300 K) δ: 63.37 (s), 47.66 (broad), 22.47 (broad), 21.61 (broad), 20.33 (broad), 13.40 - 12.90 (m), 1.49 (broad), 1.34 (broad), -0.65 (broad), -5.99 (s), -7.96 (s), -11.70 (broad), -14.01 (s), -15.07 (broad), -34.85 (broad), -39.00 (broad), -45.16 (broad). CSI-HRMS: m/z calcd for $[Ru^{IV}(O)(Py_2^{Me}tacn)](PF_6)^+$: 588.0900; found: 588.0888.tu

UNIVERSITAT ROVIRA I VIRGILI
MECHANISTIC STUDIES OF WATER OXIDATION CATALYZED BY HOMOGENEOUS IRON AND RUTHENIUM
COMPLEXES AND LIGHT-DRIVEN ORGANIC REDUCTIONS WITH A DUAL COBALT/COPPER CATALYTIC SYSTEM
Carla Casadevall Serrano

CHAPTER VI   After the O-O in Ru Catalyzed WO: a Missing Link

VI.4.2.3. Synthesis of η^2-[Ru^{IV}(OO)(Py$_2^{Me}$tacn)](PF$_6$)$_2$: η^2-1Ru^{IV}-OO

a) Synthesis from the [Ru^{II}(H$_2$O)(Py$_2^{Me}$tacn)](PF$_6$)$_2$ (1Ru^{II}-OH$_2$) complex

[Ru^{II}(H$_2$O)(Py$_2^{Me}$tacn)](PF$_6$)$_2$[21] (100 mg, 0.136 mmol) were weighed in a 100 ml Schleck flask and dissolved in 50 ml degassed MilliQ water (2.7 mM final concentration) under vigorously stirring until complete dissolution under argon atmosphere. Then, the addition of NaIO$_4$ (0.5 equiv., 500 μl of a solution of 64.17 mg in 2 ml degassed water) turned the initial green solution to pale green (formation of **1Ru^{III}-OH**). Further addition of NaIO$_4$ (4 equiv., 4000 μl of a solution of 64.17 mg in 2 ml degassed water) changed the color to yellow. The reaction was monitored by ^{1}H-NMR, a total amount of 4.5 equiv. NaIO$_4$ were needed to have enough excess to generate the Ru-peroxo intermediate. The reaction was left stirring for 2 hours at rt. Then, addition of 1.5 ml of an ammonium hexafluorophosphate saturated solution in degassed MilliQ water yielded slow precipitation of the [η^2-1Ru^{IV}-OO]$^{2+}$ complex at 5 ºC (compound stored in the fridge) under a balloon of oxygen after 24-48 h (but the mother liquid was still having color). Then the solid was filtered cold through a cannula and washed with cold degassed MilliQ water. The solid was dried under air for a couple of hours to achieve [η^2-1Ru^{IV}-OO]$^{2+}$ as a yellowish solid powder (27 mg, 26 % yield). The solid was kept at -40 ºC in the freezer of the glovebox. ^{1}H NMR (D$_2$O, 400 MHz, 298 K) δ: 8.71 (d, J = 4 Hz, 1H), 7.80-7.73 (m, 3H), 7.51-7.50 (m, 2H), 7.41-7.39 (m, 1H), 7.20-7.14 (m, 1H), 4.25 (d, J = 13.2 Hz, 1H), 4.05-4.03 (m, 2H), 3.60-3.55 (m, 2H), 3.44-3.42 (m, 3H), 3.17-3.11 (m, 4H), 3.10 (s, 3H), 2.82-2.73 (m, 1H), 1.26-1.23 (m, 2H). CSI-HRMS: m/z calcd. for [Ru^{IV}(OO)(Py$_2^{Me}$tacn)](PF$_6$)$^+$: 604.0850; found: 604.0885.

The synthesis from complex **1Ru^{II}-OH$_2$** was also done in D$_2$O to favor the precipitation of intermediate [η^2-1Ru^{IV}-OO]$^{2+}$ as follows.

[Ru^{II}(H$_2$O)(Py$_2^{Me}$tacn)](PF$_6$)$_2$[21] (21.7 mg, 0.030 mmol) were weighed in a 20 ml crimped vial and dissolved in 14.7 ml of degassed D$_2$O (2 mM final concentration) under vigorously stirring until complete dissolution under argon atmosphere. Then,

the addition of NaIO$_4$ (0.5 equiv., 50 µl of a solution of 25 mg in 0.4 ml degassed D$_2$O) turned the initial green solution to pale green (formation of **1Ru^{III}-OD**). Further addition of NaIO$_4$ (4 equiv., 400 µl of a solution of 25 mg in 0.4 ml degassed D$_2$O) changed the color to yellow. The reaction was monitored by ^{1}H-NMR, a total amount of 4.5 equiv. NaIO$_4$ were needed to have enough excess to generate the Ru-peroxo intermediate. The reaction was left stirring for 2 hours at rt. Then, the addition of 1.5 ml of an ammonium hexafluorophosphate saturated solution in degassed MilliQ water yielded slow precipitation of the **[η^2-1Ru^{IV}-OO]$^{2+}$** complex at 5 ºC (compound stored in the fridge) under a balloon of oxygen after 24 h (but the mother liquid was still having color). Then the solid was filtered cold through a cannula and washed with cold degassed MilliQ water. The solid was dried under air for a couple of hours to achieve **[η^2-1Ru^{IV}-OO]$^{2+}$** as a yellowish solid powder (6 mg, 27 % yield). The solid was kept at -40 ºC in the freezer of the glovebox. ^{1}H NMR (D$_2$O, 400 MHz, 298 K) δ: 8.71 (d, J = 4 Hz, 1H), 7.80-7.73 (m, 3H), 7.51-7.50 (m, 2H), 7.41-7.39 (m, 1H), 7.20-7.14 (m, 1H), 4.25 (d, J = 13.2 Hz, 1H), 4.05-4.03 (m, 2H), 3.60-3.55 (m, 2H), 3.44-3.42 (m, 3H), 3.17-3.11 (m, 4H), 3.10 (s, 3H), 2.82-2.73 (m, 1H), 1.26-1.23 (m, 2H). CSI-HRMS: m/z calcd. for [Ru^{IV}(OO)(Py$_2$^{Me}tacn)](PF$_6$)$^+$: 604.0850; found: 604.0885.

b) Synthesis from the **[Ru^{III}(OH)(Py$_2$^{Me}tacn)](PF$_6$)$_2$** (**1Ru^{III}-OH**) intermediate. The synthesis was done in both D$_2$O and MilliQ water but D$_2$O favors the precipitation of the intermediate.

[Ru^{III}(OH)(Py$_2$^{Me}tacn)](PF$_6$)$_2$ (21.7 mg, 0.030 mmol) were weighed in a 20 ml crimped vial and dissolved in 14.7 ml of degassed D$_2$O (2 mM final concentration) under vigorously stirring until complete dissolution under argon atmosphere. Then, the addition of NaIO$_4$ (4 equiv., 400 µl of a solution of 25 mg in 0.4 ml degassed D$_2$O) changed the color to yellow. The reaction was monitored by ^{1}H-NMR, a total amount of 4 equiv. NaIO$_4$ were needed to have enough excess to generate the Ru-peroxo intermediate from **1Ru^{III}-OH**. The reaction was left stirring for 2 hours at rt. Then, the addition of 1.5 ml of an ammonium hexafluorophosphate saturated solution

in degassed MilliQ water yielded slow precipitation of the $[\eta^2\text{-}1Ru^{IV}\text{-}OO]^{2+}$ complex at 5 ºC (compound stored in the fridge) under a balloon of oxygen after 24 h (but the mother liquid was still having color). Then the solid was filtered cold through a cannula and washed with cold degassed MilliQ water. The solid was dried under air for a couple of hours to achieve $[\eta^2\text{-}1Ru^{IV}\text{-}OO]^{2+}$ as a yellowish solid powder (5 mg, 22 % yield). The solid was kept at -40 ºC in the freezer of the glovebox. ^{1}H NMR (D_2O, 400 MHz, 298 K) δ: 8.71 (d, J = 4 Hz, 1H), 7.80-7.73 (m, 3H), 7.51-7.50 (m, 2H), 7.41-7.39 (m, 1H), 7.20-7.14 (m, 1H), 4.25 (d, J = 13.2 Hz, 1H), 4.05-4.03 (m, 2H), 3.60-3.55 (m, 2H), 3.44-3.42 (m, 3H), 3.17-3.11 (m, 4H), 3.10 (s, 3H), 2.82-2.73 (m, 1H), 1.26-1.23 (m, 2H). CSI-HRMS: m/z calcd. for $[Ru^{IV}(OO)(Py_2{}^{Me}tacn)](PF_6)^+$: 604.0850; found: 604.0885.

c) Synthesis from the $[Ru^{IV}(O)(Py_2{}^{Me}tacn)](PF_6)_2$ ($1Ru^{IV}=O$) intermediate. The synthesis was done both in D_2O and MilliQ water but D_2O favors the precipitation of the intermediate.

$[Ru^{IV}(O)(Py_2{}^{Me}tacn)](PF_6)_2$ (21.7 mg, 0.030 mmol) were weighed in a 20 ml crimped vial and dissolved in 14.7 ml of degassed D_2O (2 mM final concentration) under vigorously stirring until complete dissolution under argon atmosphere. Then, the addition of $NaIO_4$ (3 equiv., 300 μl of a solution of 25 mg in 0.4 ml degassed D_2O) changed the color to yellow. The reaction was monitored by ^{1}H-NMR, a total amount of 3 equiv. $NaIO_4$ were needed to have enough excess to generate the Ru-peroxo intermediate. The reaction was left stirring for 2 hours at rt Then, addition of 1.5 ml of an ammonium hexafluorophosphate saturated solution in degassed MilliQ water yielded slow precipitation of the $[\eta^2\text{-}1Ru^{IV}\text{-}OO]^{2+}$ complex at 5 ºC (compound stored in the fridge) under a balloon of oxygen after 24 h (but the mother liquid was still having color). Then the solid was filtered cold through a cannula and washed with cold degassed MilliQ water. The solid was dried under air for a couple of hours to achieve $[\eta^2\text{-}1Ru^{IV}\text{-}OO]^{2+}$ as a yellowish solid powder (5 mg, 22 % yield). The solid was kept at -40 ºC in the freezer of the glovebox. ^{1}H NMR (D_2O, 400 MHz, 298 K) δ: 8.71 (d, J = 4 Hz, 1H), 7.80-7.73 (m, 3H), 7.51-7.50 (m, 2H), 7.41-7.39 (m,

UNIVERSITAT ROVIRA I VIRGILI
MECHANISTIC STUDIES OF WATER OXIDATION CATALYZED BY HOMOGENEOUS IRON AND RUTHENIUM
COMPLEXES AND LIGHT-DRIVEN ORGANIC REDUCTIONS WITH A DUAL COBALT/COPPER CATALYTIC SYSTEM
Carla Casadevall Serrano

CHAPTER VI   After the O-O in Ru Catalyzed WO: a Missing Link

1H), 7.20-7.14 (m, 1H), 4.25 (d, J = 13.2 Hz, 1H), 4.05-4.03 (m, 2H), 3.60-3.55 (m, 2H), 3.44-3.42 (m, 3H), 3.17-3.11 (m, 4H), 3.10 (s, 3H), 2.82-2.73 (m, 1H), 1.26-1.23 (m, 2H). CSI-HRMS: m/z calcd for $[Ru^{IV}(OO)(Py_2^{Me}tacn)](PF_6)^+$: 604.0850; found: 604.0885.

VI.4.3. Single-Crystal X-Ray Structure Determination

Crystal preparation: Crystals of $[Ru^{IV}(O)(Py_2^{Me}tacn)](PF_6)_2$, $[Ru^{IV}(OO)(Py_2^{Me}tacn)](PF_6)_2$ and $[Ru^{IV}(OO)(Py_2^{Me}tacn)](PF_6)_{1.5}(IO_3)_{0.5}$ were grown by slow evaporation of water solvent from an NMR-type tube containing a 2mM solution of each of the intermediates generated by addition of 0.5, 1.5 and 4.5 equivalents of $NaIO_4$, to $[Ru^{II}(H_2O)(Py_2^{Me}tacn)](PF_6)_2$ in D_2O respectively, after the addition of 0.5 ml of a saturated ammonium hexafluorophosphate solution in water and left standing at 5º (fridge temperature). The crystals for this samples were selected using a Zeiss stereomicroscope using polarized light and prepared under inert conditions immersed in perfluoropolyether as protecting oil for manipulation.

Data collection: Crystal structure determinations for samples $[Ru^{IV}(O)(Py_2^{Me}tacn)](PF_6)_2$, $[Ru^{IV}(OO)(Py_2^{Me}tacn)](PF_6)_2$ and $[Ru^{IV}(OO)(Py_2^{Me}tacn)](PF_6)_{1.5}(IO_3)_{0.5}$ were carried out using a Apex DUO Kappa 4-axis goniometer equipped with an APPEX 2 4K CCD area detector, a Microfocus Source E025 IuS using MoK_α radiation, Quazar MX multilayer Optics as monochromator and an Oxford Cryosystems low-temperature device Cryostream 700 plus (T = -173 °C). *Programs used:* Bruker Device: Data collection APEX-2,[45] data reduction Bruker Saint V/.60A[46] and absorption correction SADABS[47] or TWINABS.[47] In case of $[Ru^{IV}(OO)(Py_2^{Me}tacn)](PF_6)_{1.5}(IO_3)_{0.5}$ absorption correction with Scale3 Abspack scaling algorithm.[48]

Structure Solution and Refinement: Crystal structure solution was achieved using the computer program SHELXT.[49] Visualization was performed with the program SHELXle.[50] Missing atoms were subsequently located from difference Fourier synthesis and added to the atom list. Least-squares refinement on F^2 using all

UNIVERSITAT ROVIRA I VIRGILI
MECHANISTIC STUDIES OF WATER OXIDATION CATALYZED BY HOMOGENEOUS IRON AND RUTHENIUM
COMPLEXES AND LIGHT-DRIVEN ORGANIC REDUCTIONS WITH A DUAL COBALT/COPPER CATALYTIC SYSTEM
Carla Casadevall Serrano

CHAPTER VI   After the O-O in Ru Catalyzed WO: a Missing Link

measured intensities was carried out using the program SHELXL 2015.[51] All non-hydrogen atoms were refined including anisotropic displacement parameters.

Comments to the structures: Sample **[Ru^{IV}(OO)(Py$_2$^{Me}tacn)](PF$_6$)$_{1.5}$(IO$_3$)$_{0.5}$**: The asymmetric unit contains one molecule of the metal complex, one and a half PF$_6$ anions and half IO$_3$ anion. The half PF$_6$ anion and the half IO$_3$ anion are disordered sharing the same position. In total, the disordered PF$_6$ and IO$_3$ anions are oriented each in two directions. The occupancy is: 0.25(PF$_6$):0.25(PF$_6$):0.30(IO$_3$):0.20(IO$_3$). Sample **[Ru^{IV}(OO)(Py$_2$^{Me}tacn)](PF$_6$)$_2$**: The asymmetric unit contains one molecule of the metal complex and two PF$_6$ anions. One of the PF$_6$ anions is disordered in two orientations (ratio 55:45). Sample **[Ru^{IV}(O)(Py$_2$^{Me}tacn)](PF$_6$)$_2$**: The asymmetric unit contains one molecule of the metal complex and two PF$_6$ anions. The two PF$_6$ anions are disordered in two orientations (ratios: 60:40 and 70:30). All measured samples of this compound where multi-component crystals showing high mosaicity and a weak diffraction power. The measured sample is formed by a minimum of two crystals with a ratio of 79:21. The collected data were processed with TWINABS taking into account overlapping reflections.[47] The CHECKCIF shows a B-alert which was properly commented.

VI.4.4. X-ray Absorption Spectroscopy (XAS)

XAS studies were performed together with Dr. Vlad Martin-Diaconescu from our group and in collaboration with Dr. Benedikt Lassalle-Kaiser, local contact from the SOLEIL synchrotron were we went to perform the measurements. Dr. Vlad Martin-Diaconescu fitted and analyzed all the data. Ruthenium L-edge data was collected at the SAMBA LUCIA beamline under vacuum at 80 K using a Si(111) double crystal monochromator. Data was collected in fluorescence mode at the L$_{\alpha1}$ emission line. Samples were run as solids diluted in boron nitride to minimize self-absorption effects. The data was background corrected using a linear function for the pre-edge region 10 eV below the Ru L$_3$-edge (2838 eV) and the post-edge region was "flattened" using the difference in slope and quadrature of a linear post-edge function

UNIVERSITAT ROVIRA I VIRGILI
MECHANISTIC STUDIES OF WATER OXIDATION CATALYZED BY HOMOGENEOUS IRON AND RUTHENIUM
COMPLEXES AND LIGHT-DRIVEN ORGANIC REDUCTIONS WITH A DUAL COBALT/COPPER CATALYTIC SYSTEM
Carla Casadevall Serrano

CHAPTER VI   After the O-O in Ru Catalyzed WO: a Missing Link

10 eV above the Ru L$_3$-edge.[52] Furthermore, the data was energy calibrated to the Ru L$_3$-edge maximum of Ru(bpy)$_3$Cl$_2$ taken as 2840.5 eV.[36] Spectra were fit using pseudo-voigt peak functions for the absorption features and a cumulative Lorentzian-Gaussian for the edge jump. Where necessary contributions from chloride reagents used in sample preparation were accounted for as previously described (see Annex IV section XX for further details).[53] The Ru L$_3$-edge data was then normalized by setting the edge-jump to unity. Lastly, the experimental spectra were correlated with theoretically calculated spectra following previously published procedures.[37,54] XAS spectra were calculated with the ORCA software package,[55] using previously reported geometry optimized structures,[21] using a TD-DFT method employing the Tamm-Dancoff approximation[56,57] and a B3LYP functional with a def2-TZVP basis set together with a def2-TZVP/J auxiliary basis set on all atoms,[58,59] as well as the ZORA relativistic approximation.[60,61]

VI.4.5. Raman measurements

Raman measurements were performed in collaboration with Prof. Dr. W. R. Browne at the Stratingh Institute for Chemistry at the University of Groningen. Raman spectra of the isolated solid intermediates were recorded at λ$_{exc}$ 632.8 nm (12 mW at source, Thorlabs) using a Olympus BX-51 upright microscope coupled to a Shamrock 163 spectrograph and Andor idus-420 CCD camera via an optical fiber. Raman spectra in solution were recorded at 355 nm (10 mW Cobolt Lasers) and 457 nm (50 mW, Cobolt Lasers) delivered to the sample through a 2.5 cm diameter planoconvex lens (f = 7.5 cm) and Raman scattering collected in a 180º backscattering arrangement. Raman scattering was filtered by a long pass filter (Semrock) and coupled to the spectrograph (Andor Shamrock 500 and 300 respectively) with a 2.5 cm diameter planoconvex lens (f = 10 and 7.5 cm, respectively) with a 1200 L/mm grating blazed at 500 nm, or 2400 L/mm blazed at 400 nm and acquired with an DV420A-BU2 or BU CCD camera (Andor Technology). The spectral slit width was set to 12 and 80 μm, respectively. Each spectrum was accumulated, typically 60 or 120 times with 5 s acquisition time,

UNIVERSITAT ROVIRA I VIRGILI
MECHANISTIC STUDIES OF WATER OXIDATION CATALYZED BY HOMOGENEOUS IRON AND RUTHENIUM
COMPLEXES AND LIGHT-DRIVEN ORGANIC REDUCTIONS WITH A DUAL COBALT/COPPER CATALYTIC SYSTEM
Carla Casadevall Serrano

CHAPTER VI   After the O-O in Ru Catalyzed WO: a Missing Link

resulting in a total acquisition time of between 5 to 10 min per spectrum. Data were recorded and processed using Solis (Andor Technology) with spectral calibration performed using the Raman spectrum of polystyrene for solid samples, and acetonitrile/toluene mixtures for studies in solution (that is H_2O, D_2O or $H_2^{18}O$, as indicated). For solution experiments, samples were held in 10 mm path length quartz cuvettes. The UV/Vis absorption spectra were recorded before and after each Raman measurement to verify the species formed during the reaction. Baseline correction was performed for all spectra. In addition, in the case of the monitoring of the generation of intermediates **$1Ru^{II}-OH_2$**, **$1Ru^{III}-OH$**, **$1Ru^{IV}=O$** and **η^2-$1Ru^{IV}-OO$** in solution by Raman spectroscopy, the excess of oxidant and the remaining traces of the previous intermediate (for the monitoring of the formation of **η^2-$1Ru^{IV}-OO$** from a net formation of **$1Ru^{IV}=O$**) were also subtracted when necessary. The concentrations used for solution Raman studies were 2 mM for all samples in water (H_2O, D_2O or $H_2^{18}O$), as indicated.

VI.4.6. High-Resolution Mass Spectrometry (HRMS)

All mass spectra were recorded on a MicroTOF Focus II (Bruker Daltonics) instrument with a Coldspray ionization source (CSI, Bruker Daltonics) at the Research Support Area of ICIQ. Samples were introduced into the mass spectrometer ion source by direct injection using a syringe pump (550 µl/h flow rate)[1] and were externally calibrated using a solution of proline and NaCl (adducts with sodium). The instrument was operated in the positive ion mode (m/z range: 50-3500, capillary: 4000v, end plate offset: -500v). The characterization of the WO intermediates by HRMS was done at 20 ℃ (Dry temperature 9 ℃ (+/- 1℃), sprayer temperature: 20 ℃ (+/- 0.2 ℃), the flow of nitrogen (dry): 0.4; (sprayer): 2.

CSI-HRMS characterization of the Ru intermediates. The mass spectrum of complex $[Ru^{II}(H_2O)(Py_2^{Me}tacn)](PF_6)_2$ (**$1Ru^{II}-OH_2$**) was

previously reported in chapter IV.[21] The isolated intermediates $[Ru^{III}(OH)(Py_2^{Me}tacn)](PF_6)_2$ (**1Ru^{III}-OH**) and $[Ru^{IV}(O)(Py_2^{Me}tacn)](PF_6)_2$ (**1Ru^{IV}=O**) were directly injected as dissolved in water (2 mM final concentration).

CSI-HRMS labeling studies of the formation of $^2\eta$-1Ru^{IV}-OO from 1Ru^{IV}=O in Milli-Q H$_2$O, D$_2$O and H$_2^{18}$O and from 1Ru^{IV}=^{18}O in H$_2^{18}$O, respectively. From a solution of **1Ru^{IV}=O** (2 mM) in water (250 µl of MilliQ, D$_2$O or H$_2^{18}$O, depending on the experiment) under N$_2$ an aliquot was firstly analyzed. Then oxidant was added (5 eq. of NaIO$_4$ or 5 eq. Ce(OTf)$_4$) to form the η^2-**1Ru^{IV}-OO** species (with the corresponding labeling regarding each experiment). After 30 minutes of the addition, the reaction mixture was injected to the mass spectrometer for analysis. For these studies, 5 equivalents of sacrificial oxidant were used to accelerate the formation of the Ru(IV)-peroxo species.

Kinetic studies of the η^2-1Ru^{IV}-OO generation monitored by CSI-HRMS. From a solution of **1Ru^{II}-OH$_2$** or **1Ru^{IV}=O** (2 mM) in water (250 µl of MilliQ, D$_2$O or H$_2^{18}$O, depending on the experiment) under N$_2$ an aliquot was firstly analyzed. Then the sample was titrated with NaIO$_4$ (5 eq.) to form the η^2-**1Ru^{IV}-OO** species. After each addition, an aliquot of the reaction mixture (7.5 µl) was diluted (1/10 dilution) and directly injected to the mass spectrometer for analysis. For this studies, 5 equivalents of sacrificial oxidant were used to accelerate the formation of the Ru(IV)-peroxo species.

VI.4.7. Electrochemical Studies

All electrochemical experiments were performed by using a Biologic VSP potentiostat and a three-electrode-cell configuration. A glassy carbon disk (diameter 3 mm, area 0.07 cm2) was used as the working electrode, a Pt wire as the counter electrode and Hg/Hg$_2$SO$_4$ (saturated K$_2$SO$_4$) as the reference electrode (potentials

were converted to NHE by adding 0.65 V). Cyclic voltammograms and differential pulse voltammograms were internal resistance compensated by the potentiostat in all the measurements. Glassy carbon electrodes were polished with 0.05 mm alumina (Al_2O_3) and washed water before each measurement.

VI.4.8. Computational Studies

All the geometries were optimized using Density Functional Theory (DFT) at the uM11[21] level in conjunction with the SDD basis set for the Ru[28,62] and 6-31G(d) basis set[63] for the rest of the atoms, including the effect of water solvent with polarizable continuum model PCM-SMD[64-66] of Truhlar and co-workers as implemented in the Gaussian 09d01 software.[34] Stationary points were verified by frequency analysis (see section S.I.7. Cartesian coordinates of the optimized structures).

In other previous studies, it was found that taking into account solvent effects in the optimization was essential to reproduce the experimental data.[21,67,68] The energies were further refined by single-point calculations with the cc-pVTZ dunning basis set for all atoms (E_{cc_pVTZ}). All calculations employed the spin-unrestricted formalism and spin-contaminated energies were systematically corrected by using the following equations (VI.1) and (VI.2):

$$E_{spin\,corr} = \frac{E_{cc-pVTZ} - a \cdot E_{cc-pVTZ/(S+1)}}{1-a} \tag{VI.1}$$

$$a = \frac{\langle S^2 \rangle - S \cdot (S+1)}{\langle S_{(S+1)}^2 \rangle - S \cdot (S+1)} \tag{VI.2}$$

in which $E_{spin\,corr}$ is the spin corrected electronic energy, $E_{cc-pVTZ}$ and $\langle S^2 \rangle$ are the cc-pVTZ electronic energy and square total spin angular momentum, respectively, obtained from the structure optimized at the uM11/6-31G(d) level; and $E_{cc-pVTZ/(S+1)}$ and $\langle S_{(S+1)}^2 \rangle$ are the energy and square total spin

angular momentum of the afterward unpaired spin state (S+1), respectively, computed at the same level of theory and geometry.[69]

Gibbs energy corrections at 298.15 K were obtained from gas phase frequency calculations at uM11/6-31G(d) level (G_{corr}). The solvent effects were computed at the same level by performing gas phase and solvent phase calculations and taking the difference of the resulting energies (G_{solv}).[70,71] All calculated solvation free-energies use a standard state of an ideal gas at a gas-phase concentration of 1 mol·L⁻¹ dissolving as an ideal dilute solution at a liquid-phase concentration of 1M, but for water itself a 55.6M standard state was employed. Thus, as it has been indicated by Cramer et al.,[72] we calculated the free-energy change associated with moving from a standard-state gas-phase pressure of 1 atm to a standard-state gas-phase concentration of 1M (55.6M for water), $\Delta G^{o/*}$. The value of $\Delta G^{o/*}$ at 298 K is 1.9 kcal·mol⁻¹ for 1M standard state solute and 4.3 kcal·mol⁻¹ for 55.6M standard state water. The total Gibbs free energy (G) was obtained by adding the previous corrections to the spin-corrected electronic energy $E_{spin\ corr}$ (equation VI.3):

$$G = E_{spin\ corr} + G_{corr} + G_{solv} + \Delta G^{o/*} \qquad (VI.3)$$

All energies given in this work are referred to Gibbs energies G unless otherwise noted. Since the lowest-energy spin state for transition-metal complexes is not obvious, all spin-states for each species were calculated and the respective geometries were optimized. The nature of the stationary points was established by frequency calculations in the solvent-phase, in which minima have no imaginary frequencies and transition states have one and only one. Finally, the connectivity of all transition states was confirmed by relaxing the transition state geometries towards both the reactants and the products through intrinsic reaction coordinate (IRC) calculations.

Standard reduction potentials, relative to the standard hydrogen electrode (SHE), were calculated by (equation VI.4):

$$E^o = -\frac{\Delta G^o - \Delta G^o_{SHE}}{nF} \qquad (4)$$

where ΔG^o is the free energy change associated with reduction at standard conditions, n is the number of electrons involved in the redox reaction, F is the Faraday constant and ΔG^o_{NHE} is the free energy change associated with the reduction of a proton (-4.28 eV).[73] Some oxidation events are characterized by proton-coupled electron transfer (PCET), where electron transfer and proton transfer to the solvent occur simultaneously. Thus, we must include in ΔG^o the standard free energy of a proton in solution (equation VI.5):

$$G^{H+}_{aq} = G^{H+}_{gas} + G^{H+}_{solv} \qquad (VI.5)$$

where the free energy of solvation of a proton (G^{H+}_{solv}) was taken as –265.9 kcal·mol^{-1},[73] and the gas-phase Gibbs free energy of a proton (G^{H+}_{gas}) is -6.3 kcal·mol^{-1}. The aqueous pK_a associated to the general reaction: ($XH_{aq} \rightarrow X^-_{aq} + H^+_{aq}$) were computed according to (equation VI.6):

$$pK_a = \frac{\Delta G^*}{RT \ln(10)} \qquad (VI.6)$$

where T is the temperature and R is the universal gas constant.[73][38] ΔG^* is expressed in terms of the standard free energies of the acid XH and its conjugate base X$^-$ (equation VI.7):

$$\Delta G^* = G^o(X^-) + G^{H+}_{aq} - G^o(XH) + \Delta G^{\frac{o}{*}} \qquad (VI.7)$$

VI.5. References

(1) Pantazis, D. A. *ACS Catal.* **2018**, *8*, 9477.
(2) Krewald, V.; Neese, F.; Pantazis, D. A. *Isr. J. Chem.* **2015**, *55*, 1219.
(3) Cox, N.; Pantazis, D. A.; Neese, F.; Lubitz, W. *Acc. Chem. Res.* **2013**, *46*, 1588.
(4) Lewis, N. S. *Science* **2016**, *351*.
(5) Lewis, N. S.; Nocera, D. G. *Proc. Natl. Acad. Sci. U.S.A.* **2006**, *103*, 15729.
(6) Blakemore, J. D.; Crabtree, R. H.; Brudvig, G. W. *Chem. Rev.* **2015**, *115*, 12974.

(7) Codola, Z.; Lloret-Fillol, J.; Costas, M. In *Prog. Inorg. Chem.*; John Wiley & Sons, Inc.: 2014; Vol. 59, p 447.

(8) Shaffer, D. W.; Xie, Y.; Concepcion, J. J. *Chem. Soc. Rev.* **2017**, *46*, 6170.

(9) Karkas, M. D.; Akermark, B. *Dalton. Trans.* **2016**, *45*, 14421.

(10) Das, B.; Lee, B.-L.; Karlsson, E. A.; Akermark, T.; Shatskiy, A.; Demeshko, S.; Liao, R.-Z.; Laine, T. M.; Haukka, M.; Zeglio, E.; Abdel-Magied, A. F.; Siegbahn, P. E. M.; Meyer, F.; Karkas, M. D.; Johnston, E. V.; Nordlander, E.; Akermark, B. *Dalton. Trans.* **2016**, *45*, 13289.

(11) Liu, T.; Zhang, B.; Sun, L. *Chem.—Asian J.* **2019**, *14*, 31.

(12) Karkas, M. D.; Verho, O.; Johnston, E. V.; Akermark, B. *Chem. Rev.* **2014**, *114*, 11863.

(13) Fukuzumi, S.; Hong, D. C. *Eur. J. Inorg. Chem.* **2014**, 645.

(14) Codolà, Z.; Gamba, I.; Acuña-Parés, F.; Casadevall, C.; Clémancey, M.; Latour, J.-M.; Luis, J. M.; Lloret-Fillol, J.; Costas, M. *J. Am. Chem. Soc.* **2019**, *141*, 323.

(15) Casadevall, C.; Bucci, A.; Costas, M.; Lloret-Fillol, J. In *Adv. Inorg. Chem.*; Academic Press: 2019.

(16) Zeng, Q.; Lewis, F. W.; Harwood, L. M.; Hartl, F. *Coord. Chem. Rev.* **2015**, *304-305*, 88.

(17) Wasylenko, D. J.; Palmer, R. D.; Berlinguette, C. P. *Chem. Commun.* **2013**, *49*, 218.

(18) Concepcion, J. J.; Jurss, J. W.; Brennaman, M. K.; Hoertz, P. G.; Patrocinio, A. O. T.; Murakami Iha, N. Y.; Templeton, J. L.; Meyer, T. J. *Acc. Chem. Res.* **2009**, *42*, 1954.

(19) Jurss, J. W.; Concepcion, J. J.; Norris, M. R.; Templeton, J. L.; Meyer, T. J. *Inorg. Chem.* **2010**, *49*, 3980.

(20) Kaveevivitchai, N.; Zong, R.; Tseng, H. W.; Chitta, R.; Thummel, R. P. *Inorg. Chem.* **2012**, *51*, 2930.

(21) Casadevall, C.; Codolà, Z.; Costas, M.; Lloret-Fillol, J. *Chem. Eur. J.* **2016**, *22*, 10111.

(22) Duffy, E. M.; Marsh, B. M.; Voss, J. M.; Garand, E. *Angew. Chem. Int. Ed.* **2016**, *55*, 4079.

(23) Concepcion, J. J.; Tsai, M. K.; Muckerman, J. T.; Meyer, T. J. *J. Am. Chem. Soc.* **2010**, *132*, 1545.

(24) Wasylenko, D. J.; Ganesamoorthy, C.; Henderson, M. A.; Koivisto, B. D.; Osthoff, H. D.; Berlinguette, C. P. *J. Am. Chem. Soc.* **2010**, *132*, 16094.

(25) Moonshiram, D.; Jurss, J. W.; Concepcion, J. J.; Zakharova, T.; Alperovich, I.; Meyer, T. J.; Pushkar, Y. *J. Am. Chem. Soc.* **2012**, *134*, 4625.

(26) Wang, Y.; Ahlquist, M. S. G. *Dalton. Trans.* **2014**, *43*, 13776.

(27) L. Wang, Q. W., T. V. Voorhis *Inorg. Chem.* **2010**, *49*, 4543

(28) Runhua Kang, J. Y., and Hui Chen *J. Chem. Theory Comput.* **2013**, *9*, 1872−1879.

(29) Navarro Clemente, M. E.; Juárez Saavedra, P.; Cervantes Vásquez, M.; Paz-Sandoval, M. A.; Arif, A. M.; Ernst, R. D. *Organometallics* **2002**, *21*, 592.

(30) Jia, G.; Ng, W. S.; Chu, H. S.; Wong, W.-T.; Yu, N.-T.; Williams, I. D. *Organometallics* **1999**, *18*, 3597.

(31) Lindner, E.; Haustein, M.; Fawzi, R.; Steimann, M.; Wegner, P. *Organometallics* **1994**, *13*, 5021.

(32) Shen, J.; Stevens, E. D.; Nolan, S. P. *Organometallics* **1998**, *17*, 3875.

(33) Polyansky, D. E.; Muckerman, J. T.; Rochford, J.; Zong, R.; Thummel, R. P.; Fujita, E. *J. Am. Chem. Soc.* **2011**, *133*, 14649.

(34) Gaussian 09, R. A., M. J. Frisch, G. W. Trucks, H. B. Schlegel, G. E. Scuseria, M. A. Robb, J. R. Cheeseman, G. Scalmani, V. Barone, B. Mennucci, G. A. Petersson, H. Nakatsuji, M. Caricato, X. Li, H. P. Hratchian, A. F. Izmaylov, J. Bloino, G. Zheng, J. L. Sonnenberg, M. Hada, M. Ehara, K. Toyota, R. Fukuda, J. Hasegawa, M. Ishida, T. Nakajima, Y. Honda, O. Kitao, H. Nakai, T. Vreven, J. A. Montgomery, Jr., J. E. Peralta, F. Ogliaro, M. Bearpark, J. J. Heyd, E. Brothers, K. N. Kudin, V. N. Staroverov, R. Kobayashi, J. Normand, K. Raghavachari, A. Rendell, J. C. Burant, S. S. Iyengar, J. Tomasi, M. Cossi, N. Rega, J. M. Millam, M. Klene, J. E. Knox, J. B. Cross, V. Bakken, C. Adamo, J. Jaramillo, R. Gomperts, R. E. Stratmann, O. Yazyev, A. J. Austin, R. Cammi, C. Pomelli, J. W. Ochterski, R. L. Martin, K. Morokuma, V. G. Zakrzewski, G. A. Voth, P. Salvador, J. J. Dannenberg, S. Dapprich, A. D. Daniels, Ö. Farkas, J. B. Foresman, J. V. Ortiz, J. Cioslowski, and D. J. Fox, Gaussian, Inc., Wallingford CT. **2009**.

(35) Hocking, R. K.; DeBeer George, S.; Raymond, K. N.; Hodgson, K. O.; Hedman, B.; Solomon, E. I. *J. Am. Chem. Soc.* **2010**, *132*, 4006.

(36) Gawelda, W.; Johnson, M.; de Groot, F. M. F.; Abela, R.; Bressler, C.; Chergui, M. *J. Am. Chem. Soc.* **2006**, *128*, 5001.

(37) Van Kuiken, B. E.; Valiev, M.; Daifuku, S. L.; Bannan, C.; Strader, M. L.; Cho, H.; Huse, N.; Schoenlein, R. W.; Govind, N.; Khalil, M. *J Phys Chem A* **2013**, *117*, 4444.

(38) Kim, J.-Y.; Hwang, S.-H.; Kim, S.-J.; Demazeau, G.; Choy, J.-H.; Shimada, H. *Journal of Synchrotron Radiation* **2001**, *8*, 722.

(39) Cho, J.; Sarangi, R.; Nam, W. *Acc. Chem. Res.* **2012**, *45*, 1321.

(40) Holland, P. L. *Dalton. Trans.* **2010**, *39*, 5415.

(41) Cramer, C. J.; Tolman, W. B.; Theopold, K. H.; Rheingold, A. L. *Proc. Natl. Acad. Sci.* **2003**, *100*, 3635.

(42) Planas, N.; Vigara, L.; Cady, C.; Miró, P.; Huang, P.; Hammarström, L.; Styring, S.; Leidel, N.; Dau, H.; Haumann, M.; Gagliardi, L.; Cramer, C. J.; Llobet, A. *Inorg. Chem.* **2011**, *50*, 11134.

(43) Stoll, S.; Schweiger, A. *J. Magn. Reson.* **2006**, *178*, 42.

(44) Fillol, J. L.; Codolà, Z.; Garcia-Bosch, I.; Gómez, L.; Pla, J. J.; Costas, M. *Nat. Chem.* **2011**, *3*, 807.

(45) v2013.4-1, D. c. w. A. I. v. *Bruker AXS Inc., Madison, Wisconsin, USA.* **2007**.

(46) Bruker *Data reduction with Bruker SAINT version V8.30c.* **2007**, *Bruker AXS INc., Madison, Wisconsin, USA.*

(47) V2012/1, S. *Bruker* **2001**, *Bruker AXS Inc., Madison, Wisconsin, USA. Blessing, Acta Cryst. (1995) A51 33-38.*

(48) OD), C. R.; 1.171.38.37f, Ed. 2015.

(49) Sheldrick, G. *Acta Crystallogr. Sect. A* **2015**, *71*, 3.

(50) Hubschle, C. B.; Sheldrick, G. M.; Dittrich, B. *J. Appl. Crystallogr.* **2011**, *44*, 1281.

(51) Sheldrick, G. *Acta Crystallogr. Sect. C* **2015**, *71*, 3.

(52) Ravel, B.; Newville, M. *J. Synchrotron Rad.* **2005**, *12*, 537.

(53) Delgado-Jaime, M. U.; Conrad, J. C.; Fogg, D. E.; Kennepohl, P. *Inorg. Chim. Acta* **2006**, *359*, 3042.

(54) Bjornsson, R.; Delgado-Jaime, M. U.; Lima, F. A.; Sippel, D.; Schlesier, J.; Weyhermüller, T.; Einsle, O.; Neese, F.; DeBeer, S. *Z. Anorg. Allg. Chem.* **2015**, *641*, 65.

(55) Neese, F. *Wiley Interdiscip. Rev.: Comput. Mol. Sci.* **2012**, *2*, 73.

(56) DeBeer George, S.; Petrenko, T.; Neese, F. *Inorg. Chim. Acta* **2008**, *361*, 965.

(57) DeBeer George, S.; Petrenko, T.; Neese, F. *J Phys Chem A* **2008**, *112*, 12936.

(58) Schäfer, A.; Horn, H.; Ahlrichs, R. *J Chem Phys* **1992**, *97*, 2571.

(59) Weigend, F.; Ahlrichs, R. *Phys. Chem. Chem. Phys.* **2005**, *7*, 3297.

(60) van Wüllen, C. *J Chem Phys* **1998**, *109*, 392.

(61) Pantazis, D. A.; Chen, X.-Y.; Landis, C. R.; Neese, F. *J. Chem. Theor. Comp.* **2008**, *4*, 908.

(62) Aleksandr V. Marenich, A. M., Michelle Lenz, Christopher J. Cramer, and Donald G. Truhlar *Angew. Chem. Int. Ed.* **2012**, *51*, 12810

(63) M. Dolg, U. W., H. Stoll, H. Preuss *J. Chem. Phys.* **1987**, *86*, 866

(64) P. C. Hariharan , J. A. P. *Theoret. Chimica Acta* **1973**, *28*, 213.

(65) W. J. Hehre, R. D., J. A. Pople *J. Chem. Phys.* **1972**, *56*, 2257.

(66) M. Suensson, S. H., R. D. J. Froese, T. Matsubara, S. Sieber, K. Morokuma *J. Phys. Chem.* **1996**, *100*, 19357.

(67) Acuna-Pares, F.; Codola, Z.; Costas, M.; Luis, J. M.; Lloret-Fillol, J. *Chem. Eur. J.* **2014**, *20*, 5696.

(68) Codolà, Z.; Garcia-Bosch, I.; Acuña-Parés, F.; Prat, I.; Luis, J. M.; Costas, M.; Lloret-Fillol, J. *Chem. Eur. J.* **2013**, *19*, 8042.

(69) M. Swart, M. G., J. M. Luis, M. Solà *J. Phys. Chem. A* **2010**, *114*, 7191.

(70) M. Z. Ertem, L. G., C. J. Cramer *Chem. Sci.* **2012**, *3*, 1293

(71) L. Vigara, M. Z. E., N. Planas, F. Bozoglian, N. Leidel, H. Dau, M. Haumann, L. Gagliardi, C. J. Cramer, A. Llobet, *Chem. Sci.* **2012**, *3*, 2576

(72) C. P. Kelly, C. J. C., D. G. Truhlar, *J. Phys. Chem. A* **2006**, *110*, 2493

(73) Winget, P.; Cramer, C. J.; Truhlar, D. G. *Theor. Chem. Acc.* **2004**, *112*, 217.

MECHANISTIC STUDIES OF WATER OXIDATION CATALYZED BY HOMOGENEOUS IRON AND RUTHENIUM
COMPLEXES AND LIGHT-DRIVEN ORGANIC REDUCTIONS WITH A DUAL COBALT/COPPER CATALYTIC SYSTEM

Carla Casadevall Serrano

CHAPTER VII

Development of a New *N*-Pentadentate Anionic Fe Complex as an Active Catalyst for WO: the Influence of the Ligand Scaffold and the Accessibility of Fe^{V} Species

This chapter corresponds to the following publications:

"A new N-pentadentate iron (II) complex as an active homogeneous catalyst for water oxidation"

C. Casadevall, Z. Codolà, F. Acuña-Parés, V. Martin-Diaconescu, J. M. Lluis, M. Costas, J. Lloret-Fillol; *in preparation*.

MECHANISTIC STUDIES OF WATER OXIDATION CATALYZED BY HOMOGENEOUS IRON AND RUTHENIUM
COMPLEXES AND LIGHT-DRIVEN ORGANIC REDUCTIONS WITH A DUAL COBALT/COPPER CATALYTIC SYSTEM
Carla Casadevall Serrano

UNIVERSITAT ROVIRA I VIRGILI
MECHANISTIC STUDIES OF WATER OXIDATION CATALYZED BY HOMOGENEOUS IRON AND RUTHENIUM
COMPLEXES AND LIGHT-DRIVEN ORGANIC REDUCTIONS WITH A DUAL COBALT/COPPER CATALYTIC SYSTEM
Carla Casadevall Serrano

CHAPTER VII   New anionic *N*-pentadentate active Fe-WOC

VII. Development of a New *N*-Pentadentate Anionic Fe Complex as an Active Catalyst for WO: the Influence of the Ligand Scaffold and the Accessibility of Fe^{V} Species

VII.1. General insight

As seen in the previous chapters, fundamental aspects of the metal catalyzed WO such as precise manipulation of the protons, electrons and oxidation states, still remain to be clarified and are essential for its further development.[1] The metal-catalyzed reaction usually requires intermediacy of highly reactive high oxidation states at metal centers. Stabilization of these species, while maintaining at the same time their reactivity in O-O bond formation are critical elements that require novel fundamental insights for improving the efficiency of the entire process.[2,3]

As introduced in chapter III, we and others have recently reported that iron complexes are highly efficient catalysts for WO when using chemical oxidants such as cerium(IV) ammonium nitrate (CAN) and sodium periodate ($NaIO_4$).[4-6] Interestingly, for iron complexes based on neutral aminopyridil ligands, the nature of the ligand scaffold and the coordination number play a crucial role in the catalytic outcome. In this line, iron complexes based on neutral tetradentate ligands with two *cis*- labile sites are highly active.[4,6-9] Based on mechanistic studies we have proposed that iron complexes with the general structure $[L^{N4}Fe^{V}(O)(OH)]^{2+}$ (L^{N4} = stands for a tetradentate *N*-based ligand that leaves two free *cis*-sites at the iron center) are the active species, while species in the oxidation state (IV) are not reactive enough to lead to the formation of an O-O bond and are better described as the resting state of the catalytic cycle.[10,11]

On the other hand, iron complexes with stronger chelating ligands such as neutral pentadentate nitrogen-based ligands (L^{N5}) are not active in WO,

251

under the same catalytic conditions.[4,12] These differences in reactivity have been attributed to the impossibility of the later to stabilize the high oxidation state (V) required at the metal center to access the active species, which normally require high redox potentials to be achieved ($E(L^{N5}Fe^{IV/V}) > 2$ V vs SHE).[4,12,13] Recently, pentadentate anionic ligands have been employed for iron-based WO catalysis with the aim to decrease the redox potential to access the highly oxidized active species for WO. The anionic Fe(III) complex $[Fe^{III}(dpaq)(H_2O)]^{2+}$ (dpaq = 2-[bis(pyridine-2-ylmethyl)]amino-*N*-quinolin-8-yl-acetamido) was firstly reported by Kodera and coworkers (Figure VII.1, *Left*).[14,15] This ligand is formally a derivate of the well-known TPA[16] (Tris(2-pyridylmethyl)amine) ligand where one of the pyridine arms has been replaced by a *N*-(quinolin-8-yl)acetamidyl (AQ) anionic fragment. Remarkably, the derived iron(III) metal complex was found very active and selective in C-H oxidation. Moreover, Kodera and coworkers reported experimental evidence that the ligand enables the complex reaching the high oxidation states required for alkane C-H bond oxidation.[15] On the other hand, iron(II) amidate complexes are very rare although interesting since they can serve as mimics of Bleomycin, a glycopeptide that in combination with iron activates O_2 to cause efficient double strang cleavage of DNA.[17] Later on, complex $[Fe^{III}(dpaq)(H_2O)]^{2+}$ was tested in CAN driven WO by Sun and coworkers but it resulted inactive.[18] Then, Meyer and coworkers reported that the same complex was active for electrocatalytic WO, and proposed that water oxidation occurs at a $Fe^V{=}O$ species.[19] Presumably, these species can be reached in this compound and not in neutral pentadentate ligands because the anionic nature of the ligand lowers the $E(L^{N5}Fe^{IV/V})$ red-ox potentials at the iron site.[19]

With this consideration in mind, in this chapter we designed a new iron complex with a pentadentate anionic aminopyridine ligand based on the tacn (1,4,7-triazacyclononane) and the AQ (*N*-(quinolin-8-yl)acetamidyl) moieties, aiming at surpassing the inactivity towards WO of the previously reported

[L^{N5}Fe] complexes. Herein we report that complex [Fe^{II}(AQ^{Me2}tacn)](OTf) (AQ^{Me2}tacn = 2-(4,7-dimethyl-1,4,7-triaacyclononan-1-yl)-*N*-(quinolin-8-yl)acetamide and OTf = trifluoromethanesulfonate) is a catalyst for WO when using chemical oxidants such as CAN and NaIO$_4$ (Figure VII.1, *Right*). DFT calculations suggest that the AQ^{Me2}tacn ligand is red-ox non-innocent and is oxidized under catalytic conditions forming an L·Fe^{IV}(O) species with a radical mainly centered at the ligand, reminiscent to that of cytochrome P450 Compound I (Cpd-I), being the species responsible for the O-O bond formation.

[Fe^{III}(dpaq)(H$_2$O)]$^{2+}$ **[Fe^{II}(OH$_2$)(AQ^{Me2}tacn)](OTf), 1Fe**
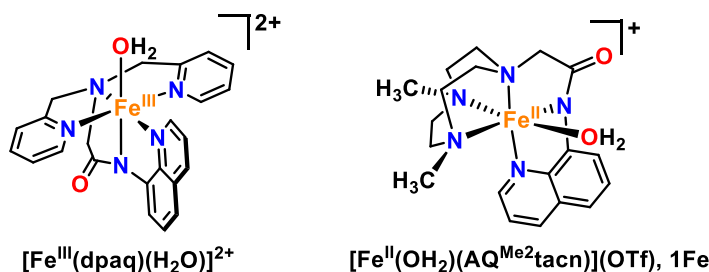
Figure VII.1. Iron complexes based on *N*-(quinolin-8-yl)acetamidyl fragment of this study. Left) iron(III) complex [Fe^{III}(dpaq)(H$_2$O)]$^{2+}$ reported by Kodera *et al*.[14] Right) New iron(II) complex based on the tacn moiety.

VII.2. Results and discussion

VII.2.1. Synthesis of ligands, complexes, and characterization

In the ligand design we took inspiration from the dpaq ligand that Kodera and coworkers recently reported (Figure VII.1).[14] In this line, we synthesized the 1-(*N*-(quinolin-8-yl)acetamidyl)-4,7-dimethyl-1,4,7-triazacyclononane (HAQ^{Me2}tacn) ligand by introducing the *N*-(quinolin-8-yl)acetamidyl fragment (AQ),[14] into the highly basic 1,4-dimethyl-1,4,7-triazacyclononane trihydrobromide (Me$_2$tacn·3HBr) moiety through alkylation in basic media (see Scheme VII.1 and Annex V section *A.V.1. Synthesis and characterization of ligands and complexes* for further information). The Me$_2$tacn·3HBr was synthesized as previously reported.[20] The ^{1}H-NMR characterization is in

UNIVERSITAT ROVIRA I VIRGILI
MECHANISTIC STUDIES OF WATER OXIDATION CATALYZED BY HOMOGENEOUS IRON AND RUTHENIUM
COMPLEXES AND LIGHT-DRIVEN ORGANIC REDUCTIONS WITH A DUAL COBALT/COPPER CATALYTIC SYSTEM
Carla Casadevall Serrano

CHAPTER VII   New anionic *N*-pentadentate active Fe-WOC

agreement with the formation of the ligand as judged by the amide signal at 11.35 ppm, the set of aromatic protons of the quinoline moiety between 8.8 and 7.4 ppm and the aliphatic protons of the tacn macrocycle between 2.8 and 3.4 ppm.
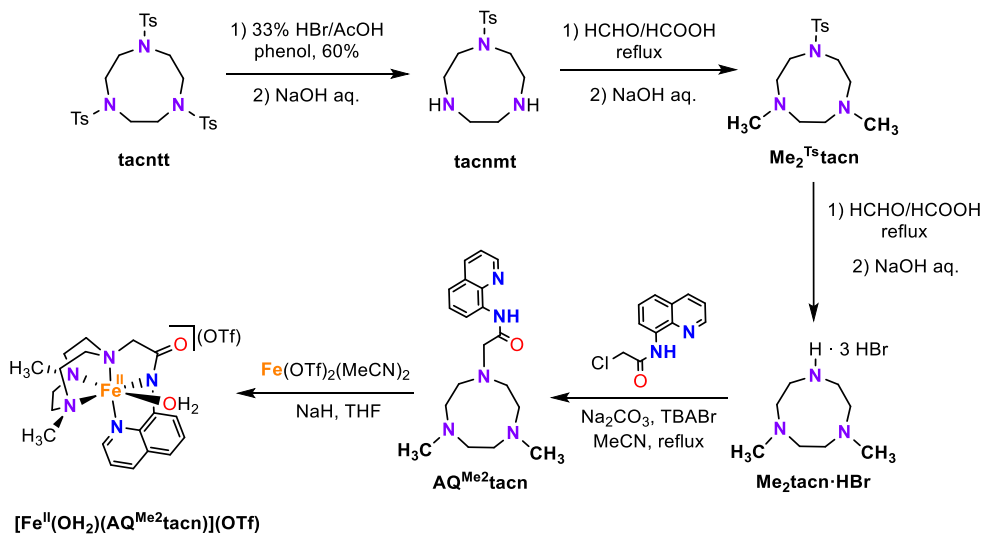
Scheme VII.1. Synthesis of the HAQ^{Me2}tacn ligand and [Fe^{II}(OH$_2$)(AQ^{Me2}tacn)](OTf) complex (**1Fe**).

Then, the reaction of the deprotonated ligand, prepared by using 1.1 equivalent of NaH, with an stoichiometric amount of Fe^{II}(OTf)$_2$(CH$_3$CN)$_2$ in THF gives a deep red solution corresponding to the [Fe^{II}(OTf)(AQ^{Me2}tacn)] complex (**1**), that could be isolated as a crystalline solid upon precipitation by adding diethyl ether and subsequent filtration (Scheme VII.1). The ^{1}H-NMR of **1Fe** in CD$_3$OD shows paramagnetically shifted peaks in the 20-190 ppm range, which is in agreement with the formation of a d^6 Fe^{II} high spin $S = 2$ complex (Figure VII.2). Interestingly, the deep-red microcrystalline iron compound turned immediately pale green when exposed to air. This is in sharp contrast with complexes with neutral ligands of general formula [Fe^{II}(OTf)(L^{N5})](OTf) which can be manipulated under air.
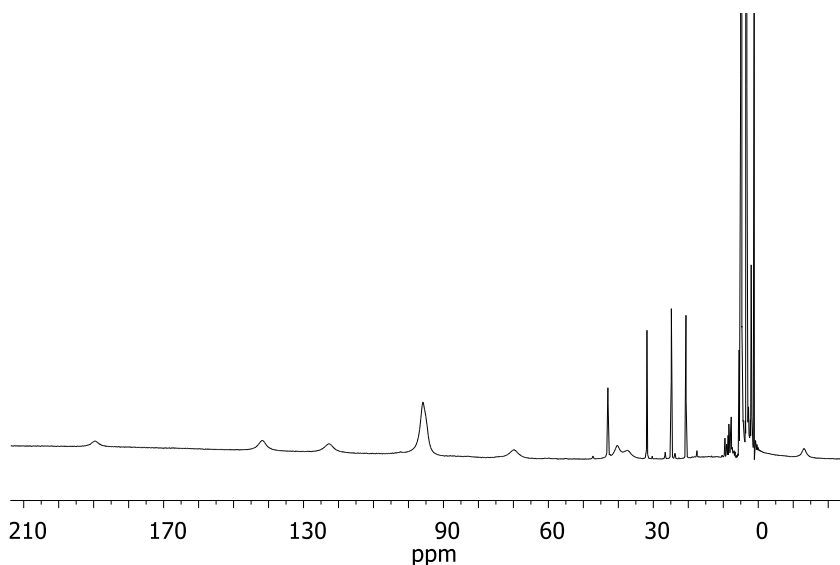
Figure VII.2. Paramagnetic ^{1}H-NMR (CD$_3$OD, 400 MHz, 300 K) of complex **1Fe** in 6 mg in 0.5 mL concentration.

The cryospray high-resolution mass spectrometry (CSI-HRMS at 25 ºC) analysis in degassed H$_2$O is dominated by the [Fe^{II}(AQ^{Me2}tacn)]$^+$ ion (calc. for C$_{19}$H$_{26}$FeN$_5$O 396.1487 m/z, found 396.1496 m/z) (Figure A.V.2). Crystals suitable for X-ray diffraction were grown by slow diffusion of diethyl ether into a solution of complex **1Fe** in DCM. X-ray diffraction analysis of a mono-crystal shows a distorted octahedral complex with the five nitrogen atoms of the AQ^{Me2}tacn ligand bonded to the iron(II) center (Figure VII.3). The three N atoms of the tacn ring cape a face of the iron coordination octahedron. The anionic amide nitrogen is *trans* to a *N*-Me group of the tacn, and a N atom of the quinolyl moiety binds trans to the *N*-atom that connects with the amide arm. The coordination sphere is completed by an amidate oxygen atom belonging to an adjacent iron complex forming a polymeric structure in the solid state (Figure VII.3). Bond distances between the N atoms of the AQ anionic fragment and the Fe center are significantly shorter than that found for the aliphatic nitrogens (Fe-N$_{amidate}$ ~ 2.1 Å vs Fe-N$_{tacn}$ ~2.2-2.3 Å). A closer look to the structure reveals an unexpected short distance for the Fe1-O1 (2.157 (4)

UNIVERSITAT ROVIRA I VIRGILI
MECHANISTIC STUDIES OF WATER OXIDATION CATALYZED BY HOMOGENEOUS IRON AND RUTHENIUM
COMPLEXES AND LIGHT-DRIVEN ORGANIC REDUCTIONS WITH A DUAL COBALT/COPPER CATALYTIC SYSTEM
Carla Casadevall Serrano

CHAPTER VII   New anionic *N*-pentadentate active Fe-WOC

Å) and similar for N1-C1 and C1-O1 distances (1.309(6) Å and 1.271(6) Å, respectively) suggesting an important charge delocalization though the N1-C1-O1 moiety (Figure VII.3). We notice that the complex presented a *cis*-disposition between the anionic group at the ligand and L_{N5} ligand-free coordination site, which is the same that is found in the structure of Bleomycin (Fe-BLM, Figure VII.3, *Right*).[21]
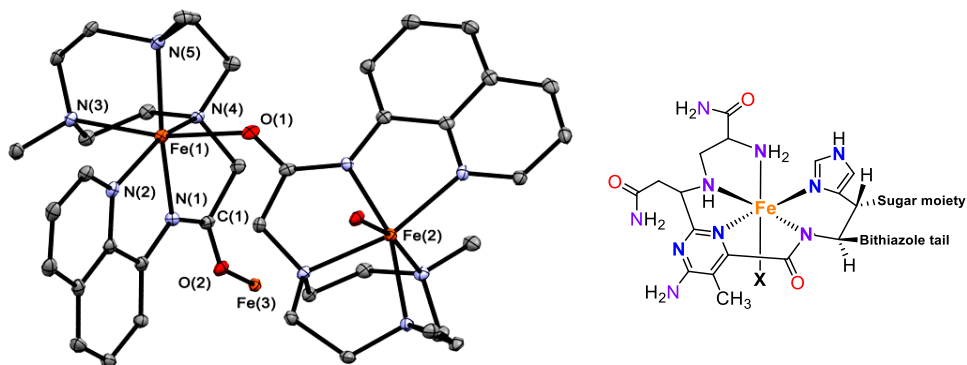
Figure VII.3. *Left*) Ortep structure with ellipsoids set at the 50% probability level of (**1Fe**)₂ from the X-ray diffraction analysis. Hydrogen atoms have been omitted for clarity. Obtained distances (Å) and bond angles (°) for **1Fe**: Fe(1)−N(1), 2.102(4); Fe(1)−N(2), 2.173(4); Fe(1)−N(3), 2.301(4); Fe(1)−N(4), 2.182(4); Fe(1)−N(6), 2.124(5); Fe(1)−O(1), 2.157(4); C(1)−N(1), 1.309(6); C(1)−O(1), 1.271(6); N(1)-Fe(1)-N(6), 76.92(17); N(1)-Fe(1)-O(1), 96.48(16); N(6)-Fe(1)-O(1), 99.96(15); N(6)-Fe(1)-N(2), 151.79(16); N(1)-Fe(1)-N(4), 158.59(15); O(1)-Fe(1)-N(3), 167.43(14). *Right*) Proposed structure of Bleomycin (Fe-BLM).[21]

VII.2.2. Water oxidation catalysis

The catalytic WO ability of complex **1Fe** was studied evaluating the O_2 formation when aqueous solutions of the complex were reacted with chemical oxidants such as CAN or $NaIO_4$. The total amount of gas produced was monitored by manometry until reaching a *plateau*. Moreover, the formation of O_2 and CO_2 was monitored and quantified *versus* time by gas chromatography (GC-TCD) and mass spectrometry by means of gas sampling from the reaction head-space (See VII.4. Experimental Section, VII.4.3.Water oxidation reactions for further details). There is an excellent agreement between the manometry and GC-TCD analysis (Table VII.1).

Table VII.1. WO catalytic activities found for the anionic complex **1Fe**.

Oxidant	Entry	[1Fe] (μM)	TON O_2[c]	TOF O_2[d]	TON O_2[e]	TON CO_2[e]
CAN[a] (pH = 0.8)	1	50	2.8 ±0.1	8 ±1	2.4 ±0.3	0.3 ±0.1
	2	100	2.2 ±0.1	7 ±2	2.0 ±0.2	0.2 ±0.0
$NaIO_4$[b] (pH = 4.5)	**3**	**12.5**	**76 ±4**	**40 ±5**	**77 ±4**	1.6 ±0.2
	4	50	40 ±2	25 ±3	42 ±1	0.9 ±0.1
	5	100	28 ±2	18 ±2	27 ±1	0.9 ±0.1

Reactions performed in Milli-Q water at 25 ºC. Values from the average of 3 experiments [a] CAN aq. solution (9.5 mL, 125 mM), initial pH = 0.8. [b] $NaIO_4$ aq. solution (9.5 mL, 250 mM), initial pH = 4.5. [c] TON (turnover number) = (n(O_2) produced / n(catalyst)) measured by manometry. [d] TOF (TON·h⁻¹) measured after 5 min of the catalyst addition. [e] Values measured by GC-TCD at the end of the reaction.
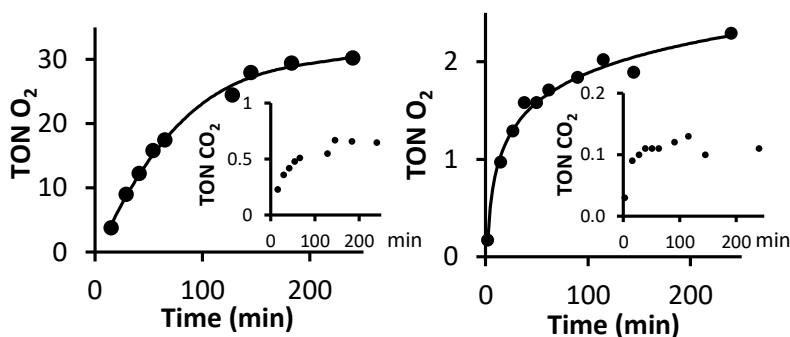
Figure VII.4. O_2 and CO_2 on-line monitoring by GC-TCD during the reaction of **1Fe** (0.1 mM) with left) NaIO4 (250 mM) and right) CAN (125 mM)

First, it is important to notice that no induction time in the O_2 detection neither generation of CO_2 was observed, an indication that the WO occurs in homogeneous phase. (Figures VII.4 and Annex V Figure A.V.4). On the other hand, few TON O_2 were obtained when using CAN as sacrificial oxidant. As previously reported, the use of $NaIO_4$ (milder oxidant) produced an increase in the TON O_2.[4] A 14-fold increase in the catalytic activity regarding the TON O_2 was observed when using $NaIO_4$ instead of CAN (Table VII.1, entries 1 and 4). In an analogous manner, we also observed an unexpected TOF growth by

more that 5-fold respect to using CAN as oxidant (Table VII.1, entries 1 and 4). To rationalize this observation we should take into account the pH imposed by the used sacrificial oxidant: pH 0.8 and 4.5 for CAN and $NaIO_4$, respectively. Therefore, we studied the change on the TON and TOF values versus pH when using $NaIO_4$ as oxidant instead of CAN. The optimum pH was found around 3 (Figure VII.5 and Annex V Figure A.V.5), which may balance the redox potential of the oxidant and the stability of the iron complex. In line with this argument, at pH 1 similar TON and TOF were recorded for both CAN (2.8, 6.8 h^{-1}) and $NaIO_4$, (4.7, 8.5 h^{-1}). The low TON and TOF may be a consequence of a partial hydrolysis of the metal due to ligand protonation.
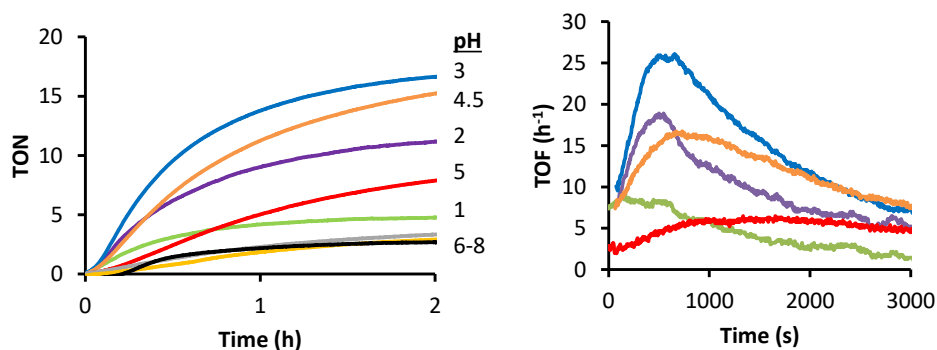
Figure VII.5. pH effect observed (*left* is TON and *right* is TOF) for the complex $Fe^{II}(OTf)(AQtacn)$ (100 µM complex, $NaIO_4$ 100mM). Acidic pH were calibrated by the addition of $HClO_4$ and basic pH were calibrated by the addition of NaOH.

At pH values higher than 3 the TON and TOF are also reduced, an aspect that has consequences with the mechanism. Moreover, the O_2 formed is systematically increased by the decrease in the catalyst concentration, clearly observed when employing $NaIO_4$ as oxidant (Table VII.1, entries 3 – 5).

VII.2.3. Mechanistic studies

First, we monitored the oxidation of complex **1Fe** under catalytic conditions by means of UV-Vis and XAS spectroscopy and CSI-HRMS spectrometry to get insights into the speciation in solution under conditions relevant to WO catalysis. Moreover, electrochemical experiments together

with DFT calculations also helped to shed some light on the intermediate formation.

VII.2.3.1. Characterization of WO intermediates

VII.2.3.1.1. Titration studies at acidic pH

A titration experiment of complex **1Fe** (1 mM, in MilliQ water at 25 ºC) with Ce^{IV} under non-buffered solution (pH = 2.9) upon subsequent addition of 0.2 equivalents of oxidant, reveals the formation of a new species (Figure VII.6a). First, the initial band at λ_{max} 507 nm ($\varepsilon = 270$ $M^{-1}cm^{-1}$) decreases in intensity upon titration with CAN (up to 1 eq.), leading to the formation of a new band in the UV-VIS at 670 nm ($\varepsilon = 900$ $M^{-1}cm^{-1}$) (Figure VII.6). CSI-HRMS analysis of the resulting solution showed a prominent peak corresponding to $[Fe^{III}(OH)(AQ^{Me2}tacn)]^+$ (**1Fe^{III}-OH**) (calc. for $C_{19}H_{27}FeN_5O_2$ 413.1514 m/z, found 413.1521 m/z) (Figure VII.7 and Figure A.V.8 and Table A.V.1).
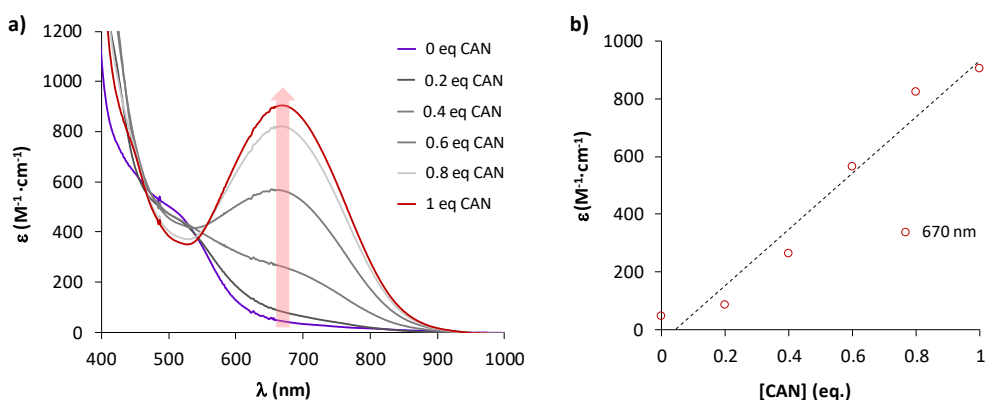
Figure VII.6. a) UV-Vis titration of **1Fe** (1 ml of 1 mM) at 298 K at pH ≈ 3 with CAN (additions of 10 µl, 0.2 eq. each, up to 1 eq.) to generate first the **1Fe^{III}-OH** species. b) ε versus CAN equivalents at 670 nm (red circles). The baseline was corrected to 0 by abs. average of the 700 - 1100 nm range. The abs values were corrected taking into account the total volume after each aliquot addition.
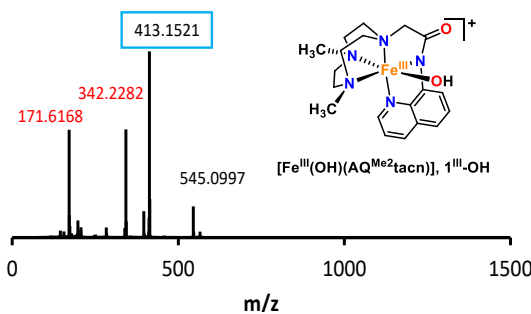
Figure VII.7. CSI-HRMS spectrum after the addition of 1 eq of **CAN** to $Fe^{II}(OTf)(AQtacn)$ (1mM, degassed MilliQ H_2O).

Further addition of CAN, up to 5 eq., decrease the band associated to **1Fe^{III}-OH** species (670 nm) from $\varepsilon = 900$ M^{-1}cm^{-1} to $\varepsilon = 600$ M^{-1}cm^{-1} (Figure VII.8). CSI-HRMS analysis of the resulting solution showed a prominent peak corresponding to $[Fe^{IV}(O)(AQ^{Me2}tacn)]^+$ (**1Fe^{IV}=O**) (calc. for $C_{19}H_{26}FeN_5O_2$ 412.1436 m/z, found 412.1431 m/z) (Figure VII.9, Figure A.V.9 and Table A.V.1). Then, CSI-HRMS at 10 eq. of CAN added shows a low intense peak for the **1Fe^{IV}=O** species. Moreover, peaks associated to mono- and dicharged protonated free ligand started to dominate the mass spectrum (Figure A.V.10 and Table A.V.1). Addition of CAN up to 20 eq. decreases the band associated to the **1Fe^{IV}=O** ($\varepsilon \approx 300$ M^{-1}cm^{-1}). This could indicate ligand dissociation at this highly acidic and oxidizing conditions (> 10 eq CAN).
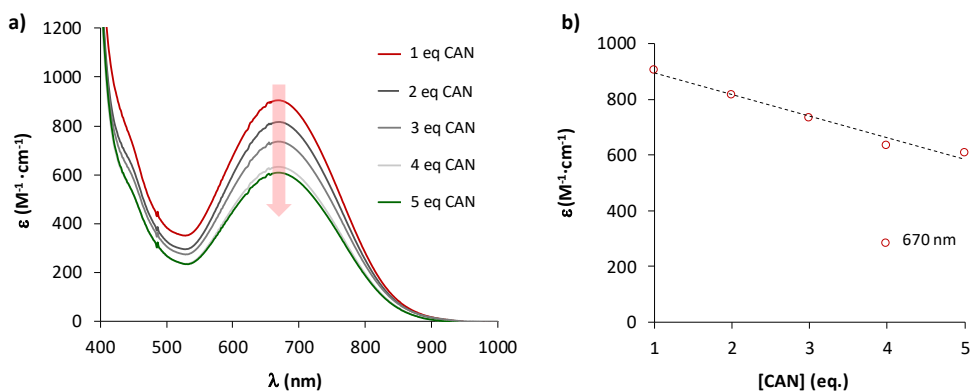
Figure VII.8. a) UV-Vis titration of **1Fe** (1 ml of 1 mM, LFeII) at 298 K at pH ≈ 3 with CAN (additions of 50 µl, 1 eq. each, up to 5 eq.) to generate first the **1Fe^{III}-OH** species. b) ε versus CAN equivalents at 670 nm (red circles). The baseline was corrected to 0 by abs. average of the 700 - 1100 nm range. The abs values were corrected taking into account the total volume after each aliquot addition.

UNIVERSITAT ROVIRA I VIRGILI
MECHANISTIC STUDIES OF WATER OXIDATION CATALYZED BY HOMOGENEOUS IRON AND RUTHENIUM
COMPLEXES AND LIGHT-DRIVEN ORGANIC REDUCTIONS WITH A DUAL COBALT/COPPER CATALYTIC SYSTEM
Carla Casadevall Serrano

CHAPTER VII   New anionic *N*-pentadentate active Fe-WOC
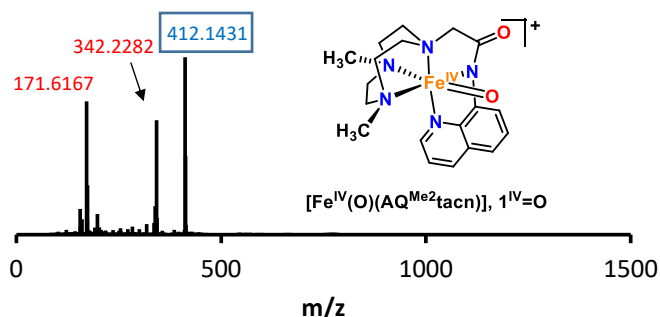
Figure VII.9. CSI-HRMS spectrum after the addition of 5 eq of **CAN** to [Fe^{II}(OTf)(AQ^{Me2}tacn)] (1mM, degassed MilliQ H$_2$O).
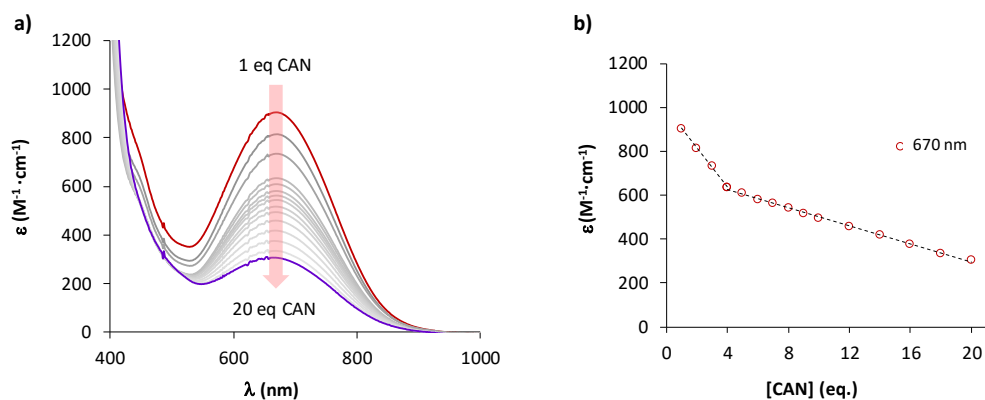
Figure VII.10. a) UV-Vis titration of **1Fe** (1 ml of 1 mM) at 298 K at pH ≈ 3 with CAN (additions of 50 µl, 1 eq. each up to 20 eq.). b) ε versus CAN equivalents at 670 nm (red circles). The base line was corrected to 0 by abs. average of the 700 - 1100 nm range. The abs values were corrected taking into account the total volume after each aliquot addition.

Analogously, the addition of 1 eq of NaIO$_4$ (0.5 mM, pH ≈ 3) was enough to detect the same peak at 412.1453 m/z, related to a **1Fe^{IV}=O** intermediate (Figure A.V.11 and Tables A.V.1 and A.V.2). This species was clearly dominant upon addition of excess of oxidant (20 eq., Figure A.V.12) and at this time almost no free ligand was detected, suggesting that the ligand is coordinated during the catalysis. Therefore, amidated anionic *N*-pentadentate iron complexes are also able to carry out WO. Likewise, titration of complex **1Fe** with NaIO$_4$ at non-buffered solution (pH ≈ 3) monitored by X-ray absorption spectroscopy (XAS) is in agreeement with the formation of further oxidized Fe(IV) species. Upon addition of 0.5 equivalents of NaIO$_4$ to **1Fe** a

clear shift to a more effectively oxidized metal center is observed. The 1s$\rightarrow$3d feature centered at 7112.5 eV in the Fe(II) complex shifts by 0.6 eV. A metal centered oxidation is further supported as a shift in the rising edge features taken both at half height ($E_0^{1/2}$) and as the first derivative of the rising edge (E_0') is apparent. Indeed 2.5 eV and 3 eV shifts in $E_0^{1/2}$ and E_0' are observed respectively (Table VII.2 and Figure VII.11), which is larger than what might be expected from a +1 formal oxidation state change. Interestingly a further addition of 0.5 eq. of $NaIO_4$ only results in a modest 0.3 eV change in both the pre-edge and rising edge energies. Further addition of excess $NaIO_4$ (up to 5 eq.), results in a further shift of the rising edges yielding values of 7123.7 eV for $E_0^{1/2}$ and 7124.2 eV for E_0'. However, in this last step, no significant shift in the pre-edge energy is observed within experimental error. In addition, the intensity (total area) of the pre-edge features remain centered around 0.15 normalized units (n.u.) below what might be expected from [Fe=X]$^{+n}$ cores (X= O,N; >19 n. u.). Lastly, although the pre-edge energies of the oxidized species are in the range of previously reported Fe(III) and Fe(IV) with values in the range of 7113-7113.4 eV,[22,23] the E0' energies with a range of 7123.6-7124.2 eV, on the other hand are reminiscent of higher Fe(IV)/Fe(V) oxidation states.[24]

Table VII.2. Experimental XANES parameters (energies are in eV).

	Pre-edge	$E_0^{1/2}$	E_0'
1Fe	7112.5	7120.1	7120.4
+ 0.5 eq $NaIO_4$	7113.1	7122.7	7123.6
+ 1.1 eq $NaIO_4$	7113.4	7122.9	7123.9
+ 5.0 eq $NaIO_4$	7113.4	7123.7	7124.2
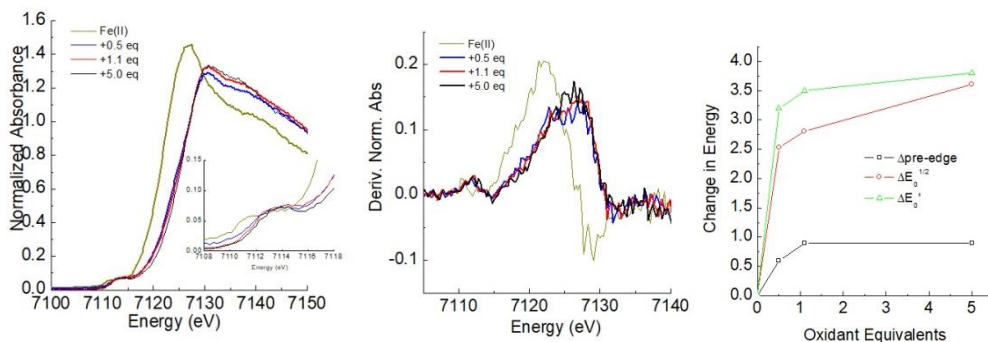
Figure VII.11. (left) XANES spectra upon addition of oxidant to **1Fe**; (center) first derivative
XANES spectra; (right) changes in XANES energies upon oxidation equivalents

In contrast, at pH 2 the behavior is different. First, the addition of
perchloric acid ($HClO_4$) down to pH 2, leads to the decrease of the initial band
of **1Fe** at λ_{max} 507 nm (ε = 270 M-1cm-1) with the concomitant formation of a
new band in the UV-VIS at 680 nm (ε = 150 $M^{-1}cm^{-1}$) (Figure 12A, red line),
most likely due to ligand protonation. Then, titration of **1Fe** at pH 2 with $NaIO_4$
(up to 0.5 eq.) leads to the increase and shift of the new band to 670 nm (ε =
270 $M^{-1}cm^{-1}$) (Figure 12A, green line), which was associated to the formation
of **1Fe^{III}-OH$_2$** species. The same was obtained with CAN (Figure A.V.6).
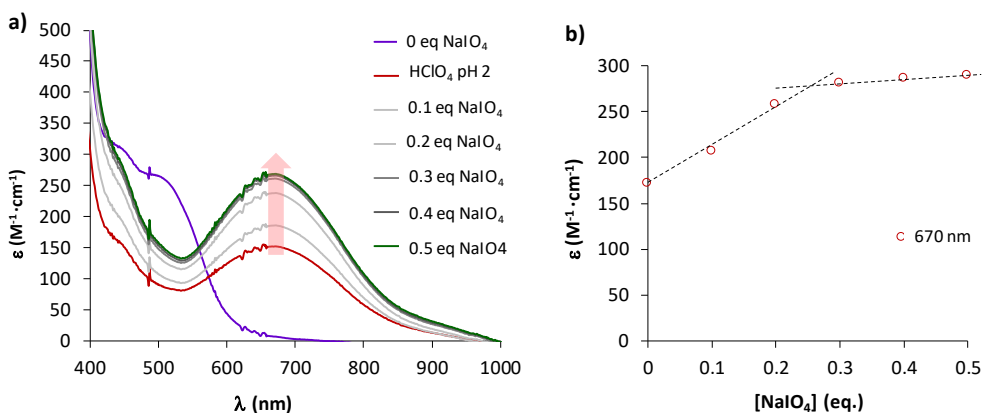
Figure VII.12A. a) UV-Vis titration of **1Fe** (1 ml of 1 mM) at 298 K at pH 2 with $NaIO_4$ (additions
of 10 µl, 0.1 eq. each) to generate first the **LH-Fe^{II}-OH$_2$** and then the **1Fe^{III}-OH$_2$** species. b) ε versus
$NaIO_4$ equivalents at 670 nm (red circles). The baseline was corrected to 0 by abs. average of the 700 -
1100 nm range. The abs values were corrected taking into account the total volume after each aliquot
addition.
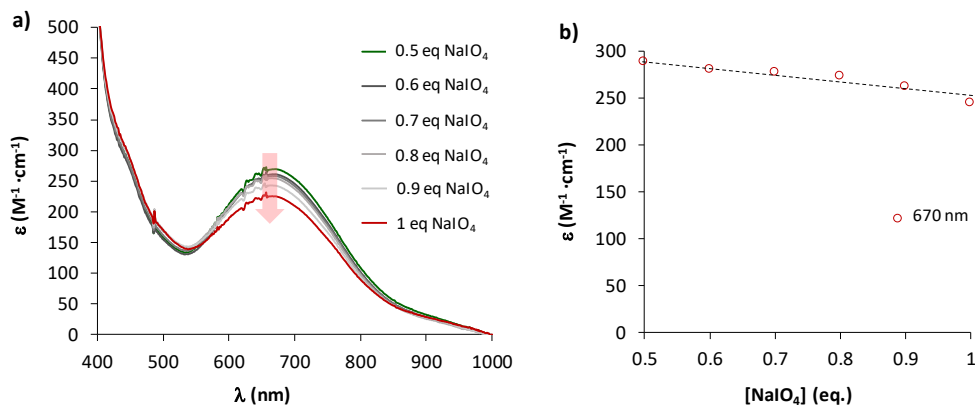
Figure VII.12B. a) UV-Vis titration of **1Fe** (1 ml of 1 mM) at 298 K at pH 2 with NaIO$_4$ (additions of 10 µl, 0.1 eq. each) to generate the **1Fe^{IV}-OH** species. b) ε versus NaIO$_4$ equivalents 670 nm (red circles). The baseline was corrected to 0 by abs. average of the 700 - 1100 nm range. The abs values were corrected taking into account the total volume after each aliquot addition.

Further addition of NaIO$_4$ (up to 1 eq.) led to the decrease of the band at 670 nm (ε = 220 M^{-1}cm^{-1}) (Figure VII.12B, red line). This was associated most likely to the formation of a **1Fe^{IV}-OH**, which is accessible under these conditions (see DFT studies section).

VII.2.3.1.2. Titration studies at basic pH

At pH 9 the behaviour is completely different. Titration of complex **1Fe** at pH 9 with NaIO$_4$ by subsequent addition of 0.05 eq., leads to the decrease of the initial band of **1Fe** at λ$_{max}$ 507 nm (ε = 270 M-1cm-1). The presence of two isosbestic points at 450 and 625 nm after the addition of 0.25 eq. NaIO$_4$ suggests the formation of a new species. In this case, since NaIO$_4$ can act as oxo transfer as well, it is like 0.5 electron have been use to oxide the starting complex **1Fe**, this behaviour is in agreement with the oxidation of **1Fe^{II}-O-1Fe^{II}** to **1Fe^{II}-O-1Fe^{III}** species, in which only one of the metal centres has been oxidized (Figure VII.13). Further addition of NaIO$_4$ up to 0.5 eq. leads to the formation of a new chromophore at λ$_{max}$ 670 nm (ε = 60 M^{-1}cm^{-1}), which is most likely associated to the formation of the **1Fe^{III}-O-1Fe^{III}** dimeric species (Figure VII.14).

264
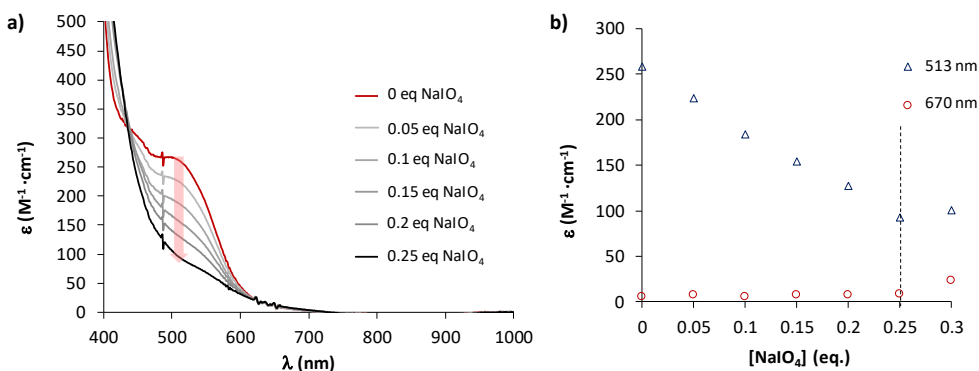
Figure VII.13. a) UV-Vis titration of **1Fe** (1 ml of 1 mM) at 298 K at pH 9 with NaIO$_4$ (additions of 5 μl, 0.05 eq. each) to generate the **1Fe^{II}-O-1Fe^{III}** species. b) ε versus NaIO$_4$ equivalents at 513 nm (blue triangles) and 670 nm (red circles). The baseline was corrected to 0 by abs. average of the 700 - 1100 nm range. The abs values were corrected taking into account the total volume after each aliquot addition.
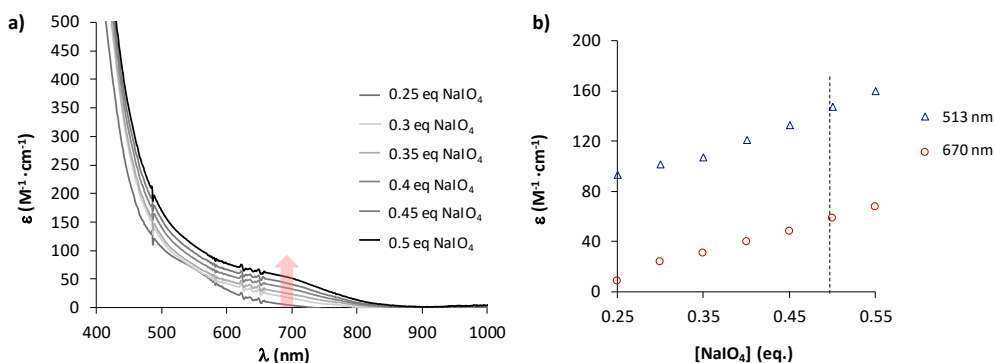
Figure VII.14. a) UV-Vis titration of **1** (1 ml of 1 mM) at 298 K at pH 9 with NaIO$_4$ (additions of 5 μl, 0.05 eq. each) to generate the **1Fe^{III}-O-1Fe^{III}** species. b) ε versus NaIO$_4$ equivalents at 513 nm (blue triangles) and 670 nm (red circles). The baseline was corrected to 0 by abs. average of the 700 - 1100 nm range. The abs values were corrected taking into account the total volume after each aliquot addition.

Subsequent titration with NaIO$_4$ from 0.5 eq. to 1 eq. leads to the increase of the band at λ$_{max}$ 670 nm (to ε = 110 M^{-1}cm^{-1}), which is most likely associated to the formation of the final formation of **1Fe^{IV}-O-1Fe^{IV}** dimeric species (Figure VII.15). Further titration did not produce significant changes in the UV-Vis spectrum (Figure A.V.7), most likely due to the inaccessibility of the active species at this high basic pH, which is also in agreement with the decrease WO activity at pH > 6 (Figure VII.5).
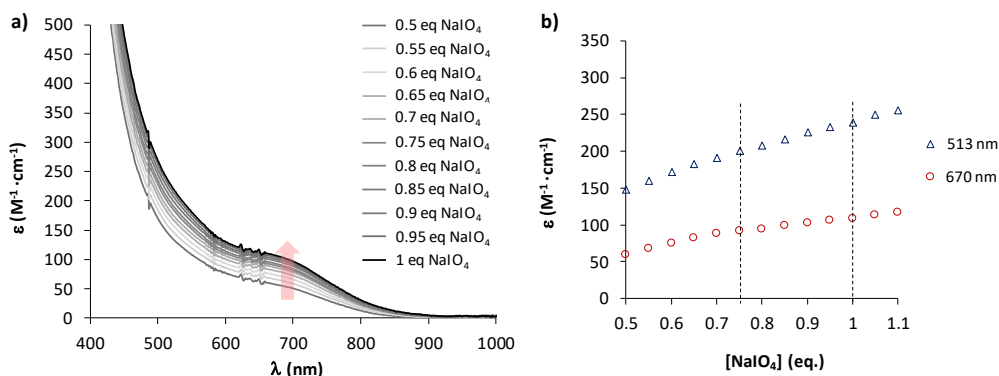
Figure VII.15. a) UV-Vis titration of **1Fe** (1 ml of 1 mM, LFeII) at 298 K at pH 9 with NaIO4 (additions of 5 µl, 0.05 eq. each) to generate the **1Fe^{II}-O-1Fe^{III}** species. b) ε versus NaIO4 equivalents at 513 nm (blue triangles) and 670 nm (red circles). The baseline was corrected to 0 by abs. average of the 700 - 1100 nm range. The abs values were corrected taking into account the total volume after each aliquot addition.

VII.2.3.2. Electrochemical studies

To get further insights into the nature of the oxidizing species in catalysis we have studied the electrochemistry in solution and the pH-redox-potential-dependence of **1Fe** by CV (cycle voltammetry), DPV (differential pulse voltammetry) and SWV (square wave voltammetry) in the pH 2-9 range (Figures VII.16, VII.17 and VII.18). The electrochemical studies were mostly performed by Dr. Zoel Codolà. First, characterization by cyclic voltammetry (CV) and differential pulse voltammetry (DPV) (in 0.1M KNO$_3$ as electrolyte) showed three distinctive waves with redox potentials of 0.28 V, 0.44 V and 0.98 V vs SHE, most likely associated to the **1Fe^{III}-OH, 1Fe^{III}-OH$_2$** and **1Fe^{IV}=O**, respectively.
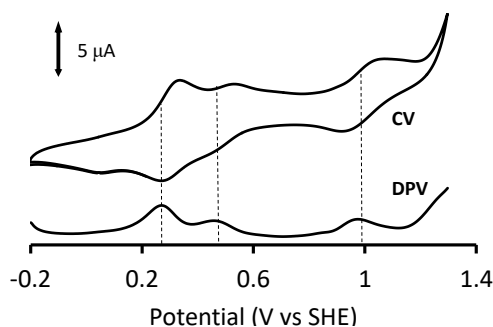
Figure VII.16. CV and DPV of complex **1Fe** (1mM) in a degassed aqueous solution of KNO_3 (0.1M). A blank experiment containing the electrolyte was subtracted from these curves. Glassy carbon, Ag/AgCl (SSCE) and Pt were the working, reference and counter electrodes. Parameters CV: Scan Rate = $100mV \cdot s^{-1}$. Parameters DPV: Increase of E = 4 mV, Amplitude = 50 mV, Pulse Width = 200 ms, Sampling Width = 16.7 ms, Pulse Period = 500 ms.

The pH of the solution modifies the relative intensity of the first (0.28 V) and second waves (0.44 V). A Pourbaix diagram of **1Fe** reveals a one electron transfer (ET) process at 0.28 V between pH 4.5 and 9, and a PCET for the species at 0.44 V from pH 2 to 5 (Figure VII.16). Interestingly, the wave at 0.28V becomes negligible at pH 3 (1eq. of acid with respect to the complex, Figures VII.17 and VII.18) and totally vanishes at pH 2 (Figure VII.17), suggesting the formation of a mono protonated compound, most likely due to ligand protonation, which is in agreement with the UV-Vis titration studies with acid at pH 2 (Figure VII.11). But unfortunately no evidence of protonated **1Fe** was found by CSI-HRMS (Figures A.V.8 – A.V.12 and Table A.V.1). At higher potentials, there is a peak at 0.98 V vs SHE that remains unaltered in the pH range between 4 and 8. In contrasts, it shifts and decreases in intensity upon addition of acid to pH 2, making complicated the Pourbaix analysis (Figure VII.17). Moreover, an additional peak at 1.48 V vs SHE was also observed by both square wave voltammetry (SWV) and DPV in the studied pH range (3 – 8), which seems to be an electron transfer process, most likely associated to the **1Fe^{IV}=O** to **1Fe^{V}=O** (better described as **1Fe^{V}=O**, see computational studies section below) oxidation process (Figure VII.19).
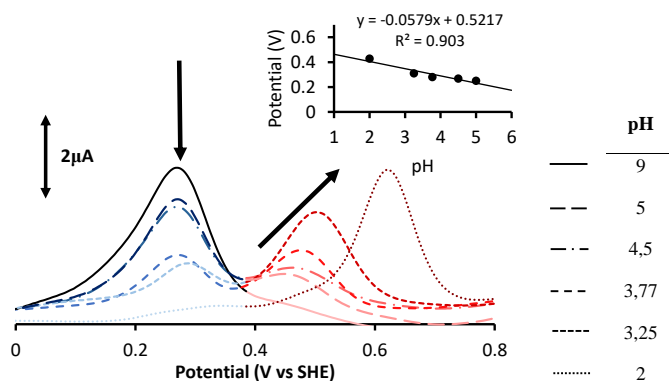
Figure VII.17. DPV of the complex [Fe^{II}(OTf)(AQ^{Me2}tacn)] (1mM) in a degassed aqueous solution of KNO$_3$ (0.1M). Evolution of the 0-0.8 V range upon addition of acid (HClO$_4$) or base (NaOH). Arrows indicate the evolution due to the increase of the [H]$^+$. Red and blue colors corresponds to the protonated and the non-protonated species, respectively. Inset, Pourbaix diagram for the protonated couple Fe$^{II/III}$ (in red). A blank experiment containing the electrolyte and the amount of acid or base required was subtracted from these curves. (Increase of E = 4 mV, Amplitude = 50 mV, Pulse Width = 200 ms, Sampling Width = 16.7 ms, Pulse Period = 500 ms).
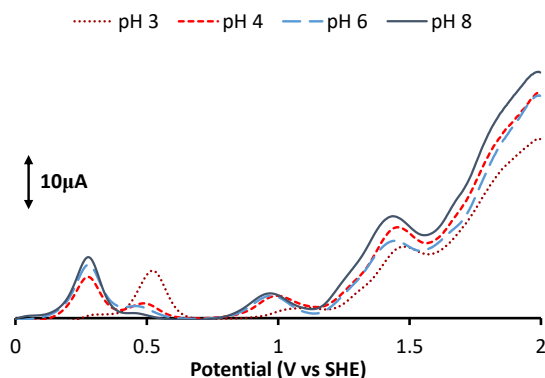
Figure VII.18. Square wave voltammetry (SWV) of the complex [Fe^{II}(OTf)(AQ^{Me2}tacn)] (1mM) in a degassed aqueous solution of KNO$_3$ (0.1M) at different pH by addition of HClO$_4$ or NaOH. A blank experiment containing the electrolyte and the amount of acid or base required was subtracted from these curves. (Increase of E = 4 mV, Amplitude = 25 mV, Freq. = 15 Hz).

Considering the relevant increase of current observed experimentally above 1.48 V vs SHE, this might be related to the onset for the catalytic WO process. It seems plausible that the introduction of a non-innocent anionic moiety in the ligand scaffold facilitates the formation of a Fe^V oxidation state which is better described as a Fe^{IV} in which the ligand has been oxidized and has one electron delocalized over the quinoline structure (**·1Fe^{IV}=O**) when using CAN or NaIO$_4$ as oxidants. Indeed,

UNIVERSITAT ROVIRA I VIRGILI
MECHANISTIC STUDIES OF WATER OXIDATION CATALYZED BY HOMOGENEOUS IRON AND RUTHENIUM
COMPLEXES AND LIGHT-DRIVEN ORGANIC REDUCTIONS WITH A DUAL COBALT/COPPER CATALYTIC SYSTEM
Carla Casadevall Serrano

CHAPTER VII   New anionic *N*-pentadentate active Fe-WOC

this is agreement with the calculated **1Fe^{IV}=O** to **1Fe^{V}=O** (·**1Fe^{IV}=O**) redox process $E^{IV/V}_{theor}$ = 1.23 V vs $E^{IV/V}_{exp}$ = 1.48 vs SHE). This is relevant, since the WO inactivity of the previously studied *N*-pentadentate iron complexes based on aminopyridyl ligands was due to the high redox $E^{(IV/V)}$ values (> 2 V vs SHE)[11,12] to access the active species, impossible to be reached under catalytic conditions with oxidants such as CAN (~1.75 V vs SHE at pH 0.9, at about 50 mM concentration)[25] or NaIO$_4$ (1.33 V vs SHE at pH 4.5).[26] Therefore, the introduction of an non-innocent anionic moiety than can be oxidise made available the Fe$^{(IV-·)}$ oxidation state (or formally Fe$^{(V)}$) when using CAN or NaIO$_4$ as oxidants.

VII.2.3.3. Computational studies

To shed some light on the potential catalytic species we calculated the DFT-redox potentials at B3LYP/cc-pVTZ//B3LYP/6-31G* level of theory including dispersion, solvent and spin contamination corrections (Figure VII.19 for the complete redox/deprotonation reaction steps). Dr. Ferran Acuña-Parés from the University of Girona performed the DFT calculations of this chapter.

As a first step to unravel the WO mechanism catalyzed by complex **1**, we investigated the potential speciation in solution under catalytic conditions. Therefore, we have evaluated the pKa, reduction potential and proton coupled electron transfer (PCET) processes for the different aquo/hydorxo/oxo Fe$^{II/III}$, Fe$^{III/IV}$ and Fe$^{IV/V}$ redox couples, respective transformations. This analysis allowed us to establish by DFT the dominant species under catalytic conditions. It is worth to note that we have examined the relative energies of all possible spin multiplicities for the iron species in oxidation states II, III, IV and V, to identify the ground spin state in each case.
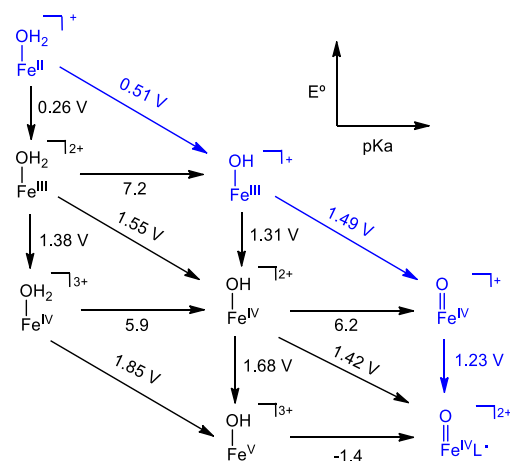
Figure VII.19. Redox potentials and pKa's relating all the possible iron intermediates that could be formed in aqueous solution from **1Fe**. Oxidation potential values correspond to the standard redox potentials relative to SHE electrode and the diagonal steps are the proton-coupled electron transfer (PCET) redox potentials at pH 3. The oxidized AQ^{Me2}tacn ligand is represented by L.

In this line, the oxidation of $[Fe^{II}(AQ^{Me2}tacn)(OH_2)]^+$ by 1e⁻ ($E^{II/III} = 0.26$ V vs SHE) was found to be more favorable than a PCET process (0.51 V at pH 3). Subsequent 1e⁻ oxidation could yield $[Fe^{IV}(AQ^{Me2}tacn)(OH_2)]^{3+}$ ($E^{III/IV} = 1.38$ V) or *via* PCET process $[Fe^{IV}(AQ^{Me2}tacn)(OH)]^{2+}$ (1.55 V at pH 3). Under catalytic conditions further oxidation and deprotonation of $[Fe^{IV}(AQ^{Me2}tacn)(OH)]^{2+}$ could take place to form $[Fe^{V}(AQ^{Me2}tacn)(O)]^{2+}$ (1.23 V at pH3, Figure VII.19). However, the analysis of the spin density distribution in the $[Fe^{V}(AQ^{Me2}tacn)(O)]^{2+}$ intermediate reveals that instead of the $Fe^{IV}=O$ moiety, the AQ^- fragment is oxidized by one electron to $AQ^\bullet$, to form $[Fe^{IV}(AQ^{Me2}tacn)^\bullet(O)]^{2+}$ ($E^{(IV/IV\bullet)} = 1.23$ V at pH 3). The radical is mainly centered at the amidated fragment but also delocalized in the aromatic system (Figure VII.20). This behavior resembles that of the $Fe^{IV}=O$ porphyrin radical cation (compound I) of the P450.[27] Further oxidation of the systems seems unviable judged by the calculated redox ($E^{(IV\bullet/V\bullet)} = 2.16$ V). In turn, these results suggest that $[Fe^{IV}(AQ^{Me2}tacn)^\bullet(O)]^{2+}$ is the species with higher oxidation state that can be formed when a large excess of CAN or NaIO₄ is present in solution and could be the active species.

UNIVERSITAT ROVIRA I VIRGILI
MECHANISTIC STUDIES OF WATER OXIDATION CATALYZED BY HOMOGENEOUS IRON AND RUTHENIUM
COMPLEXES AND LIGHT-DRIVEN ORGANIC REDUCTIONS WITH A DUAL COBALT/COPPER CATALYTIC SYSTEM
Carla Casadevall Serrano

CHAPTER VII   New anionic *N*-pentadentate active Fe-WOC
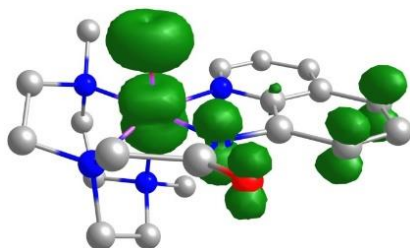
Figure VII.20. Illustration of the spin density of complex $[Fe^{IV}(AQ^{Me2}tacn)\cdot(O)]^{2+}$

The computed WNA mechanism for complex $[Fe^{IV}(AQ^{Me2}tacn)\cdot(O)]^{+2}$ gives a Gibbs energy barrier of 27.1 kcal·mol^{-1} (Figure VII.21). This energy value is higher by 8.6 kcal·mol^{-1} than the reported for the *N*-tetradentate $[Fe^{V}(Py^{Me2}tacn)(O)(OH)]^{2+}$ intermediate ($\Delta G^{\neq} = 18.5$ kcal·mol^{-1}) and then consistent with their differences in initial TOF values (8 - 40 and 222 respectively).[8,13] On the other hand, the presence of an internal base in $[Fe^{V}(Py^{Me2}tacn)(O)(OH)]^{2+}$ (the OH ligand) produces a reduction of the Gibbs energy barrier by 7.4 kcal·mol^{-1} when the WNA mechanism is assisted by the hydroxyl ligand (*cis*-assisted mechanism).[8,13] Intents to model an internal base assisted WNA mechanism assisted by the amidate group bonded to the iron center as an internal base produced in all the cases higher energetic pathways.
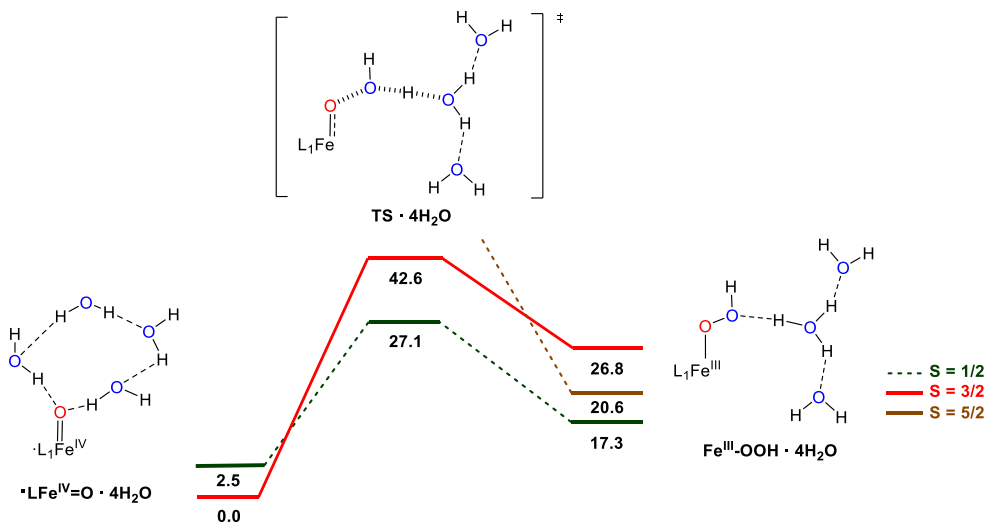
Figure VII.21. O-O bond formation free energy profiles found for $[Fe^{IV}(AQ^{Me2}tacn)\cdot(O)]^{2+}$ in the S = 1/2, 3/2 and 5/2 spin states. Gibbs energy values are given in kcal·mol^{-1}. The oxidized AQ^{Me2}tacn ligand is represented by L·.

VII.3. Conclusions

In summary, in this chapter, we synthesized and characterized the new *N*-pentadentate anionic HAQ^{Me2}tacn ligand and their corresponding iron(II) coordination complex [Fe^{II}(OTf)(AQ^{Me2}tacn)] (**1Fe**). Complex **1Fe** was found active in catalytic water oxidation when using CAN and NaIO$_4$. The lack of induction time and the apparent absence of CO$_2$ at the beginning of the reaction suggest that the catalytic species are molecular. DFT studies suggest that [Fe^{IV}(AQ^{Me2}tacn)$^•$(O)]$^{2+}$ with a radical centered on the ligand (oxidized in one electron) rather than [Fe^{V}(AQ^{Me2}tacn)(O)]$^{2+}$ is the active catalytic species. Computationally modeling of the O-O bond formation supports an external WNA mechanism through the [Fe^{IV}(AQ^{Me2}tacn)$^•$(O)]$^{2+}$ intermediate. Regarding that the Fe^{II} amidated complex **1Fe** is a rare iron complex and can be seen as a model for the anti-cancer drug Bleomycin, further studies will be carried out in our group.

Therefore, **1Fe** is the first reported non-heme iron pentacoordinate complex active for WO using CAN as a sacrificial oxidant. The negative charge and non-redox nature of the pentadentate amidated ligand may be the key factors to reduce the redox potential to form the active WO species and should be considered in future iron catalyst design for water oxidation. These results open the door for the quest of more robust WOC based in iron based on anionic pentadentate ligands.

VII.4. Experimental section

VII.4.1. General procedures

Materials. All chemical used in this study were purchased from commercial sources and used as received, without further purification. Solvents were purchased from SDS and Scharlab, purified and dried by passing through an activated alumina purification system (MBraun SPS-800) and stored in an anaerobic glovebox under

N_2. Water (18.2 MΩ·cm) was purified with a Milli-Q Millipore Gradient AIS system. Chloroacetyl chloride (98%), 8-aminoquinoline (98%), pyridine, KNO_3 (99.999% trace metals basis), Cerium(IV) ammonium nitrate (CAN, ≥99.99% trace metals basis), trifluoromethanesulfonic acid (ReagentPlus grade ≥99%), $HClO_4$ (70%, 99.999% trace metals basis) and $NaIO_4$ (ACS reagent, ≥99.8%) were purchased from Sigma-Aldrich®.

Physical Methods. UV-VIS-NIR spectra were recorded on an Agilent 8453 diode array spectrophotometer (190-1100 nm range) in 1 cm quartz cells. A cryostat from Unisoku Scientific Instruments was used for temperature control. The amount of gas generated was measured with a differential pressure transducer sensor (Honeywell-ASCX15DN, ±15 psi). Each reaction had its own reference reaction, which was connected to the other port of the sensor. Further details of the equipment are available elsewhere.[4] Cryospray High-resolution mass spectra (CRI-HRMS) were recorded on a Bruker MicrOTOF-Q II™ instrument with Cryospray ionization sources at Serveis Tècnics of the University of Girona and a MicroTOF Focus II (Bruker Daltonics) instrument with a Coldspray ionization source (CSI, Bruker Daltonics) at the Research Support Area of ICIQ. Samples were introduced into the mass spectrometer ion source by direct infusion using a syringe pump and were externally calibrated using sodium formate. The instrument was operated in the positive ion mode. The pH of the solutions was determined by a pHmeter (XS Instruments) calibrated before measurements through standard solutions at pH= 4.01, 7.00 and 10.00.

Fe K-edge X-ray absorption data was collected on 3 mM aqueous solution samples. Samples were stored at liquid nitrogen temperatures until run. Fluorescence data was collected at 77K using a liquid nitrogen cryostat and a Si(111) double crystal monochromator at Diamond beamline B18. The Athena software package was used for data calibration and normalization.[28] Energies were calibrated to the first inflection point of Co foil spectra set at 7111.2 eV

The amount of gas generated was measured with a differential pressure transducer sensor (Honeywell-ASCX15DN, ±15 psi, see Annex II Figure A.II.33). Each reaction had its own reference reaction, which was connected to the other port of the sensor. Further details of the equipment are available elsewhere.[4] Gases at the headspace were analyzed with an Agilent 7820A GC System equipped with columns Washed Molecular Sieve 5Å, 2m x 1/8'' OD, Mesh 60/80 SS and Porapak Q, 4m x 1/8'' OD, SS. Mesh: 80/100 SS and a Thermal Conductivity Detector. The quantification of the O_2 obtained was measured through the interpolation of a previous calibration using known O_2/N_2 mixtures. O_2/N_2 and CO_2/N_2 calibration was performed using previously prepared different O_2/N_2 and CO_2/N_2 mixtures.

VII.4.2. Synthesis and characterization of ligands and complexes

2-chloro-N-(quinol-8-yl)acetamide

The 2-choro-N-(quinol-8-yl)acetamide fragment was synthesized and characterized as previously described.[14]

Synthesis of 1,4-dimethyl-1,4,7-triazacyclononane trihydrobromide (Me₂tacn HBr)

Me₂tacn HBr was synthesized accordingly to the previously reported procedures from the 1,4,7-tri(*p*-toluensulfonyl)-1,4,7-triazacyclononane (tacntt) moiety.[20]

1-(*N*-(quinolin-8-yl)acetamidyl)-4,7-dimethyl-1,4,7-triazacyclononane (H-AQ^{Me2}tacn).

2-chloro-N-(quinolin-8-yl)acetamide (0.22 g, 1 mmol), 1,4-dimethyl-1,4,7-triazacyclononane trihydrobromide (0.4 g, 1mmol), Na₂CO₃ (0.9 g, 8.5 mmol) and tetrabutylammonium bromide (TBABr) (0.02 mg, 0.06 mmol) were dissolved in anhydrous acetonitrile (35mL) in a 50mL flask and the mixture was refluxed under N₂ for 20h. After cooling to room temperature, the mixture was filtered and the solvent evaporated under reduced pressure. To the obtained product (yellowish oil), NaOH (1M, 20mL) was added and the mixture was extracted with CH₂Cl₂ (3 x 20 mL). The combined organic layers were dried over anhydrous MgSO₄, the solvent
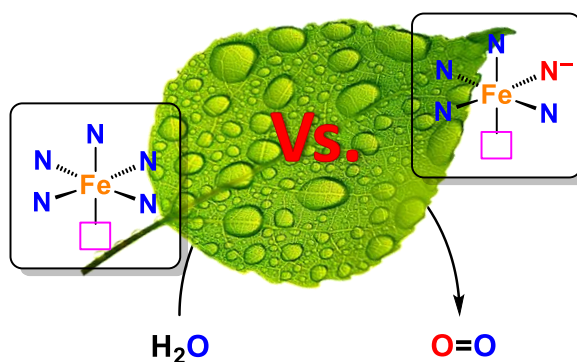
UNIVERSITAT ROVIRA I VIRGILI
MECHANISTIC STUDIES OF WATER OXIDATION CATALYZED BY HOMOGENEOUS IRON AND RUTHENIUM
COMPLEXES AND LIGHT-DRIVEN ORGANIC REDUCTIONS WITH A DUAL COBALT/COPPER CATALYTIC SYSTEM
Carla Casadevall Serrano

CHAPTER VII   New anionic *N*-pentadentate active Fe-WOC

was removed under reduced pressure and the product was extracted twice with n-hexane (50mL, overnight stirring) to yield 0.17 g of a pale yellow oil (0.5 mmols, 50 %). ^{1}H-NMR (CDCl3, 400 MHz, 298K) δ, ppm: 11.25 (s, 1H, N**H**CO), 8.74(d, J = 7.54Hz, 1H, QN-**H$_2$**), 8.68(m, 1H, QN-**H$_8$**), 8.04 (d, J = 8.14 Hz, 1H, QN-**H$_4$**) , 7.42 (m, 2H, QN-**H$_3$** and QN-**H$_7$**), 7.34 (m, 1H, QN-**H$_6$**), 3.34 (d, J = 2.18 Hz, 2H, C**H$_2$**-N)2.85 (m, 8H, N-C**H$_2$**-CH$_2$), 2.77 (m, 4H, N-C**H$_2$**-CH$_2$), 2.31 (6H, N-C**H$_3$**). ^{13}C-NMR (CDCl$_3$, 400 MHz, 300K) δ, ppm: 170.51 (N**C**O), 148.00 (QN-**C$_2$**), 138.80 (QN-**C$_2$**), 136.09 (QN-**C$_{10}$**), 134.54 (QN-**C$_4$**), 128.00 (QN-**C$_9$**), 127.25 (QN-**C$_2$**), 121.60, 121.48, 116.61, 64.45 (**C**H$_2$-N), 57.89, 57.49, 56.80(N-**C**H$_2$-C), 46.73 (N-**C**H$_3$). ESI-MS (m/z) 342.2290 m/z [AQtacn + H]$^+$.

Fe^{II}(OTf)(AQ^{Me}2tacn), 1Fe. In an anaerobic glove box, NaH (7.7 mg, 0.32mmol, 1.1 eq) was added to a vigorously stirred solution of the H-AQtacn ligand (100 mg, 0.29 mmol) in anhydrous THF (1mL). After 1 hour a solution of Fe(CH$_3$CN)$_2$(CF$_3$SO$_3$)$_2$ (128mg, 0.29 mmol) in anhydrous THF (1mL) was added dropwise. The solution turned into red immediately and it was allowed to stir for 2 hours. Precipitation in anhydrous Et$_2$O afforded a brownish powder which was recrystallized by slow Et$_2$O diffusion in CH$_2$Cl$_2$, yielding 110 mg (69%) of deep-red crystals. ^{1}H-NMR (MeOD, 400MHz, 298K) δ, ppm: 189.26, 141.58, 122.09, 95.52, 69.57, 42.92, (40.32, 36.73) 31.61, 24.77, 20.63, -13.35. CSI-HRMS (degassed D$_2$O, 298K) m/z: 396.1496 [Fe^{II}(AQtacn)]$^+$ (calc. for C$_{19}$H$_{26}$FeN$_5$O 396.1487 m/z), 957.2516 [(μ-O)Fe^{II}Fe^{III}(AQtacn)$_2$(CF$_3$SO$_3$)]$^+$ (calc. for C$_{39}$H$_{52}$F$_3$Fe$_2$N$_{10}$O$_6$S 957.2443 m/z). UV-vis (degassed D$_2$O) λ, nm (ε, M^{-1} cm^{-1}) 197 (25700), 245 (20800), 344 (shoulder, 3630).

VII.4.3.Water oxidation reactions

Water-oxidation reactions (8/run) were performed in a 15 ml vial capped with septa and equipped with stir bars. Each of the volume-calibrated vials that contained the oxidant–Milli-Q water solution (250 mM of NaIO$_4$ or 125 mM of CAN in 9.5 ml otherwise mentioned) were connected to one port of a

differential pressure transducer sensor. Each reaction had its reference reaction, which was connected to the other port of the differential pressure transducer sensors. Both vials were kept under the same experimental conditions. Stock solutions were prepared by weighing the iron catalyst (**1Fe**) inside of the glovebox. Once all the sensors were connected, 0.5 ml (otherwise mentioned) of the stock solution of the WO catalyst were added to the Milli-Q water-oxidant solution to start the on-line monitoring of the O_2 evolution. The oxygen evolution of the reactions was monitored by recording the headspace pressure increase (one-second intervals). The oxygen contained in each of the reaction vials was measured by analyzing an aliquot of the gas captured at the headspace (0.1 ml) by GC-TCD.

VII.4.4. Electrochemical Studies

Electrochemical measurements were carried out on a Workstation CH-600E series (CH Instruments). The analyte (1mM) was dissolved in a degassed aqueous solution of KNO_3 (0.1M). Electrochemistry was performed under a constant flux of N_2, employing a three-electrode setup: 3 mm diameter (S = 0.07 cm^2) Teflon-shrouded glassy carbon working electrode, a Pt wire auxiliary electrode and an Ag/AgCl reference electrode (purchased from CH Instruments). All potential values are reported with respect to SHE (Ag/AgCl + 0.199 V) unless stated. Glassy carbon electrodes were polished with 0.05 micron alumina (Al2O3) and washed water before every measurement.

VII.4.5. UV-Vis titration studies

The characterization of the WO intermediates by UV-Vis spectroscopy was done at 25 ºC and under N_2 using either $NaIO_4$ and CAN as sacrificial oxidants at a specific pH, unless otherwise indicated. To a 1 ml solution of **1Fe** (1 mM) in MilliQ-water under N_2 atmosphere in a quartz UV-vis cell (0.5 cm), subsequent additions of either $NaIO_4$ and CAN in aliquots of 5 μl (0.05 eq. respect to the iron complex). After

each addition of oxidant, the UV-Vis spectrum was let to stabilize before further titration.

VII.4.6. High resolution mass spectrometry (HRMS)

All HRMS were recorded on a Bruker MicrOTOF-Q IITM instrument with ESI or Cryospray ionization sources at Serveis Tècnics of the University of Girona. Samples were introduced into the mass spectrometer ion source by direct infusion using a syringe pump and were externally calibrated using sodium formate. The instrument was operated in the positive ion mode. The characterization of the WO intermediates by HRMS was done at 25 ºC. From a solution of **1Fe** (1 mM) in MilliQ water under N_2 an aliquot was firstly analysed. Then the sample was titrated with an oxidant (from 1 eq. of $NaIO_4$ and 1 eq. of CAN to 5 eq.).

VII.4.7. Computational details

VII.4.7.1. Geometry optimization and free energy evaluation

In this chapter, the DFT calculations were performed by Dr. Ferran Acuña-Parés, from the University of Girona. The DFT calculations were carried out using the Gaussian09 program[29] with the B3LYP hybrid exchange-correlation functional.[30-32] Geometry optimizations of iron complexes are performed using the 6-31G* 6d basis set for all atoms. Solvating water and Van der Waals dispersion effects were included in geometry optimizations through the IEFPCM-SMD polarizable continuum model[33] and the Grimme DFT-D_2 correction,[34] respectively. The nature of stationary points was established by frequency calculations in the aqueous phase, where minima have no imaginary frequencies and the transition states only one.

Single point calculations with the cc-pVTZ 6d basis set on the equilibrium geometries, including solvent and dispersion effects (E_{SP}), were used to evaluate the free energies values (G):

$$G = E_{SP} + G_{corr.} \qquad\qquad (VII.1)$$

where the Gibbs correction ($G_{corr.}$) was obtained from a thermo-statistical analysis at the B3LYP/6-31G*/IEFPCM-SMD/DFT-D$_2$ level. All calculations employ the spin-unrestricted formalism and spin-contaminated cc-pVTZ electronic energies were systematically corrected before the evaluation of the free energy values.[35]

VII.4.7.2. pK$_a$ values and redox potentials

The standard dissociation free energy change between an acid (AH) and its conjugate base (A$^-$) in aqueous phase (ΔG^o) may be expressed as:

$$\Delta G^o = G\left(A_{aq}^-\right) + G\left(H_{aq}^+\right) - G\left(AH_{aq}\right) + \Delta G^* \qquad (VII.2)$$

$$G\left(H_{aq}^+\right) = G\left(H_{gas}^+\right) + \Delta G_{solv}^{H+} \qquad (VII.3)$$

where $G\left(AH_{aq}\right)$ and $G\left(A_{aq}^-\right)$ are standard free energies of the acid and its conjugate base, respectively. The $G\left(H_{aq}^+\right)$ is the free energy of the proton in water, obtained from the experimental solvation free energy of a proton ($\Delta G_{solv}^{H+} = -265.9 \, \text{kcal} \cdot \text{mol}^{-1}$) and its gas-phase free energy at room temperature ($G\left(H_{gas}^+\right) = -6.3 \, \text{kcal} \cdot \text{mol}^{-1}$).[34] ΔG^* is the free energy change associated with the conversion from a standard-state of 1 M in the aqueous phase and 1 atm in gas phase, to 1 M in both phases. Its value is 1.89 kcal·mol^{-1} at 298.15 K. Taking into account the previous equations, the pK$_a$ can be evaluated by:

$$pK_a = \frac{\Delta G^o}{RT \ln(10)} \qquad\qquad (VII.4)$$

where *R* is the universal gas constant and *T* is the temperature.[35]

The standard one electron redox potentials relative to the SHE electrode were calculated by:

$$E^o = -\frac{\Delta G^o}{nF} + \frac{\Delta G^o_{SHE}}{F} \qquad\qquad (VII.5)$$

where ΔG^o is the standard free energy change associated with the reduction reaction, *n* the number of transferred electrons, *F* is the Faraday constant (23.06 kcal·mol^{-1} V^{-1}) and ΔG^o_{SHE} is the free energy change associated with the absolute standard potential for the hydrogen electrode in water (-98.72 kcal·mol^{-1}).[36]

V.II.5. References

(1) Blakemore, J. D.; Crabtree, R. H.; Brudvig, G. W. *Chem. Rev.* **2015**, *115*, 12974.

(2) Pantazis, D. A. *ACS Catal.* **2018**, *8*, 9477.

(3) Shaffer, D. W.; Xie, Y.; Concepcion, J. J. *Chem. Soc. Rev.* **2017**, *46*, 6170.

(4) Fillol, J. L.; Codolà, Z.; Garcia-Bosch, I.; Gómez, L.; Pla, J. J.; Costas, M. *Nat. Chem.* **2011**, *3*, 807.

(5) Z.Codolà; I. Garcia-Bosch; F. Acuña; I. Prat; J. M. Luis; M. Costas; Lloret-Fillol, J. *Chem. Eur. J.* **2013**, *19*, 8042.

(6) Liu, T.; Zhang, B.; Sun, L. *Chem.—Asian J.* **2019**, *14*, 31.

(7) Codolà, Z.; Gamba, I.; Acuña-Parés, F.; Casadevall, C.; Clémancey, M.; Latour, J.-M.; Luis, J. M.; Lloret-Fillol, J.; Costas, M. *J. Am. Chem. Soc.* **2019**, *141*, 323.

(8) Codolà, Z.; Garcia-Bosch, I.; Acuña-Parés, F.; Prat, I.; Luis, J. M.; Costas, M.; Lloret-Fillol, J. *Chem. Eur. J.* **2013**, *19*, 8042.

(9) Annunziata, A.; Esposito, R.; Gatto, G.; Cucciolito, M. E.; Tuzi, A.; Macchioni, A.; Ruffo, F. *Eur. J. Inorg. Chem.* **2018**, *2018*, 3304.

(10) Codolà, Z.; Garcia-Bosch, I.; Acuña-Parés, F.; Prat, I.; Luis, J. M.; Costas, M.; Lloret-Fillol, J. *Chem. Eur. J.* **2013**, *19*, 8042.

(11) Acuña-Parés, F.; Codolà, Z.; Costas, M.; Luis, J. M.; Lloret-Fillol, J. *Chem. Eur. J. DOI: 10.1002/chem.201304367* **2014**.

(12) Casadevall, C.; Codolà, Z.; Costas, M.; Lloret-Fillol, J. *Chem. Eur. J.* **2016**, *22*, 10111.

(13) Acuna-Pares, F.; Codola, Z.; Costas, M.; Luis, J. M.; Lloret-Fillol, J. *Chem. Eur. J.* **2014**, *20*, 5696.

(14) Hitomi, Y.; Arakawa, K.; Funabiki, T.; Kodera, M. *Angew. Chem. Int. Ed.* **2012**, *51*, 3448.

(15) Hitomi, Y.; Arakawa, K.; Kodera, M. *Chem. Commun.* **2014**, *50*, 7485.

(16) Canary, J. W.; Wang, Y.; Roy Jr, R.; Lawrence Que, Jr.; Miyake, H.

(17) Lehmann, T. E.; Ming, L.-J.; Rosen, M. E.; Que, L. *Biochemistry* **1997**, *36*, 2807.

(18) Zhang, B.; Li, F.; Yu, F.; Cui, H.; Zhou, X.; Li, H.; Wang, Y.; Sun, L. *Chem.—Asian J.* **2014**, *9*, 1515.

(19) Coggins, M. K.; Zhang, M.-T.; Vannucci, A. K.; Dares, C. J.; Meyer, J. *J. Am Chem. Soc.* **2014**, *136*, 5531−5534.

(20) Flassbeck, C.; Wieghardt, K. *Z. Anorg. Allg. Chem.* **1992**, *608*, 60.

(21) Bukowski, M. R.; Zhu, S.; Koehntop, K. D.; Brennessel, W. W.; Que, L. *JBIC Journal of Biological Inorganic Chemistry* **2004**, *9*, 39.

(22) Chandrasekaran, P.; Stieber, S. C. E.; Collins, T. J.; Que, J. L.; Neese, F.; DeBeer, S. *Dalton. Trans.* **2011**, *40*, 11070.

(23) Westre, T. E.; Kennepohl, P.; DeWitt, J. G.; Hedman, B.; Hodgson, K. O.; Solomon, E. I. *J. Am. Chem. Soc.* **1997**, *119*, 6297.

(24) Klinker, E. J.; Jackson, T. A.; Jensen, M. P.; Stubna, A.; Juhász, G.; Bominaar, E. L.; Münck, E.; Que Jr, L. *Angew. Chem. Int. Ed.* **2006**, *45*, 7394.

(25) Parent, A. R.; Crabtree, R. H.; Brudvig, G. W. *Chem. Soc. Rev.* **2013**, *42*, 2247.

(26) Parent, A. R.; Crabtree, R. H.; Brudvig, G. W. *Chemical Society Reviews* **2013**, *42*, 2247.

(27) Shaik, S.; Kumar, D.; de Visser, S. P.; Altun, A.; Thiel, W. *Chemical Reviews* **2005**, *105*, 2279.

(28) Ravel, B.; Newville, M. *J. Synchrotron Rad.* **2005**, *12*, 537.

(29) Gaussian 09, R. A., M. J. Frisch, G. W. Trucks, H. B. Schlegel, G. E. Scuseria, M. A. Robb, J. R. Cheeseman, G. Scalmani, V. Barone, B. Mennucci, G. A. Petersson, H. Nakatsuji, M. Caricato, X. Li, H. P. Hratchian, A. F. Izmaylov, J. Bloino, G. Zheng, J. L. Sonnenberg, M. Hada, M. Ehara, K. Toyota, R. Fukuda, J. Hasegawa, M. Ishida, T. Nakajima, Y. Honda, O. Kitao, H. Nakai, T. Vreven, J. A. Montgomery, Jr., J. E. Peralta, F. Ogliaro, M. Bearpark, J. J. Heyd, E. Brothers, K. N. Kudin, V. N. Staroverov, R. Kobayashi, J. Normand, K. Raghavachari, A. Rendell, J. C. Burant, S. S. Iyengar, J. Tomasi, M. Cossi, N. Rega, J. M. Millam, M. Klene, J. E. Knox, J. B. Cross, V. Bakken, C. Adamo, J. Jaramillo, R. Gomperts, R. E. Stratmann, O. Yazyev, A. J. Austin, R. Cammi, C. Pomelli, J. W. Ochterski, R. L. Martin, K. Morokuma, V. G. Zakrzewski, G. A. Voth, P. Salvador, J. J. Dannenberg, S. Dapprich, A. D. Daniels, Ö. Farkas, J. B. Foresman, J. V. Ortiz, J. Cioslowski, and D. J. Fox, Gaussian, Inc., Wallingford CT. **2009**.

(30) Becke, A. D. *J Chem Phys* **1993**, *98*, 5648.

(31) Becke, A. D. *J Chem Phys* **1993**, *98*, 1372.

(32) Lee, C.; Yang, W.; Parr, R. G. *Physical Review B* **1988**, *37*, 785.

(33) C. J. Cramer, A. V. M., D. G. Truhlar *J. Phys. Chem. B* **2009**, *113*, 6378.

(34) Schwabe, T.; Grimme, S. *Phys. Chem. Chem. Phys.* **2007**, *9*, 3397.

(35) M. Swart, M. G., J. M. Luis, M. Solà *J. Phys. Chem. A* **2010**, *114*, 7191.

(36) Winget, P.; Cramer, C. J.; Truhlar, D. G. *Theor. Chem. Acc.* **2004**, *112*, 217.

UNIVERSITAT ROVIRA I VIRGILI
MECHANISTIC STUDIES OF WATER OXIDATION CATALYZED BY HOMOGENEOUS IRON AND RUTHENIUM
COMPLEXES AND LIGHT-DRIVEN ORGANIC REDUCTIONS WITH A DUAL COBALT/COPPER CATALYTIC SYSTEM
Carla Casadevall Serrano

MECHANISTIC STUDIES OF WATER OXIDATION CATALYZED BY HOMOGENEOUS IRON AND RUTHENIUM
COMPLEXES AND LIGHT-DRIVEN ORGANIC REDUCTIONS WITH A DUAL COBALT/COPPER CATALYTIC SYSTEM
Carla Casadevall Serrano

CHAPTER VIII

Dual Co/Cu Light-driven Reduction of Aromatic Ketones and Aliphatic Aldehydes and Unprecedented Selectivity in Ketone vs Aldehyde Reduction Using H₂O and TEA as Source of Hydrides
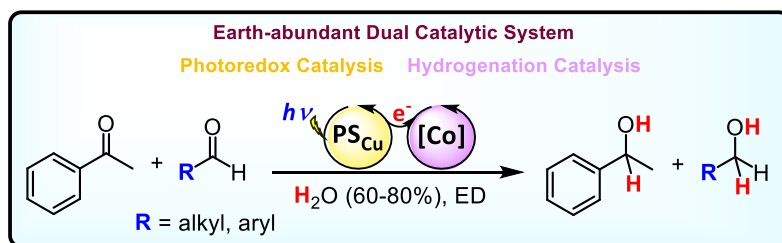
Part of this chapter corresponds to the following publication and the study has been possible thanks to the *in-house* developed photoreactors (see patent):

"Dual cobalt-copper light-driven catalytic reduction of aldehydes and aromatic ketones in aqueous media"; A. Call*, **C. Casadevall***, F. Acuña-Parés, A. Casitas, J. Lloret-Fillol; Chem. Sci., 2017, 8 (7), 4739. (* stands for equal contribution). Front cover, Highlighted in Chemistry World and Chemistry Views and Among the most downloaded articles of 2017.

Patent: "Photoreactor", J. Lloret-Fillol, **C. Casadevall**, J. L. León, A. Call, A. Casitas, J. J. Pla, J. P. Hernández, F. X. Caldentey; ICIQ, ref: 17382313.9-1370; 2017.

Patent: "A photocatalytic reduction procedure and a catalytic composition for the procedure" J. Lloret-Fillol, A. Call, **C. Casadevall**, A. Casitas; ICIQ, ref PCT/ES2017/070314, PCT international, 16/05/2017.

MECHANISTIC STUDIES OF WATER OXIDATION CATALYZED BY HOMOGENEOUS IRON AND RUTHENIUM
COMPLEXES AND LIGHT-DRIVEN ORGANIC REDUCTIONS WITH A DUAL COBALT/COPPER CATALYTIC SYSTEM
Carla Casadevall Serrano

VIII. Dual Co/Cu Light-driven Reduction of Aromatic Ketones and Aliphatic Aldehydes and Unprecedented Selectivity in Ketone vs Aldehyde Reduction Using H₂O and TEA as Source of Hydrides

VIII.1. General insight

Catalysts developed for the reduction of H_2O[1-11] and CO_2[12-19] in the context of artificial photosynthesis (AP) have the potential to provide greener light-driven methodologies for sustainable synthetic methods.[20-25] The production of fine chemicals has less scaling and economic restrictions than the synthesis of energy carriers. In this regard, using catalytic systems derived from AP to perform selective organic transformations is highly appealing.[22,23,26-35] Remarkable examples of catalytic systems based on semiconductors,[36-44] enzymes,[26-28,34,45] and more recently, homogeneous catalysts,[35,46-49] although with reduced scope or selectivity, have been shown active for specific transformations.

For instance, semiconductor materials, such as TiO_2 or CdS, provide very lower redox potentials promoting direct reduction reactions *via* one or two photoinduced electron transfer processes, but at expense of using UV light, novel metals or/and obtaining low to moderate selectivity (Scheme VIII.1).[36-42] The asymmetric reduction of acetophenones and α-ketoglutarate has been achieved coupling i) a sacrificial electron donor, ii) a photosensitizer, iii) a noble-metal-based catalyst, iv) an electron carrier and v) an enzyme that carries out the enantioselective transformation.[26-28,34,45] Results of the latter case show that selective light-driven reduction of organic substrates using water, as a formal dihydrogen source, is a feasible transformation, albeit limited to a specific substrate.[26-31,34] On the other hand, due to the complexity of these catalytic systems, optimization and mechanistic studies are difficult.

The combination of photoredox catalysts with well-defined molecular complexes is a powerful approach towards light-driven reduction of organic molecules.[50,51] The introduction of a photoredox catalytic cycle potentially enables the use of water and an electron donor as reductive equivalents, while organometallic or coordination complexes can serve as selective hydrogenation catalysts with a broad scope. In this regard, coordination complexes based on Rh,[35] Ru,[47] and Ir[48] have been explored. A remarkable example is the one reported by König and co-workers for the selective visible light photoreduction (λ = 455 nm) of aldehydes to alcohols in the presence of ketones. This catalytic system consists of proflavine (PF) as photocatalyst and [Cp*Rh^{III}(bpy)Cl]Cl as a well-known hydrogenation catalyst in the presence of triethanolamine (TEOA) as sacrificial electron donor.[35] Nevertheless, while aldehydes can be easily reduced using this system, ketones are not suitable substrates (Scheme VIII.1).
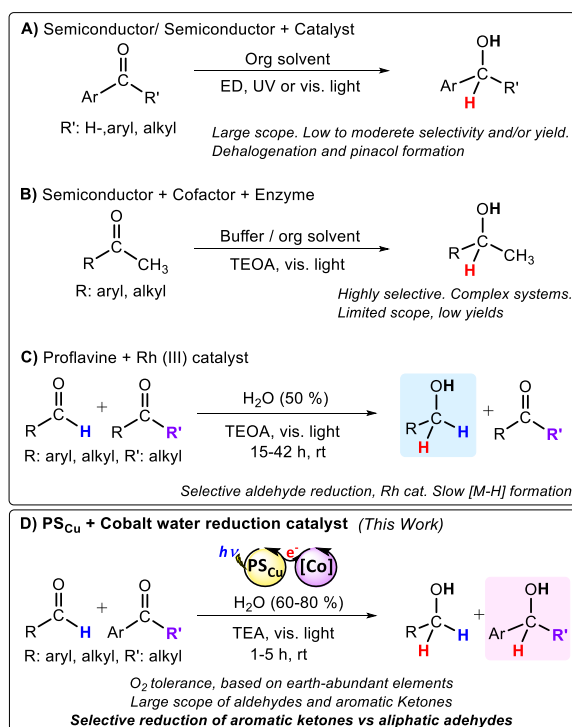
Scheme VIII.1. Methodologies for the light-driven reduction of carbonyl compounds. Abbreviations: ED: Electron Donor, TEOA: Triethanolamine, TEA: triethylamine. Selected references: A) refs 36 - 49 B) refs 26, 30, 45 and C) ref 35.

On the other hand, remarkable efforts have been focused on developing hydrogenation catalysts based on earth-abundant elements.[52-70] However, they are usually sensitive to O_2. Therefore, catalysts based on earth-abundant elements resilient to O_2 that operate in H_2O and can reduce organic substrates using light as energy source and water/electron donor as a source of hydrides could have a beneficial impact in the synthesis of drugs, pesticides and organic chemicals in general.[51,71,72] In this line, efficient catalysts for the reduction of water to hydrogen such as cobalt complexes based on glyoxime,[73] diimine-glyoxime[3] and aminopyridine[2,4] ligands are promising candidates as hydrogenation catalysts of organic substrates under similar reaction conditions.[6,8,74,75] Mechanistic investigations on these systems suggest that molecular [Co-H] species are key intermediates in the H_2 formation.[76-82] Therefore, photochemically obtained [Co-H] intermediates based on these ligands could potentially be catalytic intermediates for the reduction of organic functionalities in H_2O using amine/H_2O as a hydrides source (Scheme VIII.1).

In this chapter, a methodology to reduce aromatic ketones and both aliphatic and aromatic aldehydes by cobalt-copper dual light-driven catalysis using H_2O/(Et_3N or $^iPr_2EtN$) as a hydride source is described (Scheme VIII.2). The dual metal catalytic system is formed by an aminopyridine Co complex (**1**), initially developed for light-driven water reduction to H_2,[83] and [Cu(bathocuproine)(Xantphos)](PF_6)[84] (**PS$_{Cu}$**) (bathocuproine = 2,9-Dimethyl-4,7-diphenyl-1,10-phenanthroline and Xantphos = 4,5-Bis(diphenylphosphino)-9,9-dimethylxanthene) as photoredox catalyst (Scheme VIII.2). Reactivity and preliminary mechanistic studies suggest a common intermediate, most probably a [Co-H] as responsible for the reduction of organic substrates and water. By using water/amine and light as reductive equivalents, we achieved a selective catalytic reduction of aromatic ketones in the presence of aliphatic ketones, aliphatic aldehydes, aliphatic alkenes and alkynes. This unique selectivity is rationalized based on the mechanistic studies based on reactivity,

UNIVERSITAT ROVIRA I VIRGILI
MECHANISTIC STUDIES OF WATER OXIDATION CATALYZED BY HOMOGENEOUS IRON AND RUTHENIUM
COMPLEXES AND LIGHT-DRIVEN ORGANIC REDUCTIONS WITH A DUAL COBALT/COPPER CATALYTIC SYSTEM
Carla Casadevall Serrano

CHAPTER VIII   Unprecedented Selectivity in Ketone vs Aldehyde Photoreduction

isotopic labeling experiments, reactivity with radical clocks and computational modeling (DFT).
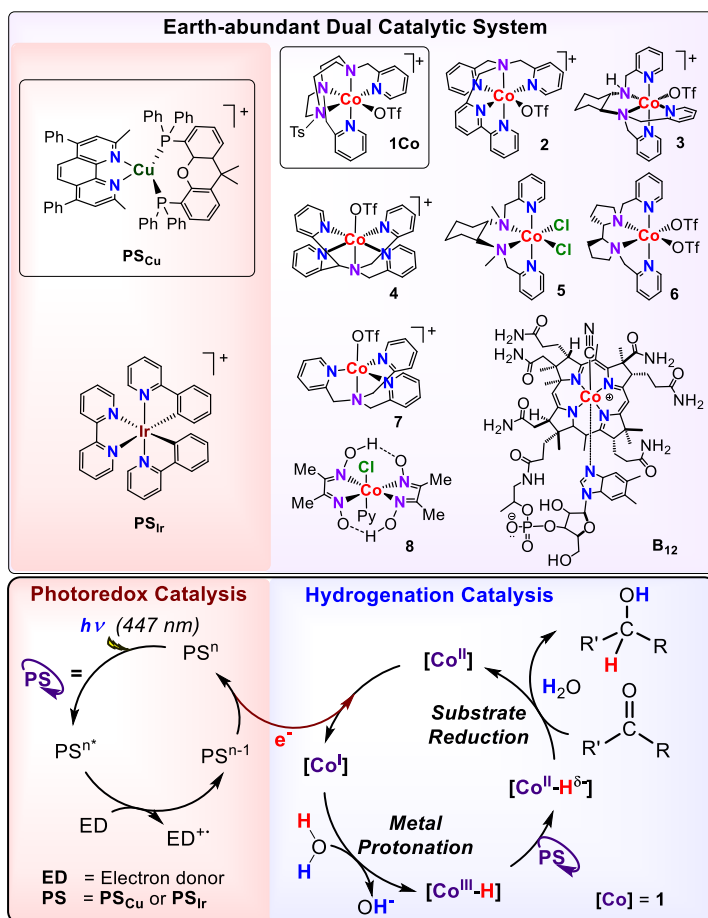
Scheme VIII.2. Earth-abundant Dual Catalytic System for the photoreduction of aromatic ketones and aldehydes.

VIII.2. Results and discussion

VIII.2.1. Synthesis of ligands, complexes, and characterization

The synthesis of the $Py_2^{Ts}tacn$ (1,4-di(picolyl)-7-(p-toluenesulfonyl)-1,4,7-triazacyclononane) ligand was performed following the previously described procedures[83] in excellent yield (94 %) from a direct dialkylation of the monotosylated

1,4,7-triazacyclononane (tacnmt) with two equivalents of 2-(chloromethyl)pyridine hydrochloride (Scheme VIII.3). NMR and elemental analysis characterization confirmed the formation of the desired compound (See Annex section *A.VI.2. Synthesis and of complexes and characterization*). Reaction of Py_2^{Ts}tacn with one equivalent of cobalt(II) triflate $(Co(OTf)_2(MeCN)_2)$ in THF at room temperature yielded complex **1Co** in 83 % yield. Characterization by NMR is in agreement with the formation of a paramagnetic d^7 high-spin Co(II), as previously reported[83] (See Annex section *A.VI.2. Synthesis and of complexes and characterization*).
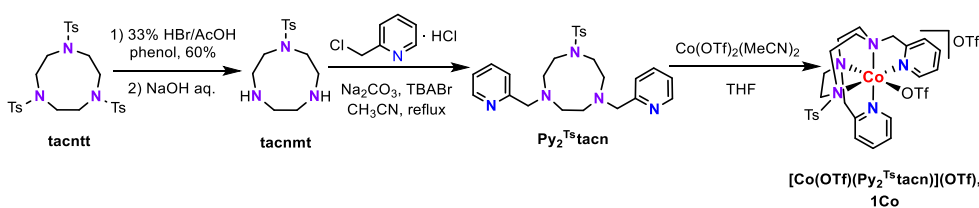
Scheme VIII.3. Synthesis of ligand Py_2^{Ts}tacn and complex **1Co**.

Photoredox catalysts $[Ir(ppy)_2(bpy)]PF_6$ (**PS$_{Ir}$**) and $[Cu(bathocuproine)(Xantphos)]PF_6$ (**PS$_{Cu}$**) were synthesized accordingly to the reported procedures.[85,86]

VIII.2.2. Precedents

For explorative purposes initially, Dr. Arnau **Call** examined the metal-catalyzed light-driven reduction of acetophenone (**9a**) as model substrate under similar conditions to those recently reported by our group for the reduction of water to H_2.[87] Acetophenone (**9a**, 66 mM), $[Co(OTf)(Py_2^{Ts}tacn)](OTf)$ ((Py_2^{Ts}tacn = 1,4-di(picolyl)-7-(*p*-toluenesulfonyl)-1,4,7-triazacyclononane, OTf = trifluoromethanesulfonate anion) (1 mol%) as reduction catalysts, $[Ir(bpy)(ppy)_2](PF_6)$ (**PS$_{Ir}$**, ppy = 2-phenylpyridine) (0.5 mol%) as photoredox catalyst and Et_3N (2.1 equiv.) as electron donor were mixed in a solvent mixture $H_2O:CH_3CN$ (3.5:1.5 mL) and irradiated for 5 h at 447 ± 20 nm using an in-house

developed high throughput photoreactor, which allows for temperature and light intensity control (Figure A.VI.1), yielding 23 % of the reduced alcohol, with quantitative recovery of the ketone **9a** (supporting information Table SI.1.1, entry 1).[88] Further optimization led to maximizing the alcohol yield up to 65% (Table SI.1.1, entry 5).[88] Control experiments demonstrated that all the components are required for the light-driven reduction of acetophenone (**9a**) (see Table SI.1.1, entries 12-14).[88] Moreover, light-dark cycles for the reduction of **9a** showed that the reaction only proceeds during light irradiation (See Figure SI.1.11),[88] this would allow for kinetic studies to get mechanistic information of the system.

An important amount of H_2 was detected in the headspace of the reaction vials. Interestingly, the substrate inhibited the hydrogen evolution. More importantly, the total amount of H_2 + **10a** formed was constant for all **9a** tested concentrations, which suggests competing-pathways with a common intermediate. Control experiments performed by Dr. Call discarded that the photogenerated H_2 is the reducing agent of acetophenone (**9a**) (See Figure SI.1.12).[88] Finally, Hg poisoning experiments did not modify the reaction outcome (61% yield **10a**), suggesting that the main catalytic activity is derived from a molecular system.[88,89]

VIII.2.3. Light-driven hydrogen evolution and ketone reduction activity of representative cobalt complexes. Choosing the right cobalt catalyst.

We hypothesized that the reaction mechanism for cobalt-catalyzed light-driven catalytic reduction of both H_2O and ketones share the same key cobalt-hydride intermediate. Therefore, a series of aminopyridine-based cobalt complexes, known to be active for water reduction, were evaluated for the photocatalytic reduction of **9a**. We studied cobalt complexes with pentadentate (**2-4**)[90-97] and tetradentate (**5-7**)[98-101] chelating nitrogen ligands as well as commercially available cobaloxime **8**[102-104] and vitamin **B₁₂** (Scheme VIII.2). Remarkably, all cobalt complexes (**1-8**) except vitamin **B₁₂** showed photocatalytic activity in the reduction of **9a** (< 0.5 % yield of **10a**) (Table SI.1.3).[88] The observed catalytic activity strongly depends on the nature

UNIVERSITAT ROVIRA I VIRGILI
MECHANISTIC STUDIES OF WATER OXIDATION CATALYZED BY HOMOGENEOUS IRON AND RUTHENIUM
COMPLEXES AND LIGHT-DRIVEN ORGANIC REDUCTIONS WITH A DUAL COBALT/COPPER CATALYTIC SYSTEM
Carla Casadevall Serrano

CHAPTER VIII   Unprecedented Selectivity in Ketone vs Aldehyde Photoreduction

of the cobalt complex employed. For instance, the most efficient complex, **1Co** (65 % yield, initial rate = 0.065 mmol **10a**·h^{-1}) is about 2 fold more reactive than complex **2**. Next, Dr. Call evaluated the selectivity of the reduction of **9a** *vs* water. Without **9a**, all complexes (except vitamin **B$_{12}$**) produced large quantities of H$_2$ under both typical conditions for H$_2$ evolution and our optimized conditions for the reduction of ketones (Figure SI.1.3 and 4). However, in the presence of **9a**, we observed notable differences in the selectivity of **9a** *vs* H$_2$O reduction among the cobalt catalysts tested, which illustrates that selectivity can be tuned by the ligand employed (Figure VIII.2). For instance, cobalt complexes bearing aminopyridine tetradentate ligands offer high selectivity towards H$_2$ evolution (Ratio(H$_2$/**10a**): 3.6–13.9), while pentadentate ones display an excellent selectivity towards the reduction of **9a** (Ratio(**10a**/H$_2$): 1.7 and 0.8 for **1Co** and **2**, respectively). Based on these results a general trend can be derived for each set of complexes: the higher is the ligands' basicity the more active is the catalyst for ketone reduction.

Among the studied complexes, **1Co** is the most active and selective catalyst towards ketone reduction. The observed selectivity is remarkable since [**9a**] (16.5 mM) is about 2500-fold lower than [H$_2$O] (> 40 M) and it is expected that M-H intermediates react very rapidly with water to form H$_2$.

VIII.2.4. Cobalt-Copper Dual Light-Driven Catalytic Reductions

Encouraged by the excellent performance of **1Co** and after further optimization studies performed by Dr. Call, we observed that the combination of complex **1Co** with photoredox catalyst [Cu(bathocuproine)(Xantphos)](PF$_6$) (**PS$_{Cu}$**), previously studied by Beller *et. al*. for the reduction of H$_2$O to H$_2$,[84] substantially improved the yield of alcohol **10a** (92%) (Table SI.1.2, entry 2).[88] In addition, control experiments showed that the reaction does not proceed in the absence of complex **1Co**. Moreover, under these conditions, the photocatalytic ketone reduction is compatible with O$_2$ (Figure A.VI.4), showing the robustness of the dual catalytic system. Indeed, the reduction of **9a** was quantitative when the reaction was carried out under air and in

non-degassed solvents in a crimped vial without headspace. We rationalize the result by the potential capacity of the catalytic system to reduce O_2 to H_2O and the remarkable stability of our catalytic system under air.[87]

With the optimized conditions in hand, a wide range of alkyl aryl ketones can be reduced to the corresponding alcohols by using **1Co** (1 mol%) and **PS$_{Cu}$** (1.5 mol%) in a H_2O:CH_3CN:Et_3N (6:4:0.2 mL) solvent mixture under N_2 and 5 h of irradiation at 447 nm. In general, isolated yields are high (Table 1), but affected by the size of the alkyl group of the ketone. The electronic effects of the substrate influence the reaction as illustrated by the lower alcohol yields observed in the case of electron rich ketones such as **9k** and **9l** (40 and 42 % respectively). The catalytic system developed is selective towards aromatic ketones. Aliphatic ketones, such as cyclohexanone (**9z**) or nonan-2-one (**9aa**) almost do not react (< 5% yield). The developed methodology tolerates fluorine and chlorine substituted aromatic rings (**9s-9x**), which are reduced to the corresponding alcohols (**10s-10x**) in high yields (81-95%) (Table 1). However, brominated substrates such as 4-bromoacetophenone (**9ab**) and 2-bromo-4-methylacetophenone (**9ac**) quantitatively give the dehalogenated products **10a** and **9p**, respectively. The expected reactivity of aromatic ketones under reductive enough photochemical conditions, is the formation of ketyl radical species *via* single electron transfer, which finally dimerize to form pinacols.[38] In this regard, efficient photoredox catalytic protocols for the reductive coupling of aldehydes and ketones have been developed by the groups of Sudo[105] and Rueping.[106] We noted that the formation of pinacols is suppressed for the tested ketones in the presence of cobalt catalyst **1Co**.

Table VIII.1. Light-driven reduction of selected aromatic ketones and aromatic and aliphatic aldehydes.
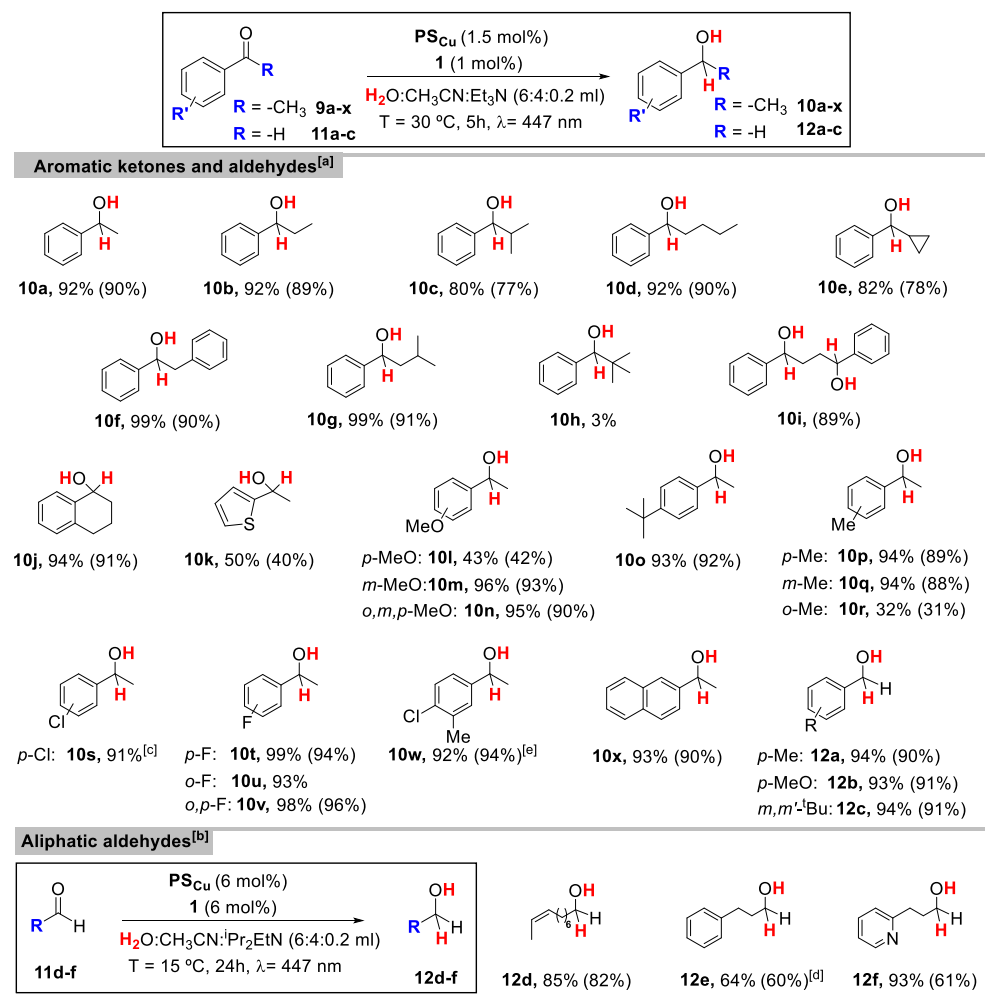
[a] Standard catalytic conditions: **1Co** (1 mol%), **PS$_{Cu}$** (1.5 mol%), Subs. (16.5 mM) in H$_2$O:CH$_3$CN:Et$_3$N (6:4:0.2 mL) irradiated (447 nm) for 5 h at 30 °C under N$_2$. [b]Optimized catalytic conditions: **1Co** (6 mol%), **PS$_{Cu}$** (6 mol%), Subs. (4.4 mM) in H$_2$O:CH$_3$CN:^{i}Pr$_2$EtN (6:4:0.2 mL) irradiated (447 nm) for 24 h at 15 °C under N$_2$. [c] Formation of **10a** was detected (5 % yield). [d]Optimized conditions using 8.7 mM of substrate. Yields after workup (average of triplicates) determined by GC analysis relative to calibrated internal standard. Isolated yields between parentheses (average of 16 reactions).

With the successful results in the reduction of aromatic keotones, mostly performed by Dr. Call, we envisioned that this methodology could be expanded to the reduction of aromatic an aliphatic aldehydes. In the first case, the catalytic dual

293

PS$_{Cu}$/1Co system can be applied for the reduction of aromatic aldehydes **11a-11c**, which are converted to the corresponding alcohols with excellent yields using the same catalytic conditions that for the reduction of ketones (Table VIII.1). On the other hand, aliphatic aldehydes (**11d-f**) were reduced with lower yields when using the same reduction conditions as ketones due to sub product formation and required further optimization (see tables VIII.2 and A.VI.2). Hydrocinnamaldehyde (**11e**) was used as a model substrate for the optimization of the catalytic conditions when using **PS$_{Cu}$** as photoredox catalyst and **1Co** as a catalyst.

We found that using a bulkier electron donor (diisopropylethylamine (DIPEA)), increasing catalyst **1Co** and photoredox catalyst **PS$_{Cu}$** loadings (up to 6%), decreasing the substrate concentration (down to 8.7 mM), and performing the reaction at lower temperature (15ºC), improved the yield of the targeted alcohol **12e** up to 64% (table VIII.2, entry 24). In the case of aliphatic aldehydes, no pinacol products were detected in either the presence or absence of cobalt catalyst. This is in agreement with the significantly lower redox potential of aliphatic aldehydes in comparison to aromatic ones or aromatic ketones.[107] The redox potential of aliphatic aldehydes **11d-f** is lower than -2 V vs SCE under catalytic conditions ($H_2O:CH_3CN:Et_3N$, 6:4:0.2)[108] (< -2.2 V vs SCE[107] in CH_3CN), while the redox potential for ketones and aromatic aldehydes is much higher (E^{red} for **9l** and **12a** are -1.74, and -1.55 V vs SCE, respectively). This serves as evidence that for the electron richest substrates the formation of the ketyl radical is not viable, while for electron poorest substrates should be considered since the redox potential of the **PS$_{Cu}$** is about -1.53 V vs SCE (Figure SI.1.14).[88] This aspect will be further addressed in the mechanistic discussion.

CHAPTER VIII   Unprecedented Selectivity in Ketone vs Aldehyde Photoreduction
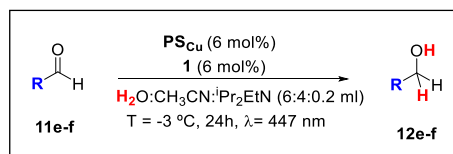
Table VIII.2. Optimization of the catalytic conditions for the photoreduction of **11e**.

Entry	[Subs] (mM)	[PS$_{Cu}$] (mol%)	[1Co] (mol %)	ED	T (ºC)	% Conv.	% alcohol	% dimer	Mass loss
1	16.5	1.5	1	TEA	30	90	23	2	65
2	16.5	1.5	1	DIPEA	30	96	44	2	50
3	8.7	1.5	1	TEA	30	82	23	3	55
4	8.7	1.5	1	DIPEA	30	93	44	3	46
5	16.5	1.5	1	TEA	15	69	13	2	54
6	16.5	1.5	1	DIPEA	15	92	45	2	45
7	8.7	1.5	1	TEA	15	61	11	3	46
8	8.7	1.5	1	DIPEA	15	86	37	2	47
9	16.5	3	3	TEA	30	97	37	2	59
10	16.5	3	3	DIPEA	30	96	47	2	47
11	8.7	3	3	TEA	30	96	36	2	57
12	8.7	3	3	DIPEA	30	97	60	3	34
13	16.5	3	3	TEA	15	79	22	2	55
14	16.5	3	3	DIPEA	15	94	52	1	41
15	8.7	3	3	TEA	15	50	12	3	35
16	8.7	3	3	DIPEA	15	95	57	2	36
17	16.5	6	6	TEA	30	98	46	2	50
18	16.5	6	6	DIPEA	30	96	48	2	47
19	8.7	6	6	TEA	30	97	45	2	50
20	8.7	6	6	DIPEA	30	97	64	2	30
21	16.5	6	6	TEA	15	87	34	1	51
22	16.5	6	6	DIPEA	15	89	38	1	49
23	8.7	6	6	TEA	15	76	30	2	44
24	**8.7**	**6**	**6**	**DIPEA**	**15**	**95**	**64**	**0**	**31**
25	4.4	6	6	DIPEA	15	99	54	0	46
26	8.7	3	3	DIPEA	-3	89	57	0	32
27	8.7	6	6	DIPEA	-3	89	57	0	31
28	4.4	3	3	DIPEA	-3	89	57	0	32
29	4.4	6	6	DIPEA	-3	91	54	0	37

Conditions: **1Co** (% mol), **PS$_{Cu}$** (% mol), substrate (mM) as indicated in the table in H$_2$O:CH$_3$CN:Et$_3$N or H$_2$O:CH$_3$CN:^{i}Pr$_2$EtN (6:4:0.2 mL) irradiated at λ= 447 nm for 5 h at 30 and 15 or for 24 h at -3 ºC under N$_2$. Yields were determined by GC analysis after reaction workup and they are relative to a calibrated internal standard. Values are average of triplicates.

VIII.2.5. Chemoselectivity
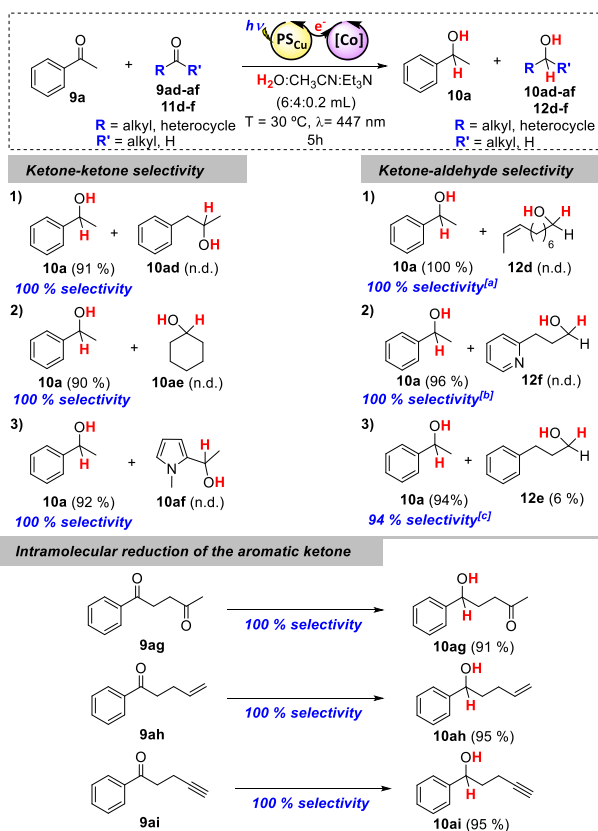
Scheme VIII.4. Competitive photoreductions. Conditions: **1Co** (1 mol%), **PS_Cu** (1.5 mol%), Substrate A + B (16.5 mM, 1:1), in $H_2O:CH_3CN:Et_3N$ (6:4:0.2 mL) irradiated (447 nm) for 5 h at 30 ºC under N_2. [a]35 [b]50 and [c]30 min reaction, respectively. The isolated products were identified and characterized by NMR.

Stoichiometric competition experiments showed that the photocatalytic system is able to reduce acetophenone (**9a**) selectively in the presence of 1-phenylpropan-2-one (**9ad**), cyclohexanone (**9ae**) or 2-acetyl-1-methylpyrrole (**9af**) (Scheme VIII.4). We also carried out competition experiments between **9a** and aliphatic aldehydes (**11d**, **11e** and **11f**) under catalytic conditions for ketone reduction (**1Co** (1 mol%), **PS_Cu** (1.5 mol%), Substrate A + B (16.5 mM, 1:1), in $H_2O:CH_3CN:Et_3N$ (6:4:0.2 mL) irradiated (447 nm) for 5 h at 30 ºC under N_2). Extraordinarily, the aromatic ketone was quantitatively reduced with an excellent unexpected selectivity in all three cases (Scheme VIII.4 and Figure VIII.1). GC monitoring of the reactions showed that **9a** was consumed and converted to **10a**, whereas the aliphatic aldehyde remained

UNIVERSITAT ROVIRA I VIRGILI
MECHANISTIC STUDIES OF WATER OXIDATION CATALYZED BY HOMOGENEOUS IRON AND RUTHENIUM
COMPLEXES AND LIGHT-DRIVEN ORGANIC REDUCTIONS WITH A DUAL COBALT/COPPER CATALYTIC SYSTEM
Carla Casadevall Serrano

CHAPTER VIII   Unprecedented Selectivity in Ketone vs Aldehyde Photoreduction

virtually intact and it did not start to react until the **9a** has been completely reduced (Figure VIII.1 and Figures A.VI.13-30). In addition, this preference for aromatic ketones is extended to aliphatic ketones, aliphatic alkenes and a aliphatic alkynes as showed by the reduction of 1-phenyl-1,4-pentanedione (**9ag**), 1-phenyl-1,4-penten-1-one (**9ah**) and 1-phenyl-4-pentyn-1-one (**9ai**) as model substrates to their corresponding aromatic alcohols (Scheme VIII.4).
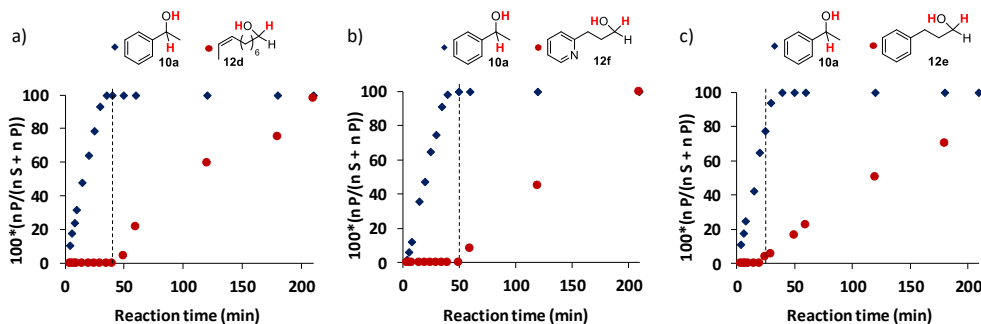
Figure VIII.1. Conditions: **1Co** (1 mol%), **PS$_{Cu}$** (1.5 mol%), total substrate concentration (16.5 mM) in H$_2$O:CH$_3$CN:^{i}Pr$_2$EtN (3:2:0.1 mL) mixture, irradiated at 447 nm for 3.5 h at 30 ºC under N$_2$. The plotted data is the ratio between the amount of the reduced product formed and the sum of the amount of the reduced product formed and the unconverted starting material. The black dotted line indicates where substrates **11d** (a), **11f** (b) and **11e** (c) start reacting.

The selective reduction of aromatic ketones versus highly reactive aliphatic aldehydes is not straightforward. Current methods rely on protection-deprotection steps or on the trapping of the aldehyde by the use of stoichiometric amounts of lanthanide salts.[109-114] The latter methodology is known as the Luche reaction, and the most common conditions are the use of 1 equiv. of CeCl$_3$ and 1.5 equiv. of NaBH$_4$ in EtOH:H$_2$O mixtures at low temperature.[109,110,114] On this basis, we compared the selectivity between our methodology and both the direct reduction with NaBH$_4$ and the Luche reaction, for the reduction of substrates **11e** and **11d** in the presence of **9a** (Scheme VIII.5). As expected, NaBH$_4$ did not yield satisfactory selectivity, however, neither did the Luche reaction, even when using less equivalents of NaBH$_4$ (see Scheme A.VI.1 in the annex for further details). In contrast, the cobalt-copper dual light-driven catalytic reduction affords an excellent selectivity (Schemes VIII.4 and VIII.5).

Scheme VIII.5. Competition experiments. [a] Light-driven conditions: **1Co** (1 mol%), **PS$_{Cu}$** (1.5 mol%), Substrate A + B (16.5 mM, 1:1), in H$_2$O:CH$_3$CN:Et$_3$N (6:4:0.2 mL)irradiated (447 nm) for 5 h at 30 ºC under N$_2$. [b]Luche reaction conditions: **CeCl$_3$·7 H$_2$O** (1 eq molar), **NaBH$_4$** (1.5 eq molar), Substrate A + B (16.5 mM, 1:1), in EtOH:H$_2$O (4:6 mL) for 15 min at 0 ºC under air. The same conditions but with **NaBH$_4$** (0.5 eq molar) are also shown. [c]**NaBH$_4$** (1 eq molar), Substrate A + B (16.5 mM, 1:1), in MeOH (10 mL) for 15 min at rt under air. [d]Analysis after 35 and [e]30 minutes of irradiation. Percentages show the conversions of the substrate from which the product derives, percentages in brackets show the yield of the reduced product.

VIII.2.6. Mechanistic investigations

We performed mechanistic studies based on isotopic labeling, radical clock experiments and computational modeling to rationalize the unique selectivity of the developed dual Cu/Co photocatalytic system and to shed some light on the mechanism of action.

VIII.2.6.1. Isotopic labeling studies

The photocatalytic reduction of several aromatic ketones (substrates **9a**, **9b** and **9j**) and aliphatic aldehyde **11d** with the dual **PS$_{Cu}$/1Co** catalytic system in D$_2$O and

UNIVERSITAT ROVIRA I VIRGILI
MECHANISTIC STUDIES OF WATER OXIDATION CATALYZED BY HOMOGENEOUS IRON AND RUTHENIUM
COMPLEXES AND LIGHT-DRIVEN ORGANIC REDUCTIONS WITH A DUAL COBALT/COPPER CATALYTIC SYSTEM
Carla Casadevall Serrano

CHAPTER VIII   Unprecedented Selectivity in Ketone vs Aldehyde Photoreduction

excess of Et$_3$N enable the incorporation of deuterium atoms in the resulting alcohol products with high yields (Scheme VIII.6). All alcohol products analyzed show nearly quantitative incorporation of deuterium atoms at the carbonyl and its α-position. Incorporation of deuterium at the α-position to the carbonyl is consistent with a keto-enol tautomerization due to the basic reaction conditions as suggested by the black experiments without cobalt. In the case of aliphatic aldehyde **11d**, the incorporation of deuterium atom into the alpha position to the carbonyl group was only about 40%. This is in contrast to the more than 90% incorporation of deuterium at the same position observed for the ketone derivatives.
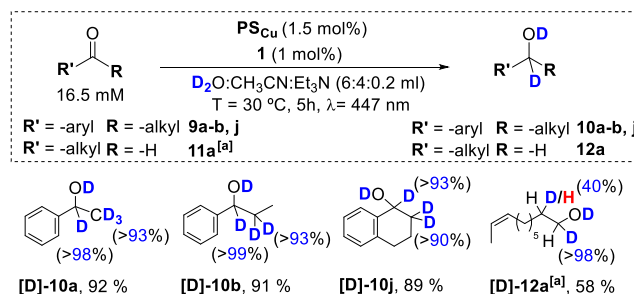
Scheme VIII.6. Deuterium labeling studies of aromatic ketones (**9a-b**, **j**), and aliphatic aldehydes (**11a**). [a] **1Co** (6 mol%), **PS$_{Cu}$** (6 mol%), Substrate (4.4 mM) in D$_2$O:CH$_3$CN:^{i}Pr$_2$EtN (6:4:0.2 mL) irradiated (447 nm) for 24 h at -3 ºC under N$_2$. [b] Conditions [a] modifying [Subs.] to 16.5 mM and 5h at 30 ºC. Isolated yields. [c] NMR yield. Deuterium insertion analyzed by NMR.

VIII.2.6.2. Radical clock experiments

Ketones containing a 2-aryl-cyclopropyl moiety at the *α*-position are commonly used as diagnostic probes for reductions involving a single electron transfer (SET) mechanism. If a SET step is involved, it will trigger cyclopropane ring opening with a rate constant in the range of 10^5-10^7 s^{-1}.[115,116, 117-120] Thus, we evaluated cyclopropyl phenyl ketone **9ai** under reaction conditions with and without cobalt catalyst **1** (Scheme VIII.7) with the aim to unravel mechanistic information of the reduction step.
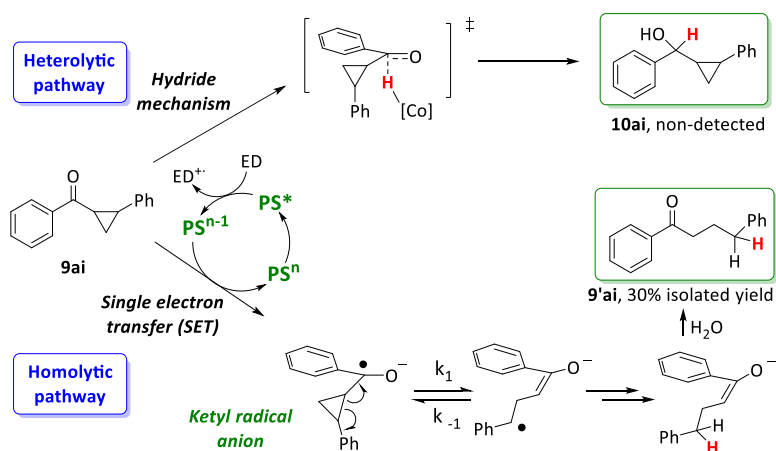
Scheme VIII.7. Possible reduction pathways for **9ai**.

In this regard, the reduction of phenyl cyclopropyl ketone **9ai** forms only the ring-opening product **9'ai** albeit in 30% yield. The same result was obtained in the absence of cobalt catalyst **1Co**. The reaction proceeds *via* a ring opening followed by a HAT from the [Co-H] intermediate to the benzylic radical (homolytic pathway) or by a reduction followed by a protonation. These results suggest that a SET from the photoredox catalyst to the ketone yields the corresponding ketyl radical anion. Indeed, this process is thermodynamically accessible ($\Delta G = 1.6$ kcal·mol^{-1}) since the redox potential of **9ai** is -1.6 V vs SCE and the $E^{1/2}$ of **PS$_{Cu}$** is only about 70 mV lower. This result indicates that, for ketones and aldehydes with similar redox potential the ketyl radical anion can be formed under catalytic conditions. However, these radical clock experiments do not allow for the discrimination between a possible interception of the ketyl radical anions by [Co-H] species via HAT and a possible direct reduction of the carbonyl groups *via* a hydride transfer mechanism.

VIII.2.6.3. DFT Modeling

In order to explain the remarkable selectivity for acetophenone (**9a**) versus water and aldehyde reduction, Dr. Ferran Acuña-Parés computed the free energy barriers associated to the reduction of water and **9a** by the cobalt(II) hydride species (**[1Co^{II}-H]**). Computational studies were conducted with the Gaussian09 software

UNIVERSITAT ROVIRA I VIRGILI
MECHANISTIC STUDIES OF WATER OXIDATION CATALYZED BY HOMOGENEOUS IRON AND RUTHENIUM
COMPLEXES AND LIGHT-DRIVEN ORGANIC REDUCTIONS WITH A DUAL COBALT/COPPER CATALYTIC SYSTEM
Carla Casadevall Serrano

CHAPTER VIII   Unprecedented Selectivity in Ketone vs Aldehyde Photoreduction

package. Geometry optimizations were performed with the B3LYP functional and the 6-31G* 6d basis set for all atoms, including the effect of the solvent (SMD implicit solvent model) and dispersion interactions (Grimme-D_2 correction). A cluster of three water molecules has been introduced into the model to account for hydrogen bonding and the micro-solvation sphere around ketone and water substrates. Free energy values (G) were obtained by including thermal ($G_{corr.}$), solvation ($G_{solv.}$) and dispersion corrections ($E_{disp.}$) to the potential energy computed with the 6-311+G** 6d basis set on equilibrium geometries:

$$G = E_{\text{6-311+G**}} + G_{corr.} + G_{solv.} + E_{disp.} \qquad \text{(VIII.1)}$$

Gibbs energies have also been adjusted to the concentration of all the species as well as to the pH of the reaction. Concentration effects were quantified by computation of the free energy change associated with the conversion from a standard state of 1 atm in gas phase to the desired concentration ($\Delta G^{o/*}$). Thus, the final absolute free energies for each species were evaluated as:

$$G_{final} = G + \Delta G^{o/*} \qquad \text{(VIII.2)}$$

See S.I. 3 for the complete computational details and Figures SI.3.2-3.5 for relevant geometrical data.[88]

Computational modeling supports that under catalytic conditions **[1Co^{II}-H]** species is easily accessible (Figure SI.3.6).[88] As expected, the initial reduction of [**1Co^{II}-NCCH$_3$**] to form [**1Co^{I}-NCCH$_3$**] by the reduced **PS$_{Cu}$**$^-$ is an exergonic process (ΔG = -3.6 kcal·mol^{-1}). Acetonitrile decoordination-protonation of [**1Co^{I}-NCCH$_3$**] to form Co^{III}-H is, under catalytic conditions (pH = 12), endergonic by 9.2 kcal·mol^{-1}, which is in agreement with reported DFT calculations on related cobalt complexes.[4,79,121] Then **[1Co^{III}-H]** can be further reduced in one electron by the reduced photosensitizer (**PS$_{Cu}$**$^-$) to **[1Co^{II}-H]** species. The overall photochemical formation of **[1Co^{II}-H]**, starting from [**1Co^{II}-NCCH$_3$**] and the copper photoredox catalyst (**PS$_{Cu}$**) as reducing agent, is thermodynamically feasible (ΔG = -12.0 kcal·mol^{-1}). It has already been reported that the heterolytic pathway for H$_2$ formation

at Co^{II}-H complexes is the most favored mechanism for cobalt complexes bearing aminopyridine ligands.[4,73,122] In our case, the protonation of the **[1Co^{II}-H]** species under catalytic conditions (pH = 12) has a low energy barrier of 12.2 kcal·mol^{-1}.

At this point, we have calculated two different reaction pathways for the reduction of **9a** starting from **[1Co^{II}-H]** (see Figures SI.3.7-3.10 for complete free energy profiles).[88] First, a hydride transfer from **[1Co^{II}-H]** to the carbonyl group of the ketone was considered (Figure VIII.2). In this mechanism, the interaction between [**1Co^{II}-H**], acetophenone and water molecules has a remarkable free energy cost of 6.4 kcal·mol^{-1}, mainly due to concentration effects. The transition state ($\Delta G^{\ddagger}$ = 11.1 kcal·mol^{-1}) is early since the metal-hydride distance is similar to the [**1Co^{II}-H**] (d(Co-H) = 1.660 Å, d(H-C) = 2.065 Å), and the metal center has a Hirshfeld charge of -0.18 and relevant spin density (Figure VIII.3.A). Finally, the hydride moiety is transferred to the ketone and the resulting negatively charged product is stabilized by an aqueous solvation sphere surrounding the oxygen atom (ΔG = -8.1 kcal·mol^{-1}). The thermodynamically feasible protonation of the alkoxide leads to the final product. For comparative reasons, the hydride transfer mechanism from a Co^{III}-H moiety has also been considered, but a $\Delta G^{\ddagger}$ > 30 kcal·mol^{-1} is obtained due to its reduced hydride character (Figure SI.3.11).[88]

Alternatively, we have explored a homolytic pathway for the ketone reduction. This mechanism starts with a single electron transfer (SET) from the reduced copper photoredox catalyst ($E_{(Exp)}$ (**PS$_{Cu}$**) = -1.53 V vs SCE) to **9a** to give a ketyl radical species (**9a^{ketyl}**), which is then trapped by the **[1Co^{II}-H]** *via* a hydrogen atom transfer (HAT) mechanism (Figure VIII.4). In this regard, DFT calculations indicate that the reduction of **9a** ($E^{o}_{(theoretical)}$ = -1.69 V, $E_{(experimental)}$ = -1.65 V vs. SCE) by **PS$_{Cu}^{-}$** to form **9a^{ketyl}** is slightly endergonic (ΔG = 3.8 kcal·mol^{-1}). Then, the subsequent HAT from Co^{II}-H to the ketyl radical **9a^{ketyl}** occurs through a transition state ($\Delta G^{\ddagger}$ = 18.3 kcal·mol^{-1}, Figure VIII.2) that is higher in free energy than the direct hydride transfer of **[1Co^{II}-H]** to **9a** by 7.2 kcal·mol^{-1}.
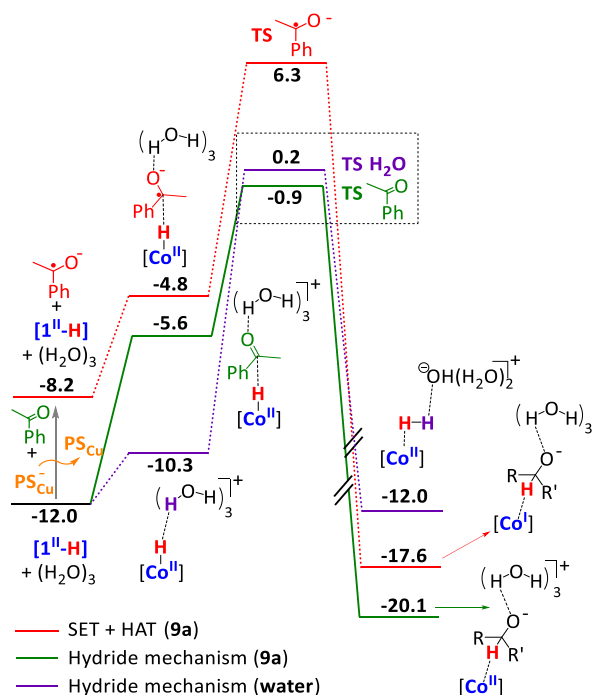
Figure VIII.2. DFT-modeled free energy profiles for the reduction of acetophenone (**9a**) and water with complex **1Co** *via* hydride transfer or homolytic SET-HAT mechanisms. Gibbs energies are in kcal·mol^{-1}.

In the late transition state structure, the transferred hydrogen (ρ(H) = -0.11) is closer to the C-O group (ρ(C-O) = 0.77) than in the previously discussed hydride pathway (d(Co-H) = 1.603 Å and d(H-C) = 1.873 Å). The ketone shows a substantial spin density (Figure VIII.3.B) and is antiferromagnetically coupled to the cobalt, evolving the final alkoxide product and the formal one-electron reduction of the cobalt center (ρ(Co) = 1.61). It has also been considered that the reduction reaction may start with a proton-coupled electron transfer to generate the O-protonated ketyl radical (ΔG = 3.8 kcal·mol^{-1} at pH = 12). However, the total energy barrier for product formation is substantially higher in free energy ($\Delta\Delta G^{\ddagger}$ = 8.4 kcal·mol^{-1}, See Figure SI.3.10).[88]
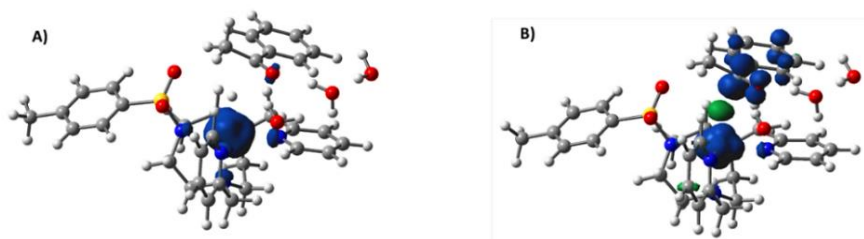
Figure VIII.3. Spin density plots (isovalue = 0.006) of transition states of **A)** hydride transfer to acetophenone and **B)** hydrogen atom transfer to a ketyl radical.

The free energy profiles for ketone and water reduction are in agreement with the observed reactivity. They start with **[1Co^{II}-H]** species as a common intermediate for both reductions. Interestingly, the kinetic barrier of the hydride transfer mechanism for **9a** ($\Delta G^{\ddagger}$ = 11.1 kcal·mol^{-1}) is lower than the one for the water reduction by 1.1 kcal·mol^{-1} (Figures VIII.2 and SI.3.12).[88] This free energy difference is in agreement with the selectivity observed. Indeed, the large water content (> 2500 fold) in comparison to acetophenone (about 15 mM) would explain the similar rates found for H$_2$ evolution and **9a** reduction.[88] However, caution should be taken since DFT calculations may fail to reproduce the electronic structure of Co(I). Therefore, the TS structure of the reaction of Co^{II}-H with the ketyl radical anion (SET+HAT mechanism from Figure VIII.2) could also be poorly described.
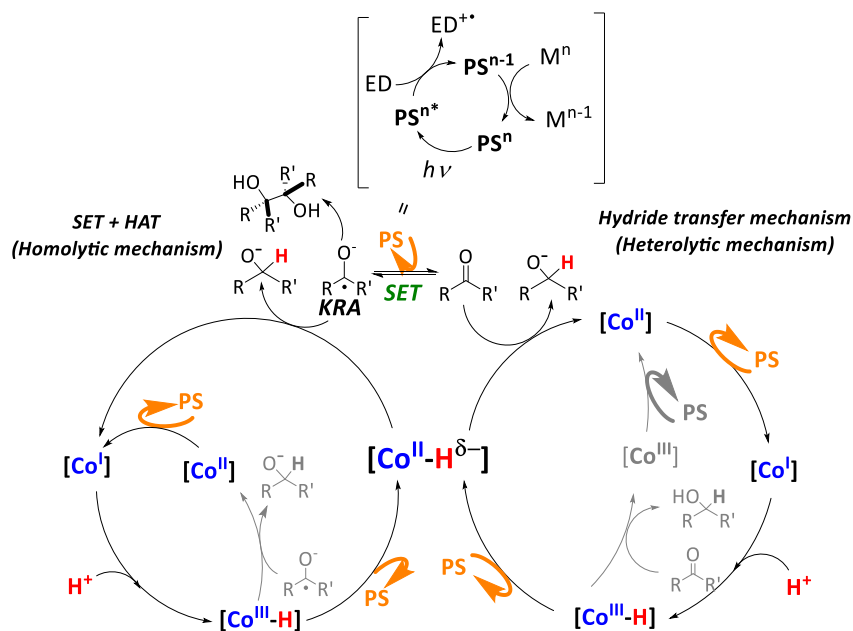
Figure VIII.4. Possible mechanistic scenarios for the photoreduction of aromatic ketones and aldehydes.

As a summary of the mechanistic studies, we propose that both mechanisms can be operative and it will strongly depend on the substrate or substrates present in solution. It is known that under catalytic conditions PS_{Cu} is excited by light (*PS_{Cu}) and reductively quenched by the electron donor (**ED**) to give PS_{Cu}^-,[123] which is reductive enough (E = -1.53 V *vs* SCE) to reduce complex **1Co** (E = -1.35 V *vs* SCE) by one electron.[87] This highly reactive low-valent intermediate, [**1Co^I**], is protonated by water to form the putative [**1Co^{III}-H**], which is easily reduced giving the active [**1Co^{II}-H**] species. Then, two different mechanistic scenarios are postulated for the reduction of ketones and aldehydes to alcohols. On the one hand, a SET-HAT mechanism, in which a single-electron transfer (SET) from PS_{Cu}^- to the substrate generates a carbonyl radical anion intermediate, which is converted into the final product by a hydrogen atom transfer (HAT) from [Co-H] species (homolytic pathway, Figure VIII.4, L*eft*). On the other hand, a direct nucleophilic attack of a putative [**1Co^{II}-H**] intermediate (heterolytic pathway, Figure VIII.4, *Right*) should be considered. Our DFT studies support the heterolytic mechanism. However, the

observed pinacol formation in absence of **1Co**, the selective reduction of acetophenone in the presence of aliphatic aldehydes, as well as the observed ring-opening products in the radical clock experiments support a SET-HAT mechanism, which should therefore be considered as well, especially for those substrates that can be easily reduced. Further studies are ongoing to clarify the feasibility of SET-HAT under our catalytic conditions.

VIII.3. Conclusions

We developed a new methodology based on a dual cobalt-copper (**1Co** and **PS$_{Cu}$**) catalytic system that is able to reduce aromatic ketones and both aromatic and aliphatic aldehydes using H_2O and an amine (Et$_3$N or ^{i}Pr$_2$EtN) as the source of hydrides and visible light as the driving force. Remarkably, the system is highly selective towards the reduction of the organic substrates in the presence of water (> 2000 fold). Moreover, replacement of H_2O by D_2O results in the formation of α,β-deuterated alcohols. Our results show that the selectivity towards the reduction of organic functionalities versus water is catalyst controlled, allowing for further improvements and developments. Moreover, the system presents a unique selectivity for the reduction of acetophenone versus aliphatic aldehydes. Indeed, this selectivity is unprecedented for metal-catalyzed transformations. The present system benefits from avoiding protecting-deprotecting steps and the use of stoichiometric amounts of lanthanides, which are required in other reduction methods of ketones and aldehydes.

Our mechanistic studies and DFT modeling suggest that the well-defined cobalt hydride is a common intermediate in the reduction of both organic substrates and water. Reactivity experiments support a hydride transfer mechanism for substrates with low redox potentials (< -2 V), such as aliphatic aldehydes. Nevertheless, both homolytic and heterolytic pathways could coexist depending on the redox potential of the substrate.

VIII.4. Experimental section

VIII.4.1. Material and Reagents

Reagents and solvents were purchased from commercial sources and used as received unless otherwise stated. Triethylamine and diisopropylethylamine were distilled over potassium hydroxide and stored under argon. Ascorbic acid (AscH) ($\geq$ 99 %) was purchased from Sigma-Aldrich® and used without further purification. Photosensitizers [Ir(bpy)(ppy)$_2$]PF$_6$ (**PS$_{Ir}$**)[124] and [Cu(bathocuproine)(Xantphos)]PF$_6$ (**PS$_{Cu}$**),[125] complexes [Co(OTf)(Py2Tstacn)](OTf) (**1Co**)[87] and [Co(OTf)$_2$(TPA)] (**6**),[126] and ligands N4Py,[127] DPA-Bpy,[128] BpcMe,[129] H-CDPy$_3$[130] and (*S,S*)-PDP[131] were synthesized according to the literature procedures.

Anhydrous acetonitrile was purchased from Sigma-Aldrich® Water (18.2 MΩ·cm) was purified with a Milli-Q Millipore Gradient AIS system. All solvents were degassed by the freeze-pump-thaw method and stored under argon.

VIII.4.2. Instrumentation

Nuclear magnetic resonance (NMR) spectra were recorded on Bruker Fourier300, AV400, AV500 and AVIII500 spectrometers using standard conditions (300 K). All ^{1}H chemical shifts are reported in ppm and have been internally calibrated to the residual protons of the deuterated solvent. The ^{13}C chemical shifts have been internally calibrated to the carbon atoms of the deuterated solvent. The coupling constants were measured in Hz.

Elemental analyses were performed using a CHNS-O EA-1108 elemental analyzer from Fisons.

Mass Spectrometry. Electrospray ionization mass spectrometry (ESI-MS) experiments were performed on a Bruker Daltonics Esquire 3000 Spectrometer using a 1 mM solution of the analyzed compound, by introducing the sample directly into the ESI-source using a syringe. High resolution mass spectra (HRMS) were recorded

on a Bruker MicroTOF-Q IITM instrument with an ESI source at Serveis Tècnics of the University of Girona. Samples were introduced into the mass spectrometer ion source by direct infusion through a syringe pump and were externally calibrated using sodium formate.

Electrochemistry. A standard three-electrode configuration was employed in conjunction with CHI Instruments potentiostat interfaced to a computer with CHI Instruments 600D software. Using one-compartment cell, all cyclic voltammetry experiments were recorded using glassy carbon working electrode which was treated between experiments by means of a sequence of polishing with MicroPolish Powder (0.05 micron) before washing and sonification. Saturated calomel electrode (SCE) and Pt wire were used as reference and counter electrodes respectively.

Gas chromatography analysis. The analysis and quantification of the starting materials and products were carried out on an Agilent 7820A gas chromatograph (HP5 column, 30m or Cyclosil-B column, 30m) and a flame ionization detector. The enantioselectivity was determined by comparison with the pure samples synthesized by the reported procedures.[132]

GC-MS spectral analyses were performed on an Agilent 7890A gas chromatograph interfaced with an Agilent 5975c MS mass spectrometer.

Parallel Pressure Transducer Hardware. The parallel pressure transducer sensors that we used for these studies is the same that was previously reported for the water oxidation studies in our group.[133] This is composed by 8 differential pressure transducers (Honeywell-ASCX15DN, ± 15 psi) connected to a hardware data-acquisition system (base on Atmega microcontroller) controlled by a home-developed software program. The differential pressure transducer Honeywell-ASCX15DN is a 100 microseconds response, signal-conditioned (high-level span, 4.5 V) output, calibrated and temperature compensated (0 ºC to 70 ºC) sensor. The differential sensor has two sensing ports that can be used for differential pressure measurements. The pressure calibrated devices to within ± 0.5 matm was offset and

UNIVERSITAT ROVIRA I VIRGILI
MECHANISTIC STUDIES OF WATER OXIDATION CATALYZED BY HOMOGENEOUS IRON AND RUTHENIUM
COMPLEXES AND LIGHT-DRIVEN ORGANIC REDUCTIONS WITH A DUAL COBALT/COPPER CATALYTIC SYSTEM
Carla Casadevall Serrano

CHAPTER VIII   Unprecedented Selectivity in Ketone vs Aldehyde Photoreduction

span calibrated *via* software with a high precision pressure transducer (PX409-030GUSB, 0.08 % Accuracy). Each of the 8 differential pressure transducers (Honeywell-ASCX15DN, ±15 psi) produce a voltage outputs that can be directly transformed to a pressure difference between the two measuring ports. The voltage outputs were digitalized with a resolution of 0.25 matm from 0 to 175 matm and 1 matm from 176 to 1000 matm using an Atmega microcontroller with an independent voltage auto-calibration. Firmware Atmega microcontroller and control software were home-developed. The sensitivity of H_2 analytics allows for quantification of the gas formed when low H_2 volumes are generated. However, it could not be discarded that small amounts of H_2 were produced by inactive complexes.

Gas chromatography identification and quantification of gases. Gases at the headspace were analyzed with an Agilent 7820A GC System equipped with columns Washed Molecular Sieve 5A, 2m x 1/8'' OD, Mesh 60/80 SS and Porapak Q, 4m x 1/8'' OD, SS. Mesh: 80/100 SS and a Thermal Conductivity Detector. The quantification of the H_2 obtained was measured through the interpolation of a previous calibration using different H_2/N_2 mixtures.

VIII.4.3. Experimental Procedures

General procedure employed in the reaction screening conditions for the light-driven reduction of aromatic ketones (9a-z) and aromatic aldehydes (11a-c). All catalytic reactions were conducted in a 20 mL septum-capped vial under vigorous stirring using an orbital stirrer and irradiating at 447 nm for 5h under nitrogen atmosphere at 30 ºC, unless otherwise indicated. The catalytic assays performed using **PS_{Ir}** (247.5 µM, 1.5 mol%) as photoredox catalyst in $H_2O:CH_3CN:Et_3N$ (8:2:0.2 mL) or (3:7:0.2 mL) reaction mixture, together with the corresponding substrate (16.5 mM) and complex **1Co** (495 µM, 3% mol). Similarly, catalytic reactions carried out using **PS_{cu}** (247.5 µM, 1.5% mol) as photoredox catalyst were performed in a $H_2O:CH_3CN:Et_3N$ (6:4:0.2 mL) reaction mixture that contained the substrate (16.5 mM) and complex **1Co** (165 µM, 1% mol). After

reaction completion, biphenyl was added as internal standard and the crude was quenched by adding 2 mL of CH_2Cl_2. The crude was purified by extraction with CH_2Cl_2 (3 x 3 mL), an aliquot of the organic phase was passed through a plug of $MgSO_4$ which was eluted with AcOEt. This sample was subjected to GC analysis to determine the conversion of **9a-z** or **11a-c$_x$** and the yield of the desired product **10a-z** or **12a-c**. All GC yields reported are an average of at least two runs.

General procedure for the reduction of aliphatic aldehydes (11d-f). All catalytic reactions were conducted in a 20 mL septum-capped vial under vigorous stirring using an orbital stirrer and irradiating at 447 nm for 24h under nitrogen atmosphere at -3ºC, unless otherwise indicated. Catalytic photoreductions were performed in H_2O:CH_3CN:^{i}Pr$_2$EtN (6:4:0.2 mL) reaction solvent mixture, substrate (4.4 mM), **PS$_{Cu}$** (261 μM, 6% mol), **1Co** (261 μM, 6% mol), unless otherwise indicated. A 447 nm LED was employed as light source. Biphenyl was added as internal standard after the reaction and the reaction was quenched by adding 2 mL of AcOEt. The crude reaction mixtures were purified by extraction with AcOEt (1 x 3 mL), the organic layer was passed through a $MgSO_4$ plug which was eluded with more AcOEt. The resulting organic solution was subjected to GC analysis to determine the conversion of **11d-f** and the yield of the desired products **12d-f** respectively. All GC yields reported are an average of at least two runs.

General procedure for product isolation. The light-driven photocatalytic reductions of targeted substrates were carried out under the optimized conditions described above. The crude mixtures of at least 16 independent reactions (equally prepared) for each compound were combined and extracted with CH_2Cl_2 (3 x 40 mL). Organic fractions were combined, dried over $MgSO_4$ and the solvent removed under reduced pressure. The resulting crude oil was purified by silica gel column chromatography with Hexane/AcOEt (9:1) to obtain the desired reduced product and the isolated yields reported are an average of at least 16 reactions.

UNIVERSITAT ROVIRA I VIRGILI
MECHANISTIC STUDIES OF WATER OXIDATION CATALYZED BY HOMOGENEOUS IRON AND RUTHENIUM
COMPLEXES AND LIGHT-DRIVEN ORGANIC REDUCTIONS WITH A DUAL COBALT/COPPER CATALYTIC SYSTEM
Carla Casadevall Serrano

CHAPTER VIII   Unprecedented Selectivity in Ketone vs Aldehyde Photoreduction

General procedure for the competition studies between acetophenone (9a) and aliphatic aldehydes (11d-e) following the Luche reaction reported conditions.[109,110,114] Catalytic reductions were performed in H_2O:EtOH (6:4 mL) reaction solvent mixture, equimolar amounts of both substrates A:B were used (8.7 mM each, total concentration 16.5 mM), $CeCl_3 \cdot 7H_2O$ (1 equivalent) and $NaBH_4$ (1.5 equivalents), unless otherwise indicated. All catalytic reactions were conducted in a 15 mL capped-vial under vigorous stirring for 15 minutes at 0ºC, unless otherwise indicated. To the equimolar mixture of substrates (ketone + aliphatic aldehyde) in H_2O:EtOH (6:4 mL), 1 equivalent of $CeCl_3 \cdot 7H_2O$ was added at r.t. and the reaction mixture was cooled down to 0 ºC. Then, 1.5 equivalents of $NaBH_4$ were added and the reaction was left stirring for 15 min at 0 ºC. Biphenyl was added as internal standard after the reaction and the reaction was quenched by adding 2 mL of acetone. Dilution with 2 ml of Brine solution and extractions with Et_2O, afforded the reaction products after the organic layer was passed through a $MgSO_4$ plug which was eluded with more Et_2O. The resulting organic solution was subjected to GC analysis to determine the conversion of **9a** and **11d/e** and the yield of the desired products **10a** and **12d/f** respectively. All GC yields reported are an average of at least two runs.

Gas-evolution monitoring studies. Each experiment was conducted in a 20 mL volume-calibrated-vial caped with a septa equipped with stir-bars and containing the solvent mixture and reagents. Each reaction vial was connected to one of the ports of a differential pressure transducer sensor (Honeywell-ASCX15DN) and the other port to a reference reaction. Reference reactions, have all components of the reaction except the catalyst. The reaction and reference vials are kept under the same experimental conditions to compensate the noise due to temperature-pressure fluctuations. In order to ensure a constant and stable irradiation, the LED sources were equipped with a water refrigeration system. This is composed for a refrigerated aluminum block by a Huber cryothermostat (refrigeration system, Minichiller -40ºC-20ºC). This block is shaken by an Orbital Shaker (IKA KS 260 Basic Package) which provides the agitation of the reaction vessels during the irradiation time. The

UNIVERSITAT ROVIRA I VIRGILI
MECHANISTIC STUDIES OF WATER OXIDATION CATALYZED BY HOMOGENEOUS IRON AND RUTHENIUM
COMPLEXES AND LIGHT-DRIVEN ORGANIC REDUCTIONS WITH A DUAL COBALT/COPPER CATALYTIC SYSTEM
Carla Casadevall Serrano

CHAPTER VIII   Unprecedented Selectivity in Ketone vs Aldehyde Photoreduction

aluminum block accommodates 16 vials (20 mL) capped with septum in which the reaction takes place. Each vial is submitted and located over a LED irradiation source (Royal-Blue Rebel LEDs ($\lambda = 447\pm20$ nm). The reaction began when the LEDs were turned on. At this point, the hydrogen evolved from the reactions was monitored by recording the increase in pressure of the headspace (1 second interval). The pressure increment is the result of the difference in pressure between the reaction and reference vials. After the hydrogen evolution reached a plateau the amount of the gas formed was measured equilibrating the pressure between reaction and reference vials. The gases at the headspace of the reaction vials and references in each of the reactions were quantified by the analysis of an aliquot of gas at the headspace (0.2 mL) by gas chromatography.

Procedure for the reduction of acetophenone (9a) in the presence of O_2. All catalytic reactions were conducted in a 20 mL septum-capped vial under vigorous stirring using an orbital stirrer and irradiating at 447 nm for 5 h at 30ºC under an atmosphere of $N_2:O_2$ of known ratio. The reactions contained **PS$_{cu}$** (247.5 μM, 1.5% mol), **1Co** (165 μM, 1% mol) and **9a** (16.5 mM) in $H_2O:CH_3CN:Et_3N$ (6:4:0.2 mL) solvent mixture and were prepared under N_2 atmosphere. Before irradiation, a known O_2 aliquot was introduced into the head space of the reaction vial with a Hamilton gas-tight syringe through the septa. The mixture was vigorously shaken during 5 min to dissolve the O_2 into the solution. Then, after 5 h of irradiation, biphenyl (16 μmol) was added as internal standard and the reaction crude was quenched with 2 mL of CH_2Cl_2. The crude was purified by extraction with CH_2Cl_2 (3 x 3 mL). An aliquot of the organic phase was passed through a plug of $MgSO_4$ and eluted with AcOEt. The conversion and yield were determined with GC analysis. All GC yields reported are an average of at least two runs.

When using **PS$_{Ir}$** (247.5 μM, 1.5 mol%) as photoredox catalyst, the reactions were performed like in the case of **PS$_{Cu}$** but with the following modification in the

reaction mixture: $H_2O:CH_3CN:Et_3N$ (8:2:0.2 mL) reaction mixture, together with substrate **9a** (16.5 mM) and complex **1Co** (495 μM, 3% mol).

Procedure for the reduction of acetophenone (9a) with non-degassed solvents prepared outside the glovebox under air exposition. All catalytic reactions were conducted in a 10 mL septum-capped vial with negligible head space under vigorous stirring using an orbital stirrer and irradiating at 447 nm for 24 h under air atmosphere at 30ºC. The reactions were carried out in a non-degased $H_2O:CH_3CN:Et_3N$ (3.6:2.4:0.12 mL) reaction mixture containing **9a** (16.5 mM), **1Co** (165 μM, 1% mol) and PS_{Cu} (247.5 μM, 1.5% mol). The reaction vials were fully filled minimizing the head space of the reaction mixture. After reaction completion, biphenyl (16 μmol) was added as internal standard and the crude was quenched by adding 2 mL of CH_2Cl_2. The crude was purified by extraction with CH_2Cl_2 (3 x 3 mL), an aliquot of the organic phase was passed through a plug of $MgSO_4$ which was eluted with AcOEt. The conversion and yield were determined with GC analysis. All GC yields reported are an average of at least two runs. The estimated concentration of O_2 in solution is about 1 mM (6 eq. regarding **1Co**).

When using PS_{Ir} (247.5 μM, 1.5 mol%), the reactions were performed like in the case of PS_{Cu} but with the following modification in the reaction mixture: $H_2O:CH_3CN:Et_3N$ (4.8:1.2:0.12 mL) reaction mixture, together with substrate **9a** (16.5 mM) and complex **1Co** (495 μM, 3% mol). The estimated concentration of O_2 in solution is about 1 mM (2 eq. regarding **1**).

VIII.4.4. Computational details

In this case, the DFT calculations were performed by Dr. Ferran Acuña-Parés, further information about the Cartesian coordintes can be found in the *SI_3_ComputaitonalMethods* in the publication[88] and in the Annex (*A.VI.12. Computaitonal studies*).

The DFT quantum mechanical exploration of ketone and water reduction mechanisms was carried out using the Gaussian09 program.[134] Geometry optimizations were performed in the unrestricted spin formalism, with the B3LYP hybrid exchange-correlation functional[135-137] and the standard 6-31G* 6d basis set for all atoms. An extra quadratic convergent SCF step was added when the first-order SCF did not converge ("scf=xqc" keyword). The solvation effect of water was introduced in geometry optimizations and energy through the IEFPCM-SMD polarizable continuum model.[138] Dispersion effects were also included using the Grimme D_2 correction.[139] The geometries have been edited with the Chemcraft program.[140]

The located stationary points were characterized by analytical frequency calculations at the same level of theory than geometry optimizations. Gibbs energy values (G) were obtained by including thermal, solvation and Grimme corrections to the potential energy computed with the 6-311+G** 6d basis set on equilibrium geometries:

$$G = E_{6\text{-}311+G^{**}} + G_{corr.} + G_{solv.} + E_{disp.} \qquad \text{(VIII.3)}$$

where the thermal correction ($G_{corr.}$) was obtained from gas phase analytical Hessians calculations at 298.15 K, the solvation energy ($G_{solv.}$) was calculated as the difference of the total free energy in gas phase and in water at the same level of theory and geometry and $E_{disp.}$ is the dispersion correction.

A cluster of three water molecules $(H_2O)_3$ is employed to model the H-H bond formation event and the microsolvation sphere around the organic substrates. Hirshfeld charges[141,142] were computed to rationalize the reactivity trends of Co-H species.

VIII.4.4.1. Protonation and redox reactions

The standard dissociation free energy change between an acid (AH) and its conjugate base (A⁻) in aqueous (ΔG*) may be expressed as:[143]

$$\Delta G^* = G(A^-_{aq}) + G(H^+_{aq}) - G(AH_{aq}) + \Delta G^{o}_* \qquad (VIII.4)$$

$$G(H^+_{aq}) = G(H^+_{gas}) + \Delta G^{H+}_{solv} \qquad (VIII.5)$$

where $G(AH_{aq})$ and $G(A^-_{aq})$ are standard free energies of the acid and its conjugate base in aqueous media, respectively. The $G(H^+_{aq})$ is the free energy of the proton in water, obtained from the experimental solvation free energy ($\Delta G^{H+}_{solv} = -265.9 \text{ kcal} \cdot \text{mol}^{-1}$)[143] and its gas-phase free energy ($G(H^+_{gas}) = -6.3 \text{ kcal} \cdot \text{mol}^{-1}$). $\Delta G^{o/*}$ is the free energy change associated with the conversion from a standard state of 1 M in the aqueous phase and 1 atm in gas phase, to the desired concentration in both phases. ΔG^* values are derived with the following expression:

$$\Delta G^{o/*} = RT \ln(24.4 * c) \qquad (VIII.6)$$

where R is the universal gas constant (1.987 cal·mol⁻¹·K⁻¹), T is the temperature in Kelvin and c the concentration in mol·L⁻¹. In the free energy balances the following concentrations were used to adjust the final free energies: 16.5 mM for acetophenone, 10^{-12} M for protons (due to the pH ≈ 12), 33.4 M for water and 7.6 M for acetonitrile (the concentrations of water and acetonitrile were derived from the 6:4 H_2O:CH_3CN solvent mixture used in catalysis). The previous concentrations translate into $\Delta G^{o/*}$ values (at 298.15 K) of -0.54 kcal·mol⁻¹ for acetophenone substrate, -14.5 kcal·mol⁻¹ for protons, 4.0 kcal·mol⁻¹ for water and 3.1 kcal·mol⁻¹ for acetonitrile. The concentration correction for a $(H_2O)_n$ water cluster can be derived with the formula 4.0/n kcal·mol⁻¹,[144] with a $\Delta G^{o/*}$ value of 1.33 kcal·mol⁻¹ when n = 3.

The standard one electron redox potentials relative to the SHE electrode were calculated by:

$$E^o = -\frac{\Delta G^0 - \Delta G_{SHE}}{F} \qquad (VIII.7)$$

where ΔG^0 is the standard free energy change associated with the reduction reaction, F is the Faraday constant (23.061 kcal·mol⁻¹V⁻¹) and ΔG_{SHE} is the free energy change associated with the proton reduction to H_2 (-4.24 eV). The

ΔG_{SHE} value was derived using the Fermi-Dirac statistics for the treatment of electron thermodynamics.[145,146]

Energetics for the reduction steps were calculated considering the experimental redox potential of the copper photosensitizer relative to the SHE electrode (E(**PS$_{Cu}$**) = -1.29 V vs. SHE). The reduction of an acetophenone molecule to the corresponding protonated ketyl radical supposes an energetic cost of 3.8 kcal·mol^{-1}. Taking into account the previous value, the relationship $\Delta G^{o} = -RTln(K)$ and a 16.5 mM for acetophenone, we derived a ketyl radical concentration of 27.5 µM, with a $\Delta G^{o/*}$ value of -4.3 kcal·mol^{-1}. The same values are obtained for the O-protonated ketyl radical at pH = 12.

VIII.5. References

(1) Simmons, T. R.; Berggren, G.; Bacchi, M.; Fontecave, M.; Artero, V. *Coord. Chem. Rev.* **2014**, *270-271*, 127.
(2) Zee, D. Z.; Chantarojsiri, T.; Long, J. R.; Chang, C. J. *Acc. Chem. Res.* **2015**, *48*, 2027.
(3) Kaeffer, N.; Chavarot-Kerlidou, M.; Artero, V. *Acc. Chem. Res.* **2015**, *48*, 1286.
(4) Queyriaux, N.; Jane, R. T.; Massin, J.; Artero, V.; Chavarot-Kerlidou, M. *Coord. Chem. Rev.* **2015**, *304-305*, 3.
(5) Wang, M.; Chen, L.; Sun, L. *Energy & Environmental Science* **2012**, *5*, 6763.
(6) McKone, J. R.; Marinescu, S. C.; Brunschwig, B. S.; Winkler, J. R.; Gray, H. B. *Chem. Sci.* **2014**, *5*, 865.
(7) Han, Z.; Eisenberg, R. *Acc. Chem. Res.* **2014**, *47*, 2537.
(8) Thoi, V. S.; Sun, Y.; Long, J. R.; Chang, C. J. *Chem. Soc. Rev.* **2013**, *42*, 2388.
(9) Eckenhoff, W. T.; Eisenberg, R. *Dalton Trans.* **2012**, *41*, 13004.
(10) Rakowski DuBois, M.; DuBois, D. L. *Chem. Soc. Rev.* **2009**, *38*, 62.
(11) Du, P.; Eisenberg, R. *Energy & Environmental Science* **2012**, *5*, 6012.
(12) Appel, A. M.; Bercaw, J. E.; Bocarsly, A. B.; Dobbek, H.; DuBois, D. L.; Dupuis, M.; Ferry, J. G.; Fujita, E.; Hille, R.; Kenis, P. J.; Kerfeld, C. A.; Morris, R. H.; Peden, C. H.; Portis, A. R.; Ragsdale, S. W.; Rauchfuss, T. B.; Reek, J. N.; Seefeldt, L. C.; Thauer, R. K.; Waldrop, G. L. *Chem. Rev.* **2013**, *113*, 6621.
(13) Izumi, Y. *Coord. Chem. Rev.* **2013**, *257*, 171.
(14) Schneider, J.; Jia, H.; Muckerman, J. T.; Fujita, E. *Chem. Soc. Rev.* **2012**, *41*, 2036.
(15) Monos, T. M.; Sun, A. C.; McAtee, R. C.; Devery, J. J., 3rd; Stephenson, C. R. *J. Org. Chem.* **2016**, *81*, 6988.
(16) Takeda, H.; Ishitani, O. *Coord. Chem. Rev.* **2010**, *254*, 346.
(17) Windle, C. D.; Perutz, R. N. *Coord. Chem. Rev.* **2012**, *256*, 2562.
(18) Qiao, J.; Liu, Y.; Hong, F.; Zhang, J. *Chem. Soc. Rev.* **2014**, *43*, 631.
(19) Costentin, C.; Robert, M.; Saveant, J. M. *Chem. Soc. Rev.* **2013**, *42*, 2423.
(20) Cook, T. R.; Dogutan, D. K.; Reece, S. Y.; Surendranath, Y.; Teets, T. S.; Nocera, D. G. *Chem. Rev.* **2010**, *110*, 6474.
(21) Joya, K. S.; Joya, Y. F.; Ocakoglu, K.; van de Krol, R. *Angew. Chem.* **2013**, *52*, 10426.
(22) Barber, J.; Tran, P. D. *J. R. Soc. Interface* **2013**, *10*, 20120984.
(23) Andreiadis, E. S.; Chavarot-Kerlidou, M.; Fontecave, M.; Artero, V. *Photochemistry and Photobiology* **2011**, *87*, 946.
(24) Lewis, N. S.; Nocera, D. G. *Proceedings of the National Academy of Sciences of the United States of America* **2006**, *103*, 15729.
(25) Rau, S.; Walther, D.; Vos, J. G. *Dalton. Trans.* **2007**, 915.

UNIVERSITAT ROVIRA I VIRGILI
MECHANISTIC STUDIES OF WATER OXIDATION CATALYZED BY HOMOGENEOUS IRON AND RUTHENIUM
COMPLEXES AND LIGHT-DRIVEN ORGANIC REDUCTIONS WITH A DUAL COBALT/COPPER CATALYTIC SYSTEM
Carla Casadevall Serrano

CHAPTER VIII   Unprecedented Selectivity in Ketone vs Aldehyde Photoreduction

(26) Choudhury, S.; Baeg, J. O.; Park, N. J.; Yadav, R. K. *Angew. Chem. Int. Ed.* **2012**, *51*, 11624.

(27) Lee, S. H.; Kim, J. H.; Park, C. B. *Chem. Eur. J.* **2013**, *19*, 4392

(28) Mifsud, M.; Gargiulo, S.; Iborra, S.; Arends, I. W.; Hollmann, F.; Corma, A. *Nature Commun.* **2014**, *5*, 3145.

(29) Kim, J. H.; Nam, D. H.; Park, C. B. *Current Opinion in Biotechnology* **2014**, *28*, 1.

(30) Liu, J.; Huang, J.; Zhou, H.; Antonietti, M. *ACS Appl. Mater. Interf.* **2014**, *6*, 8434.

(31) Bachmeier, A.; Murphy, B. J.; Armstrong, F. A. *J. Am. Chem. Soc.* **2014**, *136*, 12876.

(32) Palmisano, G.; Augugliaro, V.; Pagliaro, M.; Palmisano, L. *Chem. Commun.* **2007**, 3425.

(33) Galian, R. E.; Pérez-Prieto, J. *Energy & Environmental Science* **2010**, *3*, 1488.

(34) Macia-Agullo, J. A.; Corma, A.; Garcia, H. *Chem. Eur. J.* **2015**, *21*, 10940.

(35) Ghosh, T.; Slanina, T.; König, B. *Chem. Sci.* **2015**, *6*, 2027.

(36) Joyce-Pruden, C.; Pross, J. K.; Li, Y. *J. Org. Chem.* **1992**, *57*, 5087.

(37) Yanagida, S.; Yoshiya, M.; Shiragami, T.; Pac, C.; Mori, H.; Fujita, H. *J. Phys. Chem.* **1990**, *94*, 3104.

(38) *Photocatalytic Hydrogenation on Semiconductor Particles*; Kohtani, S.; Yoshioka, E.; Miyabe, H., Eds.; InTech, Chapters published 2012.

(39) Füldner, S.; Mild, R.; Siegmund, H. I.; Schroeder, J. A.; Gruber, M.; König, B. *Green Chemistry* **2010**, *12*, 400.

(40) Ke, X.; Sarina, S.; Zhao, J.; Zhang, X.; Chang, J.; Zhu, H. *Chemical Communications (Cambridge, United Kingdom)* **2012**, *48*, 3509.

(41) Yanagida, S.; Ishimaru, Y.; Miyake, Y.; Shiragami, T.; Pac, C.; Hashimoto, K.; Sakata, T. *J. Phys. Chem.* **1989**, *93*, 2576.

(42) Kohtani, S.; Kurokawa, T.; Yoshioka, E.; Miyabe, H. *Applied Catalysis A: General* **2016**, *521*, 68.

(43) Ke, X.; Zhang, X.; Zhao, J.; Sarina, S.; Barry, J.; Zhu, H. *Green Chemistry* **2013**, *15*, 236.

(44) Zhang, M.; Rouch, W. D.; McCulla, R. D. *Eur. J. Org. Chem.,* **2012**, *2012*, 6187.

(45) Choudhury, S.; Baeg, J.-O.; Park, N.-J.; Yadav, R. K. *Green Chemistry* **2014**, *16*, 4389.

(46) Zhong, J.-J.; Liu, Q.; Wu, C.-J.; Meng, Q.-Y.; Gao, X.-W.; Li, Z.-J.; Chen, B.; Tung, C.-H.; Wu, L.-Z. *Chemical Communications (Cambridge, United Kingdom)* **2016**, *52*, 1800.

(47) Liu, X.; Sun, D.; Yuan, R.; Fu, X.; Li, Z. *J. Catal.* **2013**, *304*, 1.

(48) Li, J.; Yang, J.; Wen, F.; Li, C. *Chem. Commun.* **2011**, *47*, 7080.

(49) Shimakoshi, H.; Hisaeda, Y. *ChemPlusChem* **2014**, *79*, 1250.

(50) Lang, X.; Zhao, J.; Chen, X. *Chem. Soc. Rev.* **2016**, *45*, 3026.

(51) Larsen, C. B.; Wenger, O. S. *Chem. Eur. J.* **2018**, *24*, 2039.

(52) Bleith, T.; Gade, L. H. *J. Am. Chem. Soc.* **2016**, *138*, 4972.

(53) Bleith, T.; Wadepohl, H.; Gade, L. H. *J. Am. Chem. Soc.* **2015**, *137*, 2456.

(54) Jochmann, P.; Stephan, D. W. *Angew. Chem. Int. Ed.* **2013**, *52*, 9831.

(55) Xu, R.; Chakraborty, S.; Bellows, S. M.; Yuan, H.; Cundari, T. R.; Jones, W. D. *ACS Catal.* **2016**, *6*, 2127.

(56) Gorgas, N.; Stöger, B.; Veiros, L. F.; Kirchner, K. *ACS Catal.* **2016**, *6*, 2664.

(57) Elangovan, S.; Wendt, B.; Topf, C.; Bachmann, S.; Scalone, M.; Spannenberg, A.; Jiao, H.; Baumann, W.; Junge, K.; Beller, M. *Adv. Synth. Catal.* **2016**, *358*, 820.

(58) Bornschein, C.; Werkmeister, S.; Wendt, B.; Jiao, H.; Alberico, E.; Baumann, W.; Junge, H.; Junge, K.; Beller, M. *Nat. Commun.* **2014**, *5*, 4111.

(59) Alberico, E.; Sponholz, P.; Cordes, C.; Nielsen, M.; Drexler, H. J.; Baumann, W.; Junge, H.; Beller, M. *Angew. Chem. Int. Ed.* **2013**, *52*, 14162.

(60) Chakraborty, S.; Leitus, G.; Milstein, D. *Chemical Communications (Cambridge, United Kingdom)* **2016**, *52*, 1812.

(61) Butschke, B.; Feller, M.; Diskin-Posner, Y.; Milstein, D. *Catal. Sci. Technol.* **2016**.

(62) Zell, T.; Ben-David, Y.; Milstein, D. *Catal. Sci. Technol.* **2015**, *5*, 822.

(63) Zell, T.; Milstein, D. *Acc. Chem. Res.* **2015**, *48*, 1979.

(64) Morris, R. H. *Acc. Chem. Res.* **2015**, *48*, 1494.

(65) Elangovan, S.; Topf, C.; Fischer, S.; Jiao, H.; Spannenberg, A.; Baumann, W.; Ludwig, R.; Junge, K.; Beller, M. *J. Am. Chem. Soc.* **2016**, *138*, 8809.

(66) Bullock, R. M. *Science* **2013**, *342*, 1054.

(67) Pellissier, H.; Clavier, H. *Chem. Rev.* **2014**, *114*, 2775.

(68) Jagadeesh, R. V.; Surkus, A.-E.; Junge, H.; Pohl, M.-M.; Radnik, J.; Rabeah, J.; Huan, H.; Schünemann, V.; Brückner, A.; Beller, M. *Science* **2013**, *342*, 1073.

(69) Kallmeier, F.; Irrgang, T.; Dietel, T.; Kempe, R. *Angew. Chem. Int. Ed.* **2016**.

(70) Le Bailly, B. A. F.; Thomas, S. P. *RSC Advances* **2011**, *1*, 1435.

(71) Ager, D. J.; de Vries, A. H.; de Vries, J. G. *Chem. Soc. Rev.* **2012**, *41*, 3340.

(72) de Vries, J. G.; Elsevier, C. J. *The Handbook of Homogeneous Hydrogenation*, 2007.

(73) Dempsey, J. L.; Brunschwig, B. S.; Winkler, J. R.; Gray, H. B. *Acc. Chem. Res.* **2009**, *42*, 1995.

(74) Artero, V.; Chavarot-Kerlidou, M.; Fontecave, M. *Angew. Chem. Int. Ed.* **2011**, *50*, 7238.

(75) Eckenhoff, W. T.; McNamara, W. R.; Du, P.; Eisenberg, R. *Biochim. Biophys. Acta* **2013**, *1827*, 958.

(76) Lo, W. K.; Castillo, C. E.; Gueret, R.; Fortage, J.; Rebarz, M.; Sliwa, M.; Thomas, F.; McAdam, C. J.; Jameson, G. B.; McMorran, D. A.; Crowley, J. D.; Collomb, M. N.; Blackman, A. G. *Inorganic Chemistry* **2016**, *55*, 4564.

(77) Moonshiram, D.; Gimbert-Surinach, C.; Guda, A.; Picon, A.; Lehmann, C. S.; Zhang, X.; Doumy, G.; March, A. M.; Benet-Buchholz, J.; Soldatov, A.; Llobet, A.; Southworth, S. H. *J. Am. Chem. Soc.* **2016**, *138*, 10586.

(78) Smolentsev, G.; Cecconi, B.; Guda, A.; Chavarot-Kerlidou, M.; van Bokhoven, J. A.; Nachtegaal, M.; Artero, V. *Chem . Eur. J.* **2015**, *21*, 15158.

(79) Artero, V.; Fontecave, M. *Coord. Chem. Rev.* **2005**, *249*, 1518.

(80) Losse, S.; Vos, J. G.; Rau, S. *Coord. Chem. Rev.* **2010**, *254*, 2492.

(81) Varma, S.; Castillo, C. E.; Stoll, T.; Fortage, J.; Blackman, A. G.; Molton, F.; Deronzier, A.; Collomb, M. N. *Phys. Chem. Chem. Phys.* **2013**, *15*, 17544.

(82) Lewandowska-Andralojc, A.; Baine, T.; Zhao, X.; Muckerman, J. T.; Fujita, E.; Polyansky, D. E. *Inorganic Chemistry* **2015**, *54*, 4310.

(83) Call, A.; Codola, Z.; Acuna-Pares, F.; Lloret-Fillol, J. *Chemistry* **2014**, *20*, 6171.

(84) Luo, S. P.; Mejia, E.; Friedrich, A.; Pazidis, A.; Junge, H.; Surkus, A. E.; Jackstell, R.; Denurra, S.; Gladiali, S.; Lochbrunner, S.; Beller, M. *Angew. Chem. Int. Ed.* **2013**, *52*, 419.

(85) Cline, E. D.; Adamson, S. E.; Bernhard, S. *Inorganic Chemistry* **2008**, *47*, 10378.

(86) Luo, S.-P.; Mejía, E.; Friedrich, A.; Pazidis, A.; Junge, H.; Surkus, A.-E.; Jackstell, R.; Denurra, S.; Gladiali, S.; Lochbrunner, S.; Beller, M. *Angew. Chem. Int. Ed.* **2013**, *52*, 419.

(87) Call, A.; Codolà, Z.; Acuña-Parés, F.; Lloret-Fillol, J. *Chem. Eur. J.* **2014**, *20*, 6171.

(88) Call, A.; Casadevall, C.; Acuña-Parés, F.; Casitas, A.; Lloret-Fillol, J. *Chemical Science* **2017**, *8*, 4739.

(89) Artero, V.; Fontecave, M. *Chem. Soc. Rev.* **2013**, *42*, 2338.

(90) Dossing, A.; Engberg, P.; Hazell, R. *Inorg. Chim. Acta* **1998**, *268*, 159.

(91) Singh, W. M.; Baine, T.; Kudo, S.; Tian, S.; Ma, X. A. N.; Zhou, H.; DeYonker, N. J.; Pham, T. C.; Bollinger, J. C.; Baker, D. L.; Yan, B.; Webster, C. E.; Zhao, X. *Angew. Chem., Int. Ed.* **2012**, *51*, 5941.

(92) Shan, B.; Baine, T.; Ma, X. A. N.; Zhao, X.; Schmehl, R. H. *Inorganic Chemistry* **2013**, *52*, 4853.

(93) Vennampalli, M.; Liang, G.; Katta, L.; Webster, C. E.; Zhao, X. *Inorganic Chemistry* **2014**, *53*, 10094.

(94) Lewandowska-Andralojc, A.; Baine, T.; Zhao, X.; Muckerman, J. T.; Fujita, E.; Polyansky, D. E. *Inorg. Chem.* **2015**, *54*, 4310.

(95) Song, X.-W.; Wen, H.-M.; Ma, C.-B.; Chen, H.; Chen, C. *New J. Chem.* **2015**, *39*, 1734.

(96) Xie, J.; Zhou, Q.; Li, C.; Wang, W.; Hou, Y.; Zhang, B.; Wang, X. *Chem. Commun. (Cambridge, U. K.)* **2014**, *50*, 6520.

(97) Lo, W. K. C.; Castillo, C. E.; Gueret, R.; Fortage, J.; Rebarz, M.; Sliwa, M.; Thomas, F.; McAdam, C. J.; Jameson, G. B.; McMorran, D. A.; Crowley, J. D.; Collomb, M.-N.; Blackman, A. G. *Inorganic Chemistry* **2016**, *55*, 4564.

(98) Fenton, R. R.; Stephens, F. S.; Vagg, R. S.; Williams, P. A. *Inorg. Chim. Acta* **1991**, *182*, 67.

(99) Kooistra, T. M.; Hekking, K. F. W.; Knijnenburg, Q.; de Bruin, B.; Budzelaar, P. H. M.; de Gelder, R.; Smits, J. M. M.; Gal, A. W. *Eur. J. Inorg. Chem.* **2003**, 648.

(100) Ward, A. L.; Elbaz, L.; Kerr, J. B.; Arnold, J. *Inorganic Chemistry* **2012**, *51*, 4694−4706.

(101) Li, Z.; Xiao, J.-D.; Jiang, H.-L. *ACS Catal.* **2016**, *6*, 5359.

(102) Du, P.; Knowles, K.; Eisenberg, R. *J. Am. Chem. Soc.* **2008**, *130*, 12576.

(103) Du, P.; Schneider, J.; Luo, G.; Brennessel, W. W.; Eisenberg, R. *Inorganic Chemistry* **2009**, *48*, 4952.

(104) McCormick, T. M.; Calitree, B. D.; Orchard, A.; Kraut, N. D.; Bright, F. V.; Detty, M. R.; Eisenberg, R. *J. Am. Chem. Soc.* **2010**, *132*, 15480.

(105) Okamoto, S.; Kojiyama, K.; Tsujioka, H.; Sudo, A. *Chem. Commun.* **2016**.

(106) Nakajima, M.; Fava, E.; Loescher, S.; Jiang, Z.; Rueping, M. *Angew. Chem. Int. Ed. Engl.* **2015**, *54*, 8828.

(107) Nicewicz, D.; Roth, H.; Romero, N. *Synlett* **2015**, *27*, 714.

(108)

(109) Gemal, A. L.; Luche, J. L. *J. Am. Chem. Soc.* **1981**, *103*, 5454.

(110) Luche, J. L.; Gemal, A. L. *J. Am. Chem. Soc.* **1979**, *101*, 5848.

(111) Abdel-Magid, A. F. **2014**, 1.

(112) Barrios, F. J.; Springer, B. C.; Colby, D. A. *Organic Letters* **2013**, *15*, 3082.

(113) Bastug, G.; Dierick, S.; Lebreux, F.; Markó, I. E. *Organic Letters* **2012**, *14*, 1306.

(114) Gemal, A. L.; Luche, J. L. *J. Org. Chem.* **1979**, *44*, 4187.

(115) Stevenson, J. P.; Jackson, W. F.; Tanko, J. M. *J. Am. Chem. Soc.* **2002**, *124*, 4271.

(116) Lu, Z.; Shen, M.; Yoon, T. P. *J. Am. Chem. Soc.* **2011**, *133*, 1162.

(117) Tanko, J. M.; Drumright, R. E. *J. Am. Chem. Soc.* **1992**, *114*, 1844.

(118) Yang, D.; Tanner, D. D. *J. Org. Chem.* **1986**, *51*, 2267.

(119) Tanko, J. M.; Drumright, R. E. *J. Am. Chem. Soc.* **1990**, *112*, 5362.

(120) Griller, D.; Ingold, K. U. *Acc. Chem. Res.* **1980**, *13*, 317.

(121) Costentin, C.; Dridi, H.; Saveant, J. M. *J. Am. Chem. Soc.* **2014**, *136*, 13727.

(122) Marinescu, S. C.; Winkler, J. R.; Gray, H. B. *Proceedings of the National Academy of Sciences of the United States of America* **2012**, *109*, 15127−15131.

(123) Fischer, S.; Hollmann, D.; Tschierlei, S.; Karnahl, M.; Rockstroh, N.; Barsch, E.; Schwarzbach, P.; Luo, S.-P.; Junge, H.; Beller, M.; Lochbrunner, S.; Ludwig, R.; Brückner, A. *ACS Catal.* **2014**, *4*, 1845.

(124) Cline, E. D.; Adamson, S. E.; Bernhard, S. *Inorg. Chem.* **2008**, *47*, 10378.

(125) Luo, S.-P.; Mejía, E.; Friedrich, A.; Pazidis, A.; Junge, H.; Surkus, A.-E.; Jackstell, R.; Denurra, S.; Gladiali, S.; Lochbrunner, S.; Beller, M. *Angew. Chem. Int. Ed.* **2013**, *52*, 419.

(126) Ward, A. L.; Elbaz, L.; Kerr, J. B.; Arnold, J. *Inorg. Chem.* **2012**, *51*, 4694−4706.

(127) Roefles, G.; Lubben, M.; Hage, R.; Jr., L. Q.; Feringa, B. L. *Chem. Eur. J.* **2000**, *6*, 2152.

(128) Radaram, B.; Ivie, J. A.; Singh, W. M.; Grudzien, R. M.; Reibenspies, J. H.; Webster, C. E.; Zhao, X. *Inorg. Chem.* **2011**, *50*, 10564.

(129) Maity, N. C.; Kumar Bera, P.; Ghosh, D.; Abdi, S. H. R.; Kureshy, R. I.; Khan, N.-u. H.; Bajaj, H. C.; Suresh, E. *Catal. Sci. Technol.* **2014**, *4*, 208.

(130) Abouelatta, A. I.; Sonk, J. A.; Hammoud, M. M.; Zurcher, D. M.; McKamie, J. J.; Schlegel, H. B.; Kodanko, J. J. *Inorg. Chem.* **2010**, *49*, 5202.

(131) Chen, M. S.; White, M. C. *Science* **2007**, *318*, 783.

(132) Wu, X.; Li, X.; Hems, W.; King, F.; Xiao, J. *Org. Biomol. Chem.* **2004**, *2*, 1818.

(133) Lloret-Fillol, J.; Codolà, Z.; Garcia-Bosch, I.; Gómez, L.; Pla, J. J.; Costas, M. *Nat. Chem.* **2011**, *3*, 807

(134) Arakawa, H.; Aresta, M.; Armor, J. N.; Barteau, M. A.; Beckman, E. J.; Bell, A. T.; Bercaw, J. E.; Creutz, C.; Dinjus, E.; Dixon, D. A. *Chem. Rev.* **2001**, *101*, 953.

(135) Becke, A. D. *J. Chem. Phys.* **1993**, *98*, 1372.

(136) Becke, A. D. *J. Chem. Phys.* **1993**, *98*, 5648.

(137) Lee, C. T.; Yang, W. T.; Parr, R. G. *Phys. Rev. B* **1988**, *37*, 785.

(138) C. J. Cramer, A. V. M., D. G. Truhlar *J. Phys. Chem. B* **2009**, *113*, 6378.

(139) Schwabe, T.; Grimme, S. *Phys. Chem. Chem. Phys.* **2007**, *9*, 3397.

(140) In *Chemcraft - graphical software for visualization of quantum chemistry computations.* .

(141) Mayer, I. *Chem. Phys. Lett.* **1983**, *97*, 270.

(142) Mayer, I. *Int. J. Quantum Chem* **1984**, *26*, 151.

(143) C. P. Kelly, C. J. C., D. G. Truhlar, *J. Phys. Chem. A* **2006**, *110*, 2493

(144) Dinescu, A.; Clark, A. E. *J Phys Chem A* **2008**, *112*, 11198.

(145) Bartmess, J. E. *J Phys Chem* **1994**, *98*, 6420.

(146) Kelly, C. P.; Cramer, C. J.; Truhlar, D. G. *J Phys Chem B* **2007**, *111*, 408.

MECHANISTIC STUDIES OF WATER OXIDATION CATALYZED BY HOMOGENEOUS IRON AND RUTHENIUM
COMPLEXES AND LIGHT-DRIVEN ORGANIC REDUCTIONS WITH A DUAL COBALT/COPPER CATALYTIC SYSTEM

Carla Casadevall Serrano

CHAPTER IX

Dual Co/Cu Light-driven Reduction of Aromatic Olefins in Aqueous Media: Reactivity, Selectivity and Mechanistic Studies

This chapter corresponds to the following publication and the study has been possible thanks to the *in-house* developed photoreactors (see patent):

"A cobalt-copper dual light-driven catalytic system for the reduction of aromatic olefins in aqueous media"; **C. Casadevall**, D. Pascual, A. Casitas, A. Call, J. Lloret-Fillol; *in progress*.

UNIVERSITAT ROVIRA I VIRGILI
MECHANISTIC STUDIES OF WATER OXIDATION CATALYZED BY HOMOGENEOUS IRON AND RUTHENIUM
COMPLEXES AND LIGHT-DRIVEN ORGANIC REDUCTIONS WITH A DUAL COBALT/COPPER CATALYTIC SYSTEM
Carla Casadevall Serrano

IX. Dual Co/Cu Light-driven Reduction of Aromatic Olefins in Aqueous Media: Reactivity, Selectivity and Mechanistic Studies

IX.1. General insight

As introduced in the previous chapter, the production of fine chemicals has less scaling and economic pressure than the synthesis of energy carriers.[1-11] However, the application of molecular catalysts designed for H_2O[12-23] and CO_2[24-32] reduction to synthetically useful transformations is still limited to few examples.[1-11,33,34] Olefin reduction is a challenging reaction to be developed in the context of artificial photosynthesis due to the susceptibility of olefins to polymerize under light-driven conditions due to radical formation *via* single electron transfer (SET) or hydrogen atom transfer (HAT) processes. Moreover, the control of the selectivity of the reduction of olefins versus water in aqueous media has fundamental mechanistic implications. There are few studies using light as driving force for the reduction of olefins.[35-37] However, there are only few reports that study the reduction of olefins in aqua media.[35,38,39]

Semiconductor materials such as TiO_2 and CdS have been used for the light-driven hydrogenation of electron deficient olefins, despite of using UV light ($\lambda = 365$ nm), noble metals and obtaining low/moderate selectivity (Scheme IX.1).[37,39,40] Other remarkable examples use Co-B_{12} complex (cyanoaquacobyrinic acid) embedded on the surface of TiO_2 (B_{12}-TiO_2 hybrid) heterogeneous catalyst for the UV light-driven reduction of alkenes to alkanes.[35,36] However, such highly energetic conditions led to important formation of dimeric products, which harm the selectivity.[41] Holland, Corma and co-workers have achieved the stereoselective hydrogenation of the conjugated C=C bond of ketoisophorone combining the photocatalytic activity of Au nanoparticles supported on TiO_2 with the enzymatic activity of oxidoreductases by means of FAD[+] as mediator and cofactor (Scheme IX.1).[3] Likewise, Hartwig, Zhao and coworkers reported a cooperative chemoenzymatic reaction that combines the

isomerization activity of C=C of an iridium photoredox catalyst with the hydrogenation activity of ene-reductases to selectively reduce electron deficient aromatic olefins to their corresponding alkanes in high enantiomeric excess (88-99 % ee).[38] These results show that selective light-driven reduction of organic substrates using water as hydrogen source is a feasible transformation, albeit very limited in substrate scope.[1-6,11,38]
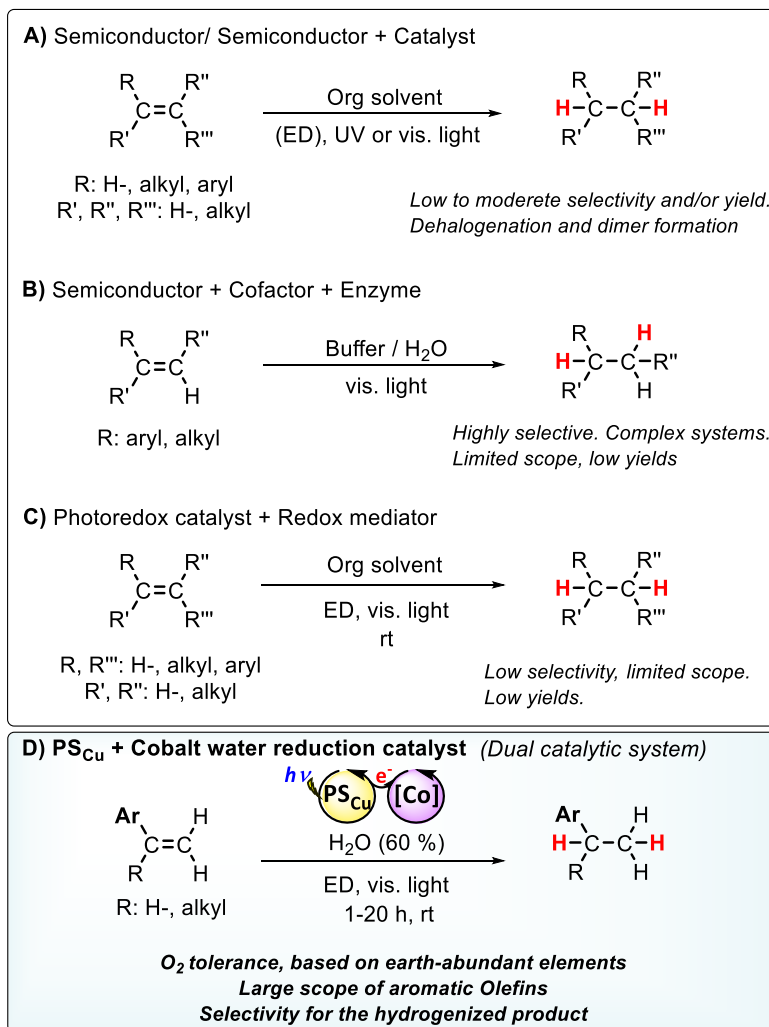
Scheme IX.1. Methodologies for the light-driven reduction of aromatic olefins. Abbreviations: ED: electron donor. Selected references: (A) ref. 4, (B) ref. 3c and (C) ref. 5. (D) Developed methodology in this study.

UNIVERSITAT ROVIRA I VIRGILI
MECHANISTIC STUDIES OF WATER OXIDATION CATALYZED BY HOMOGENEOUS IRON AND RUTHENIUM
COMPLEXES AND LIGHT-DRIVEN ORGANIC REDUCTIONS WITH A DUAL COBALT/COPPER CATALYTIC SYSTEM
Carla Casadevall Serrano

CHAPTER IX   Dual Co/Cu Light-driven Olefin Reduction

As showed in the previous chapter, an alternative approach to surpass these disadvantages is to exploit the combination of photoredox catalysts with well-defined molecular complexes based on versatile ligands.[42] This is an appealing approach since independent tuning of the photosensitizer (lifetime and redox potential) and the coordination complex (modification of the electronic and steric effects) can be rationally implemented to improve the reactivity and the selectivity of the reaction and access new activation modes and organic transformations.[43-49]

In this chapter, we present the reactivity of a dual cobalt-copper catalytic system consisting on $(Co(OTf)(Py_2{}^{Ts}tacn))(OTf)$ (**1Co**), $(Py_2{}^{Ts}tacn = 1,4$-di(picolyl)-7-(p-toluenesulfonyl)-1,4,7-triazacyclononane, OTf = trifluoromethanesulfonate anion), initially developed to reduce water to H_2,[50] and $[Cu(bathocuproine)(Xantphos)](PF_6)$[51] (**PS$_{Cu}$**) as photoredox catalyst for the photoreduction of challenging styrene derivatives (Scheme IX.2) in aqueous media using H_2O/ED (ED = electron donor, triethylamine (TEA) or N,N-diisopropylethylamine (DIPEA)) as the hydride source. This dual photocatalytic system has been already proven by our group to reduce aromatic ketones and aromatic and aliphatic aldehydes in aqueous media, with an exquisite selectivity for the aromatic ketone.[34] Styrene derivatives are challenging substrates since they are known to polymerize under light or in presence of radicals.[52] In addition, the redox potential of the one electron reduction reaction of styrene is about -2.4 V *vs* SCE, therefore its direct reduction by the photoredox catalyst is prevented (-1.53 V vs SCE). Herein we present reactivity and selectivity studies in the light-driven reduction of aromatic olefins in aqueous media using the dual Co/Cu catalytic system. Moreover, preliminary mechanistic studies have been performed on the basis on isotopic labelling, radical clock experiments and computational modelling to shed light in the reduction mechanism.

UNIVERSITAT ROVIRA I VIRGILI
MECHANISTIC STUDIES OF WATER OXIDATION CATALYZED BY HOMOGENEOUS IRON AND RUTHENIUM
COMPLEXES AND LIGHT-DRIVEN ORGANIC REDUCTIONS WITH A DUAL COBALT/COPPER CATALYTIC SYSTEM
Carla Casadevall Serrano

CHAPTER IX   Dual Co/Cu Light-driven Olefin Reduction
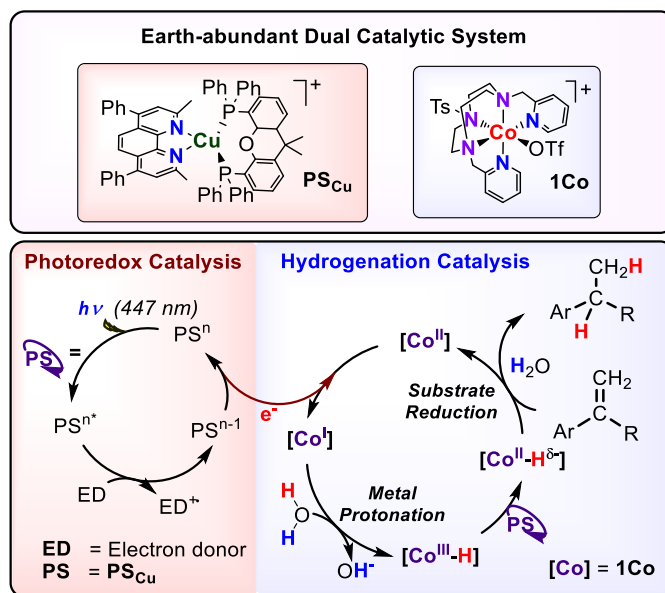
Scheme IX.2. Earth-abundant Dual Co-Cu Catalytic system for the photoreduction of aromatic olefins.

IX.2. Results and discussion

IX.2.1. Optimization of the catalytic conditions for the reduction of styrene derivatives

To test the light-driven reduction activity of the dual Co/Cu catalytic system towards aromatic olefin reduction, styrene (**13a**) was initially tested as model substrate. Interestingly, styrene (**13a**) is reduced under similar conditions ([**13a**] = 16.5 mM, [**1Co**] = 1 mol % and [**PS$_{Cu}$**] = 1.5 mol %) to that of our previously reported methodology for the visible-light reduction of carbonyl compounds using water/amine as hydride source in H$_2$O:MeCN,[43] despite obtaining moderate yield of ethylbenzene (**14a**) (67 %) accompanied with the formation of butane-2,3-diyldibenzene (**14'a**) as a by-product (11 % yield) (Table IX.1 entry 1) The observation of the latter reduced homocoupling product, albeit in small amounts, has mechanistic implications, which reveal the formation of benzylic radicals during catalysis. Nevertheless, the mass balance argues against styrene polymerization under

reaction conditions. By increasing the loading of **1Co** and **PS_Cu** (3 mol%) and reducing to half the styrene concentration (8 mM), the yield of ethylbenzene (**14a**) increased up to 86 % while by-product **14a'** diminished (4 %). Final refinement of reaction conditions by decreasing the temperature to 15ºC gave 91 % yield of **14a** without detection of dimeric products (Table IX.1 entry 8).

Table IX.1. Optimization of the catalytic conditions for the reduction of **13a** using **PS_Cu** as photoredox catalyst and **1Co** as catalyst.
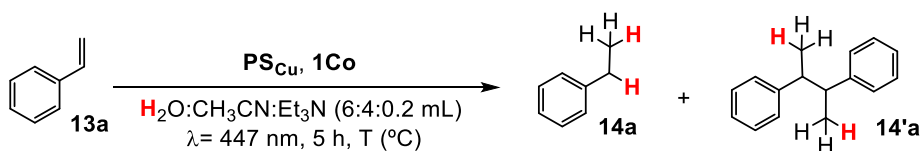
Entry	[Substrate] (mM)	Temp (ºC)	[cat] (mol %)	[PS_Cu] (mol %)	% Yield 14a	% Yield 14'a
1	16	35	1	1.5	67	11
2	32	35	3	3	64	11
3	16	35	3	3	81	6
4	8	35	3	3	86	4
5	8	35	3	3	86	4
6	8	35	3	1.5	92	4
7	8	35	3	0.75	83	7
8	8	15	3	3	91	0

Conditions: **1Co** (% mol), **PS_Cu** (% mol), substrate (mM) as indicated in the table in $H_2O:CH_3CN:Et_3N$ (6:4:0.2 mL) irradiation at $\lambda= 447$ nm for 5 h at 35 or 15 ºC under N_2. Yields were determined by GC analysis after workup of the reaction and they are relative to a calibrated internal standard. Values are average of triplicates.

It is worth to note that the same amount of reduced product (**14a**) was obtained when preparing *in situ* complex **1Co** under reaction conditions by reaction of 1 equivalent $Co(OTf)_2(MeCN)_2$ with 1 equivalent of the Py$_2$^{Ts}tacn ligand (Table A.VII.2, entry 8). Neither employing several cobalt salts as catalyst, nor in the absence of cobalt catalyst **1Co** or **PSCu** no reduction product was formed (Tables A.VII.1 and A.VII.2). Furthermore, control experiments established that the reaction is light-mediated and a reductive quenching from Et$_3$N is needed since no conversion is observed when light and/or electron-donor are not added into the reaction flask.

Additionally, the catalytic system is compatible with low concentrations of O_2, in the headspace. Indeed, the reduction of **13a** was accomplished in high yields (71%) when the reaction was prepared under air and using non-degassed solvents in a crimped vial minimizing the headspace.

IX.2.2. Influence of the structure of the cobalt catalyst

Under these optimized conditions, a variety of active tetra- and pentacoordinate cobalt complexes for water reduction (WR) to dihydrogen,[19,21,53,54] based on glyoxime,[17] diimine-glyoxime[15] and aminopyridine[14,16] ligands were tested towards the reduction of styrene (**13a**) and compared to complex **1Co** (Table IX.2 and Figure A.VII.3). This study was performed to evaluate the influence of the ligand architecture, if any, on the catalytic activity. In all cases we observed light-driven reduction of styrene (**13a**) to some extent, but the selectivity towards olefin reduction to ethylbenzene (**14a**) *versus* homocoupling product formation (**14'a**) varies depending on the nature of the complex used. Complex **1Co** is the most efficient, active and selective catalyst for olefin reduction (91 % yield of **14a** and <1 % yield **14'a**). Whereas vitamin B_{12} is the less active one, yielding only traces of both reduced and dimeric products (4 and 6 % yield, respectively). Interestingly, only catalysts based on the tacn (1,4,7-triazacyconononane) ligand are efficient under the studied conditions (yields from 76 to 91 %, Table IX.2 and Figure IX.1). However, from the catalyst series **9 – 14** we concluded that there is not an evident electronic effect in the catalytic outcome of the reaction.

UNIVERSITAT ROVIRA I VIRGILI
MECHANISTIC STUDIES OF WATER OXIDATION CATALYZED BY HOMOGENEOUS IRON AND RUTHENIUM
COMPLEXES AND LIGHT-DRIVEN ORGANIC REDUCTIONS WITH A DUAL COBALT/COPPER CATALYTIC SYSTEM
Carla Casadevall Serrano

CHAPTER IX   Dual Co/Cu Light-driven Olefin Reduction

Table IX.2. Photocatalytic reduction of styrene (**13a**) to ethylbenzene (**14a**) by the selected WR cobalt complexes.
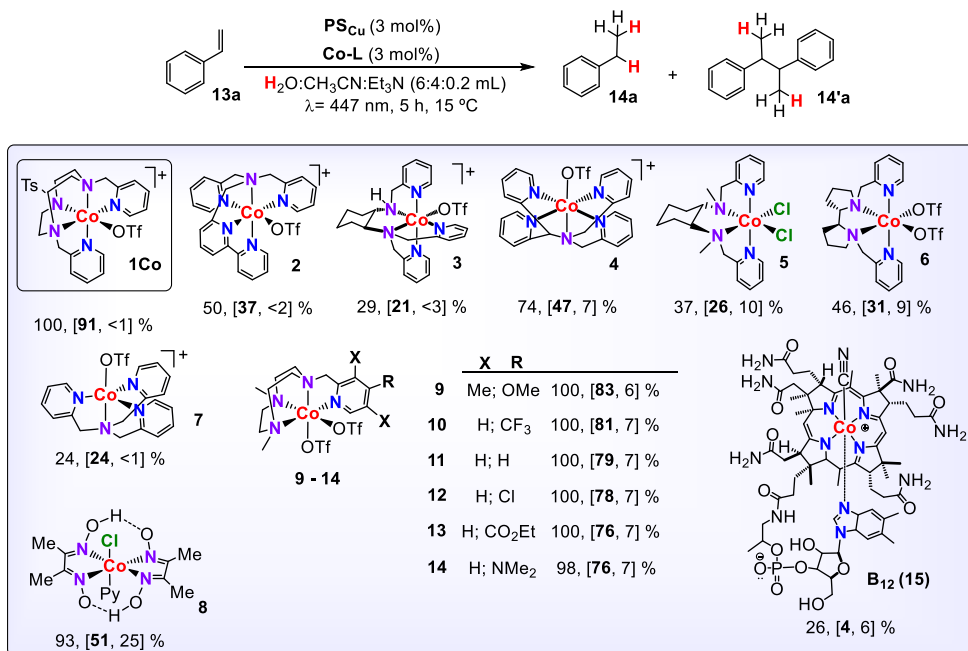
Selected WR complexes: **1Co**: [Co^{II}(OTf)(Py$_2^{Ts}$tacn)](OTf), **2**:[Co^{II}(OTf)(DPA-Bpy)](OTf), **3**: [Co^{II}(OTf)(N$_4$Py)](OTf), **4**: [Co^{II}(OTf)(H-CDPy$_3$)](OTf), **5**:[Co^{II}(OTf)$_2$(PDP)], **6**: [Co^{II}(OTf)$_2$(TPA)], **7**: [Co^{II}(Cl)$_2$(BpcMe)], **8**: [Co^{III}(Cl)(Py)(Glioxim)], **9**: [Co^{II}(OTf)$_2$(^{Me,OMe}Py^{Me2}tacn)], **10**: [Co^{II}(OTf)$_2$(^{H,CF3}Py^{Me2}tacn)], **11**: [Co^{II}(OTf)$_2$(^{H,H}Py^{Me2}tacn)], **12**: [Co^{II}(OTf)$_2$(^{H,Cl}Py^{Me2}tacn)], **13**: [Co^{II}(OTf)$_2$(^{H,CO2Et}Py^{Me2}tacn)], **14**: [Co^{II}(OTf)$_2$(^{H,NMe2}Py^{Me2}tacn)], **15**: [Co^{II}(OTf)$_2$(^{H,NO2}Py^{Me2}tacn)] and **16** vitamin **B$_{12}$**. Conditions **A**: **Co-Cat** (261 µM, 3% mol), PSCu (261 µM, 3% mol), **13a** (8.7 mM) in H$_2$O:CH$_3$CN:Et$_3$N (6:4:0.2 mL) irradiation (447 nm) for 5h at 15 ºC under N$_2$. Yields determined by GC analysis after workup relative to a calibrated internal standard. Values were average of triplicates. Reported values are as follows: % Conversion of **13a**, and % Yield of **14a** and **14'a** between brackets: Conv. **13a**, [yield **14a**, yield **14a'**] %.
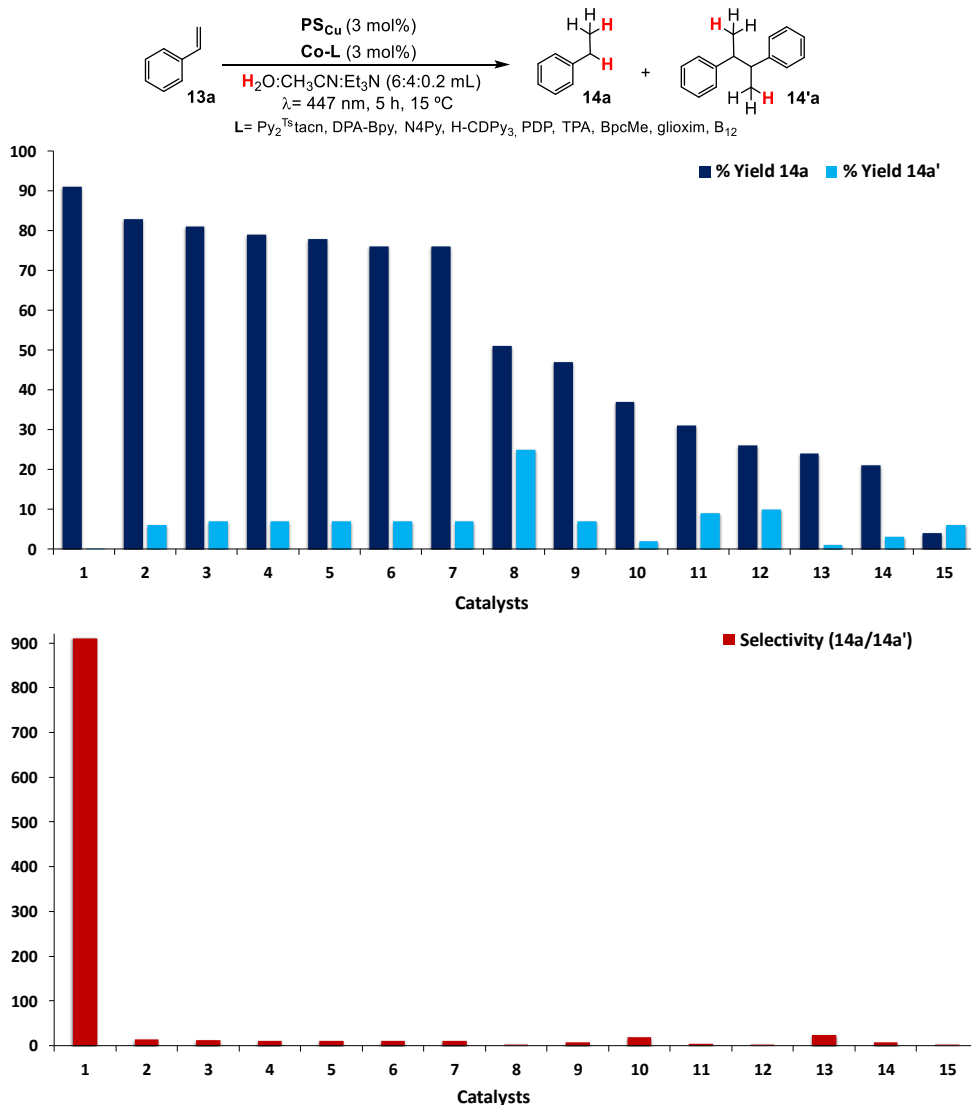
Figure IX.1. Photocatalytic activities of different cobalt-based complexes in **14a** and **14'a** formation. *Top*: **14a** and **14'a** formation activity. *Bottom*: selectivity of **14a** vs **14'a**. Conditions **A**: **Co-Cat** (261 μM, 3% mol), **PS$_{Cu}$** (261 μM, 3% mol), **13a** (8.7 mM) in H$_2$O:CH$_3$CN:Et$_3$N (6:4:0.2 mL) irradiation (447 nm) for 5h at 15 ºC under N$_2$. Yields determined by GC analysis after workup relative to a calibrated internal standard. Values were average of triplicates.

Reduction of **13a** into **14a** was always accompanied with the formation of H$_2$ as by-product, as was previously observed in the light-driven reduction of aromatic ketones[34] (Chapter VIII). The hydrogen evolved during the reaction time was monitored and quantified by analyzing an aliquot of the reaction head-space in the

UNIVERSITAT ROVIRA I VIRGILI
MECHANISTIC STUDIES OF WATER OXIDATION CATALYZED BY HOMOGENEOUS IRON AND RUTHENIUM
COMPLEXES AND LIGHT-DRIVEN ORGANIC REDUCTIONS WITH A DUAL COBALT/COPPER CATALYTIC SYSTEM
Carla Casadevall Serrano

CHAPTER IX   Dual Co/Cu Light-driven Olefin Reduction

GC-TCD (gas chromatography-Thermal Conductivity Detector, see *IX.4.
Experimental Section* for further details). As presupposed, the activity of water
reduction to H_2 is strongly dependent on the ligand scaffold. For the studied
pentacoordinate cobalt complexes, complex **1Co** is the most effective of the series in
both **14a** and H_2 formation (Figure IX.2). In this case, the presence of an electron-
withdrawing substituent in the Py ring (CO_2Et, complex **1$^{CO2Et}_{Co}$**) dramatically
decreases the formation of **14a** but also the formation of H_2. Likewise, for the studied
tetracoordinate cobalt complexes, the amount of H_2 formed follows the order **10** > **13**
> **12** > **14** > **11** > **9**, being complex **10** the most effective of the series for H_2 evolution.
In contrast, for this series, the most active system for **14a** formation is complex **9**,
which is the least active for H_2 evolution, showing more selectivity for the styrene
reduction under the catalytic conditions of study (Figure IX.3). Nevertheless,
complex **1Co** is the most efficient and active for **14a** production among all the studied
tetra- and pentacoordinate cobalt complexes under our catalytic conditions.
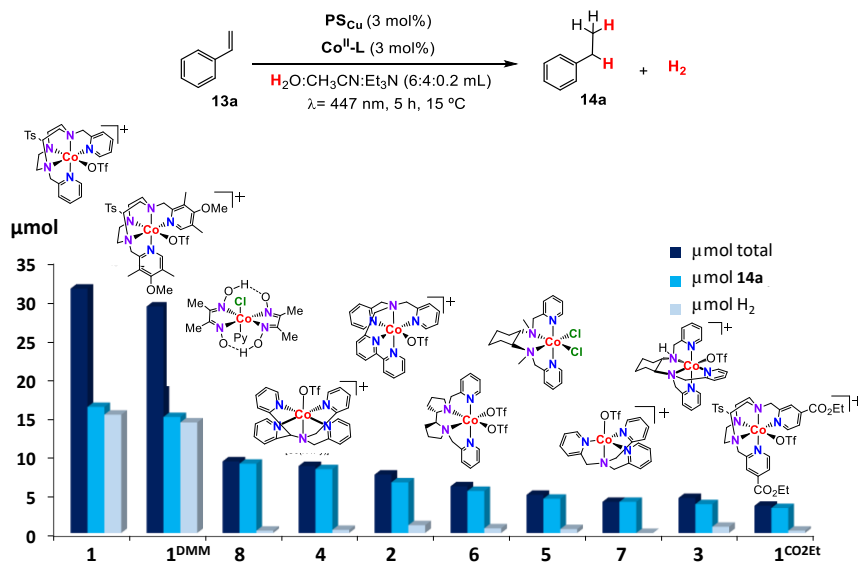
Figure IX.2. Photocatalytic activities of different pentadentate cobalt-based complexes in H_2 and **14a**
formation. [a]Conditions **A**: **Co^{II}-cat** (3 mol%), **PS$_{Cu}$** (3 mol%), Substrate (8.7 mM) in H_2O:CH_3CN:Et_3N
(6:4:0.2 mL) irradiated 5 h (447 nm) at 15 ºC under N_2. Quantity of reduced product (µmol **14a**)
determined by GC analysis after workup relative to a calibrated internal standard. H_2 was quantified by
GC-TCD analysis of an aliquot of the head-space of the reaction. Values were average of triplicates.
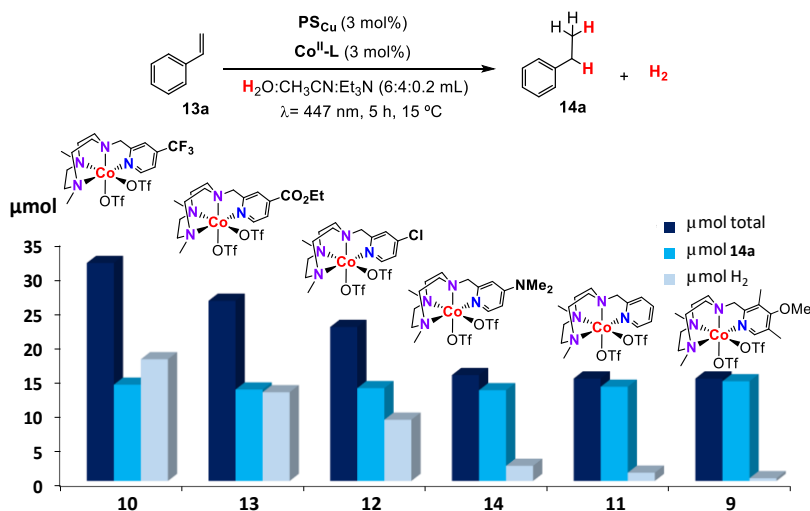
Figure IX.3. Photocatalytic activities of a family of tetradentate cobalt complexes based on the Py^{Me2}tacn ligand with different electronic effects in H$_2$ and **14a** formation. [a]Conditions **A**: **Co^{II}-cat** (3 mol%), **PS$_{Cu}$** (3 mol%), Substrate (8.7 mM) in H$_2$O:CH$_3$CN:Et$_3$N (6:4:0.2 mL) irradiated 5 h (447 nm) at 15 ºC under N$_2$. Quantity of reduced product (μmol **14a**) determined by GC analysis after workup relative to a calibrated internal standard. H$_2$ was quantified by GC-TCD analysis of an aliquot of the head-space of the reaction. Values were average of triplicates.

As a general trend, the styrene reduction activity is strongly dependent on the electronic and structural nature of the ligand scaffold coordinated to the cobalt center. For the set of complexes with pentadentate aminopyridine ligands based on the tacn moiety, the activity is related to the basicity of the ligand. Complexes **1Co** and **1^{DMM}$_{Co}$** show similar activity. The same type of trend is observed within the tetradentate **9** – **14** complexes. Moreover, tetradentate complex **9**, which is the most basic of the tetradentate series, shows the highest selectivity for styrene vs water reduction (Figure IX.3). This suggests that the light-driven styrene reduction activity can be modulated and improved by the rational design of the ligand architecture and points towards the molecularity of the active species. Due to the higher performance of complex **1Co**, we have selected it for further studies.

IX.2.3. Scope of the dual Cu/Co catalytic system

With the optimized conditions in hand, we explored the scope of the dual cobalt-copper (**1Co**/**PS$_{Cu}$**) photocatalytic system in the reduction of different styrene derivatives (**13a-l** and **15a-h**, Table IX.3). Interestingly, monosubstituted aromatic olefins with either electron withdrawing or donating groups in the aromatic ring are reduced within 5 h with excellent yields (73-99%) (Table IX.3). Substrates with electron donating substituents such as styrene (**13a**), *p*-methoxystyrene (**13b**), *p-tert*-butylstyrene (**13c**) and *p*-methylstyrene (**13d**) were reduced with similar yields: 91 – 99 % yield (Table IX.3). The lower yield obtained for *m*-methylstyrene (**13h**) and *o*-methylstyrene (**13j**) (86 % yield in both cases, Table IX.3) was attributed to the proximity of the methyl group to the double bond. Therefore, in the case of metyl-substituted styrenes, the position of the methyl group (*orto*-, *meta*- or *para*-) influences the catalytic outcome (from 99 % to 86 % yield, see table IX.3).

The selective transformation of organic molecules containing halogen atoms has interest *per se*, since dehalogenation processes can be competing pathways.[55,56] In this line, the dual catalytic system shows good tolerance in the reduction of styrene derivatives with chloride (**13f**) and fluoride (**13g**) substituents in the *para*- position, obtaining 90 and 99 % of the reduced product without dehalogenation (table IX.3). When the chloride substituent is in the *orto*- position, instead, a 86 % of the reduced product was obtained (table IX.3). In contrast, lower yield (53 %) was obtained when using *p*-bromostyerene (**13e**) that was accompanied by reduced dehalogenated product in a 18 %. The heteroaromatic substrate 2-vinylpyridine (**13l**) was also reduced in high yield (99 % **14l**, Table IX.3).

The reduction of 1,1-disubstituted aryl-alkyl olefins (**15a-c**, Table IX.3) is accompanied with the reductive coupling of two olefins (**17a-c**, Table IX.3) under the optimized catalytic conditions for styrene (**13a**) (Table IX.3, conditions A). Nevertheless, the yield of the reductive homocoupling products decreased when increasing the size of the alkyl substituent at the olefin (from -Me to ^{i}Pr), indicating

UNIVERSITAT ROVIRA I VIRGILI
MECHANISTIC STUDIES OF WATER OXIDATION CATALYZED BY HOMOGENEOUS IRON AND RUTHENIUM
COMPLEXES AND LIGHT-DRIVEN ORGANIC REDUCTIONS WITH A DUAL COBALT/COPPER CATALYTIC SYSTEM
Carla Casadevall Serrano

CHAPTER IX   Dual Co/Cu Light-driven Olefin Reduction

that steric effects on the substrate affect the product selectivity of the reaction. Actually, -^{t}Bu (**15d**) substituted aryl-alkyl olefin did not react due to the steric hindrance. Moreover, decreasing the substrate concentration of α-methylstyrene (**15a**) to half did not improve the product distribution (see annex A.VII, Table A.VII.3). We rationalized that a putative [Co-H] intermediate formed under catalytic conditions could react with the olefin *via* a HAT mechanism to the less hindered carbon, as previously observed for M-H species.[57-59] Indeed, HAT mechanism is very sensitive to steric effects.[60] This leads to the formation of benzylic radicals, which could let to the formation of reduced homocoupling products, which were also observed for styrene under non-optimized conditions and will be further discussed in this chapter. These results are also in agreement with recent reactivity reported on: i) the reduction and homo- and heterocoupling of olefins using silanes as reducing agents[61,62] and ii) on the reactivity of putative [Co-H] species with olefins by J. Norton and co-workers.[63,64] Further improvement was achieved by increasing the catalyst (**1Co**) and photoredox catalyst (**PS$_{Cu}$**) loadings up to 6% and using a bulkier electron donor (*N,N*-diisopropylethylamine, DIPEA) (see annex A.VII, Tables A.VII.4 and A.VII.5), but dimeric products were still formed. We hypothesized that the selectivity towards olefin reduction could be improved by decreasing the temperature of the reaction. The reduction of the temperature should have a higher impact in the formation rates of [Co-H] and organic radicals than in rates related to the photoredox process, which are light controlled.

UNIVERSITAT ROVIRA I VIRGILI
MECHANISTIC STUDIES OF WATER OXIDATION CATALYZED BY HOMOGENEOUS IRON AND RUTHENIUM
COMPLEXES AND LIGHT-DRIVEN ORGANIC REDUCTIONS WITH A DUAL COBALT/COPPER CATALYTIC SYSTEM
Carla Casadevall Serrano

CHAPTER IX   Dual Co/Cu Light-driven Olefin Reduction

Table IX.3. Light-driven reduction of selected aromatic mono- and 1,1-disubstituted olefins.
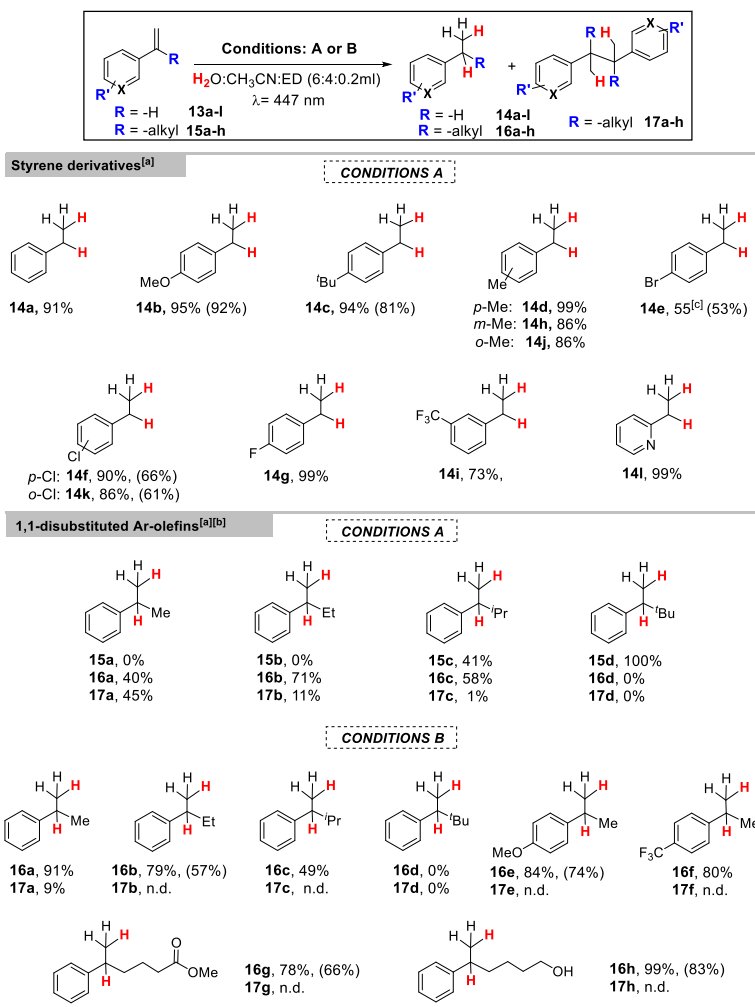
[a]Conditions **A**: **1Co** (3 mol%), **PS$_{Cu}$** (3 mol%), Substrate (8.7 mM) in H$_2$O:CH$_3$CN:Et$_3$N (6:4:0.2 mL) irradiated 5 h (447 nm) at 15 ºC under N$_2$. [b]Conditions **B**: **1Co** (6 mol%), **PS$_{Cu}$** (6 mol%), Substrate (4.4 mM) in H$_2$O:CH$_3$CN:^{i}Pr$_2$EtN (6:4:0.2 mL) irradiated 24 h (447 nm) at -3 ºC under N$_2$. Yields after workup (average of triplicates) determined by GC analysis relative to calibrated internal standard. Isolated yields between parentheses (average of 16 reactions). [c]This substrate also gave 18 % of dehalogenated product.

Therefore, two possible scenarios can be envisioned: i) the reduced **PS$_{Cu}$** could directly reduce the radical species (which derives from a first HAT from the putative [Co-H] species) yielding the reduced olefin (E = -1.44 V vs SCE for the styrene radical by DFT calculations, see Figure IX.24 and E$_{(exp)}$(**PS$_{Cu}$**) = -1.53 V vs. SCE[34]), or ii) the radical species could be more effectively trapped by either the cobalt complex or the [Co-H] leading to the reduced olefin. Both paths should prevent the

UNIVERSITAT ROVIRA I VIRGILI
MECHANISTIC STUDIES OF WATER OXIDATION CATALYZED BY HOMOGENEOUS IRON AND RUTHENIUM
COMPLEXES AND LIGHT-DRIVEN ORGANIC REDUCTIONS WITH A DUAL COBALT/COPPER CATALYTIC SYSTEM
Carla Casadevall Serrano

CHAPTER IX   Dual Co/Cu Light-driven Olefin Reduction

radical accumulation and, thus, the formation of homocoupling products. In this line, at low temperatures (-3 ºC) the dimeric products are negligible (Table IX.3, optimized conditions B and Annex VII Table A.VII.6, entry 3). Therefore, by increasing the loading of **1Co** and **PS$_{Cu}$** (6 mol%) and reducing the concentration of styrene (4.4 mM) at -3ºC and using DIPEA we could achieve excellent selectivity for the reduction of α-methylstyrene (91 % yield **16a** and 9 % yield **17a**, Table IX.3 conditions B). Additionally, the reduction of **15a** under air with non-degassed solvents yields 81% of the reduced product. This strategy could be expanded to the reduction of other 1,1-disubstituted aromatic olefins with electron donating and electron withdrawing substituents such as substrates **15e** and **15f** that were reduced in 84 and 80 % yield, respectively without any dimeric product. Under optimized conditions, the yield of the reduced product for substrates **15a** to **15d** (containing –Me, -Et, -^{i}Pr and –^{t}Bu as substituents at the alpha position, respectively) suffers from steric effects due to the proximity of the alkyl substituent to the double bond (see Table IX.3, conditions B).

On the other hand, the catalytic system is inefficient towards the reduction of 1,2-disubstituted aromatic olefins, which only yields the *trans-cis* isomerization as previously reported[65-68] and trace amount the of reduced product (Table IX.4).

Table IX.4. Light-driven reduction of selected aromatic 1,2-disubstituted olefins (**18a-e**).

18a, 20%	18b, 20%	18c, 30%	18d, 20%	[a]18e, 33%	[b]18e, 20%	[c]18e, 20%
19a, 0%	19b, 0%	19c, 0%	19d, 16%	19e, 0%	19e, 10%	19e, 18%
20a, 80%	20b, 80%	20c, 70%	20d, 40%	20e, 62%	20e, 60%	20e, 55%
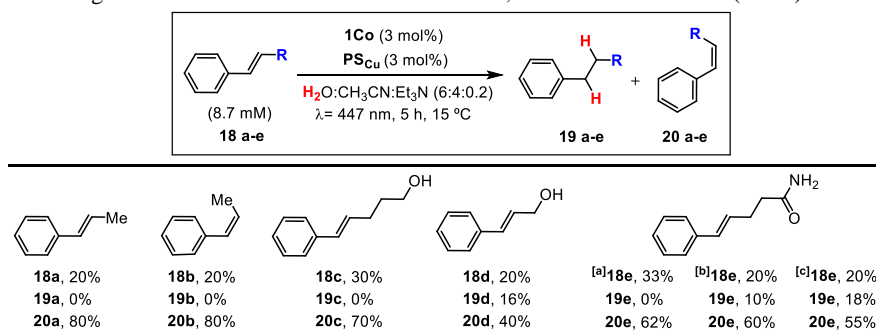
Conditions **A**: **1Co** (3% mol), **PS$_{Cu}$** (3% mol), substrate **18** (8.7 mM) in H$_2$O:CH$_3$CN:Et$_3$N (6:4:0.2 mL) irradiation at λ = 447 nm for 5h at 15 ºC under N$_2$. [a]Conditions **B**: **1Co** (6% mol),**PS$_{Cu}$** (6% mol), substrate **18** (4.4 mM) in H$_2$O:CH$_3$CN:^{i}Pr$_2$EtN (6:4:0.2 mL) irradiation at λ = 447 nm for 5 h at 15 ºC under N$_2$. [b]Catalytic conditions **B** at 50 ºC. [c]Catalytic conditions **B** at 80 ºC. Yields were determined by GC analysis after workup of the reaction and they are relative to a calibrated internal standard. Values are averages of triplicates.

UNIVERSITAT ROVIRA I VIRGILI
MECHANISTIC STUDIES OF WATER OXIDATION CATALYZED BY HOMOGENEOUS IRON AND RUTHENIUM
COMPLEXES AND LIGHT-DRIVEN ORGANIC REDUCTIONS WITH A DUAL COBALT/COPPER CATALYTIC SYSTEM
Carla Casadevall Serrano

CHAPTER IX   Dual Co/Cu Light-driven Olefin Reduction

IX.2.4. Selectivity studies

IX.2.4.1. Competition studies between aromatic olefins and ketones

In chapter VIII we observed that the organic methodology developed for the light-driven reduction of aromatic ketones and aldehydes using the dual cobalt-copper catalytic system shows an unprecedented selectivity for the reduction of aromatic ketones in front of aliphatic aldehydes.[34] We performed analogous competition studies between acetophenone (**9a**) and styrene (**13a**) and acetophenone (**9a**) and α-methylstyrene (**15a**) under the same previously reported catalytic competition conditions.[34] Interestingly, a high selectivity is obtained in the reduction of **9a** in the presence of **13a** and **15a**, 68% and 87% selectivity, respectively (Scheme IX.3). Despite the fact that in this case, the reduction of both aromatic olefins starts when acetophenone (**9a**) is still present in solution, the rate for the reduction of acetophenone differs from the rate for the reduction of the aromatic olefins (Figures IX.4 and IX.5). Therefore, a moderate to high selectivity can still be obtained. This observed behaviour has mechanistic implications. In chapter VIII, the observed selectivity between acetophenone (**9a**) and aliphatic aldehydes was rationalized on the basis on mechanistic studies. Those preliminary studies support a hydride transfer mechanism for substrates with low redox potentials (< - 2 V vs SCE), such as aliphatic aldehydes, and a single electron transfer mechanism plus a hydrogen atom transfer mechanism (SET + HAT) for substrates easier to reduce, such as acetophenone (- 1.65 V vs SCE).[34] In this case then, the observed selectivity might be also explained due to the existence of two different reduction mechanisms for acetophenone (**9a**) and the aromatic olefins, most likely a SET + HAT and a HAT + HAT, respectively.
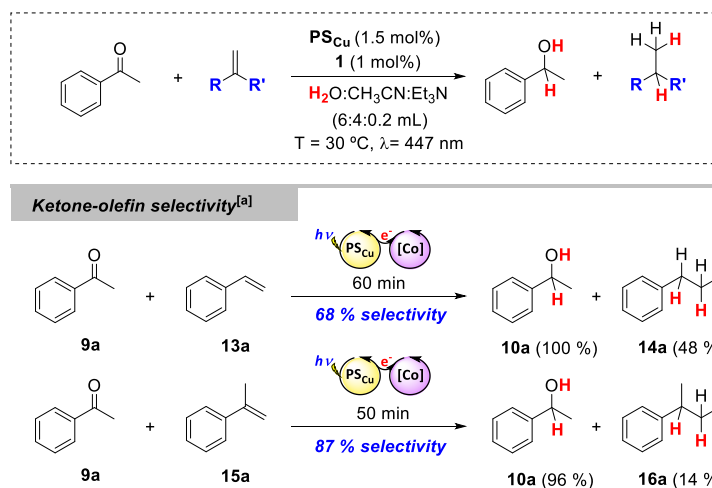
Scheme IX.3. Competitive reduction of 9a in the presence of equimolar amounts of carbonyl and alkene compounds. Conditions: **1Co** (1 mol%), **PS$_{Cu}$** (1.5 mol%), Substrate A + B (16.5 mM), A:B (1:1), in H$_2$O:CH$_3$CN:Et$_3$N (6:4:0.2 mL) irradiated (447 nm) for 5 h at 30 ºC under N$_2$.
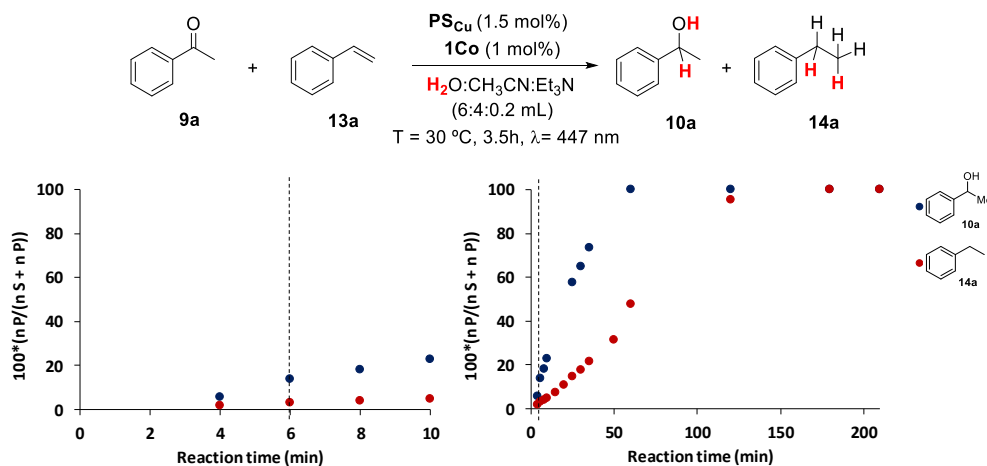
Figure IX.4. Monitoring of the competition between substrates **9a** and **13a** under catalytic conditions. *Left*: yield during the first 10 minutes of irradiation, it can be seen that the reduction of substrate **13a** starts when **9a** has not been totally reduced; *Right*, all the reaction time monitorization (3.5 hours). [a]Conditions: **1Co** (1 mol%), **PS$_{Cu}$** (1.5 mol%), Substrate A + B (16.5 mM), A:B (1:1), in H$_2$O:CH$_3$CN:Et$_3$N (6:4:0.2 mL) irradiated (447 nm) for 4 h at 30 ºC under N$_2$. [b]The plotted data is the ratio between the amount of the reduced product formed and the sum of the amount of the reduced product formed and the unconverted starting-material. [c]The black dotted line indicates the point where substrate **13a** starts reacting.

UNIVERSITAT ROVIRA I VIRGILI
MECHANISTIC STUDIES OF WATER OXIDATION CATALYZED BY HOMOGENEOUS IRON AND RUTHENIUM
COMPLEXES AND LIGHT-DRIVEN ORGANIC REDUCTIONS WITH A DUAL COBALT/COPPER CATALYTIC SYSTEM
Carla Casadevall Serrano

CHAPTER IX   Dual Co/Cu Light-driven Olefin Reduction
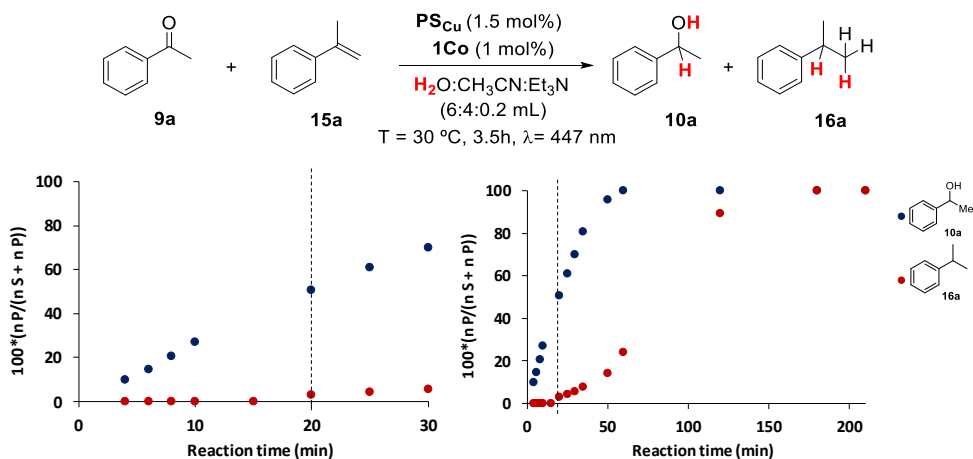
Figure IX.5. Monitoring of the competition between substrates **9a** and **15a** in the catalytic conditions. *Left*: yield during the first 30 minutes of irradiation, it can be seen that the reduction of substrate **15a** starts even when **9a** has not been totally reduced; *right*, all the reaction time monitorization (3.5 hours). [a]Conditions: **1Co** (1 mol%), **PS_Cu** (1.5mol%), Substrate A + B (16.5 mM), A:B (1:1), in $H_2O:CH_3CN:Et_3N$ (6:4:0.2 mL) irradiated (447 nm) for 4 h at 30 ºC under N_2. [b] The plotted data is the ratio between the amount of the reduced product formed and the sum of the amount of the reduced product formed and the unconverted starting-material. [c] The black dotted line indicates the point where substrate **15a** starts reacting.

IX.2.4.2. Competition studies between aromatic olefins and aliphatic aldehydes

The exquisite selectivity for the reduction of aromatic ketones in the presence of aliphatic aldehydes (100 %) and the high selectivity also observed for the reduction of aromatic ketones in front of aromatic olefins (68 – 87 %) was explained due to the distinguishable mechanisms of action depending on the redox potential of the organic substrate. Since the SET + HAT mechanism is the most accessible for substrates easier to reduce such as acetophenone (**9a**), catalytic conditions that favor a fast SET over a HAT would allow for selective reduction of the aromatic ketone. A SET mechanism is light controlled, and should not be dramatically affected by the temperature. In contrast, the reaction temperature should have a higher impact in the formation rates of the putative [Co-H] species and organic radicals and, thus, in the control of the rates of the HAT and the hydride transfer mechanisms. Attempts to selectively reduce aliphatic aldehydes in the presence of ketones were performed by

competition experiments between the aliphatic aldehyde cinnamaldehyde (**11e**) and styrene (**13a**), and cinnamaldehyde (**11e**) and α-methylstyrene (**15a**) at -3 °C and at more diluted conditions (4.35 mM of total concentration of substrates) to try to favor the differentiation of the two mechanisms of action. Nevertheless, both substrates were reduced from initial reaction times (see Figures IX.6 and IX.7) and only at high conversions of the substrates, the yield of the reduced olefins could overpass the yield of the reduced aldehydes; achieving 100 % of reduced products **14a** and **16a** but only about 70 % yield of **12e**, see Figures IX.6 and IX.7, respectively. We envision that further optimization of the catalytic conditions may led to 100 % selectivity in the reduction of the aromatic olefins in front of the aliphatic aldehydes and event to an opposite selectivity.
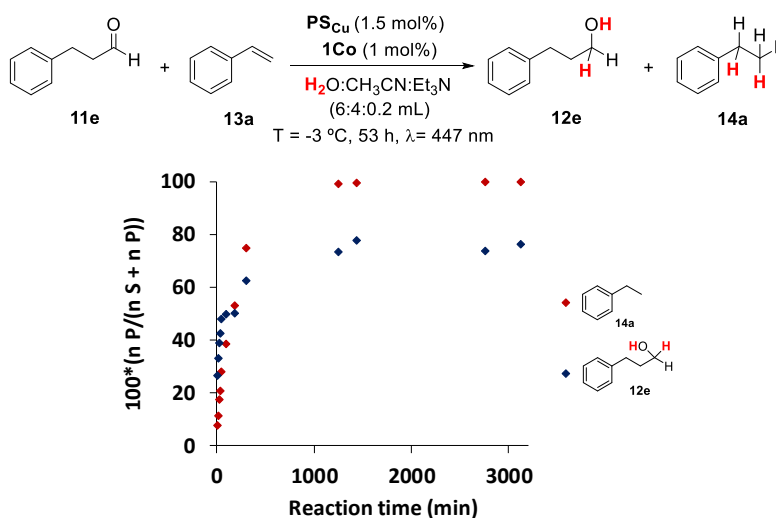
Figure IX.6. Monitoring of the competition between substrates **11e** and **13a** in the catalytic conditions along the reaction time monitorization (53 hours). [a]Conditions: **1Co** (1 mol%), **PS$_{Cu}$** (1.5mol%), Substrate A + B (4.35 mM), A:B (1:1), in H$_2$O:CH$_3$CN:Et$_3$N (6:4:0.2 mL) irradiated (447 nm) for 53 h at - 3 °C under N$_2$. [b] The plotted data is the ratio between the amount of the reduced product formed and the sum of the amount of the reduced product formed and the unconverted starting-material.
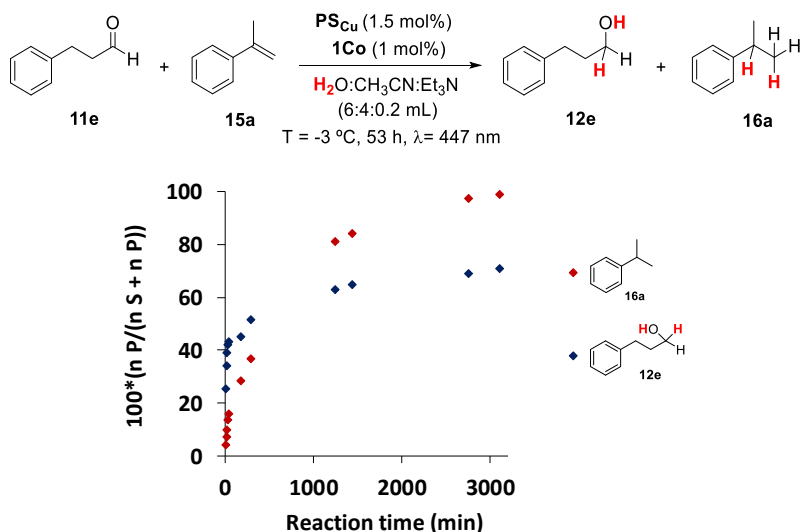
Figure IX.7. Monitoring of the competition between substrates **11e** and **15a** in the catalytic conditions along the reaction time monitorization (53 hours). [a]Conditions: **1Co** (1 mol%), **PSCu** (1.5mol%), Substrate A + B (4.35 mM), A:B (1:1), in $H_2O:CH_3CN:Et_3N$ (6:4:0.2 mL) irradiated (447 nm) for 53 h at - 3 °C under N_2. [b] The plotted data is the ratio between the amount of the reduced product formed and the sum of the amount of the reduced product formed and the unconverted starting-material.

IX.2.4.3. Competition studies between aromatic olefins

As expected, competition experiments between styrene (**13a**) and α-methylstyrene (**15a**) (Table IX. 3, conditions B) show a very similar rate for the formation of the reduced products **14a** and **16a** (Figure IX.8). These results suggest that both olefins undergo a HAT mechanism, which is the most sensitive to steric effects. Therefore, the putative [Co-H] reacts with the olefin transferring a hydrogen atom generating a benzylic radical that may subsequently undergo a second HAT yielding the reduced product.

341
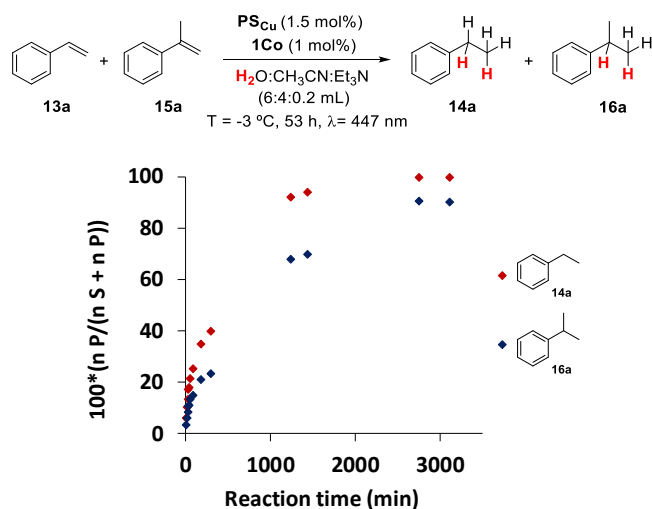
Figure IX.8. Monitoring of the competition between substrates **13a** and **15a** in the catalytic conditions along the reaction time monitorization (53 hours). [a]Conditions **B**: **1Co** (1 mol%), **PS$_{Cu}$** (1.5mol%), Substrate A + B (4.35 mM), A:B (1:1), in H$_2$O:CH$_3$CN:Et$_3$N (6:4:0.2 mL) irradiated (447 nm) for 53 h at - 3 ºC under N$_2$. [b] The plotted data is the ratio between the amount of the reduced product formed and the sum of the amount of the reduced product formed and the unconverted starting-material.

IX.2.5. Mechanistic investigations

We performed the following experiments to shed some light into the mechanism for the reduction of aromatic olefins.

IX.2.5.1. Styrene vs water reduction

As previously mentioned in this chapter, olefin reduction is always accompanied by H$_2$ evolution. However, we observed that the increase of substrate concentration inhibited the formation of H$_2$ (Figure IX.9a) while the rate of production of ethylbenzene (**14a**) was constant independently of the initial concentration of styrene (**13a**) (Figure IX.9b). This kinetic dependence can be rationalized with a common [Co-H] intermediate for both transformations. Indeed, the sum of both (H$_2$ + **14a**) decreases as the concentration of styrene increases, since the production of H$_2$ diminishes but the amount of **14a** formed remains constant (Figure IX.9b). Indeed, the independence of the formation rate of ethylbenzene (**14a**) at increasing concentrations of styrene (**13a**) is in agreement with the observed zeroth

rate order (Figure IX.9c). Moreover, kinetic studies of the reduction of **13a** under H_2 and N_2 atmosphere show the same rate and final yield of reduced product (**14a**) indicating that the hydrogen atoms incorporated in **14a** do not come from a possible molecular H_2 upon activation[71-74] (Figure IX.9d). All these results are indicative that both water reduction to H_2 and olefin reduction to alkanes share a common reaction intermediate, most likely a [Co-H] species. Moreover, taking into consideration the concentration of aromatic olefins (8.7 mM) and H_2O (55 M) under catalytic conditions, the putative [Co-H] species is highly selective for the reduction of **13a** versus H_2O.
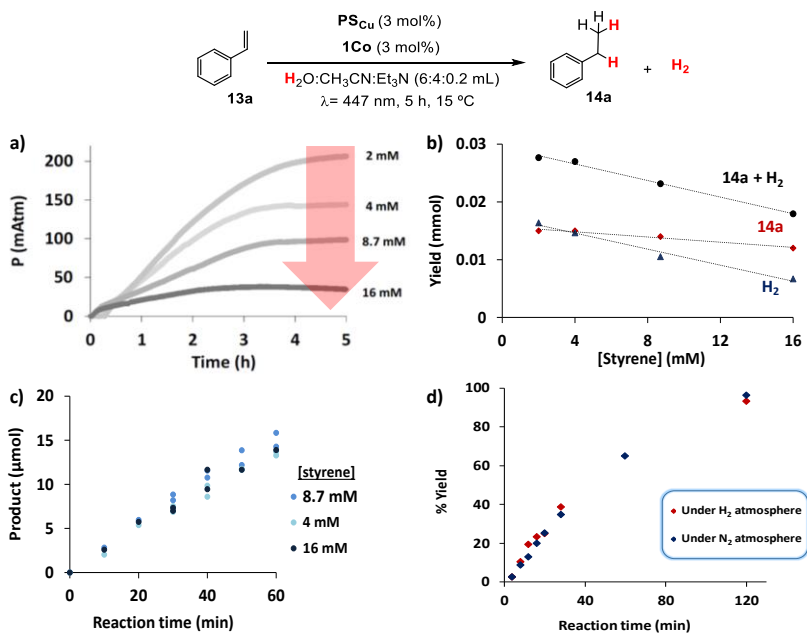
Figure IX.9. a) On-line monitoring of the photochemical H_2 production in the presence of increasing concentrations of **13a**. b) mmol of **14a** (red dots) and H_2 (blue dots) obtained under catalytic conditions and the sum of both (black dots). c) Monitoring of the formation of ethylbenzene (**14a**) at increasing concentrations of styrene (**13a**). d) Formation of **14a** (8.7 mM) catalyzed by **1Co** under H_2 (red diamonds) or N_2 (blue diamonds) atmosphere; each value of **14a** yield corresponds to an individual experiment. [a]Conditions **A**: **1Co** (3 mol%), **PS$_{Cu}$** (3 mol%), Substrate (2, 4, 8.7 and 16 mM, unless otherwise noticed) in $H_2O:CH_3CN:Et_3N$ (6:4:0.2 mL) irradiated 5 h (447 nm) at 15 ºC under N_2. The yield of **14a** was determined at several points during the kinetic study by taking aliquots of the reaction at different times. The LEDs were switched off and a new argon-purged syringe was used to take each aliquot. The yield at each time was determined by GC-FID by the ratio between the area of the substrate and the area of the reduced product.

IX.2.5.2. Molecularity of the catalytic system: Hg^0 poisoning experiments

To get insight in the nature of the active species and discard a possible formation of nanoparticles upon light irradiation along the reaction time, we performed a poisoning experiment with a large excess of Hg^0 (> 2000 eq. regarding the concentration of the cobalt catalyst) and in the absence of Hg under catalytic conditions. Hg^0 was added 15 minutes before starting the irradiation and the kinetic study. In both cases, the same amount of reduced product (**14a**) was formed with the same rate along the reaction time (Figure IX.10). Although this is not a definitive probe, nanoparticles are unlikely to be responsible for the observed light-driven reduction activity, suggesting that the activity belongs mainly to the homogeneous cobalt catalyst.[69] However, these results does not rule out the possible formation of nanoparticles derived from a decomposition process of the catalytic system, as previously demonstrated by using DLS and NTA experiments.[70]
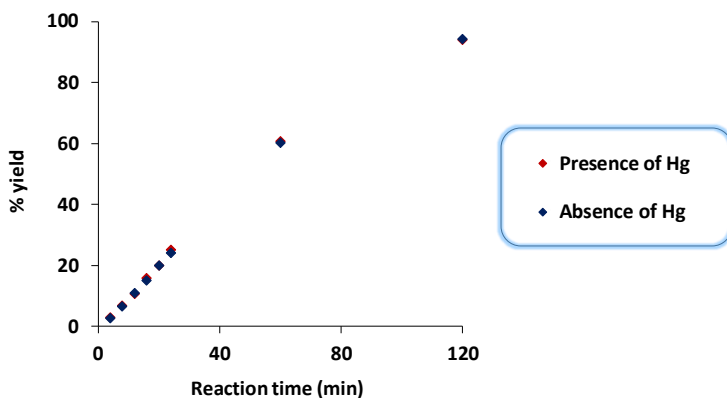
Figure IX.10. Formation of **14a** catalyzed by cobalt complex **1Co** in the absence (red diamonds) and presence of Hg(0) (>2000 eq.) (blue diamonds). Conditions: **1Co** (3% mol), **PS$_{Cu}$** (3% mol), substrate (8.7 mM) in H$_2$O:CH$_3$CN:Et$_3$N (6:4:0.2 mL) irradiation at λ = 447 nm for 2h at 15 ºC under N$_2$. The yield of **14a** was determined at several points during the kinetic study by taking aliquots of the reaction at different times. The LEDs were switched off and a new argon-purged syringe was used to take each aliquot. The yield at each time was determined by GC-FID by the ratio between the area of the substrate and the area of the reduced product. Yield of **14a**: 94% in absence of Hg(0) and 94% in the presence of Hg(0).

UNIVERSITAT ROVIRA I VIRGILI
MECHANISTIC STUDIES OF WATER OXIDATION CATALYZED BY HOMOGENEOUS IRON AND RUTHENIUM
COMPLEXES AND LIGHT-DRIVEN ORGANIC REDUCTIONS WITH A DUAL COBALT/COPPER CATALYTIC SYSTEM
Carla Casadevall Serrano

CHAPTER IX   Dual Co/Cu Light-driven Olefin Reduction

IX.2.5.3. Effect of the temperature in the photoreduction of styrene (13a) and α-methylstyrene (15a) and dimer formation

As presented at the beginning of the chapter, the product distribution in the photoreduction of styrene (**13a**) and α-methylstyrene (**15a**) is strongly dependent on the catalytic conditions. Indeed the reaction temperature has an important effect in the selectivity of the reductions for the formation of the reduced product vs the homocoupling reduced product. To get mechanistic information on the formation of benzyl radicals in the reduction of aromatic olefins with our dual cobalt-copper catalytic system we studied the effect of the temperature in the product distribution in the light-driven reduction of styrene (**13a**) and α-methlstyrene (**15a**), respectively. For both substrates, the formation of dimeric products (**17a** and **14'a**, respectively) dramatically increases with the decrease of the reduced products (**14a** and **16a**, respectively) with the increase of the temperature (Figure IX.11). However, the impact is more significant in the case of the α-methylstyrene.
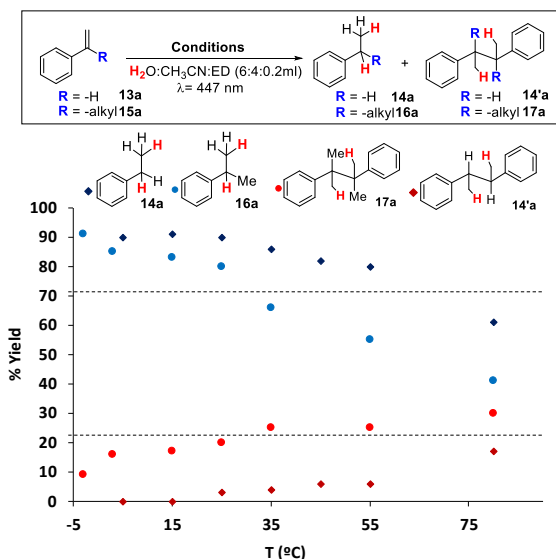
Figure IX.11. Plot of the yield of reduced products **14a** and **16a** and dimers **14a'** and **17a** *vs* the reaction temperature. Catalytic conditions **A** (**13a**): **1Co** (261 μM, 3% mol), **PS$_{Cu}$** (261 μM, 3% mol), substrate **13a** (8.7 mM) in H$_2$O:CH$_3$CN:Et$_3$N (6:4:0.2 mL); **B** (**15a**): **1Co** (261 μM, 6% mol), **PS$_{Cu}$** (261 μM, 6% mol), substrate **15a** (4.4 mM) in H$_2$O:MeCN:^{i}Pr$_2$EtN (6:4:0.2 mL) irradiation at λ = 447 nm from 2h to 24h (depending on the temperature) under N$_2$. Yields were determined by GC analysis after workup of the reaction and they were relative to a calibrated internal standard. Values are averages of triplicates.

At higher temperatures (>35 ºC) the yield of the reduced product drops in favor of the formation of the reductive homocoupling product, which could be isolated and characterized by NMR (see annex VII Figures A.VII.45-46). In addition, small quantities of trimers or higher order reduced homocoupling products were also detected by GC-MS in the reduction of α-methylstyrene (**15a**) at those high temperatures. In contrast, at low temperatures (-3 ºC) the dimeric products are negligible (Figure IX.13). On the other hand, in the case of styrene (**13a**), the yield of the reduced product significantly drops at temperatures higher than 55 ºC in favor of the formation of dimeric products (Figure IX.13). These results are consistent with a HAT mechanism.

IX.2.5.4. Isotopic labeling studies

To get an insight about the source of the hydrogen atoms incorporated into the organic unsaturated substrates upon hydrogenation, a series of deuterium isotopic labeling studies were performed using the same catalytic conditions by just changing H_2O by D_2O. The final products were recovered from the reaction mixture and characterized by ^1H-NMR and $^{13}C\{^1H\}$-NMR spectroscopy and GC-MS. First, the photocatalytic reduction of several aromatic olefins (**13b**, **15a**, **15h** and **18c**) with the dual PS_{Cu}/**1Co** catalytic system in D_2O was studied. For olefins **13b** and **15h**, we observed nearly quantitative olefin deuteration (Scheme IX.4). These results suggest that the source of hydrides (or deuterides) cannot be attributed to a molecular hydrogen activation process,[71-74] and that the H_2O solvent is the source of hydrogen atoms (or D_2O when evaluating the deuterium incorporation into the final reduced product).
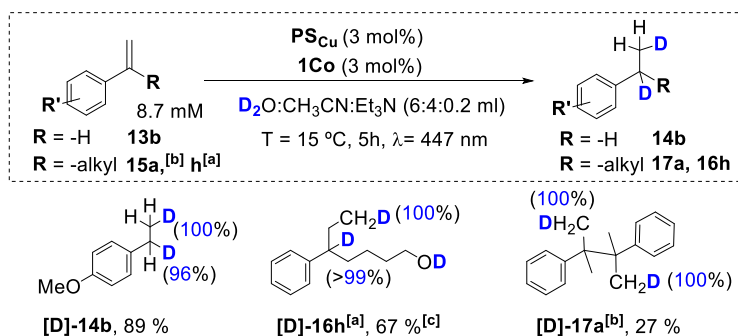
Scheme IX.4. Deuterium labeling studies of aromatic olefins (**13b**, **15a**, **h** and **18c**).[a] **1Co** (6 mol%), **PS$_{Cu}$** (6 mol%), Subs. (4.4 mM) in D$_2$O:CH$_3$CN:^{i}Pr$_2$EtN (6:4:0.2 mL) irradiated (447 nm) for 24 h at -3 ºC under N$_2$. [b] Conditions [a] modifying [Subs.] to 16 mM and 5h at 30 ºC. Isolated yields (average of 16 reactions). Deuterium insertion analyzed by NMR.

Analytics by ^{1}H-NMR and ^{13}C{^{1}H}-NMR spectroscopy show the incorporation of one deuterium atom in each alkyl site of the double bond (α and β) (Figures IX.12 – IX.15). For substrate **13b**, after the reduction under photocatalytic conditions using D$_2$O, the integrals of the ^{1}H-NMR signals attributed to the CH$_2$ and CH$_3$ hydrogens from the reduced product **[D]-14b** were reduced from 2 to 1 and from 3 to 2, respectively as compared to **14b**, indicating the deuteration of these positions when using D$_2$O (Figure IX.12). Moreover, the reduction of the ^{13}C{^{1}H}-NMR signals attributed to the CH$_2$ and CH$_3$ hydrogens from **[D]-14b** were also reduced and appeared as multiplet, confirming the deuteration of these positions when using D$_2$O (Figure IX.13). GC-MS analysis of the hydrogenated and the deuterated reduced products shows that **[D]-14b** has a mass two units higher than **14b** (138.1 vs 136.1, Figure IX.14, *inset*). Likewise, for substrate **15h**, after the reduction under photocatalytic conditions using D$_2$O, the integrals of the ^{1}H-NMR signals attributed to the CH and CH$_3$ hydrogens from the reduced product **[D]-16h** were reduced as compared to **16h**, indicating the deuteration of these positions when using D$_2$O (Figure IX.14). Moreover, the reduction of the ^{13}C{^{1}H}-NMR signals attributed to the CH from **[D]-16h** disappear in the spectrum upon reduction using D$_2$O, and the CH$_3$ hydrogens signals were also reduced, confirming the deuteration of these positions when using D$_2$O (Figure IX.15). In addition, in the ^{13}C{^{1}H}-DEPT-135-

UNIVERSITAT ROVIRA I VIRGILI
MECHANISTIC STUDIES OF WATER OXIDATION CATALYZED BY HOMOGENEOUS IRON AND RUTHENIUM
COMPLEXES AND LIGHT-DRIVEN ORGANIC REDUCTIONS WITH A DUAL COBALT/COPPER CATALYTIC SYSTEM
Carla Casadevall Serrano

CHAPTER IX   Dual Co/Cu Light-driven Olefin Reduction

NMR spectrum of **[D]-16h** the amplification of the area of the methyl with the insertion of deuterium shows the triplet due to the C-D coupling (Figure IX.17). GC-MS analysis of the hydrogenated and the deuterated reduced products shows that **[D]-16h** has a mass two units higher than **16h** (180.1 vs 178.1, Figure IX.14, *inset*).

In addition, deuterium incorporation into dimeric products was also studied. Labelling studies of α-methylstyrene (**15a**) under catalytic conditions that favour the reduced homocoupling product (high temperature and high concentration of substrate) showed the incorporation of only two deuterium atoms, each one at different methyl group of the coupling product (Scheme IX.4). The integrals of the ^{1}H-NMR signals attributed to the CH_3 hydrogens from the reduced homocoupling product **[D]-17a** were reduced as compared to **17a** from 12 to 10, indicating the deuteration of 2 of the 4 CH_3 positions in the resulting homocoupling reduced product **[D]-17a** when using D_2O (Figure IX.16). Moreover, the $^{13}C\{^1H\}$-NMR signals attributed to the CH_3 from **[D]-17a** appear as a triplet due to the C-D coupling (Figure IX.17). GC-MS analysis of the hydrogenated and the deuterated reduced products shows that **[D]-17a** has a mass two units higher than **17a** (240.0 vs 238.1, Figure IX.14, *inset*). These results supports the reaction of a [Co-D] intermediate with the olefin *via* an atom transfer (HAT) mechanism to the less hindered carbon, as in the case of H_2O.
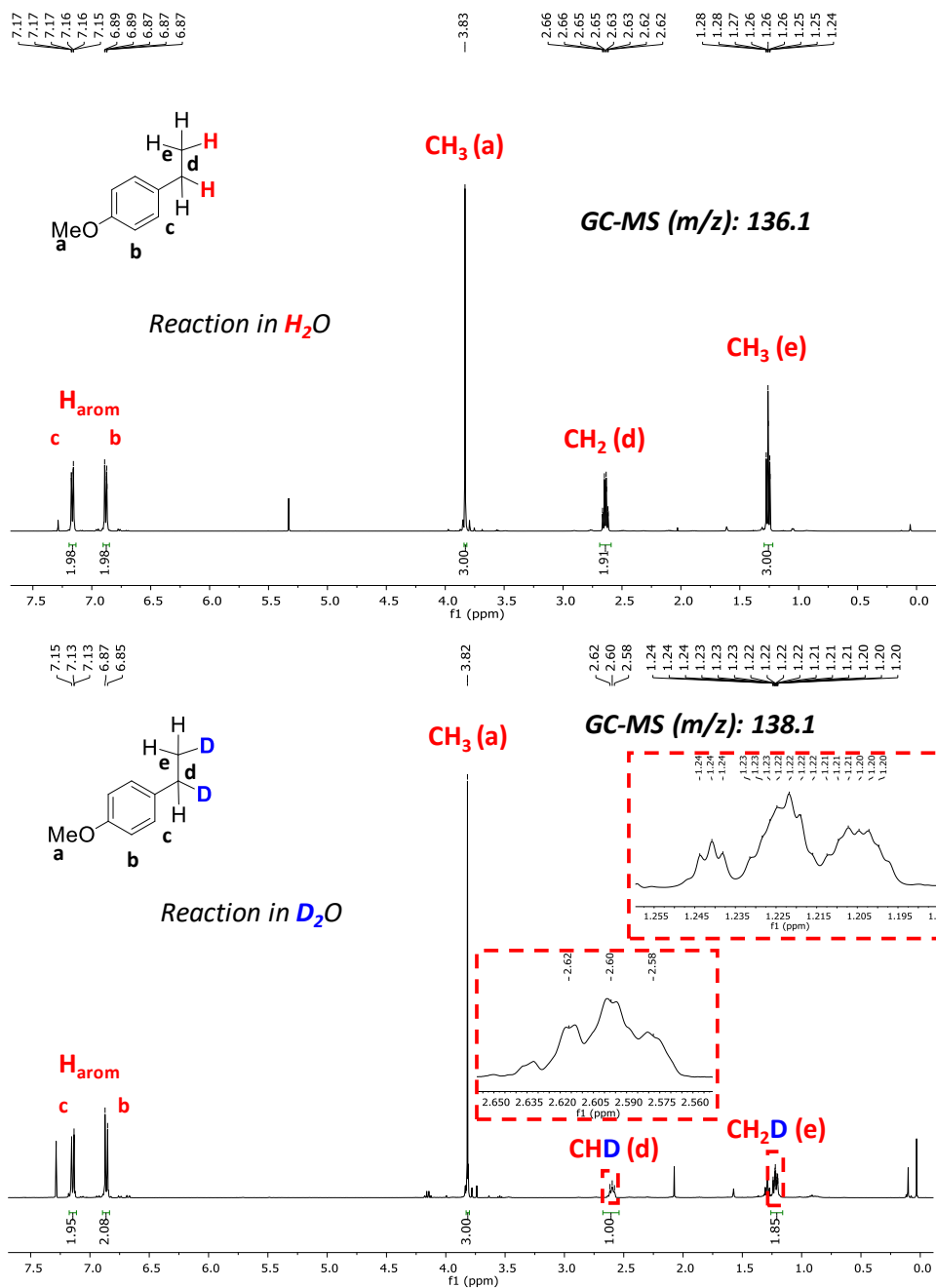
Figure IX.12. ^{1}H-NMR spectrum (CDCl$_3$, 400 MHz, 300 K) of the isolated products **14b** and **[D]-14b** using H$_2$O (Top) or D$_2$O (99.9 % in deuterium) (Bottom) in the solvent mixture, respectively. Conditions: **1Co** (3 mol%), **PS$_{Cu}$** (3 mol%), substrate (0.087 mmol, 8.7 mM) in H$_2$O (or D$_2$O):CH$_3$CN:Et$_3$N (6:4:0.2 mL) irradiated at λ = 447 nm and 15 °C for 5h, under N$_2$. Inset: amplification of the area of the –CHD and the –CH$_2$D.
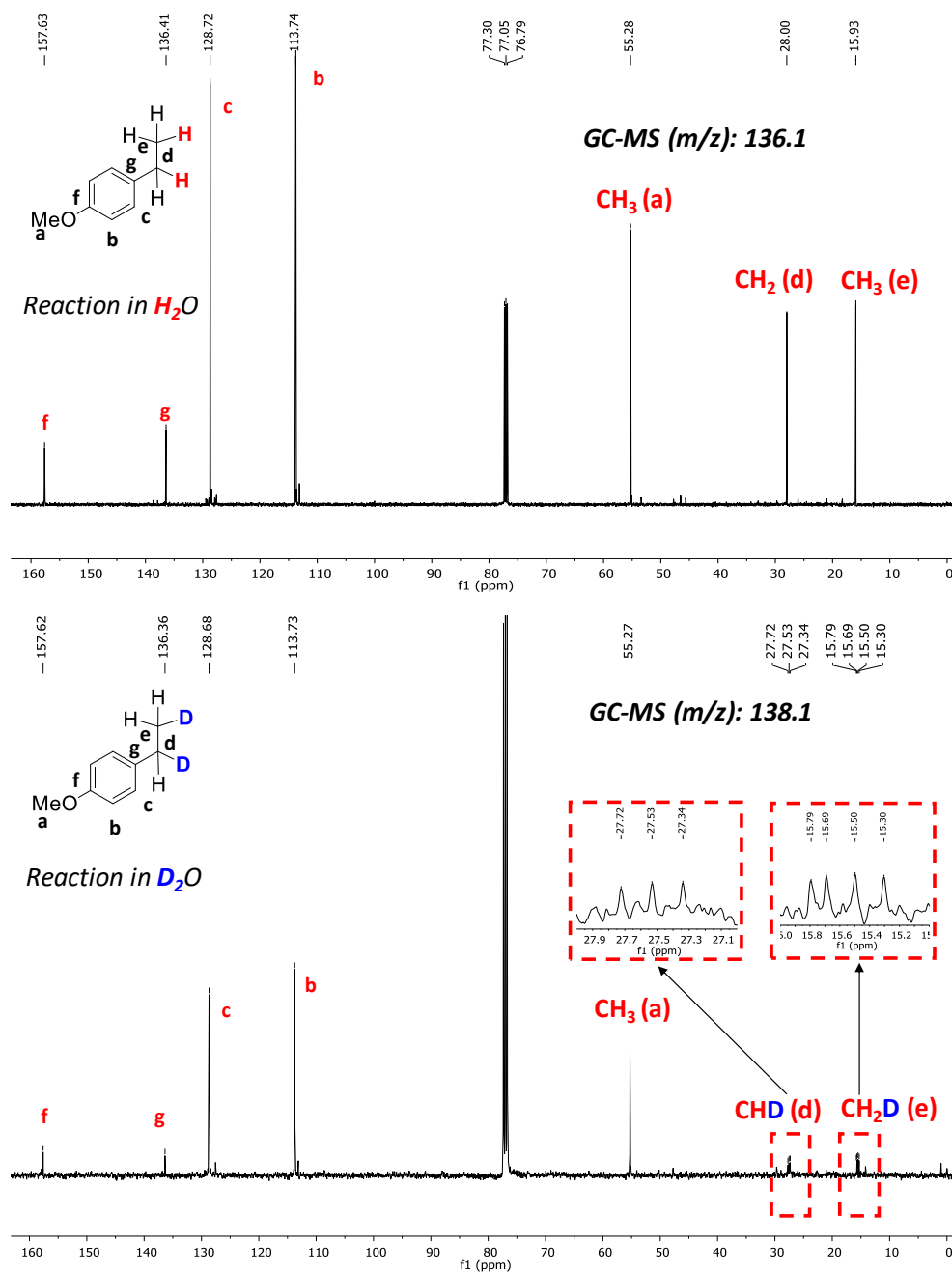
Figure IX.13. $^{13}C\{^1H\}$-NMR spectrum (CDCl3, 100.6 MHz, 300 K) of the isolated products **14b** and **[D]-14b** using H_2O (Top) or D_2O (99.9 % in deuterium) (Bottom) in the solvent mixture, respectively. Conditions: **1Co** (3 mol%), **PS_Cu** (3 mol%), substrate (0.087 mmol, 8.7 mM) in H_2O (or D_2O):CH3CN:Et3N (6:4:0.2 mL) irradiated at λ = 447 nm and 15 ºC for 5h, under N_2. Inset: amplification of the area of the –CHD and –CH2D.
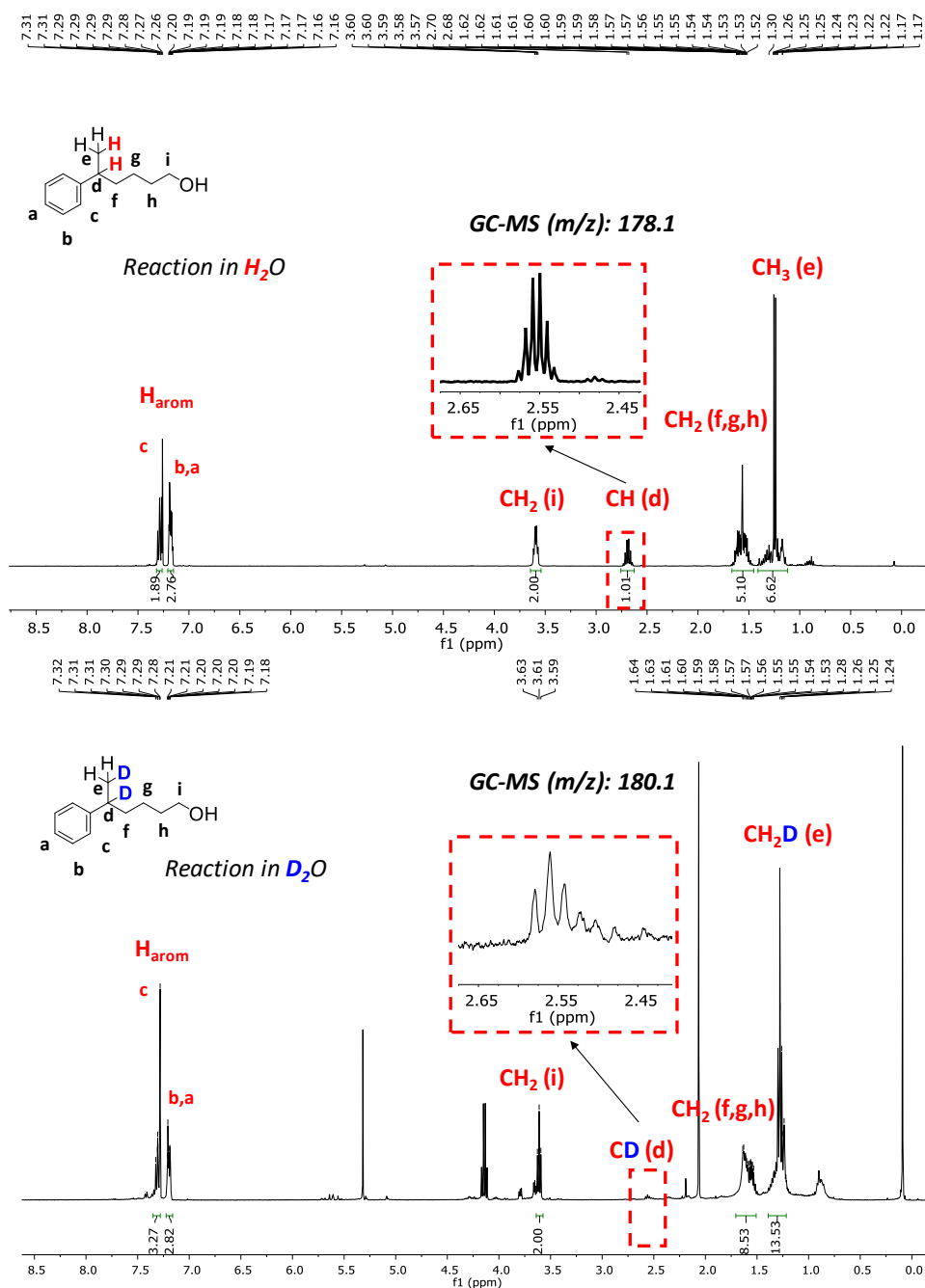
Figure IX.14. ^{1}H-NMR spectrum (CDCl$_3$, 400 MHz, 300 K) of the isolated products **16h** and **[D]-16h** using H$_2$O (Top) or D$_2$O (99.9 % in deuterium) (Bottom) in the solvent mixture, respectively. Conditions: **1Co** (6 mol%), **PS$_{Cu}$** (6 mol%), substrate (0.044 mmol, 4.4 mM) in H$_2$O (or D$_2$O):CH$_3$CN:^{i}Pr$_2$EtN (6:4:0.2 mL) irradiated at λ = 447 nm and -3 °C for 24h, under N$_2$. Inset: amplification of the area of the –CH *vs* -CD.
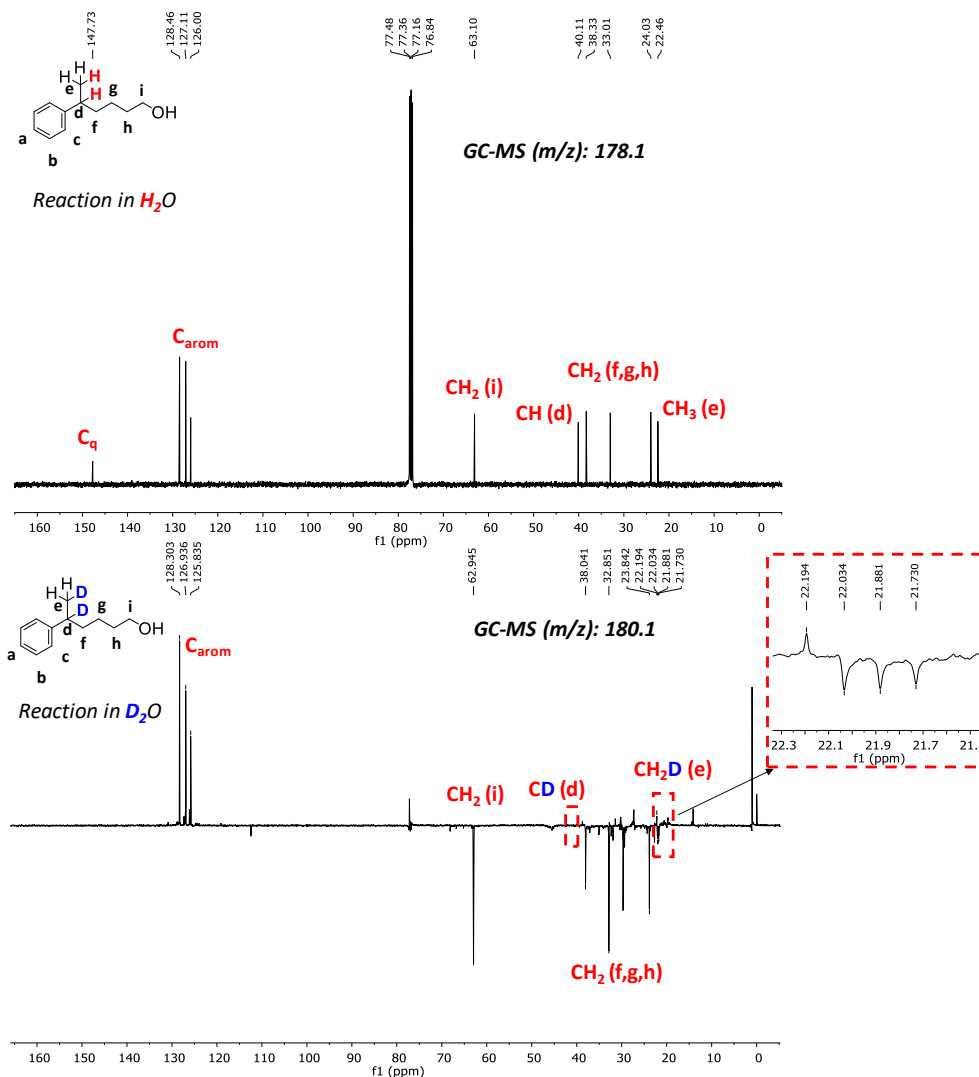
Figure IX.15. $^{13}C\{^1H\}$-NMR and $^{13}C\{^1H\}$-DEPT-135-NMR spectrum (CDCl$_3$, 100.6 MHz, 300 K) of the isolated products **16h** and **[D]-16h,** using H$_2$O (Top) or D$_2$O (99.9 % in deuterium) (Bottom) in the solvent mixture, respectively. Conditions: **1Co** (6 mol%), **PS$_{Cu}$** (6 mol%), substrate (0.044 mmol, 4.4 mM) in H$_2$O (or D$_2$O):CH$_3$CN:^{i}Pr$_2$EtN (6:4:0.2 mL) irradiated at λ = 447 nm and -3 ºC for 24h, under N$_2$. Inset: amplification of the area of the -CH$_2$D with the insertion of deuterium showing the triplet due to the C-D coupling.
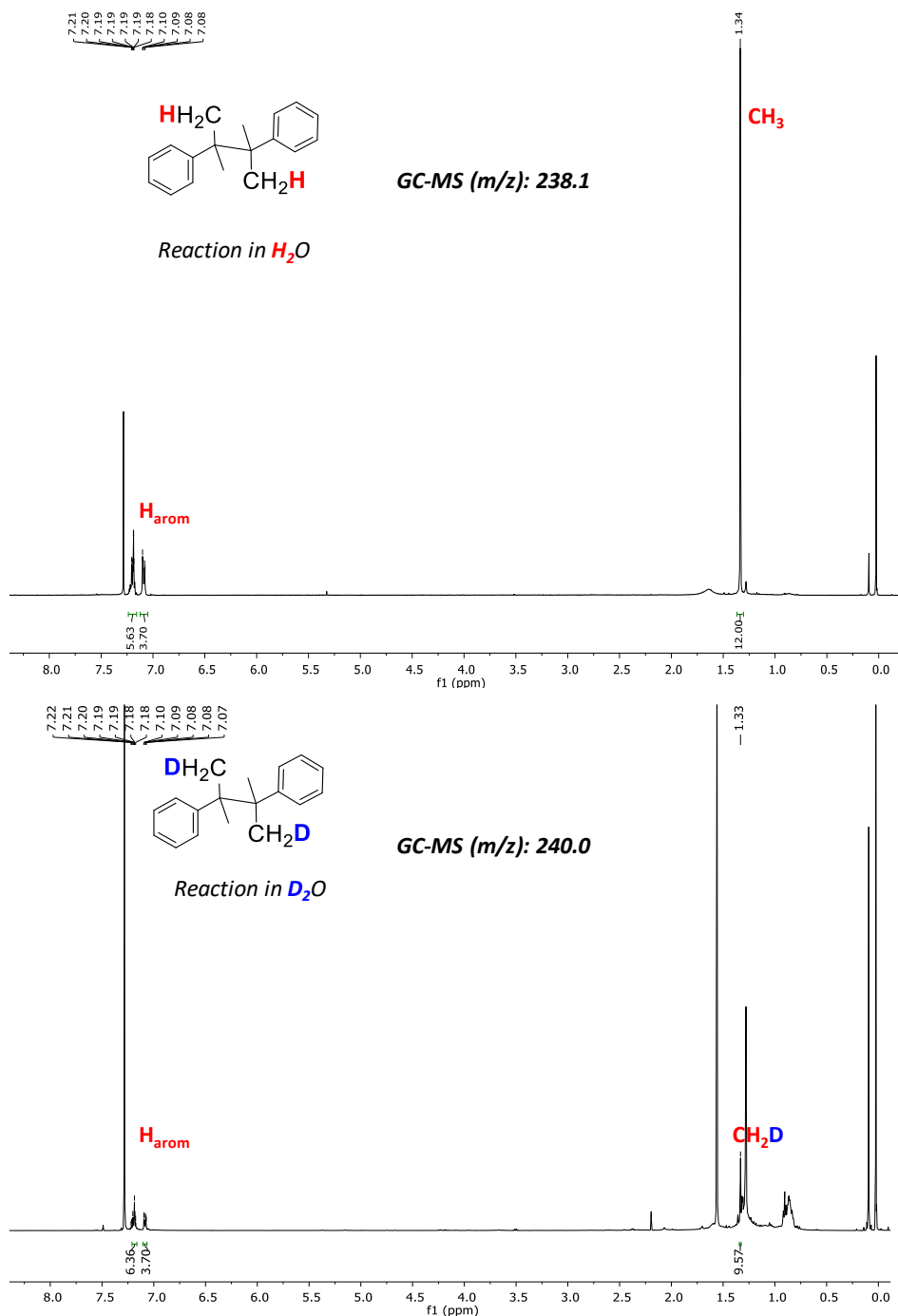
Figure IX.16. ^{1}H-NMR spectrum (CDCl$_3$, 400 MHz, 300 K) of the isolated product **17a** and **[D]-17a** using H$_2$O (Top) or D$_2$O (99.9 % in deuterium) (Bottom) in the solvent mixture, respectively. Conditions: **1Co** (6 mol%), **PS$_{Cu}$** (6 mol%), substrate (0.165 mmol, 16.5 mM) in H$_2$O (or D$_2$O):CH$_3$CN:^{i}Pr$_2$EtN (6:4:0.2 mL) irradiated at λ= 447 nm and 30 ºC for 5h, under N$_2$.

Figure IX.17. $^{13}C\{^{1}H\}$-NMR and $^{13}C\{^{1}H\}$-DEPT-135-NMR spectrum (CDCl₃, 125.8 MHz, 300 K) of the isolated product **17a** and **[D]-17a** using H₂O (Top) or D₂O (99.9 % in deuterium) (Bottom) in the solvent mixture, respectively. Conditions: **1Co** (6 mol%), **PS_{Cu}** (6 mol%), substrate (0.165 mmol, 16.5 mM) in H₂O (or D₂O):CH₃CN:^{i}Pr₂EtN (6:4:0.2 mL) irradiated at λ= 447 nm and 30 °C for 5h, under N₂. Inset: amplification of the area of the -CH₂D showing the triplet due to the C-D coupling.

Altogether is in agreement with the incorporation of the hydrogen equivalents directly from the solvent, being hydrogen when using H₂O or deuterium when using D₂O, in the hydrogenated positions. This in concordance with the same observed kinetics for the light-driven styrene (**13a**) reduction under H₂ and N₂ atmosphere (Figure IX.18).
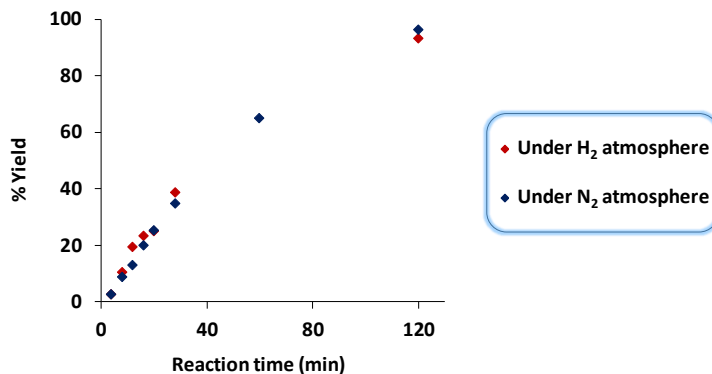
Figure IX.18. Formation of **14a** catalyzed by cobalt complex **1Co** under H_2 (red diamonds) or N_2 (blue diamonds) atmosphere. Conditions: **1Co** (3% mol), **PS$_{Cu}$** (3% mol), substrate (8.7 mM) in $H_2O:CH_3CN:Et_3N$ (6:4:0.2 mL) irradiated at $\lambda = 447$ nm for 2h at 15 ºC under N_2. Each value of **14a** yield corresponds to an individual experiment. The yield of **14a** was determined by GC analysis after the workup of the reaction and using the ratio between the substrate and the product areas. Yield of **14a**: 93% and 96% under H_2 and N_2 atmosphere, respectively.

IX.2.5.5. Radical clock experiments

We have performed experiments with 2-aryl-cyclopropyl olefins to further confirm the formation benzyl radicals in solution under catalytic conditions via a HAT mechanism from the putative [Co-H] species. Olefins containing a 2-aryl-cyclopropyl moiety at the α-position are commonly used as diagnostic probes for radicalary mechanisms in organic transformations.[75-78] For example, if a SET is involved, it will trigger the cyclopropane ring opening with a rate constant in the 10^5-10^7 s^{-1} range.[78] Under our catalytic conditions (catalytic conditions B, optimized for 1,1-disubstituted olefins) the reduction of (1-(2-phenylcyclopropyl)vinyl)benzene (**16i**) gives the ring-opening product (**17i**) in 81% yield without detection of **18i** (Scheme IX.5). Interestingly, the use of D_2O instead of H_2O in the reduction of (1-(2-phenylcyclopropyl)vinyl)benzene (**16i**) served to identify the reduced positions. Under these conditions, the deuterated ring-opening product (**[D]-17i**) was obtained in 43% (Scheme IX.5).

The integrals of the ^1H-NMR signals attributed to the CH_3 and CH_2 hydrogens from the reduced product **[D]-17i** were both reduced in one unit as compared to **17i**,

indicating the deuteration those positions in the resulting reduced product **[D]-17i** when using D_2O (Figure IX.21). Moreover, the $^{13}C\{^1H\}$-NMR signals attributed to the CH_3 and CH_2 hydrogens from **[D]-17i** appear less intense and as a triplet due to the C-D coupling (Figure IX.22). Moreover, GC-MS analysis of the hydrogenated and the deuterated reduced products show that **[D]-17i** has a mass two units higher than **17i** (224.2 vs 222.1, Figure IX.21, *inset*). Therefore, the isotopic labelling observed together with radical clock experiments provide light on the mechanism of action. These results support the reaction of a [Co-D] intermediate with (1-(2-phenylcyclopropyl)vinyl)benzene (**16i**) *via* a hydrogen atom transfer (HAT) mechanism to the less hindered carbon, as in the case of H_2O ([Co-H]). Then the cyclopropane ring opens and rearranges to the most stable radical product, generating an unsaturated radicalary intermediate (Scheme IX.5). Then, a second [Co-D] (or [Co-H]) species reacts with the latter unsaturated benzyl radical via a second HAT to generate the reduced ring-opening product **[D]-17i** (or **17i**) (Scheme IX.5). This two subsequent HAT mechanism could, in principle, be extended to the rest of aromatic olefins of study in this chapter.
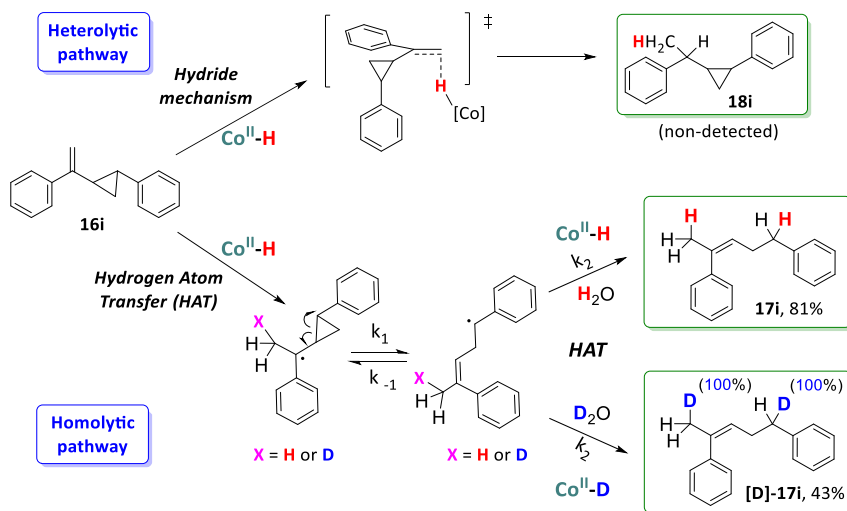
Scheme IX.5. Two possible reduction pathways for (1-(2-phenylcyclopropyl)vinyl)benzene **16i**.
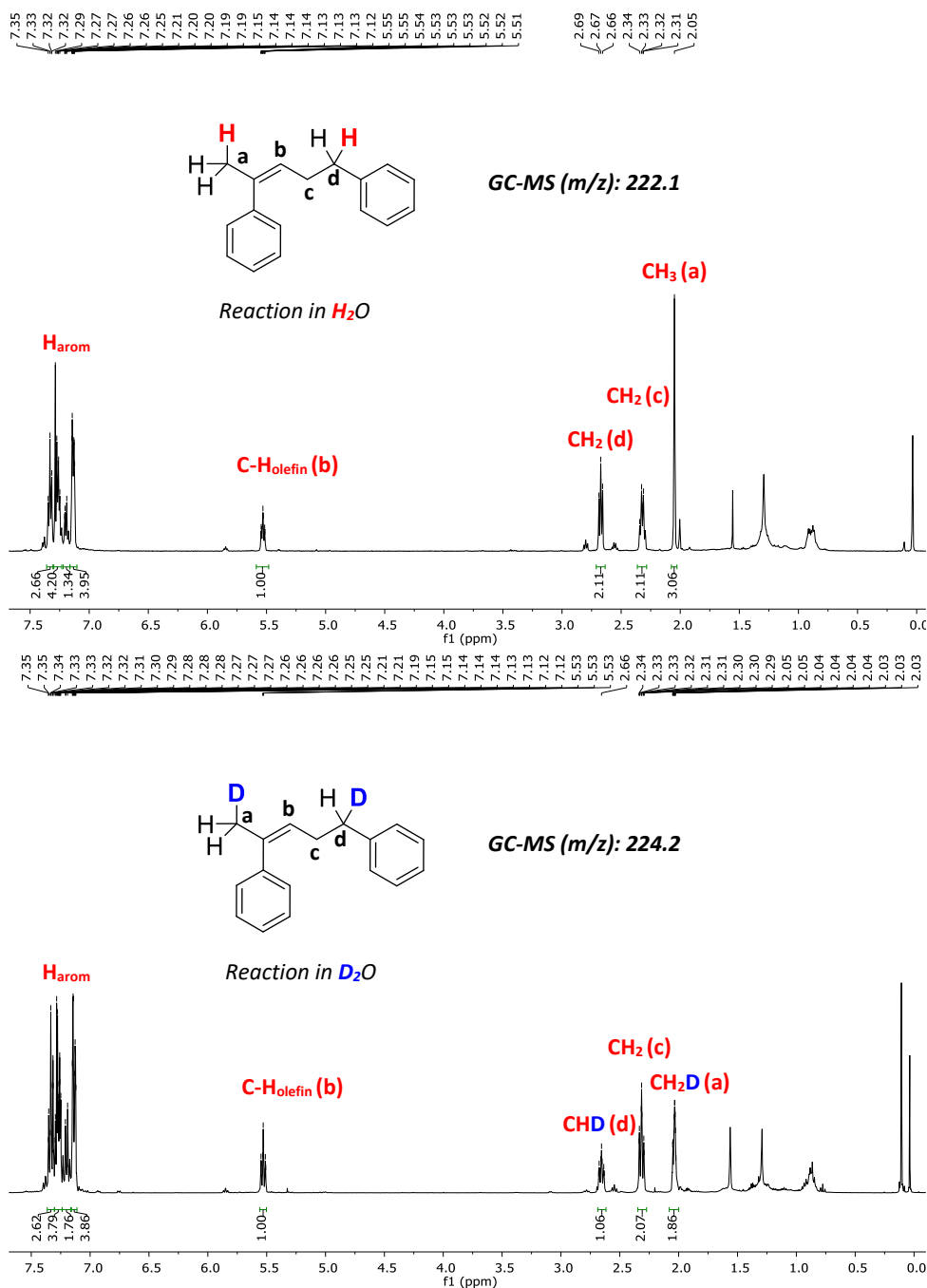
Figure IX.19. ^{1}H-NMR spectrum (CDCl$_3$, 400 MHz, 300 K) of the isolated product **17i** and **[D]-17i** using H$_2$O (Top) or D$_2$O (99.9 % in deuterium) (Bottom) in the solvent mixture, respectively. Conditions: **1Co** (6 mol%), **PS$_{Cu}$** (6 mol%), substrate (0.044 mmol, 4.4 mM) in H$_2$O (or D$_2$O):CH$_3$CN:^{i}Pr$_2$EtN (6:4:0.2 mL) irradiated at λ = 447 nm and -3 ºC for 24h, under N$_2$.

357
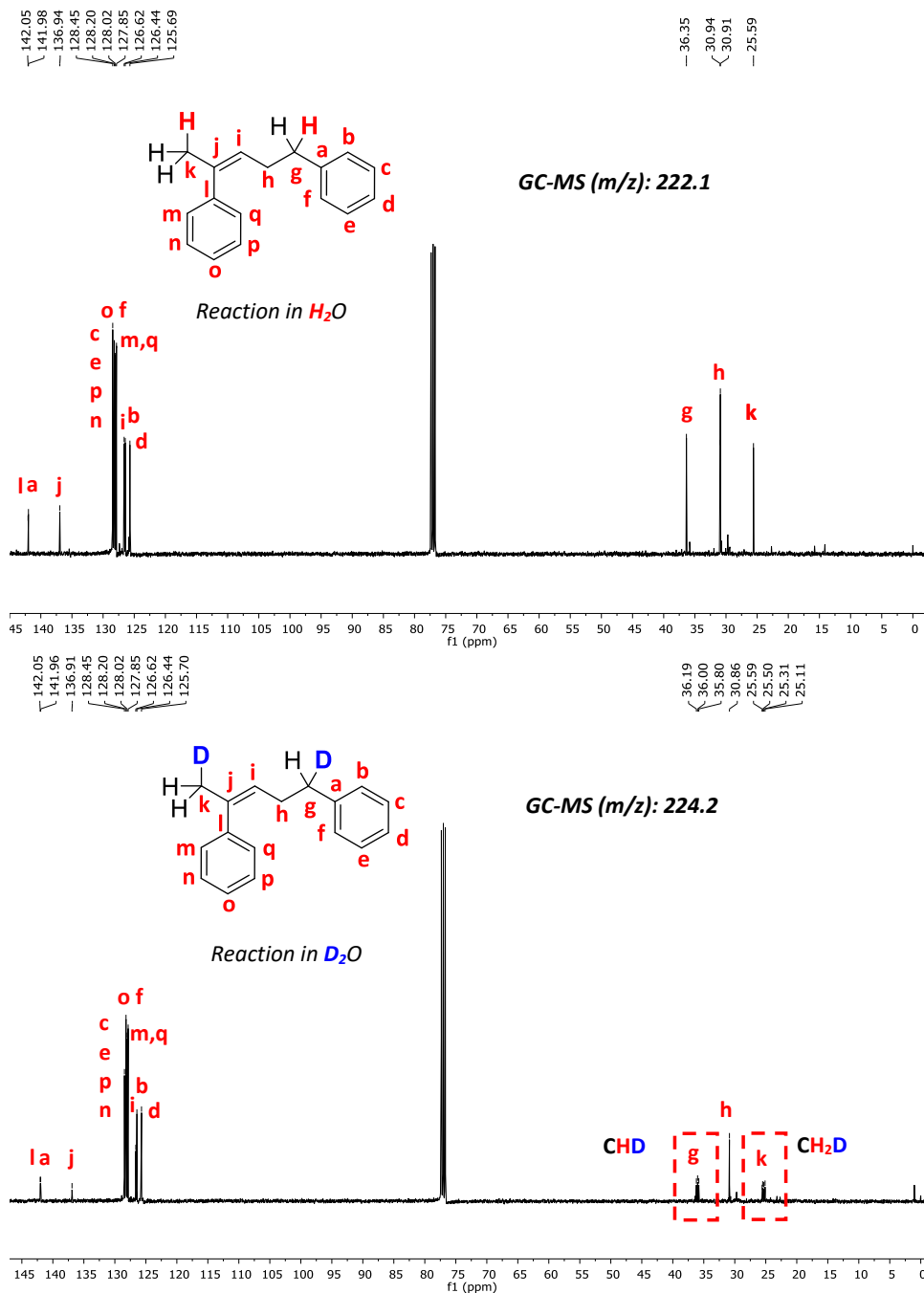
Figure IX.20. ^{13}C-NMR spectrum (CDCl$_3$, 100.6 MHz, 300 K) of the isolated product **17i** and **[D]-17i** using H$_2$O (Top) or D$_2$O (99.9 % in deuterium) (Bottom) in the solvent mixture, respectively. Conditions: **1Co** (6 mol%), **PS$_{Cu}$** (6 mol%), substrate (0.044 mmol, 4.4 mM) in H$_2$O (or D$_2$O):CH$_3$CN:^{i}Pr$_2$EtN (6:4:0.2 mL) irradiated at λ= 447 nm and -3 ºC for 24h, under N$_2$.

UNIVERSITAT ROVIRA I VIRGILI
MECHANISTIC STUDIES OF WATER OXIDATION CATALYZED BY HOMOGENEOUS IRON AND RUTHENIUM
COMPLEXES AND LIGHT-DRIVEN ORGANIC REDUCTIONS WITH A DUAL COBALT/COPPER CATALYTIC SYSTEM
Carla Casadevall Serrano

CHAPTER IX   Dual Co/Cu Light-driven Olefin Reduction

IX.2.5.6. Computational studies

In order to get a further mechanistic understanding of the mechanism for the reduction of aromatic olefins, we calculated the free energy barriers associated with the reduction of styrene (**13a**) by DFT. Geometry optimizations were performed with the B3LYP functional and the 6-31G* 6d basis set for all atoms, including the effect of the solvent (SMD implicit solvent model) and dispersion interactions (Grimme-D_2 correction) with the Gaussian09 software package (see experimental section *IX.4.4. Computational studies* for complete computational details).

It is known that under photocatalytic conditions **PS$_{Cu}$** is excited (***PS$_{Cu}$**) and reductively quenched by the **ED** to give **PS$_{Cu}$$^-$**,[79] which is reductive enough (E = -1.53 V *vs* SCE) to reduce complex **1Co** (E = -1.35 V *vs* SCE) by one electron to the highly reactive low oxidation state ([**1Co^I**]).[50] Intermediate [**1Co^I**] is protonated by water to form the putative [**1Co^{III}-H**]. [**1Co^{III}-H**] can be easily reduced under photocatalytic conditions (ΔG = -18.1 kcal·mol^{-1}) to [**1Co^{II}-H**]. Therefore, we focused the attention in the [**1Co^{II}-H**] intermediate. Indeed, the latter has been proposed as the active species in H_2 evolution and ketone reduction.[43,72,73,80,81] Then, we can envision two possible pathways for the photoreduction of olefins: A) a heterolytic mechanism where [**1Co^{II}-H**] nucleophilically attacks the double bond generating anionic species that after protonation yield the reduced alkane products (Figure IX.21.A); and B) a Hydrogen Atom Transfer (HAT) mechanism (Homolytic mechanism, Figure IX.21.B) in which the [Co-H] species transfers a hydrogen atom (H˙) to the olefin generating benzylic radical species. These benzylic radical species can follow a second HAT or, most likely, a SET + protonation can yield the reduced alkanes (Figure IX.22).

UNIVERSITAT ROVIRA I VIRGILI
MECHANISTIC STUDIES OF WATER OXIDATION CATALYZED BY HOMOGENEOUS IRON AND RUTHENIUM
COMPLEXES AND LIGHT-DRIVEN ORGANIC REDUCTIONS WITH A DUAL COBALT/COPPER CATALYTIC SYSTEM
Carla Casadevall Serrano

CHAPTER IX   Dual Co/Cu Light-driven Olefin Reduction
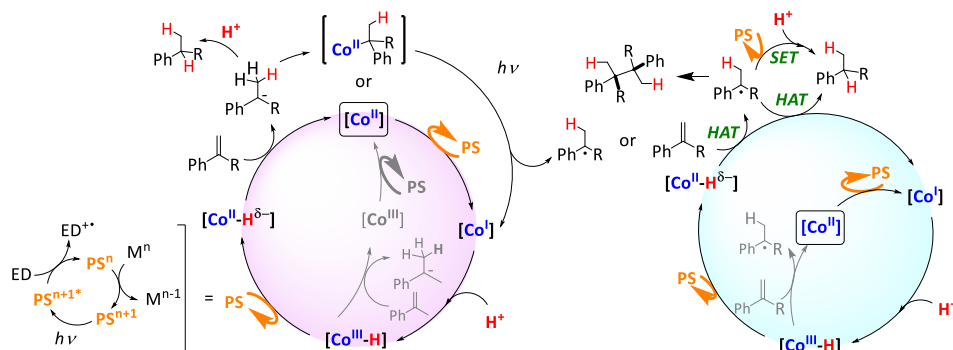
Figure IX.21. Possible mechanistic scenarios for the reduction of aromatic olefins by the light-driven dual-copper-cobalt catalytic system in aqueous media. The highlighted **[Co^{II}]** intermediate indicates the beginning of the catalytic cycles.
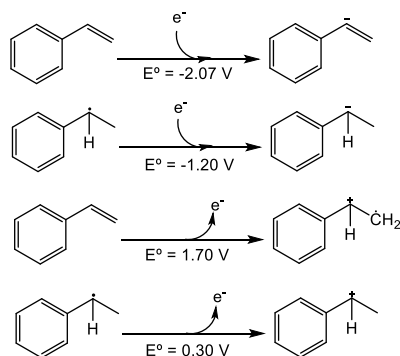
Figure IX.22. DFT calculated redox potentials for the above showed redox processes: a) from top to bottom: one electron reduction of styrene, one electron reduction of the benzylic radical, one electron oxidation of styrene and one electron oxidation of the benzylic radical. All the potentials are referred to SHE.

The formation of homocoupling products in the reduction of olefins, the labeling studies and the reduced product from the reactivity with radical clocks strongly suggest that the reduction of the olefin takes place *via* a HAT mechanism (Figure IX.21.B) from the photogenerated [**1Co^{II}-H**] species. Additionally, the formation of the corresponding organometallic species [**1Co^{II}-R**] ([**1Co^{II}-CH$_2$CH$_3$Ph**] in the case of styrene) derived from the reaction of [**1Co^{II}-H**] with the aromatic olefins is also compatible with the formation of dimers (Figure IX.21).

Indeed, Atom Transfer Radical Polymerization (ATRP) involves a chain initiation mechanism by a halogenated organic species in the presence of a metal halide, which abstracts the halide from the organohalide generating an organic radical in equilibrium with the metal halide. Nevertheless, we have explored by DFT the attack of the cobalt(II) hydride ([**1Co^{II}-H**])[34] to styrene (**13a**) as a model substrate. To this end, we pursued the following strategy in all possible spin states. First, we performed a scan shortening the distance between the hydrogen from the [Co-H] intermediate and the beta carbon of the styrene, to obtain the starting structures for the TS. In order to find the transition states it was needed to use a broken symmetry strategy. In addition, the localization of the unpaired electrons in the molecule was defined, in the calculations of the HAT mechanism, by using the graphical tool for defining fragments of the Gaussview software.

It is worth noted that the formation of [**1Co^{II}-H**] from **1Co** and **PS$_{Cu}$** as the reducing agent is thermodynamically feasible (ΔG = -12.0 kcal·mol^{-1}).[34,70] First, a hydride transfer from [**1Co^{II}-H**] to the C$_\alpha$ of the olefin was considered (Figure IX.23). The TS ($\Delta G^{\ddagger}$ = 19.0 kcal·mol^{-1}) is early since the [Co-H] distance (1.72 Å) is very similar to the initial reaction adduct (**I_S**, 1.71 Å). As expected, in the TS the metal center has a relevant spin density (ρ = 2.6) and no unpaired electrons are transferred to the substrate (Figures IX.24 and IX.25, **TS_S_hetero$_q$**). Alternatively, we have explored the HAT from [**1Co^{II}-H**] to the α carbon of the olefin (Figure IX.23). The free energy barrier ($\Delta G^{\ddagger}$ = 10.2 kcal·mol^{-1}) is lower in energy than the hydride transfer mechanism. In this TS the substrate has some spin density (ρ = -0.05) (Figure IX.24 and Figure IX.25, **TS_S_homo$_d$**), but not enough to relate the found transition state to a pure heterolytic (hydride transfer) or homolytic (HAT) mechanism.
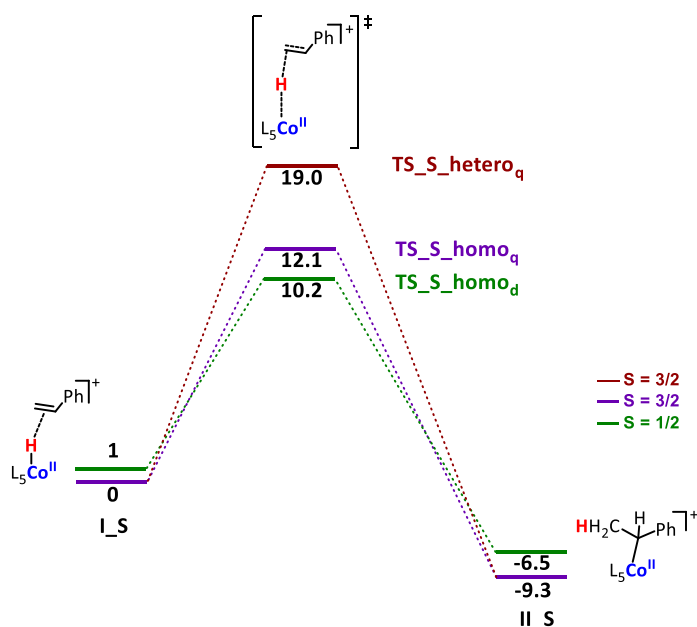
Figure IX.23. Comparison of the DFT modeled free energy profiles for hydride transfer and HAT mechanisms for styrene (**13a**) reduction under catalytic conditions (pH = 12). The L_5 label refers to the $Py_2^{Me}tacn$ ligand. Gibbs energies are in kcal·mol^{-1}.
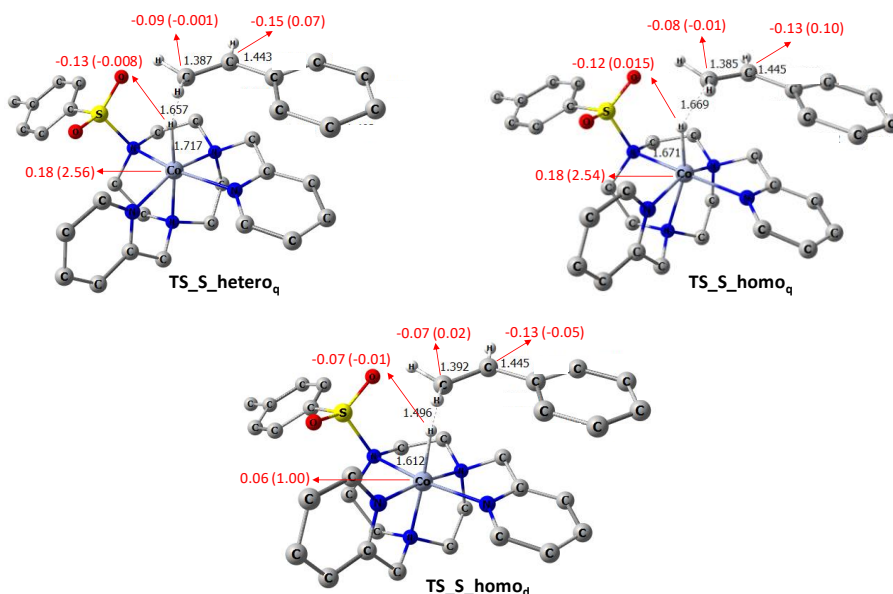
Figure IX.24. Optimized geometries of the transition state structures for the hydride mechanism (**TS_S_hetero$_q$**) and the hydrogen atom transfer mechanism (HAT, **TS_S_homo$_q$** and **TS_S_homo$_d$**) possibly involved in the photoreduction of styrene catalyzed by $[Co^{II}(H)(Py_2^{Ts}tacn)]^+$. Irrelevant hydrogen atoms are omitted for clarity. The most relevant bond distances are in Å. Hirshfeld charges and spin densities are shown in red and in brackets, respectively.
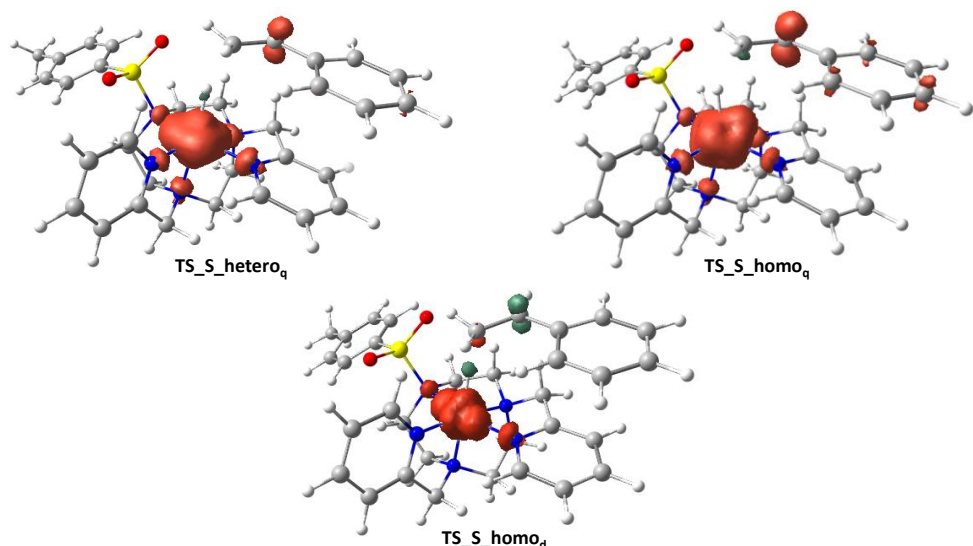
Figure IX.25. Spin density plots (isovalue = 0.006) of the transition state structures for the hydride transfer (**TS_S_hetero$_q$**) and the hydrogen atom transfer mechanisms (HAT, **TS_S_homo$_q$** and **TS_S_homo$_d$**) possibly involved in the photoreduction of styrene (**13a**) catalyzed by $[Co^{II}(H)(Py_2^{Ts}tacn)]^+$. Irrelevant hydrogen atoms are omitted for clarity.

Due to the intrinsic difficulty to differentiate between both scenarios (HAT vs hydride transfer), a detailed analysis of the bond distances, the Mulliken spin density, and charges involved in the bond-breaking/formation was done along the Intrinsic Reaction Coordinate (IRC, Figure IX.26 – IX.31). Although the detailed analysis it is not conclusive, it could be approximated to two extreme mechanisms; a homolytic HAT and a heterolytic hydride transfer mechanism.

In the case of the homolytic mechanism (HAT), the lower-in-energy transition state (**TS_S_homo$_d$**, S = 1/2), we observed a significant spin density (beta) in the alpha carbon, which is symptomatic of a radical formation (IRC point 0.4, Figure IX.26). Likewise, the beta spin on the olefin is higher (ρ = -0.46) but does not locate a full unpaired electron (green region of Figures IX.26 and IX.29). Therefore, until this point of the IRC, it can be described as a HAT. Then, the olefin suffers a fast increase of the negative charge together with a sharp decrease in the spin density. This data suggests a subsequent single electron transfer (SET) from the partial formation of a Co(I) during the HAT to the organic radical to generate an anion

363

(yellow region of Figure IX.28 and IX.29). Interesting enough, this process is thermodynamically feasible, the redox potentials calculated for both isolated fragments are: -1.59 V *vs* NHE for the Co(I) and -1.20 V *vs* NHE for the organic radical. Finally, the 2e$^-$ reduced product is reoriented to yield the organometallic species as a final product (**II_S**), which is obtained after optimization of the last point of the IRC. To conclude, the mechanism is postulated as an unusual asynchronous HAT+SET. A similar scenario is observed for the homolytic mechanism calculated in the S = 3/2 spin state (**TS_S_homo$_q$**). Nevertheless, some differences are observed. The spin density on the olefin alpha carbon is retained longer in the reaction path until the SET takes place to give the final reduced product. Further reorientation yields **II_S**. In contrast, for the calculated heterolytic mechanism, once the bond between the beta carbon and the hydrogen transferred is formed there is already a negative charge in the reduced product. This is in agreement with a hydride transfer mechanism (or with a synchronous HAT+SET), (Figure IX.31). As a summary, the lowest in energy mechanism, the **TS_S_homo$_d$** has more homolytic character than the **TS_S_hetero$_q$**.
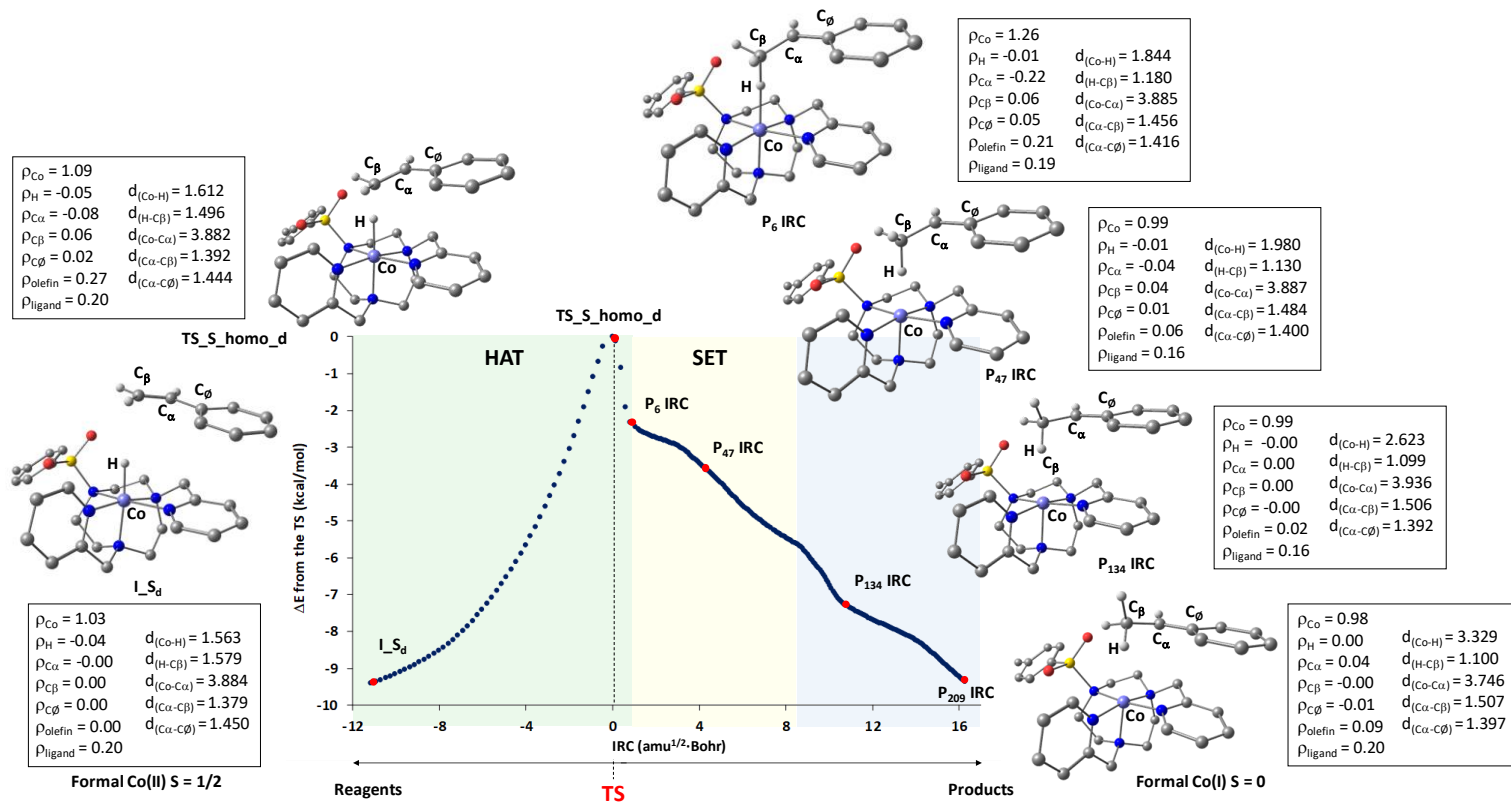
Figure IX.26. IRC connecting the TS involved in the hydrogen atom transfer mechanism (homolytic pathway, **TS_S_homo$_d$**) for the light-driven reduction of **13a** catalyzed by $[Co^{II}(H)(Py_2^{Me}tacn)]^+$ under catalytic conditions (pH = 12). Selected geometries (red dots) with corresponding Mulliken spin densities and selected bond distances along the reaction pathway illustrate the stepwise HAT + SET mechanism and the orientation of the 1e$^-$ reduced product to further give the organometallic intermediate **II_S**. Electronic energies are in kcal·mol^{-1}.

365
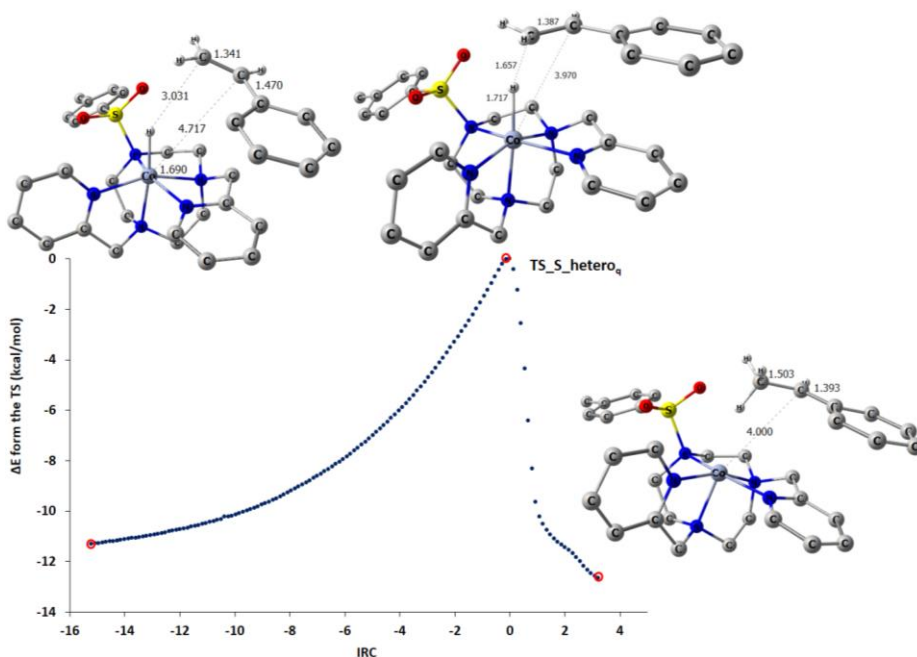
Figure IX.27. IRC connecting the TS involved in the hydride transfer mechanism (heterolytic pathway, **TS_S_hetero$_q$**) for the light-driven reduction of **13a** catalyzed by $[Co^{II}(H)(Py_2^{Me}tacn)]^+$ under catalytic conditions (pH = 12). Electronic energies are in kcal·mol^{-1}.
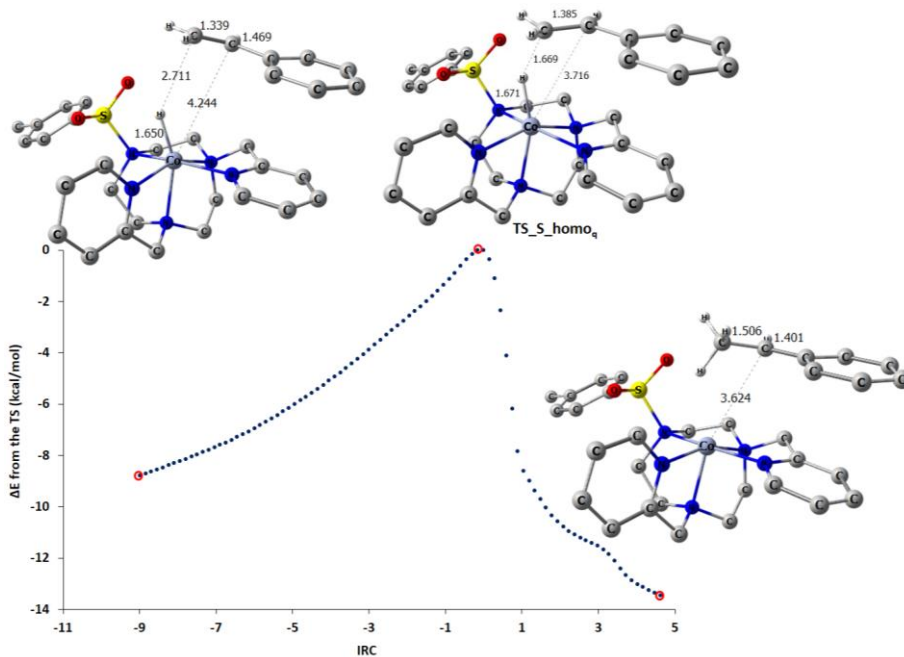
Figure IX.28. IRC connecting the TS involved in the hydrogen atom transfer mechanism (homolytic pathway, **TS_S_homo$_q$**) for the light-driven reduction of **13a** catalyzed by $[Co^{II}(H)(Py_2^{Me}tacn)]^+$ under catalytic conditions (pH = 12). Electronic energies are in kcal·mol^{-1}.
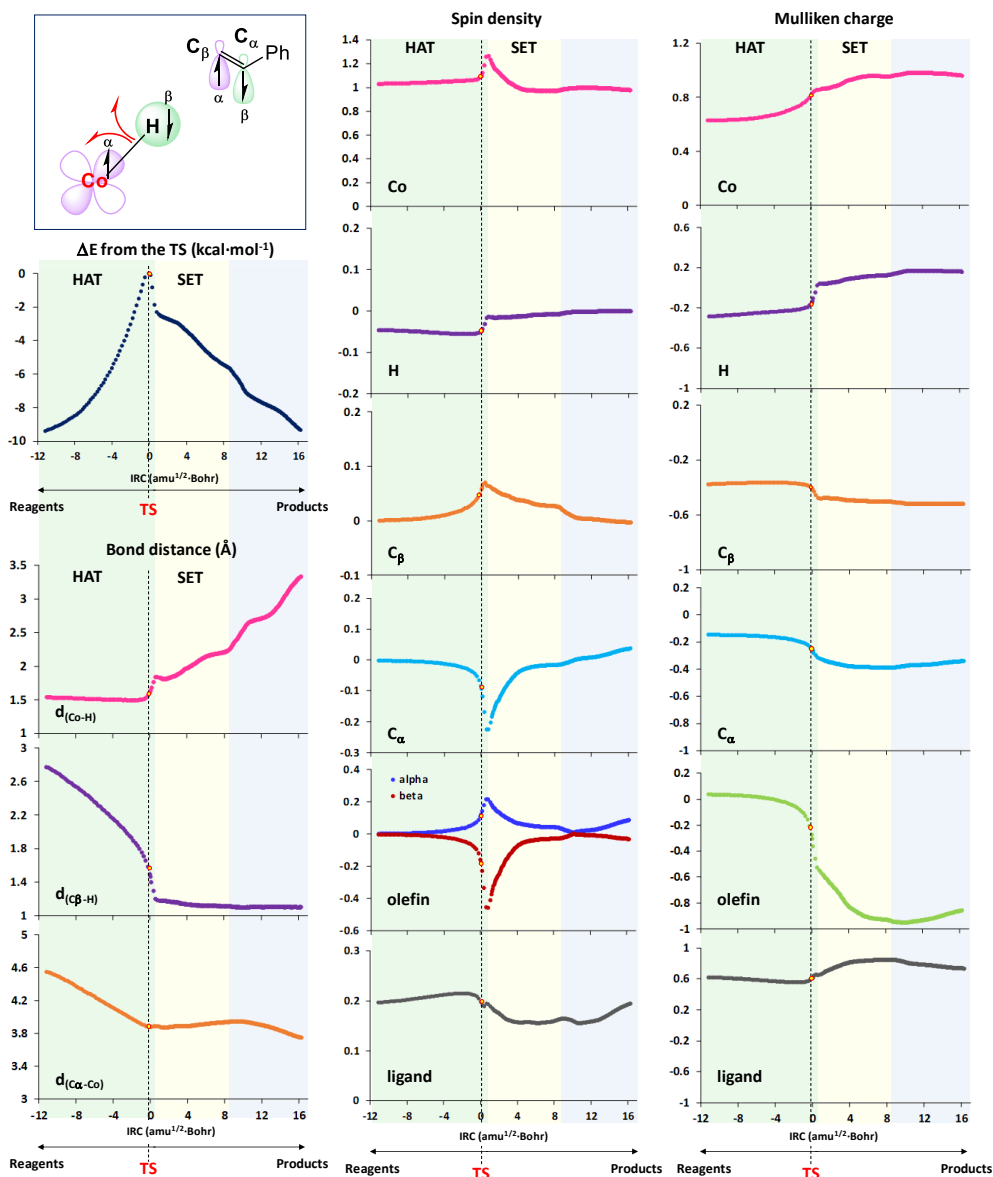
Figure IX.29. Selected bond distances (*left*) Mulliken spin densities (*middle*) and charges (*right*) along the IRC connecting the TS (highlighted dot in each plot) involved in the more homolytic mechanism (HAT) in S = 1/2 (**TS_S_homo_d**) for the light-driven reduction of **13a** catalyzed by **1Co** under catalytic conditions (pH = 12) with the reagent (*left*) and product (*right*).
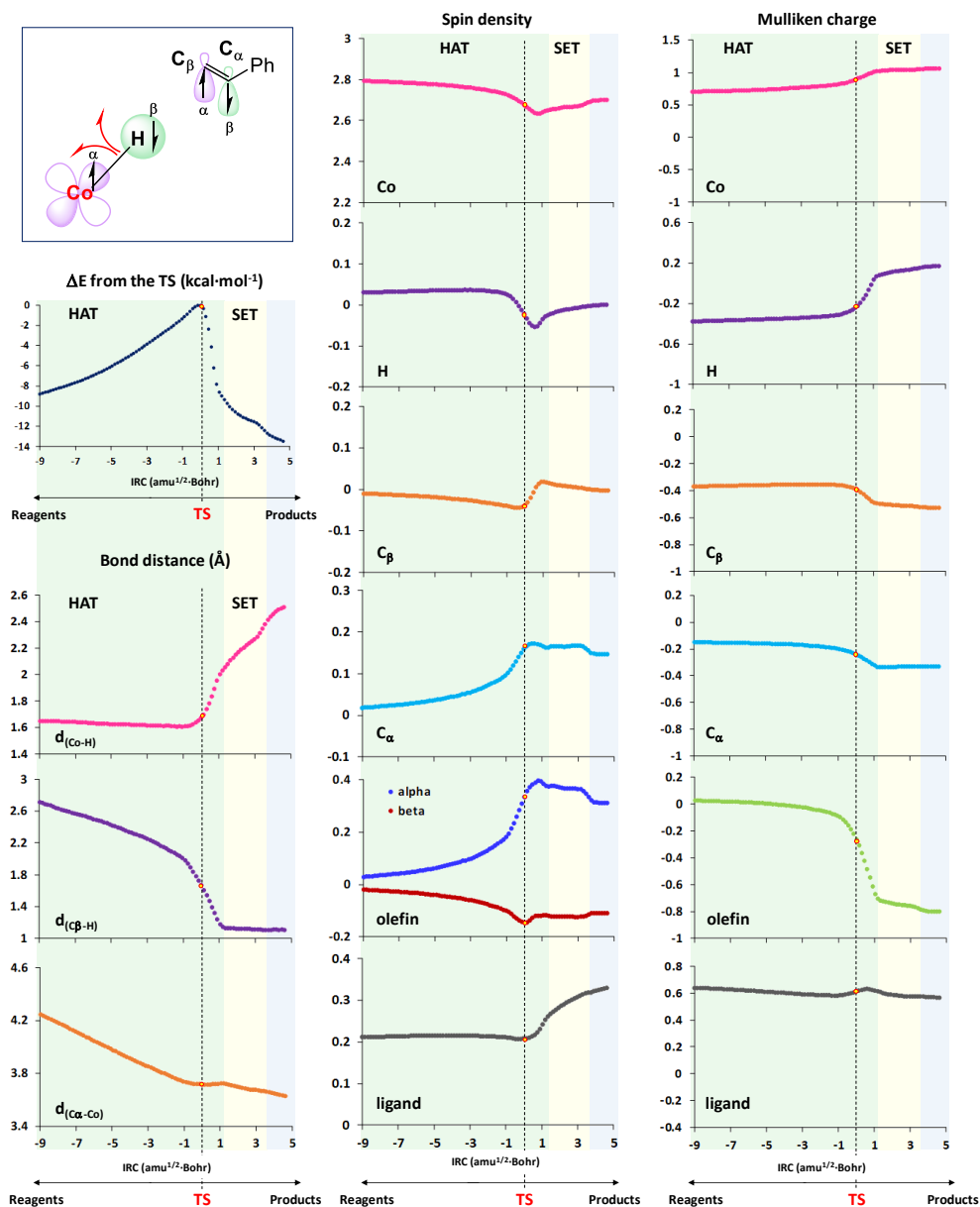
Figure IX.30. Selected bond distances (*left*) Mulliken spin densities (*middle*) and charges (*right*) along the IRC connecting the TS (highlighted dot in each plot) involved in the more homolytic mechanism (HAT) in S = 3/2 (**TS_S_homo$_q$**) for the light-driven reduction of **13a** catalyzed by **1Co** under catalytic conditions (pH = 12) with the reagent (*left*) and product (*right*).
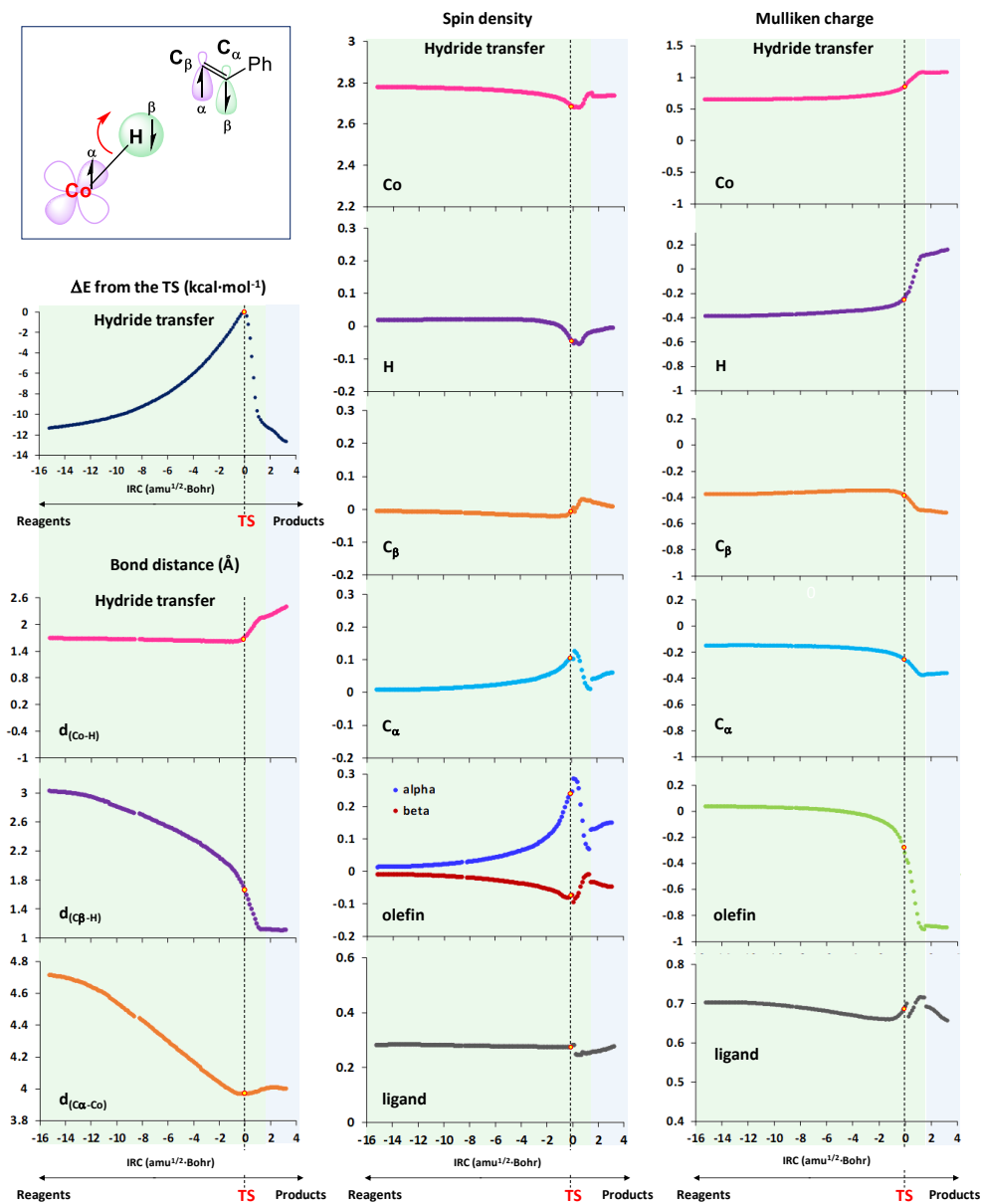
Figure IX.31. Selected bond distances (*left*) Mulliken spin densities (*middle*) and charges (*right*) along the IRC connecting the TS (highlighted dot in each plot) involved in the more heterolytic mechanism (Hydride transfer) in S = 3/2 (**TS_S_hetero$_q$**) for the light-driven reduction of **13a** catalyzed by **1Co** under catalytic conditions (pH = 12) with the reagent (*left*) and product (*right*).

Then, the final radical product is most likely trapped by the metal center, forming a Co-C bond (species **II_S$_q$**, Figure IX.32), which is barrierless. This product connects with the TS, as judged by the optimization of the last point obtained in the IRC studies and has a spin density of 0.04 in the carbon of the Co-C bond and a spin density of 2.77 in the Co, which is in agreement with the formation of a Co(II)-alkyl organometallic complex. Further release of the latter can proceed in either the radical or anionic form. And it can give rise to the reduced product by different mechanisms upon its reaction with another [**1Co^{II}-H**] via a HAT or hydride transfer. Moreover, the free organic benzylic radical can also react with the reduced species of the photoredox catalyst (**PS$_{Cu}$-**) via SET and after protonation yield the reduced product. On the other hand, the protonation of the released anionic product directly from the Co(II)-alkyl organometallic complex will also yield the alkane product (Figure IX.33). Therefore, computational studies support the idea of a HAT from [**1Co^{II}-H**] species for the light-driven reduction of aromatic olefins.
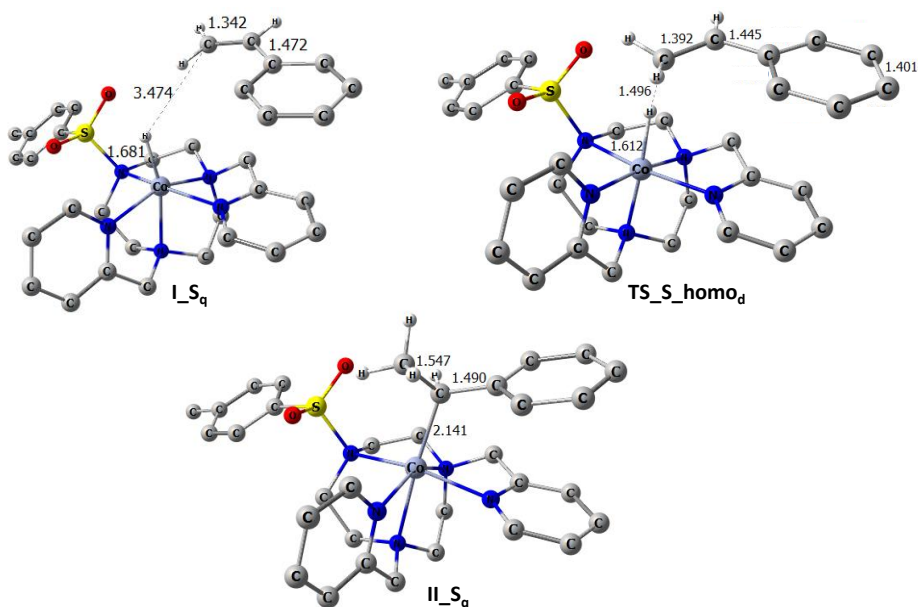
Figure IX. 32. Optimized geometries of the lowest in energy intermediates and transition state involved in the mechanism of the photoreduction of styrene (**13a**) catalyzed by [Co^{II}(H)(Py$_2$^{Me}tacn)]$^+$. Irrelevant hydrogen atoms are omitted for clarity. The most relevant bond distances are in Å.
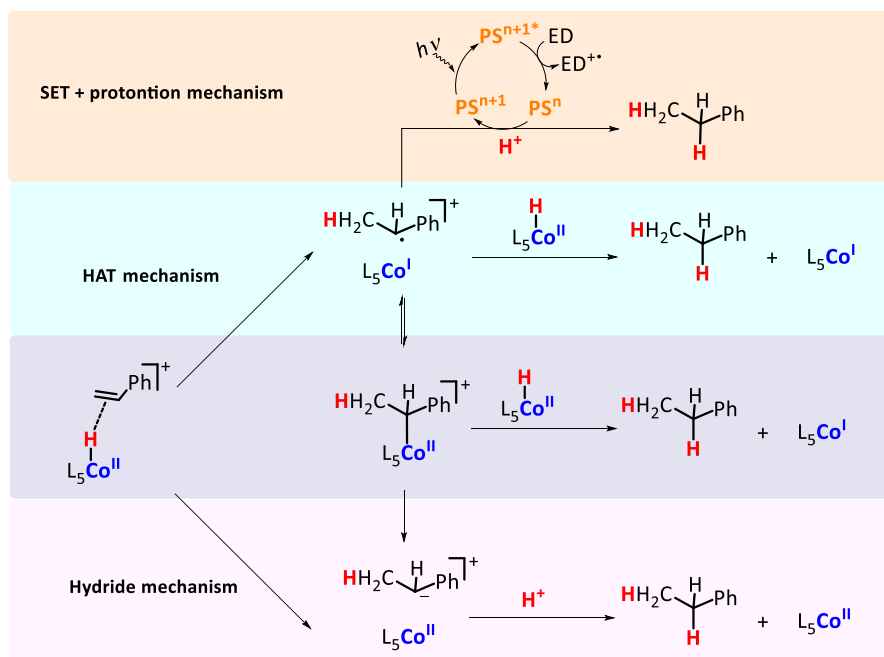
Figure IX. 33. Possible mechanistic scenarios after the release of the alkyl product from **1Co^{II}-R** in the light-driven dual-copper-cobalt catalytic reduction of styrene in aqueous media

IX.3. Conclusions

A catalytic system based on earth-abundant-elements that efficiently hydrogenates aryl olefins under simple operational conditions, just using visible light as driving-force and H$_2$O/amine (Et$_3$N or iPr$_2$EtN) as the source of hydrides has been presented in this chapter. The catalytic system involves a robust and well-defined Co complex with an aminopyridine ligand (**1Co**), initially developed for water reduction by our group, and a Cu photoredox catalyst (**PS$_{Cu}$**). In the previous chapter, we have seen that this dual system is very efficient for the reduction of aromatic ketones and aromatic and aliphatic aldehydes, with an unprecedented selectivity for the reduction of aromatic ketones. Further optimization of the catalytic conditions in aqueous media let to the reduction of a wide scope of aromatic olefins.

Our mechanistic studies based on reactivity, ligand control, selectivity, kinetics, labeling studies, reactivity with radical clocks and DFT modeling support a

UNIVERSITAT ROVIRA I VIRGILI
MECHANISTIC STUDIES OF WATER OXIDATION CATALYZED BY HOMOGENEOUS IRON AND RUTHENIUM
COMPLEXES AND LIGHT-DRIVEN ORGANIC REDUCTIONS WITH A DUAL COBALT/COPPER CATALYTIC SYSTEM
Carla Casadevall Serrano

CHAPTER IX   Dual Co/Cu Light-driven Olefin Reduction

well-defined cobalt hydride [Co-H] as the intermediate responsible for the reductions, most likely through a Hydrogen Atom Transfer (HAT) mechanism, discarding free radical diffusion as the main pathway. The different reactivity of [**1Co^{II}-H**] species depending on the redox potential of the substrate rationalizes the observed selectivity between ketones, aldehydes and olefins. Moreover, synthetically useful deuterium labeled compounds can be straightforwardly obtained replacing H_2O by D_2O as hydride source.

These results show that the selectivity of metal hydrides in basic media can be controlled and directed to the reduction of organic functionalities. For this reason, we envision that other readily available WR catalysts could be also found active in the reduction of other functional groups and more complex structures. These results pave the way for the development of selective organic reductions and solar-chemicals generation by artificial catalytic systems that operate entirely with earth-abundant elements, using visible light as the driving force and H_2O as a source of hydrides.

IX.4. Experimental Section

IX.4.1. Material and reagents

Reagents and solvents were purchased from commercial sources and used as received unless otherwise stated. Triethylamine and *di*-isopropylethylamine were distilled over potassium hydroxide and stored under argon. Ascorbic acid (AscH) (≥ 99 %) was purchased from Sigma-Aldrich® and used without further purification. Photosensitizer [Cu(bathocuproine)(Xantphos)]PF$_6$ (**PS$_{Cu}$**),[82] complexes [Co(OTf)(Py2Tstacn)](OTf) (**1Co**)[50] and [Co(OTf)$_2$(TPA)] (**6**),[83] and ligands N4Py,[84] DPA-Bpy,[85] BpcMe,[86] H-CDPy$_3$[87] and (*S*,*S*)-PDP[88] were synthesized according to the literature procedures.

Anhydrous acetonitrile was purchased from Sigma-Aldrich® Water (18.2 MΩ·cm) was purified with a Milli-Q Millipore Gradient AIS system. All solvents were degassed by the freeze-pump-thaw method and stored under argon.

IX.4.2. Instrumentation

Nuclear magnetic resonance (NMR) spectra were recorded on Bruker Fourier300, AV400, AV500 and AVIII500 spectrometers using standard conditions (300 K). All ^{1}H chemical shifts are reported in ppm and have been internally calibrated to the residual protons of the deuterated solvent. The ^{13}C chemical shifts have been internally calibrated to the carbon atoms of the deuterated solvent. The coupling constants were measured in Hz.

Elemental analyses were performed using a CHNS-O EA-1108 elemental analyzer from Fisons.

Mass Spectrometry. Electrospray ionization mass spectrometry (ESI-MS) experiments were performed on a Bruker Daltonics Esquire 3000 Spectrometer using a 1 mM solution of the analyzed compound, by introducing the sample directly into the ESI-source using a syringe. High resolution mass spectra (HRMS) were recorded on a Bruker MicroTOF-Q IITM instrument with an ESI source at Serveis Tècnics of the University of Girona. Samples were introduced into the mass spectrometer ion source by direct infusion through a syringe pump and were externally calibrated using sodium formate.

Electrochemistry. All the electrochemical experiments were carried out with a VSP potentiostat from Bio-Logic, equipped of the EC-Lab software. A standard three-electrode configuration was employed. Using one-compartment cell, all cyclic voltammetry experiments were recorded using glassy carbon working electrode which was treated between experiments by means of a sequence of polishing with MicroPolish Powder (0.05 micron) before washing and sonification. Saturated calomel electrode (SCE) and Pt wire were used as reference and counter electrodes respectively.

Gas chromatography analysis. The analysis and quantification of the starting materials and products were carried out on an Agilent 7820A gas chromatograph

(HP5 column, 30m or Cyclosil-B column, 30m) and a flame ionization detector. The enantioselectivity was determined by comparison with the pure samples synthesized by the reported procedures.[89]

GC-MS spectral analyses were performed on an Agilent 7890A gas chromatograph interfaced with an Agilent 5975c MS mass spectrometer.

Parallel Pressure Transducer Hardware. The parallel pressure transducer sensors that we used for these studies is the same that was previuosly reported for the water oxidation studies in our group.[90] This is composed by 8 differential pressure transducers (Honeywell-ASCX15DN, $\pm$ 15 psi) connected to a hardware data-acquisition system (base on Atmega microcontroller) controlled by a home-developed software program. The differential pressure transducer Honeywell-ASCX15DN is a 100 microseconds response, signal-conditioned (high level span, 4.5 V) output, calibrated and temperature compensated (0 ºC to 70 ºC) sensor. The differential sensor has two sensing ports that can be used for differential pressure measurements. The pressure calibrated devices to within $\pm$ 0.5 matm was offset and span calibrated *via* software with a high precision pressure transducer (PX409-030GUSB, 0.08 % Accuracy). Each of the 8 differential pressure transducers (Honeywell-ASCX15DN, $\pm$15 psi) produce a voltage outputs that can be directly transformed to a pressure difference between the two measuring ports. The voltage outputs were digitalized with a resolution of 0.25 matm from 0 to 175 matm and 1 matm from 176 to 1000 matm using an Atmega microcontroller with an independent voltage auto-calibration. Firmware Atmega microcontroller and control software were home-developed. The sensitivity of H_2 analytics allows for quantification of the gas formed when low H_2 volumes are generated. However, it could not be discarded that small amounts of H_2 were produced by inactive complexes.

Gas chromatography identification and quantification of gases. Gases at the headspace were analyzed with an Agilent 7820A GC System equipped with columns Washed Molecular Sieve 5A, 2m x 1/8'' OD, Mesh 60/80 SS and Porapak

UNIVERSITAT ROVIRA I VIRGILI
MECHANISTIC STUDIES OF WATER OXIDATION CATALYZED BY HOMOGENEOUS IRON AND RUTHENIUM
COMPLEXES AND LIGHT-DRIVEN ORGANIC REDUCTIONS WITH A DUAL COBALT/COPPER CATALYTIC SYSTEM
Carla Casadevall Serrano

CHAPTER IX   Dual Co/Cu Light-driven Olefin Reduction

Q, 4m x 1/8'' OD, SS. Mesh: 80/100 SS and a Thermal Conductivity Detector. The quantification of the H_2 obtained was measured through the interpolation of a previous calibration using different H_2/N_2 mixtures.

IX.4.3. Experimental Procedures

General procedure employed in reaction screening conditions for the light-driven reduction of monosubstituted aromatic alkenes (13a-l). All catalytic reactions were conducted in a 20 mL septum-capped vial under vigorous stirring using an orbital stirrer and irradiating at 447 nm for 5h under nitrogen atmosphere at 15ºC, unless otherwise indicated. Catalytic assays were performed using **PS$_{Cu}$** as photoredox catalyst (261 µM, 3% mol) in H_2O:CH_3CN:Et_3N (6:4:0.2 mL) reaction solvent mixture, together with the corresponding substrate (8.7 mM), and complex **1Co** (261 µM, 3% mol). After reaction completion, biphenyl was added as internal standard and the crude was quenched by adding 2 mL of AcOEt. The crude was purified by extraction with AcOEt (1 x 3 mL), an aliquote of the organic phase was passed through a plug of $MgSO_4$ which was eluted with AcOEt. This sample was subjected to GC analysis to determine the conversion of **13a-m** and the yield of the desired product **a-m**. All GC yields reported are an average of at least two runs.

General procedure for the reduction of 1,1-disubstituted aromatic olefins (15a-h). All catalytic reactions were conducted in a 20 mL septum-capped vial under vigorous stirring using an orbital stirrer and irradiating at 447 nm for 24h under nitrogen atmosphere at -3ºC, unless otherwise indicated. Catalytic photoreductions were performed in H_2O:CH_3CN:$^iPr_2EtN$ (6:4:0.2 mL) reaction solvent mixture, substrate (4.4 mM), **PS$_{Cu}$** (261 µM, 6% mol), **1Co** (261 µM, 6% mol), unless otherwise indicated. A 447 nm LED was employed as light source. Biphenyl was added as internal standard after the reaction and the reaction was quenched by adding 2 mL of AcOEt. The crude reaction mixtures were purified by extraction with AcOEt (1 x 3 mL), the organic layer was passed through a $MgSO_4$ plug which was eluded with more AcOEt. The resulting organic solution was subjected to GC analysis to

determine the conversion of **15a-h** and the yield of the desired products **16a-h** respectively. All GC yields reported are an average of at least two runs.

General procedure for product isolation. The light-driven photocatalytic reductions of a targeted substrate were carried out under the optimized conditions described above. The crude mixtures of at least 16 independent reactions (equally prepared) for each compound were combined and extracted with CH_2Cl_2 (3 x 40 mL). Organic fractions were combined, dried over $MgSO_4$ and the solvent removed under reduced pressure. The resulting crude oil was purified by silica gel column chromatography with Hexane/AcOEt (9:1) to obtain the desired reduced product and the isolated yields reported are an average of at least 16 reactions.

Gas-evolution monitoring studies. Each experiment was conducted in a 20 mL volume-calibrated-vial caped with a septa equipped with stir-bars and containing the solvent mixture and reagents. Each reaction vial was connected to one of the ports of a differential pressure transducer sensor (Honeywell-ASCX15DN) and the other port to a reference reaction. Reference reactions have all components of the reaction except the catalyst. The reaction and reference vials are kept under the same experimental conditions to compensate the noise due to temperature-pressure fluctuations. In order to ensure a constant and stable irradiation, the LED sources were equipped with a water refrigeration system. This is composed for a refrigerated aluminum block by a Huber cryothermostat (refrigeration system, Minichiller -40ºC-20ºC). This block is shaken by an Orbital Shaker (IKA KS 260 Basic Package) which provides the agitation of the reaction vessels during the irradiation time. The aluminum block accommodates 16 vials (20 mL) capped with septum in which the reaction takes place. Each vial is submitted and located over a LED irradiation source (Royal-Blue Rebel LEDs ($\lambda = 447\pm20$ nm). The reaction began when the LEDs were turned on. At this point, the hydrogen evolved from the reactions was monitored by recording the increase in pressure of the headspace (1 second interval). The pressure increment is the result of the difference in pressure between the reaction and reference vials. After the hydrogen evolution reached a plateau the amount of the gas formed

was measured equilibrating the pressure between reaction and reference vials. The gases at the headspace of the reaction vials and references in each of the reactions were quantified by the analysis of an aliquot of gas at the headspace (0.2 mL) by gas chromatography.

Poisoning studies with Hg^0. Catalytic reactions were performed in the presence of Hg(0) in a 10 mL septum-capped vials. Each experiment was conducted following the general procedure described above for the light-driven reduction of compounds **13x**. Hg(0) was added in large excess (>2000 eq. with respect to catalyst) before starting the reaction by weighting it directly in the reaction vial prior addition of the stock solutions of all the other components. The solution was vigorously stirred for 5 minutes with an orbital stirrer and then the kinetics were performed by irradiating with a LED at 447 nm for 2h. The yield of **14a** was determined at several points during the kinetic study by taking aliquots of the reaction at different times. The LEDs were switched off and a new argon-purged syringe was used to take each aliquot. The yield at each time was determined by GC-FID by the ratio between the area of the substrate and the area of the reduced product.

IX.4.4. Computational studies

DFT calculations for styrene (**13a**) and water reduction mechanisms were carried out using the Gaussian09 program.[91] Geometry optimizations were performed in the unrestricted spin formalism, with the B3LYP hybrid exchange-correlation functional[92-94] and the standard 6-31G* 6d basis set for all atoms. An extra quadratic convergent SCF step was added when the first-order SCF did not converge ("scf=xqc" keyword). The solvation effect of water was introduced in geometry optimizations and energy through the SMD polarizable continuum model.[95] Dispersion effects were also included using the Grimme D$_2$ correction.[96] The geometries have been edited with the Chemcraft program.[97] The located stationary points were characterized by analytical frequency calculations at the same level of theory than geometry optimizations. Gibbs energy values (G) were obtained by

including thermal, solvation and Grimme corrections to the potential energy computed with the 6-311+G** 6d basis set on equilibrium geometries:

$$G = E_{6\text{-}311+G^{**}} + G_{corr.} + G_{solv.} + E_{disp.} \qquad (IX.1)$$

where the thermal correction ($G_{corr.}$) was obtained from gas phase analytical Hessians calculations at 298.15 K, the solvation energy ($G_{solv.}$) was calculated as the difference of the total free energy in gas phase and in water at the same level of theory and geometry and $E_{disp.}$ is the dispersion correction.

A cluster of three water molecules $(H_2O)_3$ is employed to model the H-H bond formation event and the microsolvation sphere around water. Hirshfeld charges[98,99] were computed to rationalize the reactivity trends of Co-H species. Intrinsic Reaction Coordinate (IRC) calculations has been performed to verify the connectivity between the transition states and found reagent and product structures.

IX.4.4.1. Protonation and redox reactions

The standard dissociation free energy change between an acid (AH) and its conjugate base (A⁻) in aqueous (ΔG^*) may be expressed as:[100]

$$\Delta G^* = G\left(A_{aq}^-\right) + G\left(H_{aq}^+\right) - G\left(AH_{aq}\right) + \Delta G^{\frac{o}{*}} \qquad (IX.2)$$

$$G\left(H_{aq}^+\right) = G\left(H_{gas}^+\right) + \Delta G_{solv}^{H+} \qquad (IX.3)$$

where $G\left(AH_{aq}\right)$ and $G\left(A_{aq}^-\right)$ are standard free energies of the acid and its conjugate base in aqueous media, respectively. The $G\left(H_{aq}^+\right)$ is the free energy of the proton in water, obtained from the experimental solvation free energy ($\Delta G_{solv}^{H+} = -265.9\,\text{kcal}\cdot\text{mol}^{-1}$)[100] and its gas-phase free energy ($G\left(H_{gas}^+\right) = -6.3\,\text{kcal}\cdot\text{mol}^{-1}$). $\Delta G^{o/*}$ is the free energy change associated with the conversion from a standard state of 1 M in the aqueous phase and 1 atm in gas phase, to the desired concentration in both phases. ΔG^* values are derived with the following expression:

$$\Delta G^{o/*} = RT \ln(24.4 * c) \qquad (IX.4)$$

where R is the universal gas constant (1.987 cal·mol^{-1}·K^{-1}), T is the temperature in Kelvin and c the concentration in mol·L^{-1}.

In the free energy balances the following concentrations were used to adjust the final free energies: 8.7 mM for styrene, 10^{-12} M for protons (due to the pH $\approx$ 12), 33.4 M for water and 7.6 M for acetonitrile (the concentrations of water and acetonitrile were derived from the 6:4 $H_2O:CH_3CN$ solvent mixture used in catalysis). The previous concentrations translate into $\Delta G^{o/*}$ values (at 298.15 K) of -0.92 kcal·mol^{-1} for styrene substrate, -14.5 kcal·mol^{-1} for protons, 4.0 kcal·mol^{-1} for water and 3.1 kcal·mol^{-1} for acetonitrile. The concentration correction for a $(H_2O)_n$ water cluster can be derived with the formula 4.0/n kcal·mol^{-1},[101] with a $\Delta G^{o/*}$ value of 1.33 kcal·mol^{-1} when n = 3. Then, the standard one electron redox potentials relative to the SHE electrode were calculated by:

$$E^o = -\frac{\Delta G^0 - \Delta G_{SHE}}{F} \qquad (IX.5)$$

where ΔG^0 is the standard free energy change associated with the reduction reaction, F is the Faraday constant (23.061 kcal·mol^{-1}V^{-1}) and ΔG_{SHE} is the free energy change associated with the proton reduction to H_2 (-4.24 eV). The ΔG_{SHE} value was derived using the Fermi-Dirac statistics for the treatment of electron thermodynamics.[102,103]

IX.5. References

(1) Choudhury, S.; Baeg, J. O.; Park, N. J.; Yadav, R. K. *Angew. Chem. Int. Ed.* **2012**, *51*, 11624.
(2) Lee, S. H.; Kim, J. H.; Park, C. B. *Chem. Eur. J.* **2013**, *19*, 4392
(3) Mifsud, M.; Gargiulo, S.; Iborra, S.; Arends, I. W.; Hollmann, F.; Corma, A. *Nat. Commun.* **2014**, *5*, 3145.
(4) Kim, J. H.; Nam, D. H.; Park, C. B. *Current Opinion in Biotechnology* **2014**, *28*, 1.
(5) Liu, J.; Huang, J.; Zhou, H.; Antonietti, M. *ACS Appl. Mater. Interf.* **2014**, *6*, 8434.
(6) Bachmeier, A.; Murphy, B. J.; Armstrong, F. A. *J. Am. Chem. Soc.* **2014**, *136*, 12876.
(7) Palmisano, G.; Augugliaro, V.; Pagliaro, M.; Palmisano, L. *Chem. Commun.* **2007**, 3425.
(8) Galian, R. E.; Pérez-Prieto, J. *Energy & Environmental Science* **2010**, *3*, 1488.

(9) Barber, J.; Tran, P. D. *J. R. Soc. Interface* **2013**, *10*, 20120984.

(10) Andreiadis, E. S.; Chavarot-Kerlidou, M.; Fontecave, M.; Artero, V. *Photochem. Photobiol.* **2011**, *87*, 946.

(11) Macia-Agullo, J. A.; Corma, A.; Garcia, H. *Chem. Eur. J.* **2015**, *21*, 10940.

(12) Wang, M.; Chen, L.; Sun, L. *Energy & Environmental Science* **2012**, *5*, 6763.

(13) Simmons, T. R.; Berggren, G.; Bacchi, M.; Fontecave, M.; Artero, V. *Coord. Chem. Rev.* **2014**, *270-271*, 127.

(14) Zee, D. Z.; Chantarojsiri, T.; Long, J. R.; Chang, C. J. *Acc. Chem. Res.* **2015**, *48*, 2027.

(15) Kaeffer, N.; Chavarot-Kerlidou, M.; Artero, V. *Acc. Chem. Res.* **2015**, *48*, 1286.

(16) Queyriaux, N.; Jane, R. T.; Massin, J.; Artero, V.; Chavarot-Kerlidou, M. *Coord. Chem. Rev.* **2015**, *304-305*, 3.

(17) Dempsey, J. L.; Brunschwig, B. S.; Winkler, J. R.; Gray, H. B. *Acc. Chem. Res.* **2009**, *42*, 1995.

(18) Eckenhoff, W. T.; Eisenberg, R. *Dalton Trans.* **2012**, *41*, 13004.

(19) McKone, J. R.; Marinescu, S. C.; Brunschwig, B. S.; Winkler, J. R.; Gray, H. B. *Chem. Sci.* **2014**, *5*, 865.

(20) Han, Z.; Eisenberg, R. *Acc. Chem. Res.* **2014**, *47*, 2537.

(21) Thoi, V. S.; Sun, Y.; Long, J. R.; Chang, C. J. *Chem. Soc. Rev.* **2013**, *42*, 2388.

(22) Rakowski DuBois, M.; DuBois, D. L. *Chem. Soc. Rev.* **2009**, *38*, 62.

(23) Du, P.; Eisenberg, R. *Energy & Environmental Science* **2012**, *5*, 6012.

(24) Appel, A. M.; Bercaw, J. E.; Bocarsly, A. B.; Dobbek, H.; DuBois, D. L.; Dupuis, M.; Ferry, J. G.; Fujita, E.; Hille, R.; Kenis, P. J.; Kerfeld, C. A.; Morris, R. H.; Peden, C. H.; Portis, A. R.; Ragsdale, S. W.; Rauchfuss, T. B.; Reek, J. N.; Seefeldt, L. C.; Thauer, R. K.; Waldrop, G. L. *Chem. Rev.* **2013**, *113*, 6621.

(25) Izumi, Y. *Coord. Chem. Rev.* **2013**, *257*, 171.

(26) Schneider, J.; Jia, H.; Muckerman, J. T.; Fujita, E. *Chem. Soc. Rev.* **2012**, *41*, 2036.

(27) Monos, T. M.; Sun, A. C.; McAtee, R. C.; Devery, J. J., 3rd; Stephenson, C. R. *J. Org. Chem.* **2016**, *81*, 6988.

(28) Takeda, H.; Ishitani, O. *Coord. Chem. Rev.* **2010**, *254*, 346.

(29) Windle, C. D.; Perutz, R. N. *Coord. Chem. Rev.* **2012**, *256*, 2562.

(30) Qiao, J.; Liu, Y.; Hong, F.; Zhang, J. *Chem. Soc. Rev.* **2014**, *43*, 631.

(31) Costentin, C.; Robert, M.; Saveant, J. M. *Chem. Soc. Rev.* **2013**, *42*, 2423.

(32) Rakowski Dubois, M.; Dubois, D. L. *Acc. Chem. Res.* **2009**, *42*, 1974.

(33) Claros, M.; Ungeheuer, F.; Franco, F.; Martin-Diaconescu, V.; Casitas, A.; Lloret-Fillol, J. *Angew. Chem. Int. Ed.* **2019**, *58*, 4869.

(34) Call, A.; Casadevall, C.; Acuña-Parés, F.; Casitas, A.; Lloret-Fillol, J. *Chemical Science* **2017**, *8*, 4739.

(35) Shimakoshi, H.; Hisaeda, Y. *ChemPlusChem* **2014**, *79*, 1250.

(36) Tian, H.; Shimakoshi, H.; Imamura, K.; Shiota, Y.; Yoshizawa, K.; Hisaeda, Y. *Chem. Commun.* **2017**, *53*, 9478.

(37) Imamura, K.; Okubo, Y.; Ito, T.; Tanaka, A.; Hashimoto, K.; Kominami, H. *RSC Advances* **2014**, *4*, 19883.

(38) Litman, Z. C.; Wang, Y.; Zhao, H.; Hartwig, J. F. *Nature* **2018**, *560*, 355.

(39) Li, J.; Yang, J.; Wen, F.; Li, C. *Chem. Commun.* **2011**, *47*, 7080.

(40) Yamataka, H.; Seto, N.; Ichihara, J.; Hanafusa, T.; Teratani, S. *J. Chem. Soc., Chem. Commun.* **1985**, 788.

(41) Shiragami, T.; Pac, C.; Yanagida, S. *J. Phys. Chem.* **1990**, *94*, 504.

(42) Lang, X.; Zhao, J.; Chen, X. *Chem. Soc. Rev.* **2016**, *45*, 3026.

(43) Call, A.; Casadevall, C.; Acuna-Pares, F.; Casitas, A.; Lloret-Fillol, J. *Chemical Science* **2017**, *8*, 4739.

(44) Kainz, Q. M.; Matier, C. D.; Bartoszewicz, A.; Zultanski, S. L.; Peters, J. C.; Fu, G. C. *Science* **2016**, *351*, 681.

(45) Zuo, Z.; Ahneman, D. T.; Chu, L.; Terrett, J. A.; Doyle, A. G.; MacMillan, D. W. C. *Science* **2014**, *345*, 437.

(46) Shaw, M. H.; Twilton, J.; MacMillan, D. W. C. *J Phys Chem* **2016**, *81*, 6898.

(47) Skubi, K. L.; Blum, T. R.; Yoon, T. P. *Chem. Rev.* **2016**, *116*, 10035.

(48) Nielsen, M. K.; Shields, B. J.; Liu, J.; Williams, M. J.; Zacuto, M. J.; Doyle, A. G. *Angew. Chem.* **2017**, *129*, 7297.

(49) Shields, B. J.; Doyle, A. G. *J. Am. Chem. Soc.* **2016**, *138*, 12719.

(50) Call, A.; Codolà, Z.; Acuña-Parés, F.; Lloret-Fillol, J. *Chem. Eur. J.* **2014**, *20*, 6171.

(51) Luo, S. P.; Mejia, E.; Friedrich, A.; Pazidis, A.; Junge, H.; Surkus, A. E.; Jackstell, R.; Denurra, S.; Gladiali, S.; Lochbrunner, S.; Beller, M. *Angew. Chem. Int. Ed.* **2013**, *52*, 419.

(52) Perkowski, A. J.; You, W.; Nicewicz, D. A. *J. Am. Chem. Soc.* **2015**, *137*, 7580.

(53) Artero, V.; Chavarot-Kerlidou, M.; Fontecave, M. *Angew. Chem. Int. Ed.* **2011**, *50*, 7238.

(54) Eckenhoff, W. T.; McNamara, W. R.; Du, P.; Eisenberg, R. *Biochim. Biophys. Acta* **2013**, *1827*, 958.

(55) Narayanam, J. M. R.; Tucker, J. W.; Stephenson, C. R. J. *J. Am. Chem. Soc.* **2009**, *131*, 8756.

(56) Maji, T.; Karmakar, A.; Reiser, O. *J Phys Chem* **2011**, *76*, 736.

(57) Wiedner, E. S.; Chambers, M. B.; Pitman, C. L.; Bullock, R. M.; Miller, A. J.; Appel, A. M. *Chem. Rev.* **2016**, *116*, 8655.

(58) Hu, Y.; Shaw, A. P.; Estes, D. P.; Norton, J. R. *Chem. Rev.* **2016**, *116*, 8427.

(59) Crossley, S. W.; Obradors, C.; Martinez, R. M.; Shenvi, R. A. *Chem. Rev.* **2016**, *116*, 8912.

(60) Litwinienko, G.; Ingold, K. U. *Acc. Chem. Res.* **2007**, *40*, 222.

(61) Lo, J. C.; Gui, J.; Yabe, Y.; Pan, C. M.; Baran, P. S. *Nature* **2014**, *516*, 343.

(62) Lo, J. C.; Yabe, Y.; Baran, P. S. *J. Am. Chem. Soc.* **2014**, *136*, 1304.

(63) Li, G.; Han, A.; Pulling, M. E.; Estes, D. P.; Norton, J. R. *J. Am. Chem. Soc.* **2012**, *134*, 14662.

(64) Eisenberg, D. C.; Norton, J. R. *Isr. J. Chem.* **1991**, *31*, 55.

(65) Metternich, J. B.; Gilmour, R. *J. Am. Chem. Soc.* **2015**, *137*, 11254.

(66) Saltiel, J.; Hammond, G. S. *J. Am. Chem. Soc.* **1963**, *85*, 2515.

(67) Hammond, G. S.; Saltiel, J. *J. Am. Chem. Soc.* **1962**, *84*, 4983.

(68) Meng, Q.-Y.; Schirmer, T. E.; Katou, K.; König, B. *Angew. Chem. Int. Ed.* **2019**, *58*, 5723.

(69) Artero, V.; Fontecave, M. *Chem. Soc. Rev.* **2013**, *42*, 2338.

(70) Call, A.; Codola, Z.; Acuna-Pares, F.; Lloret-Fillol, J. *Chemistry* **2014**, *20*, 6171.

(71) Zhang, G.; Scott, B. L.; Hanson, S. K. *Angew. Chem. Int. Ed.* **2012**, *51*, 12102.

(72) Lin, T.-P.; Peters, J. C. *J. Am. Chem. Soc.* **2013**, *135*, 15310.

(73) Zhang, G.; Vasudevan, K. V.; Scott, B. L.; Hanson, S. K. *J. Am. Chem. Soc.* **2013**, *135*, 8668.

(74) Li, Y.; Hou, C.; Jiang, J.; Zhang, Z.; Zhao, C.; Page, A. J.; Ke, Z. *ACS Catal.* **2016**, *6*, 1655.

(75) Tanko, J. M.; Drumright, R. E. *J. Am. Chem. Soc.* **1992**, *114*, 1844.

(76) Tanko, J. M.; Drumright, R. E. *J. Am. Chem. Soc.* **1990**, *112*, 5362.

(77) Griller, D.; Ingold, K. U. *Acc. Chem. Res.* **1980**, *13*, 317.

(78) Stevenson, J. P.; Jackson, W. F.; Tanko, J. M. *J. Am. Chem. Soc.* **2002**, *124*, 4271.

(79) Fischer, S.; Hollmann, D.; Tschierlei, S.; Karnahl, M.; Rockstroh, N.; Barsch, E.; Schwarzbach, P.; Luo, S.-P.; Junge, H.; Beller, M.; Lochbrunner, S.; Ludwig, R.; Brückner, A. *ACS Catal.* **2014**, *4*, 1845.

(80) Li, F.; Jiang, Y.; Zhang, B.; Huang, F.; Gao, Y.; Sun, L. *Angew. Chem., Int. Ed.* **2012**, *51*, 2417.

(81) Jing, Y.; Chen, X.; Yang, X. *Organometallics* **2015**, *34*, 5716.

(82) Luo, S.-P.; Mejía, E.; Friedrich, A.; Pazidis, A.; Junge, H.; Surkus, A.-E.; Jackstell, R.; Denurra, S.; Gladiali, S.; Lochbrunner, S.; Beller, M. *Angew. Chem. Int. Ed.* **2013**, *52*, 419.

(83) Ward, A. L.; Elbaz, L.; Kerr, J. B.; Arnold, J. *Inorg. Chem.* **2012**, *51*, 4694−4706.

(84) Roefles, G.; Lubben, M.; Hage, R.; Jr., L. Q.; Feringa, B. L. *Chem. Eur. J.* **2000**, *6*, 2152.

(85) Radaram, B.; Ivie, J. A.; Singh, W. M.; Grudzien, R. M.; Reibenspies, J. H.; Webster, C. E.; Zhao, X. *Inorg. Chem.* **2011**, *50*, 10564.

(86) Maity, N. C.; Kumar Bera, P.; Ghosh, D.; Abdi, S. H. R.; Kureshy, R. I.; Khan, N.-u. H.; Bajaj, H. C.; Suresh, E. *Catal. Sci. Technol.* **2014**, *4*, 208.

(87) Abouelatta, A. I.; Sonk, J. A.; Hammoud, M. M.; Zurcher, D. M.; McKamie, J. J.; Schlegel, H. B.; Kodanko, J. J. *Inorg. Chem.* **2010**, *49*, 5202.

(88) Chen, M. S.; White, M. C. *Science* **2007**, *318*, 783.

(89) Wu, X.; Li, X.; Hems, W.; King, F.; Xiao, J. *Org. Biomol. Chem.* **2004**, *2*, 1818.

(90) Lloret-Fillol, J.; Codolà, Z.; Garcia-Bosch, I.; Gómez, L.; Pla, J. J.; Costas, M. *Nat. Chem.* **2011**, *3*, 807

(91) Arakawa, H.; Aresta, M.; Armor, J. N.; Barteau, M. A.; Beckman, E. J.; Bell, A. T.; Bercaw, J. E.; Creutz, C.; Dinjus, E.; Dixon, D. A. *Chem. Rev.* **2001**, *101*, 953.

(92) Becke, A. D. *J. Chem. Phys.* **1993**, *98*, 1372.

(93) Becke, A. D. *J. Chem. Phys.* **1993**, *98*, 5648.

(94) Lee, C. T.; Yang, W. T.; Parr, R. G. *Phys. Rev. B* **1988**, *37*, 785.

(95) C. J. Cramer, A. V. M., D. G. Truhlar *J. Phys. Chem. B* **2009**, *113*, 6378.

(96) Schwabe, T.; Grimme, S. *Phys. Chem. Chem. Phys.* **2007**, *9*, 3397.

(97) In *Chemcraft - graphical software for visualization of quantum chemistry computations.* .

(98) Mayer, I. *Chem. Phys. Lett.* **1983**, *97*, 270.

(99) Mayer, I. *Int. J. Quantum Chem* **1984**, *26*, 151.

(100) Kelly, C. P.; Cramer, C. J.; Truhlar, D. G. *J Phys Chem B* **2006**, *110*, 16066.

(101) Dinescu, A.; Clark, A. E. *J Phys Chem A* **2008**, *112*, 11198.

(102) Bartmess, J. E. *J Phys Chem* **1994**, *98*, 6420.

(103) Kelly, C. P.; Cramer, C. J.; Truhlar, D. G. *J Phys Chem B* **2007**, *111*, 408.

UNIVERSITAT ROVIRA I VIRGILI
MECHANISTIC STUDIES OF WATER OXIDATION CATALYZED BY HOMOGENEOUS IRON AND RUTHENIUM
COMPLEXES AND LIGHT-DRIVEN ORGANIC REDUCTIONS WITH A DUAL COBALT/COPPER CATALYTIC SYSTEM
Carla Casadevall Serrano

CHAPTER X

Synthesis, Characterization and Reactivity of Co(I), (II) and (III) Intermediates Derived From The [Co(^{X,Y}Py$_2$Tstacn)(OTf)](OTf) Complexes involved in the Light-driven Organic Transformations
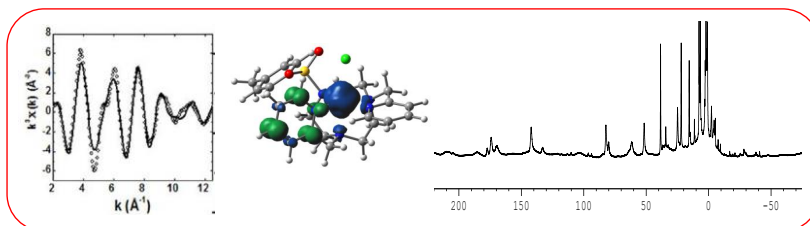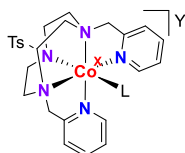
This chapter corresponds to the following publications:

"Characterization of Reduced [Co^{II}(Py$_2$Tstacn)L] Intermediates. The Unexpected Non-innocent Character of the Pyridine in Water Reduction."
C. Casadevall, A. Call, F. Acuña-Parés, V. Martin-Diaconescu, F. Franco, C. Sáenz de Pipaón, J. R. Galán-Mascarós and J. Lloret-Fillol; *in preparation*

UNIVERSITAT ROVIRA I VIRGILI

MECHANISTIC STUDIES OF WATER OXIDATION CATALYZED BY HOMOGENEOUS IRON AND RUTHENIUM
COMPLEXES AND LIGHT-DRIVEN ORGANIC REDUCTIONS WITH A DUAL COBALT/COPPER CATALYTIC SYSTEM

Carla Casadevall Serrano

X. Synthesis, Characterization and Reactivity of Co(I), (II) and (III) Intermediates Derived from the [Co(^{X,Y}Py$_2$^{TS}tacn)(OTf)](OTf) Complexes Involved in the Light-driven Organic Transformations

X.1. General insight

The development of effective catalysts for light-driven organic transformations requires a fundamental understanding of the reaction mechanisms.[1-6] Putative [Co-H] species are postulated as common intermediates in both light-driven WR[7] and the light-driven organic reductions mediated by our dual cobalt-copper catalytic system (chapters VIII and IX).[5] In this line, state of the art characterization techniques based on ESI-MS,[8,9] electrochemistry,[10,11] spectroelectrochemistry,[8,9,12,13] steady-state UV/Vis spectroscopy,[14,15] EPR,[14,16] time-resolved IR spectroscopy,[17,18] transient absorption spectroscopy[8,9,12,13] and pulse radiolysis[9] have been used to study the intermediates involved in those reactions. Despite all these studies, mechanistic comprehension is still limited most probably due to its intrinsic instability.[19,20] Characterization of Co^I intermediates is not straightforward. The *in-situ* generation of low oxidation state intermediates starting from Co^{III} or Co^{II} species by strong reducing agents (such as Co(Cp)$_2$ or Co(Cp*)$_2$,[14,20-22] Na/Hg[9]) or by bulk electrochemistry in organic solvents is still rough and only few reactivity studies have been performed so far.[23,24] Therefore, a comprehensive characterization is still missing.[25,26] Few are the pieces of evidence under photocatalytic conditions. Nevertheless, putative *in-situ* generated Co^I intermediates react with protons to yield H$_2$ and cobalt species in higher oxidation state (Co^{II} and/or Co^{III}).[11,13,14,20,21,27,28]

A remarkable result in the characterization of Co^I complexes was achieved by J. Long and C. Chang groups.[29] They reported the synthesis of [Co^I(PY$_5$Me$_2$)](BPh$_4$) by reaction of the PY$_5$Me$_2$ (PY$_5$Me$_2$ = 2,6-bis(1,1-bis(2-pyridyl)ethyl)pyridine) ligand with Co^I(PPh$_3$)$_3$Cl followed by chloride abstraction with NaBPh$_4$. The X-ray structure of the isolated [Co^I(PY$_5$Me$_2$)](BPh$_4$) shows a pentacoordinate square planar

UNIVERSITAT ROVIRA I VIRGILI
MECHANISTIC STUDIES OF WATER OXIDATION CATALYZED BY HOMOGENEOUS IRON AND RUTHENIUM
COMPLEXES AND LIGHT-DRIVEN ORGANIC REDUCTIONS WITH A DUAL COBALT/COPPER CATALYTIC SYSTEM
Carla Casadevall Serrano
CHAPTER X   Synthesis, Characterization and Reactivity of Co(I), (II) and (III) Intermediates

pyramidal cobalt complex, which reacts with protons in CH$_3$CN to form [Co^{II}(PY$_5$Me$_2$)NCCH$_3$] and 0.6 equivalents of H$_2$ for every two equivalents of Co^I (Figure X.1).
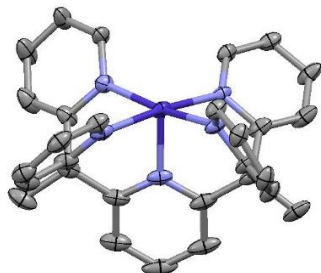
Figure X.1. Crystal structure (Ellipsoids 50 % probability level) of [Co^I(PY5Me$_2$)](BPh$_4$) complex reported by J. Long and C. Chang groups.[29] In purple, blue and grey there are the Co, N and C atoms, respectively; H atoms are omitted for clarity.

Due to the optical nature of Co^I intermediates, X-ray absorption spectroscopy (XAS) is gaining importance as a characterization technique to determine their local geometry and/or electronic structure. Recently, seminal pump-probe Laser − X-ray Transient Absorption Spectroscopy (L-XTA) (Co K-edge) studies on photosensitizer-cobaloxime systems[30,31] in non-aqueous media have revealed a change in both oxidation state and bonding.

Reaching a specific low oxidation state at the metal center is not trivial due to an inherent instability of metal complexes towards the environment. In this regard, the introduction of a redox non-innocent ligand could activate the generation of the active formal oxidation state of the complex,[32-39] by delocalizing part of the electronic density of the complexes into their structure. In the context of water reduction, pyridine-imine[40] bi-pyridine[41,42] and pyrazine[43] based ligands could act as redox non-innocent ligands. In extreme cases, even ligands such as pyridine can also act as redox non-innocent ligands.[36,37] This unusual reactivity was reported by P. Holland and co-workers in the L'Fe(pyridine)$_2$ (L' = 2,4-bis(2,6-diisopropylimino)pentyl) complex by reactivity, spectroscopy and theoretical studies (Figure X.2).
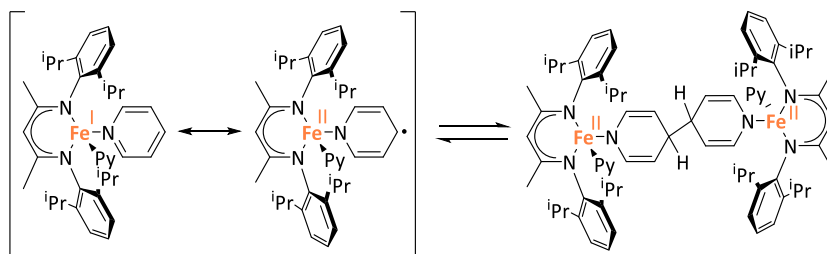
Figure X.2. Redox non-innocent nature of the L'Fe(pyridine)$_2$ (L' = 2,4-bis(2,6-diisopropylimino)pentyl) complex and the reversible C-C bond formation at the para-position of the pyridine reduction.

Taking into consideration our ongoing interest in mechanistic aspects of aminopyridine Co complexes for water and organic reductions, we sought to further explore the Co^I oxidation state derived from complex **1Co** reported in chapters VIII and IX for the light-driven organic reductions. Precedent work from Dr. Arnau Call thesis suggested the possible formation of low valent Co(I) species derived from complex [Co(Py$_2$^{TS}tacn)(OTf)](OTf) involved in the light-driven hydrogen evolution and organic reductions.[5,7] Additionally, he was able to crystallize the Co(II) species with Cl and MeCN coordinated ligands, respectively, and the Co(III) complex with a MeCN coordinated (Figure X.3). Preliminary reactivity experiments with the putative Co(I) intermediate pointed towards the formation of Co(III) species, as evidenced by NMR and EXAFS spectroscopy. However, the characterization of such intermediate is not straightforward from an electronic point of view. On the one hand, SQUID magnetometry measurements suggest the formation of new paramagnetic Co(II) species, and DFT calculations performed by Dr. Ferran Acuña suggested a strong delocalization of the electronic density into the pyridine ring. Preliminary XAS analyses suggested a reduction of the metal center but less than the expected for a one-electron reduction reaction. However, the preliminary reactivity studies showed that the system was behaving as a Co(I). At that point, we concluded that its electronic structure is better described as a formal Co(II) with an electron delocalized in the Py ring (Figure X.4).

$1_{Co}^{II}{}_{MeCN}$ $1_{Co}^{II}{}_{Cl}$ $1_{Co}^{III}{}_{MeCN}$
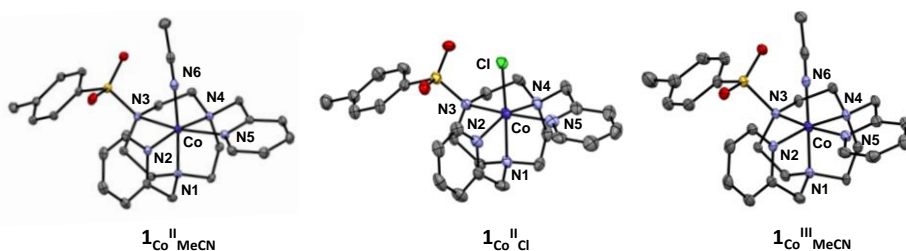
Figure X.3. Crystal structures of the cobalt complexes $1_{Co}^{II}{}_{CH3CN}$, $1_{Co}^{II}{}_{Cl}$ and $1_{Co}^{III}{}_{CH3CN}$ isolated by Dr. A. Call. Ellipsoids are drawn at the 50 % probability level. Solvent molecules and hydrogen atoms are omitted for clarity. Color code: cobalt (blue), nitrogen (light blue), oxygen (red), fluor (yellow), carbon (grey) and sulfur (orange).

Co^{II} (S = 3/2) Co^{I} (S = 1)
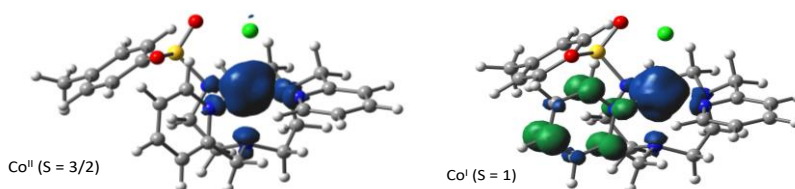
Figure X.4. Spin density obtained for the DFT modeled $1_{Co}^{I}{}_{Cl}$ and $1_{Co}^{II}{}_{Cl}$ complexes (isovalue = 0.005). Blue and green regions indicate α and β spin density, respectively.

Due to the unexpected spectroscopic features and reactivity, the most important objective of this chapter was to clarify the electronic nature of the Co(I) intermediate derived from complex [Co(Py$_2$^{TS}tacn)(OTf)](OTf) involved in the catalytic light-driven organic transformations. To this end, we describe the *in-situ* formation of the putative [Co^I] ($1_{Co}^{I}{}_{L}$, L = Cl or MeCN) intermediate under photochemical conditions by the reaction of **PS$_{Ir}$** with $1_{Co}^{II}{}_{L}$ (L = Cl or MeCN) in MeCN:H$_2$O using Et$_3$N as electron donor, and the chemical formation of $1_{Co}^{I}{}_{Cl}$ by the reaction of Py$_2$^{Ts}tacn with Co^I(PPh$_3$)$_3$Cl. We have characterized this intermediate by means of EPR, NMR and XAS and, most importantly, we have ensured that the samples are still intact after the XAS measurements by NMR analyses, which was not done previously. Then, the further reactivity of the putative Co(I) with protons and oxygen has been repeated to double-check the resulting products and reanalyze them by NMR and XAS. Moreover, to discard that a putative new Co(II) species could react similarly to a Co(I) intermediate, reactivity studies of complex $1_{Co}^{II}{}_{Cl}$ against protons have also been performed.

In addition, to validate the hypothesis of a possible delocalization of the electron density over the Py ring, we have studied the electronic effects in the formation of the putative Co(I), by the electronic modification of the $^{X,Y}Py_2^{TS}$tacn (X = -Me, Y = -OMe and X = -H, Y = -CO$_2$Et, $\mathbf{1^{DMM}}$ and $\mathbf{1^{CO2Et}}$ ligands, respectively) ligand with an electron-donating ($\mathbf{1^{DMM}}$) and an electron-withdrawing ($\mathbf{1^{CO2Et}}$) substituent in the *para* position of the Py ring. Moreover, DFT calculations of all the series for the Co(II) and Co(I) complexes at the uB3LYP/6-31+G* GD3 level of theory and including solvent (PCM, SMD = acetonitrile) have been performed. We envision that having a ligand with enough electron density on the Py ring would disfavor the electron delocalization of a putative Co(I) intermediate in the Py.

X.2. Results and discussion

X.2.1. Synthesis and characterization of Co(I), Co(II) and Co(III) complexes derived from [Co(^{X,Y}Py$_2$^{TS}tacn)(OTf)](OTf) complexes
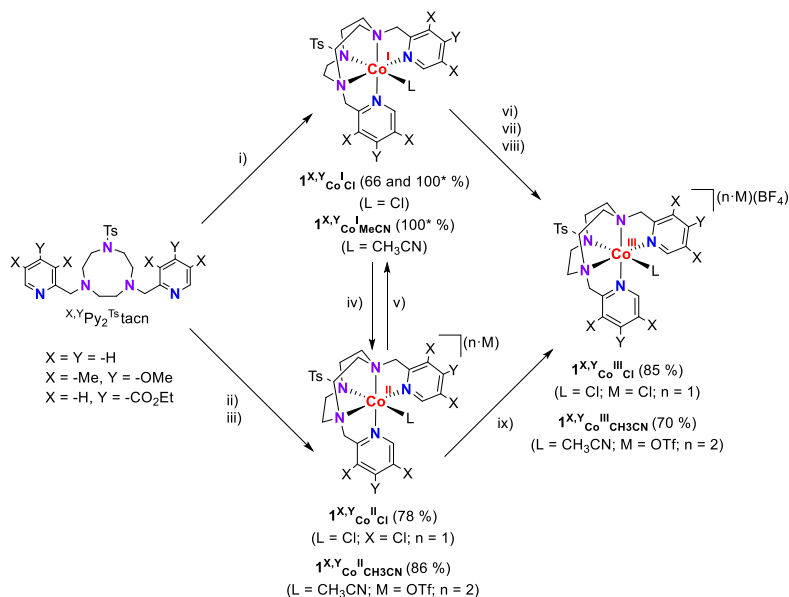
Scheme X.1. Reactivity interconversions between $\mathbf{1^{X,Y}_{Co}{}^I_L}$, $\mathbf{1^{X,Y}_{Co}{}^{II}_L}$ and $\mathbf{1^{X,Y}_{Co}{}^{III}_L}$: i) metalation with 1 equiv. of Co(PPh$_3$)$_3$Cl in dry toluene; ii) metalation with CoCl$_2$ in dry CH$_2$Cl$_2$; iii) metalation with [Co(OTf)$_2$(CH$_3$CN)$_2$] in dry CH$_3$CN, iv) 1 e$^-$ oxidation with NOBF$_4$. v) photogeneration with 1 eq. **PS$_{Ir}$** and excess of Et$_3$N in dry CH$_3$CN; vi) 1 e$^-$ oxidation with NOBF$_4$; vii) addition of 3 eq. of TFA or excess of H$_2$O, exposition to air in dry CH$_3$CN.

The Py_2^{Ts}tacn ligand was synthesized as in chapters VIII and IX and $^{X,Y}Py_2^{TS}$tacn (X = -Me, Y = -OMe (DMM) and X = -H, Y = -CO$_2$Et) ligands were synthesized following the reported procedures.[44] Complexes $1_{Co}{}^n{}_L$, $1^{DMM}{}_{Co}{}^n{}_L$ and $1^{CO2Et}{}_{Co}{}^n{}_L$ (n = 2, L = CH$_3$CN ($1_{Co}{}^{II}{}_{CH3CN}$, $1^{DMM}{}_{Co}{}^{II}{}_{CH3CN}$ and $1^{CO2Et}{}_{Co}{}^{II}{}_{CH3CN}$); L = Cl ($1_{Co}{}^{II}{}_{Cl}$, $1^{DMM}{}_{Co}{}^{II}{}_{Cl}$ and $1^{CO2Et}{}_{Co}{}^{II}{}_{Cl}$)) were synthesized by direct reaction of the Py_2^{Ts}tacn, $^{DMM}Py_2^{TS}$tacn and $^{CO2Et}Py_2^{TS}$tacn ligands with [Co(OTf)$_2$(CH$_3$CN)$_2$] and CoCl$_2$ forming $1_{Co}{}^{II}{}_L$ and $1^X{}_{Co}{}^{II}{}_L$ (X = DMM or CO$_2$Et) in excellent yields, respectively (Scheme X.1). Then, complexes $1_{Co}{}^{III}{}_L$ (for L = CH$_3$CN, $1_{Co}{}^{III}{}_{CH3CN}$, and for L = Cl, $1_{Co}{}^{III}{}_{Cl}$) were obtained by a clean reaction of respective cobalt $1_{Co}{}^{II}{}_L$ complex by 1 electron oxidation with 1 equivalent of NOBF$_4$. (Scheme X.). ^{1}H-NMR, MS-ESI and EA characterization is in agreement with the formation of the complexes. We noticed that the Cl is not replaced by CD$_3$CN in $1_{Co}{}^{II}{}_{Cl}$ (nor in $1^{DMM}{}_{Co}{}^{II}{}_{Cl}$ and $1^{CO2Et}{}_{Co}{}^{II}{}_{Cl}$) or $1_{Co}{}^{III}{}_{Cl}$ as judged by ^{1}H-NMR experiments (Figure X.5). The ^{1}H-NMR spectra of the chemically synthesized $1_{Co}{}^{II}{}_{Cl}$, $1^{DMM}{}_{Co}{}^{II}{}_{Cl}$, $1^{CO2Et}{}_{Co}{}^{II}{}_{Cl}$ and $1_{Co}{}^{II}{}_{CHCN3}$, $1^{DMM}{}_{Co}{}^{II}{}_{CHCN3}$, $1^{CO2Et}{}_{Co}{}^{II}{}_{CHCN3}$ show paramagnetic signals in the rage between 320 and -100 ppm which is in agreement with a $t_2g^5 eg^2$ or a $t_2g^6 eg^1 d^7$ Co(II) configuration (Figure X.5). The magnetic susceptibility (μ_{eff}) values for complex 1 ($1_{Co}{}^{II}{}_{CHCN3}$) were measured by ^{1}H-NMR following the Evans' method[45-47] in MeCN-d$_3$ (see experimental section for further details) at 270, 280, 290 and 298 K. Complex $1_{Co}{}^{II}{}_{CHCN3}$ presents reasonably constant μ_{eff} values (3.6 - 4.4 BM) between 270 and 298 K (Figure A.VIII.1), in good agreement with d^7 high-spin Co^{II} complexes ($t_2g^5 eg^2$) reported in the literature[48-50] and our DFT calculations. Moreover, ^{1}H-NMR spectra at varied temperatures indicate a possible dynamic behavior. The broad signals in the ^{1}H-NMR spectrum at room temperature become well defined and sharper at 235 K (Figures X.5 and A.VIII.2).
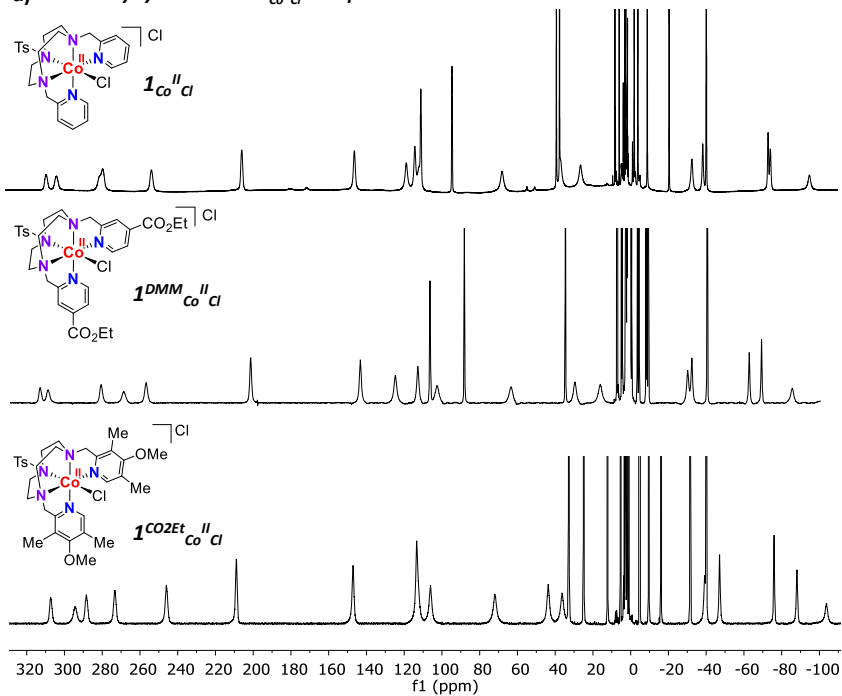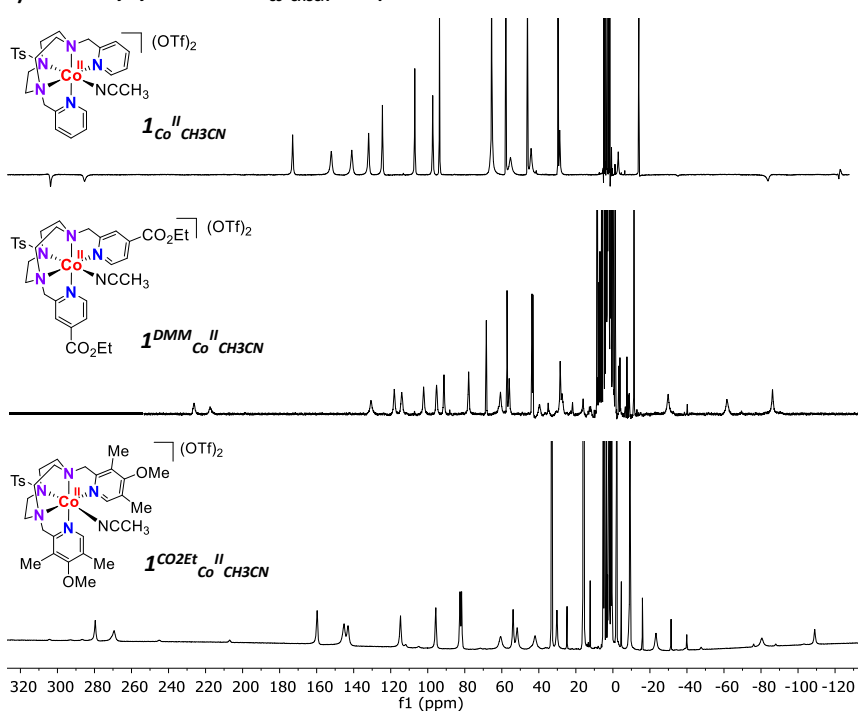
Figure X.5. ^{1}H-NMR (500 MHz, 235 K, CD$_3$CN) of the complex $1^{X,Y}_{Co^{II}_{Cl}}$ and $1^{X,Y}_{Co^{II}_{CH3CN}}$ series.

UNIVERSITAT ROVIRA I VIRGILI
MECHANISTIC STUDIES OF WATER OXIDATION CATALYZED BY HOMOGENEOUS IRON AND RUTHENIUM
COMPLEXES AND LIGHT-DRIVEN ORGANIC REDUCTIONS WITH A DUAL COBALT/COPPER CATALYTIC SYSTEM
Carla Casadevall Serrano
CHAPTER X   Synthesis, Characterization and Reactivity of Co(I), (II) and (III) Intermediates

On the other hand, the ^{1}H-NMR spectra of the chemically synthesized $\mathbf{1_{Co}^{III}_{Cl}}$, and $\mathbf{1_{Co}^{III}_{CHCN3}}$ show the formation of a diamagnetic species with signals expanding in the region form 9.5 - 1.5 ppm, which is in agreement with the formation of a low-spin d^6 configuration at the cobalt center (Figure X.5).
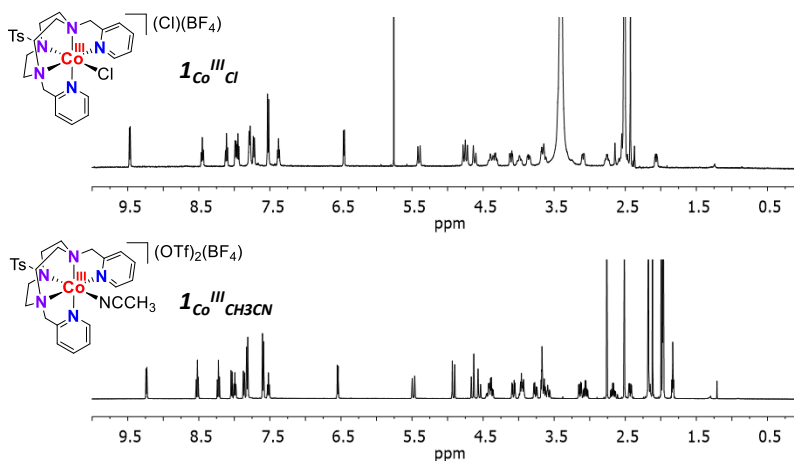
Figure X.6. ^{1}H-NMR (500 MHz, 235 K, CD$_3$CN) of the chemically synthesized $\mathbf{1_{Co}^{III}_{L}}$ complexes [Co^{III}(Py$_2^{Ts}$tacn)(Cl)](Cl)(BF$_4$) and [Co^{III}(Py$_2^{Ts}$tacn)(Cl)](OTf)$_2$(BF$_4$), respectively.

Complex $\mathbf{1_{Co}^{I}_{Cl}}$ was obtained by equimolar reaction of Co^I(PPh$_3$)$_3$Cl with the Py$_2^{Ts}$tacn ligand in dry toluene solution in 66 % yield as a deep blue solid after purification, which was highly unstable towards H$_2$O and O$_2$. The ^{1}H-NMR spectrum in CD$_3$CN shows a main set of paramagnetic signals ranged from -80 to 220 ppm (Figure X.7, *top*). Likewise, $\mathbf{1^{DMM}_{Co}^{I}_{Cl}}$ was synthesized in an analogous manner in 70 % yield. The ^{1}H-NMR spectrum of $\mathbf{1^{DMM}_{Co}^{I}_{Cl}}$ shows a set of signals in the paramagnetic region from -80 to 220 ppm, which is in agreement with the formation of a high spin d^8 Co complex and resembles the one obtained for $\mathbf{1_{Co}^{I}_{Cl}}$ (Figure X.7, *bottom*). However, in this case there is another set of small signals in the paramagnetic region at higher and lower frequencies (> 220 and < -50 ppm) that the ones associated to Co(I), most likely to traces of $\mathbf{1^{DMM}_{Co}^{II}_{Cl}}$ that might be still present due to an unclean formation of Co(I). The broad signals in the ^{1}H-NMR spectrum at room temperature become well defined and sharper at 270 K and then the signals

UNIVERSITAT ROVIRA I VIRGILI
MECHANISTIC STUDIES OF WATER OXIDATION CATALYZED BY HOMOGENEOUS IRON AND RUTHENIUM
COMPLEXES AND LIGHT-DRIVEN ORGANIC REDUCTIONS WITH A DUAL COBALT/COPPER CATALYTIC SYSTEM
Carla Casadevall Serrano

CHAPTER X   Synthesis, Characterization and Reactivity of Co(I), (II) and (III) Intermediates

become broader again at 235 K (see Annex VIII Figure A.VIII. 3). This may indicate a possible dynamic behavior.
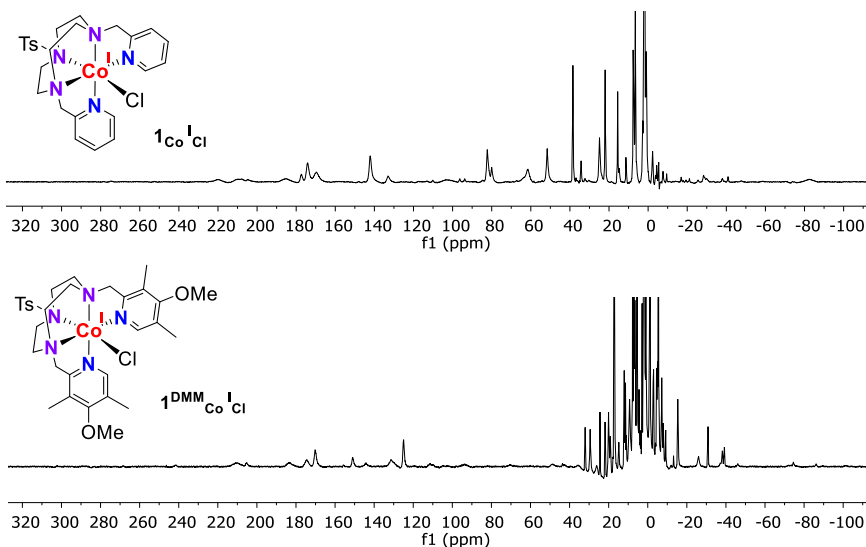
Figure X.7. ¹H-NMR (500 MHz, 235 K, CD₃CN) of the chemically synthesized **1₍Co₎ᴵ₍Cl₎** (*top*) and **1ᴰᴹᴹ₍Co₎ᴵ₍Cl₎** (*bottom*) complexes.

In order to gain some insight into the light-driven reactivity, we explored the *in situ* photogeneration of Co(I) species. The irradiation of a CD₃CN solution of **1₍Co₎ᴵᴵ₍Cl₎** (10 mM) containing **PS₍Ir₎** (10 mM) and Et₃N (120 mM) in a Young gas-tight NMR tube under Argon atmosphere during 20 min at room temperature lead to the complete disappearance of signals belonging to **1₍Co₎ᴵᴵ₍Cl₎** and the appearance of a new set of paramagnetic signals expanding from 220 to -80 ppm. The resulting ¹H-NMR spectrum was similar to the one of the chemically synthesized **1₍Co₎ᴵ₍Cl₎** but with the signals better seen and sharper at 250 K (Figure X.8). Likewise, the *in situ* photogenerated **1₍Co₎ᴵ₍CH3CN₎** complex shows a new set of ¹H-NMR paramagnetic signals in the range between 180 and -100 ppm, which is completely formed after 20 min irradiation at r.t. (Figure X.9). Moreover, the ¹H-NMR paramagnetic spectra of both Co(I) intermediates **1₍Co₎ᴵ₍Cl₎** and **1₍Co₎ᴵ₍CH3CN₎** are slightly different, suggesting that the chloride anion might still be bounded to the Co(I) center after one electron reduction (Figure X.10), which would be confirmed by EXAFS analyses (section below).

393
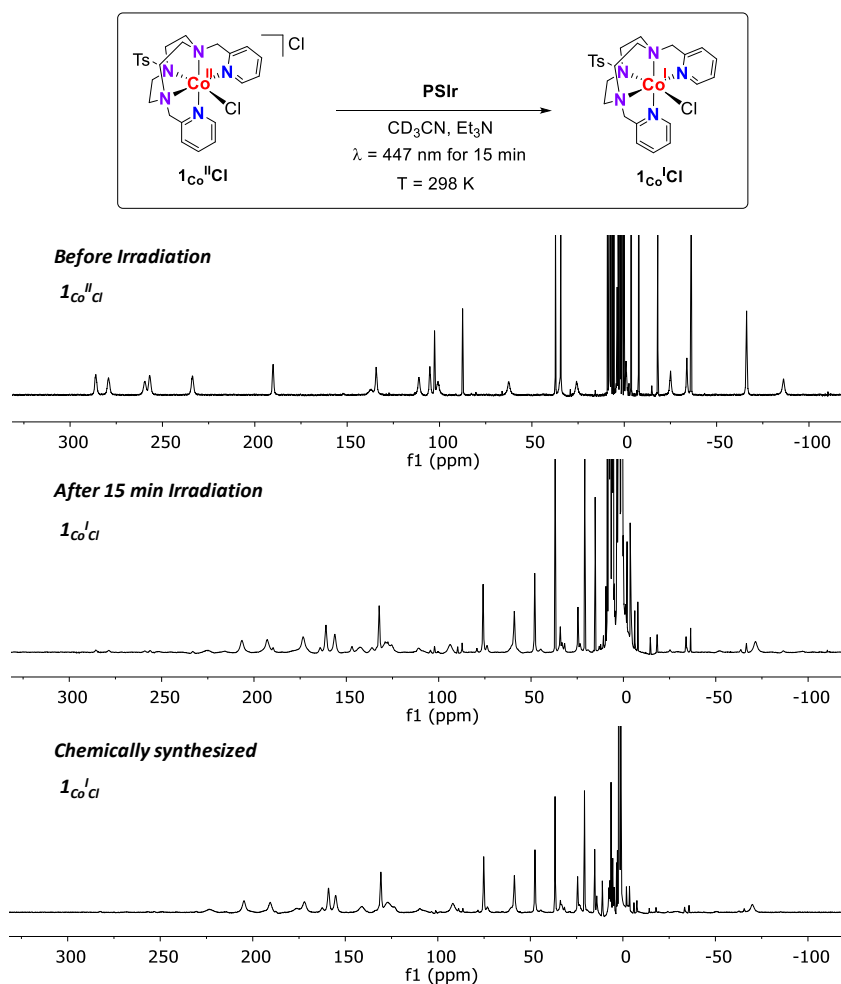
Figure X.8. Photoreduction of $1_{Co}^{II}{}_{Cl}$ to $1_{Co}^{I}{}_{Cl}$ monitored by ^{1}H-NMR (500 MHz, 250 K, CD$_3$CN). *Top*: ^{1}H-NMR paramagnetic spectrum before irradiation. *Middle:* ^{1}H-NMR paramagnetic spectrum of the monitoring of the photogeneration of $1_{Co}^{I}{}_{Cl}$ after 15 min irradiation at 298 K. *Bottom:* ^{1}H-NMR paramagnetic spectrum of the chemically synthesized $1_{Co}^{I}{}_{Cl}$ species. Conditions: $1_{Co}^{II}{}_{Cl}$ (10 mM), **PS$_{Ir}$** (10 mM), Et$_3$N (120 mM) in 1 ml CD$_3$CN irradiating at 298 K (λ = 447 nm).
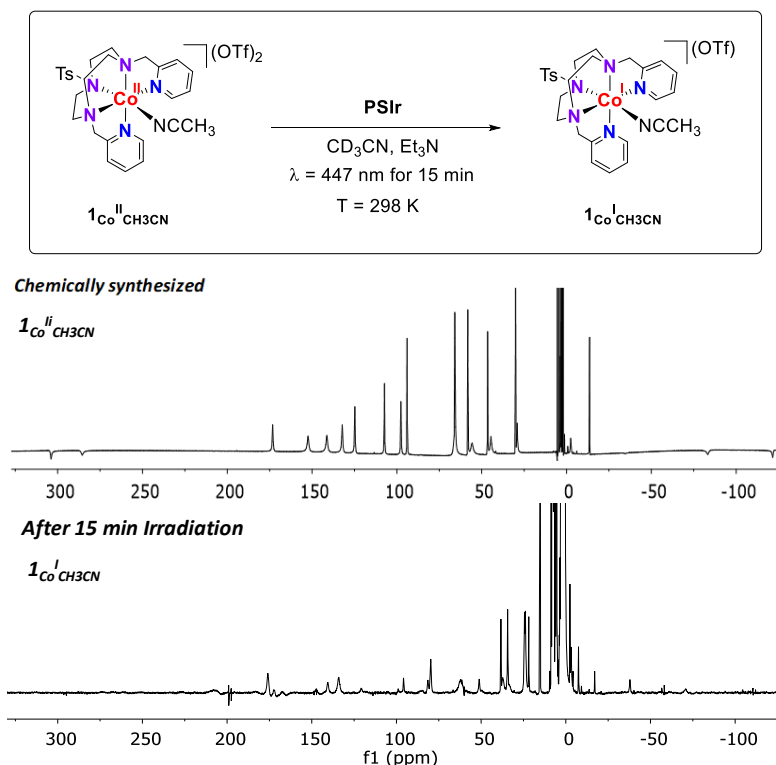
Figure X.9. Photoreduction of **1$_{Co}^{II}$CH3CN** to **1$_{Co}^{I}$CH3CN** monitored by ^{1}H-NMR (500 MHz, 235 K, CD$_3$CN). *Top*: ^{1}H-NMR paramagnetic spectrum before irradiation. *Bottom:* ^{1}H-NMR paramagnetic spectrum of the monitoring of the photogeneration of **1$_{Co}^{I}$CH3CN** after 15 min irradiation at 298 K. Conditions: **1$_{Co}^{II}$CH3CN** (10 mM), **PS$_{Ir}$** (10 mM), Et$_3$N (120 mM) in 1 ml CD$_3$CN irradiating at 298 K (λ = 447 nm).
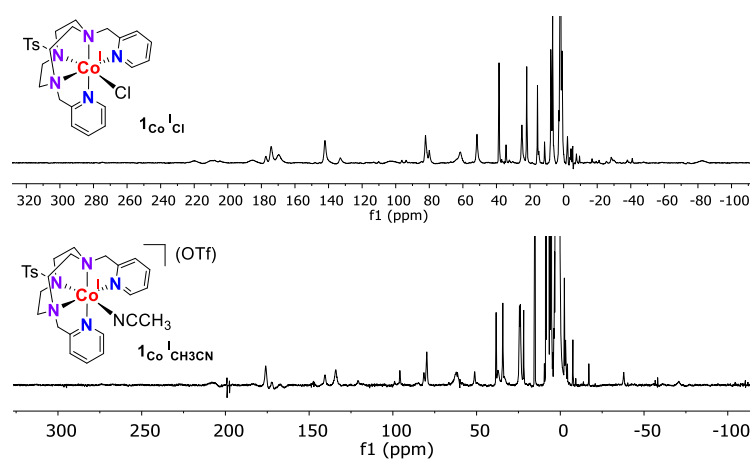
Figure X.10. ^{1}H-NMR (500 MHz, 235 K, CD$_3$CN) of the chemically synthesized **1$_{Co}^{I}$Cl** and the photogenerated **1$_{Co}^{I}$CH3CN** intermediates.

```
UNIVERSITAT ROVIRA I VIRGILI
MECHANISTIC STUDIES OF WATER OXIDATION CATALYZED BY HOMOGENEOUS IRON AND RUTHENIUM
COMPLEXES AND LIGHT-DRIVEN ORGANIC REDUCTIONS WITH A DUAL COBALT/COPPER CATALYTIC SYSTEM
Carla Casadevall Serrano
```
CHAPTER X   Synthesis, Characterization and Reactivity of Co(I), (II) and (III) Intermediates

$1^{DMM}Co^I_{Cl}$ and $1^{CO2Et}Co^I_{Cl}$ were photochemically synthesized and characterized by ^{1}H-NMR spectroscopy at 235 K (Figures X.11 and X.12 and A.VIII.4). Analogously to $1Co^I_{Cl}$, irradiation of a solution of $1^{DMM}Co^{II}_{Cl}$ and $1^{CO2Et}Co^{II}_{Cl}$ complexes (10 mM) in the presence of the PS_{Ir} (10 mM) and Et$_3$N (120 mM) as electron donor leads to the formation of a new paramagnetic species expanding from 200 – 50 ppm that is in similar to the chemically synthesized Co(I) intermediate (figures X.11 and X.12). In the case of the photogenerated $1^{DMM}Co^I_{Cl}$ complex, the ^{1}H-NMR of the photogenerated species is clearly cleaner than the chemically synthesized intermediate, suggesting a cleaner reaction (Figure X.11).
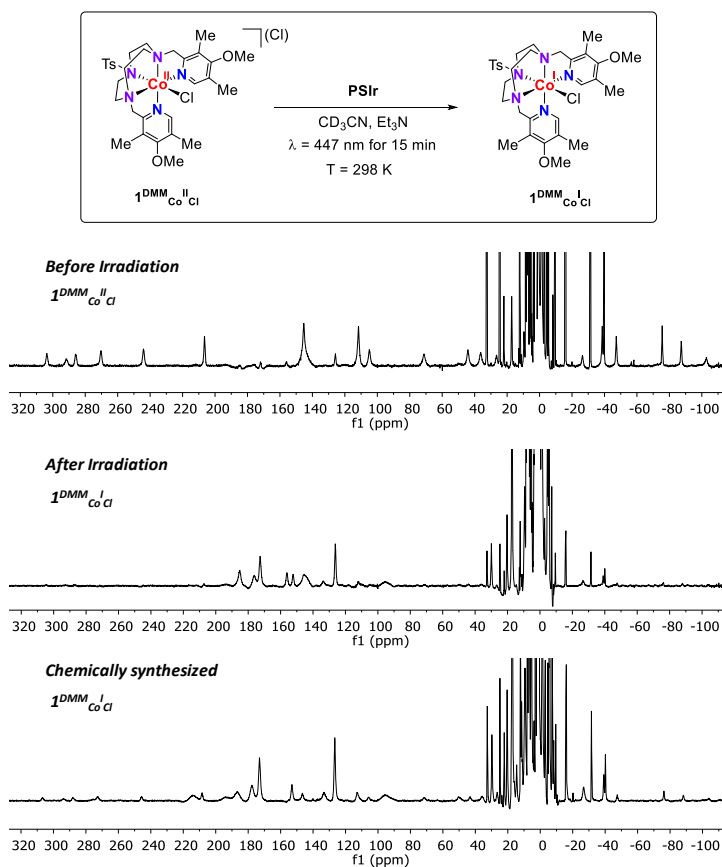
Figure X.11. Photoreduction of $1^{DMM}Co^{II}_{Cl}$ to $1^{DMM}Co^I_{Cl}$ monitored by ^{1}H-NMR (500 MHz, 235 K, CD$_3$CN). *Top*: ^{1}H-NMR paramagnetic spectrum before irradiation. *Middle:* ^{1}H-NMR paramagnetic spectrum of the photogenerated $1^{DMM}Co^I_{Cl}$. *Bottom:* ^{1}H-NMR paramagnetic spectrum of the chemically synthesized $1^{DMM}Co^I_{Cl}$. Conditions: $1^{DMM}Co^{II}_{CH3CN}$ (10 mM), PS_{Ir} (10 mM), Et$_3$N (120 mM) in 1 ml CD$_3$CN irradiating at 298 K (λ = 447 nm).
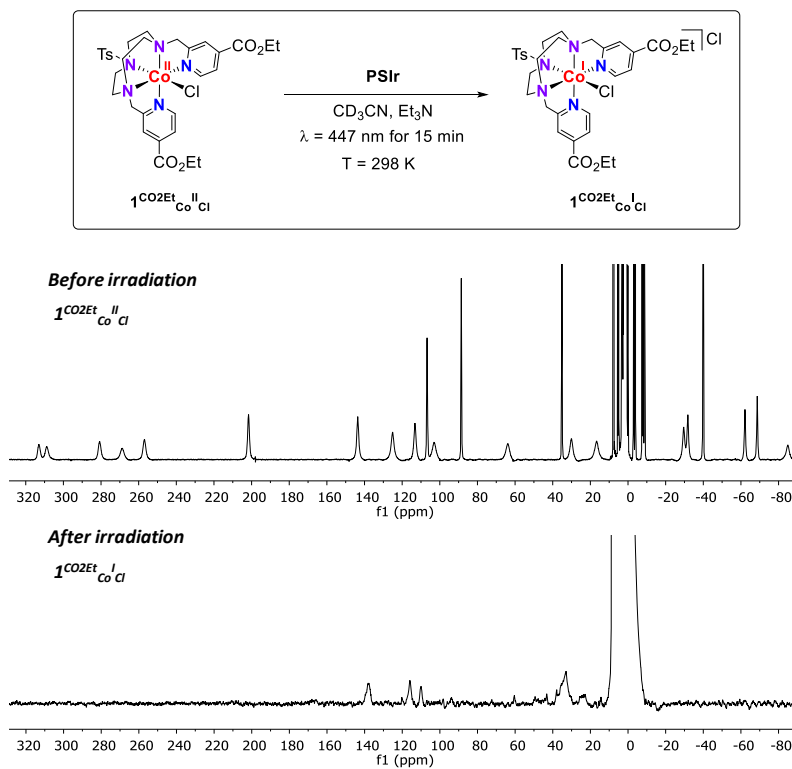
Figure X.12. Photoreduction of $1^{CO2Et}\text{Co}^{II}\text{Cl}$ to $1^{CO2Et}\text{Co}^{I}\text{Cl}$ monitored by ^{1}H-NMR (500 MHz, 235 K, CD_3CN). *Top*: ^{1}H-NMR paramagnetic spectrum before irradiation at 235 K. *Bottom:* ^{1}H-NMR paramagnetic spectrum at 235 K of the photogenerated $1^{CO2Et}\text{Co}^{I}\text{Cl}$. Conditions: $1^{CO2Et}\text{Co}^{II}\text{Cl}$ (10 mM), **PS$_{Ir}$** (10 mM), Et$_3$N (120 mM) in 1 ml CD_3CN irradiating at 298 K (λ = 447 nm).

Interestingly, both the photogenerated and the chemically synthesized ^{1}H-NMR spectra of $1^{DMM}\text{Co}^{I}\text{Cl}$ resemble that of $1\text{Co}^{I}\text{Cl}$ (Figure X.7). Taking into account the precedents of this work it could be that: i) we have formed a new paramagnetic Co(II) species in both cases, or ii) we have formed a formal Co(II) with an electron delocalized in the Py ring, or iii) we have formed Co(I) intermediates but still we need to shed light into their spectroscopic characterization. Therefore, we performed XAS analyses of the Co(I), Co(II) and Co(III) series and evaluated the samples by ^{1}H-NMR before and after the XAS analyses to ensure the integrity of them and get a clear insight into their electronic nature.

X.2.1.1. XAS characterization of Co(I), Co(II) and Co(III)

a) Effect of the ligand scaffold

First, we analyzed the $[Co(^{X,Y}Py_2^{TS}tacn)(OTf)](OTf)$ family and their coordination environment to get more insight into the oxidation state of the cobalt intermediates. We performed Co K-edge XANES (X-ray Absorption Near Edge Structure) and EXAFS (Extended X-ray Absorption Fine Structure) studies in collaboration with Dr. Vlad Martin-Diaconescu. For comparative purposes, we also analyzed the tetracoordinate Co(II) complex $[Co(Py^{Me2}tacn)(CH_3CN)_2](OTf)_2$ ($\mathbf{2_{Co}^{II}_{CH3CN}}$) that was synthesized as previously reported.[51] It is important to say that all samples were analyzed before and after the EXAFS measurements by ^{1}H-NMR, confirming that they were intact after the analyses (see experimental section Figure X.26). Moreover, Co(III) species $\mathbf{1_{Co}^{III}_{Cl}}$ and $\mathbf{1_{Co}^{III}_{CH3CN}}$ were used as standards.

Interestingly, from the perspective of Co K-edge X-ray absorption spectroscopy (Co K-edge XAS) the ligand electronic effects were small but detectable on the Co rising edge region (XANES). Incorporation of electron-withdrawing (CO_2Et) or electron donating (DMM) substituents into the pyridine ring in the pentacoordinate series $\mathbf{1^{X,Y}_{Co}^{II}_{Cl}}$ exhibits only a minor effect on the XANES spectra with E_0 values of 7718.1 eV and 7718.6 eV for complexes $\mathbf{1^{DMM}_{Co}^{II}_{Cl}}$ and $\mathbf{1^{CO2Et}_{Co}^{II}_{Cl}}$, respectively. It should be noted that an expected experimental error of 0.2 eV is within range of the value for $\mathbf{1_{Co}^{II}_{Cl}}$ (Figure X.13, *left*). Additionally, inspection of the tetra- ($\mathbf{2_{Co}^{II}_{CH3CN}}$), and pentadentate ($\mathbf{1_{Co}^{II}_{CH3CN}}$) XANES profiles suggests that the extra pyridine ligand has a significant electron donating effect reducing the effective charge on the Co center with $\mathbf{1_{Co}^{II}_{CH3CN}}$ having a rising edge centered at 7719.3 eV, about 1.8 eV lower in energy than the tetradentate $\mathbf{2_{Co}^{II}_{CH3CN}}$ ($E_0 \sim 7721.1$ eV, Figure X.13, *right*). Complex $\mathbf{1_{Co}^{II}_{CH3CN}}$ is formally more reduced than $\mathbf{2_{Co}^{II}_{CH3CN}}$ due to the presence of the extra pyridine. Additionally, the substitution of the solvent ligand in $\mathbf{1_{Co}^{II}_{CH3CN}}$ with chlorine in $\mathbf{1_{Co}^{II}_{Cl}}$ further reduces the rising

edge energy to 7718.4 eV (Figure X.13, *right*), which is expected as the chlorine coordination adds extra stabilization to the Co center.
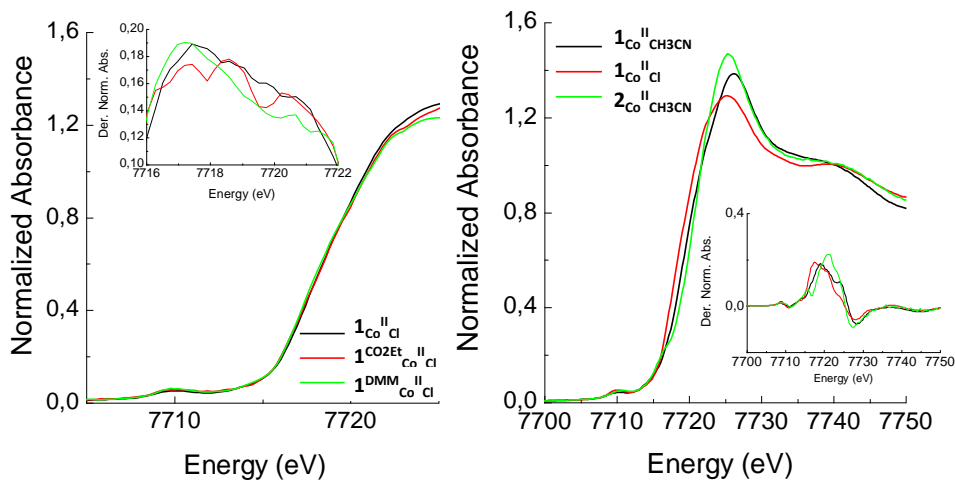
Figure X.13. Normalized cobalt-edge XANES region of the chemically synthesized *left*) $1_{Co}{}^{II}{}_{Cl}$ (black line), $1^{CO2Et}{}_{Co}{}^{II}{}_{Cl}$ (red line) and $1^{DMM}{}_{Co}{}^{II}{}_{Cl}$ (green line); *right*) $1_{Co}{}^{II}{}_{CH3CN}$ (black line), $1_{Co}{}^{II}{}_{Cl}$ (red line) and the derivative tetracoordinate Co(II) complex from the same family $[Co(Py^{Me2}tacn)(CH_3CN)_2](OTf)_2$ ($2_{Co}{}^{II}{}_{CH3CN}$, green line) for comparative purposes.

b) Characterization of Co(III) complexes

Co(III) complexes were analyzed by XAS as standard samples to set the higher energy limits at which we expect the rising-edge energies. XAS analyses for complexes $1_{Co}{}^{III}{}_{Cl}$ and $1_{Co}{}^{III}{}_{CH3CN}$ has a XANES profile consistent with a Co(III) center, having the most intense pre-edge of the series at 7710.0 eV as compared to $1_{Co}{}^{II}{}_{Cl}$ and $1_{Co}{}^{II}{}_{CH3CN}$, respectively, with rising edges at around 7719.6 eV (Figure X.14), which are around 1.2 eV higher than the ones for the Co(II) complexes, consistent with a one-electron oxidation of the metal centre. In the case of $1_{Co}{}^{III}{}_{Cl}$ the pre-edge is slightly less intense, which is most likely attributed to the electron density given by the chlorine substituent with regard to the CH3CN ligand in $1_{Co}{}^{III}{}_{CH3CN}$.
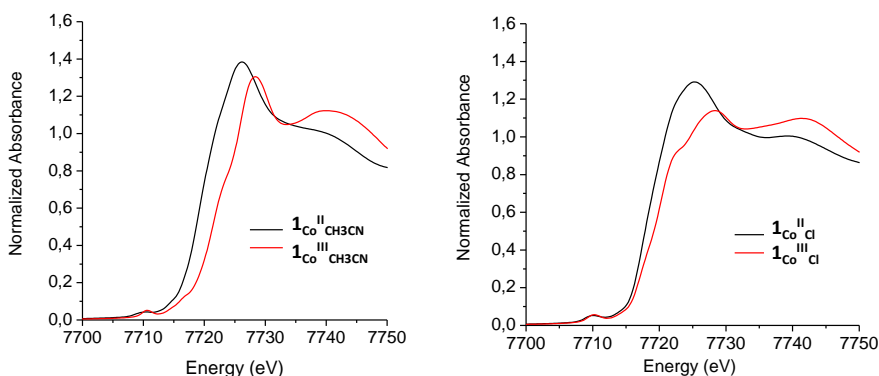
Figure X.14. Normalized cobalt-edge XANES region of the chemically synthesized *left*) $1_{Co}{}^{II}{}_{CH3CN}$ (black line) and $1_{Co}{}^{III}{}_{CH3CN}$ (red line), and *right*) $1_{Co}{}^{II}{}_{Cl}$ (black line) and $1_{Co}{}^{III}{}_{Cl}$ (red line).

c) Characterization of Co(I) intermediates

In the case of the photogenerated $1_{Co}{}^{I}{}_{CH3CN}$ upon photoreduction of $1_{Co}{}^{II}{}_{CH3CN}$ ($1_{Co}{}^{II}{}_{CH3CN}$ (15 mM), PS_{Ir} (7.5 mM), Et_3N (120 mM) in CD_3CN irradiating at 298 K (λ = 447 nm) for 15 min., see experimental section for details) a shift of 0.5 eV to lower energy (from 7719.3 to 7718.8 eV) is evident, consistent with the reduction of the metal center (Figure X.15, *left*). Likewise, in the case of the photogenerated $1_{Co}{}^{I}{}_{Cl}$ the same shift of 0.5 eV to lower energy (7717.9 eV) with respect to the initial Co(II) complex is consistent with the reduction of the metal center (Figure X.15, *right*). The extra stabilization given by the chlorine substitution is confirmed by the rising-edge at a lower energy for the $1_{Co}{}^{I}{}_{Cl}$ intermediate. A similar result is observed for the chemically synthesized $1_{Co}{}^{I}{}_{Cl}$ (starting from $(Co(I)PPh_3)_3Cl$ and the $Py_2{}^{Ts}tacn$ ligand, Figure X.15, *right*). Interestingly, in the case of the $1^{X,Y}{}_{Co}{}^{I}{}_{Cl}$ series a ~0.5 eV shift to lower energy regarding their initial Co(II) complex is observed with the rising edges centered at around 7718eV (Figure X.16).
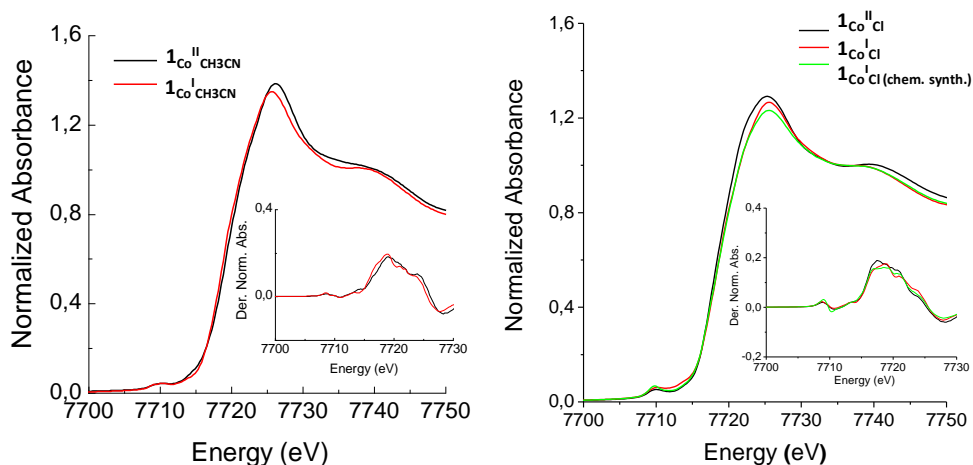
Figure X.15. Normalized cobalt-edge XANES region of *left*) the chemically synthesized $1_{Co}{}^{II}{}_{CH3CN}$ (black line) and the photogenerated $1_{Co}{}^{I}{}_{CH3CN}$ (red line), and *right*) the chemically synthesized $1_{Co}{}^{II}{}_{Cl}$ (black line), $1_{Co}{}^{I}{}_{Cl}$ (green line) and the photogenerated $1_{Co}{}^{I}{}_{Cl}$ (red line). Conditions for the photogeneration of Co(I) intermediates: $1_{Co}{}^{II}{}_{L}$ (15 mM), PS_{Ir} (7.5 mM), Et₃N (120 mM) in CD₃CN irradiating at 298 K (λ = 447 nm) for 15 min.
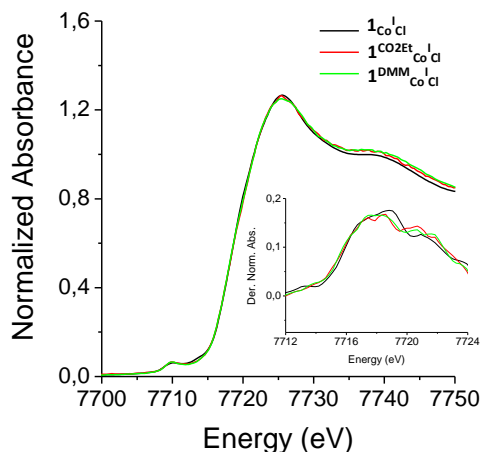
Figure X.16. Normalized cobalt-edge XANES region of the photogenerated Co(I) intermediates $1^{X,Y}{}_{Co}{}^{I}{}_{Cl}$ derived from complexes $[Co(^{X,Y}Py_2{}^{TS}tacn)(Cl)](Cl)$ (where X = Y = H for $1_{Co}{}^{I}{}_{Cl}$, X = Me and Y = OMe for $1^{DMM}{}_{Co}{}^{I}{}_{Cl}$ and X = H and Y = CO₂Et for $1^{CO2Et}{}_{Co}{}^{I}{}_{Cl}$). Conditions for the photogeneration of Co(I) intermediates: $1^{X,Y}{}_{Co}{}^{II}{}_{Cl}$ (15 mM), PS_{Ir} (7.5 mM), Et₃N (120 mM) in CD₃CN irradiating at 298 K (λ = 447 nm) for 15 min.

a) $1^{DMM}{}_{Co}{}^{I}{}_{Cl}$ Co(I) S = 1, S^2 = 2.0

b) $1_{Co}{}^{I}{}_{Cl}$ Co(I) S = 1, S^2 = 2.1

c) $1^{CO2Et}{}_{Co}{}^{I}{}_{Cl}$ Co(I) S = 1, S^2 = 2.6
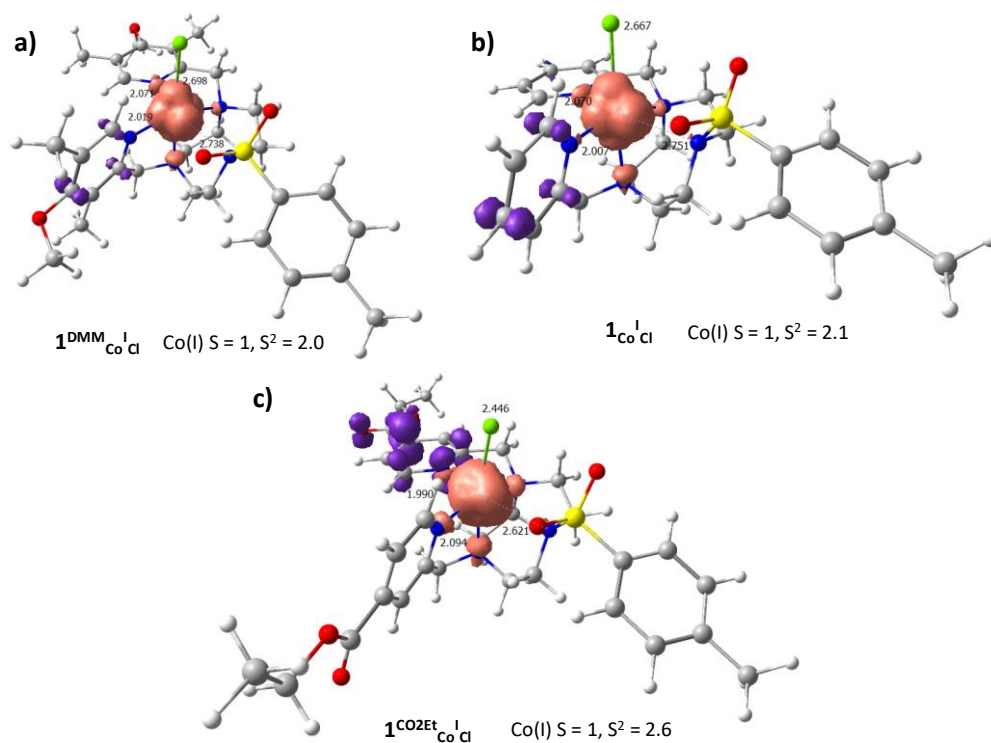
Figure X.17. Spin density obtained for the DFT modeled $1^{DMM}{}_{Co}{}^{I}{}_{Cl}$, $1_{Co}{}^{I}{}_{Cl}$ and $1^{CO2Et}{}_{Co}{}^{I}{}_{Cl}$ complexes (isovalue = 0.005). Pink and purple regions indicate α and β spin density, respectively.

At this point, DFT calculations were performed at the uB3LYP/6-31+G* GD3 level of theory and including solvent (PCM, SMD = acetonitrile) for all the series of Co(II) and Co(I) complexes derived from the $[Co(^{X,Y}Py_2{}^{Ts}tacn)Cl]Cl$ family. For the Co(I) series the complexes are better described as Co(I) intermediates in an S = 1 configuration as the lowest in energy intermediate. In all cases, the chlorine is coordinated but in favor of elongation of the Co-NTs bond distance with regard to their respective Co(II) complexes, which is also in agreement with the EXAFS analyses (see Table X.1 and annex for further details). For complex $1^{DMM}{}_{Co}{}^{I}{}_{Cl}$ and $1_{Co}{}^{I}{}_{Cl}$ there is very few spin density from the metal center delocalized on the Py ring that increases significantly when the electron-withdrawing –CO$_2$Et substituent is incorporated in the Pytacn ligand ($\rho(Py)$ = - 0.10 for $1^{DMM}{}_{Co}{}^{I}{}_{Cl}$ < $\rho(Py)$ = - 0.16 for $1_{Co}{}^{I}{}_{Cl}$ < $\rho(Py)$ = - 0.55 for $1^{CO2Et}{}_{Co}{}^{I}{}_{Cl}$, Figure X.17).

402

UNIVERSITAT ROVIRA I VIRGILI
MECHANISTIC STUDIES OF WATER OXIDATION CATALYZED BY HOMOGENEOUS IRON AND RUTHENIUM
COMPLEXES AND LIGHT-DRIVEN ORGANIC REDUCTIONS WITH A DUAL COBALT/COPPER CATALYTIC SYSTEM
Carla Casadevall Serrano

CHAPTER X   Synthesis, Characterization and Reactivity of Co(I), (II) and (III) Intermediates

Moreover, it is important to say that all samples were analyzed before and after the EXAFS measurements by ^{1}H-NMR, confirming that they were intact after the analyses (Figure X.18).
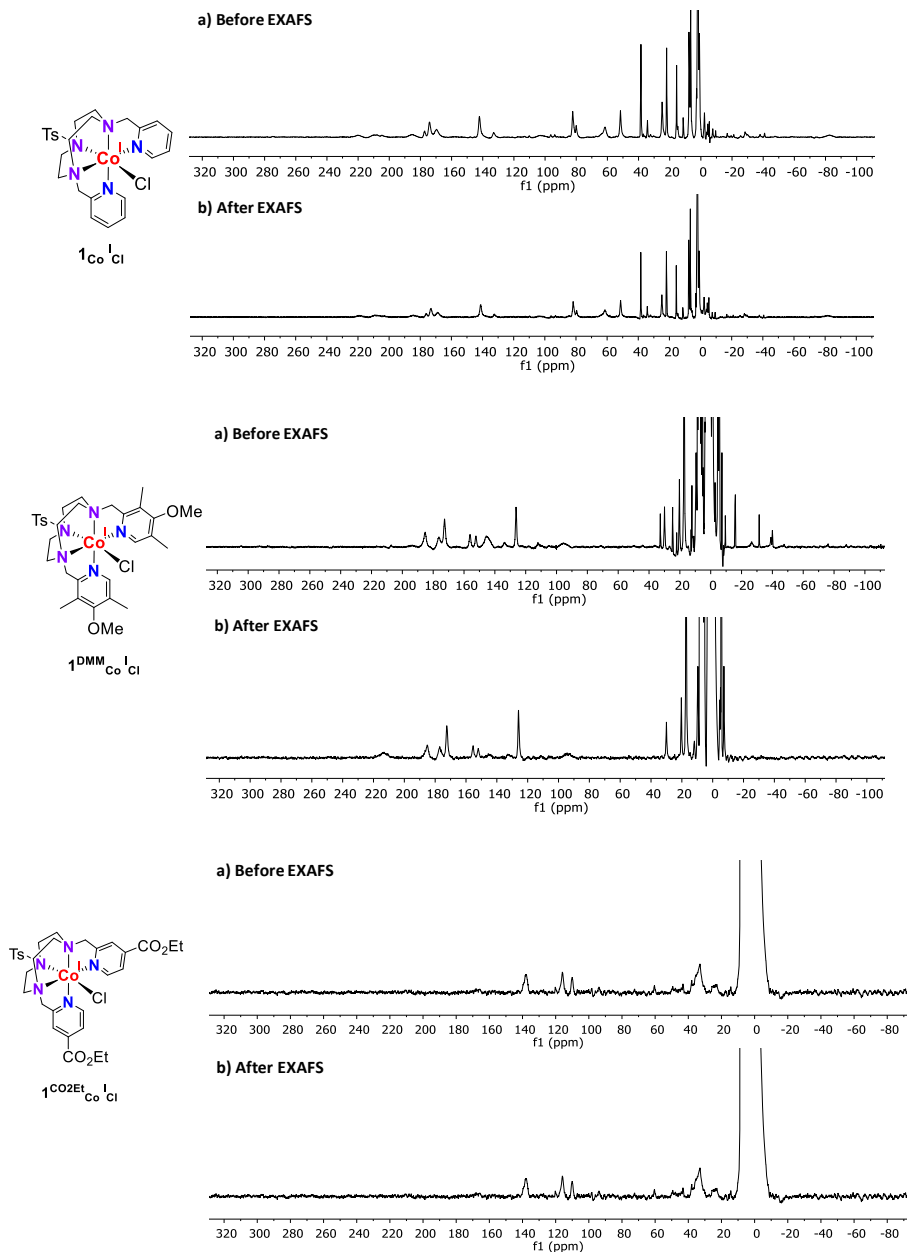
Figure X.18. ^{1}H-NMR (500 MHz, 235 K, CD$_3$CN) analyses of the synchrotron samples before and after the EXAFS measurements. From *top* to *bottom:* **1$_{Co}^{I}$$_{Cl}$**, **1$^{DMM}_{Co}^{I}$$_{Cl}$** and **1$^{CO2Et}_{Co}^{I}$$_{Cl}$**.

UNIVERSITAT ROVIRA I VIRGILI
MECHANISTIC STUDIES OF WATER OXIDATION CATALYZED BY HOMOGENEOUS IRON AND RUTHENIUM
COMPLEXES AND LIGHT-DRIVEN ORGANIC REDUCTIONS WITH A DUAL COBALT/COPPER CATALYTIC SYSTEM
Carla Casadevall Serrano

CHAPTER X   Synthesis, Characterization and Reactivity of Co(I), (II) and (III) Intermediates

d) EXAFS analysis

For the $1^{X,Y}\mathrm{_{Co}{}^{II}_{Cl}}$ and $1^{X,Y}\mathrm{_{Co}{}^{I}_{Cl}}$ series EXAFS analysis consistently suggests the presence of the Cl ion with a slight elongation upon reduction (Figure A.VIII.5). Furthermore, a clear elongation of the Co-N bonds in $1\mathrm{_{Co}{}^{II}_{CH3CN}}$ occurs upon reduction to $1\mathrm{_{Co}{}^{I}_{CH3CN}}$ consistent with theoretical predictions. However, this effect is not as clear in the $1^{X,Y}\mathrm{_{Co}{}^{II}_{Cl}}$ and $1^{X,Y}\mathrm{_{Co}{}^{I}_{Cl}}$ family of complexes. Overall EXAFS derived bond distances are consistent with structures predicted by theory.

The EXAFS analysis shows that the $1\mathrm{_{Co}{}^{II}_{CH3CN}}$ and $1^{X,Y}\mathrm{_{Co}{}^{II}_{Cl}}$ Co(II) species are consistent with the crystal structure of $1\mathrm{_{Co}{}^{II}_{Cl}}$ previously obtained by Dr. A. Call. All $1^{X,Y}\mathrm{_{Co}{}^{II}_{Cl}}$ and $1^{X,Y}\mathrm{_{Co}{}^{I}_{Cl}}$ complexes have Cl coordinated, even in their lower oxidation state Co(I). The Co(I) species can be fit as 5 coordinate with a long Co-N bond above 2.4 to 2.6 Å (Table X.1 and Table A.VIII.1 from the annex).

Table X.1. Selected theoretical and experimental distances (Å) obtained by EXAFS and X-ray.

		EXAFS			X-ray	DFT
	PATH*	r(Å)	$\sigma^2 (\times 10^3 \, \text{Å}^2)$	%R	Average dist. (Å)	Average dist. (Å)
	2 N/O	2.07	3			2.12
	1 N/O	2.43	3			2.46
$1\mathrm{_{Co}{}^{I}_{Cl}}$	1 N/O	2.14	3			2.12
	1 Cl	2.35	2			2.58
	3 N/O	2.11	5		2.130(5)	2.15
	1 N/O	2.18	5		2.130(5)	2.15
$1\mathrm{_{Co}{}^{II}_{Cl}}$	1 N/O	2.49	5	1.4	2.433(5)	2.36
	1 Cl	2.30	2		2.300(2)	2.37
	4 N/O	2.00	7			2.03
$1\mathrm{_{Co}{}^{III}_{Cl}}$	1 N/O	2.20	7			2.32
	1 Cl	2.28	1			2.25
	3 N/O	2.08	1			2.09
	1 N/O	2.24	1			2.24
$1^{DMM}\mathrm{_{Co}{}^{I}_{Cl}}$	1 N/O	2.44	1			2.73
	1 Cl	2.34	4			2.69

UNIVERSITAT ROVIRA I VIRGILI
MECHANISTIC STUDIES OF WATER OXIDATION CATALYZED BY HOMOGENEOUS IRON AND RUTHENIUM
COMPLEXES AND LIGHT-DRIVEN ORGANIC REDUCTIONS WITH A DUAL COBALT/COPPER CATALYTIC SYSTEM
Carla Casadevall Serrano

CHAPTER X   Synthesis, Characterization and Reactivity of Co(I), (II) and (III) Intermediates

	3 N/O	2.10	6	2.12
$1^{DMM}Co^{II}Cl$	1 N/O	2.16	6	2.22
	1 N/O	2.48	6	2.50
	1 Cl	2.31	1	2.36
	3 N/O	2.12	4	2.09
$1^{CO2Et}Co^{I}Cl$	1 N/O	2.19	4	2.24
	1 N/O	2.41	4	2.62
	1 Cl	2.31	5	2.45
	3 N/O	2.14	4	2.14
$1^{CO2Et}Co^{II}Cl$	1 N/O	2.21	4	2.22
	1 N/O	2.54	4	2.36
	1 Cl	2.30	1	2.37

EXAFS fits were carried out in R-space with Hanning window (dk 1), a k-weight = 2 and S_0 = 0.9. Bond distances and disorder parameters (Δr_{eff} and σ^2) were allowed to float having initial values of 0.0 Å and 0.003 Å^2 respectively, with a universal E_0 and ΔE_0 = 0 eV

X.2.2. EPR characterization of Co(II) and Co(I)

Then we have analyzed the Co(II) initial complexes $[Co(OTf)(Py_2^{Ts}tacn)](OTf)$ (1_{Co}^{II}) and $[Co(Cl)(Py_2^{Ts}tacn)](Cl)$ ($1_{Co}^{II}Cl$) (Figure X.19) by EPR. The EPR of complex $[Co(OTf)(Py_2^{Ts}tacn)](OTf)$ in isobutyronitrile shows a dominant axially symmetric signal with g-values centered around 2.2 and 2.0 similar to previously reported values of elongated distorted pseudo-octahedral Co(II) complexes. However, replacing the OTf$^-$ by a Cl$^-$ anion as the sixth ligand ($[Co(Cl)(Py_2^{Ts}tacn)](Cl)$ ($1_{Co}^{II}Cl$)) in the same solvent (isobutyronitrile) leads to a dominant broad high-spin Co(II) signal with transitions to the lower Kramer doublet (m_s ½) with simulated real g-values of 2.85, 2.22 and 1.89 and a E/D ratio of 0.041. In addition, a small low spin (1/2) Co(II) contribution to the EPR spectrum is also present with g-values and hyperfine coupling constants (A) typical of LS Co(II) systems (Figure X.19 and Table X.2).[16,23] On the other hand, the photochemically generated Co(I) intermediate $1_{Co}^{II}CH3CN$ shows a much less intense signal in the EPR maybe due to the measurement in X band, but with g values also around g = 2, which is in agreement with the formation of a d^8 Co(I) intermediate (Figure X.20).[16,23]

UNIVERSITAT ROVIRA I VIRGILI
MECHANISTIC STUDIES OF WATER OXIDATION CATALYZED BY HOMOGENEOUS IRON AND RUTHENIUM
COMPLEXES AND LIGHT-DRIVEN ORGANIC REDUCTIONS WITH A DUAL COBALT/COPPER CATALYTIC SYSTEM
Carla Casadevall Serrano

CHAPTER X   Synthesis, Characterization and Reactivity of Co(I), (II) and (III) Intermediates
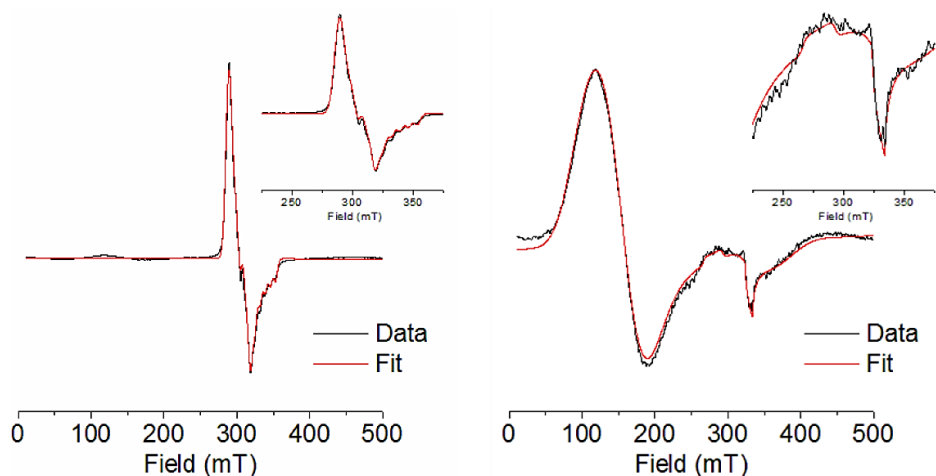
Figure X.19. EPR spectra (black line) and simulation (red line) of $[Co(OTf)(Py_2^{Ts}tacn)](OTf)$ (left) and $[Co(Cl)(Py_2^{Ts}tacn)](Cl)$ (right) (0.5 mM) in isobutyronitrile at 5 dB of power and 50 K.

Table X.2. Results from the simulation of sample EPR spectra.

Sample	Spin 3/2			Spin 1/2			Spin 1/2		
	g values g_1 g_2 g_3	E/D ratio	weight	g values g_1 g_2 g_3	A (MHz) A_1 A_2 A_3	weight	g values $g_\parallel$ $g_\perp$	A (MHz) $A_\parallel$ $A_\perp$	weight
$[Co(Cl)(Py_2^{Ts}tacn)]Cl$	2.85 2.22 1.89	0.041	1	2.39 2.06 2.03	112 6 38	0.014	-	-	-
$[Co(OTf)(Py_2^{Ts}tacn)](OTf)$	-	-	-	-	-	-	2.22 2.04	114 198	1
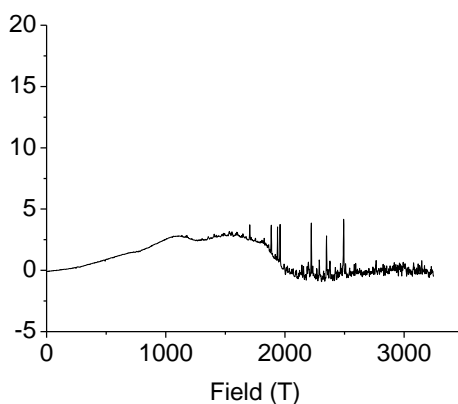
Figure X.20. EPR spectrum of the photogenerated $\mathbf{1_{Co}^{I}{}_{CH3CN}}$ (0.5 mM) in acetonitrile at 5 dB of power and 50 K. Conditions for the photogeneration of Co(I) intermediate: $\mathbf{1_{Co}^{II}{}_{CH3CN}}$ (0.5 mM), $\mathbf{PS_{Ir}}$ (0.5 mM), Et$_3$N (5 mM) in CD$_3$CN irradiating at 298 K (λ = 447 nm) for 15 min.

UNIVERSITAT ROVIRA I VIRGILI
MECHANISTIC STUDIES OF WATER OXIDATION CATALYZED BY HOMOGENEOUS IRON AND RUTHENIUM
COMPLEXES AND LIGHT-DRIVEN ORGANIC REDUCTIONS WITH A DUAL COBALT/COPPER CATALYTIC SYSTEM
Carla Casadevall Serrano

CHAPTER X   Synthesis, Characterization and Reactivity of Co(I), (II) and (III) Intermediates

X.2.3. Reactivity of the Co(I) intermediate

XANES, EXAFS and NMR characterization together with DFT calculations point to the formation of low valent Co(I) intermediates. With these results in hand, we performed some of the initially studied reactivity studies with the putative Co(I) against protons using trifluoroacetic acid (TFA) or H_2O and O_2 to double-check the products that are formed. The reactivity studies were performed at low temperature due to the inherent instability of the low valent Co(I) intermediate at r.t. Analogously, the same reactivity was studied with Co(II) to discard the formation of a possible a new Co(II) species. Then the reaction products were analyzed by ^{1}H-NMR and XAS when possible.

X.2.3.1. ^{1}H-NMR reactivity studies with Co(I) at low temperature

In all cases, the reactions were performed by adding the corresponding reagent to the Co(I) species at low temperature (-35 ºC) under Argon atmosphere inside a young gast-tight NMR tube to prevent an aerobic oxidation of the putative Co(I).

a)   Reactivity of $1_{Co}{}^{I}{}_{Cl}$ with 3eq of TFA at 238 K

The addition of 3 equivalents of TFA to $1_{Co}{}^{I}{}_{Cl}$ at 238 K vanishes the paramagnetic signals associated with $1_{Co}{}^{I}{}_{Cl}$ with the consecutive formation of a new set of diamagnetic signals in the ^{1}H-NMR spectrum (Figure X.20). This new species was attributed to the formation of Co(III) species since the new signals resemble those of the chemically synthesized Co(III) species (Figure X.6). This indicates a clear change in the speciation upon the addition of protons. Moreover, to confirm this observation, the reaction product resulting from the addition of 3 equiv. TFA to either $1_{Co}{}^{I}{}_{Cl}$ and $1_{Co}{}^{I}{}_{CH3CN}$ at 238 K was analyzed by XAS. The new compound exhibits a very intense pre-edge energy at 7710.2 eV consistent with the formation of a Co(III) species. This pre-edge energy is about 0.2 eV higher in energy than the chemically synthesized $1_{Co}{}^{III}{}_{Cl}$ and $1_{Co}{}^{III}{}_{CH3CN}$ (Figure X.21), which can be either due to experimental error. In contrast, the addition of TFA to $1_{Co}{}^{II}{}_{Cl}$ produces an apparent protonation and decoordination of one of the Py rings as judged by the appearance of

407

new paramagnetic signals in the ^{1}H-NMR spectrum (Figure X.22). Therefore, the nature of the oxidation state at metal center in the photogenerated Co(I) samples is also indirectly implied to be Co(I) as the reaction of Co(I) samples with a proton source such as trifluoroacetic acid (TFA) results in formation of Co(III) centers in both the case of the $\mathbf{1_{Co}{}^I_{CH3CN}}$ and $\mathbf{1_{Co}{}^I_{Cl}}$ complexes.
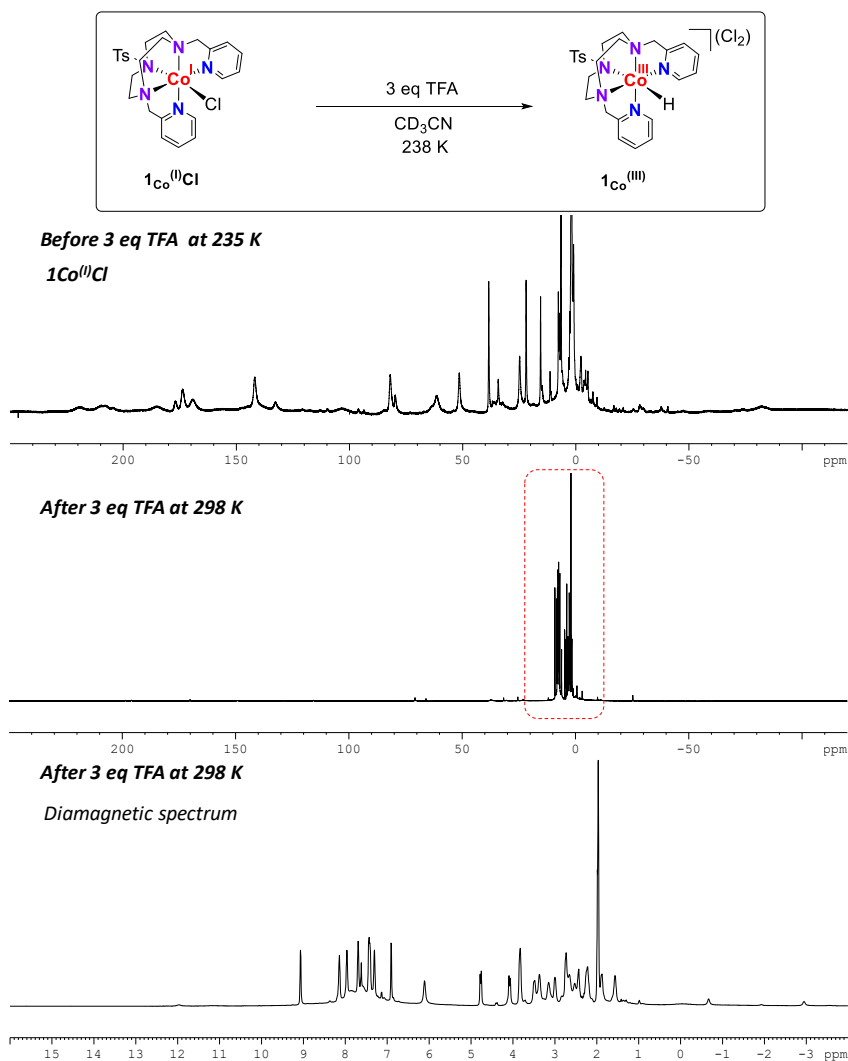
Figure X.20. Protonation of $\mathbf{1Co^ICl}$ with TFA analyzed by ^{1}H-NMR (CD$_3$CN, 500 MHz, 298 K). Top: ^{1}H-NMR paramagnetic spectrum of $\mathbf{1Co^ICl}$ before the addition of TFA (under argon at 238 K). Middle: ^{1}H-NMR paramagnetic spectrum of $\mathbf{1Co^ICl}$ after the addition of 3 eq. TFA. Bottom: ^{1}H-NMR diamagnetic spectrum of $\mathbf{1Co^ICl}$ after the addition of 3 eq. TFA.
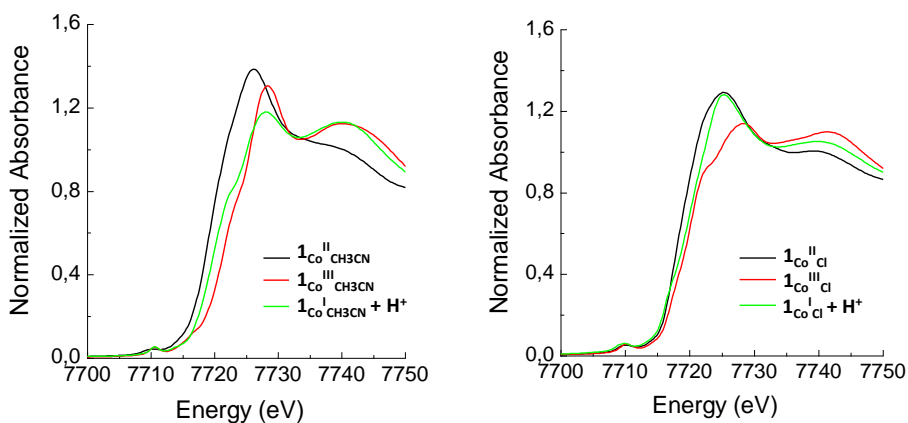
Figure X.21. Normalized cobalt-edge XANES region of the chemically synthesized $\mathbf{1_{Co}{}^{II}{}_L}$ (black line) and $\mathbf{1_{Co}{}^{III}{}_L}$ (red line) and the resulting product from the reaction of the photogenerated Co(I) $\mathbf{1_{Co}{}^{I}{}_L}$ with protons from TFA (green line) for the L = CH₃CN (*left*) and L = Cl (*right*) series. Conditions for the reaction of $\mathbf{1_{Co}{}^{I}{}_L}$ with H⁺: $\mathbf{1_{Co}{}^{II}{}_L}$ (20 mM) and slow addition of TFA (60 mM) at 238.
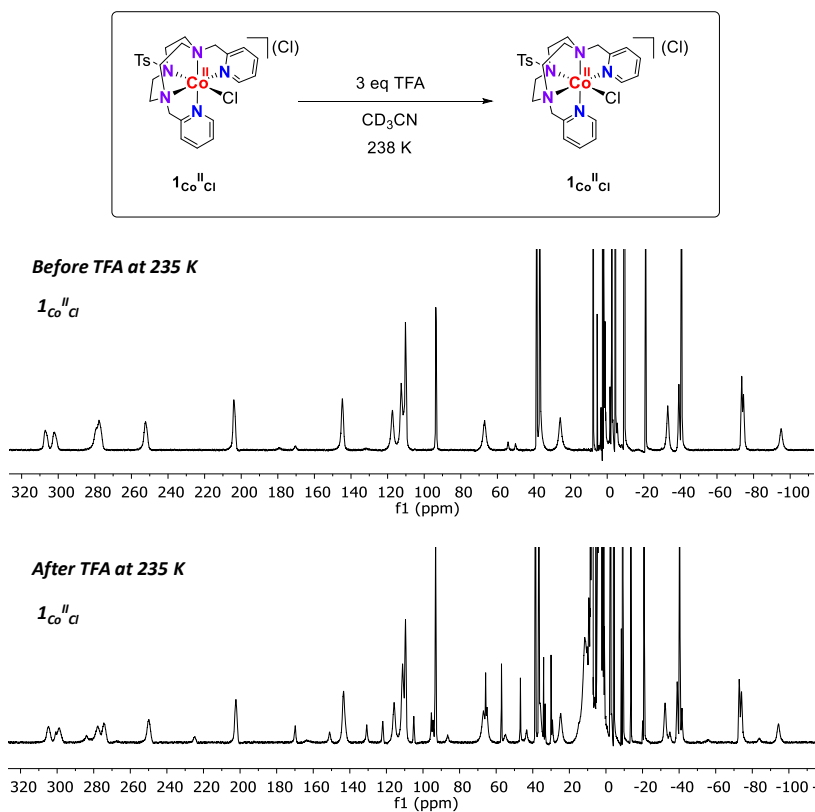
Figure X.22. Protonation of $\mathbf{1_{Co}{}^{II}Cl}$ with TFA analyzed by ¹H-NMR (CD₃CN, 500 MHz, 298 K). *Top*: ¹H-NMR paramagnetic spectrum of $\mathbf{1_{Co}{}^{II}Cl}$ before the addition of TFA (under argon at 238 K). *Bottom*: ¹H-NMR paramagnetic spectrum of $\mathbf{1_{Co}{}^{II}Cl}$ after the addition of 3 eq. TFA.

b) Reactivity of $1Co^I Cl$ with excess H_2O at 238 K

Likewise, the reaction of a slight excess of H_2O with $1_{Co}{}^I_{Cl}$ at 298 K also vanishes the initial set of paramagnetic signals associated with $1_{Co}{}^I_{Cl}$ with the concomitant formation of a new set of well-defined diamagnetic signals (Figure X.23). The new diamagnetic species was associated with the formation of Co(III) species due to the similar ^{1}H-NMR spectra to that of the chemically synthesized $1_{Co}{}^{III}_{Cl}$ and the one obtained after the reactivity with TFA (Figures X.6 and X.20). Indeed, the ^{1}H-NMR at 298 K is almost identical to the one of $1_{Co}{}^{III}_{Cl}$ (Figures X.6 and X.24). Moreover, the addition of an excess of water to $1_{Co}{}^{II}_{Cl}$ did not provoke any significant change in its paramagnetic ^{1}H-NMR spectrum (Figure X.24), as observed with TFA.
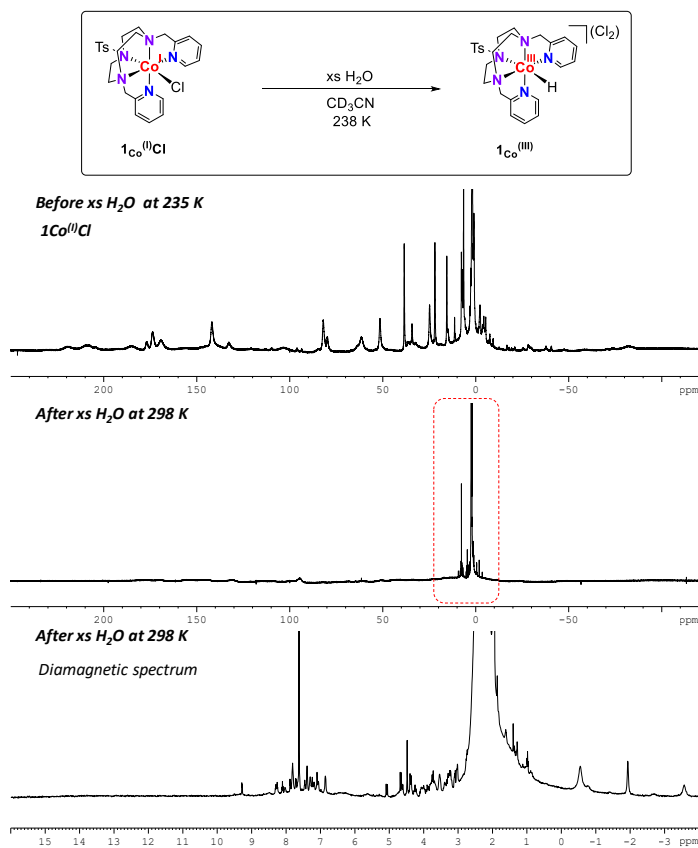
Figure X.23. Protonation of $1Co^I Cl$ with H_2O analyzed by ^{1}H-NMR (CD$_3$CN, 500 MHz, 298 K). *Top*: ^{1}H-NMR paramagnetic spectrum of $1Co^I Cl$ before the addition of an excess of H_2O. *Middle* and *bottom*: ^{1}H-NMR paramagnetic and diamagnetic spectra of $1Co^I Cl$ after the addition of an excess of H_2Oan .
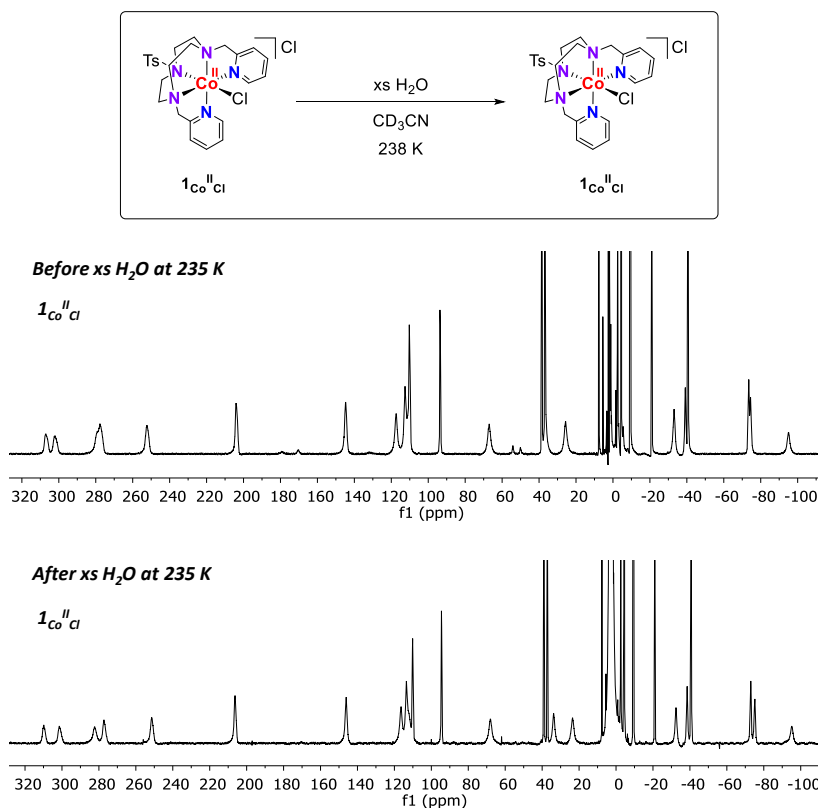
Figure X.24. Protonation of **1Co^{II}Cl** with H_2O analyzed by ^{1}H-NMR (CD$_3$CN, 500 MHz, 298 K). Top: ^{1}H-NMR paramagnetic spectrum of **1Co^{II}Cl** before the addition of an excess of H_2O (under argon at 238 K). Bottom: ^{1}H-NMR paramagnetic spectrum of **1Co^{II}Cl** after the addition of an excess of H_2O.

c) Reactivity of $1_{Co}^{I}Cl$ with O_2 at 298 K

The resulting product of the reaction of $1_{Co}^{I}Cl$ with oxygen at room temperature just by simple exposure to air results in a rapid change of the deep blue color of the putative Co(I) intermediate to a brownish one. This is an indication of the high reactivity and instability of this intermediate. The resulting compound was analyzed by XAS, showing the formation of a similar final Co(III) species (Figure X.26). Moreover, XAS analysis of the product of the reaction of $1_{Co}^{I}Cl$ with water under aerobic conditions is also in agreement with the formation of similar Co(III) species. in this case, the decrease in the pre-edge intensity is consistent with less p-d mixing into the d manifold, consistent with the presence of water as a ligand (Figure X.25).
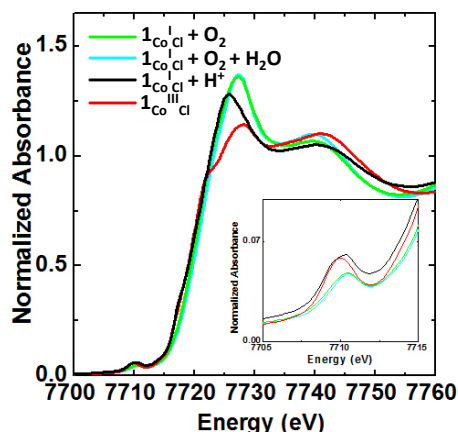
Figure X.25. Comparison between the normalized XANES region for the $1_{Co}{}^{I}_{Cl}$ reactivity against oxygen, oxygen and water, protons and the $1_{Co}{}^{III}_{Cl}$.

As a summary, the reactivity observed for Co(I) intermediates against protons, water and oxygen is characteristic of low valent Co(I) metal centers. Indeed, the reaction of Co(II) with protons or oxygen did not result in any apparent change in the ^{1}H-NMR spectra. Despite the XAS analyses shows a lower energy shift from what it is expected for a one-electron reduction (0.5 eV), the reactivity suggests that we have low valent Co(I) intermediates.

X.3. Conclusions

Detailed herein is the synthesis, characterization and reactivity of reduced intermediates ($1^{X,Y}{}_{Co}{}^{I}_{L}$, L = Cl or MeCN) derived from complex [Co(^{X,Y}Py$_2{}^{Ts}$tacn)(OTf)]OTf ($1^{X,Y}{}_{Co}$) invoked in the light-driven water reduction (WR) reaction to hydrogen and the reduction of organic substrates from chapters VIII and IX. Previous studies with complex [Co(Py$_2{}^{Ts}$tacn)(OTf)]OTf (1) suggested a strong delocalization of the spin density around the pyridine ring when the putative Co(I) intermediate is formed ($1_{Co}{}^{I}_{L}$). In this chapter we have shown that spectroscopic characterization by NMR and XAS/EXAFS of all the series of pentacoordinate complexes points to the formation of a low valent Co(I) intermediates. Additionally,

UNIVERSITAT ROVIRA I VIRGILI
MECHANISTIC STUDIES OF WATER OXIDATION CATALYZED BY HOMOGENEOUS IRON AND RUTHENIUM
COMPLEXES AND LIGHT-DRIVEN ORGANIC REDUCTIONS WITH A DUAL COBALT/COPPER CATALYTIC SYSTEM
Carla Casadevall Serrano

CHAPTER X   Synthesis, Characterization and Reactivity of Co(I), (II) and (III) Intermediates

the reactivity of the Co(I) towards protons, water and oxygen generates Co(III) species, which is in agreement with the formation of Co(I).

X.4. Experimental Section

X.4.1. Physical methods

Nuclear magnetic resonance (NMR) spectra were recorded on Bruker AV400 and AV500 spectrometers using standard conditions. All ^1H chemical shifts are reported in ppm and have been internally calibrated to the residual protons of the deuterated solvent.

XAS measurements. Co K-edge X-ray absorption data was collected on both solution samples in acetonitrile (10-15mM) and when applicable as powders diluted in boron nitride. Co(I) intermediates and photoreduced samples were treated anaerobically and were stored at liquid nitrogen temperatures until run. Data was acquired both in fluorescence and transmission modes at 77K using a liquid nitrogen cryostat and a Si(111) double crystal monochromator for Diamond and at 20 K using a liquid helium cryostat and a Si(220) double crystal monochromator for SOLEIL. The Athena software package was used for data calibration and normalization.[52] Energies were calibrated to the first inflection point of Co foil spectra set at 7709.5 eV. EXAFS analysis was carried out with the Artemis software program running the IFEFFIT engine and the FEFF6 code.[53,54] The k^2-weighted data was fit in r-space using a Hannings window (dk=1) over k-and r- ranges specified in the text The S_0^2 value was set to 0.9, and a global E_0 was employed with the initial E_0 value set to the inflection point of the rising edge. Single and multiple scattering paths were fit in terms of a Δr_{eff} and σ^2 as previously described. To assess the goodness of the fits both the R_{factor} (%R) and the reduced χ^2 (χ^2_v) were minimized, ensuring that the data was not over-fit.[55,56] Samples were either prepared as solids diluted in boron nitride or as ~15 mM solutions in acetonitrile. In addition, the integrity of the measured samples was ensured by ^1H-NMR analysis after the EXAFS analysis (ie. Figure X.26).

413
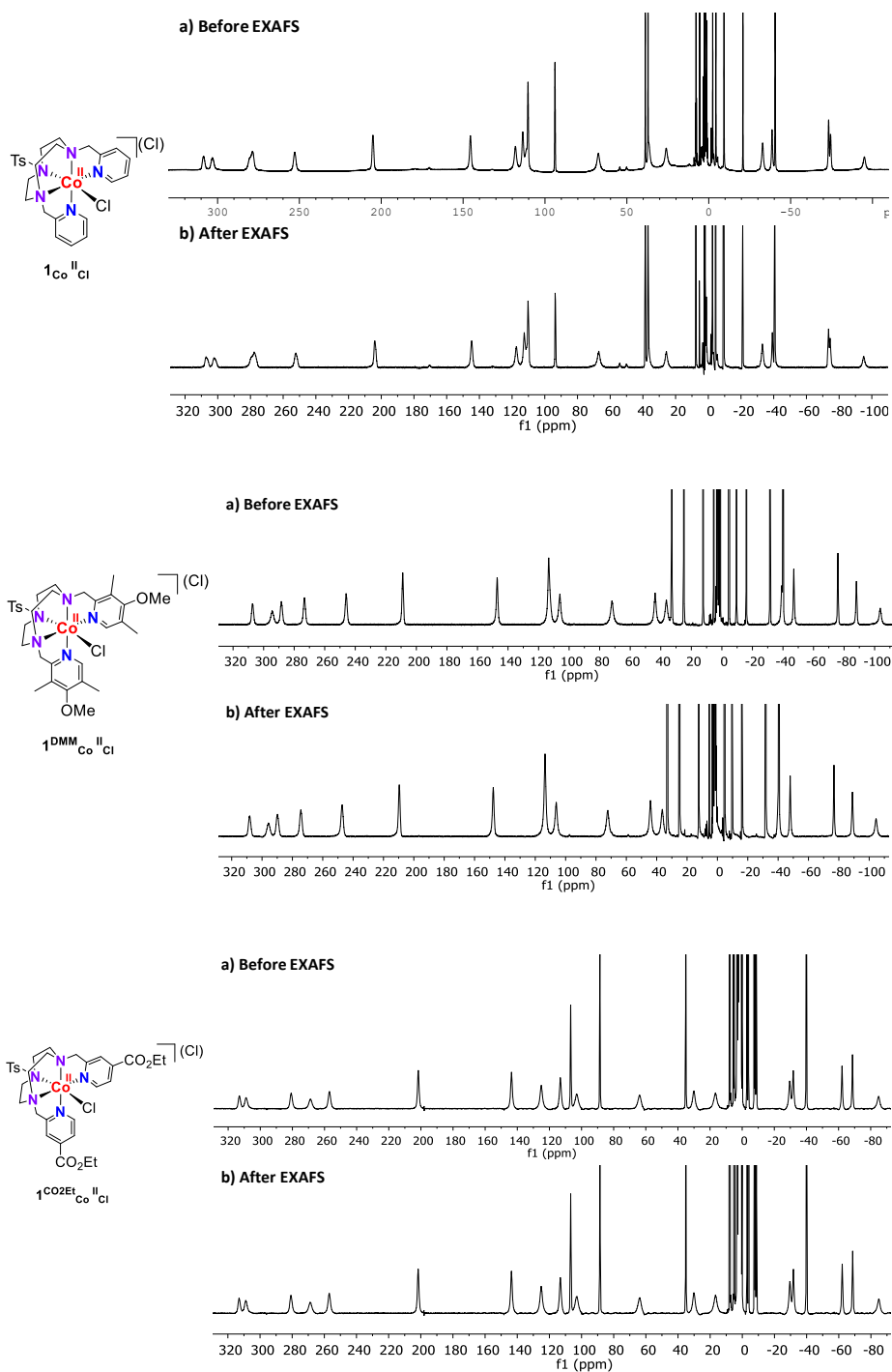
Figure X.26. ^{1}H-NMR (500 MHz, 235 K, CD$_3$CN) analyses of the synchrotron samples before and after the EXAFS measurements. From *top* to *bottom:* **1**$_{Co}{}^{II}{}_{Cl}$, **1**$^{DMM}{}_{Co}{}^{II}{}_{Cl}$ and **1**$^{CO2Et}{}_{Co}{}^{II}{}_{Cl}$.

X-Ray crystallography. Single crystals were mounted on a nylon loop for X-ray structure determination. The measurements were carried out on a BRUKER SMART APEX CCD diffractometer using graphite-monochromated $Mo_{K\alpha}$ radiation (λ=0.71073 Å). Programs used: data collection, Smart version 5.631 (Bruker AXS 1997-02); data reduction, Saint+ version 6.36A (Bruker AXS 2001); absorption correction, SADABS version 2.10 (Bruker AXS 2001). Structure solution and refinement was done using SHELXTL Version 6.14 (Bruker AXS 2000–2003). The structure was solved by direct methods and refined by full-matrix least-squares methods on F^2. The non-hydrogen atoms were refined anisotropically. The hydrogen atoms were placed in geometrically optimized position and forced to ride on the atom to which they are attached.

General procedure for the reactivity studies at low temperature monitored by NMR. In a nitrogen purged glovebox, 5.6 mg of the $1_{Co^I Cl}$ complex was weighted and dissolved in 0.5 ml degassed anhydrous CD_3CN (20 mM final concentration). The solution was introduced in a Young gas-tight NMR tube and closed under nitrogen atmosphere inside the glovebox. Then the Young-NMR tube was connected with a glass adaptor to an argon flow into a Schlenk line and after purging the atmosphere of the adaptor was opened to the argon media. Then the tube was introduced into a bath at 298 K and let reach the temperature. Then, the addition of 3 equivalents of TFA (3 μl) or excess of water (20 μl) were added and the tube was carefully closed and led react for 10 min before bringing it to the NMR unit with the bath at the same temperature (238 K). The NMR spectra was taken first at 235 K to make sure any change could be due to a warm-up of the sample. Then NMR spectra were also recorded at 298 K to better see the new formed diamagnetic species.

UNIVERSITAT ROVIRA I VIRGILI
MECHANISTIC STUDIES OF WATER OXIDATION CATALYZED BY HOMOGENEOUS IRON AND RUTHENIUM
COMPLEXES AND LIGHT-DRIVEN ORGANIC REDUCTIONS WITH A DUAL COBALT/COPPER CATALYTIC SYSTEM
Carla Casadevall Serrano

CHAPTER X   Synthesis, Characterization and Reactivity of Co(I), (II) and (III) Intermediates

X.4.2. Synthesis of complexes
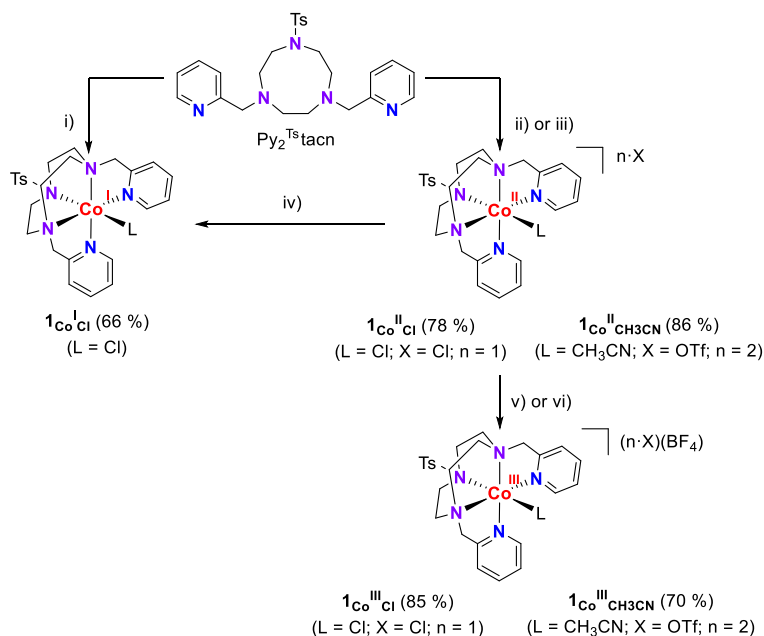
Scheme X.2. Synthesis of compounds $1_{Co}^{n}L$ (n = II or III and L = Cl or NCCH$_3$). Conditions: i) metalation with one equivalent of Co(PPh$_3$)$_3$Cl in anhydrous toluene. ii) Metalation with CoCl$_2$ in anhydrous CH$_2$Cl$_2$. iii) Metalation with [Co(OTf)$_2$(CH$_3$CN)$_2$] in anhydrous CH$_3$CN. iv) Reduction with one equivalent of KC$_8$ in anhydrous THF. v) and vi) Oxidation with 1 eq. of NOBF$_4$ in anhydrous CH$_3$CN. All reactions were performed under N$_2$ inside a glovebox at rt.

Synthesis of Co(PPh₃)₃Cl

We followed the procedure available in the literature with slight modifications.[57] CoCl$_2$·6H$_2$O (2 g, 8.47 mmol) and PPh$_3$ (6.67 g, 25.47 mmol) were mixed in 75 mL of degassed CH$_3$CN. After a few minutes a deep blue suspension was obtained attributed to the formation of Co(PPh$_3$)$_2$Cl$_2$. After stirring this solution under N2 at reflux temperature for 30 min, Zn (0.553 g, 8.46 mmol) was added directly as solid and a bright green slurry was obtained after a few minutes. After stirring for an additional 2 hours, the green product was precipitated with 50 mL EtOH:H$_2$O (1:1). This product was collected by filtration under N$_2$ using Schlenk apparatus. The resulting solid was washed with 50 mL of absolute EtOH and then slurried under N$_2$ with 2M HCl (50 mL) for 1 h. The solid was filtered under N$_2$ and

washed with H_2O (25 mL) and EtOH (25 mL), and then dried at room temperature under vacuum to yield Co(PPh3)3Cl (6.95 g, 93 % yield). The product, a bright green solid, was moderately air stable and was best stored under N_2.

Synthesis of $[Co^I(Cl)(Py_2^{Ts}tacn)]$ $(1_{Co}{}^I_{Cl})$

$Py_2^{Ts}tacn$ → [Co^I(Py$_2^{Ts}$tacn)(Cl)] $(1_{Co}{}^I_{Cl})$ (66 %)
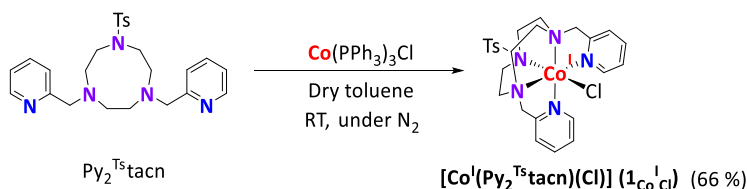
In a glovebox, a solution of $Py_2^{Ts}tacn$ (0.150 g, 0.322 mmol) in anhydrous toluene (2 mL) was added dropwise to a vigorously stirred suspension of Co(PPh$_3$)$_3$Cl (0.283 g, 0.321 mmol) in toluene (10 mL). After stirring overnight at room temperature a dark solution with a blue solid appeared. The reaction was filtered with a cannula, and the remaining blue solid was washed with 20 mL toluene and 20 mL diethyl ether to remove the residual PPh$_3$ and dried under vacuum. This solid was dissolved with anhydrous CH$_3$CN, filtered through Celite and the solvent was removed in the vacuum line affording a deep blue compound (0.119 g, 0.214 mmol, 66 % yield). ^{1}H-NMR (CD$_3$CN, 500 MHz, 235 K) δ, ppm: 219.46, 210.37, 185.77, 176.59, 173.76, 168.74, 156.87, 141.56, 132.34, 102.95, 81.89, 79.78, 60.89, 51.41, 38.37, 34.21, 24.87, 21.92, 15.59, 11.38.

Synthesis of $[Co^{II}(Cl)(Py_2^{Ts}tacn)]Cl$ $(1_{Co}{}^{II}_{Cl})$

$Py_2^{Ts}tacn$ → [Co^{II}(Py$_2^{Ts}$tacn)(Cl)](Cl) $(1_{Co}{}^{II}_{Cl})$ (78 %)
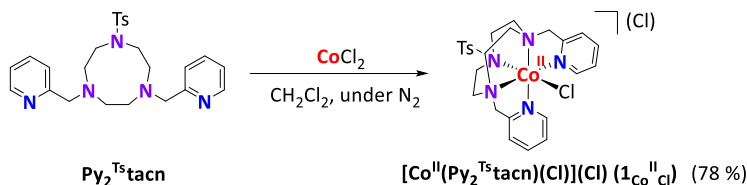
In a glovebox, a suspension of CoCl$_2$ (0.028 g, 0.215 mmol) in anhydrous CH$_2$Cl$_2$ (2 mL) was added dropwise to a vigorously stirred solution of $Py_2^{Ts}tacn$ (0.100 g, 0.215 mmol) in CH$_2$Cl$_2$ (5 mL). The cobalt chloride salt was quickly

solubilized, and after few minutes, the solution became deep purple. After stirring for an additional 3 h the solution was passed through Celite and the slow diffusion of diethyl ether over the resultant solution afforded a blue crystalline compound (0.105 g, 0.176 mmol, 78 % yield). ^{1}H-NMR (CD$_3$CN, 500 MHz, 235 K) δ, ppm: 308.68, 302.36, 278.50, 252.31, 205.39, 145.72, 118.31, 114.08, 110.15, 93.84, 67.51, 38.87, 37.11, 36.30, 26.23, -2.16, -4.41, -9.62, -20.55, -32.11, -37.64, -40.18, -72.41, -73.66, -94.47. HR-ESI-MS (m/z): 559.1213 [M - Cl]$^+$, 262.0760 [M-2·Cl]$^{2+}$.

Synthesis of [Co(Py$_2$^{Ts}tacn)(CH$_3$CN)](OTf)$_2$ (1$_{Co}^{II}_{CH3CN}$)

Py$_2$^{Ts}tacn   [Co^{II}(Py$_2$^{Ts}tacn)(CH$_3$CN)](OTf)$_2$ (1$_{Co}^{II}_{MeCN}$) (86%)
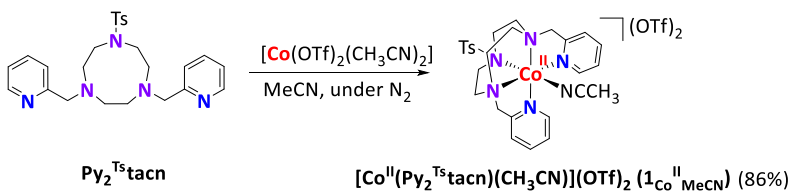
This compound was synthesized in a similar manner to the compound **1$_{Co}$** (Chapter III). In a glovebox, a suspension of [Co(OTf)$_2$(CH$_3$CN)$_2$](113 mg, 0.257 mmol) in anhydrous CH$_3$CN (2 mL) was added dropwise to a vigorously stirred solution of Py$_2$^{Ts}tacn (120 mg, 0.257 mmol) in CH$_3$CN (2 mL). The cobalt triflate salt was quickly solubilized, and after few minutes, the solution became deep red. After stirring for an additional 3 h the solution was passed through Celite and the slow diffusion of diethyl ether over the resultant solution afforded a red crystalline compound (191 mg, 0.221 mmol, 86 % yield). ^{1}H-NMR (CD$_3$CN, 500 MHz, 298 K) δ, ppm: ^{1}H-NMR (CD$_3$CN, 300 MHz, 300 K) δ, ppm: 118.28, 55.72, 3.92, 3.76, 2.22, 9.42 HR-ESI-MS (m/z): 673.1054 [M - OTf]$^+$, 262.0766 [M-2·OTf]$^{2+}$.

Synthesis of $[Co(Py_2^{Ts}tacn)(CH_3CN)](OTf)_2(BF_4)$ ($1_{Co}^{II}{}_{CH3CN}$)

$[Co^{II}(Py_2^{Ts}tacn)(CH_3CN)](OTf)_2$ $1_{Co}^{II}{}_{CH3CN}$ $[Co^{III}(Py_2^{Ts}tacn)(CH_3CN)](OTf)(BF_4)$ $1_{Co}^{III}{}_{CH3CN}$ (70 %)
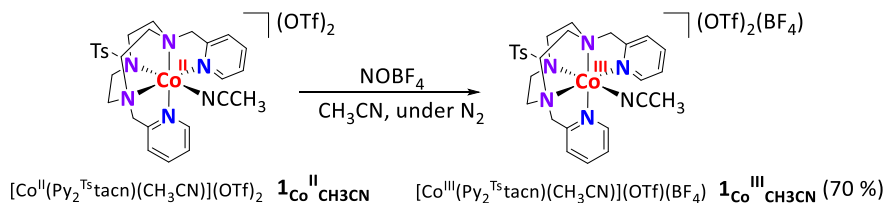
1 equivalent of $NOBF_4$ (0.030 g, 0.231 mmol) was added dropwise to 1 equivalent of $1_{Co}^{II}{}_{CH3CN}$ (0.200 g, 0.231 mmol) in 5 mL CH_3CN. The red solution of $1_{Co}^{II}{}_{CH3CN}$ intensified in color. The reaction was allowed to stir an additional 2 hours before being filtered and concentered to 1 mL. The slow diffusion of diethyl ether over this solution afforded a red crystalline compound (0.149 g, 0.156 mmol, 70 % yield). ^{1}H-NMR (CD$_3$CN, 400 MHz, 298 K) δ, ppm: 9.24, 8.52, 8.22, 8.04, 7.99, 7.87, 7.82, 7.60, 7.51, 6.55, 5.48, 4.92, 4.65, 4.40, 4.08, 3.94, 3.79, 3.68, 3.08, 2.66, 2.42.

Synthesis of $[Co(Py_2^{Ts}tacn)(Cl)](Cl)(BF_4)$ ($1_{Co}^{III}{}_{Cl}$)

$[Co^{II}(Py_2^{Ts}tacn)(Cl)](Cl)$ $1_{Co}^{II}{}_{Cl}$ $[Co^{III}(Py_2^{Ts}tacn)(Cl)](Cl)(BF_4)$ $1_{Co}^{III}{}_{Cl}$ (85 %)
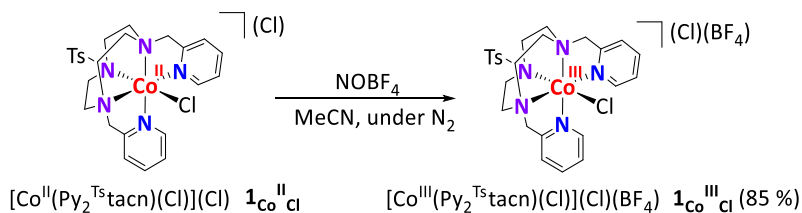
1 equivalent of $NOBF_4$ (0.039 g, 0.334 mmol) was added dropwise to a vigorously stirred solution of $1_{Co}^{II}{}_{Cl}$ (0.200 g, 0.336 mmol) in 5 mL CH_3CN. After few minutes a purple precipitate appeared. After stirring for an additional 2 hours the solution was filtered off and the resulting solid was washed with diethyl ether and dried under vacuum to yield a purple compound (0.164 g, 0.240 mmol, 85 % yield). ^{1}H-NMR (CD$_3$CN, 500 MHz, 298 K) δ, ppm: 9.45, 8.38, 8.06, 7.90, 7.77, 7.66, 7.50, 7.36, 6.42, 5.74, 5.36, 4.64, 4.33, 4.08, 3.98, 3.82, 3.60, 3.36, 3.01, 2.78.

$^{X,Y}Py_2^{TS}tacn$ (X = -Me, Y = -OMe and X = -H, Y = -CO$_2$Et) ligands were synthesized following the reported procedures.[44] Co(II), Co(III) and Co(I) complexes

with either Cl or MeCN as auxiliary ligands were synthesized analogously to the ones derived from complex **1Co** (described above).

X.4.3. Computational details

DFT calculations were carried out with the Gaussian09 program.[58] The B3LYP exchange-correlation functional[59,60] was employed for geometry optimizations of Co^n-Cl (n = 1, 2, 3) complexes, with the standard 6-31+G* 6d basis set for all atoms. The solvation effect of acetonitrile was introduced through the SMD implicit solvent model.[61] Dispersion effects were modeled with the Grimme-D_3 correction.[62] The nature of stationary points was also established by frequency calculations in solvent-phase, where all minima have no imaginary frequencies.

X.5. References

(1) Zee, D. Z.; Chantarojsiri, T.; Long, J. R.; Chang, C. J. *Acc. Chem. Res.* **2015**, *48*, 2027.
(2) Kaeffer, N.; Chavarot-Kerlidou, M.; Artero, V. *Acc. Chem. Res.* **2015**, *48*, 1286.
(3) Artero, V.; Chavarot-Kerlidou, M.; Fontecave, M. *Angew. Chem. Int. Ed.* **2011**, *50*, 7238.
(4) Wender, P. A.; Quiroz, R. V.; Stevens, M. C. *Acc. Chem. Res.* **2015**, *48*, 752.
(5) Call, A.; Casadevall, C.; Acuña-Parés, F.; Casitas, A.; Lloret-Fillol, J. *Chemical Science* **2017**, *8*, 4739.
(6) Claros, M.; Ungeheuer, F.; Franco, F.; Martin-Diaconescu, V.; Casitas, A.; Lloret-Fillol, J. *Angew. Chem. Int. Ed.* **2019**, *58*, 4869.
(7) Call, A.; Codola, Z.; Acuna-Pares, F.; Lloret-Fillol, J. *Chemistry* **2014**, *20*, 6171.
(8) Khnayzer, R. S.; Thoi, V. S.; Nippe, M.; King, A. E.; Jurss, J. W.; El Roz, K. A.; Long, J. R.; Chang, C. J.; Castellano, F. N. *Energy Environ. Sci.* **2014**, *7*, 1477.
(9) Lewandowska-Andralojc, A.; Baine, T.; Zhao, X.; Muckerman, J. T.; Fujita, E.; Polyansky, D. E. *Inorganic chemistry* **2015**, *54*, 4310.
(10) McCrory, C. C.; Uyeda, C.; Peters, J. C. *J. Am. Chem. Soc.* **2012**, *134*, 3164.
(11) Marinescu, S. C.; Winkler, J. R.; Gray, H. B. *Proc. Natl. Acad. Sci. U. S. A.* **2012**, *109*, 15127−15131.
(12) Singh, W. M.; Mirmohades, M.; Jane, R. T.; White, T. A.; Hammarstrom, L.; Thapper, A.; Lomoth, R.; Ott, S. *Chem. Commun.* **2013**, *49*, 8638.
(13) Deponti, E.; Luisa, A.; Natali, M.; Iengo, E.; Scandola, F. *Dalton Trans.* **2014**, *43*, 16345.
(14) Mandal, S.; Shikano, S.; Yamada, Y.; Lee, Y. M.; Nam, W.; Llobet, A.; Fukuzumi, S. *J. Am. Chem. Soc.* **2013**, *135*, 15294.
(15) Lazarides, T.; McCormick, T.; Du, P.; Luo, G.; Lindley, B.; Eisenberg, R. *J. Am. Chem. Soc.* **2009**, *131*, 9192.
(16) Basu, D.; Mazumder, S.; Niklas, J.; Baydoun, H.; Wanniarachchi, D.; Shi, X.; Staples, R. J.; Poluektov, O.; Schlegel, H. B.; Verani, C. N. *Chem. Sci.* **2016**.
(17) Probst, B.; Guttentag, M.; Rodenberg, A.; Hamm, P.; Alberto, R. *Inorg. Chem.* **2011**, *50*, 3404.
(18) Probst, B.; Kolano, C.; Hamm, P.; Alberto, R. *Inorg. Chem.* **2009**, *48*, 1836.
(19) Muckerman, J. T.; Fujita, E. *Chem. Commun.* **2011**, *47*, 12456.
(20) Rodenberg, A.; Orazietti, M.; Probst, B.; Bachmann, C.; Alberto, R.; Baldridge, K. K.; Hamm, P. *Inorg. Chem.* **2015**, *54*, 646.
(21) Mahammed, A.; Mondal, B.; Rana, A.; Dey, A.; Gross, Z. *Chem. Commun.* **2014**, *50*, 2725.
(22) Aoi, S.; Mase, K.; Ohkubo, K.; Fukuzumi, S. *Chem. Commun.* **2015**, *51*, 15145.
(23) Lo, W. K.; Castillo, C. E.; Gueret, R.; Fortage, J.; Rebarz, M.; Sliwa, M.; Thomas, F.; McAdam, C. J.; Jameson, G. B.; McMorran, D. A.; Crowley, J. D.; Collomb, M. N.; Blackman, A. G. *Inorg. Chem.* **2016**, *55*, 4564.
(24) Varma, S.; Castillo, C. E.; Stoll, T.; Fortage, J.; Blackman, A. G.; Molton, F.; Deronzier, A.; Collomb, M. N. *Phys. Chem. Chem. Phys.* **2013**, *15*, 17544.
(25) Lo, W. K.; Castillo, C. E.; Gueret, R.; Fortage, J.; Rebarz, M.; Sliwa, M.; Thomas, F.; McAdam, C. J.; Jameson, G. B.; McMorran, D. A.; Crowley, J. D.; Collomb, M. N.; Blackman, A. G. *Inorganic chemistry* **2016**, *55*, 4564.

(26) Varma, S.; Castillo, C. E.; Stoll, T.; Fortage, J.; Blackman, A. G.; Molton, F.; Deronzier, A.; Collomb, M. N. *Physical chemistry chemical physics : PCCP* **2013**, *15*, 17544.

(27) Mondal, B.; Sengupta, K.; Rana, A.; Mahammed, A.; Botoshansky, M.; Dey, S. G.; Gross, Z.; Dey, A. *Inorg. Chem.* **2013**, *52*, 3381.

(28) Moonshiram, D.; Gimbert-Suriñach, C.; Guda, A.; Picon, A.; Lehmann, C. S.; Zhang, X.; Doumy, G.; March, A. M.; Benet-Buchholz, J.; Soldatov, A.; Llobet, A.; Southworth, S. H. *J. Am. Chem. Soc.* **2016**, *138*, 10586.

(29) King, A. E.; Surendranath, Y.; Piro, N. A.; Bigi, J. P.; Long, J. R.; Chang, C. J. *Chem. Sci.* **2013**, *4*, 1578.

(30) Smolentsev, G.; Cecconi, B.; Guda, A.; Chavarot-Kerlidou, M.; van Bokhoven, J. A.; Nachtegaal, M.; Artero, V. *Chem . Eur. J.* **2015**, *21*, 15158.

(31) Smolentsev, G.; Guda, A.; Zhang, X.; Haldrup, K.; Andreiadis, E.; Chavarot-Kerlidou, M.; Canton, S. E.; Nachtegaal, M.; Artero, V.; Sundstrom, V. *The journal of physical chemistry. C, Nanomaterials and interfaces* **2013**, *117*, 17367.

(32) Chirik, P. J.; Wieghardt, K. *Science* **2010**, *327*, 794.

(33) Luca, O. R.; Crabtree, R. H. *Chem. Soc. Rev.* **2013**, *42*, 1440.

(34) Blanchard, S.; Derat, E.; Desage-El Murr, M.; Fensterbank, L.; Malacria, M.; Mouriès-Mansuy, V. *Eur. J. Inorg. Chem.* **2012**, *2012*, 376.

(35) Lyaskovskyy, V.; de Bruin, B. *ACS Catal.* **2012**, *2*, 270.

(36) Dugan, T. R.; Bill, E.; MacLeod, K. C.; Christian, G. J.; Cowley, R. E.; Brennessel, W. W.; Ye, S.; Neese, F.; Holland, P. L. *J. Am. Chem. Soc.* **2012**, *134*, 20352.

(37) Lewis, R. A.; MacLeod, K. C.; Mercado, B. Q.; Holland, P. L. *Chem. Commun.* **2014**, *50*, 11114.

(38) Broere, D. L. J.; Plessius, R.; Vlugt, J. I. v. d. *Chem. Soc. Rev.* **2015**, *44*, 6886.

(39) Chirik, P. J. *Acc. Chem. Res.* **2015**, *48*, 1687.

(40) Stubbert, B. D.; Peters, J. C.; Gray, H. B. *J. Am. Chem. Soc.* **2011**, *133*, 18070.

(41) Joliat, E.; Schnidrig, S.; Probst, B.; Bachmann, C.; Spingler, B.; Baldridge, K. K.; von Rohr, F.; Schilling, A.; Alberto, R. *Dalton Trans.* **2015**.

(42) Nippe, M.; Khnayzer, R. S.; Panetier, J. A.; Zee, D. Z.; Olaiya, B. S.; Head-Gordon, M.; Chang, C. J.; Castellano, F. N.; Long, J. R. *Chem. Sci.* **2013**, *4*, 3934.

(43) Jurss, J. W.; Khnayzer, R. S.; Panetier, J. A.; Roz, K. A. E.; Nichols, E. M.; Head-Gordon, M.; Long, J. R.; Castellano, F. N.; Chang, C. J. *Chem. Sci.* **2015**, *6*, 4954.

(44) Call, A.; Lloret-Fillol, J. *Chem. Commun.* **2018**, *54*, 9643.

(45) Evans, D. F. *J. Chem. Soc.* **1959**, 2003.

(46) Piguet, C. *J. Chem. Educ.* **1997**, *74*, 815.

(47) Naklicki, M. L.; White, C. A.; Plante, L. L.; Evans, C. E. B.; Crutchley, R. J. *Inorg. Chem.* **1998**, *37*, 1880.

(48) Bigi, J. P.; Hanna, T. E.; Harman, W. H.; Chang, A.; Chang, C. J. *Chem. Commun.* **2010**, *46*, 958.

(49) Das, U. K.; Bobak, J.; Fowler, C.; Hann, S. E.; Petten, C. F.; Dawe, L. N.; Decken, A.; Kerton, F. M.; Kozak, C. M. *Dalton Trans.* **2010**, *39*, 5462.

(50) Matsumoto, J.; Suzuki, T.; Kajita, Y.; Masuda, H. *Dalton Trans.* **2012**, *41*, 4107.

(51) Call, A.; Franco, F.; Kandoth, N.; Fernández, S.; González-Béjar, M.; Pérez-Prieto, J.; Luis, J. M.; Lloret-Fillol, J. *Chemical Science* **2018**, *9*, 2609.

(52) Ravel, B.; Newville, M. *Journal of Synchrotron Radiation* **2005**, *12*, 537.

(53) Newville, M. *J. Synchrotron Rad.* **2001**, *8*, 96.

(54) Rehr, J. J.; Albers, R. C. *Reviews of Modern Physics* **2000**, *72*, 621.

(55) Martin-Diaconescu, V.; Bellucci, M.; Musiani, F.; Ciurli, S.; Maroney, M. J. *J. Biol. Inorg. Chem.* **2012**, *17*, 353.

(56) Zambelli, B.; Berardi, A.; Martin-Diaconescu, V.; Mazzei, L.; Musiani, F.; Maroney, M. J.; Ciurli, S. *J. Biol. Inorg. Chem.* **2014**, *19*, 319.

(57) Liebeskind, L. S.; Baysdon, S. L.; South, M. S.; Iyer, S.; Leeds, J. P. *Tetrahedron* **1985**, *41*, 5839.

(58) Gaussian 09, R. A., M. J. Frisch, G. W. Trucks, H. B. Schlegel, G. E. Scuseria, M. A. Robb, J. R. Cheeseman, G. Scalmani, V. Barone, B. Mennucci, G. A. Petersson, H. Nakatsuji, M. Caricato, X. Li, H. P. Hratchian, A. F. Izmaylov, J. Bloino, G. Zheng, J. L. Sonnenberg, M. Hada, M. Ehara, K. Toyota, R. Fukuda, J. Hasegawa, M. Ishida, T. Nakajima, Y. Honda, O. Kitao, H. Nakai, T. Vreven, J. A. Montgomery, Jr., J. E. Peralta, F. Ogliaro, M. Bearpark, J. J. Heyd, E. Brothers, K. N. Kudin, V. N. Staroverov, R. Kobayashi, J. Normand, K. Raghavachari, A. Rendell, J. C. Burant, S. S. Iyengar, J. Tomasi, M. Cossi, N. Rega, J. M. Millam, M. Klene, J. E. Knox, J. B. Cross, V. Bakken, C. Adamo, J. Jaramillo, R. Gomperts, R. E. Stratmann, O. Yazyev, A. J. Austin, R. Cammi, C. Pomelli, J. W. Ochterski, R. L. Martin, K. Morokuma, V. G. Zakrzewski, G. A. Voth, P. Salvador, J. J. Dannenberg, S. Dapprich, A. D. Daniels, Ö. Farkas, J. B. Foresman, J. V. Ortiz, J. Cioslowski, and D. J. Fox, Gaussian, Inc., Wallingford CT. **2009**.

(59) Becke, A. D. *J Chem Phys* **1993**, *98*, 5648.

(60) Becke, A. D. *J Chem Phys* **1993**, *98*, 1372.

(61) C. J. Cramer, A. V. M., D. G. Truhlar *J. Phys. Chem. B* **2009**, *113*, 6378.

(62) Grimme, S. *J. Comput. Chem.* **2006**, *27*, 1787.

MECHANISTIC STUDIES OF WATER OXIDATION CATALYZED BY HOMOGENEOUS IRON AND RUTHENIUM
COMPLEXES AND LIGHT-DRIVEN ORGANIC REDUCTIONS WITH A DUAL COBALT/COPPER CATALYTIC SYSTEM
Carla Casadevall Serrano

CHAPTER XI

GENERAL CONCLUSIONS

UNIVERSITAT ROVIRA I VIRGILI
MECHANISTIC STUDIES OF WATER OXIDATION CATALYZED BY HOMOGENEOUS IRON AND RUTHENIUM
COMPLEXES AND LIGHT-DRIVEN ORGANIC REDUCTIONS WITH A DUAL COBALT/COPPER CATALYTIC SYSTEM
Carla Casadevall Serrano

XI. GENERAL CONCLUSIONS

In **chapter III** we have studied the decomposition paths of the neutral *N*-tetradentate iron(II) complexes **1α** and **1β** by computational analyses, which explain why the topology of the catalyst enforces different oxidation sensitive sites. This analysis has served to correlate the WO activity of complexes **1α** and **1β** with stability against oxidative damage of the ligand via aliphatic C-H oxidation. This information has served as the basis for creating a novel family of catalysts where sensitive C-H bonds have been replaced by C-D bonds. Consequently, deuterated analogs, D$_4$-α-[Fe(OTf)$_2$(mcp)] (**D$_4$-1α**) and D$_4$-β-[Fe(OTf)$_2$(mcp)] (**D$_4$-1β**), in which pseudobenzylic methylenic positions are deuterated, and D$_6$-β-[Fe(OTf)$_2$(mcp)] (D$_6$-1β), where *N*-Me groups are deuterated, exhibited informative catalytic activity with CAN. **D$_4$-1α** proves to be an extraordinarily active and efficient catalyst (up to 91% of O$_2$ yield); it exhibits initial reaction rates identical to its protio analog, but it is substantially more robust towards oxidative degradation and yields > 3400 TON (n(O$_2$)/n(Fe)), which constitutes the highest value described for a first row transition metal catalyst. Altogether evidence that the water oxidation catalytic activity is performed by a well-defined coordination complex and not by iron oxides formed after oxidative degradation of the ligands.

In **chapters IV** and **V**, in order to understand the differences in the WO catalytic activity between neutral *N*-pentadentate Fe (inactive) and Ru (active) WOCs based on the Py$_2$^{Me}tacn ligand (Py$_2$Metacn = *N*-methyl-*N',N''*-bis(2-picolyl)-1,4,7-triazacyclononane), we have reported a comprehensive mechanistic study of the Ru WOC [Ru^{II}(Py$_2$^{Me}tacn)(OH$_2$)](PF$_6$)$_2$ (**1Ru^{II}-OH$_2$**). Among all the experimental studies from **chapter IV** together with the computational modeling from **chapter V**, we propose a catalytic cycle for the Ru catalyzed WO on the basis of spectroscopic, spectrometric and computational data together with the characterization of all the intermediates starting from complex **1Ru^{II}-OH$_2$** to access the resting state of the catalytic cycle ([Ru^{IV}=O]$^{2+}$, **1Ru^{IV}=O**). The study suggests the formation of a high

valent $[Ru^V=O]^{3+}$ (**1Ru^V=O**) as the active species responsible for the O-O bond formation based on kinetic and electrochemical studies. The O-O bond formation was found to be the rate-determining step (rds). Moreover, kinetic and computational studies proved that the WO reaction catalyzed by complex **1Ru^{II}-OH$_2$** is redox-controlled and that a minimum redox potential of 1.64 V vs SHE in solution is needed to access the active species. Computational studies showed that after the O-O bond formation a $[Ru^{III}-OOH]^{2+}$ (**1Ru^{III}-OOH**) is most likely to be formed that after a PCET yields a closed shell η^2-$[Ru^{IV}-OO]^{2+}$ (η^2-**1Ru^{IV}-OO**) intermediate that after one-electron oxidation to $[Ru^{III}-O_2]^{2+}$ (**1Ru^{III}-O$_2$**) would release O_2. Moreover, we understand that the inactivity of neutral *N*-pentadentate Fe complexes based on aminopyridyl ligands is due to the high redox potential required to access the active species (> 2 V vs SHE).

Further investigations let to the characterization of an intermediate formed after the O-O bond formation, which is the rate-determining step, in **chapter VI**. The new Ru(IV) side-on peroxo intermediate η^2-$[Ru^{IV}(OO)(Py_2^{Me}tacn)](PF_6)_2$ (η^2-**1Ru^{IV}-OO**) is formed either from $[Ru^{II}(OH_2)(Py_2^{Me}tacn)](PF_6)_2$, $[Ru^{III}(OH)(Py_2^{Me}tacn)](PF_6)_2$ and $[Ru^{IV}(O)(Py_2^{Me}tacn)](PF_6)_2$ under catalytic conditions. We have reported the first example of an isolated and fully-characterized closed-shell peroxo complex η^2-$[Ru^{IV}(OO)(Py_2^{Me}tacn)](PF_6)_2$ (η^2-**1Ru^{IV}-OO**), synthesized *in operando* conditions for WO and proposed as a key intermediate after the O-O bond formation in Ru catalyzed WO. The symmetric coordination of a peroxo moiety to the Ru center for η^2-**1Ru^{IV}-OO** is confirmed by X-ray structural analysis, XAS/XANES, solid-state and solution Raman spectroscopy together with CSI-HRMS (Cryospray- High-Resolution Mass Spectrometry) and DFT. A combination of UV/Vis and Raman spectroscopy together with electrochemistry allowed for correlation of the isolated intermediates with the redox processes in solution and their connection in the catalytic cycle. Moreover, Isotopic labeling experiments allowed for the identification of the modes from the Raman spectra and direct evidence of the O-O bond formation from Ru=O by means of solution Raman spectroscopy and CSI-HRMS under catalytic conditions. Likewise, GC-MS and GC-

TCD analysis of the reaction headspace confirmed the O_2 evolution from the η^2-**1Ru^{IV}-OO** intermediate.

Along the thesis, we have seen the power of mechanistic studies to improve catalysis by rational design with a dramatic impact in the robustness of the WOC in **chapter III**. Moreover, a deep mechanistic study can also serve to elucidate a full catalytic cycle from scratch, as in **chapters IV**, **V** and **VI**. Among all the studies with *N*-tetradentate Fe(II) and *N*-pentadentate Ru(II) complexes it seems that the inactivity of neutral aminopyridyl *N*-pentadentate Fe(II) complexes for WO resides in the high oxidation state (> 2 V vs SHE) to access the active species under the catalytic conditions given by the sacrificial oxidants used (CAN or NaIO$_4$). In order to surpass this disadvantage, in **chapter VII** we have developed a new anionic *N*-pentadentate Fe(II) complex ([Fe^{II}(AQ^{Me2}tacn)(OTf)]) that is the first homogeneous anionic non-heme pentacoordinate Fe(II) complex active for WO with CAN. The negative charge and the redox non-innocent nature of the pentadentate amidated ligand seems to be key to reduce the redox potential to form the active WO species (from 2 to 1.23 V vs SHE). Spectroscopic and computational studies suggest that the high valent [Fe^{IV}(AQ^{Me2}tacn)•(O)]$^{2+}$ intermediate is potentially the active catalytic species and that the O-O bond formation could take place *via* a water nucleophilic attack mechanism. However, more studies need to be done to further conclude this hypothesis.

Water oxidation is only one of the bottlenecks to solve artificial photosynthesis. In the same line, the reduction of water to H_2 and the CO_2 reduction to other solar fuels, as well as the reduction of organic compounds to fine chemicals are also essential processes which are not fully realized. In this line, with the ligands and methods in hand, I found that similar ligand scaffolds used for WO are also viable systems to study the light-driven reduction of organic substrates. Moreover, once again, mechanistic understanding is showed to be a very powerful tool for the development of sustainable methodologies. Thus, in **chapter VIII** we have presented an efficient, general, fast, and robust light-driven methodology based on earth-

abundant elements to reduce aryl ketones, and both aryl and aliphatic aldehydes (up to 1400 TON). The catalytic system consists of a robust and well-defined aminopyridyl cobalt complex $[Co(OTf)(Py_2Tstacn)](OTf)$ (**1Co**) ($Py_2^{Ts}tacn$ = 1,4-di(picolyl)-7-(p-toluenesulfonyl)-1,4,7-triazacyclononane, OTf = trifluoromethanesulfonate anion), active for electro- and photocatalytic water reduction, and the $[Cu(bathocuproine)(Xantphos)](PF_6)$ (**PS$_{Cu}$**) photoredox catalyst. The dual cobalt–copper system (**1Co/PS$_{Cu}$**) uses visible light as the driving-force and H_2O and an electron donor (Et_3N or $^iPr_2EtN$) as the hydride source and operates in aqueous mixtures (80–60% water) with high selectivity towards the reduction of organic substrates (>2000) vs. water reduction, and tolerates O_2. High selectivity towards the hydrogenation of aryl ketones is observed in the presence of terminal olefins, aliphatic ketones, and alkynes. Remarkably, the catalytic system also shows unique and unprecedented selectivity for the reduction of acetophenone in the presence of aliphatic aldehydes in 100%. Moreover, the catalytic system provides a simple and convenient method to obtain α,β-deuterated alcohols. Both the observed reactivity and the DFT modeling support a common cobalt hydride intermediate [Co-H] as the active species. Mechanistic studies suggest alternative mechanisms depending on the redox potential of the substrate. These results show the potential of the water reduction catalyst $[Co(OTf)(Py_2Tstacn)](OTf)$ (**1Co**) and others, to develop light-driven selective organic transformations for the production of fine solar chemicals.

In **chapter IX** the dual cobalt-copper catalytic system developed in chapter VIII has been proven to efficiently hydrogenate aryl olefins using visible light as driving-force and H_2O/amine (Et_3N or $^iPr_2EtN$) as hydrogen reductive equivalents in aqueous media. In addition, synthetically useful deuterium labeled compounds can be straightforwardly obtained replacing H_2O by D_2O. Selectivity studies reinforce the hypothesis of different mechanisms for the light-driven reductive transformations depending on the redox potential of the organic substrate. Moreover, reactivity and mechanistic studies based on kinetics, isotopic labeling, reactivity with radical clocks

and computational modeling, support the formation of a [Co-H] intermediate that reacts as hydrogen transfer agent (HAT) to reduce the aryl olefins. This work is a step forward to develop light-driven selective organic methodologies towards the production of solar-fine-chemicals by the application of artificial photosynthetic schemes.

In **chapter X** we detailed the synthesis, characterization and reactivity of reduced intermediates ($\mathbf{1_{Co}^{I}L}$, L = Cl or MeCN) derived from complex [Co(OTf)(Py$_2$^{Ts}tacn)](OTf) (**1Co**) invoked in the light-driven water reduction (WR) and organic substrate reductions (chapters VIII and IX). Equivalent ^{1}H-NMR spectra are obtained by the generation of the Co(I) species under photochemical catalytic conditions and the chemically synthesized isolated Co(I). XANES and EXAFS characterization supports the formation of low valent Co(I) species. Additionally, reactivity studies show the formation of Co(III) species by ^{1}H-NMR and EXAFS analyses after protonation of Co(I) or its reaction with oxygen, showing its low valent character. The introduction of pyridine substituents at the Py$_2$^{Ts}tacn ligand by the incorporation of: i) p-CO$_2$Et and ii) 3,5-dimethyl and 4-methoxy substituents (DMM) in the Py rings; resulted in small differences in the XANES and EXAFS analyses for the Co(I) series, which are in agreement with the electronic density given to the metal center (for DMM) or withdrawn (for p-CO$_2$Et) by each ligand.

As a general conclusion, mechanistic understanding of catalytic reactions is essential to develop more robust and efficient catalysts but also to translate the catalytic activity to new methodologies. This is a step forward in the understanding and application of artificial photosynthetic schemes for the development of sustainable organic methodologies.

UNIVERSITAT ROVIRA I VIRGILI

MECHANISTIC STUDIES OF WATER OXIDATION CATALYZED BY HOMOGENEOUS IRON AND RUTHENIUM
COMPLEXES AND LIGHT-DRIVEN ORGANIC REDUCTIONS WITH A DUAL COBALT/COPPER CATALYTIC SYSTEM

Carla Casadevall Serrano

ANNEX

UNIVERSITAT ROVIRA I VIRGILI

MECHANISTIC STUDIES OF WATER OXIDATION CATALYZED BY HOMOGENEOUS IRON AND RUTHENIUM
COMPLEXES AND LIGHT-DRIVEN ORGANIC REDUCTIONS WITH A DUAL COBALT/COPPER CATALYTIC SYSTEM
Carla Casadevall Serrano

A.I. ANNEX CHAPTER III

A.I.1. Synthesis and characterization of organic ligands and Fe(II) complexes

The synthesis of ligands and complexes was described elsewhere.[1]
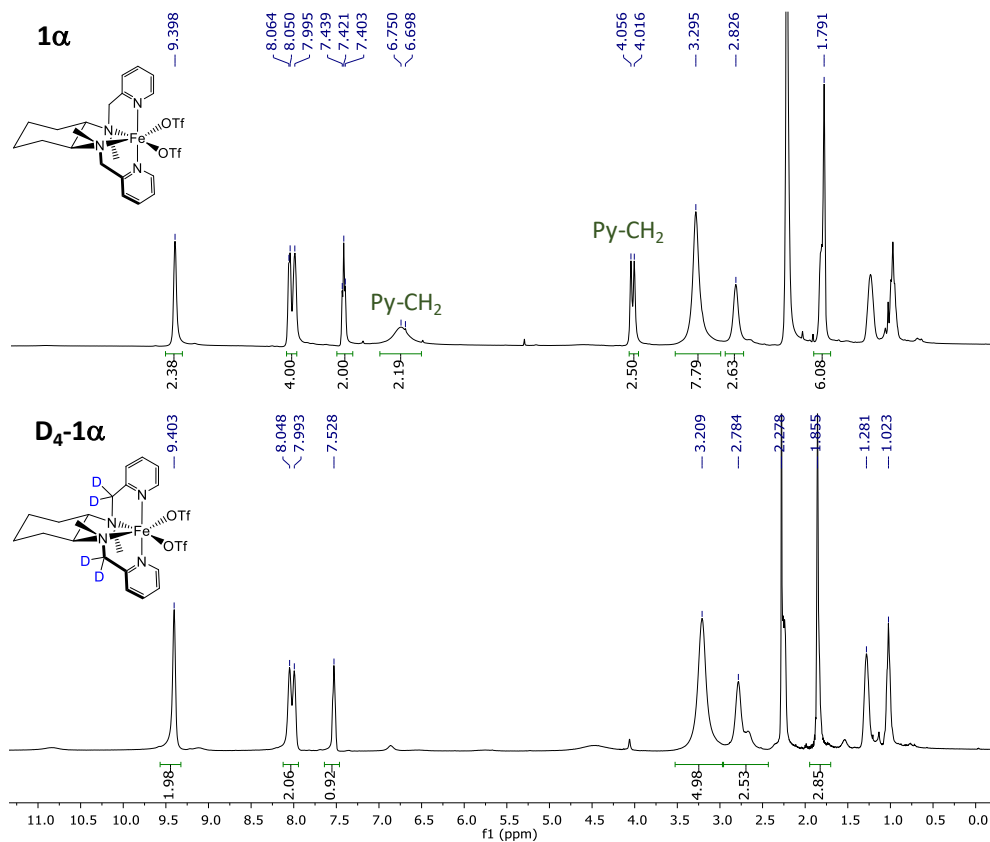
Figure A.I.1. ^{1}H-NMR (400 MHz, CD$_3$CN, 233 K) spectrum at 8 mM complex concentration from top to bottom: **1α** and **D$_4$-1α**.

ANNEX
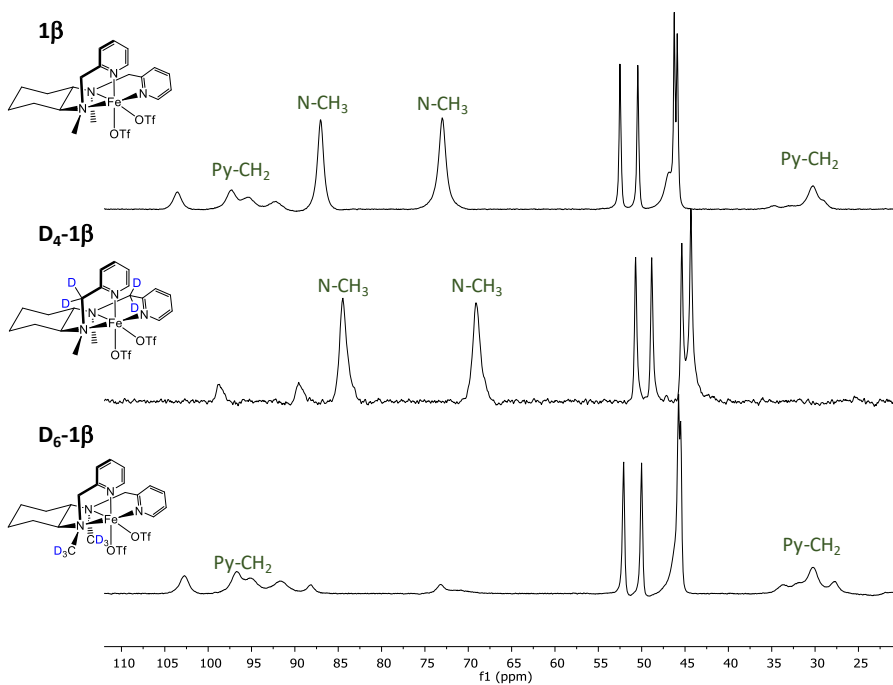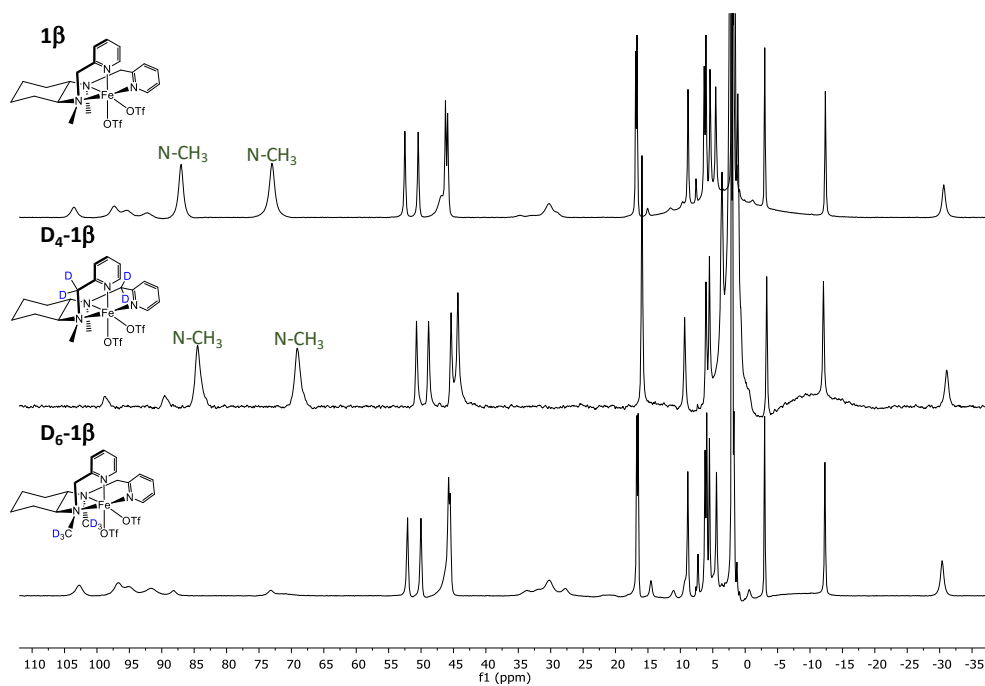
Figure A.I.2. Paramagnetic ¹H-NMR (400 MHz, CD₃CN, 298 K) spectrum at 8 mM complex concentration of **1β**, **D₄-1β** and **D₆-1β** *(top)*. (*Bottom*) magnification of the 110 to 20 ppm region.

ANNEX

A.I.2. Mössbauer characterization Fe(IV)-oxo intermediates

Mössbauer spectra were recorded at 5 K on a low field Mössbauer spectrometer equipped with a Janis CCR 5 K cryostat or at 4.2 K on a strong-field Mössbauer spectrometer equipped with an Oxford Instruments Spectromag 4000 cryostat containing an 8 T split-pair superconducting magnet. Both spectrometers were operated in a constant acceleration mode in transmission geometry. The isomer shifts were referenced against that of a metallic iron foil at room temperature. Analysis of the data was performed with the program WMOSS (WMOSS4 Mössbauer Spectral Analysis Software, www.wmosss.org, 2009-2015).
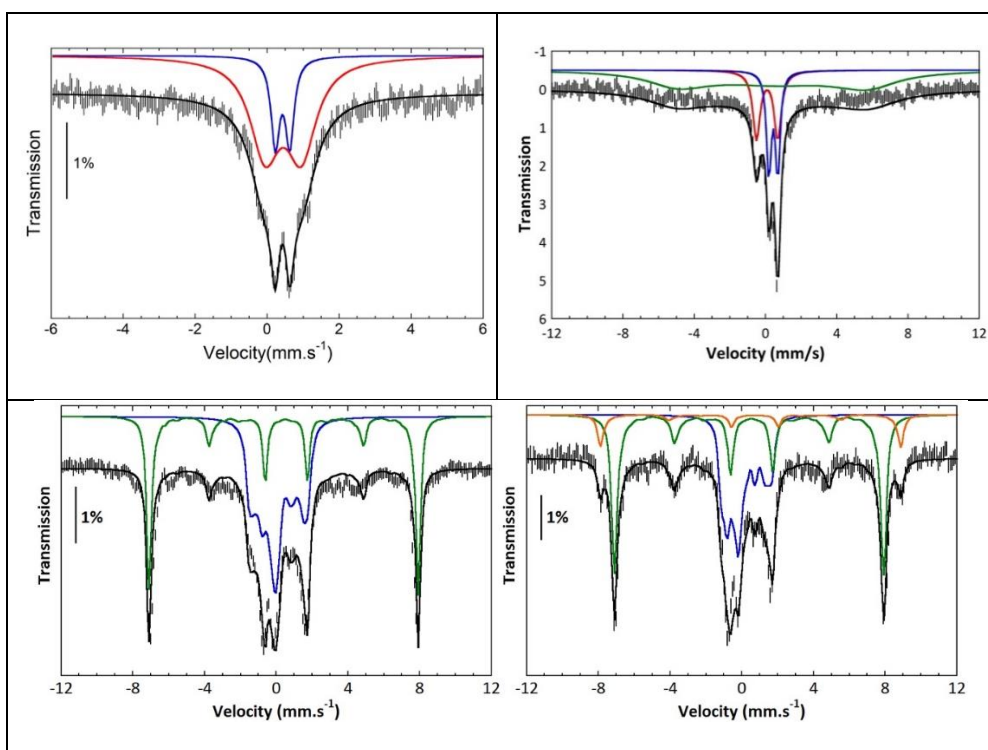
Figure A.I.3. Mössbauer spectra of **2α** (left) and **2β** (right) recorded at ca 5 K without field (top) and at 4.5 K under a field of 7 T applied parallel to the γ-rays (bottom). Hatched bars: experimental spectrum; solid lines spectra simulated with the hyperfine parameters listed in Table A.I.1. Blue line: contribution of the Fe^{IV} species; green and orange lines: contributions of Fe^{III} species; black line: overall simulations.

Table A.I.1. Hyperfine parameters deduced from the simulation of the Mössbauer spectra of **2α** and **2β**.

	D cm^{-1}	S	$g_x/g_y/g_z$	d mm s^{-1}	DE$_Q$ mm s^{-1}	G mm s^{-1}	h	Ax (T)	Ay (T)	Az (T)	%
2a											
Fe^{IV}	28	1	2.3/2.3/2.0	0.04	1.28	0.20	0.43	-29.5	-16.3	-9.5	61
Fe^{III}	5	5/2	2.0/2.0/2.0	0.46	0.30	0.15		-23.1	-23.1	-23.1	39
2b											
Fe^{IV}	28	1	2.3/2.3/2.0	0.04	1.28	0.15	0.86	-25.5	-13.7	-8.5	44
Fe^{III}	5	5/2	2.0/2.0/2.0	0.46	0.30	0.18		-23.1	-23.1	-23.1	46
Fe^{III}	5	5/2	2.0/2.0/2.0	0.60	0.50	0.17		-25.5	-25.5	-25.5	9
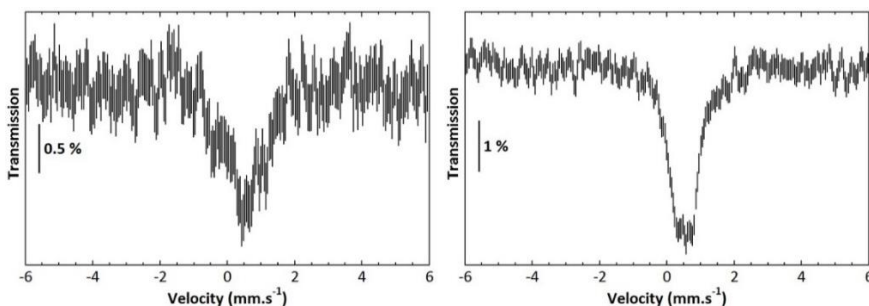
Figure A.I.4. Mössbauer spectra of **2α** (left) and **2β** (right) recorded at 80 K without field after 2 h aging of the solution.

A.I.3. Gas traces of the gaseous products in the head space during water oxidation.
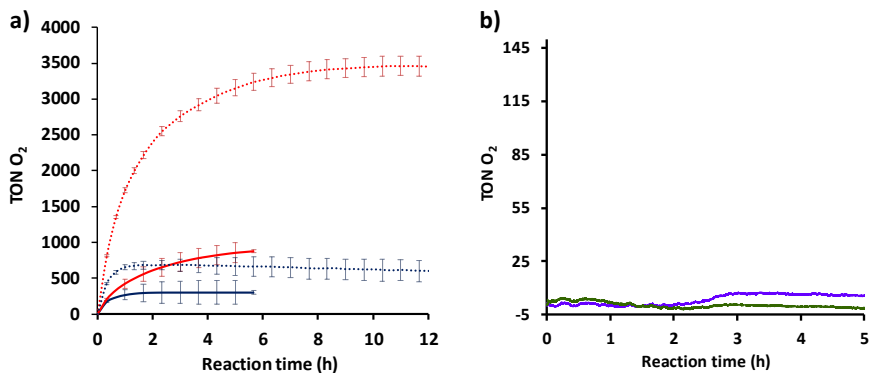
Figure A.I.5. Gas traces of the manometry monitorization when a) the iron catalyst **α-Fe(OTf)₂(mcp)** (1 μM short-dashed blue line and 12.5 μM straight blue line) and **D₄-α-Fe(OTf)₂(mcp)** (1 μM short-dashed red line and 12.5 μM straight red line) (0.5 ml of a stock solution) is added to a stirred solution of CAN (14.5 mL, final concentration 125 mM) in Milli-Q water at 25ºC and initial pH 0.8; and b) the iron catalyst **Fe(OTf)₂(mcp-Me)** (12.5 μM purple line) and **Fe(OTf)₂(mcp-Py)** (12.5 μM green line) (0.5 mL of a stock solution) is added to a stirred solution of CAN (9.5 ml, final concentration 125 mM) in Milli-Q water at 25ºC and initial pH 0.8. Vertical lines represent the error bars from the standard deviation between replicates.

436

A.I.4. DFT modelling of the degradation paths and the catalytic cycle

The mechanisms for the O-O bond formation were calculated by Dr. Ferran Acuña-Parés and the mechanism of the oxidative degradation of the catalysts by Carla Casadevall.

A.I.4.1. Relevant optimized geometries

3β-a (S = 3/2)   3β-a (S = 1/2)

3β-b (S = 3/2)   3β-b (S = 1/2)
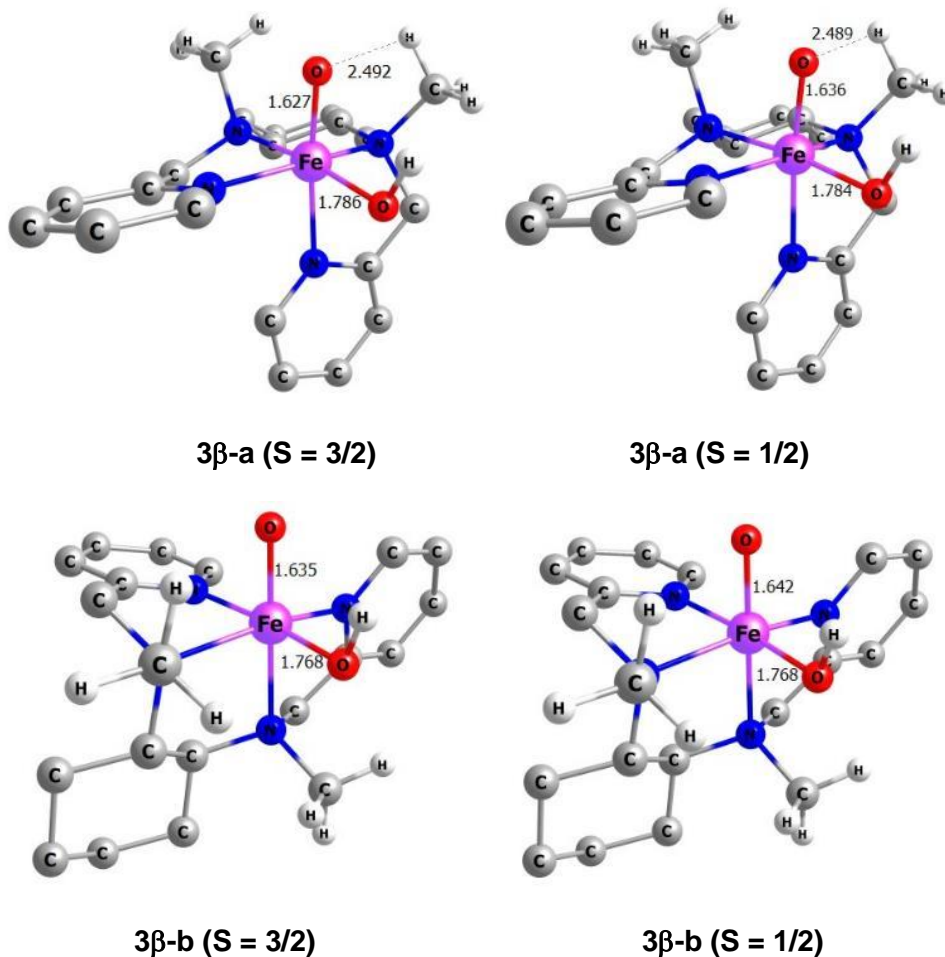
Figure A.I.6. Optimized geometries of the β-[Fe^V(O)(OH)(mcp)]$^{2+}$ (**3β**) *cis*-isomers (**a** and **b**) in the S = 1/2 and S = 3/2 spin states. The most relevant bond distances are in Å.

A.I.4.2. Free energy profiles

Figure A.I.7. a) Methyl oxidation mechanism of **3β-a** in S = 1/2 and S = 3/2 spin states. Gibbs energies are in kcal·mol⁻¹.

Figure A.I.8. Free energy profiles for the O-O bond formation mechanism performed by the **3β-a** intermediate in the S = 1/2 and S = 3/2 spin states. **L** stands for mcp ligand. Gibbs energies are in kcal·mol⁻¹.

ANNEX
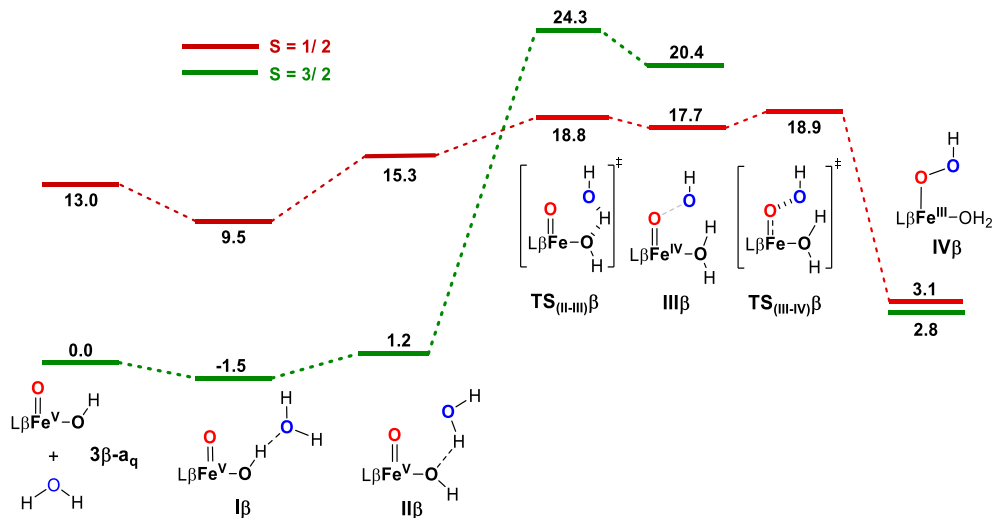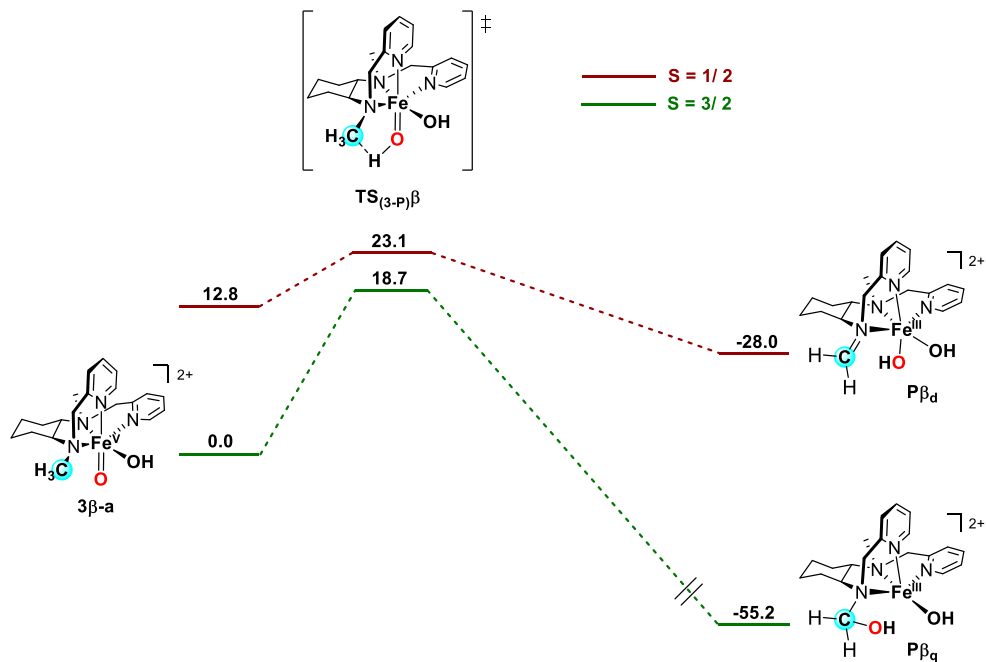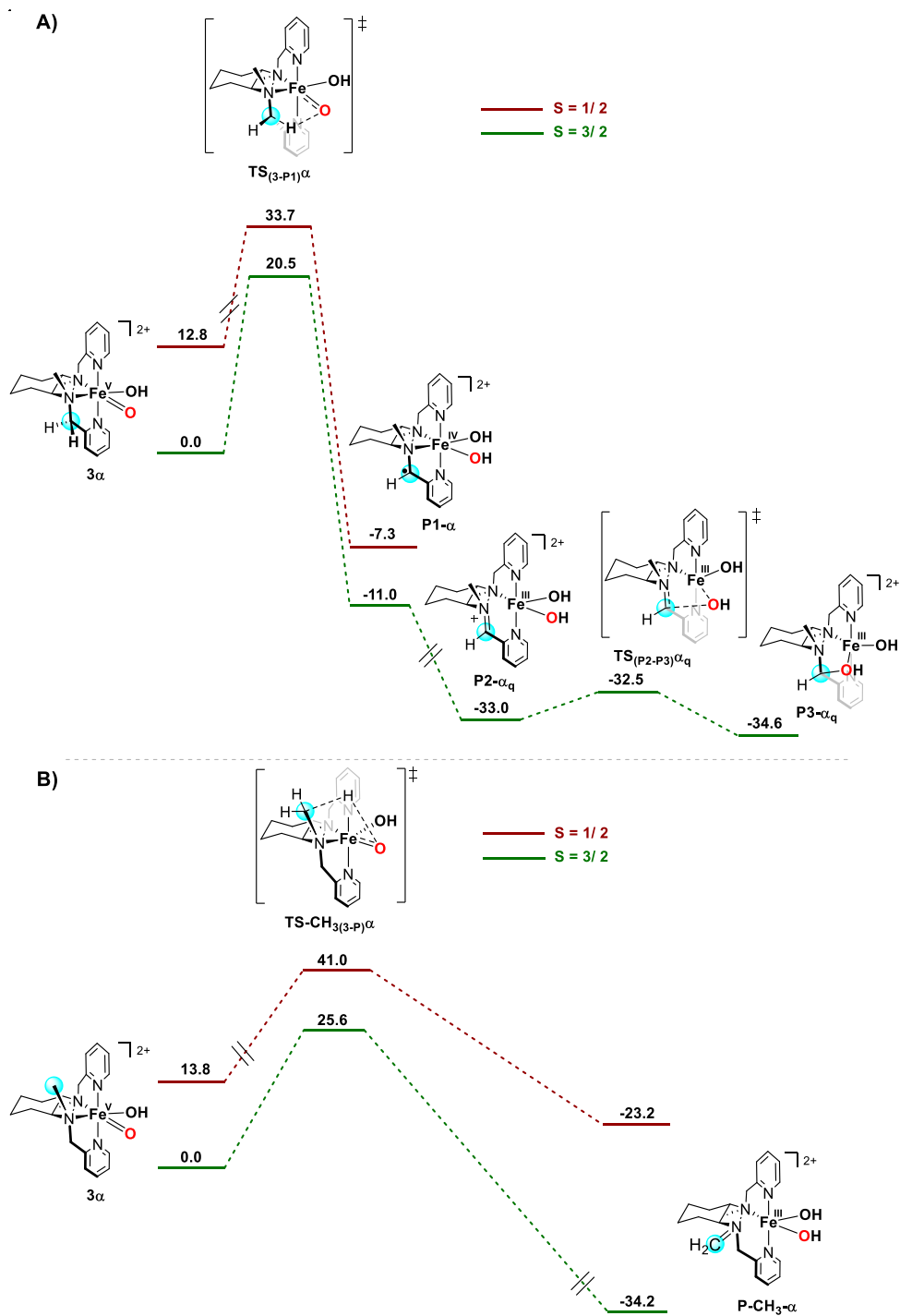
Figure A.I.9. a) Methylene oxidation mechanism by **3α** in the S = 1/2 and S = 3/2 spin states. B) Methyl oxidation mechanism by **3α** in the S = 1/2 and S = 3/2 spin states. Gibbs energies are in kcal·mol^{-1}.

ANNEX
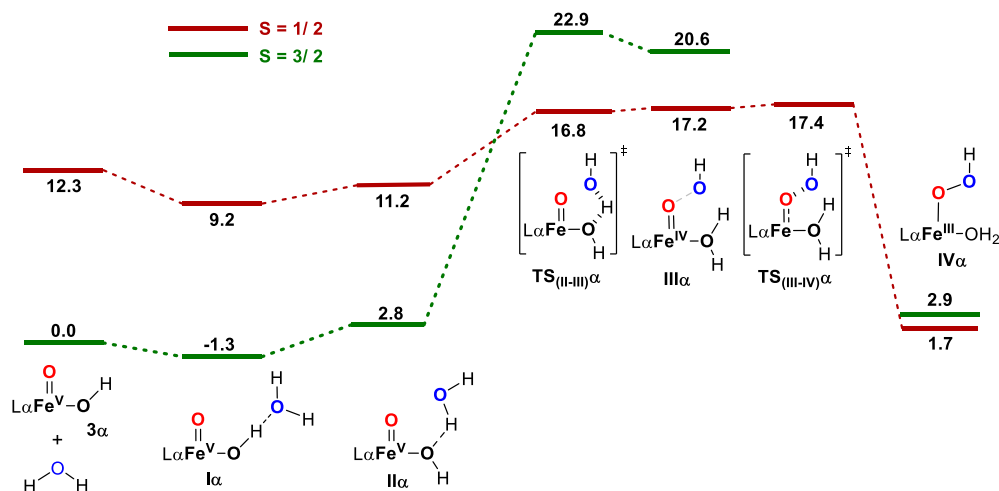
Figure A.I.10. Free energy profiles for the O-O bond formation mechanism performed by the **3α** intermediate in the S = 1/2 and S = 3/2 spin states. **L** stands for mcp ligand. ligand. Gibbs energies are in kcal·mol^{-1}.

A.I.4.3. IRC analysis

Analyses of the Intrinsic Reaction Coordinate (IRC) connecting the transitions state structures with reagents and products was performed for all cases, connecting reagents with products.

Interestingly, in the case of **3β-a$_q$** the oxidation of the methyl group yields to the ligand hydroxylation. Presumably, the beta geometry disposes in a very short distance the Fe^V-Oxo moiety and the methyl group, which forces a concerted oxidation. To better understand the direct concerted methyl hydroxylation, we carefully studied the changes in spin densities and distances of the atoms involved in the bond-breaking/forming along the IRC from **3β-a$_q$** to **Pβ$_q$**, revealing three differentiated phases (Figures A.I.11 – A.I.13). First a hydrogen atom transfer (HAT) from the starting Fe^V-Oxo to about the early transition state. During this phase the (Fe=O)···H distance is concordantly modified with the formation of an OH group, the spin density at the oxygen atom decreases and an unpaired electron is localized at the carbon atom suffering the oxidation (C$_4$, 0.67 e-). By continuing the reaction

coordinate toward products, we found a second phase were an electron is transferred from C_4 to the metal center leading to Fe^{III} species (spin density at the iron c.a. 2.81 e-). In agreement is the vanishing of the spin density over C_4 (0.05 e-) with concomitant modification of $C_4 - N_5$ distance from a typical single bound (1.50 Å) to a double bound (1.30 Å), which is consistent with the formation of an iminium cation. Finally, we illustrate the nucleophilic attack of the OH- to the $C_4 - N_5$ by the geometric changes observed.

ANNEX
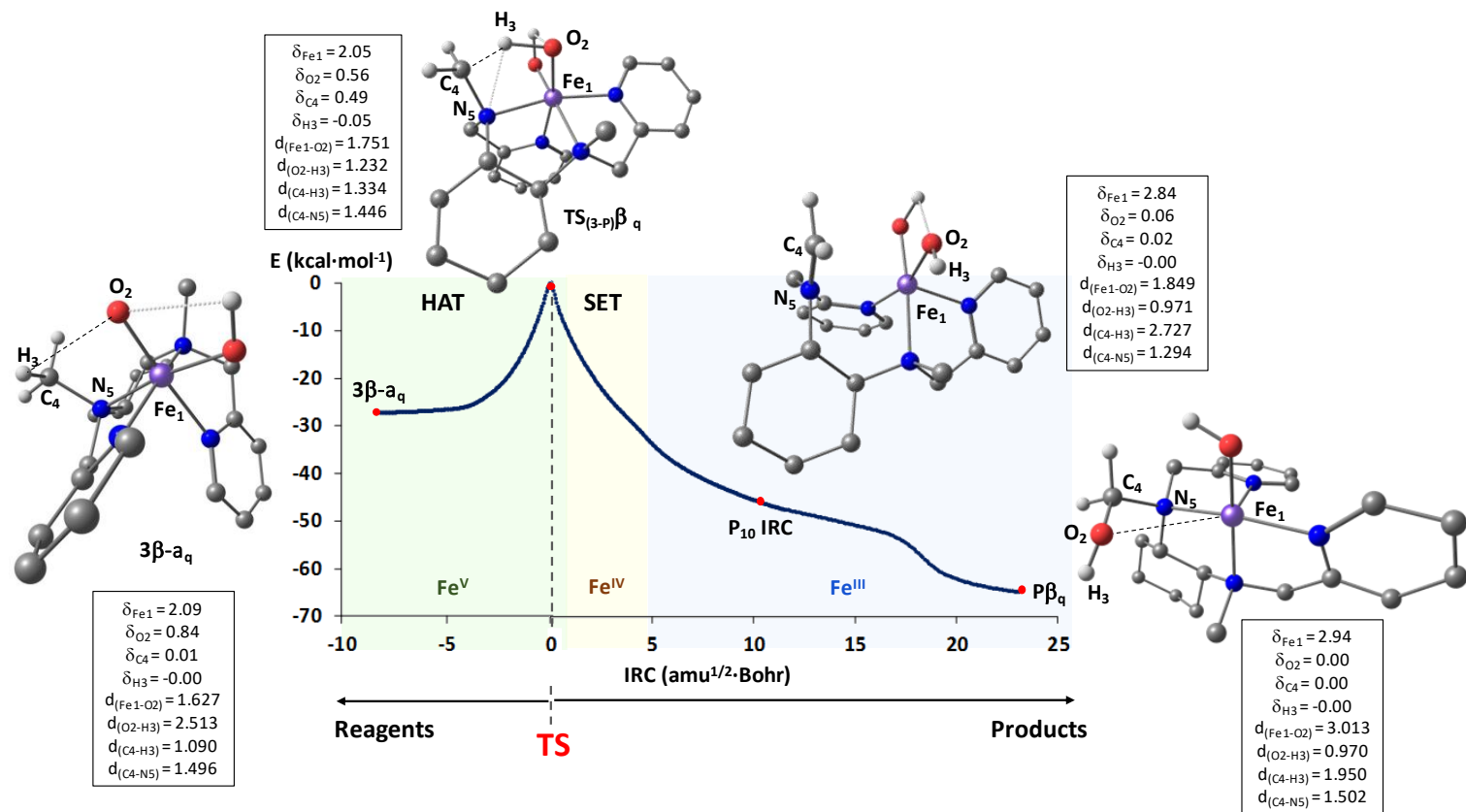
Figure A.I.11. IRCs from TS to reagent (left) and product (right) for the methyl group oxidation in **3β-a** (S = 3/2). Selected geometries (red dots) with corresponding Mulliken spin and charges along the reaction pathway illustrates the concerted C-H hydroxylation mechanism.

ANNEX
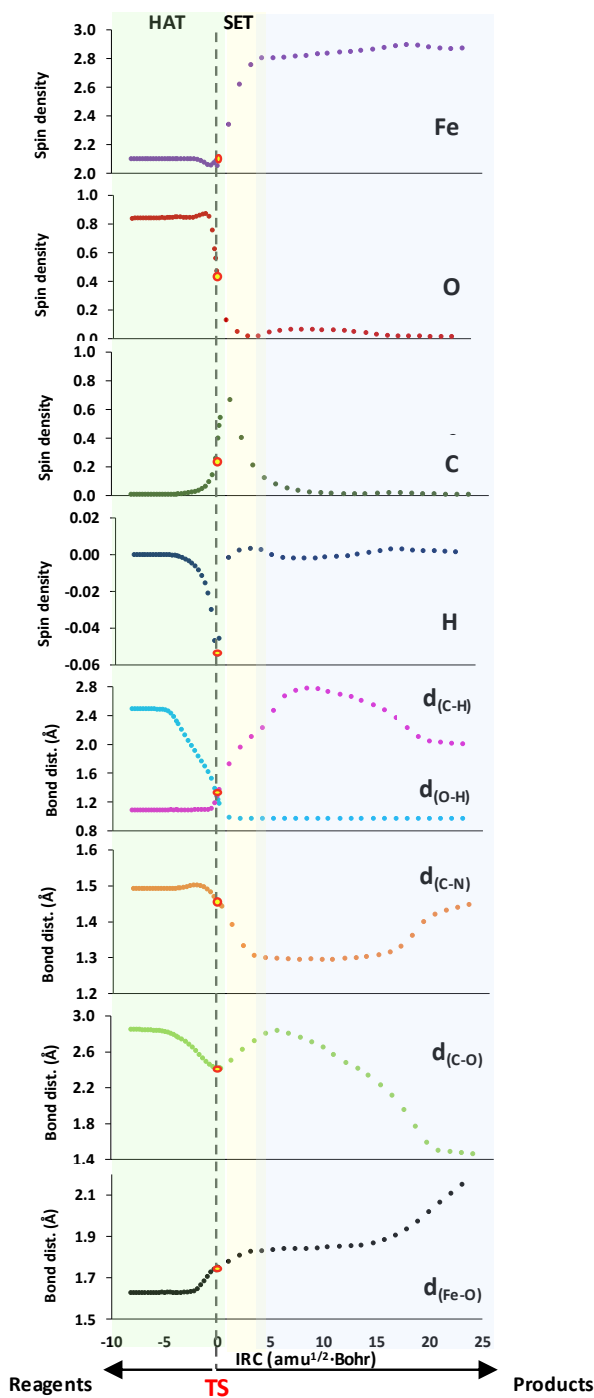
Figure A.I.12. Selected Mulliken spin densities and bond distances along the IRCs from TS (red dot) to reagent (left) and product (right) of the methyl group oxidation in **3β-a** (S = 3/2) to illustrate the concerted C-H hydroxylation mechanism.

ANNEX
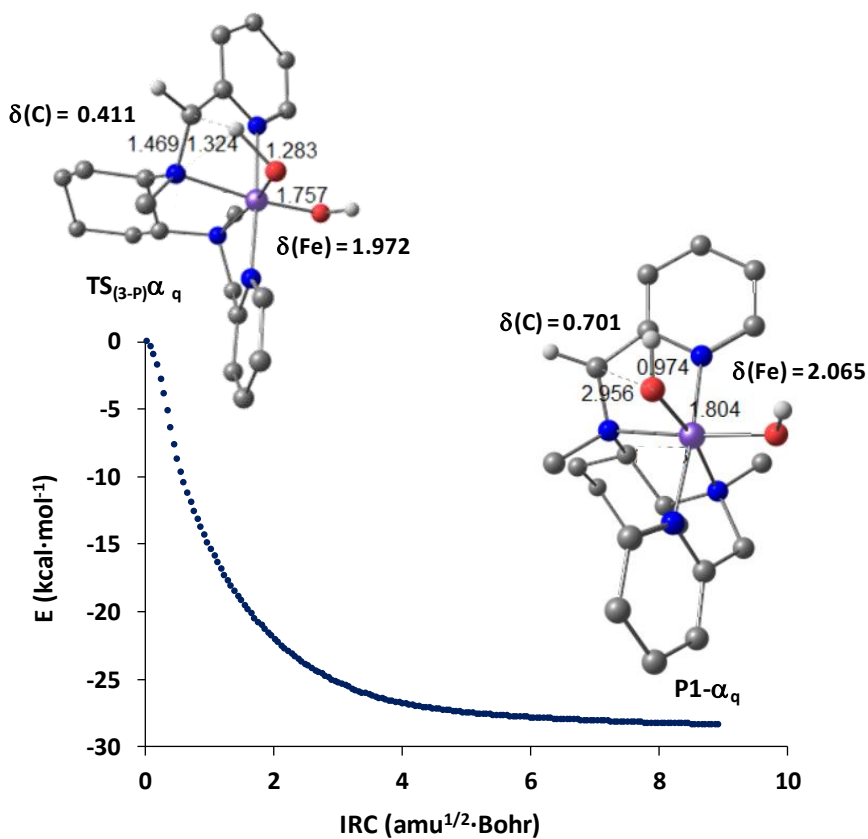
Figure A.I.13. IRC from TS to product for the methylene oxidation in **3α** (S = 3/2). Geometries represent the TS and the product.

A.I.5. References

(1) Codolà, Z.; Gamba, I.; Acuña-Parés, F.; Casadevall, C.; Clémancey, M.; Latour, J.-M.; Luis, J. M.; Lloret-Fillol, J.; Costas, M. *Journal of the American Chemical Society* **2019**, *141*, 323.

A.II. ANNEX CHAPTER IV

A.II.1. Characterization of ruthenium complexes

A.II.1.1. [Ru^{II}Cl(Py$_2^{Me}$tacn)]Cl
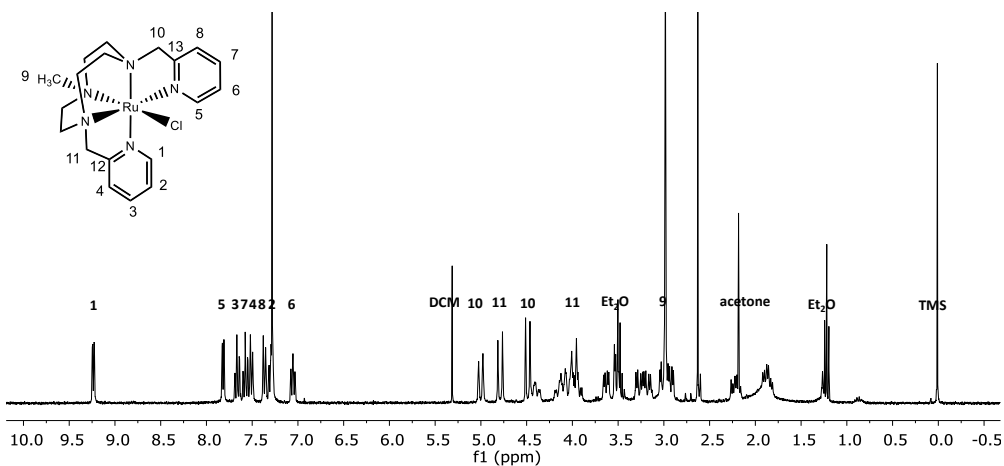
Figure A.II.1. ^{1}H-NMR (400 MHz, 298 K, CDCl$_3$) spectrum of complex [Ru^{II}Cl(Py$_2^{Me}$tacn)]Cl (**1Ru^{II}-C**). Signals at a δ between 9.5 and 7.0 ppm are due to a dissimetrisation of the ligand upon coordination to the metallic center. Methylene signals at a δ c.a. 5.0, 4.7, 4.4 and 4.0 ppm indicate that the methylenes of the pyridine alkylic arm (J = 15.0 Hz) become diastereotopic and magnetically inequivalent due to the coordination to the metallic center.

ANNEX
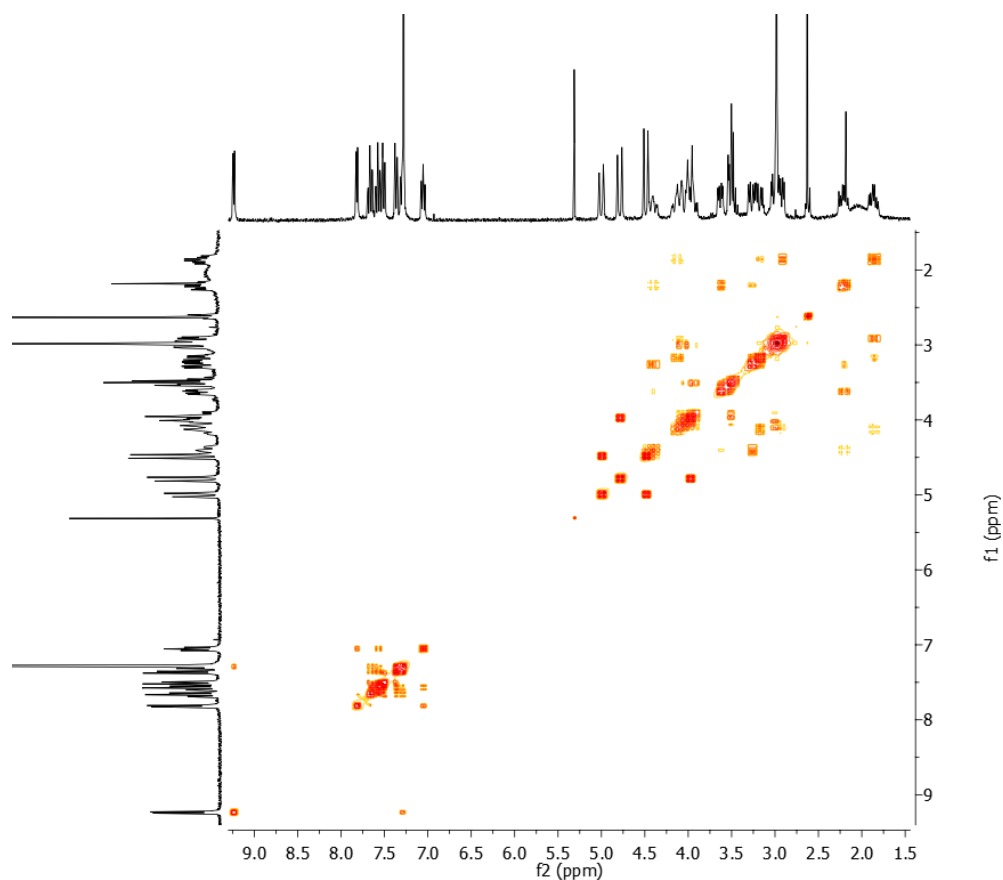
Figure A.II.2. ^{1}H-^{1}H-COSY NMR (400 MHz, 298 K, CDCl$_3$) spectrum of complex [Ru^{II}Cl(Py$_2^{Me}$tacn)]Cl (**1Ru^{II}-Cl**). Signals at a δ between 9.5 and 7.0 ppm are due to the resonances in the pyridine rings and those between 4.0 and 2.0 ppm are associated with the resonance in the tacn macrocycle. Zoom of the aromatic and the aliphatic region of the COSY spectrum are shown in the following page, respectively.
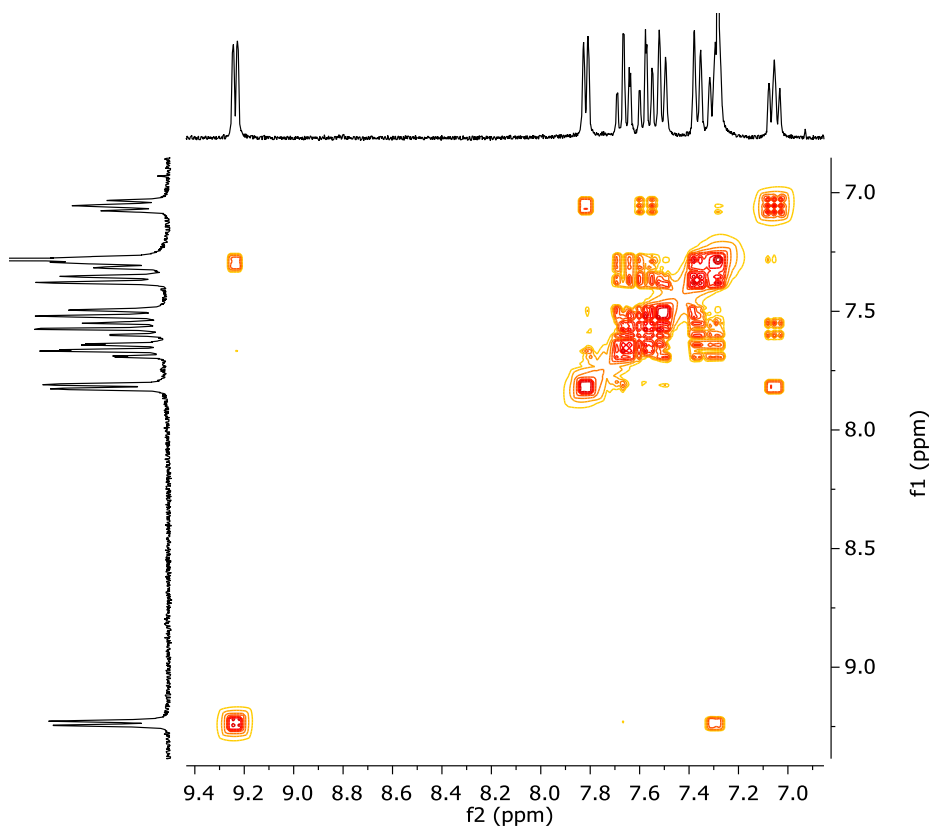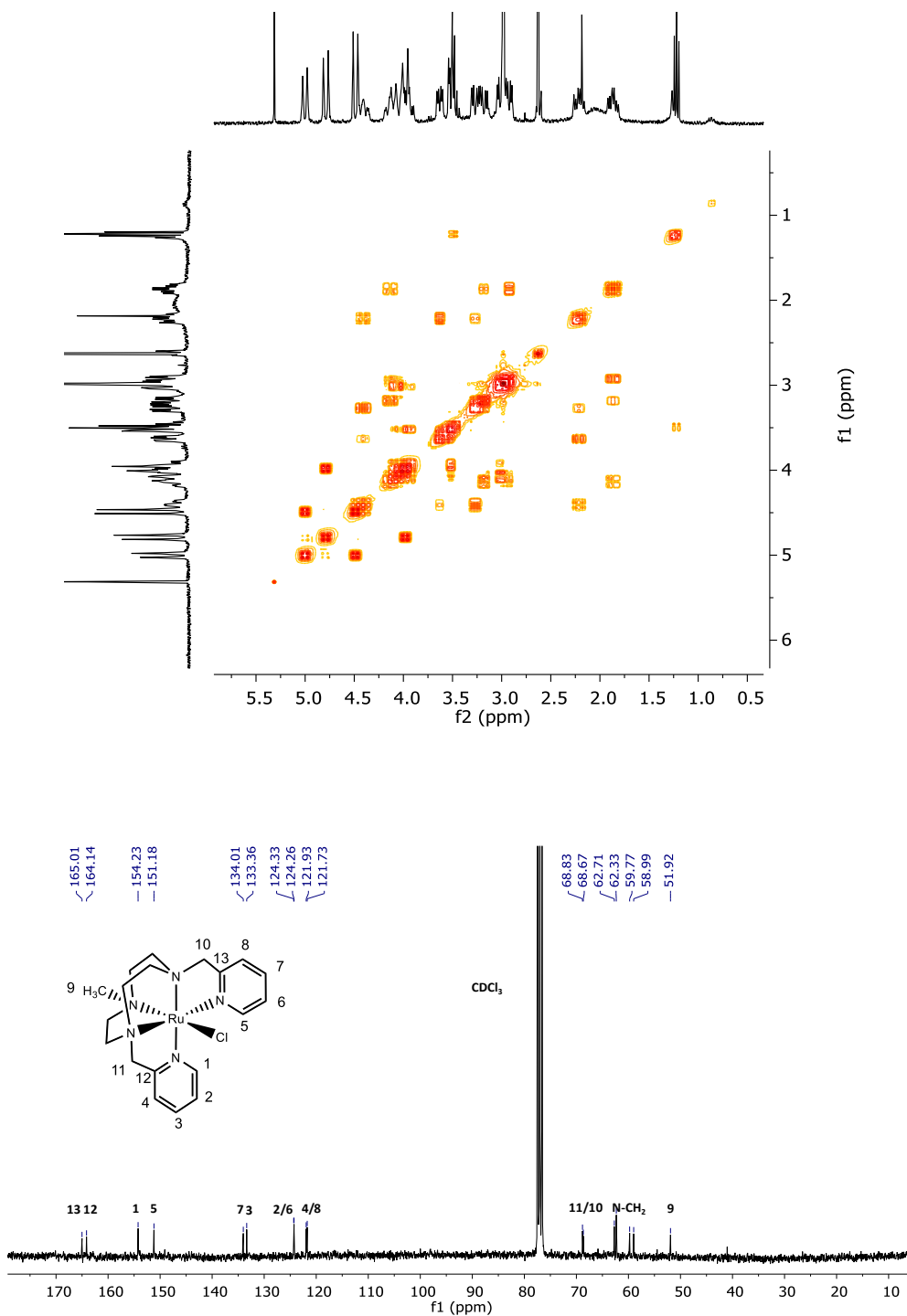
ANNEX

ANNEX

Figure A.II.3. ^{13}C-NMR (400 MHz, 298 K, CDCl$_3$) spectrum of complex [Ru^{II}Cl(Py$_2^{Me}$tacn)]Cl (**1Ru^{II}-Cl**).
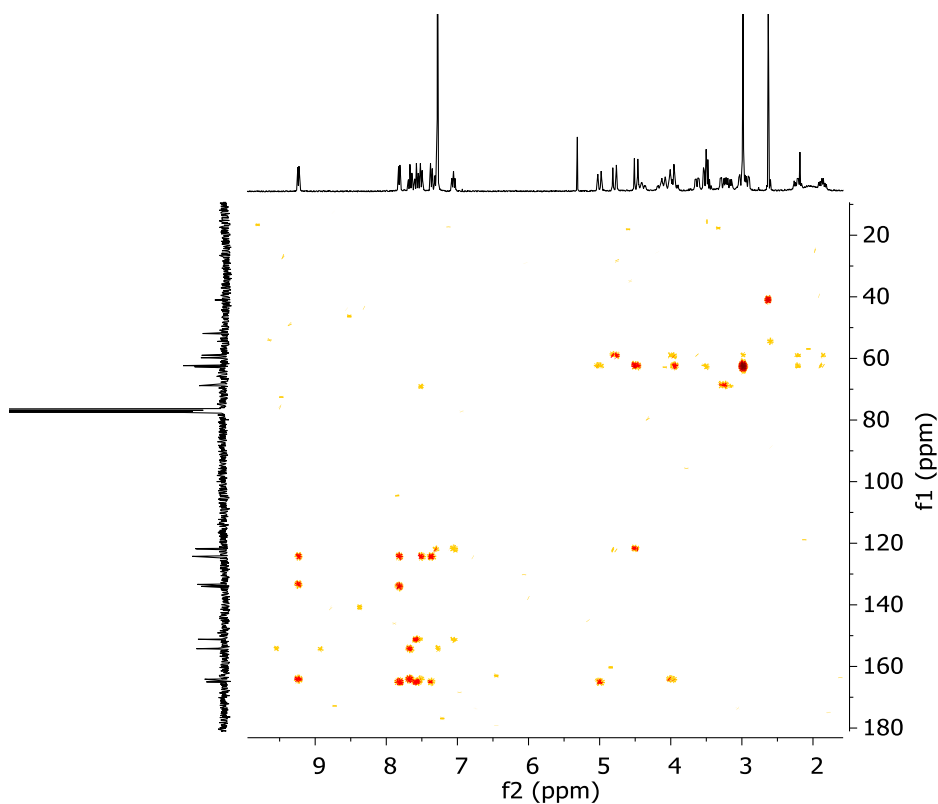
Figure A.II.4. ^{1}H-^{13}C-HMBC NMR (400 MHz, 298 K, CDCl$_3$) spectrum of complex [Ru^{II}Cl(Py$_2^{Me}$tacn)]Cl (**1Ru^{II}-Cl**). Signals between 9.5 and 7.0 ppm correspond to correlations between protons and carbons from the pyridine rings.

449
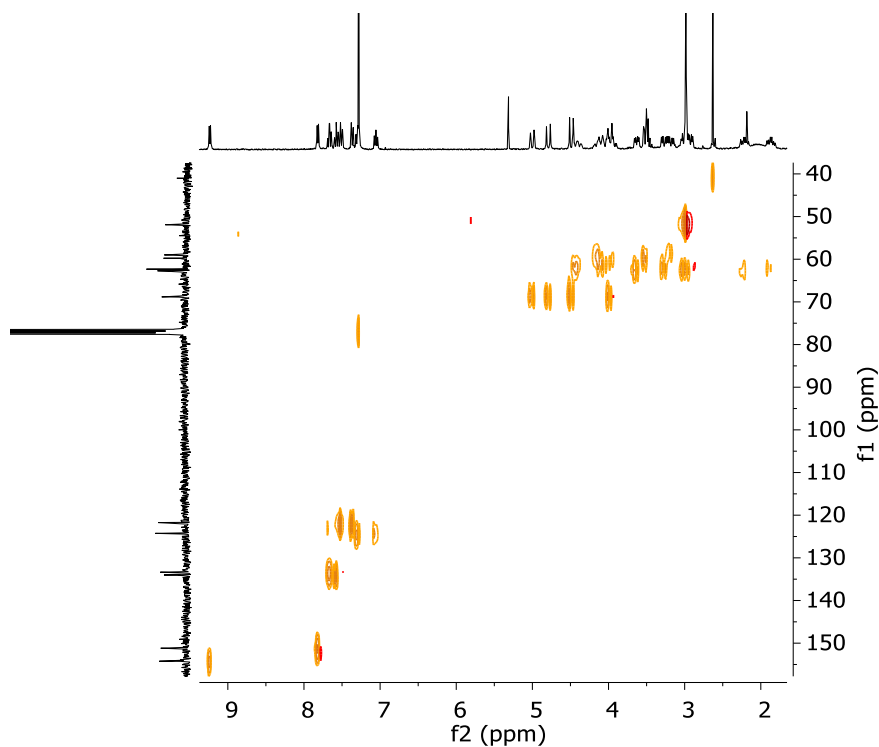
ANNEX

Figure A.II.5. ^{1}H-^{13}C-HSQC NMR (400 MHz, 298 K, CDCl$_3$) spectrum of complex [Ru^{II}Cl(Py$_2^{Me}$tacn)]Cl (**1Ru^{II}-Cl**).
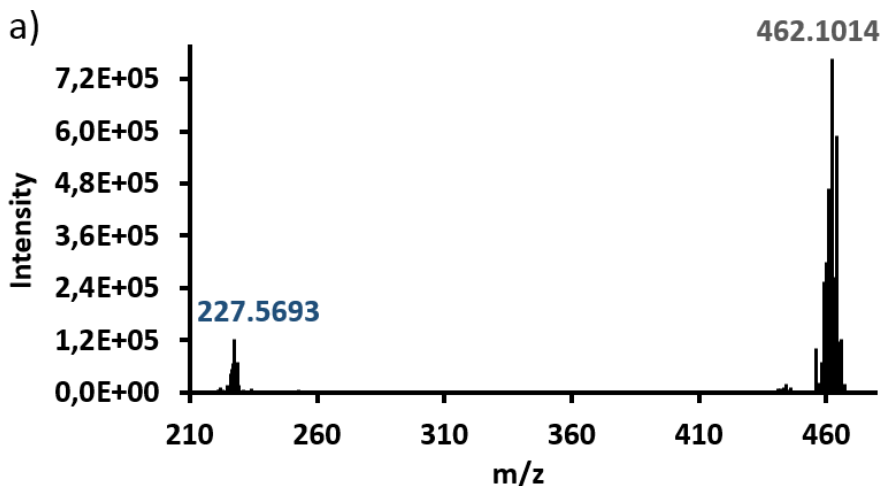
Figure A.II.6. CSI-HRMS spectrum (298 K, MilliQ water) of complex [Ru^{II}Cl(Py$_2^{Me}$tacn)]Cl (**1Ru^{II}-Cl**).

ANNEX
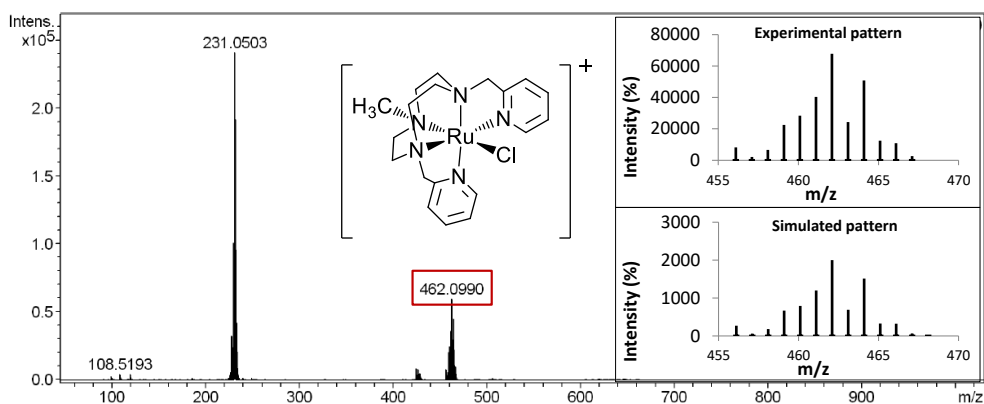
Figure A.II.7. CSI-HRMS spectrum (298 K, MeCN) of complex [Ru^{II}Cl(Py$_2^{Me}$tacn)]Cl (**1Ru^{II}-Cl**).

A.II.1.2. [Ru^{II}(OH$_2$)(Py$_2^{Me}$tacn)](PF$_6$)$_2$
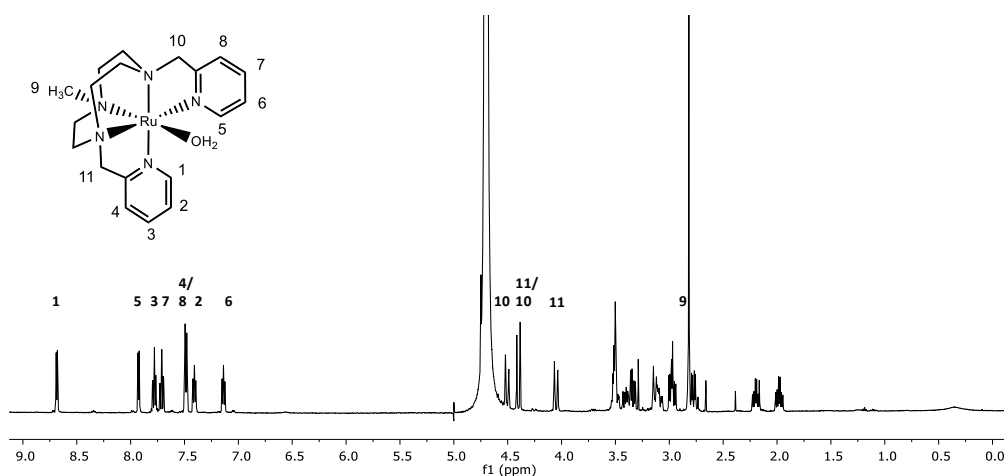
Figure A.II.8. ^{1}H-NMR (500 MHz equipped with a QNP cryoprobe, 298 K, D$_2$O) spectrum of complex [Ru^{II}(OH$_2$)(MePy$_2$tacn)](PF$_6$)$_2$ (**1Ru^{II}-OH$_2$**).
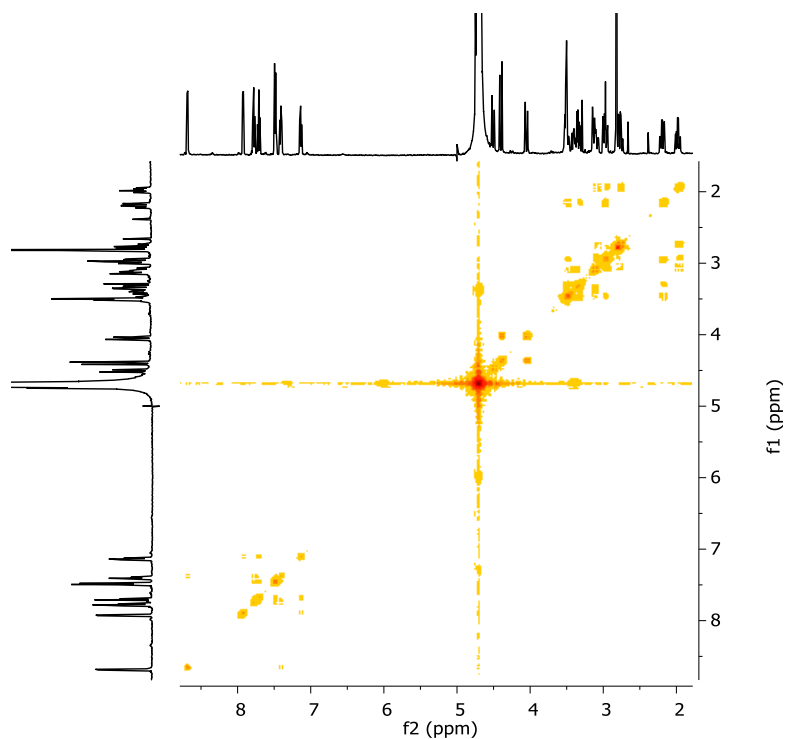
ANNEX

Figure A.II.9. ^{1}H-^{1}H-COSY NMR (400 MHz, 298 K, D$_2$O) spectrum of complex [Ru^{II}(OH$_2$)(MePy$_2$tacn)](PF$_6$)$_2$ (**1Ru^{II}-OH$_2$**). Zoom of the aromatic and the aliphatic region of the COSY spectrum are shown in the following page, respectively.
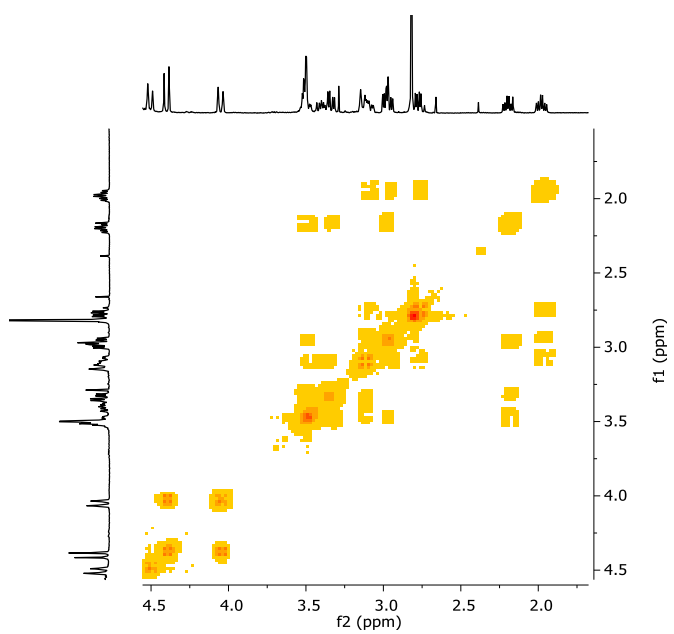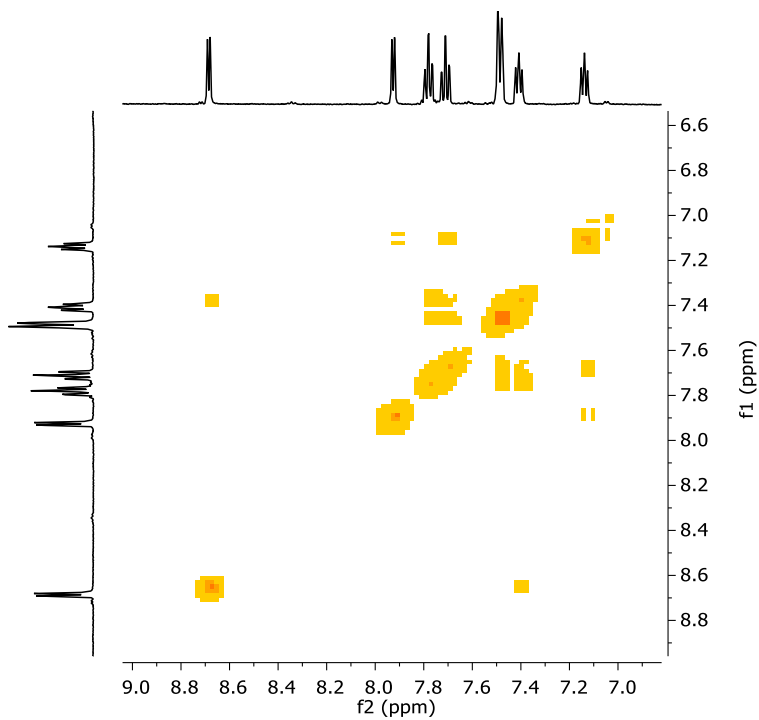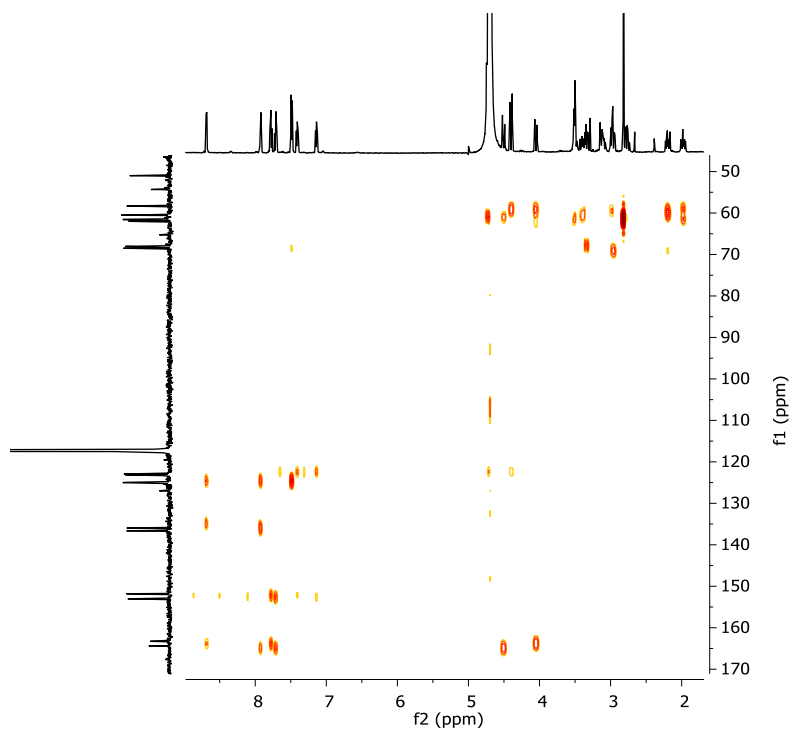
ANNEX

Figure A.II.10. ^{1}H-^{13}C-HMBC NMR (500 MHz equipped with a QNP cryoprobe, 298 K, D$_2$O) spectrum of complex [Ru^{II}(OH$_2$)(MePy$_2$tacn)](PF$_6$)$_2$ (**1Ru^{II}-OH$_2$**). Signals between 9.5 and 7.0 ppm correspond to correlations between protons and carbons from the pyridine rings.

ANNEX
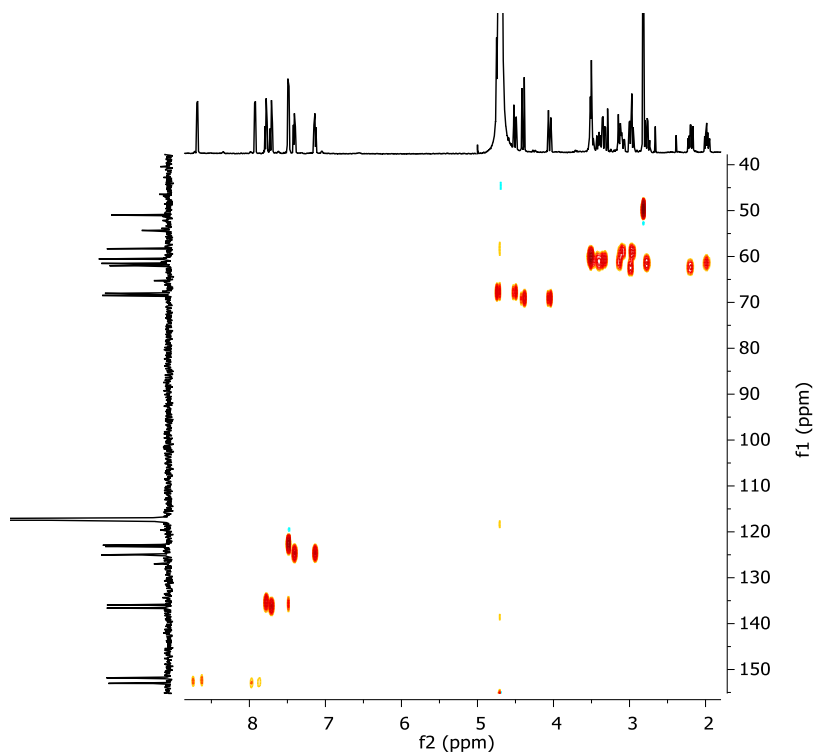
Figure A.II.11. ^{1}H-^{13}C-HSQC NMR (500 MHz equipped with a QNP cryoprobe, 298 K, D$_2$O) spectrum of complex [Ru^{II}(OH$_2$)(MePy$_2$tacn)](PF$_6$)$_2$ (**1Ru^{II}-OH$_2$**).
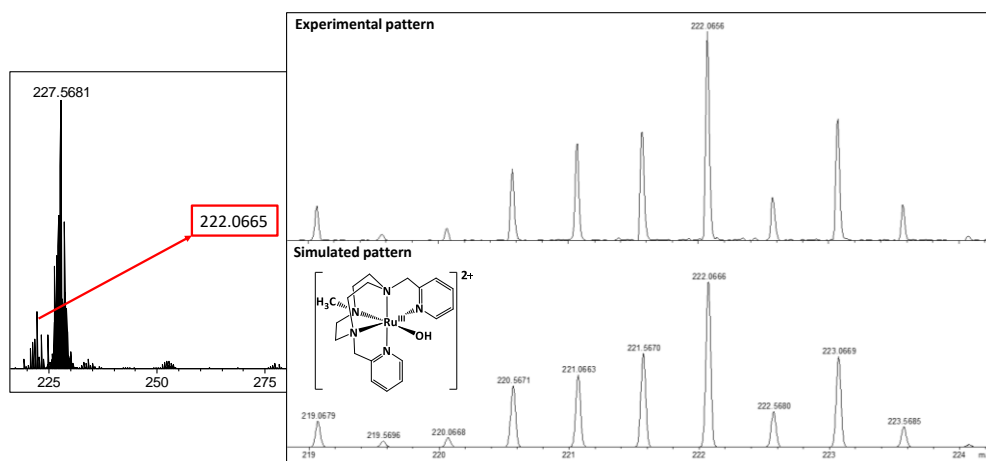
ANNEX

Figure A.II.12. CSI-HRMS spectrum (298 K, MiliQ H_2O) of complex $[Ru^{II}(H_2O)(Py_2^{Me}tacn)](PF_6)_2$ (**1Ru^{II}-OH$_2$**).

A.II.1.3. [Ru^{II}(NCCH$_3$)(Py$_2^{Me}$tacn)](PF$_6$)$_2$
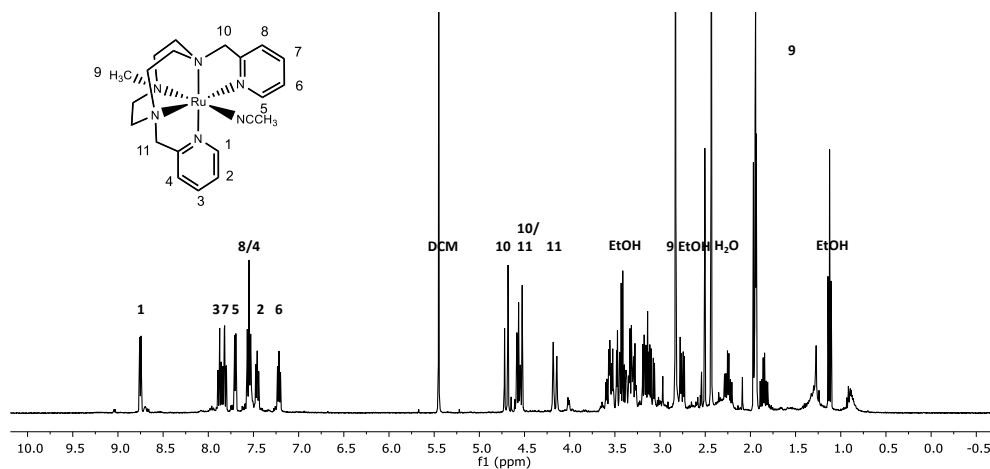
Figure A.II.13. ^{1}H-NMR (400 MHz, 298 K, CD$_3$CN) spectrum of complex $[Ru^{II}(CH_3CN)(MePy_2tacn)](OTf)_2$ (**1Ru^{II}-NCCH$_3$**).

456
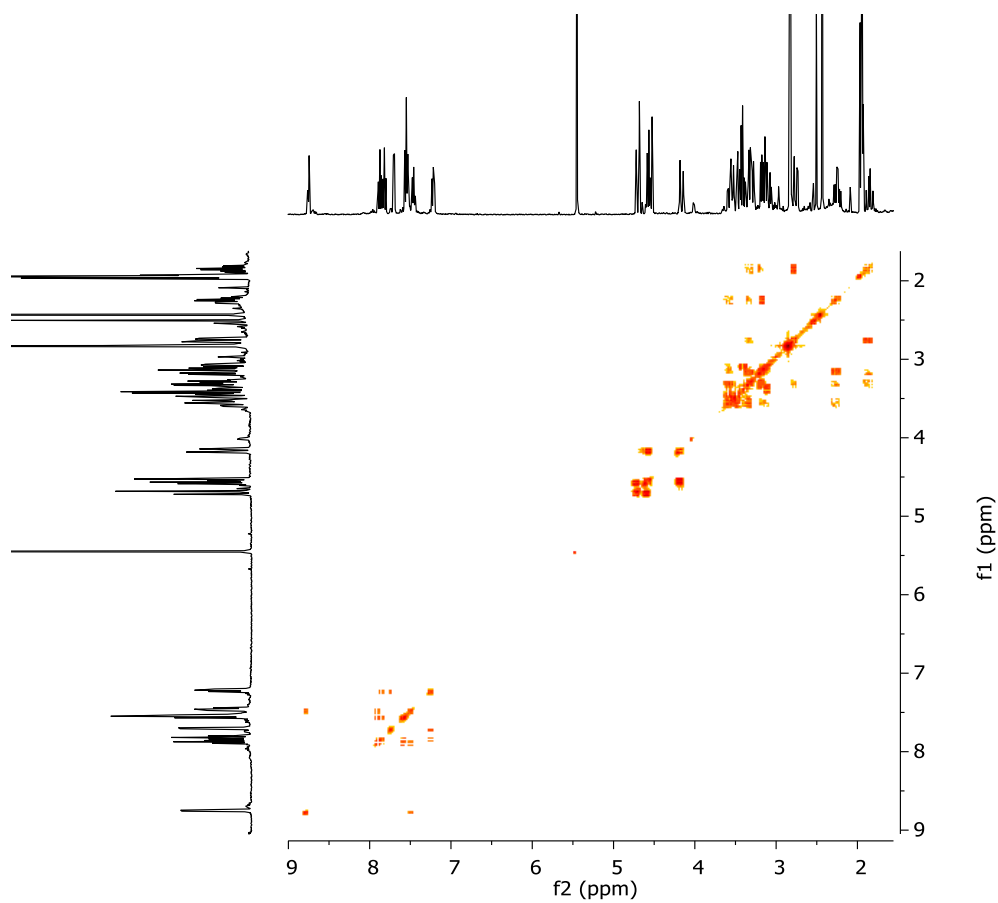
ANNEX

Figure A.II.14. ^{1}H-^{1}H-COSY NMR (400 MHz, 298 K, CD$_3$CN) spectrum of complex [Ru^{II}(CH$_3$CN)(MePy$_2$tacn)](OTf)$_2$ (**1Ru^{II}-NCCH$_3$**). Zoom of the aromatic and the aliphatic region of the COSY spectrum are shown in the following page, respectively.
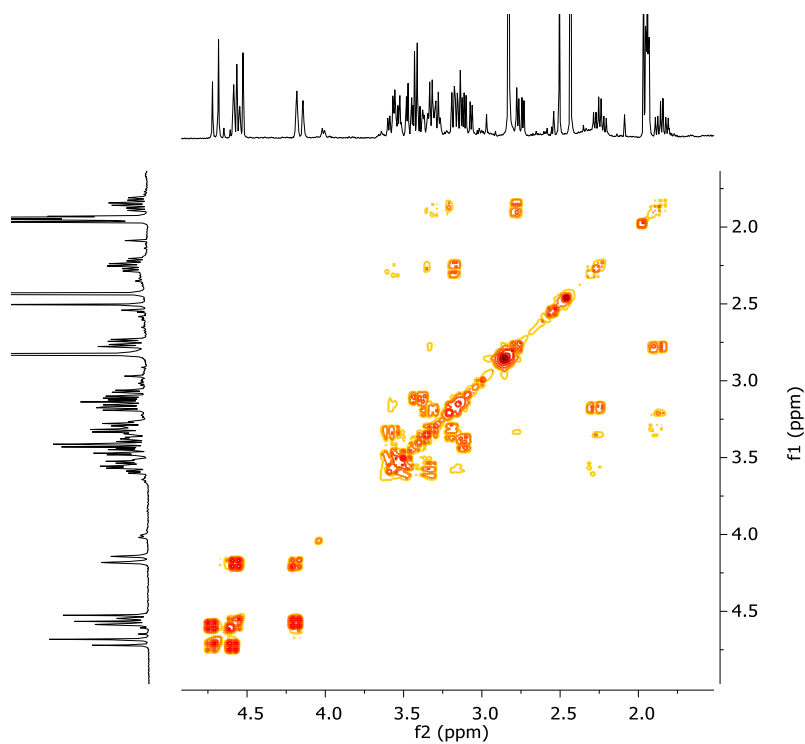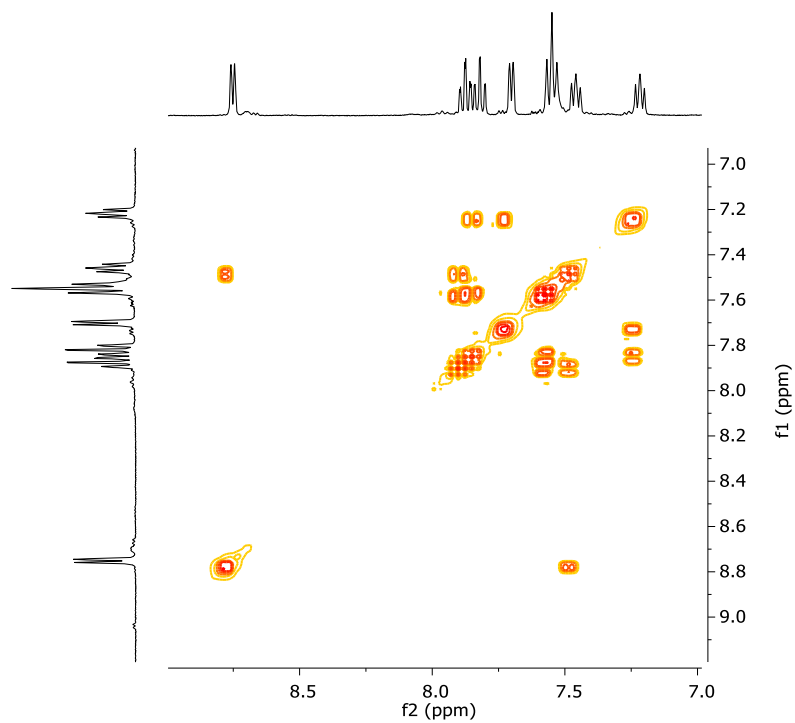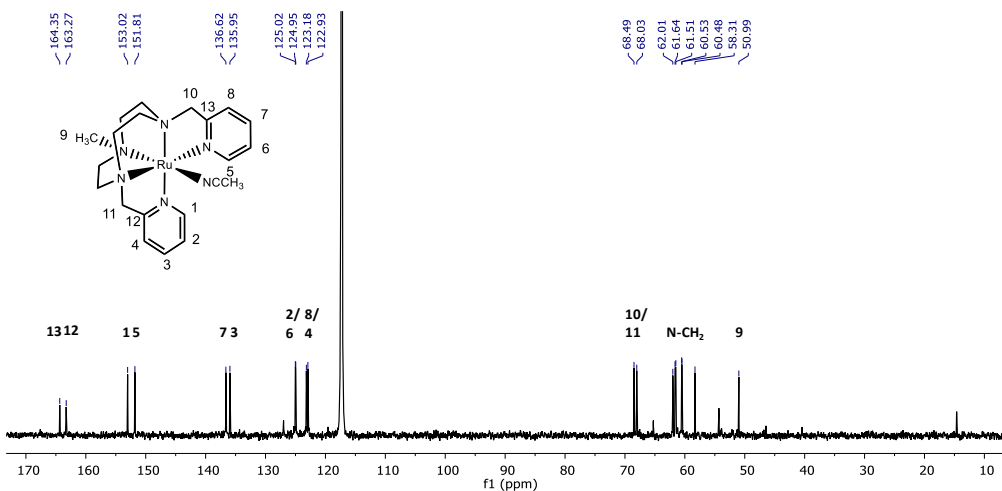
ANNEX

ANNEX

Figure A.II.15. ^{13}C-NMR (400 MHz, 298 K, CD$_3$CN) spectrum of complex [Ru^{II}(CH$_3$CN)(MePy$_2$tacn)](OTf)$_2$ (**1Ru^{II}-NCCH$_3$**).
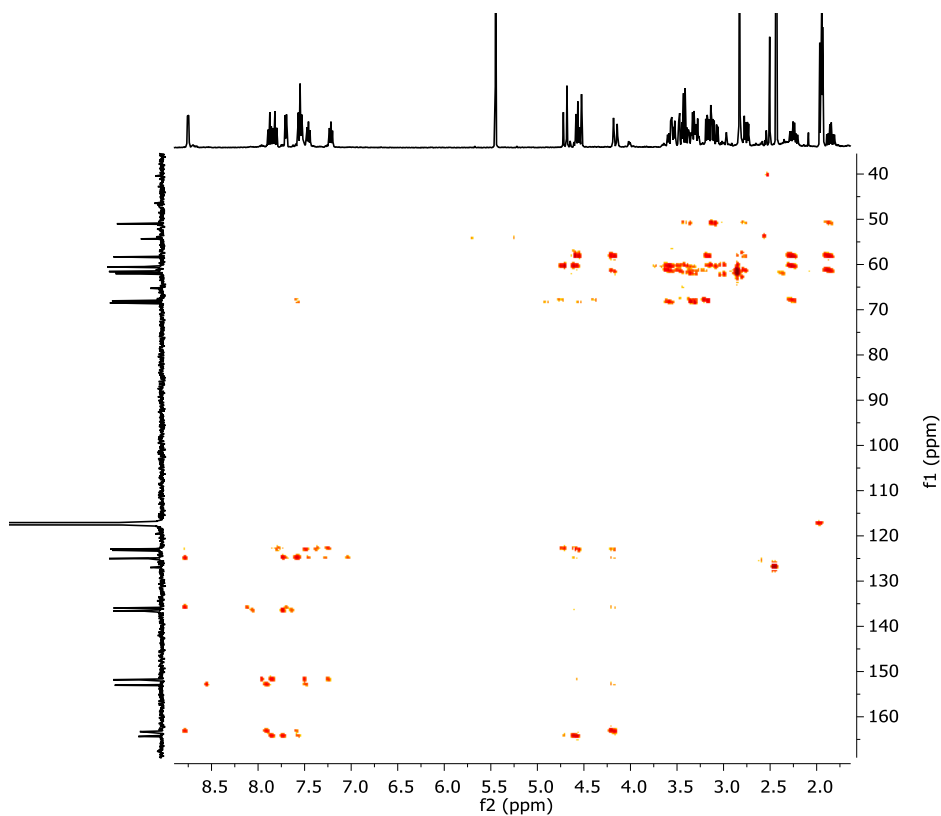
Figure A.II.16. ^{1}H-^{13}C-HMBC NMR (400 MHz, 298 K, CD$_3$CN) spectrum of complex [Ru^{II}(CH$_3$CN)(MePy$_2$tacn)](OTf)$_2$ (**1Ru^{II}-NCCH$_3$**).

459
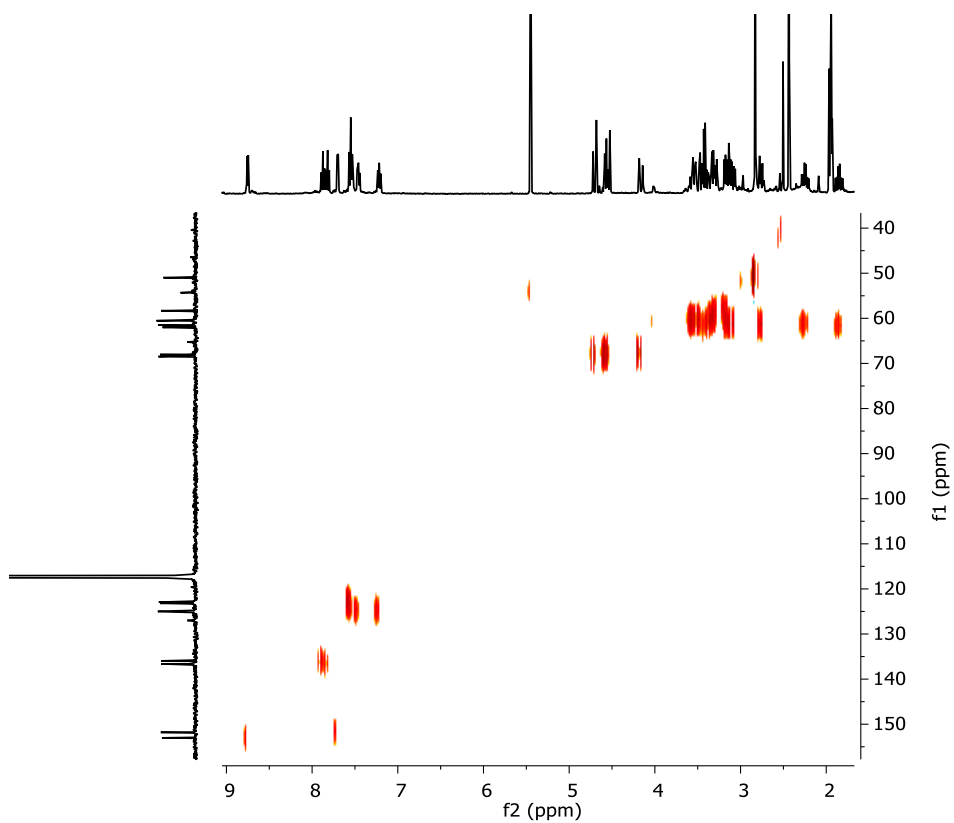
ANNEX

Figure A.II.17. ^{1}H-^{13}C-HSQC NMR (400 MHz, 298 K, CD$_3$CN) spectrum of complex [Ru^{II}(CH$_3$CN)(MePy$_2$tacn)](OTf)$_2$ (**1Ru^{II}-NCCH$_3$**).

ANNEX
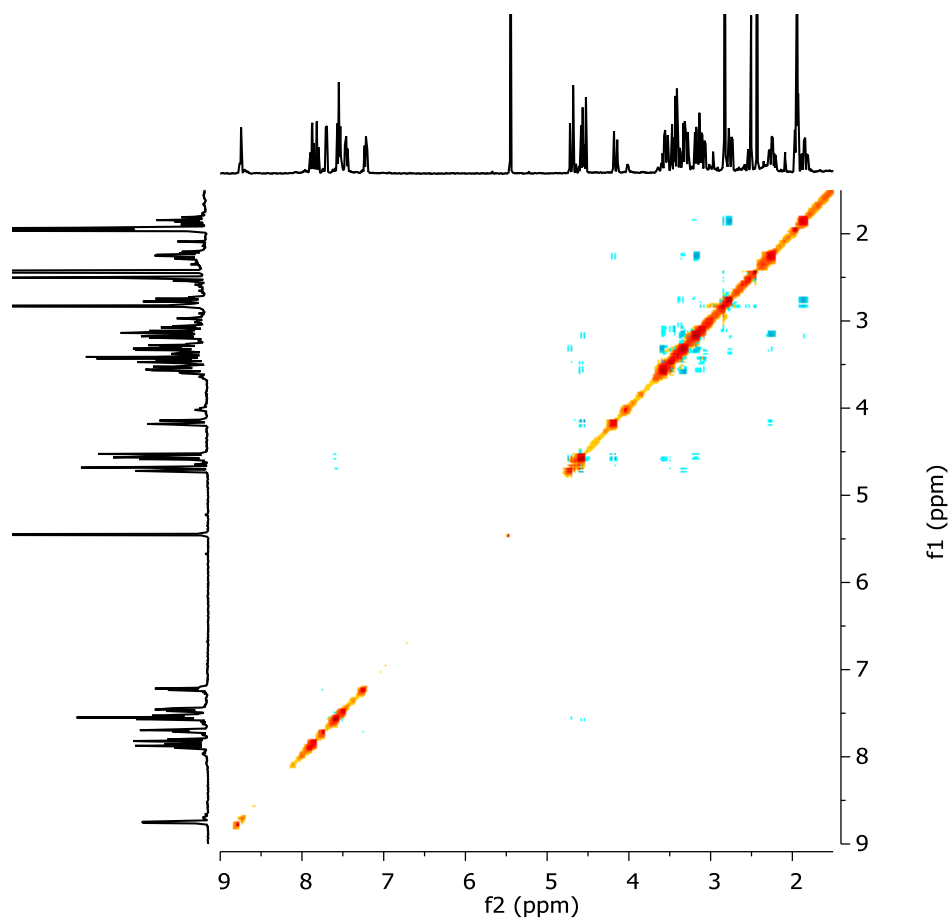
Figure A.II.18. ^{1}H-^{1}H-NOESY NMR (400 MHz, 298 K, CD$_3$CN) spectrum of complex [Ru^{II}(CH$_3$CN)(MePy$_2$tacn)](OTf)$_2$ (**1Ru^{II}-NCCH$_3$**). The signals in the aliphatic region show interaction between the methylenic protons of either the tacn macrocycle and the pyridine arms.

ANNEX
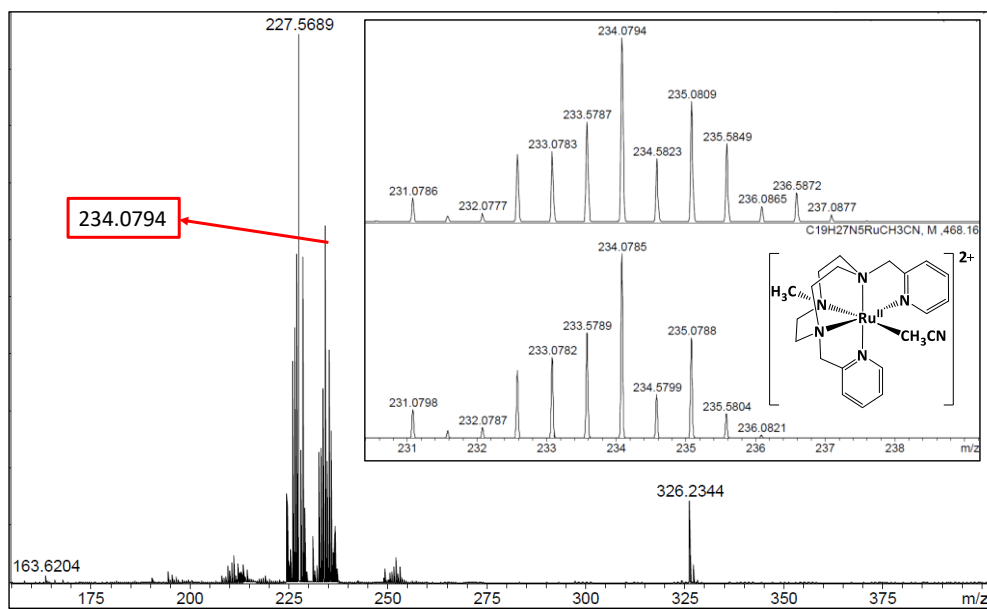
Figure A.II.19. CSI-HRMS spectrum (298 K, Milli-Q H_2O) of complex $[Ru^{II}(CH_3CN)(Py_2^{Me}tacn)](OTf)_2$ (**1Ru^{II}-NCCH$_3$**).

ANNEX

A.II.1.4. ^{1}H-NMR exchange studies [Ru^{II}(Cl)(Py$_2^{Me}$tacn)]Cl-[Ru^{II}(OH$_2$)(Py$_2^{Me}$tacn)]Cl$_2$
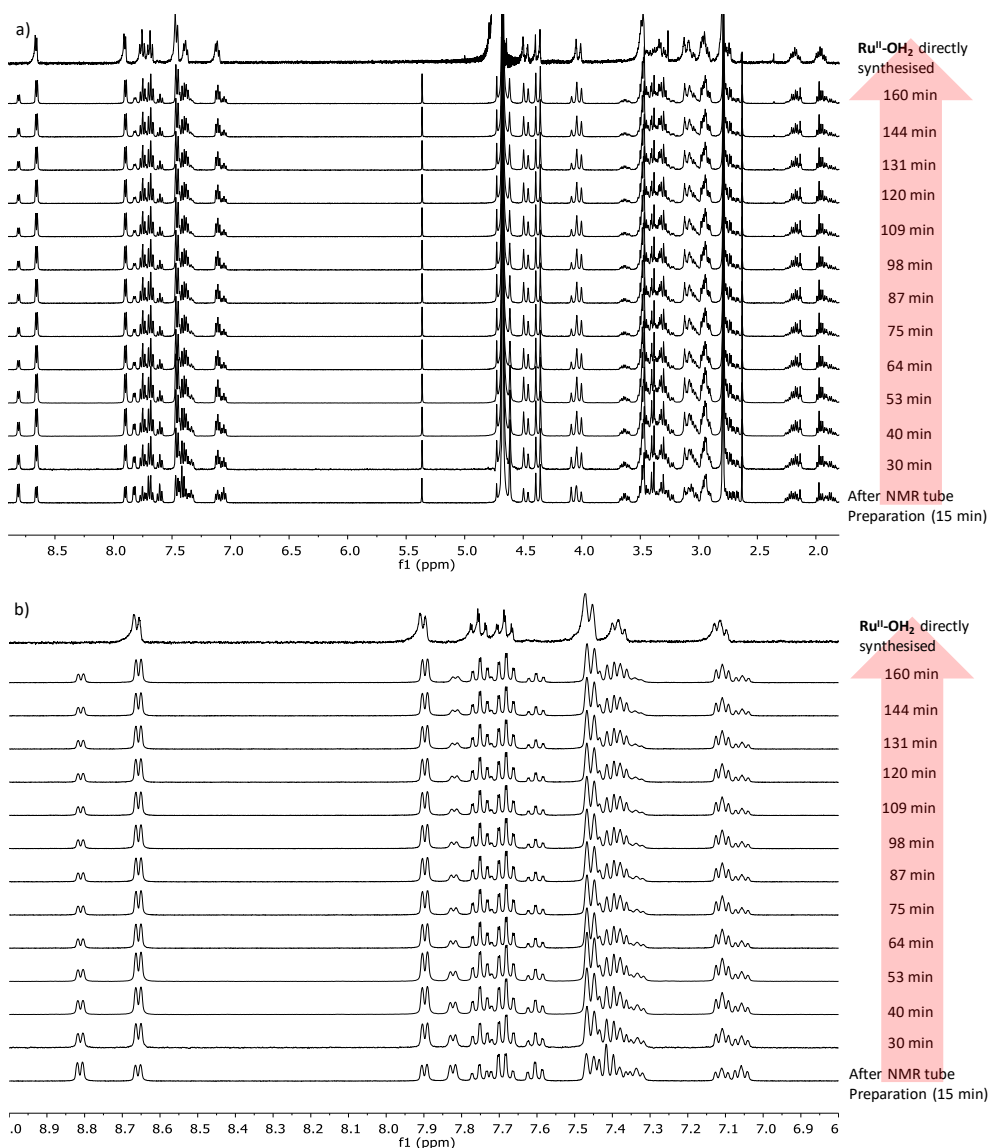
Figure A.II.20. ^{1}H-NMR monitoring of the Cl/H$_2$O exchange in complex [Ru^{II}Cl(Py$_2^{Me}$tacn)]Cl (**1Ru^{II}-Cl**) after dissolution in D$_2$O *vs* time. a) Monitoring of the signals in all diamagnetic region. b) Magnification of the aromatic region. On the top of the stacked spectra is the ^{1}H-NMR spectrum of pure [Ru^{II}(OH$_2$)(MePy$_2$tacn)](PF$_6$)$_2$ (**1Ru^{II}-OH$_2$**) complex dissolved in D$_2$O.

463

ANNEX

A.II.2. Water Oxidation Catalytic Studies

Table A.II.1. Selected WO catalytic tests for complex [$Ru^{II}Cl(Py_2^{Me}tacn)$]Cl (**1Ru^{II}-Cl**).

[cat] (μM)	Oxi/[Oxi] (mM)	Ag(OTf) (μM)	TON – O$_2$[a]	TON - CO$_2$[b]
35	(CAN) 125	-	19±2	n.d.
35	(CAN) 125	70	36±2	0.16±0.01
50	(CAN) 125	-	25±1	≈1
50	(NaIO$_4$) 125	-	≈1	n.d.
250[c]	(CAN) 12.5	-	0.2±0.1	n.d.
250[c]	(CAN) 25	-	0.3±0.2	n.d.
250[c]	(CAN) 50	-	2.6±0.2	n.d.
250[c]	(CAN) 75	-	5±1	n.d.
250[c]	(CAN) 125	-	13±1	0.03±0.06
250[c]	(CAN) 150	-	18±1	0.07±0.04
50[c]	(CAN) 75	-	7	n.d.
100[c]	(CAN) 75	-	7	n.d.
500[c]	(CAN) 75	-	2	n.d.
1000[c]	(CAN) 75	-	3	0.01
250[c] [d]	(CAN) 12.5	-	1	n.d.
250[c] [d]	(CAN) 25	-	3	n.d.
250[c] [d]	(CAN) 50	-	3.5	n.d.
250[c] [d]	(CAN) 75	-	8.5	n.d.
250[c] [d]	(CAN) 125	-	13	0.02
250[c] [d]	(CAN) 150	-	16	0.03

[a] TON (turnover number) refers to the ratio between [moles of O$_2$ produced / moles of catalyst]. [b] ratio between [moles of CO$_2$ produced / moles of catalyst]. [c] 20 ml vials were used instead of the current 15 ml vials of the other experiments. [d] The pH was adjusted at a value of 0.7 by the addition of concentrated perchloric acid (HClO$_4$). When not specified, the pH is the one given by the CAN in solution (125 mM), which is about 1.1. *Ag(OTf) (2 eq.) used as chloride scavenger.

464

ANNEX

Table A.II.2. Selected WO catalytic tests for complex $[Ru^{II}(H_2O)(Py_2^{Me}tacn)](PF_6)_2$ (**$1Ru^{II}$-OH$_2$**).

[cat] (μM)	Oxi/[Oxi] (mM)	TON – O$_2$ [a]	TON - CO$_2$ [b]
35	(CAN) 125	51±2	n.d.
25[c]	(CAN) 75	28±5	n.d
50[c]	(CAN) 75	23±3	n.d.
75[c]	(CAN) 75	21±3	n.d.
100[c]	(CAN) 75	16±1	n.d.
250[c]	(CAN) 75	9±4	n.d.
500[c]	(CAN) 75	6±3	0.04±0.04
1000[c]	(CAN) 75	3±2	0.03±0.04
250[c] [d]	(CAN) 12.5	3	0.1
250[c] [d]	(CAN) 25	9	0.2
250[c] [d]	(CAN) 50	12	0.4
250[c] [d]	(CAN) 75	20	0.1
250[c] [d]	(CAN) 125	26	0.1
250[c] [d]	(CAN) 150	29	0.2

[a] TON (turnover number) refers to the ratio between [moles of O$_2$ produced / moles of catalyst]. [b] ratio between [moles of CO$_2$ produced / moles of catalyst]. [c] 20 ml vials were used instead of the current 15 ml vials of the other experiments. [d] The pH was adjusted at 0.7 by the addition of concentrated perchloric acid (HClO$_4$). When not specified, the pH is the one given by the CAN in solution (125 mM), which is about 1.1.

ANNEX

Table A.II.3. WO tests for complexes $[Ru^{II}Cl(Py_2^{Me}tacn)]Cl$ (**1Ru^{II}-Cl**) and $[Ru^{II}(H_2O)($ $Py_2^{Me}tacn)](PF_6)_2$ (**1Ru^{II}-OH$_2$**).[a]

Catalyst	pH[b]	CAN (mM)	NaIO$_4$	TON – O$_2$[c]	TON - CO$_2$[d]
1Ru^{II}-OH$_2$[e]	0	125	-	38±3	n.d.
1Ru^{II}-OH$_2$[e]	0	-	125	n.d.	n.d.
1Ru^{II}-OH$_2$[e]	1	-	125	n.d.	n.d.
1Ru^{II}-OH$_2$[e]	1.1	125	-	51±2	n.d.
1Ru^{II}-OH$_2$[f]	1.1	125	-	n.d.	n.d.
1Ru^{II}-OH$_2$[g]	1.1	125	-	n.d.	n.d.
1Ru^{II}-OH$_2$[h]	1.1	125	-	25±5	n.d.
1Ru^{II}-Cl[i]	1.1	125	-	43±4	n.d.
1Ru^{II}-Cl[j]	1.1	125	-	40±1	n.d.

[a] The reactions were carried out by the addition of 1 ml of the stock solution of the catalyst **1Ru^{II}-OH$_2$** (35 µM final concentration) in Milli-Q water to a solution of CAN (125 mM, final concentration) in Milli-Q water (14 mL, 18.2 MΩ·cm) or otherwise noticed. [b] The pH was adjusted by addition of the needed HClO$_4$. When not specified, the pH is the one given by the CAN in solution (125 mM), which is about 1.1. [c] TON-O$_2$ (moles of O$_2$ produced / moles of catalyst) [d] and TON-CO$_2$ (moles of CO$_2$ produced / moles of catalyst) were measured by calibrated GC-TCD. A stock solution of **1Ru^{II}-OH$_2$** prepared in [e] MilliQ water (1 ml), [f] in MeCN (1 ml) and [g] in MeCN (20 µl) [h] in MeCN (1 equiv.)-12 µl of a 1:100 diluted solution of MeCN was added in 4.41 ml of the stock solution of the catalyst and left stirring for 4 hours prior addition of 1 ml of the latter to the reaction vial to analyze the effect of MeCN in catalysis. In contrast, to accelerate the exchange rate between the Cl$^-$ and the H$_2$O ligand in the **1Ru^{II}-Cl** complex and see this effect in the catalytic outcome, a stock solution of **1Ru^{II}-OH$_2$** prepared in [i] in MilliQ water and left stirring and heating at 60 ℃ for 3 hours prior addition to the reaction vial. [j] in MilliQ water and left stirring and heating at 80 ℃ for 3 hours prior to addition to the reaction vial.

ANNEX
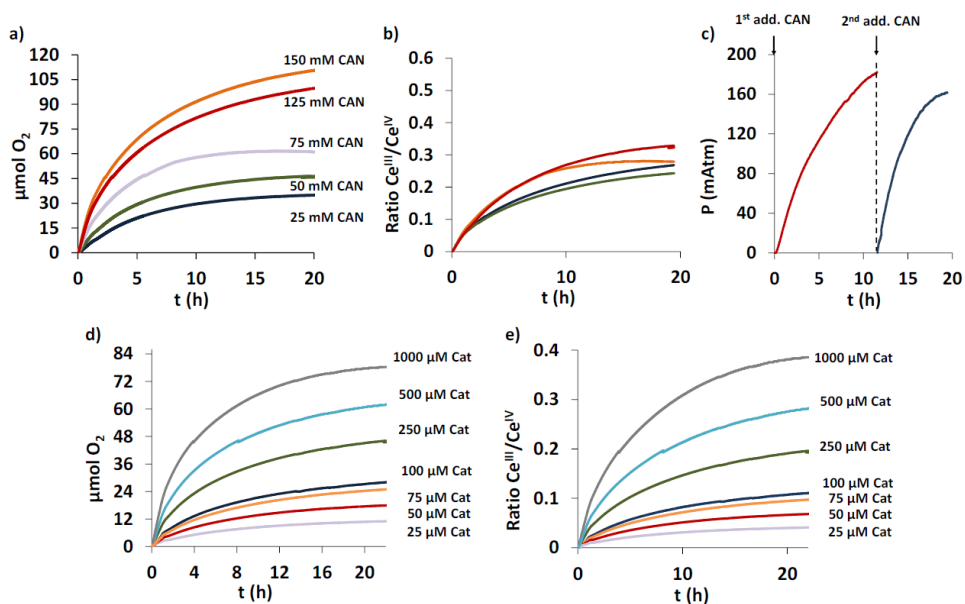
Figure A.II.21. O*n-line monitorization traces of the O₂ evolution* when either varying the CAN concentration while keeping fixed the catalyst concentration (250 μM) and the catalyst concentration while keeping fixed the concentration of CAN (75 mM). **a)** Plot of TON O₂ *vs* time at different [CAN] (250 μM **1Ru^{II}-OH₂**, pH 0.7, 25 ℃). **b)** Plot of the ratio Ce^{III}/Ce^{IV} *vs* t (h) at different [CAN] (250 μM **1Ru^{II}-OH₂**, pH 0.7, 25 ℃). **c)** Plot of the on-line pressure trace monitorization of the O₂ evolution *vs* time after two subsequent additions of the same amount of CAN (75 mM CAN, 250 μM **1Ru^{II}-OH₂**, pH 0.7, 25 ℃). **d)** Plot of TON O₂ *vs* time at different [**1Ru^{II}-OH₂**] (75 mM CAN, pH 0.7, 25 ℃). **e)** Plot of the ratio Ce^{III}/Ce^{IV} *vs* t (h) at different [**1Ru^{II}-OH₂**] (75 mM CAN, pH 0.7, 25 ℃).

ANNEX

A.II.3. Characterization of WO intermediates
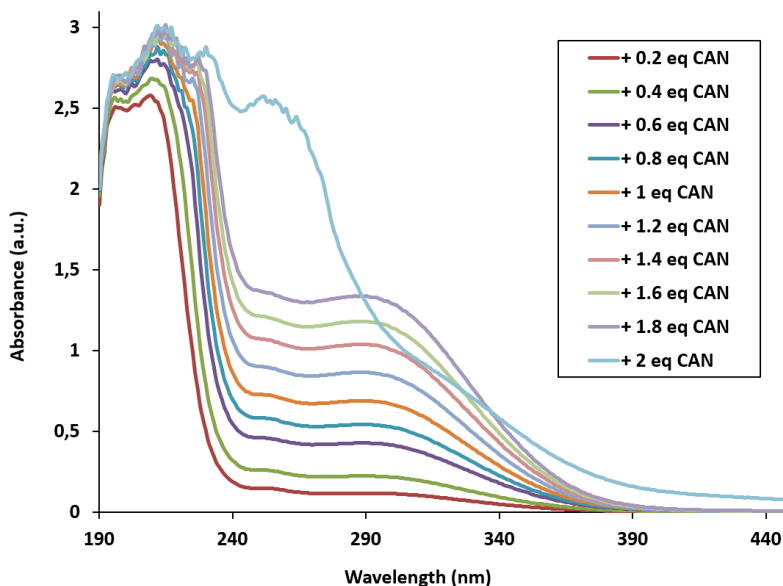
Figure A.II.22. CAN UV-Vis blank experiments at the same concentrations that those used in the titration studies at pH 0.7 (HClO$_4$) and 298 K.
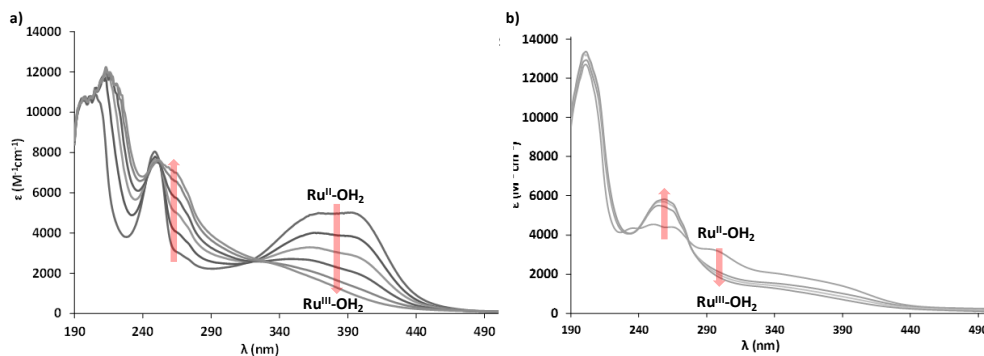
Figure A.II.23. UV-Vis spectroscopy analysis of titration reactions in 3 mL solution of ruthenium complex at 25 ºC: **a)** Titration of **1Ru^{II}-OH$_2$** (0.25 mM) by subsequent addition of CAN (15 mM, 0.1 eq. in aliquots of 5 μl) at pH 0.7 (HOTf 1.1 M) to generate the **1Ru^{III}-OH$_2$** species. Each band corresponds to the total amount of CAN (15mM) added as follows: i) 0 eq, ii) 0.2 eq, iii) 0.4 eq, iv) 0.6 eq, v) 0.8 eq, vi) 1 eq. **b)** Titration of **1Ru^{III}-OH**, previously generated by the reaction of **1Ru^{II}-OH$_2$** (0.25 mM) with NaIO$_4$ (0.6 eq. in aliquots of 5 μl each), by subsequent additions of HOTf (1.1 M) to generate the **1Ru^{III}-OH$_2$** species. Each band corresponds to the total amount of HOTf (1.1 M) added as follows: i) **1Ru^{III}-OH** + 0 μl (initial pH 6), ii) 80 μl, iii) 160 μl, iv) 200 μl (final pH c.a. 1.4).

ANNEX
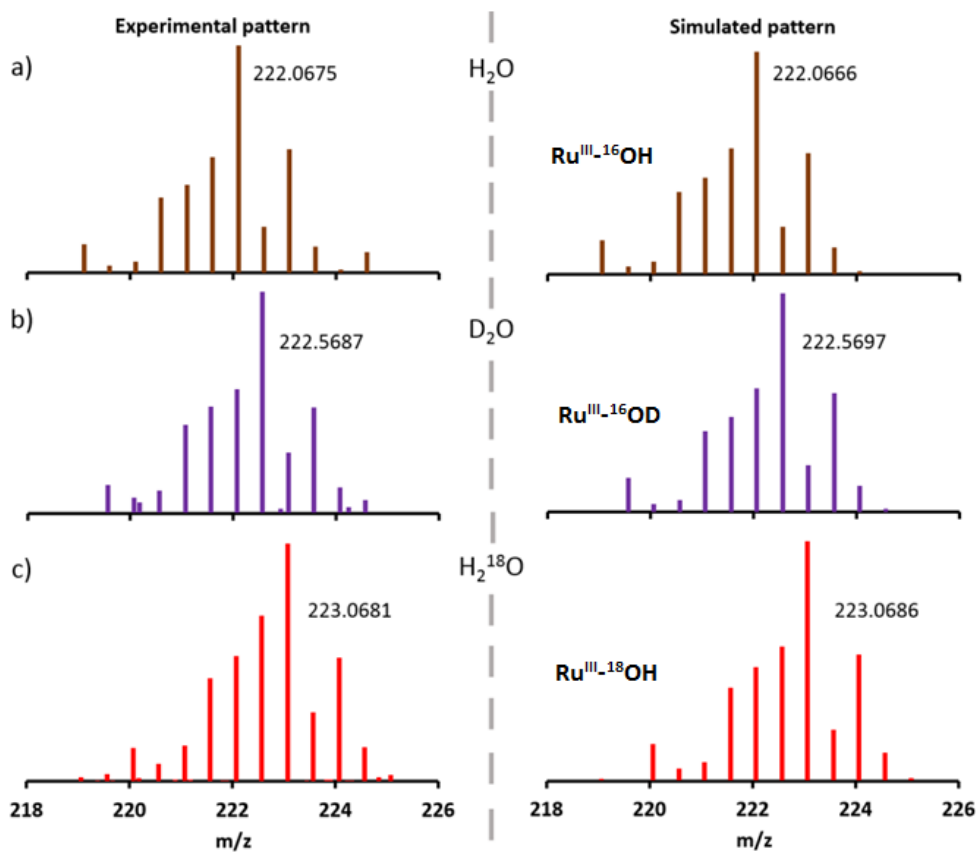
Figure A.II.24. Characterization of intermediates of complex **1Ru^{II}-OH$_2$** by CSI-HRMS at 25ºC: a), b) and c) figures represent the titration of **1Ru^{II}-OH$_2$** with CAN (1 eq.) to generate the **1Ru^{III}-OH** species in MilliQ water, D$_2$O and H$_2^{18}$O, respectively.

ANNEX
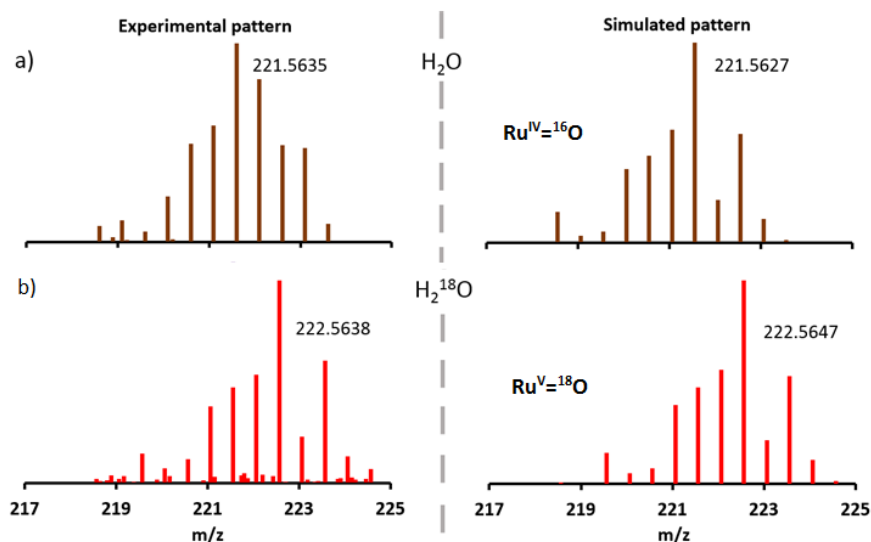
Figure A.II.25. Characterization of intermediates of complex **1Ru^{II}-OH$_2$** by CSI-HRMS at 25ºC: a), b) and c) figures represent the titration of **1Ru^{II}-OH$_2$** with CAN (4 eq.) to generate the **1Ru^{IV}=O** species in MilliQ water, D$_2$O and H$_2$^{18}O, respectively.
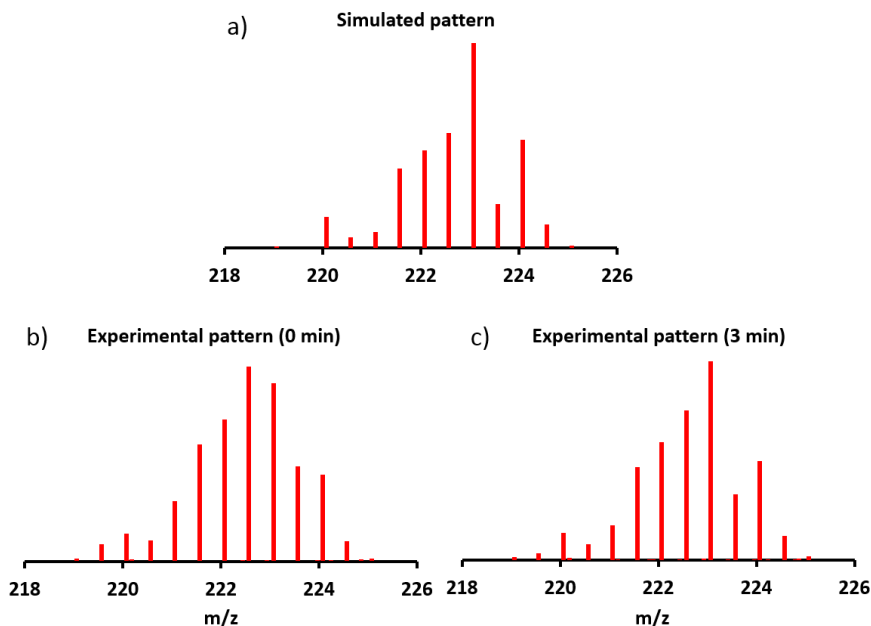
Figure A.II.26. Labelling studies of complex [RuCl(Py$_2$^{Me}tacn)]Cl by CSI-HRMS at 25ºC: a) Simulated pattern of the peak associated to the dicationic **1Ru^{IV}=^{18}O** species, b) and c) experimental patterns of the peak associated to the dicationic **1Ru^{IV}=^{18}O** species after 0 and 3 minutes of the addition of 0.5 equivalents of NaIO$_4$, respectively, in labelled water.

ANNEX
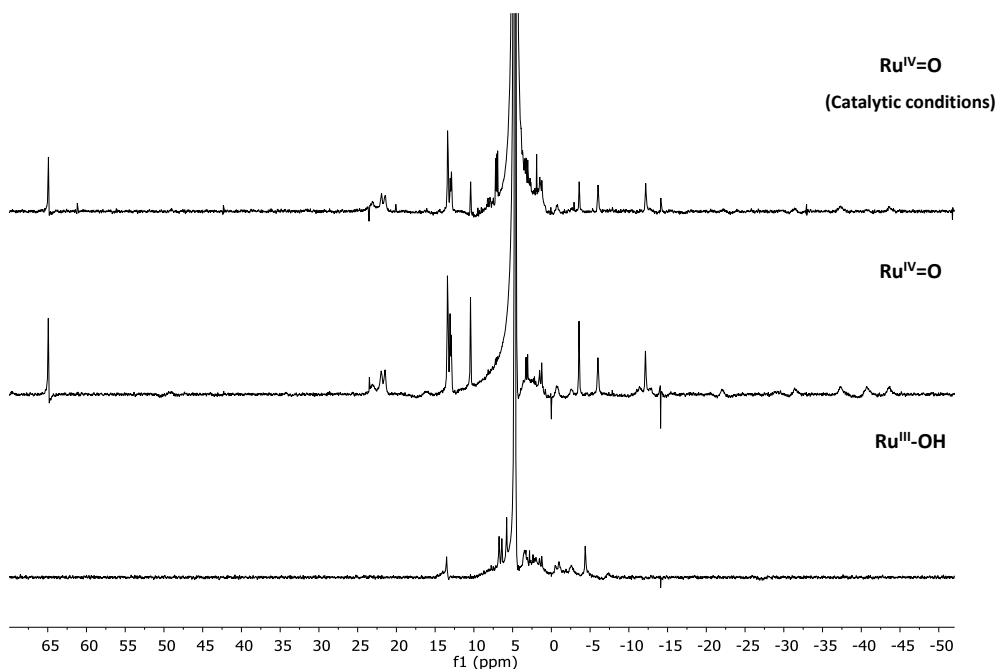
Figure A.II.27. ^{1}H-NMR (400 MHz, D$_2$O, 298 K) characterization of **1Ru^{III}-OH** and **1Ru^{IV}=O** species generated *in situ* with CAN. To a solution of **1Ru^{II}-OH$_2$** (2 mM in D$_2$O) in an NMR tube (bottom) 1 eq of CAN leads to the formation of paramagnetic **1Ru^{III}-OH** species, subsequent addition of 2 eq of CAN leads to **1Ru^{IV}=O** species (middle), and further addition of an excess of CAN (20 eq) to simulate the catalytic conditions still yields the formation of **1Ru^{IV}=O** species (top).

471

ANNEX
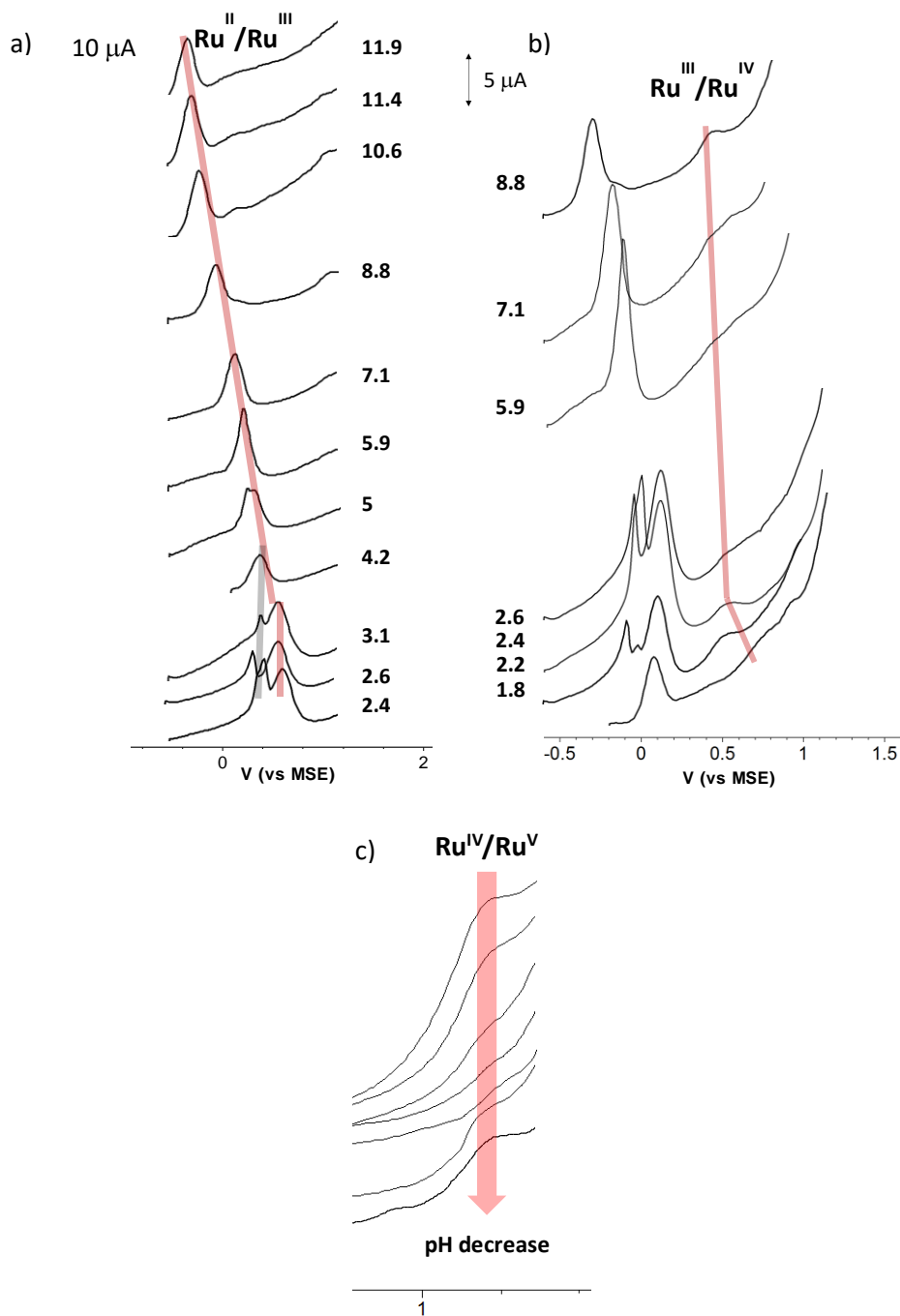
Figure A.II.28. Plots *a)*, *b)* and *c)* Square Wave Voltammetries (SWV) (298 K, under N_2, $P_H = 25$ mV and $P_W = 50$ ms) of complex **1Ru^{II}-OH$_2$** (0.5 mM) in aqueous Britton-Robinson buffer (0.1 M) and KNO$_3$ as electrolyte (0.1 M) at different pH (V *vs* MSE). *a)* **1Ru^{II}/1Ru^{III}**, *b)* **1Ru^{III}/1Ru^{IV}** and *c)* **1Ru^{IV}/1Ru^{V}** redox pairs.
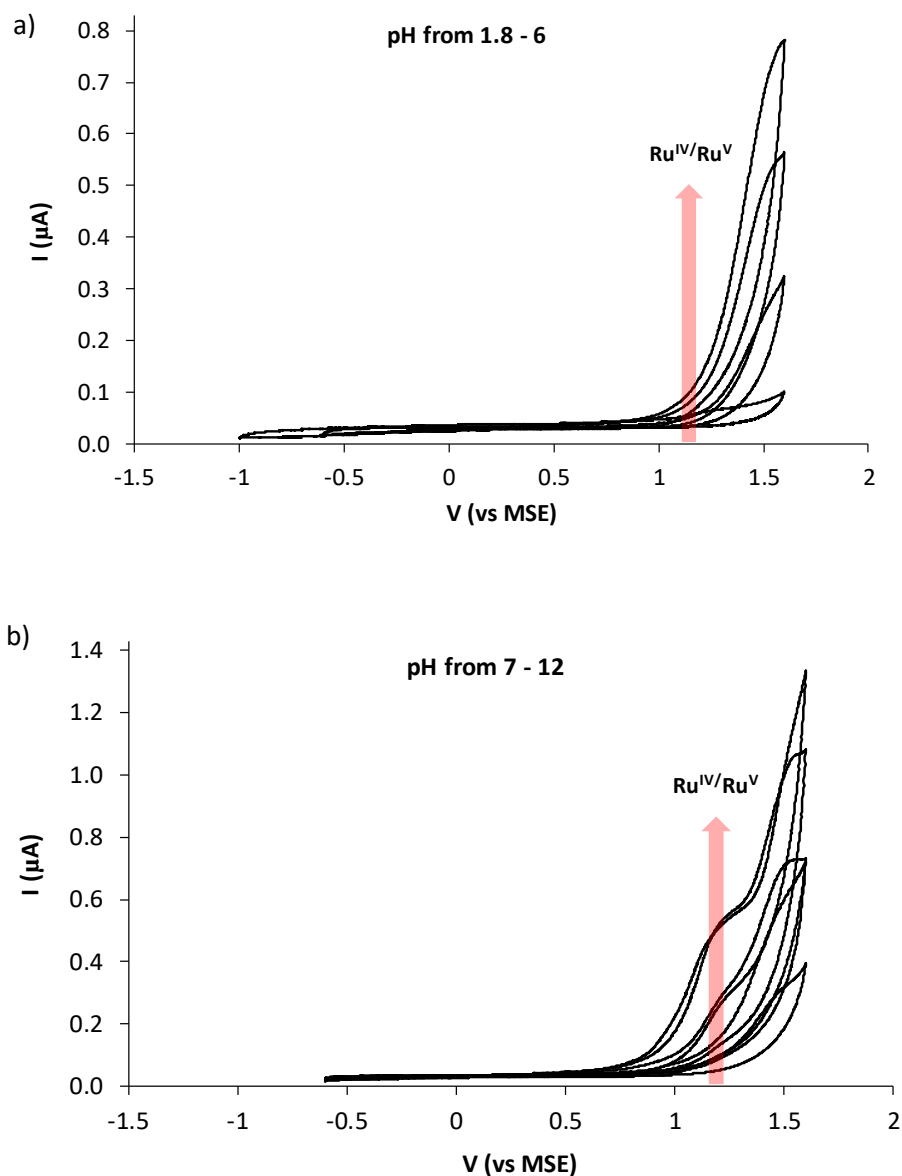
Figure A.II.29. Plots *a)* and *b)* Cyclic Voltammograms (CV) (298 K, under N_2 and 100 mV/s scan rate) of complex **1Ru^{II}-OH$_2$** (0.5 mM) in aqueous Britton-Robinson buffer (0.1 M) and KNO_3 as electrolyte (0.1 M) at different pH (V *vs* MSE).
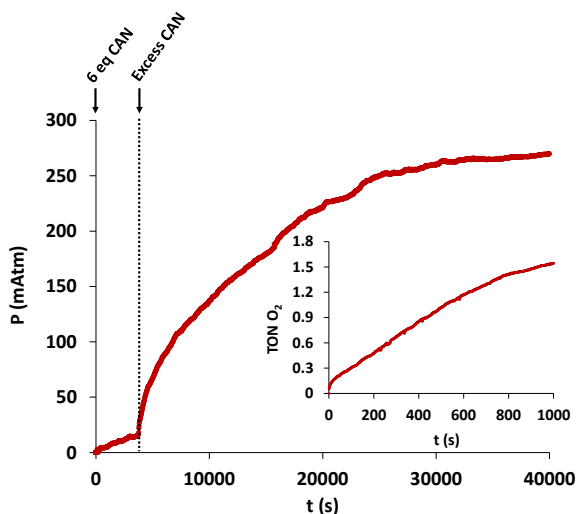
Figure A.II.30. On-line monitoring of the gas evolved from the reaction from the vial head space after both additions of CAN (6 eq in $H_2^{16}O$ to generate $1Ru^{IV}=^{16}O$ and c.a. 100 eq of CAN dissolved in $H_2^{18}O$ to the generated $H_2^{16}O$ solution of $1Ru^{IV}=^{16}O$. The inset shows the TON O_2 evolved at the beginning of the reaction. It can be seen that the first TON O_2 is generated within the first 600 (s).

A.II.4. Crystal-Structure Determination

[Ru(NCCH$_3$)(Py$_2$^{Me}tacn)](OTf)$_2$: Yellow crystals of **C$_{21}$H$_{30}$N$_6$Ru, 2(CF$_3$O$_3$S)**, were grown from slow diffusion of ether in acetonitrile, and used for low temperature (150(2) K) X-ray structure determination. The measurement was carried out on a *BRUKER SMART APEX CCD* diffractometer using graphite-monochromated Mo $K\alpha$ radiation ($\lambda = 0.71073$ Å) from an X-ray tube. The measurements were made in the range of 2.255 to 28.314° for θ. Full-sphere data collection was carried out with ω and φ scans. A total of 23993 reflections were collected of which 7498 [R(int) = 0.0658] were unique. Programs used: data collection, Smart[1]; data reduction, Saint+[2]; absorption correction, SADABS[3]. Structure solution and refinement was done using SHELXTL[4]. The structure was solved by direct methods and refined by full-matrix least-squares methods on F^2. The non-hydrogen atoms were refined anisotropically. The H-atoms were placed in geometrically optimized positions and forced to ride on the atom to which they are attached.

Final R indices [I>2sigma(I)]   **R1 = 0.0649,** wR2 = 0.1365

ANNEX

R indices (all data)   R1 = 0.0970, wR2 = 0.1533

[Ru(Cl)(Py$_2$^{Me}tacn)]$_2$(Cl)$_2$(CH$_2$Cl$_2$)$_3$(OH$_2$)$_2$: Orange crystals of **2(C$_{19}$H$_{27}$ClN$_5$Ru),** **3(CH$_2$Cl$_2$), 2(Cl), 2(OH$_2$)**, were grown from slow diffusion of ethyl ether in CH$_2$Cl$_2$, and used for low temperature (100(2) K) X-ray structure determination. The measurement was carried out on a *BRUKER SMART APEX CCD* diffractometer using graphite-monochromated Mo $K\alpha$ radiation (λ = 0.71073 Å) from an X-ray tube. The measurements were made in the range 1.74 to 28.29° for θ. Full-sphere data collection was carried out with ω and φ scans. A total of 77403 reflections were collected of which 24788 [R(int) = 0.0461] were unique. Programs used: data collection, Smart[1]; data reduction, Saint+[2]; absorption correction, SADABS[3]. Structure solution and refinement was done using SHELXTL[4]. The structure was solved by direct methods and refined by full-matrix least-squares methods on F2. The non-hydrogen atoms were refined anisotropically. The H-atoms were placed in geometrically optimized positions and forced to ride on the atom to which they are attached. The hydrogen atoms associated with the solvent waters could not be located and so are omitted from the final refinement and structure factor calculations. They are, however, included in the reported chemical formula and derived values (e.g. formula weight, F000, etc). The crystal was refined as a racemic twin in the space group P2$_1$.

Final R indices [I>2sigma(I)]   **R1 = 0.0514,** wR2 = 0.1264
R indices (all data)   R1 = 0.0639, wR2 = 0.1355

[Ru(OH)(Py$_2$^{Me}tacn)](PF$_6$)$_2$(NCCH$_3$): Yellow crystals of **C$_{19}$H$_{28}$N$_5$ORu, 2(F$_6$P),** **C$_2$H$_3$N**, were grown from slow diffusion of ethyl ether in CH$_3$CN, and used for low temperature (150(2) K) X-ray structure determination. The measurement was carried out on a *BRUKER SMART APEX CCD* diffractometer using graphite-monochromated Mo $K\alpha$ radiation (λ = 0.71073 Å) from an X-ray Tube. The measurements were made in the range of 1.429 to 27.648° for θ. Hemi-sphere data collection was carried out with ω and φ scans. A total of 17091 reflections were

ANNEX

collected of which 6622 [R(int) = 0.1708] were unique. Programs used: data collection, Smart[1]; data reduction, Saint+[2]; absorption correction, SADABS[3]. Structure solution and refinement was done using SHELXTL[4]. The structure was solved by direct methods and refined by full-matrix least-squares methods on F^2. The non-hydrogen atoms were refined anisotropically. The H-atoms were placed in geometrically optimized positions and forced to ride on the atom to which they are attached.

Final R indices [I>2sigma(I)]	**R1 = 0.0867,** wR2 = 0.1547
R indices (all data)	R1 = 0.1696, wR2 = 0.1898

Table A.II.4. Crystal data and structure refinement for $[Ru^{II}(NCCH_3)(Py_2^{Me}tacn)](OTf)_2$.

Empirical formula	$C_{23}H_{30}F_6N_6O_6RuS_2$
Molecular weight	765.72
Temperature	150(2) K
Wavelength	0.71073 Å
Crystal system, space group	Triclinic, P$\bar{1}$
Unit cell dimensions	a = 9.8609(12) Å alpha = 93.392(2) °
	b = 11.4147(13) Å beta = 95.271(2) °
	c = 13.7740(17) Å gamma = 91.283(2) °
Volume	1540.5(3) Å^3
Z, Calculated density (ρ_c)	2, 1.651 g/cm^3
μ(MoKα)	0.728 mm^{-1}
Crystal size	0.20 x 0.20 x 0.10 mm
Theta range for data collection	2.255 to 28.314 °
Limiting indices	-13<=h<=13, -15<=k<=15, -18<=l<=18
N_t	23993
N (R$_{int}$)	7498 (0.0658)
Completeness to theta =	25.242 99.7 %
Absorption correction	Empirical
Max. and min. transmission	1.0 and 0.742348
Refinement method	Full-matrix least-squares on F^2
Data / restraints / parameters	7498 / 0 / 381
GOF	1.048
R_t [$I > 2\sigma(I)$]	0.0649
wR_2 (all data)	0.1533
Largest diff. peak and hole	0.958 and -0.471 e·Å^{-3}

ANNEX

Table A.II.5. Crystal data and structure refinement for $[Ru^{II}(Cl)(Py_2^{Me}tacn)]_2(Cl)_2(CH_2Cl_2)_3(OH_2)_2$.

Empirical formula	$C_{41}H_{64}Cl_{10}N_{10}O_2Ru_2$
Molecular weight	1285.66
Temperature	173(2) K
Wavelength	0.71073 Å
Crystal system, space group	Monoclinic, P2$_1$
Unit cell dimensions	a = 9.3139(7) Å alpha = 90 °
	b = 31.031(2) Å beta = 93.6070(10) °
	c = 17.8023(14) Å gamma = 90 °
Volume	5135.0(7) Å^3
Z, Calculated density (ρ_c)	4, 1.663 g/cm^3
μ(MoKα)	1.155 mm^{-1}
Crystal size	0.38 x 0.25 x 0.18 mm
Theta range for data collection	1.74 to 28.289 °
Limiting indices	-12<=h<=12, -41<=k<=41, -23<=l<=23
N_t	77403
N (R$_{int}$)	24788 (0.0461)
Completeness to theta =	25.242 99.9 %
Absorption correction	Empirical
Max. and min. transmission	1.0 and 0.698821
Refinement method	Full-matrix least-squares on F^2
Data / restraints / parameters	24788 / 1 / 1158
GOF	1.042
R_t [$I > 2\sigma(I)$]	0.0513
wR_2 (all data)	0.1265
Largest diff. peak and hole	2.729 and -1.291 e·Å^{-3}

ANNEX

Table A.II.6. Crystal data and structure refinement for $[Ru^{III}(Cl)(Py_2^{Me}tacn)](PF_6)_2$.

Empirical formula	$C_{19}H_{27}ClF_{12}N_5P_2Ru$
Molecular weight	751.91
Temperature	130(2) K
Wavelength	0.71073 Å
Crystal system, space group	Orthorhombic, $P2_12_12_1$
Unit cell dimensions	$a = 10.9141(18)$ Å alpha = 90 °
	$b = 11.3295(18)$ Å beta = 90 °
	$c = 21.971(4)$ Å gamma = 90 °
Volume	2716.7(8) Å^3
Z, Calculated density (ρ_c)	4, 1.838 g/cm^3
μ(MoKα)	0.897 mm^{-1}
Crystal size	0.30 x 0.15 x 0.10 mm
Theta range for data collection	1.854 to 27.724 °
Limiting indices	$-11<=h<=14$, $-14<=k<=14$, $-28<=l<=15$
N_t	16541
N (R$_{int}$)	6155 (0.0576)
Completeness to theta =	25.242 100 %
Absorption correction	Empirical
Max. and min. transmission	1.0 and 0.402746
Refinement method	Full-matrix least-squares on F^2
Data / restraints / parameters	6155 / 0 / 406
GOF	1.165
R_t [$I > 2\sigma(I)$]	0.0667
wR_2 (all data)	0.1429
Largest diff. peak and hole	0.680 and -0.813 e·Å^{-3}

478

ANNEX

Table A.II.7. Crystal data and structure refinement for $[Ru^{III}(OH)(Py_2^{Me}tacn)](PF_6)_2(NCCH_3)$.

Empirical formula	$C_{21}H_{31}F_{12}N_6OP_2Ru$
Molecular weight	774.53
Temperature	130(2) K
Wavelength	0.71073 Å
Crystal system, space group	Monoclinic, P 2_1/c
Unit cell dimensions	a = 15.785(4) Å alpha = 90 °
	b = 13.494(3) Å beta = 115.485(4) °
	c = 15.256(3) Å gamma = 90 °
Volume	2933.4(11) Å^3
Z, Calculated density (ρ_c)	4, 1.754 g/cm^3
μ(MoKα)	0.748 mm^{-1}
Crystal size	0.30 x 0.12 x 0.12 mm
Theta range for data collection	1.429 to 27.648 °
Limiting indices	-20<=h<=20, -17<=k<=16, -19<=l<=18
N_t	17091
N (R$_{int}$)	6622 (0.1708)
Completeness to theta =	25.242 99.7 %
Absorption correction	Empirical
Max. and min. transmission	1.0 and 0.229498
Refinement method	Full-matrix least-squares on F^2
Data / restraints / parameters	6622 / 6 / 394
GOF	1.030
R_t [$I > 2\sigma(I)$]	0.0867
wR_2 (all data)	0.1898
Largest diff. peak and hole	1.001 and -0.811 e·Å^{-3}
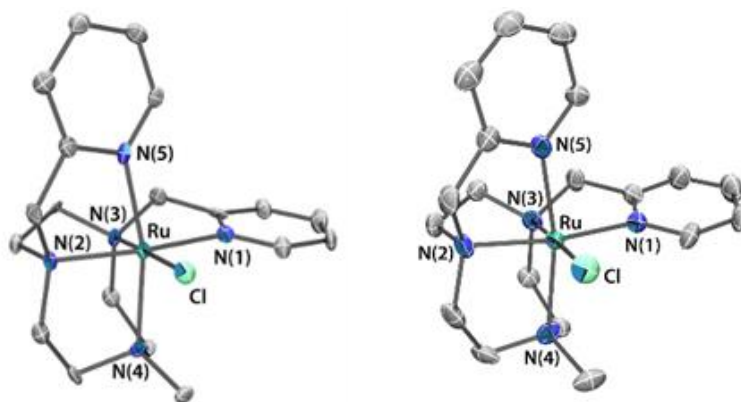
Figure A.II.31. Thermal ellipsoid plot for [Ru^{II}Cl(Py$_2^{Me}$tacn)]Cl (left) and [Ru^{III}Cl(Py$_2^{Me}$tacn)]Cl$_2$ (right) at 30 % probability. Hydrogen, anions and lattice solvents are omitted for clarity.
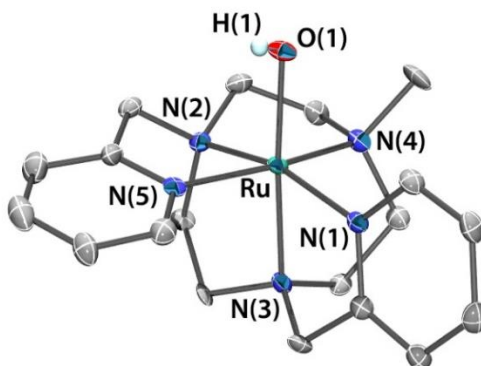
Figure A.II.32. Thermal ellipsoid plot of [Ru ^{III}(OH)(Py$_2^{Me}$tacn)](PF$_6$)$_2$(NCCH$_3$) at 30 % probability. Hydrogen, anions and lattice solvents are omitted for clarity.

A.II.5. Parallel pressure transducer equipment

The parallel pressure transducer hardware is composed of 8 differential pressure transducers (Honeywell-ASCX15DN, ±15 psi) connected to a hardware data-acquisition system (base on Atmega microcontroller) controlled by a home-developed software program. The differential pressure transducer Honeywell-ASCX15DN is a 100 microseconds response, signal-conditioned (high-level span, 4.5 V) output, calibrated and temperature compensated (0 °C to 70 °C) sensor. The differential sensor has two sensing ports that can be used for differential pressure

UNIVERSITAT ROVIRA I VIRGILI
MECHANISTIC STUDIES OF WATER OXIDATION CATALYZED BY HOMOGENEOUS IRON AND RUTHENIUM
COMPLEXES AND LIGHT-DRIVEN ORGANIC REDUCTIONS WITH A DUAL COBALT/COPPER CATALYTIC SYSTEM
Carla Casadevall Serrano

ANNEX

measurements. The pressure calibrated devices to within ± 0.5 matm was offset and span calibrated via software with a high precision pressure transducer (PX409-030GUSB, 0.08% Accuracy). Each of the 8 differential pressure transducers (HoneywellASCX15DN, ±15 psi) produce voltage outputs direct with the pressure difference between the two measuring ports. The voltage outputs were digitalized with a resolution of 0.25 matm from 0 to 175 matm and 1 matm from 176 to 1000 matm using an Atmega microcontroller with an independent voltage auto-calibration. Firmware Atmega microcontroller and control software were home developed. The sensitivity of O_2 analytics allows quantifying the gas formed when the O_2 volume are higher than 50 microL.
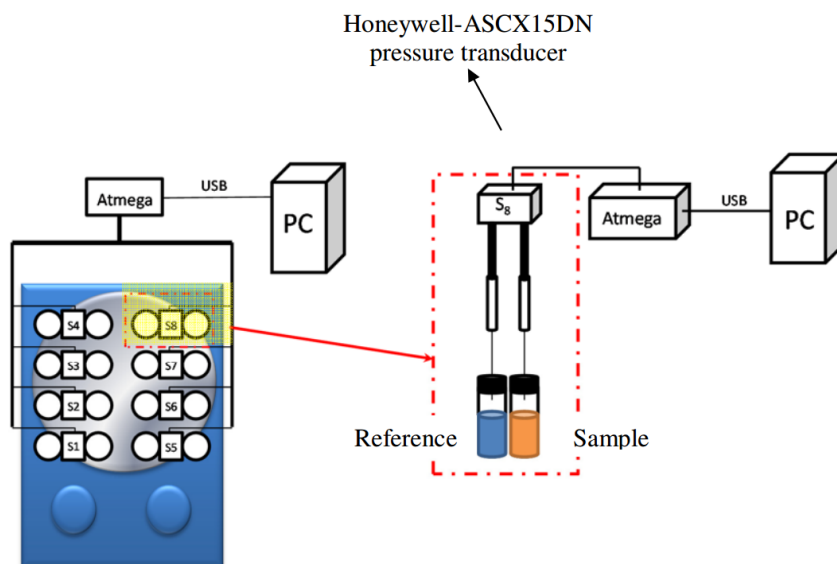
Figure A.II.33. Scheme of the parallel pressure transducer hardware.

A.II.6. References

1. Bruker Advanced X-ray Solutions. SMART: Version 5.631, 1997-2002.
2. Bruker Advanced X-ray Solutions. SAINT +, Version 6.36A, 2001.
3. G. M. Sheldrick, *Empirical Absorption Correction Program*, Universität Göttingen, 1996
Bruker Advanced X-ray Solutions. SADABS Version 2.10, 2001.
4. G. M. Sheldrick, *Program for Crystal Structure Refinement*, Universität Göttingen,
1997 Bruker Advanced X-ray Solutions. SHELXTL Version 6.14, 2000-2003.

A.III. ANNEX CHAPTER V

A.III.1. DFT optimization of intermediates and comparison with the experimental structures

Table A.III.1. Comparison between selected bond distances for solid state X-ray diffraction and the DFT modeled structures

1: L = X = Cl⁻, n = 1
2: L = H₂O, X = PF₆⁻, n = 2
3: L = CH₃CN, X = OTf⁻, n = 2
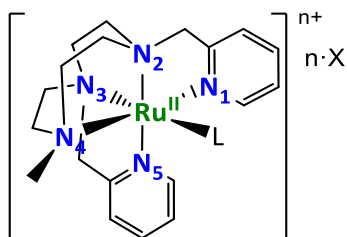
| Bond dist.[a] | X-ray structures data | | DFT data | | | | |
	$1Ru^{II}$-NCCH$_3$	$1Ru^{III}$-OH	$1Ru^{II}$-OH$_2$	$1Ru^{III}$-OH$_2$	$1Ru^{III}$-OH (d)[b] ($1Ru^{III}$-OH (q))	$1Ru^{IV}$-OH	$1Ru^{IV}$(O)
d(Ru-O/N)	2.027(4)	1.943(7)	2.234	2.194	1.931 (1.981)	1.847	1.762
d(Ru-N₁)	2.072(4)	2.074(7)	2.097	2.126	2.100 (2.166)	2.113	2.095
d(Ru-N₂)	2.072(4)	2.044(7)	2.096	2.101	2.089 (2.398)	2.083	2.085
d(Ru-N₃)	2.065(5)	2.098(8)	2.065	2.071	2.143 (2.219)	2.195	2.234
d(Ru-N₄)	2.116(4)	2.107(7)	2.156	2.142	2.146 (2.199)	2.144	2.159
d(Ru-N₅)	2.070(4)	2.063(7)	2.100	2.091	2.098 (2.548)	2.078	2.091

The theoretical modelled distances correspond to the most stable spin states. [a] bond distances are given in Å. [b] d and q represent the doublet and the quadruplet spin states.

A.IV. ANNEX CHAPTER VI

A.IV.1. NMR characterization of the isolated Ru intermediates
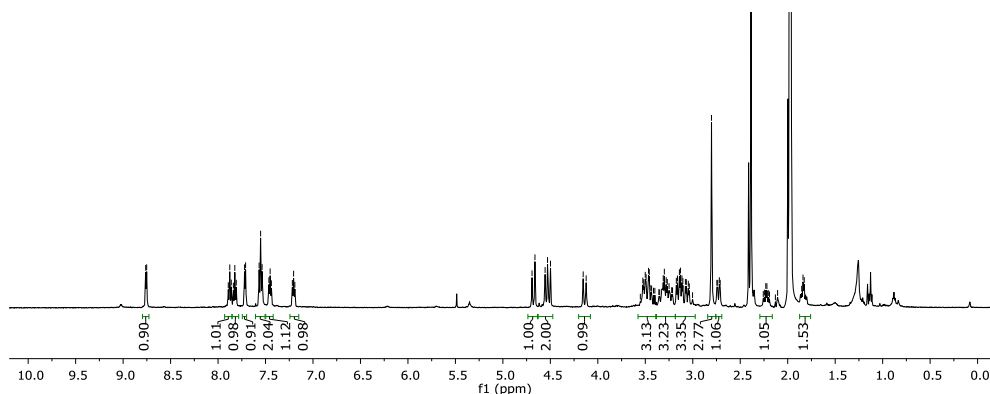
Figure A.IV.1. ^{1}H-NMR (500 MHz, 233 K, MeCN-d$_3$) spectrum of the isolated [Ru^{IV}(OO)(Py$_2^{Me}$tacn)](PF$_6$)$_2$ (**η^2-1Ru^{IV}-OO**) complex in acetonitrile that ressembles Ru(II) species with acetonitrile coordinated.
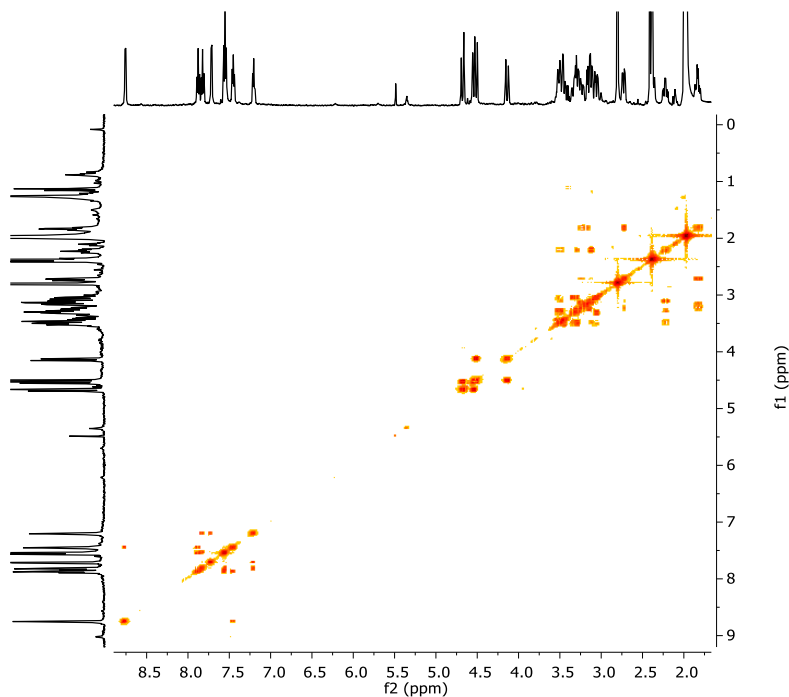
Figure A.IV.2. ^{1}H-^{1}H-COSY NMR (500 MHz, 233 K, MeCN-d$_3$) spectrum of the isolated [Ru^{IV}(OO)(Py$_2^{Me}$tacn)](PF$_6$)$_2$ (**η^2-1Ru^{IV}-OO**) complex complex in acetonitrile that ressembles Ru(II) species with acetonitrile coordinated.

483

A.IV.2. Crystal structure determination

A.IV.2.1. X-ray characterization of Ru(IV) oxo species: 1Ru^{IV}=O
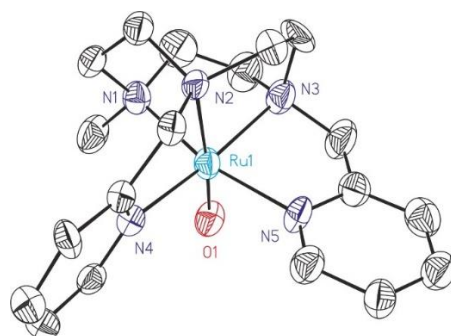
Figure A.IV.3. ORTEP drawing (thermal ellipsoids are drawn at a 50 % probability level) showing the structure of **[Ru^{IV}(O)(Py$_2^{Me}$tacn)](PF$_6$)$_2$**. PF$_6$ anions and hydrogen atoms have been omitted in the sake of clarity. Selected bond lengths (Å): Ru-O1 1.807(8), Ru-N1 2.114(11), Ru-N3 2.062(12), Ru-N4 2.057(11), Ru-N2 2.135(10), Ru-N5 2.079(11). Selected angles (º): O1-Ru-N1 93.4(5), O1-Ru-N2 175.1(4), O1-Ru-N3 96.8(5), O1-Ru-N4 98.0(5), O1-Ru-N5 89.9(5).

Table A.IV.1. Crystal data and structure refinement for [Ru^{IV}(O)(Py$_2^{Me}$tacn)](PF$_6$)$_2$.

Empirical formula	C$_{19}$H$_{26}$F$_{12}$N$_5$OP$_2$Ru	
Molecular weight	731.46	
Temperature	100(2) K	
Wavelength	0.71073 Å	
Crystal system, space group	Orthorhombic	
Space group	P2(1)2(1)2(1)	
Unit cell dimensions	a = 10.789(4)Å	α = 90 º
	b = 11.082(4)Å	β = 90 º
	c = 21.713(8)Å	γ = 90 º
Volume	2596.1(17) Å^3	
Z	4	
Calculated density (ρ_c)	1.871 Mg/m^3	
Absorption coefficient, μ(MoKα)	0.839 mm^{-1}	
F(000)	1460	
Crystal size	0.15 x 0.08 x 0.04 mm^3	
Theta range for data collection	1.876 to 24.858°.	
Limiting indices	0<=h<=12,0<=k<=13,0<=l<=25	
Reflections collected, N_t	2545	
Completeness to theta = 24.858°	99.1 %	
Absorption correction	Multi-scan	
Max. and min. transmission	0.967 and 0.744	
Refinement method	Full-matrix least-squares on F^2	
Data / restraints / parameters	2545/ 741/ 484	
GOF	1.014	
Final R incices, R_t [$I > 2\sigma(I)$] and wR_2	R1 = 0.0661, wR2 = 0.1545	
R indices (all data)	R1 = 0.1034, wR2 = 0.1724	
Flack parameter	x =0.03(8)	
Largest diff. peak and hole	0.778 and -0.662 e.Å^{-3}	

ANNEX

Table A.IV.2. Selected bond distances (Å) and angles (°) for $[Ru^{IV}(O)(Py_2^{Me}tacn)](PF_6)_2$.

Bond lengths (Å)	
Ru1-O1	1.807(8)
Ru1-N1	2.114(11)
Ru1-N3	2.062(12)
Ru1-N4	2.057(11)
Ru1-N2	2.135(10)
Ru1-N5	2.079(11)
Angles (°)	
O1-Ru1-N1	93.4(5)
O1-Ru1-N2	175.1(4)
O1-Ru1-N3	96.8(5)
O1-Ru1-N4	98.0(5)
O1-Ru1-N5	89.9(5)
N1-Ru1-N2	81.9(5)
N3-Ru1-N1	86.2(4)
N3-Ru1-N2	84.1(5)
N3-Ru1-N5	81.1(4)
N4-Ru1-N2	81.3(4)
N4-Ru1-N3	164.9(6)
N4-Ru1-N5	96.1(4)
N4-Ru1-N1	95.8(4)
N5-Ru1-N1	167.1(5)
N5-Ru1-N2	94.9(5)

A.IV.2.1. X-ray characterization of Ru(IV) peroxo species: η^2-1Ru^{IV}-OO

Since there could be doubts about if really (a Peroxo) two Oxygen atoms are linked to the Ruthenium atom its nature was carefully checked. If both Oxygen atoms are deleted and the structure is refined without them, two electron densities are obtained on the deleted positions with a similar number of electrons. Only one position corresponding to one Oxygen atom is discarded since clearly two positions appear in the electron density map. Still, it could be argued that these two positions could be a disordered Oxygen atom distributed in two positions. But this can be

485

ANNEX

clearly revoked refining the occupancy for these two atoms free and fixing the thermal displacement parameters. The occupancy obtained for both atoms is exactly 1.0 which corresponds to two full Oxygen atoms so that a single disordered Oxygen atom can also be discarded.
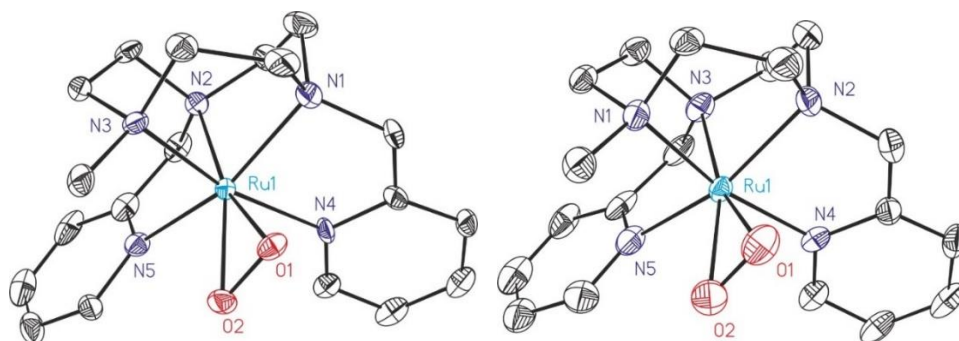
Figure A.IV.4. *left*) ORTEP drawing (thermal ellipsoids are drawn at a 50 % probability level) showing the structure of $[Ru^{IV}(OO)(Py_2^{Me}tacn)](PF_6)_{1.5}(IO_3)_{0.5}$ (**η^2-1Ru^{IV}-OO**). PF_6 anions and hydrogen atoms have been omitted in the sake of clarity. Selected bond lengths (Å): Ru-O2 1.996(6), Ru-O1 2.004(6), Ru-N4 2.075(7), Ru-N1 2.091(8), Ru-N3 2.093(7), Ru-N5 2.112(7), Ru-N2 2.118(7), O1-O2 1.367(9). Selected angles (°): O2-Ru-O1 40.0(3), O2-O1-Ru 69.7(4), O1-O2-Ru 70.3(4). *Right*) ORTEP drawing (thermal ellipsoids are drawn at a 50 % probability level) showing the structure of $[Ru^{IV}(OO)(Py_2^{Me}tacn)](PF_6)_2$ (**η^2-1Ru^{IV}-OO**). PF_6 anions and hydrogen atoms have been omitted in the sake of clarity. Selected bond lengths (Å): Ru-O1 1.995(7), Ru-O2 1.988(7), Ru-N1 2.101(8), Ru-N2 2.092(8), Ru-N3 2.112(8), Ru-N4 2.062(9), Ru-N5 2.128(9), O1-O2 1.353(10). Selected angles (°): O2-Ru-O1 39.7(3), O2-O1-Ru 69.8(4), O1-O2-Ru 70.5(4).

Figure A.IV.5. Crystals of **η^2-1Ru^{IV}-OO** observed in the microscope.

ANNEX

Table A.IV.3. Crystal data and structure refinement for $^2\eta$-[Ru^{IV}(OO)(Py$_2^{Me}$tacn)](PF$_6$)$_2$.

Empirical formula	C$_{19}$H$_{27}$F$_{12}$N$_5$O$_2$P$_2$Ru	
Molecular weight	748.46	
Temperature	100(2) K	
Wavelength	0.71073 Å	
Crystal system, space group	Trigonal	
Space group	P3(1)	
Unit cell dimensions	a = 10.8154(9)Å	α = 90 º
	b = 10.8154(9)Å	β = 90 º
	c = 19.1658(13)Å	γ = 120 º
Volume	1941.5(3) Å^3	
Z	3	
Calculated density (ρ_c)	1.920 Mg/m^3	
Absorption coefficient, μ(MoKα)	0.846 mm^{-1}	
F(000)	1122	
Crystal size	0.20 x 0.03 x 0.03 mm^3	
Theta range for data collection	2.174 to 26.379º	
Limiting indices	-13<=h<=13,-13<=k<=10,-23<=l<=21	
Reflections collected, N_t	19756	
Independent reflections, N (R$_{int}$)	5126[R(int) = 0.0672]	
Completeness to theta = 24.858°	100.0%	
Absorption correction	Empirical	
Max. and min. transmission	0.975 and 0.738	
Refinement method	Full-matrix least-squares on F^2	
Data / restraints / parameters	5126/ 292/ 425	
GOF	1.044	
Final R incices, R_t [$I > 2\sigma(I)$] and wR_2	R1 = 0.0501, wR2 = 0.1138	
R indices (all data)	R1 = 0.0671, wR2 = 0.1222	
Flack parameter	x =-0.03(2)	
Largest diff. peak and hole	1.235 and -0.705 e.Å^{-3}	

Table A.IV.4. Selected bond distances (Å) and angles (°) for $^2\eta$-[Ru^{IV}(OO)(Py$_2^{Me}$tacn)](PF$_6$)$_2$.

Bond lengths (Å)	
Ru1-O1	1.995(7)
Ru1-O2	1.988(7)
Ru1-N1	2.101(8)
Ru1-N2	2.092(8)
Ru1-N3	2.112(8)
Ru1-N4	2.062(9)
Ru1-N5	2.128(9)
O1-O2	1.353(10)
Angles (º)	
O2-Ru1-O1	39.7(3)
O2-O1-Ru1	69.8(4)
O1-O2-Ru1	70.5(4)
N1-Ru1-N3	84.6(3)

ANNEX

N1-Ru1-N5	93.4(3)
N2-Ru1-N1	83.9(3)
N2-Ru1-N3	81.9(4)
N2-Ru1-N5	159.2(3)
N3-Ru1-N5	77.3(3)
N4-Ru1-N1	166.4(3)
N4-Ru1-N2	82.7(3)
N4-Ru1-N3	96.1(3)
N4-Ru1-N5	100.0(3)

Table A.IV.5. Crystal data and structure refinement for $^2\eta$-[Ru^{IV}(OO)(Py$_2^{Me}$tacn)](PF$_6$)$_{1.5}$(IO$_3$)$_{0.5}$.

Empirical formula	**C$_{19}$H$_{27}$F$_9$I$_{0.5}$N$_5$O$_{3.5}$P$_{1.5}$Ru**	
Molecular weight	763.43	
Temperature	100(2) K	
Wavelength	0.71073 Å	
Crystal system, space group	Trigonal	
Space group	P3(2)	
Unit cell dimensions	a = 10.7837(3)Å	$\alpha = 90$ °
	b = 10.7837(3)Å	$\beta = 90$ °
	c = 19.1541(7)Å	$\gamma = 120$ °
Volume	1929.00(12) Å^3	
Z	3	
Calculated density (ρ_c)	1.972 Mg/m^3	
Absorption coefficient, μ(MoKα)	1.404 mm^{-1}	
F(000)	1134	
Crystal size	0.15 x 0.04 x 0.04 mm^3	
Theta range for data collection	2.181 to 32.367°.	
Limiting indices	-15<=h<=10,-13<=k<=14,-12<=l<=28	
Reflections collected, N_t	11693	
Independent reflections, N (R$_{int}$)	5583[R(int) = 0.0336]	
Completeness to theta = 24.858°	92.6%	
Absorption correction	Empirical	
Max. and min. transmission	0.946 and 0.728	
Refinement method	Full-matrix least-squares on F^2	
Data / restraints / parameters	5583/ 240/ 488	
GOF	1.143	
Final R incices, R_t [$I > 2\sigma(I)$] and wR_2	R1 = 0.0582, wR2 = 0.1455	
R indices (all data)	R1 = 0.0635, wR2 = 0.1522	
Flack parameter	x =0.07(3)	
Largest diff. peak and hole	1.333 and -1.606 e.Å-3	

ANNEX

Table A.IV.6. Selected bond distances (Å) and angles (°) for $^2\eta$-[Ru^{IV}(OO)(Py_2^{Me}tacn)](PF_6)$_{1.5}$(IO_3)$_{0.5}$.

Bond lengths (Å)	
Ru1-O2	1.996(6)
Ru1-O1	2.004(6)
Ru1-N4	2.075(7)
Ru1-N1	2.091(8)
Ru1-N3	2.093(7)
Ru1-N5	2.112(7)
Ru1-N2	2.118(7)
O1-O2	1.367(9)
Angles (°)	
O2-Ru1-O1	40.0(3)
O2-O1-Ru1	69.7(4)
O1-O2-Ru1	70.3(4)
N4-Ru1-N1	82.0(3)
N4-Ru1-N3	166.1(3)
N1-Ru1-N3	84.3(3)
N4-Ru1-N5	100.8(3)
N1-Ru1-N5	159.0(3)
N3-Ru1-N5	92.9(3)
N4-Ru1-N2	96.8(3)
N1-Ru1-N2	81.6(3)
N3-Ru1-N2	83.7(3)
N5-Ru1-N2	77.4(3)

Table A.IV.7. Comparison between X-ray diffraction and the DFT modeled structures.
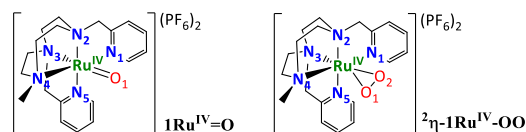
Bond dist.[a]	X-ray structures data			DFT data	
	$1Ru^{IV}=O$	$^2\eta$-$1Ru^{IV}$-OO[b]	$^2\eta$-$1Ru^{IV}$-OO[c]	$1Ru^{IV}=O$	$^2\eta$-$1Ru^{IV}$-OO
d(Ru-O$_1$)	1.807(8)	1.988(7)	1.996(6)	1.762	2.001
d(Ru-N$_1$)	2.079(11)	2.062(9)	2.075(7)	2.095	2.108
d(Ru-N$_2$)	2.062(12)	2.092(8)	2.091(8)	2.085	2.101
d(Ru-N$_3$)	2.135(10)	2.112(8)	2.118(7)	2.234	2.109
d(Ru-N$_4$)	2.114(11)	2.101(8)	2.093(7)	2.159	2.127
d(Ru-N$_5$)	2.057(11)	2.128(9)	2.112(7)	2.091	2.131
d(O$_1$–O$_2$)	-	1.353(10)	1.367(9)	-	1.352
d(Ru-O$_2$)	-	1.995(7)	2.004(6)	-	2.012

The theoretically modeled distances correspond to the most stable spin states. [a] bond distances are given in Å. [b] crystal with two PF_6 as counterions. [c] crystal with 1.5 PF_6 and 0.5 IO_3 as counterions.

ANNEX

A.IV.3. X-ray Absorption Spectroscopy (XAS)
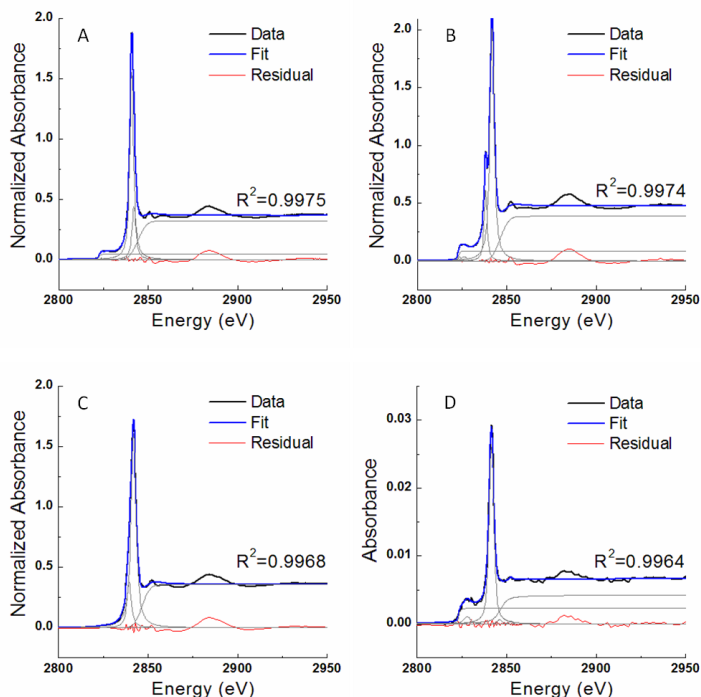
Figure A.IV.6. Ru L$_3$-edge fits for (A) **1Ru^{II}-OH$_2$**; (B) **1Ru^{III}-OH**; (C) **1Ru^{IV}=O**; (D) **η^2-1Ru^{IV}-OO**.
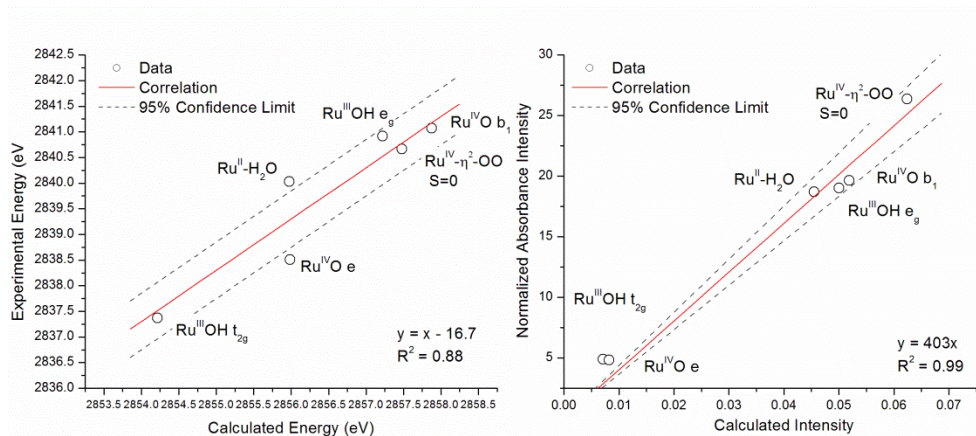
Figure A.IV.7. Correlation of theoretical transition energies and intensities to experiment. Although the theoretical spectra are calculated as an overlap of L$_3$ and L$_2$ edge transitions the high covalency of the complexes resulting in mixing of p$_{3/2}$ and p$_{1/2}$ states suggests this is a reasonable approximation yielding a good qualitative agreement to experiment for comparison purposes.[1,2]

490

ANNEX
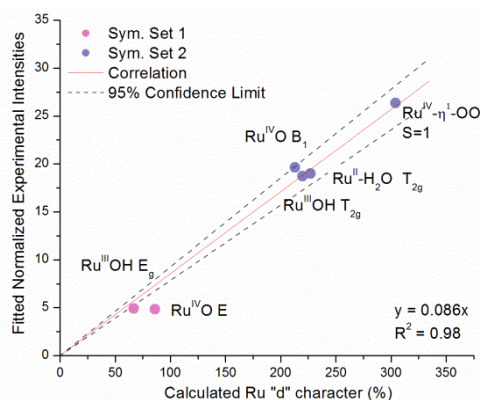
Figure A.IV.8. Correlation of theoretically calculated ground state Ru "d" character to experimentally determined L_3 edge intensities. As metal L_3-edge spectra involve dipole allowed p→d transitions the experimental intensity has previously been shown to directly correlated with the metal d character in the ground state wave function allowing further correlation of experiment and theory.[3] Intensity correlations were grouped based on experimentally resolved features and orbital symmetries derived using a first coordination shell approximations at the metal center together with theoretically predicted mixing of orbitals from the theoretically calculated L_3 edge spectra as shown in Figures 11 – 14 from chapter VI. *Symmetry set 1:* **1Ru^{III}-OH** (T_{2g}: $^\beta d_{xz/yz}$) and **1Ru^{IV}=O** (E: $^\beta d_{xz/yz}$, $^\beta d_{yz/xz}$); *Symmetry set 2:* **1Ru^{II}-OH$_2$** (T_{2g}: $d_{x^2-y^2}, d_{z^2}$), **1Ru^{III}-OH** (T_{2g}: $d_{x^2-y^2}, d_{z^2}$), **1Ru^{IV}=O** (B$_1$: $d_{x^2-y^2}$; A$_1$: d_{z^2}), **η²-1Ru^{IV}-OO** (A': $d_{xy}, d_{x^2-y^2}, d_{z^2}$), .
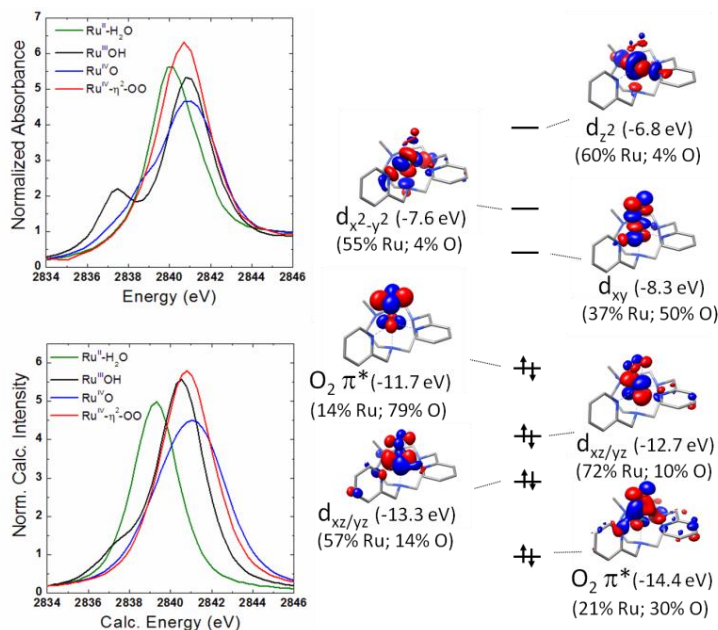
Figure A.IV.9. Experimental and theoretical Ru L_3 edge spectra for complexes **1Ru^{II}-OH$_2$** (green line), **1Ru^{III}-OH** (black line), **1Ru^{IV}=O** (blue line) and **η²-1Ru^{IV}-OO** (red line), together with a schematic representation of the Ru 3d manifold showing metal and oxygen contributions (isovalue 0.05) for **η²-1Ru^{IV}-OO**.

491
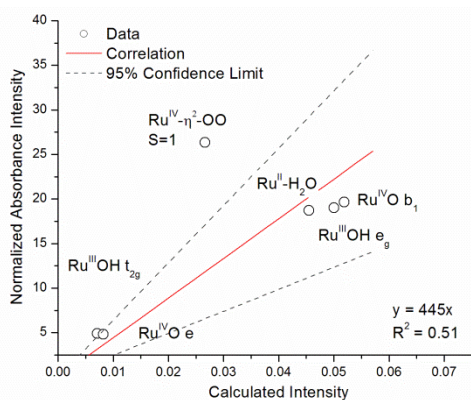
Figure A.IV.10. Correlation of theoretical transition intensities to experiment using the $^3[\eta^2\text{-}1Ru^{IV}\text{-}OO]$ (S=1) model
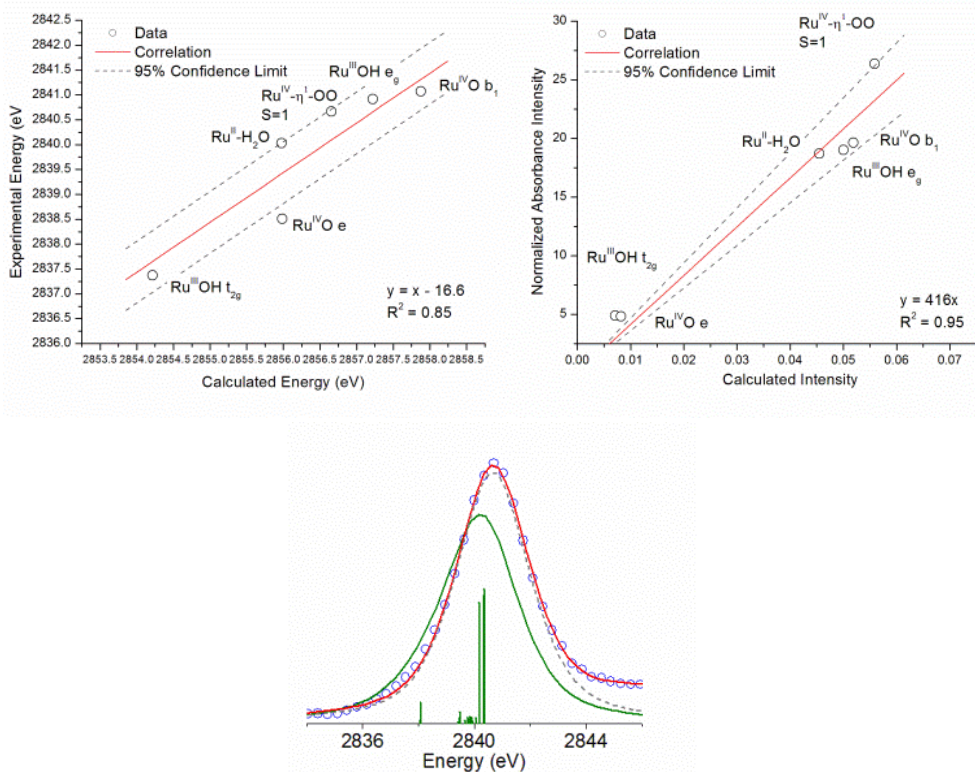
Figure A.IV.11. (*right*) Correlation of theoretical transition energies intensities to experiment using the $^3[\eta^1\text{-}1Ru^{IV}\text{-}OO]$ (S=1) model. (*left*) XANES region of Ru L$_3$-edge spectra showing edge and background subtracted experimental data (*circles*) overall fit (*red*) and fitted components (*dashed gray*) overlaid with scaled (416x) theoretical spectra having FWHM 3.1 eV and an energy shift of -16.6 eV

492

ANNEX

A.IV.4. Raman spectroscopic studies
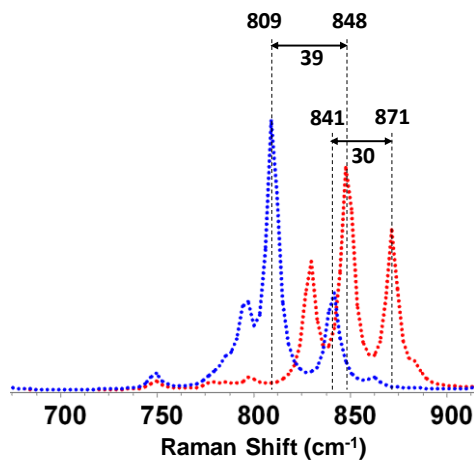
Figure A.IV.12. DFT calculated Raman spectra of **1Ru^{IV}=O** (red dotted line), **1Ru^{IV}=^{18}O** (blue dotted line) in the Ru-O stretching region.
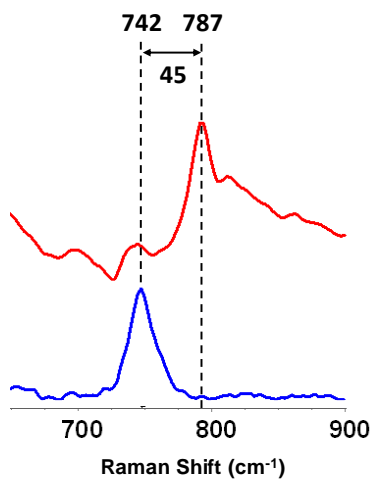
Figure A.IV.13. Solution Raman spectra of [Ru^{IV}(O)(Py$_2^{Me}$tacn)](PF$_6$)$_2$ (**1Ru^{IV}=O**) with ^{16}O (red) and ^{18}O (blue) isotopic substitution generated after the addition of NaIO4 (1.5 eq) to **1Ru^{II}-OH$_2$** in in Milli-Q H$_2$O and H$_2$^{18}O (2 mM concentration), respectively, in the measured region (λ_{exc} = 457 nm, 50 mW, rt).

493
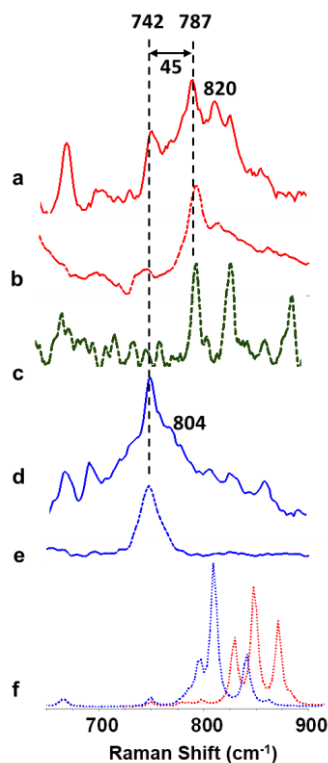
Figure A.IV.14. Comparison of solid, solution and DFT Raman spectra of [Ru^{IV}(O)(Py$_2^{Me}$tacn)](PF$_6$)$_2$ (**1Ru^{IV}=O**) in the Ru-O stretching region. Solid Raman spectrum of [Ru^{IV}(O)(Py$_2^{Me}$tacn)](PF$_6$)$_2$ (**1Ru^{IV}=O**) with ^{16}O (*a*, red). Solution Raman spectra of [Ru^{IV}(O)(Py$_2^{Me}$tacn)](PF$_6$)$_2$ (**1Ru^{IV}=O**) generated after the addition of NaIO$_4$ (1.5 eq) to **1Ru^{II}-OH$_2$** in Milli-Q H$_2$O (2 mM concentration) with ^{16}O (*b*, red dashed line) measured at λ_{exc} = 457 nm (50 mW power, rt). Raman spectrum of [Ru^{IV}(O)(Py$_2^{Me}$tacn)](PF$_6$)$_2$ (**1Ru^{IV}=O**) generated after the addition of CAN (3 eq) to **1Ru^{II}-OH$_2$** in Milli-Q H$_2$O (2 mM concentration) with ^{16}O (*c*, green dashed line) measured at λ_{exc} = 355 nm (10 mW power, rt). Solid Raman spectrum of [Ru^{IV}(^{18}O)(Py$_2^{Me}$tacn)](PF$_6$)$_2$ (**1Ru^{IV}=^{18}O**) with ^{18}O (*d*, red). Raman spectra of [Ru^{IV}(^{18}O)(Py$_2^{Me}$tacn)](PF$_6$)$_2$ (**1Ru^{IV}=^{18}O**) generated after the addition of NaI^{18}O$_4$ (1.5 eq, previously exchanged) to **1Ru^{II}-OH$_2$** in H$_2$^{18}O (2 mM concentration) (*e*, blue dashed line) measured at λ_{exc} = 457 nm (50 mW power, rt). DFT calculated Raman spectra of **1Ru^{IV}=O** (red dotted line) and **1Ru^{IV}=^{18}O** (blue dotted line) in the regions of study (*f*).

494

ANNEX
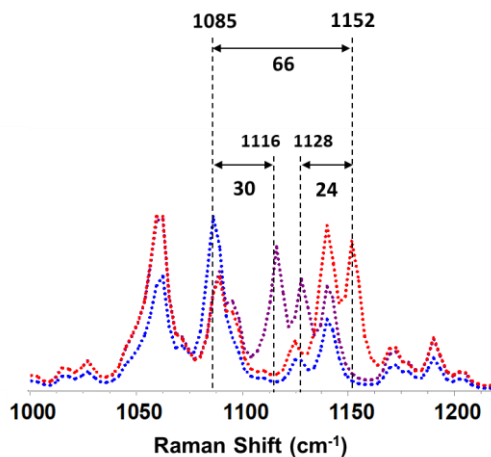
Figure A.IV.15. DFT calculated Raman spectra of η^2-**1Ru^{IV}-OO** (red dotted line), η^2-**1Ru^{IV}-^{18}OO** (purple dotted line) and η^2-**1Ru^{IV}-^{18}O^{18}O** (blue dotted line) in the O-O stretching region. Black dotted line spectrum is the ^{16}O and ^{18}O difference from the DFT calculated Raman.
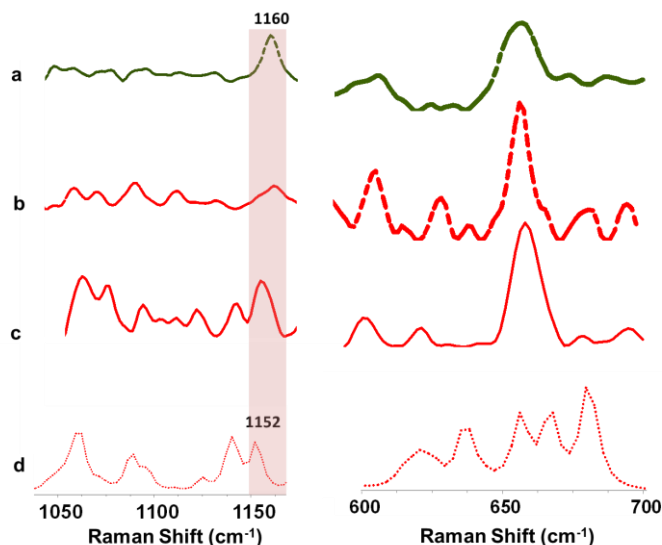
Figure A.IV.16. Comparison of the solid, solution and DFT Raman spectra of [Ru^{IV}(OO)(Py$_2$^{Me}tacn)](PF$_6$)$_2$ (η^2-**1Ru^{IV}-OO**) in the Ru-O (*left*) and O-O (*right*) stretching regions, respectively. Raman spectra of η^2-[Ru^{IV}(OO)(Py$_2$^{Me}tacn)](PF$_6$)$_2$ (η^2-**1Ru^{IV}-OO**) generated after the addition of CAN (8 eq) to **1Ru^{II}-OH$_2$** in Milli-Q H$_2$O (2 mM concentration) with ^{16}O (*a*, green) measured at λ_{exc} = 355 nm (10 mW power, rt). Raman spectra of η^2-[Ru^{IV}(OO)(Py$_2$^{Me}tacn)](PF$_6$)$_2$ (η^2-**1Ru^{IV}-OO**) generated after the addition of NaIO$_4$ (6.5 eq) to **1Ru^{II}-OH$_2$** in Milli-Q H$_2$O (2 mM concentration) with ^{16}O (*b*, red) measured at λ_{exc} = 355 nm (10 mW power, rt). Solid Raman spectra of [Ru^{IV}(OO)(Py$_2$^{Me}tacn)](PF$_6$)$_2$ (η^2-**1Ru^{IV}-OO**) (*c*) measured at λ_{exc} = 632.8 nm (12 mW power, rt). DFT calculated Raman spectra of η^2-**1Ru^{IV}-OO** in the regions of study (*d*).

ANNEX
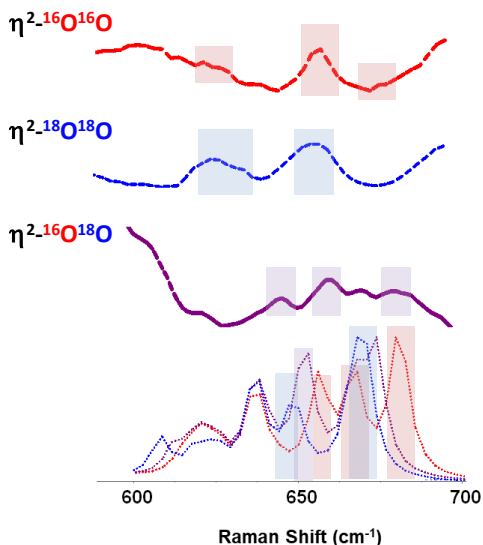
Figure A.IV.17. Comparison of the solution and DFT Raman spectra of $[Ru^{IV}(OO)(Py_2^{Me}tacn)](PF_6)_2$ (**η^2-1Ru^{IV}-OO**) in the Ru-O stretching region. Raman spectra of η^2-$[Ru^{IV}(OO)(Py_2^{Me}tacn)](PF_6)_2$ (**η^2-1Ru^{IV}-OO**) generated after the addition of NaIO$_4$ (6.5 eq) to **1Ru^{II}-OH$_2$** in Milli-Q H$_2$O (2 mM concentration) with ^{16}O (*top,* red) measured at λ_{exc} = 457 nm, (50 mW power, rt). Raman spectra of η^2-$[Ru^{IV}(^{18}O^{18}O)(Py_2^{Me}tacn)](PF_6)_2$ (**η^2-1Ru^{IV}-^{18}O^{18}O**) generated after the addition of NaI^{18}O$_4$ (6.5 eq, previously exchanged) to **1Ru^{II}-OH$_2$** in H$_2^{18}$O (2 mM concentration) (*middle*, blue) measured at λ_{exc} = 457 nm (50 mW power, rt). Raman spectra of η^2-$[Ru^{IV}(O^{18}O)(Py_2^{Me}tacn)](PF_6)_2$ (**η^2-1Ru^{IV}-O^{18}O**) generated after the addition of NaIO$_4$ (6.5 eq) to **1Ru^{IV}=^{18}O** in D$_2$O (2 mM concentration) (purple) measured at λ_{exc} = 457 nm (50 mW power, rt). DFT calculated Raman spectra of **η^2-1Ru^{IV}-OO** (red dotted line), **η^2-1Ru^{IV}-^{18}OO** (purple dotted line) and **η^2-1Ru^{IV}-^{18}O^{18}O** (blue dotted line) in the regions of study (*bottom*).
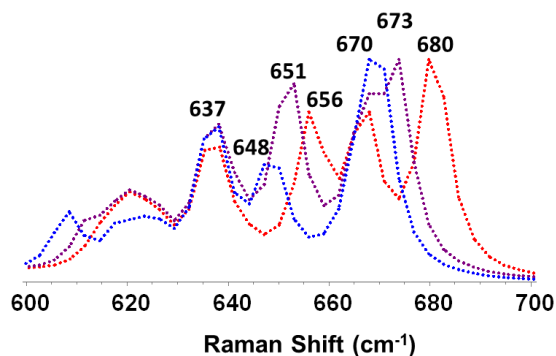
Figure A.IV.18. DFT calculated Raman spectra of **η^2-1Ru^{IV}-OO** (red dotted line), **η^2-1Ru^{IV}-^{18}OO** (purple dotted line) and **η^2-1Ru^{IV}-^{18}O^{18}O** (blue dotted line) in the Ru-O stretching region. Black dotted line spectrum is the ^{16}O and ^{18}O difference from the DFT calculated Raman.

ANNEX
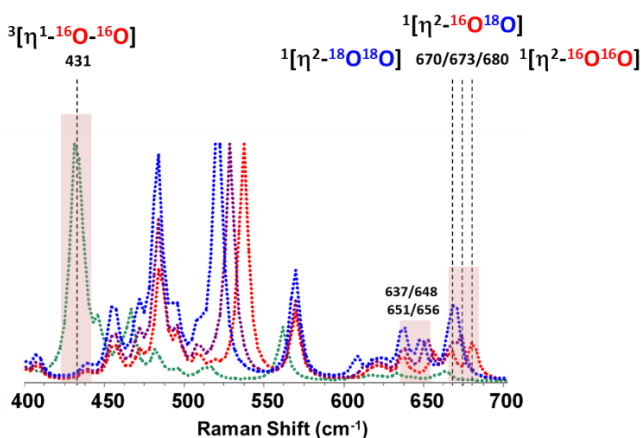
Figure A.IV.19. DFT calculated Raman spectra of η^2-**1Ru^{IV}-OO** (red dotted line), η^2-**1Ru^{IV}-^{18}OO** (purple dotted line), η^2-**1Ru^{IV}-^{18}O^{18}O** (blue dotted line) and the triplet structure of η^2-**1Ru^{IV}-OO** (η^1-**1Ru^{IV}-OO**) (green dotted line), in the Ru-O stretching region.

A.IV.5. CSI-HRMS studies

A.IV.5.1. CSI-HRMS characterization of the isolated intermediates
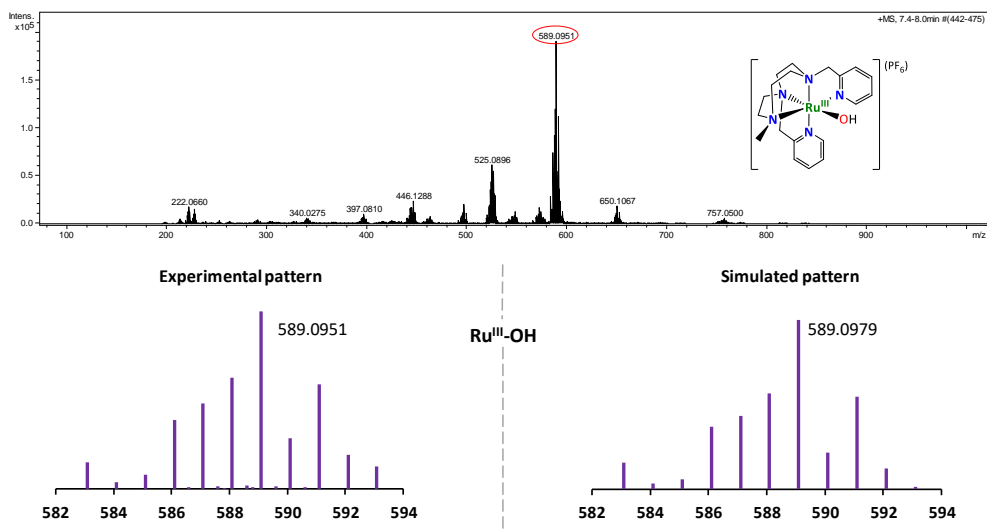
Figure A.IV.20. Characterization of the isolated complex **[Ru^{III}(OH)(Py$_2$^{Me}tacn)](PF$_6$)$_2$** (2 mM) by CSI-HRMS at 20ºC in MilliQ water.

497

ANNEX
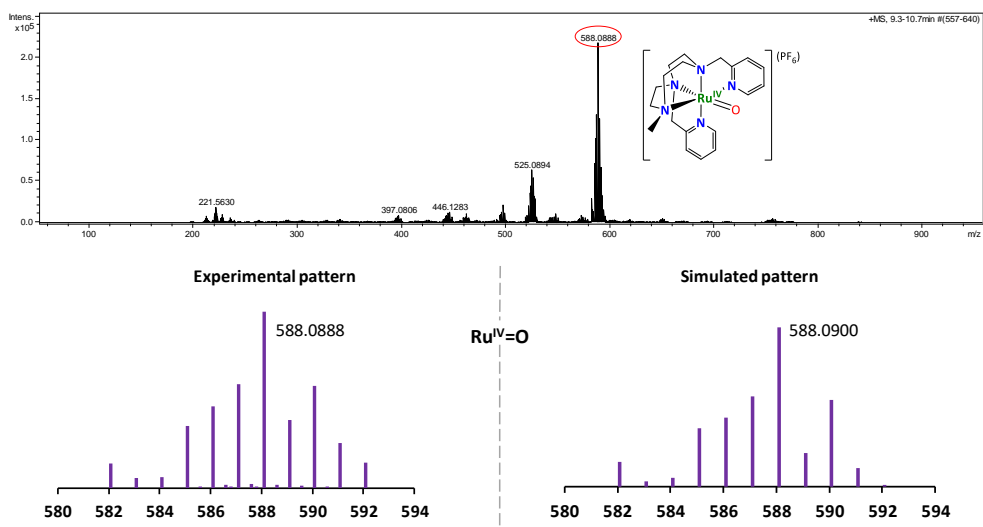
Figure A.IV.21. Characterization of the isolated complex $[Ru^{IV}(O)(Py_2^{Me}tacn)](PF_6)_2$ (2 mM) by CSI-HRMS at 20ºC in MilliQ water.
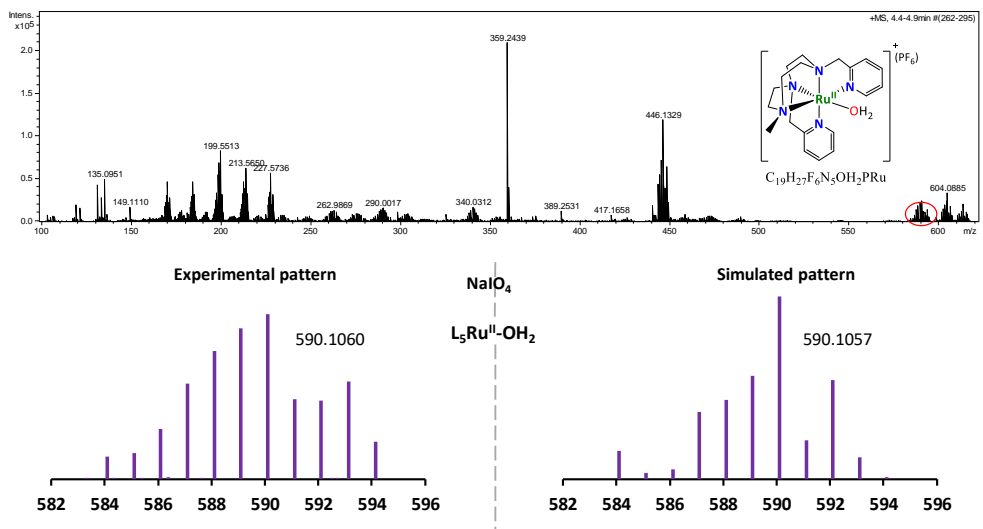
Figure A.IV.22. Characterization of the isolated crystal of complex $^2\eta$-$[Ru^{IV}(OO)(Py_2^{Me}tacn)](PF_6)_2$ (0.001 mM) by CSI-HRMS at 25ºC in D$_2$O:MeCN (1:10) solvent mixture. Peak at m/z 590.1060.

ANNEX
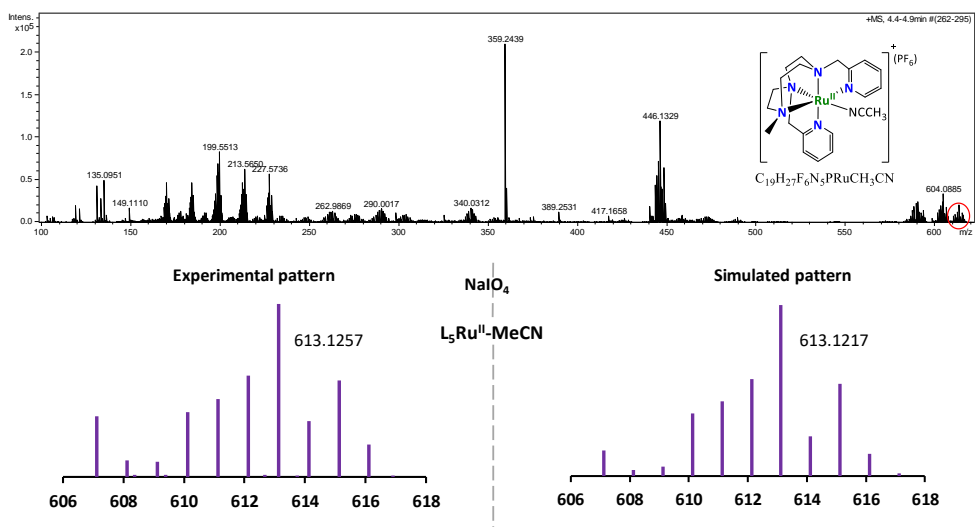
Figure A.IV.23. Characterization of the isolated crystal of complex $^2\eta\text{-}[Ru^{IV}(OO)(Py_2^{Me}tacn)](PF_6)_2$ (0.001 mM) by CSI-HRMS at 25ºC in D_2O:MeCN (1:10) solvent mixture. Peak at m/z 613.1257.
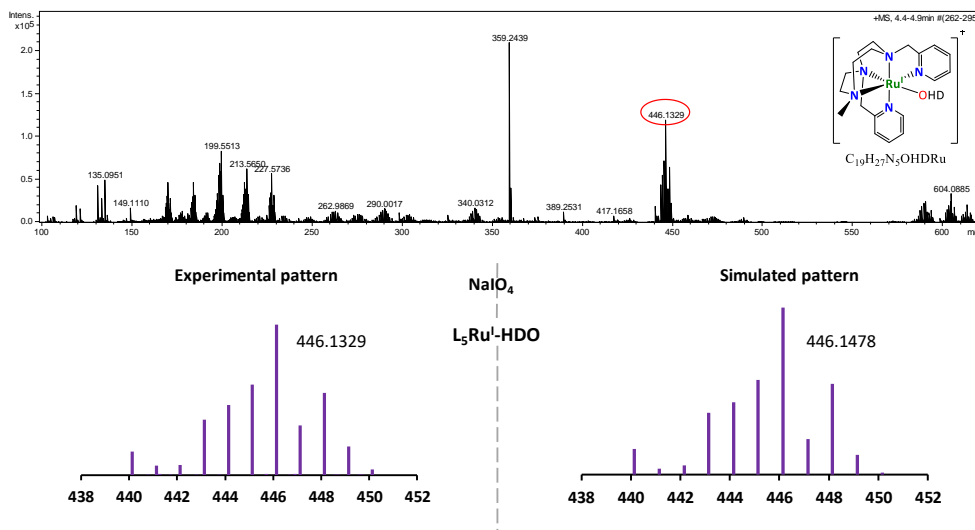
Figure A.IV.24. Characterization of the isolated crystal of complex $^2\eta\text{-}[Ru^{IV}(OO)(Py_2^{Me}tacn)](PF_6)_2$ (0.001 mM) by CSI-HRMS at 25ºC in D_2O:MeCN (1:10) solvent mixture. Peak at m/z 446.1329.

ANNEX
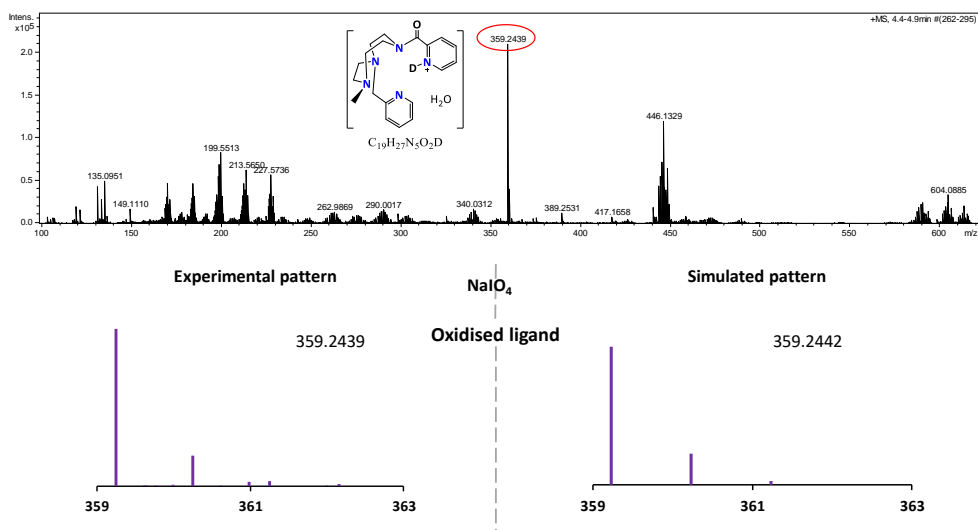
Figure A.IV.25. Characterization of the isolated crystal of complex $^2\eta$-[$Ru^{IV}(OO)(Py_2^{Me}tacn)$]($PF_6$)$_2$ (0.001 mM) by CSI-HRMS at 25ºC in D_2O:MeCN (1:10) solvent mixture. Peak at *m/z* 359.2439.
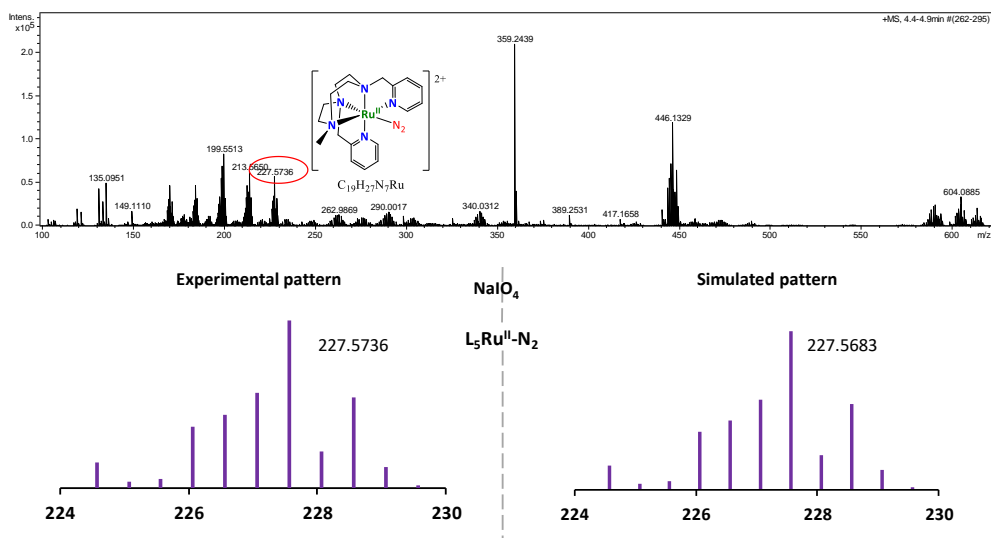
Figure A.IV.26. Characterization of the isolated crystal of complex $^2\eta$-[$Ru^{IV}(OO)(Py_2^{Me}tacn)$]($PF_6$)$_2$ (0.001 mM) by CSI-HRMS at 25ºC in D_2O:MeCN (1:10) solvent mixture. Peak at *m/z* 227.5736.

A.IV.5.2. CSI-HRMS monitoring of the formation of $^2\eta$-1^{IV}-OO from 1 in MilliQ H$_2$O
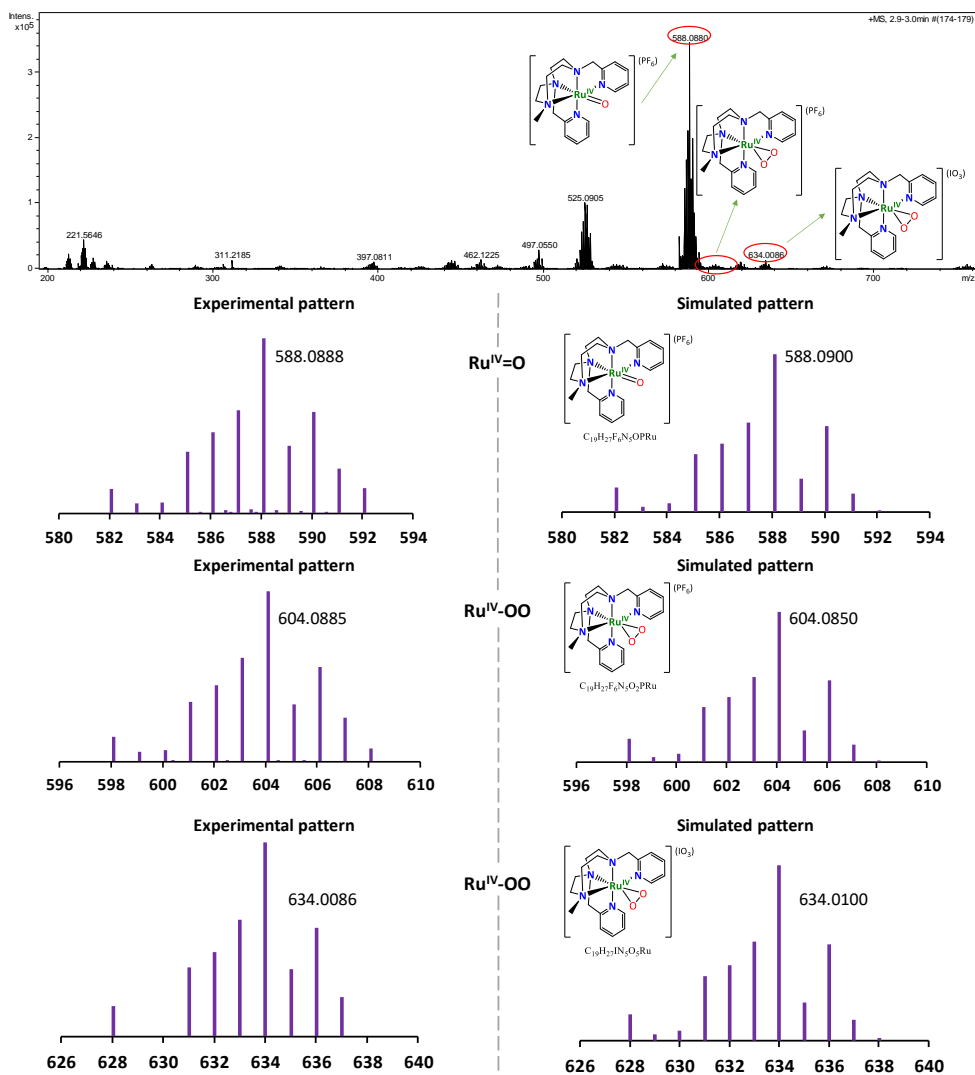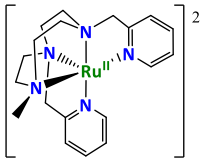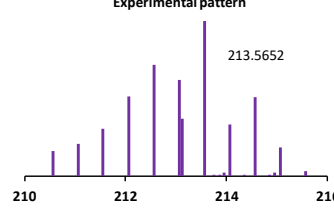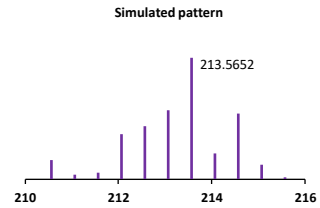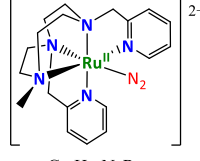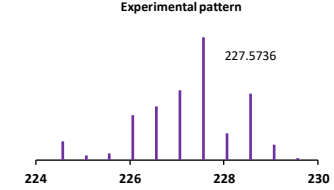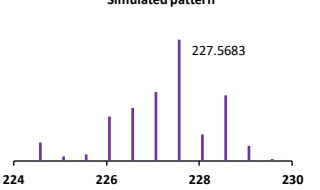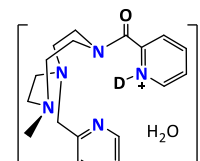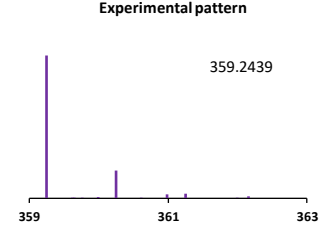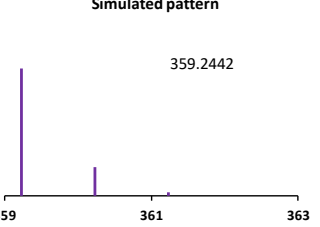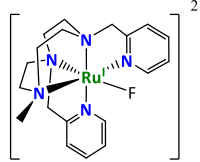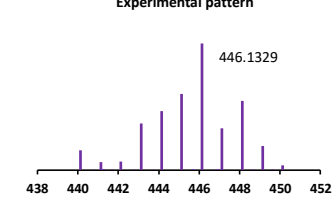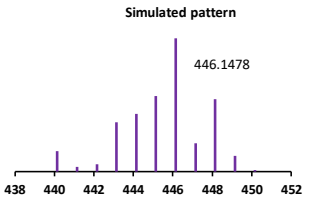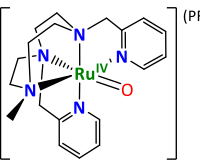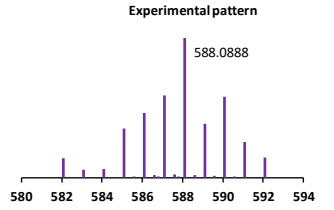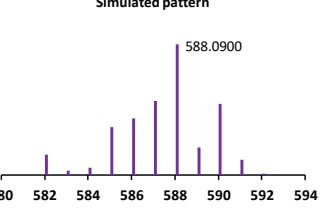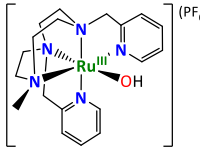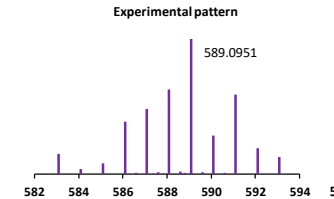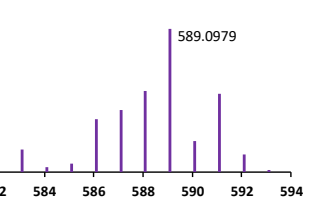
Figure A.IV.27. Monitoring of the generation of $^2\eta$-1Ru^{IV}-OO from **1** after the addition of 5 equivalents of NaIO$_4$ by CSI-HRMS at 25ºC in D$_2$O. In the full spectrum it can be seen the slow formation of the peroxide intermediate.

501

ANNEX

Table A.IV.8. Summary of the peaks found in the CSI-HRMS studies.

ANNEX

A.IV.5.3. CSI-HRMS labelling studies of the formation of $^2\eta$-1^{IV}-OO from 1^{IV}=O in Milli-Q H$_2$O, D$_2$O and H$_2$^{18}O, respectively
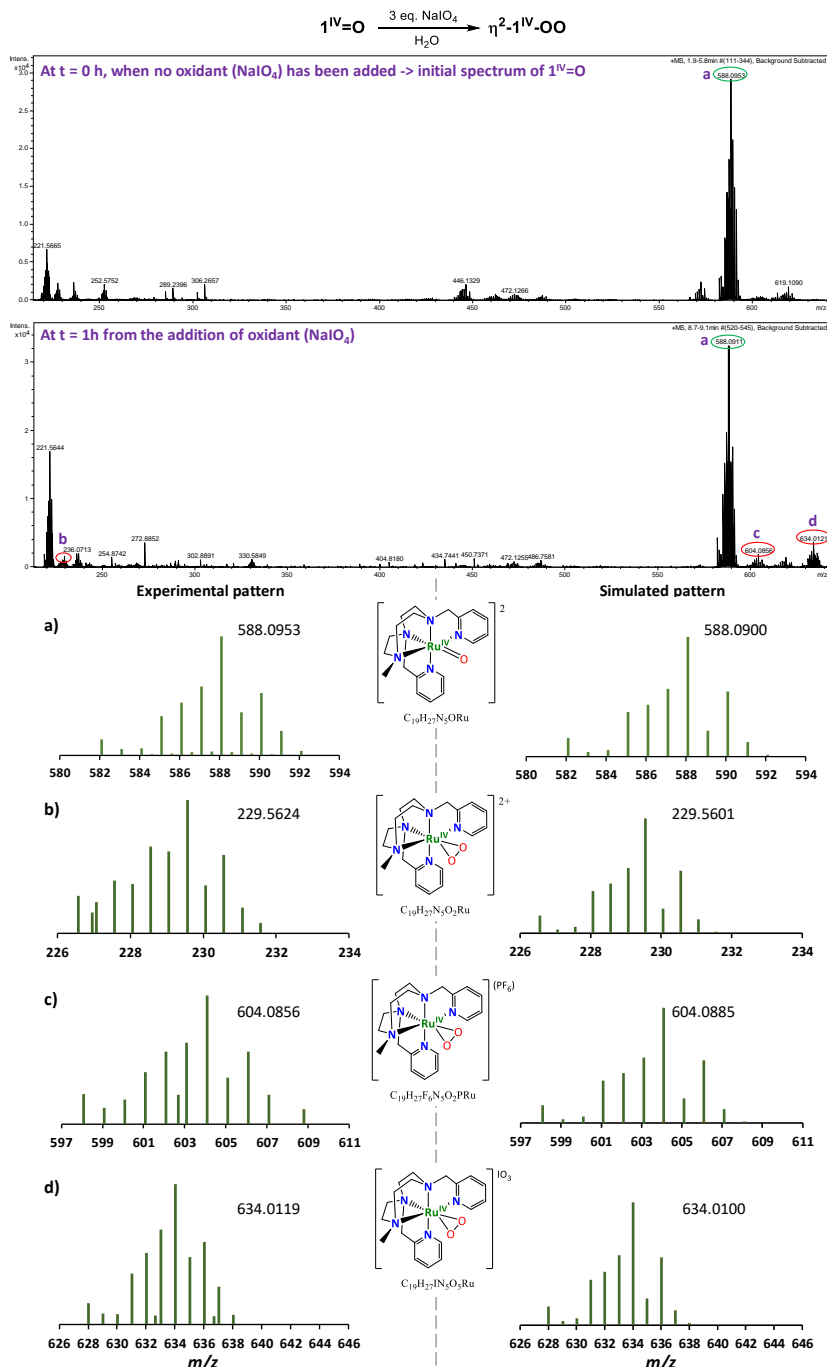
Figure A.IV.28. CSI-HRMS (293 K) monitoring of the reaction kinetics of **1Ru^{IV}=O** with NaIO$_4$ (3 eq) in MilliQ water after 60 minutes of reaction time (see the experimental section for further details).

504
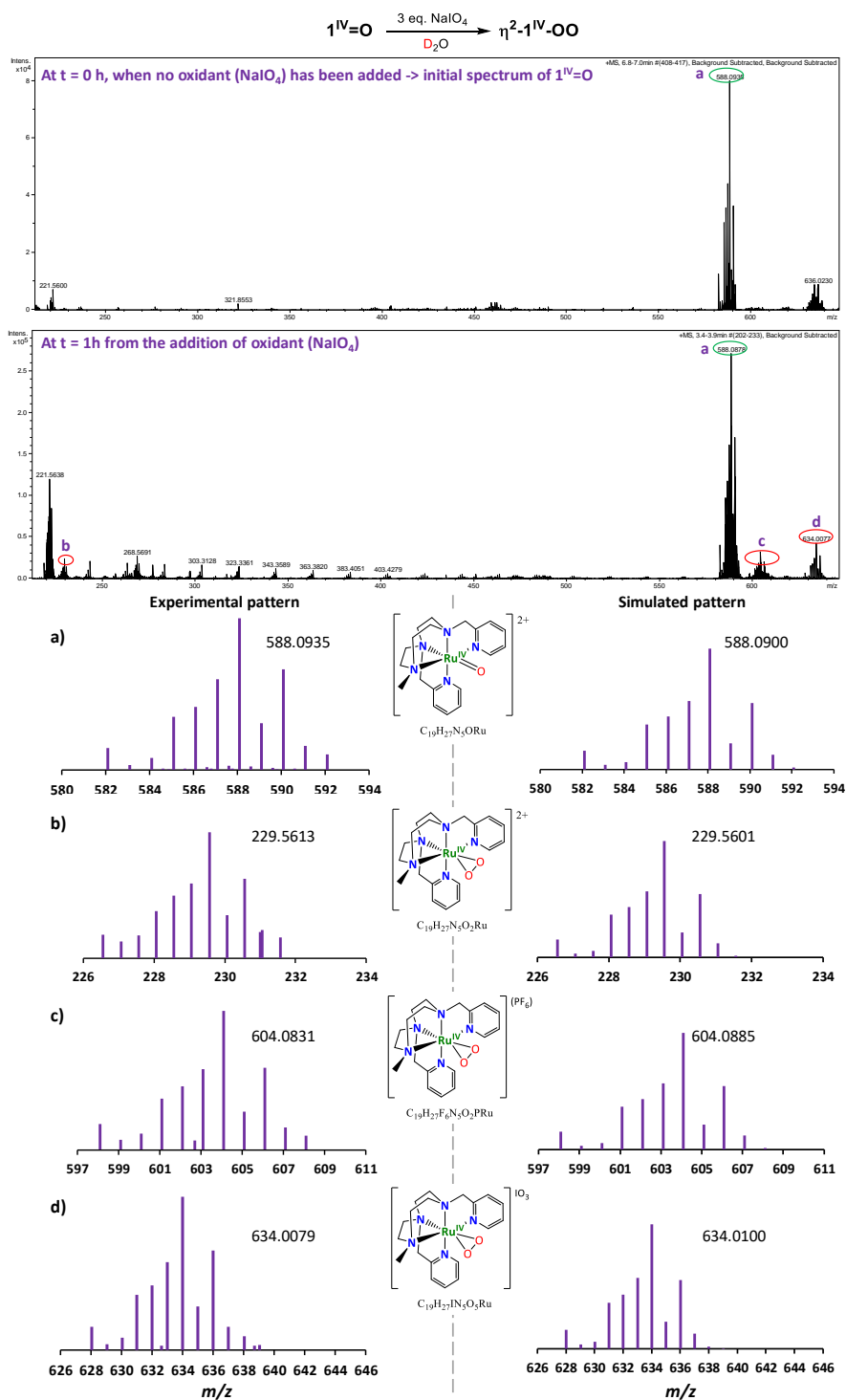
ANNEX

Figure A.IV.29. CSI-HRMS (293 K) monitoring of the reaction kinetics of **1Ru^{IV}=O** with NaIO$_4$ (3 eq) in D$_2$O after 60 minutes of reaction time (see the experimental section for further details).

505

ANNEX
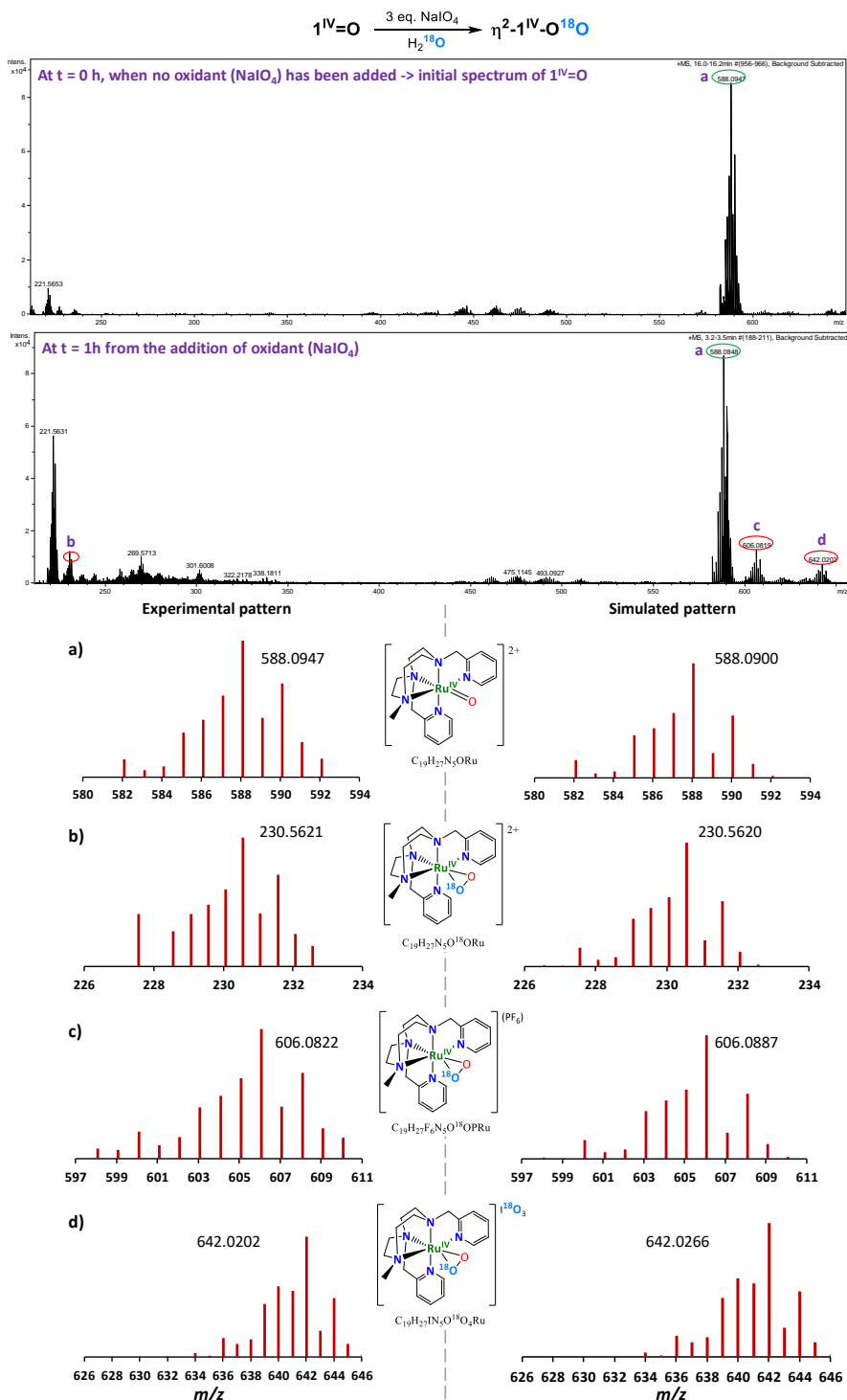
Figure A.IV.30. CSI-HRMS (293 K) monitoring of the reaction kinetics of **1Ru^{IV}=O** with NaIO$_4$ (3 eq) in H$_2{}^{18}$O after 60 minutes of reaction time (see the experimental section for further details).

506

ANNEX
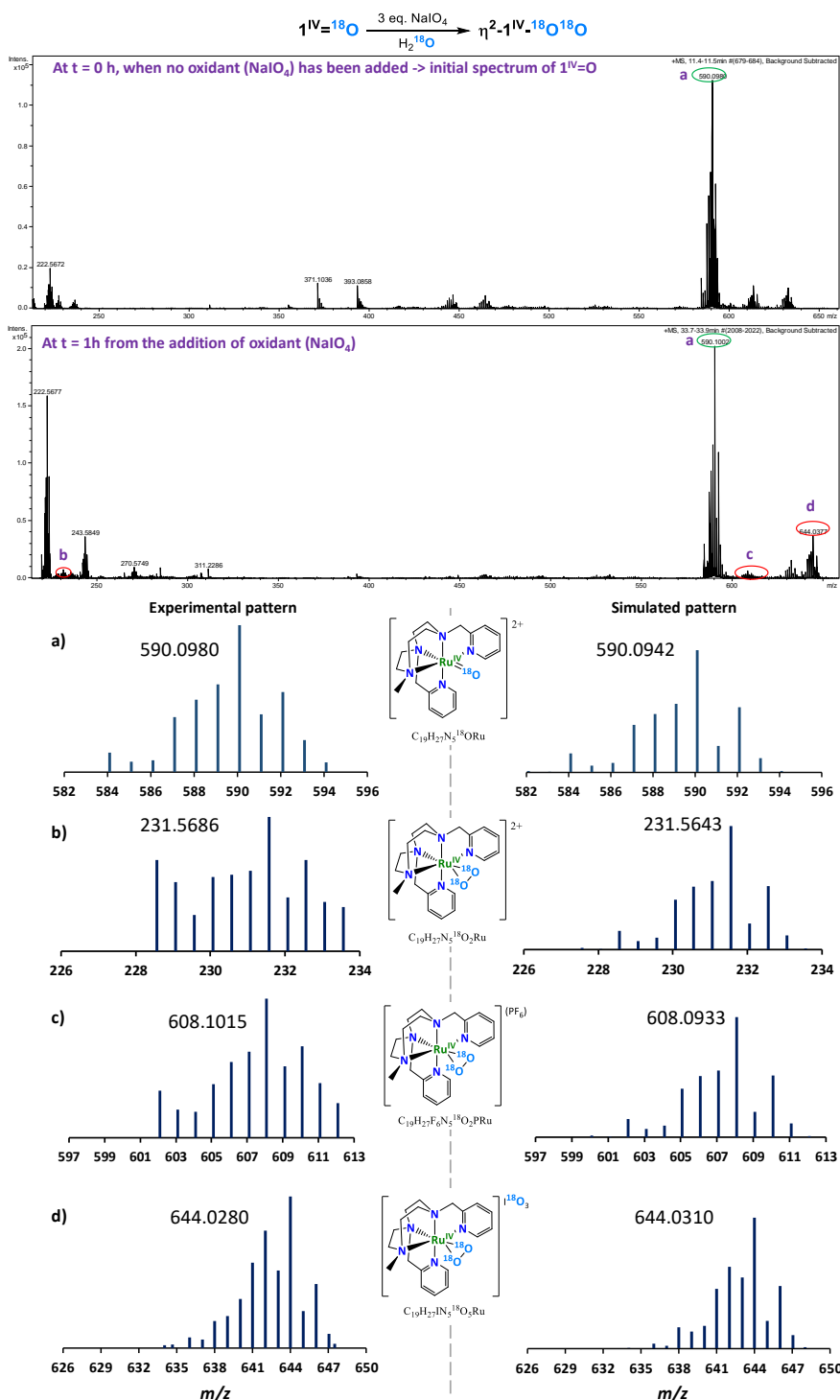
Figure A.IV.31. CSI-HRMS (293 K) monitoring of the reaction kinetics of **1Ru^{IV}=^{18}O** with NaIO$_4$ (3 eq) in H$_2^{18}$O after 60 minutes of reaction time (see the experimental section for further details).

ANNEX
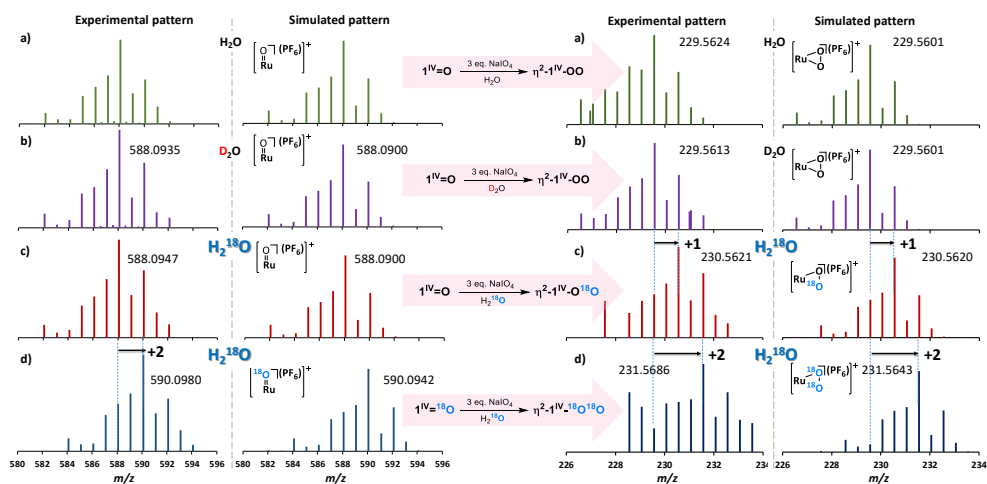
Figure A.IV.32. CSI-HRMS (293 K) of the monocharged [Ru-OO-PF$_6$]$^+$ species of a) **η^2-1Ru^{IV}-OO** generated in MilliQ H$_2$O after addition of NaIO$_4$ (5 eq.) to **1Ru^{IV}=O** (green), b) **η^2-1Ru^{IV}-OO** generated in D$_2$O after addition of NaIO$_4$ (5 eq.) to **1Ru^{IV}=O** (purple), c) **η^2-1Ru^{IV}-^{18}OO** generated in H$_2$^{18}O after addition of NaIO$_4$ (5 eq.) to **1Ru^{IV}=O** (red) and d) **η^2-1Ru^{IV}-^{18}O^{18}O** generated in H$_2$^{18}O after addition of NaIO$_4$ (5 eq.) to **1Ru^{IV}=^{18}O** (blue) (see experimental section for further details).

A.IV.5.4. CSI-HRMS labeling kinetic studies of the formation of $^2\eta$-1^{IV}-OO from 1^{IV}=O in Milli-Q H$_2$O, D$_2$O and H$_2$^{18}O, respectively
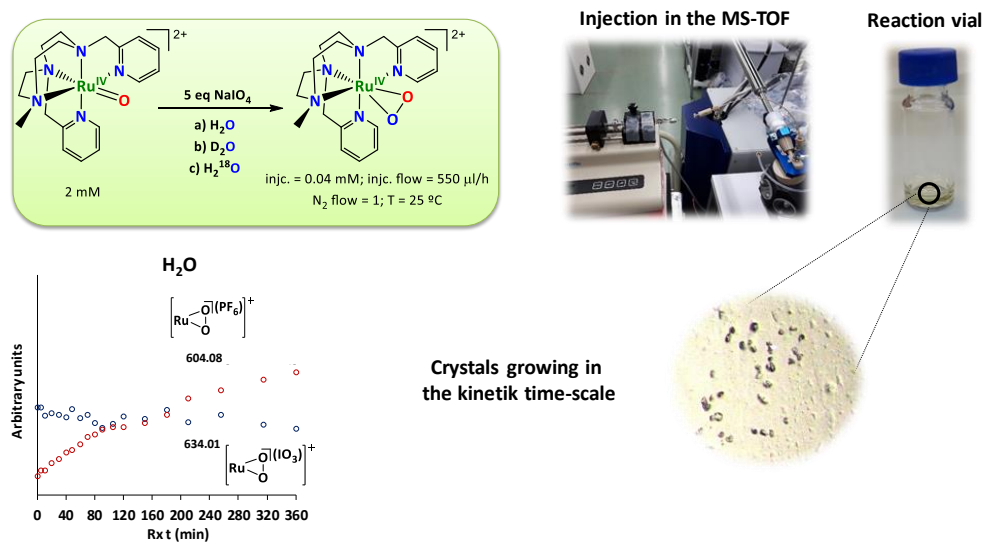
Figure A.IV.33. Reaction conditions, experimental set-up and crystals formed within the reaction time scale during the CSI-HRMS (293 K) monitoring of the reaction kinetics of **1Ru^{IV}=O** with NaIO$_4$ (5 eq) for the formation of **η^2-1Ru^{IV}-OO**.

ANNEX
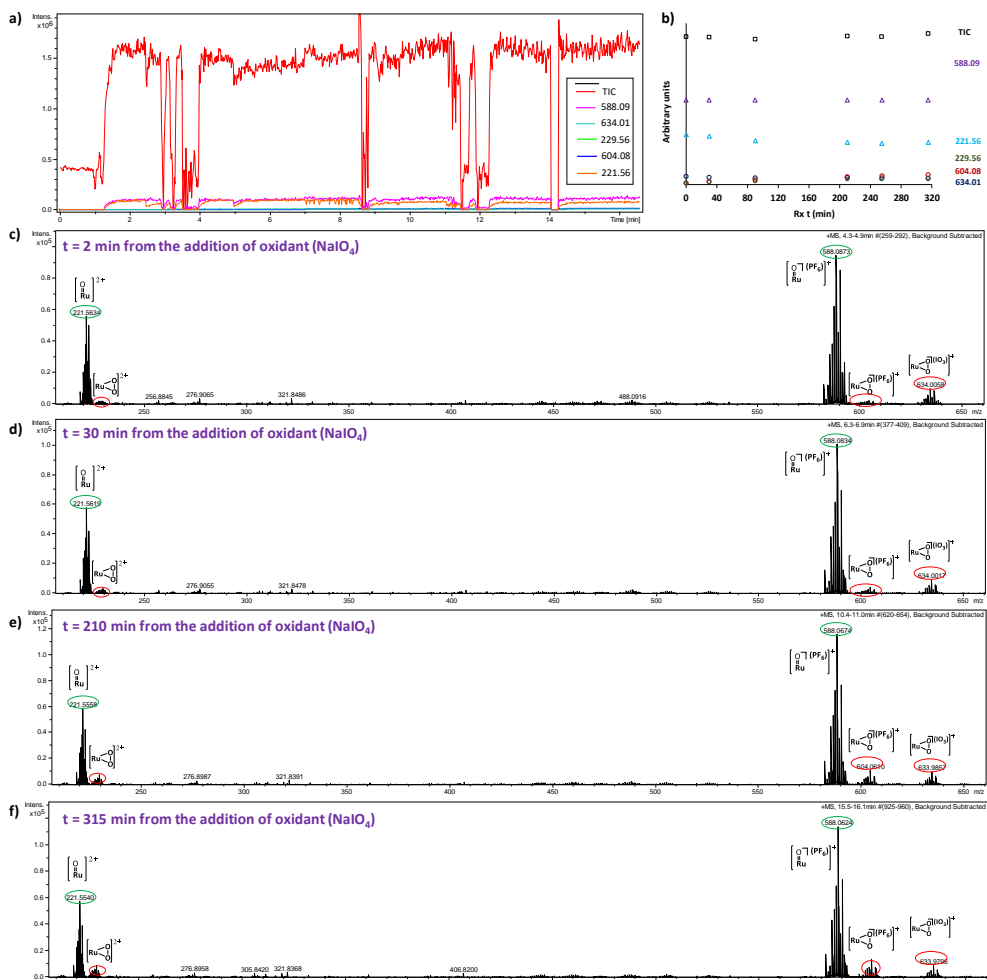
Figure A.IV.34. CSI-HRMS (293 K) monitoring of the reaction kinetics of **1Ru^{IV}=O** with NaIO$_4$ (5 eq) for the formation of **η²-1Ru^{IV}-OO** (2 mM concentration) in D$_2$O. a) and b) Representation of the TIC (Total Ion Counting) together with the other *m/z* monitored traces, showing that the TIC remains constant alons the reaction time and only the reaction species are decreasing or increasing in intensity, respectively. C) to f) Snapshots of the HRMS spectra at increasing rection times after the addition of oxidant (NaIO$_4$) to **1Ru^{IV}=O** showing the variation of intensity of the different species present in solution.
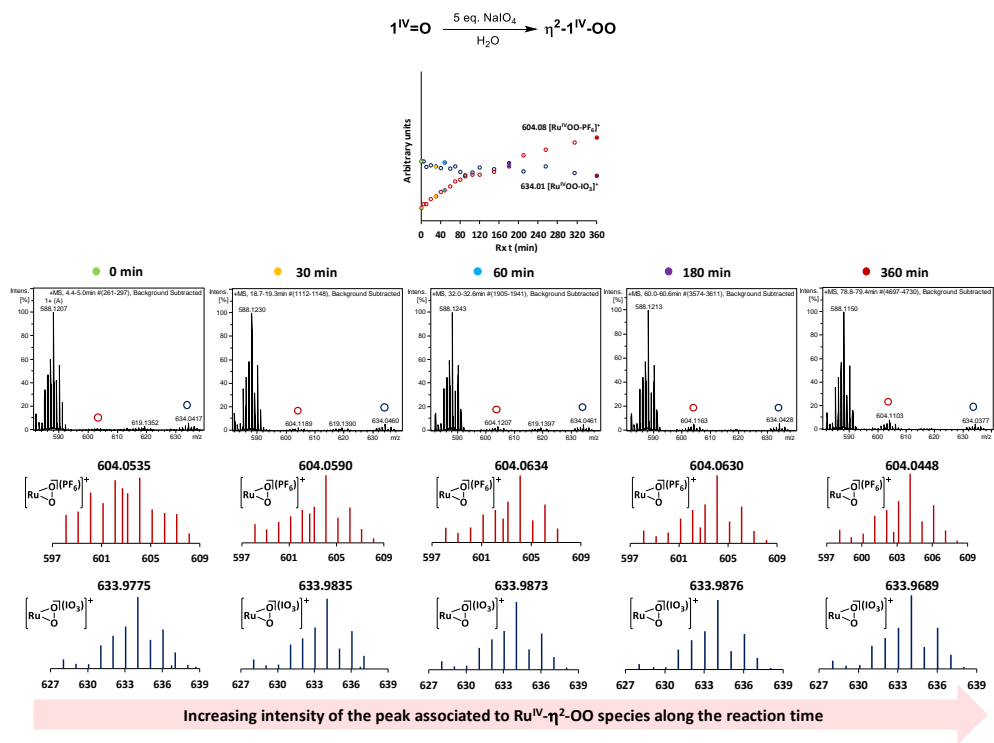
Figure A.IV.35. Snapshots of the CSI-HRMS (293 K) monitoring of the reaction kinetics of **1Ru^{IV}=O** with NaIO$_4$ (5 eq) in H$_2$O. For further details see the experimental section.

ANNEX
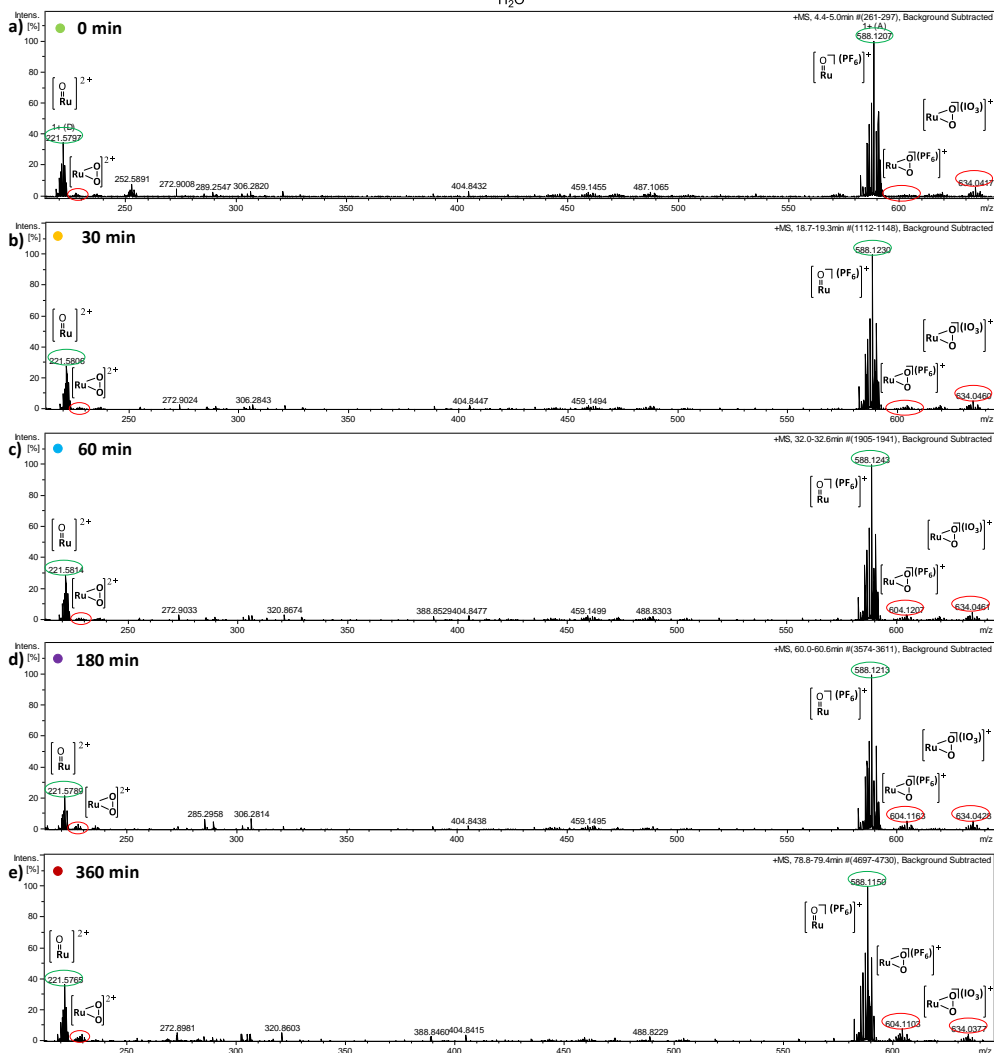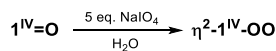
Figure A.IV.36. Snapshots of the full mass spectra of the CSI-HRMS (293 K) monitoring of the reaction kinetics of **1Ru^{IV}=O** with NaIO$_4$ (5 eq) in H$_2$O. For further details see the experimental section.

511

ANNEX
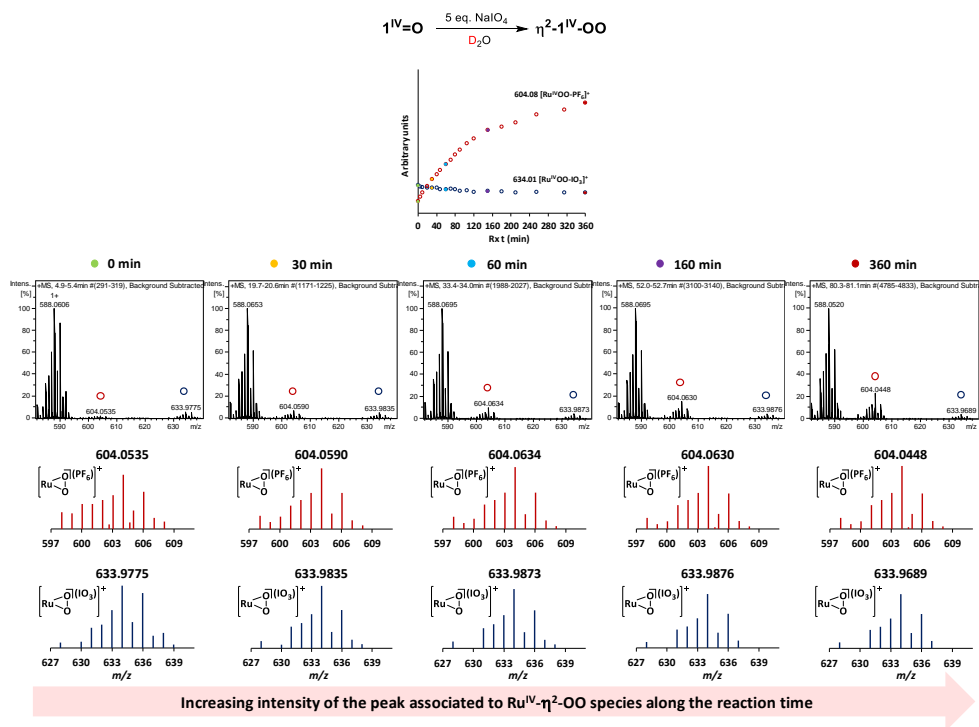
Figure A.IV.37. Snapshots of the CSI-HRMS (293 K) monitoring of the reaction kinetics of **1Ru^{IV}=O** with NaIO$_4$ (5 eq) in D$_2$O. For further details see the experimental section.

ANNEX
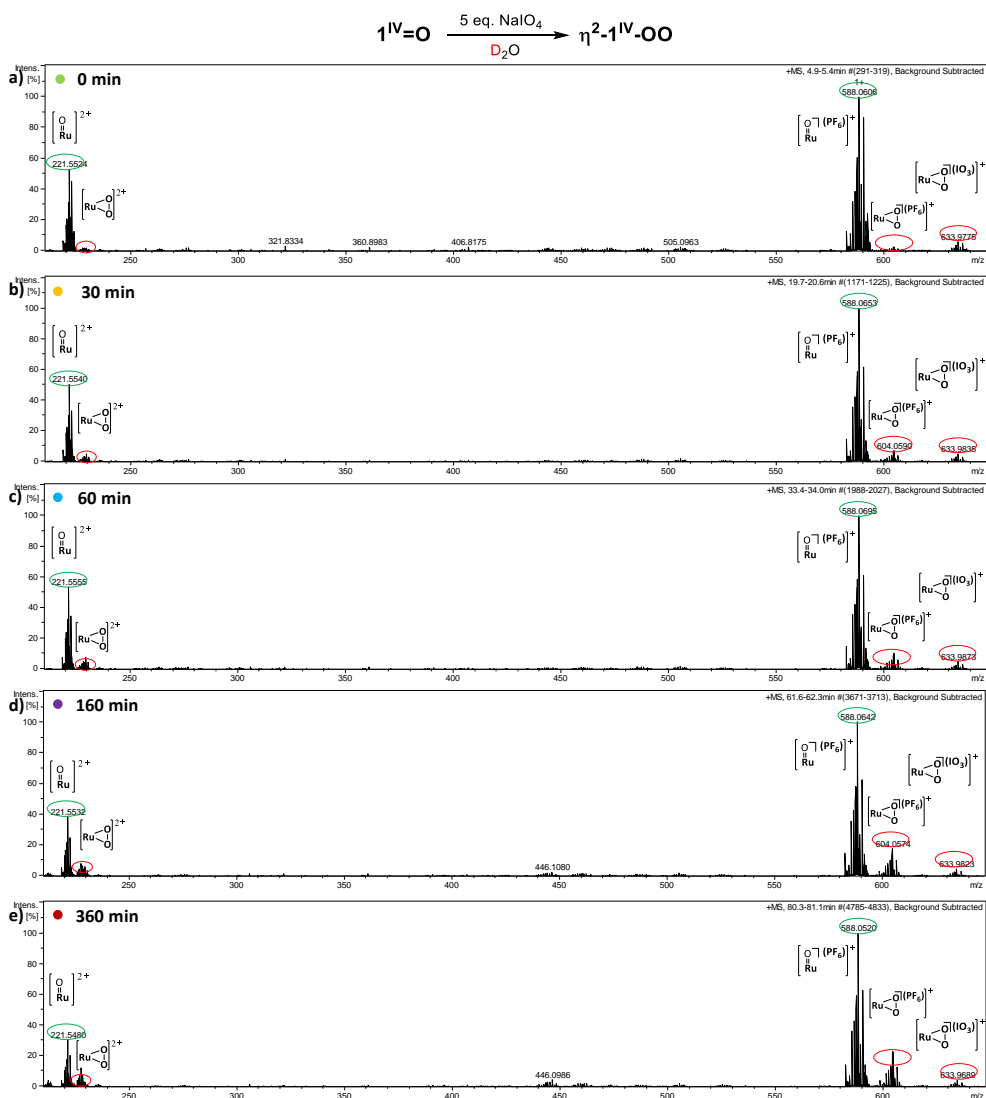
Figure A.IV.38. Snapshots of the full mass spectra of the CSI-HRMS (293 K) monitoring of the reaction kinetics of **1Ru^{IV}=O** with NaIO$_4$ (5 eq) in D$_2$O. For further details see the experimental section.

513

ANNEX
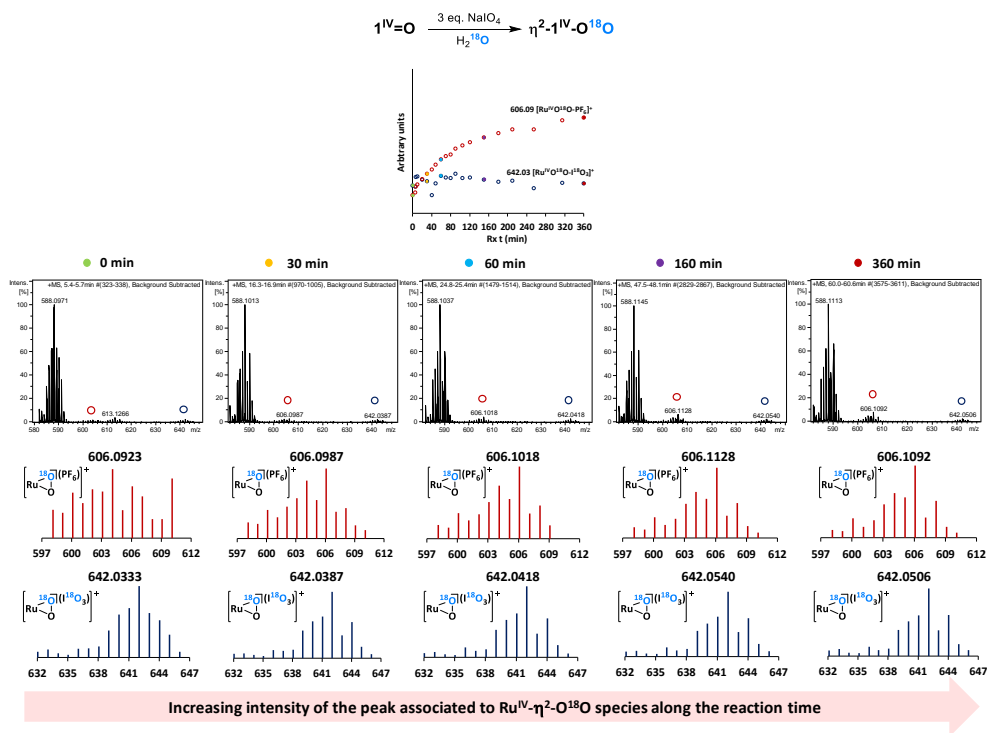
Figure A.IV.39. Snapshots of the CSI-HRMS (293 K) monitoring of the reaction kinetics of **1Ru^{IV}=O** with NaIO$_4$ (5 eq) in H$_2$^{18}O. For further details see the experimental section.

ANNEX
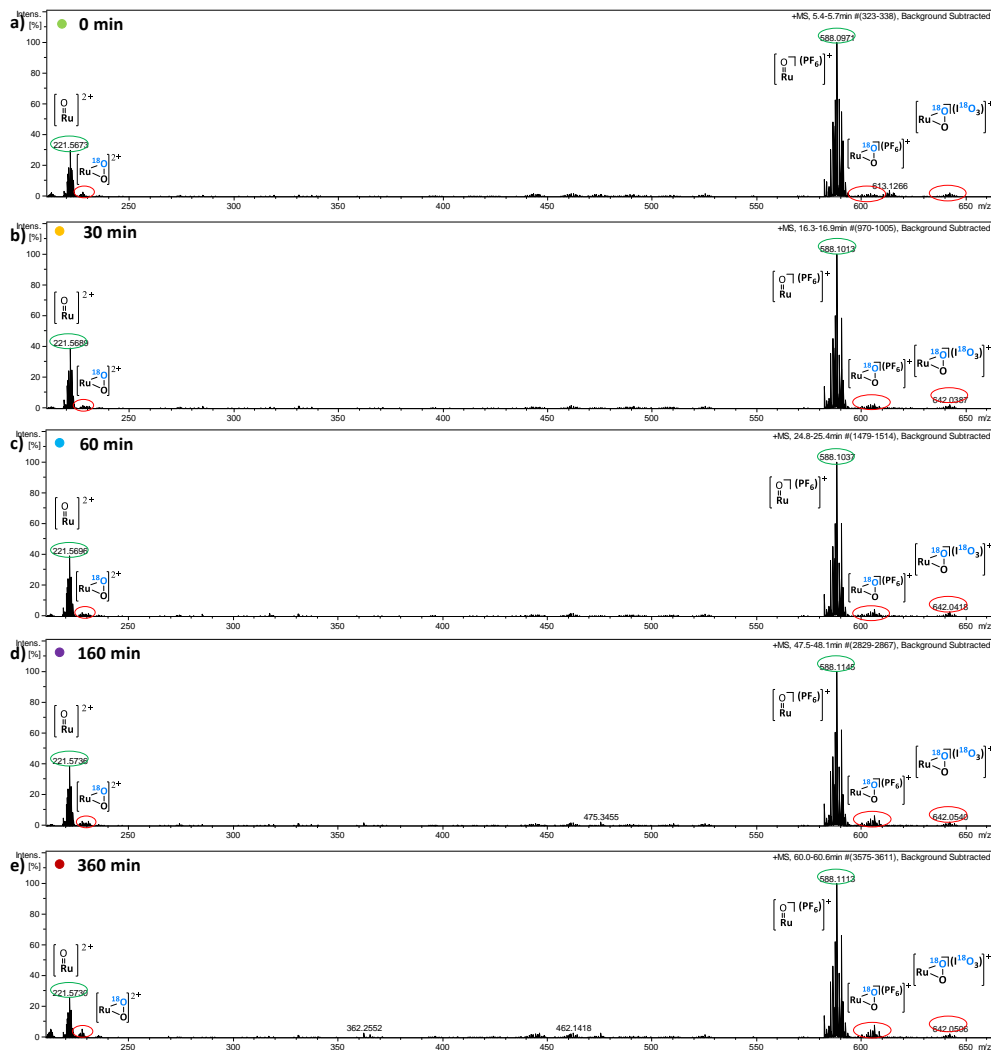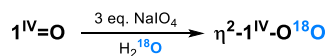
Figure A.IV.40. Snapshots of the full mass spectra of the CSI-HRMS (293 K) monitoring of the reaction kinetics of $1Ru^{IV}=O$ with $NaIO_4$ (5 eq) in $H_2^{18}O$. For further details see the experimental section.

515

ANNEX
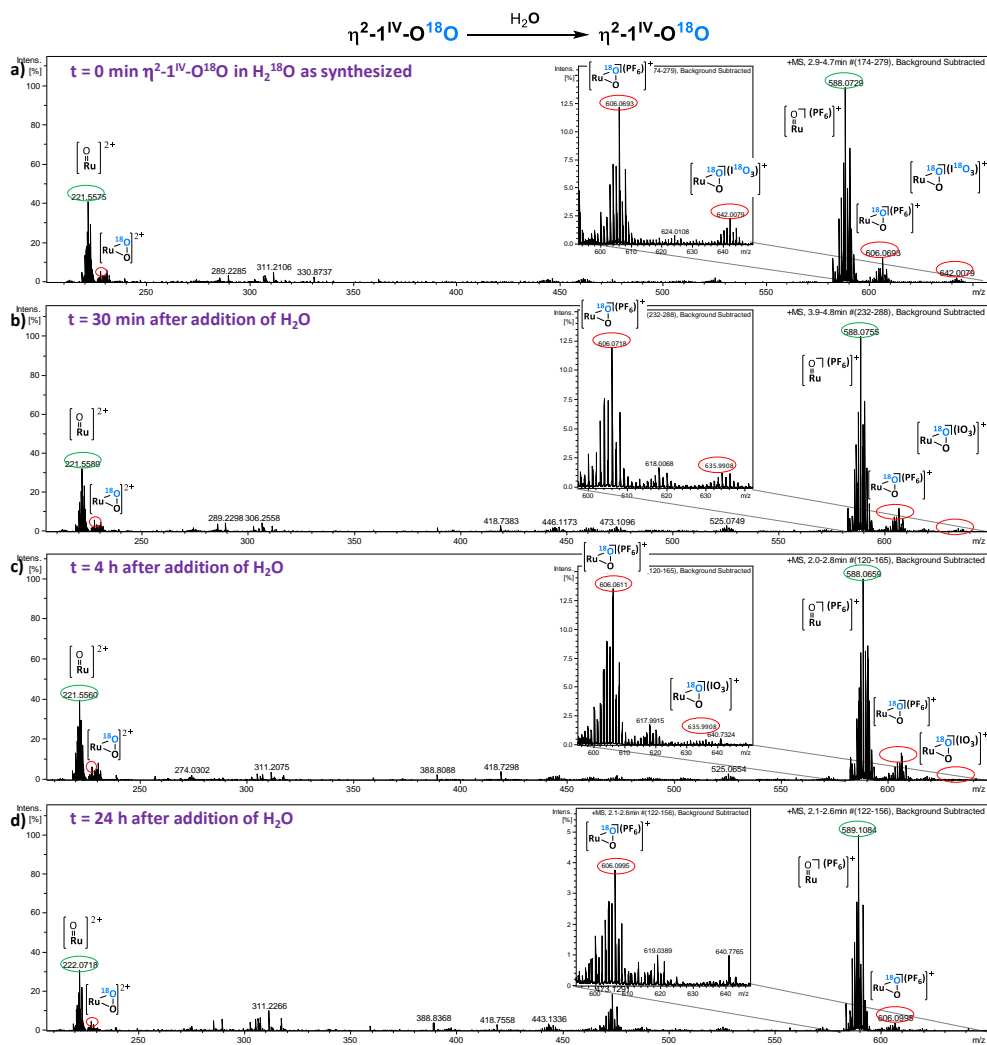
Figure A.IV.41. Snapshots of the full mass spectra of the CSI-HRMS (293 K) monitoring of the exchange of the peroxo moiety of η^2-**1Ru^{IV}-O^{18}O** (generated after the addition of 5 eq. NaIO$_4$ to **1Ru^{IV}=O** in H$_2$^{18}O) after the addition of MilliQ H$_2$O. For further details see the experimental section.

A.IV.6. Mechanistic Studies
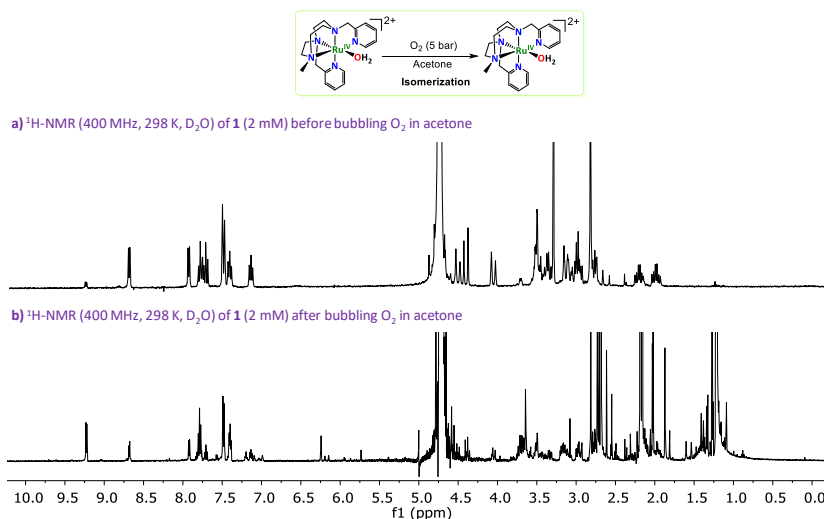
Figure A.IV.42. ^{1}H-NMR (400 MHz, 298 K, D$_2$O) spectra of the reaction of **1Ru^{II}-OH$_2$** with O$_2$ pressure in acetone at rt.
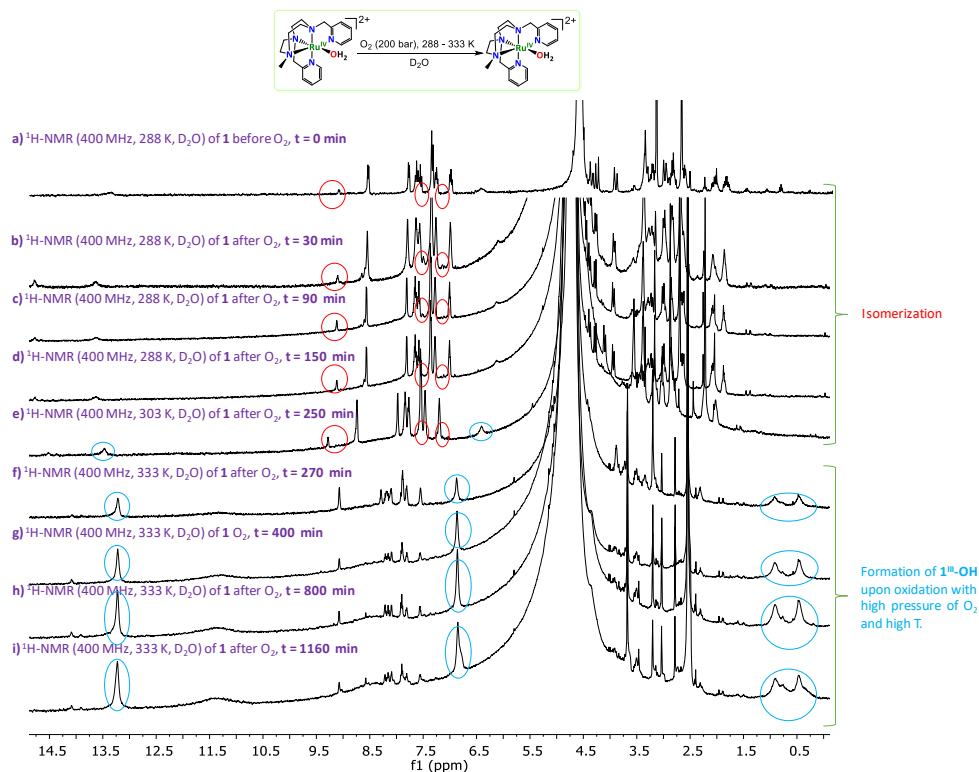
Figure A.IV.43. ^{1}H-NMR (500 MHz, from 288 to 333 K, D$_2$O) spectra of the monitoring of the reaction of **1Ru^{II}-OH$_2$** under a high pressure of O$_2$ (200 bar) in a pressurized NMR using D$_2$O as solvent (see the experimental section for further details).

517

ANNEX
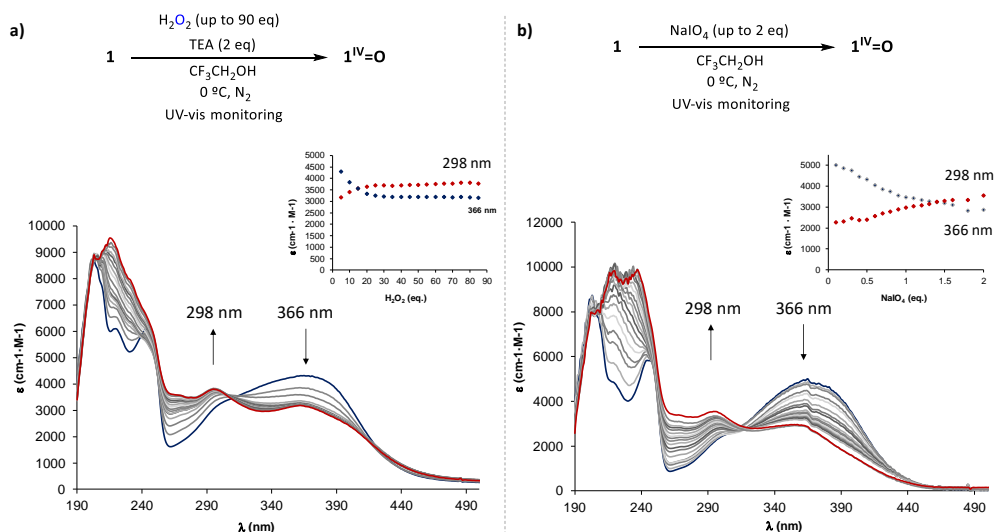
Figure A.IV.44. UV-Vis monitoring of the titration of **1Ru^{II}-OH$_2$** (3 ml of 0.25 mM in trifluoroethanol) at 273 K with a) H$_2$O$_2$ (additions of 9 µl, 5 eq. each) in 2 eq of TEA to basify the media and b) NaIO$_4$ (additions of 5 µl, 0.1 eq. each), generating most likely **1Ru^{IV}=O** in both cases. Inset: ε *versus* NaIO$_4$ equivalents at 249 nm (blue circles) and 266 nm (red triangles). Insets: ε *versus* H$_2$O$_2$ and NaIO$_4$ eq., respectively, at 298 nm (red diamonds) and 366 nm (blue diamonds). The baseline was corrected to 0 by abs. average of the 700 - 1100 nm range. The abs values were corrected taking into account the total volume after each aliquot addition.
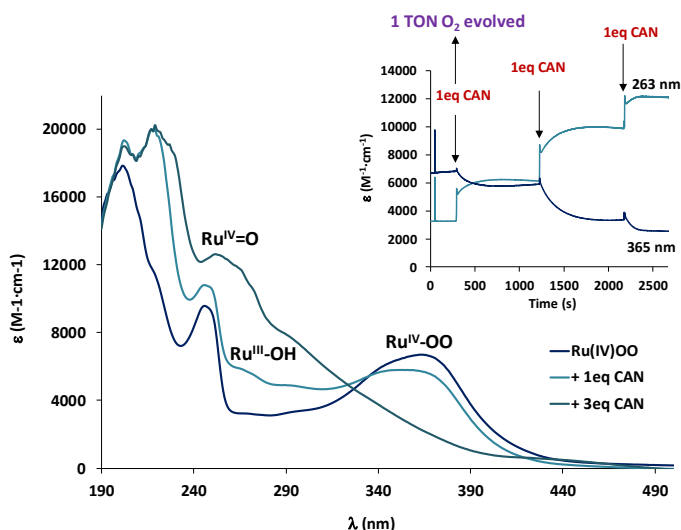
Figure A.IV.45. UV-Vis spectra of **η^2-1Ru^{IV}-OO** (dark blue line) at 0.25 mM concentration measured at 298 K in degassed MilliQ water, as well as the formed Ru(III) species after the subsequent addition of CAN (q and 3 equiv., respectively, light blue lines) with concomitant oxygen release. The inset shows the evolution of the traces at 263 and 365 nm associated with the absorbance of the initial **η^2-1Ru^{IV}-OO** complex. TON O$_2$ have been quantified by manometry and GC-TCD.

ANNEX

A.IV.7. Computational studies

O-O 1.289 Å
Ru-O 2.084 Å

O-O 1.352 Å
Ru-O 2.001 Å

O-O 1.306 Å
Ru-O 2.076 Å

$^1[Ru^{IV}(\eta^1\text{-}O_2)]^{2+}$

$^1[Ru^{IV}(\eta^2\text{-}O_2)]^{2+}$

$^3[Ru^{IV}(\eta^1\text{-}O_2)]^{2+}$

0.2 kcal·mol^{-1}

0 kcal·mol^{-1}

4.3 kcal·mol^{-1}
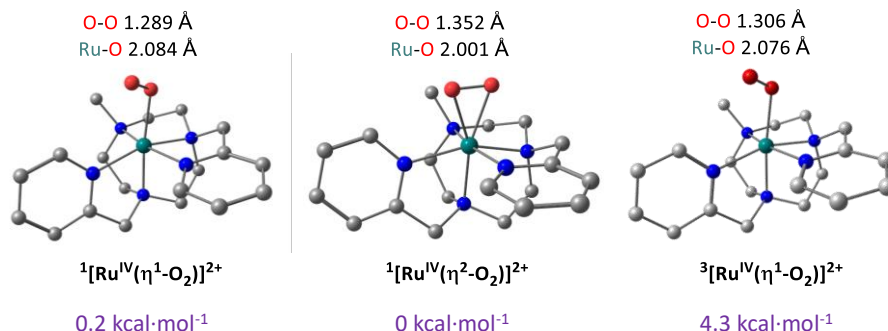
Figure A.IV.46. Optimised geometries for η^1-[Ru^{IV}(OO)(Py$_2^{Me}$tacn)]$^{2+}$ (**$^1[\eta^1\text{-}1Ru^{IV}\text{-}OO]$**), η^2-[Ru^{IV}(OO)(Py$_2^{Me}$tacn)]$^{2+}$ (**$^1[\eta^2\text{-}1Ru^{IV}\text{-}OO]$**) and η^1- [Ru^{IV}(OO)(Py$_2^{Me}$tacn)]$^{2+}$ (**$^3[\eta^1\text{-}1Ru^{IV}\text{-}OO]$**). O-O and Ru-O bond distances are given in Å. Hydrogen atoms have been omitted for clarity. Gibbs energy value differences are reported regarding the lowest in energy intermediate in kcal·mol^{-1}.
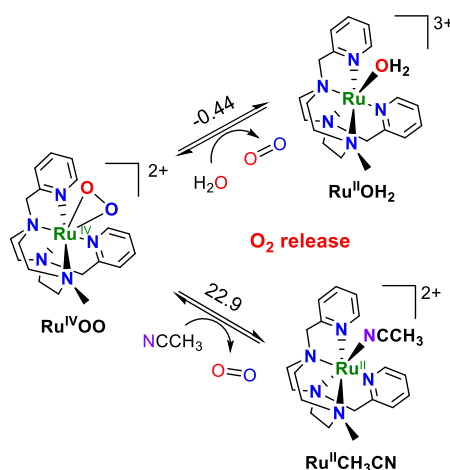
Figure A.IV.47. Thermodynamics for the decay of **η^2-1Ru^{IV}-OO** upon O$_2$ release in water and MeCN. Free energies are reported in kcal·mol^{-1}.

A.IV.8. References

(1) Bjornsson, R.; Delgado-Jaime, M. U.; Lima, F. A.; Sippel, D.; Schlesier, J.; Weyhermüller, T.; Einsle, O.; Neese, F.; DeBeer, S. *Z. Anorg. Allg. Chem.* **2015**, *641*, 65.
(2) Van Kuiken, B. E.; Valiev, M.; Daifuku, S. L.; Bannan, C.; Strader, M. L.; Cho, H.; Huse, N.; Schoenlein, R. W.; Govind, N.; Khalil, M. *J Phys Chem A* **2013**, *117*, 4444.
(3) George, S. J.; Lowery, M. D.; Solomon, E. I.; Cramer, S. P. *J. Am. Chem. Soc.* **1993**, *115*, 2968.

A.V. ANNEX CHAPTER VII

A.V.1. Synthesis and characterization of ligands and complexes
A.V.1.1. ^{1}H-NMR spectroscopic characterization
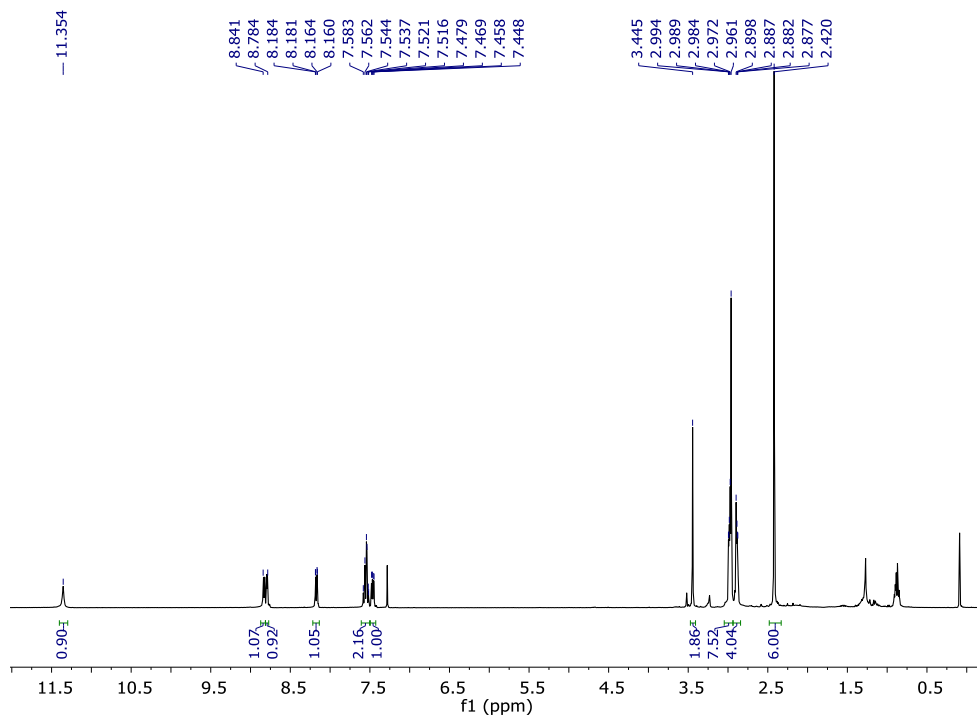
Figure A.V.1. ^{1}H-NMR (CDCl$_3$, 400 MHz, 300 K) spectrum of the H-AQ^{Me2}tacn ligand.

A.V.1.2. CSI-HRMS characterization
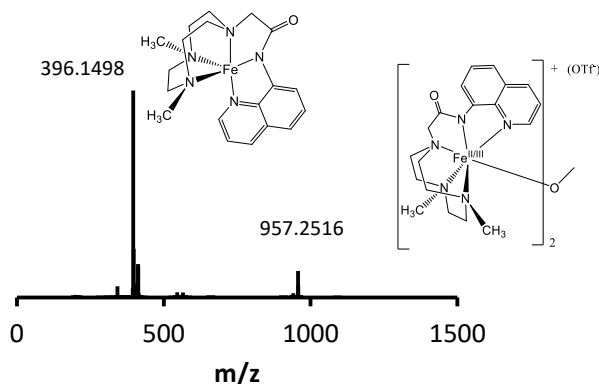
Figure A.V.2. CSI-HRMS (298 K) of complex Fe^{II}(OTf)(AQtacn) (1 mM) dissolved in 2 mL of degassed MilliQ water.

A.V.1.3. UV-Vis spectroscopic characterization
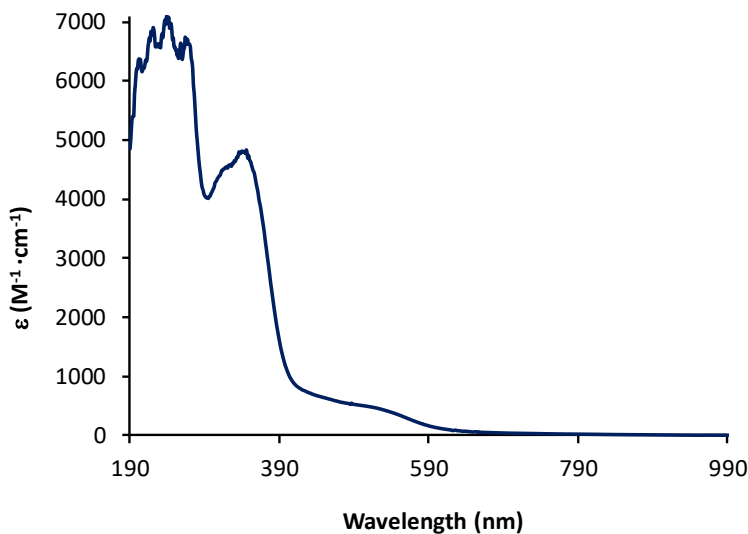
Figure A.V.3. UV-Vis spectrum of complex $Fe^{II}(OTf)(AQ^{Me2}tacn)$, 1 mL solution of 1 mM concentration of **1** in degassed water at 298K, in a 0.5 cm path UV-Vis cell.

A.V.2. Gas chromatography identification and quantification of gases

Dr. Zoel Codolà performed the following experiments.
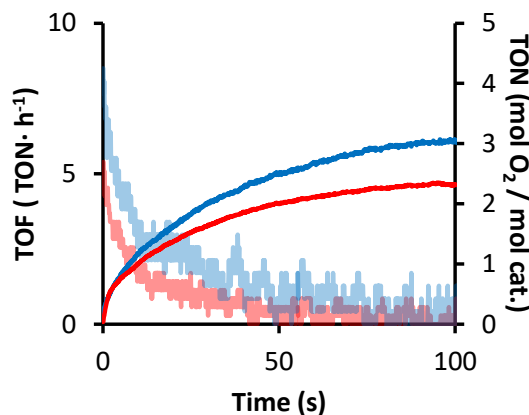
Figure A.V.4. Comparison of TON (right axis) and TOF (left axis) evolution between two samples containing 50μM (blue) and 100μM (red) of complex $Fe^{II}(OTf)(AQtacn)$. To a vial (total head space = 24.5mL) containing an aqueous solution of Ce^{IV} (18.5mL, 125mM CAN), the catalyst (0.5mL) was injected through a septum and the vial was monitored by a pressure sensor at 298K.

ANNEX
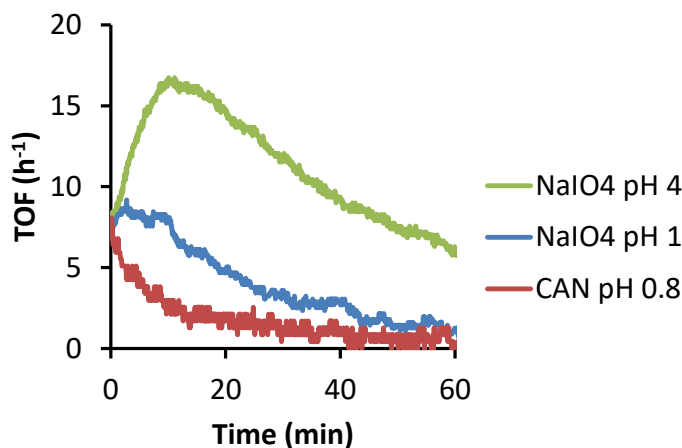
Figure A.V.5. Initial TOF profiles observed when $Fe^{II}(OTf)(AQtacn)$ (100 µM) was injected to a solution of $NaIO_4$ (250mM) at pH 4 (no additives), at pH 1 (with $HClO_4$) or to a solution of CAN (125mM) at pH 0.8.

A.V.3. Characterization of WO intermediates

A.V.3.1. UV-vis spectroscopic characterization
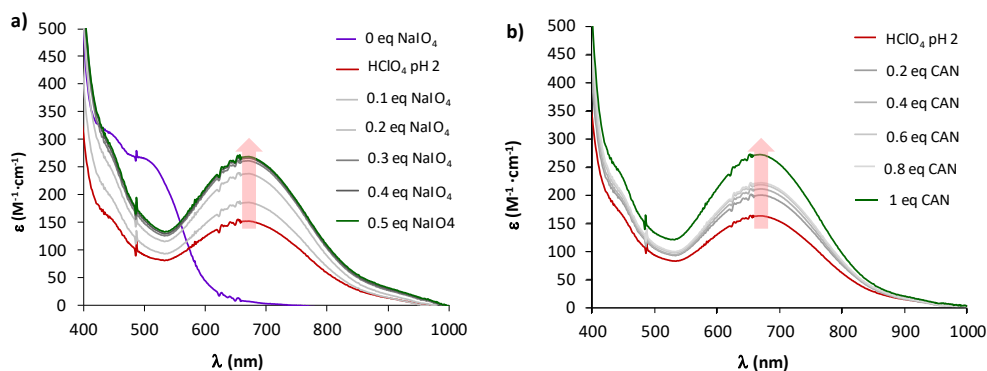
Figure A.V.6. a) UV-Vis titration of **1Fe** (1 ml of 1 mM, **1Fe^{II}**) at 298 K at pH 2 with $NaIO_4$ (additions of 10 µl, 0.1 eq. each) to generate the **1Fe^{III}-OH$_2$** species. b) ε *versus* $NaIO_4$ equivalents 670 nm (red circles). The base line was corrected to 0 by abs. average of the 700 - 1100 nm range. The abs values were corrected taking into account the total volume after each aliquot addition.

ANNEX
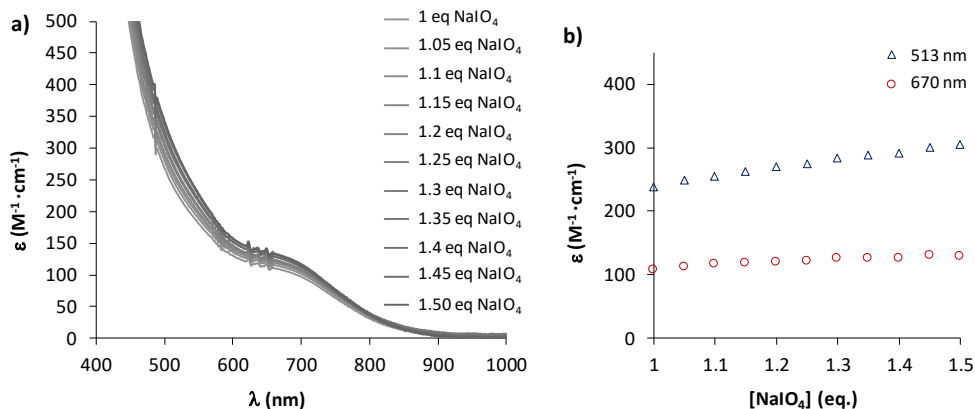
Figure A.V.7. a) UV-Vis titration of **1Fe** (1 ml of 1 mM, **1Fe^{II}**) at 298 K at pH 9 with NaIO$_4$ (additions of 5 μl, 0.05 eq. each) to generate the **1Fe^{II}-O-1Fe^{III}** species. b) ε *versus* NaIO$_4$ equivalents at 513 nm (blue triangles) and 670 nm (red circles). The base line was corrected to 0 by abs. average of the 700 - 1100 nm range. The abs values were corrected taking into account the total volume after each aliquot addition.

A.V.3.2. CSI-HRMS characterization
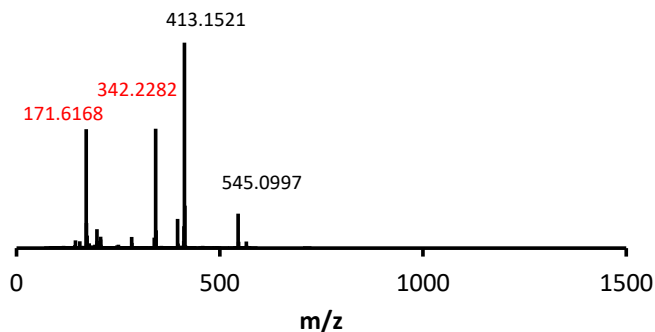
Figure A.V.8. CSI-HRMS spectrum after the addition of 1 eq of **CAN** to [Fe^{II}(OTf)(AQ^{Me2}tacn)] (1mM, degassed MilliQ H$_2$O).
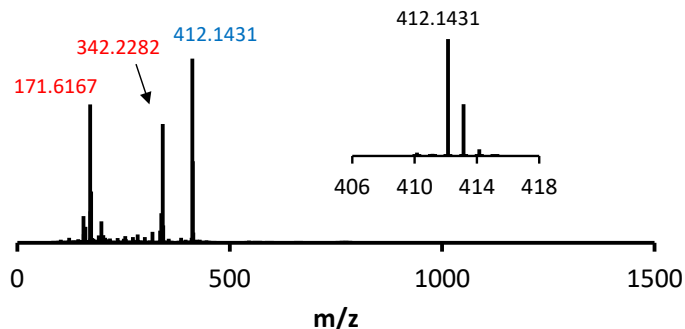
Figure A.V.9. CSI-HRMS spectrum after the addition of 5 eq of **CAN** to [Fe^{II}(OTf)(AQ^{Me2}tacn)] (1mM, degassed MilliQ H$_2$O).
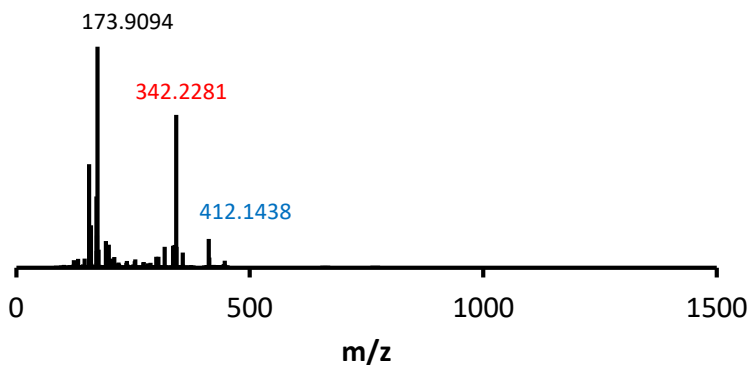
Figure A.V.10. CSI-HRMS spectrum after the addition of 10 eq of **CAN** to [Fe^{II}(OTf)(AQ^{Me2}tacn)] (1mM, degassed MilliQ H$_2$O).

Table A.V.1. Proposal structures observed in the CSI-HRMS after the addition of CAN.

m/z found	m/z calculated	Structure
171.6167	C$_{19}$H$_{28}$N$_5$O 171.6180	
342.2294	C$_{19}$H$_{28}$N$_5$O 342.2288	
412.1431	C$_{19}$H$_{26}$FeN$_5$O$_2$ 412.1436	
413.1517	C$_{19}$H$_{27}$FeN$_5$O$_2$ 413.1509	
545.1079	C$_{20}$H$_{26}$FeN$_5$O$_4$F$_3$S 546.1085	

ANNEX
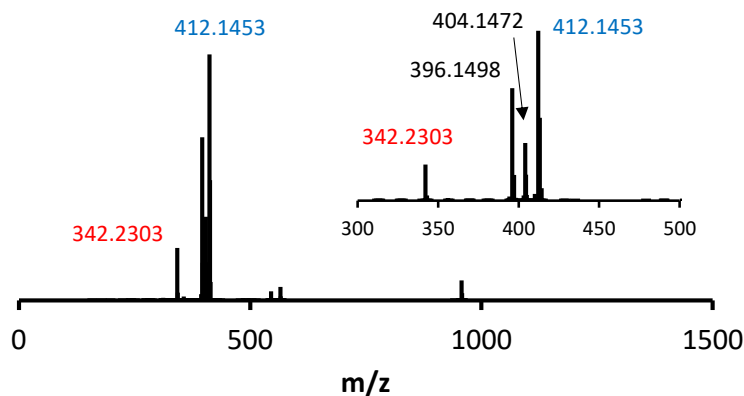
Figure A.V.11. CSI-HRMS spectrum after the addition of 1 eq of **NaIO₄** to $Fe^{II}(OTf)(AQtacn)$ (1mM, degassed MilliQ H_2O).
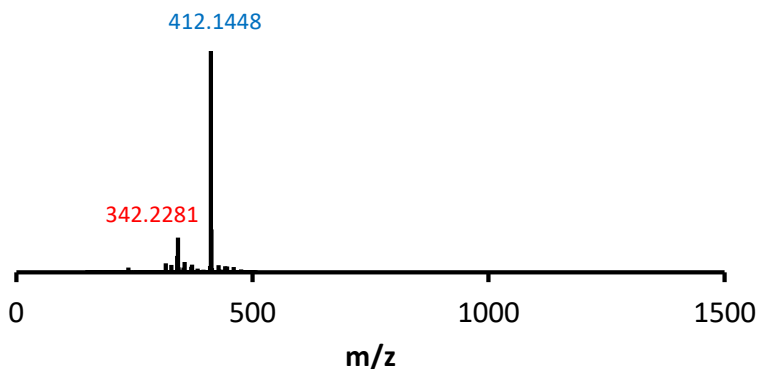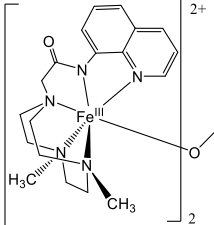
Figure A.V.12. CSI-HRMS spectrum after the addition of 20 eq of **NaIO₄** to $Fe^{II}(OTf)(AQtacn)$ (0.5mM, degassed MilliQ H_2O).

Table A.V.2. Possible structures observed in the CSI-HRMS after the addition of $NaIO_4$.

m/z found	m/z calculated	Structure
404.1472	$C_{38}H_{52}Fe_2N_{10}O_3$ 404.1462	

ANNEX

A.V.3.3. Computational studies

A.V.3.3.1. Important intermediate structures
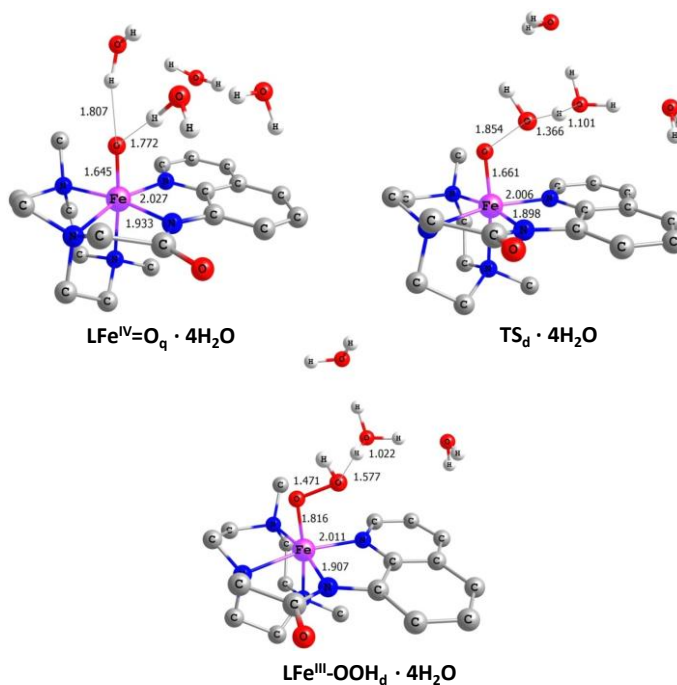
Figure A.V.13. Optimized geometries of the lowest energy species involved in the O-O bond formation mechanism performed by $[Fe^{IV}(AQ^{Me2}tacn)\cdot(O)]^{2+}$, with the most relevant bond distances (Å). Hydrogen atoms of the $AQ^{Me2}tacn$ ligand are omitted for clarity.

A.VI. ANNEX CHAPTER VIII

A.VI.1. In-house developed parallel photoreactor

Light source: The reactions were performed using Royal-Blue ($\lambda = 447 \pm 20$ nm) LUXEON Rebel ES LED, mounted on a 10mm Square Saber - 1030 mW @ 700mA (Datasheet: https://www.luxeonstar.com/assets/downloads/ds68.pdf) as a light source.

Temperature Control: Reaction temperature was controlled by a high precision thermoregulation Hubber K6 cryostat. Likewise, to guarantee a stable irradiation the temperature of the LEDs was also controlled and set up at 22 ºC.

Figure A.VI.1. In-house developed parallel photoreactor.

A.VI.2. Synthesis of complexes and characterization

A.VI.2.1. Synthesis of 1-(p-toluensulfonyl)-1,4,7-triazacyclononane, tacnmt.

527
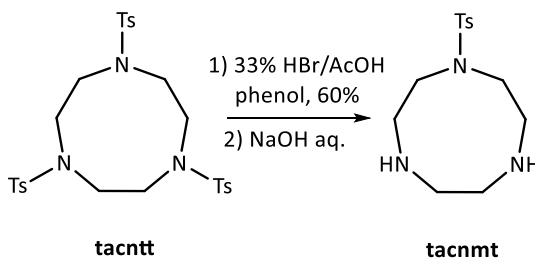
ANNEX

1-(p-toluensulfonyl)-1,4,7-triazacyclononane, tacnmt. tacntt (24.6 g, 41.6 mmol) and phenol (35.2 g, 374 mmol) were mixed in 500 mL flask. A solution of HBr in acetic acid (33%, 380 mL) was added with extreme care as an important evolution of $HBr_{(g)}$ takes place. The mixture was gently heated with stirring to 90ºC which caused the complete dissolution of all the starting reactives giving rise to the formation of a dark solution. A colorless precipitate of 1-(p-toluensulfonyl)-1,4,7-triazcyclononane·2HBr appeared within 2-4 h. After heating for 36 h, the misture was cooled to room temperature and filtered. The solid was washed with diethyl ether (125 mL) and then dissolved in aqueous NaOH 1M (320 mL). The resultant pink aqueous mixture was then extracted with CH_2Cl_2 (3x190 mL) the organic extracts dried with anhydrous $MgSO_4$, filtered and evaporated under reduced pressure. Drying the resultant oil under vacuum afforded 9.88 g the pure product (36.9 mmol, 84 %). ^{1}H-NMR (CDCl$_3$, 400 MHz, 300K) δ, ppm: 7.70 (d, J=8.2 Hz, 2H, Ar**H**), 7.34 (d, J= 8.2 Hz, 2H, Ar**H**), 3.23-3.18 (m, 4H, TsN-C**H$_2$**-CH$_2$-NH), 3.12-3.09 (m, 4H, TsN-CH$_2$-C**H$_2$**-NH), 2.90 (s, 4H, HN-C**H$_2$**-C**H$_2$**-NH), 2.44 (s, 3H, Ar-C**H$_3$**), 1.85 (s, 2H, NH).

A.VI.2.2. Synthesis and characterization of 1,4-di(picolyl)-7-(p-toluenesulfonyl)-1,4,7-triazacyclononane, Py$_2$tacnmt.

tacnmt   Na$_2$CO$_3$, TBABr   CH$_3$CN, reflux   **Py$_2$tacnmt**
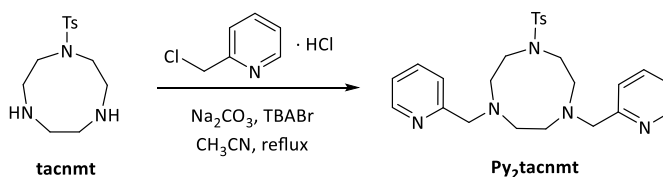
1,4-di(picolyl)-7-(p-toluenesulfonyl)-1,4,7-triazacyclononane, Py$_2$tacnmt. 2-Pycolyl chloride hydrochloride (1.16 g, 7.70 mmol), tacnmt (1 g, 3.53 mmol) and anhydrous acetonitrile (40 mL) were mixed in a 100 mL flask. Na$_2$CO$_3$ (2.05 g) and tetrabutylammonium bromide, TBABr (80 mg) were added directly as solids and the resulting mixture was heated at reflux under N$_2$ for 22 hours. After cooling to room temperature, the resulting orange mixture was filtered and the filter cake was washed with CH$_2$Cl$_2$. The combined filtrates were evaporated under reduce pressure. To the

ANNEX

resulting residue, 2 M NaOH (15 mL) was added and the mixture was extracted with CH_2Cl_2 (4 x 40 mL). The combined organic layers were dried over $MgSO_4$ and the solvent was removed under reduced pressure. The resulting residue was dissolved in the minimum amount of CH_2Cl_2 and Et_2O was added to precipitate the impurities. The mixture was filtered and the solvent from the orange filtrates was removed under reduced pressure to yield 1.54 g of a colorless solid (3.31 mmol, 94 %). ^{1}H-NMR (CDCl$_3$, 300 MHz, 300K) δ, ppm: 8.50 (d, J = 4.8 Hz, 2H, **H$_2$** of py), 7.66-7.60 (m, 4H, **H$_{Ts}$** and **H$_4$** of py), 7.47 (d, J = 7.8 Hz, 2H, **H$_{Ts}$**), 7.26 (d, 2H, J=8.4 Hz, **H$_5$** of py), 7.15-7.11 (m, 2H, **H$_3$** of py), 3.86 (s, 4H, **CH$_2$**-py), 3.22 (m, 4H, N-C**H$_2$**-CH$_2$), 3.12 (m, 4H, N-C**H$_2$**-CH$_2$), 2.79 (s, 4H, N-C**H$_2$**-CH$_2$), 2.40 (s, 3H, **CH$_3$**). ^{13}C-NMR (CDCl$_3$, 300 MHz, 300K) δ, ppm: 160, 149, 142.99, 136.40, 135.94, 129.60, 127.12, 123.23, 121.94, 63.84, 55.85, 55.79, 50.91, 21.47. ESI-MS (m/z): 466.2 [M+H]$^+$. Anal. Calcd for $C_{25}H_{31}N_5O_2S \cdot 1/2H_2O$: C, 63.27; H, 6.80; N, 14.76 %. Found: C, 63.47; H, 6.68; N, 13.91%.
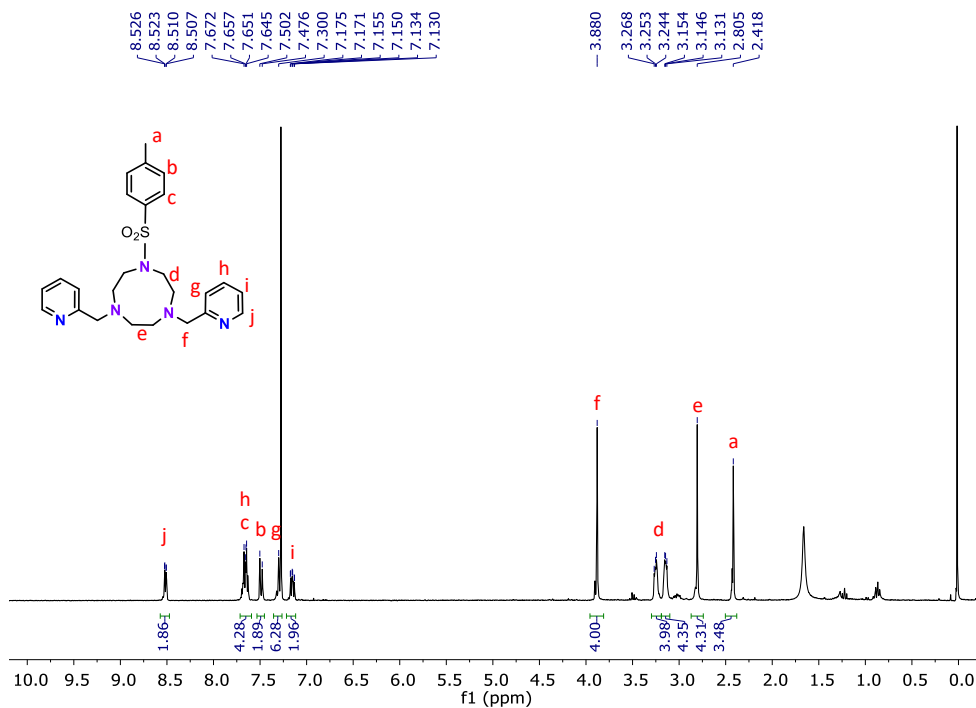
Figure A.VI.2. ^{1}H-NMR spectra (400 MHz, CD$_3$Cl) of the Py$_2$^{Ts}tacn ligand at 298 K.

ANNEX

A.VI.2.3. Synthesis and characterization of [Co(OTf)(Py₂tacnmt)](OTf), (1).

[Co(OTf)(Py₂tacnmt)](OTf), (1Co). In a glovebox, a solution of $Co(OTf)_2(MeCN)_2$ (236mg, 0.537 mmol) in anhydrous THF (1 mL) was added dropwise to a vigorously stirred solution of Py₂tacnmt (250 mg, 0.537 mmol) in THF (1 mL). After few minutes, the solution become cloudy and a pale pink precipitate appeared. After stirring overnight, the solution was filtered off and the resulting solid dried under vacuum. This solid was dissolved in CH_2Cl_2 with a few drops of CH_3CN and the slow diffusion of diethyl ether into this solution produced 355 mg of pink crystals (0.432 mmol, 83.4%). ^{1}H-NMR (CD₃CN, 400 MHz, 298K) δ, ppm: 55.24, 3.69,-9.24. Anal. Calcd for $C_{27}H_{31}F_6CoN_5O_8S_3$: C, 39.42 ; N, 8.51; H, 3.80 %. Found: C, 39.23; N, 8.56 ; H, 3.68 %. ESI-MS (m/z): 672.2 [M - OTf]$^+$, 261.5 [M-2OTf]$^{2+}$.
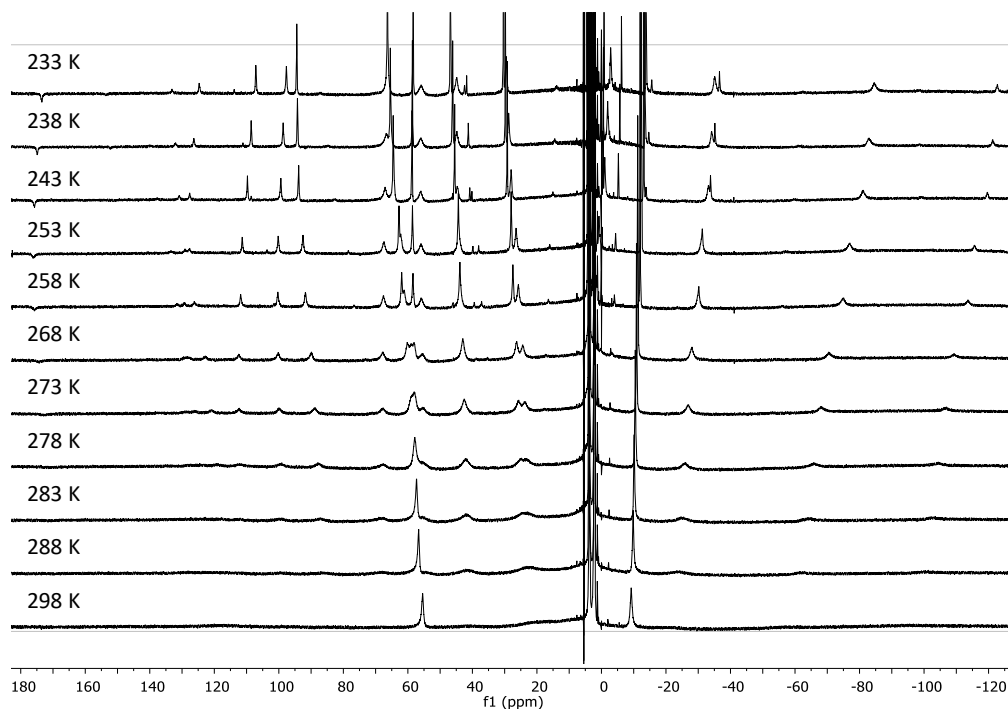
Figure A.VI.3. ^{1}H-NMR spectra (500 MHz, CD₃CN) of complex **1Co** at from 298 to 233 K.

ANNEX

Photoredox catalysts [Ir(ppy)$_2$(bpy)]PF$_6$ (**PS$_{Ir}$**) and [Cu(batocuproine)(Xantphos)]PF$_6$ (**PS$_{Cu}$**) were synthesized accordingly to the reported procedures and the characterization is also in agreement with the previously reported.[1,2]

A.VI.3. Synthesis of substrates

-Synthesis of 1-Phenylpent-4-en-1-one (9ah)
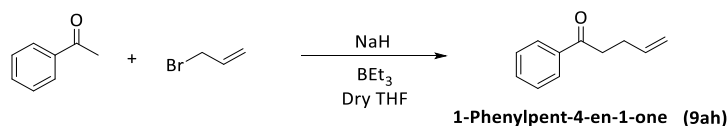
An oven-dried two-neck round-bottomed flask equipped with a stirring bar and a dropping funnel and connected to a nitrogen inlet was charged with sodium hydride (2.11 g, 52.8 mmol, 1.2 eq.) and anhydrous THF (100 mL). Then a solution of acetophenone (5.2 mL, 44 mmol, 1.0 eq.) in 20 mL of dry THF was added over the grey suspension during 20 min at 0ºC under nitrogen atmosphere. The yellow suspension formed was stirred at room temperature for 30 min and BEt$_3$ (56 mL 1M in THF, 56 mmol, 1.2 eq.) was added dropwise for 20 min. The resulting yellow solution was further stirred for 30 min and allyl bromide (5.8 mL, 68 mmol, 1.5 eq.) was added dropwise for 15 min and the resulting solution was left stirring overnight at room temperature. The reaction mixture was quenched by the addition of 50 mL of 1:1 mixture of 30 % NaOH and 30 % H$_2$O$_2$ at 0 ºC over 30 min and finally diluted with H$_2$O (100 mL). The organic layer was extracted, diluted with Et$_2$O (100 mL) and washed with H$_2$O (2 x 50 mL). All aqueous phases were combined and extracted with CH$_2$Cl$_2$ (3 x 40mL). The combined organic layers were dried over MgSO$_4$ and the solvent was removed under reduced pressure. The resulting oil product was purified by column chromatography in silica gel using hexane:AcOEt (30:1) as eluent that gave the desired product as a colorless oil (65 % yield). ^{1}H-NMR (CDCl$_3$, 300 MHz, 300 K) δ, ppm: 8.00-7.97 (m, 2H, **H$_{arom}$**), 7.61-7.55 (m, 1H, **H$_{arom}$**), 7.51-7.46 (m, 2H, **H$_{arom}$**), 5.97-5.86 (m, 1H, C**H**=CH$_2$), 5.13-5.02 (m, 2H, CH=C**H$_2$**), 3.10 (t, 2H, J = 7.2 Hz), 2.51 (q, 2H, J = 6.6 Hz).

ANNEX

-**Synthesis of 1-Phenyl-4-pentyn-1-one (9ai)**
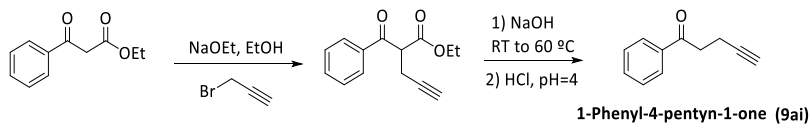
In a mixture of ethyl benzoylacetate (5.76 g, 30 mmol, 1.0 eq.) in a 50 mL of anhydrous ethanol were added 2.25 g of NaOEt (33 mmol, 1.1 eq.). After stirring the mixture for 15 min, propargyl bromide (3.76 mL, 80 % wt solution in toluene, 33 mmol, 1.1 eq.) was added dropwise at 0 ºC within 30 minutes. The resulting orange solution was stirred at room temperature for 1 day. After that, the sodium bromide was filtered off, and the solvent removed under vacuum in a rotary evaporator. To the residue was added 24 mL (60 mmol) of 10 % aq. NaOH, and the mixture was stirred 3 hour at room temperature and at 60 ºC for another 3 hours. Then, the crude mixture was cooled to ambient temperature, acidified with conc. HCl to a pH of 4 and extracted with CH_2Cl_2 (3x 50 mL). The combined organic layers were dried over $MgSO_4$ and the solvent were removed under reduced pressure. The resulting oil product was purified by silica column cromatography (Hexane:AcOEt 30:1) to afford the desired alkyne product (75 % yield) as a pale yellow solid. 1H-NMR (CDCl$_3$, 300 MHz, 300 K) δ, ppm: 8.01-7.98 (m, 2H, **H$_{arom}$**), 7.62-7.57 (m, 1H, **H$_{arom}$**), 7.52-7.46 (m, 2H, **H$_{arom}$**), 3.27 (t, 2H, J = 7.1 Hz, **CH$_2$**CH$_2$C≡CH), 2.68 (td, 2H, J = 7.1 Hz, J' = 2.7 Hz, CH$_2$**CH$_2$**C≡CH), 2.00 (t, 1H, J = 2.7 Hz, C≡C**H**).

-**Synthesis of 3-(pyridin-2-yl)propanal (11f)**
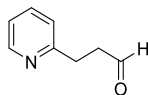
3-(pyridin-2-yl)propanal (11f) was prepared by Swern oxidation of the corresponding comercially available alcohol according to previously reported procedure.[3] ^{1}H-NMR (CDCl$_3$, 400 MHz, 300 K) δ, ppm: 9.87 (s, 1H), 8.51 (d, J = 3.9 Hz, 1H), 7.59 (td, J = 7.7, 1.9 Hz, 1H), 7.19 (d, J = 7.8 Hz, 1H), 7.12 (dd, J = 7.2, 4

Hz, 1H), 3.14 (t, $J = 7.1$ Hz, 3H), 2.95 (tt, $J = 6.4$, 0.6 Hz, 2H). $^{13}C\{^{1}H\}$-NMR (CDCl$_3$, 100.6 MHz, 300 K) δ, ppm: 201.7, 159.9, 149.4, 136.7, 123.2, 121.5, 42.8, 30,5. MS (GC): 135.1 [M].

-Synthesis of phenyl(2-phenylcyclopropyl)methanone (9aj)
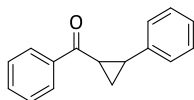
Phenyl(2-phenylcyclopropyl)methanone (9aj) was prepared according to previously reported procedure through a Corey-Chaykovsky reaction.[4] ^{1}H-NMR (CDCl$_3$, 300 MHz, 300 K) δ, ppm: 7.92 (d, $J = 7.7$ Hz, 2H), 7.48-7.35 (m, 3H), 7.26-7.09 (m, 5H), 2.83 (ddd, $J = 8.0$, 4.2, 4.0 Hz, 1H), 2.63 (m, $J = 6.9$ Hz, 1H), 1.84 (ddd, $J = 9.0$, 4.2, 4.1 Hz, 1H), 1.48 (ddd, $J = 8.0$, 6.9, 4.1 Hz, 1H).

A.VI.4. Control experimetns in the photoreduction of acetophenone (9a)

A.VI.4.1. Effect of the presence of O$_2$ in the photocatalytic reduction of acetophenone (9a)
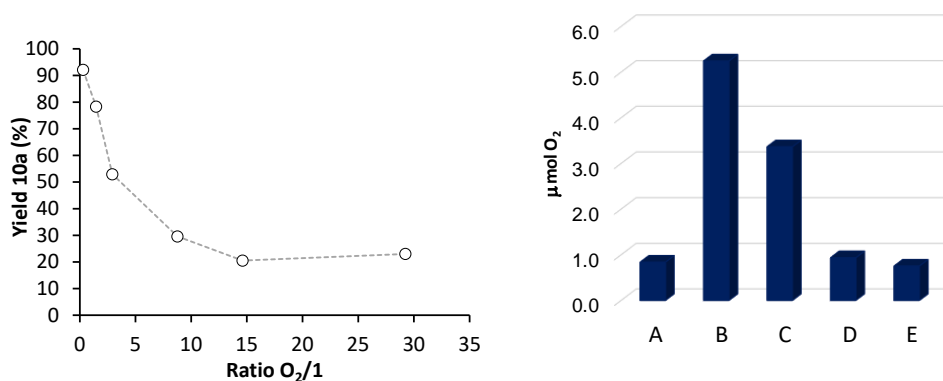
Figure A.VI.4. Right) Plot of the O$_2$/**1Co** stoichiometric ratio. O$_2$/**1Co** = (mmol O$_2$ added to the headspace versus the amount of **1Co** in solution. **Left)** n(O$_2$) measured in the headspace by CG-TDC **A)** under pure N$_2$, **B)** A + addition of 5 μmol O$_2$ (3 eq. respect the catalyst) after 1 min without shaking, **C)** B + after 5 min shaking, **D)** C + after 5 h of irradiation and **E)** C + after 24 h of irradiation. Conditions: **1Co** (1 mol%), **PS$_{Cu}$** (1.5 mol%), **9a** (16.5 mM) in H$_2$O:CH$_3$CN:Et$_3$N (6:4:0.2 mL) irradiation (447 nm) for 5 h at 30 ºC.

Quantification of the O_2 in the headspace after the reaction. The O_2 content in the headspace of reactions vials **(A-E)** prepared as described in the ***Procedure for the reduction of acetophenone (9a) in presence of O_2*** was quantified.

A) Reaction under pure N_2, before irradiation.

B) A + addition of 5 μmol O_2 (2 and 3 eq. respect the copper and cobalt catalysts, respectively) O_2 measured after 1 min without shaking.

C) B + O_2 measured after 5 min shaking.

D) C + O_2 measured after 5 h of irradiation.

E) C + O_2 measured after 24 h of irradiation (Figure SI.1.9, right).

For reactions **B**, **C**, **D** and **E** the 5 μmol of O_2 (from Air) were introduced into the reaction vial headspace using a Hamilton gas-tight syringe through the septa. The O_2 content was measured by GC-TDC. The O_2 measured after 1 min of the O_2 addition (5.2 mmol) indicates that negligible amount of O_2 was introduced into the solution. After 5 min shaking, the O_2 level at the headspace of the reaction vial dropped about 40%. After 5h irradiation the headspace O_2 level found was equivalent to the measured in pure N_2. These results support the hypothesis that when using an over stoichiometry of O_2 respect the dual catalytic system (in this experiment, 2 and 3 eq. regarding the copper and cobalt catalysts, respectively) the O_2 is being consumed during the reaction.

Table A.VI.1. O_2 introduced and **10a** yields of experiments in Figure A.VI.4.

O_2 (mmol)	$n(O_2) / n(1)$	$n(O_2) / n(9a)$	$n(O_2) / n(PS_{Cu})$	Yield $10a^{[a]}$ (%)
0.0005	0.3	0.003	0.2	92
0.0025	1.5	0.02	1	78
0.005	3	0.03	2	53
0.015	9	0.09	6	30
0.025	15	0.15	10	21
0.049	30	0.30	20	23

[a] Conditions: **1Co** (1 mol%), **PS$_{Cu}$** (1.5 mol%), **9a** (16.5 mM) in H_2O:CH_3CN:Et_3N (6:4:0.2 mL) irradiation (447 nm) for 5 h at 30 ºC.

ANNEX

In the experiments carried out with the **procedure for the reduction of acetophenone (9a) with non-degassed solvents prepared outside the glovebox under air exposition** we have estimated the oxygen content of the solutions by **1)** employing the O_2 reported concentration for pure water and acetonitrile at the reaction temperature and 1 atm of pressure.

Estimation of the oxygen content using reported concentration values in water and acetonitrile. Data extracted from *Journal of Physical and Chemical Reference Data* **2014***, 43*, 033102; doi: 10.1063/1.4883876. Solubility of O_2 at 30ºC and 1 atm:

[H_2O]: 1 mM and [CH3CN]: 1.7 mM

Estimation of n(O_2) in the reaction mixtures with PS_{Cu} taking into account the solubility in both solvents employed: V(MeCN) = 2.4 mL; V(H₂O) = 3.6 mL

$$n(O_2\ in\ MeCN) = M(M) * V(L) = 1.7 \cdot 10^{-3} * 2.4 \cdot 10^{-3} = 4.1 \cdot 10^{-6}\ mol$$

$$n(O_2\ in\ H2O) = 1 \cdot 10^{-3} * 3.6 \cdot 10^{-3} = 3.6 \cdot 10^{-6}\ mol$$

$$n(O_2\ Reac.mix.) = 7.7 * 10^{-3}\ mmol\ and\ [O_2\ Reac.mix.] \approx 1\ mM$$

Estimation of n(O_2) in the reaction mixtures with PS_{Ir} taking into account the solubility in both solvents employed: V(MeCN) = 1.2 mL; V(H₂O) = 4.8 mL

$$n(O_2\ in\ MeCN) = M(M) * V(L) = 1.7 \cdot 10^{-3} * 1.2 \cdot 10^{-3} = 2 \cdot 10^{-6}\ mol$$

$$n(O_2\ in\ H2O) = 1 \cdot 10^{-3} * 4.8 \cdot 10^{-3} = 4.8 \cdot 10^{-6}\ mol$$

$$n(O_2\ Reac.mix.) = 6.8 * 10^{-3}\ mmol\ and\ [O_2\ Reac.mix.] \approx 1\ mM$$

In the case of PS_{Cu} we estimate about 1 mM of O_2 in solution, which represents 6 equivalents regarding complex **1Co** (165 μM) and 4 equivalents regarding PS_{Cu}.(247.5 μM). When using PS_{Ir} we estimate 2 equivalents of O_2 regarding complex **1Co** (495 μM) and 4 equivalents regarding PS_{Ir}.(247.5 μM).

A.VI.5. Optimization of aliphatic aldehyde reduction

Table A.VI.2. Optimization of the catalytic conditions for the photoreduction of **11f**.

Entry	[Substrate] (mM)	[cat] (mol %)	[PS$_{Cu}$] (mol %)	ED	T (ºC)	% Conv.	% alcohol	% dimer	Mass loss
1	8.7	3	3	TEA	15	96	50	0	46
2	4.4	6	6	TEA	15	98	70	0	28
3	**4.4**	**6**	**6**	**DIPEA**	**15**	**98**	**93**	**0**	**0**

Conditions: **1Co** (% mol), **PS$_{Cu}$** (% mol), substrate (mM) as indicated in the table in H$_2$O:CH$_3$CN:Et$_3$N or H$_2$O:CH$_3$CN:^{i}Pr$_2$EtN (6:4:0.2 mL) irradiation at λ= 447 nm for 5 h at 15 ºC under N$_2$. Yields were determined by GC analysis after workup of the reaction and they are relative to a calibrated internal standard. Values were average of triplicates.

A.VI.6. NMR data of the isolated products

A.VI.6.1. Isolated alcohols

NMR spectra of the isolated alcohols from the reduction of aromatic ketons (**10a** – **12c**) were performed by Dr. Arnau Call and can be found in the supplementary electronic information of the publication *SI_1_Cat_ExpProced*.[5]

(Z)-pent-3-en-1-ol (12d) (82%). ^{1}H-NMR (CDCl$_3$, 500 MHz, 300 K) δ, ppm: 5.41-5.27 (m, 2H), 3.64 (q, *J* = 6.3 Hz, 2H), 2.08-1.98 (m, 4H), 1.61-1.53 (m, 2H), 1.41-1.28 (m, 6H), 1.25-1.20 (m, 1H), 0.95 (t, *J* = 7.5 Hz, 3H). ^{13}C{^{1}H}-NMR (CDCl$_3$, 125.8 MHz, 300 K) δ, ppm: 131.8, 129.3, 63.2, 32.9, 29.9, 29.2, 27.1, 25.8, 20.7, 14.5. MS (GC): 156.0 [M].
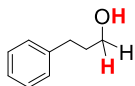
3-phenylpropan-1-ol 12e (67%). ^{1}H-NMR (CDCl$_3$, 400 MHz, 300 K) δ, ppm: 7.32-7.26 (m, 2H), 7.23-7.16 (m, 3H), 3,69 (t, *J* = 6.3 Hz, 3H), 2.72 (t, *J* = 7.7 Hz, 2H),

1.96-1.86 (m, 2H), 1.32-1.24 (m, 1H). $^{13}C\{^1H\}$-NMR (CDCl$_3$, 100.6 MHz, 300 K) δ, ppm: 142.0, 128.6, 128.5, 126.0, 62.5, 34.4, 32.2. MS (GC): 136.0 [M].
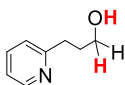
3-(pyridin-2-yl)propan-1-ol 12f (61%). ^1H-NMR (CDCl$_3$, 400 MHz, 300 K) δ, ppm: 8.49-8.47 (m, 1H), 7.64-7.59 (m, 1H), 7.19 (d, J = 7.6 Hz, 1H), 7.14-7.11 (m, 1H), 3.71 (td, J = 6 Hz, J = 1.6 Hz, 2H), 2.96 (td, J = 6.8 Hz, J = 1.6 Hz, 2H), 1.98 (m, 2H).$^{13}C\{^1H\}$-NMR (CDCl$_3$, 100.6 MHz, 300 K) δ, ppm: 161.45, 148.63, 136.81, 123.18, 121.16, 62.13, 35.21, 31.71. MS (GC): 137.1 [M].

A.VI.6.1. Characterization of 10ag, 10ah and 10ai

A) Reduction of 1-Phenyl-1,4-pentanedione (**9ag**)
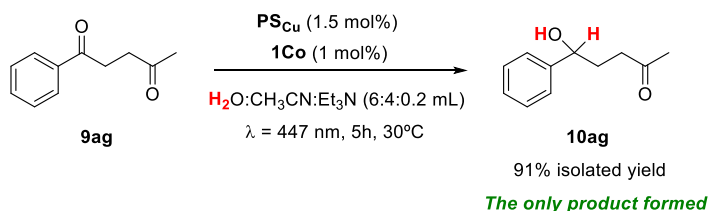
^1H-NMR (CDCl$_3$, 400 MHz, 300 K) δ, ppm: 7.39-7.28 (m, 5H, **H$_{arom}$**), 4.71 (t, J = 6.5 Hz, 1H, **CH**-CH$_2$-CH$_2$), 2.74 (br, 1H, **OH**), 2.55 (t, J = 6.5 Hz, 2H, CH-CH$_2$-**CH$_2$**), 2.14 (s, 1H, **CH$_3$**), 2.00 (m, 2H, CH-**CH$_2$**-CH$_2$). $^{13}C\{^1H\}$-NMR (CDCl$_3$, 100.6 MHz, 300 K) δ, ppm: 209.5, 144.3, 128.4, 127.5, 125.7, 73.4, 39.8, 32.6, 29.9.

B) Reduction of 1-Phenyl-4-penten-1-one (**9ah**)
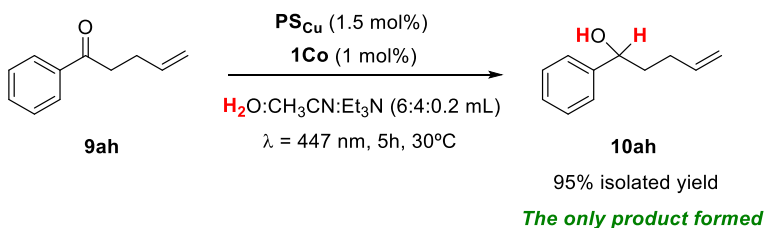
ANNEX

^{1}H-NMR (CDCl$_3$, 400 MHz, 300 K) δ, ppm: 7.39-7.30 (m, 5H, **H$_{arom}$**), 5.87 (ddt, 1H, CH$_2$-CH$_2$-**CH**=CH$_2$, J = 17.0 Hz, J = 10.0 Hz and J = 6.5 Hz), 5.09-5.05 (m, 1H, CH=CH**^{e}**H**^{f}**), 5.03-5.00 (m, 1H, CH=CH**^{e}H^f**), 4.73-4.69 (m, 1H, **CH**-CH$_2$-CH$_2$), 2.19-2.11 (m, 2H, CH-CH$_2$-**CH$_2$**), 1.94-1.81 (m, 2H, CH-**CH$_2$**-CH$_2$). ^{13}C{^{1}H}-NMR (CDCl$_3$, 100.6 MHz, 300 K) δ, ppm: 144.6, 138.2, 128.5, 127.6, 125.9, 114.9, 74.0, 38.1, 30.1.

C) Reduction of 1-Phenyl-4-pentyn-1-one (9**ai**)
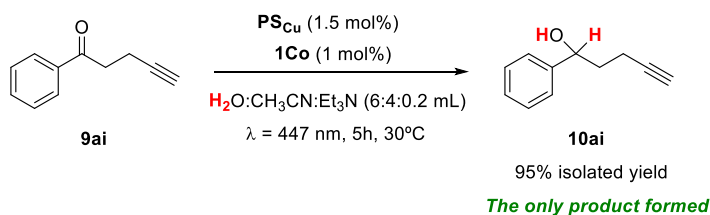
^{1}H-NMR (CDCl$_3$, 400 MHz, 300 K) δ, ppm: 7.39-7.28 (m, 5H, **H$_{arom}$**), 4.86 (dd, 1H, **CH**-CH$_2$-CH$_2$, J = 8.2 Hz, J' = 5.5 Hz), 2.41-2.22 (m, 2H, CH-CH$_2$-**CH$_2$**), 2.06-1.88 (m, 3H, CH-**CH$_2$**-CH$_2$≡-**H**).^{13}C{^{1}H}-NMR (CDCl$_3$, 400 MHz, 300 K) δ, ppm: 144.0, 128.5, 127.7, 125.8, 83.9, 73.1, 68.9, 37.3, 15.1.

A.VI.6.1. Characterization of deuterated alcohols
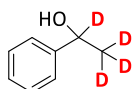
1-phenylethan-1,2,2,2-d_4-1-ol ([D]-10a). ^{1}H-NMR (CDCl$_3$, 300 MHz, 300 K) δ, ppm: 7.26-7.38 (m, 5H, **H$_{arom}$**), 2.12 (s, 1H, **OH**). ^{13}C{^{1}H}-NMR (CDCl$_3$, 75.4 MHz, 300 K) δ, ppm: 145.9 (C$_3$), 128.6 (C$_5$), 127.5 (C$_4$), 125.5 (C$_6$), 69.9 (t, J = 21.2 Hz, C$_2$), 24.3 (m, C$_1$).
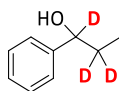
1-phenylpropan-1,2,2,-d_3-1-ol ([D]-10b). ^{1}H-NMR (CDCl$_3$, 500 MHz, 300 K) δ, ppm: 7.38-7.30 (m, 5H, **H$_{arom}$**), 1.99 (s, 1H, O**H**), 0.93 (s, 3H, C**H$_3$**). ^{13}C{^{1}H}-NMR (CDCl$_3$, 125.8 MHz, 300 K) δ, ppm: 144.5 (C$_4$), 128.4 (C$_6$), 127.5 (C$_7$), 125.9 (C$_5$), 75.5 (t, J = 22.7 Hz, C$_2$), 31.1 (m, C$_2$), 9.9 (C$_1$).
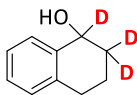
1, 2,3,4-tetrahydronaphthalen-1,2,2,-d_3-1-ol ([D]-10j). ^{1}H-NMR (CDCl$_3$, 500 MHz, 300 K) δ, ppm: 7.45 (m, 1H, **H$_{arom}$**), 7.23 (m, 2H, **H$_{arom}$**), 7.13 (m, 1H, **H$_{arom}$**), 2.88-2.75 (m, 2H, **H$_c$**), 2.02-1.76 (m, 2H, **H$_b$**). ^{13}C{^{1}H}-NMR (CDCl$_3$, 125.8 MHz, 300 K) δ, ppm: 138.7 (C$_{10}$), 137.2 (C$_5$), 129.0, 128.7, 127.56, 126.1, 67.6 (m, C$_1$), 31.6 (m, C$_2$), 29.2 (C$_4$), 18.6 (C$_3$).
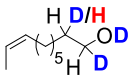
(Z)-hex-4-en-1,2-d_2-1-ol-d ([D]-12d). ^{1}H-NMR (CDCl$_3$, 400 MHz, 300 K) δ, ppm: 5.41-5.27 (m, 2H), 3.64 (q, J = 6.3 Hz, 1H), 2.08-1.98 (m, 4H), 1.61-1.53 (m, mixture of 2H and 1H with ratio 1:0.8), 1.40-1.25 (m, 7H), 0.95 (t, J = 7.5 Hz, 3H). ^{13}C{^{1}H}-NMR (CDCl$_3$, 125.8 MHz, 300 K) δ, ppm: 131.81, 129.38, 63.03-62.54 (m, **C**HD), 32.81, 32.41 (t, J = 19.1 Hz, **C**HD), 29.85, 29.19, 27.15, 25.76, 20.66, 14.52. MS (GC): 156.0 [M].

A.VI.7. Competition experiments between acetophenone and aliphatic aldehydes

A.VI.7.1. Selectivity studies using our dual catalytic system: Blank ^{1}H-NMR sutdy of the selectivity for acetophenone (9a) versus aliphatic aldehydes

We have measured the ^{1}H-NMR spectrum of substrate **11d** with and without the presence of Et$_3$N (40 μl) under catalytic conditions to discard the possible

formation of a hemiacetal, which could be responsible for the observed selectivity. Both spectra, before and after the addition of Et$_3$N (40 μl), are the same appart from the integration increase of the signals at 2.7 and 1.2 ppm, corresponding to the methyls and methylenes of Et$_3$N. The peak at 9.95 ppm corroborates the presence of the aldehyde under catalytic conditions, which rules out this possibility.
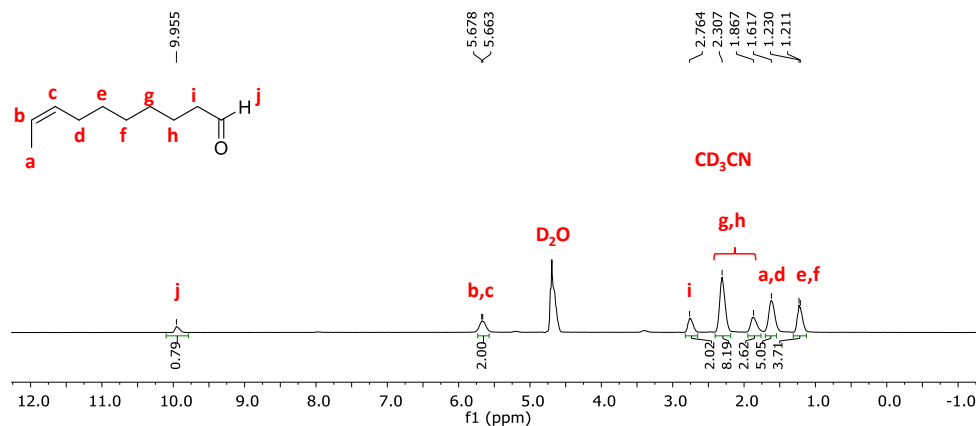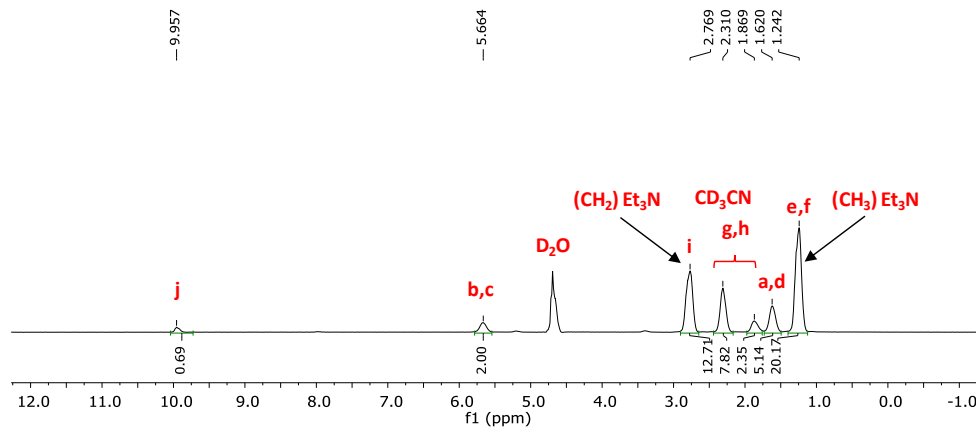
Figure A.VI.5. ^{1}H-NMR (D$_2$O:CD$_3$CN (1.2:0.8), 400 MHz, 300 K) spectrum of substrate **11d** before and after the addition of TEA (40 μl, 2 % volume). Conditions analogous to the photocatalytic competition experiments of scheme 3: **11d** (8.7 mM) in 2 ml solvent mixture of D$_2$O:CD$_3$CN (1.2:0.8) before the addition of Et$_3$N (40 μl), top, and after the addition of Et$_3$N (40 μl), bottom.

A.VI.7.2. Comparison of different methodologies in the selectivity studies

Ar-ketone-aliphatic aldehyde selectivity
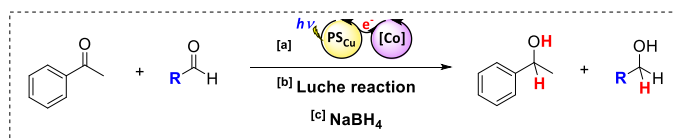
		10a	12d	Selectivity
i)	[a],[d]Light-driven	100 % (100 %)	0 % (n.d.)	100 %
ii)	[b]Luche reaction	100 % (91 %)	58 % (49 %)	1.8:1
	1 eq NaBH$_4$	100 % (95 %)	39 % (30 %)	3.2:1
	0.5 eq NaBH$_4$	100 % (87 %)	39 % (8 %)	10.9:1
	(acidic work-up) 0.5 eq NaBH$_4$	99 % (45 %)	45 % (0 %)	100 %
	0.25 eq NaBH$_4$	99 % (61 %)	52 % (0 %)	100 %
	(acidic work-up) 0.25 eq NaBH$_4$	100 % (23 %)	50 % (0 %)	100 %
iii)	[c]NaBH$_4$	56 % (51 %)	100 % (94 %)	0.6:1

Ar-ketone-aliphatic aldehyde selectivity

		10a	12e	Selectivity
i)	[a],[e]Light-driven	100 % (94 %)	6 % (6 %)	16:1
ii)	[b]Luche reaction	96 % (86 %)	64 % (13 %)	6.6:1
	1 eq NaBH$_4$	100 % (95 %)	70 % (1 %)	95:1
	0.5 eq NaBH$_4$	99 % (78 %)	69 % (0 %)	100%
	(acidic work-up) 0.5 eq NaBH$_4$	98 % (47 %)	71 % (0 %)	100%
	0.25 eq NaBH$_4$	96 % (43 %)	70 % (0 %)	100%
	(acidic work-up) 0.25 eq NaBH$_4$	98 % (27 %)	74 % (0 %)	100%
iii)	[c]NaBH$_4$	93 % (93 %)	89 % (51 %)	1.8:1

Scheme A.VI.1. Competition experiments between aromatic ketones and aliphatic aldehydes. [a] Light-driven conditions: **1Co** (1 mol%), **PS$_{Cu}$** (1.5 mol%), Substrate A + B (16.5 mM), A:B (1:1), in H$_2$O:CH$_3$CN:Et$_3$N (6:4:0.2 mL)irradiated (447 nm) for 5 h at 30 ºC under N$_2$. [b]Luche reaction conditions: **CeCl$_3$·7 H$_2$O** (1 eq molar), **NaBH$_4$** (1.5, 1, 0.5 and 0.25 eq molar, subsequently), Substrate A + B (16.5 mM), A:B (1:1), in EtOH:H$_2$O (4:6 mL) for 15 min at 0 ºC under air. In two cases (shown in brackets) an acidic work.up was used in addition to the reported procedure to dissociate the possible formed B-(OR)x when using low equivalents of **NaBH$_4$**. [c]**NaBH$_4$** (1 eq molar), Substrate A + B (16.5 mM), A:B (1:1), in MeOH (10 mL) for 15 min at rt under air. The same conditions but with **NaBH$_4$** (0.5 eq molar) are also showed in the table [d]Analysis after 35 minutes of irradiation. [e]Analysis after 30 minutes of irradiation. Percentages show the conversions of the substrate from which the product derives, percentages in brakets show the yield of the reduced product.

A.VI.8. NMR spectra of the synthesized substrates
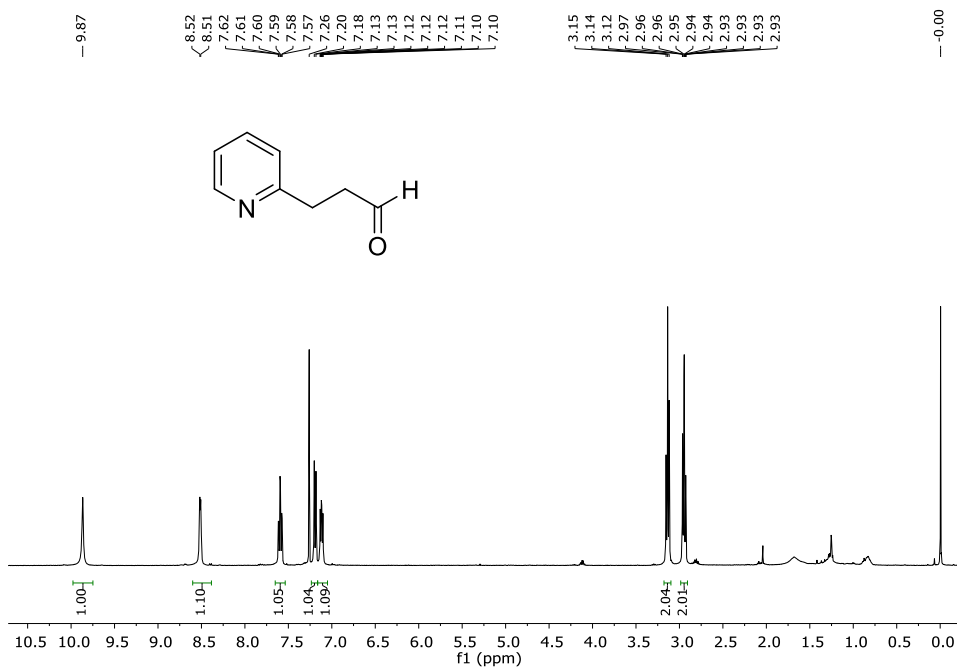
Figure SI.2.6. ^{1}H-NMR (CDCl$_3$, 400 MHz, 300 K) spectrum of substrate **11f.**
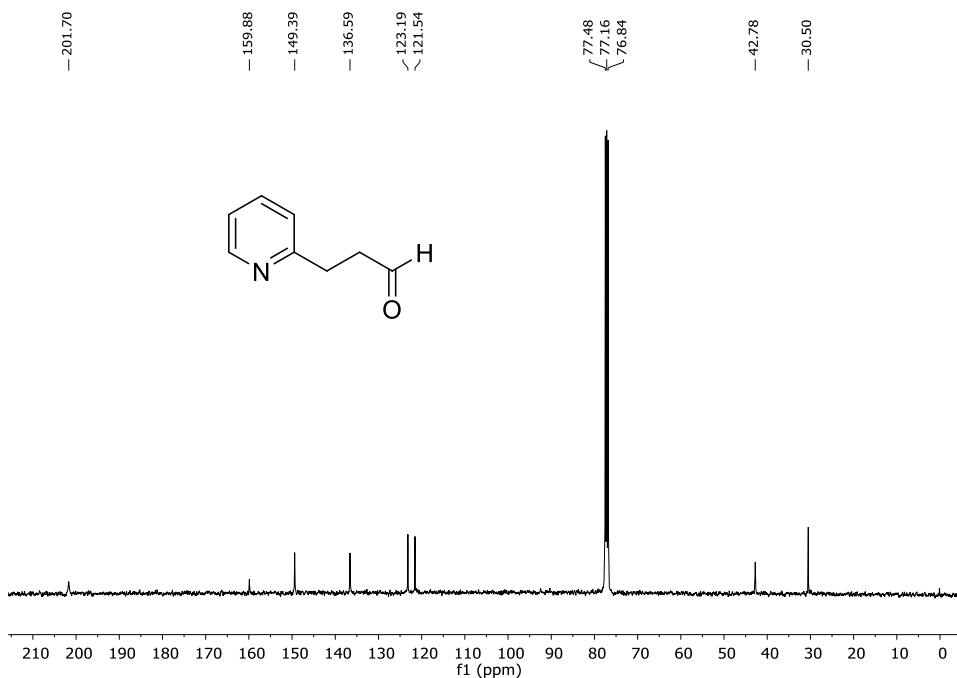
Figure A.VI.6. ^{13}C{^{1}H}-NMR (CDCl$_3$, 100.6 MHz, 300

ANNEX

A.VI.9. NMR spectra of the isolated alcohols

NMR spectra of the isolated alcohols from the reduction of aromatic ketons (**10a** – **12c**) were performed by Dr. Arnau Call and can be found in the supplementary electronic information of the publication *SI_2_NMR_and_GC_spectra*.[5]
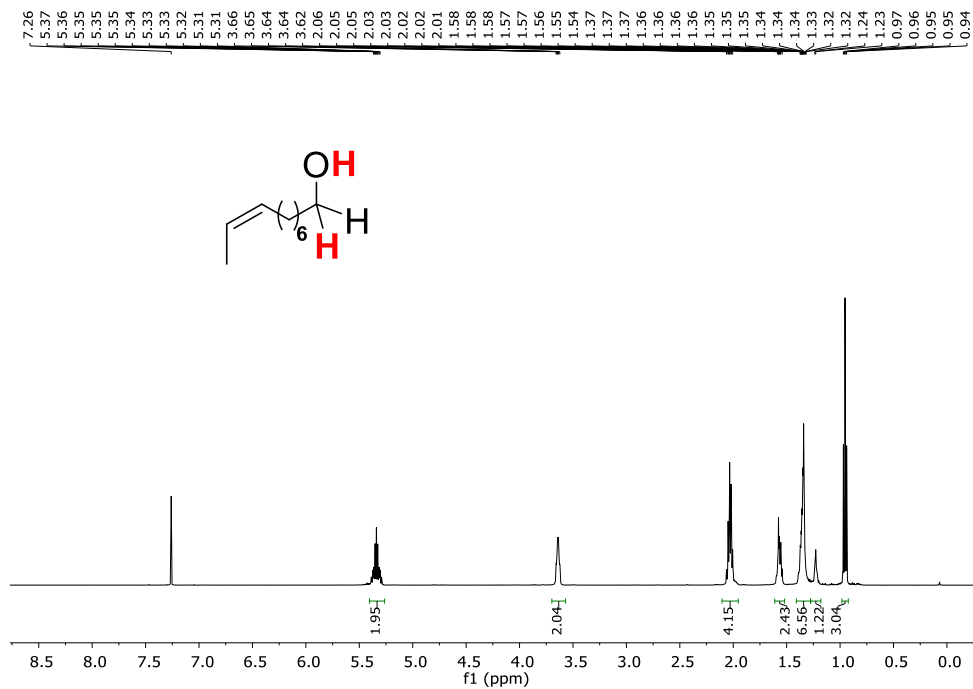
Figure A.VI.7. ^{1}H-NMR (CDCl$_3$, 500 MHz, 300 K) spectrum of product **12d.**

ANNEX
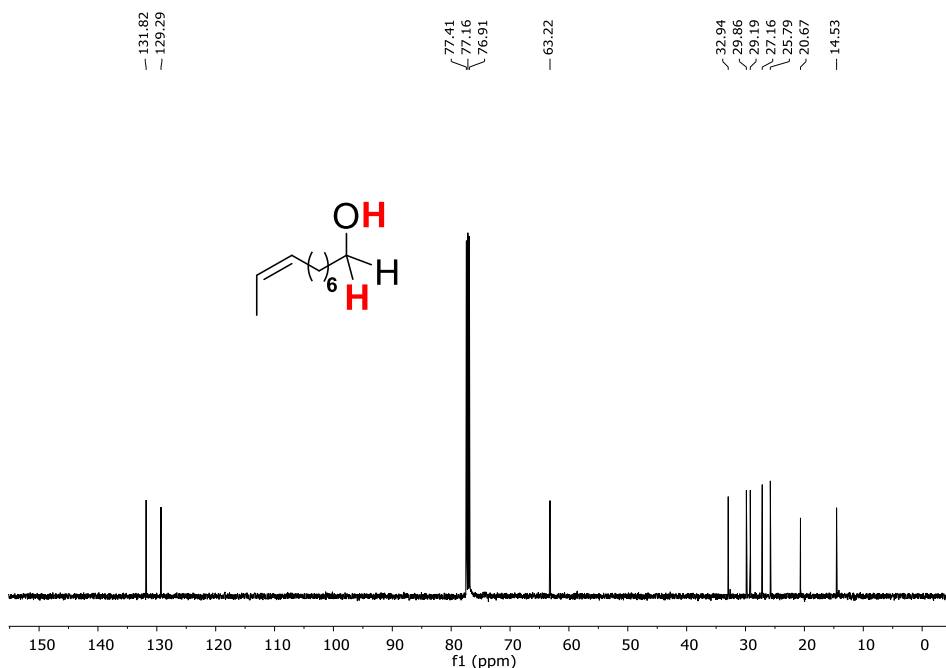
Figure A.VI.8. $^{13}C\{^{1}H\}$-NMR (CDCl$_3$, 125.8 MHz, 300 K) spectrum of product **12d.**
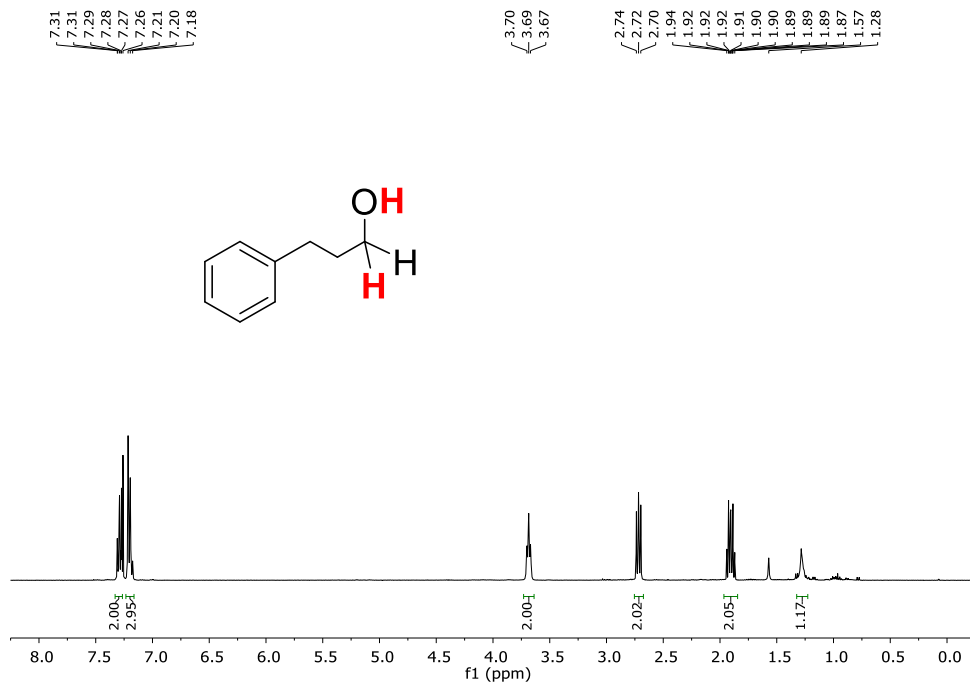
Figure A.VI.9. ^{1}H-NMR (CDCl$_3$, 400 MHz, 300 K) spectrum of product **12e.**

544
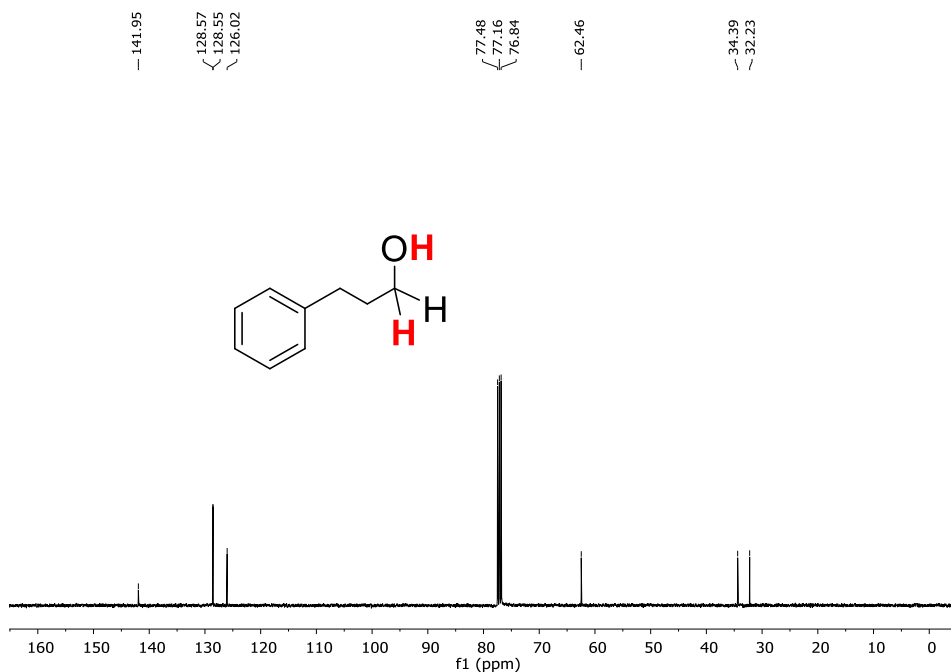
Figure A.VI.10. ^{13}C{^{1}H}-NMR (CDCl$_3$, 100.6 MHz, 300 K) spectrum of product **12e.**
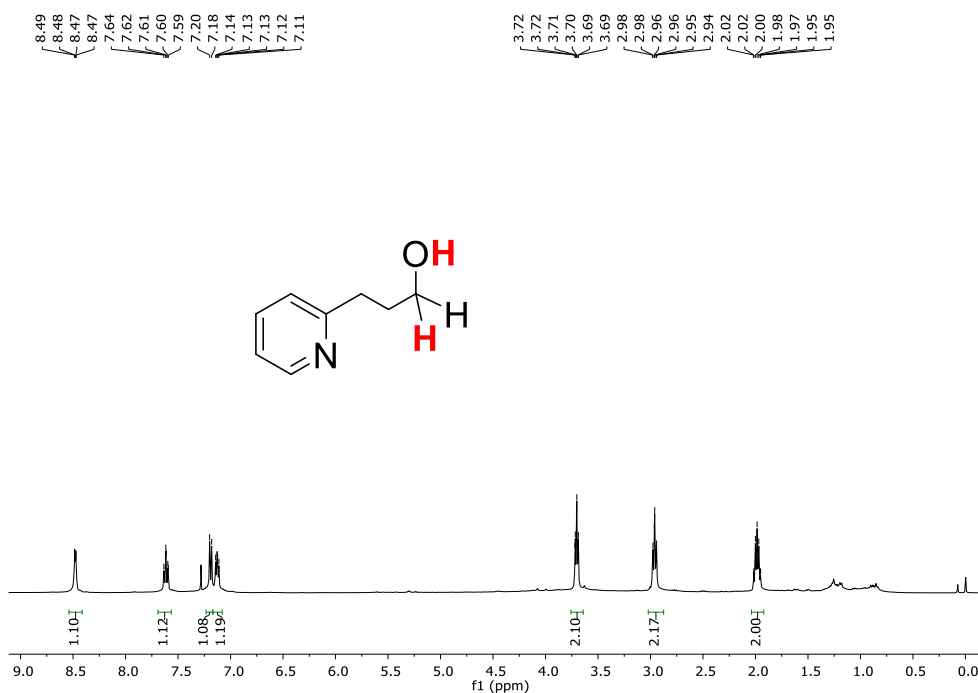
Figure A.VI.11. ^{1}H-NMR (CDCl$_3$, 400 MHz, 300 K) spectrum of product **12f.**

ANNEX
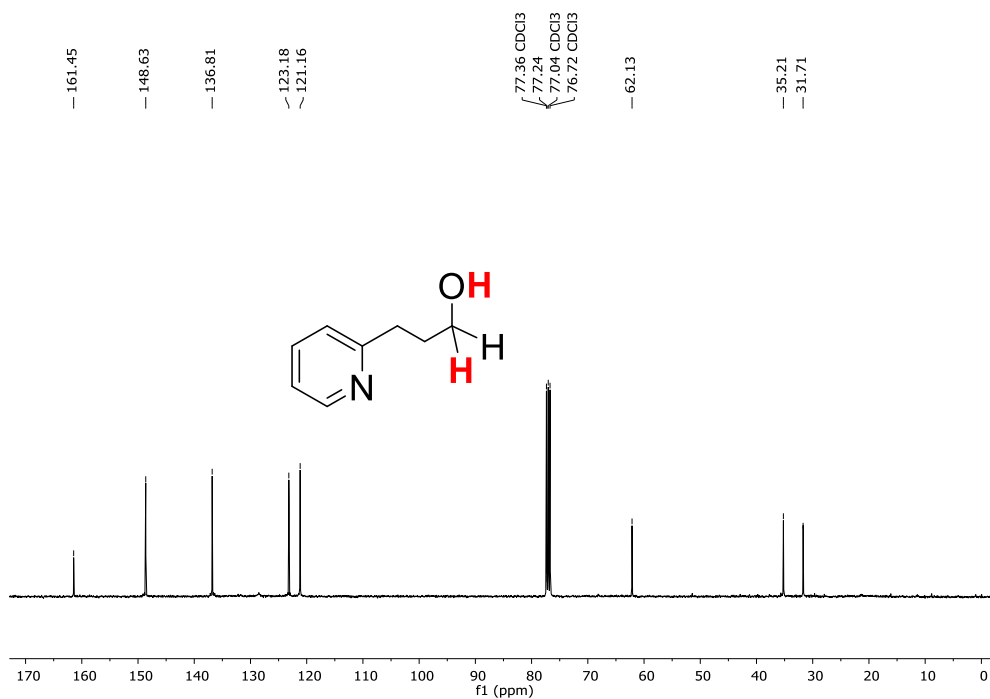
Figure A.VI.12. $^{13}C\{^{1}H\}$-NMR (CDCl$_3$, 100.6 MHz, 300 K) spectrum of product **12f.**

ANNEX

A.VI.10. Selected chromatograms of the selectivity studies

A.VI.10.1. Competition experiments between aromatic aldehydes and ketones
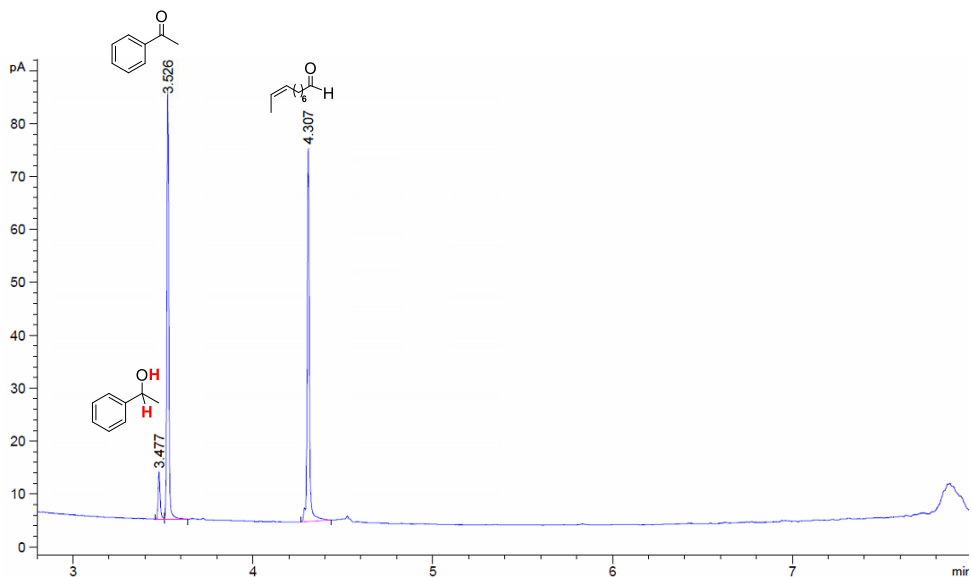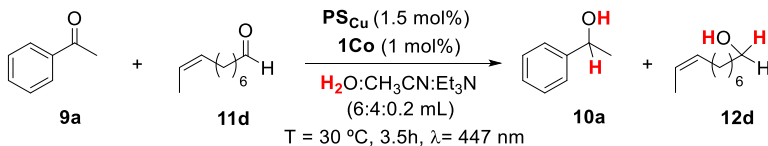
Figure A.VI.13. GC-FID chromatogram of the monitorization of the photoreduccion of acetophenone (**9a**) in the presence of (Z)-dec-8-enal (**11d**) after 4 minutes of irradiation.

547

ANNEX
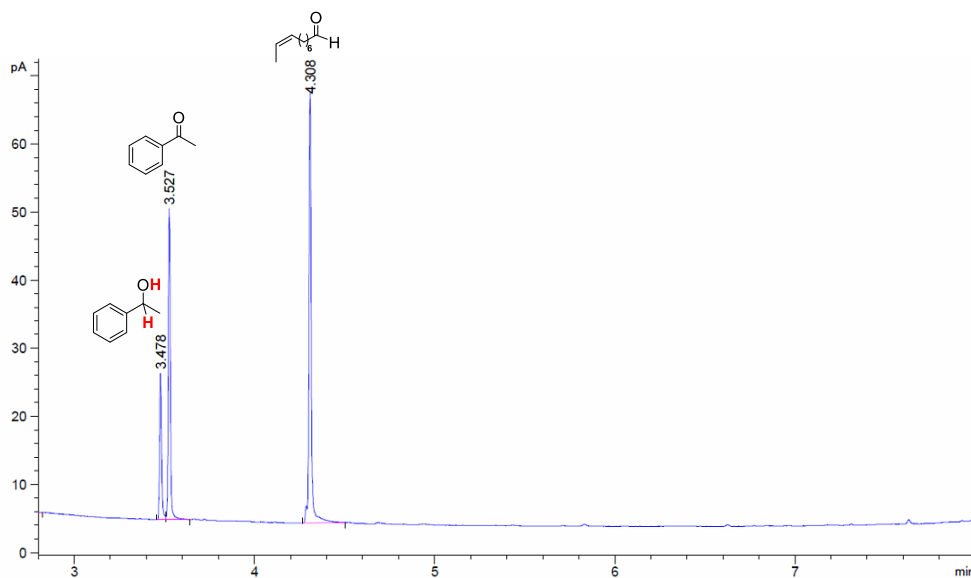
Figure A.VI.14. GC-FID chromatogram of the monitorization of the photoreduccion of acetophenone (**9a**) in the presence of (Z)-dec-8-enal (**11d**) after 10 minutes of irradiation.
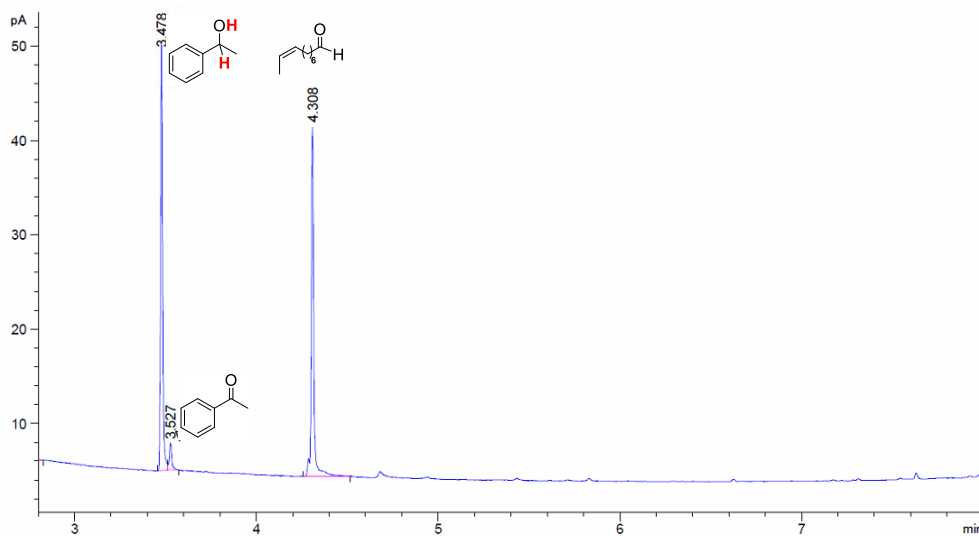
Figure A.VI.15. GC-FID chromatogram of the monitorization of the photoreduccion of acetophenone (**9a**) in the presence of (Z)-dec-8-enal (**11d**) after 30 minutes of irradiation.

ANNEX
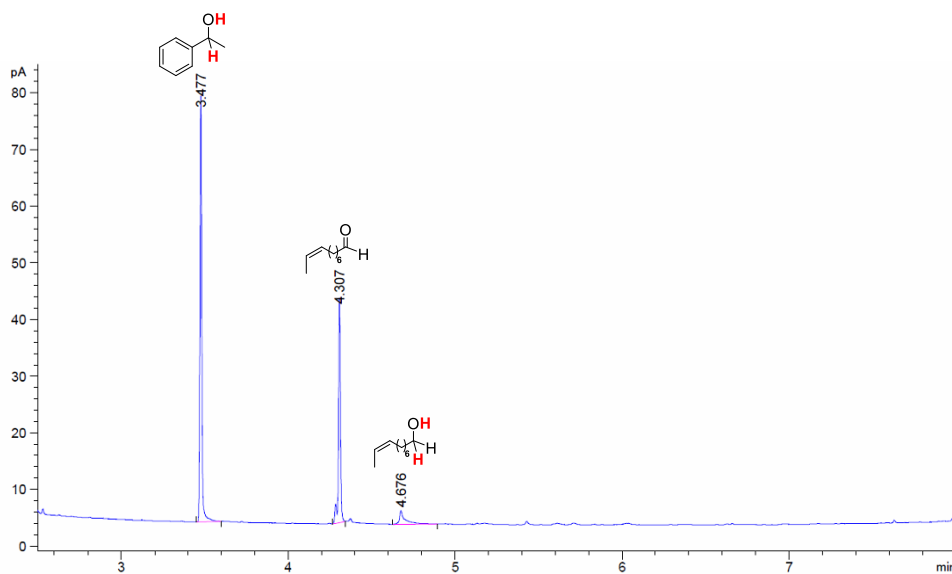
Figure A.VI.16. GC-FID chromatogram of the monitorization of the photoreduccion of acetophenone (**9a**) in the presence of (Z)-dec-8-enal (**11d**) after 50 minutes of irradiation.
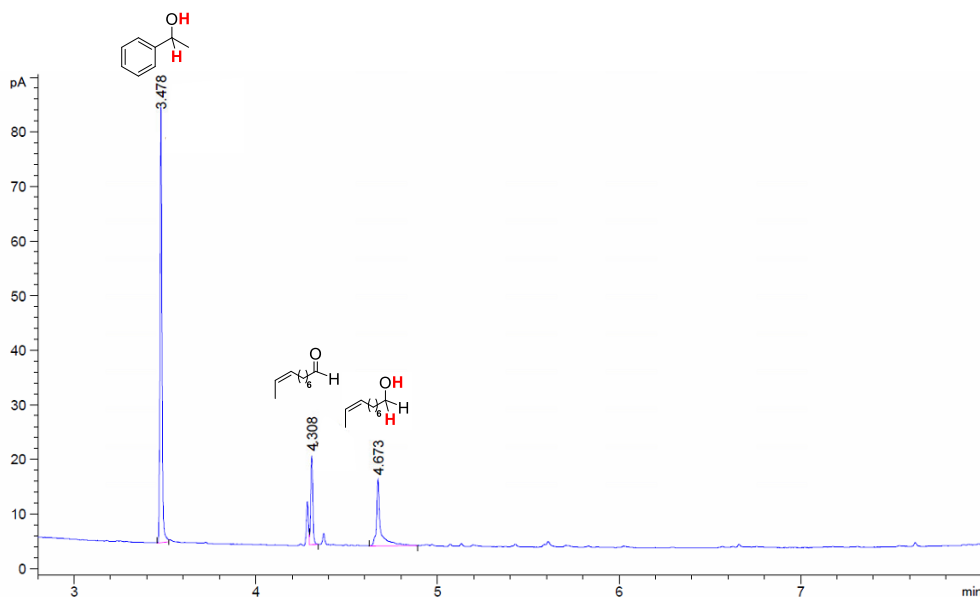
Figure A.VI.17. GC-FID chromatogram of the monitorization of the photoreduccion of acetophenone (**9a**) in the presence of (Z)-dec-8-enal (**11d**) after 120 minutes of irradiation.

549

ANNEX
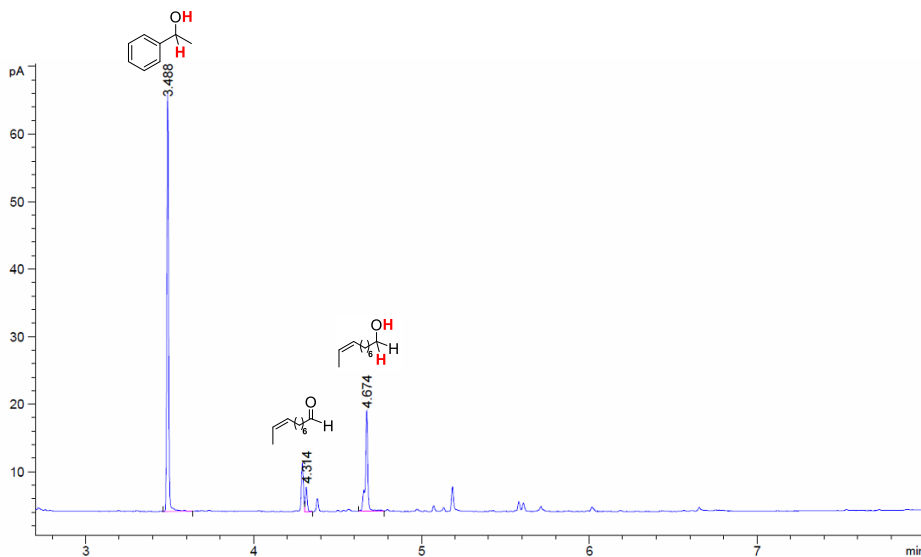
Figure A.VI.18. GC-FID chromatogram of the monitorization of the photoreduccion of acetophenone (**9a**) in the presence of (Z)-dec-8-enal (**11d**) after 210 minutes of irradiation.
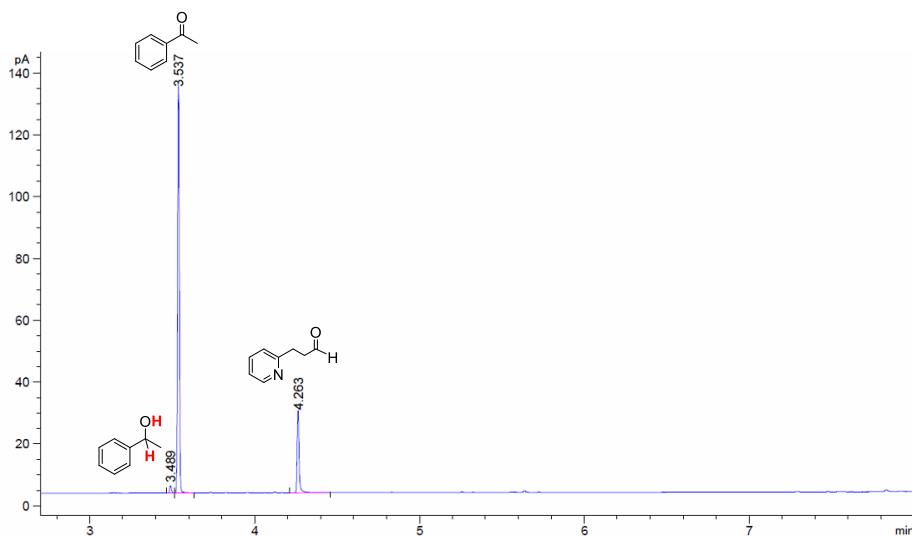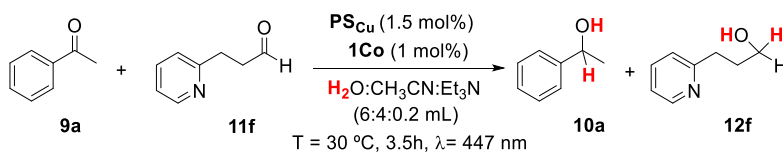
Figure A.VI.19. GC-FID chromatogram of the monitorization of the photoreduccion of acetophenone (**9a**) in the presence of 3(pydidin-2-yl)propanal (**11f**) after 4 minutes of irradiation.

550

ANNEX
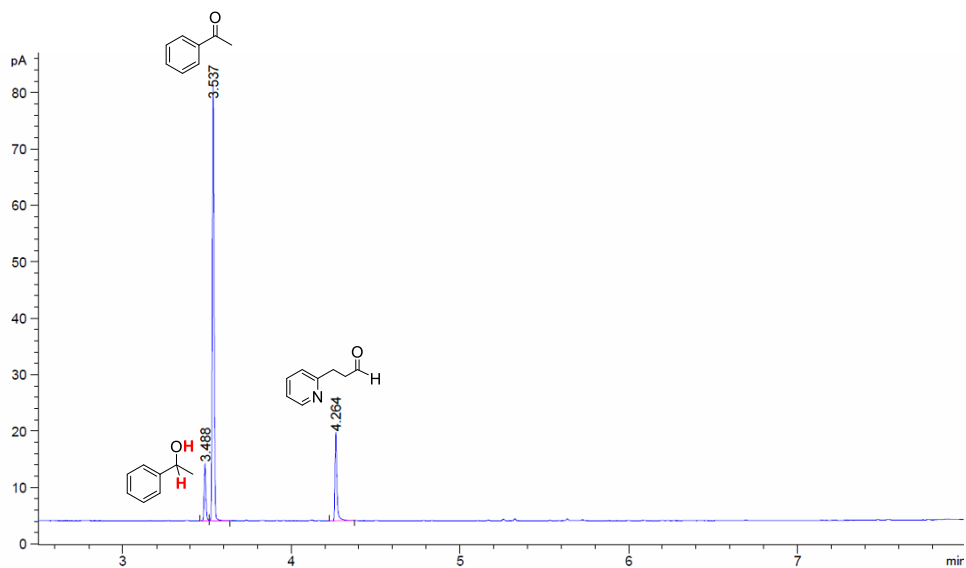
Figure A.VI.20. GC-FID chromatogram of the monitorization of the photoreduccion of acetophenone (**9a**) in the presence of 3(pydidin-2-yl)propanal (**11f**) after 10 minutes of irradiation.
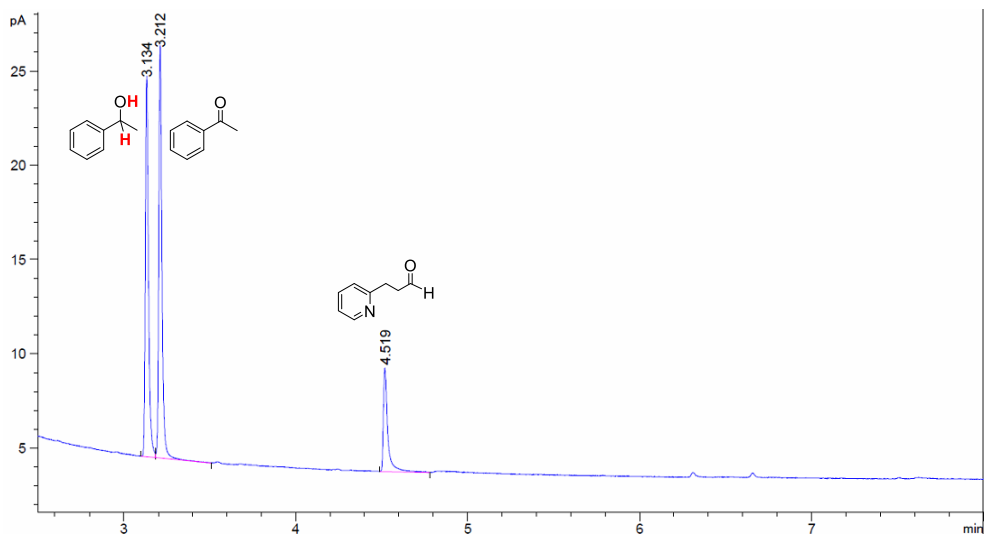
Figure A.VI.21. GC-FID chromatogram of the monitorization of the photoreduccion of acetophenone (**9a**) in the presence of 3(pydidin-2-yl)propanal (**11f**) after 20 minutes of irradiation.

ANNEX
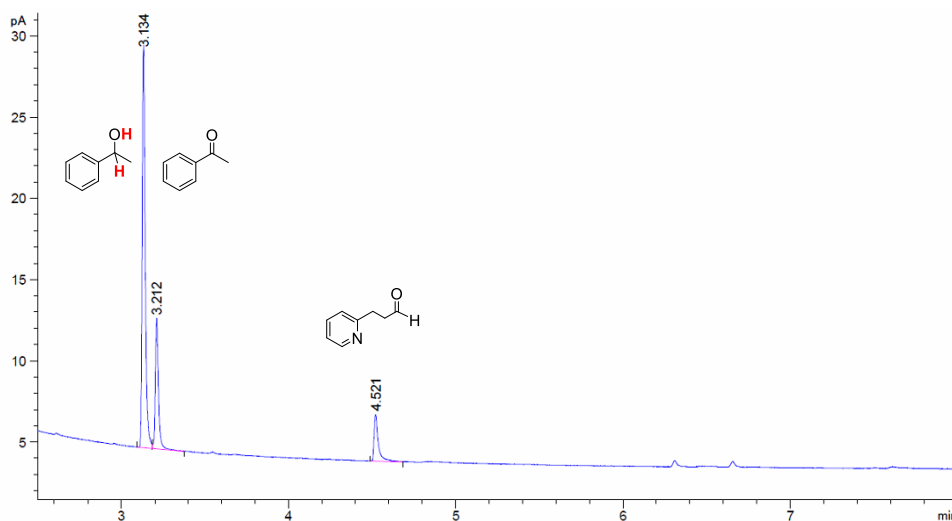
Figure A.VI.22. GC-FID chromatogram of the monitorization of the photoreduccion of acetophenone (**9a**) in the presence of 3(pydidin-2-yl)propanal (**11f**) after 30 minutes of irradiation.
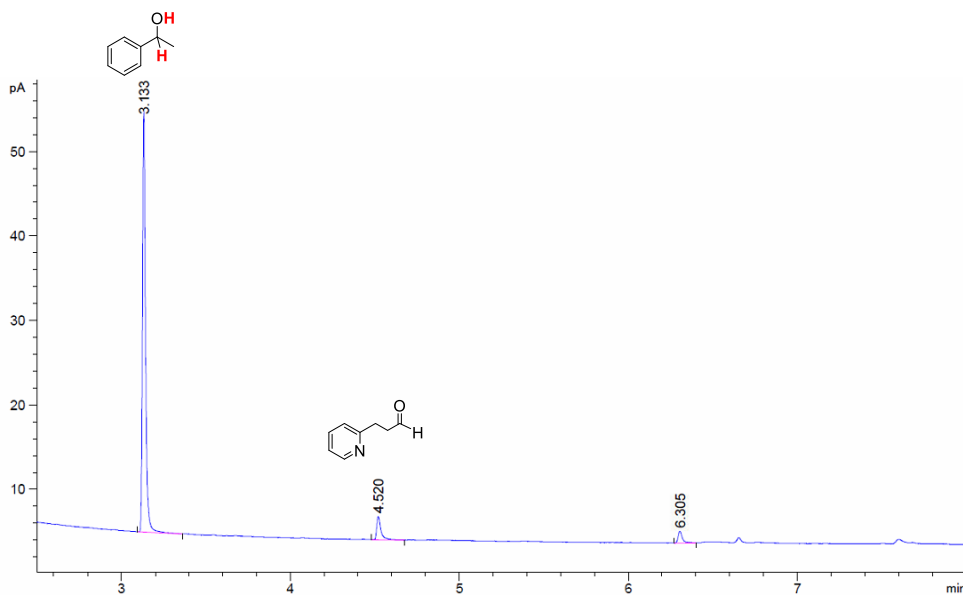
Figure A.VI.23. GC-FID chromatogram of the monitorization of the photoreduccion of acetophenone (**9a**) in the presence of 3(pydidin-2-yl)propanal (**11f**) after 50 minutes of irradiation.
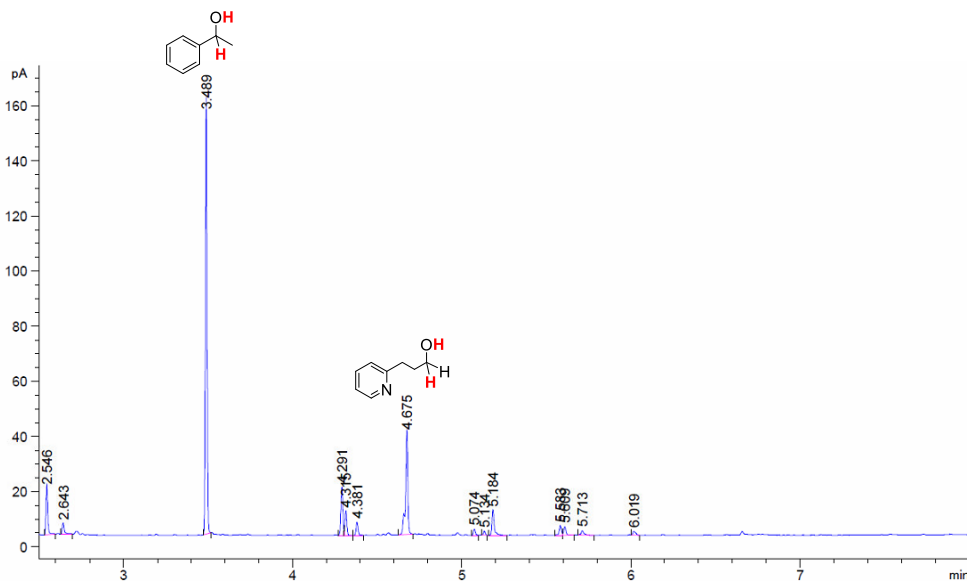
Figure A.VI.24. GC-FID chromatogram of the monitorization of the photoreduccion of acetophenone (**9a**) in the presence of 3(pydidin-2-yl)propanal (**11f**) after 210 minutes of irradiation.
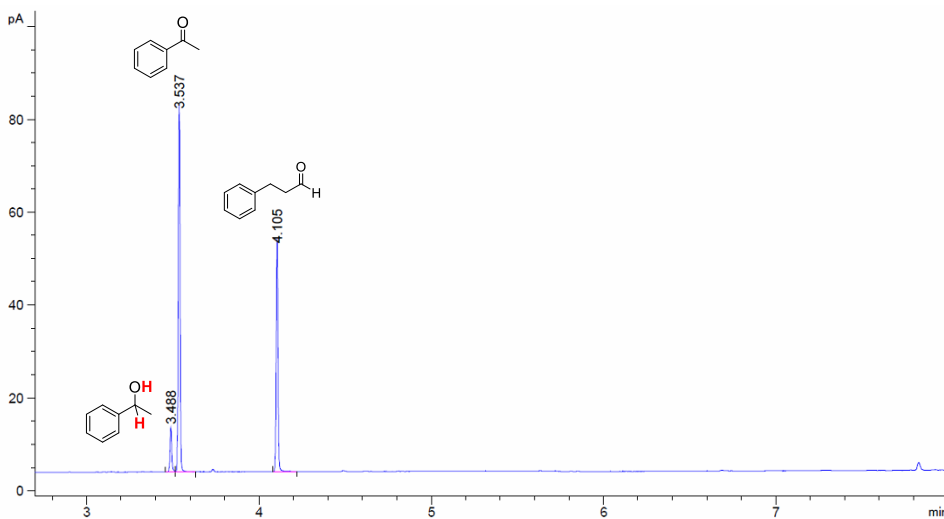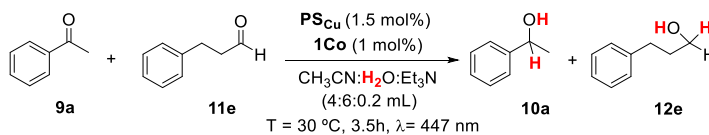
Figure A.VI.25. GC-FID chromatogram of the monitorization of the photoreduccion of acetophenone (**9a**) in the presence of 3-phenylpropanal (**11e**) after 4 minutes of irradiation.

ANNEX
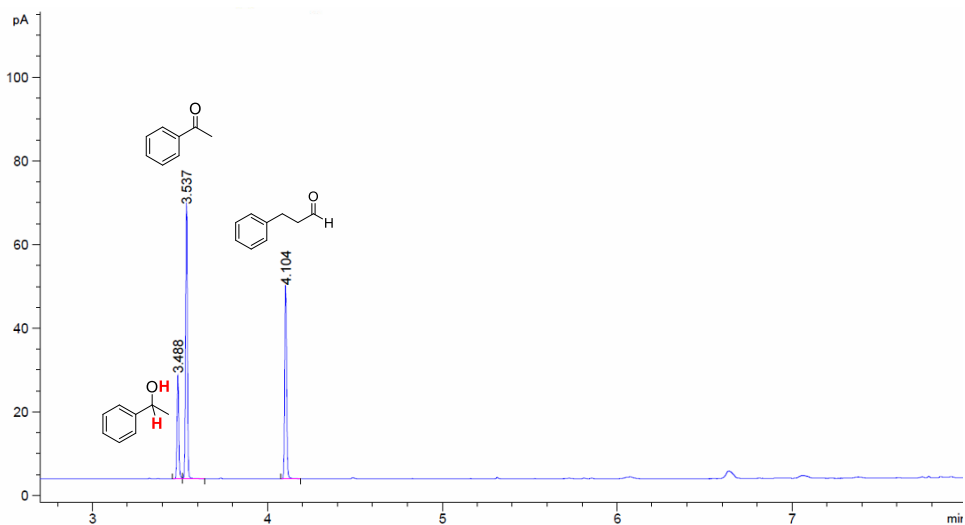
Figure A.VI.26. GC-FID chromatogram of the monitorization of the photoreduccion of acetophenone (**9a**) in the presence of 3-phenylpropanal (**11e**) after 10 minutes of irradiation.
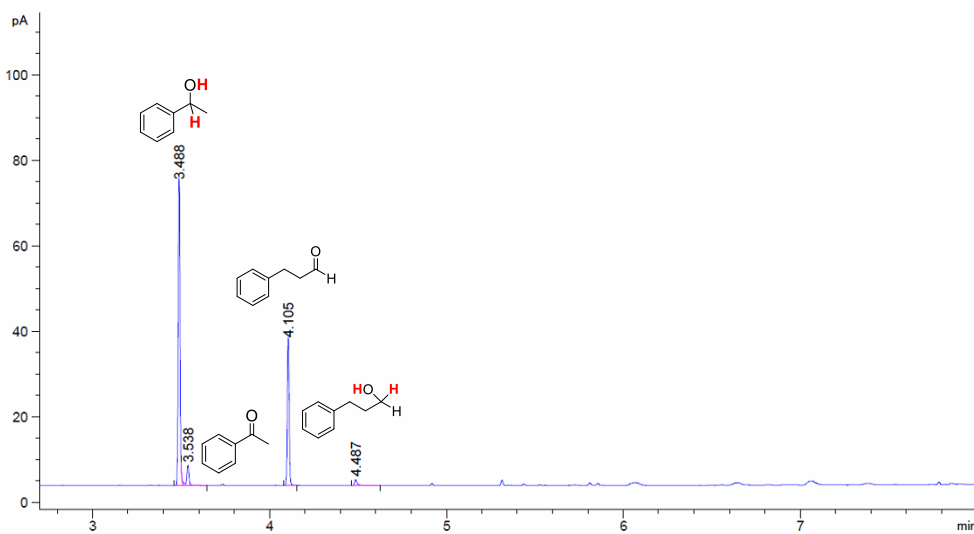
Figure A.VI.27. GC-FID chromatogram of the monitorization of the photoreduccion of acetophenone (**9a**) in the presence of 3-phenylpropanal (**11e**) after 30 minutes of irradiation.

ANNEX
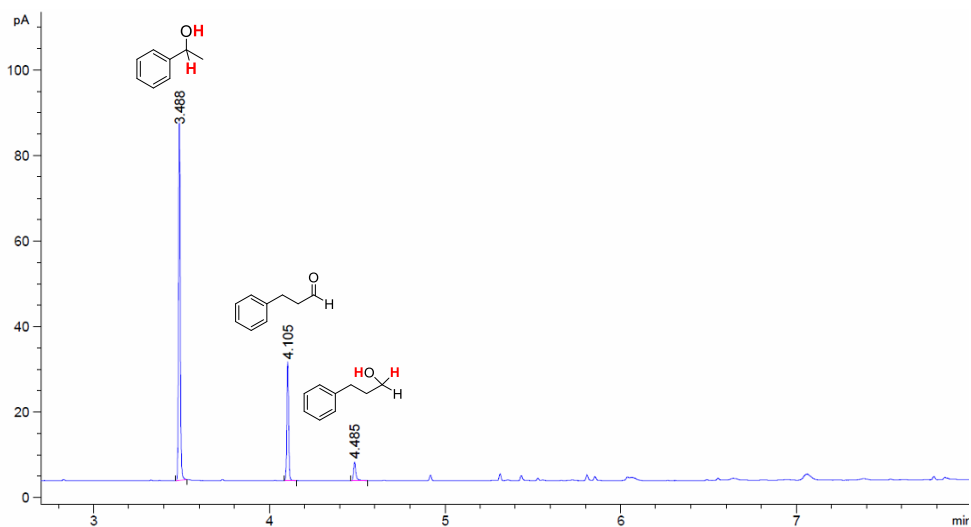
Figure A.VI.28. GC-FID chromatogram of the monitorization of the photoreduccion of acetophenone (**9a**) in the presence of 3-phenylpropanal (**11e**) after 50 minutes of irradiation.
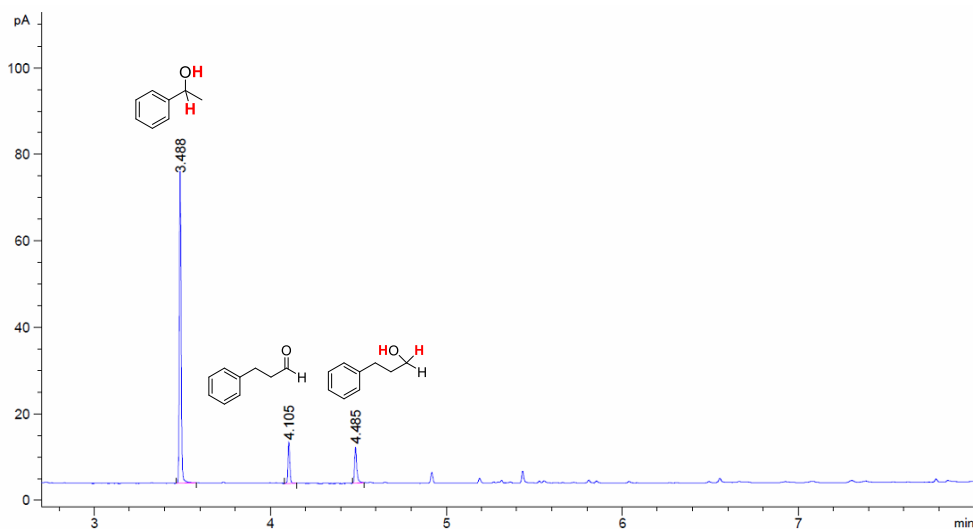
Figure A.VI.29. GC-FID chromatogram of the monitorization of the photoreduccion of acetophenone (**9a**) in the presence of 3-phenylpropanal (**11e**) after 120 minutes of irradiation.
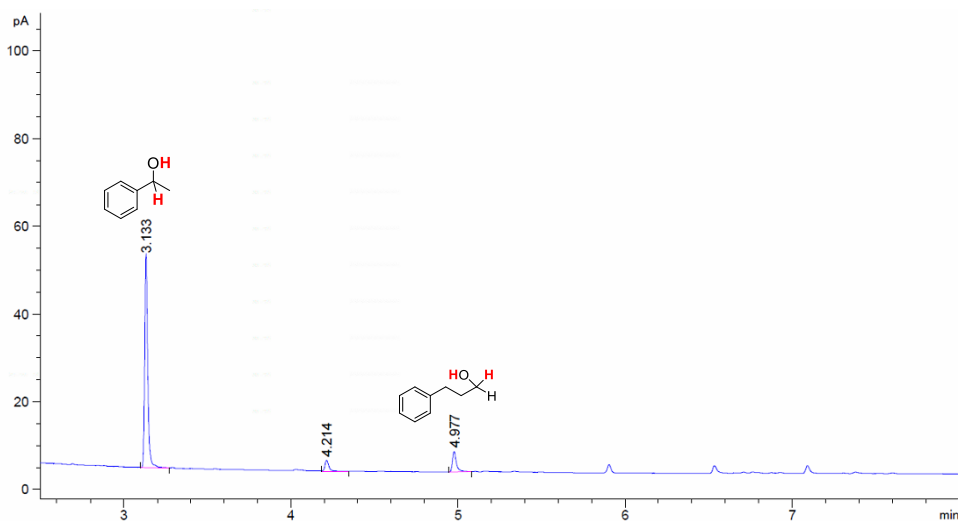
Figure A.VI.30. GC-FID chromatogram of the monitorization of the photoreduccion of acetophenone (**9a**) in the presence of 3-phenylpropanal (**11e**) after 200 minutes of irradiation.

A.VI.11. References

(1) Cline, E. D.; Adamson, S. E.; Bernhard, S. *Inorg. Chem.* **2008**, *47*, 10378.

(2) Luo, S.-P.; Mejía, E.; Friedrich, A.; Pazidis, A.; Junge, H.; Surkus, A.-E.; Jackstell, R.; Denurra, S.; Gladiali, S.; Lochbrunner, S.; Beller, M. *Angew. Chem. Int. Ed.* **2013**, *52*, 419.

(3) Hoover, J. M.; Stahl, S. S. *J. Am. Chem. Soc.* **2011**, *133*, 16901.

(4) Concellón, J. M.; Rodríguez-Solla, H.; Méjica, C.; Blanco, E. G. *J. Org. Chem.* **2007**, *9*, 2981.

(5) Call, A.; Casadevall, C.; Acuña-Parés, F.; Casitas, A.; Lloret-Fillol, J. *Chemical Science* **2017**, *8*, 4739.

A.VII. ANNEX CHAPTER IX

A.VII.1. In-house developed parallel photoreactor

Light source: The reactions were performed using Royal-Blue ($\lambda = 447 \pm 20$ nm) LUXEON Rebel ES LED, mounted on a 10mm Square Saber - 1030 mW @ 700mA (Datasheet: https://www.luxeonstar.com/assets/downloads/ds68.pdf) as a light source.

Temperature Control: Reaction temperature was controlled by a high precision thermoregulation Hubber K6 cryostat. Likewise, to guarantee a stable irradiation the temperature of the LEDs was also controlled and set up at 22 ºC.

Figure A.VII.1. In-house developed parallel photoreactor.

Figure A.VII.2. Reproducibility of the 24-well photoreactor in the photoreduction of styrene (**13a**) as model substrate. Conditions A: Co-Cat (261 μM, 3% mol), PSCu (261 μM, 3% mol), 13a (16 μmol, 8 mM) in $H_2O:CH_3CN:Et_3N$ (6:4:0.2 mL) irradiation (447 nm) for 5h at 15 ºC under N_2. Yields determined by GC analysis after workup relative to a calibrated internal standard. Values were average of triplicates. Values are ethylbenzene (**14a**) GC-FID yields.

A.VII.2. Synthesis of complexes and characterization

Complex **1** (see *chapter VIII* and annex VI section *A.VI.2. Synthesis of complexes and characterization* for further details) and the photoredox catalysts [Ir(ppy)$_2$(bpy)]PF$_6$ (**PS$_{Ir}$**) and [Cu(batocuproine)(Xantphos)]PF$_6$ (**PS$_{Cu}$**) were synthesized accordingly to the reported procedures and the characterization is also in agreement with the previously reported.[1-3] Complexes **2 – 6** were synthesized accordingly to the reported procedures and generously provided by Dr. Arnau Call.[3]

A.VII.3. Synthesis of substrates

-Synthesis of but-1-en-2-ylbenzene (15b)
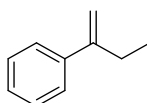
But-1-en-2-ylbenzene (15b) was prepared by a Wittig olefination according to previously reported procedure.[4] ^{1}H-NMR (CDCl$_3$, 400 MHz, 300 K) δ, ppm: 7.46-7.43 (m, 2H), 7.38-7.33 (m, 2H), 7.31-7.27 (m, 1H), 5.31-5.29 (m, 1H), 5.09-5.08 (m, 1H), 2.55 (m, 2H), 1.14 (t, $J = 7.6$ Hz, 3H). MS (GC): 132.1 [M].

-Synthesis of (3-methylbut-1-en-2-yl)benzene (15c)
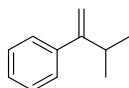
(3-methylbut-1-en-2-yl)benzene (15c) was prepared by a Wittig olefination according to previously reported procedure.[4] ^{1}H-NMR (CDCl$_3$, 400 MHz, 300 K) δ, ppm: 7.39-7.33 (m, 4H), 7.31-7.28 (m, 1H), 5.18-5.17 (m, 1H), 5.07-5.06 (m, 1H), 2.92-2.82 (m, 1H), 1.13 (d, $J = 6.8$ Hz, 6H). ^{13}C{^{1}H}-NMR (CDCl$_3$, 100.6 MHz, 300 K) δ, ppm: 155.81, 142.85, 128.11, 127.02, 126.62, 109.97, 32.35, 22.05. MS (GC): 146.1 [M].

-Synthesis of (3,3-dimethylbut-1-en-2-yl)benzene (15d)
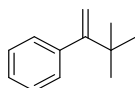
(3,3-dimethylbut-1-en-2-yl)benzene (15d) was prepared by a Wittig olefination acording to previously reported procedures.[4] ^{1}H-NMR (CDCl$_3$, 400 MHz, 300 K) δ, ppm: 7.35-7.28 (m, 3H), 7.20-7.18 (m, 2H), 5.22 (d, $J = 1.6$ Hz, 1H), 4.82 (d, $J = 1.6$ Hz), 1.17 (s, 9H). ^{13}C{^{1}H}-NMR (CDCl$_3$, 100.6 MHz, 300 K) δ, ppm: 159.85, 143.50, 129.01, 127.28, 126.24, 111.51, 36.13, 29.68. MS (GC): 160.1 [M].

-Synthesis of 1-methoxy-4-(prop-1-en-2-yl)benzene (15e)
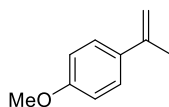
1-methoxy-4-(prop-1-en-2-yl)benzene (15e) was prepared by a Wittig olefination acording to previously reported procedures.[4] ^{1}H-NMR (CDCl$_3$, 400 MHz, 300 K) δ, ppm: 7.44-7.41 (m, 2H), 6.89-6.86 (m, 2H), 5.30-5.29 (m, 1H), 5.00-4.99 (m, 1H), 3.82 (s, 3H), 2.14-2.13 (m, 3H). ^{13}C{^{1}H}-NMR (CDCl$_3$, 100.6 MHz, 300 K) δ, ppm: 159.07, 142.56, 133.76, 126.59, 113.54, 110.66, 55.29, 21.92. MS (GC): 148.1 [M].

-Synthesis of 1-(prop-1-en-2-yl)-4-(trifluoromethyl)benzene (15f)
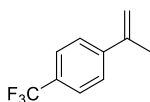
1-(prop-1-en-2-yl)-4-(trifluoromethyl)benzene (15f) was prepared by a Wittig olefination acording to previously reported procedures.[4] ^{1}H-NMR (CDCl$_3$, 400 MHz, 300 K) δ, ppm: 7.60-7.54 (m, 4H), 5.45-5.44 (m, 1H), 5.20-5.19 (m, 1H), 2.17-2.16 (m, 3H). ^{13}C{^{1}H}-NMR (CDCl$_3$, 100.6 MHz, 300 K) δ, ppm: 144.76, 142.21, 133.74 (d, J = 19.5 Hz), 132.11 (d, J = 9.96 Hz), 128.56 (q, J = 14.28 Hz), 125.77, 125.17 (q, J = 3.8 Hz), 114.55, 21.66. MS (GC): 186.1 [M].

-Synthesis of methyl-5-phenylhex-5-enoate (15g)
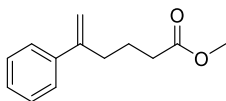
Methyl-5-phenylhex-5-enoate (15g) was prepared by Wittig olefination of the corresponding commercially available ketone according to previously reported procedure.[5] ^{1}H-NMR (CDCl$_3$, 500 MHz, 300 K) δ, ppm: 7.42-7.38 (m, 2H), 7.35-7.30 (m, 2H), 7.29-7.24 (m, 1H), 5.30 (d, J = 1.4 Hz, 1H), 5.07 (q, J = 1.3 Hz, 1H), 3.66 (s, 3H), 2.55 (td, J = 7.7, 1.2 Hz, 2H), 2.34 (t, J = 7.5 Hz, 2H), 1.79 (quint, J = 7.5 Hz, 2H). ^{13}C{^{1}H}-NMR (CDCl$_3$, 100.6 MHz, 300 K) δ, ppm: 174.17, 147.73, 141.07, 128.57, 127.69, 126.34, 113.16, 51.72, 34.82, 33.61, 23.61. MS (GC): 204.0 [M].

ANNEX

-Synthesis of 5-phenylhex-5-en-1-ol (15h)
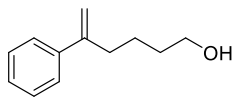
A oven-dried 50 mL two-necked round-bottomed flask equipped with a stirring bar and a dropping funnel and connected to an argon inlet was charged with dry CH_2Cl_2 (10 mL) and substrate **S1** (604 mg, 2,96 mmol). The flask was immersed in dry-ice/acetone bath. Then, a solution of DIBAL-H 1M (5,8 mL, 5,92 mmol) in THF was slowly added via the dropping funnel. After being stirred for 2h at dry ice temperature, the cooling bath was removed and the mixture allowed to warm to room temperature. The reaction was quenched with saturated ammonium chloride solution, the mixture was extracted two times with diethyl ether and the combined organic layers were washed with brine, dried over magnesium sulfate and concentrated under reduced pressure. Then, pure product was obtained in 70% (363 mg) by flash chromatography in silica gel (hexanes/ethyl acetate (80:20). ^{1}H-NMR (CDCl$_3$, 400 MHz, 300 K) δ, ppm: 7.43-7.37 (m, 2H), 7.36-7.30 (m, 2H), 7.29-7.23 (m, 1H), 5.27 (d, J = 1.5 Hz, 1H), 5.07 (q, J = 1.4 Hz, 1H), 3.64 (q, J = 5.5 Hz, 2H), 2.54 (td, J = 7.4, 1.3 Hz, 2H), 1.66-1.47 (m, 4H), 1.22-1.16 (m, 1H). ^{13}C{^{1}H}-NMR (CDCl$_3$, 100.6 MHz, 300 K) δ, ppm: 148.5, 141.4, 128.4, 127.5, 126.3, 112.6, 63.0, 35.2, 32.5, 24.5.

-Synthesis of (*E*)-5-phenylpent-4-en-1-ol (18c)
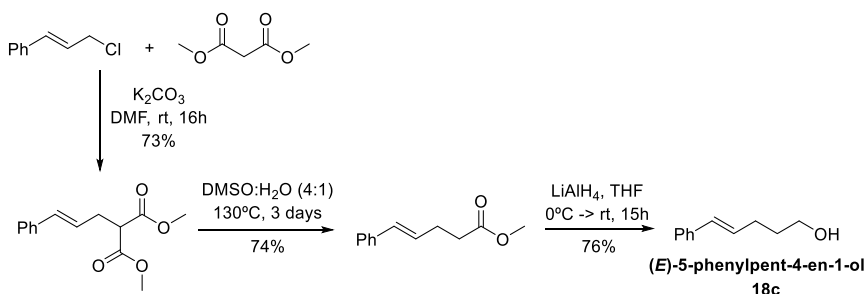
(*E*)-5-phenylpent-4-en-1-ol (18c) was prepared according to previously reported procedures.[6] ^{1}H-NMR (CDCl$_3$, 400 MHz, 300 K) δ, ppm: 7.37-7.26 (m, 4H), 7.23-7.16 (m, 1H), 6.42 (dt, J = 15.8, 1.5 Hz, 1H), 6.23 (dt, J = 15.8, 6.9 Hz, 2H),

3.71 (t, J = 6.5 Hz, 2H), 2.36- 2.27 (m, 2H), 1.81-1.71 (m, 2H), 1.44 (s br, 1H). $^{13}C\{^1H\}$-NMR (CDCl$_3$, 100.6 MHz, 300 K) δ, ppm: 137.8, 130.6, 130.2, 128.7, 127.1, 126.1, 62.6, 32.4, 29.5.

-Synthesys of (*E*)-5-phenylpent-4-enamide (18e)
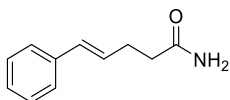
(*E*)-5-phenylpent-4-enamide (18e) was prepared according to previously reported procedures.[7] ^{1}H-NMR (CDCl$_3$, 400 MHz, 300 K) δ, ppm: 7.37-7.35 (m, 2H), 7.34-7.30 (m, 2H), 7.25-7.22 (m, 1H), 6.50-6.45 (m, 1.5 Hz, 1H), 6.28-6.22 (m, 2H), 5.56-5.51 (br m, 2H), 2.61-2.56 (m, 2H), 2.44- 2.41 (m, 2H). $^{13}C\{^1H\}$-NMR (CDCl$_3$, 100.6 MHz, 300 K) δ, ppm: 174.51, 137.26, 131.16, 128.53, 128.51, 127.22, 126.06, 35.48, 28.68. MS (GC): 175.1 [M].

-Synthesis of (1-(2-phenylcyclopropyl)vinyl)benzene (16i)
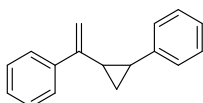
(1-(2-phenylcyclopropyl)vinyl)benzene (16i) was prepared according to previously reported procedures through a Corey-Chaykovsky reaction[8] and further Wittig olefination gave the targeted olefin.[4] ^{1}H-NMR (CDCl$_3$, 400 MHz, 300 K) δ, ppm: 7.53-7.47 (m, 1H), 7.31-7.22 (m, 5H), 7.21-7.15 (m, 1H), 7.15-7.11 (m, 2H), 5.36 (s, 1H), 5.05-5.02 (m, 1H), 2.03-1.91 (m, 2H), 1.42-1.35 (m, 1H), 1.30-1.22 (m, 2H). $^{13}C\{^1H\}$-NMR (CDCl$_3$, 100.6 MHz, 300 K) δ, ppm: 148.5, 142.7, 141.2, 128.6, 128.4, 127.7, 126.2, 125.9, 109.5, 28.0, 26.6, 16.0. MS (GC): 220.1 [M].

A.VII.4. Control experiments in the photoreduction of styrene (13a)

Styrene (**13a**) was used as a model substrate for the optimization of the catalytic conditions when using **PS$_{Cu}$** as photoredox catalyst and **1** as catalyst.

Table A.VII.1. Blank experiments for styrene (**13a**) reduction.
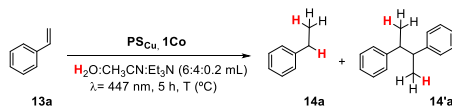
Entry	[Substrate] (mM)	[PS$_{Cu}$] (mol%)	[1Co] (mol%)	Temp. (º C)	% Conv.	% Yield 14a	% Yield 14'a
1	16	1	0	35	0	0	0
2	16	0	1.5	35	0	0	0
3	32	3	0	35	0	0	0
4	32	0	3	35	0	0	0
5	16	3	0	35	0	0	0
6	16	0	3	35	0	0	0
7	8	3	0	35	0	0	0
8	8	0	3	35	0	0	0
9	8	1.5	0	35	0	0	0
10	8	0	3	35	0	0	0
11	8	0.75	0	35	0	0	0
12	8	0	3	35	0	0	0
13	8	3	0	15	0	0	0
14	8	0	3	15	0	0	0
15	8	3	0	25	0	0	0
16	8	0	3	25	0	0	0
17	8	3	0	45	0	0	0
18	8	0	3	45	0	0	0
19	8	3	0	55	0	0	0
20	8	0	3	55	0	0	0
21	8	3	0	80	0	0	0
22	8	0	3	80	0	0	0
23	32	10	0	55	0	0	0
24	8	10	0	55	0	0	0
25	32	10	0	45	0	0	0
26	8	10	0	45	0	0	0
27	32	10	0	35	0	0	0
28	8	10	0	35	0	0	0
29	32	10	0	15	0	0	0
30	8	10	0	15	0	0	0

Conditions: **1Co** (% mol), **PS$_{Cu}$** (% mol), substrate (mM) as indicated in the table in $H_2O:CH_3CN:Et_3N$ (6:4:0.2 mL) irradiated at λ= 447 nm for 5 h at each temperature under N_2. Yields were determined by GC analysis after workup and they are relative to a calibrated internal standard. Values are average of triplicates.

Table A.VII.2. Control experiments for **13a** reduction when using **PS_{Cu}** as photoredox catalyst and different cobalt salts.
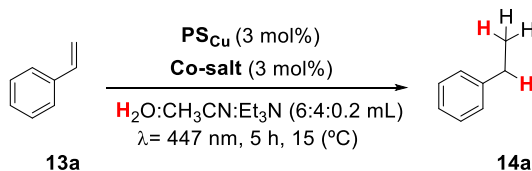
Entry	Co-Salt	% Conv. 13a	% Yield 14a
1	$Co(SO_4)$ x $7H_2O$	0	0
2	$Co(AcO)$ x $4H_2O$	0	0
3	$Co(NO_3)$ x $6H_2O$	0	0
4	$Co(acac)$	0	0
5	$CoCl_2$	0	0
6	$Co(OTf)_2(MeCN)_2$	0	0
7	1Co (preformed)	100	91
8	1Co (*in situ* generation)	100	90

Conditions: **Co-salt** (261 μM, 3% mol), (**PS_{Cu}** (261 μmol, 3% mol), substrate (0.087 mmol, 8.7 mM) in H_2O:CH_3CN:Et_3N (6:4:0.2 mL) irradiated at λ= 447 nm for 5 h at 15 °C under N_2. [b] **PS_{Cu}** (2.5 μmol, 1.5% mol), substrate (0.168 mmol, 16.5 mM) in H_2O:CH_3CN:Et_3N (6:4:0.2 mL) irradiation at λ= 447 nm for 5 h at 30 °C under N_2. Yields were determined by GC analysis after workup of the reaction and they were relative to a calibrated internal standard. Values are average of triplicates.

A.VII.5. Screening of cobalt catalysts in the reduction of styrene (13a) to ethylbenzene (14a)

L= Py$_2$^{Ts}tacn, DPA-Bpy, N4Py, H-CDPy$_3$, PDP, TPA, BpcMe, glioxim, B$_{12}$
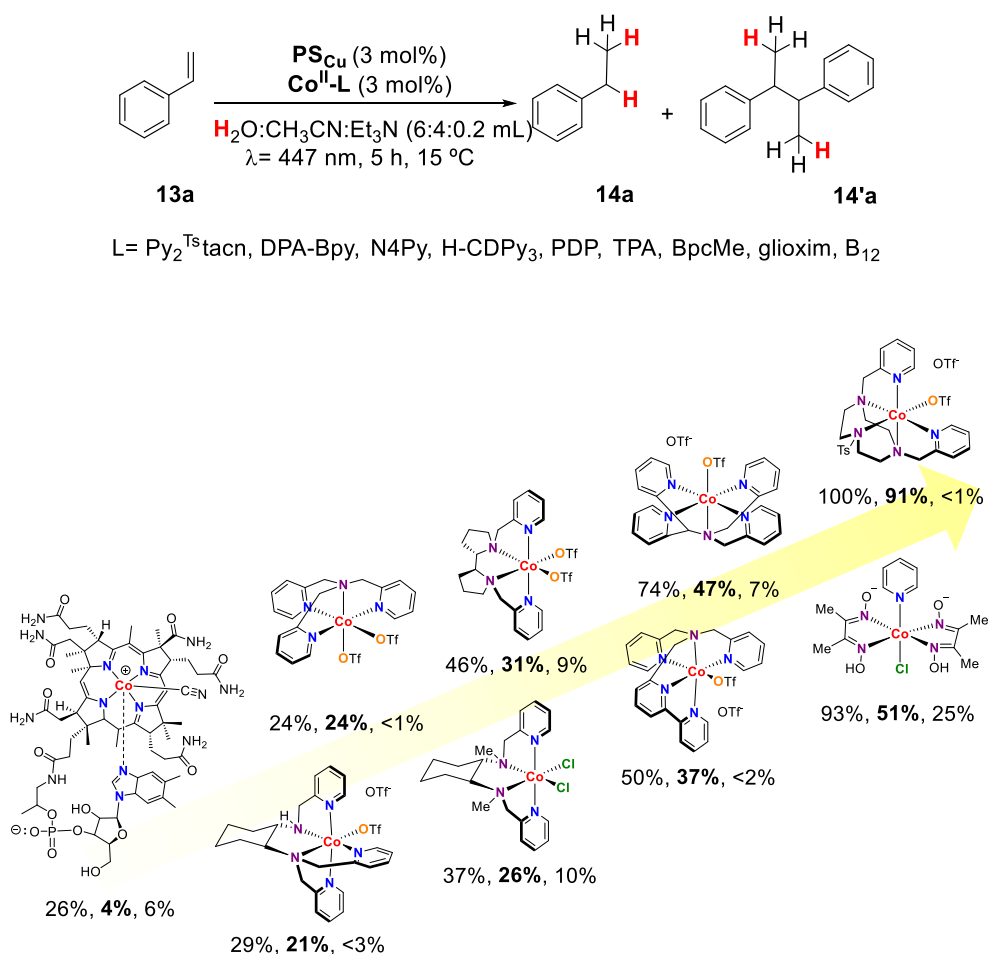
Figure A.VII.3. Photocatalytic reduction of styrene (**13a**) to ethylbenzene (**14a**) by the selected cobalt complexes. Catalytic conditions **A**: **1Co** (261 µM, 3% mol), **PS$_{Cu}$** (261 µM, 3% mol), substrate **13a** (16 µmol, 8 mM) in H$_2$O:CH$_3$CN:Et$_3$N (6:4:0.2 mL) irradiation at λ= 447 nm for 5h at 15 ºC under N$_2$. Yields determined by GC analysis after workup relative to a calibrated internal standard. Values were average of triplicates. Represented values are as follows: Conv %, % yield **14a**, % yield **14'a**.

A.VII.6. Optimization of aromatic 1,1-dibustituted olefins

α-methylstyrene (**15a**) was used as a model substrate for the optimization of the catalytic conditions when using PS_{Cu} as photoredox catalyst and **1Co** as catalyst.
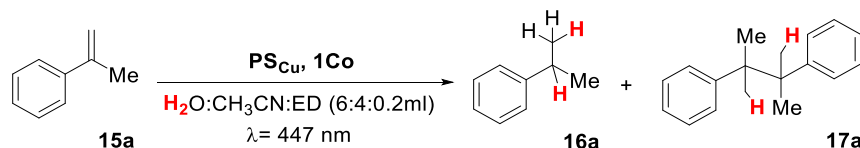
Table A.VII.3. Variation of the substrate concentration using the optimized conditions for styrene derivatives (**13a-l,** see table 4 main text) photoreduction.

Entry	[Substrate] (mM)	[PS$_{Cu}$] (mol%)	[1Co] (mol%)	ED	T (ºC)	% Conv.	% 16a	% 17a	Mass loss
1	8.7	3	3	TEA	15	100	40	45	15
2	**4.4**	**3**	**3**	**TEA**	**15**	**100**	**45**	**38**	**17**

Table A.VII.4. Variation of the electron donor (ED) using the best substrate concentration from table **SI.1.10**. (4.4 mM) and the optimized conditions for styrene derivatives (**13a-l,** see table 4 main text) photoreduction.

Entry	[Substrate] (mM)	[PS$_{Cu}$] (mol%)	[1Co] (mol %)	ED	T (ºC)	% Conv.	% 16a	% 17a	Mass loss
1	4.4	3	3	TEA	15	100	45	38	17
2	4.4	3	3	DIPEA	15	100	56	26	18
3	4.4	6	6	TEA	15	100	47	34	19
4	**4.4**	**6**	**6**	**DIPEA**	**15**	**100**	**61**	**15**	**24**

Table A.VII.5. Variation of the dual catalytic system loading using the best ED (DIPEA) and substrate concentration (4.4 mM).

Entry	[Substrate] (mM)	[PS$_{Cu}$] (mol%)	[1Co] (mol %)	ED	T (ºC)	% Conv.	% 16a	% 17a	Mass loss
1	4.4	3	3	DIPEA	15	100	56	26	18
2	4.4	3	6	DIPEA	15	100	58	19	23
3	4.4	3	12	DIPEA	15	100	60	16	24
4	4.4	6	3	DIPEA	15	100	57	20	23
5	**4.4**	**6**	**6**	**DIPEA**	**15**	**100**	**61**	**15**	**24**
6	4.4	6	12	DIPEA	15	100	61	13	26

Table A.VII.6. Variation of the temperature ED (DIPEA), substrate concentration (4.4 mM) and 6 mol% loading of the dual catalytic system.

Entry	[Substrate] (mM)	[PS$_{Cu}$] (mol%)	[1Co] (mol %)	ED	T (ºC)	% Conv.	% 16a	% 17a	Mass loss
1	4.4	6	6	DIPEA	15	100	61	15	24
2	4.4	6	6	DIPEA	3	100	85	15	0
3	4.4	6	6	DIPEA	-3	100	91	9	0

Conditions: **1Co** (% mol), **PS$_{Cu}$** (% mol), substrate (mM) in H$_2$O:CH$_3$CN:Et$_3$N or H$_2$O:CH$_3$CN:^{i}Pr$_2$EtN (6:4:0.2 mL) irradiation at λ= 447 nm for 5 h at 15 ºC or 24 h at 3 and -3 ºC under N$_2$. Yields were determined by GC analysis after workup of the reaction and they were relative to a calibrated internal standard. Values are averages by triplicates.

A.VII.7. DFT calculations

A.VII.7.1. Relevant optimized structures
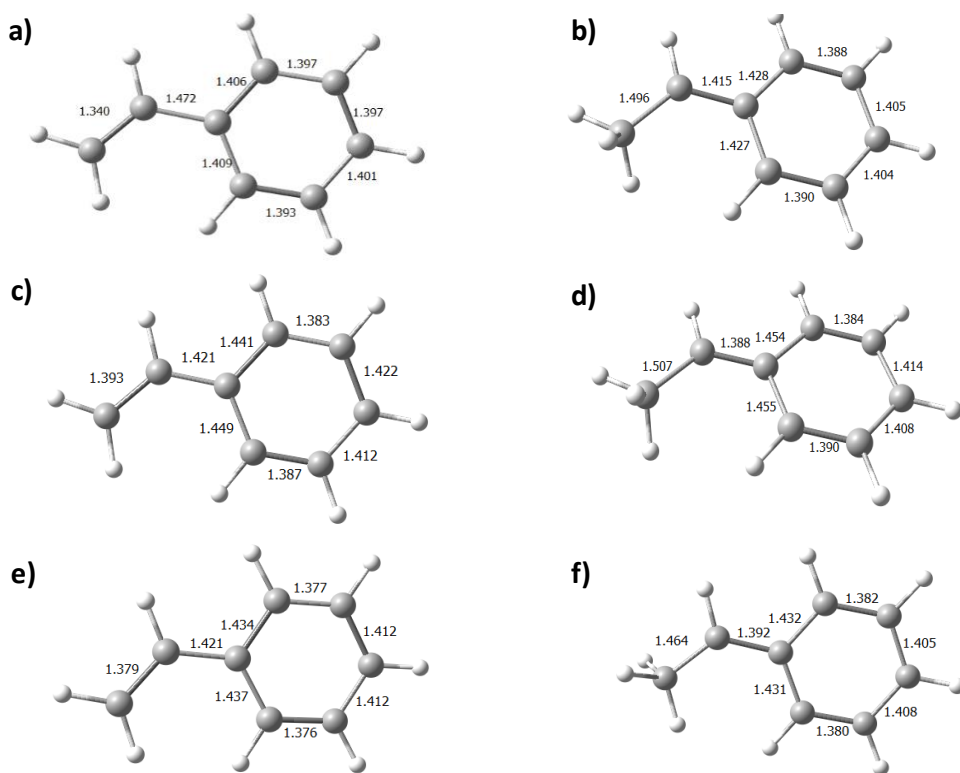
Figure A.VII.4. Optimized geometries of the lowest in energy substrate in different oxidation states: a) olefin **13a**, b) benzilyc radial, c) one electron reduced olefin and d) one electron reduced radical e) one electron oxidised olefin and f) one electron oxidised radical. The most relevant bond distances are in Å.

A.VII.8. Experimental NMR data of the synthesised substrates
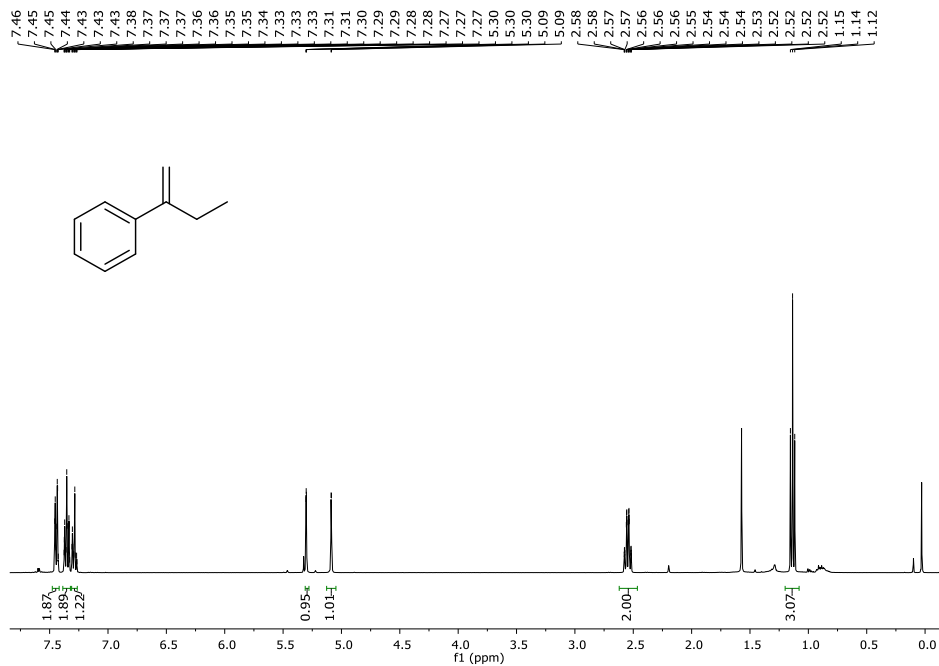
Figure A.VII.5. ^{1}H-NMR (CDCl$_3$, 400 MHz, 300 K) spectrum of substrate **15b.**
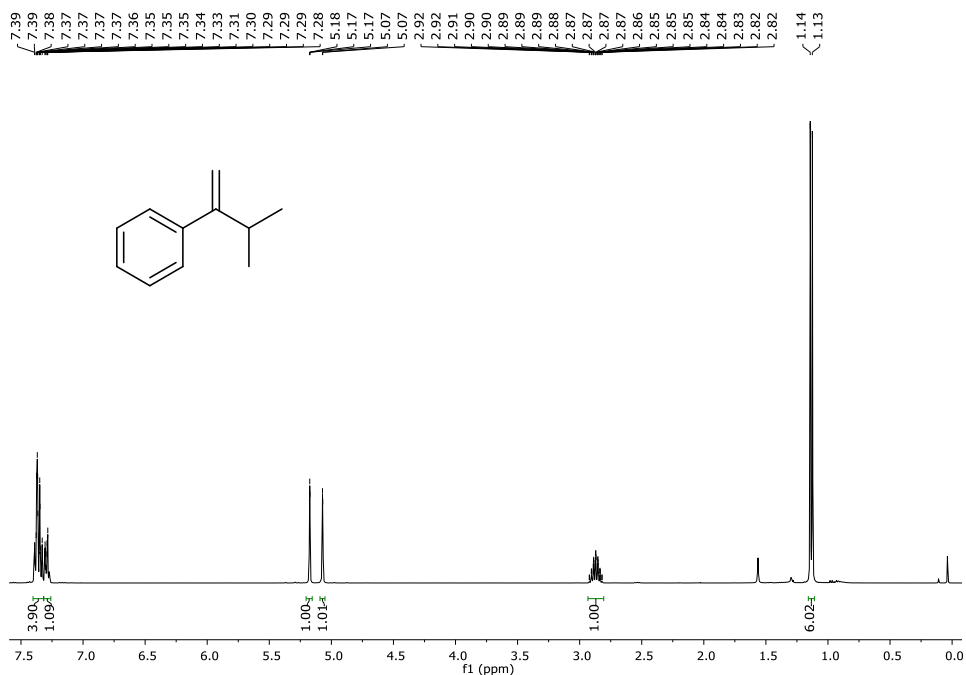
Figure A.VII.6. ^{1}H-NMR (CDCl$_3$, 400 MHz, 300 K) spectrum of substrate **15c.**

568

ANNEX
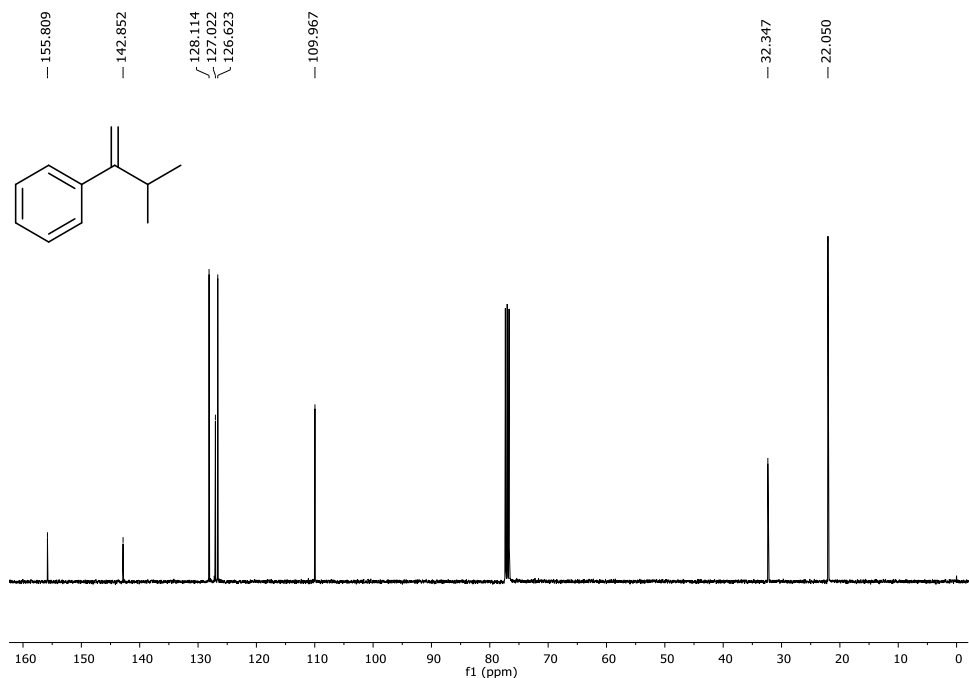
Figure A.VII.7. $^{13}C\{^1H\}$-NMR (CDCl$_3$, 100.6 MHz, 300 K) spectrum of substrate **15c.**
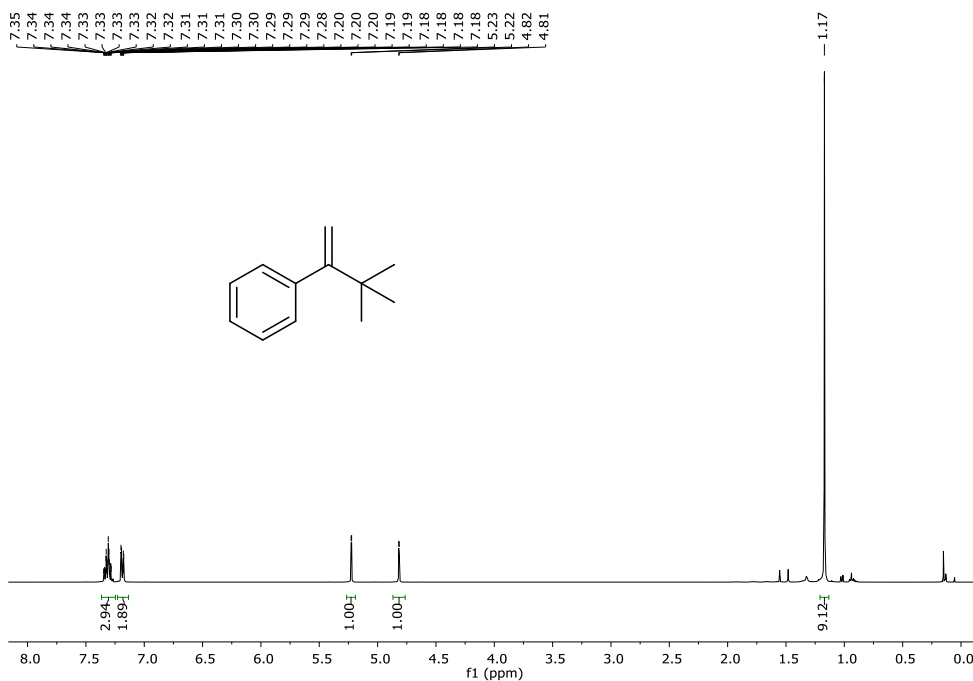
Figure A.VII.8. ^1H-NMR (CDCl$_3$, 400 MHz, 300 K) spectrum of substrate **15d.**
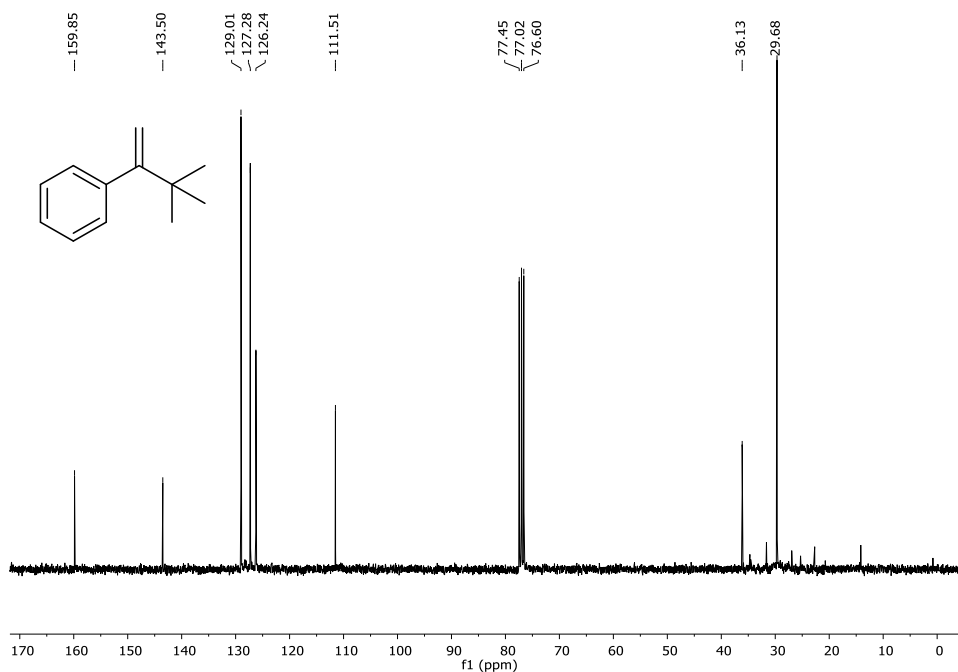
Figure A.VII.9. $^{13}C\{^1H\}$-NMR (CDCl$_3$, 100.6 MHz, 300 K) spectrum of substrate **15d.**
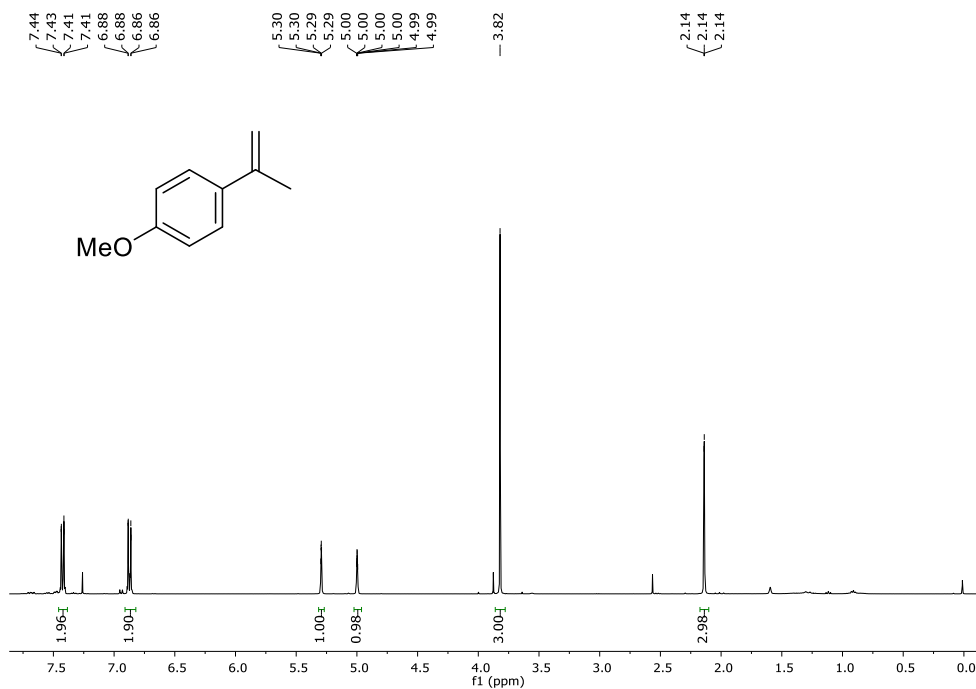
Figure A.VII.10. ^{1}H-NMR (CDCl$_3$, 400 MHz, 300 K) spectrum of substrate **15e.**

ANNEX
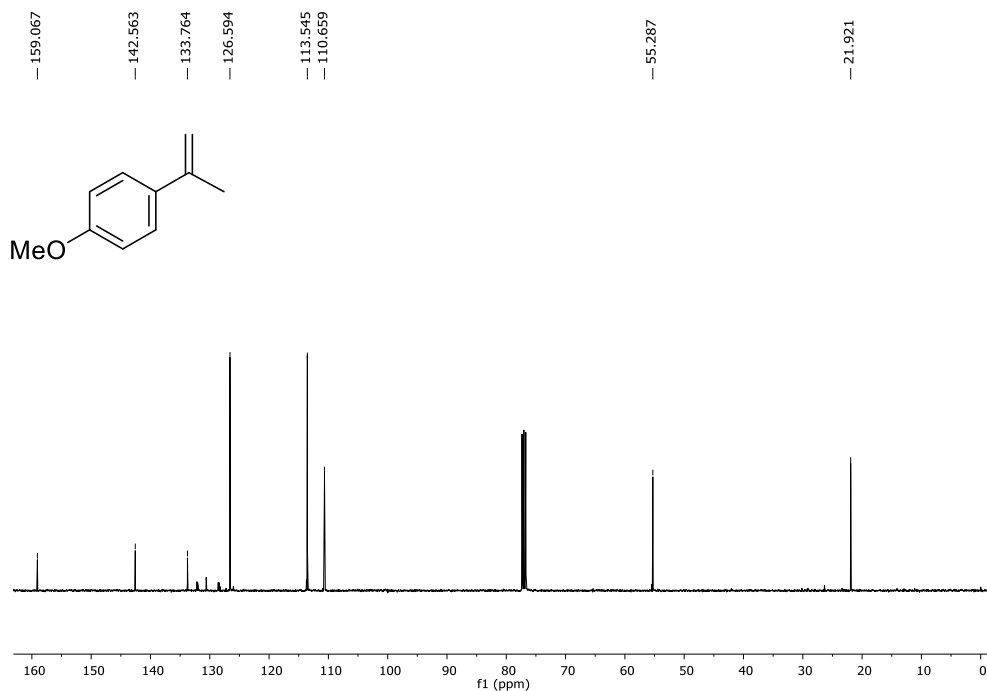
Figure A.VII.11. $^{13}C\{^1H\}$-NMR (CDCl$_3$, 100.6 MHz, 300 K) spectrum of substrate **15e.**
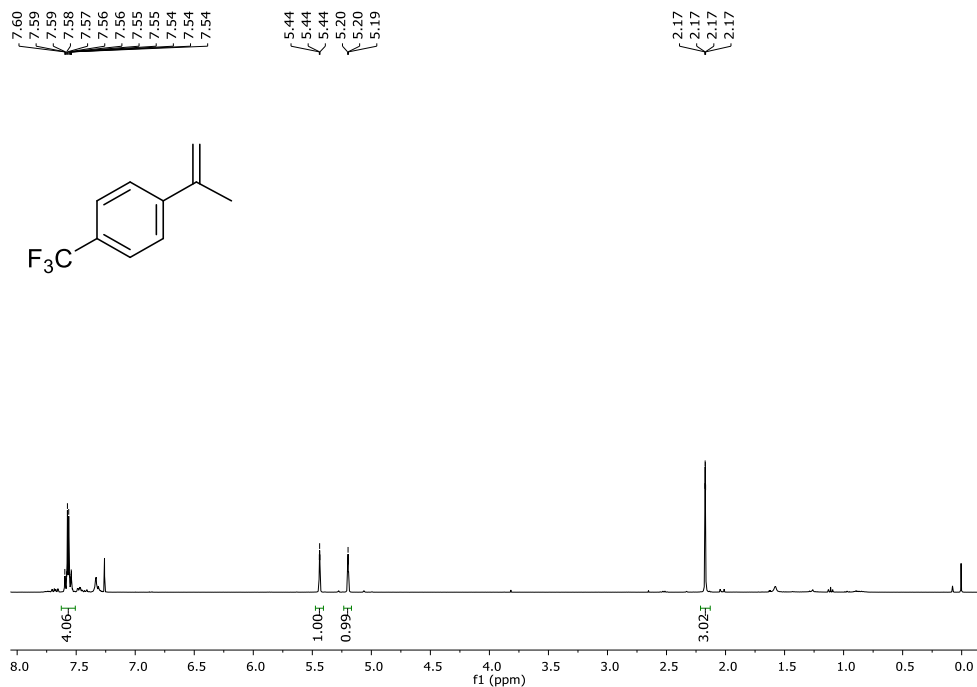
Figure A.VII.12. ^1H-NMR (CDCl$_3$, 400 MHz, 300 K) spectrum of substrate **15f.**

571
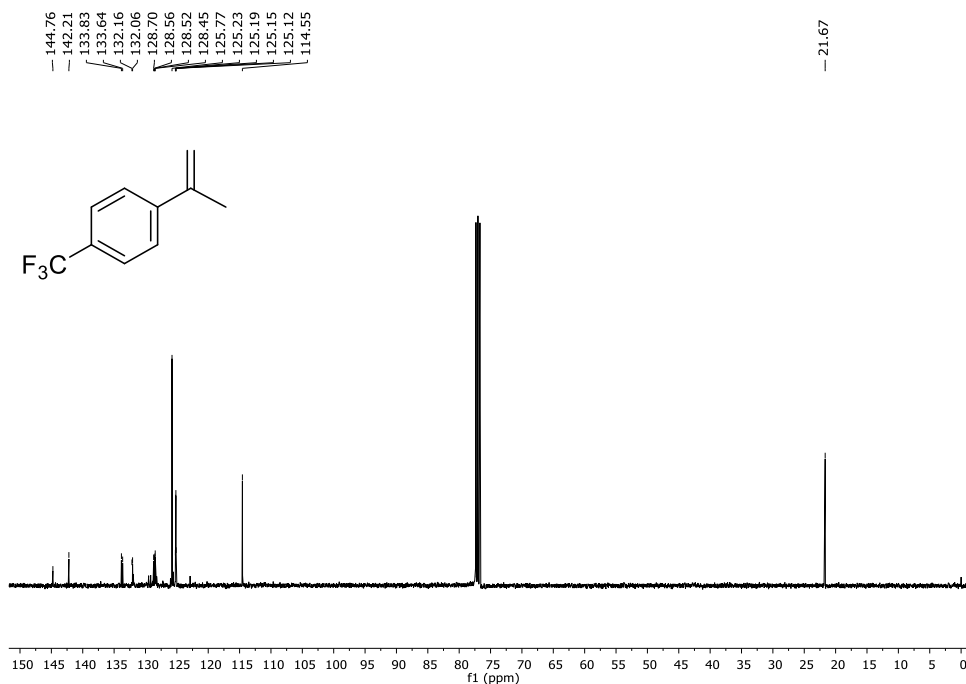
Figure A.VII.13. $^{13}C\{^1H\}$-NMR (CDCl$_3$, 100.6 MHz, 300 K) spectrum of substrate **15f.**
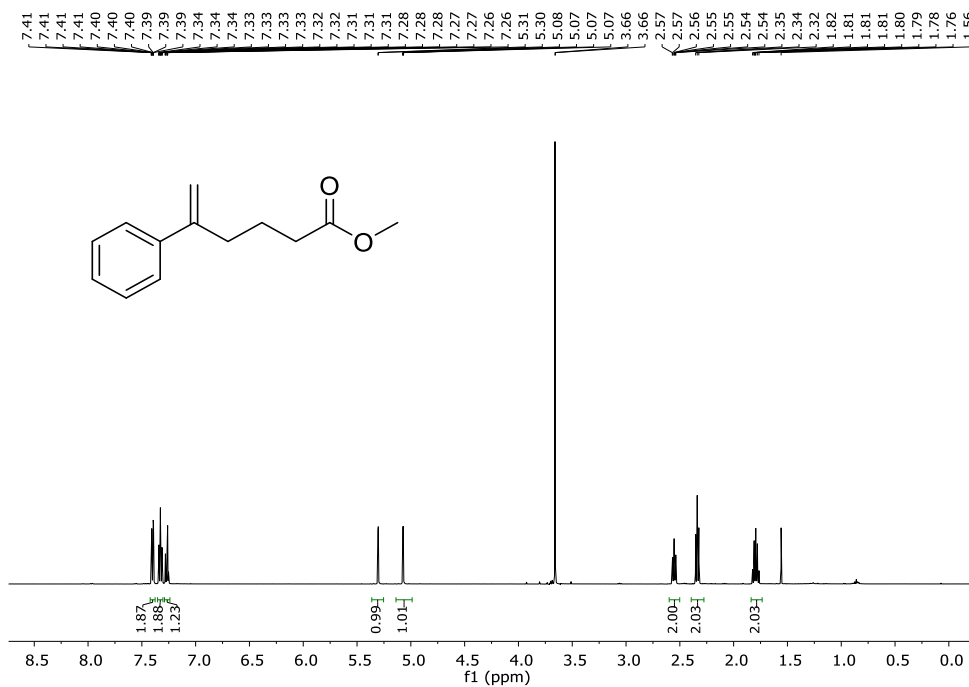
Figure A.VII.14. ^1H-NMR (CDCl$_3$, 500 MHz, 300 K) spectrum of substrate **15g.**

572
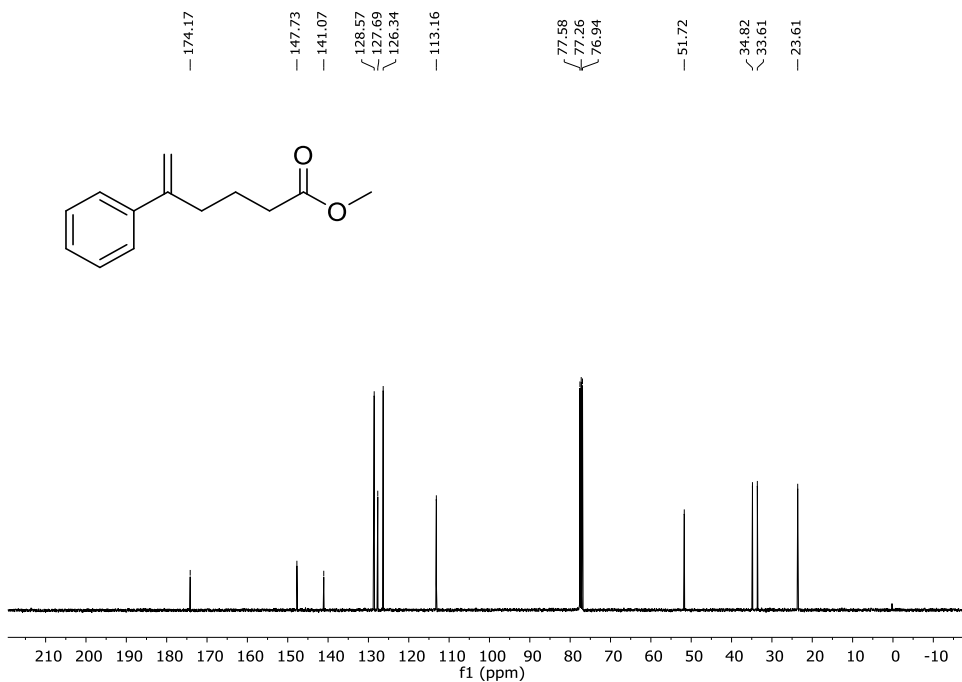
Figure A.VII.15. $^{13}C\{^1H\}$-NMR (CDCl$_3$, 100.6 MHz, 300 K) spectrum of substrate **15g.**
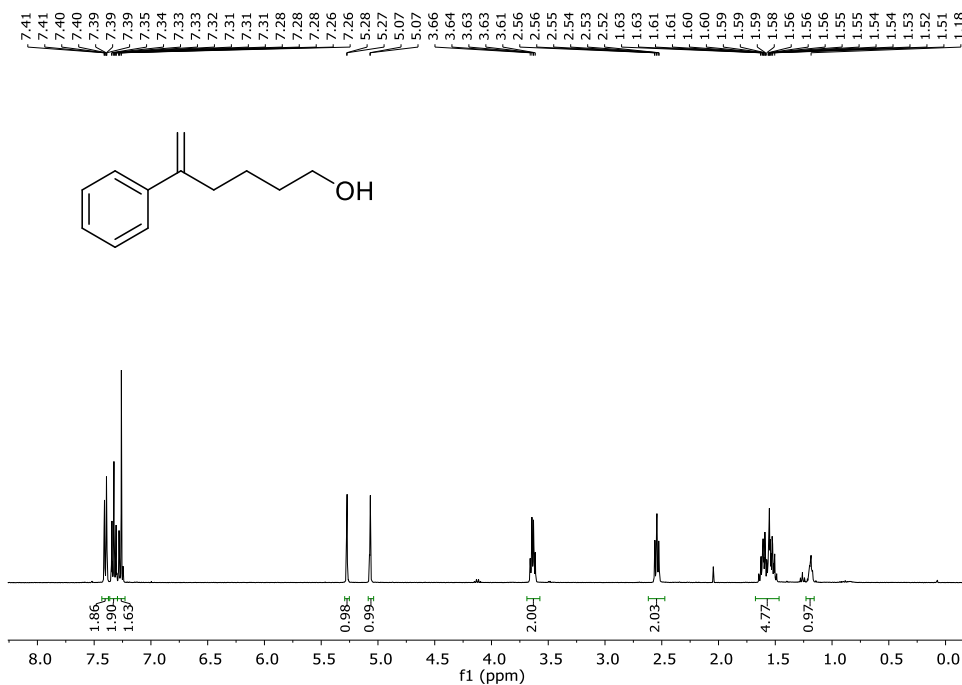
Figure A.VII.16. ^1H-NMR (CDCl$_3$, 400 MHz, 300 K) spectrum of substrate **15h.**

573
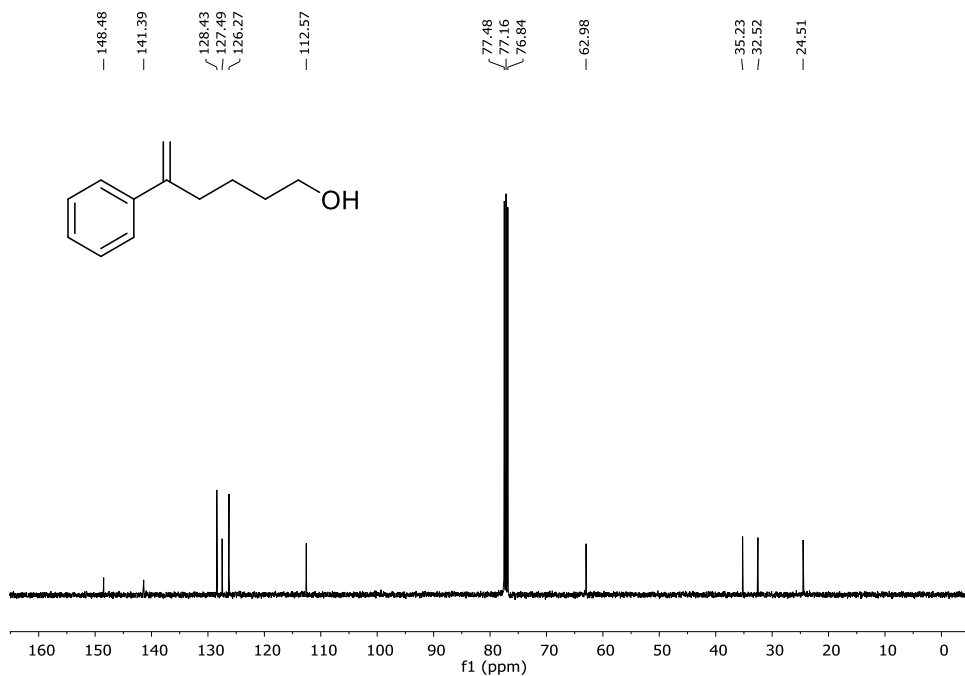
ANNEX

Figure A.VII.17. ^{13}C{^{1}H}-NMR (CDCl$_3$, 100.6 MHz, 300 K) spectrum of substrate **15h.**
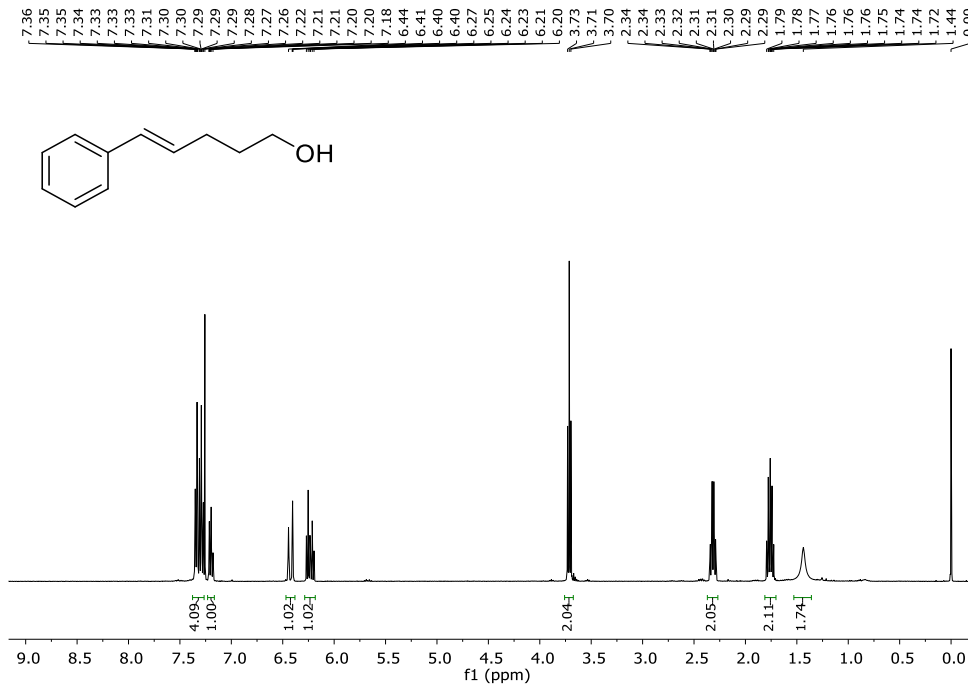
Figure A.VII.18. ^{1}H-NMR (CDCl$_3$, 400 MHz, 300 K) spectrum of substrate **18c.**

UNIVERSITAT ROVIRA I VIRGILI
MECHANISTIC STUDIES OF WATER OXIDATION CATALYZED BY HOMOGENEOUS IRON AND RUTHENIUM
COMPLEXES AND LIGHT-DRIVEN ORGANIC REDUCTIONS WITH A DUAL COBALT/COPPER CATALYTIC SYSTEM
Carla Casadevall Serrano
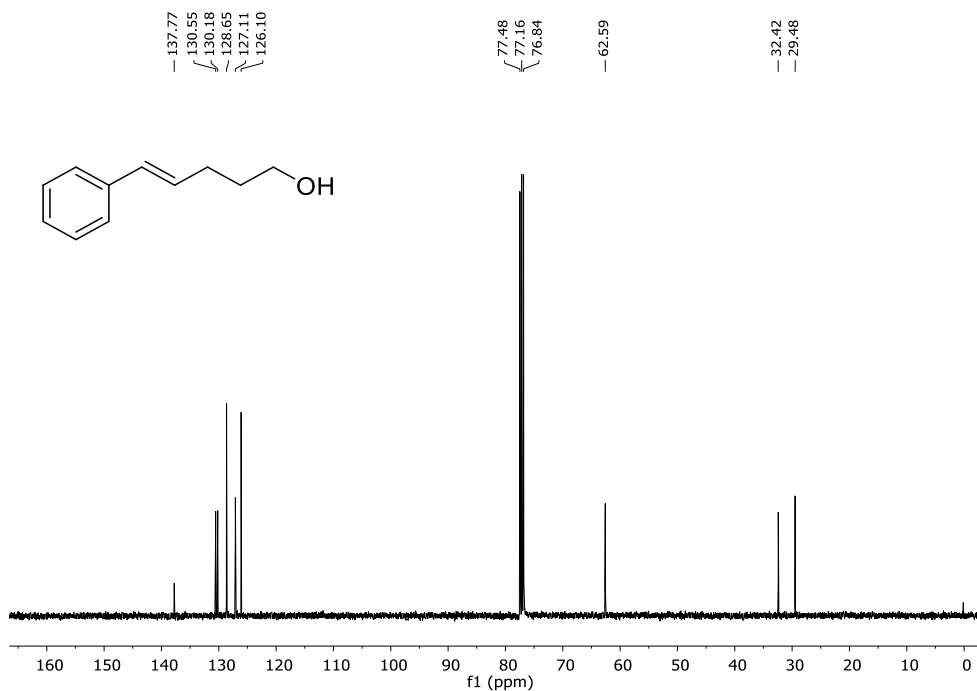
ANNEX

Figure A.VII.19. $^{13}C\{^1H\}$-NMR (CDCl$_3$, 100.6 MHz, 300 K) spectrum of substrate **18c.**
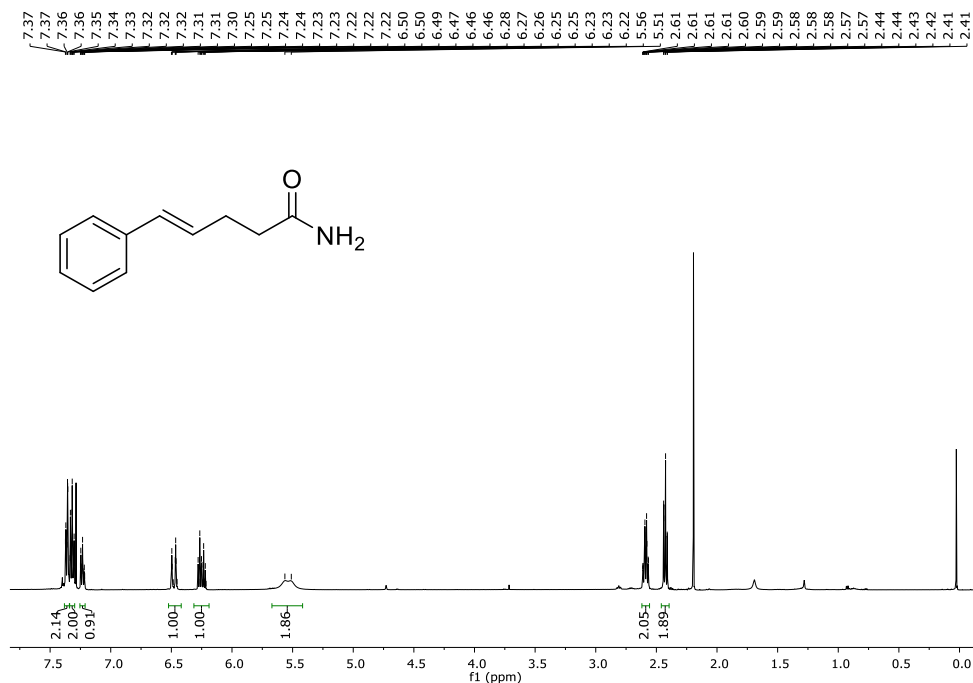
Figure A.VII.20. ^{1}H-NMR (CDCl$_3$, 400 MHz, 300 K) spectrum of substrate **18e.**

575
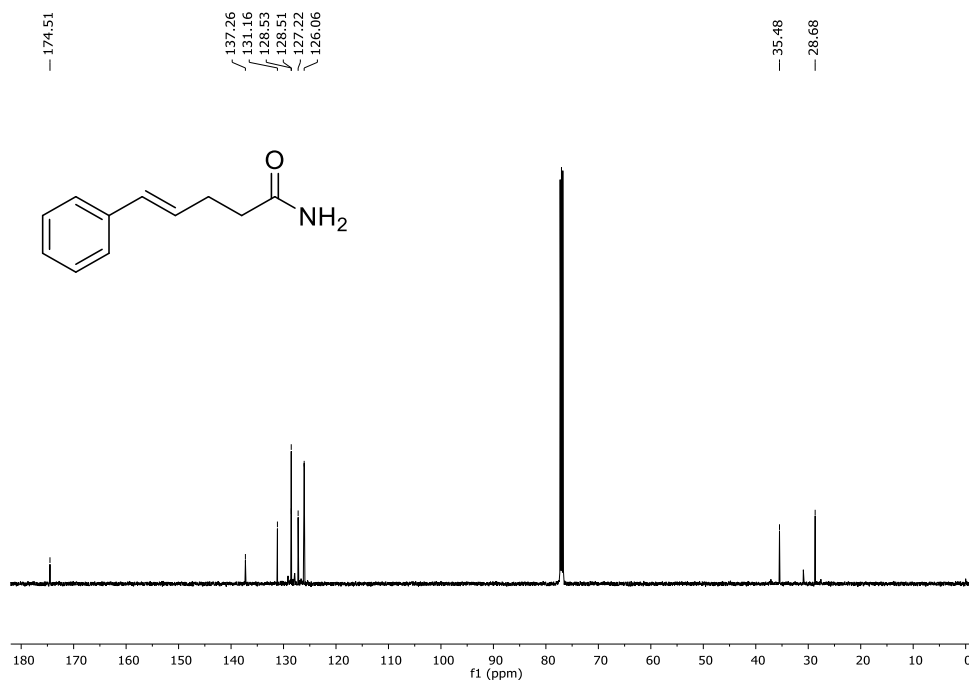
Figure A.VII.21. $^{13}C\{^{1}H\}$-NMR (CDCl$_3$, 100.6 MHz, 300 K) spectrum of substrate **18e.**
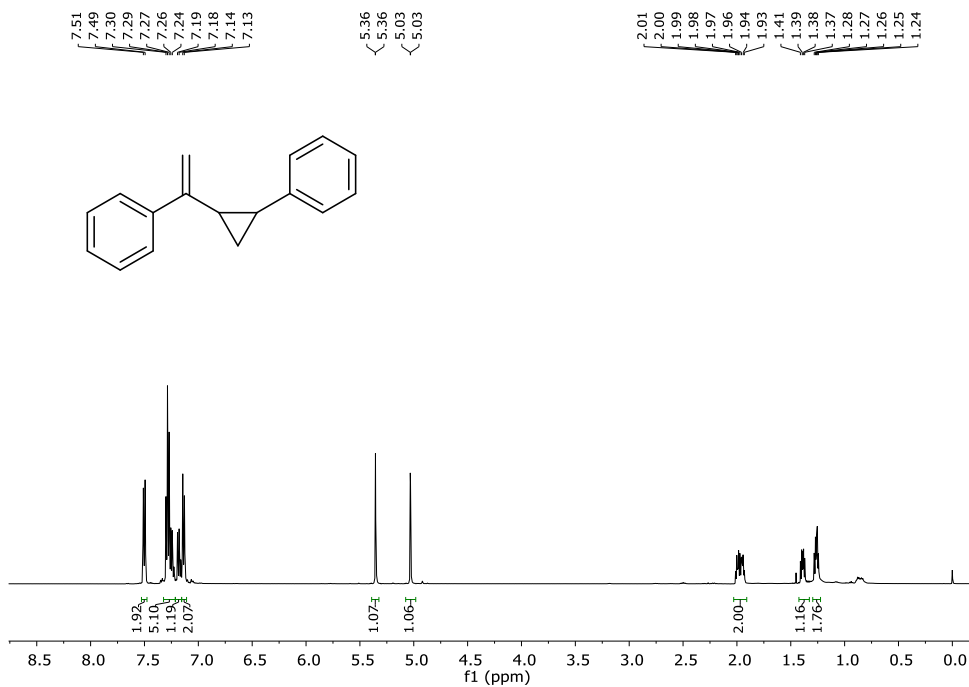
Figure A.VII.22. ^{1}H-NMR (CDCl$_3$, 500 MHz, 300 K) spectrum of substrate **16i.**

576
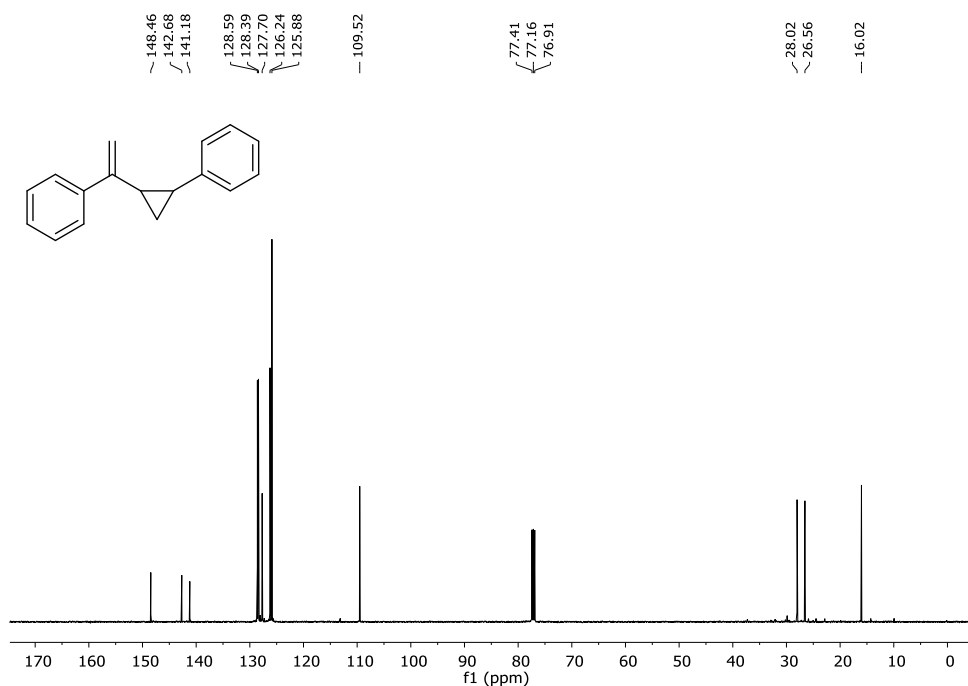
Figure A.VII.23. $^{13}C\{^1H\}$-NMR (CDCl$_3$, 125.75 MHz, 300 K) spectrum of substrate **16i.**

A.VII.9. ^{1}H- NMR spectra of the isolated alkanes
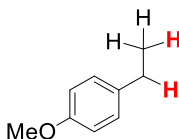
14b (92%) ^{1}H-NMR (CDCl$_3$, 400 MHz, 300 K) δ, ppm: 7.17-7.15 (m, 2H), 6.89-6.87 (m, 2H), 3.83 (s, 3H), 2.66-2.62 (m, 2H), 1.28-1.24 (m, 3H). $^{13}C\{^1H\}$-NMR (CDCl$_3$, 100.6 MHz, 300 K) δ, ppm: 157.63, 136.41, 128.72, 113.74, 55.28, 28.00, 15.93. MS (GC): 136.1 [M].
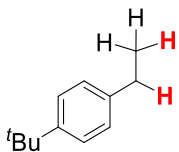
14c (81%) ^{1}H-NMR (CDCl$_3$, 400 MHz, 300 K) δ, ppm: 7.41-7.38 (m, 2H), 7.23-7.21 (m, 2H), 2.74-2.68 (m, 2H), 1.39 (s, 9H), 1.34-1.29 (m, 3H). $^{13}C\{^1H\}$-NMR (CDCl$_3$, 100.6 MHz, 300 K) δ, ppm: 148.38, 141.17, 127.54, 125.21, 34.37, 31.48, 28.31, 15.54. MS (GC): 162.1 [M].

577

ANNEX
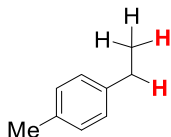
14d (92%) ^{1}H-NMR (CDCl$_3$, 300 MHz, 300 K) δ, ppm: 7.12 (s, 4H), 2.63 (q, J = 7.8 Hz, 2H), 2.34 (s, 3H), 1.24 (t, J = 7.8 Hz, 3H). MS (GC): 120.1 [M].
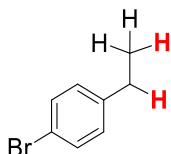
14e (53%) ^{1}H-NMR (CDCl$_3$, 300 MHz, 300 K) δ, ppm: 7.43-7.40 (m, 2H), 7.15-7.08 (m, 2H), 2.62 (q, J = 7.8 Hz, 2H), 1.24 (t, J = 7.8 Hz, 3H). ^{13}C{^{1}H}-NMR (CDCl$_3$, 75.45 MHz, 300 K) δ, ppm: 143.15, 131.32, 129.65, 119.26, 28.33, 15.48. MS (GC): 184.0 [M].
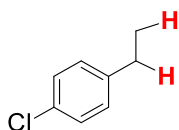
14f (66%) ^{1}H-NMR (CDCl$_3$, 400 MHz, 300 K) δ, ppm: 7.29-7.27 (m, 2H), 7.17-7.13 (m, 2H), 2.64 (q, J = 7.6 Hz, 2H), 1.25 (t, J = 7.6 Hz, 3H). ^{13}C{^{1}H}-NMR (CDCl$_3$, 100.6 MHz, 300 K) δ, ppm: 142.62, 131.25, 129.20, 128.36, 28.26, 15.52. MS (GC): 140.0 [M].
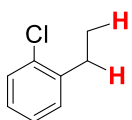
14k (61%) ^{1}H-NMR (CDCl$_3$, 400 MHz, 300 K) δ, ppm: 7.37-7.35 (m, 1H), 7.27-7.20 (m, 2H), 7.17-7.13 (m, 1H), 2.79 (q, J = 7.6 Hz, 2H), 1.26 (t, J = 7.6 Hz, 3H). ^{13}C{^{1}H}-NMR (CDCl$_3$, 100.6 MHz, 300 K) δ, ppm: 141.61, 133.79, 129.51, 129.35, 127.06, 126.80, 26.74, 14.04. MS (GC): 140.0 [M].
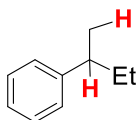
16b (57%) ^{1}H-NMR (CDCl$_3$, 400 MHz, 300 K) δ, ppm: 7.32-7.29 (m, 2H), 7.22-7.20 (m, 2H), 2.62 (sext., J = 6 Hz, 1H), 1.67-1.58 (m, 2H), 1.27 (d, J = 5.6 Hz, 3H), 0.85 (t, J = 5.6 Hz, 3H). ^{13}C{^{1}H}-NMR (CDCl$_3$, 100.6 MHz, 300 K) δ, ppm: 147.68, 128.22, 127.05, 125.74, 41.69, 31.18, 21.84, 12.26. MS (GC): 134.1 [M].
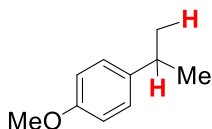
16e (74%) ^{1}H-NMR (CDCl$_3$, 400 MHz, 300 K) δ, ppm: 7.19-7.17 (m, 2H), 6.88-6.86 (m, 2H), 3.22 (s, 3H), 2.89 (sept., J = 6.8 Hz, 1H), 1.26 (s, 3H), 1.25 (s, 3H). ^{13}C{^{1}H}-NMR (CDCl$_3$, 100.6 MHz, 300 K) δ, ppm: 157.64, 141.05, 127.23, 113.68, 55.25, 33.27, 24.21. MS (GC): 150.1 [M].
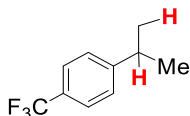
16f ^{1}H-NMR (CDCl$_3$, 400 MHz, 300 K) δ, ppm: 7.59-7.56 (m, 2H), 7.37-7.35 (m, 2H), 2.99 (sept, J = 6.8 Hz, 1H), 1.31 (s, 3H), 1.29 (s, 3H). ^{13}C{^{1}H}-NMR (CDCl$_3$, 100.6 MHz, 300 K) δ, ppm: 152.86, 133.74 (d, J = 19.4 Hz), 128.75 (d, J = 11.57 Hz), 128.48 (d, J = 6.94 Hz), 126.75, 125.24 (q, J = 3.82 Hz), 34.11, 23.74. MS (GC): 188.1 [M].
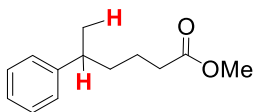
16g (66%). ^{1}H-NMR (CDCl$_3$, 400 MHz, 300 K) δ, ppm: 7.33-7.25 (m, 2H), 7.22-7.15 (m, 3H), 3.64 (s, 3H), 2.69 (sext., J = 6.9 Hz, 1H), 2.30-2.24 (m, 2H), 1.65-1.46 (m, 4H), 1.25 (d, J = 6.9 Hz, 3H). ^{13}C{^{1}H}-NMR (CDCl$_3$, 100.6 MHz, 300 K) δ, ppm: 174.2, 147.3, 128.5, 127.1, 126.1, 51.6, 39.9, 37.9, 34.3, 23.3, 22.4. GC (MS): 206.1 [M].
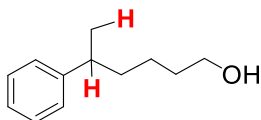
16h (83%). ^{1}H-NMR (CDCl$_3$, 400 MHz, 300 K) δ, ppm: 7.32-7.25 (m, 2H), 7.21-7.16 (m 3H), 3.59 (td, J = 6.5, 4.6 Hz, 2H), 2.69 (h, J = 7.0 Hz, 1H), 1.66-1.49 (m, 4H), 1.38-1.13 (m, 6H). ^{13}C{^{1}H}-NMR (CDCl$_3$, 100.6 MHz, 300 K) δ, ppm: 147.7, 128.5, 127.1, 126.0, 63.1, 40.1, 38.3, 33.0, 24.0, 22.5. MS (GC): 178.1 [M].
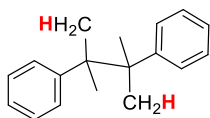
17a (45%). ^{1}H-NMR (CDCl$_3$, 500 MHz, 300 K) δ, ppm: 7.21-7.18 (m, 6H), 7.10-7.08 (m, 4H), 1.34 (s, 12H). ^{13}C{^{1}H}-NMR (CDCl$_3$, 125.75 MHz, 300 K) δ, ppm: 146.81, 128.61, 126.61, 125.46, 43.63, 25.18. MS (GC): 238.2 [M].
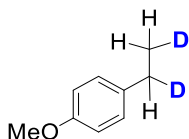
1-(ethyl-1,2-*d$_2$*)-4-methoxybenzene ([D]-14b). ^{1}H-NMR (CDCl$_3$, 400 MHz, 300 K) δ, ppm: 7.15-7.13 (m, 2H, **H$_{arom}$**), 6.87-6.85 (m, 2H, **H$_{arom}$**), 3.82 (s, 3H, O-C**H$_3$**), 2.62-2.58 (m, 2H, C**H$_2$**), 1.28-1.24 (m, 3H, C**H$_3$**). ^{13}C{^{1}H}-NMR (CDCl$_3$, 100.6 MHz, 300 K) δ, ppm: 157.62, 136.36, 128.68, 113.73, 55.27, 27.53 (t, J = 19.1 Hz, **C**HD), 15.79-15.30 (m, **C**H$_2$D).
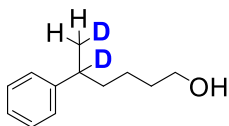
5-phenylhexan-5,6-*d$_2$*-1-ol ([D]-16h). ^{1}H-NMR (CDCl$_3$, 400 MHz, 300 K) δ, ppm: 7.32-7.28 (m, 2H, **H$_{arom}$**), 7.21-7.18 (m, 2H, **H$_{arom}$**), 3.63-3.59 (m, 2H, O-C**H$_2$**), 1.64-1.53 (m, 4H, (C**H$_2$**)$_2$), 1.28-1.24 (m, 4H, C**H$_2$D** and C**H$_2$**). ^{13}C{^{1}H}-DEPT-135-NMR (CDCl$_3$, 125.8 MHz, 300 K) δ, ppm: 128.30, 126.94, 125.84, 62.94, 38.04, 32.85, 23.84, 22.19, 21.88 (t, J = 19.2 Hz, **C**H$_2$D).
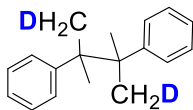
(2,3-dimethylbutane-2,3-diyl-1,4-*d$_2$*)dibenzene ([D]-17a). ^{1}H-NMR (CDCl$_3$, 400 MHz, 300 K) δ, ppm: 7.20-7.18 (m, 6H, **H$_{arom}$**), 7.10-7.08 (m, 4H, **H$_{arom}$**), 1.33 (s, 10H, (C**H$_3$**)$_2$ and (C**H$_2$D**)). ^{13}C{^{1}H}-DEPT-135-NMR (CDCl$_3$, 125.8 MHz, 300 K) δ, ppm: 128.59, 126.60, 125.45, 25.13, 24.87 (t, J = 19.2 Hz, **C**H$_2$D).
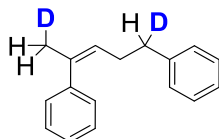
(Z)-(pent-3-ene-1,4-diyl-1,5-*d$_2$*)dibenzene ([D]-16i). ^{1}H-NMR (CDCl$_3$, 400 MHz, 300 K) δ, ppm: 7.35-7.31 (m, 2H, **H$_{arom}$**), 7.30-7.25 (m, 3H, **H$_{arom}$**), 7.21-7.19 (m, 2H, **H$_{arom}$**), 7.15-7.12 (m, 3H, **H$_{arom}$**), 5.53-5.52 (m, 1H, olefin-C**H**), 2.68-2.63 (m, 1H, C**H**D), 2.34-2.29 (m, 2H, C**H$_2$**), 2.05-2.02 (m, 2H, C**H$_2$D**). ^{13}C{^{1}H}-NMR (CDCl$_3$, 100.6 MHz, 300 K) δ, ppm: 146.81, 128.61, 126.61, 125.46, 43.63, 25.18. MS (GC): 238.2 [M].
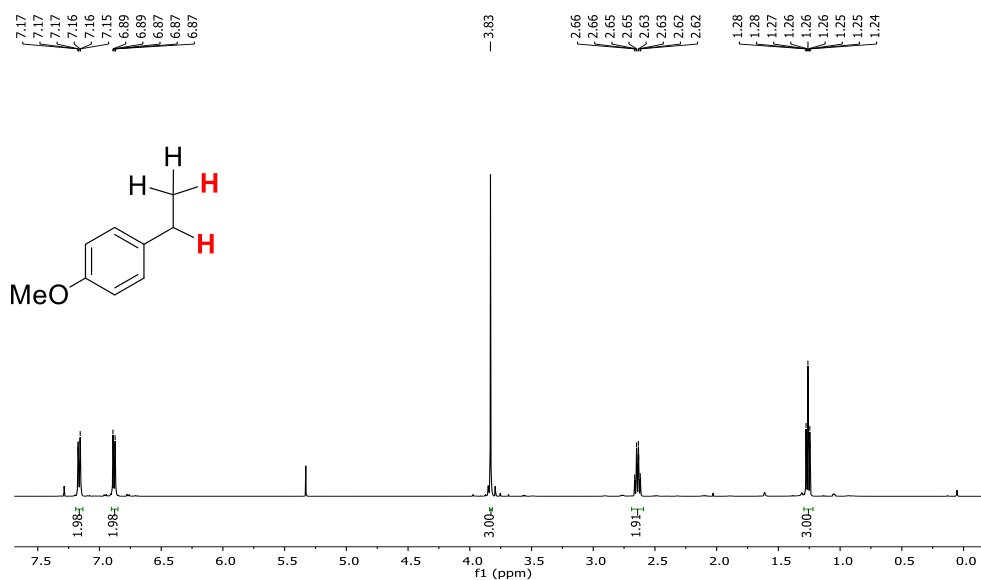
Figure A.VII.24. ^{1}H-NMR (CDCl$_3$, 400 MHz, 300 K) spectrum of product **14b.**
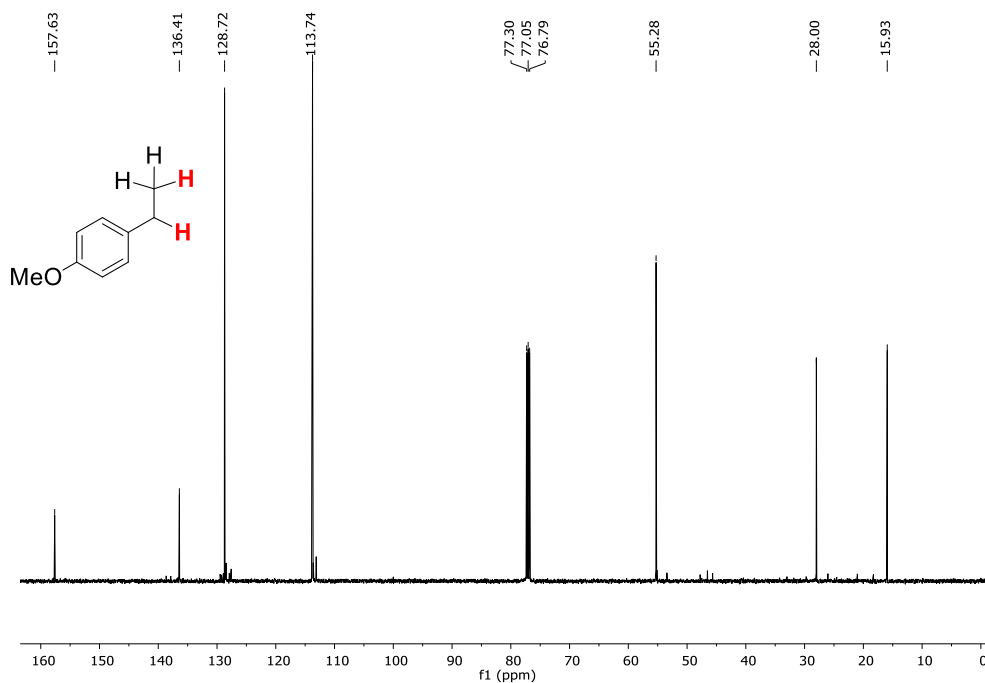
Figure A.VII.25. ^{13}C{^{1}H}-NMR (CDCl$_3$, 100.6 MHz, 300 K) spectrum of product **14b.**
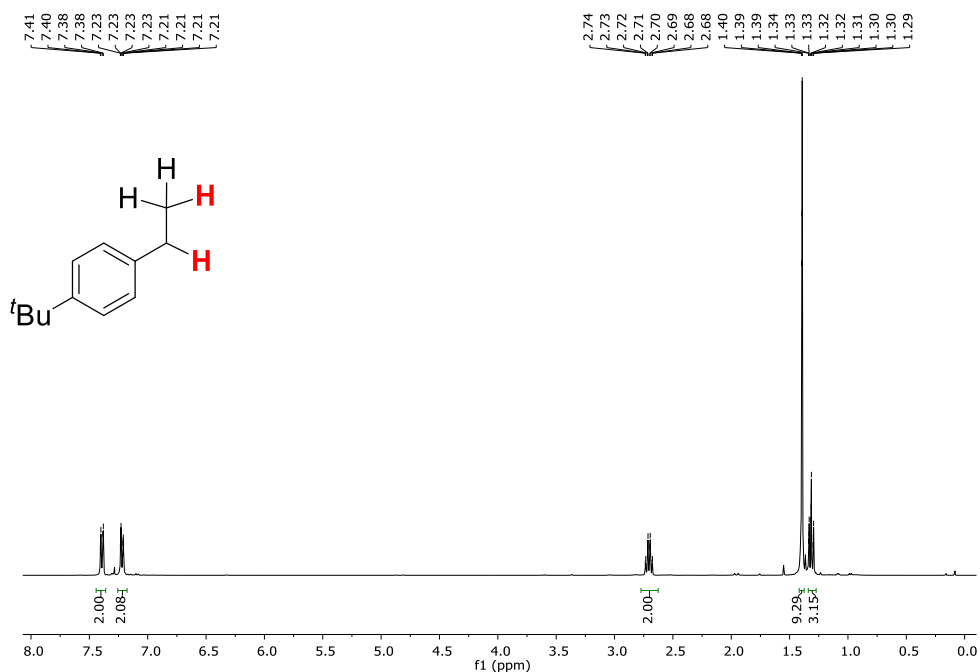
Figure A.VII.26. ^{1}H-NMR (CDCl$_3$, 400 MHz, 300 K) spectrum of product **14c**.
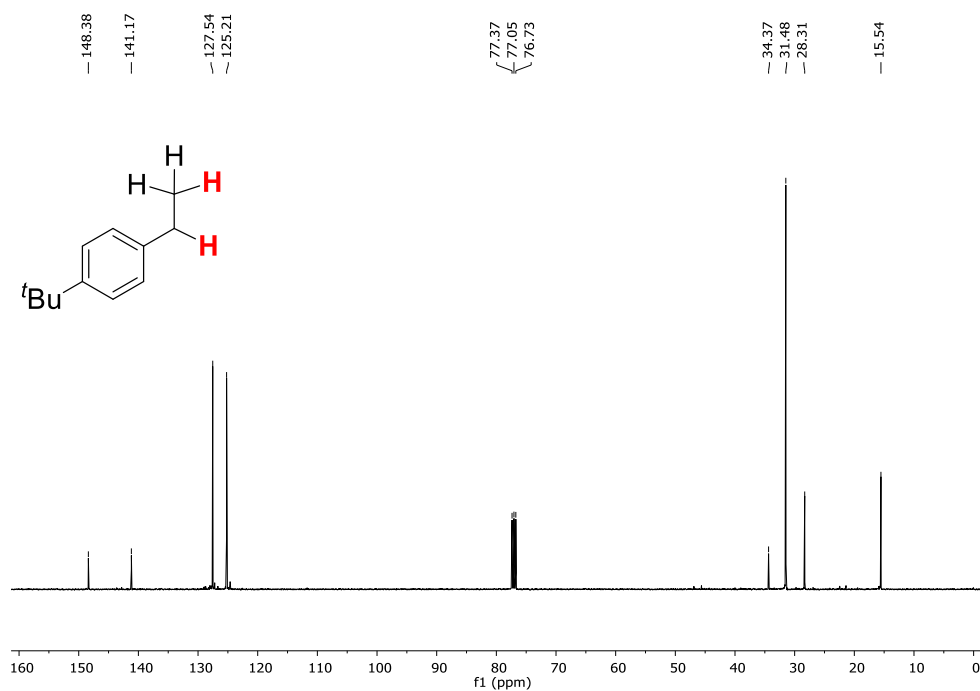
Figure A.VII.27. ^{13}C{^{1}H}-NMR (CDCl$_3$, 100.6 MHz, 300 K) spectrum of product **14c**.
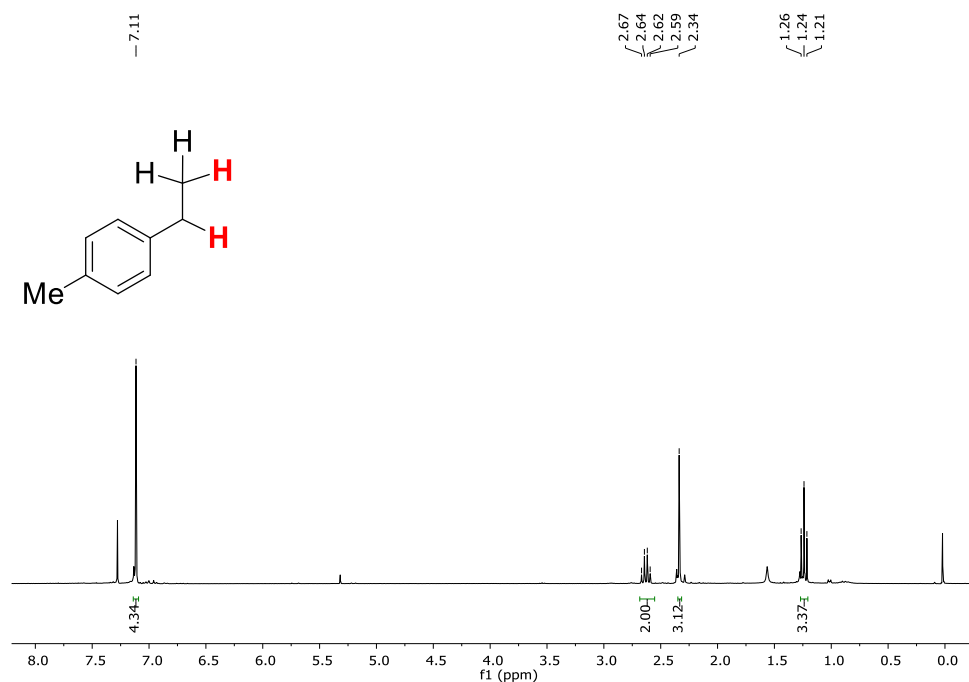
Figure A.VII.28. ^{1}H-NMR (CDCl$_3$, 400 MHz, 300 K) spectrum of product **14d.**
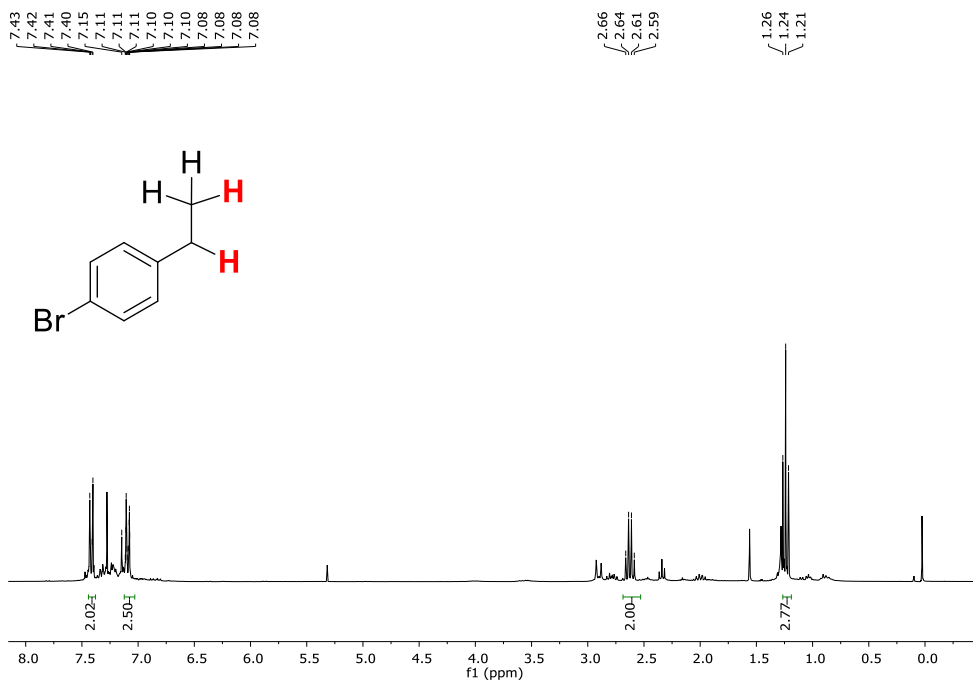
Figure A.VII.29. ^{1}H-NMR (CDCl$_3$, 400 MHz, 300 K) spectrum of product **14e.**
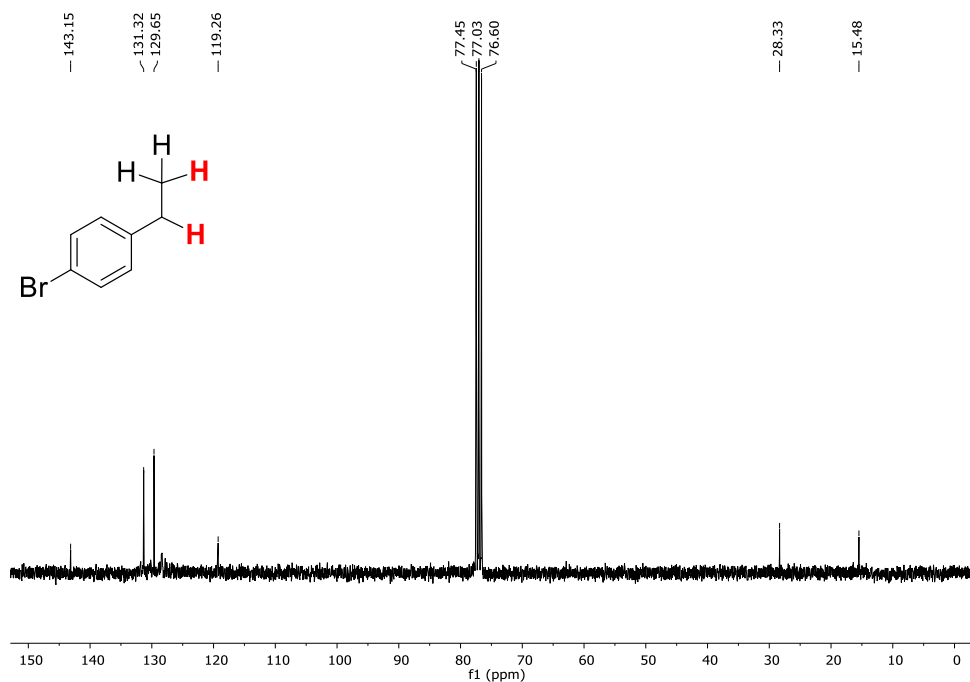
Figure A.VII.30. $^{13}C\{^{1}H\}$-NMR (CDCl$_3$, 100.6 MHz, 300 K) spectrum of product **14e.**
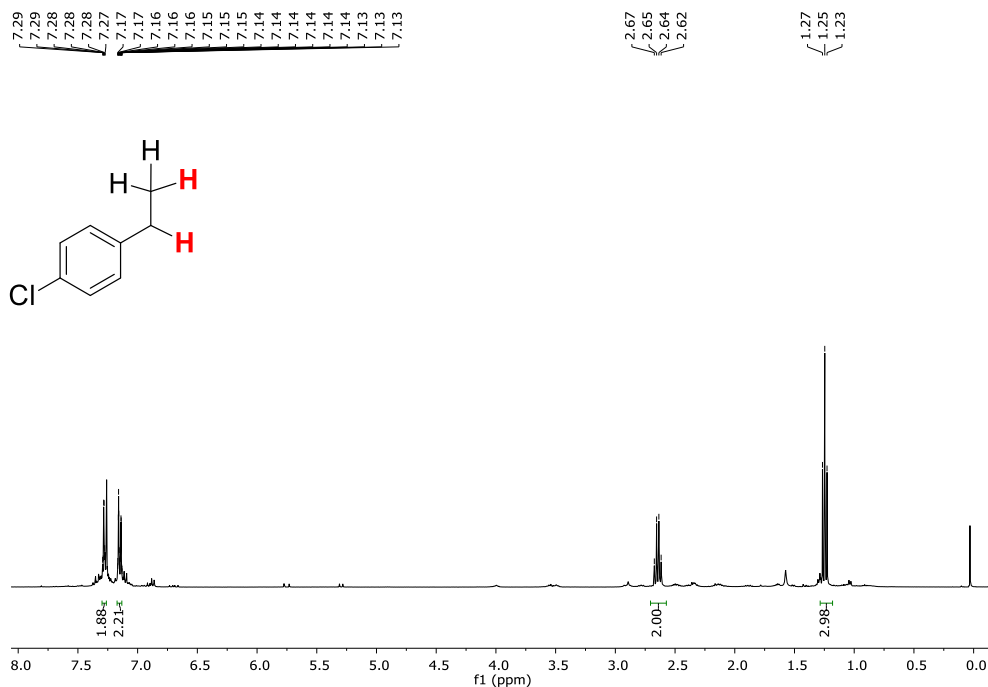
Figure A.VII.31. ^{1}H-NMR (CDCl$_3$, 400 MHz, 300 K) spectrum of product **14f.**
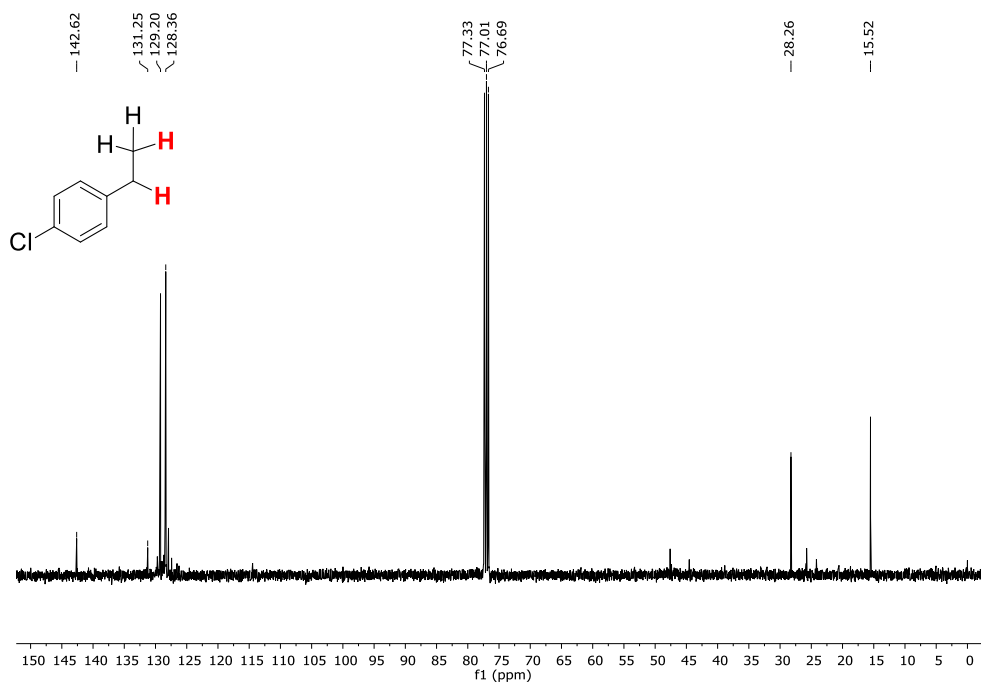
Figure A.VII.32. $^{13}C\{^{1}H\}$-NMR (CDCl$_3$, 100.6 MHz, 300 K) spectrum of product **14f.**
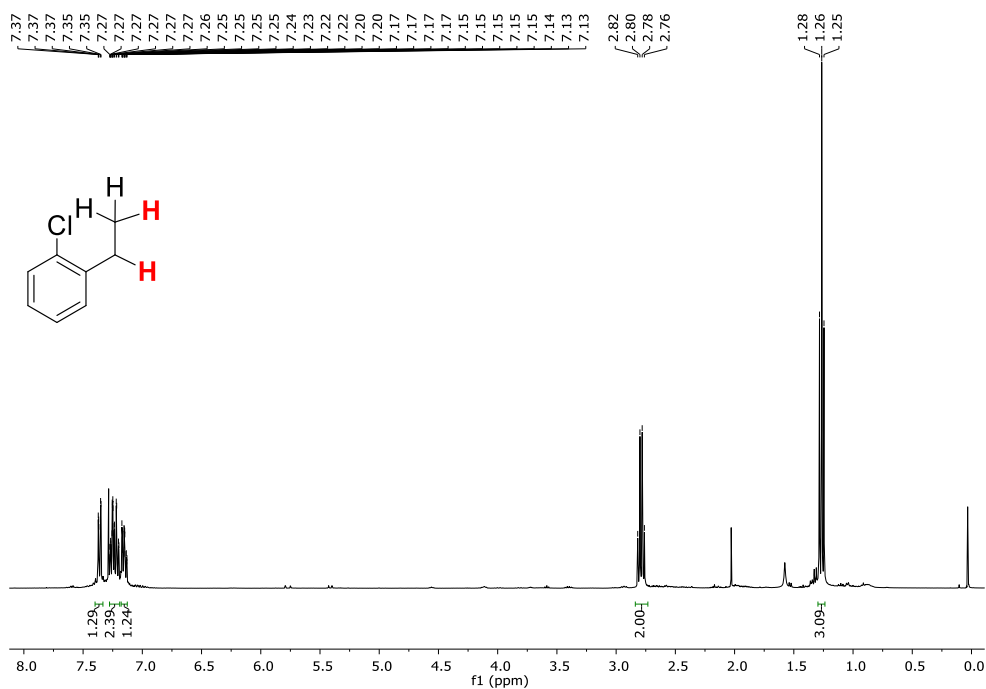
Figure A.VII.33. ^{1}H-NMR (CDCl$_3$, 400 MHz, 300 K) spectrum of product **14k.**

585
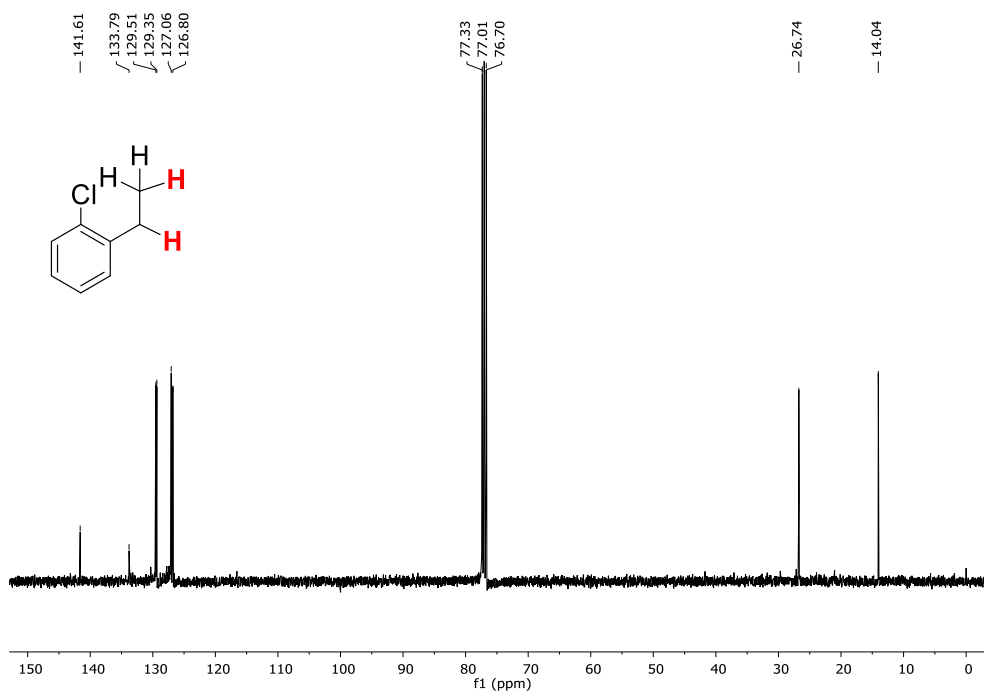
Figure A.VII.34. $^{13}C\{^{1}H\}$-NMR (CDCl$_3$, 100.6 MHz, 300 K) spectrum of product **14k.**
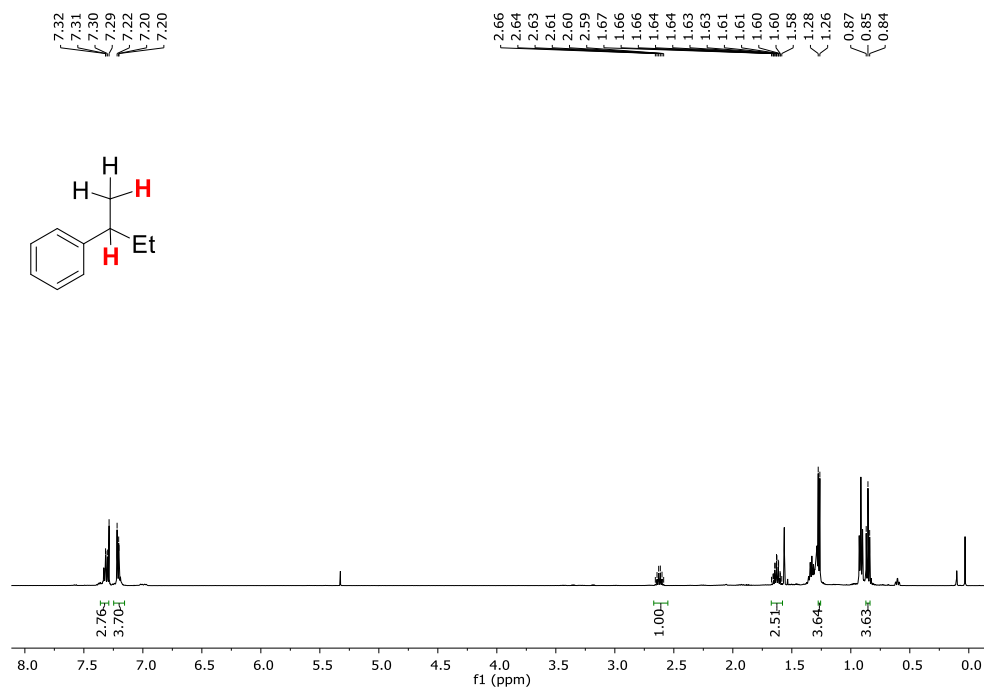
Figure A.VII.35. ^{1}H-NMR (CDCl$_3$, 400 MHz, 300 K) spectrum of product **16b.**

586
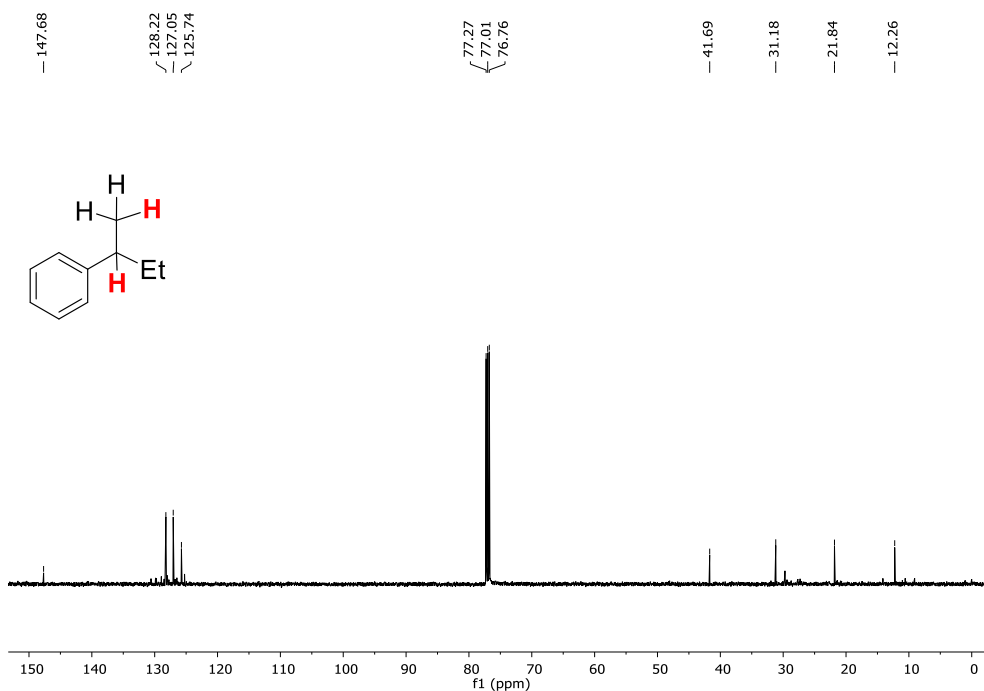
Figure A.VII.36. $^{13}C\{^1H\}$-NMR (CDCl$_3$, 100.6 MHz, 300 K) spectrum of product **16b.**
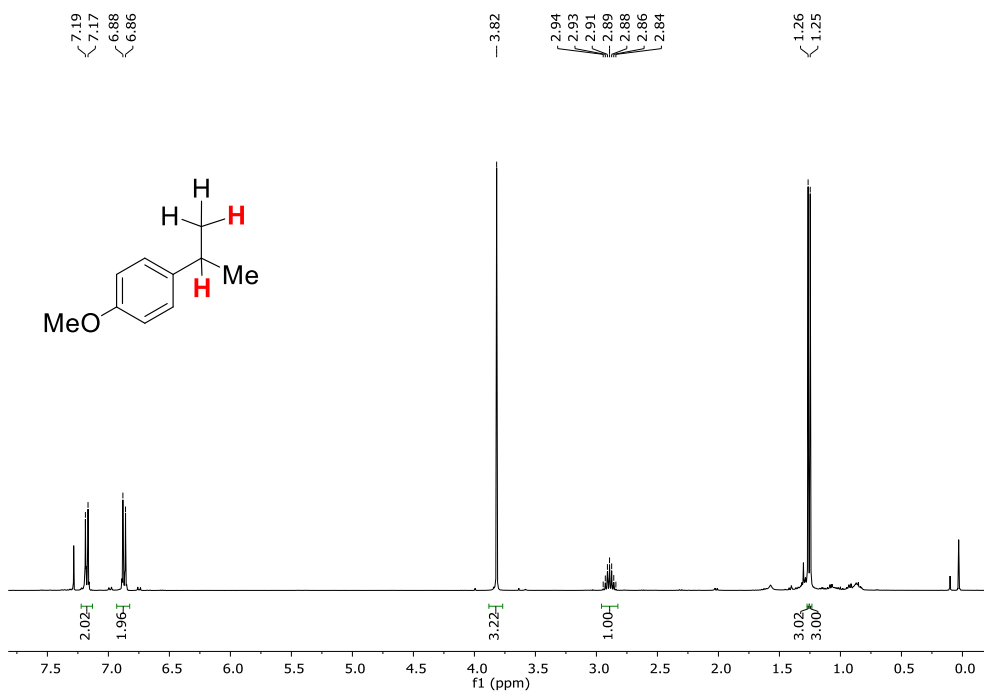
Figure A.VII.37. ^{1}H-NMR (CDCl$_3$, 400 MHz, 300 K) spectrum of product **16e.**

587
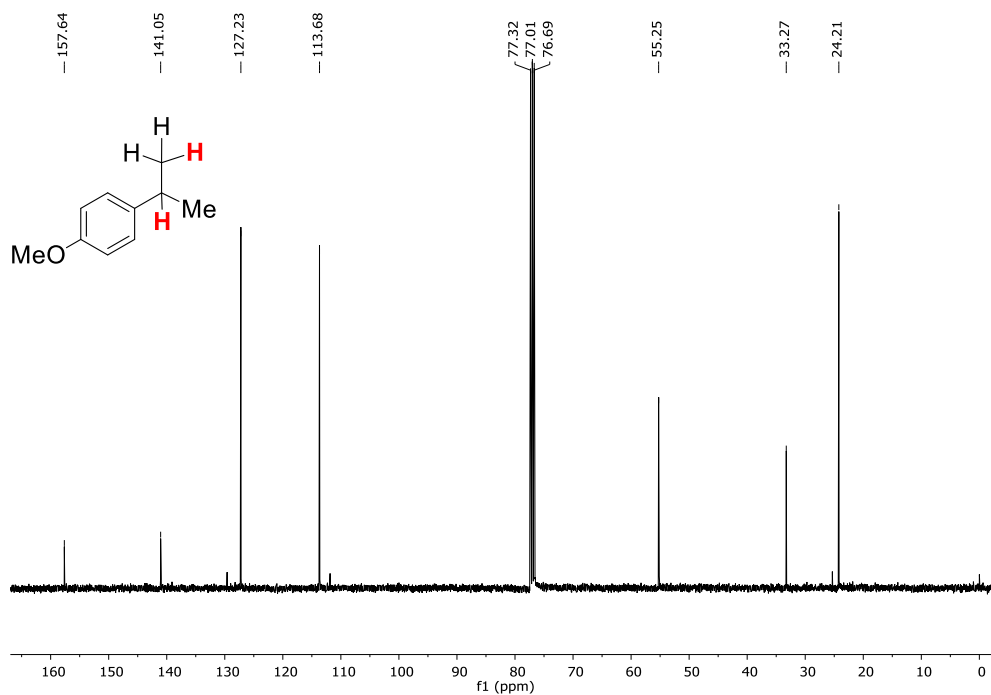
Figure A.VII.38. $^{13}C\{^1H\}$-NMR (CDCl$_3$, 100.6 MHz, 300 K) spectrum of product **16e.**
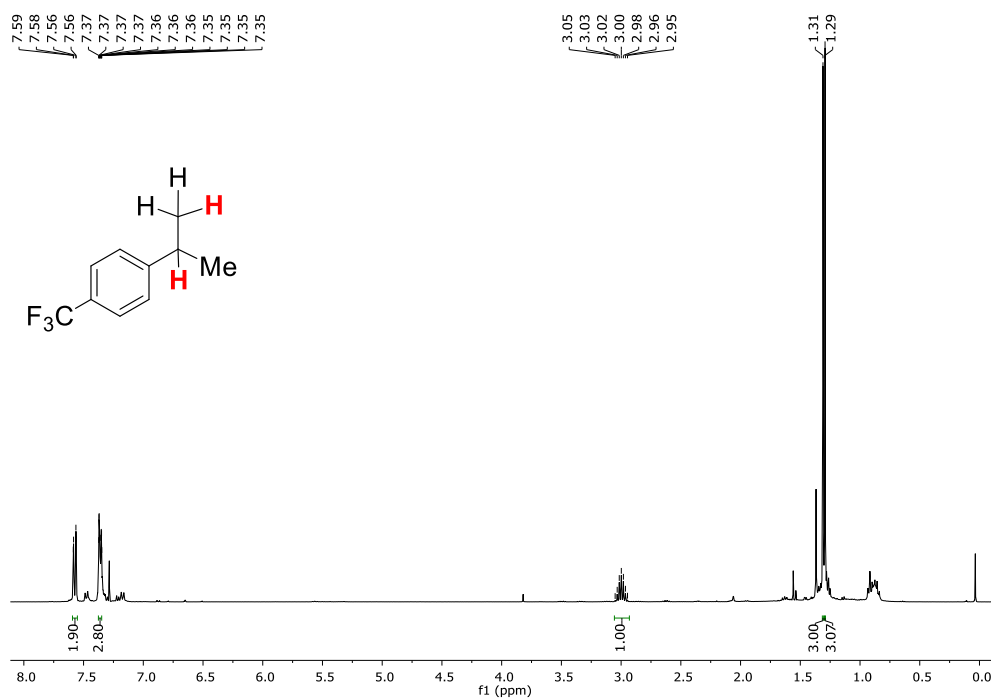
Figure A.VII.39. ^{1}H-NMR (CDCl$_3$, 400 MHz, 300 K) spectrum of product **16f.**
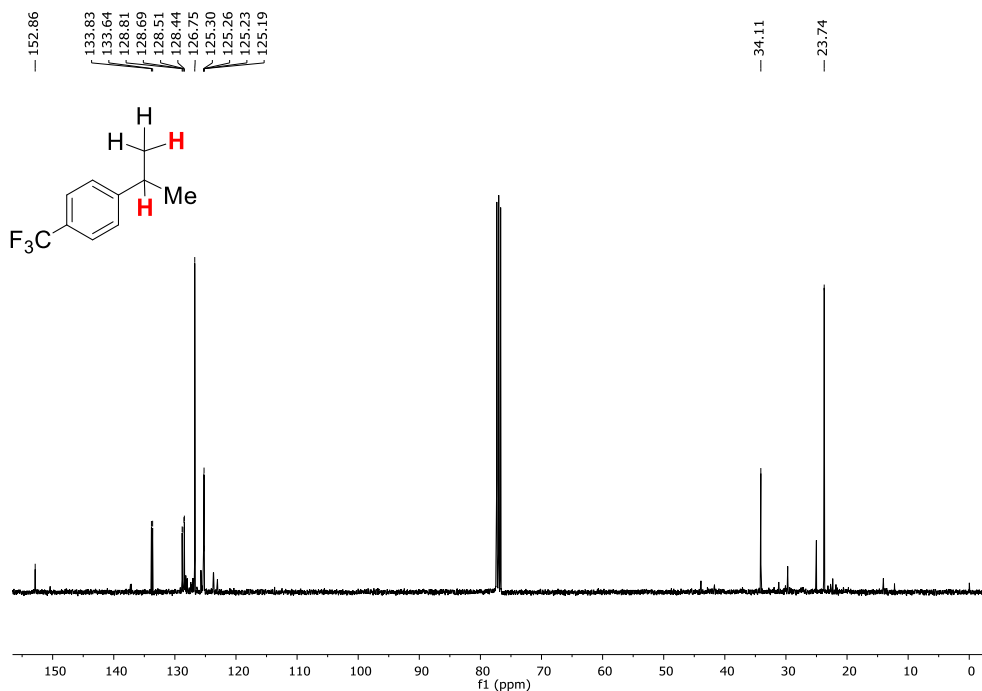
Figure A.VII.40. $^{13}C\{^1H\}$-NMR (CDCl$_3$, 100.6 MHz, 300 K) spectrum of product **16f.**
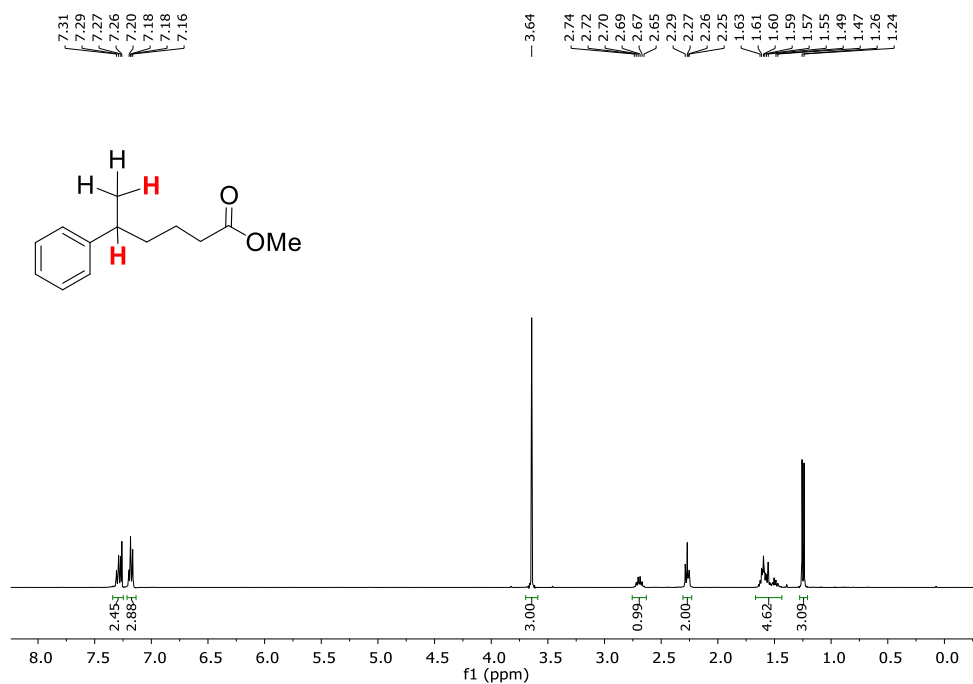
Figure A.VII.41. ^{1}H-NMR (CDCl$_3$, 400 MHz, 300 K) spectrum of product **16g.**
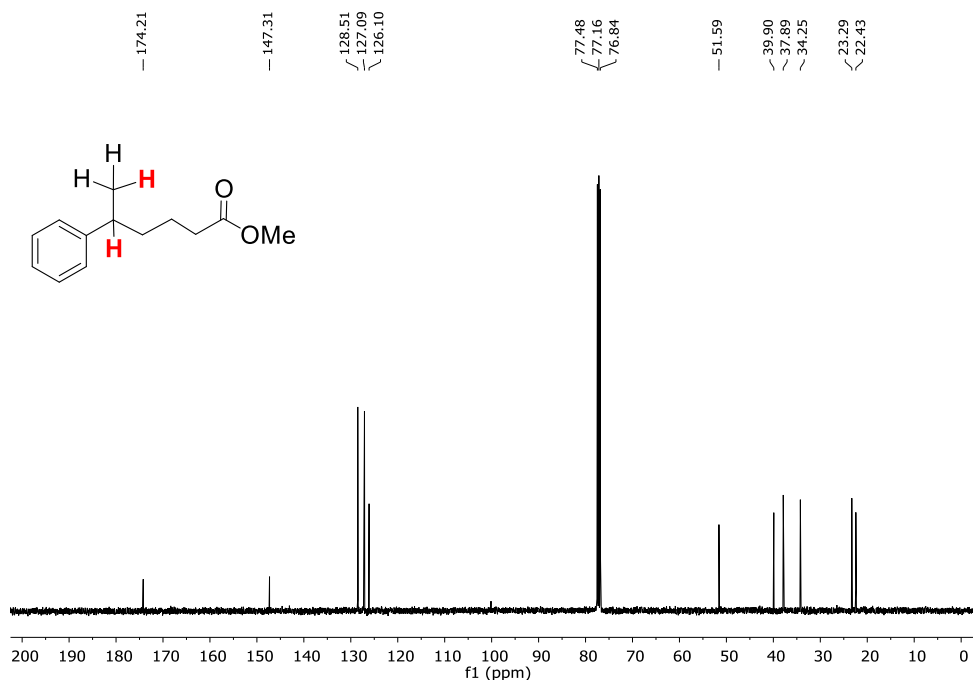
Figure A.VII.42. $^{13}C\{^1H\}$-NMR (CDCl$_3$, 100.6 MHz, 300 K) spectrum of product **16g**.
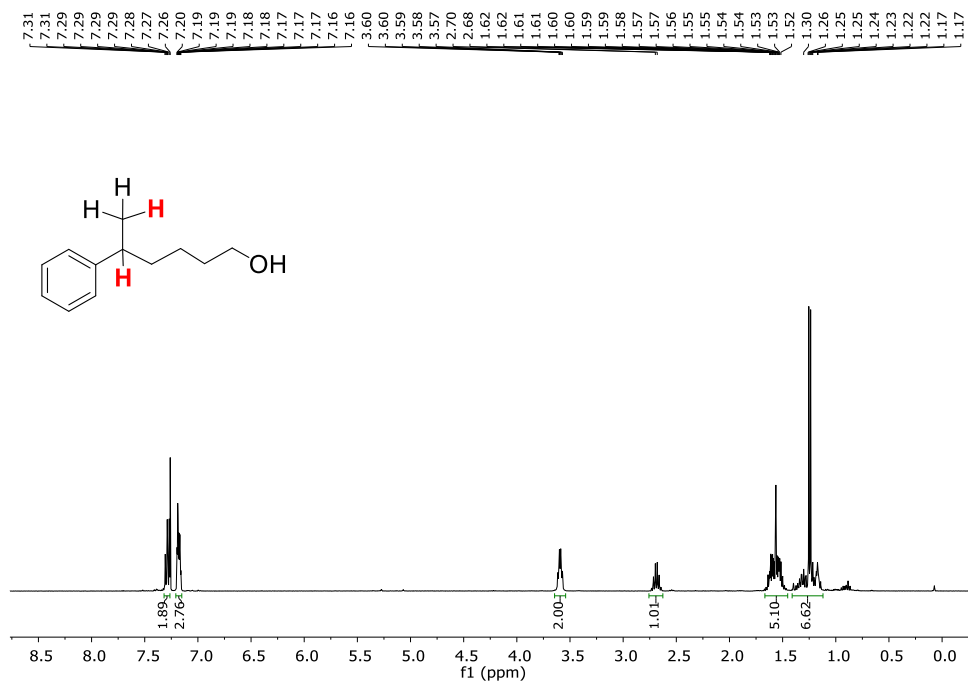
Figure A.VII.43. ^{1}H-NMR (CDCl$_3$, 400 MHz, 300 K) spectrum of product **16h**.
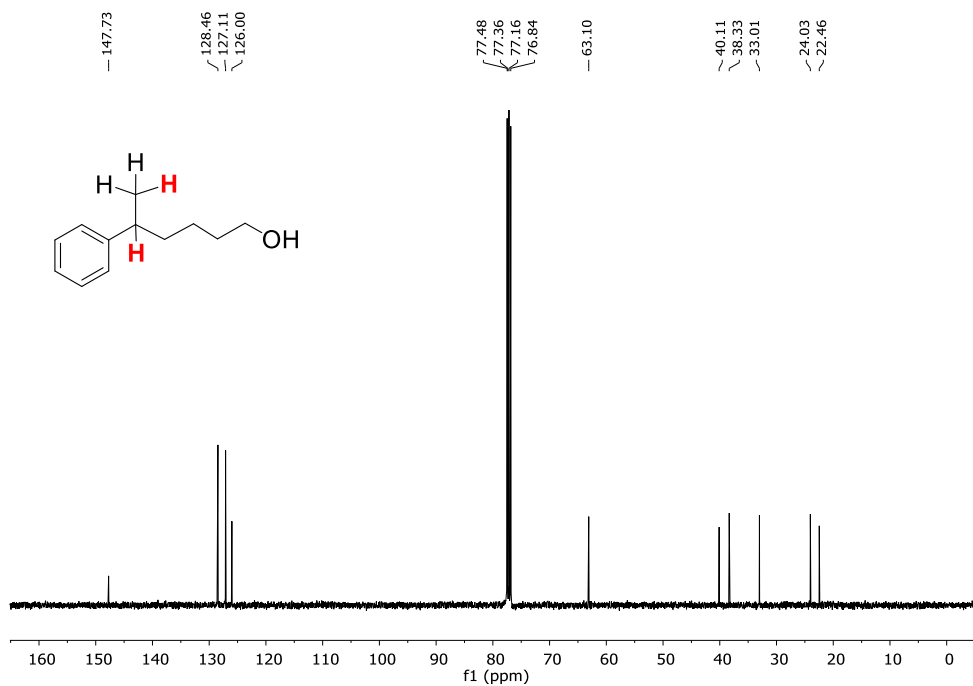
Figure A.VII.44. $^{13}C\{^1H\}$-NMR (CDCl$_3$, 100.6 MHz, 300 K) spectrum of product **16h**.
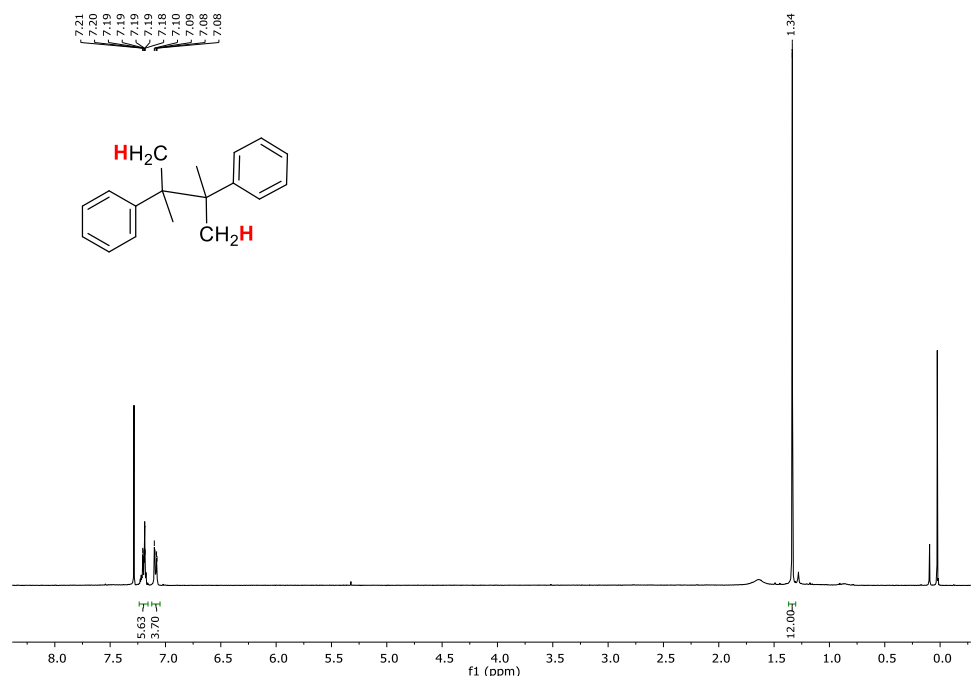
Figure A.VII.45. ^{1}H-NMR (CDCl$_3$, 500 MHz, 300 K) spectrum of product **17a**.
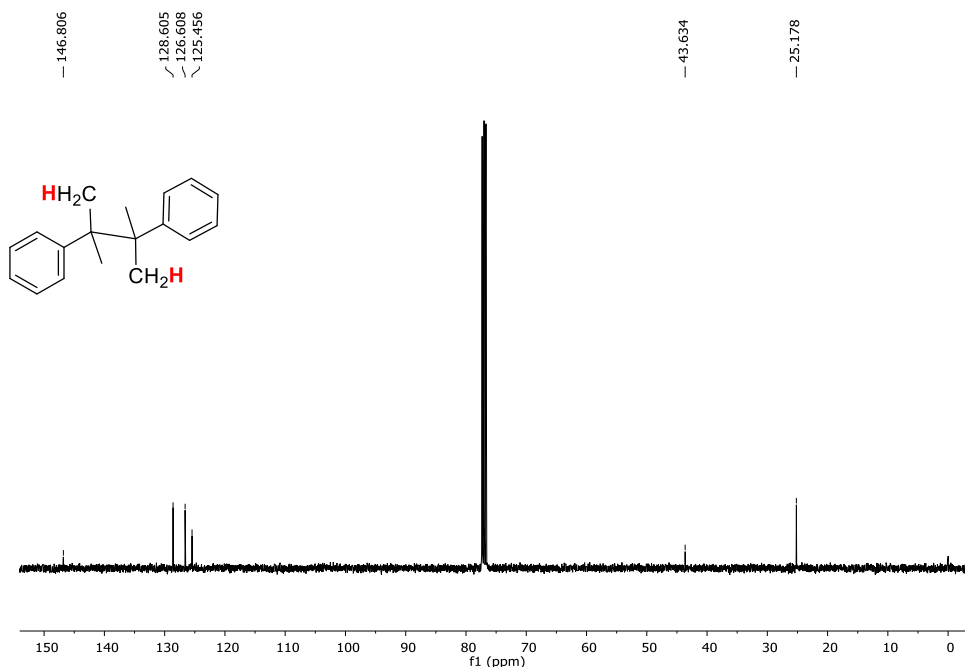
Figure A.VII.46. $^{13}C\{^1H\}$-NMR (CDCl$_3$, 125.75 MHz, 300 K) spectrum of product **17a**.

A.VII.10. NMR of the radical clock ring-opening products

(1-(2-phenylcyclopropyl)vinyl)benzene
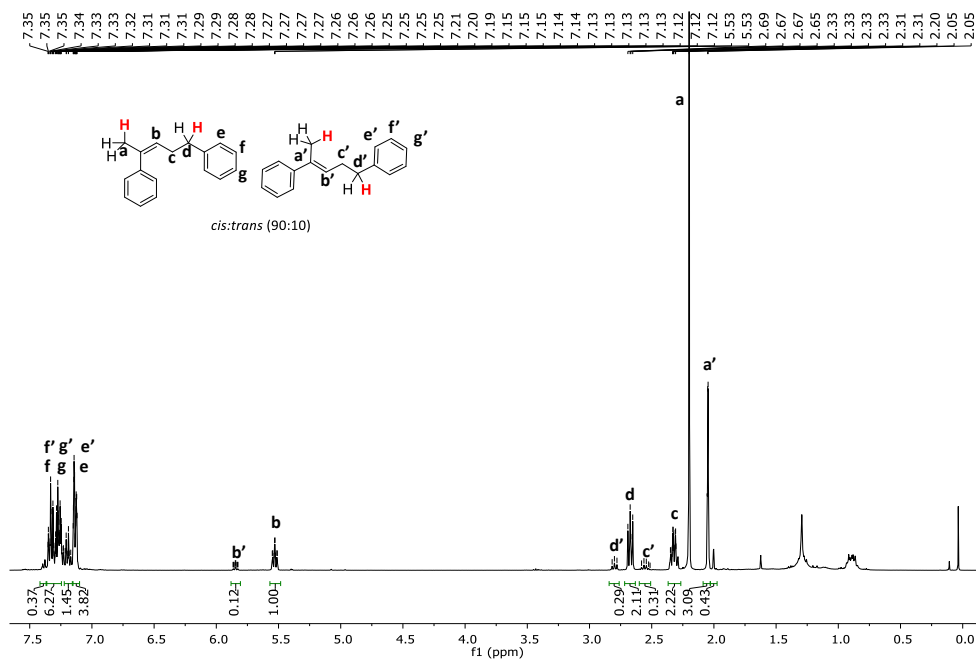
Figure A.VII.47. ^1H-NMR (CDCl$_3$, 400 MHz, 300 K) spectrum of the isolated product **17i** (in H$_2$O).
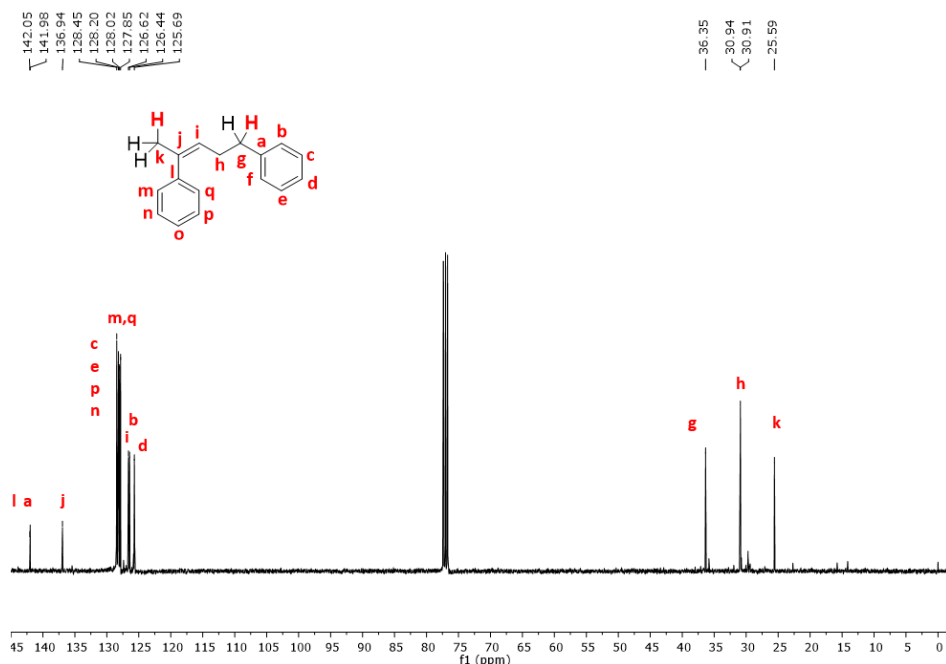
Figure A.VII.48. $^{13}C\{^1H\}$-NMR (CDCl$_3$, 100.6 MHz, 300 K) spectrum of the isolated product **17i** (in H$_2$O).
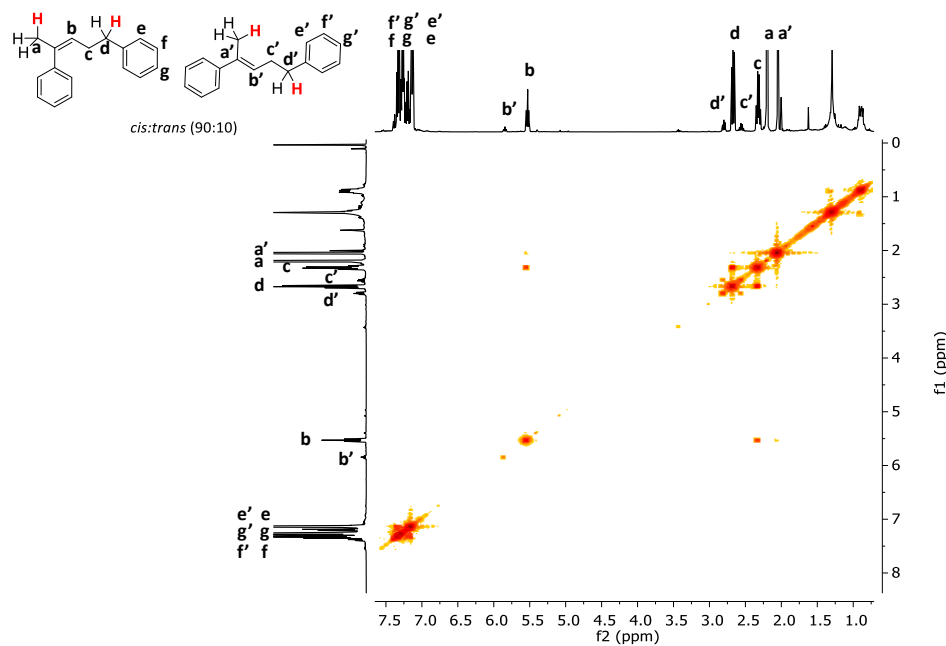
Figure A.VII.49. ^{1}H-^{1}H COSY (CDCl$_3$, 400 MHz, 300 K) spectrum of the isolated of product **17i** (in H$_2$O).
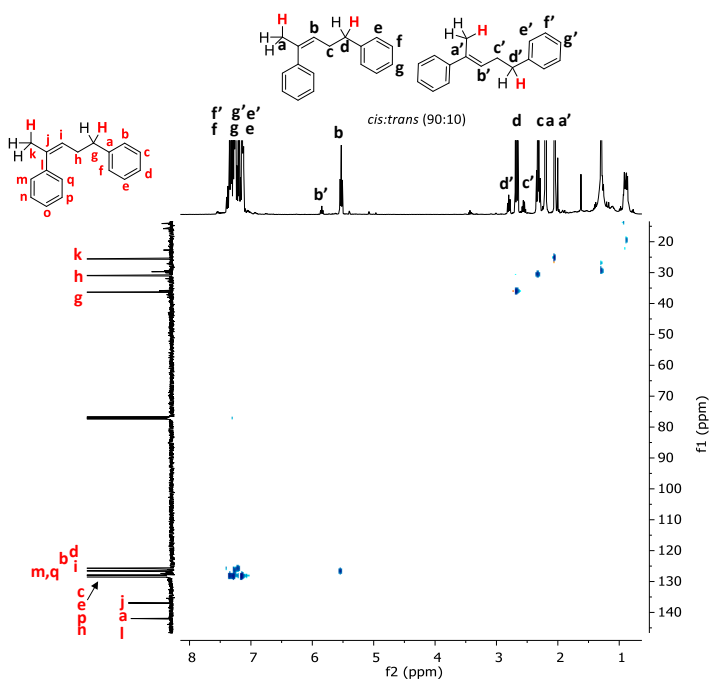
Figure A.VII.50. ^1H-^{13}C HMBC (CDCl$_3$, 400 MHz, 300 K) of the isolated product **17i** (in H$_2$O).
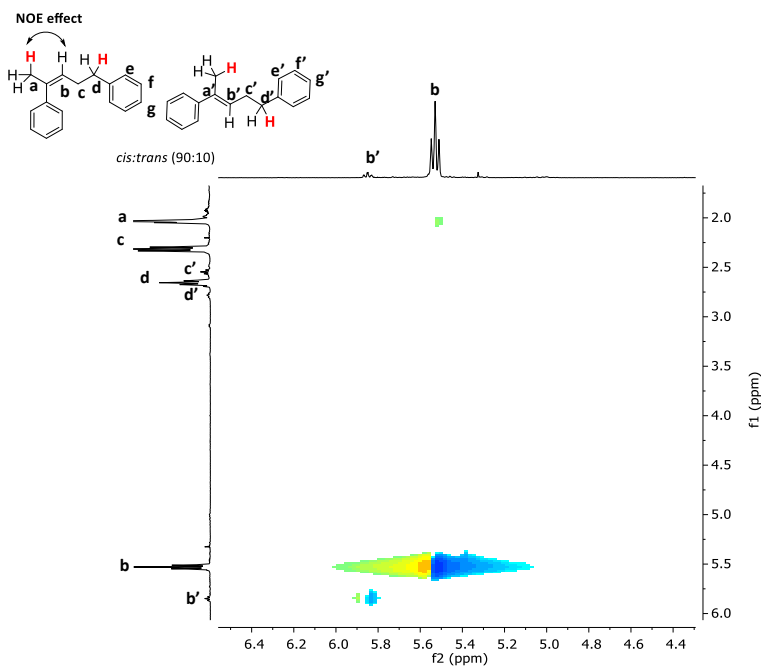
Figure A.VII.51. ^1H-NOESY (CDCl$_3$, 400 MHz, 300 K) of the isolated product **17i** (in H$_2$O).

594

A.VII.11. GC chromatograms from the catalysis
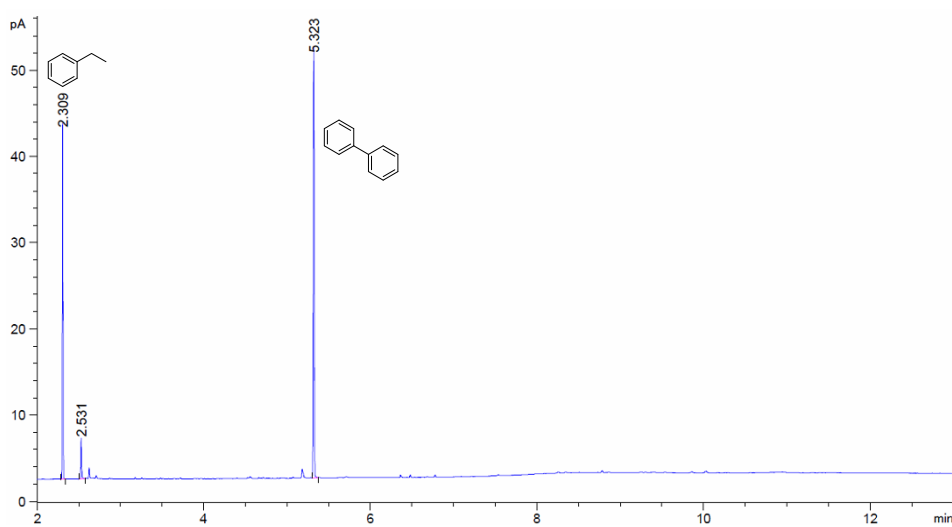
Figure A.VII.52. GC-FID chromatogram of the reduced product **14a** from the catalysis.
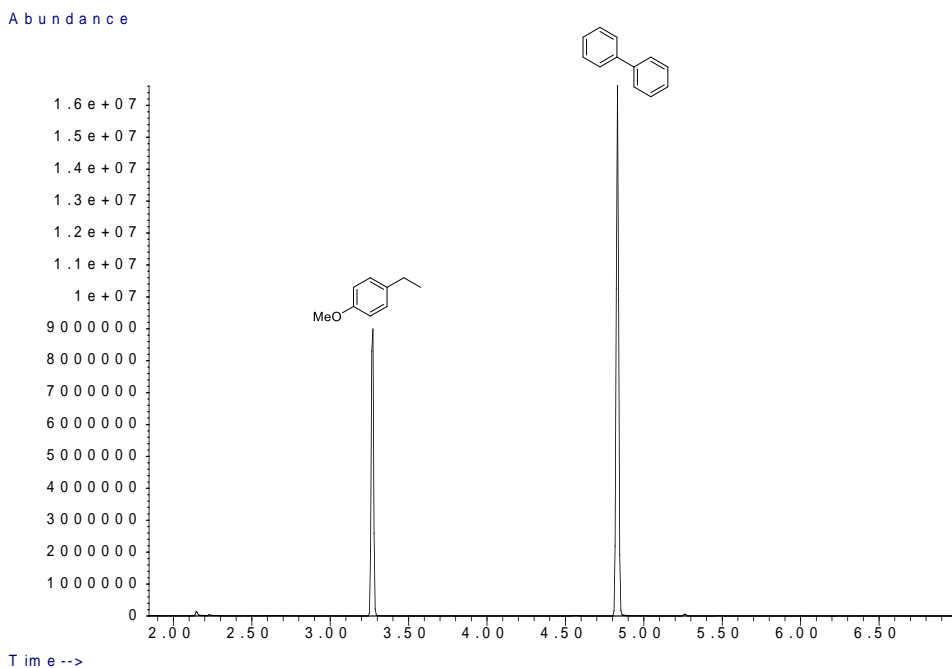
Figure A.VII.53. GC-FID chromatogram of the reduced product **14b** from the catalysis.

595
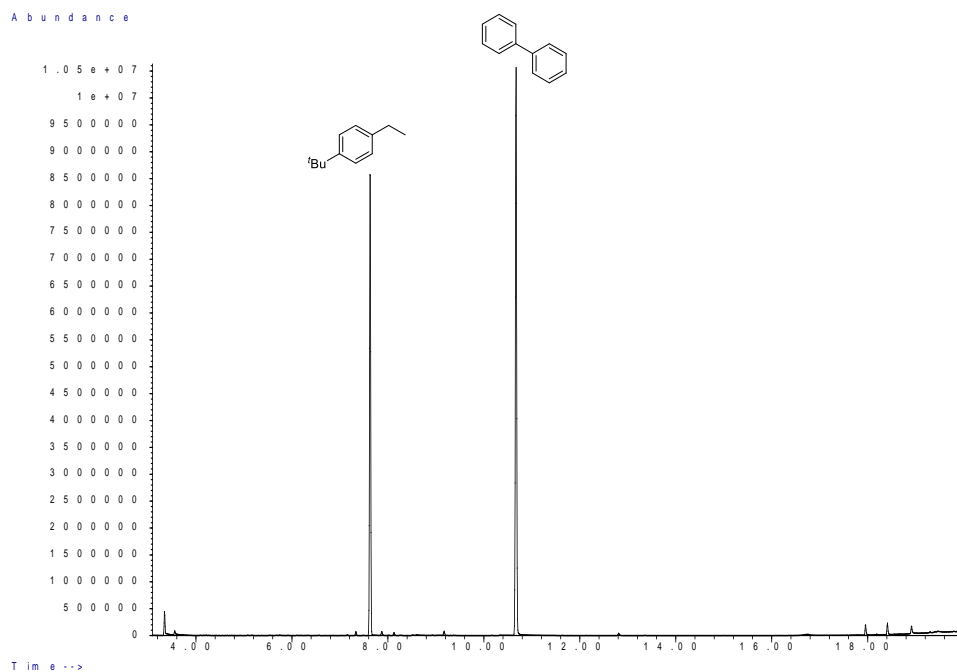
Figure A.VII.54. GC-FID chromatogram of the reduced product **14c** from the catalysis.
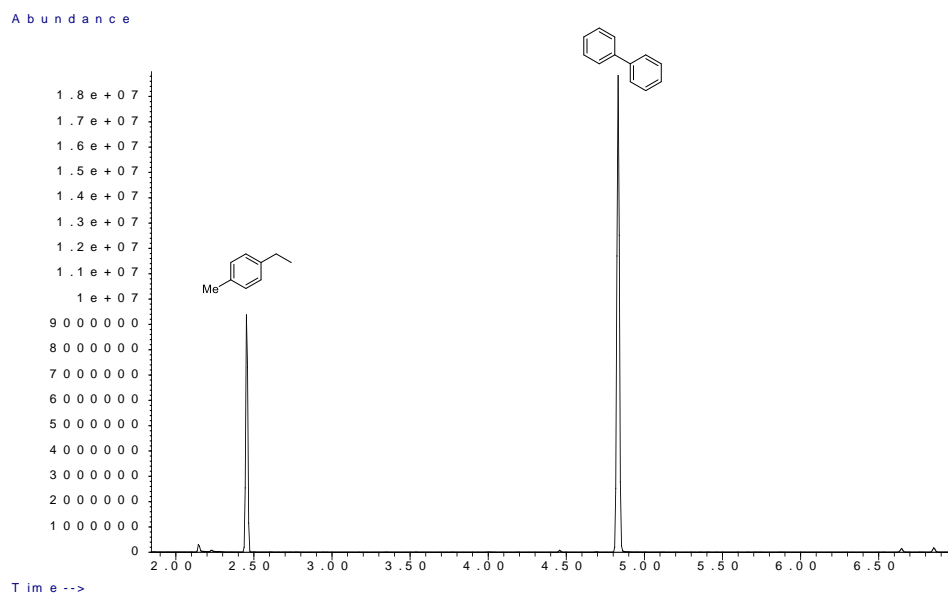
Figure A.VII.55. GC-FID chromatogram of the reduced product **14d** from the catalysis.

596

ANNEX
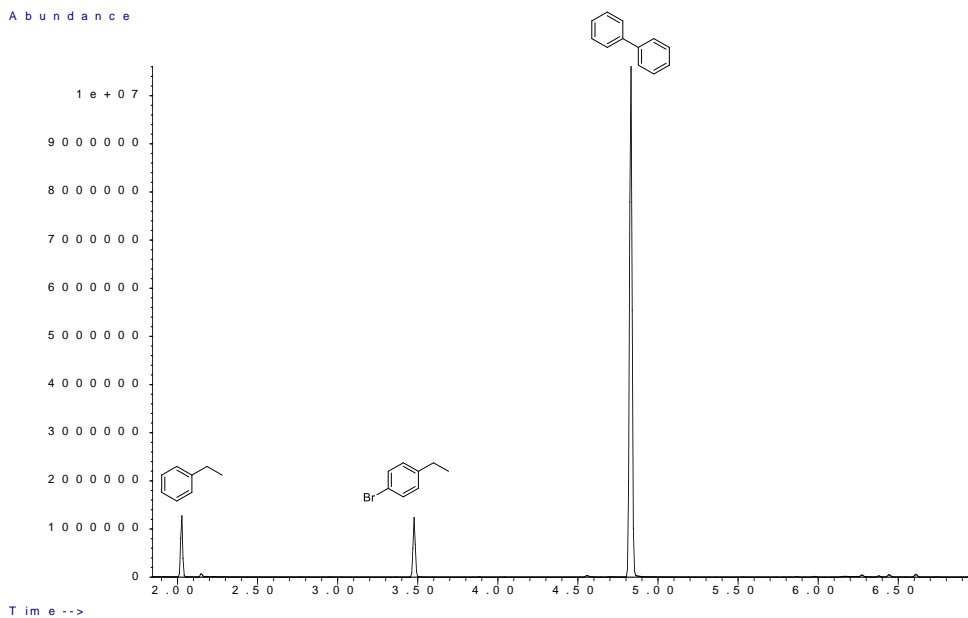
Figure A.VII.56. GC-FID chromatogram of the reduced product **14e** from the catalysis.
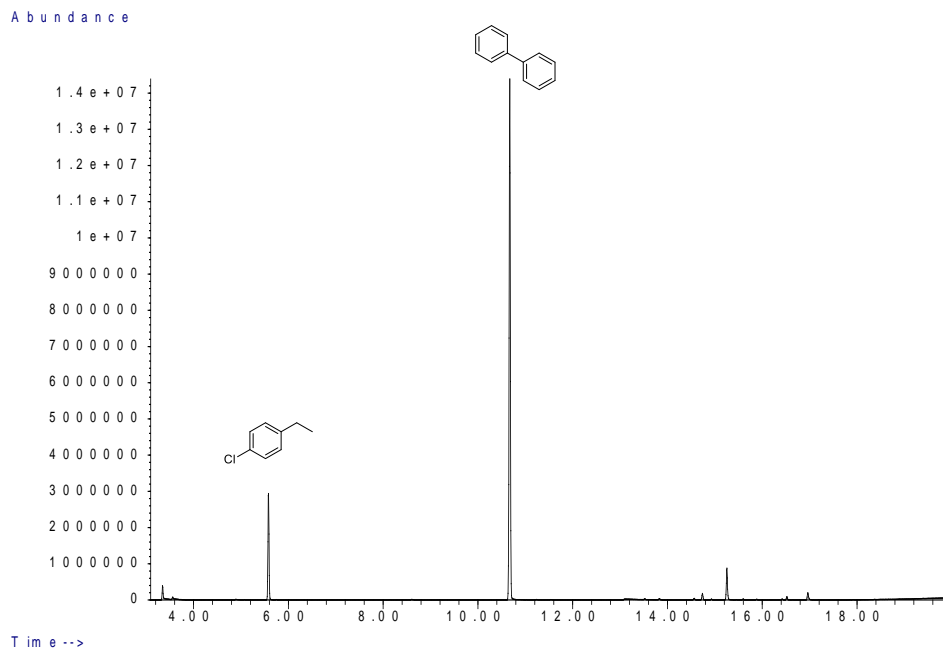
Figure A.VII.57. GC-FID chromatogram of the reduced product **14f** from the catalysis.

597

ANNEX
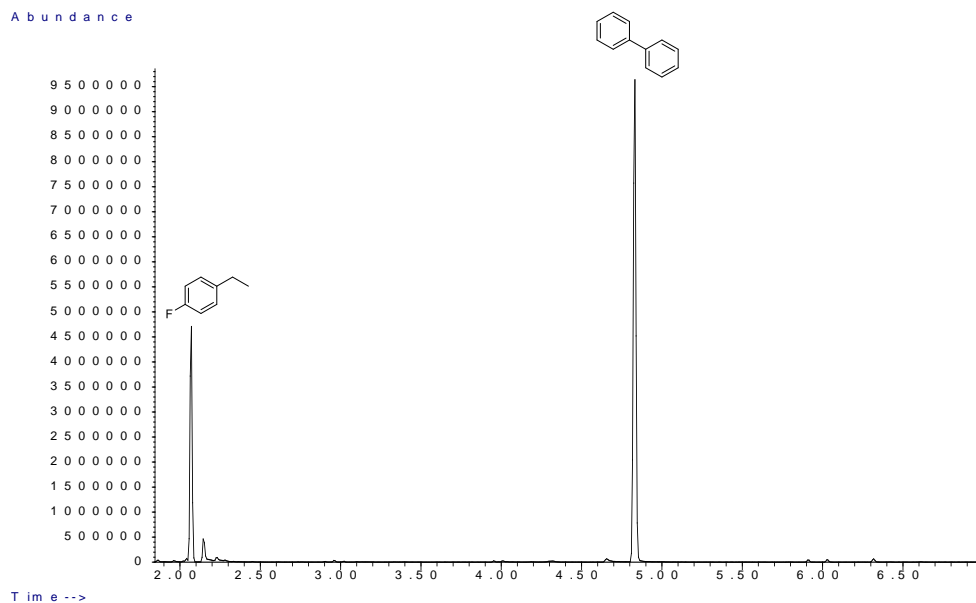
Figure A.VII.58. GC-FID chromatogram of the reduced product **14g** from the catalysis.
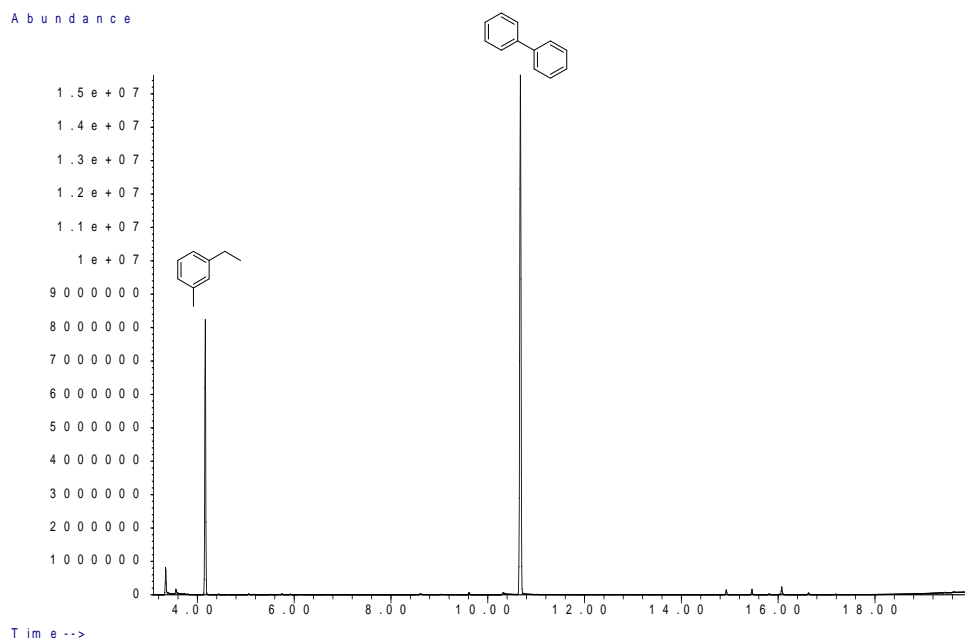
Figure A.VII.59. GC-FID chromatogram of the reduced product **14h** from the catalysis.

598
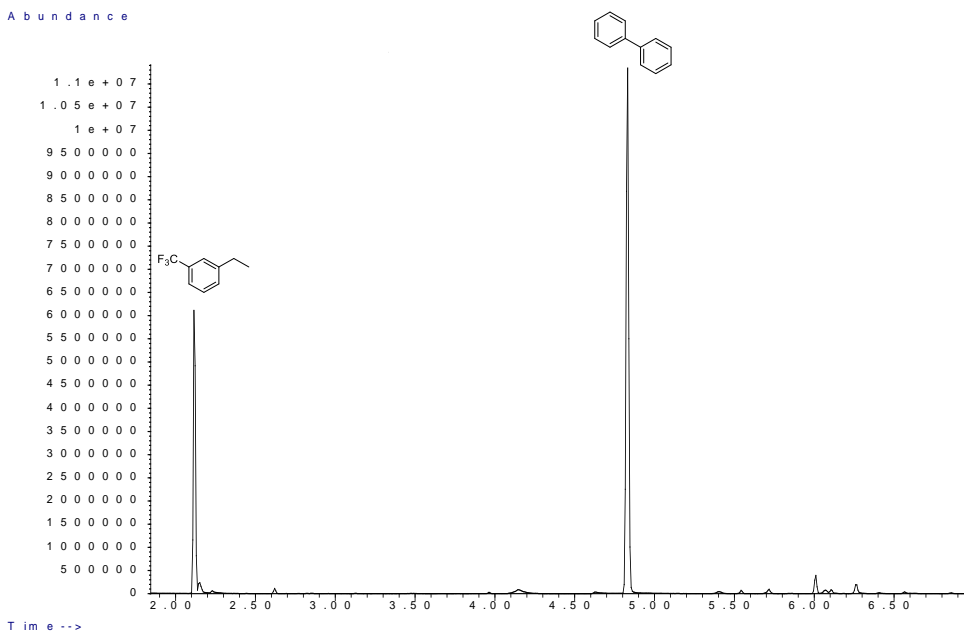
Figure A.VII.60. GC-FID chromatogram of the reduced product **14i** from the catalysis.
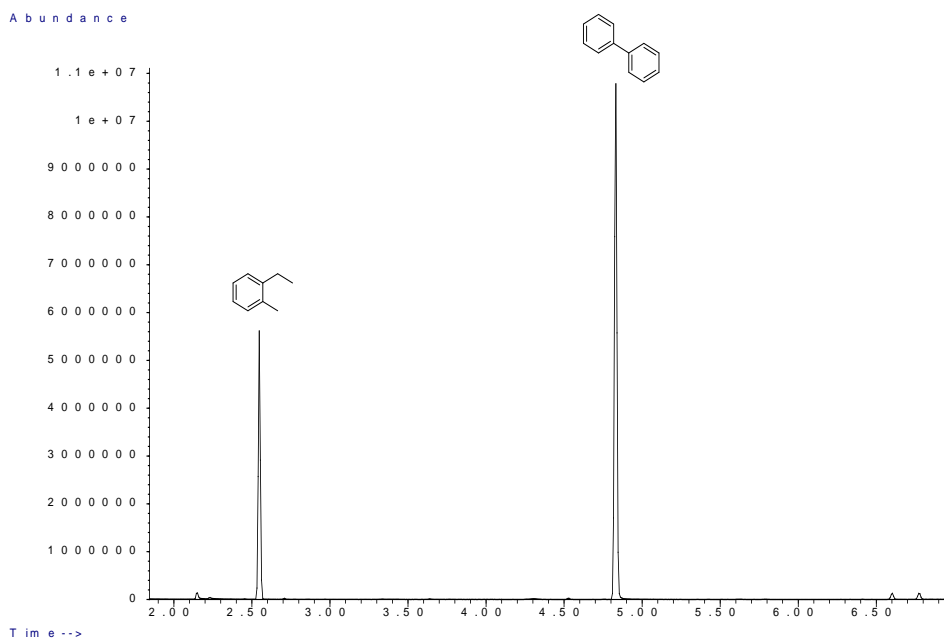
Figure A.VII.61. GC-FID chromatogram of the reduced product **14j** from the catalysis.
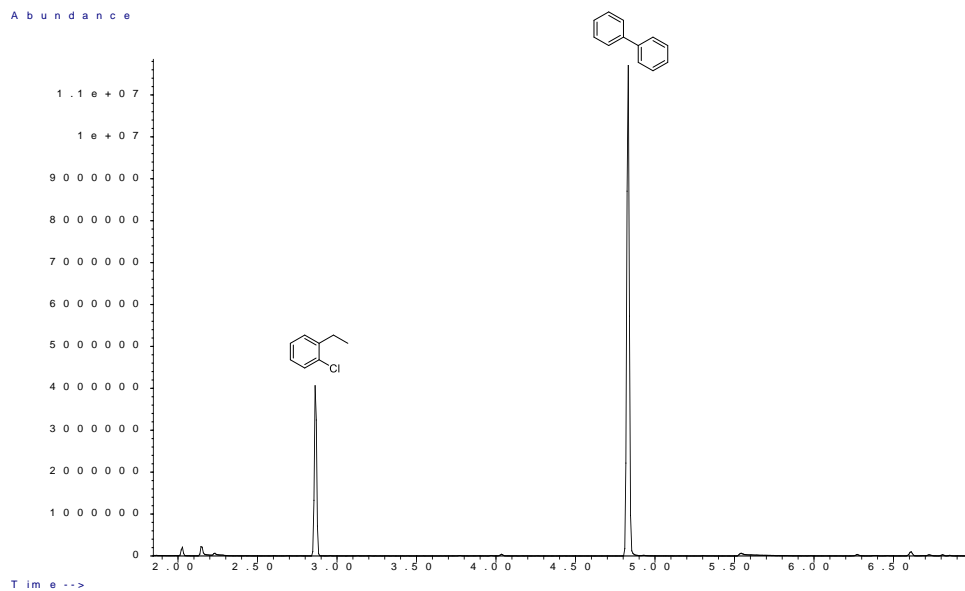
ANNEX

Figure A.VII.62. GC-FID chromatogram of the reduced product **14k** from the catalysis.
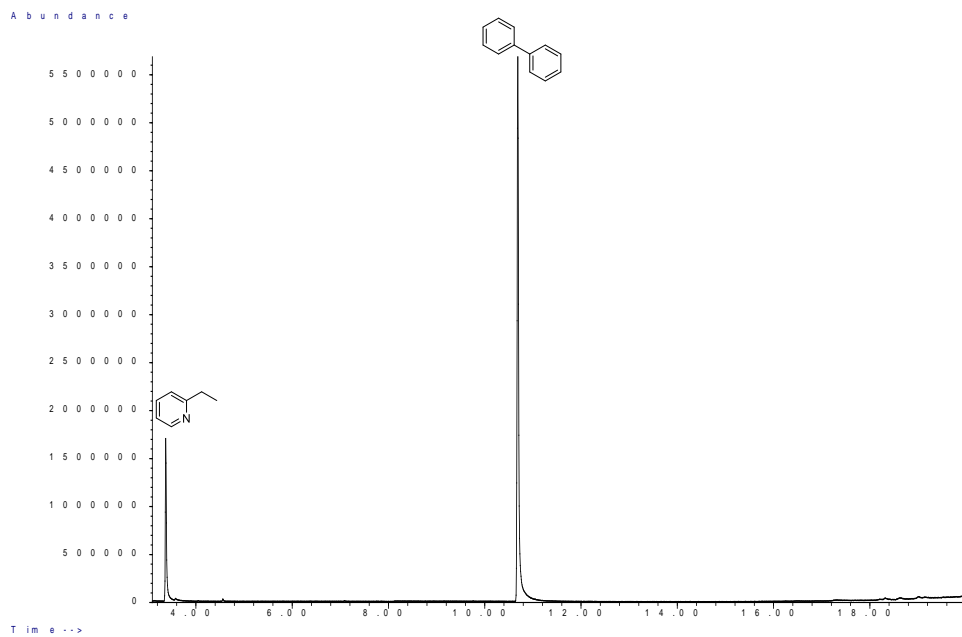
Figure A.VII.63. GC-FID chromatogram of the reduced product **14l** from the catalysis.

ANNEX
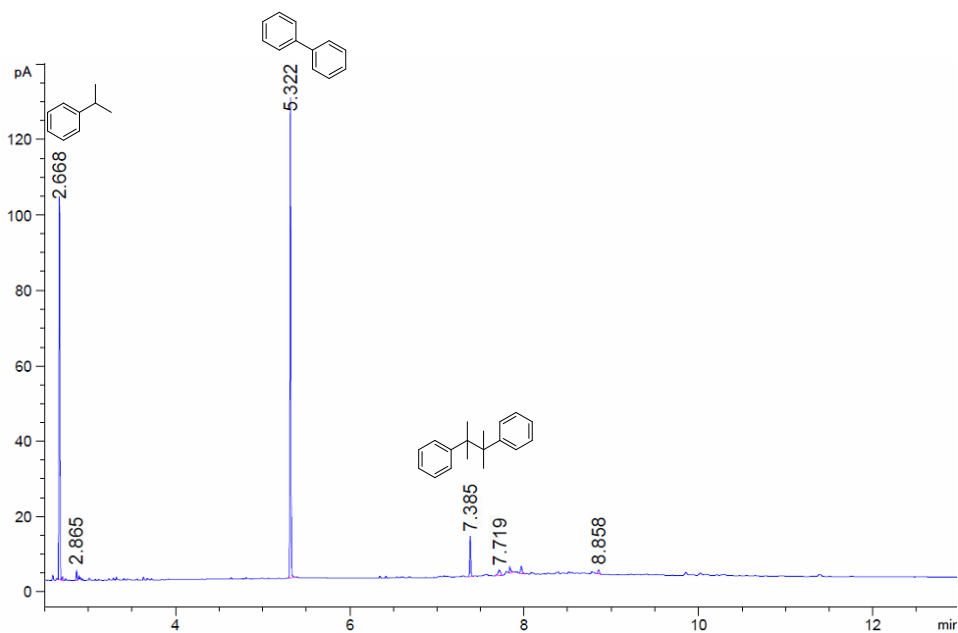
Figure A.VII.64. GC-FID chromatogram of the reduced product **16a** from the catalysis.
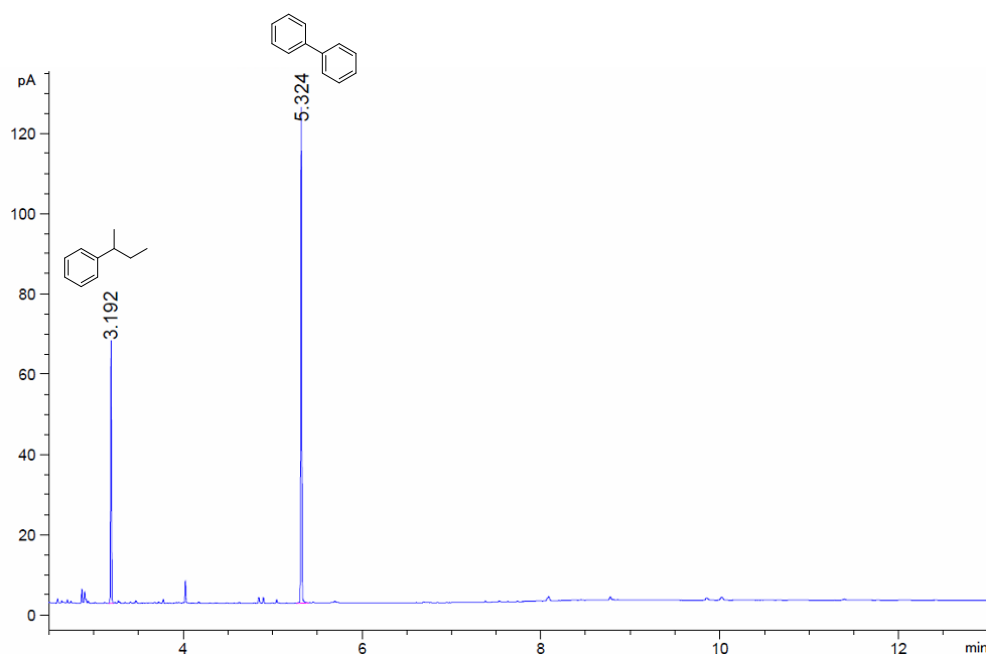
Figure A.VII.65. GC-FID chromatogram of the reduced product **16b** from the catalysis.

601
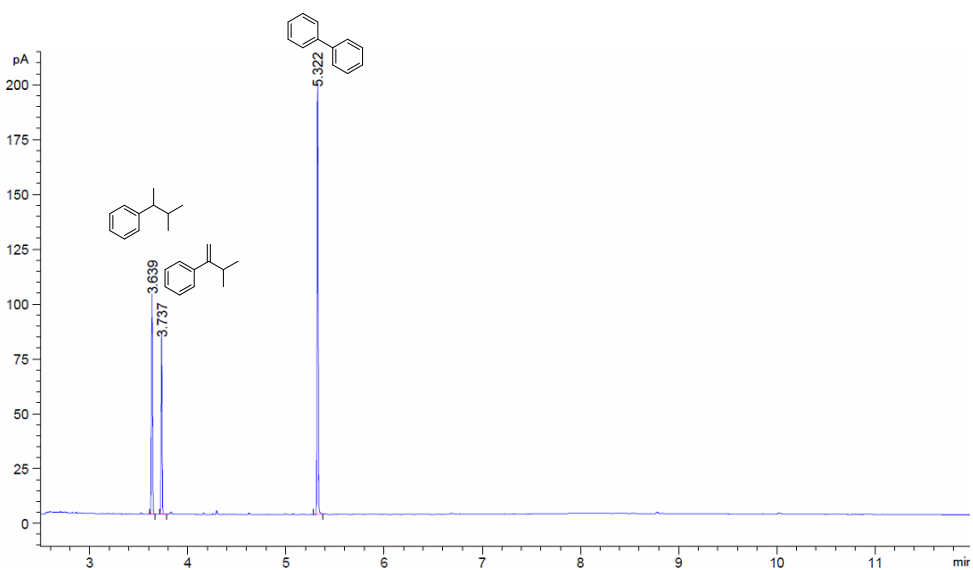
Figure A.VII.66. GC-FID chromatogram of the reduced product **16c** from the catalysis.
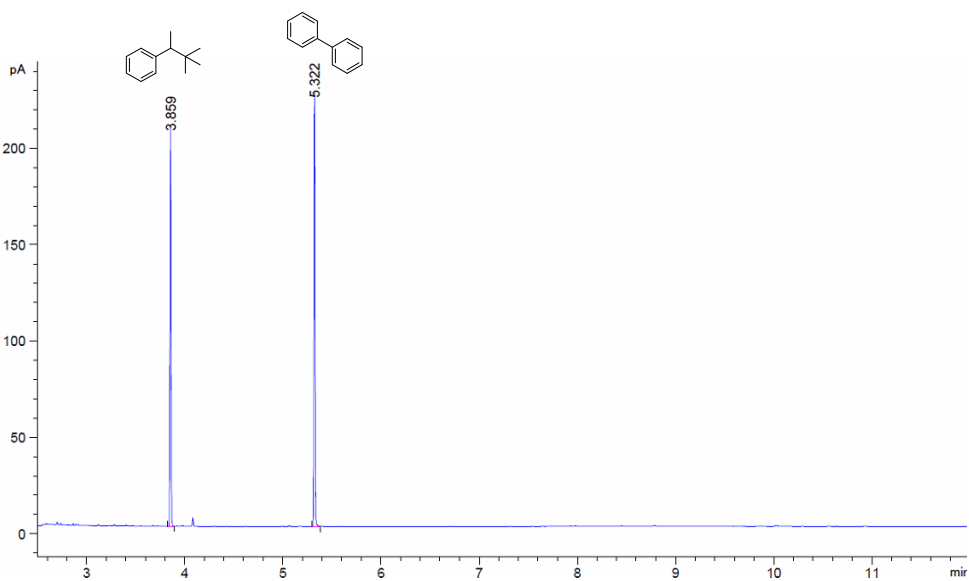
Figure A.VII.67. GC-FID chromatogram of the reduced product **16d** from the catalysis.
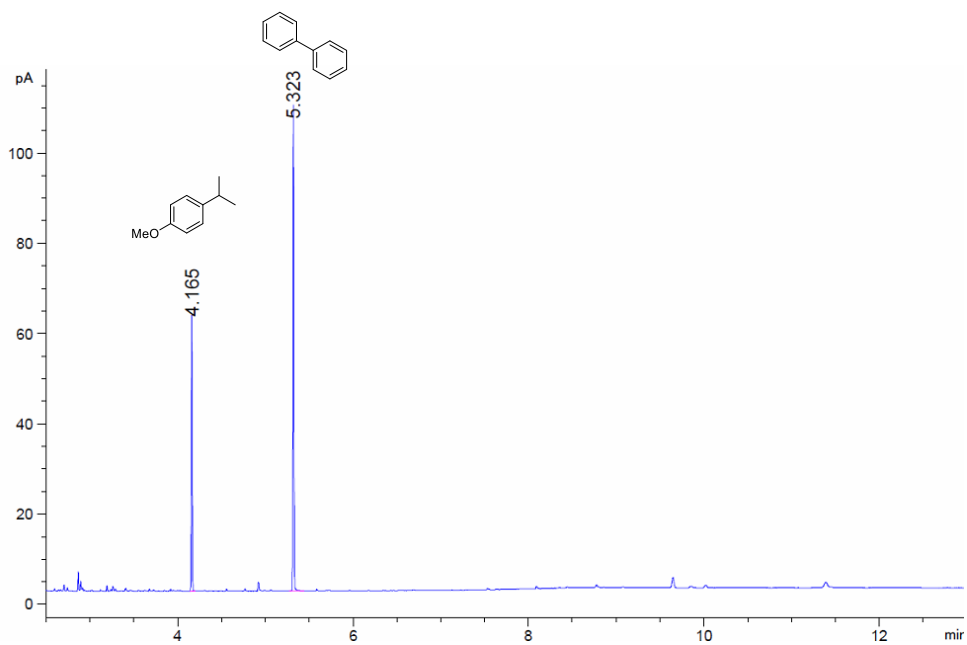
Figure A.VII.68. GC-FID chromatogram of the reduced product **16e** from the catalysis.
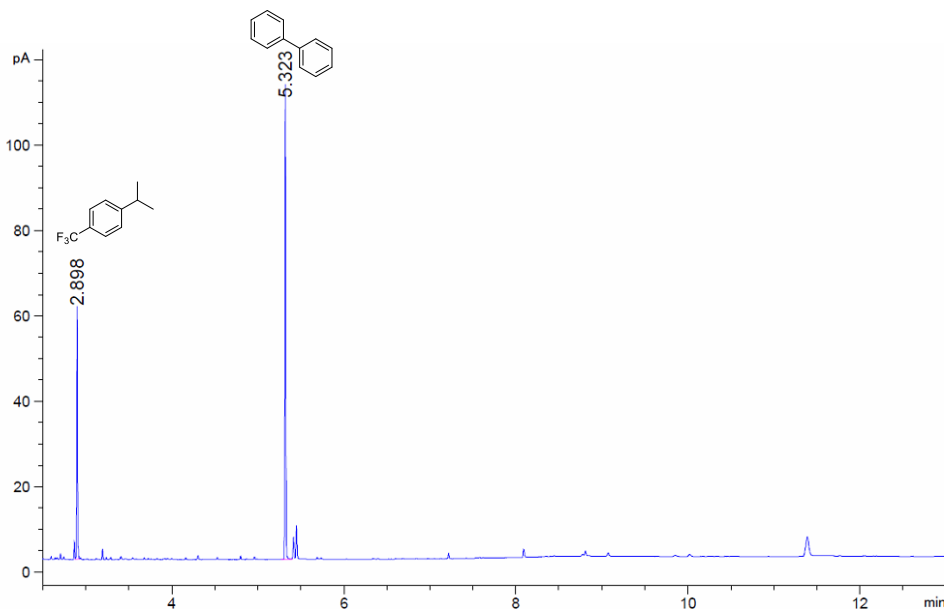
Figure A.VII.69. GC-FID chromatogram of the reduced product **16f** from the catalysis.

ANNEX
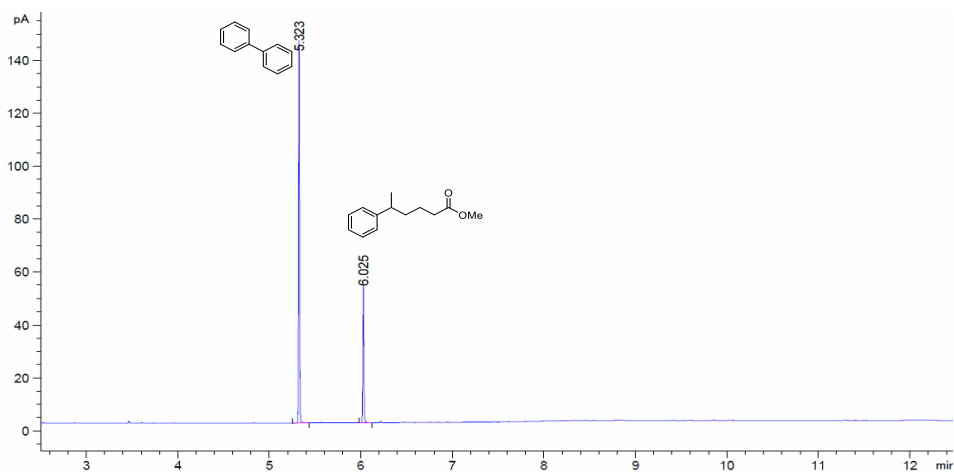
Figure A.VII.70. GC-FID chromatogram of the reduced product **16g** from the catalysis.
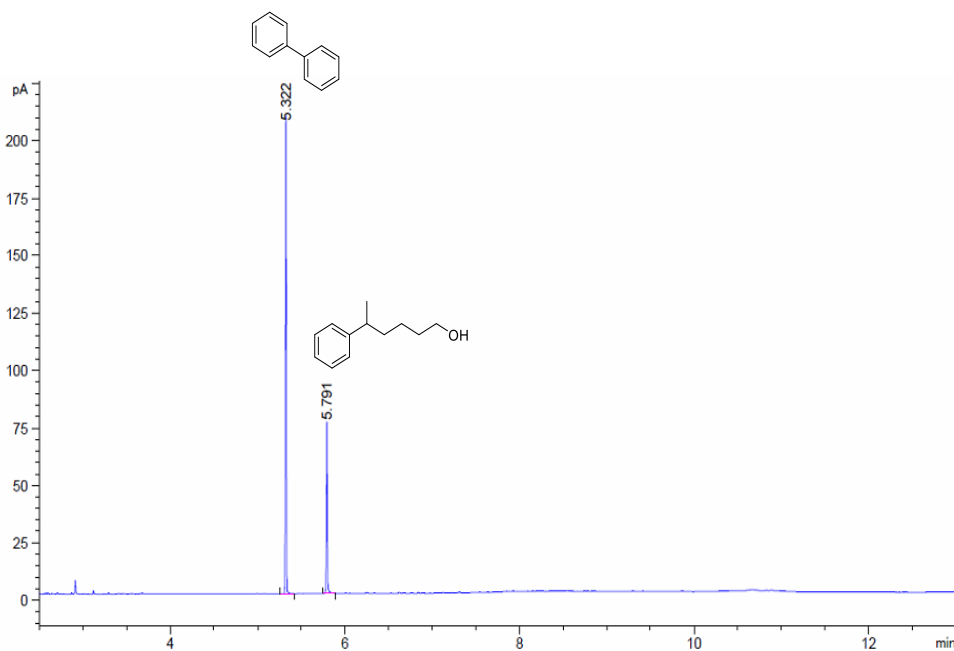
Figure A.VII.71. GC-FID chromatogram of the reduced product **16h** from the catalysis.

604

A.VII.12. Selected chromatograms of the selectivity studies
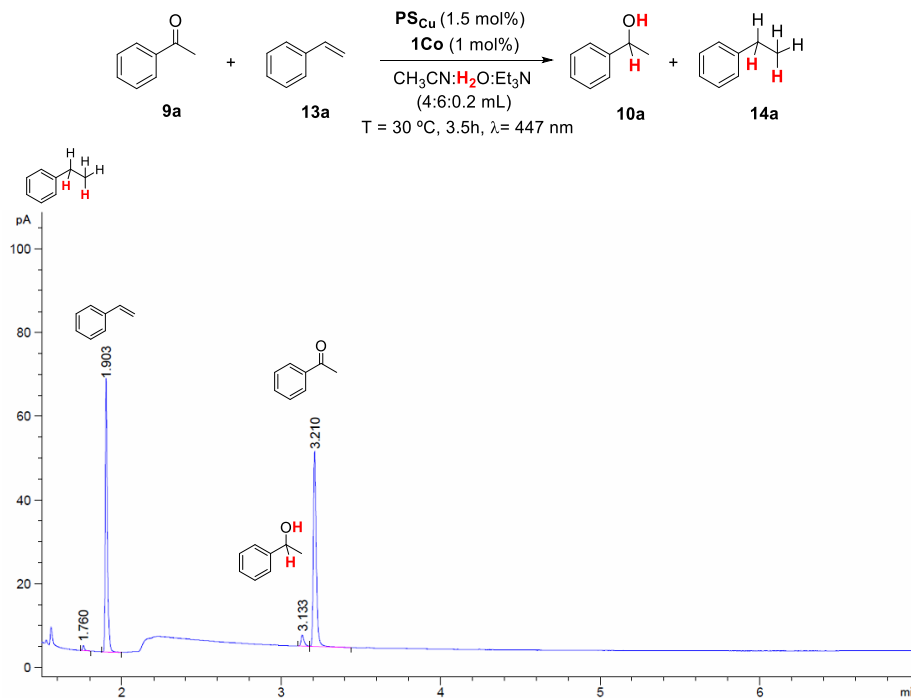
Figure A.VII.72. GC-FID chromatogram of the monitorization of the photoreduccion of acetophenone (**9a**) in the presence of styrene (**13a**) after 4 minutes of irradiation.
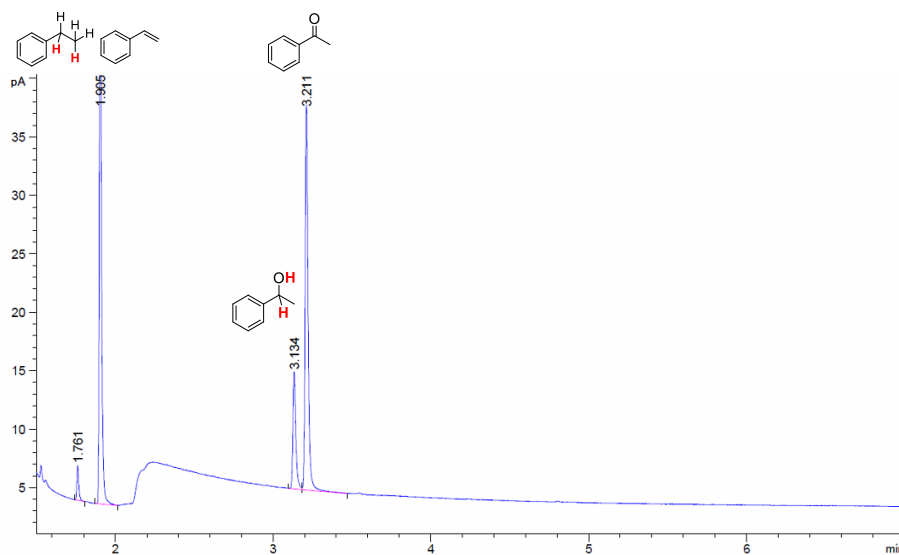
Figure A.VII.73. GC-FID chromatogram of the monitorization of the photoreduccion of acetophenone (**9a**) in the presence of styrene (**13a**) after 10 minutes of irradiation.
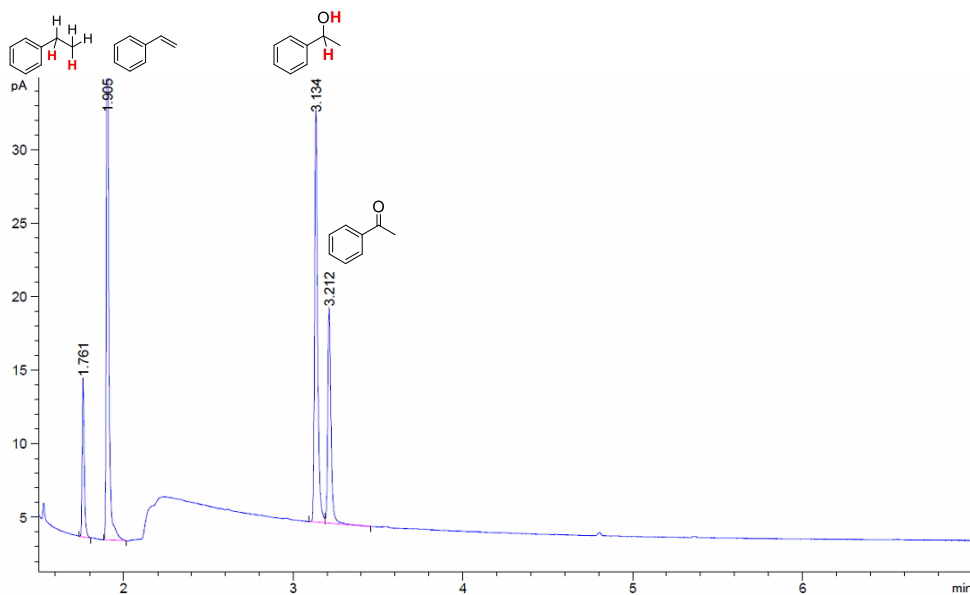
Figure A.VII.74. GC-FID chromatogram of the monitorization of the photoreduccion of acetophenone (**9a**) in the presence of styrene (**13a**) after 30 minutes of irradiation.
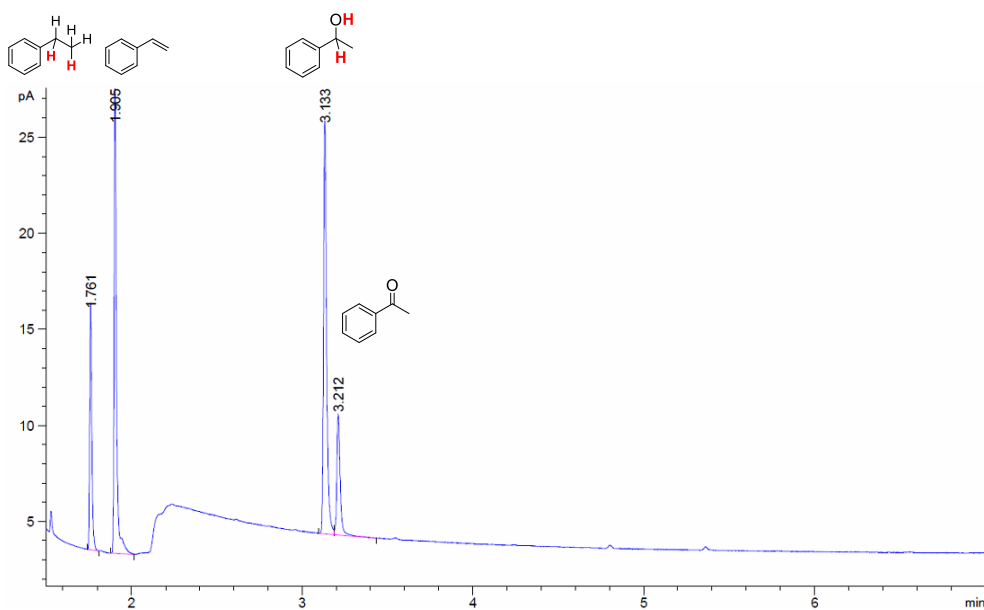
Figure A.VII.75. GC-FID chromatogram of the monitorization of the photoreduccion of acetophenone (**9a**) in the presence of styrene (**13a**) after 50 minutes of irradiation.

606
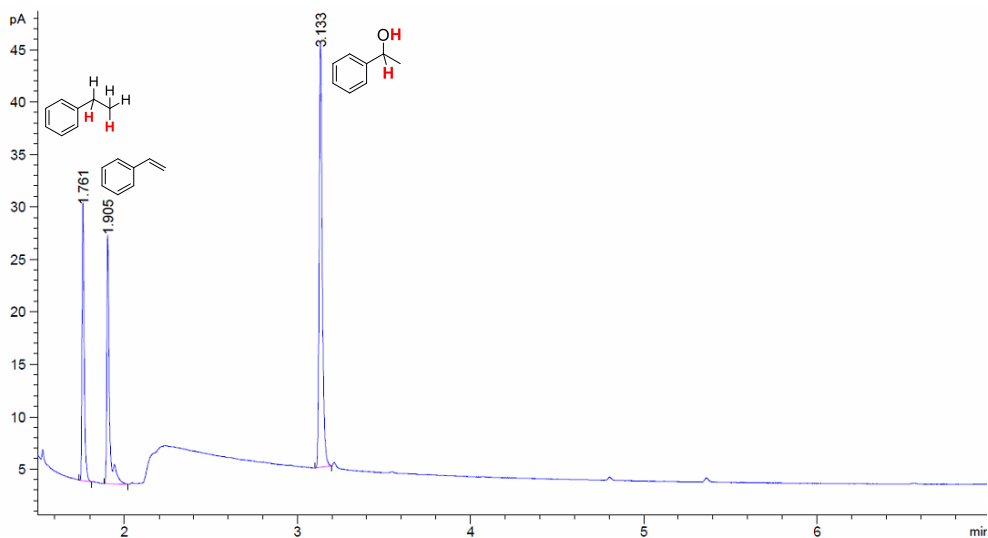
Figure A.VII.76. GC-FID chromatogram of the monitorization of the photoreduccion of acetophenone (**9a**) in the presence of styrene (**13a**) after 60 minutes of irradiation.
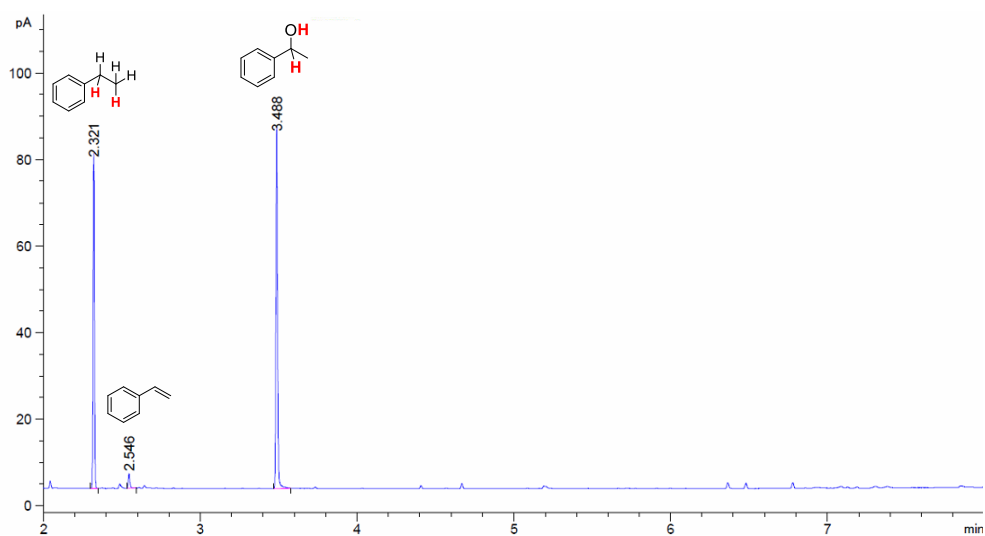
Figure A.VII.77. GC-FID chromatogram of the monitorization of the photoreduccion of acetophenone (**9a**) in the presence of styrene (**13a**) after 120 minutes of irradiation.

607

ANNEX
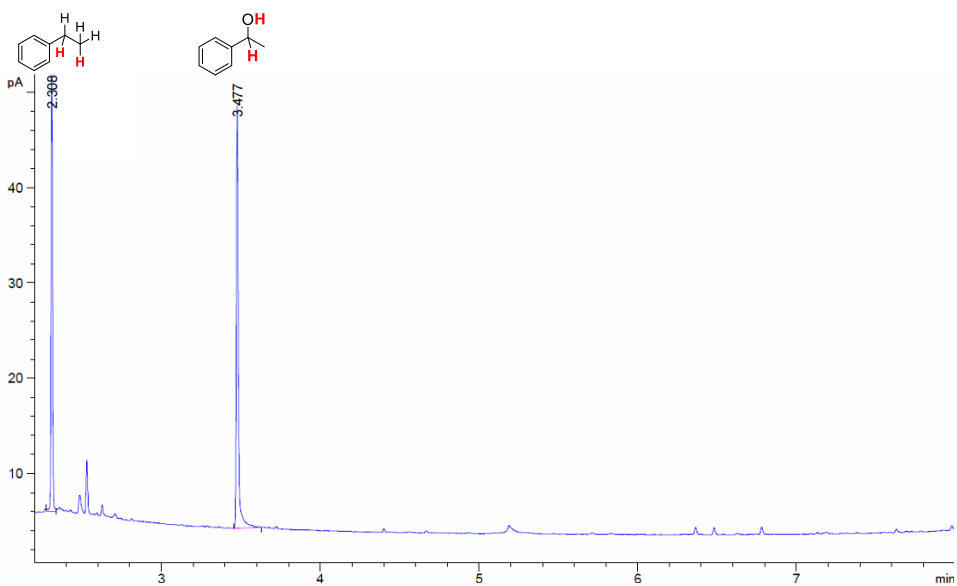
Figure A.VII.78. GC-FID chromatogram of the monitorization of the photoreduccion of acetophenone (**9a**) in the presence of styrene (**13a**) after 200 minutes of irradiation.
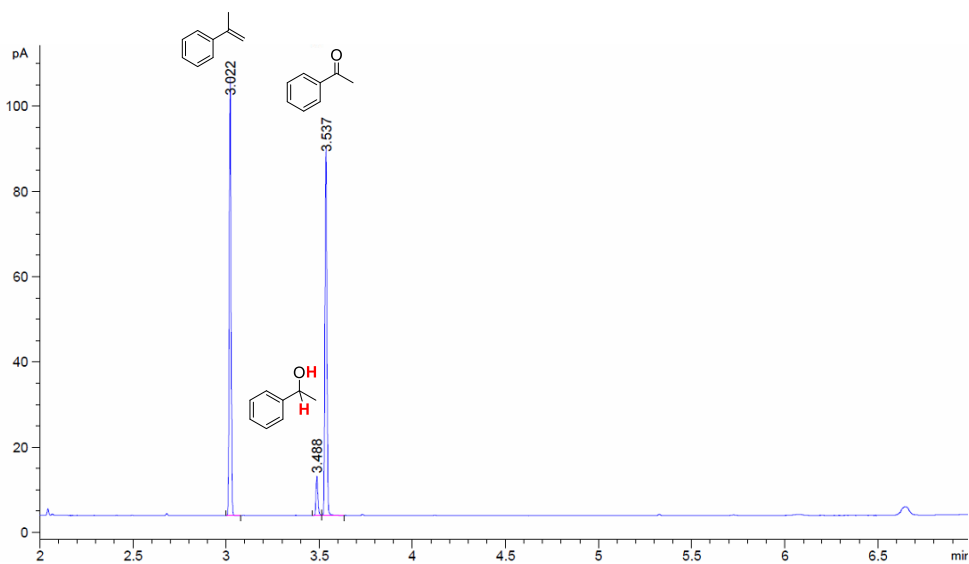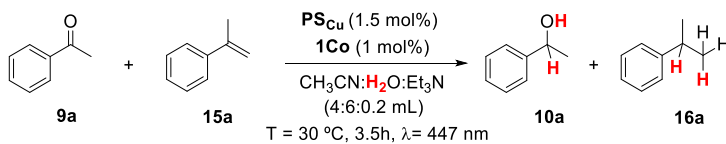
Figure A.VII.79. GC-FID chromatogram of the monitorization of the photoreduccion of acetophenone (**9a**) in the presence of α-methylstyrene (**15a**) after 4 minutes of irradiation.

ANNEX
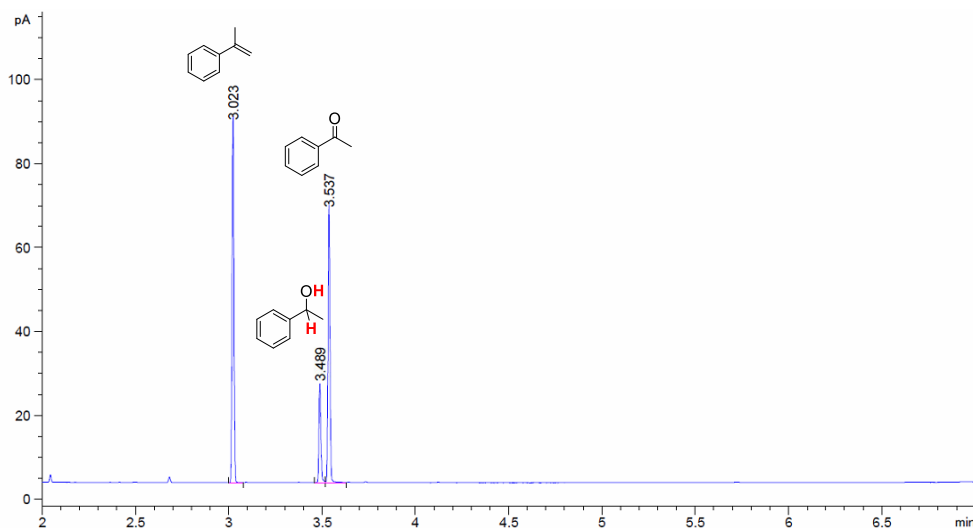
Figure A.VII.80. GC-FID chromatogram of the monitorization of the photoreduccion of acetophenone (**9a**) in the presence of α–methylstyrene (**15a**) after 10 minutes of irradiation.
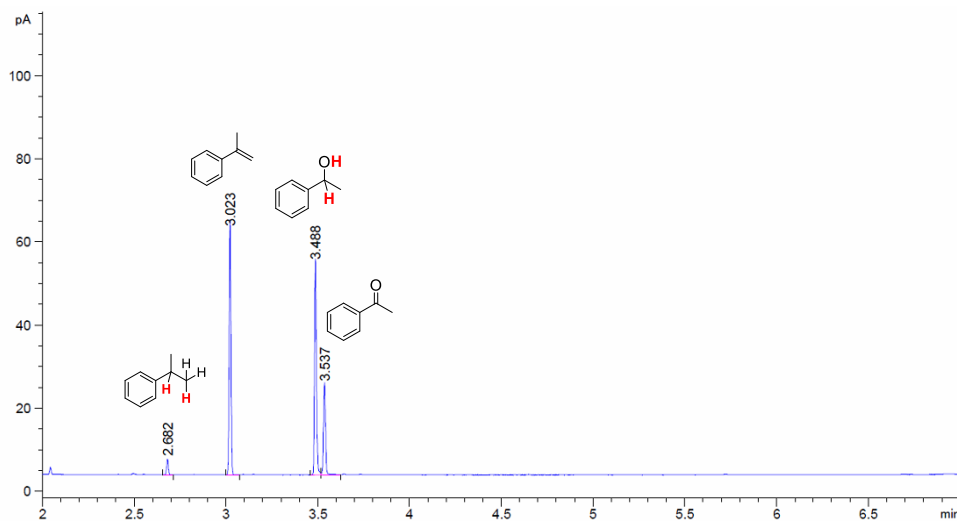
Figure A.VII.81. GC-FID chromatogram of the monitorization of the photoreduccion of acetophenone (**9a**) in the presence of α-methylstyrene (**15a**) after 30 minutes of irradiation.
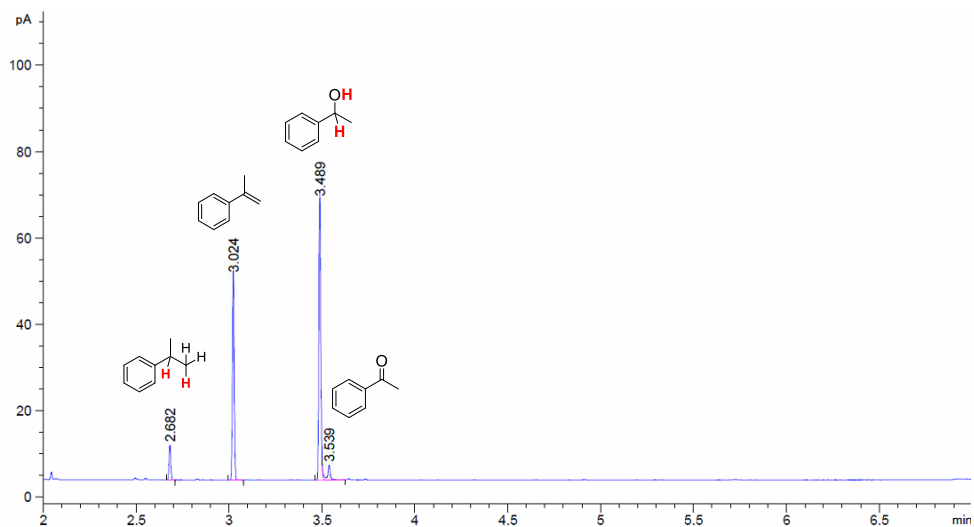
Figure A.VII.82. GC-FID chromatogram of the monitorization of the photoreduccion of acetophenone (**9a**) in the presence of α-methylstyrene (**15a**) after 50 minutes of irradiation.
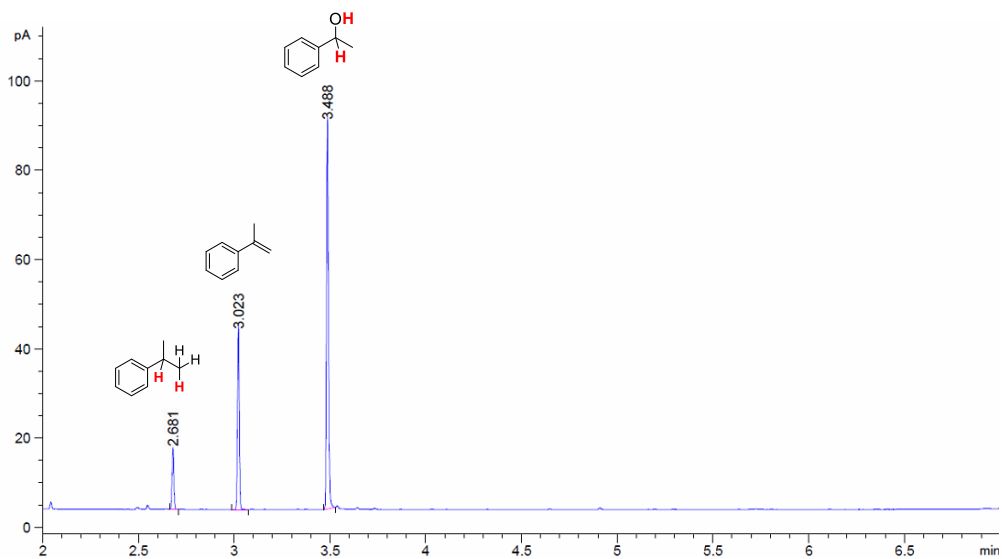
Figure A.VII.83. GC-FID chromatogram of the monitorization of the photoreduction of acetophenone (**9a**) in the presence of α-methylstyrene (**15a**) after 60 minutes of irradiation.

ANNEX
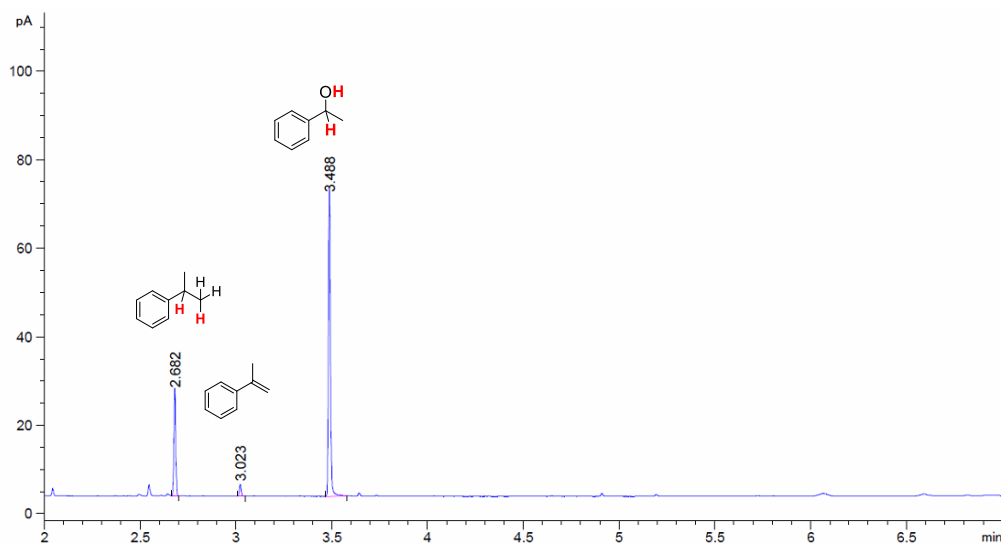
Figure A.VII.84. GC-FID chromatogram of the monitorization of the photoreduccion of acetophenone (**9a**) in the presence of α-methylstyrene (**15a**) after 120 minutes of irradiation.
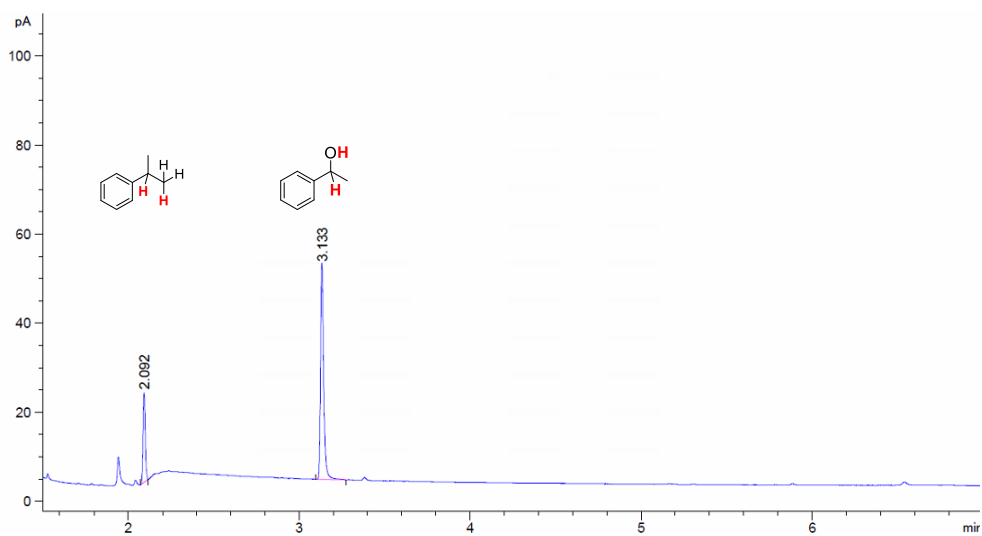
Figure A.VII.85. GC-FID chromatogram of the monitorization of the photoreduccion of acetophenone (**9a**) in the presence of α-methylstyrene (**15a**) after 210 minutes of irradiation.

611

A.VII.13. Chromatograms of the (1-(2-phenylcyclopropyl)vinyl)benzene ring-opening
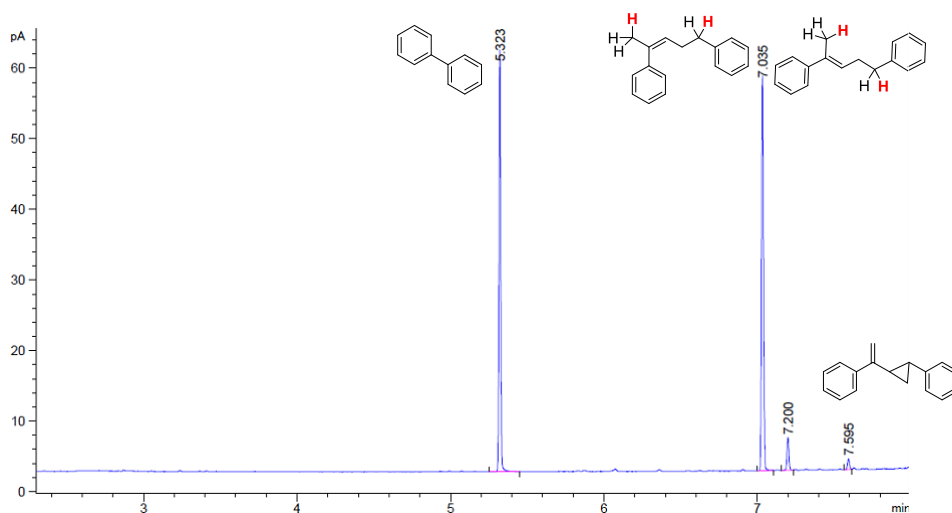
Figure A.VII.86. GC-FID chromatogram of the reduced product **17i** from the catalysis.

A.VII.14. References

(1) Cline, E. D.; Adamson, S. E.; Bernhard, S. *Inorg. Chem.* **2008**, *47*, 10378.

(2) Luo, S.-P.; Mejía, E.; Friedrich, A.; Pazidis, A.; Junge, H.; Surkus, A.-E.; Jackstell, R.; Denurra, S.; Gladiali, S.; Lochbrunner, S.; Beller, M. *Angew. Chem. Int. Ed.* **2013**, *52*, 419.

(3) Call, A.; Casadevall, C.; Acuña-Parés, F.; Casitas, A.; Lloret-Fillol, J. *Chemical Science* **2017**, *8*, 4739.

(4) McIntyre, S.; Hörmann, E.; Menges, F.; Smidt, S. P.; Pfaltz, A. *Adv. Synth. Catal.* **2005**, *347*, 282.

(5) Murai, K.; Matsushita, T.; Nakamura, A.; Fukushima, S.; Shimura, M.; Fujioka, H. *Angew. Chem. Int. Ed.* **2010**, *49*, 9174.

(6) Musacchio, A. J.; Nguyen, L. Q.; Beard, G. H.; Knowles, R. R. *J. Am. Chem. Soc.* **2014**, *136*, 12217.

(7) Denmark, S. E.; Chi, H. M. *J. Am. Chem. Soc.* **2014**, *136*, 8915.

(8) Concellón, J. M.; Rodríguez-Solla, H.; Méjica, C.; Blanco, E. G. *J. Org. Chem.* **2007**, *9*, 2981.

A.VIII. ANNEX CHAPTER X

A.VIII.1. NMR spectra
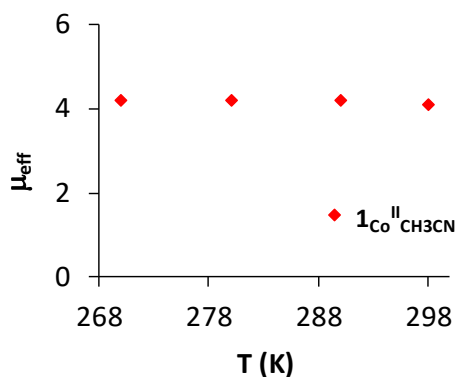
Figure A.VIII.1. Representation of the effective magnetic moment (μeff) of $1_{Co}{}^{II}{}_{CH3CN}$ in MeCN-d$_3$ as function of temperature.
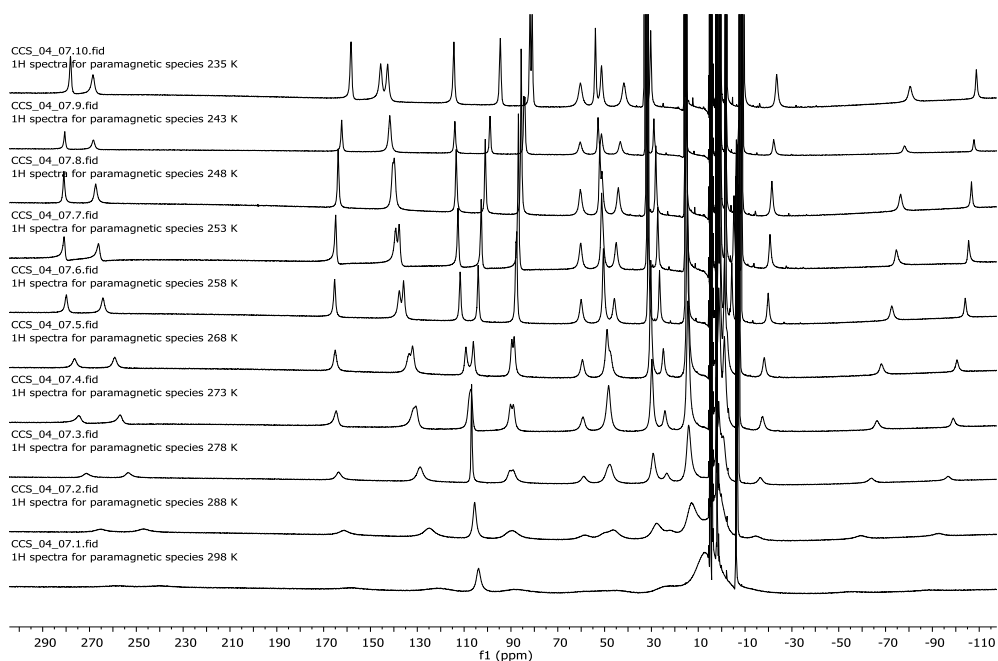
Figure A.VIII.2. Variable temperature ^{1}H-NMR (500 MHz, CD$_3$CN) of the chemically synthesized [Co^{II}(^{Me,OMe}Py$_2$^{Ts}tacn)(CH$_3$CN)](OTf)$_2$ complex ($1^{DMM}{}_{Co}{}^{II}{}_{CH3CN}$). From top to bottom: 235 – 298 K.

ANNEX
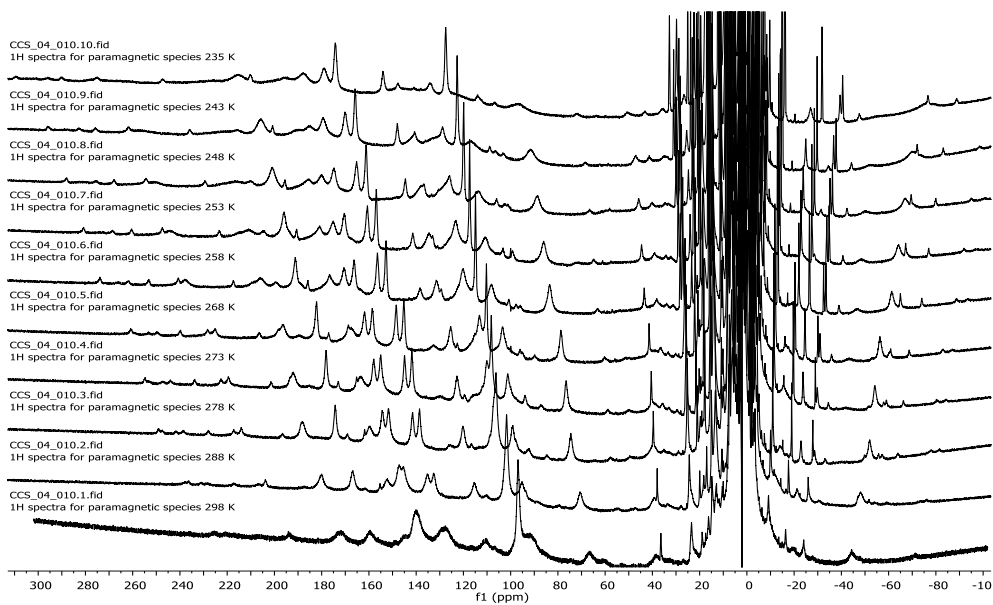
Figure A.VIII.3. Variable temperature ^{1}H-NMR (500 MHz, CD$_3$CN) of the chemically synthesized [Co^I(^{Me,OMe}Py$_2$^{Ts}tacn)(Cl)] complex (**1^{DMM}$_{Co}^{I}_{Cl}$**). From top to bottom: 235 – 298 K.

ANNEX
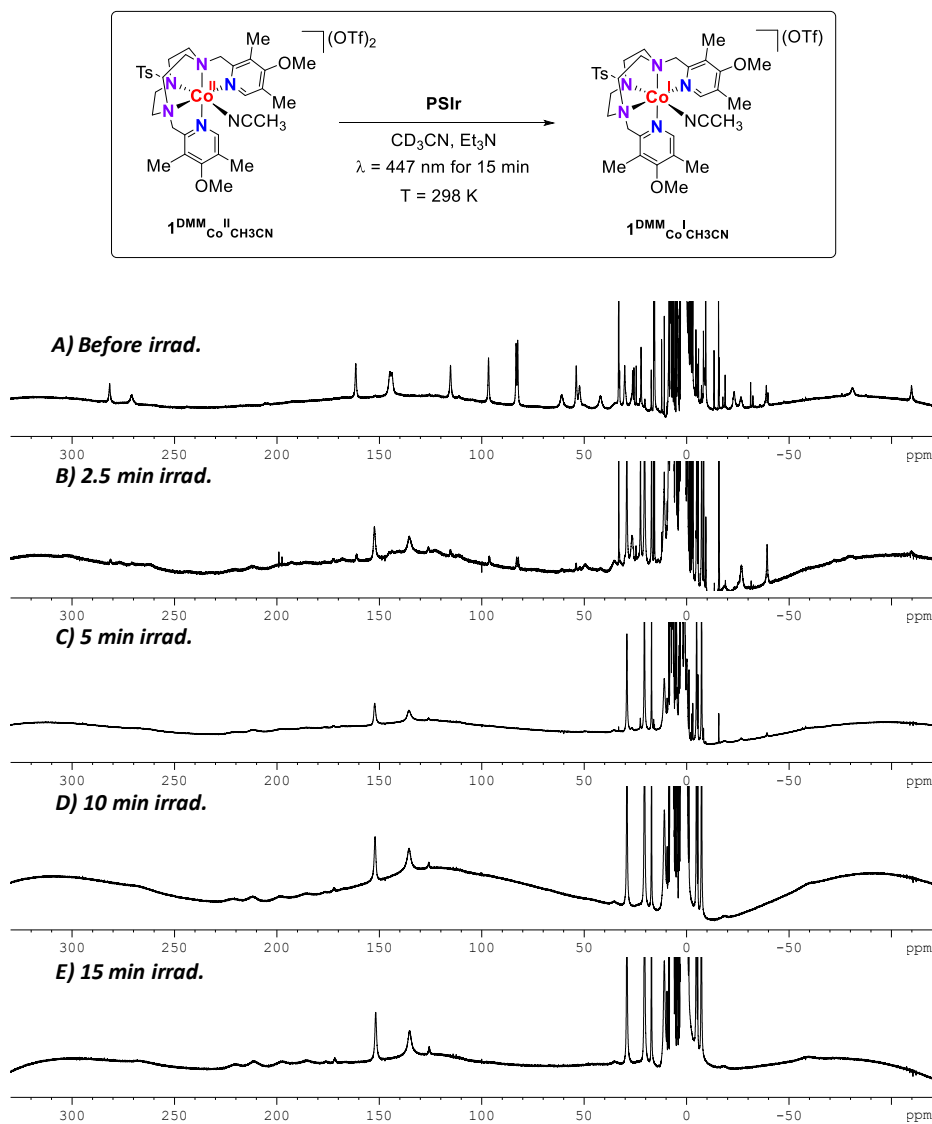
Figure A.VIII.4. Photoreduction of $1^{DMM}Co^{II}_{CH3CN}$ to $1^{DMM}Co^{I}_{CH3CN}$. *Top*: ^{1}H-NMR paramagnetic spectrum before irradiation at 235 K. *Middle:* ^{1}H-NMR paramagnetic spectra at 235 K of the monitorization of the photogeneration of $1^{DMM}Co^{I}_{CH3CN}$. *Bottom:* ^{1}H-NMR paramagnetic spectrum of the chemically synthesized $1^{DMM}Co^{I}_{CH3CN}$ species at 235 K. Conditions: $1^{DMM}Co^{II}_{CH3CN}$ (10 mM), **PS$_{Ir}$** (10 mM), Et$_3$N (120 mM) in CD$_3$CN irradiating at 298 K (λ = 447 nm).
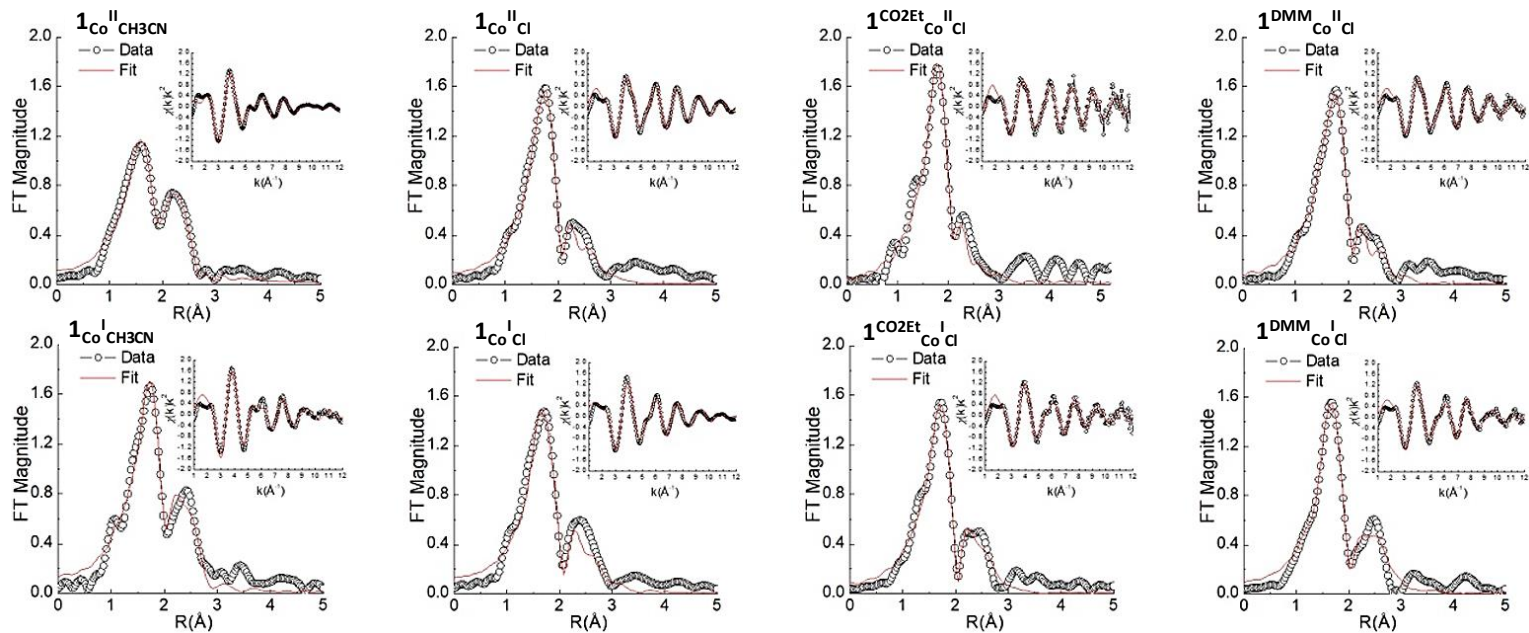
ANNEX

Figure A.VIII.5. Fourier transformed EXAFS data and fits with the inset showing the k-space spectra. Experimental data (circles) and Fit (red).

ANNEX

Table A.VIII.1. Selected EXAFS fits. Fits carried out in r-space with a Hanning window (dk 1), a k-weight = 2 and S_0 = 0.9. Bond distances and disorder parameters (Δr_{eff} and σ^2) were allowed to float having initial values of 0.0 Å and 0.003 Å^2 respectively, with a universal E_0 and ΔE_0 = 0 eV. (σ^2 reported as x10^3 Å^2).

Sample	Δk	Δr	Var.	R_{FACTOR}	ΔE_0	M-Cl N	r(Å)	σ^2	M-N/O N	r(Å)	σ^2	M-N/O N	r(Å)	σ^2	M-N N	r(Å)	σ^2	M--C N	r(Å)	σ^2	M--C N	r(Å)	σ^2	M--C-N--M N	r(Å)	σ^2
1Co(II)Cl	2-13.5	1-2.8	8	0.013	3	1	2.30	2	3	2.11	5	1	2.18	5	1	2.49	5	2	3.01	6	3	3.10	6	10	3.25	6
1^{CO2Et}Co(II)Cl	2-12.5	1-3.2	8	0.028	3	1	2.30	1	3	2.14	4	1	2.21	4	1	2.54	4	2	3.06	12	3	3.19	12	10	3.44	12
1^{DMM}Co(II)Cl	2-13	1-3.2	8	0.014	2	1	2.31	1	3	2.10	6	1	2.16	6	1	2.48	6	2	3.00	7	3	3.08	7	10	3.33	7
1Co(II)CH3CN	2-13.5	1-3.2	7	0.010	-2	-	-	-	1	2.03	8	4	2.09	8	1	2.46	13	4	2.93	8	2	2.92	8	12	3.35	8
1Co(I)Cl	2-13.5	1-2.8	7	0.025	1	1	2.35	2	2	2.07	3	1	2.14	3	1	2.43	3	2	2.95	3	3	3.10	3	12	3.25	3
1^{CO2Et}Co(I)Cl	2-12.5	1-2.8	7	0.016	4	1	2.31	5	3	2.12	4	1	2.19	4	1	2.41	4	2	2.93	3	3	3.06	6	8	3.25	3
1^{DMM}Co(I)Cl	2-12	1-3.2	7	0.019	3	1	2.34	4	3	2.08	1	1	2.24	1	1	2.44	1	2	2.96	3	3	3.04	1	8	3.25	1
1Co(I)CH3CN	2-13	1-3.2	8	0.024	1	-	-	-	1	2.14	2	4	2.18	3	1	2.64	1	4	3.01	6	2	2.95	6	12	3.40	6

Although EXAFS cannot differentiate between O/N/C scattering paths, chemical intuition was used for description. M is the absorber element, in this case Co.

A.IX. Cartesian coordinates from all chapters

In parenthesis are the Gibbs energies (G) in hartrees and the spin state of each intermediate, unless otherwise indicated.

A.IX.1.Corrdinates from chapter III

3α (S = 1/2)

(G = -2412.641725) (doublet)

Fe 0.1277558614 -1.1506761819 0.0217017231
C -2.5221684048 -1.7498232684 1.2845635366
H -1.9194016134 -2.1191587646 2.1031421129
N -1.8677686671 -1.2327874049 0.2274152335
N -0.4508144006 0.3223339736 -1.3432552719
C -3.9088344031 -1.7922117833 1.331132756
N 0.3459483869 0.5561040044 1.3107706213
N 2.0855864968 -0.8143855856 -0.1290590763
O 0.1219024747 -2.2470589469 -1.16168535
C -4.6377527141 -1.2785830917 0.2581927312
C -3.9548914475 -0.7347954589 -0.8289429459
H -4.4784494035 -0.3091995781 -1.677607245
C -2.5665265948 -0.7331273458 -0.8182739545
C -1.7234005809 -0.196009861 -1.9302555088
H -1.469513786 -0.9995240075 -2.6284962796
H -2.2329089301 0.5985284527 -2.4815523279
C 0.552719911 0.4746334193 -2.4351967102
H 0.7927266608 -0.5169854554 -2.8176855353
H 1.4484714529 0.960619755 -2.0497665483
C -0.727111947 1.6256823997 -0.6183885892
C 0.3255520226 1.8050305873 0.4615706836
C -0.6632961615 0.5858256663 2.4013350648
H -0.6782247228 -0.3955719145 2.874259813
H -1.6459400209 0.8216112435 1.9921616273
C 1.6979276634 0.3971280379 1.9148763435
H 1.6324644639 -0.3557424122 2.7053123759
H 2.0302665348 1.3381756736 2.362809365
C 2.6437982126 -0.0711209069 0.8540173132
C 4.0058354277 0.2041039864 0.861799077
H 4.4156671876 0.8192736505 1.6550398476
C 4.8084878996 -0.3149771816 -0.1524641463
C 4.2239525382 -1.0936495993 -1.1527005016
C 2.8565592409 -1.3230709384 -1.1112282404
H 2.3514564749 -1.9144309815 -1.864283822
O 0.3977401776 -2.1171293207 1.4893565987
H -5.7228270955 -1.29171336 0.2717276917
H -4.3972369828 -2.215985805 2.2010683428
H 5.8742992158 -0.110661498 -0.1647054461
H 4.8095071761 -1.5176115382 -1.9603924553
H -0.3848656825 1.3391352922 3.1444586359
H 0.1207888865 1.0764681769 -3.2395935348
H -0.1160225234 -2.9473321931 1.4545898717
C -0.7937198047 2.8441059799 -1.5494936004
C -1.052372834 4.1167154941 -0.7322194993
C 0.0568412517 4.3045206068 0.3101355929
C 0.0958438955 3.0980947175 1.2563006085
H 1.0236356306 4.4090387535 -0.2011873483

H -0.1108180405 5.2162921868 0.8945326872
H -1.0974844245 4.975514132 -1.411483374
H -2.0230695279 4.0422292141 -0.2231925723
H 0.1629927878 2.960020851 -2.0685331334
H -1.5743580382 2.6902670916 -2.301701849
H 0.8840304501 3.2084146829 2.0085688914
H -0.8650893875 3.0397676318 1.7777604772
H 1.3045598183 1.8683306119 -0.0225525916
H -1.7002090606 1.5068041099 -0.1337286663

3α (S = 3/2)

(G = -2412.662144) (quadruplet)

Fe 0.1304606252 -1.13049904 0.0414675591
C -2.4975961951 -1.7349150943 1.2878086444
H -1.8706273282 -2.1149119743 2.0832257951
N -1.8616502673 -1.2002235483 0.2287894359
N -0.4444623105 0.3174340683 -1.3626802663
C -3.883861173 -1.7907448531 1.3380088938
N 0.3541729032 0.5668965549 1.3135372395
N 2.0824070043 -0.7853048135 -0.1496662117
O 0.1263135393 -2.3103505353 -1.0929273421
C -4.6216896889 -1.2845348597 0.267153689
C -3.9514344444 -0.7403062586 -0.8281813031
H -4.4842858988 -0.33087314 -1.6789511706
C -2.5634557065 -0.7213098422 -0.8235201308
C -1.7184506367 -0.2065419411 -1.9429785354
H -1.4657220852 -1.0270056086 -2.6217714117
H -2.2212670755 0.5794500442 -2.5125469568
C 0.5512090385 0.4591425282 -2.4599324004
H 0.7917682145 -0.5388197858 -2.8263765559
H 1.4462644481 0.9553449211 -2.085708264
C -0.7214648201 1.6227547016 -0.6363621304
C 0.3269973385 1.8100904004 0.4482468958
C -0.6466762347 0.6014660648 2.4107151275
H -0.6640632862 -0.3803130757 2.8843316893
H -1.6303798093 0.8412097619 2.0062450125
C 1.7131361343 0.4148665095 1.9038257123
H 1.659755582 -0.3472164604 2.6873146866
H 2.0453692353 1.3543138851 2.3550497239
C 2.6494137484 -0.0433703902 0.8305150948
C 4.0115780003 0.2283570228 0.8219693919
H 4.432304791 0.8422773193 1.6103822312
C 4.8007080618 -0.2947985463 -0.20121919
C 4.2054957211 -1.0772902443 -1.1927416171
C 2.8388532287 -1.305338423 -1.137026506
H 2.3223561063 -1.90245293 -1.8775328316
O 0.3738043593 -2.1443427795 1.4811696227
H -5.7064755751 -1.3104169583 0.2852412076
H -4.3655966467 -2.2244724705 2.2067929475
H 5.8667166947 -0.0927574818 -0.2258149667
H 4.7830785828 -1.5067118197 -2.0032039947
H -0.3610586267 1.3531316094 3.1528262977

ANNEX

```
H  0.1135237381  1.0458835998 -3.2725897326
H  0.43395619   -3.0836046622  1.2230148572
C -0.7873587733  2.8368056087 -1.5725837741
C -1.0506088412  4.1131959443 -0.7627677296
C  0.0538449409  4.3081342263  0.2831664611
C  0.0920056973  3.1061258671  1.2353055737
H  1.0224968929  4.412191608  -0.2247082039
H -0.1179183726  5.2223449232  0.8625218885
H -1.0945586723  4.9684646568 -1.4465489533
H -2.0232603423  4.039648873  -0.2573330628
H  0.170355914   2.9500343538 -2.0906164108
H -1.5663702077  2.677247655  -2.325262879
H  0.8776543394  3.2215082788  1.9894359124
H -0.8704519456  3.0473925568  1.7540735573
H  1.3064664126  1.8737854866 -0.0349353909
H -1.6952985188  1.5044655071 -0.1531802262


3β-a (S = 1/2)
(G = -2412.637817) (doublet)


Fe  0.5407699625 -0.0824804726  1.0587262692
O   1.0473075646  1.2152216577  2.1704748486
O   0.8022917006 -1.2916255998  2.1298709147
N  -0.0330805718 -1.386261516  -0.4488943527
N  -1.4550652511  0.0605237313  1.4630451677
N   0.096262869   1.5101144541 -0.2080387056
N   2.2831611995 -0.3248152126  0.1577430888
C  -1.4610567554 -1.0465227603 -0.7888977404
H  -1.428860301  -0.0968979431 -1.3248825407
C  -2.1517357263 -2.075326874  -1.6914153642
H  -1.5766101272 -2.1850586981 -2.6173258583
H  -2.1808622311 -3.0475721421 -1.1885180906
C  -3.5925988004 -1.6282323864 -1.9759978497
H  -3.5818232041 -0.6764405813 -2.5244465355
H  -4.0836174253 -2.3733263581 -2.6119537864
C  -4.3625319709 -1.4497614304 -0.6614677549
H  -4.4165514467 -2.4120342346 -0.1345936342
H  -5.3886505299 -1.1194394086 -0.8580915434
C  -3.6650194493 -0.4117885129  0.2309912175
H  -4.2044374869 -0.2711471876  1.1734256273
H  -3.6499861353  0.5448371982 -0.3041612988
C  -2.227446319  -0.8625024963  0.5161257
H  -2.2623791291 -1.82331114    1.0339331924
C   0.1309859534 -2.8081871449 -0.0106395624
H  -0.0981914471 -3.4727074882 -0.8470923139
H  -0.528724166  -3.0159310869  0.8304738892
H   1.1677344315 -2.9570790634  0.2936939048
C  -1.7709861451 -0.3146806985  2.8720931468
H  -2.8387207188 -0.1491615039  3.0519725065
H  -1.1741754036  0.3098622465  3.5389208546
H  -1.5218637504 -1.3656111843  3.0206607156
C   0.8812908386 -1.1626889893 -1.6088890058
H   0.5261196176 -0.3006497207 -2.1804878748
H   0.8771661698 -2.0292831628 -2.2756164687
C   2.2541035113 -0.8873664011 -1.0731622734
C   3.4275504819 -1.1192557878 -1.7790493985
H   3.3737624272 -1.5753720573 -2.7612594871
C   4.6443423895 -0.75395155   -1.2045061057
H   5.5726942839 -0.9242837472 -1.7402203933
C   4.6572841132 -0.1759502938  0.066726127
H   5.5832466322  0.1176978088  0.5479132139
C   3.4532780239  0.0212794126  0.7279975358
```

```
C  -1.7750312937  1.5127357816  1.290486866
H  -1.3593821198  2.0253879396  2.1628189459
H  -2.8532236608  1.6737726762  1.2870499789
C  -1.1073466703  2.0594670764  0.0705004554
C  -1.6320517498  3.107732571  -0.6743831258
H  -2.6115158072  3.5002089014 -0.4246018173
C  -0.874538821   3.6304722695 -1.7218339453
H  -1.2607256765  4.4478685046 -2.3224969264
C   0.3874696105  3.0936469259 -1.9787264004
H   1.0177720204  3.4792230195 -2.7719664014
C   0.838273616   2.0332519508 -1.2019450408
H   1.8123368301  1.5954688942 -1.3787848998
H   3.3951062302  0.4578816306  1.7170633257
H   1.3088408137  0.8401141845  3.0342090037


3β-a (S = 3/2)
(G = -2412.658219) (quadruplet)


Fe  0.5405143227 -0.0472593088  1.0708049917
O   1.0341337715  1.2953632414  2.1362121134
O   0.8007015876 -1.2207772962  2.1677632773
N  -0.0248728347 -1.4008540468 -0.4168172447
N  -1.4652748887  0.0947416687  1.4591711969
N   0.0800452213  1.5061563495 -0.2566734344
N   2.2888265912 -0.3053770402  0.1645422502
C  -1.4548582277 -1.0773311392 -0.7642601061
H  -1.4286523065 -0.143118024  -1.3266145968
C  -2.1366782766 -2.1365396328 -1.6389498609
H  -1.559491663  -2.2661558527 -2.5608622507
H  -2.1579046873 -3.0945393714 -1.1092232674
C  -3.5806717871 -1.7086358114 -1.9362150608
H  -3.5773153117 -0.7720586829 -2.5102196019
H  -4.064517467  -2.4750667298 -2.5519463257
C  -4.3527206481 -1.5015909249 -0.6274202927
H  -4.398976353  -2.4494440373 -0.0744820932
H  -5.3813445119 -1.1847902561 -0.832883778
C  -3.6651266199 -0.4333373837  0.2366229393
H  -4.2061149144 -0.2718556932  1.1746254815
H  -3.6570206986  0.5082730133 -0.3245056961
C  -2.2239421171 -0.8647379691  0.5344747154
H  -2.2500161058 -1.8098465609  1.0804865727
C   0.1499373618 -2.8064597258  0.0651740411
H  -0.0737728058 -3.4951316014 -0.7531333004
H  -0.5091566157 -2.9943765868  0.910972739
H   1.187196705  -2.9385843733  0.3743990246
C  -1.7798798367 -0.2412642689  2.8774256188
H  -2.8490378887 -0.0757313018  3.0487750112
H  -1.1885312717  0.4070341564  3.5259818516
H  -1.525113476  -1.2857518061  3.0565079635
C   0.8915254787 -1.2002970439 -1.5798413081
H   0.5308959857 -0.356713925  -2.1748933731
H   0.8935308359 -2.0849719165 -2.2223664933
C   2.261940568  -0.9027461565 -1.0503508467
C   3.4381360532 -1.1470272811 -1.7470744518
H   3.3888835537 -1.6310257005 -2.7160881275
C   4.6516898734 -0.7580680831 -1.1808093462
H   5.5817658788 -0.9380779314 -1.7102946868
C   4.6600520013 -0.1439004487  0.0733997975
H   5.5836110189  0.1691604205  0.5468134036
C   3.4540516147  0.0649208689  0.7276638361
C  -1.7916744486  1.5397304344  1.2420434909
H  -1.3801072522  2.0806176133  2.0987114855
```

ANNEX

```
H  -2.8712709707   1.6911628332   1.2339638692
C  -1.1279528585   2.0534715287   0.0057713893
C  -1.6598689709   3.0750291316  -0.7702826209
H  -2.6424137489   3.4674101327  -0.5328634341
C  -0.9051497403   3.5720891341  -1.8322448636
H  -1.297100968    4.3683171924  -2.4570726327
C   0.3612232241   3.0379152227  -2.0725012889
H   0.9892086251   3.4048524226  -2.8763182564
C   0.8198102369   2.0044235147  -1.2645842809
H   1.7974982254   1.5692399827  -1.4273003638
H   3.3892942995   0.5305259201   1.703055915
H   1.2754412376   0.9416851302   3.0131753046
```

3β-b (S = 1/2)

(G = -2412.631922) (doublet)

```
26    0.567124000   -0.038233000    1.050259000
8     1.055979000    1.043726000    2.184611000
8     0.757788000   -1.443298000    2.105887000
7    -0.011656000   -1.388873000   -0.481506000
7    -1.432206000    0.157967000    1.428526000
7     0.173649000    1.578991000   -0.190017000
7     2.325901000   -0.281471000    0.185164000
6    -1.421338000   -0.986278000   -0.846012000
1    -1.331537000   -0.047464000   -1.396483000
6    -2.160202000   -1.986340000   -1.752625000
1    -1.585761000   -2.130128000   -2.674493000
1    -2.235327000   -2.959008000   -1.255234000
6    -3.578219000   -1.489126000   -2.066907000
1    -3.527001000   -0.558742000   -2.648759000
1    -4.089540000   -2.230016000   -2.691963000
6    -4.362471000   -1.246047000   -0.773664000
1    -4.496943000   -2.195952000   -0.238944000
1    -5.362967000   -0.858323000   -0.996290000
6    -3.630636000   -0.240688000    0.129566000
1    -4.188727000   -0.084770000    1.058679000
1    -3.580717000    0.719508000   -0.396441000
6    -2.211084000   -0.741630000    0.445961000
1    -2.296419000   -1.691492000    0.978465000
6     0.089855000   -2.826744000   -0.082705000
1    -0.123511000   -3.462310000   -0.945452000
1    -0.604775000   -3.055292000    0.723036000
1     1.105023000   -3.030733000    0.256359000
6    -1.787147000   -0.241300000    2.826889000
1    -2.852719000   -0.056214000    2.994034000
1    -1.201645000    0.353717000    3.528319000
1    -1.568163000   -1.298444000    2.966696000
6     0.954946000   -1.171196000   -1.599192000
1     0.634936000   -0.309569000   -2.193088000
1     0.982223000   -2.032085000   -2.272615000
6     2.315923000   -0.904571000   -1.018977000
6     3.507066000   -1.206990000   -1.669506000
1     3.473861000   -1.712750000   -2.628042000
6     4.716149000   -0.851843000   -1.074949000
1     5.654475000   -1.080650000   -1.569815000
6     4.707592000   -0.206150000    0.162267000
1     5.626407000    0.084961000    0.658175000
6     3.490679000    0.062729000    0.770205000
6    -1.715241000    1.621297000    1.291015000
1    -1.333282000    2.103036000    2.196578000
1    -2.787960000    1.811223000    1.251976000
6    -0.990523000    2.194962000    0.118014000
```

3β-b (S = 3/2)

(G = -2412.652531) (quadruplet)

```
6    -1.421446000    3.333924000   -0.553396000
1    -2.370102000    3.783761000   -0.282316000
6    -0.614727000    3.875564000   -1.550333000
1    -0.928256000    4.765117000   -2.087053000
6     0.602561000    3.261408000   -1.839149000
1     1.271805000    3.653408000   -2.596410000
6     0.963871000    2.116511000   -1.141921000
1     1.906899000    1.628593000   -1.347498000
1     3.423054000    0.554337000    1.732838000
1     1.007837000   -1.144335000    3.002362000

26    0.570358000   -0.035521000    1.057992000
8     1.055409000    1.045392000    2.185003000
8     0.759775000   -1.445187000    2.108356000
7    -0.007600000   -1.393617000   -0.484156000
7    -1.435231000    0.154652000    1.431729000
7     0.161651000    1.579765000   -0.199884000
7     2.332882000   -0.274003000    0.181212000
6    -1.417713000   -0.990521000   -0.847120000
1    -1.328954000   -0.052012000   -1.397921000
6    -2.155310000   -1.992135000   -1.753466000
1    -1.580114000   -2.134830000   -2.674946000
1    -2.229042000   -2.964571000   -1.255579000
6    -3.573658000   -1.496194000   -2.067957000
1    -3.523680000   -0.565929000   -2.649955000
1    -4.083752000   -2.238016000   -2.692842000
6    -4.358269000   -1.254196000   -0.774916000
1    -4.491943000   -2.204051000   -0.240050000
1    -5.358952000   -0.866951000   -0.997403000
6    -3.628304000   -0.247702000    0.128657000
1    -4.186346000   -0.093341000    1.057925000
1    -3.578628000    0.712686000   -0.396874000
6    -2.208261000   -0.748222000    0.444801000
1    -2.291869000   -1.697509000    0.978194000
6     0.095358000   -2.829638000   -0.079609000
1    -0.119799000   -3.466961000   -0.940624000
1    -0.597853000   -3.055377000    0.727885000
1     1.111319000   -3.031665000    0.257515000
6    -1.785742000   -0.248919000    2.828623000
1    -2.853024000   -0.069991000    2.992450000
1    -1.205385000    0.350254000    3.530457000
1    -1.560610000   -1.304415000    2.967074000
6     0.961481000   -1.176509000   -1.600163000
1     0.639472000   -0.319151000   -2.199116000
1     0.992455000   -2.040763000   -2.268967000
6     2.321496000   -0.903632000   -1.020174000
6     3.513759000   -1.204078000   -1.669153000
1     3.482371000   -1.714246000   -2.625407000
6     4.721651000   -0.842125000   -1.075825000
1     5.660485000   -1.070618000   -1.569844000
6     4.712381000   -0.189985000    0.158107000
1     5.630645000    0.107324000    0.651261000
6     3.495188000    0.078065000    0.765621000
6    -1.717378000    1.619201000    1.295814000
1    -1.332295000    2.100103000    2.200175000
1    -2.791106000    1.804918000    1.262100000
6    -1.000423000    2.194299000    0.119206000
6    -1.434749000    3.335328000   -0.546273000
1    -2.381212000    3.785097000   -0.267602000
```

```
6   -0.634123000    3.878945000   -1.547126000
1   -0.950610000    4.770323000   -2.078995000
6    0.580580000    3.264829000   -1.846774000
1    1.244478000    3.658478000   -2.607844000
6    0.946503000    2.117694000   -1.155666000
1    1.887416000    1.629166000   -1.369492000
1    3.423933000    0.574685000    1.725465000
1    1.052760000   -1.135341000    2.986355000
```

TS$_d$-CH$_{3(3-P1)}$α

(G = -2412.596719) (doublet)

```
Fe   0.1101235259   -1.196471963    0.2134419863
C    2.7112008972   -1.711821559   -1.1015169853
H    2.1201729342   -2.360568785   -1.7347153456
N    2.0621292364   -1.0655472686  -0.1107866778
N    0.5481976756    0.6354764162    1.3758193758
C    4.0664617109   -1.5302760121  -1.3343516002
N   -0.3208641794    0.2816412572   -1.2852873953
N   -1.8986720873   -1.1518039157    0.2577233967
O    0.195911441    -1.7959761478    1.7741552841
C    4.7748375521   -0.6353693763   -0.5319388703
C    4.0983578075    0.0491164659    0.4756067754
H    4.6000997478    0.767889352     1.1141474126
C    2.7425451714   -0.189148484     0.6665177432
C    1.9748573739    0.4735146979    1.7717316912
H    2.0169867295   -0.1583625693    2.663757482
H    2.4020120554    1.4491851448    2.0196709276
C   -0.3276509105    0.4454769088    2.4637804864
H   -0.2417620329   -0.895452795     2.5033749495
H   -1.3632969116    0.7050646429    2.2572460868
C    0.3658202566    1.8535713011    0.490618951
C   -0.6700737073    1.5720793474   -0.5797345062
C    0.7408266309    0.4494519245   -2.3102596797
H    1.0076734116   -0.5376342034   -2.6901537674
H    1.6151372403    0.9277132121   -1.867701262
C   -1.5354121341   -0.2757658259   -1.9475457596
H   -1.2151041777   -1.1212924251   -2.563762118
H   -1.9982859815    0.4718759056   -2.5983160978
C   -2.4848993421   -0.748067514    -0.8915238191
C   -3.8631340559   -0.7890360694   -1.0607354833
H   -4.2930529645   -0.4388901015   -1.9926076588
C   -4.6550105367   -1.2781661484   -0.0232171908
C   -4.0416077581   -1.7053292151    1.1555194225
C   -2.6589251988   -1.6318858408    1.260335174
H   -2.1402607014   -1.9616254207    2.1511571563
O   -0.1260090258   -2.7411254636   -0.6957548172
H    5.8333812154   -0.4619366804   -0.6970387051
H    4.5438985705   -2.0726897501   -2.1421885222
H   -5.7340303939   -1.3214577947   -0.1316892626
H   -4.6172332822   -2.0935621732    1.9880314192
H    0.3625634082    1.0589857333   -3.1372236656
H    0.0584895864    0.6644503792    3.4626259015
H    0.6935778378   -3.2631302138   -0.7390501242
C    0.0241576236    3.1017208308    1.3082342948
C   -0.1463963431    4.3119702032    0.3803573423
C   -1.2013770874    4.0226314232   -0.694934897
C   -0.806958617     2.784353691    -1.5129283079
H   -2.1749468259    3.8506563712   -0.2158955737
H   -1.3085332272    4.8816597146   -1.3667253804
H   -0.4292925998    5.1872297355    0.9762626159
H    0.8134191052    4.5369301376   -0.104540786
```

```
H   -0.9142255758    2.9219649797    1.8484008348
H    0.8152380379    3.2727806906    2.0466614253
H   -1.5507390235    2.574788292    -2.2881672949
H    0.1529769459    2.9764464738   -2.0050115311
H   -1.6320298303    1.4087375958   -0.0864517057
H    1.3367627825    1.993697888     0.0076816555
```

P$_d$-CH$_3$-α

(G = -2412.716545) (doublet)

```
Fe  -0.0738149803   -1.1840534582   -0.0888878284
C   -2.7963257188   -1.4234354394    1.0613175743
H   -2.2612341539   -2.0263278178    1.7820722457
N   -2.0609172171   -0.8717275143    0.0751735897
N   -0.512238562     0.8878264232   -1.4700243715
C   -4.1664048542   -1.2263702498    1.1783258864
N    0.4368814298    0.315499871     1.2756535354
N    1.9207388652   -1.2772249351   -0.2716255325
O   -0.435662268    -2.1665063672   -1.5668254513
C   -4.811692413    -0.4097391516    0.2522110416
C   -4.0544690114    0.1814960718    -0.7571397957
H   -4.5022285067    0.8416697906    -1.4918443825
C   -2.6899529505   -0.0771392312    -0.8213529523
C   -1.8702320049    0.5147781454    -1.9358905163
H   -1.7599348357   -0.1884466991   -2.7637343635
H   -2.334304212     1.4338377089   -2.3034277097
C    0.5418517619    0.4879868392   -2.1036088372
H    0.2109928543   -2.8794846789   -1.6992881503
H    1.5107915027    0.8896342951   -1.8297965988
C   -0.4263000451    1.9639330541   -0.4245548321
C    0.6605049686    1.6628159476    0.614973418
C   -0.5599474142    0.4050782325    2.3800394654
H   -0.7720254697   -0.6090318047    2.7172291578
H   -1.4738470377    0.876840559     2.017623478
C    1.7262541498   -0.1728095129    1.8561472331
H    1.4783663314   -0.9769327478    2.5542432641
H    2.2334695308    0.6189752259    2.4137330138
C    2.5924015871   -0.7170800321    0.7606577209
C    3.9816749946   -0.6689702786    0.7917446551
H    4.478571533    -0.199491472     1.6337088962
C    4.7006323737   -1.219748881    -0.2679781237
C    4.0041290665   -1.7826788769   -1.338506127
C    2.615710233    -1.7837719741   -1.3091543531
H    2.0396270703   -2.1770515316   -2.1375457622
O    0.0281104612   -2.4783487558    1.1641971652
H   -5.8788096019   -0.2242160776    0.3199091283
H   -4.7043459707   -1.7010111455    1.9911300814
H    5.7857479695   -1.1948111475   -0.2661134616
H    4.5200715791   -2.2046688801   -2.1935865713
H   -0.1505004906    0.9848403141    3.2124529623
H    0.4403282678   -0.2116947629   -2.924779969
H   -0.7207034512   -3.087609835     1.0461088004
C   -0.1737334799    3.2938083527   -1.1545867833
O   -0.0586065683    4.445909705    -0.1540557817
C    1.0434065472    4.1485794024    0.8680735968
C    0.7404599744    2.8373221152    1.6051747402
H    2.0100433914    4.0682522694    0.3525375639
H    1.1210448901    4.961977269     1.5980235709
H    0.1528977228    5.372267868    -0.6996786814
H   -1.0163284068    4.5769006588    0.3673562928
H    0.7654482978    3.1991369237   -1.7144994596
H   -0.9870224983    3.4591572594   -1.8692390784
```

ANNEX

```
H  1.5103355869  2.6246475313  2.3528091439
H -0.2173803255  2.9414441772  2.1257282252
H  1.6261348642  1.5986900575  0.1053689371
H -1.4033413562  1.987227191   0.0616530903
```

TS_q-CH_{3(3-P1)}α

$TS_q\text{-}CH_{3(3\text{-}P1)}\alpha$

(G = -2412.621218) (quadruplet)

```
Fe  0.1172485879 -1.1120879763  0.2154316567
C   2.7312777559 -1.6612800094 -1.0929951817
H   2.1350039185 -2.308870063  -1.7217712651
N   2.0841715015 -1.0039311064 -0.1073445713
N   0.5521823002  0.6006725613  1.3322420474
C   4.0901851017 -1.4919337815 -1.3124592844
N  -0.3387608329  0.2559680472 -1.2982836587
N  -1.9031427459 -1.1296381266  0.2727664609
O   0.1880218234 -1.9104746323  1.782220006
C   4.8020102857 -0.6029603388 -0.5054344729
C   4.1282849076  0.0849598148  0.5017053527
H   4.6328721255  0.7938144299  1.14877304
C   2.76983843  -0.1424013982  0.6800453437
C   1.9728419811  0.4856153975  1.7747510881
H   2.0100485928 -0.1634714953  2.6551519205
H   2.3577091321  1.4698427149  2.0540306428
C  -0.3318206683  0.3830263979  2.4515248477
H  -0.1955208876 -0.9229729057  2.5164261367
H  -1.371650108   0.6131718937  2.2324859158
C   0.3595089042  1.8357239345  0.483201816
C  -0.6789071706  1.5573758102 -0.5904494415
C   0.7082867142  0.4252176152 -2.3396866258
H   0.974415733  -0.5629588831 -2.7164221726
H   1.5839441541  0.9131114971 -1.9110122608
C  -1.5652190613 -0.2890633072 -1.9495654568
H  -1.2609323119 -1.1295111629 -2.5794676843
H  -2.028825822   0.4705435602 -2.5850269159
C  -2.5003629647 -0.7634884167 -0.8838325599
C  -3.8771857716 -0.8445714576 -1.04801994
H  -4.3180658801 -0.5240088955 -1.9853686379
C  -4.6537638924 -1.3349877353  0.0003494772
C  -4.0272953519 -1.7247494847  1.1849795415
C  -2.6471338382 -1.6128606963  1.2855675598
H  -2.1163980769 -1.9149875101  2.1786296056
O  -0.0385442226 -2.5550394221 -0.8481394035
H   5.863074465  -0.4400929165 -0.6650327745
H   4.569045477  -2.0406613411 -2.1152096702
H  -5.7313838684 -1.4092883965 -0.1048151783
H  -4.589859916  -2.113304637   2.0261876304
H   0.3112881752  1.0286578323 -3.161368123
H   0.0425201006  0.7169642791  3.4225508096
H   0.6425582638 -3.2069904085 -0.6015474722
C  -0.0027390548  3.0675654667  1.314751008
C  -0.1781167017  4.2857634871  0.3962918943
C  -1.2184703954  3.9996498422 -0.6945578751
C  -0.813919402   2.769088967  -1.5207677485
H  -2.1970318245  3.820335023  -0.2286200904
H  -1.3207034    4.8643098524 -1.3598201849
H  -0.4768280927  5.1523891314  0.9968139745
H   0.7848420768  4.5247802617 -0.0753260422
H  -0.9426459636  2.8717305342  1.8458509218
H   0.7813529035  3.2414190939  2.060003824
H  -1.5540182293  2.5631814278 -2.3005198954
H   0.1480344842  2.9662255427 -2.0070716652
```

P_q-CH₃-α

$P_q\text{-}CH_3\text{-}\alpha$

(G = -2412.699058) (quadruplet)

```
Fe -0.1017110683 -1.4464732533  0.1449779821
C  -2.8698494472 -1.3831495048  0.9315852863
H  -2.3592767925 -2.0455639797  1.619537729
N  -2.091976634  -0.8138892901 -0.0162079812
N  -0.5095028813  1.0545027734 -1.6245391213
C  -4.2334444463 -1.1431644614  1.0333034002
N   0.4211767928  0.2839807478  1.2725915639
N   1.9184274095 -1.3570571351 -0.2455515995
O  -0.4581428501 -2.7100356173 -1.1016712827
C  -4.8269747105 -0.2635782651  0.1301880379
C  -4.0284034558  0.3307228028 -0.8439994037
H  -4.4423499245  1.0272959849 -1.5649727423
C  -2.6696051342  0.023792526  -0.9012865286
C  -1.8566347476  0.6029949483 -2.0311941022
H  -1.7379459464 -0.1280643317 -2.8351138527
H  -2.371059877   1.4828450751 -2.4269348054
C   0.5272700296  0.7078603205 -2.2940170258
H   0.2936636453 -3.3227677505 -1.17712817
H   1.5034344006  1.0924085398 -2.0157096915
C  -0.428172977   2.0080362576 -0.4663657637
C   0.6470155052  1.6273725306  0.5726320176
C  -0.5689844263  0.4121969521  2.3809489678
H  -0.8093009532 -0.5906503773  2.7326699353
H  -1.4702286259  0.8976493884  2.0036798981
C   1.7388768553 -0.1701994306  1.8329211965
H   1.5259702733 -0.9835467876  2.531647661
H   2.2390298725  0.6315591122  2.3803371331
C   2.5951882823 -0.6768930167  0.7072727961
C   3.9652656766 -0.4654115912  0.6142781165
H   4.4747533416  0.0948088769  1.390651678
C   4.6474416867 -0.966068736  -0.4962182253
C   3.9385571812 -1.6509697585 -1.4851839932
C   2.5681674096 -1.8222182586 -1.3269069119
H   1.9637584608 -2.3280988837 -2.0715356169
O  -0.0567759164 -2.5657524629  1.6535592413
H  -5.8873329541 -0.0385071291  0.1838407619
H  -4.8053900443 -1.6338114055  1.8129105503
H   5.7167777295 -0.8080336572 -0.5963681226
H   4.4314054966 -2.0377555281 -2.3701101835
H  -0.1507279702  0.9943866636  3.206553691
H   0.4203170883  0.0354517559 -3.1394559958
H  -0.5260609225 -3.3910726842  1.4466616885
C  -0.1749607546  3.397973265  -1.0928052739
C  -0.0204016602  4.4931293562 -0.0396090136
C   1.1030907537  4.112687516   0.9250095781
C   0.7631949393  2.7793301999  1.5954637805
H   2.0510535686  4.0290607448  0.3762944404
H   1.2298478393  4.8786546979  1.6983289539
H   0.189957003   5.4439146647 -0.5422850789
H  -0.958717063   4.6100365689  0.5190801835
H   0.7468980336  3.3360722055 -1.685119725
H  -1.0036176475  3.6118547118 -1.7764232383
H   1.5173702429  2.5229844834  2.3441032932
H  -0.1935257046  2.8972758721  2.1150354048
H   1.6052146479  1.5404032158  0.0545109254
H  -1.4106276301  1.9948665383  0.0082775571
```

ANNEX

TS$_{(3-P)d}$α
(G =-2412.608472) (doublet)

```
Fe  0.1356245376 -1.1847097406  0.0640518467
C  -2.5800552057 -1.6344896288  1.3462015616
H  -2.0518244027 -1.9252188155  2.2452026319
N  -1.8472314899 -1.2206538914  0.3059656655
N  -0.3869121504  0.2707128024 -1.3153572878
C  -3.9729975789 -1.693370673   1.2795194684
N   0.4166287603  0.5000488576  1.3259526598
N   2.0964425134 -0.9494567398 -0.1410995941
O  -0.0038673747 -2.1526553479 -1.3058169457
C  -4.6223954477 -1.3204334779  0.1016843072
C  -3.8640258405 -0.8923261238 -0.9861156632
H  -4.3157939732 -0.5806932019 -1.9207489496
C  -2.4792056154 -0.8388977617 -0.8426081428
C  -1.5400732362 -0.4306637806 -1.8736700393
H  -0.9065241612 -1.5743425477 -2.0373289412
H  -1.9197777876 -0.0802690655 -2.8338326093
C   0.6206663325  0.4970564423 -2.389714798
H   0.9361000219 -0.4729257236 -2.7725468558
H   1.4771634192  1.0321379633 -1.9811962764
C  -0.7529577504  1.5519410969 -0.573868268
C   0.3206462226  1.7565501526  0.4896124214
C  -0.5255771621  0.5010403484  2.4761606995
H  -0.4995126926 -0.4920223232  2.924780585
H  -1.5332520425  0.7368764934  2.1345203649
C   1.802467786   0.3529353073  1.8581283592
H   1.7696267251 -0.3818232601  2.6678850319
H   2.1564814282  1.3039363965  2.2669988378
C   2.6973390779 -0.1540330317  0.7717223695
C   4.0581761887  0.122742344   0.7079938261
H   4.4995650681  0.7811448928  1.4480296051
C   4.8187906199 -0.4548228947 -0.3069897699
C   4.1929019942 -1.2905750891 -1.2334892383
C   2.8268780506 -1.5115340594 -1.1237793245
H   2.2877012669 -2.1367916106 -1.8240769721
O   0.4776134454 -2.2999377538  1.4265804937
H  -5.7042823102 -1.3612525416  0.0325748883
H  -4.5264324069 -2.040058859   2.1446718329
H   5.8829336027 -0.2527083101 -0.3760644389
H   4.7450679936 -1.7615627235 -2.0387768212
H  -0.2086800105  1.2447786322  3.21348193
H   0.1667601158  1.0747438885 -3.1988582903
H  -0.2946909229 -2.842794909   1.663776496
C  -0.9119268992  2.7694321621 -1.4881787943
C  -1.1990617858  4.0181925933 -0.6419699296
C  -0.0654399983  4.2420024003  0.3656817414
C   0.0570244581  3.0328065907  1.3025615077
H   0.8792878575  4.3910015178 -0.1749221631
H  -0.2525402998  5.1415989203  0.962890515
H  -1.3042497663  4.8844081943 -1.3048651092
H  -2.1479956588  3.8924819189 -0.1029803715
H   0.0150668427  2.9398422472 -2.0447535108
H  -1.7140237546  2.5767989391 -2.2089639034
H   0.866116861   3.1706800462  2.0283505775
H  -0.8816581576  2.9278383816  1.8565450057
H   1.2867488273  1.8662662694 -0.0104088522
H  -1.7074051343  1.3680640861 -0.0768983695
```

P1α

(G = -2412.673822) (doublet)

```
Fe  0.0819903661 -1.0422923945  0.1041128517
C  -2.5478559285 -1.7684696373  1.2626763403
H  -1.9467426451 -2.0954365546  2.1017631563
N  -1.8935731082 -1.1626065367  0.2669003668
N  -0.5154774647  0.3956738956 -1.314327854
C  -3.9232996786 -1.994729157   1.2065382794
N   0.3780757427  0.5959855377  1.3413674927
N   2.0342931141 -0.7747951364 -0.1604293045
O   0.084972165  -2.3302375786 -1.1538145898
C  -4.637521888  -1.599788401   0.674412789
C  -3.9692697494 -0.970723645  -0.9721509389
H  -4.4798755205 -0.6329505439 -1.8669552294
C  -2.5834619741 -0.736253658  -0.8487862968
C  -1.801850079  -0.0430827504 -1.7795960981
H  -0.7845749301 -2.445877294  -1.5776481522
H  -2.146442234   0.2727625091 -2.756991926
C   0.4326459166  0.4965984888 -2.4608617867
H   0.6064243334 -0.5129277083 -2.8323300378
H   1.3673491243  0.9415828299 -2.1197336386
C  -0.7133613678  1.7218005085 -0.5603713747
C   0.3767908785  1.8511775441  0.4862756734
C  -0.6153822959  0.6436658956  2.447818249
H  -0.6499664372 -0.3422460799  2.9115541656
H  -1.5970237814  0.9044067787  2.0512582706
C   1.7406911189  0.3995174205  1.9148665576
H   1.6717063087 -0.3664697069  2.6921935493
H   2.1011471435  1.325888013   2.3705337779
C   2.6472717684 -0.0706255468  0.820120757
C   4.0150630407  0.1660706751  0.7890284103
H   4.4700738296  0.749098733   1.5819211419
C   4.7652250248 -0.349898595  -0.2672765352
C   4.124156861  -1.0852879261 -1.26595715
C   2.752505232  -1.279280351  -1.1819670064
H   2.1991634171 -1.8417519615 -1.9218605097
O   0.3533814833 -2.1029703659  1.4992220218
H  -5.7051581956 -1.7812697532 -0.0004658527
H  -4.4106312063 -2.4905664233  2.0379493004
H   5.8355848036 -0.1759500964 -0.3128694094
H   4.6705511739 -1.5031540886 -2.1037339349
H  -0.3060552509  1.3830816827  3.1919471754
H  -0.0087942084  1.1117019825 -3.2491917748
H   0.1845796931 -3.0256613791  1.2295114256
C  -0.7654364573  2.9341394253 -1.493410587
C  -0.942603556   4.2179863097 -0.6712877586
C   0.1978210351  4.3570577118  0.344151498
C   0.2144154802  3.1482822131  1.2901363512
H   1.1561323173  4.4241581937 -0.1886716102
H   0.0796946655  5.2731080919  0.9338433475
H  -0.965039988   5.0787936457 -1.3489291491
H  -1.9031821042  4.1869053919 -0.1392341911
H   0.1739450685  3.0053725892 -2.0519494615
H  -1.5820300905  2.800811506  -2.2113176618
H   1.0254818801  3.2289630143  2.0214780667
H  -0.7346932377  3.1220050466  1.8358856763
H   1.344573211   1.878478154  -0.0228114415
H  -1.6734238198  1.6280954813 -0.04738892
```

TS$_{(3-P1)q}$α
(G = -2412.629517) (quadruplet)

ANNEX

```
Fe  0.1421188986 -1.1512505919  0.1223552392
C  -2.5644202671 -1.605867262   1.3611744266
H  -2.0037438453 -1.8951385873  2.2404775998
N  -1.8542374978 -1.1915721423  0.305012922
N  -0.3850571097  0.2533734274 -1.3221630213
C  -3.955342579  -1.6744582318  1.3055436938
N   0.4345979122  0.5158001559  1.3417382787
N   2.0970524861 -0.9180224684 -0.1354480137
O   0.0397731586 -2.2445927404 -1.2528638469
C  -4.6095151557 -1.3211157747  0.1240798817
C  -3.8625772117 -0.9079035953 -0.9802324934
H  -4.3266812748 -0.6248137983 -1.9179178736
C  -2.4795125257 -0.8489215265 -0.852663194
C  -1.5128164668 -0.4967425678 -1.8884487601
H  -0.8482757747 -1.6520411872 -1.9622308317
H  -1.8609096701 -0.1780971246 -2.8698884936
C   0.6294555023  0.4680338315 -2.3912394382
H   0.9467735105 -0.5071367888 -2.7589468354
H   1.4824166694  1.0152904284 -1.9913413082
C  -0.7548106723  1.5295177426 -0.5850934938
C   0.3151017898  1.7642901978  0.4771182841
C  -0.4995679629  0.5324474734  2.5007949098
H  -0.4712701206 -0.4504000797  2.9710881258
H  -1.5094249411  0.760748406   2.1612514655
C   1.8273094514  0.3944037828  1.8596297203
H   1.8161936698 -0.3326029925  2.6783681886
H   2.1765229034  1.3532897836  2.252968563
C   2.7101274223 -0.1157475839  0.7658140364
C   4.0698913883  0.1545709787  0.6789955079
H   4.5250032894  0.8171372641  1.4067088095
C   4.8120845827 -0.4354414228 -0.343134924
C   4.1721449933 -1.2799914537 -1.2526912331
C   2.8079428439 -1.4961048932 -1.1235044039
H   2.2523523081 -2.1264606308 -1.805907744
O   0.3284104361 -2.2738454225  1.4836551199
H  -5.6916903754 -1.3701250361  0.061098273
H  -4.5033780413 -2.0128489537  2.1774006661
H   5.8753153783 -0.2359969757 -0.4309684471
H   4.7125122618 -1.7606225377 -2.060120509
H  -0.1770770606  1.2894662581  3.2214711775
H   0.1725074736  1.0304996279 -3.2094369397
H   0.3847823862 -3.1936298683  1.1614477575
C  -0.9299556904  2.7362609609 -1.5123607639
C  -1.2326237993  3.9903844799 -0.6810611065
C  -0.1004335583  4.2412091214  0.3218371268
C   0.0386302932  3.0456297578  1.2747663647
H   0.8415505268  4.3950221318 -0.222125505
H  -0.2977646373  5.1455860488  0.908312967
H  -1.3507028653  4.8477961255 -1.3531789536
H  -2.1787899406  3.8579551027 -0.1387793036
H  -0.0063252239  2.9109066539 -2.0733999741
H  -1.7307810691  2.5219678171 -2.2287345323
H   0.8471766625  3.204242536   1.9966261651
H  -0.8978010937  2.9376407713  1.8318264025
H   1.2806649709  1.8792921945 -0.0226934848
H  -1.7066317387  1.3418761781 -0.0848942444
```

P1-α_q

(G = -2412.679708) (quadruplet)

```
Fe  -0.020487000 -1.132510000  0.110031000
C   -2.768731000 -1.411415000  1.248834000
```

```
H  -2.233601000 -1.810501000  2.101498000
N  -2.018020000 -0.947680000  0.244741000
N  -0.434428000  0.399621000 -1.336742000
C  -4.163252000 -1.410498000  1.184987000
N   0.495733000  0.458511000  1.340612000
N   1.936447000 -1.140051000 -0.192223000
O  -0.236782000 -2.399054000 -1.152923000
C  -4.794176000 -0.939895000  0.028399000
C  -4.023041000 -0.458036000 -1.021707000
H  -4.466854000 -0.060735000 -1.927730000
C  -2.623915000 -0.448392000 -0.886596000
C  -1.723434000  0.074667000 -1.834690000
H  -1.173264000 -2.633044000 -1.283155000
H  -1.966566000  0.267986000 -2.872310000
C   0.563289000  0.431448000 -2.442638000
H   0.663626000 -0.584662000 -2.823979000
H   1.520846000  0.790423000 -2.066744000
C  -0.508269000  1.707357000 -0.525384000
C   0.612362000  1.712449000  0.496340000
C  -0.449986000  0.611950000  2.477637000
H  -0.595049000 -0.368316000  2.931290000
H  -1.401808000  0.998582000  2.112813000
C   1.845234000  0.100484000  1.867572000
H   1.709451000 -0.644840000  2.656670000
H   2.332965000  0.979002000  2.298792000
C   2.654694000 -0.493441000  0.756056000
C   4.041032000 -0.436848000  0.693889000
H   4.584685000  0.102543000  1.461554000
C   4.696012000 -1.077929000 -0.357214000
C   3.944977000 -1.755072000 -1.320293000
C   2.561799000 -1.765518000 -1.207909000
H   1.924951000 -2.270979000 -1.921809000
O   0.066048000 -2.211291000  1.523578000
H  -5.876609000 -0.946117000 -0.047891000
H  -4.731501000 -1.796780000  2.023176000
H   5.778774000 -1.046255000 -0.425727000
H   4.415909000 -2.266224000 -2.152146000
H  -0.032457000  1.298295000  3.219745000
H   0.204541000  1.089598000 -3.238382000
H   0.017825000 -3.136065000  1.216382000
C  -0.490216000  2.942720000 -1.429312000
C  -0.526010000  4.215643000 -0.572532000
C   0.666932000  4.230784000  0.389865000
C   0.607667000  3.010350000  1.318189000
H   1.601593000  4.216578000 -0.187353000
H   0.663361000  5.143335000  0.996556000
H  -0.505498000  5.091724000 -1.230431000
H  -1.461162000  4.251213000  0.002654000
H   0.430801000  2.952016000 -2.021283000
H  -1.341374000  2.893293000 -2.117146000
H   1.450814000  2.999066000  2.017077000
H  -0.316649000  3.069029000  1.901948000
H   1.567279000  1.641109000 -0.031579000
H  -1.462412000  1.674301000  0.005808000
```

P2-α_q

(G = -2412.715022) (quadruplet)

```
Fe  -0.018816000 -1.465883000 -0.341297000
C    2.890218000 -1.334432000 -1.075922000
H    2.490928000 -1.738638000 -1.998066000
N    1.987203000 -0.956307000 -0.157512000
```

ANNEX

N	0.466176000	0.788585000	1.667303000
C	4.262149000	-1.223513000	-0.850005000
N	-0.437580000	0.319952000	-1.345539000
N	-1.953021000	-1.191846000	0.204595000
O	0.219635000	-2.678062000	0.997990000
C	4.714085000	-0.736158000	0.374218000
C	3.780061000	-0.361581000	1.344054000
H	4.077174000	0.021675000	2.313862000
C	2.434794000	-0.471069000	1.024712000
C	1.360104000	-0.096399000	1.957128000
H	1.155840000	-2.928136000	1.086581000
H	1.272700000	-0.614112000	2.908615000
C	-0.689139000	0.947354000	2.584408000
H	-0.848680000	0.003156000	3.104385000
H	-1.570550000	1.203639000	1.996919000
C	0.606222000	1.763838000	0.522513000
C	-0.495852000	1.625718000	-0.547209000
C	0.497720000	0.409316000	-2.504872000
H	0.622261000	-0.593756000	-2.913821000
H	1.461158000	0.789897000	-2.162925000
C	-1.822794000	0.030969000	-1.847340000
H	-1.737504000	-0.760771000	-2.597306000
H	-2.263641000	0.910523000	-2.323005000
C	-2.646736000	-0.447238000	-0.686403000
C	-3.992853000	-0.161148000	-0.502190000
H	-4.516272000	0.448260000	-1.230690000
C	-4.632287000	-0.659595000	0.634595000
C	-3.906119000	-1.419321000	1.554194000
C	-2.560535000	-1.665276000	1.305532000
H	-1.938538000	-2.243942000	1.978286000
O	-0.138518000	-2.574474000	-1.845561000
H	5.776074000	-0.652324000	0.579900000
H	4.955602000	-1.532653000	-1.623730000
H	-5.682991000	-0.446741000	0.805538000
H	-4.368361000	-1.812332000	2.452717000
H	0.091747000	1.064998000	-3.279570000
H	-0.470301000	1.744999000	3.296640000
H	-0.184574000	-3.504635000	-1.567473000
C	0.618531000	3.163011000	1.186443000
C	0.657741000	4.298485000	0.164314000
C	-0.550729000	4.173830000	-0.761643000
C	-0.460865000	2.839149000	-1.501027000
H	-1.477445000	4.228028000	-0.174304000
H	-0.569470000	4.986739000	-1.496169000
H	0.653453000	5.252274000	0.703716000
H	1.581862000	4.250357000	-0.427047000
H	-0.291937000	3.288335000	1.780085000
H	1.477686000	3.201809000	1.863602000
H	-1.275074000	2.737077000	-2.224181000
H	0.481284000	2.837885000	-2.057087000
H	-1.462866000	1.628346000	-0.040875000
H	1.578984000	1.584950000	0.064771000

TS$_{(P2-P3)}\alpha_q$

(G = -2412.713916) (quadruplet)

Fe	0.2436156748	-1.5476432422	0.1824221593
C	-2.5483699057	-1.8852807513	1.1183944594
H	-2.010965068	-2.3646744633	1.9269843543
N	-1.7860069448	-1.3532984003	0.147718602
N	-0.7889289249	0.8770191189	-1.7438894571
C	-3.9389818602	-1.833227903	1.0771643294

N	0.3743554275	0.3930612587	1.2433792897
N	2.1660330454	-1.160108869	-0.1186092033
O	0.1236478425	-2.2533658921	-1.5225215504
C	-4.5630010552	-1.2297131483	-0.0119834435
C	-3.7761626551	-0.6867843862	-1.0309331317
H	-4.2139587033	-0.2070960719	-1.899080016
C	-2.3958239272	-0.7554460964	-0.9039614832
C	-1.4995439306	-0.1812767036	-1.9347892022
H	-0.7239034434	-2.7115913752	-1.6551021674
H	-1.4487335237	-0.6573648248	-2.908380092
C	0.1937892744	1.2596703343	-2.7840210458
H	0.4955405287	0.3594725338	-3.3195501876
H	1.058131876	1.7097499036	-2.2951870314
C	-0.9175508793	1.7545774195	-0.5254360047
C	0.3044420248	1.6863439013	0.435336046
C	-0.5966286033	0.3685169952	2.3698347142
H	-0.6342057158	-0.6506255395	2.7560775739
H	-1.5866227891	0.6623028249	2.0180196472
C	1.7503157253	0.2247181127	1.8025184275
H	1.6840464353	-0.553384518	2.5695051517
H	2.1195056434	1.136486344	2.2771575326
C	2.6875336673	-0.2446126588	0.7320325891
C	4.0064170115	0.1765109366	0.6204925328
H	4.3867860237	0.9219695209	1.3099814744
C	4.8060871488	-0.3703091214	-0.3840953522
C	4.2599028391	-1.3159161507	-1.2536452969
C	2.9293038786	-1.6835499564	-1.0960773769
H	2.4403505662	-2.3948288086	-1.7498202996
O	0.3926395859	-2.6199657474	1.6971391913
H	-5.6450867017	-1.182863072	-0.0756909194
H	-4.5116363587	-2.2720387011	1.8862944142
H	5.8394768298	-0.0557378008	-0.4917470834
H	4.847018908	-1.7600490272	-2.0495738772
H	-0.2856752692	1.0391158388	3.1767992257
H	-0.2602845413	1.9795604306	-3.4675405218
H	1.1384791098	-3.2407263084	1.6362112745
C	-1.2037243731	3.1660555431	-1.0970963764
C	-1.2158001125	4.2589234045	-0.0323914124
C	0.135354151	4.2525258049	0.6781601935
C	0.3022187611	2.9088328115	1.3870315159
H	0.9405393295	4.4116443732	-0.0523530549
H	0.1951148546	5.0545559938	1.4227207483
H	-1.4118286639	5.2204526831	-0.5203188492
H	-2.0176481787	4.0809985872	0.6968815108
H	-0.4254298885	3.431391331	-1.8186004302
H	-2.1566324051	3.1109004347	-1.6336126398
H	1.2248053433	2.8999494862	1.9726088327
H	-0.5333998773	2.8173140345	2.0869995406
H	1.2188987707	1.713303035	-0.1632768498
H	-1.8078809774	1.4204245413	0.0078300256

P3-α_q

(G = -2412.717301) (quadruplet)

Fe	0.4779366567	-1.4746837885	0.1694808768
C	-2.217587327	-2.2648816624	1.152333276
H	-1.6502481523	-2.6052835249	2.0100419027
N	-1.5057802836	-1.6995922115	0.1605263834
N	-1.2374057522	0.8810063056	-1.7754176439
C	-3.5973746464	-2.4009285328	1.0670326813
N	0.330803293	0.5022183936	1.258150317
N	2.3566245081	-0.880303574	0.000737659

ANNEX

```
O  0.1436096524 -1.0770675778 -1.7476453879
C -4.250439937  -1.9427310387 -0.0782542875
C -3.5073288455 -1.3480813058 -1.1000881463
H -3.9776266637 -0.9645547652 -1.9986013718
C -2.1335754889 -1.2360919962 -0.9464817256
C -1.2554260864 -0.5146559254 -1.941199218
H  0.2338199904 -1.9134314661 -2.249712466
H -1.5068819159 -0.7713345318 -2.9721573281
C -0.3539026712  1.5391261942 -2.7434778695
H -0.6272676121  1.2088591937 -3.7521228542
H  0.7047995244  1.3005251378 -2.5787785735
C -1.3116209726  1.4962653887 -0.4217827445
C  0.0777151402  1.6645160324  0.3036644769
C -0.626004001   0.417096879   2.3855210724
H -0.4586072804 -0.5359990825  2.8910378968
H -1.6544550936  0.4478262522  2.0275861999
C  1.7090214188  0.5506149007  1.8222539226
H  1.7491787324 -0.1930035927  2.6258243112
H  1.9417635042  1.5263314822  2.2550029337
C  2.7185322309  0.1620420275  0.7823860502
C  3.9531524754  0.7784512868  0.6205468264
H  4.212080969   1.6237779299  1.2485081971
C  4.8261746545  0.2952320363 -0.3552571565
C  4.4387824374 -0.7835375936 -1.1539490197
C  3.1826647805 -1.3419454986 -0.95742375
H  2.8081934846 -2.1645973174 -1.5569930377
O  0.7419443222 -2.4564481985  1.6418724122
H -5.3267590242 -2.0428567913 -0.1745682913
H -4.1414826399 -2.860583761   1.884286709
H  5.795430744   0.7625304592 -0.4985738399
H  5.0883363666 -1.1796058055 -1.9261329631
H -0.4744383691  1.2335225841  3.1010188484
H -0.4752728943  2.6223836936 -2.6861841519
H  1.677581027  -2.4788374787  1.9103807892
C -2.1783585237  2.7749227188 -0.5664701562
C -1.9582027021  3.8241325115  0.5187925858
C -0.4774871527  4.2003045297  0.5139208741
C  0.3358138971  3.0142484249  1.0321107149
H -0.1756677712  4.4661257951 -0.5092943171
H -0.278246308   5.0693452522  1.1523497036
H -2.5945930675  4.6934621917  0.3141878663
H -2.2362515622  3.4327832837  1.5081195185
H -1.9654446181  3.2601250314 -1.5248235158
H -3.2231865262  2.4465197815 -0.6074946624
H  1.4080625763  3.2298688993  0.9749406245
H  0.0929574477  2.9060847121  2.0941199913
H  0.8502568665  1.5610706061 -0.4613624129
H -1.9154068114  0.8207430677  0.1779942701
```

TS(3-P)βd
(G = -2412.621366) (doublet)

```
O  1.0903190477  1.3231289687  2.1353575718
O  0.6939183506 -1.2383356559  2.243132062
N  0.0209466177 -1.3019746005 -0.4703973012
N -1.3994936981  0.1163525135  1.4622446368
N  0.1157778256  1.5800888725 -0.2275979294
N  2.3373680245 -0.3348446447  0.2073303251
C -1.4161542464 -0.9923328862 -0.7937430565
H -1.413650347  -0.0420335875 -1.3299880772
C -2.1048511569 -2.0377854579 -1.6779145371
H -1.5514557289 -2.1346889367 -2.6181816649
```

```
H -2.0979477838 -3.0097077987 -1.173377158
C -3.5632545028 -1.6258711682 -1.9236485786
H -3.5913972665 -0.6707602101 -2.4655634416
H -4.0504234515 -2.3799815802 -2.5518138776
C -4.3066477589 -1.4754289702 -0.5894150126
H -4.3187640267 -2.4410973064 -0.0664203711
H -5.346536128  -1.1750714105 -0.7594070542
C -3.6174690223 -0.4216458647  0.2909200614
H -4.1253876033 -0.3065898232  1.2549797836
H -3.6484125668  0.5392155031 -0.2353776996
C -2.1629184785 -0.8304309016  0.5290178207
H -2.1560693894 -1.791509512   1.0463153567
C  0.2136029218 -2.7186719337 -0.0274296806
H  0.02891755  -3.3804857755 -0.8774817539
H -0.4620776887 -2.9532332848  0.791017593
H  1.2424923924 -2.8413076487  0.3112762922
C -1.4629816219 -0.3522745399  2.8414398863
H -2.3074093808 -1.0063462993  3.0632083623
H -1.2653880049  0.4351584746  3.5668847122
H -0.3863345354 -1.0911386673  2.8651653942
C  0.9465238065 -1.0651237474 -1.6187197975
H  0.6089491534 -0.186563688  -2.1742375825
H  0.9342309518 -1.918085293  -2.302878338
C  2.3194508429 -0.8409055193 -1.0494371312
C  3.5004196629 -1.1046570102 -1.7302492083
H  3.455708062  -1.5185431422 -2.7314909052
C  4.7160111652 -0.8376895732 -1.0999348762
H  5.651003633  -1.0370734454 -1.6137128741
C  4.7187636414 -0.3237865897  0.198364018
H  5.6435821339 -0.1098935098  0.7219554377
C  3.5044658526 -0.0858746905  0.8286558523
C -1.7509906805  1.5662474589  1.3041614736
H -1.3383632671  2.0867421798  2.1715477048
H -2.8309348415  1.7106331795  1.2996860474
C -1.0925311601  2.1154150832  0.0713746425
C -1.6286242249  3.1594501544 -0.6698466648
H -2.6086040081  3.5468809098 -0.4145070175
C -0.8815236064  3.6889090863 -1.7228594856
H -1.2795128368  4.5036505807 -2.3192497463
C  0.3837210496  3.1657479494 -1.9934829284
H  1.0025320213  3.5591649742 -2.7917581625
C  0.8501408173  2.1075366397 -1.2237234501
H  1.824765773   1.6689863076 -1.4015303435
H  3.435787905   0.3159233465  1.8322265113
H  1.3562481111  0.9032959588  2.9755943706
```

Pβd
(G = -2412.702781) (doublet)

```
Fe  0.8876997343  0.1949680264  1.1561361681
O   1.4909825779  1.5442653016  2.1922637085
O   1.1337420235 -1.0867559061  2.4222920071
N  -0.0662848201 -1.2662745275 -0.239935149
N  -2.071361098  -0.0170562033  1.5818154015
N   0.0016464617  1.5737159084 -0.0393132788
N   2.431591543  -0.2669363875  0.0941953918
C  -1.4776052984 -0.9774893553 -0.6970164198
H  -1.4369395214 -0.0196311418 -1.2146719271
C  -2.0363607754 -1.9996926743 -1.7121848854
H  -1.3189863831 -2.1399332857 -2.5247545949
H  -2.1855165818 -2.9677778268 -1.2202487154
C  -3.3747351732 -1.5101093464 -2.2813554788
```

ANNEX

```
H  -3.2184242088  -0.5549350103  -2.8012849812
H  -3.7424077993  -2.2329611427  -3.0184069511
C  -4.3995425174  -1.3199318682  -1.1604314588
H  -4.6191839754  -2.2911026937  -0.6969683563
H  -5.3400941109  -0.9192344275  -1.5547740374
C  -3.855795259  -0.3637363347  -0.0928991449
H  -4.5586824171  -0.2671523286   0.7408209085
H  -3.7083390515   0.6280562795  -0.5354269848
C  -2.5109864414  -0.8803387176   0.4465690811
H  -2.6539944306  -1.8736336836   0.8758269963
C   0.0535387316  -2.6415448323   0.3169421687
H  -0.2226816828  -3.3833126211  -0.4389547081
H  -0.5851379995  -2.7479229086   1.1934777846
H   1.0896006368  -2.8056001214   0.6144665076
C  -1.8036319828  -0.5356322232   2.726498358
H  -1.8976970263  -1.6082016672   2.8603792234
H  -1.4984241251   0.10343776     3.548870317
H   1.0597636687  -0.6334132739   3.2806045237
C   0.8206728329  -1.1827218715  -1.4411919022
H   0.5046821326  -0.3272012115  -2.0477730595
H   0.7350222614  -2.0792576609  -2.0614105689
C   2.2471647795  -0.9794686247  -1.0362172837
C   3.3256445475  -1.4291363252  -1.7904377276
H   3.1391550575  -2.009670543   -2.6872580262
C   4.6183687033  -1.1202166896  -1.3713740132
H   5.4748205557  -1.4595474477  -1.945305669
C   4.7977806933  -0.37552093    -0.2029860843
H   5.7866806341  -0.1161031678   0.1576938709
C   3.6801733606   0.0283786832   0.5128136553
C  -2.0173210219   1.4652278973   1.4067119777
H  -1.5508752256   1.8703491527   2.3082356321
H  -3.0513542924   1.8102846955   1.3613079745
C  -1.2736133408   1.9716954225   0.1889353554
C  -1.8967866359   2.9074673274  -0.631064662
H  -2.9240503833   3.1881940082  -0.4268880561
C  -1.1925384814   3.4668919668  -1.6976409682
H  -1.6669778547   4.1989773286  -2.3430874033
C   0.1225509354   3.0662167041  -1.9166216788
H   0.715226136    3.4700998438  -2.7296000922
C   0.6786321649   2.1148233682  -1.0685829653
H   1.695909691    1.7683477662  -1.2094981236
H   3.7555563928   0.6023598047   1.4273296145
H   2.1539626595   1.2284587363   2.8302867295
```

TS$_{(3-P)}$β$_q$

(G = -2412.628428) (quadruplet)

```
Fe   0.5760077411   0.069111268    1.030696705
O    1.0758229766   1.3883274072   2.1198398977
O    0.688993276   -1.1390159388   2.2934723041
N    0.029728863   -1.3226315657  -0.4206055235
N   -1.4269028982   0.1401555573   1.470499848
N    0.1073308022   1.5661510741  -0.2606750035
N    2.3498523457  -0.3138701607   0.2083047757
C   -1.4058800011  -1.0248789374  -0.7630086135
H   -1.4005226143  -0.0897801968  -1.3248726462
C   -2.0821798705  -2.0954918794  -1.6266033781
H   -1.5173848708  -2.2154550876  -2.5573541584
H   -2.0779753429  -3.0537155752  -1.0963043328
C   -3.5382713147  -1.693329122   -1.9014299565
H   -3.5606067011  -0.7540559865  -2.4705864319
H   -4.0166708103  -2.4656284398  -2.5140080277
```

```
C   -4.2987942    -1.5065349237  -0.5817065893
H   -4.3191982038  -2.4576293067  -0.0329911965
H   -5.33597271   -1.2100614676  -0.7737120608
C   -3.6213741581  -0.4303109774   0.2803451212
H   -4.1398389534  -0.2941346742   1.2359482529
H   -3.6472949085   0.5185087742   -0.2677116225
C   -2.1690939082  -0.8316380655   0.5457148488
H   -2.1668893074  -1.7806077673   1.0846508894
C    0.2250655498  -2.7198285396   0.0771799451
H    0.0404046511  -3.4172052996  -0.7438428695
C   -0.4491090185  -2.9219647132   0.9058898869
H    1.2548396902  -2.8259237735   0.4190422342
C   -1.5065857137  -0.2919177117   2.8484142494
H   -2.3108293109  -0.9939305178   3.0699506409
H   -1.3532786376   0.5121528204   3.566049339
H   -0.3755506314  -0.9978369878   2.8980334086
C    0.9539069922  -1.1259457087  -1.5779204458
H    0.6112780454  -0.269675825   -2.1647099999
H    0.9423645882  -2.0033064045  -2.2304663249
C    2.3281779006  -0.8709741028  -1.0258142122
C    3.5062905548  -1.1427191741  -1.7088323623
H    3.4582572042  -1.5970702156  -2.6922674689
C    4.7234197322  -0.8256300411  -1.1054450464
H    5.656299839   -1.0295026014  -1.6213208056
C    4.7304488646  -0.2541603523   0.1684927574
H    5.6566439647   0.0007237703   0.6709656333
C    3.5186586803  -0.0130540176   0.8028211518
C   -1.7631108236   1.5888094767   1.2691584753
H   -1.3514437102   2.1289099118   2.124946709
H   -2.8428597643   1.7358903692   1.2572272242
C   -1.1025984493   2.1044436735   0.0233991968
C   -1.6456809103   3.1224471908  -0.7484188947
H   -2.6268893193   3.5126708147  -0.5022871657
C   -0.9050820911   3.6208906416  -1.8209133252
H   -1.3090300737   4.414266148   -2.4416068761
C    0.3604536679   3.0931291583  -2.0801535424
H    0.9740799629   3.461832194   -2.8940949916
C    0.8344958122   2.0627197355  -1.2778530035
H    1.8102829765   1.623285366   -1.4462483971
H    3.4530777375   0.4289655082   1.7895978627
H    1.3340328087   0.9959901995   2.9743549441
```

Pβ$_q$

(G = -2412.746115) (quadruplet)

```
Fe   0.6603695998  -0.1549334967   0.9964785529
O    1.3573403363   0.6834345429   2.4276535516
O   -0.8940632576  -1.5342635864   3.1792279518
N    0.0639512328  -1.4213038386  -0.4709501722
N   -1.3550430399   0.0447015776   1.4373645554
N    0.1616950535   1.5665990085   -0.2642379201
N    2.4211066189  -0.3270480214   0.0378205523
C   -1.3661419079  -1.0952367157  -0.8065332024
H   -1.3325584915  -0.158701411   -1.3672255603
C   -2.0667126662  -2.1463436837  -1.6739236209
H   -1.4918485002  -2.3011628483  -2.5936845099
H   -2.1090305365  -3.0986375873  -1.1330291744
C   -3.4977317728  -1.6843687289  -1.9841323841
H   -3.4611372964  -0.7556204844  -2.5699521113
H   -4.0018513194  -2.4423556776  -2.5942888136
C   -4.2773205077  -1.4345574766  -0.6862070281
H   -4.364065642   -2.376219908   -0.1270233825
```

```
H  -5.2922706656  -1.0866690707  -0.9093774873
C  -3.562577446   -0.3889680872   0.1838790988
H  -4.1047136119  -0.217711654    1.1205105178
H  -3.5226006731   0.5584670025  -0.3664193096
C  -2.1394645271  -0.8645012976   0.4922581749
H  -2.214943903   -1.825143192    1.0074360397
C   0.2427260601  -2.7971774389   0.0836099538
H  -0.01934338    -3.5410597689  -0.673233629
H  -0.3795355435  -2.9188416265   0.9701317374
H   1.2916449325  -2.9180489469   0.3656496548
C  -1.6226594869  -0.3775211094   2.8543895678
H  -2.700534422   -0.5256761119   2.9779858568
H  -1.2830106957   0.4223475503   3.5131653537
H  -1.4056053966  -2.315093751    2.912592752
C   0.9645456091  -1.2614966311  -1.6507854143
H   0.5903124687  -0.4335250809  -2.261768155
H   0.9571268066  -2.1647960719  -2.2677714938
C   2.3504232166  -0.92632574    -1.1763671238
C   3.4865911295  -1.1193652365  -1.952990418
H   3.3968960942  -1.6086689182  -2.9167334224
C   4.7152747684  -0.6671531742  -1.4723859789
H   5.6152217201  -0.8050441011  -2.0633145865
C   4.776230642   -0.0384397514  -0.2262922846
H   5.7131305933   0.3266511695   0.1788776781
C   3.6059303199   0.1105268648   0.505484858
C  -1.6735890274   1.4976295033   1.2846931536
H  -1.2059464878   2.0113802127   2.1310049665
H  -2.7483151355   1.6793587021   1.3311965089
C  -1.0682417823   2.0410757632   0.0213091817
C  -1.6938694968   2.994884055   -0.773008208
H  -2.69161484    3.3346749374  -0.517318336
C  -1.0137001012   3.4855458862  -1.8889240907
H  -1.4803608564   4.2254700071  -2.5317258404
C   0.2698393518   3.0132375118  -2.167388299
H   0.8346014413   3.3729915718  -3.0202748869
C   0.821913673    2.0491050823  -1.3300513444
H   1.8126290159   1.6479614508  -1.2503102346
H   3.5859975985   0.5792037043   1.4821417933
H   0.7095551339   1.0030571206   3.0785135231
```

Iα_d

(G = -2489.108621) (doublet)

```
26  -0.037561000  -0.942509000  -0.007374000
6   -2.782532000  -1.260295000   1.112419000
1   -2.252399000  -1.802150000   1.884851000
7   -2.030549000  -0.720747000   0.133730000
7   -0.326307000   0.684727000  -1.329876000
6   -4.163496000  -1.123316000   1.120772000
7    0.534676000   0.568826000   1.348460000
7    1.921219000  -1.066821000  -0.246583000
8   -0.330271000  -2.060659000  -1.284953000
6   -4.779112000  -0.408399000   0.093347000
6   -3.993917000   0.145588000  -0.914928000
1   -4.431894000   0.712331000  -1.729033000
6   -2.615951000  -0.037447000  -0.873978000
6   -1.675739000   0.449874000  -1.931261000
1   -1.571995000  -0.314632000  -2.706859000
1   -2.043699000   1.360930000  -2.410448000
6    0.671622000   0.717360000  -2.437618000
1    0.725899000  -0.276123000  -2.882531000
1    1.651620000   1.007355000  -2.061182000
```

```
6  -0.352146000   1.963302000  -0.504158000
6   0.714281000   1.874855000   0.584254000
6  -0.408186000   0.687454000   2.496043000
1  -0.597419000  -0.310337000   2.890777000
1  -1.346370000   1.134124000   2.167434000
6   1.860009000   0.108050000   1.860224000
1   1.682491000  -0.648647000   2.630361000
1   2.405186000   0.933223000   2.326910000
6   2.651381000  -0.509494000   0.746721000
6   4.040595000  -0.577349000   0.734696000
1   4.602143000  -0.109441000   1.535604000
6   4.678175000  -1.251312000  -0.304022000
6   3.911154000  -1.838126000  -1.311531000
6   2.531036000  -1.725115000  -1.253764000
1   1.889501000  -2.157704000  -2.012550000
8  -0.014675000  -2.066063000   1.326226000
1  -5.856640000  -0.280430000   0.078705000
1  -4.736383000  -1.570314000   1.925102000
1   5.761090000  -1.317566000  -0.327717000
1   4.367886000  -2.374418000  -2.135238000
1   0.031162000   1.301316000   3.286961000
1   0.352516000   1.426568000  -3.205611000
1  -1.747544000  -4.408090000   0.509586000
6  -0.199422000   3.248170000  -1.338442000
6  -0.220295000   4.487836000  -0.434018000
6   0.881652000   4.399756000   0.626227000
6   0.714953000   3.130211000   1.474188000
1   1.864731000   4.396753000   0.136099000
1   0.854897000   5.275353000   1.284890000
1  -0.089236000   5.383004000  -1.052557000
1  -1.199182000   4.577271000   0.056356000
1   0.753737000   3.229420000  -1.877004000
1  -0.998849000   3.304894000  -2.084744000
1   1.515936000   3.056860000   2.217501000
1  -0.233052000   3.200599000   2.017426000
1   1.694249000   1.803114000   0.101792000
1  -1.334930000   1.981810000  -0.022756000
1  -0.273507000  -2.992247000   1.019264000
8  -0.800567000  -4.401584000   0.283599000
1  -0.776892000  -3.942780000  -0.579784000
```

Iα_q

(G = -2489.125500) (quadruplet)

```
26  -0.026993000  -0.971781000  -0.048710000
6   -2.748461000  -1.322481000   1.115259000
1   -2.199707000  -1.857973000   1.878952000
7   -2.018305000  -0.765048000   0.130398000
7   -0.357321000   0.673413000  -1.340643000
6   -4.131652000  -1.212491000   1.136017000
7    0.495218000   0.570913000   1.355326000
7    1.958634000  -0.987301000  -0.240201000
8   -0.223977000  -2.041967000  -1.273127000
6   -4.770317000  -0.510278000   0.114192000
6   -4.006223000   0.057914000  -0.902713000
1   -4.463569000   0.613623000  -1.713675000
6   -2.624829000  -0.095889000  -0.874711000
6   -1.701358000   0.403910000  -1.938893000
1   -1.580844000  -0.366631000  -2.706674000
1   -2.090419000   1.302165000  -2.425432000
6    0.636012000   0.742660000  -2.450158000
1    0.717490000  -0.245149000  -2.903223000
```

1	1.607922000	1.058680000	-2.073611000
6	-0.416820000	1.944427000	-0.503303000
6	0.645087000	1.879072000	0.593514000
6	-0.459617000	0.658655000	2.493977000
1	-0.626377000	-0.346040000	2.882104000
1	-1.406003000	1.085074000	2.162256000
6	1.824142000	0.147216000	1.882759000
1	1.659560000	-0.632253000	2.633063000
1	2.332399000	0.979960000	2.377617000
6	2.653143000	-0.417379000	0.770887000
6	4.044057000	-0.423109000	0.770656000
1	4.576123000	0.053941000	1.586143000
6	4.720805000	-1.045927000	-0.275089000
6	3.989573000	-1.647623000	-1.300037000
6	2.604969000	-1.601118000	-1.251999000
1	1.986679000	-2.054288000	-2.016771000
8	0.024635000	-2.104777000	1.292778000
1	-5.850286000	-0.404250000	0.109402000
1	-4.687943000	-1.672126000	1.944823000
1	5.805821000	-1.061871000	-0.290048000
1	4.476778000	-2.147468000	-2.129210000
1	-0.043290000	1.277589000	3.293821000
1	0.294071000	1.449126000	-3.211031000
1	-1.466862000	-4.606507000	0.483512000
6	-0.292315000	3.237014000	-1.330924000
6	-0.352096000	4.472470000	-0.422814000
6	0.746827000	4.409797000	0.642439000
6	0.608217000	3.133538000	1.484582000
1	1.731929000	4.433840000	0.156885000
1	0.694656000	5.282303000	1.303673000
1	-0.242465000	5.372663000	-1.038257000
1	-1.335355000	4.533864000	0.063115000
1	0.664920000	3.246043000	-1.862187000
1	-1.087552000	3.275016000	-2.082780000
1	1.406749000	3.078185000	2.232042000
1	-0.343979000	3.177816000	2.023369000
1	1.629261000	1.833990000	0.116300000
1	-1.402350000	1.936041000	-0.027635000
1	-0.140552000	-3.041392000	0.964253000
8	-0.520004000	-4.529001000	0.270629000
1	-0.522650000	-4.187803000	-0.642585000

1	0.586938000	-0.437655000	-2.896935000
1	1.597892000	0.821436000	-2.146143000
6	-0.310152000	1.935940000	-0.572318000
6	0.761475000	1.842726000	0.508048000
6	-0.441001000	0.788243000	2.450777000
1	-0.669602000	-0.183042000	2.888314000
1	-1.356804000	1.252686000	2.087120000
6	1.816055000	0.113757000	1.907670000
1	1.593111000	-0.611331000	2.695764000
1	2.356466000	0.945547000	2.367519000
6	2.629345000	-0.547933000	0.838251000
6	4.018360000	-0.617450000	0.852118000
1	4.567428000	-0.129798000	1.649920000
6	4.671240000	-1.313699000	-0.162151000
6	3.916308000	-1.919006000	-1.166749000
6	2.534209000	-1.806248000	-1.128912000
1	1.901619000	-2.256119000	-1.883615000
8	-0.089283000	-2.181532000	1.361021000
1	-5.860114000	-0.179211000	0.321205000
1	-4.702562000	-1.477994000	2.137079000
1	5.754410000	-1.380119000	-0.169927000
1	4.383098000	-2.470415000	-1.974849000
1	0.008106000	1.421430000	3.220527000
1	0.285342000	1.271549000	-3.264918000
1	-0.772133000	-3.508056000	0.382015000
6	-0.103311000	3.172071000	-1.466414000
6	-0.056414000	4.450294000	-0.617827000
6	1.049964000	4.356694000	0.437027000
6	0.832199000	3.134989000	1.341415000
1	2.027272000	4.285428000	-0.059291000
1	1.070244000	5.260378000	1.056792000
1	0.111039000	5.309733000	-1.276879000
1	-1.025499000	4.607769000	-0.125175000
1	0.842369000	3.082913000	-2.011261000
1	-0.907503000	3.233606000	-2.207293000
1	1.637639000	3.056386000	2.079179000
1	-0.105186000	3.274102000	1.890109000
1	1.731356000	1.697787000	0.021470000
1	-1.284741000	2.030417000	-0.084097000
1	0.797051000	-2.558815000	1.507994000
8	-1.099339000	-3.982212000	-0.425045000
1	-0.303809000	-4.418069000	-0.779457000

IIα_d

(G = -2489.105559) (doublet)

26	-0.092994000	-0.966701000	-0.002316000
6	-2.773001000	-1.216812000	1.250652000
1	-2.225834000	-1.765617000	2.005841000
7	-2.046824000	-0.701017000	0.240816000
7	-0.364527000	0.621708000	-1.341767000
6	-4.149278000	-1.050744000	1.308697000
7	0.521564000	0.583698000	1.329518000
7	1.907422000	-1.128463000	-0.146637000
8	-0.317882000	-2.006190000	-1.278710000
6	-4.785848000	-0.331221000	0.297174000
6	-4.027879000	0.193512000	-0.747660000
1	-4.486110000	0.756526000	-1.553091000
6	-2.653733000	-0.017566000	-0.756027000
6	-1.750904000	0.420642000	-1.868190000
1	-1.711615000	-0.362244000	-2.631621000
1	-2.114927000	1.334124000	-2.345606000
6	0.592615000	0.571621000	-2.484265000

IIα_q

(G = -2489.118829) (quadruplet)

26	-0.172038000	-0.956869000	-0.074123000
6	-2.894952000	-0.804666000	1.132912000
1	-2.458939000	-1.441607000	1.890049000
7	-2.085327000	-0.398217000	0.136033000
7	-0.199186000	0.711776000	-1.344714000
6	-4.227954000	-0.422352000	1.177729000
7	0.607821000	0.454371000	1.355620000
7	1.780932000	-1.330663000	-0.227869000
8	-0.533875000	-1.914691000	-1.351131000
6	-4.733629000	0.393509000	0.166334000
6	-3.890103000	0.802280000	-0.864529000
1	-4.242023000	1.438352000	-1.668929000
6	-2.565600000	0.382112000	-0.858332000
6	-1.577564000	0.700743000	-1.932733000
1	-1.609338000	-0.076452000	-2.702249000
1	-1.791542000	1.659339000	-2.412368000

ANNEX

6	0.784851000	0.580767000	-2.460541000
1	0.665857000	-0.402612000	-2.914041000
1	1.801319000	0.700869000	-2.088627000
6	-0.007924000	1.977932000	-0.514465000
6	1.013766000	1.705828000	0.584646000
6	-0.317852000	0.754851000	2.486911000
1	-0.678144000	-0.181281000	2.916513000
1	-1.166604000	1.339108000	2.133887000
6	1.841978000	-0.187619000	1.898986000
1	1.554942000	-0.901785000	2.678102000
1	2.491127000	0.555254000	2.371031000
6	2.555857000	-0.911747000	0.799087000
6	3.917122000	-1.194422000	0.825984000
1	4.516350000	-0.831156000	1.653491000
6	4.476868000	-1.940442000	-0.208048000
6	3.660338000	-2.384790000	-1.248615000
6	2.312553000	-2.062442000	-1.228635000
1	1.634741000	-2.382444000	-2.009902000
8	-0.359246000	-2.299289000	1.103517000
1	-5.771539000	0.709554000	0.179982000
1	-4.849023000	-0.765384000	1.997142000
1	5.536903000	-2.172417000	-0.202030000
1	4.053746000	-2.971887000	-2.070356000
1	0.205339000	1.307795000	3.271073000
1	0.580499000	1.340078000	-3.219029000
1	-1.702357000	-3.528573000	0.596884000
6	0.380878000	3.211639000	-1.350640000
6	0.569995000	4.439400000	-0.448159000
6	1.628836000	4.160767000	0.622040000
6	1.227529000	2.946866000	1.470647000
1	2.600445000	3.980218000	0.142626000
1	1.751463000	5.030006000	1.277920000
1	0.862444000	5.293414000	-1.069524000
1	-0.381899000	4.702664000	0.032443000
1	1.322454000	3.022057000	-1.875848000
1	-0.387159000	3.404620000	-2.106417000
1	1.993565000	2.735524000	2.223942000
1	0.301154000	3.189944000	2.001084000
1	1.969436000	1.462374000	0.110085000
1	-0.978857000	2.171645000	-0.048384000
1	-0.278503000	-2.052638000	2.043722000
8	-2.445099000	-4.027003000	0.198862000
1	-2.026745000	-4.478266000	-0.552045000

TS(II-III)α_d

d
(G = -2489.096554) (doublet)

26	-0.026834000	-0.953579000	-0.023383000
6	-2.692550000	-1.386162000	1.241362000
1	-2.116230000	-1.877996000	2.013883000
7	-1.996596000	-0.838759000	0.226568000
7	-0.403915000	0.577538000	-1.342042000
6	-4.078369000	-1.322931000	1.285614000
7	0.472012000	0.605918000	1.340155000
7	1.978564000	-0.973908000	-0.166578000
8	-0.182398000	-2.080032000	-1.211785000
6	-4.758079000	-0.674502000	0.254642000
6	-4.031936000	-0.114897000	-0.794828000
1	-4.523824000	0.396586000	-1.614687000
6	-2.646140000	-0.222615000	-0.786833000
6	-1.761542000	0.265126000	-1.892369000

1	-1.647377000	-0.525292000	-2.640501000
1	-2.181426000	1.141198000	-2.393145000
6	0.566220000	0.618867000	-2.474341000
1	0.659836000	-0.386641000	-2.884558000
1	1.539025000	0.966284000	-2.128167000
6	-0.471233000	1.889811000	-0.563660000
6	0.597668000	1.885413000	0.526736000
6	-0.488158000	0.722551000	2.475191000
1	-0.631503000	-0.267151000	2.909059000
1	-1.444463000	1.110987000	2.126460000
6	1.810111000	0.246053000	1.897416000
1	1.661949000	-0.495474000	2.689667000
1	2.288269000	1.117157000	2.354391000
6	2.662192000	-0.347873000	0.817230000
6	4.053064000	-0.321078000	0.829211000
1	4.568774000	0.201452000	1.627271000
6	4.750355000	-0.971306000	-0.185675000
6	4.036460000	-1.629608000	-1.187323000
6	2.649797000	-1.609779000	-1.147623000
1	2.046820000	-2.102954000	-1.899551000
8	0.080735000	-2.308004000	1.336232000
1	-5.840993000	-0.604255000	0.267310000
1	-4.606026000	-1.773858000	2.118190000
1	5.835595000	-0.963527000	-0.195378000
1	4.539231000	-2.150624000	-1.994060000
1	-0.086437000	1.386752000	3.245435000
1	0.198074000	1.285104000	-3.258392000
1	-0.217909000	-3.204527000	0.647888000
6	-0.366726000	3.144378000	-1.448779000
6	-0.437686000	4.418246000	-0.594741000
6	0.664455000	4.415463000	0.469596000
6	0.544318000	3.174494000	1.365055000
1	1.648324000	4.431837000	-0.018765000
1	0.601568000	5.314589000	1.093078000
1	-0.340796000	5.291738000	-1.249486000
1	-1.420277000	4.489193000	-0.108784000
1	0.587238000	3.141828000	-1.986024000
1	-1.166673000	3.139865000	-2.196429000
1	1.343498000	3.162724000	2.113600000
1	-0.408581000	3.228156000	1.901745000
1	1.579089000	1.834155000	0.044434000
1	-1.453958000	1.893175000	-0.082635000
1	0.991273000	-2.506527000	1.621066000
8	-0.586720000	-3.900597000	-0.337602000
1	0.238902000	-4.245260000	-0.731734000

TS(II-III)α_q

(G = -2489.086857) (quadruplet)

26	-0.029901000	-0.948594000	-0.029333000
6	-2.711559000	-1.341737000	1.225383000
1	-2.146315000	-1.845888000	1.998257000
7	-2.003193000	-0.805972000	0.213030000
7	-0.385499000	0.589767000	-1.341428000
6	-4.096198000	-1.253124000	1.268607000
7	0.491005000	0.588484000	1.341925000
7	1.969462000	-1.009183000	-0.177034000
8	-0.218455000	-2.089664000	-1.285621000
6	-4.762905000	-0.588956000	0.239340000
6	-4.024658000	-0.039511000	-0.807038000
1	-4.505390000	0.484364000	-1.625717000
6	-2.641183000	-0.174058000	-0.797470000

6	-1.745023000	0.300192000	-1.899027000
1	-1.639691000	-0.491412000	-2.646979000
1	-2.148084000	1.183522000	-2.400850000
6	0.590117000	0.622405000	-2.469148000
1	0.676228000	-0.384112000	-2.878231000
1	1.564189000	0.962357000	-2.119095000
6	-0.436715000	1.897764000	-0.554619000
6	0.631631000	1.872854000	0.535528000
6	-0.465096000	0.710677000	2.479716000
1	-0.619227000	-0.279868000	2.907740000
1	-1.416866000	1.113394000	2.135027000
6	1.826025000	0.207021000	1.892309000
1	1.670188000	-0.534134000	2.683146000
1	2.318257000	1.070248000	2.349297000
6	2.665278000	-0.396009000	0.806978000
6	4.056396000	-0.389813000	0.815928000
1	4.581390000	0.122276000	1.614707000
6	4.742207000	-1.046578000	-0.202592000
6	4.016498000	-1.690294000	-1.205083000
6	2.630416000	-1.650193000	-1.162057000
1	2.018995000	-2.131244000	-1.915158000
8	0.057002000	-2.288102000	1.335804000
1	-5.844301000	-0.498203000	0.251074000
1	-4.632563000	-1.696627000	2.099638000
1	5.827421000	-1.054788000	-0.214393000
1	4.509547000	-2.215840000	-2.014874000
1	-0.052334000	1.365089000	3.252436000
1	0.230327000	1.290905000	-3.255241000
1	-0.337040000	-3.200262000	0.682648000
6	-0.316584000	3.156004000	-1.432278000
6	-0.371534000	4.425279000	-0.570390000
6	0.729662000	4.401732000	0.494603000
6	0.593685000	3.156692000	1.382615000
1	1.713967000	4.408747000	0.006937000
1	0.677769000	5.297529000	1.123875000
1	-0.262678000	5.301613000	-1.219416000
1	-1.353562000	4.505845000	-0.084814000
1	0.637132000	3.144335000	-1.969899000
1	-1.116801000	3.166204000	-2.179613000
1	1.392309000	3.130483000	2.131343000
1	-0.358825000	3.218549000	1.919096000
1	1.612675000	1.812696000	0.053623000
1	-1.419235000	1.909675000	-0.073457000
1	0.965140000	-2.529271000	1.593020000
8	-0.801352000	-3.903974000	-0.213992000
1	-0.027953000	-4.332576000	-0.634290000

IIIαd

(G = -2489.095952) (doublet)

26	-0.041169000	-0.946383000	-0.021582000
6	-2.716529000	-1.308699000	1.257865000
1	-2.153788000	-1.801245000	2.040072000
7	-2.007200000	-0.788290000	0.237909000
7	-0.384171000	0.570993000	-1.340824000
6	-4.101005000	-1.219337000	1.299018000
7	0.499267000	0.598947000	1.343529000
7	1.966456000	-1.010395000	-0.171706000
8	-0.223042000	-2.088016000	-1.184965000
6	-4.766948000	-0.570769000	0.259181000
6	-4.028260000	-0.037243000	-0.795024000
1	-4.508821000	0.474310000	-1.621553000

6	-2.644741000	-0.171968000	-0.782649000
6	-1.748703000	0.286831000	-1.891198000
1	-1.651886000	-0.510487000	-2.634031000
1	-2.147131000	1.169571000	-2.397654000
6	0.584586000	0.589620000	-2.475000000
1	0.655683000	-0.418537000	-2.882592000
1	1.564887000	0.917682000	-2.131299000
6	-0.425035000	1.888779000	-0.567232000
6	0.644608000	1.871462000	0.522954000
6	-0.451222000	0.738111000	2.483531000
1	-0.608618000	-0.246877000	2.923678000
1	-1.403318000	1.139596000	2.137963000
6	1.833245000	0.215977000	1.893372000
1	1.676417000	-0.517271000	2.691884000
1	2.333937000	1.079184000	2.341683000
6	2.666899000	-0.402221000	0.811457000
6	4.058319000	-0.410976000	0.823731000
1	4.587037000	0.097920000	1.622157000
6	4.739303000	-1.077710000	-0.191302000
6	4.008664000	-1.716385000	-1.193691000
6	2.623160000	-1.661310000	-1.152948000
1	2.008397000	-2.139959000	-1.904737000
8	0.059064000	-2.318148000	1.390769000
1	-5.848354000	-0.479902000	0.268915000
1	-4.638104000	-1.650081000	2.136248000
1	5.824415000	-1.097448000	-0.200804000
1	4.497845000	-2.249225000	-2.001087000
1	-0.035640000	1.399478000	3.248966000
1	0.228667000	1.261777000	-3.259551000
1	-0.282493000	-3.119901000	0.840168000
6	-0.298530000	3.136497000	-1.459146000
6	-0.347293000	4.416257000	-0.612548000
6	0.754336000	4.400601000	0.452092000
6	0.613341000	3.166167000	1.353527000
1	1.738347000	4.397855000	-0.036280000
1	0.706542000	5.303957000	1.070836000
1	-0.235127000	5.284154000	-1.272302000
1	-1.328738000	4.506965000	-0.127537000
1	0.655223000	3.113965000	-1.996439000
1	-1.098444000	3.142666000	-2.206845000
1	1.412216000	3.144828000	2.102237000
1	-0.338417000	3.238726000	1.890195000
1	1.624421000	1.801996000	0.039530000
1	-1.406699000	1.912219000	-0.084733000
1	0.965276000	-2.561460000	1.656290000
8	-0.855765000	-3.858609000	-0.401919000
1	-0.075087000	-4.271218000	-0.821607000

IIIαq

(G = -2489.090451) (quadruplet)

26	0.109138000	-1.008203000	-0.015922000
6	-2.698261000	-1.671317000	1.239178000
1	-2.090259000	-2.125078000	2.011630000
7	-2.035813000	-1.063857000	0.236796000
7	-0.581152000	0.582452000	-1.368294000
6	-4.085787000	-1.718187000	1.277264000
7	0.428585000	0.651958000	1.301305000
7	2.171936000	-0.784472000	-0.155490000
8	0.069587000	-2.122090000	-1.219143000
6	-4.806058000	-1.111224000	0.247886000
6	-4.115548000	-0.481573000	-0.784888000

631

ANNEX

1	-4.638928000	0.007499000	-1.599475000
6	-2.722733000	-0.483156000	-0.765718000
6	-1.897759000	0.115064000	-1.874226000
1	-1.711057000	-0.652098000	-2.633004000
1	-2.439521000	0.931564000	-2.362420000
6	0.360751000	0.716748000	-2.513112000
1	0.549838000	-0.276104000	-2.923741000
1	1.303174000	1.149971000	-2.177333000
6	-0.739611000	1.853838000	-0.557820000
6	0.373288000	1.940295000	0.491232000
6	-0.540472000	0.628277000	2.436975000
1	-0.563554000	-0.380029000	2.851528000
1	-1.536851000	0.901374000	2.092374000
6	1.804634000	0.467206000	1.865432000
1	1.739960000	-0.276649000	2.666818000
1	2.164433000	1.396402000	2.315333000
6	2.744722000	-0.032778000	0.809587000
6	4.116401000	0.200535000	0.822836000
1	4.549205000	0.816148000	1.603688000
6	4.904917000	-0.366173000	-0.176811000
6	4.302997000	-1.144362000	-1.167544000
6	2.928804000	-1.330320000	-1.127616000
1	2.404021000	-1.916394000	-1.872842000
8	0.220955000	-2.505576000	1.501324000
1	-5.891495000	-1.123696000	0.251708000
1	-4.584101000	-2.216603000	2.101147000
1	5.976921000	-0.196677000	-0.186331000
1	4.883105000	-1.597777000	-1.963148000
1	-0.224954000	1.322815000	3.220394000
1	-0.069193000	1.347157000	-3.297270000
1	0.419851000	-3.280417000	0.893426000
6	-0.795321000	3.133885000	-1.413126000
6	-0.953958000	4.381733000	-0.533357000
6	0.183569000	4.466946000	0.488372000
6	0.222510000	3.203936000	1.359091000
1	1.141994000	4.589436000	-0.034406000
1	0.057649000	5.343205000	1.134651000
1	-0.966643000	5.272410000	-1.172179000
1	-1.918367000	4.349704000	-0.008252000
1	0.130927000	3.233039000	-1.989319000
1	-1.620690000	3.062611000	-2.129454000
1	1.046777000	3.263519000	2.077587000
1	-0.709024000	3.148924000	1.932722000
1	1.334078000	1.995941000	-0.030383000
1	-1.696791000	1.755517000	-0.036059000
1	0.987305000	-2.410918000	2.094980000
8	0.497595000	-4.077163000	-0.582948000
1	1.422104000	-3.901679000	-0.854284000

6	-4.030776000	-0.051221000	-0.786576000
1	-4.513367000	0.457087000	-1.613944000
6	-2.646742000	-0.181730000	-0.774702000
6	-1.753962000	0.277365000	-1.886230000
1	-1.658744000	-0.520609000	-2.628591000
1	-2.155874000	1.158585000	-2.392735000
6	0.577250000	0.579898000	-2.477592000
1	0.647915000	-0.429359000	-2.882869000
1	1.558536000	0.908509000	-2.137139000
6	-0.428596000	1.884822000	-0.572775000
6	0.640998000	1.870962000	0.517534000
6	-0.456208000	0.744380000	2.481206000
1	-0.613430000	-0.238871000	2.925250000
1	-1.408338000	1.143868000	2.133463000
6	1.829048000	0.221664000	1.895778000
1	1.671737000	-0.510753000	2.694964000
1	2.326903000	1.086573000	2.343896000
6	2.665590000	-0.396769000	0.816340000
6	4.056967000	-0.404066000	0.830735000
1	4.584237000	0.106674000	1.628948000
6	4.739843000	-1.072216000	-0.182153000
6	4.010969000	-1.713839000	-1.183930000
6	2.625279000	-1.659860000	-1.145029000
1	2.011999000	-2.141582000	-1.896085000
8	0.060931000	-2.323570000	1.396139000
1	-5.849078000	-0.496908000	0.279161000
1	-4.634550000	-1.660161000	2.148012000
1	5.824990000	-1.091033000	-0.190289000
1	4.501691000	-2.248171000	-1.989416000
1	-0.041587000	1.409070000	3.244275000
1	0.220045000	1.249693000	-3.263627000
1	-0.266191000	-3.117658000	0.832453000
6	-0.301915000	3.129643000	-1.468586000
6	-0.349644000	4.412448000	-0.626517000
6	0.752073000	4.399708000	0.438100000
6	0.610323000	3.168459000	1.343705000
1	1.736054000	4.394598000	-0.050337000
1	0.704979000	5.305236000	1.053724000
1	-0.237007000	5.278066000	-1.289197000
1	-1.330947000	4.505503000	-0.141631000
1	0.651509000	3.104919000	-2.006421000
1	-1.102212000	3.133569000	-2.215929000
1	1.409010000	3.149515000	2.092687000
1	-0.341518000	3.243404000	1.879932000
1	1.620749000	1.799293000	0.034288000
1	-1.410181000	1.910691000	-0.090093000
1	0.966667000	-2.562022000	1.667367000
8	-0.820871000	-3.805708000	-0.463100000
1	-0.042145000	-4.232258000	-0.871547000

TS(iII-IV)αd
(G = -2489.095652) (doublet)

26	-0.041334000	-0.944839000	-0.012880000
6	-2.714360000	-1.314532000	1.268028000
1	-2.149738000	-1.804136000	2.050720000
7	-2.006651000	-0.793860000	0.246971000
7	-0.388184000	0.564025000	-1.340712000
6	-4.099021000	-1.229355000	1.309797000
7	0.495207000	0.601219000	1.342405000
7	1.966567000	-1.006971000	-0.166521000
8	-0.219345000	-2.091091000	-1.181348000
6	-4.767406000	-0.584659000	0.269043000

IVαd
(G = -2489.120592) (doublet)

26	-0.059556000	-0.924440000	0.039796000
6	-2.762680000	-1.205671000	1.315913000
1	-2.223367000	-1.690462000	2.119606000
7	-2.024296000	-0.742797000	0.287575000
7	-0.358161000	0.536466000	-1.338757000
6	-4.143750000	-1.075536000	1.346505000
7	0.521836000	0.578809000	1.352041000
7	1.934960000	-1.071364000	-0.163399000
8	-0.311445000	-2.220615000	-1.196116000

ANNEX

6	-4.784414000	-0.438300000	0.283444000		8	-0.272722000	-2.270402000	-1.245994000
6	-4.021461000	0.042348000	-0.777768000		6	-4.854987000	-0.338566000	0.278105000
1	-4.480231000	0.547517000	-1.620666000		6	-4.080904000	0.178410000	-0.756783000
6	-2.641343000	-0.133936000	-0.750534000		1	-4.526659000	0.749790000	-1.564011000
6	-1.735175000	0.284809000	-1.869944000		6	-2.704725000	-0.042662000	-0.752047000
1	-1.668119000	-0.524054000	-2.602928000		6	-1.811611000	0.435080000	-1.867319000
1	-2.118100000	1.169946000	-2.385682000		1	-1.764299000	-0.339080000	-2.640533000
6	0.593494000	0.502121000	-2.483318000		1	-2.226349000	1.335201000	-2.334196000
1	0.628689000	-0.516260000	-2.871340000		6	0.514670000	0.622415000	-2.514533000
1	1.589013000	0.802637000	-2.158137000		1	0.519920000	-0.391852000	-2.918942000
6	-0.349593000	1.868459000	-0.593027000		1	1.522159000	0.872952000	-2.180045000
6	0.716326000	1.829176000	0.502793000		6	-0.359909000	1.930977000	-0.554080000
6	-0.414397000	0.780869000	2.492061000		6	0.749802000	1.802744000	0.500190000
1	-0.605182000	-0.186401000	2.957537000		6	-0.379876000	0.711860000	2.471102000
1	-1.354447000	1.204103000	2.139119000		1	-0.592640000	-0.266238000	2.902653000
6	1.843119000	0.153048000	1.903254000		1	-1.309349000	1.164895000	2.127738000
1	1.659071000	-0.576061000	2.699664000		6	1.879728000	0.082547000	1.874462000
1	2.370460000	0.999425000	2.353376000		1	1.680886000	-0.666823000	2.648017000
6	2.658276000	-0.492820000	0.821701000		1	2.402112000	0.915725000	2.352802000
6	4.048503000	-0.551263000	0.841162000		6	2.712971000	-0.541892000	0.792914000
1	4.592696000	-0.063387000	1.642473000		6	4.103839000	-0.524922000	0.778372000
6	4.709269000	-1.241514000	-0.171834000		1	4.643809000	-0.000494000	1.558950000
6	3.958486000	-1.851606000	-1.176932000		6	4.773936000	-1.185786000	-0.250115000
6	2.575234000	-1.744824000	-1.140038000		6	4.038334000	-1.840794000	-1.238998000
1	1.949779000	-2.204543000	-1.894634000		6	2.652575000	-1.814257000	-1.167087000
8	-0.012705000	-2.337798000	1.457173000		1	2.028108000	-2.304205000	-1.904828000
1	-5.862585000	-0.313551000	0.282782000		8	-0.178156000	-2.518494000	1.719433000
1	-4.698364000	-1.463956000	2.193139000		1	-5.928373000	-0.177524000	0.293364000
1	5.792982000	-1.301606000	-0.177108000		1	-4.789085000	-1.474034000	2.126172000
1	4.430567000	-2.401774000	-1.983025000		1	5.858909000	-1.183938000	-0.282696000
1	0.024876000	1.446666000	3.240229000		1	4.524812000	-2.361554000	-2.055889000
1	0.255665000	1.166737000	-3.282949000		1	0.070270000	1.344521000	3.241456000
1	-0.458636000	-3.079252000	0.972178000		1	0.218005000	1.313999000	-3.310091000
6	-0.174970000	3.095656000	-1.504166000		1	-0.543143000	-3.265847000	1.207018000
6	-0.170803000	4.392158000	-0.682634000		6	-0.186643000	3.205906000	-1.401540000
6	0.929389000	4.350815000	0.382847000		6	-0.095673000	4.459162000	-0.522717000
6	0.738674000	3.140143000	1.307239000		6	1.052144000	4.322869000	0.481464000
1	1.912251000	4.297658000	-0.105169000		6	0.856625000	3.077234000	1.357699000
1	0.920139000	5.267127000	0.984254000		1	2.007195000	4.256299000	-0.057515000
1	-0.023511000	5.243628000	-1.356915000		1	1.109536000	5.208016000	1.125580000
1	-1.147553000	4.531653000	-0.199394000		1	0.051034000	5.339132000	-1.159821000
1	0.775808000	3.025440000	-2.043371000		1	-1.041344000	4.608477000	0.016467000
1	-0.975560000	3.119226000	-2.251333000		1	0.732017000	3.131447000	-1.994352000
1	1.536529000	3.102157000	2.056612000		1	-1.022028000	3.288651000	-2.105930000
1	-0.208822000	3.262066000	1.843154000		1	1.683559000	2.979807000	2.069266000
1	1.692766000	1.709584000	0.022324000		1	-0.061847000	3.209221000	1.939748000
1	-1.329890000	1.940903000	-0.111450000		1	1.701726000	1.665573000	-0.022994000
1	0.874679000	-2.677996000	1.676141000		1	-1.318111000	2.003597000	-0.028987000
8	-1.128881000	-3.322211000	-0.684297000		1	0.708647000	-2.809490000	1.996883000
1	-0.632389000	-4.089342000	-1.029824000		8	-1.238332000	-3.285935000	-0.876033000
					1	-0.677535000	-4.085765000	-0.901486000

IVα_q
(G = -2489.118694) (quadruplet)

26	-0.027004000	-1.008510000	0.023480000
6	-2.852270000	-1.229057000	1.243755000
1	-2.323025000	-1.773529000	2.015195000
7	-2.103833000	-0.732516000	0.238800000
7	-0.434369000	0.666605000	-1.373554000
6	-4.228642000	-1.057143000	1.296833000
7	0.557540000	0.529831000	1.327448000
7	2.009314000	-1.177028000	-0.170804000

Iβ_d
(G = -2489.104099) (doublet)

26	0.552741000	-0.245613000	-0.669553000
8	1.237291000	-1.882569000	-1.253638000
8	0.880018000	0.507673000	-2.103518000
7	-0.159578000	1.502619000	0.174537000
7	-1.391317000	-0.648371000	-1.206556000
7	0.043026000	-1.351823000	0.988446000
7	2.250848000	0.388926000	0.151377000

ANNEX

6	-1.623350000	1.253719000	0.458888000	7	2.221420000	0.481329000	-0.032367000
1	-1.649435000	0.577633000	1.316863000	6	-1.650121000	1.275518000	-0.156690000
6	-2.408952000	2.523723000	0.830716000	1	-1.646838000	1.018650000	0.904417000
1	-1.960166000	2.978117000	1.720556000	6	-2.493445000	2.551753000	-0.323997000
1	-2.346595000	3.254153000	0.017444000	1	-2.051839000	3.360672000	0.268059000
6	-3.887708000	2.189343000	1.075158000	1	-2.494173000	2.868206000	-1.372157000
1	-3.980731000	1.526784000	1.946249000	6	-3.943905000	2.289925000	0.109235000
1	-4.429506000	3.111240000	1.314566000	1	-3.975858000	2.061974000	1.183111000
6	-4.493797000	1.507605000	-0.155659000	1	-4.533285000	3.201173000	-0.042703000
1	-4.464942000	2.197196000	-1.010154000	6	-4.545537000	1.124557000	-0.683096000
1	-5.545863000	1.256593000	0.019294000	1	-4.605569000	1.392280000	-1.746516000
6	-3.720535000	0.224842000	-0.496584000	1	-5.567629000	0.917481000	-0.346607000
1	-4.157555000	-0.269816000	-1.369913000	6	-3.700839000	-0.148618000	-0.515309000
1	-3.803377000	-0.461082000	0.354195000	1	-4.125323000	-0.970396000	-1.101021000
6	-2.242123000	0.552145000	-0.759824000	1	-3.721574000	-0.439891000	0.540675000
1	-2.191125000	1.237251000	-1.609462000	6	-2.252088000	0.117477000	-0.956299000
6	0.068044000	2.679291000	-0.735364000	1	-2.263788000	0.395239000	-2.012323000
1	-0.150594000	3.603289000	-0.196233000	6	-0.018833000	2.110204000	-1.866619000
1	-0.571103000	2.602611000	-1.613637000	1	-0.370962000	3.141337000	-1.790617000
1	1.111230000	2.697959000	-1.049419000	1	-0.566702000	1.586822000	-2.647693000
6	-1.556450000	-0.841565000	-2.678198000	1	1.040562000	2.119771000	-2.121398000
1	-2.595973000	-1.107117000	-2.894471000	6	-1.485304000	-1.878267000	-2.192015000
1	-0.900338000	-1.647229000	-3.005805000	1	-2.511412000	-2.249559000	-2.275977000
1	-1.297778000	0.079978000	-3.196976000	1	-0.792000000	-2.719408000	-2.193964000
6	0.669336000	1.712988000	1.405497000	1	-1.262430000	-1.216243000	-3.027387000
1	0.309132000	1.042795000	2.190668000	6	0.590919000	2.188768000	0.469418000
1	0.562279000	2.737082000	1.771366000	1	0.188286000	1.985318000	1.465379000
6	2.099789000	1.394508000	1.058334000	1	0.500878000	3.264033000	0.294872000
6	3.217183000	2.045791000	1.595780000	6	2.025039000	1.749891000	0.397709000
1	3.074597000	2.850477000	2.309163000	6	3.100202000	2.544505000	0.781135000
6	4.505873000	1.642112000	1.189511000	1	2.917238000	3.559344000	1.116665000
1	5.383176000	2.138551000	1.593068000	6	4.387900000	2.016737000	0.721744000
6	4.646124000	0.607474000	0.251298000	1	5.239110000	2.621658000	1.016925000
1	5.621694000	0.277157000	-0.088443000	6	4.572160000	0.709392000	0.269378000
6	3.490750000	-0.004605000	-0.257207000	1	5.558845000	0.265976000	0.200929000
6	-1.739832000	-1.941720000	-0.537268000	6	3.463999000	-0.034192000	-0.107534000
1	-1.355253000	-2.742918000	-1.173413000	6	-1.633701000	-2.072391000	0.214688000
1	-2.821144000	-2.071563000	-0.479199000	1	-1.126671000	-3.010171000	-0.029033000
6	-1.092038000	-2.073321000	0.805639000	1	-2.701872000	-2.284245000	0.266649000
6	-1.554483000	-2.969945000	1.777500000	6	-1.088111000	-1.571319000	1.515921000
1	-2.474072000	-3.518088000	1.601952000	6	-1.617690000	-1.944530000	2.747412000
6	-0.808046000	-3.149712000	2.951595000	1	-2.517206000	-2.549280000	2.782787000
1	-1.147349000	-3.841562000	3.716440000	6	-0.968010000	-1.537507000	3.910242000
6	0.385608000	-2.432695000	3.117025000	1	-1.361015000	-1.815156000	4.883020000
1	1.002868000	-2.550810000	4.000566000	6	0.195885000	-0.776851000	3.804450000
6	0.781004000	-1.542560000	2.116588000	1	0.742413000	-0.449625000	4.681602000
1	1.699819000	-0.976569000	2.210900000	6	0.657692000	-0.428823000	2.541878000
1	3.524256000	-0.808590000	-0.984833000	1	1.561373000	0.157224000	2.427625000
1	1.464081000	-1.784438000	-2.211059000	1	3.546718000	-1.048165000	-0.477930000
8	1.862544000	-1.557995000	-3.962940000	1	1.689775000	-2.458976000	-1.235863000
1	2.812657000	-1.350969000	-3.930331000	8	2.462463000	-2.922033000	-2.680997000
1	1.447787000	-0.692832000	-4.135980000	1	3.403474000	-2.796384000	-2.465828000
				1	2.230662000	-2.111061000	-3.168043000

Iβq
(G = -2489.121663) (quadruplet)

26	0.595360000	-0.522197000	-0.599594000
8	1.273875000	-2.137122000	-0.382532000
8	0.962335000	-0.414453000	-2.182654000
7	-0.196471000	1.425121000	-0.547790000
7	-1.339602000	-1.124177000	-0.908977000
7	0.019056000	-0.803700000	1.416472000

IIβd
(G = -2489.094766) (doublet)

26	0.561295000	-0.261017000	0.781047000
8	1.340632000	0.658370000	2.183597000
8	0.817651000	-1.779233000	1.385303000
7	-0.146525000	-1.116282000	-0.970748000
7	-1.406404000	-0.217395000	1.415009000

ANNEX

7	0.016057000	1.645225000	0.069692000
7	2.251527000	-0.183986000	-0.253053000
6	-1.603939000	-0.718883000	-1.068230000
1	-1.611459000	0.338603000	-1.337930000
6	-2.391954000	-1.481938000	-2.147694000
1	-1.919189000	-1.317141000	-3.122212000
1	-2.365457000	-2.556967000	-1.942825000
6	-3.858850000	-1.029224000	-2.167739000
1	-3.920887000	0.027706000	-2.460010000
1	-4.400649000	-1.604223000	-2.927167000
6	-4.498188000	-1.219955000	-0.788859000
1	-4.516699000	-2.288002000	-0.533692000
1	-5.537618000	-0.873151000	-0.795833000
6	-3.720656000	-0.440097000	0.282544000
1	-4.175310000	-0.584348000	1.268105000
1	-3.782810000	0.626472000	0.038143000
6	-2.249659000	-0.888866000	0.313948000
1	-2.225145000	-1.949685000	0.574440000
6	0.045631000	-2.604948000	-0.984785000
1	-0.243665000	-3.000475000	-1.960503000
1	-0.551238000	-3.073863000	-0.204344000
1	1.098166000	-2.829350000	-0.816098000
6	-1.615205000	-0.956829000	2.697759000
1	-2.655598000	-0.847909000	3.019111000
1	-0.958734000	-0.542379000	3.464296000
1	-1.381562000	-2.009756000	2.550890000
6	0.698990000	-0.555462000	-2.072031000
1	0.314587000	0.427262000	-2.359868000
1	0.647600000	-1.195663000	-2.956439000
6	2.115089000	-0.428777000	-1.579797000
6	3.228302000	-0.492370000	-2.409991000
1	3.094265000	-0.695426000	-3.466751000
6	4.494446000	-0.296061000	-1.860854000
1	5.375308000	-0.344101000	-2.492894000
6	4.617295000	-0.043173000	-0.494393000
1	5.584388000	0.112669000	-0.030185000
6	3.470412000	0.002841000	0.285478000
6	-1.747648000	1.218755000	1.653674000
1	-1.337299000	1.494272000	2.631419000
1	-2.826412000	1.358983000	1.724281000
6	-1.129016000	2.106838000	0.620497000
6	-1.636727000	3.366938000	0.318958000
1	-2.567724000	3.687860000	0.773145000
6	-0.926168000	4.191301000	-0.548806000
1	-1.301933000	5.178137000	-0.799123000
6	0.277697000	3.731292000	-1.081199000
1	0.875479000	4.342222000	-1.747865000
6	0.715197000	2.456252000	-0.751210000
1	1.648633000	2.079472000	-1.148387000
1	3.504395000	0.190102000	1.350943000
1	0.701104000	0.926366000	2.866170000
8	2.232169000	-1.645687000	3.166279000
1	2.034813000	-0.691167000	2.951890000
1	2.970473000	-1.866405000	2.570554000

IIβ_q

(G = -2489.117368) (quadruplet)

26	0.584066000	0.628354000	0.495602000
8	1.264987000	2.230560000	0.061001000
8	0.835979000	0.891144000	2.083631000
7	-0.116919000	-1.303494000	0.846254000

7	-1.390065000	1.197417000	0.569737000
7	0.133716000	0.452446000	-1.553873000
7	2.281852000	-0.385965000	0.259119000
6	-1.556269000	-1.319429000	0.370850000
1	-1.508326000	-1.301886000	-0.719326000
6	-2.342623000	-2.574022000	0.790195000
1	-1.837713000	-3.465948000	0.404340000
1	-2.368633000	-2.652003000	1.882112000
6	-3.785505000	-2.496423000	0.270156000
1	-3.787430000	-2.513532000	-0.827949000
1	-4.333054000	-3.384110000	0.606108000
6	-4.473428000	-1.220449000	0.766199000
1	-4.559458000	-1.247033000	1.860603000
1	-5.491247000	-1.152594000	0.366113000
6	-3.687677000	0.029305000	0.336292000
1	-4.175818000	0.935247000	0.709165000
1	-3.683645000	0.074081000	-0.758502000
6	-2.246768000	-0.048596000	0.867635000
1	-2.290222000	-0.081571000	1.958282000
6	0.024019000	-1.671227000	2.292651000
1	-0.254392000	-2.718242000	2.427097000
1	-0.605180000	-1.035666000	2.912017000
1	1.064223000	-1.544915000	2.591096000
6	-1.638729000	2.216609000	1.635622000
1	-2.683025000	2.539955000	1.580959000
1	-0.981708000	3.071960000	1.483013000
1	-1.441309000	1.771593000	2.609842000
6	0.753298000	-2.232057000	0.054003000
1	0.407531000	-2.252175000	-0.983378000
1	0.677174000	-3.249739000	0.444319000
6	2.164087000	-1.726894000	0.115328000
6	3.292510000	-2.528870000	-0.008454000
1	3.173678000	-3.601116000	-0.117186000
6	4.551773000	-1.932270000	0.015076000
1	5.444556000	-2.541917000	-0.077925000
6	4.653394000	-0.549020000	0.167887000
1	5.614645000	-0.049088000	0.194907000
6	3.493202000	0.201420000	0.292726000
6	-1.661395000	1.840228000	-0.756196000
1	-1.216909000	2.839136000	-0.716733000
1	-2.733379000	1.969759000	-0.907659000
6	-1.017025000	1.087086000	-1.877468000
6	-1.495511000	1.125119000	-3.182453000
1	-2.430183000	1.632309000	-3.394780000
6	-0.748927000	0.519961000	-4.190801000
1	-1.099623000	0.537085000	-5.217571000
6	0.457584000	-0.097898000	-3.862874000
1	1.078686000	-0.567593000	-4.616878000
6	0.865727000	-0.114073000	-2.536381000
1	1.799210000	-0.583821000	-2.252283000
1	3.506192000	1.276738000	0.417168000
1	1.335611000	2.348214000	-0.905252000
8	1.147634000	4.407436000	1.864412000
1	1.223673000	3.694913000	1.195779000
1	1.011044000	3.907802000	2.685851000

TS_{(II-III)}β_d

(G = -2489.089220) (doublet)

26	0.545389000	-0.175066000	0.804330000
8	1.336412000	0.948977000	2.159242000
8	0.844831000	-1.515282000	1.699816000

ANNEX

7	-0.149980000	-1.289174000	-0.762242000
7	-1.422941000	0.007589000	1.405920000
7	0.060027000	1.629650000	-0.164907000
7	2.249349000	-0.264480000	-0.209492000
6	-1.594821000	-0.879350000	-0.961944000
1	-1.559765000	0.117474000	-1.407493000
6	-2.385983000	-1.793437000	-1.913644000
1	-1.889128000	-1.821879000	-2.889521000
1	-2.405753000	-2.815215000	-1.520513000
6	-3.833060000	-1.300085000	-2.054070000
1	-3.845680000	-0.309239000	-2.527894000
1	-4.381534000	-1.979208000	-2.716556000
6	-4.512328000	-1.221731000	-0.682793000
1	-4.587471000	-2.227597000	-0.248223000
1	-5.534263000	-0.838354000	-0.781375000
6	-3.724011000	-0.302082000	0.262170000
1	-4.204442000	-0.258573000	1.245281000
1	-3.734032000	0.708691000	-0.161350000
6	-2.275496000	-0.796266000	0.409729000
1	-2.304510000	-1.801638000	0.836259000
6	0.002570000	-2.758666000	-0.505299000
1	-0.300546000	-3.317933000	-1.392758000
1	-0.599120000	-3.061296000	0.349814000
1	1.050166000	-2.973270000	-0.297724000
6	-1.656060000	-0.528763000	2.781838000
1	-2.697141000	-0.355991000	3.072851000
1	-0.996460000	-0.015694000	3.482881000
1	-1.440969000	-1.595796000	2.794536000
6	0.711094000	-0.953374000	-1.941539000
1	0.334109000	-0.041370000	-2.413208000
1	0.664059000	-1.749739000	-2.688377000
6	2.122773000	-0.736510000	-1.473418000
6	3.237835000	-0.932034000	-2.280889000
1	3.107820000	-1.317885000	-3.285970000
6	4.499842000	-0.622675000	-1.777287000
1	5.382286000	-0.766921000	-2.392280000
6	4.615823000	-0.132958000	-0.476132000
1	5.579465000	0.116679000	-0.047125000
6	3.466882000	0.028744000	0.285524000
6	-1.734521000	1.469344000	1.432489000
1	-1.335048000	1.872495000	2.369164000
1	-2.810277000	1.643570000	1.464719000
6	-1.080483000	2.190824000	0.296042000
6	-1.554155000	3.406011000	-0.189492000
1	-2.482012000	3.811862000	0.198319000
6	-0.815860000	4.080044000	-1.158289000
1	-1.164852000	5.028505000	-1.553704000
6	0.380462000	3.520221000	-1.605252000
1	0.997150000	4.013163000	-2.348075000
6	0.784189000	2.297632000	-1.087720000
1	1.709456000	1.842620000	-1.416322000
1	3.500978000	0.397254000	1.302765000
1	0.704528000	1.445853000	2.708424000
8	1.998353000	-1.025110000	3.339339000
1	1.746663000	0.069991000	2.853663000
1	2.796099000	-1.331940000	2.864950000

TS(II-III)βq
(G = -2489.080456) (quadruplet)

26	0.530164000	-0.135606000	0.784377000
8	1.343431000	0.998307000	2.110516000

8	0.861048000	-1.499722000	1.744044000
7	-0.163693000	-1.294633000	-0.739496000
7	-1.423793000	0.070855000	1.393514000
7	0.087294000	1.641091000	-0.205376000
7	2.241928000	-0.307891000	-0.208324000
6	-1.612508000	-0.898846000	-0.938697000
1	-1.587593000	0.086047000	-1.411507000
6	-2.404580000	-1.844904000	-1.857870000
1	-1.918591000	-1.891601000	-2.838514000
1	-2.406377000	-2.856758000	-1.439567000
6	-3.860052000	-1.376089000	-1.993139000
1	-3.894070000	-0.398741000	-2.493370000
1	-4.406215000	-2.081152000	-2.629895000
6	-4.522427000	-1.270830000	-0.615557000
1	-4.575537000	-2.265031000	-0.151963000
1	-5.551421000	-0.905928000	-0.710516000
6	-3.735932000	-0.311692000	0.290599000
1	-4.206259000	-0.240275000	1.276874000
1	-3.764069000	0.683406000	-0.167651000
6	-2.278963000	-0.780685000	0.438011000
1	-2.287932000	-1.770345000	0.900815000
6	0.000421000	-2.757351000	-0.450014000
1	-0.292827000	-3.332937000	-1.330529000
1	-0.604036000	-3.050452000	0.405565000
1	1.047916000	-2.960961000	-0.232235000
6	-1.643318000	-0.404634000	2.793704000
1	-2.682558000	-0.225822000	3.087732000
1	-0.979415000	0.143749000	3.463205000
1	-1.420757000	-1.469009000	2.850541000
6	0.693048000	-0.981547000	-1.930519000
1	0.325021000	-0.069032000	-2.407877000
1	0.628681000	-1.785215000	-2.668139000
6	2.110108000	-0.785877000	-1.468307000
6	3.223054000	-1.015884000	-2.269393000
1	3.088113000	-1.404690000	-3.272693000
6	4.489958000	-0.738621000	-1.759268000
1	5.371988000	-0.909051000	-2.368131000
6	4.611492000	-0.249641000	-0.458221000
1	5.579645000	-0.028897000	-0.023413000
6	3.463149000	-0.051827000	0.296227000
6	-1.746456000	1.531250000	1.353532000
1	-1.382213000	1.974627000	2.286052000
1	-2.823484000	1.698012000	1.345018000
6	-1.063827000	2.215721000	0.210991000
6	-1.521756000	3.416908000	-0.321845000
1	-2.458445000	3.834988000	0.030187000
6	-0.756187000	4.062661000	-1.288640000
1	-1.092343000	5.000440000	-1.719108000
6	0.450775000	3.489449000	-1.688068000
1	1.087751000	3.961721000	-2.427147000
6	0.838024000	2.281227000	-1.126966000
1	1.769786000	1.814362000	-1.418586000
1	3.500647000	0.319586000	1.312379000
1	0.742343000	1.592790000	2.592168000
8	1.960248000	-0.857557000	3.497019000
1	1.704969000	0.171218000	2.887940000
1	2.788910000	-1.176508000	3.084331000

IIIβd
(G = -2489.091067) (doublet)

26	0.534531000	-0.176848000	0.799993000

ANNEX

8	1.367034000	0.962001000	2.212280000
8	0.800689000	-1.518495000	1.693611000
7	-0.156031000	-1.262439000	-0.772495000
7	-1.441944000	0.014537000	1.393183000
7	0.078575000	1.655650000	-0.131784000
7	2.249411000	-0.276870000	-0.206244000
6	-1.604818000	-0.863332000	-0.969460000
1	-1.578785000	0.140011000	-1.401922000
6	-2.384407000	-1.774231000	-1.934022000
1	-1.888447000	-1.782037000	-2.910711000
1	-2.389687000	-2.801554000	-1.555528000
6	-3.839163000	-1.302198000	-2.066500000
1	-3.868695000	-0.304813000	-2.525694000
1	-4.376792000	-1.980635000	-2.738531000
6	-4.516998000	-1.254839000	-0.693200000
1	-4.571623000	-2.267462000	-0.271312000
1	-5.546275000	-0.889698000	-0.784577000
6	-3.742736000	-0.331106000	0.258919000
1	-4.222630000	-0.301362000	1.242810000
1	-3.771546000	0.681723000	-0.158569000
6	-2.285125000	-0.800428000	0.402349000
1	-2.296034000	-1.807896000	0.824885000
6	0.009161000	-2.735973000	-0.545977000
1	-0.285988000	-3.278678000	-1.446128000
1	-0.592056000	-3.061003000	0.300954000
1	1.057754000	-2.945520000	-0.339320000
6	-1.673107000	-0.508676000	2.773725000
1	-2.711182000	-0.327544000	3.070971000
1	-1.005387000	0.006110000	3.465846000
1	-1.464254000	-1.576845000	2.794938000
6	0.699247000	-0.898913000	-1.948717000
1	0.330738000	0.031708000	-2.389743000
1	0.636968000	-1.671049000	-2.719395000
6	2.114776000	-0.714343000	-1.481501000
6	3.223345000	-0.911872000	-2.297363000
1	3.082893000	-1.270627000	-3.311041000
6	4.492493000	-0.641613000	-1.789781000
1	5.370882000	-0.788369000	-2.409979000
6	4.619606000	-0.187954000	-0.476819000
1	5.588648000	0.030397000	-0.042859000
6	3.475011000	-0.021889000	0.290764000
6	-1.768053000	1.473749000	1.406697000
1	-1.408371000	1.878851000	2.358042000
1	-2.845179000	1.640227000	1.398349000
6	-1.077679000	2.207570000	0.299511000
6	-1.538727000	3.429071000	-0.183639000
1	-2.480322000	3.826758000	0.178898000
6	-0.770381000	4.120169000	-1.116011000
1	-1.108710000	5.073975000	-1.507973000
6	0.442079000	3.570190000	-1.531394000
1	1.081641000	4.076409000	-2.245423000
6	0.830434000	2.340096000	-1.020186000
1	1.765465000	1.889411000	-1.327331000
1	3.524392000	0.319169000	1.316718000
1	0.764447000	1.486460000	2.769978000
8	2.015599000	-1.221621000	3.311648000
1	1.727959000	0.215489000	2.819310000
1	2.775995000	-1.495703000	2.761214000

IIIβ_q
(G = -2489.086636) (quadruplet)

26	0.526419000	-0.185984000	0.765810000
8	1.417320000	0.977090000	2.188639000
8	0.839579000	-1.507230000	1.688837000
7	-0.196471000	-1.242213000	-0.792487000
7	-1.431938000	0.031175000	1.397162000
7	0.111666000	1.670794000	-0.128279000
7	2.226387000	-0.319237000	-0.255929000
6	-1.652789000	-0.849920000	-0.953055000
1	-1.643904000	0.155847000	-1.381649000
6	-2.449632000	-1.763369000	-1.900951000
1	-1.982070000	-1.758967000	-2.891000000
1	-2.430647000	-2.793076000	-1.529643000
6	-3.914238000	-1.310640000	-1.986807000
1	-3.971451000	-0.311224000	-2.438943000
1	-4.462048000	-1.992849000	-2.646730000
6	-4.551125000	-1.281212000	-0.593696000
1	-4.575689000	-2.296831000	-0.175977000
1	-5.588688000	-0.933311000	-0.652495000
6	-3.763578000	-0.349127000	0.338974000
1	-4.214139000	-0.330001000	1.336809000
1	-3.822602000	0.664406000	-0.073285000
6	-2.294844000	-0.795440000	0.437320000
1	-2.277921000	-1.802409000	0.861077000
6	-0.018475000	-2.717703000	-0.583295000
1	-0.319850000	-3.250177000	-1.487407000
1	-0.608222000	-3.055977000	0.265747000
1	1.033228000	-2.921939000	-0.389388000
6	-1.634780000	-0.469502000	2.789802000
1	-2.664117000	-0.280122000	3.111380000
1	-0.947488000	0.051847000	3.457412000
1	-1.428983000	-1.538256000	2.821407000
6	0.634190000	-0.861132000	-1.982183000
1	0.269059000	0.086846000	-2.387917000
1	0.539391000	-1.612213000	-2.770183000
6	2.063289000	-0.715399000	-1.540397000
6	3.154329000	-0.919136000	-2.378150000
1	2.990403000	-1.242447000	-3.400238000
6	4.437341000	-0.704936000	-1.878603000
1	5.303351000	-0.858278000	-2.514437000
6	4.594388000	-0.301560000	-0.552385000
1	5.575431000	-0.131400000	-0.123662000
6	3.464627000	-0.122945000	0.234617000
6	-1.751798000	1.492742000	1.392386000
1	-1.387922000	1.904584000	2.339564000
1	-2.827511000	1.666839000	1.380360000
6	-1.053321000	2.218590000	0.284062000
6	-1.514083000	3.434639000	-0.213440000
1	-2.463075000	3.829641000	0.132537000
6	-0.735375000	4.124542000	-1.138155000
1	-1.073369000	5.073938000	-1.541079000
6	0.487214000	3.580118000	-1.531395000
1	1.134530000	4.086991000	-2.237949000
6	0.873865000	2.354557000	-1.008160000
1	1.815146000	1.905300000	-1.298617000
1	3.537618000	0.182129000	1.270533000
1	0.833637000	1.552516000	2.715381000
8	2.248300000	-1.137712000	3.573899000
1	1.781945000	0.306657000	2.838911000
1	2.929366000	-1.422312000	2.926087000

TS_(III-IV)β_d
(G = -2489.089076) (doublet)

ANNEX

(G = -2489.114310) (doublet)

26	0.534733000	-0.181274000	0.805712000	26	0.527135000	-0.120996000	0.811280000
8	1.374082000	0.923359000	2.244459000	8	1.366999000	0.976760000	2.286079000
8	0.782739000	-1.549923000	1.678883000	8	0.777127000	-1.620114000	1.801797000
7	-0.150544000	-1.249868000	-0.783416000	7	-0.126674000	-1.241963000	-0.751588000
7	-1.447577000	-0.005462000	1.392912000	7	-1.465693000	-0.006268000	1.382027000
7	0.076356000	1.658960000	-0.100239000	7	0.071038000	1.680182000	-0.067985000
7	2.253286000	-0.260072000	-0.197689000	7	2.277034000	-0.229512000	-0.146795000
6	-1.598130000	-0.849158000	-0.982089000	6	-1.571435000	-0.860966000	-0.985325000
1	-1.571035000	0.160436000	-1.399740000	1	-1.547918000	0.147265000	-1.407573000
6	-2.373285000	-1.745807000	-1.963437000	6	-2.322143000	-1.767384000	-1.975953000
1	-1.872682000	-1.739427000	-2.937814000	1	-1.804093000	-1.763229000	-2.941456000
1	-2.380583000	-2.778662000	-1.600381000	1	-2.328746000	-2.799063000	-1.608865000
6	-3.827415000	-1.271953000	-2.096244000	6	-3.777308000	-1.307019000	-2.138878000
1	-3.854615000	-0.267971000	-2.541012000	1	-3.804765000	-0.305288000	-2.589053000
1	-4.361822000	-1.940420000	-2.780748000	1	-4.294191000	-1.982675000	-2.829982000
6	-4.512083000	-1.244341000	-0.725723000	6	-4.487728000	-1.277727000	-0.781092000
1	-4.568437000	-2.262979000	-0.318689000	1	-4.543107000	-2.295248000	-0.370736000
1	-5.541078000	-0.878308000	-0.816930000	1	-5.518256000	-0.921640000	-0.893447000
6	-3.742581000	-0.334535000	0.243523000	6	-3.743177000	-0.358067000	0.198642000
1	-4.227191000	-0.319696000	1.225478000	1	-4.246695000	-0.343276000	1.171302000
1	-3.769951000	0.684546000	-0.158563000	1	-3.772726000	0.659809000	-0.206825000
6	-2.285480000	-0.805663000	0.387014000	6	-2.284370000	-0.814150000	0.370904000
1	-2.298708000	-1.819354000	0.794453000	1	-2.297835000	-1.827050000	0.781652000
6	0.013763000	-2.726353000	-0.578668000	6	0.046081000	-2.713388000	-0.535868000
1	-0.280710000	-3.257069000	-1.486171000	1	-0.234421000	-3.255287000	-1.441575000
1	-0.588287000	-3.063776000	0.263027000	1	-0.560810000	-3.051564000	0.302016000
1	1.062114000	-2.939508000	-0.374306000	1	1.092808000	-2.918590000	-0.316977000
6	-1.685556000	-0.547799000	2.764593000	6	-1.722495000	-0.542488000	2.751364000
1	-2.724528000	-0.368978000	3.060246000	1	-2.765761000	-0.365616000	3.034851000
1	-1.020148000	-0.044050000	3.467064000	1	-1.067460000	-0.034430000	3.461341000
1	-1.478896000	-1.616529000	2.772585000	1	-1.512779000	-1.610104000	2.770497000
6	0.708946000	-0.870493000	-1.951036000	6	0.748480000	-0.866632000	-1.908257000
1	0.341526000	0.065608000	-2.381518000	1	0.387429000	0.071085000	-2.341714000
1	0.651239000	-1.632173000	-2.732521000	1	0.702762000	-1.626074000	-2.693330000
6	2.122590000	-0.688245000	-1.476904000	6	2.158855000	-0.680405000	-1.420196000
6	3.233211000	-0.876047000	-2.292350000	6	3.275142000	-0.884704000	-2.224632000
1	3.095536000	-1.227944000	-3.308809000	1	3.144807000	-1.254230000	-3.235878000
6	4.500713000	-0.604454000	-1.781447000	6	4.539867000	-0.605842000	-1.710694000
1	5.380435000	-0.743853000	-2.401466000	1	5.423779000	-0.757188000	-2.322049000
6	4.624174000	-0.157762000	-0.465799000	6	4.653943000	-0.134636000	-0.402898000
1	5.591599000	0.063094000	-0.029507000	1	5.618476000	0.094019000	0.036025000
6	3.477826000	-0.001448000	0.301194000	6	3.500967000	0.036833000	0.351332000
6	-1.774849000	1.453273000	1.427654000	6	-1.811346000	1.448519000	1.411057000
1	-1.409834000	1.842730000	2.383773000	1	-1.453857000	1.841168000	2.369296000
1	-2.851824000	1.620737000	1.424018000	1	-2.889258000	1.611189000	1.397589000
6	-1.083936000	2.202171000	0.331604000	6	-1.113117000	2.202809000	0.323434000
6	-1.547640000	3.427106000	-0.140059000	6	-1.589225000	3.411523000	-0.176949000
1	-2.492530000	3.816767000	0.222618000	1	-2.551920000	3.785091000	0.154802000
6	-0.778120000	4.131640000	-1.061325000	6	-0.810227000	4.120990000	-1.086589000
1	-1.118621000	5.088276000	-1.444417000	1	-1.160817000	5.064500000	-1.492556000
6	0.438248000	3.590850000	-1.476997000	6	0.428744000	3.601817000	-1.460526000
1	1.079168000	4.107027000	-2.182641000	1	1.077564000	4.122452000	-2.155677000
6	0.829095000	2.356563000	-0.977695000	6	0.833038000	2.383459000	-0.932419000
1	1.767038000	1.913222000	-1.286302000	1	1.788275000	1.955629000	-1.208390000
1	3.524996000	0.335313000	1.328676000	1	3.542893000	0.397698000	1.371203000
1	0.772637000	1.421378000	2.827366000	1	0.758129000	1.470096000	2.864976000
8	1.992518000	-1.336027000	3.191647000	8	1.824901000	-1.505071000	2.808406000
1	1.735173000	0.152190000	2.814577000	1	1.731651000	0.242459000	2.845397000
1	2.754658000	-1.586958000	2.633393000	1	2.623891000	-1.790928000	2.323238000

IVβ_d

638

IVβ$_q$

(G = -2489.114769) (quadruplet)

26	0.602965000	0.264517000	0.910566000
8	1.411960000	1.885432000	2.070744000
8	0.974850000	-0.969932000	2.171594000
7	-0.075534000	-1.419701000	-0.423578000
7	-1.564241000	0.283137000	1.369543000
7	-0.009984000	1.675419000	-0.440542000
7	2.368786000	-0.229465000	-0.211597000
6	-1.523612000	-1.151961000	-0.722793000
1	-1.532239000	-0.281740000	-1.385560000
6	-2.232230000	-2.307947000	-1.457832000
1	-1.692773000	-2.531449000	-2.385326000
1	-2.204177000	-3.212614000	-0.840140000
6	-3.699677000	-1.974273000	-1.754621000
1	-3.756424000	-1.123383000	-2.447543000
1	-4.172137000	-2.826767000	-2.256810000
6	-4.442645000	-1.630885000	-0.459987000
1	-4.468069000	-2.512456000	0.195489000
1	-5.483772000	-1.360919000	-0.672268000
6	-3.753913000	-0.465050000	0.261766000
1	-4.279586000	-0.226635000	1.193257000
1	-3.814319000	0.418610000	-0.384773000
6	-2.279923000	-0.790058000	0.570630000
1	-2.265758000	-1.668493000	1.221394000
6	0.156049000	-2.745347000	0.208543000
1	-0.084059000	-3.557211000	-0.485096000
1	-0.445936000	-2.848697000	1.111074000
1	1.207850000	-2.832006000	0.482192000
6	-1.806264000	0.076095000	2.821234000
1	-2.867791000	0.209190000	3.063453000
1	-1.220088000	0.799958000	3.391863000
1	-1.495647000	-0.930251000	3.101956000
6	0.763229000	-1.332978000	-1.646439000
1	0.380688000	-0.526042000	-2.280313000
1	0.711401000	-2.257023000	-2.231977000
6	2.196415000	-1.032852000	-1.278893000
6	3.285111000	-1.513280000	-2.003172000
1	3.118580000	-2.166625000	-2.852991000
6	4.571882000	-1.145243000	-1.614426000
1	5.433627000	-1.510033000	-2.164660000
6	4.740304000	-0.313692000	-0.506068000
1	5.724845000	-0.009633000	-0.168611000
6	3.610037000	0.122385000	0.173281000
6	-1.938072000	1.682828000	1.022609000
1	-1.585621000	2.316648000	1.844401000
1	-3.019434000	1.823758000	0.965922000
6	-1.259225000	2.153983000	-0.231333000
6	-1.829448000	3.097092000	-1.082163000
1	-2.838215000	3.445709000	-0.889560000
6	-1.088826000	3.577354000	-2.159354000
1	-1.516747000	4.310737000	-2.835482000
6	0.208557000	3.104101000	-2.351723000
1	0.826467000	3.455836000	-3.170084000
6	0.712466000	2.153912000	-1.474089000
1	1.714052000	1.759844000	-1.593332000
1	3.681672000	0.764342000	1.045184000
1	0.688837000	2.453041000	2.394640000
8	1.836256000	-0.471124000	3.218270000
1	1.692679000	1.343087000	2.843130000
1	2.726008000	-0.702071000	2.883178000

H$_2$O

(G = -76.469236) (singlet)

8	0.000000000	0.121388000	0.000000000
1	0.757404000	-0.485552000	0.000000000
1	-0.757404000	-0.485552000	0.000000000

A.IX.2. Corrdinates from chapter V

In parenthesis are indicated the most stable spin multiplicity and the corrected free energies (G), given in kcal·mol^{-1}.

1Ru^{II}-OH$_2$ complex

[(Py$_2$^{Me}tacn)Ru^{II}-OH$_2$]$^{2+}$ (singlet, G = -743252.672)

Ru	0.007834000	-0.284578000	-0.402008000
N	-1.699106000	0.991815000	-0.414238000
N	-0.337186000	-0.201968000	1.653649000
N	-1.101859000	-2.121055000	-0.255589000
N	1.650367000	-1.494100000	0.125226000
N	1.547823000	1.194229000	-0.374935000
C	-2.550071000	1.269702000	-1.410759000
H	-2.280252000	0.891830000	-2.398575000
C	-3.712829000	2.004443000	-1.216689000
H	-4.369979000	2.208137000	-2.060992000
C	-4.012233000	2.453161000	0.064933000
H	-4.921340000	3.024115000	0.255951000
C	-3.135032000	2.157880000	1.104712000
H	-3.334070000	2.484317000	2.125528000
C	-1.983141000	1.431988000	0.832467000
C	-0.951815000	1.125619000	1.897616000
H	-1.395025000	1.184184000	2.902898000
H	-0.153470000	1.880669000	1.834484000
C	-1.255392000	-1.312292000	2.077479000
H	-1.968937000	-0.936187000	2.824223000
H	-0.653030000	-2.080514000	2.577512000
C	-2.013923000	-1.912455000	0.895111000
H	-2.482687000	-2.863482000	1.201011000
H	-2.811117000	-1.235557000	0.556684000
C	-1.879103000	-2.439781000	-1.465864000
H	-2.513193000	-3.326896000	-1.299772000
H	-1.188016000	-2.646798000	-2.293894000
H	-2.514809000	-1.582365000	-1.727143000
C	-0.113478000	-3.217239000	0.024196000
H	-0.417681000	-4.131476000	-0.505895000
H	-0.142849000	-3.457249000	1.093688000
C	1.307370000	-2.840367000	-0.398434000
H	2.019262000	-3.603422000	-0.042170000
H	1.376631000	-2.791248000	-1.494332000
C	1.786485000	-1.481587000	1.622424000
H	2.848788000	-1.397639000	1.894436000
H	1.441151000	-2.448703000	2.007782000
C	1.006584000	-0.334934000	2.280781000
H	0.918487000	-0.518793000	3.363480000
H	1.531715000	0.618354000	2.138803000

```
C    2.820322000   -0.878053000   -0.535141000
H    2.755299000   -1.106499000   -1.609988000
H    3.768547000   -1.287393000   -0.153909000
C    2.775031000    0.626225000   -0.354667000
C    3.926022000    1.387529000   -0.198602000
H    4.896753000    0.892458000   -0.173914000
C    3.813084000    2.768753000   -0.070701000
H    4.703936000    3.385062000    0.054440000
C    2.549250000    3.348054000   -0.098050000
H    2.411714000    4.423883000    0.001281000
C    1.441699000    2.523304000   -0.248402000
H    0.427679000    2.928790000   -0.266825000
O    0.272005000   -0.374299000   -2.638957000
H   -0.598819000   -0.501786000   -3.051801000
H    0.791325000   -1.152122000   -2.906207000
```

$[(Py_2{}^{Me}tacn)Ru^{III}\text{-}OH_2]^{3+}$ (doblet, G = -743142.5019)

```
Ru   0.021052000   -0.300946000   -0.440201000
N   -1.671237000    0.989137000   -0.364419000
N   -0.396218000   -0.278255000    1.648923000
N   -1.090705000   -2.115774000   -0.377922000
N    1.630754000   -1.489255000    0.127140000
N    1.522092000    1.201418000   -0.349948000
C   -2.454745000    1.304431000   -1.405575000
H   -2.143530000    0.923400000   -2.379136000
C   -3.597877000    2.074176000   -1.248367000
H   -4.209535000    2.313332000   -2.116787000
C   -3.939081000    2.512966000    0.027375000
H   -4.836512000    3.111915000    0.184335000
C   -3.125937000    2.174841000    1.104666000
H   -3.361456000    2.493433000    2.119751000
C   -1.990976000    1.411195000    0.875402000
C   -1.007992000    1.040264000    1.957874000
H   -1.482711000    1.032140000    2.948609000
H   -0.206254000    1.794941000    1.969011000
C   -1.326634000   -1.409979000    1.990958000
H   -2.069677000   -1.062820000    2.721311000
H   -0.741913000   -2.195416000    2.484460000
C   -2.040313000   -1.958532000    0.756915000
H   -2.508440000   -2.926268000    0.998358000
H   -2.831251000   -1.272717000    0.423767000
C   -1.838398000   -2.386368000   -1.623471000
H   -2.466830000   -3.281810000   -1.496884000
H   -1.126787000   -2.549998000   -2.441227000
H   -2.472767000   -1.522284000   -1.861462000
C   -0.109146000   -3.228837000   -0.114700000
H   -0.392517000   -4.110225000   -0.705538000
H   -0.182041000   -3.523697000    0.938213000
C    1.321466000   -2.826762000   -0.468122000
H    2.035085000   -3.579976000   -0.102306000
H    1.435319000   -2.727543000   -1.555168000
C    1.720838000   -1.555468000    1.633106000
H    2.775745000   -1.497157000    1.931114000
H    1.352357000   -2.537246000    1.951079000
C    0.934507000   -0.431500000    2.305993000
H    0.812633000   -0.645876000    3.378312000
H    1.465322000    0.523600000    2.204821000
C    2.834685000   -0.848786000   -0.467976000
H    2.838735000   -1.083075000   -1.542129000
H    3.753037000   -1.251227000   -0.019257000
C    2.757227000    0.653864000   -0.300342000
C    3.889340000    1.441373000   -0.145344000
```

```
H    4.869973000    0.968650000   -0.096968000
C    3.742361000    2.821789000   -0.052840000
H    4.618074000    3.459582000    0.070581000
C    2.468333000    3.376968000   -0.114157000
H    2.310041000    4.452012000   -0.045152000
C    1.378728000    2.530105000   -0.259955000
H    0.356531000    2.911444000   -0.304523000
O    0.361522000   -0.448521000   -2.389253000
H    0.929792000    0.287325000   -2.669377000
```

$[(Py_2{}^{Me}tacn)Ru^{III}\text{-}OH]^{2+}$ (doblet, G = -743142.5019)

```
Ru   0.021052000   -0.300946000   -0.440201000
N   -1.671237000    0.989137000   -0.364419000
N   -0.396218000   -0.278255000    1.648923000
N   -1.090705000   -2.115774000   -0.377922000
N    1.630754000   -1.489255000    0.127140000
N    1.522092000    1.201418000   -0.349948000
C   -2.454745000    1.304431000   -1.405575000
H   -2.143530000    0.923400000   -2.379136000
C   -3.597877000    2.074176000   -1.248367000
H   -4.209535000    2.313332000   -2.116787000
C   -3.939081000    2.512966000    0.027375000
H   -4.836512000    3.111915000    0.184335000
C   -3.125937000    2.174841000    1.104666000
H   -3.361456000    2.493433000    2.119751000
C   -1.990976000    1.411195000    0.875402000
C   -1.007992000    1.040264000    1.957874000
H   -1.482711000    1.032140000    2.948609000
H   -0.206254000    1.794941000    1.969011000
C   -1.326634000   -1.409979000    1.990958000
H   -2.069677000   -1.062820000    2.721311000
H   -0.741913000   -2.195416000    2.484460000
C   -2.040313000   -1.958532000    0.756915000
H   -2.508440000   -2.926268000    0.998358000
H   -2.831251000   -1.272717000    0.423767000
C   -1.838398000   -2.386368000   -1.623471000
H   -2.466830000   -3.281810000   -1.496884000
H   -1.126787000   -2.549998000   -2.441227000
H   -2.472767000   -1.522284000   -1.861462000
C   -0.109146000   -3.228837000   -0.114700000
H   -0.392517000   -4.110225000   -0.705538000
H   -0.182041000   -3.523697000    0.938213000
C    1.321466000   -2.826762000   -0.468122000
H    2.035085000   -3.579976000   -0.102306000
H    1.435319000   -2.727543000   -1.555168000
C    1.720838000   -1.555468000    1.633106000
H    2.775745000   -1.497157000    1.931114000
H    1.352357000   -2.537246000    1.951079000
C    0.934507000   -0.431500000    2.305993000
H    0.812633000   -0.645876000    3.378312000
H    1.465322000    0.523600000    2.204821000
C    2.834685000   -0.848786000   -0.467976000
H    2.838735000   -1.083075000   -1.542129000
H    3.753037000   -1.251227000   -0.019257000
C    2.757227000    0.653864000   -0.300342000
C    3.889340000    1.441373000   -0.145344000
H    4.869973000    0.968650000   -0.096968000
C    3.742361000    2.821789000   -0.052840000
H    4.618074000    3.459582000    0.070581000
C    2.468333000    3.376968000   -0.114157000
H    2.310041000    4.452012000   -0.045152000
```

ANNEX

C	1.378728000	2.530105000	-0.259955000
H	0.356531000	2.911444000	-0.304523000
O	0.361522000	-0.448521000	-2.389253000
H	0.929792000	0.287325000	-2.669377000

[(Py$_2$^{Me}tacn)Ru^{IV}=O]$^{2+}$ (triplet, G = -742465.9589)

Ru	0.021148000	-0.304657000	-0.500181000
N	-1.679470000	0.972752000	-0.399392000
N	-0.339463000	-0.228299000	1.661303000
N	-1.088696000	-2.115959000	-0.298018000
N	1.641384000	-1.484308000	0.060830000
N	1.520776000	1.194035000	-0.380221000
C	-2.497372000	1.255021000	-1.423678000
H	-2.211413000	0.850957000	-2.395647000
C	-3.640868000	2.020084000	-1.251820000
H	-4.280654000	2.232286000	-2.106815000
C	-3.946162000	2.489018000	0.022207000
H	-4.842801000	3.085719000	0.191733000
C	-3.098772000	2.183205000	1.082422000
H	-3.307348000	2.524616000	2.096024000
C	-1.964211000	1.422257000	0.841190000
C	-0.958236000	1.093677000	1.922904000
H	-1.428233000	1.122854000	2.915885000
H	-0.164848000	1.857416000	1.905338000
C	-1.248124000	-1.351981000	2.062151000
H	-1.971444000	-0.991284000	2.806044000
H	-0.644678000	-2.121387000	2.558164000
C	-1.999184000	-1.933362000	0.866924000
H	-2.449868000	-2.900184000	1.140042000
H	-2.805468000	-1.261851000	0.541758000
C	-1.894401000	-2.424025000	-1.503611000
H	-2.512421000	-3.314374000	-1.312659000
H	-1.219347000	-2.613728000	-2.345813000
H	-2.541216000	-1.568846000	-1.737473000
C	-0.094840000	-3.227421000	-0.052706000
H	-0.411906000	-4.118394000	-0.610273000
H	-0.121542000	-3.496501000	1.008890000
C	1.316878000	-2.837438000	-0.483115000
H	2.046293000	-3.579277000	-0.125933000
H	1.382364000	-2.767171000	-1.576736000
C	1.781867000	-1.501210000	1.568415000
H	2.847580000	-1.432582000	1.823460000
H	1.431705000	-2.475840000	1.925754000
C	1.017732000	-0.366415000	2.258604000
H	0.949899000	-0.575695000	3.336918000
H	1.540892000	0.590037000	2.131884000
C	2.822849000	-0.853406000	-0.582787000
H	2.772001000	-1.069344000	-1.659557000
H	3.756371000	-1.270592000	-0.182022000
C	2.757051000	0.643544000	-0.378583000
C	3.890382000	1.428128000	-0.231741000
H	4.872373000	0.956291000	-0.224008000
C	3.743162000	2.804976000	-0.092531000
H	4.621206000	3.440061000	0.027854000
C	2.468159000	3.360903000	-0.103684000
H	2.311256000	4.433062000	0.001445000
C	1.375293000	2.519470000	-0.249021000
H	0.353740000	2.903498000	-0.264714000
O	0.216007000	-0.469066000	-2.250254000

[(Py$_2$^{Me}tacn)(H$_2$O)$_4$Ru^{IV}=O]$^{2+}$ (triplet, G = -934324.9063)

Ru	-0.544756000	-0.339427000	-0.325576000
N	-1.796183000	1.384535000	-0.264629000
N	-1.595611000	-0.632210000	1.577846000
N	-2.094858000	-1.633321000	-1.009657000
N	0.407225000	-2.106835000	0.215661000
N	1.145251000	0.458865000	0.675290000
C	-2.138662000	2.138423000	-1.318648000
H	-1.673663000	1.879099000	-2.270933000
C	-3.040929000	3.184890000	-1.203351000
H	-3.291577000	3.778324000	-2.081054000
C	-3.609933000	3.443097000	0.039598000
H	-4.326299000	4.255851000	0.161693000
C	-3.266280000	2.644275000	1.125575000
H	-3.702300000	2.804676000	2.111233000
C	-2.350021000	1.618287000	0.944721000
C	-1.890120000	0.730489000	2.081598000
H	-2.644170000	0.704993000	2.881786000
H	-0.967026000	1.150882000	2.507951000
C	-2.850380000	-1.418645000	1.345388000
H	-3.662040000	-1.007370000	1.961170000
H	-2.682444000	-2.446569000	1.689600000
C	-3.268503000	-1.400271000	-0.122111000
H	-4.030466000	-2.173424000	-0.305683000
H	-3.695761000	-0.427366000	-0.401484000
C	-2.483406000	-1.365741000	-2.414439000
H	-3.347132000	-1.993601000	-2.680504000
H	-1.638444000	-1.601844000	-3.071321000
H	-2.749038000	-0.306860000	-2.524696000
C	-1.586050000	-3.049792000	-0.883185000
H	-1.922470000	-3.628643000	-1.753445000
H	-2.048699000	-3.508240000	-0.001987000
C	-0.062369000	-3.101524000	-0.795927000
H	0.273375000	-4.112827000	-0.522708000
H	0.388006000	-2.821719000	-1.757205000
C	0.017904000	-2.511498000	1.620620000
H	0.912995000	-2.871908000	2.144291000
H	-0.669215000	-3.361667000	1.543731000
C	-0.618668000	-1.371349000	2.424135000
H	-1.112078000	-1.783917000	3.316991000
H	0.144515000	-0.658089000	2.758180000
C	1.858709000	-1.801575000	0.121860000
H	2.117661000	-1.725085000	-0.944137000
H	2.460458000	-2.600661000	0.576648000
C	2.128329000	-0.465115000	0.777715000
C	3.329808000	-0.164692000	1.401197000
H	4.105843000	-0.927570000	1.467292000
C	3.520859000	1.115984000	1.912991000
H	4.460152000	1.373721000	2.404459000
C	2.508133000	2.061173000	1.790327000
H	2.619885000	3.073014000	2.176001000
C	1.326562000	1.691557000	1.165365000
H	0.497444000	2.391692000	1.051498000
O	0.205780000	-0.180551000	-1.920131000
O	1.029144000	2.856090000	-1.717089000
H	0.560161000	2.520095000	-2.495583000
H	1.807722000	2.261476000	-1.638919000
O	3.328160000	1.272958000	-1.632195000
H	4.028597000	1.544065000	-1.009297000
H	3.454126000	0.303251000	-1.673990000
O	5.814197000	1.069491000	-0.265411000
H	6.134750000	1.011143000	0.648235000
H	6.583515000	1.349230000	-0.786805000

ANNEX

O	4.597247000	-1.232206000	-1.286439000
H	5.017073000	-1.430756000	-2.137639000
H	5.158937000	-0.529931000	-0.890071000

[(Py$_2$^{Me}tacn)Ru^V=O]$^{3+}$ (doublet, G = -742323.9341)

Ru	0.021152000	-0.315809000	-0.580207000
N	-1.636860000	0.978259000	-0.313505000
N	-0.339703000	-0.190598000	1.627420000
N	-1.140060000	-2.090652000	-0.343937000
N	1.566842000	-1.486527000	0.183458000
N	1.505362000	1.177331000	-0.412859000
C	-2.421268000	1.232351000	-1.375772000
H	-2.128380000	0.776979000	-2.322393000
C	-3.544463000	2.030282000	-1.245806000
H	-4.168954000	2.219870000	-2.116890000
C	-3.851539000	2.561987000	0.004408000
H	-4.737243000	3.183941000	0.135056000
C	-3.025372000	2.291342000	1.090017000
H	-3.233956000	2.685405000	2.083835000
C	-1.911380000	1.490926000	0.898751000
C	-0.903822000	1.147850000	1.949667000
H	-1.334386000	1.152352000	2.959581000
H	-0.091433000	1.890562000	1.921332000
C	-1.310775000	-1.282557000	2.006390000
H	-2.036115000	-0.881365000	2.725678000
H	-0.752864000	-2.066546000	2.529874000
C	-2.061770000	-1.850497000	0.805466000
H	-2.538893000	-2.801066000	1.086609000
H	-2.846738000	-1.166942000	0.457560000
C	-1.931677000	-2.408347000	-1.560043000
H	-2.557673000	-3.289095000	-1.357466000
H	-1.245325000	-2.620604000	-2.387660000
H	-2.569376000	-1.553174000	-1.814754000
C	-0.177223000	-3.224640000	-0.045999000
H	-0.464783000	-4.094768000	-0.648140000
H	-0.295859000	-3.514129000	1.003387000
C	1.269162000	-2.859894000	-0.362686000
H	1.959217000	-3.579939000	0.097889000
H	1.446982000	-2.829092000	-1.443464000
C	1.670237000	-1.540358000	1.692036000
H	2.732036000	-1.552222000	1.962816000
H	1.234335000	-2.487262000	2.024146000
C	0.965196000	-0.357112000	2.315151000
H	0.815461000	-0.524378000	3.391429000
H	1.543033000	0.566320000	2.185202000
C	2.805856000	-0.877379000	-0.406904000
H	2.844295000	-1.157313000	-1.468719000
H	3.691501000	-1.280320000	0.098003000
C	2.736101000	0.625791000	-0.295725000
C	3.859577000	1.421340000	-0.150165000
H	4.838855000	0.954684000	-0.051660000
C	3.704865000	2.805094000	-0.138876000
H	4.576635000	3.450048000	-0.027463000
C	2.434973000	3.357522000	-0.268987000
H	2.276895000	4.434390000	-0.266680000
C	1.347613000	2.508882000	-0.402395000
H	0.329074000	2.885705000	-0.509441000
O	0.521022000	-0.757078000	-2.119221000

[(Py$_2$^{Me}tacn)(H$_2$O)$_4$Ru^V=O]$^{2+}$ (doublet, G =-934183.5452)

Ru	-0.509411000	-0.323837000	-0.405398000
N	-1.826193000	1.328853000	-0.210111000
N	-1.496644000	-0.530648000	1.600450000
N	-2.071601000	-1.669030000	-0.948562000
N	0.394829000	-2.036011000	0.356038000
N	1.133882000	0.565354000	0.565918000
C	-2.199298000	1.988149000	-1.321051000
H	-1.769947000	1.648767000	-2.263536000
C	-3.101312000	3.035193000	-1.251005000
H	-3.390757000	3.552299000	-2.163972000
C	-3.624820000	3.390773000	-0.010601000
H	-4.343942000	4.206142000	0.069282000
C	-3.234584000	2.692189000	1.126871000
H	-3.631922000	2.930976000	2.112445000
C	-2.325979000	1.654818000	0.995621000
C	-1.795942000	0.828204000	2.125057000
H	-2.502934000	0.772705000	2.963870000
H	-0.864563000	1.281459000	2.495426000
C	-2.765437000	-1.327198000	1.418762000
H	-3.562468000	-0.876901000	2.024462000
H	-2.593455000	-2.332560000	1.820181000
C	-3.219830000	-1.391828000	-0.035786000
H	-3.968024000	-2.189709000	-0.151782000
H	-3.676317000	-0.448749000	-0.362804000
C	-2.506632000	-1.482719000	-2.358060000
H	-3.354447000	-2.152615000	-2.559781000
H	-1.671761000	-1.725992000	-3.025155000
H	-2.814985000	-0.441663000	-2.510082000
C	-1.548692000	-3.079597000	-0.759100000
H	-1.826295000	-3.676152000	-1.636498000
H	-2.059577000	-3.527150000	0.100275000
C	-0.032862000	-3.116798000	-0.601034000
H	0.291483000	-4.087508000	-0.201994000
H	0.473192000	-2.932200000	-1.555509000
C	0.012285000	-2.415715000	1.769331000
H	0.904308000	-2.804558000	2.273001000
H	-0.714229000	-3.231911000	1.712300000
C	-0.550505000	-1.222981000	2.511107000
H	-1.066013000	-1.550208000	3.425549000
H	0.238625000	-0.514973000	2.793022000
C	1.863185000	-1.727915000	0.272527000
H	2.156374000	-1.752208000	-0.786173000
H	2.433935000	-2.491305000	0.815380000
C	2.107281000	-0.341515000	0.813599000
C	3.270348000	0.024951000	1.468689000
H	4.037334000	-0.724288000	1.662437000
C	3.432796000	1.354563000	1.850835000
H	4.342764000	1.666234000	2.365085000
C	2.433780000	2.280085000	1.568589000
H	2.529029000	3.327714000	1.848185000
C	1.285716000	1.846945000	0.924368000
H	0.465608000	2.527133000	0.689100000
O	0.317742000	-0.547905000	-1.851439000
O	0.873483000	2.419097000	-2.148328000
H	0.418527000	1.909388000	-2.835603000
H	1.686744000	1.897104000	-1.966748000
O	3.273185000	1.053681000	-1.759540000
H	3.902889000	1.454840000	-1.131411000
H	3.474780000	0.098785000	-1.672489000
O	5.707903000	1.173917000	-0.292058000
H	6.080860000	1.274748000	0.597952000
H	6.431449000	1.401723000	-0.897362000

O	4.603221000	-1.301987000	-0.993932000
H	5.083412000	-1.622641000	-1.773215000
H	5.133228000	-0.539587000	-0.671620000

TS, [(Py$_2^{Me}$tacn)(H$_2$O)$_3$Ru^V-O--O-H]$^{3+}$

(doublet, G = -934161.0034)

Ru	-0.537226000	-0.318676000	-0.297406000
N	-1.592930000	1.520091000	-0.248286000
N	-1.626991000	-0.479637000	1.568508000
N	-2.182454000	-1.473537000	-0.998241000
N	0.233450000	-2.150591000	0.311752000
N	1.203335000	0.370096000	0.651976000
C	-1.791164000	2.294301000	-1.324802000
H	-1.315663000	1.969456000	-2.251278000
C	-2.563139000	3.443037000	-1.249353000
H	-2.705317000	4.055576000	-2.138069000
C	-3.148662000	3.777792000	-0.031727000
H	-3.769137000	4.670014000	0.055088000
C	-2.944942000	2.960122000	1.075953000
H	-3.393583000	3.184639000	2.043049000
C	-2.152521000	1.831115000	0.937704000
C	-1.804781000	0.908307000	2.078549000
H	-2.567628000	0.937838000	2.868388000
H	-0.850824000	1.239652000	2.516686000
C	-2.952550000	-1.150344000	1.334436000
H	-3.724198000	-0.651386000	1.935071000
H	-2.883032000	-2.180310000	1.702054000
C	-3.346778000	-1.118463000	-0.137666000
H	-4.170979000	-1.824182000	-0.322083000
H	-3.680291000	-0.116636000	-0.440935000
C	-2.510467000	-1.185104000	-2.415665000
H	-3.423042000	-1.731546000	-2.695893000
H	-1.677077000	-1.508697000	-3.050421000
H	-2.673370000	-0.106985000	-2.541174000
C	-1.804846000	-2.929660000	-0.843843000
H	-2.156808000	-3.481192000	-1.725137000
H	-2.341076000	-3.339324000	0.019369000
C	-0.294926000	-3.120989000	-0.700523000
H	-0.067205000	-4.150812000	-0.390177000
H	0.216775000	-2.911787000	-1.649417000
C	-0.230429000	-2.505677000	1.707897000
H	0.610796000	-2.952704000	2.252131000
H	-1.000575000	-3.279652000	1.617569000
C	-0.751459000	-1.288462000	2.467191000
H	-1.310067000	-1.611664000	3.357664000
H	0.076003000	-0.646651000	2.796923000
C	1.713217000	-1.977448000	0.267919000
H	2.022958000	-1.976705000	-0.787196000
H	2.217436000	-2.804439000	0.784004000
C	2.080378000	-0.637614000	0.868082000
C	3.274045000	-0.408676000	1.535846000
H	3.955833000	-1.239665000	1.714876000
C	3.573907000	0.884687000	1.952759000
H	4.508950000	1.087592000	2.475604000
C	2.678405000	1.918299000	1.688761000
H	2.887290000	2.944643000	1.987174000
C	1.494283000	1.621683000	1.035729000
H	0.751765000	2.389411000	0.808995000
O	0.234555000	-0.371896000	-1.871288000
O	1.120079000	1.237501000	-2.274875000
H	1.038023000	1.197233000	-3.246239000

H	2.081140000	0.948824000	-2.048011000
O	3.551602000	0.622014000	-1.732081000
H	4.008656000	1.295631000	-1.173695000
H	3.833630000	-0.262737000	-1.400438000
O	4.976236000	2.569877000	-0.371133000
H	4.324163000	3.255761000	-0.157340000
H	5.481810000	2.939634000	-1.112453000
O	4.575391000	-1.820699000	-0.900844000
H	5.049714000	-2.108833000	-1.697285000
H	5.273663000	-1.509014000	-0.303223000

[(Py$_2^{Me}$tacn)Ru^{III}-OOH]$^{2+}$ (doublet, G = -790021.1634)

Ru	0.009665000	-0.314263000	-0.345426000
N	-1.663618000	0.992412000	-0.227966000
N	-0.446885000	-0.442123000	1.725370000
N	-1.101782000	-2.125014000	-0.432724000
N	1.612897000	-1.553118000	0.129254000
N	1.511469000	1.162874000	-0.089854000
C	-2.413427000	1.398768000	-1.261092000
H	-2.083243000	1.082951000	-2.252328000
C	-3.544510000	2.179803000	-1.074868000
H	-4.128316000	2.498016000	-1.937101000
C	-3.908778000	2.529793000	0.221667000
H	-4.797282000	3.135794000	0.400923000
C	-3.133532000	2.091768000	1.291210000
H	-3.391423000	2.337595000	2.320986000
C	-2.007413000	1.323361000	1.033225000
C	-1.059667000	0.856039000	2.113070000
H	-1.567396000	0.781095000	3.084422000
H	-0.253784000	1.599887000	2.208886000
C	-1.380774000	-1.593907000	1.973617000
H	-2.133885000	-1.300270000	2.716873000
H	-0.801557000	-2.414242000	2.414166000
C	-2.074081000	-2.044743000	0.691406000
H	-2.554485000	-3.023241000	0.849051000
H	-2.850968000	-1.327796000	0.392499000
C	-1.831330000	-2.300153000	-1.707103000
H	-2.465491000	-3.198654000	-1.653008000
H	-1.107656000	-2.412008000	-2.523475000
H	-2.458146000	-1.417642000	-1.891532000
C	-0.129957000	-3.260217000	-0.239059000
H	-0.418222000	-4.098262000	-0.887948000
H	-0.208336000	-3.622123000	0.792459000
C	1.301535000	-2.839283000	-0.563236000
H	2.013449000	-3.621906000	-0.260414000
H	1.410880000	-2.654914000	-1.640869000
C	1.683160000	-1.719077000	1.628821000
H	2.733524000	-1.669846000	1.944620000
H	1.324167000	-2.724175000	1.876574000
C	0.881132000	-0.651416000	2.378191000
H	0.748526000	-0.951974000	3.428131000
H	1.411469000	0.308373000	2.362542000
C	2.820779000	-0.870975000	-0.403823000
H	2.828373000	-1.011001000	-1.494963000
H	3.737839000	-1.311712000	0.010778000
C	2.745277000	0.613632000	-0.111250000
C	3.881762000	1.390181000	0.070755000
H	4.863397000	0.917355000	0.056823000
C	3.737035000	2.759282000	0.268389000
H	4.615559000	3.388184000	0.415429000
C	2.461394000	3.316329000	0.279031000

H	2.305624000	4.383541000	0.428359000
C	1.369429000	2.481486000	0.096568000
H	0.346856000	2.865095000	0.096180000
O	0.295713000	-0.287469000	-2.281385000
O	0.531687000	1.043290000	-2.755226000
H	0.062902000	1.033997000	-3.607911000

[(Py$_2$^{Me}tacn)(H$_2$O)$_4$Ru^{III}-OOH]$^{2+}$ (doublet, G = -934183.4767)

Ru	-0.546038000	-0.332125000	-0.244532000
N	-1.706172000	1.440112000	-0.362436000
N	-1.669505000	-0.482128000	1.548364000
N	-2.034664000	-1.665739000	-0.970588000
N	0.395581000	-2.062101000	0.422424000
N	1.149311000	0.539719000	0.699685000
C	-1.900227000	2.174313000	-1.465713000
H	-1.375434000	1.845432000	-2.364631000
C	-2.720278000	3.292793000	-1.457219000
H	-2.852399000	3.873394000	-2.368715000
C	-3.363103000	3.640763000	-0.272594000
H	-4.019476000	4.510538000	-0.234969000
C	-3.168704000	2.863559000	0.865407000
H	-3.660847000	3.099766000	1.808475000
C	-2.324291000	1.765047000	0.790779000
C	-1.976738000	0.906220000	1.984946000
H	-2.780941000	0.916135000	2.733794000
H	-1.073654000	1.322692000	2.456141000
C	-2.922843000	-1.278848000	1.305886000
H	-3.758558000	-0.817726000	1.848278000
H	-2.783166000	-2.279665000	1.732214000
C	-3.257898000	-1.364656000	-0.179068000
H	-4.020079000	-2.141494000	-0.347850000
H	-3.655049000	-0.409590000	-0.549399000
C	-2.317550000	-1.482128000	-2.411095000
H	-3.167926000	-2.115213000	-2.707927000
H	-1.430360000	-1.764847000	-2.990280000
H	-2.558203000	-0.427801000	-2.601640000
C	-1.544749000	-3.067883000	-0.718421000
H	-1.838596000	-3.711359000	-1.558793000
H	-2.047906000	-3.464560000	0.170829000
C	-0.027145000	-3.108322000	-0.555787000
H	0.300663000	-4.104297000	-0.221881000
H	0.464514000	-2.872365000	-1.509767000
C	-0.073519000	-2.372592000	1.823327000
H	0.787253000	-2.691781000	2.425625000
H	-0.757928000	-3.226094000	1.769272000
C	-0.747701000	-1.175143000	2.501223000
H	-1.301837000	-1.514814000	3.388789000
H	0.000661000	-0.442359000	2.826508000
C	1.851756000	-1.768419000	0.381969000
H	2.160798000	-1.779238000	-0.673481000
H	2.425363000	-2.531726000	0.925573000
C	2.106233000	-0.383018000	0.939529000
C	3.274510000	-0.048174000	1.612285000
H	4.024951000	-0.815723000	1.798466000
C	3.456237000	1.265103000	2.033624000
H	4.365001000	1.549795000	2.564863000
C	2.470484000	2.211713000	1.765615000
H	2.578882000	3.251054000	2.072859000
C	1.328124000	1.808206000	1.091182000
H	0.524631000	2.509037000	0.854910000

O	0.376313000	-0.259573000	-1.981351000
O	1.115585000	0.961144000	-2.117031000
H	1.014630000	1.160882000	-3.066506000
H	2.714777000	0.592074000	-1.877211000
O	3.717261000	0.509281000	-1.826837000
H	4.095962000	1.306621000	-1.288646000
H	4.016468000	-0.373026000	-1.394965000
O	4.724570000	2.519661000	-0.583593000
H	3.980739000	3.044443000	-0.243525000
H	5.113601000	3.063115000	-1.289883000
O	4.654896000	-1.684531000	-0.811660000
H	4.416421000	-2.396258000	-1.429114000
H	5.616250000	-1.579616000	-0.911634000

[(Py$_2$^{Me}tacn)(H$_2$O)$_4$Ru^{III}-OO·]$^{2+}$ (singlet, G = -789630.8132)

Ru	0.019794000	-0.324585000	-0.349088000
N	-1.680811000	0.975112000	-0.258727000
N	-0.451060000	-0.398767000	1.711716000
N	-0.981690000	-2.182201000	-0.387790000
N	1.682240000	-1.444621000	0.203050000
N	1.443254000	1.243017000	-0.154715000
C	-2.425631000	1.341910000	-1.310671000
H	-2.046814000	1.054294000	-2.291992000
C	-3.607983000	2.050346000	-1.151051000
H	-4.187440000	2.335335000	-2.027613000
C	-4.027267000	2.372019000	0.135926000
H	-4.956196000	2.920435000	0.294244000
C	-3.252150000	1.981420000	1.223984000
H	-3.548124000	2.208689000	2.247689000
C	-2.076779000	1.283686000	0.992273000
C	-1.123432000	0.874790000	2.084550000
H	-1.630121000	0.783199000	3.054342000
H	-0.352615000	1.655035000	2.175747000
C	-1.329054000	-1.592291000	1.987796000
H	-2.104479000	-1.312726000	2.712588000
H	-0.713128000	-2.366419000	2.460519000
C	-1.979972000	-2.120190000	0.714025000
H	-2.408873000	-3.117945000	0.895451000
H	-2.787314000	-1.454757000	0.378365000
C	-1.663183000	-2.391016000	-1.686388000
H	-2.267755000	-3.309763000	-1.648247000
H	-0.906867000	-2.481074000	-2.475924000
H	-2.311288000	-1.529389000	-1.897643000
C	0.043163000	-3.262403000	-0.161803000
H	-0.185350000	-4.118932000	-0.809641000
H	-0.041411000	-3.617470000	0.871493000
C	1.455811000	-2.764667000	-0.467361000
H	2.205854000	-3.494311000	-0.128906000
H	1.581155000	-2.603696000	-1.546558000
C	1.722886000	-1.585438000	1.706139000
H	2.763797000	-1.501285000	2.043482000
H	1.383767000	-2.594414000	1.963812000
C	0.872867000	-0.524071000	2.398470000
H	0.727043000	-0.785168000	3.456878000
H	1.365152000	0.455268000	2.349831000
C	2.877278000	-0.721202000	-0.312910000
H	2.953153000	-0.918984000	-1.391395000
H	3.791826000	-1.087808000	0.171920000
C	2.707094000	0.769110000	-0.105727000

C	3.785907000	1.622645000	0.077539000
H	4.794267000	1.212429000	0.125010000
C	3.550911000	2.988875000	0.199291000
H	4.384263000	3.676286000	0.346714000
C	2.245622000	3.466433000	0.135866000
H	2.020822000	4.527887000	0.226324000
C	1.213151000	2.557663000	-0.038744000
H	0.170051000	2.875914000	-0.088182000
O	0.677830000	-0.427526000	-2.315547000
O	0.249259000	0.607227000	-2.988250000

[(Py$_2^{Me}$tacn)(H$_2$O)$_4$Ru^{IV}-OO]$^{2+}$ (singlet, G = -789631.0057)

Ru	0.034860000	-0.280736000	-0.396646000
N	-1.705669000	0.942554000	-0.276986000
N	-0.381581000	-0.248379000	1.671027000
N	-1.069229000	-2.097839000	-0.351202000
N	1.629850000	-1.469230000	0.280319000
N	1.516759000	1.214438000	-0.294714000
C	-2.532399000	1.204922000	-1.301115000
H	-2.256986000	0.794962000	-2.271646000
C	-3.683920000	1.958471000	-1.130699000
H	-4.327382000	2.149727000	-1.987846000
C	-3.993771000	2.441592000	0.136057000
H	-4.896989000	3.029620000	0.300090000
C	-3.139238000	2.157358000	1.196092000
H	-3.343964000	2.505617000	2.207862000
C	-1.999520000	1.407882000	0.953356000
C	-0.980138000	1.074606000	1.999600000
H	-1.410026000	1.058318000	3.009884000
H	-0.180343000	1.830545000	1.975730000
C	-1.338760000	-1.371625000	2.006138000
H	-2.089126000	-0.999111000	2.715235000
H	-0.771241000	-2.150977000	2.526727000
C	-2.035349000	-1.936140000	0.769937000
H	-2.492836000	-2.906301000	1.019263000
H	-2.831646000	-1.265469000	0.421592000
C	-1.797367000	-2.373497000	-1.608990000
H	-2.377219000	-3.303494000	-1.506994000
H	-1.073320000	-2.479212000	-2.425572000
H	-2.478369000	-1.540595000	-1.824904000
C	-0.091402000	-3.213886000	-0.062129000
H	-0.338258000	-4.076659000	-0.694141000
H	-0.232543000	-3.537267000	0.975625000
C	1.366508000	-2.820127000	-0.311725000
H	2.038745000	-3.562459000	0.142587000
H	1.579850000	-2.763658000	-1.383335000
C	1.669037000	-1.559623000	1.784917000
H	2.713489000	-1.560926000	2.119047000
H	1.234712000	-2.520200000	2.081171000
C	0.911588000	-0.401841000	2.399594000
H	0.720872000	-0.574199000	3.468698000
H	1.469861000	0.536250000	2.291744000
C	2.869953000	-0.821114000	-0.241708000
H	2.992879000	-1.114807000	-1.291571000
H	3.746748000	-1.173119000	0.317004000
C	2.754484000	0.687237000	-0.172525000
C	3.869928000	1.503447000	-0.046473000
H	4.855965000	1.052411000	0.062026000
C	3.700591000	2.884366000	-0.063188000
H	4.564165000	3.542850000	0.033903000

C	2.421749000	3.415076000	-0.199601000
H	2.247899000	4.489684000	-0.215349000
C	1.348699000	2.543059000	-0.308227000
H	0.321354000	2.900499000	-0.406059000
O	0.803731000	-0.789665000	-2.184548000
O	-0.150614000	0.154484000	-2.340866000

[(Py$_2^{Me}$tacn)Ru^{III}-O$_2$]$^{3+}$ (quadruplet, G = -789514.6408)

Ru	-0.014328000	-0.354229000	-0.328681000
N	-1.659006000	0.973110000	-0.195278000
N	-0.459417000	-0.554854000	1.665765000
N	-0.981495000	-2.211818000	-0.489350000
N	1.675305000	-1.482158000	0.139463000
N	1.411708000	1.206110000	-0.032021000
C	-2.344324000	1.447444000	-1.244612000
H	-1.947967000	1.210454000	-2.233289000
C	-3.500418000	2.191690000	-1.066707000
H	-4.039300000	2.567714000	-1.934682000
C	-3.946609000	2.432754000	0.229662000
H	-4.856061000	3.009774000	0.398796000
C	-3.227854000	1.932353000	1.313007000
H	-3.548465000	2.102766000	2.340052000
C	-2.076564000	1.202726000	1.064543000
C	-1.146151000	0.693775000	2.130719000
H	-1.663413000	0.507398000	3.080192000
H	-0.376225000	1.459359000	2.307336000
C	-1.332033000	-1.773084000	1.895771000
H	-2.093461000	-1.525985000	2.644642000
H	-0.701741000	-2.562336000	2.320743000
C	-1.989309000	-2.227908000	0.603351000
H	-2.408650000	-3.238236000	0.721752000
H	-2.799070000	-1.547066000	0.307979000
C	-1.635932000	-2.314388000	-1.814149000
H	-2.233149000	-3.237108000	-1.863073000
H	-0.859432000	-2.334742000	-2.589998000
H	-2.287670000	-1.443078000	-1.965431000
C	0.054663000	-3.293308000	-0.331781000
H	-0.172787000	-4.111979000	-1.027033000
H	-0.018824000	-3.705738000	0.680669000
C	1.453065000	-2.753384000	-0.622258000
H	2.222367000	-3.491621000	-0.352649000
H	1.550306000	-2.506113000	-1.688986000
C	1.731873000	-1.712522000	1.628909000
H	2.771210000	-1.615837000	1.967961000
H	1.421666000	-2.742847000	1.833875000
C	0.859286000	-0.707470000	2.372072000
H	0.680985000	-1.031689000	3.406849000
H	1.337315000	0.278945000	2.394945000
C	2.852584000	-0.719873000	-0.353541000
H	2.885234000	-0.825375000	-1.448242000
H	3.783400000	-1.124193000	0.065716000
C	2.681593000	0.744600000	-0.022068000
C	3.751344000	1.591374000	0.224410000
H	4.763048000	1.187505000	0.242156000
C	3.502840000	2.943228000	0.443596000
H	4.329013000	3.626393000	0.641739000
C	2.193552000	3.411992000	0.407441000
H	1.958646000	4.463203000	0.565191000
C	1.168452000	2.509573000	0.169600000
H	0.125270000	2.827793000	0.135767000
O	0.459135000	0.066285000	-2.753611000

ANNEX

O	0.615637000	1.218532000	-3.031245000

H₂O (singlet, G = -47968.7312)

O	0.000000000	0.000000000	0.119648000
H	0.000000000	0.761424000	-0.478593000
H	0.000000000	-0.761424000	-0.478593000

(H₂O)₄ (singlet, G = -191859.6716)

O	1.416766000	2.121366000	-1.469570000
H	0.727859000	1.481170000	-1.697880000
H	2.221525000	1.771353000	-1.913048000
O	3.742560000	1.116829000	-2.652619000
H	4.375422000	1.519324000	-2.027525000
H	3.691912000	0.201840000	-2.304037000
O	5.392465000	1.258801000	-0.356892000
H	5.062085000	1.683098000	0.450273000
H	6.358811000	1.278176000	-0.275020000
O	4.169968000	-1.158887000	-1.059360000
H	4.825237000	-1.637577000	-1.590181000
H	4.680055000	-0.425125000	-0.652198000

H₂O⁺·(H₂O)₂ (singlet, G = -144164.3027)

H	2.753368000	0.528127000	-1.767276000
O	3.725090000	0.511872000	-1.868242000
H	4.115320000	1.329637000	-1.341606000
H	4.079548000	-0.373747000	-1.433987000
O	4.714458000	2.484796000	-0.608457000
H	3.978967000	2.992875000	-0.226032000
H	5.100849000	3.071770000	-1.280688000
O	4.610942000	-1.631228000	-0.827156000
H	4.391895000	-2.350189000	-1.443956000
H	5.580506000	-1.562150000	-0.859668000

O₂ (singlet, G = -94346.1689)

O	0.000000000	0.000000000	0.597893000
O	0.000000000	0.000000000	-0.597893000

1Feᴵᴵ-OTf complex

[(Py₂ᴹᵉtacn)Feᴵⱽ=O] (triplet, G = -1476453.9567)

Fe	0.037344000	-0.335385000	-0.446602000
N	-1.537672000	0.892376000	-0.361200000
N	-0.350695000	-0.435161000	1.621028000
N	-1.067361000	-2.072340000	-0.506855000
N	1.607593000	-1.497603000	-0.027762000
N	1.398485000	1.139962000	-0.246082000
C	-2.238662000	1.314495000	-1.432226000
H	-1.891713000	0.965055000	-2.396942000
C	-3.340595000	2.149266000	-1.304835000
H	-3.877080000	2.464851000	-2.192475000
C	-3.733078000	2.557682000	-0.030340000
H	-4.595895000	3.202716000	0.101357000
C	-3.004489000	2.125593000	1.075990000
H	-3.275654000	2.422102000	2.083432000
C	-1.903291000	1.298728000	0.880033000
C	-0.995718000	0.853353000	1.996128000

H	-1.537524000	0.766207000	2.942200000
H	-0.214506000	1.607348000	2.139476000
C	-1.268728000	-1.596691000	1.912404000
H	-1.987038000	-1.314156000	2.686275000
H	-0.669968000	-2.412171000	2.318363000
C	-2.004632000	-2.036822000	0.657237000
H	-2.452460000	-3.026046000	0.806392000
H	-2.807780000	-1.342287000	0.407037000
C	-1.863686000	-2.228713000	-1.754838000
H	-2.473798000	-3.135979000	-1.682015000
H	-1.190964000	-2.309857000	-2.607819000
H	-2.517651000	-1.366315000	-1.885414000
C	-0.096065000	-3.232990000	-0.388237000
H	-0.403958000	-4.030777000	-1.068556000
H	-0.156608000	-3.639231000	0.621283000
C	1.323103000	-2.795204000	-0.718927000
H	2.045905000	-3.558086000	-0.410213000
H	1.434619000	-2.621416000	-1.789513000
C	1.760027000	-1.684806000	1.474542000
H	2.820166000	-1.640864000	1.734692000
H	1.414437000	-2.687335000	1.724812000
C	0.985866000	-0.628120000	2.257710000
H	0.881414000	-0.937016000	3.303718000
H	1.508105000	0.328340000	2.241197000
C	2.796840000	-0.799896000	-0.597757000
H	2.808130000	-0.975529000	-1.677557000
H	3.722725000	-1.204756000	-0.180018000
C	2.668855000	0.677036000	-0.349228000
C	3.762580000	1.534516000	-0.298934000
H	4.764654000	1.126012000	-0.371855000
C	3.544674000	2.903520000	-0.160633000
H	4.384264000	3.590119000	-0.120375000
C	2.235826000	3.376341000	-0.076558000
H	2.018035000	4.433305000	0.026378000
C	1.189283000	2.464873000	-0.120966000
H	0.160929000	2.798685000	-0.063109000
O	0.232146000	-0.310814000	-2.069701000

[(Py₂ᴹᵉtacn)Feⱽ=O] (quadruplet, G = -1476305.6573)

N	-1.530927000	0.890926000	-0.353040000
N	-0.369315000	-0.446657000	1.617711000
N	-1.043022000	-2.098668000	-0.515160000
N	1.609117000	-1.477084000	-0.030477000
N	1.405673000	1.136566000	-0.225842000
C	-2.193661000	1.327126000	-1.451552000
H	-1.823439000	0.984993000	-2.409819000
C	-3.290086000	2.164063000	-1.338767000
H	-3.801025000	2.493786000	-2.235767000
C	-3.712316000	2.559876000	-0.067955000
H	-4.574285000	3.208968000	0.045895000
C	-3.020188000	2.115659000	1.058050000
H	-3.317803000	2.407085000	2.059108000
C	-1.922052000	1.284839000	0.892549000
C	-1.041668000	0.827193000	2.017827000
H	-1.606476000	0.693903000	2.943217000
H	-0.280321000	1.590025000	2.208941000
C	-1.275033000	-1.629879000	1.900000000
H	-2.000002000	-1.354992000	2.668200000
H	-0.665165000	-2.435231000	2.307034000
C	-1.998605000	-2.066999000	0.640569000
H	-2.422918000	-3.068249000	0.770218000

ANNEX

H	-2.810047000	-1.387914000	0.377883000
C	-1.804374000	-2.242403000	-1.792478000
H	-2.395075000	-3.161902000	-1.726772000
H	-1.106346000	-2.313162000	-2.626224000
H	-2.472217000	-1.392372000	-1.926459000
C	-0.050139000	-3.251068000	-0.384931000
H	-0.359872000	-4.047891000	-1.063816000
H	-0.109993000	-3.643907000	0.628400000
C	1.344758000	-2.782549000	-0.732617000
H	2.099255000	-3.513070000	-0.424092000
H	1.443449000	-2.601745000	-1.803324000
C	1.767835000	-1.658687000	1.481151000
H	2.828346000	-1.577914000	1.726387000
H	1.455068000	-2.673028000	1.724336000
C	0.971387000	-0.622849000	2.263556000
H	0.852256000	-0.947233000	3.302065000
H	1.475631000	0.342483000	2.266283000
C	2.798796000	-0.781694000	-0.622835000
H	2.791678000	-0.952777000	-1.703492000
H	3.715749000	-1.212253000	-0.213589000
C	2.678568000	0.683788000	-0.355464000
C	3.759381000	1.554154000	-0.310363000
H	4.763888000	1.156153000	-0.401192000
C	3.524360000	2.918169000	-0.153013000
H	4.355462000	3.614769000	-0.117264000
C	2.211942000	3.374687000	-0.044818000
H	1.980829000	4.427093000	0.072028000
C	1.171516000	2.457434000	-0.084498000
H	0.142725000	2.783335000	-0.010349000
O	0.211073000	-0.290654000	-2.049382000
Fe	0.004956000	-0.327479000	-0.422369000

A.IX.3. Corrdinates from chapter VI

In parenthesis are indicated the most stable spin multiplicity and the corrected free energies (G), given in kcal·mol^{-1}.

^{1}[η^1-1Ru^{IV}-OO] (singlet, G = -789630.8132)

44	0.019794000	-0.324585000	-0.349088000
7	-1.680811000	0.975112000	-0.258727000
7	-0.451060000	-0.398767000	1.711716000
7	-0.981690000	-2.182201000	-0.387790000
7	1.682240000	-1.444621000	0.203050000
7	1.443254000	1.243017000	-0.154715000
6	-2.425631000	1.341910000	-1.310671000
1	-2.046814000	1.054294000	-2.291992000
6	-3.607983000	2.050346000	-1.151051000
1	-4.187440000	2.335335000	-2.027613000
6	-4.027267000	2.372019000	0.135926000
1	-4.956196000	2.920435000	0.294244000
6	-3.252150000	1.981420000	1.223984000
1	-3.548124000	2.208689000	2.247689000
6	-2.076779000	1.283686000	0.992273000
6	-1.123432000	0.874790000	2.084550000
1	-1.630121000	0.783199000	3.054342000
1	-0.352615000	1.655035000	2.175747000
6	-1.329054000	-1.592291000	1.987796000
1	-2.104479000	-1.312726000	2.712588000
1	-0.713128000	-2.366419000	2.460519000
6	-1.979972000	-2.120190000	0.714025000

1	-2.408873000	-3.117945000	0.895451000
1	-2.787314000	-1.454757000	0.378365000
6	-1.663183000	-2.391016000	-1.686388000
1	-2.267755000	-3.309763000	-1.648247000
1	-0.906867000	-2.481074000	-2.475924000
1	-2.311288000	-1.529389000	-1.897643000
6	0.043163000	-3.262403000	-0.161803000
1	-0.185350000	-4.118932000	-0.809641000
1	-0.041411000	-3.617470000	0.871493000
6	1.455811000	-2.764667000	-0.467361000
1	2.205854000	-3.494311000	-0.128906000
1	1.581155000	-2.603696000	-1.546558000
6	1.722886000	-1.585438000	1.706139000
1	2.763797000	-1.501285000	2.043482000
1	1.383767000	-2.594414000	1.963812000
6	0.872867000	-0.524071000	2.398470000
1	0.727043000	-0.785168000	3.456878000
1	1.365152000	0.455268000	2.349831000
6	2.877278000	-0.721200000	-0.312910000
1	2.953153000	-0.918984000	-1.391395000
1	3.791826000	-1.087808000	0.171920000
6	2.707094000	0.769110000	-0.105727000
6	3.785907000	1.622645000	0.077539000
1	4.794267000	1.212429000	0.125010000
6	3.550911000	2.988875000	0.199291000
1	4.384263000	3.676286000	0.346714000
6	2.245622000	3.466433000	0.135866000
1	2.020822000	4.527887000	0.226324000
6	1.213151000	2.557663000	-0.038744000
1	0.170051000	2.875914000	-0.088182000
8	0.677830000	-0.427526000	-2.315547000
8	0.249259000	0.607227000	-2.988250000

^{3}[η^1-1Ru^{IV}-OO] (triplet, G = -789626.7156)

44	0.019794000	-0.324585000	-0.349088000
7	-1.680811000	0.975112000	-0.258727000
7	-0.451060000	-0.398767000	1.711716000
7	-0.981690000	-2.182201000	-0.387790000
7	1.682240000	-1.444621000	0.203050000
7	1.443254000	1.243017000	-0.154715000
6	-2.425631000	1.341910000	-1.310671000
1	-2.046814000	1.054294000	-2.291992000
6	-3.607983000	2.050346000	-1.151051000
1	-4.187440000	2.335335000	-2.027613000
6	-4.027267000	2.372019000	0.135926000
1	-4.956196000	2.920435000	0.294244000
6	-3.252150000	1.981420000	1.223984000
1	-3.548124000	2.208689000	2.247689000
6	-2.076779000	1.283686000	0.992273000
6	-1.123432000	0.874790000	2.084550000
1	-1.630121000	0.783199000	3.054342000
1	-0.352615000	1.655035000	2.175747000
6	-1.329054000	-1.592291000	1.987796000
1	-2.104479000	-1.312726000	2.712588000
1	-0.713128000	-2.366419000	2.460519000
6	-1.979972000	-2.120190000	0.714025000
1	-2.408873000	-3.117945000	0.895451000
1	-2.787314000	-1.454757000	0.378365000
6	-1.663183000	-2.391016000	-1.686388000
1	-2.267755000	-3.309763000	-1.648247000
1	-0.906867000	-2.481074000	-2.475924000
1	-2.311288000	-1.529389000	-1.897643000
6	0.043163000	-3.262403000	-0.161803000
1	-0.185350000	-4.118932000	-0.809641000
1	-0.041411000	-3.617470000	0.871493000
6	1.455811000	-2.764667000	-0.467361000
1	2.205854000	-3.494311000	-0.128906000
1	1.581155000	-2.603696000	-1.546558000
6	1.722886000	-1.585438000	1.706139000

1	2.763797000	-1.501285000	2.043482000
1	1.383767000	-2.594414000	1.963812000
6	0.872867000	-0.524071000	2.398470000
1	0.727043000	-0.785168000	3.456878000
1	1.365152000	0.455268000	2.349831000
6	2.877278000	-0.721202000	-0.312910000
1	2.953153000	-0.918984000	-1.391395000
1	3.791826000	-1.087808000	0.171920000
6	2.707094000	0.769110000	-0.105727000
6	3.785907000	1.622645000	0.077539000
1	4.794267000	1.212429000	0.125010000
6	3.550911000	2.988875000	0.199291000
1	4.384263000	3.676286000	0.346714000
6	2.245622000	3.466433000	0.135866000
1	2.020822000	4.527887000	0.226324000
6	1.213151000	2.557663000	-0.038744000
1	0.170051000	2.875914000	-0.088182000
8	0.677830000	-0.427526000	-2.315547000
8	0.249259000	0.607227000	-2.988250000

$^{1}[\eta^{2}\text{-}1Ru^{IV}\text{-}OO]$ (singlet, G = -789631.0057)

44	0.034860000	-0.280736000	-0.396646000
7	-1.705669000	0.942554000	-0.276986000
7	-0.381581000	-0.248379000	1.671027000
7	-1.069229000	-2.097839000	-0.351202000
7	1.629850000	-1.469230000	0.280319000
7	1.516759000	1.214438000	-0.294714000
6	-2.532399000	1.204922000	-1.301115000
1	-2.256986000	0.794962000	-2.271646000
6	-3.683920000	1.958471000	-1.130699000
1	-4.327382000	2.149727000	-1.987846000
6	-3.993771000	2.441592000	0.136057000
1	-4.896989000	3.029620000	0.300090000
6	-3.139238000	2.157358000	1.196092000
1	-3.343964000	2.505617000	2.207862000
6	-1.999520000	1.407882000	0.953356000
6	-0.980138000	1.074606000	1.999600000
1	-1.410026000	1.058318000	3.009884000
1	-0.180343000	1.830545000	1.975730000
6	-1.338760000	-1.371625000	2.006138000
1	-2.089126000	-0.999110000	2.715235000
1	-0.771241000	-2.150977000	2.526727000
6	-2.035349000	-1.936140000	0.769937000
1	-2.492836000	-2.906301000	1.019263000
1	-2.831646000	-1.265469000	0.421592000
6	-1.797367000	-2.373497000	-1.608990000
1	-2.377219000	-3.303494000	-1.506994000
1	-1.073320000	-2.479212000	-2.425572000
1	-2.478369000	-1.540595000	-1.824904000
6	-0.091402000	-3.213886000	-0.062129000
1	-0.338258000	-4.076659000	-0.694141000
1	-0.232543000	-3.537267000	0.975625000
6	1.366508000	-2.820127000	-0.311725000
1	2.038745000	-3.562459000	0.142587000
1	1.579850000	-2.763658000	-1.383335000
6	1.669037000	-1.559623000	1.784917000
1	2.713489000	-1.560926000	2.119047000
1	1.234712000	-2.520200000	2.081171000
6	0.911588000	-0.401841000	2.399594000
1	0.720872000	-0.574199000	3.468698000
1	1.469861000	0.536250000	2.291744000
6	2.869953000	-0.821114000	-0.241708000
1	2.992879000	-1.114807000	-1.291571000

1	3.746748000	-1.173119000	0.317004000
6	2.754484000	0.687237000	-0.172525000
6	3.869928000	1.503447000	-0.046473000
1	4.855965000	1.052412000	0.062026000
6	3.700591000	2.884366000	-0.063188000
1	4.564165000	3.542851000	0.033903000
6	2.421749000	3.415076000	-0.199601000
1	2.247898000	4.489684000	-0.215349000
6	1.348699000	2.543059000	-0.308227000
1	0.321354000	2.900499000	-0.406059000
8	0.803731000	-0.789665000	-2.184548000
8	-0.150614000	0.154484000	-2.340866000

$1Ru^{III}\text{-}OOH$ (doblet, G = -934183.4767)

Ru	-0.546038000	-0.332125000	-0.244532000
N	-1.706172000	1.440112000	-0.362436000
N	-1.669505000	-0.482128000	1.548364000
N	-2.034664000	-1.665739000	-0.970588000
N	0.395581000	-2.062101000	0.422424000
N	1.149311000	0.539719000	0.699685000
C	-1.900227000	2.174313000	-1.465713000
H	-1.375434000	1.845432000	-2.364631000
C	-2.720278000	3.292793000	-1.457219000
H	-2.852399000	3.873394000	-2.368715000
C	-3.363103000	3.640763000	-0.272594000
H	-4.019476000	4.510538000	-0.234969000
C	-3.168704000	2.863559000	0.865407000
H	-3.660847000	3.099766000	1.808475000
C	-2.324291000	1.765047000	0.790779000
C	-1.976738000	0.906220000	1.984946000
H	-2.780941000	0.916135000	2.733794000
H	-1.073654000	1.322692000	2.456141000
C	-2.922843000	-1.278848000	1.305886000
H	-3.758558000	-0.817726000	1.848278000
H	-2.783166000	-2.279650000	1.732214000
C	-3.257898000	-1.364656000	-0.179068000
H	-4.020079000	-2.141494000	-0.347850000
H	-3.655049000	-0.409590000	-0.549399000
C	-2.317550000	-1.482128000	-2.411095000
H	-3.167926000	-2.115213000	-2.707927000
H	-1.430360000	-1.764847000	-2.990280000
H	-2.558203000	-0.427801000	-2.601640000
C	-1.544749000	-3.067883000	-0.718421000
H	-1.838596000	-3.711359000	-1.558793000
H	-2.047906000	-3.464560000	0.170829000
C	-0.027145000	-3.108322000	-0.555787000
H	0.300663000	-4.104297000	-0.221881000
H	0.464514000	-2.872365000	-1.509767000
C	-0.073519000	-2.372592000	1.823327000
H	0.787253000	-2.691781000	2.425625000
H	-0.757928000	-3.226094000	1.769272000
C	-0.747701000	-1.175143000	2.501223000
H	-1.301837000	-1.514814000	3.388789000
H	0.000661000	-0.442359000	2.826508000
C	1.851756000	-1.768419000	0.381969000
H	2.160798000	-1.779238000	-0.673481000
H	2.425363000	-2.531726000	0.925573000
C	2.106233000	-0.383018000	0.939529000
C	3.274510000	-0.048174000	1.612285000
H	4.024951000	-0.815723000	1.798466000
C	3.456237000	1.265103000	2.033624000

ANNEX

H	4.365001000	1.549795000	2.564863000
C	2.470484000	2.211713000	1.765615000
H	2.578882000	3.251054000	2.072859000
C	1.328124000	1.808206000	1.091182000
H	0.524631000	2.509037000	0.854910000
O	0.376313000	-0.259573000	-1.981351000
O	1.115585000	0.961144000	-2.117031000
H	1.014630000	1.160882000	-3.066506000
H	2.714777000	0.592074000	-1.877211000
O	3.717261000	0.509281000	-1.826837000
H	4.095962000	1.306621000	-1.288646000
H	4.016468000	-0.373026000	-1.394965000
O	4.724570000	2.519661000	-0.583593000
H	3.980739000	3.044443000	-0.243525000
H	5.113601000	3.063115000	-1.289883000
O	4.654896000	-1.684531000	-0.811660000
H	4.416421000	-2.396258000	-1.429114000
H	5.616250000	-1.579616000	-0.911634000

1Ru^{IV}-OOH (triplet, G = -934045.5454)

44	0.808398000	-0.255374000	0.274517000
7	0.973067000	1.861947000	0.089618000
7	1.824651000	-0.148519000	-1.522147000
7	2.740855000	-0.638010000	1.039977000
7	0.754919000	-2.312513000	-0.084584000
7	-1.130860000	-0.461643000	-0.602071000
6	0.855239000	2.769889000	1.067777000
1	0.528567000	2.398934000	2.039195000
6	1.142580000	4.109586000	0.847874000
1	1.036704000	4.823681000	1.662591000
6	1.567129000	4.505994000	-0.416265000
1	1.802962000	5.551242000	-0.617253000
6	1.696188000	3.555696000	-1.425568000
1	2.033089000	3.825438000	-2.426009000
6	1.390738000	2.235642000	-1.140205000
6	1.428855000	1.136330000	-2.170127000
1	2.107825000	1.373885000	-2.999174000
1	0.416076000	1.010809000	-2.581470000
6	3.320141000	-0.219903000	-1.309378000
1	3.811071000	0.497619000	-1.978003000
1	3.656230000	-1.219872000	-1.606676000
6	3.684259000	0.074864000	0.137741000
1	4.718489000	-0.239022000	0.344035000
1	3.598119000	1.147655000	0.358190000
6	2.840068000	-0.119694000	2.425730000
1	3.865386000	-0.259864000	2.798820000
1	2.133841000	-0.669506000	3.060806000
1	2.590364000	0.949517000	2.436023000
6	2.956374000	-2.128237000	1.031699000
1	3.514131000	-2.413041000	1.933550000
1	3.585137000	-2.389954000	0.173781000
6	1.625453000	-2.872155000	1.001743000
1	1.781395000	-3.948813000	0.841226000
1	1.086480000	-2.724327000	1.948443000
6	1.326229000	-2.580340000	-1.458690000
1	0.726287000	-3.354449000	-1.953284000
1	2.334743000	-2.989895000	-1.336125000
6	1.337907000	-1.322040000	-2.323160000
1	1.986376000	-1.465938000	-3.198732000
1	0.327403000	-1.084983000	-2.677040000

6	-0.655143000	-2.765223000	0.030779000
1	-0.897806000	-2.857883000	1.099240000
1	-0.791215000	-3.750394000	-0.434372000
6	-1.578525000	-1.734975000	-0.578268000
6	-2.853761000	-2.056626000	-1.022978000
1	-3.182085000	-3.095426000	-1.000946000
6	-3.686223000	-1.037648000	-1.474318000
1	-4.694555000	-1.265941000	-1.820638000
6	-3.219296000	0.274635000	-1.477964000
1	-3.842375000	1.101262000	-1.818872000
6	-1.930302000	0.525307000	-1.035016000
1	-1.514005000	1.534852000	-1.020109000
8	-0.522179000	-0.515944000	2.003350000
8	-1.209309000	0.580264000	2.154831000
1	-2.142988000	0.272643000	2.428538000
1	-4.334442000	2.163779000	0.553806000
8	-4.979194000	1.569393000	0.986700000
1	-5.598239000	1.134962000	0.232727000
1	-4.455998000	0.829017000	1.444009000
8	-6.447893000	0.480865000	-0.726573000
1	-6.219486000	0.803717000	-1.615411000
1	-7.361779000	0.776581000	-0.570853000
8	-3.614883000	-0.327793000	2.195748000
1	-4.067051000	-0.645441000	2.997748000
1	-3.546365000	-1.094205000	1.597073000

1Ru^{II}-NCCH_3 (in MeCN)

(singlet, G = -778585.1328)

44	-0.001324000	-0.282512000	0.111752000
7	-1.489195000	1.236313000	0.075502000
6	-1.341814000	2.562224000	0.187564000
1	-0.323245000	2.918437000	0.357739000
7	-1.584274000	-1.374882000	-0.738996000
6	-2.414955000	3.438808000	0.089779000
1	-2.248305000	4.510858000	0.187750000
7	0.601253000	0.009936000	-1.879077000
6	-3.682976000	2.916084000	-0.141106000
1	-4.546685000	3.575680000	-0.233720000
7	1.096041000	-2.117304000	-0.099079000
6	-3.836859000	1.537453000	-0.256470000
1	-4.813431000	1.088842000	-0.440407000
7	1.703992000	0.933220000	0.465369000
6	-2.720842000	0.719356000	-0.132866000
7	-0.519287000	-0.616878000	2.107138000
6	-2.821883000	-0.794530000	-0.173546000
1	-2.920326000	-1.162627000	0.858866000
1	-3.714373000	-1.108104000	-0.736606000
6	-1.526998000	-1.209995000	-2.233052000
1	-2.544881000	-1.079363000	-2.627552000
1	-1.140577000	-2.140823000	-2.665033000
6	-0.661985000	-0.018416000	-2.666929000
1	-0.452284000	-0.085375000	-3.746505000
1	-1.187243000	0.926190000	-2.478409000
6	1.538498000	-1.082050000	-2.304874000
1	2.341404000	-0.658676000	-2.925268000
1	0.980493000	-1.778558000	-2.942167000
6	2.141402000	-1.816688000	-1.109287000
1	2.631027000	-2.744517000	-1.450944000
1	2.899544000	-1.195766000	-0.611452000

ANNEX

6	1.729969000	-2.587154000	1.146940000
1	2.374607000	-3.459362000	0.947097000
1	0.949264000	-2.873341000	1.862833000
1	2.333318000	-1.775504000	1.575569000
6	0.129107000	-3.151796000	-0.604132000
1	0.285746000	-3.285581000	-1.681193000
1	0.351513000	-4.121060000	-0.134929000
6	-1.327573000	-2.777218000	-0.315208000
1	-2.003669000	-3.481547000	-0.827623000
1	-1.521773000	-2.824878000	0.765469000
6	1.264020000	1.336792000	-1.894459000
1	0.474409000	2.102818000	-1.852543000
1	1.838633000	1.490214000	-2.820432000
6	2.150073000	1.503687000	-0.676463000
6	3.329854000	2.236326000	-0.708962000
1	3.667177000	2.671045000	-1.650156000
6	4.057137000	2.400302000	0.466985000
1	4.985725000	2.972250000	0.464242000
6	3.585621000	1.821343000	1.640295000
1	4.123300000	1.923622000	2.582149000
6	2.405301000	1.089832000	1.595057000
1	1.998150000	0.603502000	2.483599000
6	-0.799247000	-0.780472000	3.213948000
6	-1.148162000	-0.996797000	4.613662000
1	-2.036328000	-0.403526000	4.862449000
1	-0.309151000	-0.688604000	5.249222000
1	-1.359633000	-2.061099000	4.773620000

$^1[\eta^2\text{-}1Ru^{IV}\text{-}OO]$ (in MeCN)

(singlet, G = -789640.1327)

44	0.040090000	-0.276041000	-0.383410000
7	-1.706693000	0.942653000	-0.273368000
7	-0.406659000	-0.288667000	1.677313000
7	-1.049653000	-2.099804000	-0.395778000
7	1.639110000	-1.464458000	0.283310000
7	1.508868000	1.228045000	-0.251932000
6	-2.512608000	1.236643000	-1.305454000
1	-2.217142000	0.852064000	-2.280776000
6	-3.667869000	1.985681000	-1.136454000
1	-4.294220000	2.202379000	-2.000613000
6	-4.002545000	2.432896000	0.137248000
1	-4.909196000	3.016498000	0.300375000
6	-3.168067000	2.119132000	1.205139000
1	-3.392442000	2.441253000	2.221666000
6	-2.022600000	1.376976000	0.963114000
6	-1.018080000	1.024814000	2.019437000
1	-1.463734000	0.991002000	3.022698000
1	-0.220893000	1.784042000	2.017369000
6	-1.359670000	-1.425362000	1.973420000
1	-2.124520000	-1.074608000	2.678344000
1	-0.792403000	-2.212369000	2.483280000
6	-2.033197000	-1.969583000	0.713988000
1	-2.487903000	-2.947727000	0.936986000
1	-2.827965000	-1.296650000	0.366913000
6	-1.753527000	-2.350060000	-1.672526000
1	-2.316548000	-3.293797000	-1.609160000
1	-1.011691000	-2.409907000	-2.477605000
1	-2.445603000	-1.522629000	-1.872046000
6	-0.067048000	-3.214020000	-0.115909000

1	-0.299448000	-4.066762000	-0.767272000
1	-0.218710000	-3.555763000	0.914630000
6	1.391861000	-2.805090000	-0.338757000
1	2.063545000	-3.552797000	0.108156000
1	1.614675000	-2.722934000	-1.406743000
6	1.659726000	-1.583646000	1.786078000
1	2.699837000	-1.575184000	2.134282000
1	1.235991000	-2.556369000	2.057903000
6	0.878812000	-0.448932000	2.417913000
1	0.677936000	-0.649180000	3.480442000
1	1.427959000	0.496978000	2.337943000
6	2.878733000	-0.798516000	-0.217256000
1	3.015252000	-1.081914000	-1.268601000
1	3.752799000	-1.145828000	0.348902000
6	2.751168000	0.709996000	-0.144986000
6	3.863253000	1.534428000	-0.037031000
1	4.853969000	1.090689000	0.060660000
6	3.685299000	2.914162000	-0.062134000
1	4.546100000	3.578888000	0.018708000
6	2.401207000	3.435571000	-0.187764000
1	2.220343000	4.509161000	-0.212034000
6	1.332668000	2.555257000	-0.275739000
1	0.301214000	2.903441000	-0.362945000
8	0.824450000	-0.757165000	-2.172487000
8	-0.133334000	0.174336000	-2.324039000

O_2 (in MeCN)

(singlet, G = -94315.4753)

8	0.000000000	0.000000000	0.599464000
8	0.000000000	0.000000000	-0.599464000

CH_3CN (in MeCN)

(singlet, G = -83283.3989)

7	-1.435655000	-0.000010000	0.000014000
6	-0.279634000	0.000068000	-0.000050000
6	1.180834000	0.000016000	-0.000050000
1	1.547154000	-0.197151000	1.014681000
1	1.547886000	0.977227000	-0.336527000
1	1.547345000	-0.780509000	-0.677646000

$1Ru^{II}\text{-}OH_2$ (in H_2O)

(singlet, G = -743253.814)

Ru	0.007834000	-0.284578000	-0.402008000
N	-1.699106000	0.991815000	-0.414238000
N	-0.337186000	-0.201968000	1.653649000
N	-1.101859000	-2.121055000	-0.255589000
N	1.650367000	-1.494100000	0.125226000
N	1.547823000	1.194229000	-0.374935000
C	-2.550071000	1.269702000	-1.410759000
H	-2.280252000	0.891830000	-2.398575000
C	-3.712829000	2.004443000	-1.216689000
H	-4.369979000	2.208137000	-2.060992000
C	-4.012233000	2.453161000	0.064933000
H	-4.921340000	3.024115000	0.255951000
C	-3.135032000	2.157880000	1.104712000

ANNEX

H	-3.334070000	2.484317000	2.125528000
C	-1.983141000	1.431988000	0.832467000
C	-0.951815000	1.125619000	1.897616000
H	-1.395025000	1.184184000	2.902898000
H	-0.153470000	1.880669000	1.834484000
C	-1.255392000	-1.312292000	2.077479000
H	-1.968937000	-0.936187000	2.824223000
H	-0.653030000	-2.080514000	2.577512000
C	-2.013923000	-1.912455000	0.895111000
H	-2.482687000	-2.863482000	1.201011000
H	-2.811117000	-1.235557000	0.556684000
C	-1.879103000	-2.439781000	-1.465864000
H	-2.513193000	-3.326896000	-1.299772000
H	-1.188016000	-2.646798000	-2.293894000
H	-2.514809000	-1.582365000	-1.727143000
C	-0.113478000	-3.217239000	0.024196000
H	-0.417681000	-4.131476000	-0.505895000
H	-0.142849000	-3.457249000	1.093688000
C	1.307370000	-2.840367000	-0.398434000
H	2.019262000	-3.603422000	-0.042170000
H	1.376631000	-2.791248000	-1.494332000
C	1.786485000	-1.481587000	1.622424000
H	2.848788000	-1.397639000	1.894436000
H	1.441151000	-2.448703000	2.007782000
C	1.006584000	-0.334934000	2.280781000
H	0.918487000	-0.518793000	3.363480000
H	1.531715000	0.618354000	2.138803000
C	2.820322000	-0.878053000	-0.535141000
H	2.755299000	-1.106499000	-1.609988000
H	3.768547000	-1.287393000	-0.153909000
C	2.775031000	0.626225000	-0.354667000
C	3.926022000	1.387529000	-0.198602000
H	4.896753000	0.892458000	-0.173914000
C	3.813084000	2.768753000	-0.070701000
H	4.703936000	3.385062000	0.054440000
C	2.549250000	3.348054000	-0.098050000
H	2.411714000	4.423883000	0.001281000
C	1.441699000	2.523304000	-0.248402000
H	0.427679000	2.928790000	-0.266825000
O	0.272005000	-0.374299000	-2.638957000
H	-0.598819000	-0.501786000	-3.051801000
H	0.791325000	-1.152122000	-2.906207000

O₂ (in H₂O)

(singlet, G = -94346.1689)

O	0.000000000	0.000000000	0.597893000
O	0.000000000	0.000000000	-0.597893000

H₂O (in H₂O)

(singlet, G = -47968.7312)

O	0.000000000	0.000000000	0.119648000
H	0.000000000	0.761424000	-0.478593000
H	0.000000000	-0.761424000	-0.478593000

H₂O⁺·(H₂O)₂

(singlet, G = -144164.3027)

H	2.753368000	0.528127000	-1.767276000
O	3.725090000	0.511872000	-1.868242000
H	4.115320000	1.329637000	-1.341606000
H	4.079548000	-0.373747000	-1.433987000
O	4.714458000	2.484796000	-0.608457000
H	3.978967000	2.992875000	-0.226032000
H	5.100849000	3.071770000	-1.280688000
O	4.610942000	-1.631228000	-0.827156000
H	4.391895000	-2.350189000	-1.443956000
H	5.580506000	-1.562150000	-0.85966800

A.IX.4. Corrdinates from chapter VII

[Feᴵᴵ(H₂O)(AQtacn)]⁺

(G= -2428.981823) (quintuplet)

7	-1.258868000	-0.808775000	1.692323000
6	-2.683782000	-1.224190000	1.650406000
6	-3.043284000	-1.840721000	0.296555000
7	-2.563604000	-1.065610000	-0.879948000
6	-3.384889000	0.124917000	-1.216327000
6	-3.323963000	1.244291000	-0.175297000
7	-1.936774000	1.499990000	0.292446000
6	-1.054595000	0.460198000	2.421330000
6	-1.812203000	1.637990000	1.770485000
6	-1.313197000	2.626484000	-0.418124000
6	0.215406000	2.625535000	-0.276134000
7	0.724832000	1.384646000	-0.172177000
26	-0.590394000	-0.268104000	-0.364389000
6	-0.428924000	-1.874343000	2.273200000
6	-2.543821000	-1.967410000	-2.052282000
8	-0.148146000	0.068331000	-2.641456000
1	-3.320182000	-0.373516000	1.881292000
1	-2.884725000	-1.971782000	2.429323000
1	-4.130208000	-1.994514000	0.232347000
1	-2.559696000	-2.820627000	0.233520000
1	-4.433878000	-0.169965000	-1.371729000
1	-2.998712000	0.505822000	-2.166946000
1	-3.960358000	1.000840000	0.674296000
1	-3.750206000	2.149444000	-0.627064000
1	0.021375000	0.656332000	2.398884000
1	-1.364555000	0.365970000	3.473340000
1	-1.268523000	2.558093000	2.009279000
1	-2.807091000	1.739861000	2.213990000
1	-1.548082000	2.524951000	-1.485407000
1	-0.550461000	-2.785771000	1.679794000
1	0.621584000	-1.573727000	2.243436000
1	-0.720419000	-2.080762000	3.315250000
1	-1.850681000	-2.791827000	-1.858224000
1	-3.546164000	-2.377347000	-2.249767000
1	-2.206211000	-1.416687000	-2.933403000
8	0.816801000	3.721972000	-0.321417000
6	2.080129000	1.087825000	-0.061569000
6	2.393509000	-0.318721000	-0.119890000
6	3.138933000	1.977269000	0.119900000
6	3.739873000	-0.772928000	0.005311000
6	4.470208000	1.515414000	0.242817000
1	2.934984000	3.037334000	0.165380000
6	1.612035000	-2.500113000	-0.342328000
6	3.972052000	-2.170868000	-0.059051000
6	4.780885000	0.173488000	0.188326000
1	5.260826000	2.247819000	0.383883000
6	2.912757000	-3.034393000	-0.234488000
1	0.752780000	-3.153586000	-0.467750000
1	4.990087000	-2.539931000	0.033650000

ANNEX

1	5.804176000	-0.178521000	0.282696000
1	3.057340000	-4.108402000	-0.284944000
7	1.357518000	-1.198918000	-0.295229000
1	-1.703338000	3.594379000	-0.072363000
1	0.476521000	0.801367000	-2.496017000
1	-0.939694000	0.505362000	-2.998595000

[Fe^{III}(H$_2$O)(AQtacn)]$^{2+}$

(G= -2428.814812) (sextuplet)

7	-1.035315000	-0.753875000	1.677758000
6	-2.449712000	-1.240719000	1.771221000
6	-2.912228000	-1.872700000	0.461341000
7	-2.573336000	-1.083838000	-0.765420000
6	-3.481239000	0.056781000	-1.056165000
6	-3.379533000	1.160889000	-0.012984000
7	-1.950891000	1.447457000	0.322937000
6	-0.846416000	0.535051000	2.396251000
6	-1.702614000	1.658472000	1.784501000
6	-1.425476000	2.562866000	-0.491730000
6	0.099433000	2.592214000	-0.445100000
7	0.630335000	1.358641000	-0.222815000
26	-0.589680000	-0.259953000	-0.399870000
6	-0.115221000	-1.771271000	2.239954000
6	-2.581958000	-2.024243000	-1.915633000
8	-0.341842000	-0.115000000	-2.554353000
1	-3.092107000	-0.419975000	2.077354000
1	-2.518921000	-1.998851000	2.558638000
1	-3.993568000	-2.054394000	0.492248000
1	-2.403766000	-2.834235000	0.350018000
1	-4.516976000	-0.300534000	-1.125895000
1	-3.182089000	0.447231000	-2.033281000
1	-3.919238000	0.882010000	0.889548000
1	-3.860055000	2.065400000	-0.402369000
1	0.214456000	0.780521000	2.318131000
1	-1.099748000	0.405911000	3.456259000
1	-1.181827000	2.607855000	1.933640000
1	-2.662300000	1.736494000	2.299684000
1	-1.735008000	2.403437000	-1.531809000
1	-0.225249000	-2.701197000	1.676688000
1	0.912999000	-1.413467000	2.161751000
1	-0.363681000	-1.946933000	3.294738000
1	-1.778280000	-2.753964000	-1.782458000
1	-3.546915000	-2.546319000	-1.963254000
1	-2.426578000	-1.476190000	-2.846108000
8	0.705584000	3.653456000	-0.643729000
6	1.998813000	1.107180000	-0.087441000
6	2.352478000	-0.277074000	-0.156124000
6	3.013039000	2.029439000	0.144701000
6	3.702287000	-0.701899000	-0.015623000
6	4.354821000	1.603084000	0.292471000
1	2.775280000	3.081554000	0.211982000
6	1.611288000	-2.474378000	-0.447449000
6	3.959495000	-2.091935000	-0.109673000
6	4.708074000	0.272812000	0.212523000
1	5.117234000	2.355471000	0.472269000
6	2.921649000	-2.975418000	-0.330419000
1	0.763731000	-3.134952000	-0.603205000
1	4.981516000	-2.445645000	-0.005862000
1	5.739485000	-0.047837000	0.322235000
1	3.093583000	-4.043024000	-0.407702000
7	1.342316000	-1.177108000	-0.362062000
1	-1.824755000	3.524442000	-0.149193000
1	0.408660000	0.488874000	-2.709935000
1	-1.107753000	0.355587000	-2.933340000

[Fe^{III}(OH)(AQtacn)]$^+$

(G = -2428.368403) (sextuplet)

7	-1.020285000	-0.779973000	1.641483000
6	-2.443413000	-1.196832000	1.796194000
6	-2.969043000	-1.841309000	0.520708000
7	-2.658130000	-1.074319000	-0.715255000
6	-3.533451000	0.095956000	-0.977370000
6	-3.333156000	1.243091000	0.010282000
7	-1.886786000	1.481698000	0.304286000
6	-0.751401000	0.495238000	2.342609000
6	-1.592969000	1.646546000	1.766773000
6	-1.349651000	2.627493000	-0.459983000
6	0.179937000	2.625238000	-0.415869000
7	0.683778000	1.383333000	-0.236365000
26	-0.608265000	-0.229769000	-0.549461000
6	-0.132147000	-1.833210000	2.172433000
6	-2.750006000	-2.008555000	-1.862258000
8	-0.572902000	-0.033945000	-2.429532000
1	-3.046822000	-0.340768000	2.085980000
1	-2.532189000	-1.922560000	2.613703000
1	-4.052470000	-2.004701000	0.597685000
1	-2.484653000	-2.815512000	0.405961000
1	-4.588082000	-0.213673000	-0.970988000
1	-3.280732000	0.442438000	-1.982294000
1	-3.865640000	1.041082000	0.938170000
1	-3.782291000	2.147555000	-0.415420000
1	0.312654000	0.705161000	2.216228000
1	-0.961372000	0.392195000	3.416939000
1	-1.046631000	2.579952000	1.926399000
1	-2.535703000	1.740080000	2.310224000
1	-1.673094000	2.531825000	-1.502305000
1	-0.287029000	-2.755854000	1.606580000
1	0.908300000	-1.518078000	2.073698000
1	-0.354918000	-2.015412000	3.233828000
1	-1.996334000	-2.792956000	-1.743310000
1	-3.749135000	-2.465732000	-1.900957000
1	-2.561098000	-1.467330000	-2.789718000
8	0.798081000	3.694149000	-0.570198000
6	2.039797000	1.089652000	-0.106741000
6	2.353552000	-0.307832000	-0.180579000
6	3.087797000	1.976602000	0.122242000
6	3.691114000	-0.774139000	-0.036454000
6	4.414998000	1.507716000	0.271763000
1	2.885176000	3.036168000	0.185460000
6	1.555216000	-2.478505000	-0.495745000
6	3.909466000	-2.171284000	-0.136108000
6	4.727068000	0.166943000	0.195151000
1	5.201499000	2.235765000	0.449984000
6	2.848964000	-3.022207000	-0.369201000
1	0.690451000	-3.113417000	-0.665424000
1	4.920649000	-2.553992000	-0.027686000
1	5.747756000	-0.186544000	0.306131000
1	2.989301000	-4.094252000	-0.451988000
7	1.321655000	-1.177123000	-0.401183000
1	-1.724835000	3.578838000	-0.063265000
1	0.083052000	0.643146000	-2.667648000

[Fe^{IV}(OH$_2$)(AQtacn)]$^{3+}$

(G = -2428.606599) (quintuplet)

7	-0.992650000	-0.766667000	1.660535000
6	-2.421568000	-1.198873000	1.822465000
6	-2.961232000	-1.821120000	0.539387000
7	-2.657431000	-1.036406000	-0.699231000

ANNEX

6	-3.524135000	0.148506000	-0.943233000
6	-3.333587000	1.233614000	0.103366000
7	-1.876198000	1.471733000	0.366478000
6	-0.716113000	0.503860000	2.382191000
6	-1.546021000	1.668776000	1.815860000
6	-1.384917000	2.582966000	-0.472237000
6	0.127955000	2.609071000	-0.517926000
7	0.673669000	1.336678000	-0.294768000
26	-0.647144000	-0.317370000	-0.438862000
6	-0.092565000	-1.833759000	2.167728000
6	-2.752976000	-1.960406000	-1.860503000
8	-0.429023000	-0.171017000	-2.574909000
1	-3.015241000	-0.351003000	2.149569000
1	-2.480986000	-1.947453000	2.618847000
1	-4.044716000	-1.969851000	0.616910000
1	-2.484932000	-2.795316000	0.401952000
1	-4.575578000	-0.163484000	-0.974659000
1	-3.241595000	0.535283000	-1.926997000
1	-3.833706000	0.970085000	1.032023000
1	-3.797777000	2.158315000	-0.255730000
1	0.351772000	0.702375000	2.270842000
1	-0.934511000	0.372873000	3.448992000
1	-0.973451000	2.591850000	1.936535000
1	-2.475836000	1.792148000	2.374202000
1	-1.736859000	2.425122000	-1.499671000
1	-0.252117000	-2.740383000	1.578892000
1	0.944665000	-1.507969000	2.079518000
1	-0.323861000	-2.031053000	3.221802000
1	-1.983219000	-2.731004000	-1.765837000
1	-3.745020000	-2.430040000	-1.871927000
1	-2.606278000	-1.403604000	-2.786668000
8	0.760830000	3.609256000	-0.814958000
6	1.975689000	1.094250000	-0.089105000
6	2.347898000	-0.308424000	-0.169722000
6	2.992486000	2.046890000	0.214772000
6	3.691978000	-0.709224000	-0.017475000
6	4.308852000	1.633601000	0.377603000
1	2.726989000	3.089205000	0.319633000
6	1.647591000	-2.492833000	-0.524776000
6	3.985424000	-2.085539000	-0.139615000
6	4.672328000	0.287295000	0.258845000
1	5.069765000	2.371465000	0.607003000
6	2.958057000	-2.977851000	-0.399823000
1	0.810128000	-3.156967000	-0.711333000
1	5.011094000	-2.423635000	-0.029187000
1	5.705681000	-0.018336000	0.388643000
1	3.145686000	-4.040419000	-0.501364000
7	1.359181000	-1.193915000	-0.410981000
1	-1.763192000	3.547127000	-0.115796000
1	0.407176000	0.273780000	-2.809200000
1	-1.129662000	0.421817000	-2.908685000

[Fe^{IV}(OH)(AQtacn)]$^{2+}$

(G= -2428,163122) (triplet)

7	-0.935143000	-0.473469000	1.670857000
6	-2.258367000	-1.186785000	1.774558000
6	-2.429370000	-2.098069000	0.581665000
7	-2.141989000	-1.374912000	-0.695801000
6	-3.244717000	-0.459297000	-1.163833000
6	-3.344120000	0.860068000	-0.399236000
7	-1.986945000	1.352003000	0.049756000
6	-1.011353000	0.866479000	2.314071000
6	-1.968702000	1.749689000	1.524526000
6	-1.477998000	2.510472000	-0.740810000
6	0.022100000	2.625900000	-0.484794000
7	0.566415000	1.395472000	-0.153898000
26	-0.582007000	-0.062006000	-0.357499000
6	0.099222000	-1.272629000	2.383803000

6	-1.982725000	-2.401392000	-1.765163000
8	-0.574213000	0.093301000	-2.133240000
1	-3.063063000	-0.459076000	1.840029000
1	-2.275826000	-1.769802000	2.699968000
1	-3.441078000	-2.516902000	0.547653000
1	-1.707545000	-2.916175000	0.642609000
1	-4.196339000	-0.997519000	-1.099389000
1	-3.030312000	-0.249471000	-2.210730000
1	-3.987050000	0.755897000	0.471493000
1	-3.794423000	1.613463000	-1.050205000
1	-0.002069000	1.279266000	2.314580000
1	-1.353931000	0.752287000	3.348670000
1	-1.654353000	2.791112000	1.608705000
1	-2.984272000	1.685116000	1.912049000
1	-1.636369000	2.311006000	-1.803348000
1	0.113868000	-2.289881000	1.991787000
1	1.074168000	-0.800561000	2.257339000
1	-0.163132000	-1.297809000	3.447571000
1	-1.214576000	-3.119379000	-1.480770000
1	-2.936739000	-2.927786000	-1.889114000
1	-1.704538000	-1.912257000	-2.697774000
8	0.641948000	3.673590000	-0.620347000
6	1.930712000	1.114032000	-0.077859000
6	2.193814000	-0.278278000	-0.163496000
6	2.992284000	1.995652000	0.080094000
6	3.515973000	-0.783330000	-0.085400000
6	4.313317000	1.493539000	0.146432000
1	2.810120000	3.058208000	0.157718000
6	1.291903000	-2.422186000	-0.329175000
6	3.681118000	-2.187159000	-0.142854000
6	4.582378000	0.141867000	0.067602000
1	5.128445000	2.199345000	0.271219000
6	2.570924000	-2.999961000	-0.258471000
1	0.411037000	-3.047046000	-0.389107000
1	4.680465000	-2.607897000	-0.083822000
1	5.598080000	-0.235475000	0.131178000
1	2.658109000	-4.079699000	-0.291107000
7	1.104903000	-1.104782000	-0.296232000
1	-1.998841000	3.428576000	-0.458288000
1	0.151416000	0.657616000	-2.457989000

[Fe^{IV}(O)(AQtacn)]$^+$

(G = -2427.718978) (triplet)

7	-0.904837000	-0.469392000	1.678391000
6	-2.228386000	-1.158007000	1.813694000
6	-2.436202000	-2.084747000	0.636604000
7	-2.180872000	-1.381988000	-0.652735000
6	-3.285253000	-0.460633000	-1.099052000
6	-3.341268000	0.892645000	-0.381267000
7	-1.972827000	1.370599000	0.032133000
6	-0.958595000	0.873426000	2.297102000
6	-1.916241000	1.761719000	1.506095000
6	-1.457811000	2.530093000	-0.754001000
6	0.055019000	2.631525000	-0.518159000
7	0.581251000	1.429349000	-0.167540000
26	-0.596330000	-0.058339000	-0.440594000
6	0.131687000	-1.271130000	2.367195000
6	-2.065931000	-2.416108000	-1.714791000
8	-0.598016000	0.117398000	-2.072267000
1	-3.025481000	-0.419103000	1.868597000
1	-2.256342000	-1.726701000	2.749827000
1	-3.448982000	-2.505589000	0.641758000
1	-1.713721000	-2.903749000	0.690135000
1	-4.245803000	-0.977657000	-0.989275000
1	-3.104432000	-0.285197000	-2.159119000
1	-3.977877000	0.831505000	0.499663000
1	-3.790615000	1.626624000	-1.055731000
1	0.053539000	1.278812000	2.273850000

1	-1.288408000	0.798002000	3.341452000
1	-1.588059000	2.799788000	1.586132000
1	-2.924764000	1.714175000	1.916049000
1	-1.633819000	2.337530000	-1.814798000
1	0.142175000	-2.285387000	1.964022000
1	1.107940000	-0.805650000	2.218288000
1	-0.094132000	-1.312286000	3.440938000
1	-1.322264000	-3.160488000	-1.431064000
1	-3.034819000	-2.915937000	-1.842870000
1	-1.768595000	-1.936584000	-2.647620000
8	0.663769000	3.697257000	-0.685094000
6	1.935063000	1.115836000	-0.092629000
6	2.186636000	-0.284639000	-0.194114000
6	3.010286000	1.976153000	0.085235000
6	3.506011000	-0.801921000	-0.090769000
6	4.325489000	1.459010000	0.169817000
1	2.838797000	3.040770000	0.165890000
6	1.280503000	-2.420886000	-0.415639000
6	3.663069000	-2.208645000	-0.157663000
6	4.581793000	0.105700000	0.089731000
1	5.146578000	2.155748000	0.311633000
6	2.554772000	-3.012756000	-0.311592000
1	0.396843000	-3.036716000	-0.518717000
1	4.659157000	-2.634475000	-0.077020000
1	5.591533000	-0.285233000	0.169329000
1	2.636850000	-4.092918000	-0.353724000
7	1.097667000	-1.107876000	-0.373877000
1	-1.963242000	3.455631000	-0.462678000

[Fe^V(OH)(AQtacn)]$^{3+}$

(G = -2427.943949) (doublet)

7	-0.942799000	-0.480840000	1.664443000
6	-2.275248000	-1.185626000	1.758948000
6	-2.440414000	-2.095473000	0.566531000
7	-2.146987000	-1.367142000	-0.710715000
6	-3.241940000	-0.443259000	-1.188418000
6	-3.336387000	0.875888000	-0.425422000
7	-1.975558000	1.353944000	0.041975000
6	-1.008161000	0.864024000	2.305263000
6	-1.971521000	1.743354000	1.523338000
6	-1.461065000	2.520848000	-0.734466000
6	0.022796000	2.670600000	-0.436570000
7	0.602395000	1.391769000	-0.169816000
26	-0.592990000	-0.081387000	-0.359593000
6	0.081491000	-1.289693000	2.386277000
6	-1.972006000	-2.392372000	-1.781399000
8	-0.573629000	0.089536000	-2.119541000
1	-3.075291000	-0.452958000	1.818889000
1	-2.298301000	-1.767261000	2.684406000
1	-3.453473000	-2.507899000	0.520280000
1	-1.721027000	-2.915585000	0.626240000
1	-4.193839000	-0.979499000	-1.123396000
1	-3.021904000	-0.238586000	-2.234873000
1	-3.988066000	0.781441000	0.439289000
1	-3.766163000	1.635480000	-1.082311000
1	0.003615000	1.272067000	2.304137000
1	-1.344530000	0.749842000	3.341301000
1	-1.673431000	2.788736000	1.616977000
1	-2.988020000	1.662175000	1.903628000
1	-1.580150000	2.320569000	-1.802907000
1	0.088655000	-2.307898000	1.996798000
1	1.060977000	-0.823624000	2.275721000
1	-0.196990000	-1.309397000	3.445444000
1	-1.195631000	-3.099969000	-1.493235000
1	-2.922165000	-2.925753000	-1.899708000
1	-1.701139000	-1.900258000	-2.714450000
8	0.638208000	3.710680000	-0.478704000
6	1.916892000	1.111833000	-0.107477000
6	2.186774000	-0.306763000	-0.159905000

6	3.003124000	2.023799000	0.004592000
6	3.504404000	-0.793083000	-0.073351000
6	4.298578000	1.531508000	0.082341000
1	2.806954000	3.085547000	0.043694000
6	1.311702000	-2.453295000	-0.295467000
6	3.697790000	-2.190600000	-0.104766000
6	4.562624000	0.154457000	0.048936000
1	5.124508000	2.227311000	0.178630000
6	2.590877000	-3.017131000	-0.211031000
1	0.432352000	-3.081268000	-0.351485000
1	4.702310000	-2.595672000	-0.037401000
1	5.582192000	-0.211154000	0.117104000
1	2.688946000	-4.095973000	-0.227413000
7	1.112814000	-1.129273000	-0.285022000
1	-2.004520000	3.429634000	-0.466656000
1	0.164333000	0.620997000	-2.477106000

[Fe^{IV}(O)(AQtacn$^•$)]$^{2+}$

(G = -2427.516311) (quadruplet)

7	-0.909876000	-0.510845000	1.661750000
6	-2.236816000	-1.208162000	1.770030000
6	-2.428816000	-2.102814000	0.565581000
7	-2.158887000	-1.361861000	-0.704368000
6	-3.265686000	-0.436826000	-1.147217000
6	-3.343908000	0.885855000	-0.381911000
7	-1.976426000	1.357676000	0.056366000
6	-0.964654000	0.825306000	2.304422000
6	-1.935607000	1.719307000	1.540869000
6	-1.475661000	2.538581000	-0.705407000
6	0.026464000	2.670614000	-0.467859000
7	0.604854000	1.409841000	-0.198879000
26	-0.609013000	-0.074222000	-0.415354000
6	0.116970000	-1.324323000	2.359307000
6	-2.009657000	-2.367740000	-1.793763000
8	-0.568300000	0.196445000	-2.039289000
1	-3.036167000	-0.474267000	1.843048000
1	-2.264722000	-1.803027000	2.688618000
1	-3.440880000	-2.522210000	0.540754000
1	-1.705374000	-2.921646000	0.602988000
1	-4.220154000	-0.968833000	-1.070820000
1	-3.065067000	-0.223826000	-2.196898000
1	-3.980853000	0.787552000	0.494420000
1	-3.793976000	1.642430000	-1.029551000
1	0.047650000	1.233289000	2.283290000
1	-1.283018000	0.729259000	3.349598000
1	-1.627497000	2.761157000	1.647553000
1	-2.944090000	1.643095000	1.944892000
1	-1.636536000	2.366763000	-1.772517000
1	0.125832000	-2.335787000	1.949986000
1	1.097351000	-0.861075000	2.234248000
1	-0.130442000	-1.370299000	3.427024000
1	-1.245950000	-3.095990000	-1.522817000
1	-2.965472000	-2.886944000	-1.933773000
1	-1.722485000	-1.857902000	-2.713811000
8	0.636010000	3.720085000	-0.553555000
6	1.916400000	1.119502000	-0.124303000
6	2.177400000	-0.301354000	-0.186387000
6	3.003854000	2.018258000	0.009026000
6	3.495648000	-0.791078000	-0.076969000
6	4.301253000	1.518181000	0.113233000
1	2.813228000	3.081228000	0.052121000
6	1.309219000	-2.442134000	-0.389941000
6	3.687493000	-2.189846000	-0.124821000
6	4.557530000	0.147389000	0.077860000
1	5.126102000	2.212206000	0.232968000
6	2.586507000	-3.012319000	-0.274754000
1	0.433325000	-3.069733000	-0.487642000
1	4.690505000	-2.595881000	-0.038993000

```
1    5.572192000   -0.227481000    0.167041000
1    2.684816000   -4.091082000   -0.305598000
7    1.104475000   -1.123945000   -0.364289000
1   -1.992228000    3.452134000   -0.400230000
```

(·LFe^IV=O·4H2O)_q

(G = -2733.385673)

```
7    1.646468000   -0.680782000   -1.785419000
6    2.765393000   -1.668516000   -1.553269000
6    2.635368000   -2.304387000   -0.181257000
7    2.358643000   -1.259177000    0.850111000
6    3.574603000   -0.379696000    1.077283000
6    3.169463000    1.086529000    1.133372000
7    2.247928000    1.357668000   -0.014182000
6    2.175156000    0.585300000   -2.378257000
6    2.982547000    1.340329000   -1.337459000
6    1.487745000    2.630293000    0.133335000
6    0.191016000    2.565227000   -0.658763000
7   -0.285385000    1.237486000   -0.720894000
26   0.859636000   -0.081425000    0.106354000
6    0.677932000   -1.272882000   -2.745988000
6    2.007215000   -1.912258000    2.141402000
8    0.373339000    0.364952000    1.612760000
1    3.720438000   -1.155447000   -1.664775000
1    2.728826000   -2.444911000   -2.321587000
1    3.549685000   -2.848333000    0.082549000
1    1.800037000   -3.006099000   -0.166876000
1    4.295767000   -0.558515000    0.280619000
1    4.054289000   -0.667038000    2.015813000
1    4.046327000    1.739357000    1.073077000
1    2.613455000    1.298309000    2.046427000
1    1.317716000    1.172648000   -2.714045000
1    2.798629000    0.358233000   -3.250373000
1    3.157226000    2.367449000   -1.666291000
1    3.956804000    0.878969000   -1.184354000
1    1.198245000    2.744009000    1.183163000
1    0.314986000   -2.225859000   -2.358186000
1   -0.157749000   -0.587357000   -2.898298000
1    1.183113000   -1.438584000   -3.704929000
1    1.065449000   -2.451057000    2.039885000
1    2.807727000   -2.609519000    2.414640000
1    1.905103000   -1.143542000    2.908190000
8   -0.382368000    3.542772000   -1.099729000
6   -1.514654000    0.839879000   -1.080227000
6   -1.761864000   -0.559730000   -0.800647000
6   -2.542104000    1.620640000   -1.676762000
6   -2.999472000   -1.144346000   -1.140837000
6   -3.753961000    1.023979000   -2.011466000
1   -2.364836000    2.667101000   -1.877631000
6   -0.969405000   -2.550826000    0.069826000
6   -3.190601000   -2.512076000   -0.849987000
6   -3.992788000   -0.330377000   -1.758479000
1   -4.527209000    1.623590000   -2.478947000
6   -2.167310000   -3.211425000   -0.240270000
1   -0.167800000   -3.091041000    0.554213000
1   -4.132256000   -2.988254000   -1.104214000
1   -4.942887000   -0.782831000   -2.024201000
1   -2.266890000   -4.260838000    0.010804000
7   -0.757331000   -1.262138000   -0.208081000
1    2.086967000    3.491450000   -0.170832000
8   -1.299040000    2.416989000    2.375769000
1   -1.155452000    3.141632000    1.744213000
1   -0.702931000    1.699262000    2.059954000
8   -2.729960000   -1.189241000    2.501660000
1   -3.096239000   -0.347406000    2.139612000
1   -2.045055000   -0.875189000    3.131802000
8   -3.682648000    1.282864000    1.664695000
1   -3.739587000    1.300494000    0.696871000
8   -0.628244000   -0.173200000    4.122112000
```

```
1   -0.128962000   -0.126510000    3.277931000
1   -1.023132000    0.714460000    4.173821000
1   -2.826901000    1.742001000    1.868574000
```

(·LFe^IV=O·4H2O)_d

(G = -2733.381714)
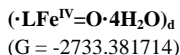
```
7    1.648967000    0.268772000   -1.902234000
6    2.768891000   -0.707740000   -2.172966000
6    2.636437000   -1.929104000   -1.282915000
7    2.354931000   -1.513757000    0.123840000
6    3.565269000   -0.851510000    0.755784000
6    3.156161000    0.406420000    1.510346000
7    2.237915000    1.199613000    0.635749000
6    2.175530000    1.663882000   -1.808741000
6    2.976821000    1.824371000   -0.529235000
6    1.481937000    2.245172000    1.377068000
6    0.192372000    2.580130000    0.644622000
7   -0.289831000    1.444768000   -0.045801000
26   0.844191000   -0.115325000    0.049035000
6    0.681874000    0.213547000   -3.029811000
6    2.006249000   -2.714666000    0.929107000
8    0.382392000   -0.485634000    1.582151000
1    3.724480000   -0.208146000   -2.012812000
1    2.740490000   -1.011821000   -3.222251000
1    3.552127000   -2.530941000   -1.313916000
1    1.803245000   -2.552723000   -1.611404000
1    4.291860000   -0.624281000   -0.023760000
1    4.041270000   -1.553372000    1.444564000
1    4.032646000    1.006292000    1.776153000
1    2.598322000    0.151395000    2.411378000
1    1.316812000    2.338739000   -1.823546000
1    2.802619000    1.886397000   -2.679456000
1    3.149383000    2.882323000   -0.319106000
1    3.951389000    1.346176000   -0.612154000
1    1.183843000    1.837803000    2.348926000
1    0.322548000   -0.809014000   -3.152449000
1   -0.156023000    0.884740000   -2.832062000
1    1.188247000    0.533907000   -3.948313000
1    1.073716000   -3.146806000    0.567299000
1    2.815444000   -3.449126000    0.841820000
1    1.886982000   -2.416294000    1.970818000
8   -0.375222000    3.652045000    0.726337000
6   -1.522075000    1.276523000   -0.543502000
6   -1.779765000   -0.084945000   -0.970995000
6   -2.550122000    2.251970000   -0.678367000
6   -3.022486000   -0.429707000   -1.541079000
6   -3.771098000    1.890732000   -1.236168000
1   -2.367234000    3.264161000   -0.348707000
6   -0.990733000   -2.247736000   -1.184197000
6   -3.218184000   -1.765913000   -1.951381000
6   -4.016309000    0.582558000   -1.670506000
1   -4.547807000    2.640454000   -1.339538000
6   -2.193047000   -2.673752000   -1.767694000
1   -0.184907000   -2.952585000   -1.033965000
1   -4.163503000   -2.057358000   -2.397988000
1   -4.973524000    0.318195000   -2.108360000
1   -2.294205000   -3.712498000   -2.059181000
7   -0.776436000   -0.986272000   -0.801725000
1    2.086694000    3.141601000    1.531342000
8   -1.305414000    0.935065000    3.198286000
1   -1.169798000    1.879719000    3.015074000
1   -0.704283000    0.470940000    2.567367000
8   -2.613839000   -2.331223000    1.687506000
1   -3.024155000   -1.436094000    1.758231000
1   -1.950449000   -2.324974000    2.412267000
8   -3.684145000    0.198994000    2.090240000
1   -3.769380000    0.663308000    1.243402000
8   -0.537337000   -2.102307000    3.606379000
```

1	-0.058094000	-1.680111000	2.859704000
1	-0.938164000	-1.334417000	4.049516000
1	-2.836173000	0.544098000	2.473997000

(TS·4H₂O)_q

(G = -2733.317780)

7	1.992745000	-1.309020000	1.118921000
6	2.998762000	-0.637311000	2.000598000
6	2.617243000	0.815253000	2.239631000
7	2.286455000	1.510613000	0.957556000
6	3.512752000	1.657521000	0.075783000
6	3.191382000	1.266967000	-1.362363000
7	2.429932000	-0.018264000	-1.346785000
6	2.635659000	-2.100280000	0.041460000
6	3.317297000	-1.176206000	-0.957797000
6	1.718561000	-0.309527000	-2.622646000
6	0.493511000	-1.180478000	-2.349851000
7	0.022482000	-0.998168000	-1.080198000
26	0.917897000	0.302612000	-0.038361000
6	1.136606000	-2.196934000	1.933470000
6	1.769951000	2.871129000	1.268625000
8	0.271397000	1.687232000	-0.902051000
1	3.990029000	-0.713090000	1.551247000
1	3.052596000	-1.151597000	2.965506000
1	3.433374000	1.347420000	2.743470000
1	1.727287000	0.868961000	2.869531000
1	4.317258000	1.043873000	0.480795000
1	3.855859000	2.694638000	0.104491000
1	4.109069000	1.155861000	-1.950545000
1	2.549548000	2.016301000	-1.825022000
1	1.851607000	-2.682173000	-0.447130000
1	3.374915000	-2.795738000	0.460068000
1	3.590384000	-1.734922000	-1.856510000
1	4.236714000	-0.770136000	-0.539400000
1	1.357925000	0.634621000	-3.039884000
1	0.656347000	-1.613824000	2.722225000
1	0.376082000	-2.653603000	1.297907000
1	1.748452000	-2.987892000	2.388564000
1	0.827908000	2.796194000	1.812129000
1	2.509311000	3.402897000	1.880009000
1	1.607001000	3.407972000	0.334082000
8	-0.002105000	-1.894570000	-3.224984000
6	-1.155576000	-1.531000000	-0.558588000
6	-1.525115000	-0.932590000	0.681284000
6	-1.945814000	-2.548673000	-1.076049000
6	-2.691069000	-1.349259000	1.374625000
6	-3.102626000	-2.971327000	-0.375525000
1	-1.674013000	-3.021491000	-2.008928000
6	-1.000592000	0.620152000	2.330617000
6	-2.992128000	-0.701622000	2.596709000
6	-3.481367000	-2.391318000	0.818449000
1	-3.700037000	-3.772232000	-0.800363000
6	-2.151349000	0.282477000	3.068667000
1	-0.325556000	1.380035000	2.702172000
1	-3.881390000	-0.994368000	3.147404000
1	-4.368533000	-2.719376000	1.351187000
1	-2.348006000	0.800542000	4.000443000
7	-0.685702000	0.034926000	1.181435000
1	2.383056000	-0.789432000	-3.346190000
8	-0.940767000	2.093213000	-2.113357000
1	-0.673447000	3.031735000	-2.159323000
1	-2.019096000	2.041714000	-1.080156000
8	-2.776469000	1.944154000	-0.362512000
1	-3.360585000	1.171525000	-0.704307000
1	-3.346908000	2.794593000	-0.402838000
8	-4.169317000	0.011739000	-1.380398000
1	-4.297530000	-0.657929000	-0.683689000
8	-4.258245000	4.085778000	-0.482272000
1	-4.153079000	4.388724000	-1.401664000

1	-5.163637000	3.727992000	-0.462685000
1	-3.502087000	-0.398511000	-1.959690000

(TS·4H₂O)_d

(G = -2733.342417)

7	1.917639000	-1.197811000	1.265224000
6	2.913377000	-0.477617000	2.135945000
6	2.567649000	0.996468000	2.223866000
7	2.271354000	1.538932000	0.866858000
6	3.521847000	1.591406000	0.012797000
6	3.242133000	1.053354000	-1.385348000
7	2.476548000	-0.223273000	-1.260403000
6	2.615559000	-2.132820000	0.332323000
6	3.350961000	-1.334171000	-0.728420000
6	1.810058000	-0.638819000	-2.526572000
6	0.559793000	-1.461181000	-2.224238000
7	0.077407000	-1.211187000	-0.976709000
26	0.940639000	0.191467000	-0.033787000
6	1.014864000	-1.997583000	2.133247000
6	1.742391000	2.920763000	0.997142000
8	0.397414000	1.439953000	-0.984288000
1	3.914445000	-0.624364000	1.731034000
1	2.909300000	-0.916776000	3.137203000
1	3.390665000	1.559458000	2.680348000
1	1.672388000	1.136163000	2.832648000
1	4.312948000	1.022144000	0.499685000
1	3.869878000	2.625067000	-0.056183000
1	4.174638000	0.880800000	-1.933602000
1	2.616600000	1.750067000	-1.943730000
1	1.856392000	-2.770501000	-0.121222000
1	3.319999000	-2.760568000	0.890592000
1	3.650011000	-1.984637000	-1.554114000
1	4.258129000	-0.890790000	-0.320189000
1	1.475719000	0.262624000	-3.047893000
1	0.540222000	-1.341052000	-2.864054000
1	0.257126000	-2.485668000	1.519712000
1	1.604462000	-2.760508000	2.656376000
1	0.784958000	2.906766000	1.517842000
1	2.459921000	3.531957000	1.558141000
1	1.602765000	3.339599000	-0.000728000
8	0.057000000	-2.194482000	-3.082799000
6	-1.179595000	-1.586975000	-0.510581000
6	-1.585858000	-0.843547000	0.635065000
6	-2.033012000	-2.558172000	-1.015083000
6	-2.833290000	-1.091430000	1.264650000
6	-3.280824000	-2.798605000	-0.389671000
1	-1.743161000	-3.132122000	-1.883554000
6	-1.056680000	0.829433000	2.161622000
6	-3.167111000	-0.301032000	2.390204000
6	-3.682096000	-2.095416000	0.727758000
1	-3.927129000	-3.565560000	-0.806079000
6	-2.280777000	0.654880000	2.834925000
1	-0.355671000	1.575287000	2.510169000
1	-4.119657000	-0.460747000	2.887364000
1	-4.638060000	-2.286249000	1.205454000
1	-2.499042000	1.280739000	3.692670000
7	-0.710715000	0.108620000	1.101638000
1	2.498756000	-1.188935000	-3.173056000
8	-1.131110000	1.160255000	-1.995822000
1	-0.974311000	1.984824000	-2.496175000
1	-2.016731000	1.569932000	-1.039898000
8	-2.738487000	2.011610000	-0.334889000
1	-3.598120000	1.470071000	-0.407479000
1	-2.913624000	2.918963000	-0.755976000
8	-4.932487000	0.576367000	-0.542629000
1	-5.242706000	0.517713000	0.378440000
8	-2.903181000	4.250494000	-1.697179000
1	-2.261646000	4.839364000	-1.262307000
1	-2.410609000	3.901772000	-2.462119000

ANNEX

1	-4.580636000	-0.317137000	-0.712166000

$(Fe^{III}-OOH \cdot H_3O^+ \cdot 2H_2O)_q$

(G = -2733.342970)

7	1.954458000	-1.402775000	1.107984000
6	2.972392000	-0.778879000	1.998049000
6	2.628023000	0.680729000	2.260732000
7	2.331618000	1.421181000	0.993727000
6	3.571771000	1.536447000	0.122491000
6	3.261891000	1.176452000	-1.327361000
7	2.459205000	-0.080893000	-1.354575000
6	2.559399000	-2.186984000	0.010253000
6	3.285001000	-1.274539000	-0.974121000
6	1.734551000	-0.313076000	-2.630048000
6	0.456160000	-1.113717000	-2.377352000
7	-0.038512000	-0.901903000	-1.120371000
26	0.906390000	0.326270000	-0.045360000
6	1.052066000	-2.260366000	1.897044000
6	1.876649000	2.792400000	1.352043000
8	0.359859000	1.966830000	-0.958527000
1	3.963962000	-0.871647000	1.551403000
1	3.014046000	-1.306505000	2.957539000
1	3.451611000	1.180031000	2.786205000
1	1.731531000	0.745481000	2.881085000
1	4.350067000	0.890688000	0.528955000
1	3.950601000	2.560744000	0.169194000
1	4.189580000	1.056062000	-1.899381000
1	2.654210000	1.956837000	-1.784831000
1	1.749140000	-2.720142000	-0.492752000
1	3.270085000	-2.929061000	0.400614000
1	3.544513000	-1.838544000	-1.874902000
1	4.218796000	-0.917552000	-0.540794000
1	1.429879000	0.655710000	-3.037359000
1	0.583397000	-1.666170000	2.685089000
1	0.278780000	-2.675109000	1.246886000
1	1.615663000	-3.086065000	2.356015000
1	0.936218000	2.736619000	1.902158000
1	2.641144000	3.273344000	1.974767000
1	1.731566000	3.368984000	0.437967000
8	-0.054623000	-1.803613000	-3.264094000
6	-1.226645000	-1.432438000	-0.609681000
6	-1.585484000	-0.877193000	0.655080000
6	-2.036709000	-2.419770000	-1.157360000
6	-2.753102000	-1.305763000	1.339298000
6	-3.191570000	-2.859259000	-0.461483000
1	-1.780390000	-2.862323000	-2.109067000
6	-1.030331000	0.605444000	2.357144000
6	-3.039747000	-0.694956000	2.584426000
6	-3.557860000	-2.319465000	0.754018000
1	-3.799375000	-3.637819000	-0.912609000
6	-2.185244000	0.262039000	3.087516000
1	-0.334053000	1.337082000	2.749823000
1	-3.930390000	-0.995678000	3.128859000
1	-4.446035000	-2.656411000	1.279801000
1	-2.374124000	0.748986000	4.037681000
7	-0.731092000	0.057010000	1.187084000
1	2.363506000	-0.823793000	-3.365448000
8	-0.770198000	1.785797000	-1.872434000
1	-0.751335000	2.631871000	-2.358667000
1	-2.000332000	1.897326000	-0.899843000
8	-2.807386000	1.935976000	-0.269758000
1	-3.455441000	1.216204000	-0.626685000
1	-3.252370000	2.855293000	-0.410914000
8	-4.344712000	0.126461000	-1.279105000
1	-4.673973000	-0.408757000	-0.534469000
8	-3.902955000	4.249020000	-0.647163000
1	-3.221932000	4.894281000	-0.385930000
1	-3.941830000	4.335299000	-1.616315000

1	-3.689734000	-0.463023000	-1.697119000

$(Fe^{III}-OOH H_3O^+ \cdot 2H_2O)_d$

(G = -2733.358138)

7	1.820047000	-0.897450000	1.503948000
6	2.503783000	0.060213000	2.447426000
6	1.882386000	1.440929000	2.343553000
7	1.724857000	1.828748000	0.912003000
6	3.067985000	2.085388000	0.264634000
6	3.130414000	1.424562000	-1.108117000
7	2.614401000	0.031824000	-0.984832000
6	2.833720000	-1.717553000	0.771941000
6	3.576912000	-0.848007000	-0.229998000
6	2.257309000	-0.593909000	-2.289171000
6	1.146446000	-1.630947000	-2.107732000
7	0.412038000	-1.398038000	-0.992956000
26	0.857846000	0.178257000	-0.017366000
6	0.965221000	-1.820316000	2.292790000
6	0.926669000	3.078535000	0.834690000
8	0.213207000	1.286739000	-1.303058000
1	3.568319000	0.093938000	2.214959000
1	2.413940000	-0.309101000	3.472757000
1	2.498114000	2.180005000	2.871339000
1	0.886645000	1.438225000	2.790427000
1	3.856631000	1.707935000	0.915680000
1	3.226509000	3.162706000	0.162623000
1	4.155217000	1.425599000	-1.496814000
1	2.478978000	1.947520000	-1.809882000
1	2.293954000	-2.516971000	0.263713000
1	3.537915000	-2.162481000	1.485017000
1	4.129667000	-1.475569000	-0.934209000
1	4.306206000	-0.214355000	0.273547000
1	1.858523000	0.185040000	-2.945043000
1	0.240753000	-1.242505000	2.869517000
1	0.444760000	-2.499429000	1.616324000
1	1.594918000	-2.402130000	2.977365000
1	-0.082016000	2.901475000	1.207394000
1	1.410304000	3.857830000	1.437381000
1	0.873228000	3.399678000	-0.205978000
8	0.958320000	-2.508031000	-2.964907000
6	-0.794032000	-2.011656000	-0.671926000
6	-1.515666000	-1.305255000	0.336340000
6	-1.336896000	-3.182521000	-1.186049000
6	-2.756450000	-1.795359000	0.825512000
6	-2.582002000	-3.656694000	-0.707903000
1	-0.804041000	-3.732773000	-1.948723000
6	-1.573100000	0.518444000	1.773842000
6	-3.388359000	-1.059694000	1.859394000
6	-3.284503000	-2.991935000	0.275677000
1	-2.981263000	-4.575054000	-1.128696000
6	-2.798370000	0.093127000	2.329081000
1	-1.105524000	1.424340000	2.134080000
1	-4.330862000	-1.414870000	2.266635000
1	-4.233557000	-3.367758000	0.645657000
1	-3.251373000	0.685129000	3.116499000
7	-0.939589000	-0.151904000	0.821204000
1	3.133278000	-1.040812000	-2.768134000
8	-1.124672000	0.934283000	-1.802747000
1	-1.081847000	1.309136000	-2.703520000
1	-2.002840000	1.928457000	-0.949673000
8	-2.556125000	2.566144000	-0.374533000
1	-3.465565000	2.097742000	-0.242491000
1	-2.708732000	3.417941000	-0.936268000
8	-4.785116000	1.291625000	-0.079272000
1	-4.681279000	0.868441000	0.792071000
8	-2.903989000	4.679915000	-1.818653000
1	-1.999964000	4.986333000	-2.012317000
1	-3.216743000	4.328297000	-2.671281000
1	-4.670336000	0.551592000	-0.702541000

ANNEX

(Fe^{III}-OOH· H$_3$O$^+$·2H$_2$O)$_{sext}$

(G = -2733.352913)

7	1.679334000	-1.199281000	1.531384000
6	2.679736000	-0.492125000	2.384779000
6	2.453252000	1.009505000	2.335849000
7	2.400449000	1.515312000	0.936749000
6	3.692187000	1.344462000	0.199980000
6	3.461926000	0.728532000	-1.179394000
7	2.560779000	-0.448785000	-1.080376000
6	2.310282000	-2.228859000	0.668996000
6	3.213272000	-1.600510000	-0.386928000
6	2.011383000	-0.852557000	-2.389996000
6	0.693231000	-1.611984000	-2.235305000
7	0.002645000	-1.234122000	-1.133622000
26	0.763617000	0.302153000	0.036743000
6	0.672323000	-1.851090000	2.396974000
6	2.004650000	2.942422000	0.966647000
8	0.622442000	1.702617000	-1.295801000
1	3.689374000	-0.747274000	2.060023000
1	2.593013000	-0.828338000	3.423491000
1	3.239354000	1.532043000	2.897675000
1	1.483090000	1.246565000	2.787384000
1	4.369303000	0.726840000	0.790656000
1	4.180712000	2.316482000	0.077551000
1	4.423178000	0.444155000	-1.627280000
1	2.970371000	1.455461000	-1.827960000
1	1.502097000	-2.785954000	0.192073000
1	2.899932000	-2.925292000	1.281463000
1	3.487130000	-2.367827000	-1.118865000
1	4.141831000	-1.252131000	0.067741000
1	1.795926000	0.051314000	-2.968589000
1	0.193499000	-1.099028000	3.028501000
1	-0.082566000	-2.339352000	1.777535000
1	1.158089000	-2.603965000	3.033773000
1	1.003835000	3.029019000	1.400260000
1	2.717818000	3.515947000	1.574821000
1	1.994076000	3.335398000	-0.050777000
8	0.350033000	-2.420531000	-3.115117000
6	-1.242089000	-1.747421000	-0.771749000
6	-1.845385000	-1.080340000	0.343692000
6	-1.931503000	-2.823824000	-1.324143000
6	-3.080575000	-1.519047000	0.897887000
6	-3.173881000	-3.241472000	-0.787308000
1	-1.511675000	-3.350890000	-2.168282000
6	-1.647142000	0.616751000	1.934819000
6	-3.570723000	-0.820766000	2.031134000
6	-3.748218000	-2.618239000	0.300253000
1	-3.676445000	-4.085519000	-1.251108000
6	-2.862725000	0.247387000	2.546158000
1	-1.047985000	1.437627000	2.318191000
1	-4.506695000	-1.139292000	2.481698000
1	-4.695595000	-2.950634000	0.713467000
1	-3.215847000	0.797495000	3.411181000
7	-1.162249000	-0.027587000	0.882447000
1	2.725735000	-1.464569000	-2.952396000
8	-0.610514000	1.601058000	-2.071837000
1	-0.418322000	2.215133000	-2.806297000
1	-1.574951000	2.375377000	-1.083025000
8	-2.160145000	2.823853000	-0.378299000
1	-3.038124000	2.281688000	-0.359971000
1	-2.371628000	3.779691000	-0.708422000
8	-4.295327000	1.376796000	-0.369495000
1	-4.379684000	1.098900000	0.560451000
8	-2.673990000	5.218209000	-1.188167000
1	-1.820911000	5.686156000	-1.146067000
1	-2.845627000	5.134330000	-2.143029000
1	-4.003051000	0.564733000	-0.821603000

A.IX.5.Coordinates from chapter VIII

I_heter$_d$

(G = -3791.292338) (doublet)

27	-0.242997000	0.653873000	-0.548285000
16	2.654586000	-0.547864000	0.844631000
7	2.076085000	0.027704000	-0.655041000
8	2.422967000	0.511291000	1.837900000
7	-0.111639000	2.148128000	0.656210000
7	-2.327481000	0.769215000	-1.043607000
7	0.337079000	1.963649000	-1.967637000
7	-0.308391000	-0.698338000	-2.060927000
8	2.047710000	-1.875556000	1.040129000
6	2.599828000	1.374316000	-1.010239000
1	3.660003000	1.327722000	-1.289662000
1	2.493314000	2.007109000	-0.128376000
6	-1.629138000	-1.360200000	-1.933363000
1	-1.579360000	-2.010131000	-1.057782000
1	-1.850021000	-1.979180000	-2.812238000
6	0.021639000	3.344340000	0.023503000
6	-3.237504000	1.722021000	-0.792488000
1	-2.880684000	2.593438000	-0.252524000
6	-0.080169000	2.132225000	2.003993000
1	-0.198422000	1.161724000	2.466648000
6	-0.147414000	3.278266000	-1.470924000
1	-1.218227000	3.340352000	-1.692684000
1	0.350207000	4.115402000	-1.973736000
6	-4.027533000	-0.532818000	-2.130886000
1	-4.293569000	-1.443527000	-2.657411000
6	1.820599000	1.971802000	-2.176607000
1	2.172356000	2.998081000	-2.325630000
1	2.045582000	1.425858000	-3.093551000
6	-4.974263000	0.454848000	-1.860159000
1	-6.006500000	0.327479000	-2.170413000
6	2.137895000	-1.017362000	-1.719079000
1	2.883887000	-1.784516000	-1.489609000
1	2.475927000	-0.539340000	-2.638402000
6	4.410371000	-0.753959000	0.635862000
6	-0.363726000	1.531036000	-3.209182000
1	0.027685000	2.058870000	-4.088198000
1	-1.417837000	1.781363000	-3.098984000
6	-0.191857000	0.021047000	-3.381903000
1	-0.942950000	-0.359123000	-4.082268000
1	0.785066000	-0.199344000	-3.813368000
6	4.921089000	-2.003360000	0.271100000
1	4.263671000	-2.861791000	0.186065000
6	-2.713566000	-0.336008000	-1.712147000
6	0.779974000	-1.693469000	-1.898592000
1	0.824722000	-2.365498000	-2.766547000
1	0.552230000	-2.281035000	-1.007900000
6	5.241392000	0.364924000	0.767488000
1	4.831478000	1.325242000	1.061052000
6	-4.569350000	1.614037000	-1.190695000
1	-5.268818000	2.413922000	-0.970271000
6	0.253335000	4.506677000	2.111391000
1	0.401670000	5.422483000	2.675407000
6	0.092622000	3.283607000	2.763639000
1	0.103913000	3.213133000	3.846068000
6	0.216825000	4.533381000	0.715972000
1	0.331489000	5.459407000	0.161981000
6	6.290278000	-2.126844000	0.039625000
1	6.701679000	-3.094598000	-0.233397000
6	7.147517000	-1.022737000	0.157774000
6	6.605639000	0.217985000	0.530399000

ANNEX

1	7.262784000	1.076437000	0.638392000
6	8.619831000	-1.156820000	-0.130273000
1	8.961050000	-2.186488000	0.023023000
1	9.209461000	-0.486543000	0.505503000
1	8.831078000	-0.888419000	-1.174981000
6	-1.939738000	-1.377856000	2.502339000
8	-2.779564000	-0.490540000	2.708912000
6	-2.189862000	-2.452294000	1.506239000
6	-1.217759000	-3.429685000	1.227685000
6	-3.409729000	-2.483919000	0.812243000
6	-1.468711000	-4.415234000	0.273019000
1	-0.262890000	-3.411462000	1.740917000
6	-3.663233000	-3.472832000	-0.134305000
1	-4.155613000	-1.726102000	1.001089000
6	-2.691825000	-4.441453000	-0.407415000
1	-0.709561000	-5.160895000	0.056301000
1	-4.611923000	-3.469844000	-0.663256000
1	-2.882295000	-5.209658000	-1.151535000
6	-0.665184000	-1.400959000	3.304448000
1	0.205369000	-1.352340000	2.642580000
1	-0.655455000	-0.553891000	3.995136000
1	-0.600149000	-2.340495000	3.868639000
1	-0.513046000	-0.366354000	0.572123000
1	-4.444258000	-0.009348000	2.071233000
8	-5.233484000	0.484338000	1.751592000
1	-4.971645000	0.740101000	0.848158000
1	-6.203985000	-0.906406000	0.910474000
1	-4.015352000	2.025981000	2.285451000
8	-3.141625000	2.372283000	2.549679000
8	-6.587844000	-1.571694000	0.298434000
1	-2.665146000	1.549274000	2.761959000
1	-6.293888000	-2.415535000	0.677212000

I_heter$_q$

(G = -3791.293083) (quartet)

27	-0.132165000	-0.125000000	-0.322210000
16	2.998157000	-0.355855000	1.170990000
7	2.336673000	-0.468059000	-0.408602000
8	2.584563000	0.948046000	1.713361000
7	-0.023187000	1.937912000	-0.060239000
7	-2.097120000	-0.461719000	-1.016627000
7	0.460203000	0.628991000	-2.406119000
7	0.123454000	-2.001729000	-1.491558000
8	2.624537000	-1.594306000	1.872579000
6	2.718200000	0.691026000	-1.262001000
1	3.786231000	0.659233000	-1.512941000
1	2.516491000	1.595434000	-0.687585000
6	-1.142773000	-2.677760000	-1.143369000
1	-1.115497000	-2.908990000	-0.072010000
1	-1.270673000	-3.613391000	-1.704114000
6	0.020797000	2.700853000	-1.171878000
6	-3.060352000	0.445903000	-1.242476000
1	-2.866546000	1.458123000	-0.899616000
6	0.054555000	2.530798000	1.143777000
1	0.018796000	1.870394000	2.001292000
6	-0.167969000	1.960125000	-2.473496000
1	-1.244364000	1.821309000	-2.627010000
1	0.215666000	2.554349000	-3.313628000
6	-3.452345000	-2.137866000	-2.070471000
1	-3.558545000	-3.170119000	-2.386835000
6	1.932931000	0.719372000	-2.571935000
1	2.201256000	1.652548000	-3.082833000
1	2.268167000	-0.090155000	-3.221623000
6	-4.443065000	-1.190298000	-2.326581000

1	-5.350622000	-1.471032000	-2.852287000
6	2.558375000	-1.819711000	-1.011109000
1	3.374207000	-2.350526000	-0.511929000
1	2.885177000	-1.675591000	-2.040808000
6	4.766896000	-0.344199000	0.963670000
6	-0.134926000	-0.333244000	-3.355881000
1	0.209623000	-0.146528000	-4.382942000
1	-1.216636000	-0.196514000	-3.336840000
6	0.225195000	-1.773102000	-2.960738000
1	-0.436458000	-2.462851000	-3.498149000
1	1.241170000	-2.004439000	-3.284293000
6	5.471711000	-1.549909000	1.017683000
1	4.958247000	-2.479456000	1.238073000
6	-2.292478000	-1.737593000	-1.415899000
6	1.301969000	-2.689904000	-0.936670000
1	1.502964000	-3.634801000	-1.462856000
1	1.085697000	-2.912099000	0.110593000
6	5.413241000	0.868734000	0.696038000
1	4.851758000	1.796087000	0.665298000
6	-4.242519000	0.124060000	-1.906447000
1	-4.980804000	0.893061000	-2.110279000
6	0.260043000	4.696343000	0.140122000
1	0.380084000	5.772920000	0.215586000
6	0.187983000	3.907543000	1.289975000
1	0.244809000	4.343565000	2.281597000
6	0.178538000	4.082478000	-1.109712000
1	0.228496000	4.657143000	-2.028723000
6	6.849559000	-1.531433000	0.802411000
1	7.410927000	-2.460450000	0.846314000
6	7.524905000	-0.332635000	0.534083000
1	6.788915000	0.862918000	0.484711000
1	7.302705000	1.798430000	0.280766000
6	9.015334000	-0.315931000	0.318865000
1	9.413028000	-1.332090000	0.225844000
1	9.521811000	0.174191000	1.161475000
1	9.274691000	0.248735000	-0.585193000
6	-2.726956000	0.423346000	2.584343000
8	-3.171547000	1.451256000	2.055161000
6	-3.223083000	-0.922271000	2.201618000
6	-2.564843000	-2.087841000	2.631940000
6	-4.343382000	-1.040293000	1.363009000
6	-3.011603000	-3.341732000	2.214023000
1	-1.697650000	-2.017393000	3.278667000
6	-4.801692000	-2.291370000	0.963523000
1	-4.857070000	-0.154549000	1.022535000
6	-4.130371000	-3.446358000	1.380744000
1	-2.489256000	-4.236404000	2.540013000
1	-5.672849000	-2.358398000	0.319366000
1	-4.477514000	-4.424122000	1.058324000
6	-1.652436000	0.531880000	3.634362000
1	-0.736760000	0.053401000	3.265012000
1	-1.456951000	1.584639000	3.851724000
1	-1.957326000	0.004970000	4.546622000
1	-0.120377000	-0.813951000	1.199999000
1	-4.660101000	1.884410000	1.125130000
8	-5.361081000	2.323206000	0.586926000
1	-5.279221000	1.882409000	-0.275258000
1	-6.745860000	0.986811000	0.831251000
1	-3.869150000	3.440621000	0.068211000
8	-2.956892000	3.765030000	-0.077146000
8	-7.299170000	0.186321000	0.714803000
1	-2.454379000	3.255475000	0.579672000
1	-7.013018000	-0.382733000	1.447349000

TS_heter$_d$

(G = -3791.280906) (doublet)

UNIVERSITAT ROVIRA I VIRGILI
MECHANISTIC STUDIES OF WATER OXIDATION CATALYZED BY HOMOGENEOUS IRON AND RUTHENIUM
COMPLEXES AND LIGHT-DRIVEN ORGANIC REDUCTIONS WITH A DUAL COBALT/COPPER CATALYTIC SYSTEM
Carla Casadevall Serrano

ANNEX

27	0.317599000	0.505641000	0.548334000
16	-2.670640000	-0.554970000	-0.929722000
7	-2.010750000	-0.127401000	0.593814000
8	-2.411539000	0.569541000	-1.840149000
7	0.117635000	2.157672000	-0.457701000
7	2.373103000	0.533514000	1.031057000
7	-0.255358000	1.650529000	2.109017000
7	0.362362000	-0.993010000	1.957327000
8	-2.132612000	-1.890303000	-1.240713000
6	-2.526714000	1.179635000	1.089319000
1	-3.582590000	1.103818000	1.376826000
1	-2.432743000	1.895824000	0.272534000
6	1.691944000	-1.638811000	1.840263000
1	1.670834000	-2.281014000	0.961733000
1	1.903004000	-2.270290000	2.711668000
6	0.008663000	3.264531000	0.324236000
6	3.280445000	1.495267000	0.801372000
1	2.921844000	2.375779000	0.277641000
6	-0.027675000	2.309669000	-1.786144000
1	0.067408000	1.413352000	-2.373017000
6	0.259209000	3.004523000	1.778295000
1	1.341344000	2.997096000	1.945687000
1	-0.181953000	3.775825000	2.418822000
6	4.076084000	-0.787463000	2.087432000
1	4.344809000	-1.710862000	2.589868000
6	-1.743524000	1.666781000	2.304007000
1	-2.077046000	2.685085000	2.527829000
1	-1.986098000	1.057310000	3.174877000
6	5.017780000	0.210984000	1.845144000
1	6.048462000	0.083996000	2.161148000
6	-2.078517000	-1.269787000	1.556755000
1	-2.821163000	-2.011370000	1.249945000
1	-2.426487000	-0.883561000	2.514298000
6	-4.427082000	-0.699553000	-0.685492000
6	0.423258000	1.096896000	3.311649000
1	0.037979000	1.562028000	4.227293000
1	1.485177000	1.326886000	3.228363000
6	0.207351000	-0.408559000	3.340807000
1	0.922989000	-0.872741000	4.026014000
1	-0.787159000	-0.646097000	3.717006000
6	-4.978807000	-1.948695000	-0.384318000
1	-4.354720000	-2.835299000	-0.360855000
6	2.763519000	-0.591390000	1.662833000
6	-0.723425000	-1.963276000	1.670057000
1	-0.775980000	-2.729618000	2.455237000
1	-0.484708000	-2.444339000	0.719634000
6	-5.217374000	0.454426000	-0.744104000
1	-4.775404000	1.413567000	-0.991456000
6	4.609962000	1.382381000	1.200454000
1	5.305858000	2.192436000	1.004466000
6	-0.420913000	4.666924000	-1.573876000
1	-0.637962000	5.638968000	-2.006017000
6	-0.291466000	3.538219000	-2.381180000
1	-0.396625000	3.595760000	-3.459113000
6	-0.267385000	4.522805000	-0.194175000
1	-0.358819000	5.367139000	0.480854000
6	-6.348548000	-2.034756000	-0.140972000
1	-6.792545000	-3.000831000	0.082139000
6	-7.165855000	-0.895692000	-0.186808000
6	-6.583000000	0.343851000	-0.496719000
1	-7.209125000	1.230190000	-0.548978000
6	-8.639538000	-0.993403000	0.107904000
1	-9.009334000	-2.010734000	-0.059904000
1	-9.213189000	-0.296922000	-0.514332000
1	-8.837788000	-0.734528000	1.157469000
6	1.636468000	-0.799483000	-2.098259000

8	2.484668000	0.130662000	-2.268628000
6	2.085130000	-2.082779000	-1.448231000
6	1.228448000	-3.191959000	-1.344643000
6	3.385407000	-2.182283000	-0.941196000
6	1.665197000	-4.366539000	-0.731057000
1	0.211372000	-3.129338000	-1.715424000
6	3.823300000	-3.356319000	-0.326336000
1	4.051088000	-1.334258000	-1.004827000
6	2.964417000	-4.452561000	-0.215584000
1	0.988664000	-5.212566000	-0.646791000
1	4.831487000	-3.400967000	0.076462000
1	3.299860000	-5.365075000	0.269505000
6	0.537079000	-0.945603000	-3.146007000
1	-0.404956000	-1.310871000	-2.739530000
1	0.377624000	0.004958000	-3.660480000
1	0.898211000	-1.670005000	-3.890114000
1	0.658790000	-0.357503000	-0.805636000
1	4.226776000	0.424152000	-2.047832000
8	5.135964000	0.806613000	-1.961911000
1	5.121733000	1.172644000	-1.060596000
1	6.093750000	-0.629760000	-1.294826000
1	3.909875000	2.597123000	-2.249264000
8	2.975169000	2.853203000	-2.342385000
8	6.548619000	-1.355235000	-0.809249000
1	2.548397000	1.972251000	-2.410348000
1	6.179995000	-2.153283000	-1.220306000

TS_heter$_q$

(G = -3791.285555) (quartet)

27	0.256618000	0.443618000	0.434710000
16	-2.608687000	-0.617562000	-0.884587000
7	-1.996572000	-0.121359000	0.654335000
8	-2.342916000	0.487876000	-1.816298000
7	0.076523000	2.339851000	-0.517157000
7	2.304033000	0.515631000	0.962752000
7	-0.346295000	1.770406000	2.133055000
7	0.330817000	-0.958602000	2.126394000
8	-2.032650000	-1.948066000	-1.137811000
6	-2.567818000	1.188594000	1.092818000
1	-3.627515000	1.082197000	1.353209000
1	-2.475744000	1.879330000	0.253806000
6	1.663348000	-1.577258000	1.979422000
1	1.628490000	-2.231111000	1.103591000
1	1.927810000	-2.187533000	2.852931000
6	-0.126153000	3.392344000	0.302177000
6	3.171565000	1.499541000	0.679273000
1	2.797829000	2.300411000	0.049323000
6	-0.046153000	2.510702000	-1.842828000
1	0.139529000	1.632292000	-2.451064000
6	0.125880000	3.122211000	1.764560000
1	1.209622000	3.154740000	1.927960000
1	-0.332972000	3.898132000	2.390387000
6	4.004285000	-0.598910000	2.233397000
1	4.288767000	-1.449390000	2.843901000
6	-1.822372000	1.739272000	2.309548000
1	-2.207285000	2.749018000	2.495013000
1	-2.063581000	1.147653000	3.193963000
6	4.909441000	0.417740000	1.931656000
1	5.927522000	0.376814000	2.305938000
6	-2.098376000	-1.225763000	1.666878000
1	-2.841859000	-1.970384000	1.369355000
1	-2.465550000	-0.792474000	2.596677000
6	-4.366675000	-0.788523000	-0.679863000
6	0.371305000	1.242876000	3.316258000

ANNEX

1	0.031484000	1.731056000	4.240211000
1	1.430553000	1.468457000	3.182926000
6	0.176812000	-0.270777000	3.439210000
1	0.902199000	-0.665484000	4.160489000
1	-0.813458000	-0.491072000	3.840402000
6	-4.902348000	-2.040998000	-0.367435000
1	-4.261458000	-2.913526000	-0.302184000
6	2.706869000	-0.514676000	1.733949000
6	-0.755250000	-1.926245000	1.860569000
1	-0.850720000	-2.655739000	2.677435000
1	-0.498084000	-2.460578000	0.942775000
6	-5.176086000	0.349311000	-0.787630000
1	-4.744323000	1.311881000	-1.039527000
6	4.481203000	1.497290000	1.154479000
1	5.147063000	2.319532000	0.910982000
6	-0.625583000	4.818006000	-1.562381000
1	-0.910523000	5.784291000	-1.967874000
6	-0.394096000	3.733036000	-2.409318000
1	-0.484433000	3.825255000	-3.486305000
6	-0.486899000	4.645814000	-0.183990000
1	-0.655088000	5.462644000	0.510347000
6	-6.277450000	-2.148590000	-0.162297000
1	-6.709610000	-3.117128000	0.072506000
6	-7.113916000	-1.027877000	-0.260372000
6	-6.545374000	0.217063000	-0.578974000
1	-7.185953000	1.090171000	-0.667311000
6	-8.596289000	-1.145856000	-0.023661000
1	-9.160433000	-0.666398000	-0.833082000
1	-8.879169000	-0.640996000	0.910011000
1	-8.903644000	-2.194411000	0.047629000
6	1.855884000	-1.064400000	-2.414672000
8	2.657394000	-0.119467000	-2.586524000
6	2.238668000	-2.217993000	-1.542508000
6	1.412899000	-3.346305000	-1.393255000
6	3.466147000	-2.183559000	-0.864497000
6	1.809657000	-4.407480000	-0.579388000
1	0.454541000	-3.393774000	-1.898029000
6	3.864658000	-3.245706000	-0.054299000
1	4.105273000	-1.317572000	-0.956746000
6	3.037379000	-4.362423000	0.092697000
1	1.159000000	-5.269995000	-0.466330000
1	4.813883000	-3.185452000	0.470501000
1	3.340829000	-5.188743000	0.729459000
6	0.688790000	-1.203310000	-3.366774000
1	-0.184677000	-1.671588000	-2.912326000
1	0.417933000	-0.215804000	-3.750169000
1	1.021019000	-1.826498000	-4.211576000
1	0.544623000	-0.407308000	-0.961361000
1	4.358443000	0.341170000	-2.148954000
8	5.210969000	0.800914000	-1.961375000
1	5.066145000	1.157019000	-1.067412000
1	6.167074000	-0.537408000	-1.137531000
1	3.892111000	2.441950000	-2.410813000
8	2.962999000	2.678945000	-2.582925000
8	6.593430000	-1.245188000	-0.558996000
1	2.560511000	1.794248000	-2.691502000
1	6.257083000	-2.082500000	-0.916111000

II_heter$_d$

(G = -3791.308208) (doublet)

27	0.161890000	0.602183000	0.691549000
16	-2.509467000	-0.284988000	-0.936899000
7	-1.925591000	0.238075000	0.654664000
8	-2.383795000	0.872579000	-1.829953000
7	0.147231000	2.116602000	-0.534420000

7	2.096206000	0.629203000	0.943328000
7	-0.379123000	2.055550000	2.138255000
7	0.197314000	-0.686592000	2.184282000
8	-1.756278000	-1.516779000	-1.210702000
6	-2.557881000	1.545689000	1.047828000
1	-3.620894000	1.402559000	1.266128000
1	-2.448675000	2.225041000	0.203360000
6	1.514174000	-1.378316000	2.120726000
1	1.457241000	-2.138001000	1.338034000
1	1.750539000	-1.874386000	3.067324000
6	0.054078000	3.321591000	0.085570000
6	2.974972000	1.539830000	0.479104000
1	2.578488000	2.317948000	-0.159195000
6	0.185677000	2.078476000	-1.878547000
1	0.286568000	1.102062000	-2.330425000
6	0.184524000	3.302178000	1.589120000
1	1.254188000	3.324479000	1.828554000
1	-0.276039000	4.193432000	2.031797000
6	3.895855000	-0.486762000	2.081735000
6	4.212203000	-1.312247000	2.709588000
6	-1.854201000	2.114712000	2.280882000
1	-2.189392000	3.149196000	2.416706000
1	-2.148280000	1.564111000	3.175378000
6	4.801047000	0.457371000	1.601375000
1	5.854447000	0.387493000	1.851575000
6	-2.196067000	-0.858163000	1.671972000
1	-2.975118000	-1.543056000	1.330455000
1	-2.588826000	-0.378746000	2.567098000
6	-4.230934000	-0.667702000	-0.738419000
6	0.308504000	1.547982000	3.347138000
1	-0.018901000	2.069410000	4.256104000
1	1.377288000	1.723154000	3.213641000
6	0.038951000	0.050321000	3.498481000
1	0.724495000	-0.373188000	4.237704000
1	-0.972540000	-0.119147000	3.867763000
6	-4.624169000	-1.999448000	-0.576308000
1	-3.887884000	-2.795891000	-0.582391000
6	2.556284000	-0.374684000	1.730305000
6	-0.924092000	-1.637040000	1.952882000
1	-1.066840000	-2.291353000	2.821444000
1	-0.661751000	-2.245038000	1.085003000
6	-5.160313000	0.380335000	-0.749470000
1	-4.839951000	1.406240000	-0.894526000
6	4.327826000	1.491439000	0.791691000
1	4.993152000	2.250562000	0.393327000
6	-0.049955000	4.458881000	-2.027109000
1	-0.140396000	5.371976000	-2.607382000
6	0.093530000	3.225197000	-2.658745000
1	0.133051000	3.139208000	-3.738708000
6	-0.065061000	4.505079000	-0.632363000
1	-0.158549000	5.443083000	-0.095487000
6	-5.979891000	-2.279734000	-0.421032000
1	-6.303002000	-3.310069000	-0.304132000
6	-6.935753000	-1.253124000	-0.417395000
6	-6.507898000	0.074404000	-0.586906000
1	-7.242392000	0.874712000	-0.598944000
6	-8.395030000	-1.563961000	-0.219862000
1	-8.609204000	-2.614046000	-0.445343000
1	-9.022484000	-0.926163000	-0.853222000
1	-8.687513000	-1.376972000	0.822794000
6	1.609954000	-1.149180000	-2.054538000
8	2.643247000	-0.248597000	-2.252648000
6	1.987261000	-2.354619000	-1.186194000
6	1.046181000	-3.359539000	-0.898848000
6	3.249473000	-2.446434000	-0.593368000
6	1.363530000	-4.419997000	-0.046689000

ANNEX

1	0.050430000	-3.299785000	-1.327116000
6	3.573447000	-3.504087000	0.262877000
1	3.974830000	-1.667608000	-0.776328000
6	2.632583000	-4.497462000	0.541367000
1	0.617391000	-5.181252000	0.167591000
1	4.558856000	-3.532856000	0.722108000
1	2.877440000	-5.317355000	1.211504000
6	1.012410000	-1.606908000	-3.401661000
1	0.162155000	-2.288955000	-3.281503000
1	0.671348000	-0.724349000	-3.958818000
1	1.787347000	-2.111731000	-3.994572000
1	0.776179000	-0.670413000	-1.495200000
1	4.234818000	-0.207783000	-2.192496000
8	5.205022000	0.094476000	-2.127304000
1	5.153874000	0.771774000	-1.432239000
1	6.026594000	-1.076183000	-1.046558000
1	4.116241000	2.017573000	-2.910635000
8	3.172374000	2.247407000	-2.888482000
8	6.446759000	-1.681876000	-0.386823000
1	2.768124000	1.347923000	-2.707383000
1	6.096803000	-2.550011000	-0.642881000

II_heter_q

(G = -3791.316152) (quartet)

27	0.367142000	0.452438000	0.577829000
16	-2.611038000	-0.432246000	-0.999998000
7	-1.951631000	-0.046898000	0.563268000
8	-2.393422000	0.752144000	-1.842133000
7	0.184809000	2.271257000	-0.431287000
7	2.369221000	0.363763000	1.144835000
7	-0.295339000	1.683933000	2.215129000
7	0.292779000	-1.061199000	2.136137000
8	-1.999499000	-1.716877000	-1.372113000
6	-2.501715000	1.250392000	1.073633000
1	-3.567490000	1.148580000	1.308458000
1	-2.379838000	1.988051000	0.280992000
6	1.603356000	-1.740340000	2.053397000
1	1.586135000	-2.396224000	1.178850000
1	1.794591000	-2.356646000	2.940606000
6	0.011746000	3.317294000	0.409711000
6	3.306568000	1.280564000	0.849128000
1	2.976208000	2.135155000	0.267759000
6	0.049923000	2.462385000	-1.753229000
1	0.216021000	1.595585000	-2.379670000
6	0.250746000	3.019469000	1.871161000
1	1.333283000	2.990494000	2.041433000
1	-0.176799000	3.803536000	2.506622000
6	4.012873000	-0.946504000	2.286017000
1	4.249549000	-1.843042000	2.848976000
6	-1.779062000	1.714201000	2.337787000
1	-2.119559000	2.733539000	2.551938000
1	-2.073031000	1.100167000	3.189340000
6	4.991282000	-0.006371000	1.966638000
1	6.018958000	-0.156535000	2.282078000
6	-2.122513000	-1.199364000	1.521777000
1	-2.867699000	-1.910139000	1.155690000
1	-2.526818000	-0.800222000	2.451113000
6	-4.354127000	-0.668219000	-0.753968000
6	0.347193000	1.095173000	3.415752000
1	-0.025887000	1.566161000	4.334203000
1	1.418372000	1.288461000	3.341462000
6	0.088532000	-0.414714000	3.468565000
1	0.759878000	-0.862605000	4.209095000
1	-0.929847000	-0.614131000	3.806050000

6	-4.846496000	-1.959762000	-0.540896000
1	-4.181872000	-2.816102000	-0.577665000
6	2.707882000	-0.733122000	1.849121000
6	-0.819783000	-1.960781000	1.752858000
1	-0.994367000	-2.725917000	2.521745000
1	-0.526373000	-2.458330000	0.824862000
6	-5.194722000	0.451234000	-0.734463000
1	-4.798440000	1.443485000	-0.920206000
6	4.631261000	1.134853000	1.243601000
1	5.361256000	1.893345000	0.980667000
6	-0.478586000	4.777388000	-1.429351000
1	-0.748772000	5.754919000	-1.817248000
6	-0.280128000	3.701174000	-2.293684000
1	-0.381266000	3.810844000	-3.367826000
6	-0.327723000	4.582800000	-0.054767000
1	-0.473136000	5.391490000	0.653660000
6	-6.208844000	-2.123541000	-0.298022000
1	-6.607544000	-3.121450000	-0.139327000
6	-7.075509000	-1.021332000	-0.260052000
6	-6.551546000	0.261845000	-0.488672000
1	-7.217121000	1.120398000	-0.477550000
6	-8.540081000	-1.203197000	0.038383000
1	-8.853699000	-2.238501000	-0.132580000
1	-9.153679000	-0.537478000	-0.579683000
1	-8.748271000	-0.957292000	1.089007000
6	1.563007000	-0.732155000	-2.284920000
8	2.475097000	0.304837000	-2.174746000
6	1.969837000	-2.001694000	-1.524649000
6	1.069173000	-3.071984000	-1.390569000
6	3.240692000	-2.136395000	-0.959106000
6	1.436013000	-4.242762000	-0.722241000
1	0.071623000	-2.983126000	-1.810120000
6	3.615954000	-3.304961000	-0.288548000
1	3.936994000	-1.313692000	-1.024785000
6	2.716780000	-4.366905000	-0.168485000
1	0.720466000	-5.055743000	-0.626101000
1	4.607495000	-3.369046000	0.153334000
1	3.001869000	-5.274500000	0.357083000
6	1.288411000	-1.088221000	-3.762386000
1	0.531602000	-1.876561000	-3.865731000
1	0.935752000	-0.192781000	-4.291331000
1	2.217737000	-1.429223000	-4.239226000
1	0.577799000	-0.436773000	-1.858315000
1	4.067054000	0.371856000	-2.210478000
8	5.042065000	0.664630000	-2.122186000
1	5.023621000	1.176617000	-1.296289000
1	5.948623000	-0.670094000	-1.314161000
1	3.930575000	2.666073000	-2.494760000
8	2.982938000	2.873883000	-2.435014000
8	6.415821000	-1.364087000	-0.787399000
1	2.593429000	1.952507000	-2.426700000
1	6.031486000	-2.185914000	-1.131690000

I_Co(III)_heter_s

(G =-3791.159912) (singlet)

27	0.071771000	0.454995000	0.711381000
16	-2.532339000	-0.439251000	-0.957329000
7	-1.934791000	0.078215000	0.659771000
8	-2.266555000	0.676913000	-1.868306000
7	0.082107000	1.999381000	-0.458370000
7	1.993553000	0.538732000	0.965185000
7	-0.385670000	1.811076000	2.163382000
7	0.141406000	-0.890275000	2.130316000
8	-1.923107000	-1.755194000	-1.184918000
6	-2.579080000	1.376621000	1.067492000

ANNEX

1	-3.642383000	1.227034000	1.275433000
1	-2.463276000	2.072983000	0.237505000
6	1.461183000	-1.557190000	1.983716000
1	1.398151000	-2.220635000	1.118359000
1	1.709951000	-2.149739000	2.869039000
6	0.058672000	3.188152000	0.197443000
6	2.844241000	1.511887000	0.586414000
1	2.452863000	2.302164000	-0.037314000
6	0.174237000	1.994391000	-1.800733000
1	0.214770000	1.026322000	-2.271261000
6	0.174888000	3.101756000	1.695449000
1	1.240426000	3.124281000	1.950383000
1	-0.302051000	3.954512000	2.188797000
6	3.799171000	-0.560813000	2.111059000
1	4.127420000	-1.408380000	2.701740000
6	-1.874354000	1.896438000	2.315224000
1	-2.178847000	2.932907000	2.486731000
1	-2.171759000	1.325508000	3.194623000
6	4.670637000	0.463256000	1.746073000
1	5.710462000	0.439049000	2.053756000
6	-2.237179000	-1.038460000	1.649372000
1	-3.036108000	-1.687593000	1.288323000
1	-2.611344000	-0.576387000	2.560570000
6	-4.286159000	-0.622972000	-0.765476000
6	0.275956000	1.284597000	3.389171000
1	-0.096432000	1.789744000	4.287630000
1	1.344026000	1.483959000	3.298558000
6	0.016414000	-0.218049000	3.487508000
1	0.724432000	-0.675829000	4.183083000
1	-0.985576000	-0.410437000	3.870473000
6	-4.823226000	-1.892067000	-0.525266000
1	-4.178961000	-2.762756000	-0.469319000
6	2.474902000	-0.495569000	1.701183000
6	-0.977793000	-1.842981000	1.895617000
1	-1.105330000	-2.507314000	2.757422000
1	-0.729436000	-2.432122000	1.012325000
6	-5.095388000	0.515321000	-0.868190000
1	-4.662407000	1.487964000	-1.074555000
6	4.179212000	1.515439000	0.973344000
1	4.814323000	2.337977000	0.660164000
6	0.132489000	4.390174000	-1.876940000
1	0.141860000	5.323549000	-2.430955000
6	0.209435000	3.167306000	-2.543370000
1	0.292843000	3.111624000	-3.622769000
6	0.058665000	4.398740000	-0.484380000
1	0.021345000	5.324775000	0.078978000
6	-6.202631000	-2.012470000	-0.375869000
1	-6.637196000	-2.991685000	-0.197259000
6	-7.040883000	-0.890210000	-0.458348000
6	-6.469850000	0.367791000	-0.712830000
1	-7.112659000	1.239416000	-0.794844000
6	-8.526332000	-1.024099000	-0.258837000
1	-8.864382000	-2.043968000	-0.471178000
1	-9.074425000	-0.322663000	-0.897934000
1	-8.790849000	-0.793869000	0.782765000
6	1.976743000	-1.124723000	-2.391874000
8	2.728270000	-0.141340000	-2.401842000
6	2.226109000	-2.269879000	-1.481166000
6	1.295860000	-3.317421000	-1.353319000
6	3.407933000	-2.304529000	-0.725432000
6	1.552949000	-4.378564000	-0.485221000
1	0.370857000	-3.298134000	-1.918987000
6	3.670141000	-3.370617000	0.130494000
1	4.118131000	-1.493779000	-0.803550000
6	2.742111000	-4.410510000	0.252772000
1	0.826859000	-5.179457000	-0.382816000

1	4.590439000	-3.377007000	0.707258000
1	2.939626000	-5.239912000	0.925860000
6	0.799640000	-1.183143000	-3.328881000
1	-0.135476000	-1.203351000	-2.757423000
1	0.812595000	-0.313548000	-3.990501000
1	0.836997000	-2.105605000	-3.920914000
1	0.321830000	-0.523391000	-0.348726000
6	4.498991000	0.195614000	-1.989311000
8	5.395830000	0.589362000	-1.897649000
1	5.339459000	1.050765000	-1.043802000
1	6.233424000	-2.308019000	-0.626372000
8	6.558523000	-1.459256000	-0.285889000
1	6.215152000	-0.812270000	-0.940572000
1	4.266497000	2.249513000	-2.437490000
8	3.405827000	2.705039000	-2.495316000
1	2.795951000	1.951623000	-2.580077000

I_Co(III)_heter$_t$

(G =-3791.134213) (triplet)

27	0.132826000	0.482409000	0.635411000
16	-2.587030000	-0.466241000	-0.923620000
7	-2.008996000	0.007697000	0.670429000
8	-2.276738000	0.657077000	-1.814664000
7	0.170631000	2.149438000	-0.473576000
7	2.178564000	0.360209000	0.994525000
7	-0.307313000	1.760114000	2.162188000
7	0.155573000	-0.980792000	2.161070000
8	-1.992032000	-1.787336000	-1.165195000
6	-2.558893000	1.340510000	1.096681000
1	-3.622382000	1.253894000	1.342347000
1	-2.437047000	2.027372000	0.258608000
6	1.452332000	-1.684746000	2.025147000
1	1.381534000	-2.344824000	1.156715000
1	1.668554000	-2.293101000	2.910237000
6	0.155930000	3.277293000	0.281663000
6	3.086260000	1.293937000	0.665243000
1	2.754306000	2.093428000	0.012799000
6	0.180007000	2.253427000	-1.816918000
1	0.188894000	1.325108000	-2.366616000
6	0.280724000	3.071834000	1.768198000
1	1.348562000	3.049521000	2.013579000
1	-0.173966000	3.896086000	2.325971000
6	3.839981000	-0.819456000	2.250914000
1	4.092791000	-1.675112000	2.867303000
6	-1.801502000	1.851706000	2.321910000
1	-2.093388000	2.891791000	2.492552000
1	-2.087260000	1.289226000	3.210419000
6	4.783418000	0.154373000	1.925839000
1	5.802207000	0.075990000	2.291278000
6	-2.257291000	-1.093609000	1.669495000
1	-3.050547000	-1.763974000	1.330932000
1	-2.623538000	-0.631802000	2.585013000
6	-4.344427000	-0.625220000	-0.759310000
6	0.345319000	1.198466000	3.381760000
1	0.002167000	1.725672000	4.279202000
1	1.418812000	1.356723000	3.275658000
6	0.038125000	-0.293597000	3.495402000
1	0.728852000	-0.751770000	4.210041000
1	-0.969894000	-0.449883000	3.880337000
6	-4.898967000	-1.884474000	-0.507494000
1	-4.267736000	-2.764685000	-0.454224000
6	2.542912000	-0.681443000	1.769649000
6	-0.984427000	-1.895748000	1.904965000
1	-1.132525000	-2.580218000	2.749130000

1	-0.746147000	-2.474166000	1.010526000
6	-5.136004000	0.526020000	-0.852285000
1	-4.688770000	1.491577000	-1.062225000
6	4.396005000	1.236233000	1.131991000
1	5.093642000	2.025761000	0.870507000
6	0.129535000	4.645571000	-1.687161000
1	0.106428000	5.621784000	-2.161252000
6	0.166777000	3.483167000	-2.459669000
1	0.181149000	3.522264000	-3.542976000
6	0.122902000	4.540866000	-0.296582000
1	0.099656000	5.418372000	0.340434000
6	-6.278760000	-1.982554000	-0.343730000
1	-6.727081000	-2.954053000	-0.156839000
6	-7.100017000	-0.847634000	-0.421542000
6	-6.511513000	0.400656000	-0.683704000
1	-7.141191000	1.282372000	-0.760327000
6	-8.585656000	-0.958416000	-0.207491000
1	-8.940150000	-1.974663000	-0.410314000
1	-9.129511000	-0.253449000	-0.846376000
1	-8.837747000	-0.717749000	0.834833000
6	1.908692000	-0.992308000	-2.497747000
8	2.706604000	-0.045873000	-2.516703000
6	2.135077000	-2.171306000	-1.623807000
6	1.176411000	-3.196080000	-1.519381000
6	3.327948000	-2.269718000	-0.889923000
6	1.418624000	-4.300439000	-0.702454000
1	0.243514000	-3.127865000	-2.067492000
6	3.574683000	-3.378638000	-0.085814000
1	4.062417000	-1.478845000	-0.949132000
6	2.620490000	-4.397931000	0.008466000
1	0.672013000	-5.084681000	-0.620944000
1	4.503972000	-3.435294000	0.473210000
1	2.807360000	-5.261424000	0.640475000
6	0.692951000	-0.968012000	-3.385706000
1	-0.219176000	-0.959040000	-2.777991000
1	0.722587000	-0.082325000	-4.024874000
1	0.661031000	-1.873041000	-4.004327000
1	0.357637000	-0.359416000	-0.544547000
1	4.474096000	0.238300000	-2.069878000
8	5.367089000	0.617365000	-1.903265000
1	5.302574000	0.908592000	-0.977727000
1	6.145581000	-2.418138000	-0.882420000
8	6.520411000	-1.605378000	-0.507204000
1	6.197750000	-0.910131000	-1.119946000
1	4.255933000	2.349913000	-2.182388000
8	3.397523000	2.800484000	-2.294465000
1	2.812265000	2.047124000	-2.487506000

TS_Co(III)_heter$_t$

(G =-3791.108659) (triplet)

27	0.288177000	0.371695000	0.531279000
16	-2.647658000	-0.533074000	-1.029104000
7	-1.924062000	-0.206039000	0.542717000
8	-2.349372000	0.644206000	-1.853757000
7	0.099285000	2.240112000	-0.332177000
7	2.294248000	0.276848000	0.946779000
7	-0.242003000	1.448587000	2.232570000
7	0.325447000	-1.245706000	1.996238000
8	-2.130175000	-1.855151000	-1.412002000
6	-2.484028000	1.062564000	1.122385000
1	-3.539409000	0.929684000	1.382228000
1	-2.398177000	1.834602000	0.357272000
6	1.661393000	-1.865341000	1.867787000
1	1.655712000	-2.509136000	0.987298000

1	1.902740000	-2.486013000	2.737961000
6	0.039999000	3.233982000	0.588932000
6	3.165160000	1.259514000	0.659840000
1	2.795571000	2.074437000	0.046923000
6	-0.068477000	2.549607000	-1.629442000
1	-0.021226000	1.729108000	-2.325822000
6	0.305743000	2.812893000	2.005172000
1	1.389775000	2.769997000	2.157957000
1	-0.111348000	3.526594000	2.723155000
6	4.000191000	-0.894183000	2.145681000
1	4.288400000	-1.767673000	2.720331000
6	-1.735042000	1.479249000	2.385438000
1	-2.058129000	2.492462000	2.642482000
1	-2.008768000	0.834932000	3.220290000
6	4.904973000	0.127861000	1.863176000
1	5.926741000	0.071070000	2.224421000
6	-2.084380000	-1.406350000	1.444622000
1	-2.834073000	-2.096623000	1.051729000
1	-2.472905000	-1.056263000	2.399614000
6	-4.395459000	-0.643142000	-0.754639000
6	0.411627000	0.800665000	3.403307000
1	0.046651000	1.246379000	4.335909000
1	1.483267000	0.988991000	3.325775000
6	0.132983000	-0.696210000	3.377868000
1	0.804226000	-1.201132000	4.079296000
1	-0.883841000	-0.906773000	3.709494000
6	-4.974578000	-1.896194000	-0.533182000
1	-4.371876000	-2.797206000	-0.561516000
6	2.697689000	-0.789321000	1.670395000
6	-0.768354000	-2.161394000	1.597426000
1	-0.898915000	-2.964368000	2.334525000
1	-0.489896000	-2.602411000	0.637368000
6	-5.155061000	0.534302000	-0.743885000
1	-4.689023000	1.495672000	-0.930420000
6	4.477585000	1.227835000	1.117107000
1	5.146419000	2.051598000	0.888992000
6	-0.373634000	4.869819000	-1.114710000
1	-0.564583000	5.894544000	-1.417784000
6	-0.304605000	3.848812000	-2.061874000
1	-0.433132000	4.044741000	-3.120430000
6	-0.200065000	4.554944000	0.233076000
1	-0.250133000	5.313359000	1.006808000
6	-6.346601000	-1.962352000	-0.296530000
1	-6.814632000	-2.928306000	-0.130663000
6	-7.134989000	-0.803070000	-0.275461000
6	-6.521466000	0.440850000	-0.503866000
1	-7.124976000	1.344114000	-0.498847000
6	-8.615835000	-0.879036000	-0.017333000
1	-8.948929000	-1.917511000	0.078851000
1	-9.176081000	-0.404588000	-0.832993000
1	-8.875932000	-0.343900000	0.905480000
6	1.646488000	-0.600050000	-2.073572000
8	2.525085000	0.332811000	-2.219653000
6	2.096067000	-1.928560000	-1.511024000
6	1.225035000	-3.030592000	-1.475193000
6	3.397161000	-2.062081000	-1.012689000
6	1.664706000	-4.252778000	-0.964111000
1	0.205663000	-2.934039000	-1.831165000
6	3.832563000	-3.280635000	-0.495733000
1	4.063146000	-1.210177000	-1.018027000
6	2.968248000	-4.380953000	-0.471180000
1	0.986202000	-5.100485000	-0.938944000
1	4.841732000	-3.363037000	-0.102104000
1	3.304804000	-5.329961000	-0.063595000
6	0.556049000	-0.670749000	-3.149752000
1	-0.382668000	-1.081102000	-2.783189000

ANNEX

1	0.392448000	0.318731000	-3.579918000
1	0.940424000	-1.327311000	-3.941010000
1	0.948827000	-0.173623000	-0.983310000
1	4.324909000	0.637873000	-2.044363000
8	5.240037000	1.000772000	-2.057046000
1	5.303231000	1.464805000	-1.205881000
1	6.198832000	-1.983316000	-1.271973000
8	6.536256000	-1.195123000	-0.817301000
1	6.117591000	-0.457929000	-1.317248000
1	3.918705000	2.840956000	-2.212720000
8	2.977383000	3.088147000	-2.205389000
1	2.553725000	2.210107000	-2.291033000

III_Co(III)_heter$_s$

(G =-3791.116184) (singlet)

27	0.102954000	0.630691000	0.748508000
16	-2.531944000	-0.256678000	-1.000022000
7	-1.916472000	0.245010000	0.642934000
8	-2.421881000	0.937464000	-1.840643000
7	0.094759000	2.120256000	-0.493526000
7	2.016491000	0.712250000	0.979057000
7	-0.325317000	1.946464000	2.091847000
7	0.174761000	-0.702253000	2.181620000
8	-1.758227000	-1.465987000	-1.296761000
6	-2.558930000	1.540384000	1.047717000
1	-3.614766000	1.385151000	1.287504000
1	-2.469035000	2.233867000	0.213125000
6	1.506284000	-1.368633000	2.076482000
1	1.447091000	-2.127957000	1.293847000
1	1.766313000	-1.861791000	3.016675000
6	0.069312000	3.325566000	0.126946000
6	2.867422000	1.621340000	0.460838000
1	2.449599000	2.425657000	-0.124655000
6	0.139149000	2.055053000	-1.834875000
1	0.193847000	1.069938000	-2.273801000
6	0.245292000	3.246115000	1.613021000
1	1.315044000	3.248799000	1.843888000
1	-0.220681000	4.079196000	2.143312000
6	3.875746000	-0.483830000	1.907892000
1	4.226677000	-1.347538000	2.460689000
6	-1.828502000	2.061490000	2.269970000
1	-2.083733000	3.109507000	2.435940000
1	-2.108912000	1.509042000	3.164181000
6	4.752708000	0.476386000	1.406692000
1	5.820044000	0.383417000	1.573864000
6	-2.205493000	-0.876122000	1.635862000
1	-2.976424000	-1.550413000	1.260372000
1	-2.614659000	-0.421448000	2.536208000
6	-4.238099000	-0.651343000	-0.764424000
6	0.318948000	1.474763000	3.363484000
1	-0.079252000	2.052754000	4.202642000
1	1.389710000	1.655193000	3.281153000
6	0.016970000	-0.008539000	3.520238000
1	0.700329000	-0.455384000	4.245055000
1	-0.997368000	-0.175020000	3.879448000
6	-4.615649000	-1.992048000	-0.631280000
1	-3.872375000	-2.781631000	-0.657059000
6	2.516599000	-0.343100000	1.672130000
6	-0.936380000	-1.657844000	1.901011000
1	-1.069063000	-2.341991000	2.745695000
1	-0.654166000	-2.226277000	1.012512000
6	-5.174812000	0.391357000	-0.752197000
1	-4.864160000	1.422722000	-0.878078000
6	4.236642000	1.543274000	0.672608000

1	4.878768000	2.304285000	0.242818000
6	0.021861000	4.446659000	-1.985420000
1	-0.020324000	5.358740000	-2.571999000
6	0.110042000	3.205501000	-2.613714000
1	0.153766000	3.115901000	-3.692754000
6	0.008289000	4.509655000	-0.589928000
1	-0.029397000	5.454135000	-0.058691000
6	-5.967652000	-2.286181000	-0.479328000
1	-6.281668000	-3.321354000	-0.384832000
6	-6.932376000	-1.267409000	-0.452423000
6	-6.517761000	0.068270000	-0.593633000
1	-7.259732000	0.861408000	-0.588393000
6	-8.388004000	-1.595207000	-0.261477000
1	-8.589285000	-2.647113000	-0.489445000
1	-9.019193000	-0.962199000	-0.895895000
1	-8.685100000	-1.411817000	0.780444000
6	1.675220000	-1.086524000	-1.892115000
8	2.679422000	-0.158311000	-1.926388000
6	2.027517000	-2.368595000	-1.133798000
6	1.055534000	-3.357822000	-0.905979000
6	3.293354000	-2.536113000	-0.567764000
6	1.344257000	-4.475545000	-0.119854000
1	0.059266000	-3.234839000	-1.320570000
6	3.588629000	-3.652559000	0.221175000
1	4.039719000	-1.769487000	-0.714193000
6	2.613932000	-4.625508000	0.453497000
1	0.575934000	-5.224137000	0.056848000
1	4.578001000	-3.745221000	0.663796000
1	2.834897000	-5.489132000	1.075201000
6	1.131185000	-1.406162000	-3.302176000
1	0.291503000	-2.110413000	-3.276698000
1	0.796491000	-0.477837000	-3.782954000
1	1.937027000	-1.839145000	-3.909871000
1	0.785832000	-0.693368000	-1.325576000
1	4.280936000	-0.199490000	-2.105373000
8	5.264163000	0.044564000	-2.135575000
1	5.302460000	0.790777000	-1.514502000
1	6.062325000	-1.103880000	-1.019393000
1	4.141368000	2.041540000	-2.932384000
8	3.214611000	2.284180000	-2.771643000
8	6.475940000	-1.709032000	-0.354629000
1	2.827509000	1.399182000	-2.511675000
1	6.137322000	-2.579448000	-0.618965000

II_Co(III)_heter$_t$

(G = -3791.117875) (triplet)

27	0.207299000	0.425113000	0.592978000
16	-2.598405000	-0.551077000	-0.961314000
7	-1.983712000	-0.133477000	0.620150000
8	-2.279059000	0.592904000	-1.825911000
7	0.115257000	2.284652000	-0.384825000
7	2.246641000	0.341774000	0.969190000
7	-0.379560000	1.652177000	2.242199000
7	0.252770000	-1.088197000	2.160238000
8	-2.021792000	-1.872288000	-1.253529000
6	-2.573518000	1.159021000	1.110650000
1	-3.637743000	1.030600000	1.335640000
1	-2.460557000	1.890124000	0.309377000
6	1.584782000	-1.717633000	2.037761000
1	1.560518000	-2.383484000	1.171882000
1	1.834628000	-2.313984000	2.923368000
6	-0.034705000	3.325242000	0.465301000
6	3.126631000	1.305991000	0.648490000
1	2.767543000	2.082827000	-0.017154000
6	0.064446000	2.510508000	-1.709067000

665

1	0.181110000	1.646619000	-2.349438000
6	0.137857000	3.006732000	1.929811000
1	1.212645000	3.012280000	2.145714000
1	-0.335790000	3.770793000	2.556590000
6	3.925931000	-0.742549000	2.289418000
1	4.197997000	-1.572189000	2.932824000
6	-1.865241000	1.649442000	2.374695000
1	-2.229894000	2.661269000	2.581230000
1	-2.142659000	1.033715000	3.230683000
6	4.842656000	0.252441000	1.953632000
1	5.857903000	0.215675000	2.335583000
6	-2.157024000	-1.282319000	1.585586000
1	-2.901061000	-1.994571000	1.220588000
1	-2.559422000	-0.876929000	2.512643000
6	-4.356301000	-0.701180000	-0.788814000
6	0.298746000	1.064862000	3.427399000
1	-0.048044000	1.539182000	4.354068000
1	1.366716000	1.263689000	3.317452000
6	0.058741000	-0.444578000	3.494374000
1	0.747593000	-0.880677000	4.225999000
1	-0.951607000	-0.656831000	3.846949000
6	-4.913004000	-1.958419000	-0.535295000
1	-4.286264000	-2.842716000	-0.496138000
6	2.633208000	-0.665823000	1.780116000
6	-0.842253000	-2.023922000	1.811606000
1	-0.988333000	-2.777192000	2.597344000
1	-0.554097000	-2.530495000	0.887165000
6	-5.145135000	0.454202000	-0.862332000
1	-4.695250000	1.418924000	-1.070341000
6	4.432487000	1.304491000	1.130310000
1	5.109233000	2.108231000	0.857741000
6	-0.314808000	4.850645000	-1.366186000
1	-0.489757000	5.852152000	-1.747325000
6	-0.142820000	3.777712000	-2.241621000
1	-0.173899000	3.911783000	-3.317257000
6	-0.261100000	4.619917000	0.008809000
1	-0.389266000	5.424081000	0.725695000
6	-6.291606000	-2.051221000	-0.351529000
1	-6.741709000	-3.021022000	-0.160288000
6	-7.108800000	-0.913546000	-0.412974000
6	-6.518022000	0.334595000	-0.675096000
1	-7.143740000	1.220653000	-0.734584000
6	-8.594958000	-1.016920000	-0.197702000
1	-8.912059000	-2.061797000	-0.117903000
1	-9.142142000	-0.543957000	-1.022668000
1	-8.887503000	-0.495603000	0.723622000
6	1.834995000	-0.751692000	-2.340604000
8	2.911413000	-0.161875000	-2.957185000
6	2.166200000	-2.006592000	-1.545732000
6	1.251570000	-3.062427000	-1.423801000
6	3.406052000	-2.106399000	-0.902212000
6	1.589571000	-4.209620000	-0.697175000
1	0.277507000	-3.000588000	-1.895090000
6	3.743294000	-3.247456000	-0.175349000
1	4.109140000	-1.285378000	-0.956462000
6	2.837184000	-4.308991000	-0.075678000
1	0.872840000	-5.022022000	-0.615731000
1	4.707031000	-3.295142000	0.323851000
1	3.095749000	-5.198075000	0.492655000
6	0.639670000	-0.856958000	-3.305776000
1	-0.280462000	-1.058816000	-2.756111000
1	0.534100000	0.085400000	-3.851029000
1	0.818245000	-1.668235000	-4.020030000
1	1.564246000	0.046708000	-1.602589000
1	4.635453000	0.258970000	-2.344047000
8	5.358946000	0.803785000	-1.964791000

1	5.052598000	0.950024000	-1.052479000
1	6.212294000	-2.170892000	-0.958636000
8	6.608229000	-1.378800000	-0.561511000
1	6.291218000	-0.660314000	-1.148466000
1	4.019357000	2.292243000	-2.342713000
8	3.141926000	2.682811000	-2.521605000
1	2.657575000	1.918028000	-2.880051000

I_homo$_s$

(G = -3791.400991) (singlet)

27	0.205434000	0.822805000	0.446905000
16	-2.689984000	-0.535584000	-0.891275000
7	-2.097106000	0.089629000	0.582747000
8	-2.586662000	0.538146000	-1.891332000
7	-0.034907000	2.278686000	-0.785976000
7	2.288872000	1.057901000	0.927739000
7	-0.430560000	2.125907000	1.846342000
7	0.350136000	-0.493436000	1.976109000
8	-1.983905000	-1.808387000	-1.113378000
6	-2.677287000	1.414480000	0.932936000
1	-3.728555000	1.321014000	1.233904000
1	-2.618596000	2.040273000	0.042083000
6	1.700330000	-1.093340000	1.844326000
1	1.678970000	-1.753631000	0.975523000
1	1.955325000	-1.690116000	2.728912000
6	-0.210900000	3.480317000	-0.174553000
6	3.155423000	2.042315000	0.645249000
1	2.750799000	2.895260000	0.107974000
6	-0.105902000	2.228725000	-2.131913000
1	0.036839000	1.251160000	-2.574047000
6	-0.014184000	3.451487000	1.317654000
1	1.056153000	3.565648000	1.520626000
1	-0.541866000	4.274855000	1.812688000
6	4.060796000	-0.159070000	1.998860000
1	4.377133000	-1.053935000	2.523898000
6	-1.909057000	2.066094000	2.076654000
1	-2.307477000	3.076884000	2.214979000
1	-2.093204000	1.525752000	3.006134000
6	4.958569000	0.868446000	1.707326000
1	6.000098000	0.787492000	2.002251000
6	-2.083243000	-0.940657000	1.663750000
1	-2.788506000	-1.751683000	1.457049000
1	-2.437513000	-0.467658000	2.580077000
6	-4.412347000	-0.885064000	-0.606951000
6	0.301504000	1.752733000	3.088698000
1	-0.110637000	2.276239000	3.960901000
1	1.339925000	2.056369000	2.965659000
6	0.211405000	0.238530000	3.287633000
1	0.991821000	-0.088782000	3.982688000
1	-0.746491000	-0.028124000	3.735910000
6	-4.802142000	-2.172814000	-0.226585000
1	-4.073343000	-2.974455000	-0.175946000
6	2.732410000	-0.022791000	1.601339000
6	-0.689795000	-1.542516000	1.836197000
1	-0.693313000	-2.204955000	2.712871000
1	-0.439135000	-2.130458000	0.952231000
6	-5.337699000	0.161880000	-0.694420000
1	-5.023074000	1.152709000	-1.004125000
6	4.496910000	1.996635000	1.021582000
1	5.158969000	2.820583000	0.777018000
6	-0.541928000	4.585019000	-2.279635000
1	-0.743478000	5.480701000	-2.859334000
6	-0.347494000	3.355151000	-2.910155000
1	-0.388296000	3.260642000	-3.990104000

ANNEX

6	-0.475390000	4.644197000	-0.886383000
1	-0.619913000	5.575925000	-0.349133000
6	-6.144416000	-2.408753000	0.066702000
1	-6.461354000	-3.407613000	0.353467000
6	-7.093644000	-1.378356000	-0.004237000
6	-6.672966000	-0.097035000	-0.395232000
1	-7.402491000	0.704833000	-0.468697000
6	-8.534326000	-1.632931000	0.354272000
1	-8.798816000	-2.685997000	0.208224000
1	-9.206067000	-1.009143000	-0.246339000
1	-8.714318000	-1.388231000	1.410579000
6	2.396224000	-1.686824000	-2.528087000
8	3.460282000	-0.984657000	-2.855900000
6	2.380897000	-2.590824000	-1.427752000
6	1.215371000	-3.351369000	-1.076518000
6	3.531602000	-2.772688000	-0.594135000
6	1.220909000	-4.219363000	0.007932000
1	0.308068000	-3.237362000	-1.661237000
6	3.520745000	-3.641325000	0.485621000
1	4.421269000	-2.197915000	-0.803751000
6	2.368966000	-4.385701000	0.806243000
1	0.314697000	-4.773319000	0.245526000
1	4.417761000	-3.727553000	1.096543000
1	2.360214000	-5.061897000	1.656511000
6	1.149229000	-1.488845000	-3.365774000
1	0.329985000	-1.046390000	-2.778446000
1	1.375749000	-0.820503000	-4.203698000
1	0.767165000	-2.437562000	-3.772009000
1	0.549949000	-0.205123000	-0.651045000
1	4.795779000	-0.518630000	-1.924336000
8	5.552026000	-0.076081000	-1.440172000
1	5.095717000	0.395870000	-0.723920000
1	6.251746000	-1.273090000	-0.254529000
1	3.791917000	1.815333000	-1.898844000
8	3.135131000	1.681395000	-2.600313000
8	6.564866000	-1.880224000	0.458170000
1	3.200296000	0.701748000	-2.769689000
1	6.342759000	-2.758359000	0.109761000

TS_homo$_s$

(G = -3791.376265) (singlet)

27	0.368092000	0.560683000	0.502166000
16	-2.643401000	-0.597202000	-0.905224000
7	-1.989547000	-0.126646000	0.601999000
8	-2.396452000	0.503837000	-1.848816000
7	0.116442000	2.198363000	-0.511508000
7	2.353897000	0.600436000	1.032007000
7	-0.298596000	1.733055000	2.107656000
7	0.382155000	-0.945143000	2.007193000
8	-2.098756000	-1.937439000	-1.185941000
6	-2.524260000	1.187451000	1.059292000
1	-3.587730000	1.108661000	1.319153000
1	-2.415056000	1.885858000	0.229150000
6	1.715872000	-1.567875000	1.886295000
1	1.700836000	-2.216102000	1.009213000
1	1.954786000	-2.187505000	2.761862000
6	-0.075844000	3.302190000	0.264799000
6	3.250642000	1.571197000	0.783178000
1	2.873280000	2.439569000	0.252798000
6	-0.024782000	2.348872000	-1.844628000
1	0.156952000	1.463940000	-2.433197000
6	0.190226000	3.075160000	1.726257000
1	1.274904000	3.084398000	1.881586000
1	-0.251004000	3.868831000	2.342984000

6	4.089681000	-0.678194000	2.095248000
1	4.374823000	-1.590125000	2.610176000
6	-1.776308000	1.713594000	2.281911000
1	-2.150146000	2.725032000	2.482091000
1	-2.022235000	1.111528000	3.158159000
6	5.018673000	0.325842000	1.825490000
1	6.055178000	0.215592000	2.128717000
6	-2.049922000	-1.241075000	1.595876000
1	-2.788290000	-1.995996000	1.311094000
1	-2.400310000	-0.829027000	2.541904000
6	-4.401675000	-0.752395000	-0.667314000
6	0.397682000	1.200596000	3.299077000
1	0.021353000	1.657362000	4.225127000
1	1.454941000	1.449573000	3.202767000
6	0.220841000	-0.315626000	3.359314000
1	0.948673000	-0.737597000	4.061724000
1	-0.767087000	-0.561388000	3.750294000
6	-4.942832000	-1.997393000	-0.324062000
1	-4.309085000	-2.875670000	-0.269145000
6	2.769777000	-0.507481000	1.683365000
6	-0.691724000	-1.923319000	1.740240000
1	-0.758958000	-2.672057000	2.544064000
1	-0.445617000	-2.433247000	0.806370000
6	-5.203649000	0.389071000	-0.760855000
1	-4.771455000	1.345973000	-1.032936000
6	4.585469000	1.482422000	1.169392000
1	5.267567000	2.298478000	0.950454000
6	-0.602182000	4.670666000	-1.639056000
1	-0.890429000	5.623471000	-2.072666000
6	-0.378767000	3.552938000	-2.443279000
1	-0.477278000	3.602915000	-3.522815000
6	-0.443219000	4.535179000	-0.257720000
1	-0.599436000	5.371100000	0.416849000
6	-6.309808000	-2.090202000	-0.077983000
1	-6.741711000	-3.053084000	0.181379000
6	-7.141012000	-0.961192000	-0.164910000
6	-6.570366000	0.272257000	-0.510483000
1	-7.205228000	1.150496000	-0.585999000
6	-8.618341000	-1.085124000	0.102217000
1	-9.119629000	-0.115103000	0.018415000
1	-8.799234000	-1.486356000	1.107756000
1	-9.084279000	-1.779059000	-0.609571000
6	1.669089000	-0.856962000	-2.098872000
8	2.591229000	0.069354000	-2.356781000
6	2.100451000	-2.116442000	-1.467005000
6	1.226148000	-3.225946000	-1.325926000
6	3.391806000	-2.239902000	-0.904080000
6	1.625228000	-4.378470000	-0.652471000
1	0.219970000	-3.171090000	-1.728519000
6	3.787772000	-3.394568000	-0.233650000
1	4.076725000	-1.407976000	-0.970056000
6	2.910573000	-4.479155000	-0.096114000
1	0.927108000	-5.207395000	-0.555815000
1	4.786190000	-3.438510000	0.196970000
1	3.216342000	-5.378315000	0.431949000
6	0.587681000	-1.000864000	-3.172307000
1	-0.368606000	-1.349065000	-2.776095000
1	0.427975000	-0.040473000	-3.672789000
1	0.916940000	-1.717230000	-3.942648000
1	0.780245000	-0.282557000	-0.854560000
1	4.208641000	0.299748000	-2.072654000
8	5.137890000	0.664597000	-1.934093000
1	5.074535000	1.059290000	-1.045665000
1	6.091168000	-0.715361000	-1.224625000
1	3.920088000	2.515028000	-2.280885000
8	2.979955000	2.717486000	-2.428373000

8	6.557651000	-1.429218000	-0.728024000
1	2.604586000	1.797514000	-2.450572000
1	6.154830000	-2.235005000	-1.089318000

II_homo$_s$

(G = -3791.404444) (singlet)

27	-0.242319000	0.680924000	-0.511550000
16	2.554291000	-0.362787000	0.887506000
7	1.871460000	0.219850000	-0.625570000
8	2.465452000	0.744282000	1.848097000
7	-0.086505000	2.127834000	0.776735000
7	-2.143288000	0.766002000	-0.591816000
7	0.312553000	2.170767000	-1.930650000
7	-0.388125000	-0.558416000	-2.061060000
8	1.849493000	-1.624807000	1.154565000
6	2.520142000	1.522222000	-1.011624000
1	3.566057000	1.359975000	-1.291681000
1	2.475277000	2.174733000	-0.139921000
6	-1.738249000	-1.185921000	-1.910786000
1	-1.655711000	-1.886947000	-1.076248000
1	-2.024879000	-1.730343000	-2.818048000
6	0.032742000	3.354965000	0.213083000
6	-2.924135000	1.870955000	-0.275767000
1	-2.516751000	2.536484000	0.474593000
6	-0.090738000	2.019493000	2.116612000
1	-0.202573000	1.016844000	2.511044000
6	-0.148749000	3.413703000	-1.287605000
1	-1.225083000	3.511524000	-1.473560000
1	0.346124000	4.300830000	-1.702198000
6	-3.890993000	0.139445000	-2.189125000
1	-4.225712000	-0.571653000	-2.939778000
6	1.769854000	2.161627000	-2.177931000
1	2.152940000	3.180946000	-2.309677000
1	1.974567000	1.622107000	-3.104235000
6	-4.682468000	1.262695000	-1.842086000
1	-5.644981000	1.447680000	-2.305969000
6	2.026358000	-0.844749000	-1.697314000
1	2.788086000	-1.579353000	-1.427457000
1	2.388519000	-0.350114000	-2.597932000
6	4.269314000	-0.703604000	0.571767000
6	-0.490257000	1.736900000	-3.095394000
1	-0.224051000	2.289560000	-4.007087000
1	-1.537034000	1.935520000	-2.861049000
6	-0.295552000	0.235741000	-3.338831000
1	-1.053136000	-0.117069000	-4.045831000
1	0.678812000	0.050747000	-3.793592000
6	4.669749000	-2.007716000	0.263486000
1	3.947441000	-2.816784000	0.250378000
6	-2.682135000	-0.079056000	-1.575182000
6	0.703055000	-1.553048000	-1.939109000
1	0.777471000	-2.176366000	-2.840119000
1	0.465317000	-2.191172000	-1.085912000
6	5.186051000	0.354478000	0.616006000
1	4.862869000	1.357174000	0.873566000
6	-4.142483000	2.137834000	-0.866246000
1	-4.687100000	3.022927000	-0.547007000
6	0.208211000	4.383339000	2.376379000
1	0.332293000	5.264042000	2.999270000
6	0.048383000	3.122864000	2.951801000
1	0.035321000	2.987350000	4.027769000
6	0.198843000	4.499447000	0.985320000
1	0.306057000	5.461754000	0.495337000
6	6.014826000	-2.247270000	-0.010217000
1	6.340876000	-3.256859000	-0.243332000

6	6.955492000	-1.206906000	0.013887000
6	6.523630000	0.090043000	0.337448000
1	7.246996000	0.899772000	0.374661000
6	8.400150000	-1.467307000	-0.320565000
1	8.658919000	-2.520497000	-0.167079000
1	9.063879000	-0.842888000	0.288412000
1	8.596786000	-1.224417000	-1.374250000
6	-1.967035000	-1.364369000	2.221643000
8	-3.216202000	-0.953690000	2.697563000
6	-2.052345000	-2.603718000	1.317531000
6	-0.914392000	-3.347701000	0.961545000
6	-3.271509000	-2.958271000	0.724876000
6	-0.989929000	-4.384287000	0.026656000
1	0.047316000	-3.105509000	1.396274000
6	-3.352356000	-3.984070000	-0.220890000
1	-4.163141000	-2.409556000	0.990648000
6	-2.209090000	-4.701629000	-0.580721000
1	-0.090388000	-4.936434000	-0.235174000
1	-4.310332000	-4.205210000	-0.685606000
1	-2.265104000	-5.496716000	-1.319827000
6	-1.007147000	-1.572752000	3.407982000
1	0.010080000	-1.835567000	3.096855000
1	-0.953102000	-0.639208000	3.983289000
1	-1.389341000	-2.362449000	4.069289000
1	-1.500922000	-0.587760000	1.573498000
1	-4.359091000	-0.496412000	1.712396000
8	-5.175308000	-0.137152000	1.203252000
1	-4.794843000	0.512063000	0.586688000
1	-5.731226000	-1.298028000	0.003668000
1	-3.705808000	1.824630000	2.178805000
8	-3.228011000	1.634561000	3.002497000
8	-6.060222000	-1.935398000	-0.682486000
1	-3.170326000	0.616847000	2.964658000
1	-6.065138000	-2.781454000	-0.207933000

I_homo$_t$

(G = -3791.406244) (triplet)

27	0.205434000	0.822805000	0.446905000
16	-2.689984000	-0.535584000	-0.891275000
7	-2.097106000	0.089629000	0.582747000
8	-2.586662000	0.538146000	-1.891332000
7	-0.034907000	2.278686000	-0.785976000
7	2.288872000	1.057901000	0.927739000
7	-0.430560000	2.125907000	1.846342000
7	0.350136000	-0.493436000	1.976109000
8	-1.983905000	-1.808387000	-1.113378000
6	-2.677287000	1.414480000	0.932936000
1	-3.728555000	1.321014000	1.233940000
1	-2.618596000	2.040273000	0.042083000
6	1.700330000	-1.093340000	1.844326000
1	1.678970000	-1.753631000	0.975523000
1	1.955325000	-1.690116000	2.728912000
6	-0.210900000	3.480317000	-0.174553000
6	3.155423000	2.042315000	0.645240000
1	2.750799000	2.895260000	0.107974000
6	-0.105902000	2.228725000	-2.131913000
1	0.036839000	1.251160000	-2.574047000
6	-0.014184000	3.451487000	1.317654000
1	1.056153000	3.565648000	1.520626000
1	-0.541866000	4.274855000	1.812688000
6	4.060796000	-0.159070000	1.998860000
1	4.377133000	-1.053935000	2.523898000
6	-1.909057000	2.066094000	2.076654000
1	-2.307477000	3.076884000	2.214979000
1	-2.093204000	1.525752000	3.006134000

ANNEX

6	4.958569000	0.868446000	1.707326000
1	6.000098000	0.787492000	2.002251000
6	-2.083243000	-0.940657000	1.663750000
1	-2.788506000	-1.751683000	1.457049000
1	-2.437513000	-0.467658000	2.580077000
6	-4.412347000	-0.885064000	-0.606951000
6	0.301504000	1.752733000	3.088698000
1	-0.110637000	2.276239000	3.960901000
1	1.339925000	2.056369000	2.965659000
6	0.211405000	0.238530000	3.287633000
1	0.991821000	-0.088782000	3.982688000
1	-0.746491000	-0.028124000	3.735910000
6	-4.802142000	-2.172814000	-0.226585000
1	-4.073343000	-2.974455000	-0.175946000
6	2.732410000	-0.022791000	1.601339000
6	-0.689795000	-1.542516000	1.836197000
1	-0.693313000	-2.204955000	2.712871000
1	-0.439135000	-2.130458000	0.952231000
6	-5.337699000	0.161880000	-0.694420000
1	-5.023074000	1.152709000	-1.004125000
6	4.496910000	1.996635000	1.021582000
1	5.158969000	2.820583000	0.777018000
6	-0.541928000	4.585019000	-2.279635000
1	-0.743478000	5.480701000	-2.859334000
6	-0.347494000	3.355151000	-2.910155000
1	-0.388296000	3.260642000	-3.990104000
6	-0.475390000	4.644197000	-0.886383000
1	-0.619913000	5.575925000	-0.349133000
6	-6.144416000	-2.408753000	0.066702000
1	-6.461354000	-3.407613000	0.353467000
6	-7.093644000	-1.378356000	-0.004237000
6	-6.672966000	-0.097035000	-0.395232000
1	-7.402491000	0.704833000	-0.468697000
6	-8.534326000	-1.632931000	0.354272000
1	-8.798816000	-2.685997000	0.208224000
1	-9.206067000	-1.009143000	-0.246339000
1	-8.714318000	-1.388231000	1.410579000
6	2.396224000	-1.686824000	-2.528087000
8	3.460282000	-0.984657000	-2.855900000
6	2.380897000	-2.590824000	-1.427752000
6	1.215371000	-3.351369000	-1.076518000
6	3.531602000	-2.772688000	-0.594135000
6	1.220909000	-4.219363000	0.007932000
1	0.308068000	-3.237362000	-1.661237000
6	3.520745000	-3.641325000	0.485621000
1	4.421269000	-2.197915000	-0.803751000
6	2.368966000	-4.385701000	0.806243000
1	0.314697000	-4.773319000	0.245526000
1	4.417761000	-3.727553000	1.096543000
1	2.360214000	-5.061897000	1.656511000
6	1.149229000	-1.488845000	-3.365774000
1	0.329985000	-1.046390000	-2.778446000
1	1.375749000	-0.820503000	-4.203698000
1	0.767165000	-2.437562000	-3.772009000
1	0.549949000	-0.205123000	-0.651045000
1	4.795779000	-0.518630000	-1.924336000
8	5.552026000	-0.076081000	-1.440172000
1	5.095717000	0.395870000	-0.723920000
1	6.251746000	-1.273090000	-0.254529000
1	3.791917000	1.815333000	-1.898844000
8	3.135131000	1.681395000	-2.600313000
8	6.564866000	-1.880224000	0.458170000
1	3.200296000	0.701748000	-2.769689000
1	6.342759000	-2.758359000	0.109761000

TS_homo_t

(G = -3791.388688) (triplet)

27	0.323311000	0.554275000	0.492823000
16	-2.584954000	-0.603187000	-0.877351000
7	-1.964073000	-0.104029000	0.641168000
8	-2.331059000	0.484482000	-1.833592000
7	0.105481000	2.220380000	-0.520977000
7	2.303929000	0.581190000	1.012198000
7	-0.294670000	1.759749000	2.118140000
7	0.351329000	-0.948813000	2.086410000
8	-2.024619000	-1.942870000	-1.125113000
6	-2.515902000	1.213879000	1.070618000
1	-3.580362000	1.129584000	1.323605000
1	-2.404953000	1.899889000	0.230539000
6	1.682093000	-1.562264000	1.942793000
1	1.651997000	-2.219024000	1.070621000
1	1.949396000	-2.171833000	2.818328000
6	-0.067567000	3.324610000	0.261003000
6	3.195911000	1.547806000	0.726527000
1	2.813741000	2.391450000	0.160899000
6	-0.028745000	2.384208000	-1.855544000
1	0.136371000	1.498046000	-2.450424000
6	0.206912000	3.092440000	1.721681000
1	1.293319000	3.088243000	1.866790000
1	-0.216838000	3.894989000	2.339811000
6	4.048362000	-0.644305000	2.123406000
1	4.338913000	-1.534808000	2.671812000
6	-1.772162000	1.758014000	2.289276000
1	-2.138848000	2.775899000	2.469879000
1	-2.027146000	1.172821000	3.174491000
6	4.970469000	0.357906000	1.822619000
1	6.006184000	0.268679000	2.135192000
6	-2.070114000	-1.203876000	1.651145000
1	-2.825720000	-1.941619000	1.366410000
1	-2.422213000	-0.765993000	2.584648000
6	-4.346607000	-0.765417000	-0.669347000
6	0.399122000	1.233722000	3.313666000
1	0.037993000	1.713942000	4.234275000
1	1.459596000	1.463758000	3.205238000
6	0.202806000	-0.281210000	3.412776000
1	0.926802000	-0.690635000	4.128150000
1	-0.788108000	-0.501120000	3.813189000
6	-4.890227000	-2.008408000	-0.332351000
1	-4.255338000	-2.884727000	-0.260120000
6	2.728605000	-0.500845000	1.701995000
6	-0.730803000	-1.913635000	1.831608000
1	-0.828519000	-2.643638000	2.650306000
1	-0.485208000	-2.451041000	0.912986000
6	-5.150066000	0.376313000	-0.779478000
1	-4.713762000	1.333384000	-1.044284000
6	4.529458000	1.484923000	1.121612000
1	5.205067000	2.298923000	0.875782000
6	-0.569172000	4.714665000	-1.635827000
1	-0.840960000	5.674764000	-2.063945000
6	-0.359269000	3.597719000	-2.447057000
1	-0.451847000	3.657478000	-3.526870000
6	-0.415618000	4.566263000	-0.254464000
1	-0.558652000	5.400779000	0.425189000
6	-6.263273000	-2.102716000	-0.107430000
1	-6.698603000	-3.063651000	0.152074000
6	-7.093073000	-0.977488000	-0.212290000
6	-6.518043000	0.258482000	-0.551369000
1	-7.152211000	1.136658000	-0.636626000
6	-8.578085000	-1.087749000	0.012695000
1	-9.116259000	-1.059963000	-0.944862000
1	-8.946491000	-0.248404000	0.614588000

ANNEX

```
1    -8.834440000   -2.025591000    0.516956000
6     1.701395000   -0.938447000   -2.219504000
8     2.587558000    0.003917000   -2.424209000
6     2.091041000   -2.153061000   -1.493502000
6     1.229180000   -3.273859000   -1.365805000
6     3.356947000   -2.237176000   -0.866872000
6     1.613843000   -4.398001000   -0.640077000
1     0.245003000   -3.250642000   -1.821642000
6     3.739199000   -3.366771000   -0.147659000
1     4.031186000   -1.395838000   -0.926216000
6     2.873731000   -4.460854000   -0.021997000
1     0.926264000   -5.236534000   -0.553561000
1     4.716016000   -3.380974000    0.331007000
1     3.168198000   -5.340087000    0.544504000
6     0.592228000   -1.059505000   -3.254435000
1    -0.341965000   -1.444345000   -2.840633000
1     0.398570000   -0.081735000   -3.706400000
1     0.909956000   -1.738389000   -4.063807000
1     0.619342000   -0.301586000   -0.829432000
1     4.232324000    0.263029000   -2.109789000
8     5.146617000    0.641600000   -1.954790000
1     5.060533000    1.028151000   -1.065841000
1     6.079002000   -0.743451000   -1.201383000
1     3.923909000    2.460895000   -2.337015000
8     2.991016000    2.679404000   -2.507324000
8     6.524570000   -1.450936000   -0.679051000
1     2.599411000    1.772147000   -2.540612000
1     6.107109000   -2.258628000   -1.018809000
```

II_homo$_t$

(G = -3791.426684) (triplet)

```
27    0.322504000    0.550226000    0.539744000
16   -2.572385000   -0.424497000   -0.916594000
7    -1.954921000    0.027470000    0.627938000
8    -2.374561000    0.720209000   -1.817300000
7     0.198716000    2.198473000   -0.498700000
7     2.299919000    0.431003000    1.059670000
7    -0.289991000    1.805093000    2.185619000
7     0.254258000   -0.962164000    2.172622000
8    -1.934358000   -1.713392000   -1.233821000
6    -2.487300000    1.354980000    1.069150000
1    -3.559059000    1.285692000    1.292040000
1    -2.335173000    2.051291000    0.245348000
6     1.558413000   -1.635322000    2.069108000
1     1.519397000   -2.308549000    1.208331000
1     1.783283000   -2.237185000    2.961705000
6     0.034235000    3.317980000    0.285254000
6     3.243597000    1.340195000    0.746397000
1     2.915869000    2.167179000    0.124707000
6     0.082906000    2.382489000   -1.845488000
1     0.247554000    1.501326000   -2.453805000
6     0.294172000    3.090077000    1.751652000
1     1.378646000    3.011095000    1.900079000
1    -0.074342000    3.935026000    2.350610000
6     3.953862000   -0.806057000    2.287964000
1     4.187827000   -1.674801000    2.895202000
6    -1.761197000    1.865764000    2.316051000
1    -2.094439000    2.898004000    2.485502000
1    -2.067896000    1.290510000    3.191697000
6     4.931278000    0.129995000    1.950247000
1     5.954344000    0.008683000    2.292408000
6    -2.154396000   -1.080133000    1.623514000
1    -2.932725000   -1.776917000    1.299770000
1    -2.525728000   -0.629959000    2.543422000
6    -4.321064000   -0.687867000   -0.714273000
```

```
6     0.366216000    1.237354000    3.376680000
1     0.032626000    1.727726000    4.303588000
1     1.439017000    1.408148000    3.270659000
6     0.093067000   -0.269370000    3.479802000
1     0.773298000   -0.700538000    4.225307000
1    -0.919990000   -0.437814000    3.850968000
6    -4.805286000   -1.980975000   -0.495211000
1    -4.128584000   -2.828604000   -0.498850000
6     2.654669000   -0.628460000    1.819923000
6    -0.866491000   -1.862067000    1.862116000
1    -1.048704000   -2.591095000    2.667487000
1    -0.607607000   -2.409384000    0.952332000
6    -5.177323000    0.419935000   -0.731721000
1    -4.789037000    1.415211000   -0.918872000
6     4.563616000    1.232220000    1.171924000
1     5.285532000    1.993765000    0.892692000
6    -0.436247000    4.724485000   -1.617130000
1    -0.691110000    5.689790000   -2.043341000
6    -0.226850000    3.601046000   -2.428810000
1    -0.302848000    3.666100000   -3.510408000
6    -0.295194000    4.560046000   -0.230890000
1    -0.431283000    5.392863000    0.453571000
6    -6.172577000   -2.159762000   -0.290545000
1    -6.563209000   -3.160688000   -0.129960000
6    -7.054165000   -1.069019000   -0.294018000
6    -6.538695000    0.217308000   -0.523091000
1    -7.214670000    1.067754000   -0.542559000
6    -8.525447000   -1.265439000   -0.039532000
1    -8.822393000   -2.305311000   -0.213049000
1    -9.127431000   -0.611206000   -0.681001000
1    -8.770244000   -1.015243000    1.002186000
6     1.578248000   -0.858953000   -2.260316000
8     2.558926000    0.117331000   -2.291733000
6     1.970316000   -2.111540000   -1.463825000
6     1.060626000   -3.170586000   -1.296814000
6     3.229867000   -2.229071000   -0.868814000
6     1.407162000   -4.311297000   -0.568801000
1     0.069208000   -3.095948000   -1.732352000
6     3.584829000   -3.368673000   -0.139766000
1     3.932102000   -1.413411000   -0.954734000
6     2.676680000   -4.418089000    0.013303000
1     0.684374000   -5.114901000   -0.449386000
1     4.567389000   -3.419029000    0.323391000
1     2.946356000   -5.302774000    0.584329000
6     1.146690000   -1.259422000   -3.688115000
1     0.331710000   -1.994365000   -3.688508000
1     0.808158000   -0.364213000   -4.226227000
1     2.003430000   -1.685043000   -4.228688000
1     0.658969000   -0.473354000   -1.764563000
1     4.143775000    0.186672000   -2.205667000
8     5.104648000    0.503189000   -2.067996000
1     5.026852000    1.005012000   -1.238880000
1     5.977461000   -0.820594000   -1.209538000
1     4.026157000    2.445624000   -2.562323000
8     3.083428000    2.682746000   -2.587453000
8     6.419571000   -1.508906000   -0.654731000
1     2.670111000    1.772016000   -2.546816000
1     6.027158000   -2.331906000   -0.986704000
```

I_homo$_{quint}$

(G = -3791.389625) (quintuplet)

```
27    0.146271000    0.763096000    0.221086000
16   -2.632583000   -0.756333000   -0.901822000
7    -2.013491000   -0.093404000    0.575001000
8    -2.542625000    0.313269000   -1.906646000
```

ANNEX

7	-0.337565000	2.531094000	-0.826714000
7	2.163014000	1.155544000	0.746299000
7	-0.575993000	2.084628000	1.877302000
7	0.441817000	-0.543625000	1.972400000
8	-1.923278000	-2.027842000	-1.112366000
6	-2.732778000	1.158416000	0.963632000
1	-3.760358000	0.935302000	1.272842000
1	-2.756702000	1.801963000	0.083360000
6	1.837764000	-0.993128000	1.802960000
1	1.864853000	-1.674006000	0.948573000
1	2.201565000	-1.533401000	2.685664000
6	-0.591797000	3.609909000	-0.056030000
6	2.886326000	2.237894000	0.417089000
1	2.378312000	2.988959000	-0.179687000
6	-0.520727000	2.616715000	-2.154910000
1	-0.307760000	1.716181000	-2.719219000
6	-0.287328000	3.454446000	1.415046000
1	0.784869000	3.638897000	1.550134000
1	-0.828892000	4.209507000	1.999998000
6	4.046233000	0.272795000	1.935698000
1	4.465842000	-0.531299000	2.529866000
6	-2.026762000	1.875351000	2.113712000
1	-2.536744000	2.835895000	2.256027000
1	-2.162484000	1.314244000	3.039864000
6	4.798869000	1.397581000	1.596186000
1	5.830197000	1.485908000	1.922490000
6	-1.940705000	-1.139859000	1.649360000
1	-2.598720000	-1.984962000	1.428554000
1	-2.323985000	-0.697453000	2.568237000
6	-4.348515000	-1.102024000	-0.586133000
6	0.234372000	1.714513000	3.058351000
1	-0.149728000	2.192532000	3.970603000
1	1.248785000	2.077568000	2.889634000
6	0.253293000	0.194647000	3.255539000
1	1.056349000	-0.061191000	3.956739000
1	-0.679413000	-0.133136000	3.717427000
6	-4.726151000	-2.378056000	-0.156431000
1	-3.990226000	-3.170153000	-0.070697000
6	2.726901000	0.187245000	1.498879000
6	-0.514771000	-1.658750000	1.821734000
1	-0.486905000	-2.333584000	2.689678000
1	-0.225272000	-2.223050000	0.932357000
6	-5.283350000	-0.069766000	-0.725452000
1	-4.976170000	0.910538000	-1.073261000
6	4.207481000	2.403316000	0.825798000
1	4.755088000	3.295102000	0.540958000
6	-1.232076000	4.896617000	-1.978271000
1	-1.587208000	5.820512000	-2.425047000
6	-0.962165000	3.781411000	-2.773996000
1	-1.096861000	3.807551000	-3.849904000
6	-1.046558000	4.808872000	-0.598226000
1	-1.249595000	5.650087000	0.056510000
6	-6.067435000	-2.615337000	0.138093000
1	-6.376146000	-3.604851000	0.463344000
6	-7.026783000	-1.598455000	0.018161000
6	-6.617576000	-0.330399000	-0.423974000
1	-7.354928000	0.459632000	-0.535835000
6	-8.466576000	-1.853887000	0.378434000
1	-8.731034000	-2.906725000	0.230237000
1	-9.139206000	-1.228197000	-0.218557000
1	-8.643318000	-1.613459000	1.436273000
6	2.645023000	-2.014665000	-2.494536000
8	3.532500000	-1.132948000	-2.903613000
6	2.772915000	-2.724482000	-1.266171000
6	1.762221000	-3.625421000	-0.787652000
6	3.923840000	-2.562850000	-0.428149000

6	1.917763000	-4.313364000	0.409555000
1	0.851903000	-3.761471000	-1.363917000
6	4.066556000	-3.259896000	0.760699000
1	4.694256000	-1.870171000	-0.730898000
6	3.071148000	-4.153729000	1.201081000
1	1.125795000	-4.982422000	0.740827000
1	4.960145000	-3.092001000	1.359644000
1	3.180832000	-4.694740000	2.136760000
6	1.439505000	-2.239291000	-3.382995000
1	0.533851000	-1.769049000	-2.966766000
1	1.628978000	-1.797434000	-4.367857000
1	1.212932000	-3.306367000	-3.516518000
1	0.488397000	-0.240329000	-1.089708000
1	4.698400000	-0.280219000	-2.025436000
8	5.330952000	0.367563000	-1.595326000
1	4.796938000	0.736197000	-0.872920000
1	6.333325000	-0.562964000	-0.368660000
1	3.427242000	1.757045000	-2.338670000
8	2.702116000	1.459213000	-2.911892000
8	6.784390000	-1.030034000	0.373809000
1	2.904274000	0.489845000	-3.002059000
1	6.704663000	-1.964692000	0.124928000

TS_homo_{quint}

TS_homo_{quint}

(G = -3791.362011) (quintuplet)

27	0.284834000	0.545380000	0.411417000
16	-2.589458000	-0.664730000	-0.878528000
7	-1.989667000	-0.139565000	0.651723000
8	-2.344310000	0.427395000	-1.832137000
7	0.181905000	2.342466000	-0.545055000
7	2.296570000	0.584512000	1.011905000
7	-0.374532000	1.790029000	2.123362000
7	0.342716000	-0.937775000	2.102653000
8	-2.002884000	-1.993823000	-1.116695000
6	-2.572011000	1.172042000	1.068806000
1	-3.637066000	1.067266000	1.308581000
1	-2.458301000	1.855239000	0.226329000
6	1.679478000	-1.544572000	1.967618000
1	1.660715000	-2.201098000	1.093146000
1	1.943204000	-2.151121000	2.845027000
6	-0.235962000	3.386521000	0.283897000
6	3.163525000	1.568665000	0.720185000
1	2.766672000	2.383282000	0.124587000
6	0.025273000	2.549538000	-1.901667000
1	0.379236000	1.741306000	-2.535247000
6	0.082351000	3.147541000	1.729151000
1	1.171921000	3.160032000	1.868440000
1	-0.357652000	3.921593000	2.373554000
6	4.028812000	-0.579365000	2.187967000
1	4.326265000	-1.449996000	2.762800000
6	-1.846539000	1.739743000	2.289422000
1	-2.248118000	2.746961000	2.458053000
1	-2.090920000	1.154110000	3.177880000
6	4.931282000	0.439850000	1.887945000
1	5.960426000	0.381401000	2.228046000
6	-2.078525000	-1.235296000	1.669679000
1	-2.820868000	-1.987027000	1.386177000
1	-2.439894000	-0.797342000	2.599539000
6	-4.347104000	-0.849619000	-0.671054000
6	0.342450000	1.271148000	3.303791000
1	-0.014019000	1.738978000	4.233339000
1	1.397082000	1.524527000	3.183402000
6	0.182331000	-0.248626000	3.415805000
1	0.915935000	-0.632951000	4.135139000
1	-0.802525000	-0.486766000	3.820359000

ANNEX

6	-4.874170000	-2.101741000	-0.343313000
1	-4.226810000	-2.968683000	-0.267808000
6	2.716358000	-0.474048000	1.731910000
6	-0.727977000	-1.921387000	1.854584000
1	-0.808925000	-2.645502000	2.679126000
1	-0.473829000	-2.460597000	0.939208000
6	-5.165709000	0.280403000	-0.792412000
1	-4.741069000	1.242911000	-1.056215000
6	4.487349000	1.542253000	1.151390000
1	5.152594000	2.364337000	0.905549000
6	-1.035637000	4.707585000	-1.583322000
1	-1.520238000	5.594573000	-1.977939000
6	-0.548556000	3.677316000	-2.438998000
1	-0.628974000	3.766004000	-3.519779000
6	-0.849767000	4.523418000	-0.190285000
1	-1.164857000	5.281591000	0.523604000
6	-6.248597000	-2.217155000	-0.136488000
1	-6.673567000	-3.186015000	0.110016000
6	-7.093496000	-1.103967000	-0.247744000
6	-6.534037000	0.140915000	-0.581846000
1	-7.181062000	1.008160000	-0.680974000
6	-8.575002000	-1.229269000	-0.008252000
1	-9.143166000	-0.750127000	-0.815013000
1	-8.858265000	-0.728504000	0.927594000
1	-8.877591000	-2.279374000	0.061137000
6	1.873849000	-1.017566000	-2.348627000
8	2.682081000	-0.051406000	-2.511965000
6	2.262497000	-2.180479000	-1.516935000
6	1.441940000	-3.323294000	-1.385327000
6	3.491018000	-2.165018000	-0.828450000
6	1.838856000	-4.396203000	-0.590167000
1	0.484263000	-3.367059000	-1.892209000
6	3.888599000	-3.241522000	-0.038588000
1	4.128342000	-1.295516000	-0.896244000
6	3.065764000	-4.366192000	0.089019000
1	1.187963000	-5.261668000	-0.496476000
1	4.836958000	-3.187696000	0.489714000
1	3.369405000	-5.203799000	0.710764000
6	0.734037000	-1.155779000	-3.337525000
1	-0.140838000	-1.657474000	-2.920911000
1	0.441493000	-0.163006000	-3.691801000
1	1.090515000	-1.737894000	-4.202658000
1	0.538866000	-0.396841000	-0.927924000
1	4.366962000	0.328577000	-2.117289000
8	5.238968000	0.763298000	-1.933276000
1	5.100100000	1.138155000	-1.045820000
1	6.191422000	-0.601598000	-1.121531000
1	4.034323000	2.448927000	-2.423112000
8	3.106536000	2.720101000	-2.546586000
8	6.628061000	-1.281772000	-0.560063000
1	2.663717000	1.847796000	-2.600041000
1	6.256055000	-2.110717000	-0.901266000

II_homo_{quint}

(G = -3791.394785) (quintuplet)

27	0.420612000	0.443968000	0.548278000
16	-2.628922000	-0.502034000	-0.924463000
7	-1.932166000	-0.050763000	0.600542000
8	-2.390693000	0.623114000	-1.840058000
7	0.210407000	2.202180000	-0.560935000
7	2.345550000	0.453248000	1.049705000
7	-0.221133000	1.744146000	2.129481000
7	0.323426000	-1.009649000	2.160724000
8	-2.065879000	-1.825702000	-1.234527000

6	-2.453559000	1.279822000	1.052658000
1	-3.516909000	1.209106000	1.309781000
1	-2.332192000	1.973110000	0.220615000
6	1.652029000	-1.660741000	2.032399000
1	1.603260000	-2.271353000	1.124969000
1	1.859107000	-2.319746000	2.887791000
6	0.075658000	3.284927000	0.239957000
6	3.320753000	1.406618000	0.787360000
1	3.018386000	2.213376000	0.125529000
6	0.046786000	2.353669000	-1.884249000
1	0.177606000	1.463496000	-2.486642000
6	0.341320000	3.046828000	1.708618000
1	1.426555000	2.998413000	1.854748000
1	-0.054856000	3.871245000	2.313614000
6	3.971967000	-0.719361000	2.432420000
1	4.187513000	-1.574525000	3.070135000
6	-1.700639000	1.795340000	2.278729000
1	-2.028239000	2.826609000	2.453994000
1	-1.984056000	1.221277000	3.161448000
6	4.971759000	0.262514000	2.163826000
1	5.967819000	0.192231000	2.587166000
6	-2.097136000	-1.153417000	1.614467000
1	-2.863589000	-1.866901000	1.300549000
1	-2.469982000	-0.702730000	2.533699000
6	-4.377328000	-0.662324000	-0.649497000
6	0.437052000	1.197204000	3.343016000
1	0.081895000	1.710565000	4.246305000
1	1.507409000	1.371702000	3.236150000
6	0.168356000	-0.309985000	3.464439000
1	0.862538000	-0.730015000	4.202225000
1	-0.840065000	-0.482518000	3.845890000
6	-4.915351000	-1.920102000	-0.359596000
1	-4.281472000	-2.800061000	-0.343021000
6	2.722232000	-0.614589000	1.879223000
6	-0.794543000	-1.916353000	1.851203000
1	-0.965526000	-2.646949000	2.656343000
1	-0.528703000	-2.460655000	0.940933000
6	-5.178884000	0.484136000	-0.703533000
1	-4.747635000	1.448628000	-0.948239000
6	4.591071000	1.344711000	1.310101000
1	5.296784000	2.135991000	1.065266000
6	-0.427732000	4.690584000	-1.639293000
1	-0.686200000	5.659140000	-2.056875000
6	-0.270998000	3.578208000	-2.465279000
1	-0.394157000	3.648828000	-3.540630000
6	-0.249716000	4.540497000	-0.262661000
1	-0.362752000	5.376680000	0.419616000
6	-6.283724000	-2.021752000	-0.116503000
1	-6.717810000	-2.993945000	0.098950000
6	-7.112244000	-0.890250000	-0.153315000
6	-6.542694000	0.357460000	-0.455288000
1	-7.177984000	1.237451000	-0.501975000
6	-8.584377000	-1.004622000	0.141993000
1	-8.946230000	-2.022190000	-0.040830000
1	-9.164405000	-0.302913000	-0.468214000
1	-8.781891000	-0.763758000	1.195967000
6	1.529995000	-0.847744000	-2.340572000
8	2.483625000	0.153571000	-2.318312000
6	1.928333000	-2.112596000	-1.565837000
6	1.017479000	-3.172398000	-1.413762000
6	3.192094000	-2.243709000	-0.983548000
6	1.365663000	-4.325250000	-0.706394000
1	0.024526000	-3.087523000	-1.845179000
6	3.549946000	-3.395875000	-0.276417000
1	3.894935000	-1.427855000	-1.058544000
6	2.638649000	-4.444404000	-0.133862000

ANNEX

1	0.642442000	-5.129967000	-0.596910000
1	4.536704000	-3.456066000	0.176599000
1	2.909099000	-5.339458000	0.420488000
6	1.148036000	-1.223377000	-3.789720000
1	0.355081000	-1.981163000	-3.829863000
1	0.798704000	-0.324555000	-4.315051000
1	2.031621000	-1.610278000	-4.315842000
1	0.583639000	-0.505171000	-1.860956000
1	4.083345000	0.275464000	-2.143942000
8	5.009870000	0.628645000	-1.919101000
1	4.856770000	0.989289000	-1.023228000
1	5.915893000	-0.759127000	-1.184901000
1	3.930964000	2.475485000	-2.411302000
8	3.009585000	2.718697000	-2.611233000
8	6.360190000	-1.485370000	-0.683659000
1	2.592377000	1.809924000	-2.604920000
1	5.988210000	-2.283215000	-1.091802000

I_H_homo$_s$

(G = -3791.848114) (singlet)

27	0.188215000	-0.229832000	0.693849000
16	-2.759946000	0.065805000	-1.043174000
7	-2.189672000	-0.436783000	0.488365000
8	-2.380670000	1.477336000	-1.207370000
7	0.300161000	1.700165000	0.604387000
7	2.237982000	-0.738711000	1.113991000
7	-0.277526000	0.077772000	2.632209000
7	-0.037365000	-2.207175000	1.155640000
8	-2.282186000	-0.934665000	-2.011515000
6	-2.544017000	0.506083000	1.584381000
1	-3.613457000	0.453133000	1.824806000
1	-2.308975000	1.511540000	1.235188000
6	1.202247000	-2.861005000	0.667103000
1	1.179505000	-2.840361000	-0.428092000
1	1.258181000	-3.905257000	0.999567000
6	0.312484000	2.296311000	1.827398000
6	3.273347000	0.039175000	1.457866000
1	3.108410000	1.110221000	1.402908000
6	0.270793000	2.493547000	-0.485478000
1	0.260106000	1.984644000	-1.436736000
6	0.428337000	1.337823000	2.979659000
1	1.487075000	1.096484000	3.120025000
1	0.052927000	1.776156000	3.911459000
6	3.579509000	-2.677801000	1.566825000
1	3.653351000	-3.760089000	1.591928000
6	-1.756211000	0.197567000	2.853653000
1	-1.962364000	0.992938000	3.577602000
1	-2.114185000	-0.732481000	3.296334000
6	4.649463000	-1.863874000	1.942330000
1	5.584311000	-2.303953000	2.276601000
6	-2.467828000	-1.882971000	0.737308000
1	-3.291813000	-2.247890000	0.116731000
1	-2.809034000	-1.983056000	1.767764000
6	-4.535928000	-0.033817000	-0.960237000
6	0.262141000	-1.093412000	3.376175000
1	-0.104260000	-1.105374000	4.410448000
1	1.347202000	-1.002602000	3.398611000
6	-0.153261000	-2.372907000	2.651229000
1	0.470927000	-3.208085000	2.985512000
1	-1.184323000	-2.627575000	2.898077000
6	-5.186307000	-1.182663000	-1.418234000
1	-4.622520000	-1.987554000	-1.877215000
6	2.399073000	-2.077329000	1.142606000
6	-1.232741000	-2.741436000	0.463495000

1	-1.440639000	-3.773444000	0.778010000
1	-1.019062000	-2.732602000	-0.606287000
6	-5.244879000	1.021901000	-0.372683000
1	-4.726657000	1.910607000	-0.028947000
6	4.498256000	-0.478756000	1.876256000
1	5.306915000	0.193708000	2.140679000
6	0.229688000	4.488126000	0.850938000
1	0.196672000	5.568963000	0.947004000
6	0.235394000	3.881801000	-0.404882000
1	0.228007000	4.466199000	-1.317727000
6	0.268608000	3.676531000	1.986440000
1	0.264672000	4.096367000	2.986858000
6	-6.572602000	-1.266648000	-1.287638000
1	-7.091210000	-2.152179000	-1.644123000
6	-7.309413000	-0.225998000	-0.705657000
6	-6.627125000	0.915914000	-0.252584000
1	-7.189049000	1.730440000	0.196415000
6	-8.807376000	-0.314608000	-0.575644000
1	-9.121664000	-0.119841000	0.457461000
1	-9.173666000	-1.302574000	-0.873745000
1	-9.295451000	0.438816000	-1.208268000
6	2.622685000	0.517241000	-2.613784000
8	3.261421000	1.542235000	-1.973097000
6	2.986419000	-0.841939000	-2.464177000
6	2.181782000	-1.852749000	-3.080535000
6	4.112788000	-1.281245000	-1.704559000
6	2.478685000	-3.199679000	-2.927290000
1	1.317375000	-1.560383000	-3.667412000
6	4.398437000	-2.633354000	-1.571336000
1	4.756372000	-0.563122000	-1.209781000
6	3.588777000	-3.610192000	-2.170726000
1	1.840242000	-3.941944000	-3.400401000
1	5.258324000	-2.933360000	-0.978930000
1	3.816937000	-4.665473000	-2.052057000
6	1.476805000	0.980713000	-3.458055000
1	1.398280000	2.070711000	-3.414201000
1	1.602986000	0.679975000	-4.507891000
1	0.525872000	0.547903000	-3.114706000
1	0.367450000	-0.448677000	-0.827967000
1	4.070778000	1.306364000	-1.445343000
6	2.865062000	2.793877000	-0.185068000
8	3.387326000	3.364045000	0.407433000
1	5.904480000	2.246531000	-0.960182000
8	5.418980000	1.652908000	-0.362196000
1	4.832489000	2.264142000	0.144165000
1	2.948499000	3.310401000	-2.467037000
8	2.659700000	4.242926000	-2.541565000
1	2.493728000	4.476583000	-1.613826000
1	2.888733000	3.336515000	1.242002000

TS_H_homo$_s$

(G = -3791.835250) (singlet)

27	0.417652000	0.216007000	0.704550000
16	-2.586958000	-0.329148000	-0.961130000
7	-1.937096000	-0.277096000	0.622793000
8	-2.262684000	0.952173000	-1.605901000
7	0.317936000	2.048882000	0.082760000
7	2.447985000	0.028395000	1.190968000
7	-0.145550000	1.038868000	2.510552000
7	0.353915000	-1.559824000	1.761116000
8	-2.113072000	-1.591442000	-1.553365000
6	-2.401000000	0.917108000	1.385186000
1	-3.467670000	0.838064000	1.629771000
1	-2.246748000	1.786149000	0.744853000
6	1.651837000	-2.223672000	1.497592000

1	1.626299000	-2.607222000	0.475479000
1	1.814351000	-3.067855000	2.179588000
6	0.268097000	2.968128000	1.084613000
6	3.404059000	0.970190000	1.195424000
1	3.106927000	1.950738000	0.840272000
6	0.223046000	2.498918000	-1.183149000
1	0.280422000	1.748571000	-1.951648000
6	0.450761000	2.394514000	2.461036000
1	1.525512000	2.289259000	2.645281000
1	0.036720000	3.055572000	3.232230000
6	4.036187000	-1.541598000	2.073605000
1	4.239108000	-2.552856000	2.410893000
6	-1.626294000	1.088546000	2.689072000
1	-1.923545000	2.049172000	3.124772000
1	-1.920335000	0.317279000	3.402121000
6	5.026359000	-0.558806000	2.076521000
1	6.028395000	-0.787950000	2.426860000
6	-2.085121000	-1.595794000	1.312764000
1	-2.876215000	-2.201968000	0.862340000
1	-2.406818000	-1.402826000	2.335364000
6	-4.353477000	-0.430925000	-0.763978000
6	0.494365000	0.189397000	3.545332000
1	0.128549000	0.439093000	4.549984000
1	1.566907000	0.380900000	3.513962000
6	0.217562000	-1.279118000	3.236312000
1	0.911881000	-1.909408000	3.801731000
1	-0.786649000	-1.551034000	3.562749000
6	-4.972078000	-1.683771000	-0.734593000
1	-4.394767000	-2.586494000	-0.901125000
6	2.765049000	-1.214384000	1.610925000
6	-0.776367000	-2.381638000	1.270386000
1	-0.888326000	-3.295659000	1.870541000
1	-0.553197000	-2.659808000	0.238440000
6	-5.082449000	0.748551000	-0.563222000
1	-4.588355000	1.713667000	-0.593197000
6	4.705364000	0.722633000	1.623970000
1	5.443159000	1.517754000	1.601869000
6	0.026554000	4.782353000	-0.472677000
1	-0.087018000	5.840963000	-0.685478000
6	0.082750000	3.844645000	-1.502653000
1	0.037992000	4.134949000	-2.546487000
6	0.117249000	4.328434000	0.844816000
1	0.074912000	5.012880000	1.685958000
6	-6.346391000	-1.748522000	-0.504713000
1	-6.841144000	-2.715397000	-0.484456000
6	-7.102161000	-0.585801000	-0.299964000
6	-6.452124000	0.659458000	-0.335005000
1	-7.028715000	1.567709000	-0.182060000
6	-8.586723000	-0.658700000	-0.057245000
1	-8.861888000	-0.106571000	0.850266000
1	-8.920897000	-1.696120000	0.048725000
1	-9.138162000	-0.203065000	-0.890566000
6	1.666031000	-0.651511000	-2.154996000
8	2.482170000	0.485811000	-2.217192000
6	2.272789000	-1.932181000	-1.847948000
6	1.518408000	-3.126420000	-2.022679000
6	3.559132000	-2.063296000	-1.265834000
6	2.018302000	-4.362410000	-1.626708000
1	0.523912000	-3.074664000	-2.452868000
6	4.052050000	-3.306671000	-0.878447000
1	4.173911000	-1.190073000	-1.079538000
6	3.291212000	-4.469770000	-1.046985000
1	1.408542000	-5.251653000	-1.768620000
1	5.038996000	-3.364054000	-0.425931000
1	3.678631000	-5.435763000	-0.735731000
6	0.620361000	-0.588978000	-3.244117000

1	0.293831000	0.439799000	-3.416246000
1	1.035708000	-0.963226000	-4.193539000
1	-0.260253000	-1.181858000	-2.994231000
1	0.749756000	-0.352776000	-0.779795000
1	3.408676000	0.363636000	-1.903892000
1	2.692788000	2.385762000	-1.424466000
8	3.284471000	3.158693000	-1.355569000
1	5.299560000	1.167588000	-2.512557000
8	5.102643000	1.038369000	-1.569109000
1	4.685102000	1.888639000	-1.306626000
1	2.096382000	1.740973000	-3.530199000
8	1.880451000	2.563903000	-4.017667000
1	2.121005000	3.242825000	-3.365209000
1	2.925291000	3.650192000	-0.597119000

II_H_homo$_s$

(G = -3791.869972) (singlet)

27	0.363194000	-0.361420000	-0.809325000
16	-2.404417000	0.202606000	0.861739000
7	-1.788270000	-0.112379000	-0.752261000
8	-2.070288000	-0.970445000	1.679436000
7	0.454148000	-2.023505000	0.239562000
7	2.251570000	-0.189081000	-0.961555000
7	-0.122426000	-1.678390000	-2.410326000
7	0.271807000	1.102203000	-2.171745000
8	-1.862362000	1.523111000	1.214166000
6	-2.319057000	-1.417918000	-1.276939000
1	-3.393213000	-1.343067000	-1.477237000
1	-2.145378000	-2.168422000	-0.505604000
6	1.556843000	1.847977000	-2.003212000
1	1.454959000	2.426212000	-1.081206000
1	1.733791000	2.531115000	-2.842484000
6	0.454217000	-3.146141000	-0.518075000
6	3.173530000	-1.219665000	-0.824847000
1	2.895474000	-2.007545000	-0.137992000
6	0.555664000	-2.148379000	1.575932000
1	0.569242000	-1.230561000	2.147936000
6	0.527731000	-2.938069000	-2.012498000
1	1.592598000	-2.863362000	-2.264611000
1	0.115691000	-3.804048000	-2.545933000
6	3.816521000	0.823588000	-2.551318000
1	4.015624000	1.647945000	-3.232007000
6	-1.588061000	-1.811727000	-2.562214000
1	-1.864635000	-2.845173000	-2.803812000
1	-1.918940000	-1.190116000	-3.396291000
6	4.750226000	-0.224723000	-2.379133000
1	5.693993000	-0.239804000	-2.913805000
6	-2.127156000	1.059544000	-1.653428000
1	-2.949381000	1.653714000	-1.248617000
1	-2.488272000	0.651812000	-2.596184000
6	-4.170638000	0.318899000	0.718987000
6	0.532562000	-0.991755000	-3.545420000
1	0.251278000	-1.437490000	-4.509721000
1	1.610665000	-1.099805000	-3.412757000
6	0.166518000	0.496240000	-3.546891000
1	0.827396000	1.030525000	-4.236671000
1	-0.853821000	0.632102000	-3.909596000
6	-4.768225000	1.573949000	0.570601000
1	-4.166231000	2.476040000	0.582055000
6	2.629684000	0.821886000	-1.857376000
6	-0.905221000	1.943138000	-1.852037000
1	-1.102956000	2.674200000	-2.647464000
1	-0.682264000	2.478210000	-0.926981000
6	-4.929089000	-0.859326000	0.725370000
1	-4.450148000	-1.823493000	0.856050000

ANNEX

6	4.378954000	-1.261055000	-1.490950000
1	5.042457000	-2.102163000	-1.305064000
6	0.613237000	-4.539928000	1.433987000
1	0.670663000	-5.520572000	1.896524000
6	0.650950000	-3.381261000	2.210306000
1	0.752583000	-3.413217000	3.288705000
6	0.511675000	-4.416543000	0.048773000
1	0.494311000	-5.287627000	-0.598194000
6	-6.152896000	1.641904000	0.422940000
1	-6.631947000	2.610275000	0.310770000
6	-6.938736000	0.481244000	0.418975000
6	-6.308523000	-0.765545000	0.575653000
1	-6.909021000	-1.670942000	0.583768000
6	-8.432903000	0.559273000	0.253101000
1	-8.752411000	0.007761000	-0.640786000
1	-8.767066000	1.597659000	0.158583000
1	-8.944165000	0.104671000	1.111481000
6	1.565220000	1.331849000	2.246006000
8	2.738806000	0.729673000	2.815316000
6	1.876589000	2.617059000	1.485886000
6	0.853430000	3.532423000	1.187691000
6	3.158010000	2.863770000	0.973446000
6	1.103845000	4.656012000	0.395993000
1	-0.152394000	3.361978000	1.553865000
6	3.408424000	3.983233000	0.174662000
1	3.967820000	2.171932000	1.177143000
6	2.382681000	4.884385000	-0.119883000
1	0.294096000	5.346454000	0.175049000
1	4.407767000	4.145486000	-0.220755000
1	2.576236000	5.752372000	-0.744304000
6	0.599896000	1.514093000	3.412971000
1	0.389582000	0.538925000	3.864894000
1	1.053581000	2.165088000	4.170542000
1	-0.345905000	1.949919000	3.089571000
1	1.131190000	0.638161000	1.510395000
1	3.372937000	0.439315000	2.121894000
1	2.991419000	-1.882281000	2.108508000
8	3.788207000	-2.405532000	2.300297000
1	5.446642000	0.200887000	2.356385000
8	5.065820000	-0.077918000	1.506443000
1	4.787522000	-1.008982000	1.671823000
1	2.270282000	-0.631396000	3.926571000
8	2.008668000	-1.366375000	4.528459000
1	2.479114000	-2.127815000	4.151323000
1	3.719634000	-3.140878000	1.667158000

I_H_homo$_t$

(G = -3791.849121) (triplet)

27	-0.189486000	-0.229297000	-0.694804000
16	2.761190000	0.062503000	1.038141000
7	2.188815000	-0.438168000	-0.493172000
8	2.381850000	1.473741000	1.204619000
7	-0.299863000	1.700566000	-0.602929000
7	-2.240156000	-0.736594000	-1.113030000
7	0.273685000	0.080319000	-2.633577000
7	0.034316000	-2.206109000	-1.159265000
8	2.284921000	-0.939291000	2.005875000
6	2.542137000	0.505746000	-1.588542000
1	3.611198000	0.452319000	-1.830594000
1	2.308329000	1.510963000	-1.237812000
6	-1.204929000	-2.859857000	-0.669705000
1	-1.180808000	-2.840214000	0.425464000
1	-1.261789000	-3.903763000	-1.003094000
6	-0.313545000	2.298291000	-1.825142000
6	-3.275701000	0.042101000	-1.454526000

1	-3.110157000	1.112968000	-1.398593000
6	-0.268416000	2.492481000	0.487949000
1	-0.256655000	1.982236000	1.438445000
6	-0.431732000	1.341346000	-2.978420000
1	-1.490849000	1.100961000	-3.117602000
1	-0.057271000	1.780539000	-3.910197000
6	-3.583191000	-2.674579000	-1.566291000
1	-3.657491000	-3.756807000	-1.592539000
6	1.752156000	0.199254000	-2.856974000
1	1.957871000	0.995184000	-3.580440000
1	2.108809000	-0.730608000	-3.301111000
6	-4.653266000	-1.859757000	-1.939475000
1	-5.588751000	-2.298999000	-2.273067000
6	2.465715000	-1.884231000	-0.744180000
1	3.290209000	-2.250457000	-0.125088000
1	2.805414000	-1.983309000	-1.775228000
6	4.537252000	-0.036148000	0.954005000
6	-0.267802000	-1.089580000	-3.378248000
1	0.097332000	-1.100646000	-4.412877000
1	-1.352816000	-0.997919000	-3.399251000
6	0.147773000	-2.370174000	-2.655268000
1	-0.477432000	-3.204609000	-2.989506000
1	1.178297000	-2.625171000	-2.903952000
6	5.189048000	-1.186912000	1.409156000
1	4.625061000	-1.994055000	1.863939000
6	-2.401947000	-2.075091000	-1.142879000
6	1.230396000	-2.742186000	-0.469685000
1	1.437001000	-3.773894000	-0.785993000
1	1.018314000	-2.734615000	0.600429000
6	5.244618000	1.020047000	0.368417000
6	4.725924000	1.908128000	0.023783000
6	-4.501384000	-0.474790000	-1.871875000
1	-5.310117000	0.198363000	-2.134299000
6	-0.227889000	4.488779000	-0.845930000
1	-0.194318000	5.569721000	-0.940613000
6	-0.232225000	3.880809000	0.409092000
1	-0.223328000	4.464088000	1.322608000
6	-0.268963000	3.678690000	-1.982441000
1	-0.266179000	4.099852000	-2.982305000
6	6.574047000	-1.269586000	1.278800000
1	7.092867000	-2.157025000	1.630706000
6	7.311065000	-0.224631000	0.701372000
6	6.628301000	0.915176000	0.248227000
1	7.189798000	1.728858000	-0.202403000
6	8.810858000	-0.310856000	0.596333000
1	9.180004000	0.267232000	-0.258151000
1	9.140996000	-1.350737000	0.494643000
1	9.282851000	0.097658000	1.500987000
6	-2.617902000	0.514839000	2.615174000
8	-3.255893000	1.540677000	1.975090000
6	-2.983719000	-0.843906000	2.466091000
6	-2.180431000	-1.855704000	3.082576000
6	-4.110567000	-1.281732000	1.706449000
6	-2.478857000	-3.202267000	2.929188000
1	-1.315784000	-1.564338000	3.669614000
6	-4.397837000	-2.633535000	1.573064000
1	-4.753158000	-0.562798000	1.211587000
6	-3.589345000	-3.611373000	2.172353000
1	-1.841407000	-3.945360000	3.402341000
1	-5.258021000	-2.932469000	0.980550000
1	-3.818687000	-4.666375000	2.053480000
6	-1.471927000	0.976995000	3.460015000
1	-1.392078000	2.066899000	3.416050000
1	-1.599377000	0.676732000	4.509847000
1	-0.521281000	0.543019000	3.117467000
1	-0.366219000	-0.449281000	0.827152000

ANNEX

1	-4.067009000	1.306164000	1.449422000
1	-2.861389000	2.795753000	0.187071000
8	-3.384959000	3.367065000	-0.403151000
1	-5.901609000	2.248699000	0.967689000
8	-5.416242000	1.656009000	0.368671000
1	-4.830064000	2.268046000	-0.137086000
1	-2.943101000	3.307911000	2.470151000
8	-2.655126000	4.240605000	2.546438000
1	-2.491078000	4.476785000	1.618995000
1	-2.889700000	3.338859000	-1.239674000

TS_H_homo$_t$

(G = -3791.843674) (triplet)

27	0.420355000	0.213675000	0.693157000
16	-2.561830000	-0.287651000	-0.940048000
7	-1.923426000	-0.252372000	0.648704000
8	-2.219805000	0.992990000	-1.576737000
7	0.365718000	2.074110000	0.110206000
7	2.435356000	-0.060241000	1.186027000
7	-0.086402000	1.010576000	2.527130000
7	0.314016000	-1.621142000	1.780872000
8	-2.096711000	-1.552085000	-1.535329000
6	-2.352343000	0.954161000	1.411884000
1	-3.419981000	0.904473000	1.660660000
1	-2.175630000	1.819495000	0.772732000
6	1.592923000	-2.299235000	1.488418000
1	1.545878000	-2.669148000	0.461298000
1	1.759163000	-3.154771000	2.156927000
6	0.363118000	2.967021000	1.137325000
6	3.410236000	0.862412000	1.193011000
1	3.129797000	1.850199000	0.844373000
6	0.279859000	2.565431000	-1.142705000
1	0.296565000	1.834632000	-1.934059000
6	0.544437000	2.351324000	2.497065000
1	1.617890000	2.213254000	2.667276000
1	0.158280000	3.005132000	3.288883000
6	3.995723000	-1.667218000	2.049057000
1	4.179963000	-2.684125000	2.380273000
6	-1.565970000	1.100172000	2.712452000
1	-1.834598000	2.067377000	3.152168000
1	-1.878669000	0.335868000	3.424906000
6	5.004690000	-0.703513000	2.057843000
1	6.002588000	-0.954778000	2.404055000
6	-2.119360000	-1.565323000	1.337595000
1	-2.934873000	-2.139870000	0.888845000
1	-2.431231000	-1.358600000	2.360771000
6	-4.330882000	-0.374290000	-0.758240000
6	0.530364000	0.133681000	3.553570000
1	0.180870000	0.393628000	4.561605000
1	1.608459000	0.289296000	3.515903000
6	0.203905000	-1.328504000	3.248273000
1	0.884395000	-1.975970000	3.813009000
1	-0.804523000	-1.566714000	3.588834000
6	-4.962173000	-1.621182000	-0.757961000
1	-4.392491000	-2.526236000	-0.937696000
6	2.728763000	-1.312277000	1.594454000
6	-0.841580000	-2.401515000	1.297717000
1	-0.994521000	-3.308387000	1.901313000
1	-0.632477000	-2.695605000	0.266909000
6	-5.049310000	0.808182000	-0.538589000
1	-4.545875000	1.768911000	-0.546914000
6	4.707269000	0.587612000	1.617012000
1	5.459900000	1.368822000	1.599303000
6	0.183543000	4.834811000	-0.365171000
1	0.112555000	5.902835000	-0.547088000

6	0.194128000	3.924653000	-1.422200000
1	0.151690000	4.248180000	-2.456534000
6	0.265795000	4.338879000	0.938087000
1	0.259267000	5.000130000	1.798840000
6	-6.338392000	-1.676857000	-0.537900000
1	-6.842844000	-2.638932000	-0.539925000
6	-7.083804000	-0.511016000	-0.314029000
6	-6.421308000	0.728120000	-0.320205000
1	-6.989881000	1.638739000	-0.152138000
6	-8.570453000	-0.574843000	-0.081752000
1	-8.848881000	-0.020962000	0.823573000
1	-8.911411000	-1.610376000	0.021438000
1	-9.113413000	-0.116594000	-0.919304000
6	1.667259000	-0.621578000	-2.288585000
8	2.508180000	0.477697000	-2.317684000
6	2.182159000	-1.924266000	-1.928699000
6	1.358936000	-3.071393000	-2.098588000
6	3.452817000	-2.118407000	-1.332834000
6	1.782822000	-4.329496000	-1.685236000
1	0.374261000	-2.962900000	-2.540199000
6	3.868955000	-3.384351000	-0.927463000
1	4.115615000	-1.279074000	-1.157025000
6	3.042967000	-4.501586000	-1.093010000
1	1.124937000	-5.184187000	-1.822405000
1	4.845757000	-3.494332000	-0.463430000
1	3.370836000	-5.484811000	-0.767659000
6	0.581731000	-0.492255000	-3.324316000
1	0.351258000	0.559877000	-3.510199000
1	0.912011000	-0.931934000	-4.279323000
1	-0.336683000	-0.993467000	-3.016420000
1	0.660109000	-0.292755000	-0.782693000
1	3.414922000	0.343573000	-1.946508000
1	2.743229000	2.399046000	-1.406372000
8	3.379695000	3.129658000	-1.300108000
1	5.339125000	1.073842000	-2.477369000
8	5.091290000	0.920941000	-1.549402000
1	4.716831000	1.785545000	-1.268285000
1	2.124728000	1.837671000	-3.549215000
8	1.904143000	2.678338000	-4.000415000
1	2.129207000	3.332961000	-3.318917000
1	3.045214000	3.603723000	-0.519529000

II_H_homo$_t$

(G = -3791.898314) (triplet)

27	0.246879000	-0.082871000	0.738571000
16	-2.556071000	-0.022242000	-1.024055000
7	-2.036598000	-0.316698000	0.597566000
8	-2.192772000	1.362116000	-1.355714000
7	0.365940000	1.862277000	0.530606000
7	2.161293000	-0.757348000	1.014992000
7	-0.250605000	0.412045000	2.761544000
7	-0.098957000	-2.160036000	1.590023000
8	-1.987187000	-1.127983000	-1.815147000
6	-2.429156000	0.772429000	1.548406000
1	-3.511662000	0.756803000	1.723652000
1	-2.152989000	1.718625000	1.085646000
6	1.101928000	-2.926015000	1.224608000
1	0.996098000	-3.245828000	0.183848000
1	1.219044000	-3.828621000	1.841080000
6	0.365968000	2.539955000	1.732699000
6	3.234113000	0.054298000	1.043657000
1	3.043869000	1.090920000	0.793142000
6	0.304073000	2.645629000	-0.589947000
1	0.301903000	2.116940000	-1.530427000
6	0.528768000	1.654360000	2.936764000

ANNEX

1	1.582824000	1.357163000	3.009005000
1	0.256134000	2.187476000	3.858337000
6	3.580349000	-2.586484000	1.655742000
1	3.666618000	-3.642003000	1.893804000
6	-1.711316000	0.625981000	2.899066000
1	-1.915938000	1.539631000	3.471444000
1	-2.142658000	-0.201934000	3.464509000
6	4.688845000	-1.740133000	1.682196000
1	5.670305000	-2.125466000	1.942054000
6	-2.459264000	-1.689331000	1.040639000
1	-3.301449000	-2.061773000	0.450300000
1	-2.832612000	-1.599888000	2.060367000
6	-4.330094000	-0.152340000	-1.024618000
6	0.258177000	-0.696319000	3.589663000
1	-0.029939000	-0.586143000	4.645742000
1	1.348696000	-0.668024000	3.529732000
6	-0.243124000	-2.044461000	3.066798000
1	0.313793000	-2.845299000	3.569107000
1	-1.291962000	-2.183998000	3.336358000
6	-4.942256000	-1.345145000	-1.417023000
1	-4.345740000	-2.179312000	-1.770323000
6	2.334962000	-2.062935000	1.318995000
6	-1.311248000	-2.686272000	0.945954000
1	-1.638476000	-3.637700000	1.393469000
1	-1.078549000	-2.859237000	-0.107417000
6	-5.078119000	0.940390000	-0.566873000
1	-4.588064000	1.862260000	-0.272904000
6	4.510051000	-0.390755000	1.372473000
1	5.338288000	0.307939000	1.370893000
6	0.172012000	4.699980000	0.669031000
1	0.091821000	5.780736000	0.724038000
6	0.200825000	4.028630000	-0.560830000
1	0.154388000	4.568710000	-1.501984000
6	0.258985000	3.916253000	1.831108000
1	0.247340000	4.368146000	2.819076000
6	-6.332556000	-1.436731000	-1.352983000
1	-6.823206000	-2.356298000	-1.659137000
6	-7.108712000	-0.362000000	-0.897413000
6	-6.463147000	0.823812000	-0.507790000
1	-7.055603000	1.664120000	-0.156279000
6	-8.609837000	-0.462471000	-0.836795000
1	-8.983970000	-0.140655000	0.143055000
1	-8.945845000	-1.487888000	-1.022795000
1	-9.071195000	0.191692000	-1.588897000
6	2.209311000	0.277774000	-2.247085000
8	3.299439000	1.150505000	-2.575665000
6	2.645608000	-1.178238000	-2.160407000
6	1.681347000	-2.197144000	-2.152941000
6	3.996399000	-1.532235000	-2.055946000
6	2.060323000	-3.538341000	-2.065604000
1	0.626920000	-1.943388000	-2.208576000
6	4.376982000	-2.873501000	-1.949491000
1	4.755364000	-0.757324000	-2.053134000
6	3.411083000	-3.883114000	-1.958052000
1	1.297391000	-4.312532000	-2.067623000
1	5.430233000	-3.127173000	-1.861554000
1	3.706675000	-4.926015000	-1.882394000
6	1.141487000	0.497459000	-3.319364000
1	0.966842000	1.570711000	-3.446198000
1	1.473066000	0.082309000	-4.278790000
1	0.198687000	0.021275000	-3.034083000
1	1.800130000	0.558665000	-1.268528000
1	3.924868000	1.233733000	-1.814168000
1	2.688455000	3.049401000	-0.360458000
8	3.348661000	3.453979000	0.229824000
1	5.671870000	2.365896000	-1.421865000

8	5.271007000	1.772595000	-0.763954000
1	4.668453000	2.369565000	-0.255326000
1	2.723851000	2.826443000	-2.787826000
8	2.426585000	3.741653000	-3.008611000
1	2.247180000	4.140969000	-2.143849000
1	2.962568000	3.317268000	1.112536000

I_H_homo_{quint}

(G = -3791.838648) (quintuplet)

27	-0.085259000	-0.425131000	-0.331525000
16	2.866362000	0.045844000	1.211929000
7	2.270955000	-0.601462000	-0.279639000
8	2.349668000	1.419932000	1.303664000
7	-0.275614000	1.644692000	-0.690056000
7	-2.049797000	-1.080894000	-0.848088000
7	0.436155000	-0.289359000	-2.519958000
7	0.240533000	-2.544795000	-0.842234000
8	2.534139000	-0.938361000	2.252896000
6	2.640505000	0.265350000	-1.439774000
1	3.718118000	0.217892000	-1.634020000
1	2.372502000	1.288712000	-1.174391000
6	-0.989452000	-3.179052000	-0.321466000
1	-0.972754000	-3.095354000	0.772043000
1	-1.046927000	-4.240895000	-0.594383000
6	-0.221094000	2.020339000	-1.986824000
6	-3.059030000	-0.324894000	-1.305598000
1	-2.909639000	0.748344000	-1.273528000
6	-0.301781000	2.589410000	0.264237000
1	-0.345190000	2.228910000	1.284197000
6	-0.284696000	0.902705000	-3.000398000
1	-1.339362000	0.634387000	-3.129482000
1	0.091105000	1.246092000	-3.973219000
6	-3.323157000	-3.049244000	-1.347533000
1	-3.381048000	-4.132625000	-1.348517000
6	1.902479000	-0.155697000	-2.707453000
1	2.125664000	0.592873000	-3.477252000
1	2.302391000	-1.103743000	-3.070753000
6	-4.360961000	-2.261795000	-1.849067000
1	-5.256200000	-2.725712000	-2.251852000
6	2.633082000	-2.052005000	-0.423344000
1	3.467152000	-2.319831000	0.231011000
1	2.992651000	-2.207160000	-1.439972000
6	4.635895000	0.111742000	1.037748000
6	-0.074533000	-1.537558000	-3.127807000
1	0.276468000	-1.648692000	-4.163512000
1	-1.163079000	-1.478621000	-3.146531000
6	0.375036000	-2.757990000	-2.314757000
1	-0.215506000	-3.628237000	-2.623789000
1	1.415898000	-2.991712000	-2.543975000
6	5.410268000	-0.959586000	1.492781000
1	4.945656000	-1.800527000	1.995657000
6	-2.183877000	-2.424616000	-0.852431000
6	1.446593000	-2.960733000	-0.100746000
1	1.724843000	-3.998783000	-0.333018000
1	1.217349000	-2.887374000	0.964523000
6	5.215009000	1.213543000	0.396950000
1	4.600282000	2.038733000	0.054253000
6	-4.229427000	-0.874104000	-1.822814000
1	-5.014107000	-0.219665000	-2.184040000
6	-0.196974000	4.340782000	-1.364724000
1	-0.160702000	5.392569000	-1.631939000
6	-0.268387000	3.949634000	-0.027528000
1	-0.311069000	4.675789000	0.775790000
6	-0.171371000	3.361286000	-2.359677000
1	-0.115001000	3.622735000	-3.411274000

ANNEX

6	6.790518000	-0.917406000	1.301497000
1	7.404422000	-1.741841000	1.652915000
6	7.400114000	0.172265000	0.663207000
6	6.594892000	1.232578000	0.215622000
1	7.057034000	2.081587000	-0.280311000
6	8.893896000	0.221651000	0.480015000
1	9.155804000	0.646070000	-0.496216000
1	9.336382000	-0.776520000	0.566526000
1	9.353249000	0.860840000	1.246929000
6	-3.130227000	1.039472000	2.343138000
8	-3.789066000	1.974482000	1.589857000
6	-3.467888000	-0.335772000	2.346497000
6	-2.694297000	-1.251406000	3.128570000
6	-4.543622000	-0.885900000	1.583645000
6	-2.962241000	-2.613373000	3.117132000
1	-1.877863000	-0.875256000	3.735133000
6	-4.798113000	-2.250726000	1.587136000
1	-5.172697000	-0.242139000	0.981021000
6	-4.012363000	-3.134189000	2.343468000
1	-2.348787000	-3.279803000	3.718853000
1	-5.615884000	-2.635816000	0.983931000
1	-4.215474000	-4.201165000	2.333668000
6	-2.072371000	1.643583000	3.214113000
1	-1.913149000	2.689194000	2.935659000
1	-2.350810000	1.606371000	4.278465000
1	-1.119865000	1.108428000	3.109789000
1	-0.233049000	-0.451297000	1.347972000
1	-4.480326000	1.630233000	0.963810000
1	-2.996516000	2.765329000	-0.309074000
8	-3.371084000	3.196412000	-1.098391000
1	-6.161042000	2.399471000	-0.116284000
8	-5.573065000	1.690426000	-0.428044000
1	-4.872443000	2.174598000	-0.927339000
1	-3.349045000	3.821783000	1.712362000
8	-2.978781000	4.721459000	1.612059000
1	-2.726349000	4.735832000	0.674091000
1	-2.737561000	2.979179000	-1.803011000

TS_H_homo$_{quint}$

(G = -3791.814436) (quintuplet)

27	0.444185000	0.194894000	0.590461000
16	-2.520536000	-0.389705000	-0.930559000
7	-1.885092000	-0.297763000	0.674785000
8	-2.178812000	0.880390000	-1.588242000
7	0.323040000	2.254441000	0.091895000
7	2.427031000	-0.017094000	1.211795000
7	-0.136058000	1.100383000	2.537367000
7	0.349457000	-1.604143000	1.884875000
8	-2.036509000	-1.664416000	-1.483023000
6	-2.377600000	0.912244000	1.401093000
1	-3.444179000	0.815021000	1.635831000
1	-2.235584000	1.765635000	0.737223000
6	1.643394000	-2.263655000	1.606738000
1	1.597248000	-2.654827000	0.582504000
1	1.830114000	-3.099340000	2.294109000
6	0.218110000	3.093016000	1.144407000
6	3.383367000	0.931491000	1.166315000
1	3.073092000	1.900496000	0.791816000
6	0.219681000	2.747294000	-1.151989000
1	0.335860000	2.033113000	-1.957385000
6	0.435033000	2.461054000	2.497421000
1	1.516653000	2.375593000	2.653480000
1	0.029159000	3.098386000	3.293473000
6	4.037754000	-1.560740000	2.097834000
1	4.250332000	-2.561297000	2.460322000

6	-1.612359000	1.129519000	2.705685000
1	-1.933564000	2.095856000	3.112292000
1	-1.902337000	0.373871000	3.437010000
6	5.029703000	-0.579583000	2.040215000
1	6.042097000	-0.799334000	2.364888000
6	-2.078669000	-1.594934000	1.405527000
1	-2.876582000	-2.191578000	0.954687000
1	-2.417480000	-1.357938000	2.413140000
6	-4.287649000	-0.482442000	-0.751984000
6	0.517671000	0.260584000	3.566776000
1	0.179246000	0.534117000	4.575845000
1	1.590999000	0.443809000	3.508537000
6	0.229315000	-1.224711000	3.325176000
1	0.922554000	-1.821733000	3.928895000
1	-0.775533000	-1.467706000	3.675004000
6	-4.910521000	-1.735572000	-0.724129000
1	-4.330607000	-2.641303000	-0.862832000
6	2.752668000	-1.251373000	1.670939000
6	-0.793118000	-2.418111000	1.426227000
1	-0.946372000	-3.295174000	2.071485000
1	-0.564296000	-2.760330000	0.413861000
6	-5.015709000	0.701164000	-0.593844000
1	-4.518734000	1.664626000	-0.627460000
6	4.691589000	0.693573000	1.565926000
1	5.425705000	1.489801000	1.505857000
6	-0.118715000	4.966005000	-0.319020000
1	-0.297472000	6.025690000	-0.475801000
6	0.007986000	4.098589000	-1.404693000
1	-0.048293000	4.450342000	-2.429153000
6	-0.012890000	4.454912000	0.976553000
1	-0.102135000	5.095441000	1.847952000
6	-6.288876000	-1.792758000	-0.537402000
1	-6.787461000	-2.758029000	-0.523603000
6	-7.047440000	-0.622401000	-0.372461000
6	-6.394416000	0.618518000	-0.407301000
1	-6.974395000	1.529674000	-0.291870000
6	-8.534600000	-0.707640000	-0.152587000
1	-9.008064000	0.274387000	-0.256436000
1	-8.752584000	-1.086891000	0.855150000
1	-8.996138000	-1.401308000	-0.865787000
6	1.693897000	-0.707976000	-2.322297000
8	2.535093000	0.404266000	-2.440163000
6	2.260922000	-1.985873000	-1.966445000
6	1.426115000	-3.146414000	-1.952650000
6	3.565336000	-2.133932000	-1.408771000
6	1.878367000	-4.359996000	-1.446923000
1	0.413099000	-3.084386000	-2.336405000
6	4.004320000	-3.352719000	-0.908595000
1	4.242503000	-1.288229000	-1.352279000
6	3.172783000	-4.486619000	-0.915890000
1	1.210214000	-5.218771000	-1.457541000
1	5.007821000	-3.420172000	-0.494030000
1	3.521789000	-5.435972000	-0.519736000
6	0.622546000	-0.607198000	-3.380886000
1	0.213378000	0.408290000	-3.398698000
1	1.046005000	-0.824999000	-4.372947000
1	-0.202769000	-1.293997000	-3.188909000
1	0.788762000	-0.333644000	-1.071073000
1	3.413225000	0.316628000	-2.003054000
1	2.696621000	2.345160000	-1.493170000
8	3.294977000	3.114320000	-1.457006000
1	5.325281000	1.092890000	-2.537484000
8	5.106820000	0.985899000	-1.595888000
1	4.681172000	1.841298000	-1.363859000
1	1.999347000	1.777571000	-3.617530000
8	1.728398000	2.626667000	-4.023482000

ANNEX

1	2.054490000	3.266794000	-3.368214000
1	2.987043000	3.608210000	-0.677951000

II_H_homo$_{quint}$

(G = -3791.866418) (quintuplet)

27	0.402717000	-0.005907000	0.745611000
16	-2.546499000	-0.067753000	-0.986963000
7	-1.936407000	-0.262339000	0.622365000
8	-2.148085000	1.277943000	-1.422830000
7	0.431020000	2.060903000	0.415923000
7	2.316209000	-0.459759000	1.095939000
7	-0.123692000	0.661986000	2.713752000
7	0.125413000	-1.954115000	1.696484000
8	-2.061095000	-1.246661000	-1.722672000
6	-2.342310000	0.867915000	1.521513000
1	-3.417963000	0.825355000	1.727696000
1	-2.114691000	1.794385000	0.994534000
6	1.380292000	-2.666735000	1.331312000
1	1.301937000	-2.890520000	0.260888000
1	1.475821000	-3.611280000	1.884478000
6	0.483502000	2.762194000	1.570060000
6	3.381118000	0.426607000	1.204975000
1	3.191600000	1.430329000	0.843282000
6	0.398356000	2.729640000	-0.749608000
1	0.348849000	2.127099000	-1.644874000
6	0.601192000	1.946751000	2.836553000
1	1.663416000	1.715330000	2.980550000
1	0.254572000	2.524050000	3.702421000
6	3.737439000	-2.154875000	2.118527000
1	3.829924000	-3.181819000	2.466938000
6	-1.594749000	0.827929000	2.859476000
1	-1.822446000	1.763897000	3.382655000
1	-1.979448000	0.018789000	3.481581000
6	4.835057000	-1.245946000	2.209942000
1	5.786229000	-1.541797000	2.639663000
6	-2.271432000	-1.627576000	1.162775000
1	-3.105844000	-2.076070000	0.616818000
1	-2.621547000	-1.495393000	2.186168000
6	-4.316565000	-0.141833000	-0.865228000
6	0.431800000	-0.376826000	3.616206000
1	0.121176000	-0.202412000	4.655007000
1	1.518275000	-0.303202000	3.556886000
6	-0.001907000	-1.777049000	3.170699000
1	0.619776000	-2.514924000	3.691390000
1	-1.035059000	-1.967641000	3.467498000
6	-4.970642000	-1.358157000	-1.079560000
1	-4.412265000	-2.240151000	-1.373660000
6	2.547983000	-1.757522000	1.565642000
6	-1.071600000	-2.567886000	1.094307000
1	-1.338002000	-3.511874000	1.591826000
1	-0.839564000	-2.779434000	0.047129000
6	-5.016303000	1.014933000	-0.497580000
1	-4.493275000	1.952762000	-0.344899000
6	4.603814000	0.076754000	1.725932000
1	5.388615000	0.829329000	1.763538000
6	0.482815000	4.844160000	0.370316000
1	0.504062000	5.929693000	0.356502000
6	0.431256000	4.117599000	-0.819819000
1	0.431845000	4.602837000	-1.789356000
6	0.501488000	4.154629000	1.583187000
1	0.534520000	4.678691000	2.532754000
6	-6.355244000	-1.408741000	-0.923220000
1	-6.878939000	-2.344930000	-1.093701000
6	-7.083992000	-0.270319000	-0.551676000
6	-6.396921000	0.938350000	-0.345660000

1	-6.953520000	1.828586000	-0.065964000
6	-8.577267000	-0.332616000	-0.370717000
1	-8.846981000	-0.144516000	0.676986000
1	-8.970333000	-1.313618000	-0.657141000
1	-9.075356000	0.436379000	-0.974453000
6	1.915944000	-0.072914000	-2.446278000
8	3.082298000	0.510451000	-3.069659000
6	2.126460000	-1.558804000	-2.174894000
6	1.170953000	-2.527535000	-2.516033000
6	3.307782000	-1.978960000	-1.546931000
6	1.395067000	-3.881708000	-2.242381000
1	0.244303000	-2.233051000	-2.995816000
6	3.535803000	-3.327651000	-1.274144000
1	4.050159000	-1.243239000	-1.255426000
6	2.579681000	-4.287720000	-1.623972000
1	0.641744000	-4.616059000	-2.515691000
1	4.454804000	-3.627235000	-0.777886000
1	2.754329000	-5.338765000	-1.409681000
6	0.738547000	0.226148000	-3.364351000
1	0.705459000	1.297940000	-3.577053000
1	0.847536000	-0.314942000	-4.312149000
1	-0.204629000	-0.069001000	-2.899221000
1	1.759852000	0.423997000	-1.479146000
1	3.802838000	0.606120000	-2.400347000
1	2.896550000	2.400019000	-1.063923000
8	3.535712000	3.113083000	-0.893506000
1	5.758955000	1.424292000	-2.199174000
8	5.290197000	1.024773000	-1.446410000
1	4.849295000	1.791666000	-1.018901000
1	2.643757000	2.262022000	-3.426016000
8	2.366633000	3.199019000	-3.557465000
1	2.641914000	3.613175000	-2.721334000
1	3.220807000	3.499661000	-0.057995000

H$_2$O_I_heter$_d$

(G = -3406.377530) (doublet)

27	-1.012577000	-0.051469000	-0.172757000
16	2.193073000	-0.003701000	1.032379000
7	1.359977000	-0.292037000	-0.430177000
8	1.862992000	1.364591000	1.457346000
7	-1.103615000	1.830173000	0.217342000
7	-3.113324000	-0.485372000	-0.283300000
7	-0.886442000	0.525606000	-2.098298000
7	-0.931169000	-1.939521000	-0.902177000
8	1.879451000	-1.139405000	1.918534000
6	1.542981000	0.789781000	-1.436329000
1	2.551195000	0.762758000	-1.868838000
1	1.400823000	1.740646000	-0.921738000
6	-2.057640000	-2.655012000	-0.252434000
1	-1.784992000	-2.803479000	0.798712000
1	-2.223783000	-3.636073000	-0.714768000
6	-1.305939000	2.602843000	-0.881987000
6	-4.179696000	0.327460000	-0.248572000
1	-3.970052000	1.393056000	-0.257984000
6	-0.936207000	2.439264000	1.407965000
1	-0.773500000	1.782748000	2.251838000
6	-1.599024000	1.830200000	-2.139338000
1	-2.673597000	1.619951000	-2.161470000
1	-1.349944000	2.405929000	-3.037781000
6	-4.587417000	-2.380157000	-0.261439000
1	-4.701337000	-3.459474000	-0.275275000
6	0.530804000	0.658714000	-2.570403000
1	0.628048000	1.541673000	-3.210457000
1	0.769659000	-0.206629000	-3.189423000
6	-5.693412000	-1.530989000	-0.201154000

1	-6.698757000	-1.939764000	-0.165693000
6	1.547948000	-1.689243000	-0.921247000
1	2.462030000	-2.138667000	-0.520969000
1	1.687589000	-1.646292000	-2.001166000
6	3.925566000	-0.076371000	0.631802000
6	-1.595814000	-0.532879000	-2.871925000
1	-1.418468000	-0.418200000	-3.948513000
1	-2.662770000	-0.421521000	-2.684675000
6	-1.112380000	-1.904840000	-2.401433000
1	-1.826628000	-2.675497000	-2.708339000
1	-0.158160000	-2.146928000	-2.871456000
6	4.629360000	-1.268821000	0.820609000
1	4.144060000	-2.129057000	1.268377000
6	-3.312627000	-1.818519000	-0.296670000
6	0.361898000	-2.574122000	-0.541818000
1	0.469708000	-3.545550000	-1.042898000
1	0.355846000	-2.732670000	0.535650000
6	4.534845000	1.051776000	0.067621000
1	3.977591000	1.973179000	-0.062217000
6	-5.487351000	-0.149301000	-0.199448000
1	-6.318733000	0.547150000	-0.166421000
6	-1.139310000	4.614829000	0.414824000
1	-1.144895000	5.697913000	0.490256000
6	-0.955108000	3.822084000	1.548604000
1	-0.817794000	4.262306000	2.530458000
6	-1.315722000	3.991224000	-0.821289000
1	-1.464772000	4.563539000	-1.731007000
6	5.970482000	-1.323032000	0.441399000
1	6.532766000	-2.240252000	0.591769000
6	6.607464000	-0.211626000	-0.127593000
6	5.873405000	0.973190000	-0.304825000
1	6.360848000	1.843165000	-0.736455000
6	8.050425000	-0.279293000	-0.552911000
1	8.530142000	-1.191915000	-0.183803000
1	8.608254000	0.589202000	-0.181913000
1	8.129910000	-0.270199000	-1.648584000
1	-0.868535000	-0.461154000	1.314073000
8	-2.691550000	-1.014743000	2.776985000
1	-3.378554000	-1.498869000	2.286884000
1	-2.041696000	-0.735347000	2.061871000
1	-3.475182000	0.621877000	2.791938000
8	-3.879032000	1.515763000	2.695336000
1	-4.619327000	1.347462000	2.090881000
8	-0.411897000	-2.759087000	2.970092000
1	-1.280234000	-2.307392000	3.005061000
1	0.150775000	-2.090601000	2.538298000
6	1.292946000	2.813900000	0.693056000
6	4.065322000	0.410655000	0.133332000
1	3.792841000	1.440779000	-0.072651000
6	0.995763000	2.625165000	-1.604747000
1	0.882805000	1.950854000	-2.446816000
6	1.569343000	2.083562000	1.985572000
1	2.647239000	1.887521000	2.023112000
1	1.320779000	2.718403000	2.845667000
6	4.608051000	-2.218257000	0.680137000
1	4.776274000	-3.265891000	0.907569000
6	-0.553909000	0.943731000	2.443486000
1	-0.705034000	1.901340000	2.955926000
1	-0.805860000	0.164566000	3.164410000
6	5.668818000	-1.321234000	0.547090000
1	6.692836000	-1.662117000	0.665331000
6	-1.510970000	-1.608981000	1.067768000
1	-2.430437000	-2.083476000	0.714526000
1	-1.665697000	-1.413752000	2.128239000
6	-3.887048000	-0.171383000	-0.630348000
6	1.575001000	-0.194568000	2.889829000
1	1.423186000	0.023366000	3.956290000
1	2.640593000	-0.108213000	2.676542000
6	1.101262000	-1.623309000	2.600179000
1	1.818530000	-2.327084000	3.038342000
1	0.145438000	-1.806473000	3.094178000
6	-4.601493000	-1.372372000	-0.611652000
1	-4.133458000	-2.297418000	-0.930131000
6	3.306044000	-1.750424000	0.522179000
6	-0.339650000	-2.560204000	0.838092000
1	-0.484103000	-3.453056000	1.463171000
1	-0.315503000	-2.866462000	-0.207509000
6	-4.474014000	1.038203000	-0.236220000
1	-3.907945000	1.962906000	-0.264117000
6	5.393939000	0.020896000	0.275225000
1	6.187164000	0.754308000	0.178107000
6	1.090388000	4.808653000	-0.626602000
1	1.056787000	5.890902000	-0.709524000
6	0.962941000	4.006217000	-1.762497000
1	0.830932000	4.437507000	-2.748930000
6	1.254784000	4.203890000	0.619779000
1	1.353424000	4.791159000	1.526870000
6	-5.929792000	-1.354206000	-0.187580000
1	-6.498773000	-2.279296000	-0.171964000
6	-6.544087000	-0.161530000	0.218464000
6	-5.800316000	1.030447000	0.183784000
1	-6.269577000	1.961657000	0.489031000
6	-7.976730000	-0.147428000	0.681829000
1	-8.408053000	-1.153716000	0.664149000
1	-8.586072000	0.503946000	0.041830000
1	-8.050132000	0.245887000	1.703986000
1	0.869547000	-0.489922000	-1.651969000
8	2.658200000	-1.733249000	-2.703868000
1	3.288134000	-2.069661000	-2.043527000
1	1.978711000	-1.214762000	-2.155282000
1	3.507068000	-0.133332000	-3.008166000
8	3.878784000	0.778713000	-3.018990000
1	4.577584000	0.728024000	-2.347199000
8	0.326162000	-3.396571000	-2.560935000
1	1.203967000	-2.971804000	-2.662997000
1	-0.242278000	-2.644047000	-2.316767000

H₂O_II_heterq

(G = -3406.366295) (quartet)

27	0.991602000	-0.029533000	-0.040473000
16	-2.171054000	-0.185033000	-1.094011000
7	-1.283373000	-0.284986000	0.392910000
8	-1.825010000	1.111425000	-1.695060000
7	1.159132000	2.040616000	-0.405481000
7	3.046421000	-0.455634000	0.245474000
7	0.866271000	0.786738000	2.036738000
7	0.945326000	-1.897568000	1.139896000
8	-1.896845000	-1.435313000	-1.821649000
6	-1.528834000	0.906284000	1.266935000
1	-2.551355000	0.892402000	1.660649000
1	-1.395501000	1.793845000	0.647151000
6	2.095586000	-2.650983000	0.602097000
1	1.834908000	-2.973785000	-0.413072000
1	2.317762000	-3.541735000	1.204606000

H₂O_TS_heterd

(G = -3406.360360) (doublet)

27	-0.995267000	-0.066350000	-0.210618000
16	2.128227000	-0.069621000	1.071841000

7	1.249837000	-0.242593000	-0.423961000
8	1.788383000	1.258225000	1.599565000
7	-1.084243000	1.772046000	0.348841000
7	-3.008100000	-0.337711000	-0.253829000
7	-0.832534000	0.732419000	-2.119661000
7	-0.979392000	-1.827339000	-1.094913000
8	1.817879000	-1.274608000	1.857628000
6	1.549382000	0.887270000	-1.361026000
1	2.575690000	0.818048000	-1.736988000
1	1.431830000	1.814282000	-0.799024000
6	-2.143881000	-2.564060000	-0.525574000
1	-1.873630000	-2.855180000	0.495419000
1	-2.362791000	-3.466546000	-1.105681000
6	-1.263681000	2.656591000	-0.664532000
6	-3.993549000	0.566138000	-0.135997000
1	-3.688800000	1.594790000	0.020686000
6	-0.981088000	2.232167000	1.610276000
1	-0.836548000	1.483721000	2.377223000
6	-1.508904000	2.047873000	-2.019916000
1	-2.587628000	1.883833000	-2.121174000
1	-1.200699000	2.727447000	-2.822294000
6	-4.646145000	-2.066879000	-0.548508000
1	-4.856950000	-3.117048000	-0.720759000
6	0.587526000	0.867651000	-2.546494000
1	0.728746000	1.794853000	-3.111701000
1	0.831181000	0.046457000	-3.220883000
6	-5.669479000	-1.127270000	-0.414846000
1	-6.708349000	-1.435780000	-0.478637000
6	1.485508000	-1.607143000	-1.023063000
1	2.391268000	-2.070827000	-0.624480000
1	1.660630000	-1.474029000	-2.090031000
6	3.847553000	-0.099323000	0.628150000
6	-1.572196000	-0.246797000	-2.958996000
1	-1.404930000	-0.064175000	-4.027820000
1	-2.635172000	-0.125310000	-2.749537000
6	-1.124673000	-1.661020000	-2.594661000
1	-1.847960000	-2.388563000	-2.973452000
1	-0.164434000	-1.891892000	-3.057100000
6	4.554525000	-1.303905000	0.690506000
1	4.076022000	-2.206893000	1.053811000
6	-3.327054000	-1.635692000	-0.460502000
6	0.296772000	-2.518949000	-0.753811000
1	0.395795000	-3.441335000	-1.338714000
1	0.254025000	-2.770485000	0.305517000
6	4.449014000	1.084423000	0.181845000
1	3.889510000	2.013013000	0.152591000
6	-5.338016000	0.213267000	-0.208388000
1	-6.101364000	0.977053000	-0.107262000
6	-1.197730000	4.502041000	0.868403000
1	-1.233774000	5.568363000	1.069118000
6	-1.039354000	3.587334000	1.910095000
1	-0.953230000	3.911994000	2.941071000
6	-1.310575000	4.027224000	-0.438131000
1	-1.441679000	4.700255000	-1.278736000
6	5.889990000	-1.315368000	0.290957000
1	6.455137000	-2.241581000	0.340773000
6	6.518078000	-0.149903000	-0.171714000
6	5.782672000	1.046463000	-0.212543000
1	6.264208000	1.958063000	-0.555035000
6	7.951100000	-0.176412000	-0.633195000
1	8.464259000	-1.076591000	-0.278793000
1	8.493507000	0.707988000	-0.278691000
1	7.999198000	-0.168813000	-1.731007000
1	-0.684662000	-0.573247000	1.505839000
8	-2.512483000	-1.669698000	2.757067000
1	-3.102873000	-2.022655000	2.073030000

1	-1.341324000	-0.899518000	1.824702000
1	-3.217430000	-0.218527000	2.953324000
8	-3.657185000	0.694870000	3.007368000
1	-4.405606000	0.601962000	2.396696000
8	-0.394696000	-3.263426000	2.637448000
1	-1.236693000	-2.711351000	2.714797000
1	0.267162000	-2.591377000	2.402469000

H$_2$O_TS_heter$_q$

(G = -3406.360789) (quartet)

27	-1.002041000	-0.024487000	-0.035973000
16	2.142329000	-0.165299000	1.055591000
7	1.239094000	-0.281764000	-0.431376000
8	1.793113000	1.137873000	1.638015000
7	-1.133344000	2.002821000	0.383871000
7	-3.053405000	-0.449409000	-0.193202000
7	-0.905860000	0.770367000	-2.071563000
7	-0.986457000	-1.906931000	-1.157888000
8	1.854325000	-1.403932000	1.795893000
6	1.497739000	0.893530000	-1.328098000
1	2.516553000	0.853077000	-1.728384000
1	1.385143000	1.793492000	-0.722391000
6	-2.133966000	-2.651341000	-0.597511000
1	-1.851873000	-2.987208000	0.407296000
1	-2.380225000	-3.532944000	-1.203061000
6	-1.305500000	2.786393000	-0.704180000
6	-4.059448000	0.423656000	-0.027096000
1	-3.772408000	1.450817000	0.172918000
6	-0.948812000	2.574542000	1.587182000
1	-0.804426000	1.893622000	2.417578000
6	-1.604948000	2.070061000	-2.000125000
1	-2.683821000	1.876634000	-2.023754000
1	-1.364626000	2.710124000	-2.857907000
6	-4.642435000	-2.196714000	-0.580855000
1	-4.827312000	-3.240431000	-0.812797000
6	0.511520000	0.923340000	-2.497084000
1	0.654833000	1.876384000	-3.019020000
1	0.752917000	0.136696000	-3.213044000
6	-5.689526000	-1.294824000	-0.388919000
1	-6.720022000	-1.627781000	-0.465976000
6	1.470257000	-1.615698000	-1.093470000
1	2.391625000	-2.081690000	-0.734257000
1	1.622546000	-1.431260000	-2.156121000
6	3.855907000	-0.165257000	0.593363000
6	-1.632043000	-0.214697000	-2.909159000
1	-1.499977000	-0.000382000	-3.978226000
1	-2.693032000	-0.126316000	-2.673011000
6	-1.153207000	-1.642191000	-2.619479000
1	-1.873633000	-2.348953000	-3.046550000
1	-0.199998000	-1.827331000	-3.117750000
6	4.570042000	-1.366457000	0.617521000
1	4.095811000	-2.284147000	0.947757000
6	-3.331909000	-1.740027000	-0.471205000
6	0.301961000	-2.566077000	-0.851194000
1	0.444426000	-3.465240000	-1.466564000
1	0.279486000	-2.859233000	0.198615000
6	4.448806000	1.036512000	0.184199000
1	3.882138000	1.961274000	0.180720000
6	-5.394529000	0.041789000	-0.111279000
1	-6.178039000	0.778074000	0.030772000
6	-1.097808000	4.766751000	0.634888000
1	-1.077228000	5.848306000	0.729683000
6	-0.932192000	3.953692000	1.758303000
1	-0.782891000	4.375998000	2.745955000

ANNEX

6	-1.283823000	4.174904000	-0.614526000
1	-1.412315000	4.770961000	-1.511968000
6	5.907024000	-1.355967000	0.222406000
1	6.477313000	-2.280134000	0.240808000
6	6.529189000	-0.171386000	-0.195546000
6	5.783565000	1.020019000	-0.206811000
1	6.259005000	1.944358000	-0.522965000
6	7.973448000	-0.164343000	-0.620522000
1	8.401425000	-1.171510000	-0.584272000
1	8.566612000	0.489294000	0.032415000
1	8.075672000	0.223327000	-1.642237000
1	-0.764833000	-0.524891000	1.651279000
8	-2.440489000	-1.659334000	2.755443000
1	-3.051839000	-1.972605000	2.068577000
1	-1.451953000	-0.950263000	1.993200000
1	-3.128671000	-0.153726000	3.025046000
8	-3.496628000	0.778021000	3.106899000
1	-4.276514000	0.752312000	2.530037000
8	-0.371336000	-3.367717000	2.555244000
1	-1.193055000	-2.808678000	2.671800000
1	0.293080000	-2.700206000	2.311922000

H$_2$O_II_heter$_d$
(G = -3406.373572) (doublet)

27	0.902668000	0.084914000	0.257954000
16	-2.064707000	-0.211055000	-1.021924000
7	-1.192642000	-0.065762000	0.511225000
8	-1.794282000	1.024027000	-1.766143000
7	0.952785000	1.806857000	-0.643470000
7	2.848935000	-0.134100000	0.185672000
7	0.775252000	1.261999000	2.021013000
7	0.979317000	-1.480748000	1.459889000
8	-1.643195000	-1.509609000	-1.567444000
6	-1.578388000	1.202591000	1.223701000
1	-2.613090000	1.141357000	1.574444000
1	-1.483771000	2.018692000	0.507282000
6	2.152222000	-2.278259000	1.006563000
1	1.860385000	-2.809135000	0.095613000
1	2.453280000	-3.011630000	1.761517000
6	1.129777000	2.863978000	0.188313000
6	3.776114000	0.773235000	-0.177173000
1	3.410232000	1.716521000	-0.561773000
6	0.884336000	2.025283000	-1.970248000
1	0.763298000	1.149066000	-2.592117000
6	1.402735000	2.539678000	1.637950000
1	2.488250000	2.432731000	1.747573000
1	1.086053000	3.364689000	2.286989000
6	4.611379000	-1.652769000	0.790341000
1	4.892662000	-2.623125000	1.184905000
6	-0.645169000	1.429797000	2.413876000
1	-0.824569000	2.439290000	2.800425000
1	-0.876443000	0.734012000	3.221213000
6	5.567671000	-0.709336000	0.415597000
1	6.625921000	-0.931974000	0.509444000
6	-1.464258000	-1.296744000	1.359936000
1	-2.375555000	-1.809860000	1.045390000
1	-1.644703000	-0.954219000	2.377436000
6	-3.789649000	-0.275337000	-0.613747000
6	1.565313000	0.453993000	2.979146000
1	1.440338000	0.805201000	4.011891000
1	2.617040000	0.557720000	2.704558000
6	1.146202000	-1.015722000	2.892100000
1	1.892560000	-1.640881000	3.390159000
1	0.199730000	-1.172055000	3.410928000

6	-4.426640000	-1.516510000	-0.510842000
1	-3.878449000	-2.434911000	-0.690889000
6	3.264751000	-1.332840000	0.665090000
6	-0.285519000	-2.247979000	1.283806000
1	-0.378556000	-3.024222000	2.053137000
1	-0.246969000	-2.723232000	0.303862000
6	-4.478423000	0.926533000	-0.409472000
1	-3.972807000	1.880584000	-0.510220000
6	5.140581000	0.527291000	-0.071779000
1	5.846078000	1.293510000	-0.372874000
6	1.094559000	4.393463000	-1.663478000
1	1.140111000	5.403883000	-2.057937000
6	0.958513000	3.299236000	-2.518894000
1	0.901431000	3.423708000	-3.594530000
6	1.182202000	4.168875000	-0.290496000
1	1.307512000	4.985934000	0.412287000
6	-5.782549000	-1.544992000	-0.193728000
1	-6.294412000	-2.500131000	-0.119851000
6	-6.500496000	-0.359187000	0.024400000
6	-5.832333000	0.870620000	-0.092509000
1	-6.383219000	1.794226000	0.060155000
6	-7.958069000	-0.403034000	0.397269000
1	-8.437128000	-1.311029000	0.015186000
1	-8.490040000	0.473932000	0.011977000
1	-8.070487000	-0.402720000	1.490638000
1	0.720500000	-0.923337000	-2.166272000
8	3.091479000	-3.231838000	-2.092599000
1	3.498519000	-3.286638000	-1.215015000
1	1.420961000	-1.163732000	-2.140305000
1	3.552222000	-1.827662000	-2.579844000
8	3.866714000	-0.898031000	-2.902735000
1	4.522141000	-0.649849000	-2.232536000
8	0.591889000	-3.827908000	-1.726903000
1	1.584790000	-3.588299000	-1.867197000
1	0.153923000	-2.964230000	-1.777737000

H$_2$O_II_heter$_q$
(G = -3406.380229) (quartet)

27	-1.012796000	-0.015083000	-0.071491000
16	2.174784000	-0.181169000	1.064718000
7	1.254651000	-0.276399000	-0.410510000
8	1.857432000	1.128708000	1.650899000
7	-1.069853000	2.023804000	0.411798000
7	-3.054914000	-0.407935000	-0.154410000
7	-0.862096000	0.807127000	-2.063294000
7	-1.019067000	-1.862154000	-1.212360000
8	1.843211000	-1.411112000	1.802236000
6	1.533350000	0.898645000	-1.301309000
1	2.554562000	0.845846000	-1.694189000
1	1.427571000	1.798115000	-0.694339000
6	-2.187761000	-2.600084000	-0.681237000
1	-1.922488000	-2.969370000	0.316051000
1	-2.447559000	-3.456727000	-1.315149000
6	-1.203808000	2.819639000	-0.674406000
6	-4.038443000	0.486261000	0.035663000
1	-3.726639000	1.488772000	0.309922000
6	-0.889308000	2.593387000	1.617099000
1	-0.790047000	1.916349000	2.455771000
6	-1.531928000	2.125960000	-1.974025000
1	-2.614702000	1.955108000	-1.990722000
1	-1.279963000	2.762101000	-2.830385000
6	-4.683020000	-2.073463000	-0.706142000
1	-4.892484000	-3.093631000	-1.010150000
6	0.561760000	0.943338000	-2.478910000

ANNEX

1	0.717791000	1.895786000	-2.997151000
1	0.797174000	0.155343000	-3.194487000
6	-5.707237000	-1.150288000	-0.489706000
1	-6.744400000	-1.443072000	-0.621614000
6	1.454349000	-1.610809000	-1.086803000
1	2.351559000	-2.111608000	-0.713456000
1	1.635708000	-1.419966000	-2.144102000
6	3.887219000	-0.226251000	0.606806000
6	-1.606939000	-0.139329000	-2.933371000
1	-1.466931000	0.108349000	-3.993382000
1	-2.666340000	-0.037107000	-2.693080000
6	-1.153767000	-1.578921000	-2.673094000
1	-1.879226000	-2.266281000	-3.121699000
1	-0.195058000	-1.773052000	-3.157394000
6	4.572048000	-1.444798000	0.641164000
1	4.073127000	-2.349399000	0.971121000
6	-3.363935000	-1.667156000	-0.528697000
6	0.258381000	-2.537010000	-0.881112000
1	0.400579000	-3.433635000	-1.499514000
1	0.204644000	-2.838693000	0.165711000
6	4.512701000	0.960429000	0.203787000
1	3.969539000	1.899199000	0.197634000
6	-5.380981000	0.155974000	-0.119600000
1	-6.145774000	0.907718000	0.041794000
6	-0.938528000	4.792888000	0.664832000
1	-0.878532000	5.872810000	0.760358000
6	-0.824170000	3.971914000	1.787773000
1	-0.677852000	4.385565000	2.779539000
6	-1.129945000	4.206276000	-0.585440000
1	-1.227331000	4.803778000	-1.485805000
6	5.913373000	-1.466156000	0.263972000
1	6.463416000	-2.402128000	0.297135000
6	6.567869000	-0.297114000	-0.150873000
6	5.851769000	0.911457000	-0.171057000
1	6.354035000	1.824507000	-0.477921000
6	8.009979000	-0.333788000	-0.581399000
1	8.508709000	-1.237530000	-0.215406000
1	8.550954000	0.546910000	-0.216077000
1	8.081819000	-0.328932000	-1.677926000
1	-0.360533000	-0.130906000	2.517845000
8	-2.960500000	-2.001441000	2.764329000
1	-3.475886000	-2.203887000	1.968822000
1	-1.031876000	-0.437409000	2.592149000
1	-3.305103000	-0.493223000	2.991011000
8	-3.533164000	0.504742000	3.122381000
1	-4.328720000	0.613652000	2.578313000
8	-0.647930000	-3.145236000	2.421497000
1	-1.557526000	-2.680471000	2.534937000
1	-0.038866000	-2.409329000	2.247810000

[Co^{II}(CH₃CN)(Py₂^{Ts}tacn)]²⁺

$[Co^{II}(CH_3CN)(Py_2^{Ts}tacn)]^{2+}$
(G = -3309.075646) (doublet)

27	-1.224635000	-0.048518000	0.011022000
16	2.137479000	-0.103040000	1.045925000
7	1.126396000	-0.381885000	-0.323010000
8	1.845138000	1.263234000	1.504240000
7	-1.185596000	1.865279000	0.373197000
7	-3.363409000	-0.383738000	0.063978000
7	-1.179145000	0.499874000	-1.892292000
7	-1.271756000	-1.931460000	-0.689077000
8	1.920518000	-1.242844000	1.951222000
6	1.298458000	0.672182000	-1.364528000
1	2.273904000	0.583689000	-1.857233000
1	1.238545000	1.637643000	-0.860852000

6	-2.417087000	-2.602802000	-0.010230000
1	-2.130304000	-2.781652000	1.030863000
1	-2.630191000	-3.568946000	-0.479968000
6	-1.427716000	2.621507000	-0.727427000
6	-4.383636000	0.486553000	0.069170000
1	-4.117478000	1.537429000	0.142004000
6	-0.880089000	2.483548000	1.530173000
1	-0.691342000	1.844096000	2.381675000
6	-1.844679000	1.834545000	-1.934828000
1	-2.926063000	1.670334000	-1.880612000
1	-1.626364000	2.362595000	-2.868204000
6	-4.927526000	-2.190633000	-0.143701000
1	-5.096246000	-3.258422000	-0.240217000
6	0.222600000	0.573800000	-2.438785000
1	0.314358000	1.447928000	-3.089555000
1	0.392196000	-0.304113000	-3.061484000
6	-5.987664000	-1.282411000	-0.129904000
1	-7.011416000	-1.634943000	-0.211704000
6	1.220685000	-1.796045000	-0.807544000
1	2.124029000	-2.288656000	-0.437764000
1	1.313834000	-1.776560000	-1.893054000
6	3.805326000	-0.169236000	0.435371000
6	-1.963670000	-0.531927000	-2.637886000
1	-1.826725000	-0.410802000	-3.718375000
1	-3.016546000	-0.383261000	-2.403449000
6	-1.500945000	-1.912502000	-2.186529000
1	-2.247695000	-2.664554000	-2.455877000
1	-0.572110000	-2.188727000	-2.685789000
6	4.498885000	-1.382829000	0.470866000
1	4.052866000	-2.260955000	0.924794000
6	-3.628270000	-1.702085000	-0.040169000
6	0.011237000	-2.609930000	-0.351435000
1	0.045380000	-3.604061000	-0.813035000
1	0.042114000	-2.722922000	0.733289000
6	4.371321000	0.982379000	-0.125024000
1	3.824256000	1.918744000	-0.132446000
6	-5.713236000	0.081730000	-0.020519000
1	-6.507679000	0.820348000	-0.013518000
6	-1.038637000	4.644353000	0.499060000
1	-0.974625000	5.726973000	0.546794000
6	-0.806938000	3.867406000	1.634492000
1	-0.561023000	4.318267000	2.589598000
6	-1.353927000	4.008580000	-0.702070000
1	-1.542272000	4.569329000	-1.611240000
6	5.783372000	-1.435211000	-0.068142000
1	6.338083000	-2.368715000	-0.039000000
6	6.375077000	-0.301052000	-0.643009000
6	5.655246000	0.905128000	-0.656963000
1	6.109585000	1.793476000	-1.086758000
6	7.750742000	-0.374262000	-1.251222000
1	8.287112000	-1.265625000	-0.908916000
1	8.340291000	0.515394000	-1.000061000
1	7.682350000	-0.420356000	-2.346990000
6	-0.876023000	-0.879522000	2.922772000
7	-1.086967000	-0.565664000	1.830756000
6	-0.570821000	-1.268535000	4.285499000
1	0.311541000	-0.714854000	4.625551000
1	-1.421035000	-1.042670000	4.938251000
1	-0.360258000	-2.343400000	4.317400000

[Co^{II}(CH₃CN)(Py₂^{Ts}tacn)]²⁺

$[Co^{II}(CH_3CN)(Py_2^{Ts}tacn)]^{2+}$
(G = -3309.078216) (quartet)

27	-1.179906000	-0.098565000	0.118849000
16	2.082525000	-0.221804000	1.047634000

ANNEX

7	1.053671000	-0.460313000	-0.342698000
8	1.735244000	1.107113000	1.571006000
7	-1.236402000	1.982178000	0.367667000
7	-3.266911000	-0.474511000	0.194822000
7	-1.167115000	0.517533000	-1.961279000
7	-1.286532000	-2.049501000	-0.806873000
8	1.902771000	-1.415922000	1.887071000
6	1.278687000	0.618450000	-1.362109000
1	2.269163000	0.512818000	-1.817833000
1	1.224091000	1.573511000	-0.837732000
6	-2.434484000	-2.711353000	-0.144476000
1	-2.132028000	-2.959830000	0.879528000
1	-2.713997000	-3.639360000	-0.657192000
6	-1.417214000	2.671203000	-0.780409000
6	-4.234271000	0.452711000	0.278165000
1	-3.906882000	1.466061000	0.490572000
6	-0.991836000	2.654009000	1.506774000
1	-0.859114000	2.049990000	2.397699000
6	-1.810167000	1.852765000	-1.987486000
1	-2.895862000	1.705253000	-1.945632000
1	-1.582749000	2.392273000	-2.914203000
6	-4.919700000	-2.141949000	-0.283101000
1	-5.144623000	-3.177411000	-0.516133000
6	0.231121000	0.571512000	-2.473118000
1	0.375333000	1.463293000	-3.092530000
1	0.403763000	-0.289592000	-3.119520000
6	-5.925670000	-1.177788000	-0.192507000
1	-6.963794000	-1.453474000	-0.351241000
6	1.190407000	-1.856509000	-0.889915000
1	2.104422000	-2.335315000	-0.530694000
1	1.294779000	-1.781518000	-1.971494000
6	3.743867000	-0.198805000	0.424468000
6	-1.974837000	-0.509382000	-2.668059000
1	-1.903269000	-0.387257000	-3.756612000
1	-3.015685000	-0.364480000	-2.375706000
6	-1.512639000	-1.917630000	-2.282020000
1	-2.265720000	-2.641690000	-2.610776000
1	-0.587436000	-2.167811000	-2.803092000
6	4.465735000	-1.394784000	0.366386000
1	4.043750000	-2.315631000	0.753595000
6	-3.599189000	-1.753224000	-0.084074000
6	-0.002517000	-2.723137000	-0.494092000
1	0.072112000	-3.690643000	-1.007791000
1	0.021517000	-2.895724000	0.585030000
6	4.277523000	1.006619000	-0.048949000
1	3.705406000	1.925829000	0.011518000
6	-5.579143000	0.143263000	0.094707000
1	-6.329185000	0.923331000	0.167515000
6	-1.068994000	4.754915000	0.358485000
1	-0.994540000	5.838120000	0.350838000
6	-0.905295000	4.040773000	1.547418000
1	-0.705552000	4.543369000	2.487480000
6	-1.329858000	4.059751000	-0.822286000
1	-1.467800000	4.576319000	-1.766379000
6	5.748334000	-1.373854000	-0.179236000
1	6.324756000	-2.293269000	-0.224491000
6	6.309220000	-0.184966000	-0.666630000
6	5.559885000	1.001412000	-0.587927000
1	5.989822000	1.929938000	-0.953090000
6	7.687417000	-0.170942000	-1.272486000
1	8.185586000	-1.138169000	-1.148461000
1	8.308202000	0.607805000	-0.812303000
1	7.632642000	0.052666000	-2.346385000
6	-0.735833000	-0.848473000	3.178537000
7	-1.040529000	-0.552936000	2.102471000
6	-0.339458000	-1.220946000	4.521896000

1	0.560619000	-0.661855000	4.800842000
1	-1.149421000	-0.990832000	5.222565000
1	-0.125185000	-2.295173000	4.549914000

$[Co^{II}(H_2O)(Py_2^{Ts}tacn)]^{2+}$
(G = -3252.754191) (doublet)

27	1.213341000	-0.103063000	-0.177110000
16	-2.092548000	0.213122000	-1.057404000
7	-1.094069000	-0.312433000	0.239822000
8	-1.847479000	1.651144000	-1.226632000
7	1.293671000	1.829040000	-0.302584000
7	3.279180000	-0.518413000	-0.484525000
7	1.292228000	0.200327000	1.788829000
7	1.190001000	-2.059039000	0.274134000
8	-1.775185000	-0.709254000	-2.170801000
6	-1.181477000	0.586954000	1.428885000
1	-2.144789000	0.469037000	1.938780000
1	-1.086748000	1.611681000	1.070369000
6	2.258487000	-2.697960000	-0.547214000
1	1.899537000	-2.751026000	-1.580421000
1	2.452832000	-3.719869000	-0.205627000
6	1.617713000	2.432077000	0.869418000
6	4.326755000	0.319139000	-0.454705000
1	4.091196000	1.379746000	-0.435376000
6	1.003837000	2.597638000	-1.369409000
1	0.751948000	2.069286000	-2.279120000
6	2.035529000	1.481340000	1.953492000
1	3.101476000	1.266619000	1.820422000
1	1.895020000	1.904308000	2.953218000
6	4.790039000	-2.383615000	-0.473611000
1	4.927001000	-3.459956000	-0.468897000
6	-0.068281000	0.276686000	2.423389000
1	-0.073388000	1.057323000	3.189616000
1	-0.269710000	-0.665392000	2.932111000
6	5.878074000	-1.508396000	-0.449254000
1	6.892172000	-1.895819000	-0.428450000
6	-1.274651000	-1.775442000	0.529675000
1	-2.228219000	-2.147770000	0.144285000
1	-1.324102000	-1.892113000	1.611818000
6	-3.773607000	-0.044607000	-0.557611000
6	2.060978000	-0.957889000	2.334091000
1	2.011322000	-0.975719000	3.429033000
1	3.101305000	-0.832572000	2.034614000
6	1.493541000	-2.244520000	1.745170000
1	2.209511000	-3.060656000	1.876228000
1	0.578600000	-2.539878000	2.259044000
6	-4.445479000	-1.206092000	-0.948548000
1	-3.963981000	-1.930740000	-1.595954000
6	3.505769000	-1.849805000	-0.493724000
6	-0.148823000	-2.607446000	-0.078661000
1	-0.240750000	-3.645318000	0.263927000
1	-0.229384000	-2.585787000	-1.166654000
6	-4.375429000	0.913472000	0.269219000
1	-3.843645000	1.815176000	0.553462000
6	5.644420000	-0.132277000	-0.441184000
1	6.462188000	0.579971000	-0.415820000
6	1.331685000	4.606562000	-0.098520000
1	1.339125000	5.689053000	-0.016701000
6	1.020801000	3.986554000	-1.309085000
1	0.782777000	4.563071000	-2.196244000
6	1.633917000	3.813773000	1.009173000
1	1.885091000	4.249723000	1.970152000
6	-5.751841000	-1.401802000	-0.502491000
1	-6.292023000	-2.293987000	-0.805873000

ANNEX

6	-6.382253000	-0.464605000	0.328184000
6	-5.678317000	0.692658000	0.703112000
1	-6.161511000	1.430330000	1.337586000
6	-7.786322000	-0.689857000	0.822700000
1	-8.260405000	-1.529041000	0.303234000
1	-8.399046000	0.208420000	0.678996000
1	-7.782864000	-0.910239000	1.898842000
8	0.974104000	-0.311790000	-2.188502000
1	0.082722000	-0.647485000	-2.428474000
1	1.608320000	-0.910057000	-2.618912000

[Co^{II}(H$_2$O)(Py$_2$^{Ts}tacn)]$^{2+}$
(G = -3252.755099) (quartet)

27	1.213150000	-0.123291000	-0.314434000
16	-2.076794000	0.059416000	-1.171304000
7	-1.030891000	-0.390221000	0.150676000
8	-1.791651000	1.470549000	-1.459027000
7	1.291398000	1.976790000	-0.338933000
7	3.252373000	-0.532417000	-0.474508000
7	1.255716000	0.254912000	1.810072000
7	1.237854000	-2.182936000	0.395322000
8	-1.818162000	-0.960060000	-2.210102000
6	-1.196016000	0.557524000	1.303669000
1	-2.180149000	0.427279000	1.767251000
1	-1.116650000	1.568349000	0.903396000
6	2.357432000	-2.790950000	-0.351381000
1	2.026381000	-2.953440000	-1.383610000
1	2.647694000	-3.762519000	0.067426000
6	1.547830000	2.516624000	0.873022000
6	4.250125000	0.367856000	-0.503683000
1	3.949577000	1.408524000	-0.575911000
6	0.993305000	2.792332000	-1.364146000
1	0.791391000	2.308851000	-2.313624000
6	1.972411000	1.543932000	1.948233000
1	3.042651000	1.346667000	1.816015000
1	1.831444000	1.977530000	2.945132000
6	4.858638000	-2.298415000	-0.297069000
1	5.057445000	-3.360699000	-0.201632000
6	-0.125760000	0.329097000	2.368005000
1	-0.197912000	1.153060000	3.086146000
1	-0.334065000	-0.587335000	2.920334000
6	5.894690000	-1.363450000	-0.334968000
1	6.927940000	-1.691435000	-0.274441000
6	-1.221545000	-1.843309000	0.516334000
1	-2.161098000	-2.232255000	0.116167000
1	-1.313971000	-1.899562000	1.600187000
6	-3.739668000	-0.110248000	-0.585321000
6	2.018100000	-0.881270000	2.391382000
1	1.964370000	-0.865604000	3.487403000
1	3.062218000	-0.758878000	2.099469000
6	1.477632000	-2.218166000	1.868027000
1	2.195319000	-3.008606000	2.114769000
1	0.545744000	-2.471096000	2.375878000
6	-4.432568000	-1.303722000	-0.809967000
1	-3.980918000	-2.106857000	-1.381760000
6	3.543841000	-1.849529000	-0.368455000
6	-0.080785000	-2.717937000	0.000463000
1	-0.235788000	-3.740181000	0.373380000
1	-0.107884000	-2.732930000	-1.091823000
6	-4.307611000	0.950398000	0.133469000
1	-3.760023000	1.874113000	0.285286000
6	5.587960000	-0.005448000	-0.438835000
1	6.364457000	0.751243000	-0.461813000
6	1.187124000	4.733327000	0.027650000

1	1.139718000	5.808050000	0.175291000
6	0.939188000	4.176017000	-1.227862000
1	0.697528000	4.795554000	-2.084710000
6	1.494170000	3.889358000	1.095328000
1	1.692157000	4.278913000	2.088541000
6	-5.722303000	-1.430230000	-0.297230000
1	-6.278375000	-2.347124000	-0.469043000
6	-6.316612000	-0.391730000	0.433741000
6	-5.595130000	0.797091000	0.636257000
1	-6.052331000	1.611238000	1.191560000
6	-7.701617000	-0.541803000	1.002853000
1	-8.186871000	-1.449565000	0.629745000
1	-8.324585000	0.324475000	0.748395000
1	-7.661044000	-0.598867000	2.099020000
8	0.942959000	-0.499550000	-2.461329000
1	0.055312000	-0.899032000	-2.583674000
1	1.566657000	-1.204144000	-2.709981000

[Co^{I}(CH$_3$CN)(Py$_2$^{Ts}tacn)]$^+$
(G =-3309.192573) (triplet)

27	-1.365749000	-0.030624000	0.281503000
16	2.127036000	-0.281105000	1.020026000
7	1.060270000	-0.474905000	-0.302594000
8	1.858070000	1.047725000	1.594337000
7	-1.232906000	2.001359000	0.463194000
7	-3.378541000	-0.385896000	0.203380000
7	-1.243642000	0.540346000	-1.876379000
7	-1.377868000	-2.013068000	-0.721846000
8	1.981519000	-1.482450000	1.860804000
6	1.210047000	0.627429000	-1.295581000
1	2.190427000	0.579232000	-1.787051000
1	1.137230000	1.567069000	-0.746689000
6	-2.525758000	-2.629768000	-0.030562000
1	-2.228859000	-2.796194000	1.011975000
1	-2.801384000	-3.598257000	-0.472855000
6	-1.343015000	2.686619000	-0.705054000
6	-4.371977000	0.526755000	0.164536000
1	-4.078228000	1.551555000	0.373116000
6	-0.814954000	2.681652000	1.551317000
1	-0.741260000	2.103002000	2.467056000
6	-1.870021000	1.874704000	-1.862408000
1	-2.946998000	1.730134000	-1.716521000
1	-1.724254000	2.411019000	-2.810928000
6	-4.991655000	-2.082075000	-0.374824000
1	-5.185488000	-3.127027000	-0.597035000
6	0.142920000	0.586202000	-2.388965000
1	0.294580000	1.478695000	-3.010277000
1	0.312065000	-0.273105000	-3.040499000
6	-6.014812000	-1.128673000	-0.404515000
1	-7.033459000	-1.417574000	-0.645074000
6	1.102380000	-1.863317000	-0.853782000
1	2.007468000	-2.392140000	-0.540939000
1	1.162860000	-1.792556000	-1.939434000
6	3.775246000	-0.279028000	0.342329000
6	-2.057254000	-0.469168000	-2.579594000
1	-1.980684000	-0.364027000	-3.672386000
6	-3.099105000	-0.306389000	-2.300570000
6	-1.624659000	-1.889507000	-2.182567000
1	-2.401413000	-2.596145000	-2.501439000
1	-0.717061000	-2.163813000	-2.723891000
6	4.472698000	-1.485782000	0.237007000
1	4.044143000	-2.404766000	0.621529000
6	-3.698005000	-1.679784000	-0.066587000
6	-0.108144000	-2.682548000	-0.406371000

685

ANNEX

1	-0.041020000	-3.678522000	-0.872529000
1	-0.065455000	-2.805823000	0.678873000
6	4.319676000	0.921378000	-0.130457000
1	3.769111000	1.850772000	-0.033881000
6	-5.692550000	0.202800000	-0.131732000
1	-6.447284000	0.982643000	-0.152415000
6	-0.584680000	4.727122000	0.316530000
1	-0.325735000	5.779919000	0.255597000
6	-0.487037000	4.033144000	1.525012000
1	-0.154708000	4.525007000	2.433744000
6	-1.021592000	4.034509000	-0.815986000
1	-1.112832000	4.525876000	-1.779932000
6	5.738844000	-1.481257000	-0.347721000
1	6.295363000	-2.410918000	-0.426080000
6	6.309592000	-0.295407000	-0.830487000
6	5.584999000	0.902184000	-0.710041000
1	6.021591000	1.828960000	-1.072408000
6	7.671429000	-0.296611000	-1.474130000
1	8.160487000	-1.270521000	-1.365627000
1	8.315206000	0.471995000	-1.028553000
1	7.592201000	-0.069918000	-2.545934000
6	-0.640527000	-0.839624000	3.155874000
7	-1.010485000	-0.560325000	2.085802000
6	-0.123153000	-1.199824000	4.466265000
1	0.817733000	-0.668123000	4.652103000
1	-0.842368000	-0.934038000	5.249814000
1	0.067031000	-2.278998000	4.511070000

[Co^I(H$_2$O)(Py$_2^{Ts}$tacn)]$^+$

(G = -3252.873019) (triplet)

27	1.258045000	-0.022030000	-0.340344000
16	-2.057147000	0.067015000	-1.123060000
7	-1.031411000	-0.368778000	0.185152000
8	-1.820762000	1.488216000	-1.410314000
7	1.286882000	1.924726000	-0.371731000
7	3.256865000	-0.536354000	-0.506877000
7	1.282110000	0.264862000	1.831211000
7	1.232841000	-2.146619000	0.365402000
8	-1.782864000	-0.934423000	-2.177851000
6	-1.153535000	0.590341000	1.327886000
1	-2.139429000	0.501959000	1.800444000
1	-1.038016000	1.593065000	0.917443000
6	2.326308000	-2.764248000	-0.405618000
1	1.982318000	-2.885704000	-1.439599000
1	2.590032000	-3.760083000	-0.022201000
6	1.509133000	2.507374000	0.861600000
6	4.282292000	0.336277000	-0.494739000
1	4.009415000	1.384373000	-0.577045000
6	0.967491000	2.783696000	-1.391174000
1	0.815873000	2.318889000	-2.359895000
6	2.004764000	1.549870000	1.913186000
1	3.060867000	1.331819000	1.709111000
1	1.937973000	1.997786000	2.915248000
6	4.835412000	-2.333517000	-0.263096000
1	5.005475000	-3.400455000	-0.157666000
6	-0.081821000	0.348787000	2.391985000
1	-0.155657000	1.176085000	3.110212000
1	-0.301525000	-0.565089000	2.947165000
6	5.894727000	-1.422956000	-0.258926000
1	6.918566000	-1.770103000	-0.156916000
6	-1.214233000	-1.813798000	0.551438000
1	-2.167181000	-2.206152000	0.184898000
1	-1.270363000	-1.872102000	1.637783000
6	-3.733241000	-0.136792000	-0.569631000
6	2.048866000	-0.872430000	2.367994000

1	2.031293000	-0.896802000	3.468142000
1	3.086031000	-0.747783000	2.051330000
6	1.502698000	-2.202029000	1.828724000
1	2.225813000	-2.996428000	2.052352000
1	0.582714000	-2.465278000	2.354487000
6	-4.408853000	-1.334202000	-0.820383000
1	-3.940049000	-2.119555000	-1.403005000
6	3.534717000	-1.856731000	-0.391522000
6	-0.087057000	-2.681722000	-0.000390000
1	-0.234528000	-3.710273000	0.364333000
1	-0.146040000	-2.686687000	-1.091818000
6	-4.323828000	0.898776000	0.166793000
1	-3.790922000	1.827230000	0.340891000
6	5.610867000	-0.060805000	-0.375987000
1	6.399823000	0.684170000	-0.367575000
6	1.003632000	4.723758000	0.043690000
1	0.883798000	5.790136000	0.206597000
6	0.823090000	4.150399000	-1.226932000
1	0.564299000	4.762484000	-2.086708000
6	1.357480000	3.861495000	1.096683000
1	1.529342000	4.239623000	2.101160000
6	-5.701544000	-1.489989000	-0.321254000
1	-6.242386000	-2.411786000	-0.515304000
6	-6.317163000	-0.475441000	0.424919000
6	-5.613484000	0.718658000	0.656350000
1	-6.085943000	1.515821000	1.223692000
6	-7.705157000	-0.655804000	0.979507000
1	-8.167560000	-1.573058000	0.600343000
1	-8.344641000	0.196624000	0.718623000
1	-7.676552000	-0.713006000	2.076002000
8	0.977484000	-0.449712000	-2.555546000
1	0.085898000	-0.848718000	-2.613971000
1	1.587141000	-1.179742000	-2.749353000

[Co^{II}(H)(Py$_2^{Ts}$tacn)]$^+$

(G = -3176.994155) (doublet)

27	1.259371000	-0.081944000	-0.304627000
16	-2.064949000	0.083222000	-1.192351000
7	-1.078847000	-0.413949000	0.112971000
8	-1.796673000	1.512473000	-1.413775000
7	1.273948000	1.847866000	-0.390026000
7	3.376671000	-0.468646000	-0.442785000
7	1.286390000	0.181021000	1.694318000
7	1.270914000	-2.064418000	0.138860000
8	-1.828471000	-0.880973000	-2.279095000
6	-1.189216000	0.487261000	1.293260000
1	-2.156941000	0.364280000	1.795621000
1	-1.106200000	1.511390000	0.928853000
6	2.364420000	-2.643930000	-0.680365000
1	2.029652000	-2.635858000	-1.723292000
1	2.571945000	-3.680988000	-0.388419000
6	1.555854000	2.437213000	0.802735000
6	4.426745000	0.363102000	-0.374860000
1	4.192605000	1.419585000	-0.273030000
6	0.976503000	2.643417000	-1.437988000
1	0.754894000	2.133869000	-2.366397000
6	1.983932000	1.480489000	1.881329000
1	3.057620000	1.298945000	1.764597000
1	1.818210000	1.893807000	2.882612000
6	4.891132000	-2.324654000	-0.606102000
1	5.027402000	-3.398466000	-0.687519000
6	-0.083707000	0.204991000	2.302563000
1	-0.133255000	0.974123000	3.080211000
1	-0.262263000	-0.750803000	2.795348000

ANNEX

6	5.980843000	-1.454559000	-0.538690000
1	6.995203000	-1.841117000	-0.569062000
6	-1.201763000	-1.878008000	0.384872000
1	-2.138645000	-2.285016000	-0.007814000
1	-1.248914000	-2.013019000	1.465134000
6	-3.743992000	-0.098549000	-0.627837000
6	2.071862000	-0.962214000	2.238258000
1	1.988117000	-1.011118000	3.331220000
1	3.117233000	-0.799152000	1.979847000
6	1.565193000	-2.258867000	1.606779000
1	2.310991000	-3.049551000	1.737282000
1	0.657495000	-2.597236000	2.108067000
6	-4.443650000	-1.273403000	-0.915483000
1	-3.994340000	-2.043234000	-1.533272000
6	3.605227000	-1.792582000	-0.561962000
6	-0.038393000	-2.656076000	-0.229935000
1	-0.098004000	-3.703499000	0.095686000
1	-0.117517000	-2.616064000	-1.317348000
6	-4.309351000	0.915231000	0.156592000
1	-3.758227000	1.826336000	0.363498000
6	5.745716000	-0.083060000	-0.423704000
1	6.563231000	0.627833000	-0.362890000
6	1.217156000	4.630236000	-0.112284000
1	1.189232000	5.709975000	-0.002142000
6	0.948069000	4.030375000	-1.343195000
1	0.707684000	4.621565000	-2.220422000
6	1.523556000	3.815365000	0.978400000
1	1.741907000	4.232729000	1.955923000
6	-5.733780000	-1.427806000	-0.408118000
1	-6.292000000	-2.332666000	-0.631202000
6	-6.324745000	-0.432896000	0.382629000
6	-5.597258000	0.738474000	0.653096000
1	-6.049364000	1.520648000	1.256949000
6	-7.712097000	-0.609372000	0.941189000
1	-8.180603000	-1.521544000	0.557080000
1	-8.348385000	0.247416000	0.685994000
1	-7.681906000	-0.672522000	2.037173000
1	1.107366000	-0.275913000	-1.853210000

6	4.965070000	-2.217184000	-0.401200000
1	5.180838000	-3.279603000	-0.354445000
6	-0.094805000	0.245310000	2.253448000
1	-0.214596000	1.061386000	2.976183000
1	-0.257379000	-0.682172000	2.804682000
6	5.984290000	-1.263556000	-0.377021000
1	7.023038000	-1.573645000	-0.315599000
6	-1.122480000	-1.988908000	0.429129000
1	-2.054627000	-2.417782000	0.051110000
1	-1.184255000	-2.049240000	1.515157000
6	-3.694347000	-0.207220000	-0.628878000
6	2.091636000	-0.862365000	2.248889000
1	2.040495000	-0.879534000	3.346678000
1	3.129939000	-0.689595000	1.964373000
6	1.613821000	-2.212436000	1.703990000
1	2.372160000	-2.972599000	1.924183000
1	0.706499000	-2.519887000	2.226484000
6	-4.428538000	-1.391038000	-0.744431000
1	-4.016194000	-2.248145000	-1.265411000
6	3.643658000	-1.787572000	-0.478116000
6	0.051181000	-2.802579000	-0.114085000
1	-0.015197000	-3.827540000	0.277782000
1	-0.011938000	-2.837393000	-1.203961000
6	-4.215655000	0.917919000	0.022193000
1	-3.636793000	1.832301000	0.093455000
6	5.648682000	0.090839000	-0.419020000
1	6.408335000	0.864624000	-0.390999000
6	0.994418000	4.745126000	0.016321000
1	0.887698000	5.811369000	0.192621000
6	0.777202000	4.210026000	-1.254697000
1	0.502992000	4.839028000	-2.094713000
6	1.346539000	3.890864000	1.061813000
1	1.522780000	4.264407000	2.065225000
6	-5.709354000	-1.440567000	-0.195207000
1	-6.295043000	-2.351012000	-0.284350000
6	-6.257393000	-0.332304000	0.466010000
6	-5.496040000	0.844521000	0.561765000
1	-5.915359000	1.712961000	1.062194000
6	-7.632820000	-0.397688000	1.075264000
1	-8.173641000	-1.287540000	0.736440000
1	-8.218316000	0.493272000	0.817801000
1	-7.565787000	-0.435124000	2.171186000
1	1.052824000	-0.321421000	-2.211231000

[Co^{II}(H)(Py$_2^{Ts}$tacn)]$^+$

(G = -3176.983890) (quartet)

27	1.234578000	-0.104244000	-0.521051000
16	-2.038127000	-0.140709000	-1.272117000
7	-0.997272000	-0.537591000	0.057745000
8	-1.726083000	1.249535000	-1.635759000
7	1.248468000	2.010730000	-0.423064000
7	3.322291000	-0.476447000	-0.520373000
7	1.280170000	0.242403000	1.692516000
7	1.340543000	-2.171242000	0.235021000
8	-1.869981000	-1.217106000	-2.259436000
6	-1.180468000	0.418382000	1.193960000
1	-2.156790000	0.271747000	1.669816000
1	-1.136139000	1.424873000	0.776350000
6	2.469437000	-2.735929000	-0.533315000
1	2.145582000	-2.831395000	-1.576757000
1	2.756302000	-3.729612000	-0.165140000
6	1.473673000	2.528775000	0.804248000
6	4.303068000	0.439974000	-0.485479000
1	3.985096000	1.478045000	-0.504434000
6	0.908993000	2.836280000	-1.427692000
1	0.738753000	2.365739000	-2.389904000
6	1.939971000	1.550513000	1.855332000
1	3.017537000	1.405505000	1.716325000
1	1.788294000	1.964776000	2.860484000

[Co^{III}(H)(Py$_2^{Ts}$tacn)]$^{2+}$

(G = -3176.857570) (singlet)

27	1.112567000	-0.247786000	-0.171457000
16	-1.902907000	0.244455000	-1.175047000
7	-0.892570000	-0.381033000	0.180631000
8	-1.601237000	1.674971000	-1.276948000
7	1.237415000	1.676352000	-0.243320000
7	3.015293000	-0.449269000	-0.519781000
7	1.281783000	0.006679000	1.841681000
7	1.166166000	-2.172679000	0.154112000
8	-1.640151000	-0.660863000	-2.299226000
6	-1.127941000	0.439986000	1.421831000
1	-2.131974000	0.257307000	1.814705000
1	-1.028543000	1.489042000	1.144633000
6	2.236421000	-2.701967000	-0.733714000
1	1.841466000	-2.720564000	-1.755288000
1	2.526965000	-3.716634000	-0.445670000
6	1.613117000	2.251953000	0.926824000
6	3.971504000	0.501306000	-0.534005000
1	3.652671000	1.527154000	-0.412381000

ANNEX

```
6    1.081441000    2.444849000    -1.337843000
1    0.811944000    1.927256000    -2.247860000
6    1.991996000    1.296276000    2.027903000
1    3.068252000    1.108615000    1.947572000
1    1.803514000    1.724130000    3.017583000
6    4.711384000    -2.122512000    -0.841130000
1    4.952351000    -3.174020000    -0.951995000
6    -0.082631000    0.052419000    2.458778000
1    -0.104845000    0.778347000    3.276652000
1    -0.308124000    -0.922828000    2.888593000
6    5.697965000    -1.137446000    -0.847804000
1    6.743044000    -1.405639000    -0.965264000
6    -1.240270000    -1.847217000    0.404362000
1    -2.213260000    -2.096180000    -0.021797000
1    -1.329001000    -2.005681000    1.477960000
6    -3.580782000    0.047444000    -0.631189000
6    2.062284000    -1.180898000    2.289354000
1    2.025219000    -1.293025000    3.378814000
1    3.099246000    -1.022652000    1.990648000
6    1.497656000    -2.432384000    1.615393000
1    2.219755000    -3.249932000    1.682753000
1    0.587245000    -2.764212000    2.114586000
6    -4.312393000    -1.067034000    -1.052555000
1    -3.866467000    -1.803949000    -1.711662000
6    3.384644000    -1.744673000    -0.685847000
6    -0.168199000    -2.721023000    -0.214289000
1    -0.269912000    -3.756012000    0.129995000
1    -0.245998000    -2.687635000    -1.300986000
6    -4.139300000    1.025949000    0.201962000
1    -3.565772000    1.895845000    0.502718000
6    5.316673000    0.195649000    -0.699369000
1    6.044402000    0.999316000    -0.701496000
6    1.589795000    4.425854000    -0.086559000
1    1.718669000    5.501779000    -0.022617000
6    1.255226000    3.822031000    -1.299469000
1    1.123960000    4.403134000    -2.205288000
6    1.773957000    3.627566000    1.042006000
1    2.061052000    4.050774000    1.998479000
6    -5.628979000    -1.202752000    -0.616768000
1    -6.212537000    -2.060169000    -0.938905000
6    -6.213826000    -0.249321000    0.228851000
6    -5.454011000    0.864863000    0.625050000
1    -5.902539000    1.616735000    1.268144000
6    -7.628864000    -0.410911000    0.714852000
1    -8.132435000    -1.237669000    0.203447000
1    -8.203877000    0.509223000    1.553940000
1    -7.641251000    -0.614711000    1.794074000
1    0.917304000    -0.419432000    -1.617632000
```

[Co^{III}(H)(Py$_2$^{Ts}tacn)]$^{2+}$

(G = -3176.832278) (triplet)

```
27    1.148457000    -0.140567000    -0.243456000
16    -1.967192000    0.095702000    -1.203329000
7    -0.981481000    -0.418396000    0.166459000
8    -1.643612000    1.510802000    -1.416399000
7    1.291348000    1.858444000    -0.319527000
7    3.149668000    -0.540740000    -0.632813000
7    1.308976000    0.137448000    1.770664000
7    1.209397000    -2.192575000    0.258255000
8    -1.699890000    -0.893380000    -2.255196000
6    -1.150886000    0.492769000    1.350811000
1    -2.133579000    0.342869000    1.809959000
1    -1.074353000    1.518151000    0.988364000
6    2.283138000    -2.784877000    -0.576938000
```

```
1    1.895452000    -2.885772000    -1.596878000
1    2.568674000    -3.776951000    -0.211110000
6    1.624622000    2.405403000    0.877583000
6    4.127788000    0.378186000    -0.712106000
1    3.814041000    1.416370000    -0.726319000
6    1.046551000    2.663740000    -1.372123000
1    0.795504000    2.169449000    -2.301048000
6    2.038442000    1.425271000    1.943549000
1    3.108311000    1.225875000    1.813774000
1    1.891196000    1.832998000    2.948274000
6    4.785766000    -2.286089000    -0.656339000
1    5.000622000    -3.348878000    -0.624328000
6    -0.064023000    0.206718000    2.383235000
1    -0.092283000    0.997830000    3.137760000
1    -0.263548000    -0.732330000    2.897963000
6    5.803909000    -1.334684000    -0.731728000
1    6.843004000    -1.647421000    -0.760737000
6    -1.230344000    -1.871227000    0.488199000
1    -2.193465000    -2.204354000    0.094032000
1    -1.298139000    -1.960679000    1.571474000
6    -3.646555000    -0.053948000    -0.655251000
6    2.091870000    -1.023904000    2.288326000
1    2.073428000    -1.042167000    3.383965000
1    3.123325000    -0.890280000    1.960114000
6    1.523485000    -2.325521000    1.725438000
1    2.246672000    -3.132433000    1.878016000
1    0.613748000    -2.609718000    2.255158000
6    -4.370204000    -1.206961000    -0.973844000
1    -3.924796000    -1.988348000    -1.579788000
6    3.465652000    -1.852386000    -0.610646000
6    -0.124182000    -2.749190000    -0.083440000
1    -0.233022000    -3.769227000    0.304809000
1    -0.202009000    -2.768721000    -1.171562000
6    -4.202157000    0.979476000    0.110442000
1    -3.631411000    1.873901000    0.335507000
6    5.470491000    0.020341000    -0.764865000
1    6.230913000    0.791297000    -0.822099000
6    1.409750000    4.614487000    -0.027850000
1    1.445161000    5.693059000    0.089939000
6    1.102105000    4.046803000    -1.266149000
1    0.899747000    4.661134000    -2.136269000
6    1.677461000    3.782015000    1.059002000
1    1.931762000    4.183409000    2.033904000
6    -5.678900000    -1.321224000    -0.508912000
1    -6.258011000    -2.206498000    -0.754811000
6    -6.262390000    -0.309566000    0.267183000
6    -5.509422000    0.839277000    0.564428000
1    -5.957688000    1.634071000    1.153910000
6    -7.667628000    -0.449281000    0.787372000
1    -8.192499000    -1.274760000    0.295376000
1    -8.235446000    0.476265000    0.634274000
1    -7.656486000    -0.647532000    1.867917000
1    0.968536000    -0.228937000    -1.703741000
```

H$_2$O

(G =-76.468827) (singlet)

```
8    0.000000000    0.000000000    0.121359000
1    0.000000000    0.757766000    -0.485437000
1    0.000000000    -0.757766000    -0.485437000
```

(H$_2$O)$_3$

(G = -229.388173) (singlet)

ANNEX

8	1.432539000	-1.037400000	0.002469000
1	1.335635000	-0.065848000	-0.085725000
8	-1.460496000	-0.566402000	-0.002749000
1	0.495613000	-1.302201000	0.011285000
1	-1.934604000	-0.426529000	0.834122000
8	0.303114000	1.560259000	-0.102813000
1	0.479151000	1.696894000	0.842870000
1	-0.432739000	0.899253000	-0.093608000
1	-2.144316000	-0.453224000	-0.684198000

CH$_3$CN

(G = -132.782109) (singlet)

6	0.000000000	0.000000000	0.276959000
7	0.000000000	0.000000000	1.440477000
6	0.000000000	0.000000000	-1.180973000
1	0.000000000	1.030628000	-1.553086000
1	0.892550000	-0.515314000	-1.553086000
1	-0.892550000	-0.515314000	-1.553086000

Acetophenone (9a)

(G = -384.922192) (singlet)

6	2.587772000	0.119064000	-0.000005000
6	1.810554000	1.281268000	0.000047000
6	0.418155000	1.190364000	0.000048000
6	-0.209275000	-0.067389000	0.000005000
6	0.581583000	-1.230001000	-0.000043000
6	1.971002000	-1.138089000	-0.000052000
1	3.671907000	0.191684000	-0.000010000
1	2.288279000	2.256711000	0.000086000
1	-0.177549000	2.097150000	0.000087000
1	0.091961000	-2.198529000	-0.000080000
1	2.574852000	-2.041124000	-0.000095000
8	-2.230089000	-1.311664000	0.000107000
6	-1.695042000	-0.200805000	0.000007000
6	-2.532958000	1.056379000	-0.000093000
1	-2.303374000	1.666646000	0.882410000
1	-2.303307000	1.666558000	-0.882638000
1	-3.592809000	0.789468000	-0.000114000

Ketyl radical (9a^{ketyl})

(G = -385.024638) (doublet)

6	2.617047000	0.110918000	0.000095000
6	1.818579000	1.273773000	0.000098000
6	0.432934000	1.197905000	-0.000031000
6	-0.249046000	-0.068670000	-0.000183000
6	0.588159000	-1.238444000	-0.000141000
6	1.969987000	-1.144323000	-0.000011000
1	3.701616000	0.178944000	0.000199000
1	2.295321000	2.253127000	0.000195000
1	-0.149411000	2.115614000	-0.000027000
1	0.105861000	-2.212436000	-0.000241000
1	2.566214000	-2.056106000	0.000004000
8	-2.280405000	-1.333790000	0.000318000
6	-1.672478000	-0.188465000	-0.000339000
6	-2.515211000	1.082612000	0.000014000
1	-2.319830000	1.714707000	0.880529000
1	-2.319773000	1.715202000	-0.880127000
1	-3.576582000	0.809432000	-0.000082000

O-protonated ketyl radical

(G = -385.481597) (doublet)

6	-2.662136000	-0.053950000	0.002060000
6	-1.920127000	-1.246471000	0.012302000
6	-0.532085000	-1.224957000	0.008893000
6	0.185983000	0.010945000	-0.008320000
6	-0.589258000	1.213813000	-0.013932000
6	-1.976793000	1.171556000	-0.010231000
1	-3.748069000	-0.079505000	0.005530000
1	-2.435412000	-2.203887000	0.026473000
1	0.010639000	-2.164119000	0.026897000
1	-0.080902000	2.171919000	-0.025235000
1	-2.536436000	2.104004000	-0.016675000
8	2.182497000	1.299613000	0.037176000
6	1.599989000	0.050581000	-0.016872000
6	2.530146000	-1.117056000	-0.015998000
1	2.959979000	-1.288133000	0.984211000
1	2.036933000	-2.037996000	-0.335967000
1	3.370584000	-0.924736000	-0.699091000
1	3.148389000	1.198787000	-0.010968000

C-deprotonated alcohol

(G = -385.584845) (singlet)

6	2.685824000	0.044656000	-0.031943000
6	1.930230000	1.239916000	-0.023837000
6	0.547047000	1.244364000	0.016081000
6	-0.232806000	0.012569000	0.060441000
6	0.577149000	-1.201430000	0.043145000
6	1.962677000	-1.164987000	0.000989000
1	3.771814000	0.058862000	-0.066410000
1	2.448908000	2.199353000	-0.056160000
1	0.023146000	2.197910000	0.006033000
1	0.069764000	-2.162476000	0.083600000
1	2.504694000	-2.112180000	-0.005717000
8	-2.272949000	-1.298701000	0.023447000
6	-1.613040000	-0.027144000	0.103565000
6	-2.559701000	1.123622000	-0.033182000
1	-3.437062000	1.010796000	0.626807000
1	-2.078041000	2.071509000	0.236752000
1	-2.970931000	1.252554000	-1.057265000
1	-1.932982000	-1.756105000	-0.766768000

A.IX.6.Coordinates from chapter IX

Olefin 13a

(G = -309.643622) (singlet)

6	-1.953896000	-0.539797000	-0.000067000
6	-0.515429000	-0.227381000	-0.000045000
6	0.408858000	-1.287383000	0.000004000
6	-0.019332000	1.091130000	-0.000061000
6	1.784198000	-1.044007000	0.000039000
1	0.037529000	-2.309688000	-0.000007000
6	1.352546000	1.334841000	-0.000014000
1	-0.712245000	1.927733000	-0.000124000
6	2.262086000	0.269066000	0.000037000
1	2.480104000	-1.878839000	0.000072000
1	1.716222000	2.359059000	-0.000043000
1	3.331254000	0.463039000	0.000070000
6	-2.963751000	0.341060000	0.000089000

ANNEX

1	-2.800291000	1.416753000	0.000262000
1	-3.996332000	0.001243000	0.000073000
1	-2.187922000	-1.604477000	-0.000201000

1	3.095958000	0.789989000	0.994506000
1	3.901503000	-0.144745000	-0.276110000
1	2.774706000	1.166896000	-0.696804000

Reduced Olefin 13a

(G = -309.723511) (singlet)

6	-1.938156000	-0.548113000	-0.000003000
6	-0.548135000	-0.253790000	-0.000124000
6	0.440817000	-1.301816000	-0.000092000
6	-0.021318000	1.096413000	-0.000212000
6	1.798659000	-1.039110000	0.000071000
1	0.092175000	-2.335543000	-0.000207000
6	1.344160000	1.342002000	0.000021000
1	-0.716556000	1.933584000	-0.000515000
6	2.290912000	0.294668000	0.000154000
1	2.500925000	-1.872676000	0.000047000
1	1.692234000	2.375634000	-0.000067000
1	3.358067000	0.500055000	0.000421000
6	-3.008079000	0.344246000	0.000044000
1	-2.863948000	1.423463000	0.000556000
1	-4.034378000	-0.016482000	0.000719000
1	-2.181683000	-1.615026000	-0.000103000

Oxidised Olefin 13a

(G = -309.425258) (singlet)

6	-1.901915000	-0.568687000	-0.000065000
6	-0.520341000	-0.237775000	-0.001100000
6	0.427188000	-1.314134000	-0.000527000
6	-0.039042000	1.116085000	-0.000943000
6	1.779250000	-1.052158000	0.000368000
1	0.053614000	-2.333316000	-0.000959000
6	1.314809000	1.363903000	-0.000044000
1	-0.742393000	1.940365000	-0.001145000
6	2.228505000	0.286897000	0.000781000
1	2.499557000	-1.863201000	0.001159000
1	1.685439000	2.383198000	-0.000100000
1	3.294728000	0.491938000	0.001809000
6	-2.938655000	0.340488000	0.001034000
1	-2.775989000	1.413863000	0.000614000
1	-3.965364000	-0.012892000	0.001753000
1	-2.148390000	-1.627673000	-0.000149000

Radical of 13a

(G = -310.220540) (singlet)

6	1.832624000	-0.651834000	-0.006133000
6	0.462698000	-0.299093000	-0.002019000
6	-0.541309000	-1.313894000	0.000729000
6	0.022565000	1.058414000	0.000163000
6	-1.891088000	-0.990782000	0.000800000
1	-0.226514000	-2.354997000	0.001437000
6	-1.331908000	1.369521000	0.000182000
1	0.760254000	1.855330000	0.003392000
6	-2.300489000	0.353489000	-0.000324000
1	-2.634920000	-1.783662000	0.001890000
1	-1.642996000	2.411288000	0.001291000
1	-3.357518000	0.604232000	-0.000710000
6	2.955939000	0.335471000	-0.001248000
1	2.075333000	-1.712078000	0.018207000

Reduced Radical of 13a

(G = -310.332253) (singlet)

6	-1.846497000	-0.673468000	0.006976000
6	-0.501252000	-0.332937000	-0.001453000
6	0.566505000	-1.319758000	-0.004205000
6	-0.029674000	1.043367000	-0.005351000
6	1.905969000	-0.971192000	-0.000087000
1	0.286919000	-2.374381000	-0.007533000
6	1.322358000	1.364117000	0.000793000
1	-0.765902000	1.845053000	-0.011918000
6	2.327927000	0.378423000	0.004643000
1	2.653156000	-1.766163000	-0.001363000
1	1.607803000	2.417398000	0.000366000
1	3.382263000	0.642214000	0.007434000
6	-2.951164000	0.350933000	0.000885000
1	-2.121153000	-1.728491000	-0.004728000
1	-2.990791000	0.975208000	-0.916446000
1	-3.935803000	-0.129254000	0.089521000
1	-2.881534000	1.081511000	0.831465000

Oxidised Radical of 13a

(G = -310.053698) (singlet)

6	-1.800736000	-0.583712000	-0.000013000
6	-0.450241000	-0.246454000	-0.000033000
6	0.504183000	-1.313596000	-0.000051000
6	0.008143000	1.108853000	-0.000076000
6	1.857487000	-1.034856000	0.000029000
1	0.142699000	-2.337432000	-0.000122000
6	1.363200000	1.370822000	-0.000010000
1	-0.707642000	1.922568000	-0.000091000
6	2.282336000	0.303988000	0.000068000
1	2.586808000	-1.837722000	0.000085000
1	1.724667000	2.393414000	-0.000043000
1	3.346288000	0.522639000	0.000099000
6	-2.959193000	0.311363000	0.000058000
1	-2.032144000	-1.648360000	-0.000063000
1	-2.724760000	1.376284000	-0.000147000
1	-3.583694000	0.054956000	-0.871661000
1	-3.583297000	0.055205000	0.872110000

I_S$_q$

(G = -3486.630730) (quadruplet)

27	0.522313000	0.514242000	-0.053411000
16	-2.501583000	-0.749252000	-1.021076000
7	-1.734599000	-0.158629000	0.407168000
8	-2.457291000	0.340637000	-2.008058000
7	0.081187000	2.382651000	-1.025297000
7	2.569141000	0.826158000	0.404263000
7	-0.055816000	1.897174000	1.669789000
7	0.751680000	-0.786411000	1.693000000
8	-1.869003000	-2.043874000	-1.321850000
6	-2.325632000	1.141103000	0.851501000
1	-3.348288000	0.995648000	1.220251000

ANNEX

1	-2.351829000	1.796087000	-0.019791000
6	2.115368000	-1.308959000	1.459584000
1	2.068021000	-1.965544000	0.587109000
1	2.474201000	-1.897840000	2.314018000
6	-0.063680000	3.458405000	-0.225418000
6	3.358226000	1.864048000	0.089378000
1	2.903326000	2.640777000	-0.518709000
6	-0.188510000	2.507757000	-2.335209000
1	-0.067059000	1.607251000	-2.927902000
6	0.316882000	3.249814000	1.219197000
1	1.406259000	3.343532000	1.295688000
1	-0.128843000	4.029327000	1.851037000
6	4.374550000	-0.150116000	1.641397000
1	4.734761000	-0.968570000	2.255504000
6	-1.507781000	1.790986000	1.967464000
1	-1.936252000	2.785988000	2.139122000
1	-1.640605000	1.234401000	2.896611000
6	5.193787000	0.930189000	1.312578000
1	6.218001000	0.969653000	1.670648000
6	-1.674694000	-1.220397000	1.466110000
1	-2.394874000	-2.020453000	1.274734000
1	-1.982259000	-0.764737000	2.407355000
6	-4.200757000	-1.043487000	-0.578844000
6	0.766510000	1.453774000	2.816653000
1	0.453669000	1.948513000	3.746988000
1	1.799255000	1.738904000	2.614687000
6	0.669948000	-0.063689000	2.994508000
1	1.475672000	-0.394660000	3.660439000
1	-0.267465000	-0.325631000	3.487075000
6	-4.594217000	-2.322916000	-0.170027000
1	-3.883967000	-3.142627000	-0.170274000
6	3.067316000	-0.171541000	1.166700000
6	-0.279698000	-1.834328000	1.566003000
1	-0.259999000	-2.526871000	2.419941000
1	-0.066090000	-2.398006000	0.654145000
6	-5.101355000	0.026147000	-0.597013000
1	-4.783655000	1.010738000	-0.922258000
6	4.676959000	1.959883000	0.524694000
1	5.277464000	2.821127000	0.252078000
6	-0.756988000	4.820506000	-2.077014000
1	-1.090261000	5.770792000	-2.483471000
6	-0.598683000	3.708365000	-2.906284000
1	-0.800441000	3.762064000	-3.970795000
6	-0.488048000	4.691815000	-0.714194000
1	-0.604690000	5.526830000	-0.030866000
6	-5.914837000	-2.524730000	0.222286000
1	-6.233381000	-3.514304000	0.538418000
6	-6.842478000	-1.470756000	0.214251000
6	-6.418111000	-0.199538000	-0.199466000
1	-7.128768000	0.622104000	-0.210402000
6	-8.271370000	-1.711887000	0.624050000
1	-8.320874000	-2.316923000	1.537437000
1	-8.808352000	-2.263587000	-0.159815000
1	-8.798682000	-0.767413000	0.794954000
1	0.591880000	-0.338567000	-1.500434000
6	2.724144000	-3.919226000	-1.010119000
6	3.825265000	-2.949581000	-1.123799000
6	3.674895000	-1.693052000	-1.743248000
6	5.078325000	-3.277865000	-0.576836000
6	4.741228000	-0.799806000	-1.808188000
1	2.713973000	-1.412338000	-2.162882000
6	6.147115000	-2.381013000	-0.638980000

1	5.206751000	-4.245417000	-0.096958000
6	5.981993000	-1.137908000	-1.254779000
1	4.602581000	0.168777000	-2.280328000
1	7.105862000	-2.652269000	-0.205048000
1	6.809245000	-0.435177000	-1.299729000
6	1.434505000	-3.703484000	-1.311060000
1	0.696183000	-4.490546000	-1.179183000
1	1.075353000	-2.746745000	-1.683630000
1	3.015186000	-4.892620000	-0.614906000

II_S$_q$

(G = -3486.645483) (quadruplet)

27	0.727715000	0.189074000	0.026918000
16	-2.454785000	-0.660988000	-1.033130000
7	-1.618962000	-0.208792000	0.413168000
8	-2.276325000	0.458078000	-1.974210000
7	0.646167000	2.197942000	-0.801589000
7	2.736843000	0.305185000	0.782338000
7	0.194735000	1.595360000	1.868901000
7	0.714113000	-1.161416000	1.870658000
8	-1.967772000	-2.004504000	-1.380352000
6	-2.070689000	1.144813000	0.872715000
1	-3.128328000	1.120251000	1.161551000
1	-1.946743000	1.824165000	0.029335000
6	2.021688000	-1.818144000	1.730501000
1	1.965936000	-2.498090000	0.878315000
1	2.277113000	-2.413503000	2.618648000
6	0.490466000	3.224418000	0.061649000
6	3.655028000	1.241065000	0.507202000
1	3.298260000	2.109882000	-0.037903000
6	0.453425000	2.432470000	-2.112306000
1	0.572954000	1.584451000	-2.771903000
6	0.756131000	2.906391000	1.507681000
1	1.841854000	2.858754000	1.646681000
1	0.371315000	3.708705000	2.152271000
6	4.424255000	-0.998956000	1.869774000
1	4.684193000	-1.899824000	2.416660000
6	-1.271075000	1.654894000	2.066757000
1	-1.597167000	2.687313000	2.247271000
1	-1.537467000	1.089624000	2.961658000
6	5.382100000	-0.028795000	1.571231000
1	6.414589000	-0.164409000	1.879265000
6	-1.730012000	-1.297907000	1.446275000
1	-2.509030000	-2.016553000	1.179881000
1	-2.058719000	-0.840745000	2.378942000
6	-4.180583000	-0.774157000	-0.613388000
6	0.874943000	1.035841000	3.053783000
1	0.548584000	1.539244000	3.976022000
1	1.944732000	1.209271000	2.939514000
6	0.599841000	-0.462051000	3.176377000
1	1.300428000	-0.893845000	3.901812000
1	-0.399611000	-0.623544000	3.582769000
6	-4.720347000	-2.014649000	-0.258011000
1	-4.108472000	-2.909534000	-0.282914000
6	3.107671000	-0.797104000	1.462558000
6	-0.420637000	-2.066735000	1.620183000
1	-0.554228000	-2.788551000	2.440176000
1	-0.206314000	-2.620917000	0.704335000
6	-4.958955000	0.389215000	-0.613613000
1	-4.529357000	1.340160000	-0.908629000

ANNEX

6	4.989032000	1.121646000	0.885647000
1	5.696803000	1.906787000	0.641749000
6	-0.049649000	4.742679000	-1.721662000
1	-0.326990000	5.731409000	-2.074868000
6	0.111856000	3.684420000	-2.615585000
1	-0.031761000	3.815405000	-3.682823000
6	0.142705000	4.505123000	-0.360895000
1	0.020049000	5.292585000	0.375733000
6	-6.064173000	-2.081689000	0.102956000
1	-6.498794000	-3.040910000	0.369636000
6	-6.867918000	-0.931740000	0.121425000
6	-6.299245000	0.297984000	-0.246584000
1	-6.916792000	1.191770000	-0.250567000
6	-8.310556000	-1.012408000	0.544798000
1	-8.725744000	-2.005769000	0.342274000
1	-8.916076000	-0.258277000	0.029710000
1	-8.402878000	-0.827826000	1.624424000
1	-0.250414000	-0.497049000	-2.850277000
6	1.274944000	-1.273096000	-1.438042000
6	2.717095000	-1.636056000	-1.536398000
6	3.678572000	-0.708114000	-1.996124000
6	3.199476000	-2.914020000	-1.183782000
6	5.033137000	-1.025826000	-2.071535000
1	3.346211000	0.289495000	-2.275530000
6	4.558216000	-3.237980000	-1.244272000
1	2.484960000	-3.667342000	-0.855959000
6	5.489309000	-2.294416000	-1.686981000
1	5.741762000	-0.277260000	-2.419696000
1	4.886749000	-4.233773000	-0.953957000
1	6.546990000	-2.539827000	-1.736938000
6	0.761929000	-0.908159000	-2.851536000
1	0.755469000	-1.786299000	-3.523001000
1	1.417354000	-0.168189000	-3.328363000
1	0.731479000	-2.176701000	-1.124629000

TS_S_hetero$_q$

(G = -3486.600444) (quadruplet)

27	0.436576000	0.425101000	0.096493000
16	-2.458519000	-0.833808000	-0.951838000
7	-1.731822000	-0.248143000	0.514659000
8	-2.299588000	0.240352000	-1.942889000
7	0.109606000	2.207794000	-0.948006000
7	2.500181000	0.644657000	0.477757000
7	-0.095462000	1.788107000	1.774621000
7	0.720891000	-0.920240000	1.804517000
8	-1.870058000	-2.158727000	-1.197991000
6	-2.351009000	1.043516000	0.953311000
1	-3.376489000	0.880616000	1.302919000
1	-2.371593000	1.701682000	0.083608000
6	2.077019000	-1.462252000	1.576749000
1	2.027497000	-2.135485000	0.714089000
1	2.438795000	-2.026922000	2.446117000
6	-0.059760000	3.300541000	-0.170887000
6	3.273406000	1.681438000	0.120575000
1	2.798402000	2.442005000	-0.492071000
6	-0.083355000	2.309246000	-2.274565000
1	0.069372000	1.399468000	-2.844920000
6	0.276635000	3.130727000	1.292742000
1	1.362724000	3.239779000	1.394671000
1	-0.192978000	3.925529000	1.886502000

6	4.340709000	-0.293496000	1.689885000
1	4.719491000	-1.096114000	2.313530000
6	-1.545488000	1.690857000	2.079145000
1	-1.971194000	2.686406000	2.253073000
1	-1.679184000	1.129607000	3.005319000
6	5.145671000	0.782493000	1.314653000
1	6.178679000	0.834666000	1.644431000
6	-1.708940000	-1.319742000	1.569219000
1	-2.443556000	-2.101643000	1.359149000
1	-2.017342000	-0.861960000	2.508694000
6	-4.187827000	-1.036801000	-0.594512000
6	0.739563000	1.340113000	2.911129000
1	0.444052000	1.836651000	3.845957000
1	1.770989000	1.618346000	2.691942000
6	0.640422000	-0.178596000	3.098796000
1	1.447597000	-0.502715000	3.766142000
1	-0.296140000	-0.435208000	3.596202000
6	-4.658894000	-2.286386000	-0.182913000
1	-3.987334000	-3.135690000	-0.118563000
6	3.023211000	-0.334159000	1.245404000
6	-0.324469000	-1.955474000	1.678907000
1	-0.317608000	-2.643969000	2.535983000
1	-0.115256000	-2.523214000	0.769026000
6	-5.039385000	0.070068000	-0.702011000
1	-4.656628000	1.030152000	-1.030562000
6	4.603176000	1.790670000	0.515774000
1	5.191965000	2.647036000	0.205226000
6	-0.657721000	4.625851000	-2.081367000
1	-0.966952000	5.569668000	-2.520470000
6	-0.462621000	3.500137000	-2.884163000
1	-0.608572000	3.538229000	-3.958199000
6	-0.452804000	4.524540000	-0.704899000
1	-0.592340000	5.375718000	-0.046589000
6	-6.012845000	-2.423291000	0.121588000
1	-6.395376000	-3.390217000	0.435541000
6	-6.890673000	-1.334762000	0.024219000
6	-6.385941000	-0.090999000	-0.392299000
1	-7.059590000	0.757297000	-0.477331000
6	-8.352090000	-1.486266000	0.353327000
1	-8.588440000	-2.515910000	0.641134000
1	-8.975108000	-1.213430000	-0.508257000
1	-8.634451000	-0.820421000	1.179174000
1	0.690179000	-0.632231000	-1.232412000
6	2.299765000	-2.611818000	-1.655519000
6	3.690194000	-2.295690000	-1.434648000
6	4.305078000	-1.100355000	-1.895708000
6	4.516751000	-3.195378000	-0.710702000
6	5.654698000	-0.843752000	-1.667073000
1	3.710566000	-0.365427000	-2.431916000
6	5.864863000	-2.931501000	-0.481262000
1	4.072802000	-4.112924000	-0.328386000
6	6.453930000	-1.753419000	-0.960699000
1	6.087142000	0.085027000	-2.032753000
1	6.461832000	-3.648383000	0.078916000
1	7.504930000	-1.545024000	-0.779917000
6	1.370538000	-1.761786000	-2.236490000
1	0.389181000	-2.157592000	-2.484056000
1	1.712217000	-0.972960000	-2.904556000
1	1.939025000	-3.521229000	-1.174335000

TS_S_homo$_q$

ANNEX

(G = -3486.611462) (quadruplet)

27	0.523334000	0.370284000	0.078955000
16	-2.475575000	-0.786480000	-0.962659000
7	-1.723075000	-0.229433000	0.491476000
8	-2.330699000	0.290834000	-1.953640000
7	0.267387000	2.237348000	-0.925960000
7	2.575770000	0.565141000	0.472582000
7	-0.017214000	1.765983000	1.773571000
7	0.717244000	-0.958927000	1.799915000
8	-1.913226000	-2.119810000	-1.230629000
6	-2.291093000	1.083532000	0.931239000
1	-3.324193000	0.962937000	1.278470000
1	-2.282087000	1.744088000	0.063073000
6	2.065458000	-1.528324000	1.579317000
1	2.003444000	-2.196519000	0.714233000
1	2.406959000	-2.107556000	2.447180000
6	0.086903000	3.315081000	-0.134496000
6	3.382121000	1.585785000	0.146227000
1	2.944641000	2.352726000	-0.486304000
6	0.076689000	2.367269000	-2.249713000
1	0.227363000	1.466413000	-2.835977000
6	0.403746000	3.106852000	1.325942000
1	1.492034000	3.173740000	1.440033000
1	-0.044457000	3.901732000	1.936031000
6	4.349004000	-0.409520000	1.754225000
1	4.688767000	-1.217337000	2.393587000
6	-1.472442000	1.703086000	2.063161000
1	-1.872783000	2.708938000	2.238192000
1	-1.629929000	1.142652000	2.986341000
6	5.187539000	0.652263000	1.412653000
1	6.207340000	0.685326000	1.783908000
6	-1.721786000	-1.301123000	1.542647000
1	-2.468831000	-2.071405000	1.332592000
1	-2.022994000	-0.842373000	2.484263000
6	-4.204884000	-0.973143000	-0.583940000
6	0.792452000	1.286090000	2.917266000
1	0.503559000	1.790645000	3.850014000
1	1.834676000	1.530975000	2.709031000
6	0.642519000	-0.227725000	3.097144000
1	1.428468000	-0.582072000	3.774718000
1	-0.309002000	-0.455886000	3.578946000
6	-4.687686000	-2.219177000	-0.169925000
1	-4.026391000	-3.077368000	-0.120425000
6	3.047216000	-0.422399000	1.263277000
6	-0.351120000	-1.965999000	1.652975000
1	-0.365576000	-2.669029000	2.498439000
1	-0.149508000	-2.524387000	0.735249000
6	-5.042468000	0.144242000	-0.667080000
1	-4.652736000	1.102375000	-0.993029000
6	4.695711000	1.672901000	0.596808000
1	5.312784000	2.519077000	0.314213000
6	-0.500983000	4.681262000	-2.019467000
1	-0.810303000	5.632582000	-2.442108000
6	-0.296631000	3.570487000	-2.840585000
1	-0.435657000	3.627117000	-3.914959000
6	-0.306561000	4.550207000	-0.644230000
1	-0.456466000	5.385183000	0.032677000
6	-6.036229000	-2.339850000	0.157961000
1	-6.424564000	-3.303082000	0.477013000
6	-6.902694000	-1.238518000	0.079142000

6	-6.387233000	-0.000151000	-0.333895000
1	-7.048869000	0.859218000	-0.396247000
6	-8.365659000	-1.391620000	0.400969000
1	-8.520284000	-2.130394000	1.195571000
1	-8.916410000	-1.740127000	-0.483999000
1	-8.804521000	-0.436690000	0.710173000
1	0.489609000	-0.427776000	-1.389129000
6	2.055310000	-2.472539000	-1.760196000
6	3.461341000	-2.256032000	-1.508297000
6	4.162029000	-1.096814000	-1.932530000
6	4.209348000	-3.227067000	-0.793824000
6	5.522087000	-0.939598000	-1.679752000
1	3.626492000	-0.311435000	-2.458492000
6	5.569755000	-3.064058000	-0.540217000
1	3.695861000	-4.119329000	-0.440191000
6	6.244477000	-1.919429000	-0.984434000
1	6.023669000	-0.035239000	-2.016760000
1	6.107541000	-3.833212000	0.010087000
1	7.304555000	-1.787848000	-0.785456000
6	1.198942000	-1.573854000	-2.373807000
1	0.209085000	-1.914055000	-2.664171000
1	1.608515000	-0.785413000	-3.003039000
1	1.628923000	-3.372858000	-1.317314000

TS_S_homo$_d$

(G = -3486.614497) (doublet)

27	0.460502000	0.503472000	0.257489000
16	-2.531368000	-0.712534000	-0.981270000
7	-1.833961000	-0.149189000	0.475702000
8	-2.390930000	0.367156000	-1.969973000
7	0.236372000	1.991270000	-0.936453000
7	2.567772000	0.663004000	0.595328000
7	-0.064220000	1.804119000	1.718141000
7	0.640946000	-0.846422000	1.739184000
8	-1.925260000	-2.027922000	-1.245513000
6	-2.364021000	1.180536000	0.890068000
1	-3.402200000	1.101482000	1.235702000
1	-2.330263000	1.829794000	0.014510000
6	1.970758000	-1.469840000	1.527393000
1	1.901859000	-2.080341000	0.620705000
1	2.244289000	-2.116888000	2.370112000
6	0.126357000	3.184657000	-0.293475000
6	3.427267000	1.653311000	0.317676000
1	3.025112000	2.487662000	-0.251444000
6	0.123430000	1.975820000	-2.279794000
1	0.204741000	1.005725000	-2.751787000
6	0.370564000	3.123512000	1.191769000
1	1.449722000	3.209200000	1.359649000
1	-0.117766000	3.954368000	1.714105000
6	4.314671000	-0.493015000	1.768354000
1	4.620896000	-1.361187000	2.342786000
6	-1.529556000	1.782524000	2.015671000
1	-1.891603000	2.800713000	2.192963000
1	-1.690182000	1.225628000	2.939926000
6	5.206996000	0.538827000	1.472925000
1	6.235525000	0.490210000	1.817480000
6	-1.811494000	-1.210095000	1.528761000
1	-2.555177000	-1.988667000	1.335170000
1	-2.100523000	-0.750535000	2.473846000
6	-4.260670000	-0.946262000	-0.631654000

ANNEX

6	0.721369000	1.370344000	2.905653000
1	0.382769000	1.883120000	3.814864000
1	1.762840000	1.635113000	2.729019000
6	0.583332000	-0.143816000	3.073619000
1	1.380597000	-0.516802000	3.724563000
1	-0.362683000	-0.388140000	3.557834000
6	-4.720146000	-2.208811000	-0.242944000
1	-4.044532000	-3.057075000	-0.222220000
6	3.006655000	-0.398118000	1.302855000
6	-0.433046000	-1.861438000	1.614300000
1	-0.414926000	-2.556400000	2.464721000
1	-0.243406000	-2.419693000	0.695412000
6	-5.117732000	0.159011000	-0.682418000
1	-4.748816000	1.129423000	-0.996588000
6	4.756723000	1.633998000	0.733443000
1	5.416420000	2.458723000	0.484720000
6	-0.219386000	4.349867000	-2.364450000
1	-0.400632000	5.266095000	-2.918030000
6	-0.091383000	3.128212000	-3.027241000
1	-0.167712000	3.059539000	-4.107159000
6	-0.111641000	4.373399000	-0.973033000
1	-0.203721000	5.297374000	-0.411494000
6	-6.063613000	-2.358770000	0.095366000
1	-6.435008000	-3.336815000	0.388422000
6	-6.945922000	-1.268261000	0.060592000
6	-6.456335000	-0.014586000	-0.338832000
1	-7.134215000	0.833301000	-0.383490000
6	-8.386611000	-1.433484000	0.467601000
1	-8.740900000	-2.450160000	0.264377000
1	-9.029748000	-0.718435000	-0.057363000
1	-8.502304000	-1.251995000	1.545495000
1	0.743506000	-0.577145000	-0.904693000
6	2.139400000	-2.404650000	-1.690151000
6	3.557982000	-2.245712000	-1.466919000
6	4.276123000	-1.072133000	-1.817193000
6	4.303312000	-3.290327000	-0.861366000
6	5.644231000	-0.962481000	-1.586231000
1	3.749717000	-0.237868000	-2.271489000
6	5.672084000	-3.173752000	-0.626768000
1	3.780041000	-4.199205000	-0.569786000
6	6.360737000	-2.008834000	-0.988763000
1	6.157779000	-0.045428000	-1.866105000
1	6.205964000	-3.996317000	-0.155494000
1	7.427564000	-1.915237000	-0.804946000
6	1.270843000	-1.378618000	-2.052650000
1	0.272124000	-1.647895000	-2.390852000
1	1.683604000	-0.507442000	-2.561251000
1	1.713081000	-3.360431000	-1.385874000

H₂O
(G =-76.468827) (singlet)

8	0.000000000	0.000000000	0.121359000
1	0.000000000	0.757766000	-0.485437000
1	0.000000000	-0.757766000	-0.485437000

(H₂O)₃
(G = -229.388173) (singlet)

8	1.432539000	-1.037400000	0.002469000
1	1.335635000	-0.065848000	-0.085725000

8	-1.460496000	-0.566402000	-0.002749000
1	0.495613000	-1.302201000	0.011285000
1	-1.934604000	-0.426529000	0.834122000
8	0.303114000	1.560259000	-0.102813000
1	0.479151000	1.696894000	0.842870000
1	-0.432739000	0.899253000	-0.093608000
1	-2.144316000	-0.453224000	-0.684198000

A.IX.7.Coordinates from chapter X

$\mathbf{1_{Co}{}^{II}_{Cl}}$ (G = -2282045.18, quadruplet)

27	1.306648000	-0.057506000	0.289131000
7	1.376925000	-2.082028000	-0.537666000
7	-1.094888000	-0.543932000	-0.192060000
7	1.156270000	0.390912000	-1.895194000
7	3.391241000	-0.387798000	0.187907000
7	1.067089000	2.021079000	0.297526000
16	-2.148564000	-0.246199000	1.157724000
8	-1.982121000	-1.387005000	2.067230000
8	-1.866387000	1.126615000	1.599202000
6	1.583977000	-2.053655000	-2.021408000
1	0.669335000	-2.393973000	-2.508582000
1	2.366786000	-2.766156000	-2.303405000
6	1.975241000	-0.661936000	-2.540678000
1	3.018999000	-0.455360000	-2.305812000
1	1.866292000	-0.639357000	-3.634313000
6	-0.252568000	0.368859000	-2.382093000
1	-0.402046000	-0.535026000	-2.973261000
1	-0.428341000	1.211281000	-3.061600000
6	-1.315042000	0.450480000	-1.284677000
1	-1.305430000	1.437168000	-0.822176000
1	-2.291426000	0.295840000	-1.761056000
6	-1.124651000	-1.980654000	-0.621731000
1	-1.225342000	-2.003670000	-1.706708000
1	-2.006087000	-2.492366000	-0.229276000
6	0.111219000	-2.744399000	-0.142243000
1	0.095774000	-2.777152000	0.949325000
1	0.062455000	-3.773083000	-0.528482000
6	2.550612000	-2.662240000	0.154592000
1	2.837830000	-3.627481000	-0.281767000
1	2.273135000	-2.829414000	1.200418000
6	3.715426000	-1.695908000	0.135095000
6	5.045113000	-2.115652000	0.113981000
6	6.058099000	-1.156047000	0.168838000
6	5.713519000	0.196371000	0.234842000
6	4.362957000	0.536248000	0.238505000
1	4.032424000	1.570098000	0.277862000
6	1.758861000	1.735616000	-2.008139000
1	1.555034000	2.194064000	-2.984269000
1	2.844519000	1.627543000	-1.915319000
6	1.285146000	2.632272000	-0.886343000
6	1.125480000	4.008841000	-1.037059000
6	0.745322000	4.769996000	0.070073000
6	0.529567000	4.131611000	1.293469000
6	0.696790000	2.751329000	1.362795000
1	0.527113000	2.191423000	2.274805000
6	-3.823490000	-0.286372000	0.521350000
6	-4.390711000	0.885729000	0.012746000
1	-3.830127000	1.814783000	0.013010000
6	-5.694589000	0.846052000	-0.483501000
1	-6.141080000	1.756736000	-0.874879000
6	-6.438825000	-0.344316000	-0.477420000
6	-5.843650000	-1.505409000	0.046855000
1	-6.409950000	-2.433535000	0.072195000
6	-4.542655000	-1.487704000	0.545898000
1	-4.102306000	-2.386037000	0.965828000

ANNEX

6	-7.846290000	-0.389084000	-1.016411000
1	-8.532725000	-0.833416000	-0.285265000
1	-7.895699000	-1.008424000	-1.921724000
1	-8.211336000	0.611238000	-1.270044000
17	1.314523000	-0.510944000	2.606589000
1	6.470105000	0.973705000	0.275637000
1	5.275904000	-3.175221000	0.055409000
1	0.229027000	4.685664000	2.177206000
1	1.295255000	4.468376000	-2.006196000
1	0.613760000	5.844566000	-0.023293000
1	7.101237000	-1.459604000	0.154523000

1$_{Co}^{I}$$_{Cl}$ (G = -2282104.61, triplet)

27	1.459245000	0.047290000	0.279202000
7	1.359088000	-2.044106000	-0.487464000
7	-1.198374000	-0.504749000	-0.165683000
7	1.095177000	0.400691000	-1.931063000
7	3.473802000	-0.406212000	0.139657000
7	1.244677000	2.042507000	0.318498000
16	-2.238975000	-0.195137000	1.149533000
8	-2.051898000	-1.297580000	2.106007000
8	-2.011053000	1.199804000	1.558798000
6	1.539050000	-2.051130000	-1.967466000
1	0.623621000	-2.418715000	-2.435795000
1	2.328251000	-2.759431000	-2.249627000
6	1.902724000	-0.668597000	-2.543628000
1	2.949172000	-0.448222000	-2.331013000
1	1.783725000	-0.701300000	-3.639598000
6	-0.314187000	0.365712000	-2.375132000
1	-0.485398000	-0.554903000	-2.936315000
1	-0.514272000	1.187441000	-3.077704000
6	-1.358177000	0.490950000	-1.261785000
1	-1.294980000	1.477569000	-0.802731000
1	-2.344717000	0.390147000	-1.737082000
6	-1.161856000	-1.942057000	-0.559596000
1	-1.254120000	-1.995669000	-1.644593000
1	-2.027530000	-2.480321000	-0.163987000
6	0.092245000	-2.664998000	-0.055269000
1	0.082664000	-2.642781000	1.037207000
1	0.026537000	-3.716924000	-0.383572000
6	2.520577000	-2.634983000	0.204236000
1	2.755176000	-3.644031000	-0.169343000
1	2.262392000	-2.709528000	1.266251000
6	3.731802000	-1.734574000	0.088664000
6	5.030136000	-2.231641000	-0.025364000
6	6.103594000	-1.337157000	-0.072495000
6	5.836361000	0.033783000	-0.011428000
6	4.510642000	0.450581000	0.090737000
1	4.250001000	1.504914000	0.131573000
6	1.695906000	1.742037000	-2.044958000
1	1.481690000	2.215803000	-3.015176000
1	2.781632000	1.617961000	-1.965231000
6	1.247609000	2.635568000	-0.909196000
6	0.896044000	3.969630000	-1.090447000
6	0.542769000	4.747934000	0.019403000
6	0.554840000	4.145020000	1.282119000
6	0.905677000	2.802045000	1.385536000
1	0.919484000	2.282481000	2.338313000
6	-3.921756000	-0.301168000	0.529170000
6	-4.518915000	0.833012000	-0.029084000
1	-3.983491000	1.776308000	-0.061599000
6	-5.819204000	0.740446000	-0.528999000
1	-6.287647000	1.623542000	-0.956678000
6	-6.532259000	-0.467595000	-0.480659000
6	-5.908348000	-1.590960000	0.089853000
1	-6.450009000	-2.532397000	0.148390000
6	-4.610246000	-1.518698000	0.593703000
1	-4.147870000	-2.388611000	1.048473000
6	-7.933795000	-0.569662000	-1.028491000

1	-8.603878000	-1.056445000	-0.309620000
1	-7.949687000	-1.174567000	-1.945004000
1	-8.343166000	0.416766000	-1.269757000
17	1.644715000	-0.421548000	2.897903000
1	6.634863000	0.769356000	-0.048158000
1	5.192498000	-3.304858000	-0.078154000
1	0.290067000	4.702243000	2.176717000
1	0.897549000	4.391128000	-2.092417000
1	0.263612000	5.791152000	-0.100839000
1	7.123305000	-1.702115000	-0.160862000

1^{DMM}$_{Co}^{II}$$_{Cl}$ (G =-2524480.74, quadruplet)

27	-0.688291000	-0.359092000	-0.306591000
7	-1.020629000	-2.351891000	0.510134000
7	1.634592000	-1.155824000	0.185134000
7	-0.501235000	0.074703000	1.868531000
7	-2.792286000	-0.427205000	-0.214464000
7	-0.179319000	1.665164000	-0.306607000
16	2.735561000	-0.994135000	-1.148383000
8	-6.879140000	-0.979568000	-0.360703000
8	0.658543000	5.702651000	-0.096100000
8	2.451376000	-2.112071000	-2.057664000
8	2.629584000	0.398983000	-1.602569000
6	-1.233179000	-2.294515000	1.991611000
1	-0.371043000	-2.746100000	2.483300000
1	-2.100063000	-2.904234000	2.268925000
6	-1.452635000	-0.864608000	2.506832000
1	-2.459176000	-0.529732000	2.258254000
1	-1.353446000	-0.854415000	3.601829000
6	0.888398000	-0.132719000	2.365393000
1	0.912340000	-1.045804000	2.960982000
1	1.169632000	0.681087000	3.044182000
6	1.963441000	-0.193180000	1.279387000
1	2.084766000	0.784800000	0.813921000
1	2.906658000	-0.467832000	1.768663000
1	1.473822000	-2.584052000	0.612276000
1	1.573486000	-2.625786000	1.696914000
1	2.279988000	-3.205569000	0.216289000
6	0.149266000	-3.178344000	0.128137000
1	0.167347000	-3.218661000	-0.963116000
1	0.057885000	-4.202514000	0.518890000
6	-2.255012000	-2.787324000	-0.184788000
1	-2.652686000	-3.698905000	0.275192000
1	-1.996029000	-3.018977000	-1.223130000
6	-3.289646000	-1.677247000	-0.198282000
6	-4.668129000	-1.931939000	-0.246993000
6	-5.518448000	-0.812915000	-0.286462000
6	-5.007008000	0.496629000	-0.312311000
6	-3.621541000	0.624344000	-0.278173000
1	-3.148497000	1.602280000	-0.298219000
6	-5.210259000	-3.338889000	-0.277516000
1	-6.274514000	-3.341623000	-0.523389000
1	-5.083007000	-3.836287000	0.692530000
1	-4.688268000	-3.944779000	-1.026492000
6	-7.527731000	-1.195419000	0.910390000
1	-8.591507000	-1.311009000	0.692393000
1	-7.375376000	-0.334166000	1.571945000
1	-7.148907000	-2.102209000	1.396402000
6	-5.915014000	1.693668000	-0.391030000
1	-5.337941000	2.622379000	-0.336331000
1	-6.648269000	1.693392000	0.423389000
1	-6.480095000	1.694721000	-1.331285000
6	-0.924257000	1.486290000	1.989565000
1	-0.641687000	1.896256000	2.965484000
1	-2.017136000	1.522730000	1.927151000
6	-0.361758000	2.321186000	0.856380000
6	-0.100314000	3.691747000	0.990560000
6	0.396470000	4.356209000	-0.144322000
6	0.584277000	3.682803000	-1.363448000

ANNEX

6	0.272259000	2.327369000	-1.383605000
1	0.398119000	1.731304000	-2.279777000
6	-0.360419000	4.421453000	2.285202000
1	-0.287810000	5.502236000	2.144228000
1	0.359906000	4.129425000	3.059819000
1	-1.362246000	4.196282000	2.667529000
6	1.956912000	6.041594000	0.435746000
1	2.010669000	7.132333000	0.431564000
1	2.751738000	5.627699000	-0.196284000
1	2.071703000	5.669016000	1.460477000
6	1.087534000	4.396979000	-2.588503000
1	1.194945000	3.699563000	-3.425347000
1	2.060657000	4.867452000	-2.406076000
1	0.397079000	5.194260000	-2.889628000
6	4.380873000	-1.233171000	-0.477694000
6	5.076250000	-0.135899000	0.044637000
1	4.633798000	0.854887000	0.028189000
6	6.349140000	-0.333873000	0.576122000
1	6.895793000	0.516366000	0.977266000
6	6.939408000	-1.609877000	0.595825000
6	6.221503000	-2.689115000	0.056511000
1	6.667679000	-3.680453000	0.048215000
6	4.945172000	-2.512417000	-0.480303000
1	4.408814000	-3.352231000	-0.909712000
6	8.307501000	-1.810051000	1.197113000
1	8.759539000	-2.748957000	0.861086000
1	8.244392000	-1.843109000	2.293462000
1	8.980365000	-0.984954000	0.936784000
17	-0.723925000	-0.828318000	-2.625692000

$1^{DMM}_{Co}{}^{I}_{Cl}$ (G =-2524536.76, triplet)

27	-0.877782000	-0.163385000	-0.299362000
7	-1.158809000	-2.215788000	0.463342000
7	1.632630000	-1.149484000	0.170483000
7	-0.500562000	0.163393000	1.889027000
7	-2.943640000	-0.266827000	-0.203833000
7	-0.311859000	1.774020000	-0.354199000
16	2.729891000	-1.034990000	-1.128238000
8	-7.050498000	-0.866827000	-0.223472000
8	1.491246000	5.508673000	-0.004925000
8	2.378005000	-2.101418000	-2.079484000
8	2.747649000	0.372725000	-1.555677000
6	-1.355972000	-2.174121000	1.940638000
1	-0.521071000	-2.685854000	2.423645000
1	-2.257426000	-2.735507000	2.218195000
6	-1.487618000	-0.743740000	2.498657000
1	-2.477516000	-0.351842000	2.264379000
1	-1.392837000	-0.783706000	3.597231000
6	0.874644000	-0.108043000	2.355880000
1	0.877487000	-1.036054000	2.930508000
1	1.205314000	0.676120000	3.052033000
6	1.938760000	-0.177442000	1.257175000
1	2.043978000	0.798767000	0.783757000
1	2.889429000	-0.431804000	1.748180000
6	1.341866000	-2.554072000	0.574607000
1	1.413048000	-2.616287000	1.660932000
1	2.105546000	-3.236791000	0.191874000
6	-0.012706000	-3.052471000	0.058320000
1	0.015782000	-3.045101000	-1.033871000
1	-0.135702000	-4.096169000	0.397238000
6	-2.394711000	-2.622610000	-0.234100000
1	-2.788461000	-3.562841000	0.176564000
1	-2.137554000	-2.790067000	-1.286062000
6	-3.439433000	-1.522324000	-0.188511000
6	-4.817891000	-1.790798000	-0.193573000
6	-5.684232000	-0.683831000	-0.187864000
6	-5.184472000	0.629539000	-0.206401000
6	-3.798740000	0.769716000	-0.217236000
1	-3.341499000	1.756127000	-0.237885000

6	-5.351041000	-3.202995000	-0.227485000
1	-6.426195000	-3.209468000	-0.422164000
1	-5.175160000	-3.721584000	0.723855000
1	-4.862670000	-3.790804000	-1.012984000
6	-7.655748000	-1.081427000	1.065617000
1	-8.728247000	-1.188742000	0.886688000
1	-7.475310000	-0.225316000	1.727699000
1	-7.268124000	-1.993264000	1.536664000
6	-6.103987000	1.821393000	-0.236882000
1	-5.531695000	2.753950000	-0.188862000
1	-6.810364000	1.808255000	0.601242000
1	-6.701419000	1.834405000	-1.157224000
6	-0.864235000	1.590701000	1.987528000
1	-0.599812000	2.004487000	2.968989000
1	-1.952858000	1.655558000	1.880827000
6	-0.236578000	2.385918000	0.857139000
6	0.352766000	3.644848000	1.035499000
6	0.901174000	4.264184000	-0.103652000
6	0.818396000	3.655387000	-1.367301000
6	0.195301000	2.412317000	-1.428462000
1	0.103829000	1.874737000	-2.367634000
6	0.400139000	4.319366000	2.387208000
1	0.763978000	5.345746000	2.297607000
1	1.062476000	3.784066000	3.079271000
1	-0.593176000	4.354306000	2.848621000
6	2.883049000	5.470011000	0.359582000
1	3.227022000	6.507247000	0.373377000
1	3.463411000	4.898624000	-0.375801000
1	3.017406000	5.024031000	1.353255000
6	1.380851000	4.314824000	-2.599113000
1	1.185759000	3.704543000	-3.487235000
1	2.465357000	4.458766000	-2.518193000
1	0.938593000	5.305978000	-2.757730000
6	4.359706000	-1.415127000	-0.473929000
6	5.129992000	-0.392465000	0.088283000
1	4.762775000	0.628760000	0.102052000
6	6.384494000	-0.699384000	0.618825000
1	6.987303000	0.096245000	1.049940000
6	6.881604000	-2.012057000	0.597299000
6	6.087739000	-3.019029000	0.020938000
1	6.461433000	-4.039755000	-0.017264000
6	4.832162000	-2.732659000	-0.513234000
1	4.236940000	-3.516241000	-0.970676000
6	8.231037000	-2.346461000	1.182827000
1	8.820922000	-2.960778000	0.491894000
1	8.118185000	-2.923445000	2.110493000
1	8.802652000	-1.442269000	1.416373000
17	-1.115476000	-0.649478000	-2.942362000

$1^{CO2Et}_{Co}{}^{II}_{Cl}$ (G =-2617406.01, quadruplet)

27	0.494438000	-0.457656000	0.211643000
7	1.423573000	-2.309244000	-0.421364000
7	-1.433044000	-1.770146000	-0.138368000
7	0.261691000	-0.244289000	-1.988412000
7	2.586951000	0.100174000	0.156153000
7	-0.304773000	1.486588000	0.065582000
16	-2.549964000	-1.741633000	1.216554000
8	-2.026298000	-2.692712000	2.204352000
8	-2.732956000	-0.320541000	1.541610000
8	1.596922000	-2.346424000	-1.908237000
1	0.874718000	-3.047443000	-2.327339000
1	2.589229000	-2.736134000	-2.158902000
6	1.434996000	-0.964052000	-2.549340000
1	2.316593000	-0.356856000	-2.344813000
1	1.347828000	-1.074524000	-3.639244000
6	-1.024138000	-0.843150000	-2.441368000
1	-0.813571000	-1.787153000	-2.944532000
1	-1.502380000	-0.197084000	-3.186289000
6	-2.032525000	-1.062982000	-1.316044000

ANNEX

```
 1   -2.403371000   -0.104795000   -0.950235000
 1   -2.874893000   -1.633778000   -1.724174000
 6   -0.931565000   -3.159124000   -0.425675000
 1   -1.016976000   -3.332623000   -1.498169000
 1   -1.562964000   -3.910658000    0.052036000
 6    0.499549000   -3.360824000    0.075834000
 1    0.502165000   -3.299703000    1.166321000
 1    0.841577000   -4.361890000   -0.223751000
 6    2.724326000   -2.322318000    0.283367000
 1    3.381193000   -3.115739000   -0.094035000
 1    2.525871000   -2.516338000    1.342211000
 6    3.402235000   -0.971599000    0.186106000
 6    4.789531000   -0.835757000    0.180597000
 6    5.342213000    0.449108000    0.159635000
 6    4.486912000    1.556142000    0.139272000
 6    3.113969000    1.332556000    0.133939000
 1    2.405254000    2.154543000    0.109067000
 6    0.330629000    1.210352000   -2.253372000
 1   -0.055827000    1.462036000   -3.248384000
 1    1.384168000    1.506564000   -2.224172000
 6   -0.389153000    1.993010000   -1.181891000
 6   -1.052056000    3.189016000   -1.440851000
 6   -1.636316000    3.884384000   -0.378164000
 6   -1.535077000    3.358056000    0.914263000
 6   -0.863637000    2.152074000    1.088946000
 1   -0.767172000    1.684052000    2.061420000
 6   -4.107261000   -2.376377000    0.601468000
 6   -5.043619000   -1.488864000    0.062993000
 1   -4.836396000   -0.424423000    0.027625000
 6   -6.251671000   -1.992710000   -0.420070000
 1   -6.984764000   -1.305515000   -0.834895000
 6   -6.536463000   -3.366851000   -0.373681000
 6   -5.578336000   -4.232892000    0.182552000
 1   -5.788364000   -5.298247000    0.240771000
 6   -4.365865000   -3.750618000    0.671541000
 1   -3.644617000   -4.427903000    1.116559000
 6   -7.833351000   -3.913469000   -0.914534000
 1   -8.289044000   -4.618864000   -0.209560000
 1   -7.659362000   -4.460961000   -1.850664000
 1   -8.552218000   -3.113976000   -1.120769000
17    0.694168000   -0.657443000    2.568723000
 1    4.881883000    2.565767000    0.120831000
 1    5.418898000   -1.718278000    0.191192000
 1   -1.973078000    3.861764000    1.767646000
 1   -1.116094000    3.569853000   -2.454469000
 6    6.824614000    0.682894000    0.153859000
 8    7.327902000    1.795200000    0.145891000
 8    7.520765000   -0.457576000    0.159199000
 6    8.977258000   -0.351900000    0.158189000
 1    9.278313000    0.206652000   -0.733381000
 1    9.278659000    0.212390000    1.046060000
 6   -2.353375000    5.169875000   -0.671412000
 8   -2.448874000    5.643658000   -1.792646000
 8   -2.868868000    5.727214000    0.427447000
 6   -3.585186000    6.989566000    0.262236000
 1   -2.901551000    7.711656000   -0.194461000
 1   -4.424240000    6.818741000   -0.419204000
 6    9.530144000   -1.760931000    0.162631000
 1    9.207932000   -2.308339000    1.055621000
 1    9.208734000   -2.313675000   -0.727381000
 1   10.625669000   -1.715427000    0.162992000
 6   -4.045134000    7.429172000    1.635277000
 1   -4.718444000    6.688862000    2.081980000
 1   -3.192155000    7.583854000    2.305541000
 1   -4.588025000    8.377288000    1.543077000
```

$1^{CO2Et}{}_{Co}{}^{I}{}_{Cl}$ (G =-2617473.03, triplet)

```
27    0.710621000   -0.251414000    0.359351000
 7    1.554409000   -2.186602000   -0.239755000
 7   -1.373194000   -1.771621000   -0.107710000
 7    0.408219000   -0.137772000   -1.858122000
 7    2.634534000    0.256323000    0.323513000
 7   -0.330296000    1.559421000    0.207759000
16   -2.533796000   -1.798483000    1.166938000
 8   -2.019597000   -2.714894000    2.193579000
 8   -2.837970000   -0.394679000    1.480524000
 6    1.806042000   -2.198307000   -1.710331000
 1    1.140210000   -2.926380000   -2.176262000
 1    2.827445000   -2.541372000   -1.915057000
 6    1.621058000   -0.818458000   -2.368502000
 1    2.474428000   -0.181187000   -2.138042000
 1    1.580408000   -0.945899000   -3.460921000
 6   -0.832631000   -0.778982000   -2.360381000
 1   -0.569680000   -1.715490000   -2.853923000
 1   -1.298217000   -0.150108000   -3.129963000
 6   -1.895619000   -1.035581000   -1.294852000
 1   -2.293291000   -0.088913000   -0.928110000
 1   -2.711279000   -1.593283000   -1.774299000
 6   -0.774300000   -3.116173000   -0.375137000
 1   -0.788649000   -3.283507000   -1.452241000
 1   -1.386230000   -3.911398000    0.057345000
 6    0.637102000   -3.253357000    0.206469000
 1    0.570075000   -3.178945000    1.294244000
 1    1.019773000   -4.252670000   -0.057229000
 6    2.817293000   -2.157494000    0.535142000
 1    3.490945000   -2.978343000    0.249442000
 1    2.543821000   -2.281559000    1.587854000
 6    3.496748000   -0.816285000    0.359231000
 6    4.862224000   -0.677736000    0.239073000
 6    5.442079000    0.615528000    0.099374000
 6    4.542966000    1.716498000    0.069422000
 6    3.187567000    1.497050000    0.177606000
 1    2.479211000    2.320618000    0.157798000
 6    0.416131000    1.320918000   -2.088303000
 1    0.086402000    1.581764000   -3.102969000
 1    1.447490000    1.669546000   -1.973474000
 6   -0.428149000    2.034695000   -1.054598000
 6   -1.229057000    3.128919000   -1.364674000
 6   -1.939710000    3.765809000   -0.340400000
 6   -1.822768000    3.277219000    0.966307000
 6   -1.013039000    2.167036000    1.190083000
 1   -0.901374000    1.725722000    2.174176000
 6   -4.022179000   -2.533163000    0.480133000
 6   -4.971346000   -1.712755000   -0.136381000
 1   -4.824823000   -0.638305000   -0.176323000
 6   -6.113701000   -2.293247000   -0.690066000
 1   -6.855892000   -1.656036000   -1.164673000
 6   -6.321137000   -3.680689000   -0.638883000
 6   -5.353407000   -4.480000000   -0.005322000
 1   -5.504306000   -5.555287000    0.056560000
 6   -4.206506000   -3.919105000    0.554524000
 1   -3.476963000   -4.546405000    1.056105000
 6   -7.545728000   -4.310665000   -1.253691000
 1   -8.008462000   -5.028344000   -0.565739000
 1   -7.279937000   -4.863510000   -2.164749000
 1   -8.292962000   -3.557342000   -1.523541000
17    0.618534000   -0.570723000    2.782431000
 1    4.922057000    2.728032000   -0.037478000
 1    5.489790000   -1.562849000    0.249445000
 1   -2.355368000    3.735223000    1.791583000
 1   -1.304909000    3.478933000   -2.388794000
 6    6.873728000    0.845183000   -0.017936000
 8    7.407271000    1.956156000   -0.127790000
 8    7.602596000   -0.307127000    0.002117000
 6    9.039826000   -0.176171000   -0.099618000
 1    9.285115000    0.363580000   -1.020854000
 1    9.403462000    0.413533000    0.749404000
 6   -2.804638000    4.936707000   -0.690164000
 8   -2.940289000    5.358032000   -1.829277000
 8   -3.409769000    5.465855000    0.379474000
```

ANNEX

6	-4.284697000	6.610574000	0.147806000
1	-3.689644000	7.409224000	-0.305891000
1	-5.062673000	6.307924000	-0.559859000
6	9.625518000	-1.574786000	-0.099420000
1	9.367058000	-2.110663000	0.821500000
1	9.260683000	-2.153859000	-0.955829000
1	10.718518000	-1.512481000	-0.166089000
6	-4.860205000	7.018599000	1.487186000
1	-5.445098000	6.204478000	1.929929000
1	-4.066761000	7.304982000	2.186774000
1	-5.521885000	7.881076000	1.344369000

UNIVERSITAT ROVIRA I VIRGILI

MECHANISTIC STUDIES OF WATER OXIDATION CATALYZED BY HOMOGENEOUS IRON AND RUTHENIUM
COMPLEXES AND LIGHT-DRIVEN ORGANIC REDUCTIONS WITH A DUAL COBALT/COPPER CATALYTIC SYSTEM
Carla Casadevall Serrano

UNIVERSITAT ROVIRA I VIRGILI
MECHANISTIC STUDIES OF WATER OXIDATION CATALYZED BY HOMOGENEOUS IRON AND RUTHENIUM
COMPLEXES AND LIGHT-DRIVEN ORGANIC REDUCTIONS WITH A DUAL COBALT/COPPER CATALYTIC SYSTEM
Carla Casadevall Serrano

UNIVERSITAT
ROVIRA i VIRGILI